ELSEVIER

Volume 79, Nos. 2–4, October/December 2008

ISSN 0079-6611

PROGRESS IN OCEANOGRAPHY

Special Issue

The Northern Humboldt Current System: Ocean Dynamics, Ecosystem Processes, and Fisheries

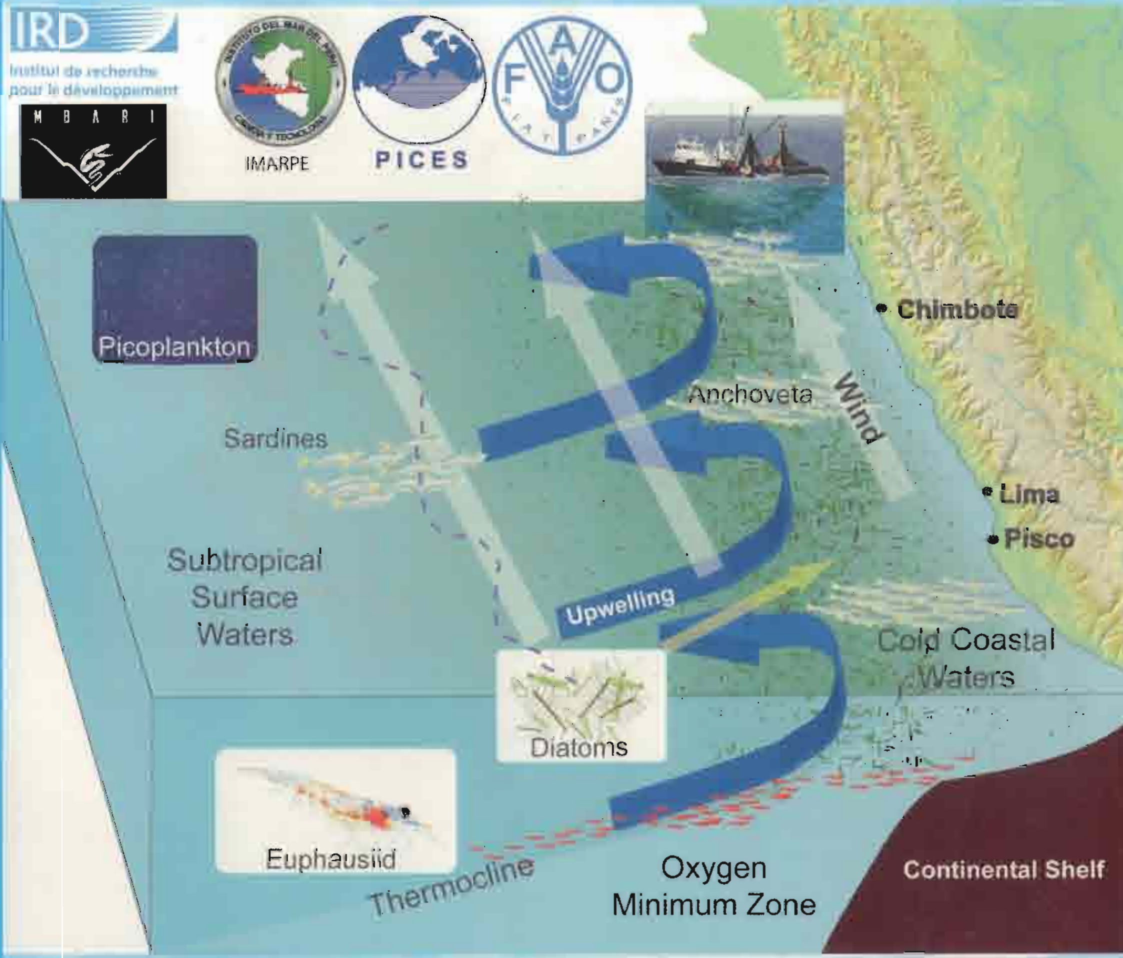

www.elsevier.com/locate/pocean

PROGRESS IN OCEANOGRAPHY

Aims and Scope
Progress in Oceanography is a journal designed for lengthy papers or collections of papers and complements the major research journals which publish shorter works. Contributions are either a review of an aspect of oceanography or a treatise on an expanding oceanographic subject. The articles cover the entire spectrum of disciplines within the science of oceanography.

Funding body agreements and policies
Elsevier has established agreements and developed policies to allow authors whose articles appear in journals published by Elsevier, to comply with potential manuscript archiving requirements as specified as conditions of their grant awards. To learn more about existing agreements and policies please visit http://www.elsevier.com/fundingbodies

For a full Guide for Authors please visit the journal homepage at: http://www.elsevier.com/locate/pocean

Publication information: *Progress in Oceanography* (ISSN 0079-6611). For 2008, volumes 76–79 are scheduled for publication. Subscription prices are available upon request from the Publisher or from the Regional Sales Office nearest you or from this journal's website (http://www.elsevier.com/locate/pocean). Further information is available on this journal and other Elsevier products through Elsevier's website (http://www.elsevier.com). Subscriptions are accepted on a prepaid basis only and are entered on a calendar year basis. Issues are sent by standard mail (surface within Europe, air delivery outside Europe). Priority rates are available upon request. Claims for missing issues should be made within six months of the date of dispatch.

Orders, claims, and journal enquiries: please contact the Regional Sales Office nearest you:

Orlando: Elsevier, Customer Service Department, 6277 Sea Harbor Drive, Orlando, FL 32887-4800, USA; phone: (877) 8397126 or (800) 6542452 [toll free numbers for US customers]; (+1) (407) 3454020 or (+1) (407) 3454000 [customers outside US]; fax: (+1) (407) 3631354 or (+1) (407) 3639661; e-mail: usjcs@elsevier.com or elspcs@elsevier.com

Amsterdam: Elsevier, Customer Service Department, PO Box 211, 1000 AE Amsterdam, The Netherlands; phone: (+31) (20) 4853757; fax: (+31) (20) 4853432; e-mail: JournalsCustomerServiceEMEA@elsevier.com

Tokyo: Elsevier, Customer Service Department, 4F Higashi-Azabu, 1-Chome Bldg, 1-9-15 Higashi-Azabu, Minato-ku, Tokyo 106-0044, Japan; phone: (+81) (3) 5561 5037; fax: (+81) (3) 5561 5047; e-mail: JournalsCustomerServiceJapan@elsevier.com

Singapore: Elsevier, Customer Service Department, 3 Killiney Road, #08-01 Winsland House I, Singapore 239519; phone: (+65) 63490222; fax: (+65) 67331510; e-mail: JournalsCustomerServiceAPAC@elsevier.com

USA mailing notice: *Progress in Oceanography* (ISSN 0079-6611) is published sixteen times a year monthly plus additional issues in March, June, September and October by Elsevier Ltd. (The Boulevard, Langford Lane, Kidlington, Oxford OX5 1GB, UK). Periodical postage paid at Rahway NJ and additional mailing offices.
USA POSTMASTER: Send change of address to *Progress in Oceanography*, Elsevier, 6277 Sea Harbor Drive, Orlando, FL 32887-4800.
AIRFREIGHT AND MAILING: in the USA by Mercury International Limited, 365, Blair Road, Avenel, NJ 07001

Front Cover Image
Winds, upwelling, water types and important biological components of the Northern Humboldt Current System (graphics by Shannon Boedecker).

PROGRESS IN OCEANOGRAPHY

The Northern Humboldt Current System: Ocean Dynamics, Ecosystem Processes, and Fisheries

Volume 79, Nos. 2–4, October/December 2008

CONTENTS

(*Continued on inside back cover*)

For a full Guide for Authors please visit the journal homepage at: http://www.elsevier.com/locate/pocean

Progress in Oceanography is indexed/abstracted in: Appl. Mech. Rev., CABS, Curr. Cont. Ind. Sci. Rev., Curr. Cont./Phy. Chem. & Earth Sci., Curr. Cont. Sci. Cit. Ind., Curr. Cont. SCISEARCH Data. Environ. Per. Bibl., Geo. Abstr., Geo. Bib. & Indx, INSPEC Data., Meteor. & Geoastrophys. Abstr., Ocean Lit. Rev./Marine Lit. Rev. and *Res. Alert. Also covered in the abstract and citation database SCOPUS®. Full text available on ScienceDirect®.*

Printed by Polestar Wheatons Ltd, Exeter, UK

0079-6611(200810/12)79:2-4;1-C

(Continued from outside back cover)

Progress in Oceanography 79 (2008) 95–105

Contents lists available at ScienceDirect

Progress in Oceanography

journal homepage: www.elsevier.com/locate/pocean

Editorial

The northern Humboldt Current System: Brief history, present status and a view towards the future

1. Introduction

The tropical ocean off the west coast of South America is notable for several reasons. First, it is unusually cool for an ocean that is so close to the equator with sea surface temperatures at 5 °S off Peru as cool as 16 °C when most other tropical locations are in excess of 25 °C. Upwelling of cool waters brings phytoplankton nutrients to the surface, dramatically increasing biological productivity in this low-latitude region of few storms. Second, as a result of the enhanced productivity, the northern Humboldt Current System (HCS) off Peru produces more fish per unit area than any other region in the world oceans (Fig. 1), representing less than 0.1% of the world ocean surface but presently producing about 10% of the world fish catch. Third, as a result of sinking and decay of surface-derived primary production and poor ventilation, surface oxygenated waters overlie an intense and extremely shallow Oxygen Minimum Zone (OMZ). The OMZ forms a barrier to some animals, concentrating living resources near the surface. At the other end of the spectrum different forms of marine life have adapted to this harsh environment, some utilizing it as a refuge from predation. The OMZ also affects global nutrient budgets, as nitrate instead of oxygen is used by bacteria as a terminal electron acceptor. Fourth, beneath the OMZ, in layered continental shelf sediments the absence of oxygen preserves dead organisms, creating a record of past ecosystem and climate changes. Fifth, through ocean/atmosphere coupling, the northern HCS is intimately linked to equatorial Pacific dynamics and is subject to large interannual to multidecadal fluctuations in climate, ecosystems and its fisheries.

New *in situ* and satellite observing capabilities, long-term and multi-variable data series, improved analysis, and modelling have opened new windows into the dynamics of the northern HCS. Fishery management is also evolving from a single-species approach towards one that where the ecosystem is the unit of management. This holistic approach, likely to be embraced in the 21st century, appears to be particularly appropriate for the northern HCS where strong temporal variability including El Niño, the Pacific Decadal Oscillation (PDO, or El Viejo/La Vieja) and global change, constitutes a major challenge. In this context, there was a clear need to begin a new integration and synthesis of the Humboldt Current System. The present collection of research papers resulted from the "International Conference on The Humboldt Current System: Climate, ocean dynamics, ecosystem processes, and fisheries" organized by the *Institut de Recherche pour le Développement* (IRD), the Instituto del Mar del Perú (IMARPE) and the *Food and Agriculture Organisation* (FAO) in Lima in late 2006 and highlight these developments. The focus of this special issue is on the northern Humboldt Current System (HCS) off Peru and complements a 2007 compilation in the same journal for the central and southern upwelling region off Chile (Escribano and Schneider, 2007). In this introductory paper we provide a brief overview of the "ecological and socio-economic" history of the northern HCS. The papers are then introduced in the context of: (1) the impacts of natural environmental rhythms and human exploitation; (2) new observations and models; and (3) the ecosystem as the management unit. A section on future research directions concludes the introduction to the special issue. The papers in the special issue are organized starting with physics and chemistry, then lower trophic biology to fish. These mostly data papers are followed by modelling and then socio-economic papers.

2. A brief history of ecology and exploitation of living marine resources

The first "artistic" descriptions of the biological richness of the northern HCS and its importance to humans can be found in the pottery left behind by native South Americans well before America was discovered by the Europeans (Rostworowski, 2005). Coastal pre-Inca and Inca communities depended heavily on ocean resources for their survival. The modern world became aware of the incredible biological productivity of the northern HCS with the discovery of tremendous deposits of seabird droppings or guano (Cushman, 2003). The extraction of the seabird excrement (guano, derived from an Inca word, comes primarily from the cormorant *Phalacrocorax bouganville*, common name Guanay) for fertilizer, played an important role in the Peruvian economy. The guano was exported worldwide and played a role in the survival of Europeans during the 19th century. The first marine biology scientific research entity in Peru was the Marine Biology Laboratory (Laboratorio de Biología Marina) established by the Compañia Administradora de Guano to study and preserve this important resource. With the aid of international scientists the first ecosystem perspective of the HCS was published in 1948 with the seabirds occupying a central role (Fig. 2). During the 1940s and 1950s a fishery developed on species like bonito (*Sarda chilensis chilensis*) and tuna (primarily *Thunnus albacore*) driven by the high demand of the liver oil of these species in the US market during World War II and later the Korean war. The end of the Korean War increased demand for guano and coincidentally the strong El Niño of

0079-6611/$ - see front matter © 2008 Elsevier Ltd. All rights reserved.
doi:10.1016/j.pocean.2008.10.012

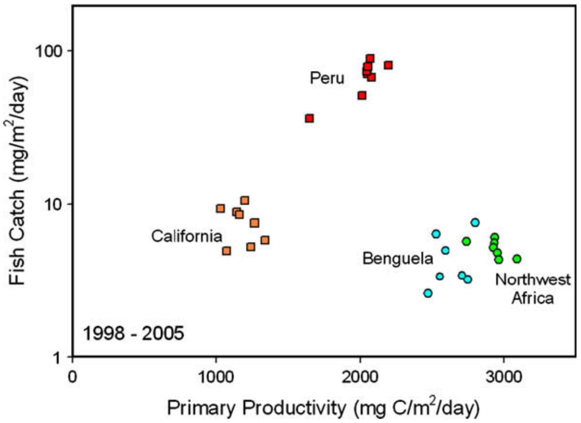

Fig. 1. Fish catch versus primary productivity for the four main eastern boundary coastal upwelling ecosystems for the years 1998–2005. It was assumed that the reported fish catches (Fish and Agriculture Organization, FAO) were made within 100 km from the coast. The catches were then normalized by area. Primary productivity was estimated from satellite remote sensing of chlorophyll and the Behrenfeld and Falkowski (1997) model. Even during the El Niño year of 1998 Peru fish catch still exceeded that from the other areas by several fold. Is Peru exceedingly efficient in the transfer of primary production to fish or are Benguela and Northwest Africa exceedingly inefficient?

1957–1958 led to a dramatic decrease in seabird populations. The present day anchovy or anchoveta (*Engraulis ringens*) fishery started around the same period in 1955. This was an important period for the ecosystem as managers pondered if the primary objective was seabirds (guano) or anchoveta (fish meal). In 1954 the Peruvian Navy with input from the Compañía Administradora de Guano and the government entity that managed fishing and hunting established the Consejo de Investigaciones Hidrobiológicas (CIH). The CIH was directed to coordinate and intensify hydrobiological studies with the goal of improving the use and sustainment of living marine resources. In 1959, as the anchoveta fishery continued to develop, Peru requested technical assistance for CIH from the Food and Agriculture Organization of the United Nations (FAO) to develop a National Fishery Plan. Soon after the Instituto de Investigaciones de los Recursos Marinos (IREMAR) was created with programs dealing with oceanography, fisheries biology, biology of whales, fishery economics and fishery technology. In their final report FAO recommended the fusion of CIH and IREMAR into a single institution. Accordingly in July of 1964 the Instituto del Mar del Perú (IMARPE) was created and began operation in September of 1965. A number of the early IMARPE scientists traced their roots to the Biology Department of the Compañía Administradora de Guano. IMARPE continues to conduct research on the northern HCS and its fisheries today.

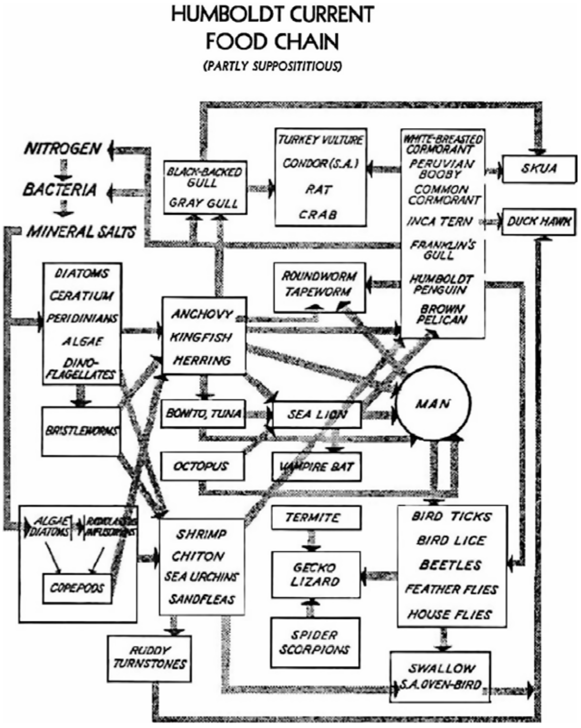

Fig. 2. First "ecosystem-based" diagram for the northern Humboldt Current System developed when seabirds were the focus of management (from Vogt, 1948).

The anchoveta fishery continued to grow during the 1960s to a peak harvest of 12 million tons per year in 1970 accounting for 20% of the world catch. The seminal paper of Ryther (1969), regarding primary productivity, trophic levels and fish productivity in coastal upwelling ecosystems, was developed based on an expedition to Peru during this period of record harvest. A number of international expeditions to the northern HCS followed and continue to present. However, seven years after IMARPE's formation, the anchoveta population collapsed during the 1972 El Niño. An outstanding synthesis of the dynamics of the Peruvian Upwelling Ecosystem focused on anchoveta and its crash was produced by IMARPE in conjunction with ICLARM (now World Fish Center) and the *Deutsche Gesellschaft für Technische Zusammenarbeit* (GTZ) during the mid 1980s and published as conference proceedings in 1987 and 1989 (Pauly and Tsukayama, 1987; Pauly et al., 1989a,b). These publications continue to serve as major references for the northern HCS. Since the 1980s, important technical and conceptual advances have transformed many areas of marine sciences. These advances have clarified important links and feedbacks between climate, ocean circulation, biogeochemical cycles, trophic webs and fish production. In addition, decades-long time series data are now revealing environmental and climactic variability beyond the interannual scale of El Niño.

3. Impacts of natural environmental rhythms and human exploitation on the ecosystem

The northern HCS is the region where El Niño, and climate variability in general, is most notable (Fig. 3); sea surface temperature (SST) anomalies greater than 10 °C have been observed during strong El Niño events (Barber and Chavez, 1983). The modern strong El Niño events include those beginning during 1925, 1941, 1957, 1982 and 1997. It was the strong 1957–1958 El Niño that led to the realization that El Niño was more than just the intensification of a tropical coastal current (Chavez, 1986) but was linked to changes in the global atmosphere (Bjerknes, 1966). The 1957–1958 El Niño resulted in strong declines in seabirds (see Fig. 1 of Chavez et al., 2003; Jahncke et al., 2004) and contributed, as described above, to the development of the most intense and successful fishery in the world. It was another El Niño in 1972 that was associated with a large and persistent decline in anchoveta. The collapse led to a vigorous scientific debate regarding causes: natural climate variability or over-fishing. The following 15–20 years saw a dramatic rise in sardine (*Sardinops sagax*) populations. It took over 10 years for scientists to notice that the same type of variability was also being experienced off California and Japan (Kawasaki, 1983; Lluch-Belda et al., 1992) and 30 years before a longer period (~50 year) natural climate phenomena (Mantua et al., 1997) was implicated in the fluctuations of anchoveta and sardine (Chavez et al., 2003; Alheit and Niquen, 2004). These large-scale, long-term changes in Pacific ecosystems became widely known as "regime shifts". The topic remains hotly debated; did the Pacific transition

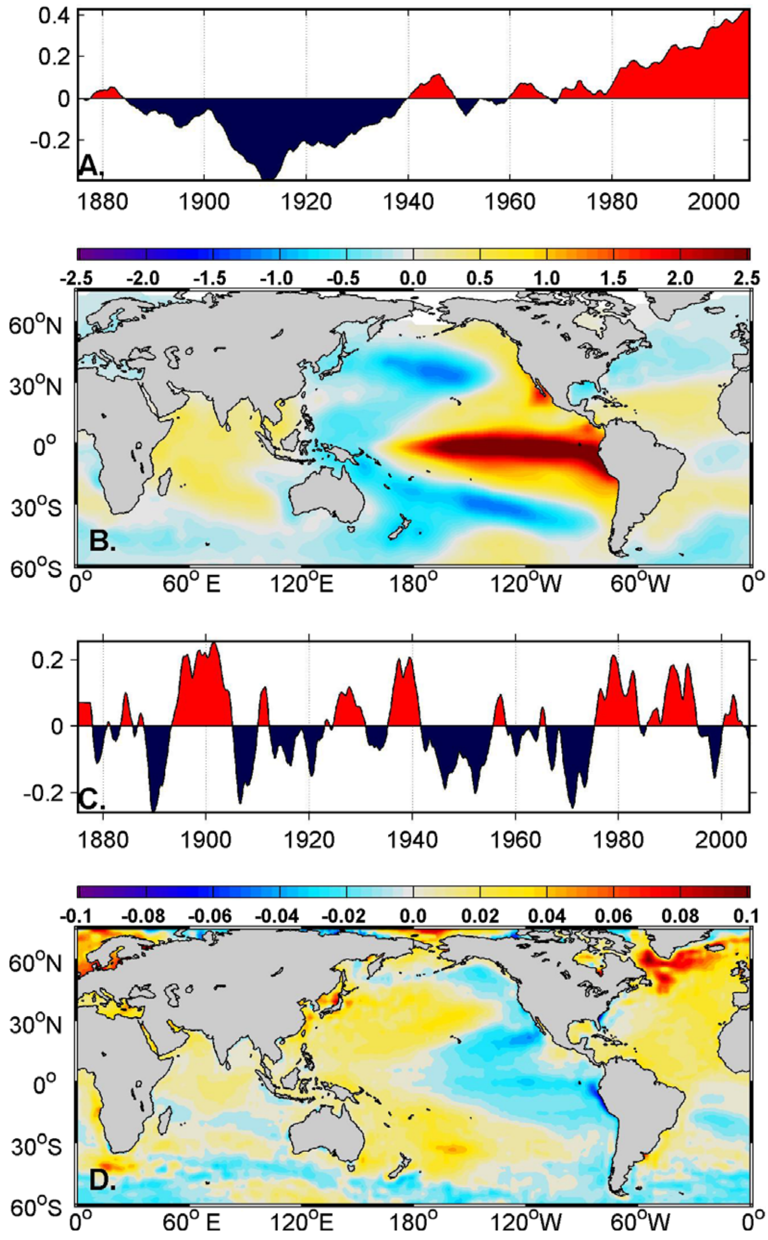

Fig. 3. Top panel shows the trend in sea surface temperature (SST) for the global ocean in 2 × 2 degree bins from 1875 to 2007. The warming over the last several decades is notable. The first empirical orthogonal function (EOF) of the SST time series was calculated after the trend and the seasonal cycle were removed (a la Mantua et al., 1997 for the Pacific Decadal Oscillation). The second panel shows the spatial pattern of the EOF with the northern HCS showing the highest variance relative to any coastal area of the world ocean. The time series of the EOF is shown in the third panel with a warm eastern Pacific from the mid 1970s to the mid 1990s. The bottom panel shows the trend of SST in 1 × 1 degree bins from 1981 to June 2008. Over this period, and primarily over the last decade the eastern Pacific, and the northern HCS in particular, has cooled (negative trend) while the majority of the ocean warmed. The long term SST records are from Woodruff et al. (2008) and the recent SST trend from Reynolds et al. (2007).

from a cool eastern Pacific (La Vieja) to warm eastern Pacific (El Viejo) in the early 1970s and then to a cool eastern Pacific again in the early to mid 1990s (Fig. 3)? Several papers in this issue examine changes that occurred during this period (Ayón et al., 2008b; Bakun and Weeks, 2008; Bertrand et al., 2008b; Guénette et al., 2008; Swartzman et al., 2008). Finally, information collected from anoxic sediments off Peru and Chile have uncovered even longer term and more dramatic changes (Gutiérrez et al., 2008; Sifeddine et al., 2008; Valdés et al., 2008). During the 400 years of the Little Ice Age (LIA) primary productivity was low in the northern HCS, the OMZ region was more oxygenated, and the abundance of small pelagics was greatly reduced. This changed at the end of LIA, circa 1820, to the present condition: high primary productivity, a very intense and shallow OMZ, and abundant small pelagic fish. This super regime shift showed that both anchovies and sardines were favoured after 1820. Multi-decadal variability (Chavez et al., 2003) was still apparent, but overwhelmed by the centennial scale changes. Are these trends continuing, what will happen with climate change (Fig. 3) and how will future changes influence the harvest of marine living resources? Will there be other tipping-points like the one at the end of LIA in the near future? Are ecological disturbances associated with large interannual to multi-decadal climate fluctuations responsible for the extremely high levels of fish production? Does environmental variability explain the Peruvian 'anchoveta paradox', that is why are fish abundance and production in the northern HCS so much higher than other coastal upwelling ecosystems (Fig. 2)? These questions will form the basis of future research.

4. New observations and models

This section highlights new findings regarding living marine resources and the environment that they are an integral part of Bertrand et al. (2008a) integrate observations and show how anchoveta are impacted by processes occurring along a spectrum of temporal and spatial scales. These processes include internal waves with periods of minutes and sizes of meters to the global climate variations described in the previous section with periods ranging from the interannual to centennial. A multi-scale (meter to entire coastline) observational effort allowed Bertrand et al. (2008a) to construct a conceptual model with management implications. The new and revealing aspects came from the small scale surveys that showed how anchoveta and other members of the living ecosystem "organize" around the rapidly varying environmental landscape. The animals leave their imprint on the physical environment, as evidenced by measurements of the partial pressure of carbon dioxide (pCO_2). Another example of a small scale but important observation, with significant impacts on ecosystem dynamics, concerns anchoveta diet. Earlier studies had shown an overwhelming numerical dominance of phytoplankton in stomach contents (e.g. Pauly et al., 1989b; Rojas de Mendiola, 1989) and led to the belief that the large populations of anchoveta were supported by an unusually short and efficient food chain (Ryther, 1969). From the analysis of a large number of stomach contents and, most importantly, by conversion of the contents to carbon equivalents, Espinoza and Bertrand (2008) show that the most important source of calories for anchoveta are zooplankton – primarily euphausiids and large copepods. Anchoveta, as indicated by its long intestine typical of herbivorous organisms, still consumes phytoplankton for important nutrients but zooplankton for energy. This new information changes previously developed and widely held paradigms for the northern HCS. Questions that immediately come to mind are: Are there more zooplankton off Peru than in any of the other coastal upwelling systems? Or perhaps, are zooplankton more concentrated and available to anchoveta? Ayón et al. (2008a) provide a review of zooplankton research for the northern HCS and leave it clear that new technologies are required to deal with the difficulties of zooplankton sampling.

One model for colonization of pelagic habitat suggests that fish first colonize favourable habitat then move to less favourable habitat as populations expand (MacCall, 1990). Information collected for anchoveta suggest a tight link to particular water masses, irrespective of population size (Bertrand et al., 2004; Swartzman et al., 2008). Salinity is a good proxy for the anchoveta-favoured water mass, Cold (upwelled) Coastal Wasters (CCW), as anchoveta is abundant and well fed over a wide (14–23 °C) temperature range (Gutiérrez et al., 2008b). Sardines seem to have greater affinity for the high salinity Subtropical Surface Waters (SSW) although not as strong as anchoveta for CCW (Swartzman et al., 2008). CCW are associated with a shallow oxycline that may favour anchoveta. Plankton size-structure is also different with larger plankton being favoured in the CCW (high nutrients) and smaller plankton in the SSW (more oligotrophic). What combination of properties selects for anchoveta and sardine is still under investigation.

Within the CCW habitat (Swartzman et al., 2008), anchoveta (i) forage efficiently under a variety of different environmental conditions (Espinoza and Bertrand, 2008), (ii) utilize food from various trophic levels and select high energy food types (Espinoza and Bertrand, 2008), (iii) concentrate in refuge areas when conditions are adverse (Bertrand et al., 2004), (iv) adapt their reproductive behaviour (Buitrón and Perea, 2000), and (v) distribute its population over a large temperature range (Gutiérrez et al., 2008b). This combination of characteristics may help explain the Peruvian 'anchoveta paradox': how anchoveta achieves such enormous concentrations when they (i) are only capable of very short migrations and therefore cannot actively escape adverse conditions, and (ii) are mainly distributed in dense surface aggregations, have very slow avoidance reactions and are highly accessible to predators (fish, cephalopods, birds, mammals and fishers) (Gerlotto et al., 2006).

Bakun and Weeks (2008) suggest two processes that might explain the dramatic fish productivity of the northern HCS. The northern HCS is the upwelling system that is nearest to the equator and is also a region of relatively weak but steady upwelling favourable winds. Because of the proximity to the equator the area of upwelling is large so even with weak winds large quantities of nutrients are upwelled but turbulence is low. Under these conditions the so called environmental window (Cury and Roy, 1989) for fish production is optimized. Second, Bakun and Weeks postulate that the close connection between Peru and the equatorial Pacific exposes the region to strong interannual variability. These sporadic and recurrent disruptions or ecosystem 're-sets' could keep the northern HCS from mature succesional states and favor the rapidly growing 'r' populations like anchoveta (Chavez, 1987). Chaigneau et al. (2008) are the first to analyze eddy activity from 15 years of altimeter data off Peru; somewhat surprisingly they find highest activity during the strong El Niño of 1997–1998. A next step would be to compare eddy activity for the major coastal upwelling systems.

The role of the ocean in modulating increasing concentrations of CO_2 in the atmosphere has led to an explosive growth of regional measurements of sea surface pCO_2. Based primarily from observations off Oregon, Hales et al. (2005) suggested that coastal upwelling systems were sinks for atmospheric CO_2. The comprehensive observations from the coast of Peru reported by Friederich et al. (2008) sharply disagree with that generalization and show that the northern HCS is a strong source of CO_2 to the atmosphere. The authors suggest several factors that could contribute to the maintenance of sea surface pCO_2 levels well above those of the atmosphere in spite of elevated uptake of CO_2 by phytoplankton: (1) upwelling source waters are affected by OMZ denitrification, contain low concentrations of pre-formed nitrate and have excess inorganic carbon relative to nitrogen; (2) iron limitation of primary production enhanced by offshore upwelling, driven by the curl of the wind stress, that does not recruit continental shelf iron (Johnson et al., 1999) and (3) rapid sea surface warming that reduces CO_2 solubility. In a modelling study Echevin et al. (2008) were able to reproduce a seasonal chlorophyll cycle that is out of phase with the upwelling seasonal cycle and nutrients (Pennington et al., 2006). The authors conclude that either (or both) light limitation by deeper mixing (first suggested by Calienes et al., 1985) during strong upwelling or iron limitation could be responsible for the out of phase relationship. Clearly the topic of regulation of primary productivity in the northern HCS requires further study.

In another combined observation and modelling study, Bertrand et al. (2008b) show the impact of equatorially-generated Kelvin Waves (KW) on the distribution of anchoveta and its primary consumer, the fishers. New tools like satellite vessel monitoring systems (VMS) are now routinely deployed on fishing vessels and in the northern HCS provide real-time positions of anchoveta seiners. Bertrand et al. (2008b) combine VMS information, oceanographic data and model output to show that large-scale oceanic KW forcing is both detectable and significant in the spatial organization of the ecosystem, including the distributions of anchoveta and the fishers. These results provide evidence for a bottom-up control of the system via "behavioural cascades" (see Frontier, 1987; Russel et al., 1992) that can produce contrasting 'ecosystem scenarios' under upwelling or downwelling KW conditions.

Bottom-up forcing in the northern HCS is evident at interannual (Barber and Chavez, 1983), multidecadal (Chavez et al., 2003; Alheit and Niquen, 2004) and now at centennial time scales (Gutiérrez et al., in press; Sifeddine et al., 2008; Valdés et al., 2008). This bottom-up control observed with *in situ* data was also simulated with trophic models at the scale of a bay (Taylor et al., 2008b) and for the entire northern HCS (Taylor et al., 2008a). The example provided by Bertrand et al. (2008b) makes it abundantly clear that there is also strong bottom-up forcing in the northern HCS at the intraseasonal time scale, but what about top-down effects? The large concentrations of plankton foraging fish in the northern HCS, and the other coastal upwelling ecosystems (Fig. 2 and 4), could drive a top-down control of zooplankton, the so-called wasp-waist hypothesis (Cury et al., 2000, 2003). Ayón et al. (2008b) combined zooplankton data (1961–2005) with simultaneous acoustic fish observations from 40 pelagic surveys (1983–2005) and Peruvian landing statistics (1961–2005). They showed that on a regional scale zooplankton and anchoveta fluctuated in phase (i.e. bottom-up forcing), but in dense schools anchoveta often induced a local reduction in zooplankton abundance.

An area of explosive progress during the last several decades has been in the development and use of numerical models. The role of models in research and management is several-fold. First, they serve as tests of our understanding of how ecosystems function: what are the drivers, why they are the way they are, why they change, etc. Models lead to new observations, improved understanding, new ecosystem rules, and iteratively to improved models. Second, models serve as integrators and interpolators of sparse information. The ocean, because of its challenges to observation (opacity to light, corrosive water, etc.), will always remain under sampled; models can interpolate the sparse data and generate views of the system that are in many ways analogous to satellite images but in three dimensions. Finally, given enough scientific

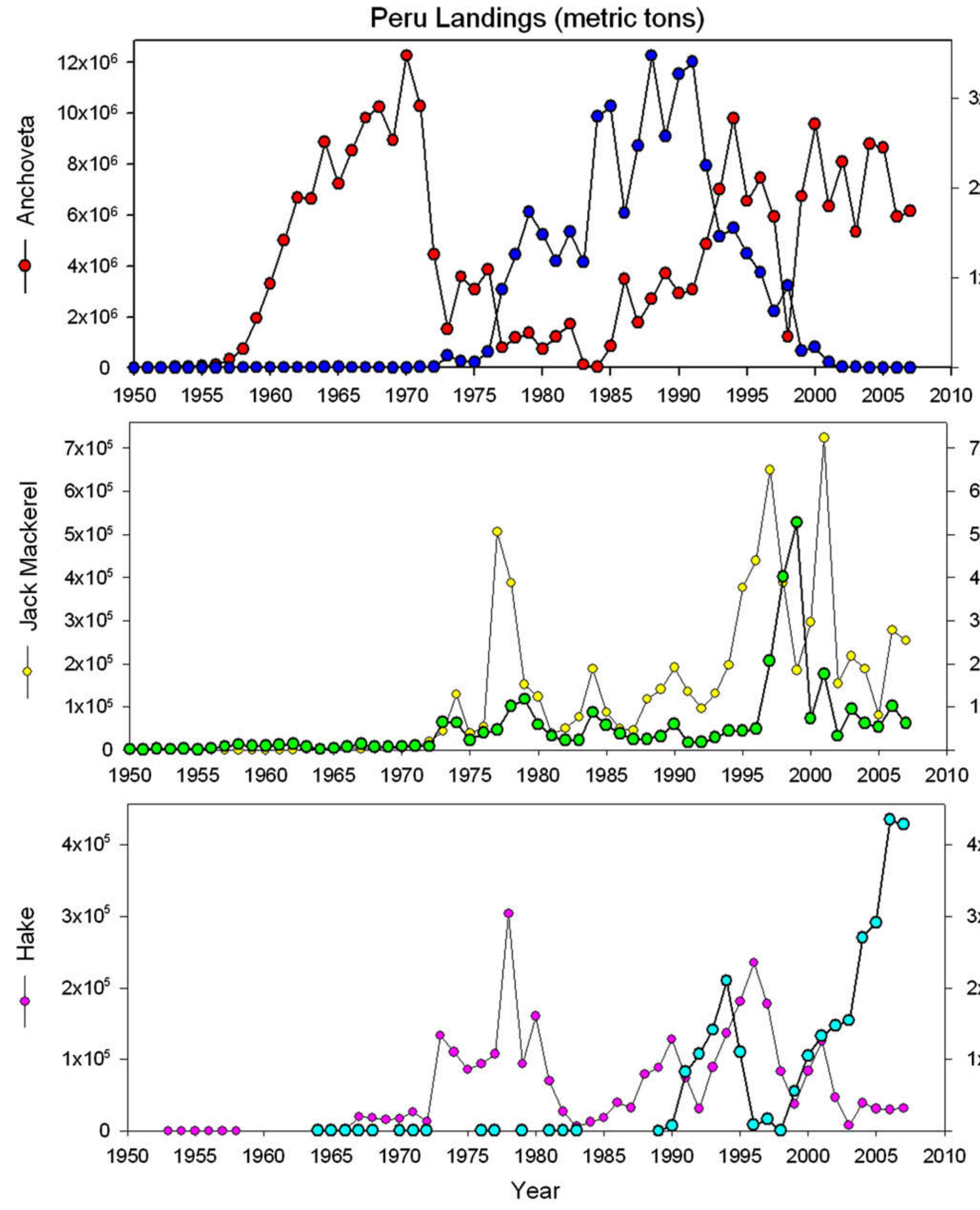

Fig. 4. Landings of anchoveta (*Engraulis ringens*), sardine (*Sardinops sagax*), jurel or jack mackerel (*Trachurus murphyi*), caballa or mackerel (*Scomber japonicus*), merluza or hake (*Merluccius gayi*) and Pota or the jumbo squid (*Doscidicus gigas*) for the period of 1950 to the present. The landings likely reflect fluctuations in abundance after 1965 for anchoveta, early 1970s for the remainder of the species and perhaps later for jack mackerel, mackerel and the jumbo squid.

progress the models can forecast the future and predict ecological responses to natural climate variability and global change. While models are an integral part of the future, it is also important to consider their present-day shortcomings. The quality (here defined as the ability to realistically simulate the ecosystem) of a model is directly proportional to the amount of available *in situ* data. The northern HCS, with its rich data, is an ideal region for model development and use. Physical (ocean and atmosphere) modelling is currently far ahead of ecological modelling. This is partly driven by the number of variables needed for physics (temperature and salinity), compared to biology (a potentially unlimited number), which increases complexity and cost. Finally, the models are only able to simulate known processes for which equations have been developed; new processes or significant errors in ecological theory are obviously problems for accurate predictions. A case in point is provided by Espinoza and Bertrand (2008) who show that euphausiids and large copepods are the dominant caloric prey for anchoveta. Yet trophic models can be tuned to simulate long-term dynamics of the ecosystem using phytoplankton as the major source of food for anchoveta. Either what the anchoveta eats is not particularly important to the ecosystem or there are still fundamental problems with the models. It is evident that modelling will continue to advance in parallel to and with the advent of new observations.

The models can be organized into several categories. First are physical ocean models. These models are driven by atmospheric forcing (wind and heat) typically provided by data-assimilating atmospheric models or model-aided reanalysis of observations. The resolution of the model (meters to kilometres in the horizontal and meters in the vertical) is usually constrained by computational power and the resolution of the atmospheric forcing. A widely used model in the northern HCS is the Regional Ocean Modelling System (ROMS; Colas et al., 2008) although it is certainly not the only one (see Dewitte et al., 2008). Simple pelagic ecosystem models (referred to as NPZ for Nutrient, Phytoplankton, Zooplankton) were first conceptualized in the 1940s (Riley, 1946) and have more recently directly coupled to physical circulation models such as ROMS (see Echevin et al., 2008, for example). Original formulations had one phytoplankton and one zooplankton group but in order to simulate global satellite chlorophyll there was a need to include two size classes each of phytoplankton and zooplankton. This type of ecosystem model is presently the most common and able to simulate a small-sized tightly coupled (oceanic) food web and a large-sized decoupled (coastal) food web. Adding NPZ to a physical model increases computational requirements by at least five fold. A present-day weakness of the coupled models is the lack of zooplankton data for validation. The output of the coupled models can be used to drive Individual Based Models (IBM) where a single species is followed over time: the coupled model provides physiological (temperature) and energetic (PZ) growth constraints; predatory losses are provided externally (see Brochier et al., 2008 as an example). The final group of models focus on trophic interactions with the most popular being those of the ECOPATH family (Christensen and Pauly, 1992; Walters and Christensen, 2007). Several papers in this issue apply these models (Guénette et al., 2008; Tam et al., 2008; Taylor et al., 2008a,b). These models are able to deal with a large number of trophic levels (hence the use of the descriptor) and components but because of their complexity are not able to resolve time or space with the necessary resolution. Time and space are typically treated discretely, for example El Niño versus normal (see, for example, Tam et al., 2008; Taylor et al., 2008a). Newer versions include the ability to treat time and space more explicitly but not at the level of the coupled models. Available *in situ* data for many, if not most, of the trophic components and their rates is sparse. A new generation of models attempts to embed "trophic" fishery models in the three dimensional coupled circulation models described above (Fulton et al., 2004; Travers et al., 2007) but these have yet to be applied to the northern HCS.

5. The northern Humboldt Current System as a management unit

Research over the past decades in the northern HCS has focused on exploited living resources, i.e. a few number of species like anchoveta, sardine, jurel or jack mackerel (*Trachurus murphyi*), caballa or mackerel (*Scomber japonicus*), merluza or hake (*Merluccius gayi*) and more recently the jumbo squid or 'pota' (*Doscidicus gigas*) (Fig. 4). As can be gleaned from Fig. 4, landings have fluctuated quite dramatically over the last decades driven by the large year to year variability of the northern HCS (Fig. 3). Is the ecosystem more sensitive to the environmental variability as a result of human exploitation of the resources? The Ecosystem Approach to Fisheries (FAO, 1995) stresses the importance of managing the resources by considering the whole ecosystem that the exploited populations and their fishers are an integral part of. The expectation is that such informed management system will facilitate the long term sustainability of fish stocks by understanding and protecting the ecosystem of which the fish are dependent, while at the same time maximizing economic and societal benefits and preventing wasteful overinvestment of economic resources. EAF and its close relative Ecosystem-Based Management (EBM) have and will continue to be daunting tasks given that resources, technologies and management theory are not yet at a level needed to implement these systems effectively. Given the unique monitoring system, the well understood climate variability and the developing ecological theory (summarized well in this special issue) the northern HCS is a strong candidate for this approach. Routine physical (temperature, salinity), chemical (nutrients and oxygen) and biological (chlorophyll, zooplankton biovolume) oceanographic information has and continues to be collected. An even more intense observation effort is in place for the marine living resources. Evolving technical capabilities, including tagging and tracking individual animals (modern tags can also record environmental data), will go a long way in improving our knowledge of the abundance and distribution of the so-called charismatic and sometimes threatened species (i.e. seabirds, marine mammals, turtles, etc.). The final frontier lies in the mero and macro zooplankton (copepods, euphausiids, larger crustaceans, fish larvae) and smaller fish all with behavioural attributes.

Technological advances in acoustics have facilitated collection of information on the mero and macro zooplankton (copepods, euphausiids, larger crustaceans, fish larvae) and smaller fish. Acoustics can now provide qualitative and quantitative data on diverse species from zooplankton to large fish (and even mammals), and given well-designed surveys, can document their interactions (Bertrand et al., 2008a). Acoustics have been used to document the dramatic changes in the pelagic red crab or 'munida' *Pleuroncodes monodon* (a macro-zooplankton) population, after the 1997–98 El Niño (Gutiérrez et al., 2008b). Munida has been exploited for decades in central Chile where its adult population is demersal. High munida concentrations were rarely reported off Peru but recently its populations experienced exponential growth, presumably in response to the cooling trends shown in Fig. 3; 1998–2005 acoustic biomass estimates range from 0.6 to 3.4 million tons. The increase in population and range was accompanied by a change in the crab's ecology, going to a complete pelagic life cycle in Peru because the intense OMZ in this region restricts its demersal habitat. As described above the munida not only increased in abundance but extended its range towards the equator as the eastern Pacific cooled during La Vieja (Fig. 3). But is it really La Vieja or the beginning of the effects of man-induced global warming? Global warming may differentially heat land and sea, intensify coastal upwelling winds (Bakun, 1990) and perhaps cool coastal upwelling regions in the face of a general global warming trend (Fig. 3). Acoustics allowed Gutiérrez et al. (2008b) to simultaneously observe anchoveta and munida and the data clearly show that they often share the same habitat. Climatic changes have resulted in an environment where these two species now overlap even though munida is restricted to the very cold CCW whereas anchoveta tolerates a much broader temperature range. Anchoveta and munida are both prey for apex predators, they both feed on the same planktonic organisms and munida forages on anchoveta eggs and larvae so their affinity for the same habitat has important ecological consequences. More information on euphausiids, the key prey of anchoveta, is critically needed. Presently acoustic devices can only be deployed routinely on ships but there is hope that acoustic devices or other technologies for sensing zooplankton can be made routinely available for autonomous platforms like floats, gliders and moorings.

Anderson et al. (2008) has shown that commercial fishing results in a decrease in average body size and age of maturity of the exploited fish stock. This can lead to age-truncated or juvenescent populations that can become increasingly unstable. Peruvian hake (*Merluccius gayi peruanus*) have been intensively fished since the early 1970s (Fig. 4C) and show juvenescent characteristics: a drastic reduction in mean hake size, an early age of maturation, with the percentage of mature hake at 2 years changing from ~zero during the 1980s to >60% in the early 2000s. Additionally the proportion of females in catches increased from ~40% at the beginning of 1990 to ~100% at the beginning of 2000 (Guevara-Carrasco and Lleonart, 2008; Ballón et al., 2008). Ballón et al. (2008) showed that the few remaining large females in the population currently make low investments in egg production. The lack of males in the population could mean sperm limitation. In addition the lack of male pheromones should impact female spawning and lead the large females to reallocate resources from reproduction to growth or survival. Not surprisingly, large females had high condition factors and low gonosomatic indices when large males were scarce. The hake habitat is restricted to northern Peru (typically north of 6 °S) where waters are ventilated (and oxygenated) by the Equatorial Undercurrent. Ballón et al. (2008) also show that El Niño negatively affects hake's condition factor and reproduction even though El Niño increases geographical range and habitat of hake by oxygenating the central and southern Peru coastal waters (Espino, 1990). These results with hake illustrate how fishing and environmental variability can interact and impact populations in unexpected and complex ways.

In addition to the above factors, the jumbo squid, an important predator of hake (Zeidberg and Robison, 2007) seems to have increased in abundance over the past decade (Fig. 4C). Argüelles et al. (2008) showed that during 1989–1999, mature jumbo squid (*Dosidicus gigas*) where of medium size (~40 cm), but from 2001 on, mature squid were larger (~80 cm). Argüelles et al. (2008) hypothesize that the change in size and the increase in numbers was caused by a parallel increase in mesopelagic (lanterfish in particular) fishes that are prey for the jumbo squid. The size increase also suggests that squid are not over-exploited in the northern HCS. Unlike hake, squid is an 'r' species that grows very fast (like anchoveta) and is therefore more resilient to fishing pressures. Jumbo squid have not only increased rapidly off Peru but also off Chile, Mexico and the United States (Zeidberg and Robison, 2007; Bograd et al., 2008). Bograd et al. (2008) suggest that changes in the geographical distribution of the jumbo squid may be related to the expansion of eastern Pacific OMZ. If true hake may be further impacted since the small area of high productivity and oxygen off northern Peru (4–6 °S) where hake thrive may be shrinking.

In northern HCS off Peru, fisheries decisions are made in quasi real-time using the most recent observations. It is probably the only place in the world where this rapidly 'adaptive' management style is possible. Government bureaucracy and slow data analysis usually mean that management decisions are implemented for yesterday's conditions and problems. However, there is still a need for reliable predictors of future conditions to support the decision making process. These must include our developing understanding of interannual, multidecadal and centennial climate variability. Forecasting climate effects on fishery stocks clearly is a daunting task, but this should be an area of continued emphasis. Kelvin waves (KW) and interannual variability are areas where immediate gains are possible. As Bertrand et al. (2008b) have shown there is a predictable northern HCS ecosystem response to coastal KWs of equatorial origin. These KWs are excited in the western equatorial Pacific, are observed by the TOGA-TAO array and satellite altimetry, and travel across the Pacific to the northern HCS in about two months. To the extent that there is a predictable response, this two month window could be used to make management decisions. If environmental conditions could be predicted six to nine months in advance, such as predicting El Niño, further measures could be taken. Jarre et al. (2008) compared two knowledge-based systems (rule-based Boolean and fuzzy logic models) that would use multiple data sets and indices to aid the decision support system. The comparison was made for fisheries in the southern Benguela but it has applications for the northern HCS. These new efforts could be implemented into an easy to use "dashboard" to support the decision makers.

The satellite vessel monitoring systems (VMS) have provided unique data regarding fishery effort and as Bertrand et al. (2008c) show, on the spatial distribution of resources. VMS data provide robust, reliable, real-time, and low-cost information for scientific and management purposes (Bertrand et al., 2007). Bertrand et al. (2008c) used artificial neural networks (ANN) with VMS data to estimate the position of fishing operations for the entire fleet of Peruvian anchovy purse-seiners. The ANN was trained on a sample of fishing trips with known fishing set positions from an at-sea observer program. The ANN correctly identified 83% of the real fishing sets and largely outperformed comparative linear models. Bertrand et al. (2008c) quantified the extent to which the distribution of purse-seine sets describes anchovy distribution and found that location yields valuable information on the distribution of the Peruvian anchoveta stock and ultimately on its vulnerability to the fishery. A fishery that at present has too much capacity: Fréon et al. (2008) estimated the present overcapacity of the Peruvian purse seiner anchoveta fleet at over 300%, in other words the fleet has the capacity to capture over 30 million tonnes per year even though current quotas have ranged from 5 to 8 million tons. This overcapacity was economically driven by the classical "tragedy of the commons" i.e. the race to catch a larger share of a global annual quota and its roots can be traced to the inability of fisheries managers, under several administrations, to enforce laws controlling the expansion of the fleet and fish processing plants.

Under the present system the fishing year is divided into two semesters (April–September and October–March) or fishing seasons, with long-established closures coinciding with the two main spawning periods in winter and summer. The quota or total allowable catch (TAC) was assigned or adjusted by management at the beginning of each fishing period, formerly by season and over the last few years by month. When the TAC for a period is reached (or the period ends) the fishery is closed. Several periods make up the fishing season. Since there is a single quota for all there is a premium on skilled captains and high capacity. A new individual quota (IQ) system, where the TAC is distributed among registered fishing vessels holding a valid fishing license, is about to be implemented. Removing the need to race to harvest as much as possible is expected to eventually result in a significant reduction in the size of the fleet, but may also lead to new socio-economic, biological and ecosystem challenges especially if, as in the past, the system is not properly enforced. If properly administered the IQ system should result in similar economic benefits to the fishery as do individual transferable quotas (ITQs) (Costello et al., 2008) but perhaps not to the shortcomings: concentration of ownership into a few large companies, the loss of fishery benefits to local communities, and the development of speculative bubbles (see Hilborn et al., 2005 for a review). The implementation of the IQ system provides an opportunity to study how anchoveta and the ecosystem respond to a measured change. Under the present system the effective fishing season is about 50 days a year (Fréon et al., 2008) and one would expect the duration of the fishing season to increase under the IQ system. The consequences could be positive or negative and as far as we know no such "controlled" experiment has been carried out. For example, longer, less intense fishing might not be as traumatic to anchoveta but more days at sea may lead to more stress on the ecosystem as a whole. After several years of data collection the pros and cons of the IQ system should be evaluated.

The examples given above illustrate the challenge of implementing a management system that is ecosystem focused. It is noteworthy that this special issue has no contributions regarding the so-called called charismatic and sometimes threatened species (i.e. seabirds, marine mammals, turtles, etc.) and how they fit into the management equation needs to be considered. Although the challenge is monumental if it can be accomplished anywhere it might be in the northern HCS.

6. Future directions

Several future research problems have been highlighted throughout this introduction to the special issue on the northern HCS. Many can be linked to the unique features of this region: (1) intense primary productivity and an efficient but still poorly defined "trophic" transfer to small pelagic fish that supports the largest fishery in the world (Fig. 1); (2) the greatest level of interannual variability for any coastal region in the world ocean (Fig. 3); and (3) an intense, shallow and 'acidic' oxygen minimum zone (OMZ; Fig. 5). While these three processes, high biological productivity, interannual variability and oxygen minima, are not independent, we treat each separately in the following paragraphs.

Several hypotheses have attempted to explain the uniquely high productivity of small pelagic fish productivity in the northern HCS – or what has been termed the 'Peruvian anchoveta paradox': (1) the northern HCS may simply have higher levels of primary productivity and therefore fish productivity than other coastal upwelling ecosystems; (2) anchovy off Peru, but not the other upwelling ecosystems, have been suggested to feed directly on phytoplankton, primarily diatoms, and hence there is a very short and efficient food chain; (3) the combination of high primary productivity and relatively weak winds may lead to longer residence times, a less turbulent environment, and optimal conditions for fish growth, reproduction and egg and larval retention (Bakun and Parrish, 1982; Bakun and Weeks, 2008); (4) the OMZ could concentrate prey and at the same time reduce predation on zooplankton and small pelagic fish; and (5) the high levels of northern HCS interannual variability lead to a the pelagic ecosystem that is always in an 'r' state favouring fast growing fish like anchoveta (Chavez, 1987) and keeping long-lived ocean dwelling predators (on the small pelagic) from getting established (Bakun and Weeks, 2008). As Bakun and Weeks (2008) remind us the spectre of climate change is on the horizon making them wonder if the changes it brings will "shift Peru's marine ecosystem out of its current sweet-spot?"

The first hypothesis regarding increased fish production off Peru can now be safely rejected as estimates of primary productivity (Carr, 2001) and nutrient supply (Messie et al., 2008) indicate that

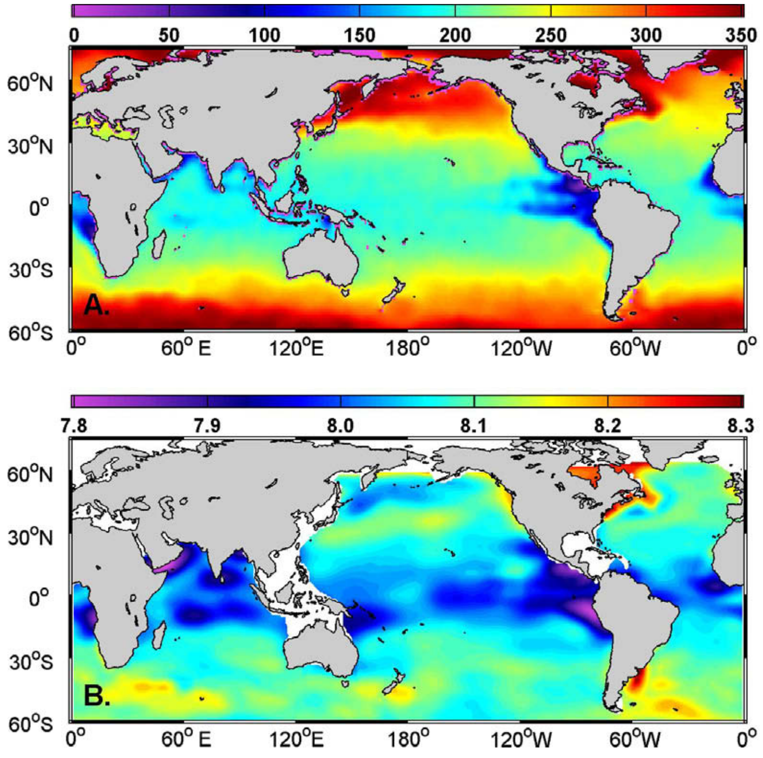

Fig. 5. Global distributions of 50 meter oxygen (μmol/kg, top) and pH (bottom). Note the very low oxygen and pH at this shallow depth off the northern HCS. The oxygen is from Conkright et al. (2002). The pH was calculated from total carbon dioxide and alkalinity found in the GLODAP database (Key et al., 2004) and temperature, salinity and nutrients in Conkright et al. (2002).

the Northwest Africa and Benguela coastal upwelling ecosystem have greater or similar levels as Peru (Fig. 1). Is Peru exceedingly efficient in the transfer of primary production to fish or are Benguela and Northwest Africa exceedingly inefficient? Paradoxically primary productivity off Peru appears limited during the winter months (Pennington et al., 2006), either by iron or light (Echevin et al., 2008; Friederich et al., 2008); Peru appears to be the only coastal upwelling ecosystem where upwelling and primary productivity are out of phase. The second, ‘short food chain’ hypothesis has now been discredited by Espinoza and Bertrand (2008), who show that anchovy get most of their caloric energy from zooplankton as in other upwelling ecosystems. One difference is that in the northern HCS euphausiids are the favoured prey of anchoveta, in contrast to Northwest Africa and Benguela. The Peruvian anchoveta paradox must be explained by some combination of the remaining hypotheses which concern (1) the efficient transfer of primary production to fish through zooplankton, in particular euphausiids, via an optimal environmental window, (2) the OMZ impacts predation on prey and predators of the small pelagic fish and (3) the high interannual variability.

There is growing awareness that environmental variability plays a dominant role in the functioning and structure of marine ecosystems and that this variability is much greater than previously thought. El Niño has been and remains the classic example of the impact of climate variability on ocean ecosystems (Barber and Chavez, 1983). However, longer and more subtle changes in the environment seem to drive stronger and more profound changes on marine living resources (Lluch-Belda et al., 1992; Chavez et al., 2003; Alheit and Niquen, 2004) leading to the so-called “regime-shifts.” New time series from cores from the marine sediments underlying the Peru OMZ have revealed dramatic and sustained shifts (Gutiérrez et al., 2008; Sifeddine et al., 2008). It appears as if the current “sweet-spot” of fish productivity has come and gone in the past before the advent of anthropogenic influences. Will similar tipping-points (Gladwell, 2000) be reached in the future? And if so, when will they occur and will we predict them? Management plans will have to developed considering this shifting environmental baseline.

Environmental variability leaves its imprint on the ecosystem and the OMZ. Benthic communities on the continental shelf shift dramatically from those dominated by the few organisms capable of withstanding the dominant anoxic conditions to a diverse community during El Niño when oxygen levels over the shelf increase dramatically (Arntz et al., 2006; Gutiérrez et al., 2008a; Tarazona et al., 1988). The oxygenation during El Niño “cleans” not only the benthic but pelagic ecosystem on interannual scales (Chavez, 1987). Similar changes occur at multidecadal and centennial time scales. However, during recent centuries, the northern HCS OMZ has confined most oxygen-requiring animals to shallow surface waters, providing a refuge from predation and competition to those that can cope with low oxygen conditions. The impacts of the OMZ on benthic communities are relatively well documented but as discussed above the full impact of the intense and shallow OMZ on the pelagic ecosystem remains unclear. For example, the role of the OMZ on zooplankton growth and survival remains unresolved given the paucity of studies in the northern HCS. An early study suggests that a large fraction of the zooplankton community is limited in its vertical distribution by the OMZ (Judkins, 1980). In northern Chile on the other hand a large number of zooplankton can penetrate the OMZ as part of their vertical migrations while a smaller fraction is restricted to the upper oxygenated layer (Escribano et al. in press). Are the zooplankton further protected from grazing while in the OMZ? Are they eventually more accessible to the anchoveta? A number of bacterial processes and biogeochemical cycling, not discussed in this special issue, are enhanced in the OMZ making this region important for global nitrogen budgets for example (Codispoti et al., 1986).

Recent reports suggest that OMZs are growing either in response to the longer term centennial scale changes (Gutiérrez et al., 2008) or anthropogenic influences (Stramma et al., 2008). Such an expansion must certainly have consequences for the global nitrogen cycles discussed above, further removing nitrate via denitrification. Can this expansion help explain the shrinkage of the habitat of hake and other demersal fauna in northern Peru? The natural process of photosynthesis, carbon fixation and oxygen production, at the surface and sinking and decay of surface-derived primary production to depth, where oxygen is consumed and carbon dioxide respired, act to “acidify” the deep ocean. Regions of low oxygen are therefore regions of low pH (Fig. 5). How fast will the slow diffusion of anthropogenically-derived atmospheric CO_2 into the ocean (Feely et al., 2008) further acidify northern HCS ecosystems and what will be the consequences? Is the acidic northern HCS OMZ a window into the future of other ecosystems that currently have higher oxygen and pH?

In summary, the northern HCS off Peru is intensively studied because of its unusual dynamics and astounding fish productivity. It is a turbid green-to-brown ecosystem with more “substance” than “beauty” – very different than stereotypical tropical systems where diversity and colour dominate. Indeed, in the northern HCS productivity is high at the expense of diversity. Interannually and multidecadally, the northern HCS changes from higher biological productivity and lower diversity during cool periods to lower productivity and higher biodiversity during warm periods (El Niño and El Viejo). In terms of marine living resources, the northern HCS is perhaps the best monitored large ecosystem in the world, allowing for unusually effective management of fisheries in spite of internal (economic) and external (environmental) challenges. The continued collection of time series data is strongly encouraged together with the application of new and evolving technologies for observation, modelling and management. In the present environment scientific/management strategy iterates between observations, basic ecosystem rules and single-purpose models or management practices. In the future fully integrated and adaptive observation, modelling and management systems will be required with greater reliance on autonomous observing systems like floats, gliders and moorings. We wonder what changes, in the environment, and the integrated management system, the next decades will bring, and hope that the next synthesis will be as positive as this one.

Acknowledgments

Support for the conference, the special issue and this paper came from the Institut de Recherche pour le Développement (IRD), the Instituto del Mar del Perú (IMARPE), the Food and Agriculture Organisation of the United Nations (FAO), the International Council for the Exploration of the Sea (ICES), the North Pacific Marine Science Organization (PICES), the Global Ocean Ecosystem Dynamics (GLOBEC) program, the Integrated Marine Biogeochemistry and Ecosystem Research (IMBER) program, the European network of excellence EUR-OCEAN, the Centre National d’Etudes Spatiales (CNES, France), the Peruvian Consejo Nacional de Ciencia, Tecnología e Innovación Tecnológica (CONCYTEC), the French Ministère des Affaires Étrangères (MAE), the French Embassy in Peru, and the Alliance Française of Lima, the National Aeronautics and Space Administration (NASA, USA), and the David and Lucile Packard Foundation. The 300 participants in the conference are warmly thanked as are the large number of reviewers. J.T. Pennington served as the copy editor and Shannon Boedecker supported the editorial office. Figures in this paper were prepared by Dorota Kolber and Reiko Michisaki.

References

Alheit, J., Niquen, M., 2004. Regime shifts in the Humboldt Current ecosystem. Progress in Oceanography 60, 201–222.

Anderson, C.N.K., Hsieh, C.-H., Sandin, S.A., Hewitt, R., Hollowed, A., Beddington, J., May, R.M., Sugihara, G., 2008. Why fishing magnifies fluctuations in fish abundance. Nature 452, 835–839.

Argüelles, J., Tafur, R., Taipe, A., Villegas, P., Keyl, F., Dominguez, N., Salazar, M., 2008. Size increment of Jumbo flying squid Dosidicus gigas mature females in Peruvian waters, 1989-2004. Progress in Oceanography 79, 308–312.

Arntz, W.E., Gallardo, V.A., Gutiérrez, D., Isla, E., Levin, L.A., Mendo, J., Neira, C., Rowe, G.T., Tarazona, J., Wolff, M., 2006. El Niño and similar perturbation effects on the benthos of the Humboldt, California, and Benguela Current upwelling ecosystems. Advances in Geosciences 6, 243–265.

Ayón, P., Criales-Hernandez, M.I., Schwamborn, R., Hirche, H.-J., 2008a. Zooplankton research off Peru: a review. Progress in Oceanography 79, 238–255.

Ayón, P., Swartzman, G., Bertrand, A., Gutiérrez, M., Bertrand, S., 2008b. Zooplankton and forage fish species off Peru: large-scale bottom-up forcing and local-scale depletion. Progress in Oceanography 79, 208–214.

Bakun, A., 1990. Global climate change and intensification of coastal ocean upwelling. Science 247, 198–201.

Bakun, A., Parrish, R.H., 1982. Turbulence, transport, and pelagic fish in the California and Peru Current systems. CalCOFI Reports 23, 99–112.

Bakun, A., Weeks, S.J., 2008. The marine ecosystem off Peru: what are the secrets of its fishery productivity and what might its future hold? Progress in Oceanography 79, 290–299.

Ballón, M., Wosnitza-Mendo, C., Guevara-Carrasco, R., Bertrand, A., 2008. The impact of overfishing and El Niño on the condition factor and reproductive success of Peruvian hake. Merluccius gayi peruanus Progress in Oceanography 79, 300–307.

Barber, R.T., Chavez, F.P., 1983. Biological consequences of El Niño. Science 222, 1203–1210.

Behrenfeld, M.J., Falkowski, P.G., 1997. Photosynthetic rates derived from satellite-based chlorophyll concentration. Limnology and Oceanography 42, 1–20.

Bertrand, A., Segura, M., Gutiérrez, M., Vásquez, L., 2004. From small-scale habitat loopholes to decadal cycles: a habitat-based hypothesis explaining fluctuation in pelagic fish populations off Peru. Fish and Fisheries 5, 296–316.

Bertrand, S., Bertrand, A., Guevara-Carrasco, R., Gerlotto, F., 2007. Scale invariant movements of fishermen: the same foraging strategy as natural predators. Ecological Applications 17, 331–337.

Bertrand, A., Gerlotto, F., Bertrand, S., Gutiérrez, M., Alza, L., Chipollini, A., Díaz, E., Espinoza, P., Ledesma, L., Quesquén, R., Peraltilla, S., Chavez., F., 2008a. Schooling behaviour and environmental forcing in relation to anchoveta distribution: an analysis across multiple spatial scales. Progress in Oceanography 79, 264–277.

Bertrand, S., Dewitte, B., Tam, J., Diáz, E., Bertrand, A., 2008b. Impacts of Kelvin wave forcing in the Peru Humboldt Current system: scenarios of spatial reorganizations from physics to fishers. Progress in Oceanography 79, 278–289.

Bertrand, S., Díaz, E., Lengaigne, M., 2008c. Patterns in the spatial distribution of Peruvian anchovy (*Engraulis ringens*) revealed by spatially explicit fishing data. Progress in Oceanography 79, 379–389.

Bjerknes, J., 1966. A possible response of the atmospheric Hadley circulation to equatorial anomalies of ocean temperature. Tellus 18, 820–829.

Bograd, S., Castro, C.G., Di Lorenzo, E., Palacios, D.M., Bailey, H., Gilly, W., Chavez F.P., 2008. Oxygen declines and the shoaling of the hypoxic boundary in the California current. Geophysical Research Letters 35, L12607, doi:10.1029/2008GL034185.

Brochier, T., Lett, C., Tam, J., Fréon, P., Colas, F., Ayón, P., 2008. An individual-based model study of anchovy early life history in the northern Humboldt Current system. Progress in Oceanography 79, 313–325.

Buitrón, B., Perea, A., 2000. Aspectos reproductivos de la anchoveta peruana durante el período 1992–2000. Boletín del Instituto del Mar del Perú 19, 45–54.

Calienes, R., Guillen, O., Lostaunau, N., 1985. Variabilidad espacio-temporal de clorofila, produccıón primaria y nutrientes frente a la costa peruana. Boletín del Instituto del Mar del Perú 10.

Chaigneau, A., Gizolme, A., Grados, C., 2008. Mesoscale eddies off Peru in altimeter records: identification algorithms and eddy spatio-temporal patterns. Progress in Oceanography 79, 106–119.

Chavez, F.P., 1986. The legitimate El Niño Current. Tropical ocean–atmosphere newsletter 34, 1.

Chavez, F.P., 1987. El Niño y la Oscilacion del Sur. Investigacion y Ciencia (Spanish edition of Scientific American) 128, 46–55.

Chavez, F.P., Ryan, J., Lluch-Cota, S.E., Niquen, M., 2003. From anchovies to sardines and back: multidecadal change in the Pacifc Ocean. Science 299, 217–221.

Christensen, V., Pauly, D., 1992. ECOPATH II a software for balancing steady-state ecosystem models and calculating network characteristics. Ecological Modelling 61, 169–185.

Codispoti, L.A., Friederich, G.E., Packard, T.T., Glover, H.E., Kelly, P.J., Spinrad, R.W., Barber, R.T., Elkins, J.W., Ward, B.B., Lipschultz, F., Lostaunau, N., 1986. High nitrite levels off Northern Peru: a signal of instability in the marine denitrification rate. Science 233, 1200–1202.

Colas, F., Capet, X., McWilliams, J.C., Shchepetkin, A., 2008. 1997–98 El Niño off Peru: A Numerical Study. Progress in Oceanography 79, 138–155.

Conkright, M.E., Locarnini, R.A., Garcia, H.E., O'Brien, T.D., Boyer, T.P., Stephens, C., Antonov, J.I., 2002. World Ocean Atlas 2001: Objective Analyses, Data Statistics, and Figures, CD-ROM Documentation. National Oceanographic Data Center, Silver Spring, MD. 17.

Costello, C., Gaines, S.D., Lynham, J., 2008. Can catch shares prevent fisheries collapse? Science 321, 1678–1681.

Cury, P., Roy, C., 1989. Optimal environmental window and pelagic fish recruitment success in upwelling areas. Canadian Journal of Fisheries and Aquatic Sciences 46, 670–680.

Cury, P., Bakun, A., Crawford, R.J.M., Jarre, A., Quiñones, R.A., Shannon, L.J., Verheye, H.M., 2000. Small pelagics in upwelling systems: patterns of interaction and structural changes in "wasp-waist" ecosystems. ICES Journal of Marine Science 57, 603–618.

Cury, P., Shannon, L., Shin, Y.-J., 2003. The functioning of marine ecosystems: a fisheries perspective. In: Sinclair, M., Valdimarsson, G. (Eds.), Responsible Fisheries in the Marine Ecosystem, pp. 103–141.

Cushman, G.T., 2003. The lords of guano [electronic resource]: science and the management of Peru's marine environment, 1800–1973. Doctoral dissertation, The University of Texas at Austin. <http://hdl.handle.net/2152/241>.

Dewitte, B., Ramos, M., Echevin, V., Pizarro, O., du Penhoat, Y., 2008. Vertical structure variability in a seasonal simulation of a medium-resolution regional model of the Eastern South Pacific. Progress in Oceanography 79, 120–137.

Echevin, V., Aumont, O., Ledesma, J., Flores, G., 2008. The seasonal cycle of surface chlorophyll in the Peru upwelling system: a modelling study. Progress in Oceanography 79, 167–176.

Escribano, R., Schneider, W., 2007. The structure and functioning of the coastal upwelling in Central/Southern Chile. Progress in Oceanography 75, 343–602.

Escribano, R., Hidalgo, P., Krautz, C., in press. Zooplankton associated with the oxygen minimum zone system in the northern upwelling region of Chile during March 2000. Deep Sea Research II.

Espino, M., 1990. "El Niño": su impacto sobre los peces demersales del Perú. Boletín Instituto del Mar del Perú 14, 3–10.

Espinoza, P., Bertrand, A., 2008. Revisiting Peruvian anchovy (*Engraulis ringens*) trophodynamics provides a new vision of the Humboldt Current system. Progress in Oceanography 79, 215–227.

FAO, 1995. Code of conduct for responsible fisheries. Food and Agriculture Organization, Rome.

Feely, R.A., Sabine, C.L., Hernandez-Ayon, J.M., Ianson, D., Hales, B., 2008. Evidence for upwelling of corrosive "acidified" water onto the continental shelf. Science 320, 1490–1492.

Fréon, P., Bouchon, M., Mullon, C., García, C., Ñiquen, M., 2008. Interdecadal variability of anchoveta abundance and overcapacity of the fishery in Peru. Progress in Oceanography 79, 401–412.

Friederich, G.E., Ledesma, J., Ulloa, O., Chavez, F.P., 2008. Air–sea carbon dioxide fluxes in the coastal southeastern tropical pacific. Progress in Oceanography 79, 156–166.

Frontier, S., 1987. Applications of fractal theory to ecology. In: Legendre, P., Legendre, L. (Eds.), Developments in Numerical Ecology. Springer-Verlag, Berlin, pp. 335–378.

Gerlotto, F., Bertrand, S., Bez, N., Gutiérrez, M., 2006. Waves of agitation inside anchovy schools observed with multibeam sonar: a way to transmit information in response to predation. ICES Journal of Marine Science 63, 1405–1417.

Gladwell, M., 2000. The Tipping Point: How Little Things Can Make a Big Difference. Little, Brown, Boston.

Guénette, S., Christensen, V., Pauly, D., 2008. Trophic modelling of the Peruvian upwelling ecosystem: towards reconciliation of multiple datasets. Progress in Oceanography 79, 326–335.

Guevara-Carrasco, R., Lleonart, J., 2008. Dynamics and Fishery of the Peruvian hake: between the nature and the man. Journal of Marine Systems 71, 249–259.

Gutiérrez, D., Sifeddine, A., Field, D.B., Ortlieb, L., Vargas, G., Chávez, F., Velazco, F., Ferreira, V., Tapia, P., Salvatteci, R., Boucher, H., Morales, M.C., Valdés, J., Reyss, J.-L., Campusano, A., Boussafir, M., Mandeng-Yogo, M., García, M., Baumgartner, T., 2008. Rapid reorganization in ocean biogeochemistry off Peru towards the end of the Little Ice Age. Biogeosciences Discussions 5, 3919–3943.

Gutiérrez, D., Enríquez, E., Purca, S., Quipúzcoa, L., Marquina, R., Flores, G., Graco, M. 2008a. Remotely-driven temporal variations of the subsurface dissolved oxygen content and responses of the continental shelf benthic subsystem off Central Peru. Progress in Oceanography.

Gutiérrez, M., Ramirez, A., Bertrand, S., Morón, O., Bertrand, A., 2008b. Ecological niches and areas of overlap of the squat lobster 'munida' (*Pleuroncodes monodon*) and anchoveta (*Engraulis ringens*) off Peru. Progress in Oceanography 79, 256–263.

Hales, B., Takahashi, T., Bandstra, L., 2005. Atmospheric CO_2 uptake by a coastal upwelling system. Global Biogeochemical Cycles 19. doi:10.1029/2004GB002295 (GB1009).

Hilborn, R., Parrish, J.K., Litle, K., 2005. Fishing rights or fishing wrongs? Reviews in Fish Biology and Fisheries 15, 191–199.

Jahncke, J., Checkley Jr., D.M., Hunt Jr., G.L., 2004. Trends in carbon flux to seabirds in the Peruvian upwelling system: effects of wind and fisheries on population regulation. Fisheries Oceanography 13, 208–223.

Jarre, A., Paterson, B., Moloney, C.L., Miller, D.C.M., Field, J.G., Starfield, A.M., 2008. Knowledge-based systems as decision support tools in an Ecosystem Approach to Fisheries: comparing a fuzzy-logic and a rule-based approach. Progress in Oceanography 79, 390–400.

Judkins, D.C., 1980. Vertical distribution of zooplankton in relation to the oxygen minimum off Peru. Deep Sea Research 27, 475–487.

Kawasaki, T., 1983. Why do some pelagic fishes have wide fluctuations in their numbers? Biological basis of fluctuation from the viewpoint of evolutionary ecology. In: Sharp, G.D., Csirke, J. (Eds.) Reports of the expert consultation to examine changes in abundance and species composition of neritic fish resources. FAO Fisheries Report 291, pp. 1065–1080.

Key, R.M., Kozyr, A., Sabine, C.L., Lee, K., Wanninkhof, R., Bullister, J.L., Feely, R.A., Millero F.J., Mordy C., Peng, T.-H., 2004. A global ocean carbon climatology: Results from Global Data Analysis Project, (GLODAP), Global Biogeochemical Cycles, 18, GB4031, doi:10.1029/2004GB002247.

Lluch-Belda, D., Schwartzlose, R.A., Serra, R., Parrish, R., Kawasaki, T., Hedgecock, D., Crawford, R.J.M., 1992. Sardine and anchovy regime fluctuations of abundance in four regions of the world oceans: a workshop report. Fisheries Oceanography 1, 339–347.

MacCall, A.D., 1990. Dynamic Geography of Marine Fish Populations: Books in Recruitment Fishery Oceanography. University of Washington Press, Washington.

Mantua, N.J., Hare, S.R., Zhang, Y., Wallace, J.M., Francis, R.C., 1997. A Pacific interdecadal oscillation with impacts on salmon production. Bulletin of the American Meteorological Society 78, 1069–1079.

Messie, M., Ledesma, J., Kolber, D., Chavez, F., 2008. Nitrate supply and potential primary productivity estimates in four eastern boundary upwelling systems. In: Eastern boundary upwelling ecosystems, integrative and comparative approaches. Abstracts Book, vol. 145. GLOBEC IPO, Plymouth United Kingdom.

Pauly, D., Tsukayama, I. (Eds.) 1987. The Peruvian anchoveta and its upwelling ecosystem: three decades of change. ICLARM Studies and Reviews 15.

Pauly, D., Muck, P., Mendo, J., Tsukayama, I. (Eds.), 1989a. The Peruvian upwelling ecosystem: dynamics and interactions. ICLARM Conference Proceedings 18.

Pauly, D., Jarre, A., Luna, S., Sambilay jr., V., Rojas de Mendiola, B., Alamo, A., 1989b. On the quantity and types of food ingested by Peruvian anchoveta, 1953–1982. In: Pauly, D., Muck, P., Mendo, J., Tsukayama, I. (Eds.), The Peruvian upwelling ecosystem: dynamics and interactions. ICLARM Conference Proceedings 18, pp. 109–124.

Pennington, J.T., Mahoney, K.L., Kuwahara, V.S., Kolber, D.D., Calienes, R., Chavez, F.P., 2006. Primary production in the eastern tropical Pacific: a review. Progress in Oceanography 69, 285–317.

Reynolds, R.W., Smith, T.M., Liu, C., Chelton, D.B., Casey, K.S., Schlax, M.G., 2007. Daily high-resolution blended analyses for sea surface temperature. Journal of Climate 20, 5473–5496.

Riley, G.A., 1946. Factors controlling phytoplankton populations on Georges Bank. Journal of Marine Research 6, 54–73.

Rojas de Mendiola, B., 1989. Stomach contents of anchoveta (*Engraulis ringens*), 1953–1974. In: Pauly, D., Muck, P., Mendo, J., Tsukayama, I. (Eds.), The Peruvian Upwelling Ecosystem: Dynamics and Interactions. ICLARM Conference Proceedings 18, pp. 97–104.

Rostworowski, M., 2005. Recursos naturales renovables y pesca, siglos XVI y XVII; Curacas y sucesiones, costa norte. Obras completas IV; Historia Andina, 29. LIMA, IEP.

Russel, R.W., Hunt, G.L., Coyle, K.O., Cooney, R.T., 1992. Foraging in a fractal environment: spatial patterns in a marine predator–prey system. Landscape Ecology 7, 195–209.

Ryther, J.H., 1969. Photosynthesis and fish production in the sea. Science 166, 72–76.

Sifeddine, A., Gutiérrez, D., Ortlieb, L., Boucher, H., Velazco, F., Field, D., Vargas, G., Boussafir, M., Salvatteci, R., Ferreira, V., García, M., Valdes, J., Caquineau, S., Mandeng Yogo, M., Cetin, F., Solis, J., Soler, P., Baumgartner, T., 2008. Laminated sediments from the central Peruvian continental slope: a 500 year record of upwelling system productivity, terrestrial runoff and redox conditions. Progress in Oceanography.

Stramma, L., Johnson, G.C., Sprintall, J., Mohrholz, V., 2008. Expanding oxygen-minimum zones in the tropical oceans. Science 320, 655–658.

Swartzman, G., Bertrand, A., Gutiérrez, M., Bertrand, S., Vasquez, L., 2008. The relationship of anchovy and sardine to water masses in the Peruvian Humboldt Current System from 1983–2005. Progress in Oceanography.

Tam, J., Taylor, M.H., Blaskovic, V., Espinoza, P., Ballón, R.M., Díaz, E., Wosnitza-Mendo, C., Argüelles, J., Purca, S., Ayón, P., Quipuzcoa, L., Gutiérrez, D., Goya, E., Ochoa, N., Wolff, M., 2008. Trophic modeling of the Northern Humboldt Current Ecosystem, Part I: Comparing trophic linkages under La Niña and El Niño conditions. Progress in Oceanography.

Tarazona, J., Salzwedel, H., Arntz, W., 1988. Oscillations of macrobenthos in shallow waters of the Peruvian central coast induced by El Niño 1982–1983. Journal of Marine Research 46, 593–611.

Taylor, M.H., Tam, J., Blaskovic, V., Espinoza, P., Ballón, R.M., Wosnitza-Mendo, C., Argüelles, J., Díaz, E., Purca, S., Ochoa, N., Ayón, A., Goya, E., Quipuzcoa, L., Gutiérrez, D., Wolff, M., 2008a. Trophic modeling of the Northern Humboldt Current Ecosystem, Part II: Elucidating ecosystem dynamics from 1995–2004 with a focus on the impact of ENSO. Progress in Oceanography.

Taylor, M.H., Wolff, M., Mendo, J., Yamashiro, C., 2008b. Changes in trophic flow structure of Independence Bay (Peru) over an ENSO cycle. Progress in Oceanography.

Travers, M., Shin, Y.-J., Jennings, S., Cury, P., 2007. Towards end-to-end models for investigating the effects of climate and fishing in marine ecosystems. Progress in Oceanography 75, 751–770.

Valdés, J., Ortlieb, L., Gutiérrez, D., Marinovic, L. Vargas, G., Sifeddine, A., 2008. 250 years of sardine and anchovy scale deposition record in Mejillones Bay, Northern Chile. Progress in Oceanography.

Vogt, W., 1948. Road to Survival. William Sloane, New York.

Walters, C., Christensen, V., 2007. Adding realism to foraging arena predictions of trophic flow rates in Ecosim ecosystem models: shared foraging arenas and bout feeding. Ecological Modelling 209, 342–350.

Woodruff, S.D., Diaz, H.F., Kent, E.C., Reynolds, R.W., Worley, S.J., 2008. Climate Variability and Extremes during the Past 100 Years. Advances in Global Change Research. In: Brönnimann, S., Luterbacher, J., Ewen, T., Diaz, H.F., Stolarski, R.S., Neu, U. (Eds.), The Evolving SST Record from ICOADS. Springer, pp. 65–83.

Zeidberg, L.D., Robison, B.H., 2007. Invasive range expansion by the Humboldt squid, Dosidicus gigas, in the eastern North Pacific. Proceedings of the National Academy of Sciences 104, 12948–12950.

Francisco P. Chavez [1]
Monterey Bay Aquarium Research Institute,
7700 Sandholdt Rd. Moss Landing,
CA 95039, USA
Tel.: +1 831 775 1709
E-mail address: chfr@mbari.org

Arnaud Bertrand [1]
Institut de Recherche pour le Développement (IRD),
CRH, Avenue Jean Monnet, BP 171,
34203 Sète Cedex,
France
Instituto del Mar del Perú,
Esquina Gamarra y Gral. Valle s/n,
Apartado 22, Callao, Lima,
Peru
Tel.: +33 (0)4 99 57 32 00
E-mail address: Arnaud.Bertrand@ird.fr

Renato Guevara-Carrasco
Instituto del Mar del Perú,
Esquina Gamarra y Gral. Valle s/n,
Apartado 22, Callao, Lima,
Peru

Pierre Soler
IRD, 44 bd de Dunkerque,
CS 90009, 13572 Marseille Cedex 02,
France

Jorge Csirke
Organización de las Naciones Unidas
para la Agricultura y la Alimentación (FAO),
Viale delle Terme di Caracalla,
00153 Roma,
Italy

---

[1] These authors contributed equally to the volume and the introductory paper.

Progress in Oceanography 79 (2008) 106–119

Contents lists available at ScienceDirect

Progress in Oceanography

journal homepage: www.elsevier.com/locate/pocean

Mesoscale eddies off Peru in altimeter records: Identification algorithms and eddy spatio-temporal patterns

Alexis Chaigneau [a,b,*], Arnaud Gizolme [a,b], Carmen Grados [b]

[a] *Institut de Recherche pour le Développement (IRD), Laboratoire d'Océanographie et de Climatologie: Expérimentation et Analyse Numérique (LOCEAN), UMR CNRS, Université P. et M. Curie, IRD, MNHN, Paris, France*

[b] *Instituto del MAR del PEru (IMARPE), Esquina general Gamarra y Valle, Callao, Peru*

ARTICLE INFO

Article history:
Accepted 14 October 2008
Available online 21 October 2008

Keywords:
Mesoscale activity
Eddy identification algorithms
Eddy characteristics
Eddy life cycles
Spatio-temporal variability
Eastern South-Pacific
Humboldt current systems

ABSTRACT

Relatively little is known about coherent vortices in the eastern South-Pacific along the Peruvian coast, even with regard to basic facts about their frequency of occurrence, longevity and structure. This study addresses these issues with nearly 15 years of relatively high-resolution satellite altimetry measurements.

We first compare two distinct automated methods for eddy identification. The objective validation protocol shows that the rarely-used geometrical or "*winding-angle method*", based on the curvature of the streamline functions, is more accurate than the commonly-used "*Okubo–Weiss algorithm*", which defines a vortex as a simple connected region with values of Okubo–Weiss parameter weaker than a given threshold.

We then investigate vortices off Peru using more than 20,000 mesoscale eddies identified by the winding-angle method. Coherent eddies, characterized by a high ratio of vorticity to deformation rate, are typically formed along the coast and propagate westward at 3–6 cm s^{-1}. The vortices have a mean radius of 80 km, increasing northward, and are most frequently observed off of Chimbote (9°S) and south of San Juan (15°S). The mean eddy lifetime is about 1 month, but if eddies survive at least 2 months, the probability for surviving an additional week (or month) is constant at 90% (or 67%). Anticyclonic eddies tend to propagate northwestward whereas cyclonic vortices migrate southwestward. In general, cyclones and anticyclones are similar, except for eddies surviving at least 6 months. In this case, after a similar 3–4 months of radius and amplitude growth, amplitudes (or sizes) decay particularly rapidly for anticyclonic (or cyclonic) eddies. In terms of intensity, cyclonic eddies show a rapid decay during the first 3 months before arriving at a quasi-constant value, whereas anticyclones exhibit steady decline. Finally, eddy temporal variations were examined at seasonal and interannual scales in the "coastal" region favorable to the formation of energetic mesoscale structures. On seasonal scales, eddy activity is maximal in fall and minimum in spring. At interannual scales, the eddy activity index was maximal during the strong El Niño of 1997–1998 but another strong maximum of eddy activity also occurred late in 2004. These temporal variations are probably associated with the intensification of the upwelling thermal front and with the passage of coastal-trapped waves which generate baroclinic instabilities. Further investigation of the mechanisms involved on the eddy genesis is needed.

1. Introduction

The eastern South-Pacific Ocean (ESP), as the World Ocean in general, is a turbulent system which exhibits, superimposed on the large-scale Peru–Chile Current System (Strub et al., 1998), mesoscale variability composed of eddies or vortices (Hormazabal et al., 2004; Chaigneau and Pizarro, 2005c), meanders or fronts (Chaigneau and Pizarro, 2005a), and squirts and filaments (Thomas, 1999). Compared to other ocean basins, the ESP is characterized by relatively low levels of eddy kinetic energy (EKE) (Stammer, 1997, 1998; Stammer and Wunsch, 1999; Le Traon and Morrow, 2001; Stammer et al., 2006; Pascual et al., 2006), varying from 200–300 $cm^2\ s^{-2}$ along the continental coast to 50–100 $cm^2\ s^{-2}$ in the interior ocean (Hormazabal et al., 2004; Chaigneau and Pizarro, 2005b). Long-lived energetic eddies, having a lifetime higher than 3 months, can nevertheless be generated near the coast and propagate long distances offshore (Chaigneau and Pizarro, 2005c).

Eddies are generally more energetic than the surrounding currents and are an important component of dynamical oceanography at all scales. In particular they can transport heat, mass, momentum, and biogeochemical properties from their regions of forma-

---

[*] Corresponding author. Address: Instituto del MAR del PEru (IMARPE), Esquina general Gamarra y Valle, Callao, Peru. Tel.: +51 1 429 60 69/76 30 (anexo 265).
E-mail address: alexis.chaigneau@ird.fr (A. Chaigneau).

0079-6611/$ - see front matter © 2008 Elsevier Ltd. All rights reserved.
doi:10.1016/j.pocean.2008.10.013

tion to remote areas where they can then impact budgets of the tracers (Bryan, 1996; Wunsch, 1999; Roemmich and Gilson, 2001; Jayne and Marotzke, 2002; Qiu and Chen, 2005). In the ESP, the offshore propagation of mesoscale structures can extend the area of high primary productivity (Thomas et al., 1994; Chavez, 1995; Loubere, 2000) through advection of phytoplankton biomass and nutrient-enriched coastal water. It is also hypothesized that the variability of the highly pronounced subsurface oxygen minimum zone observed in the Peru–Chile Current System (Helly and Levin, 2004) is modulated by the westward motions of mesoscale eddies. In the vertical, eddy pumping may be an important mechanism for bringing nutrient-enriched subsurface water into the euphotic zone as observed in other areas of the world ocean (Falkowski et al., 1991; McGillicuddy et al., 1998; Siegel et al., 1999). Finally, mesoscale processes impact marine ecosystems (Logerwell and Smith, 2001; Spear et al., 2001; Bakun, 2006; Sasai et al., 2006) and the management of various marine activities such as fisheries, pollution monitoring, or offshore industry.

Despite the importance of the mesoscale dynamics, only a few works have investigated eddy characteristics of the ESP and none of them have focused on the Peruvian oceanic region which is one of the most productive of the world. Recently, Chaigneau and Pizarro (2005c) used near-surface drifters and satellite altimetry to provide the mean Chile–Peru Current eddy characteristics in a region south of 10°S, but basic questions remain. In particular, mean eddy properties such as geographical distribution, frequency of occurrence, lifespan, and propagation velocity field are all undescribed. Growth and decay of long-lived eddies and the temporal variations of eddy activity and characteristics are also poorly documented. Over the last two decades, satellite altimetry, due to its global and regular monitoring with relatively high resolution, has given considerable insight into mesoscale dynamics. The aim of this study is to use nearly 15 years of altimetry to quantitatively investigate the mesoscale activity and examine its spatio-temporal variability in a region offshore from Peru. The results should be useful for the validation of regional oceanic model simulations, and also to better examine relationships between mesoscale dynamics and marine ecosystems.

Mesoscale vortices cannot be identified and extracted from geophysical turbulent flow as observed by satellite altimetry without suitable definition and a competitive identification algorithm. A multitude of different techniques for automatic identification of eddies have been proposed, based either on physical or geometric criteria of the flow field. Physical criteria require the calculation of dynamical properties, and eddies are identified where thresholds of calculated properties are exceeded. Dynamical properties of the flow field that have been used to identify eddies include pressure or sea-level anomaly magnitude (Jeong and Hussain, 1995; Fang and Morrow, 2003; Morrow et al., 2004a; Chaigneau and Pizarro, 2005c), high vorticity magnitude (Hussain and Huyakawa, 1987), or high normalized helicity (Buning, 1989; Sadarjoen et al., 1998). Other physical criteria based in particular on the velocity gradient tensor or rate-of-deformation tensor have also been used to study coherent oceanic structures (Isern-Fontanet et al., 2003, 2004, 2006; Morrow et al., 2004b; Chelton et al., 2007). However, as mentioned by Sadarjoen (1999), these physical criteria often fail to locate vortices and eddy identification may be inaccurate (Basdevant and Philipovitch, 1994). Furthermore, arbitrarily varying thresholds may need to be used for these methods, requiring a user interaction which leads to a non-fully automated and subjective process.

A second type of eddy identification techniques is based on geometry of the flow. As vortices consist of quasi-circular flow patterns, geometric criteria use the shape or curvature of instantaneous streamlines. These vortex-identification methods consist to release a large number of streamlines over the velocity field of the study domain and select the curves having circular or closed geometry. To this end, two different techniques can be used: (1) the "*curvature center method*" (Leeuw and Post, 1995) or (2) the "*winding-angle method*" (Sadarjoen and Post, 2000), which detects closed streamlines via measuring cumulative changes in streamline direction as represented by the winding-angle (see Appendix). As noted by Sadarjoen (1999) and Guo (2004), these geometrical methods and in particular the winding-angle method, look promising to detect weak vortices.

The first goal of this study is to compare physical and geometrical vortex-identification methods. After having established the suitability of the geometrical method to extract eddies from sea-level anomaly (SLA) maps, we apply this rather rarely-used algorithm to investigate eddy activity off Peru. The paper is organized as follows. Under Section 2, we describe the satellite data set and computation of the different eddy kinematics. Vortex censuses, which involve objective identification and tracking algorithms, are also described in Section 2. In Section 3 we compare both of the eddy detection schemes using an objective protocol of validation. Section 4 deals with the main eddy properties of the study region whereas Section 5 focuses on the genesis, the propagation and the growth and decay of long-lived eddies. The temporal variations of eddy characteristics and eddy activity are investigated in Section 6. A summary of the results is provided in Section 7, along with ideas for future research.

2. Data and methods

2.1. Altimetry data and inferred eddy kinematic properties

Combining data from different satellite missions improves the estimation of mesoscale signals (Le Traon and Dibarboure, 1999; Le Traon et al., 2001; Chelton and Schlax, 2003; Pascual et al., 2006). The altimeter data used in this study are the combined Topex/Poseidon (T/P), ERS-1/2, Jason-1 and Envisat product as provided by Collecte Localisation Satellite (CLS) – Space of Oceanography Division of Toulouse, France. This AVISO delayed-time altimeter dataset provides a homogeneous, inter-calibrated and highly accurate long time-series of SLA data spanning roughly 14 years from October 1992 to August 2006 (datasource: http://www.jason.oceanobs.com).

As explained by Ducet et al. (2000), SLA alongtrack measurements are first filtered with a Lanczos filter having a typical cutoff wavelength of 200–300 km in the study region. These filtered data are then subsampled every 35–50 km and mapped through an objective technique used to combine the distinct satellite alongtrack measurements. This method takes into account long wavelength error uncorrelated noise due to residual orbit errors but also tidal or inverse barometer errors, and high frequency ocean signals (Le Traon et al., 1998). Finally, the merged-satellite product results in 723 weekly SLA maps which are computed relative to a seven year mean (January 1993–December 1999) and distributed on a regular $0.25° \times 0.25°$ grid.

During the ERS-1 ice-monitoring and geodetic mission (26 December 1993–31 March 1995), there were no ERS data available for ocean mesoscale studies. For this period, T/P data alone were used in the merged product and the spatial and temporal decorrelation scales lead to a reduction in EKE levels of around 30% globally (Ducet et al., 2000). Since our study region (3°S–20°S; 70°W–90°W, see Fig. 1) extends near the equator where the T/P groundtrack coverage is coarse (200–300 km), we can expect some reduction in EKE and in the number of identified eddies during the period with only T/P data. We will return to this point during the discussion on the temporal evolution of eddy characteristics in Section 6.

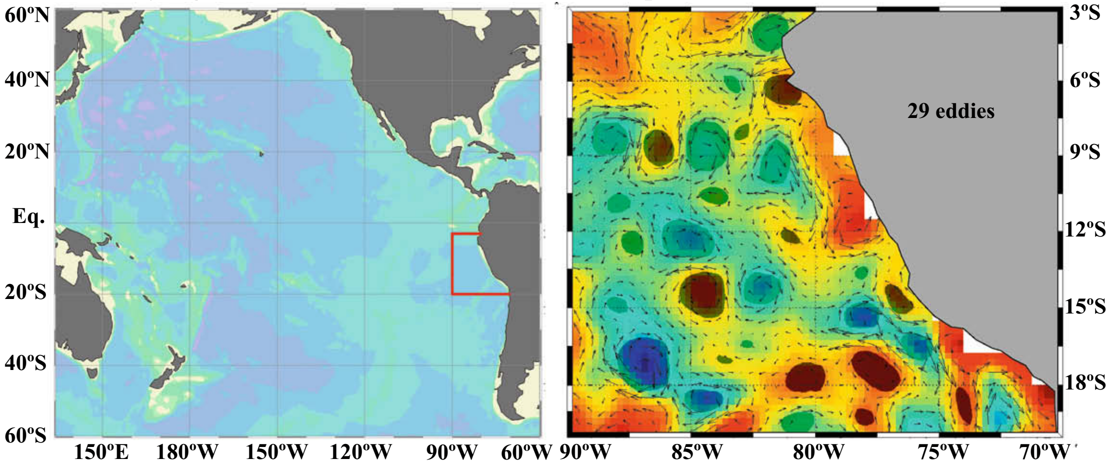
(a) Study region

(b) Expert

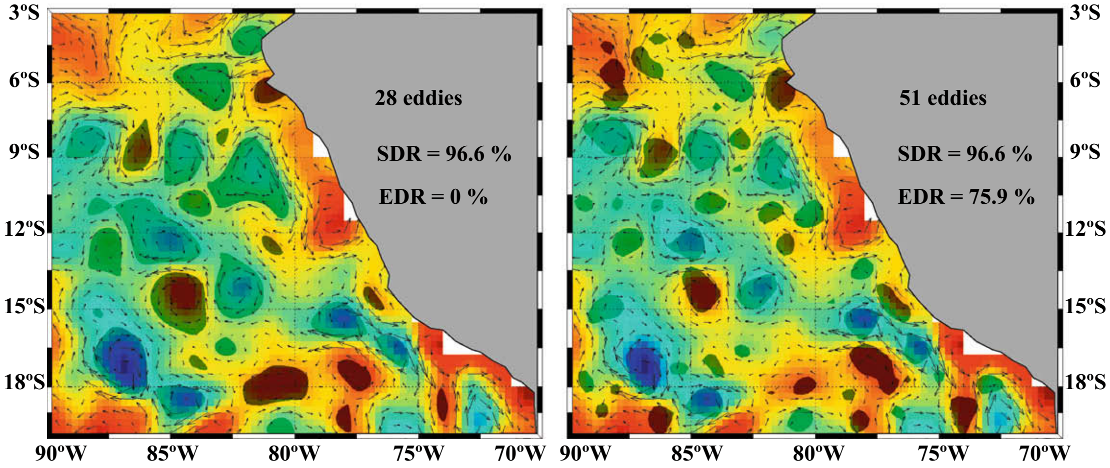
(c) WA Algorithm

(d) OW Algorithm

Fig. 1. (a) Study region (red box) and illustrative example for the detection of vortices by (b) one of the experts, (c) the "*winding-angle method*" and (d) the "*Okubo–Weiss method*". Shown are the SLAs (colour shading), the associated geostrophic currents (black quivers) and the identified eddies (light shading). Clockwise rotating structures correspond to cyclonic eddies in the southern hemisphere. The numbers of identified eddies and success and excess detection rates are also indicated.

Considering only the balance between the Coriolis force and the pressure gradient, residual sea-surface geostrophic velocity components (U', V') can be computed from the SLA gradients as

$$U' = -\frac{g}{f}\frac{\partial(SLA)}{\partial y},$$

$$V' = \frac{g}{f}\frac{\partial(SLA)}{\partial x},$$

where g is the acceleration due to gravity, f is the Coriolis parameter, and ∂x and ∂y are the eastward and northward distances. The swirl velocity V_θ of each detected eddy (see Section 3.2) corresponds to the geostrophic velocity amplitude $(V_\theta = \sqrt{U'^2 + V'^2})$.

It is important to note that f tends to zero near the equator and the geostrophic approximation will not be valid north of ~5°S. Consequently, north of 5°S we followed Lagerloef et al. (1999) to compute velocity components on a β-plane; this did not affect significantly the statistical results of this study. We thus assumed that the geostrophic approximation can be applied in the entire study region between 3°S and 20°S and the velocity fields were computed from the definitions given above. Also, the geostrophic approximation for deriving eddy velocities is valid only if centrifugal force and friction are neglected. The comparison of the relative and planetary vorticities (ξ and f, respectively) in the ESP shows that the vorticity rate $(|\frac{\xi}{f}|)$, equivalent to the Rossby number, increases when eddy radius decreases (Chaigneau and Pizarro, 2005c): at a radius of 100 km the relative vorticity is about 1% of f and at a radius of 10 km the rate increases to 10%. Since the results of this study are only based on vortices having a radius larger than 35 km (see Section 4.1) which correspond to vorticity rates smaller than 5%, we argue that ageostrophic processes can be neglected.

EKE is computed from velocity components using the classical relation

$$\mathrm{EKE} = \frac{1}{2}(U'^2 + V'^2).$$

To investigate the principal eddy characteristics of the study region we also compute their vorticity and deformation rates. First, in the local Cartesian (x, y) coordinate system, the gradients of geostrophic components are

$$g_{11} = \frac{\partial U'}{\partial x}; \quad g_{12} = \frac{\partial U'}{\partial y}; \quad g_{21} = \frac{\partial V'}{\partial x}; \quad g_{22} = \frac{\partial V'}{\partial y}.$$

Within a 7-day period, it is assumed that g_{11}, g_{12}, g_{21} and g_{22} are constants with respect to location and time. Using these gradients, we can determine the vorticity by

$$\omega = g_{21} - g_{12},$$

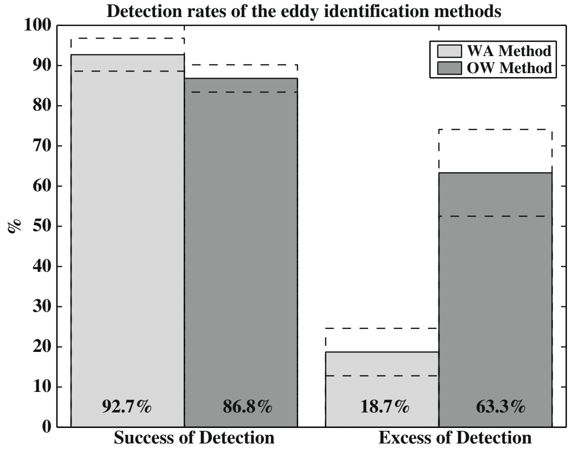

Fig. 2. Detection rates of both the *winding-angle* and *Okubo–Weiss* eddy identification methods. The gray-shading bars and black numbers correspond to the mean values and the means ± one standard deviation are displayed by dashed lines.

the shearing deformation rate (or the shear component of strain) by

$$s_s = g_{21} + g_{12},$$

the stretching deformation rate (or the normal component of strain) by

$$s_n = g_{11} - g_{22},$$

the total deformation rate by

$$s = \sqrt{s_s^2 + s_n^2}$$

and the divergence by

$$\psi = g_{11} + g_{22}.$$

By definition, in the southern hemisphere the vorticity is positive for an anticyclonic (warm-core, or high-pressure) eddy, and is negative for a cyclonic (cold-core, or low-pressure) eddy.

2.2. Eddy identification algorithms and eddy property determination

One of the aims of this study is to compare and quantify the efficiency of two automated methods for eddy identification. The first is based on geometric criteria and was motivated by the following concrete definition of a vortex provided by Robinson (1991):

> *“A vortex exists when instantaneous streamlines mapped onto a plane normal to the vortex core exhibit a roughly circular or spiral pattern (...)”*

This definition suggests the use of streamline function curvatures for the detection of mesoscale eddies and is achieved using the winding-angle (WA) detection algorithm (Sadarjoen et al., 1998; Sadarjoen and Post, 2000; Sadarjoen, 1999; Guo, 2004). This method (hereinafter referred as “*WA method*”) characterizes an eddy structure by a point that defines its center and by a closed streamline contour corresponding to the eddy edge. The inner points bordered by this contour line belong to the eddy and determine its surface area. For each SLA map, possible cyclonic (or anticyclonic) eddy centers are identified finding local SLA minima (or maxima) in an arbitrary chosen 1.25° × 1.25° latitude–longitude moving window. Then, streamlines are computed, following the trajectories of virtual particles released in the geostrophic current field from every 0.25° × 0.25° grid point. The step size and the number of steps for the integration of the streamlines must be chosen carefully. The step size should be chosen as small as possible to achieve the highest accuracy while the number of steps should be as high as possible to ensure that paths are long enough, particularly in regions of low velocity magnitude. Here, each streamline is constructed using arbitrary chosen values of 1200 vertices with a constant step size of 0.05 (one twentieth of a cell grid corresponding approximately to 1.35 km). The maximum streamline length is thus of order of 1600 km corresponding to a maximum detectable eddy radius of ∼250 km. This value is larger than both the estimated size of the visually identified eddies and the larger Rossby radius of deformation of 225 km observed in the study region (Chelton et al., 1998; see also Fig. 3b).

Then, the eddy identification process consists of two main stages: the *selection* of streamlines associated with eddies and the *clustering* of distinct streamlines corresponding to the same vortex. In the first stage, *selection*, streamlines having a high winding-angle $|\alpha| \geq 2\pi$ (see Appendix for definition of α), corresponding to a fully closed curve, are associated with an eddy center. In the second stage, *clustering*, the streamlines belonging to a given eddy are grouped. Thus, each cluster consists of closed streamlines rotating around the same vortex center. For each cluster, the outer streamline corresponds to the eddy edge. As noted by Isern-fontanet et al. (2003), when a vortex is embedded in background flow, the total streamfunction field does not necessarily exhibit a clear extreme at the eddy center. Consequently, the contours obtained with the WA in the SLA fields are not always associated with closed contours in the total streamfunction field. However, the main statistics obtained from SLA maps and discussed in this paper were also computed from the total streamfunction field adding the barotropic currents of the Rio05 combined mean dynamic topography (Rio and Hernandez, 2004; Rio et al., 2007) produced by CLS Space Oceanography Division (not shown). As no significant differences were observed and as we are interested in eddy dynamics without the influence of large-scale currents, we preferred using the streamfunctions computed from the SLAs.

While WA method is based on geometrical criteria, the second eddy identification method examined is based on a physical criterion. It detects vortices using the properties of the Okubo–Weiss parameter (Okubo, 1970; Weiss, 1991) which indexes the relative importance of strain and vorticity in the flow as

$$W = s_s^2 + s_n^2 - \omega^2,$$

where s_s, s_n and ω are, respectively, the shearing deformation rate, the straining deformation rate and the vorticity defined in Section 2.1.

As suggested in previous marine studies (Isern-Fontanet et al., 2003, 2006; Morrow et al., 2004b; Chelton et al., 2007), a vortex exists where rotation dominates, corresponding to negative W values. More precisely, a vortex is defined as a region having the same sign of vorticity and with values of the OW parameter smaller in magnitude than a threshold $W_0 = -0.2\sigma_W$, σ_W being the spatial standard deviation of W. The geostrophic velocity fields derived from SLA maps are used to compute σ_W at each time, and closed contours of $W = W_0$ are assigned to eddies. This second vortex-identification algorithm is hereinafter referred as “*OW method*”.

The two eddy identification algorithms described above are applied to the entire altimetry dataset to detect eddy edges in the study region. After a vortex edge is identified, several eddy properties are computed. The position of the vortex center is determined as the position of the maximum absolute value of SLA inside the eddy. The vortex area (A) corresponds to the area delimited by eddy edge whereas its apparent radius (R) corresponds to the radius of an equivalent circular vortex having the same area

$$R = \sqrt{\frac{A}{\pi}}.$$

By analogy with atmospheric studies of cyclone activity (e.g. Nielsen and Dole, 1992; Zhang et al., 2004; Wang et al, 2006), we define the vortex amplitude as the absolute value of the SLA difference between the eddy center and the averaged SLA along the eddy edge:

$$\text{Amplitude} = |SLA_{center} - \overline{SLA_{edge}}|.$$

Eddy intensity (EI), or energy density, corresponds to the mean EKE over the vortex ($\overline{\text{EKE}}$) normalized by its area

$$\text{EI} = \frac{\overline{\text{EKE}}}{A} = \frac{\overline{\text{EKE}}}{\pi R^2}.$$

Finally, to measure the overall eddy activity in the study region, we use an eddy activity index (EAI) that is defined as

$$\text{EAI} = N\overline{\text{EI}} = \sum_{i=1}^{N} \text{EI}_i,$$

where N denote the number of identified eddies in the domain shown in Fig. 1, and $\overline{\text{EI}}$ corresponds to the mean intensity of these eddies. In other words, the EAI is defined as the count of eddies multiplied by their mean intensity, or equivalently, the sum of the eddy intensities in a particular time (one week in our case).

Both these properties and the different eddy kinematics described in Section 2.1 (e.g. swirl velocity, EKE, divergence, vorticity, straining and shearing deformation rates) are computed for each detected vortex. In addition to these various properties, we also analyzed the eddy occurrence frequency and its distribution as the eddy life span and eddy characteristics along their tracks.

2.3. Eddy-tracking algorithm

Note that an "eddy" refers to a single minimum or maximum SLA center identified at a specific location and time, while an eddy track consists of the trajectory of an eddy during its lifetime. An eddy track usually lasts more than one observation interval (one week in this study) and therefore, the number of eddy tracks is usually smaller than counts of eddies. The eddy tracking algorithm used in this study is adapted from Penven et al. (2005) and minimizes a distance D between the detected eddies of two consecutive maps. For each eddy (e_1) identified on a given map at time t_1 and for each eddy (e_2) identified on the next map at time t_2 and rotating in the same sense than e_1, the nondimensional distance D_{e_1,e_2} is defined as

$$D_{e_1,e_2} = \sqrt{\left(\frac{\Delta D}{D_0}\right)^2 + \left(\frac{\Delta R}{R_0}\right)^2 + \left(\frac{\Delta \xi}{\xi_0}\right)^2 + \left(\frac{\Delta \text{EKE}}{\text{EKE}_0}\right)^2},$$

where ΔD is the spatial distance between e_1 and e_2, and ΔR, $\Delta\xi$ and ΔEKE are, respectively, the radius, the vorticity and the EKE variations between e_1 and e_2. D_0, R_0, ξ_0 and EKE_0 are, respectively, the characteristic length scale ($D_0 = 100$ km), characteristic radius ($R_0 = 50$ km), characteristic vorticity ($\xi_0 = 10^{-6}\ \text{s}^{-1}$) and characteristic EKE ($\text{EKE}_0 = 100\ \text{cm}^2\ \text{s}^{-2}$). D_{e_1,e_2} represents the degree of similarity between two eddies (smaller values indicate higher similitude between e_1 and e_2). Thus, the algorithm selects the eddy pair (e_1,e_2) that minimize D_{e_1,e_2} and considers this pair to be the same eddy that is tracked from t_1 to t_2. Since the propagation speed of the mesoscale eddies is expected to be a few tens of kilometers per week (Chaigneau and Pizarro, 2005c) and to avoid jumping from one track to another, the searched distance ΔD was restricted to 150 km. Vortices may also disappear between consecutive maps, in particular if they pass into the gaps between satellite groundtracks. To minimize this problem, we search for the same eddy for two weeks after its disappearance.

3. Comparison between the winding-angle and the Okubo–Weiss eddy identification methods

3.1. Validation protocol of the eddy identification methods

Since our goal is to automatically identify mesoscale eddies in a large volume of data, it is imperative that we validate both identification methods. The validation protocol, adapted from Segond (2006), verifies presence of the identified vortices using the following objective methodology:

(1) On the 723 available SLA maps, 10 are randomly chosen and sent to five oceanographic experts. These maps contain both the SLA field and the derived geostrophic currents.
(2) For each map, all experts draw by hand the eddy contours they identified.
(3) Their maps are then digitized and compared with the eddy contours determined by both the automated algorithms. For each map and for each vortex, rates of covering (Ae ∩ Am and Am ∩ Ae) are computed between the eddy area identified by the expert (Ae) and the corresponding area of the identification methods (Am). If one of these rates of covering are higher than a given threshold (50% in our case), the vortex is considered as correctly detected since the expert cannot determine the eddy envelop with high accuracy.
(4) Two different quantities are then estimated to validate and quantify the efficiency of both the OW and the WA eddy identification methods: the success of detection rate (SDR) and the excess of detection rate (EDR). These rates are defined as

$$\text{SDR} = \frac{N_c}{N_e},$$
$$\text{EDR} = \frac{N_{om}}{N_e},$$

where Nc corresponds to the common eddies identified by both the expert and the automated method, Ne corresponds to the total number of eddies identified by the expert and Nom (or Noe) corresponds to the number of eddies identified only by the method (or only by the expert). Note that the method can sometimes merge two close eddies identified as splitted by the expert. In this case it accounts for 1 in Nc and 1 in Noe. In contrast, if the method splits two close eddies identified as only one by the expert, both Nc and Nom are increased by 1.

3.2. Efficiency of the WA and OW methods for the detection of mesoscale vortices

Fig. 1 shows the SLA map and associated geostrophic currents for the 8th August of 2004 in the study region which extends from Northern Chile to Ecuador and from the coast to 90°W, covering a maritime area of ~2.8×10^6 km^2. Eddy contours identified by one of the experts (Fig. 1b) and by both the WA (Fig. 1c) and the OW methods (Fig. 1d) are shaded gray. This expert detected 29 eddies ($N_e = 29$) on this particular map (16 cyclonic and 13 anticyclonic), one more than the WA method. All the 28 structures identified by this algorithm are considered as common with the expert, but a small cyclonic vortex centered at ~14°S–78°W (Fig. 1b) is not identified by the WA method (Fig. 1c). Consequently in this example, $N_c = 28$, $N_{oe} = 1$ and $N_{om} = 0$, leading to an important SDR of 96.6%, and a null EDR. The WA method missed a small cyclonic eddy identified by the expert at 13.5°S and 78°W.

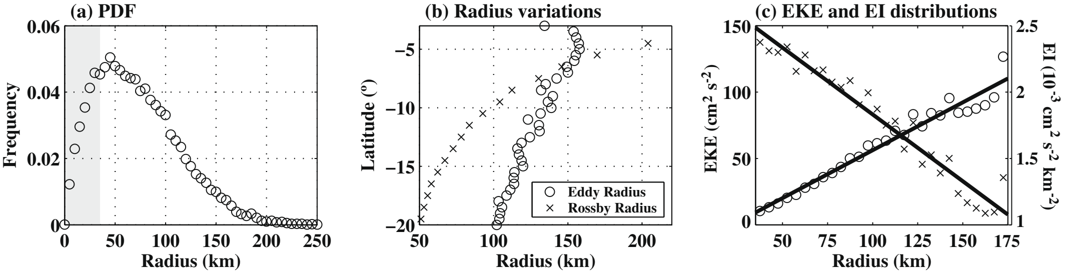

Fig. 3. Radius distributions. (a) Probability density function (PDF) of the radius sizes; The shaded region corresponds to eddy radii smaller than 35 km. (b) Meridional variation of eddy radii, for eddies with amplitude higher than 2 cm (circles); averaged Rossby radii from Chelton et al. (1998) are indicated by crosses. (c) Mean distributions of EKE (circles and left axis) and EI (crosses and right axis) as functions of eddy radii; solid lines are linear fits (for EKE, $r^2 = 97.8\%$ and an rms difference of 29.7 cm^2 s^{-2} km^{-2}; for EI, $r^2 = 97.2\%$ and an rms difference of 0.4×10^{-3} cm^2 s^{-2} km^{-2}).

In contrast, the OW method identified more structures than the expert. Among the 51 vortices identified by the OW algorithm, 28 structures are common with the expert ($N_c = 28$) leading to the same SDR of 96.6% obtained with the WA algorithm. However, 22 vortices are added by the OW method ($N_{om} = 22$) which leads to a strong EDR of 75.9%. The well-developed anticyclonic eddy located at the northeastern edge of the study region (Fig. 1b) is missed by the OW method ($N_{oe} = 1$). Even though we observed the same success of detection rate in both methods, the strong excess of detection of the OW algorithm in this particular example suggests a lack of efficiency of this method. But are these preliminary conclusions valid only for this particular example, or is the WA method constantly more efficient to detect vortices?

To answer, the mean detection rates (SDR and EDR) were estimated from the expert maps (50 maps in total) and the results are presented in Fig. 2a. The SDR is equivalent for both methods with mean values of 92.7% for the WA method and 86.8% for the OW algorithm. On average, only 0.8% (or 0%) of the experts' eddies are merged by the WA (or the OW) algorithm and 2% (or ∼ 6%) are erroneously split into two eddies. The EDR which is less than 20% for the WA method reaches 63% for the identification algorithm based on the OW parameter. With OW's EDR value of 63% and a tendency to erroneously split eddies, it is evident that the OW method over-detects. This problem was also noted by Isern-Fontanet et al. (2006) who applied the OW algorithm to vortices of the Mediterranean Sea. The SDR to EDR ratio, equivalent to a signal to noise ratio, is of 5 for the WA method and 1.4 for the OW method. These values also confirm that the automated method based on the OW parameter is not adequate to detect "true" mesoscale eddies while the WA technique is both more efficient and more conservative. Finally, although the OW algorithm identifies too many vortices, this method also fails to identify some eddies with a default of detection rate (DDR = 1 − SDR) of 13.2%. Note that the above results do not strongly depend on the choice of the selected threshold W_0 for the OW method, since the signal to noise ratio varies from 1 to 3 for W_0 varying from of $-0.05\sigma_w$ to $-\sigma_w$ (not shown). However the best compromise is effectively a W_0 value in the range $-0.3\sigma_w \leqslant -W_0 \leqslant 0.2\sigma_w$ since the success of detection rate decreases drastically outside these limits. It is also important to keep in mind that experts may, for example, miss some eddies or merge or split close eddies. As the experts do not have the possibility to correct themselves after inspection of the automatically identified eddy contours, the obtained signal to noise ratio of 5 with the WA method can be considered as a minimum value.

Finally, as the expert maps are the basis for estimating the efficiency of the automated algorithms, it is important to estimate the reliability of the expert eddy-identifications. In order to intercompare the tracking results from the different experts, Table 1 shows for each evaluated map the percentages of eddies detected by only one expert or commonly by between 2 and 5 experts. On average (last column of Table 1), 33–34 distinct eddies are identified by the experts on each given map. Around 11% of these 33 eddies are identified by only one expert whereas nearly 85% are detected by at least three of the five experts, and about 70% by all the five experts. Despite the rather good agreement between the experts, we note that 10–20% of the eddies are only identified by 1–2 experts. This suggests that 10–20% of the vortices may have a weak SLA signature and could be then considered as spurious or at least suspicious. Thus, the value of 20% can be considered as an upper limit for an acceptable error of the automated algorithms. As shown in Fig. 2, the 10–20% range is of the same order of magnitude than the DDR of both the automated methods; furthermore, the EDR of 18.7% of the WA algorithm is also in the acceptable error range set by the experts, which again confirm the good efficiency of this method compared to the OW algorithm. Thus, based on the results of this objective comparison, the WA algorithm is retained for this study and is applied to the 723 SLA maps in order to provide a reliable description and confident statistics of the mesoscale activity off Peru.

4. Mean eddy properties

4.1. Eddy radius

The probability density function of eddy radii shows a non-Gaussian distribution with a strong asymmetry (Fig. 3a). The majority of the detected eddies have a radius of ∼50 km and vortices with a radius higher than 175 km are very infrequent. Even if the WA algorithm can detect small-scale vortices of few km (Fig. 3a), the combination of the Lanczos filter with the truncation step size used for subsampling the alongtrack altimetric data (see Section 2.1) suggests that the SLA maps cannot correctly resolve mesoscale structures having a diameter smaller than 70 km. Hence, all the results discussed hereafter are based on vortices with radii ranging from 35 to 250 km. This restriction removes around 20% of the ∼25,000 vortices originally identified, but does not alter our main conclusions. The remaining cyclones and anticyclones have an average radius of 80–85 km. This mean size is relatively homogeneous over the whole spatial domain. However, considering the 35% of eddies having an SLA amplitude higher than 2 cm, Fig. 3b shows that radii increase by a factor of 1.6 from ∼100 km at 20°S to ∼160 km at 3°S. This increase is small compared to the factor of 4.5 increase in the Rossby radius of deformation (Fig. 3, 20°S vs. 3°S) that is often associated with eddy size. However, the regional study of Penven et al. (2005), performed with a high-resolution model, noted a similar equatorward increase of both the eddy radii and the characteristic eddy length-scales computed from the autocorrelation functions of surface current anomalies (Stammer, 1997). The modeled eddies exhibit typical radii of 70–80 km at 20°S and of 100–120 km at 3°S leading to a factor increase of ~1.5, similar to our observations. Other studies, based on altimetry alongtrack measurements (Stammer, 1997, 1998) or on a merged-satellite product (Chelton et al., 2007), have also identified similarly weak equatorward increases in eddy lengthscales.

The mean EKE and EI distributions as function of eddy radius are shown in Fig. 3c. The mean EKE (or EI) increases (or decreases) quasi-linearly from ~10 $cm^2 s^{-2}$ (or from 2.5 × 10^{-3} $cm^2 s^{-2} km^{-2}$) for eddy radii of 35 km to ~110 $cm^2 s^{-2}$ (or to 10^{-3} $cm^2 s^{-2} km^{-2}$) for radii of 175 km. Higher discrepancies between the linear fit and the data are observed for eddy radii higher than 150 km due to a reduced number of eddies detected in this range of size (Fig. 3a). The intensity distribution is mainly explained by the relatively weak EKE range observed in the study region and the relatively large range of eddy radius. For example, eddies have a mean EKE varying of a factor 10 (from ~10 to ~100 $cm^2 s^{-2}$) while their area vary by a factor of ~25. It is then obvious that for a same EKE range, the most energetic or most intense eddies correspond to smaller structures.

4.2. Eddy frequency

A total of 10,113 cyclones and 9842 anticyclones were identified, which corresponds to 2129 cyclone tracks and 2112 anticyclone tracks, or about 14 cyclones and anticyclones per week. These numbers indicate that there is no preference for the eddy polarity. The mesoscale structures cover an average total area of around 6.5 × 10^5 km^2, representing ~25% of the study region. Fig. 4a shows the geographical distribution of the frequency of these ~20,000 identified eddies. Its interpretation is straightforward since it corresponds at every location to the percentage of time instants that the point is located within a vortex. The mean eddy frequency over the domain is of 25.7%, in agreement with the rough estimate of the mean area they cover. Mesoscale structures are commonly observed south of 15°S where eddy frequency is of order of 30–50% but also offshore of Chimbote at around 9°S–82°W (Fig. 4a). These regions also correspond to local maxima in EKE of order of 100–150 $cm^2 s^{-2}$ (Fig. 4c). The mean spatial correlation between the eddy frequency and EKE distributions decreases from 40% south of 12°S to less than 20% in the 8°S–12°S latitude band (not shown). North of 8°S, the eddy frequency decreases to 20–25% (Fig. 4a and b) whereas EKE values are higher than 200 $cm^2 s^{-2}$ (Fig. 4c). In this northern region, the two fields are anticorrelated at −20% which suggests than the high SLA variance observed north of 8°S is rather associated with equatorial long-wave dynamics than energetic mesoscale eddies. Strong minima of eddy occurrence, with values weaker than 5–10%, take place all along the coast. The reason is that eddies are not fully developed in these coastal regions so that the WA algorithm cannot find closed streamlines. Finally, no significant difference was observed between the distribution of cyclonic and anticyclonic eddy frequencies nor in terms of seasonal variability.

4.3. Eddy lifespan

The lifespan distribution of the 4241 eddy trajectories is shown in Fig. 5a. The average lifetime of an eddy is 33 days and the median lifetime is of 14 days, without important difference between the two types of eddies. The seasonal variation of mean eddy lifespan was also insignificant with values of 33–35 days all year. For lifetimes shorter than 2 months, eddy numbers exhibit steep declines (Fig. 5a). Longer lifetimes are well approximated by expo-

Table 1
Percentage of eddies identified by only one expert and commonly by between 2 and 5 experts for each evaluated map. Numbers into brackets denote the number of distinct identified eddies.

	Map #1 (32)	Map #2 (37)	Map #3 (31)	Map #4 (31)	Map #5 (28)	Map #6 (38)	Map #7 (35)	Map #8 (36)	Map #9 (32)	Map #10 (33)	Average (33.3 ± 3.1)
1 expert	9.4	21.6	16.1	16.1	0	2.6	11.4	11.1	9.4	12.1	10.9 ± 6.3
2 experts	6.2	2.7	6.5	12.9	7.1	5.3	2.9	8.3	3.1	6.1	6.1 ± 3.1
3 experts	3.1	5.4	6.5	3.2	0	5.3	11.4	5.6	0	6.1	4.7 ± 3.3
4 experts	6.2	13.5	3.2	3.2	7.1	13.2	14.3	5.6	6.2	21.2	9.4 ± 5.9
5 experts	75.1	56.8	67.7	64.6	85.8	73.6	60.0	69.4	81.3	54.5	68.9 ± 10.3

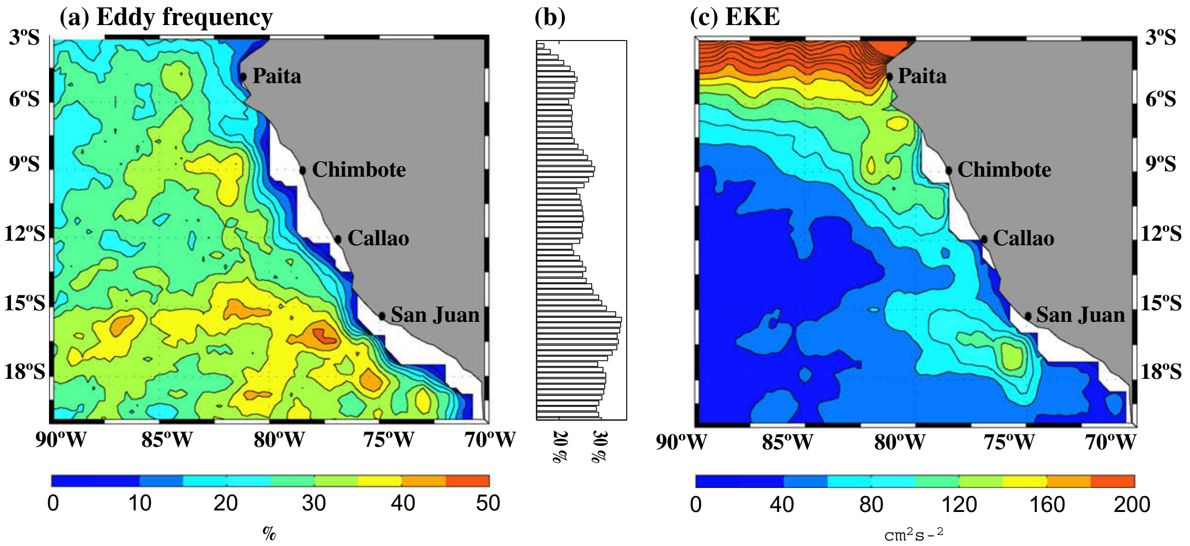

Fig. 4. (a) Mean regional climatology of eddy frequency (in %) for October 1992–August 2006. (b) Meridional variations of mean eddy frequencies (in %). (c) Spatial distribution of mean EKE (in $cm^2 s^{-2}$) from satellite altimeter measurements.

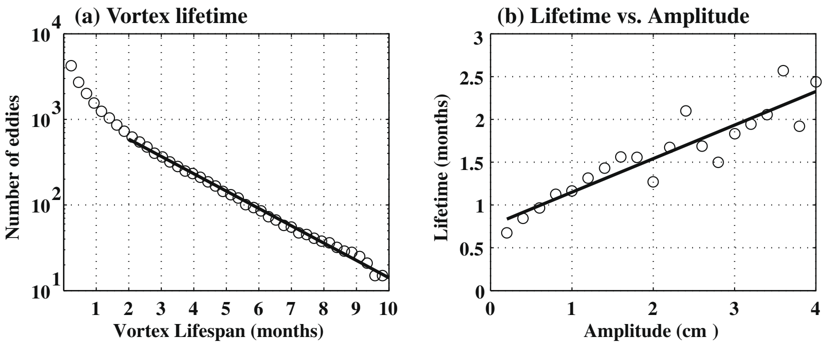

Fig. 5. (a) Vortex lifespan distribution (black circles, logarithmic scale); heavy line is a linear fit (r^2 = 99.6% and an rms difference of 12 days). (b) Variation of vortex lifespan as function of eddy amplitude; heavy line is a linear fit (r^2 = 91.8% and an rms difference of 6 days).

nentially decaying distributions (black solid line in Fig. 5a) with a correlation coefficient of 99.7% and a root mean square (rms) difference of 12 days. This distribution implies constant probability for surviving an additional week (month) of 90% (67%). In order to assess the dependence of survivability on eddy strength, we calculate 7-day survival probabilities for tracks lasting at least 2 months as function of EI (not shown). Survival probabilities increase from 85% for eddy intensities weaker than $10^{-3}\,\mathrm{cm^2\,s^{-2}\,km^{-2}}$ to 92% for intensities higher $3 \times 10^{-3}\,\mathrm{cm^2\,s^{-2}\,km^{-2}}$. Another monotonic relationship is observed between eddy lifetimes and eddy amplitudes at the time they are formed (Fig. 5b). Eddy lifespan increases on average from less than 1 month for a very weak eddy having “birth amplitude” of 0.5 cm to 2–3 months for a more developed eddy having initial amplitude higher than 3 cm. However, no interesting relationship was found between “birth intensity” and eddy lifespan. Finally, eddy lifetimes not only depend on their amplitude but also on their place of birth, showing a clear dependence with the latitude: eddies generated south of 15°S have a mean lifetime of 50–60 days, whereas eddies formed north of 5°S exist for an average of 10–15 days. This short near-equator lifespan also confirms that the high EKE values observed in the northern part of the study region (Fig. 4c) are not associated with eddies but rather with other processes such as equatorial long-waves or tropical instability waves.

4.4. Eddy kinematics

Table 2 shows the statistics of eddy kinematic parameters over the study region. Cyclonic and anticyclonic eddies have similar average vorticities of order of $2.5 \times 10^{-6}\,\mathrm{s^{-1}}$ in absolute value. On average, the shearing and stretching deformations rates and the divergences of both types of eddies are several order of magnitude smaller than the vorticities. However, a total deformation rate of $\sim 10^{-6}\,\mathrm{s^{-1}}$ suggests than eddies tend to be deformed and are not perfectly circular. Fig. 6a shows the distribution of both the vorticity and the total deformation rate as function of EI. The total deformation increases by a factor 4 from around 0.6×10^{-6} to $2.4 \times 10^{-6}\,\mathrm{s^{-1}}$ whereas the vorticity increases by a factor 6 from 1×10^{-6} to $6 \times 10^{-6}\,\mathrm{s^{-1}}$. As the ratio between the deformation rate and the vorticity decreases from 0.6 to 0.4, the most intense eddies should be less deformed and more circular. To verify this hypothesis and better investigate the eddy shape, we use the least squares method to fit ellipses to the ~20,000 eddy edges. The non-circular shape of these vortices is confirmed by a mean ellipse eccentricity of 1.65 for both types of eddies. As expected, the mean ellipse eccentricity slightly decreases with the EI (Fig. 6b): weakly intense eddies (EI < $0.8 \times 10^{-3}\,\mathrm{cm^2\,s^{-2}\,km^{-2}}$) have an eccentricity of more than 1.7 whereas strong energetic eddies (EI > $4 \times 10^{-3}\,\mathrm{cm^2\,km^{-2}}$) are more circular with a mean eccentricity of ~1.55.

Table 2
Mean statistics of the eddy kinematics for the time period October 1992–August 2006.

	Mean	Standard deviation	Minimum	Maximum
10,113 Cold-Core Cyclonic eddies (Unit: $10^{-6}\,s^{-1}$)				
Vorticity	−2.523	1.165	−17.392	−0.525
Shearing deformation	0.047	0.846	−6.330	6.840
Stretching deformation	0.115	0.872	−5.424	6.377
Total deformation	1.001	0.700	0.010	6.875
Divergence	5×10^{-5}	0.006	−0.235	0.079
9842 Warm-Core Anticyclonic eddies (Unit: $10^{-6}\,s^{-1}$)				
Vorticity	2.449	1.272	0.528	21.724
Shearing deformation	−0.044	0.836	−7.570	4.588
Stretching deformation	−0.009	0.847	−5.190	4.625
Total deformation	0.968	0.693	0.006	7.571
Divergence	-1×10^{-5}	0.006	−0.137	0.076

Finally, other kinematics properties have been studied such as the mean distribution of the rotation velocity or of the EKE across eddies. Average swirling velocities V_θ increase outward to a maximum of around $10\,\mathrm{cm\,s^{-1}}$ at the eddy edges (not shown), in agreement with the results of Chaigneau and Pizarro (2005c) obtained from surface drifters and altimetry measurements. EKE which is negligible at the eddy center also increases outward to a mean value of $\sim 70\,\mathrm{cm^2\,s^{-2}}$ at the eddy edges. However, averaged values of EKE inside the detected eddies are relatively small with values of $37 \pm 69\,\mathrm{cm^3\,s^{-2}}$ for cyclonic eddies and $42 \pm 59\,\mathrm{cm^2\,s^{-2}}$ for anticyclones.

Section 4 has been devoted to a detailed investigation of mean eddy properties (radius, frequency, lifetime and kinematics) in the study region. We will now focus in Section 5 on the genesis and on the propagation mode of “non-stationary” eddies. Section 5 also deals with the evolution of the characteristics of long-lived eddies (radius, amplitude, intensity and vorticity).

5. Eddy life cycles

5.1. Genesis and propagation

The geographical distribution of the points of eddy genesis is presented in Fig. 7 in color shading. The location of genesis corresponds to the initial point of an eddy track having a minimum lifetime of 1 month. This threshold on the lifespan is imposed to select only the “non-stationary” or propagating eddies. Eddy genesis is more frequent near the coast than in the interior ocean, with five

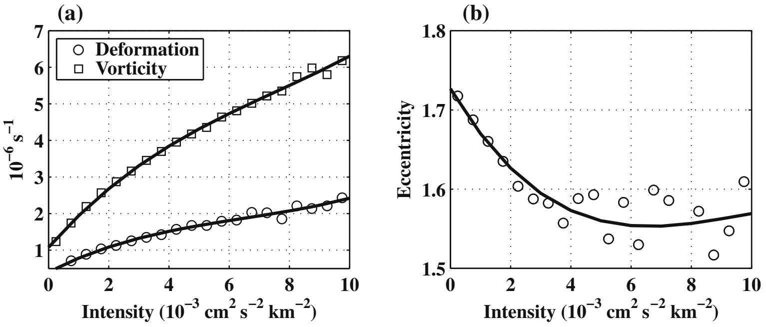

Fig. 6. (a) Eddy vorticity (black squares) and total deformation rate (black circles) as functions of EI; Solid lines shows third-order polynomial fits (for vorticity, $r^2 = 99.9\%$ and an rms difference of 7.9×10^{-8} s^{-1}; for deformation rate $r^2 = 99.3\%$ and an rms difference of 6.6×10^{-8} s^{-1}). (b) Variation of fitted ellipse eccentricity (no unit) as function of EI; Solid line shows third-order polynomial fit ($r^2 = 85.8\%$ and an rms difference of 0.03).

pronounced maxima nearshore between 6°S and 20°S. The temporal variations of eddy genesis are examined in further detail in Section 6. The coastal formation of eddies may be due to interactions of the Peru–Chile Current system with the coastline, presence of the strong upwelling front, or the high-temporal variability of the coastal flow (Pizarro et al., 2002). The intensification of the poleward subsurface Peru–Chile Undercurrent by the downwelling Kelvin waves of equatorial origin can also destabilize the near-surface coastal circulation (Shaffer et al., 1997; Zamudio et al., 2001) and generate eddies. Despite these pronounced maxima along the coast, eddy genesis also occurs offshore (Fig. 7). Additional localized maxima of eddy genesis with weaker amplitudes appear for instance in the entire region between 9°S and 14°S.

Fig. 7 also displays the mean eddy velocity propagation field (black arrows) computed by a centered difference scheme at each 7-day eddy displacement. Eddies propagate offshore quasi zonally over the entire study region, except north of 9°S where a southwestward component is observed. On average, eddy propagation velocities increase equatorward from a mean value of around 3 cm s^{-1} at 20°S to 5–6 cm s^{-1} north of 9°S, substantially weaker than the eddy-edge swirl velocities of ~10 cm s^{-1} (see Section 4.4). This velocity difference confirms eddy coherence with a clear separation between the rotating core and the surrounding advective flow. These eddy propagation velocities of 3–6 cm s^{-1} are of the same order of the estimates of Chaigneau and Pizarro (2005c); the northward increase in velocity is consistent with the meridional changes of eddy motions on a β-plane (Cushman-Roisin, 1994). However, the observed eddy propagation speeds are systematically lower than both the energetic large-scale Rossby wave zonal wave speeds of 10–30 cm s^{-1} (Maharaj et al., 2005; Chelton et al., 2007) and the westward South-Equatorial Current of ~8 cm s^{-1} observed in the region from near-surface drifter measurements (Chaigneau and Pizarro; 2005b). Thus, as also mentioned by Chelton et al. (2007), the observed SLA variability at these low latitudes consists of a superposition of fast-propagating Rossby waves and slowly-propagating mesoscale eddies. Differences between cyclonic and anticyclonic eddy pathways of long-lived vortices are investigated in Section 5.2.

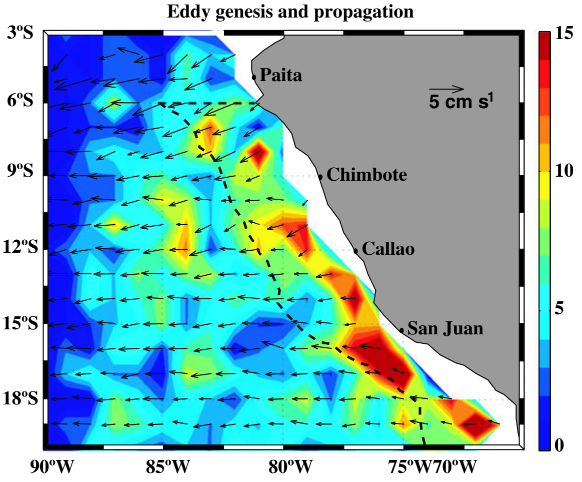

Fig. 7. Regional climatology of eddy genesis, October 1992–August 2006. Units are number of events. Only eddies having a lifetime higher than 1 month are included. Average motion vectors for eddy centers are superimposed (black quivers). Bold dashed lines delimit the "coastal region" where temporal eddy characteristics variations are investigated in Section 6 and Figs. 9 and 10.

5.2. Growth and decay of long-lived eddies

Average eddy characteristics over 6-months of life are shown in Fig. 8. This analysis is based on 32 (or 39) long-lived cyclonic (or anticyclonic) eddies. Both types exhibit similar growth rates in terms of radius and SLA amplitude (Fig. 8a and b). Long-lived eddy radii increase at a rate of ~12–15 km per month whereas the amplitudes grow by ~1 cm per month. The growth phase of 3 months is however shorter for anticyclonic eddies, with a maximum mean radius of 100 km and amplitude of ~4 cm. In contrast, cyclonic eddies are fully developed after a growing phase of 4 months, with typical radii of 120 km and SLA amplitudes of 4.5 cm. The decay phases of the two eddy types are also distinct. After 3–4 months of propagation, anticyclonic eddies tend to maintain their size whereas their amplitudes decay (~2 cm). In contrast, cyclonic eddies decay slowly in terms of SLA amplitude (Fig. 8b) but rapidly decrease in size (Fig. 8a). After 6 months of propagation the SLA amplitudes of cyclones are still two times higher (~4 cm) than at the time of their genesis (~2 cm). Finally, the temporal evolution of the mean energy density also depends on direction of rotation (Fig. 8c). While the intensity of anticyclonic vortices decays quasi-linearly by about 70% in 180 days, the cyclones intensity decays by 50% during the first 80 days before reaching a near-constant value of 1.8×10^{-3} cm^2 s^{-2} km^{-2}. Further investigation is needed to determine the physical processes involved in these differing evolutions, but similar differences in eddy characteristics have been observed for atmospheric vortices (Hakim and Canavan, 2005).

Fig. 8d shows the average meridional propagation of long-lived eddies. During the first 50 days, eddies formed near the coast propagate offshore remaining close to their latitude of birth. After this period however, a clear separation is observed: cyclonic eddies continue westward during four more months before turning slightly southward, whereas anticyclonic eddies move preferentially northwestward with a meridional displace-

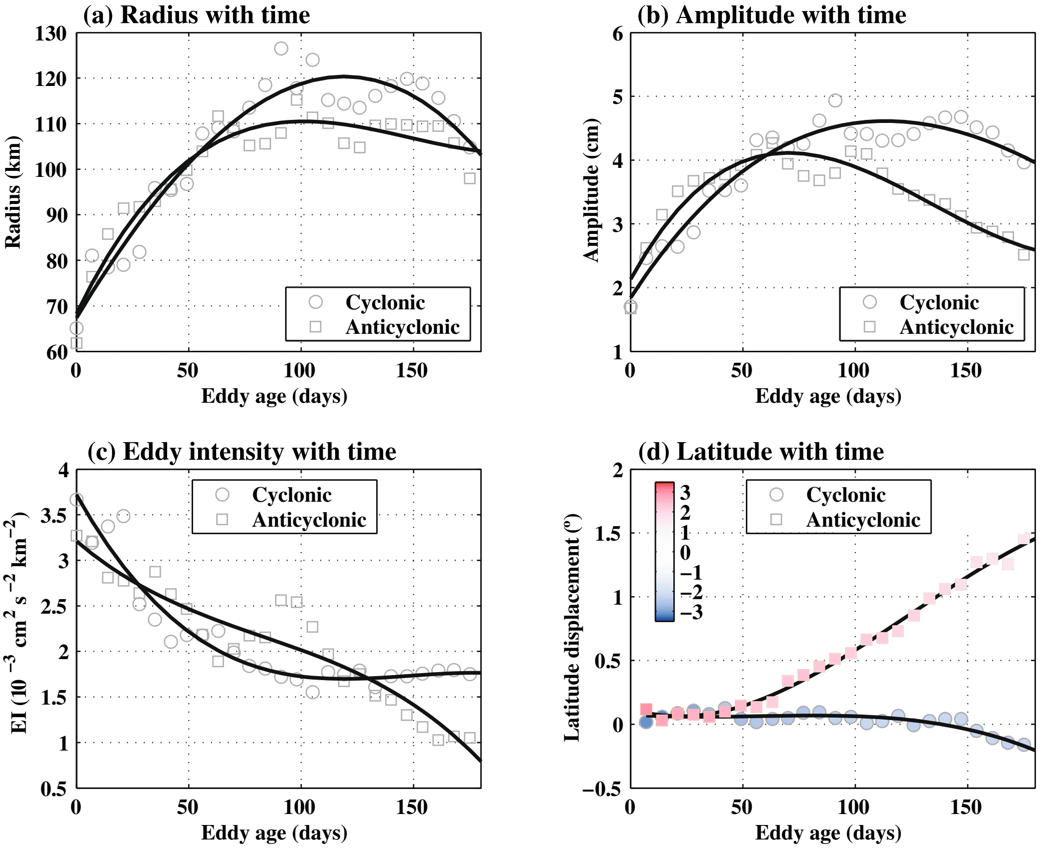

Fig. 8. Ensemble-mean properties of long-lived eddies over 180 days: (a) radius, (b) amplitude, (c) intensity, and (d) latitude. Cyclonic eddies are depicted by circles and anticyclonic eddies by squares. Solid lines are third-order polynomial fits. Colours in (d) show the evolution of vorticity (in 10^{-6} s^{-1}). All included vortices survived a minimum of 180 days so that the population is constant for all times displayed.

ment rate of 1.5° in 4 months corresponding to a northward velocity component of ~10 km per week. After 6 months, both types of eddies have traveled 750 km offshore (not shown) but anticyclonic vortices are found on average 1.7° further north than the cyclones. This divergence in eddy pathways, related to the β effect (Cushman-Roisin, 1994), has been previously observed in the ESP (Chaigneau and Pizarro, 2005c), in other eastern boundary current systems (Morrow et al., 2004b) and in the global ocean (Chelton et al., 2007). Pathway divergence may have important repercussions in tracer budgets, leading for example to a net equatorward heat transport. Finally, as the warm anticyclonic (or cold cyclonic) eddies move equatorward (or poleward) they are subject in the southern hemisphere to a higher (or lower) planetary vorticity *f*. In order to maintain their absolute vorticity, their relative vorticity ξ may decrease (or increase). As shown in Fig. 8d, the relative vorticity of long-lived anticyclones, averaged over the eddy area, decreased in average from 3.3×10^{-6} to 1.7×10^{-6} s^{-1} after 6 months. In contrast, the relative vorticity of long-lived cyclones increased from an averaged value of -3.5×10^{-6} to -2.2×10^{-6} s^{-1}. However, even considering the vorticity of the mean large-scale circulation, the temporal evolution of the absolute vorticity ($\xi + f$) does not remain constant, which suggests that the vertical eddy extent may also change during the vortex propagation, in order to conserve the potential vorticity.

Section 5 has given results on the locations of eddy genesis, on the propagation modes and on the life-cycle of long-lived eddies. However, the relatively high-temporal resolution of the altimetry dataset also allows temporal variability of eddies to be examined, since 1992. The next section examines temporal variations at seasonal and interannual scales.

6. Temporal evolution of the mesoscale eddy characteristics

In this section, we consider the ~4500 eddies located south of 6°S and less than 4° offshore the South-American coast. This sub-domain corresponds to the main region of eddy genesis (see black dashed line in Fig. 7); the temporal variations discussed below concern the newly-formed or “young” eddies of this region.

6.1. Seasonal cycle

Fig. 9 shows the mean seasonal cycle of coastal eddy properties. The number of coastal eddy and their size do not significantly vary seasonally, with values of 5.7–6.1 generated eddies per week having mean radii of 77–81 km year around (Fig. 9a and b). In contrast, SLA amplitudes (Fig. 9c) between eddy centers and eddy edges are 25% higher during fall (~2.1 cm) than during spring (~1.7 cm). The combination of increase SLA gradients and unchanged radii results in higher levels of EKE and EI during fall (Fig. 9d and e). The EKE and EI are, respectively, 45% and 50% stronger during this season than spring. Finally, as eddies are slightly more numerous and more intense during fall, the EAI is also maximal during this season (Fig. 9f). During fall, mesoscale vortices are ~35% more active than in summer and winter and 65% more active than in spring.

The enhanced EI and eddy activity during fall may be related to the strength of the thermal front separating the cold upwelled coastal water from warmer offshore water. Firstly, the annual amplitudes of both the sea-surface temperature (SST) and the upper layer heat content are maximal around 300–500 km offshore and minimal along the coast (Takahashi, 2005). Due to the ocean’s

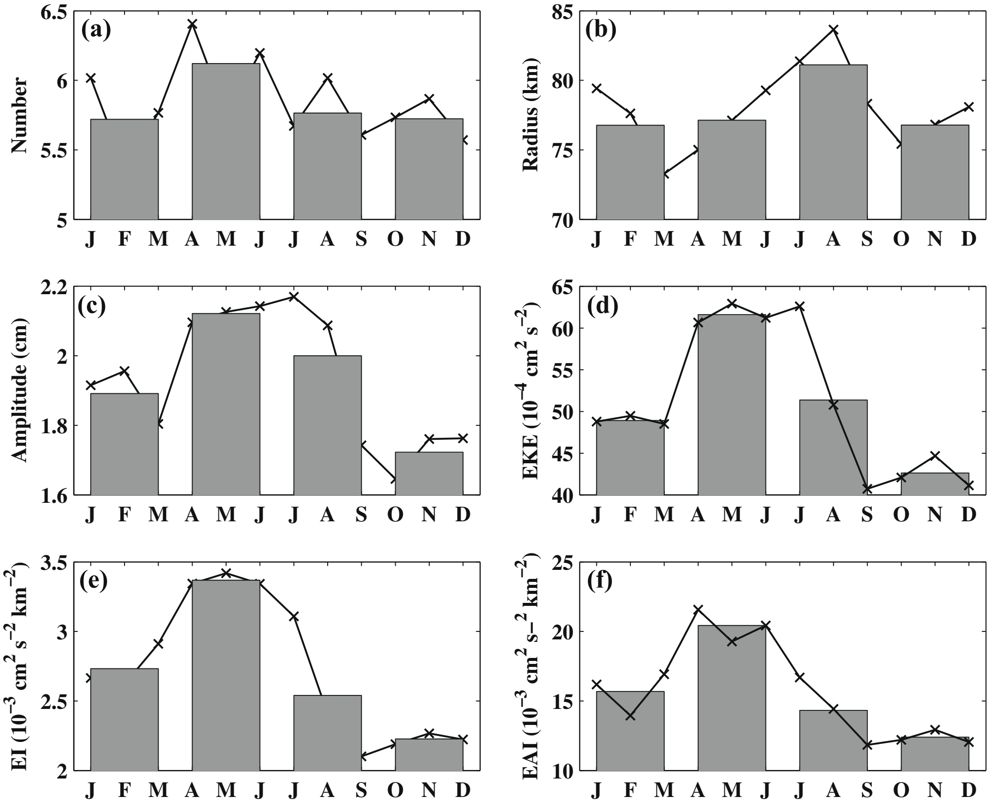

Fig. 9. Seasonal cycles of newly-formed coastal eddies: (a) number of eddies, (b) radius (km), (c) amplitude (cm), (d) EKE (cm^2 s^{-2}), (e) EI (10^{-3} cm^2 s^{-2} km^{-2}), and (f) EAI (10^{-3} cm^2 s^{-2} km^{-2}). Vertical bars indicate seasonal (3-month) averages whereas black lines show the monthly variations.

thermal inertia, the mean SST reaches its maximum value between March and May (Mitchell and Wallace, 1992) producing strong zonal SST gradients with an associated strong thermal front during this period. Based on 3 years of remote sensing data, Carr et al. (2002) observed that the maximal frontal gradients along the Peruvian coast take place in later summer and fall. Secondly, frontal intensity is also reinforced at the end of summer by a stronger inshore advection of equatorial and subtropical waters (Grados, 1989; Vázquez and García, 2001), principally observed near Chimbote (9°S) and between 15°S and 20°S (Grados, 1989; Takahashi, 2005). This latter region also corresponds to the northern limit of the cold Chile–Peru Current which turns westward at about 9°S to feed the South-Equatorial Current (Strub et al., 1998; Chaigneau and Pizarro, 2005b). The seasonal variations of frontal intensity driven by atmospheric fluxes and advective processes could thus enhance generation of baroclinic instabilities during fall and could explain the seasonal variations observed in Fig. 9. However, this interpretation requires further investigation, probably with satellite SST data, historical in-situ hydrographic data and a high-resolution regional model.

6.2. Interannual variations

To remove the intraseasonal and seasonal fluctuations of eddy properties and investigate only interannual variations, we applied a one-year running-mean to the original time-series (Fig. 10). The study time period (1992–2006) includes the years when only T/P data alone were available (December 1993–March 1995; see Section 2.1) and distinct phases of warm (or cold) El Niño Southern Oscillation associated with El Niño (or La Niña). Within the period of altimetry measurements, a very strong El Niño occurred in 1997–1998 followed by a weak event in 2002–2003 (ENFEN, 2003). In contrast, relatively cold La Niña events took place in 1995–1996 and 1998–2000 (McPhaden, 2006).

During the T/P alone period, eddies appear less numerous (Fig. 10a) with weakened SLA amplitude (Fig. 10c), leading to slightly less energetic and intense eddies (Fig. 10d and e). The EAI was consequently reduced by 35% during this period (Fig. 10f). As mentioned in Section 2.1, the coarse resolution of T/P groundtracks (typically 200–300 km in the study region) leads, on average over the World Ocean, to a reduction in EKE of 30%. In the study area, the EKE decreases by 20% from a local maximum of ~ 45 cm^2 s^{-2} in summer of 1994 to a minimum of $\sim$35 cm^2 s^{-2} in summer of 1995. In contrast, during the strong El Niño period both the eddy amplitude, the EKE and the EI are strongly increased. However the combination with a relatively weak number of eddies (Fig. 10a) does not lead to an exceptional peak in the EAI in 1997–1998. During the strong El Niño period, the EAI is of $\sim$22 × 10^{-3} cm^2 s^{-2} km^{-2}, 40% higher than the mean value observed between 1992 and 2006. These observed variations were not reproduced during the weak El Niño event of 2002–2003 which was associated with rather weak EAI values of $\sim$15 × 10^{-3} cm^2 s^{-2} km^{-2}. This may indicate that the 2002–2003 event did not significantly impact on the oceanographic conditions along the Peruvian coast. During the relatively cold La Niña period of 1995–1996, eddy SLA amplitudes and the EAI also exhibit weak values, but we cannot provide any strong conclusion since this period includes the summer of 1995 where ERS-1 data is not available. Furthermore this relatively weak eddy activity period was not reproduced during La Niña event of 1998–2000. Finally, an increase of the EAI was observed for a one-year period starting in winter of 2004 (Fig. 10f) associated with an increase number of vortices during this period (Fig. 10a). The maximum EAI values observed in spring 2004 (October–November) coincides with reduced

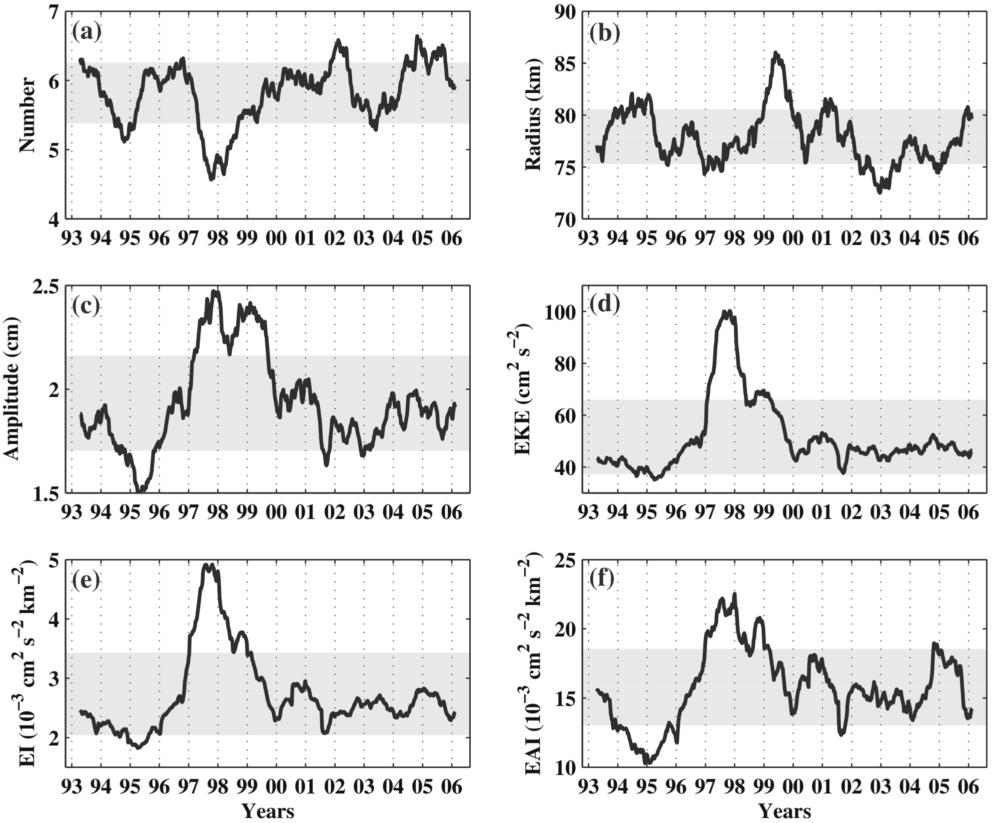

Fig. 10. Interannual variations of newly-formed coastal eddies, October 1992–August 2006: (a) number of eddies, (b) radius (km), (c) amplitude (cm), (d) EKE (cm^2 s^{-2}), (e) EI (10^{-3} cm^2 s^{-2} km^{-2}), and (f) EAI (10^{-3} cm^2 s^{-2} km^{-2}). Average values ± one standard deviation shaded in gray. These interannual variations have been computed through a one-year running-mean of the original data.

upwelling areas and an important inshore advection of warmer and saltier subtropical waters from Chimbote to 16°S (IMARPE, 2005). This local scenario was the consequence of the southward propagation of a coastal-trapped wave forced at the equator by a large-scale equatorial Kelvin wave. However, the physical mechanisms responsible of the observed eddy activity variations at interannual scales are not completely understood and further investigation is needed.

7. Summary and future work

This study investigates the eddy population off Peru using nearly 15 years of satellite altimetry measurements with high spatio-temporal resolution. The first part compares two distinct automated eddy identification methods. When considering that "*a vortex exists when instantaneous streamlines mapped onto a plane normal to the vortex core exhibit a roughly circular or spiral pattern* (...)" (Robinson, 1991), the geometrical method using the streamline function curvatures to identify eddies appears much more efficient than the algorithm based on the value of the Okubo–Weiss parameter. With a success of detection/excess of detection ratio of 5, we strongly recommend the use of the "winding-angle" method for the detection of eddy edges.

A second part provides an analysis of the mean eddy properties offshore the Peruvian coast. Around 14 cyclonic and 14 anticyclonic eddies with radii higher than 35 km were identified on each weekly map, providing more than 20,000 eddies to be studied (October 1992–August 2006). In general, no significant difference is observed between cyclonic and anticyclonic eddies in terms of mean characteristics, occurrence frequency and formation region. The typical size of the well-developed eddies having amplitudes higher than 2 cm increases equatorward from a minimum value of ~100 km at 20°S to a maximum of ~160 km north of 5°S. However, considering all eddies, their mean radius is ~80 km and mean lifetime ~1 month. They also exhibit a time-independent 1-week survival probability of 90%, for lifetimes greater than around 2 months. Eddies, which are more frequently observed south of 15°S and offshore Chimbote (9°S) than in the rest of the study domain, are rather coherent since the vorticity/total deformation ratio increases from 1.5 to 2.5 with increase EI.

Long-lived eddies are principally formed near the coast and propagate offshore at mean speeds of 3–6 cm s^{-1}. During the first 3–4 months of westward propagation, cyclonic and anticyclonic long-lived eddies exhibit a growing phase where both their radii and SLA amplitudes increase by a factor ~2–3. Then, both types of eddies show a decaying phase impacting the amplitudes of anticyclonic and the sizes of the cyclonic vortices. However in terms of EI (e.g. energy density), cyclonic eddies show a rapid decay during the first 3 months before stabilizing at a quasi-constant value, whereas anticyclones exhibit a regular decline. Finally, the displacement of long-lived eddies confirm the divergence observed in previous studies (Morrow et al., 2004b; Chaigneau and Pizarro, 2005c): anticyclonic eddies propagate preferentially northwestward while cyclonic eddies migrate in the southwestward direction. During propagation their relative vorticities increase in response to latitudinal changes in planetary vorticity.

Temporal variations of the most energetic eddies show an important variability at seasonal scales. Eddies are slightly more numerous and intense in fall, leading to a strong EAI. This EAI, 65% stronger in fall than during spring, may be related to seasonal variations of the thermal front intensity. At interannual scales, eddy activity and eddy characteristics in general are strongly decreased in 1994–1995 due to inconsistency of the data set, being affected by the T/P alone measurements. In contrast, the EAI reaches its maximum value during the strong El Niño event of 1997–1998 and another clear maximum is observed at the end of 2004 possibly due to the passage of a coastal-trapped wave.

The results may be useful for the validation of high-resolution regional models and could be of interest to the biological community to investigate links between ecosystems and mesoscale activity along the highly productive Peruvian coast. However, owing to limited resolution and necessary interpolation, the altimetry mapped data impose space and timescale limitations and miss small-scale vortices. In particular, based on satellite-tracked drifter trajectories, Chaigneau and Pizarro (2005c) have shown than the typical eddy radius of the ESP is about 20 km, and that 70% of eddies have a radius smaller than 35 km. Thus once validated, regional models could help to document, for example, the impacts of smaller vortices on the offshore transport of coastal water properties, on physical budgets (heat, salt, mass, etc.), and on productivity and ecosystems.

The results also raise a number of additional questions that require future research. For example, the respective roles of local versus remote forcing of equatorial origin on eddy genesis and the effects of this forcing on both cyclonic and anticyclonic vortices. Similarly, general mechanisms contributing to the growth and decay of eddies need be examined in detail. Another unresolved problem concerns the merging of eddies which can be an important process to the vortex phenomenology. The particular case of dipolar eddies should also be investigated since convergence/divergence lines between eddies, by analogy of the Rossby wave–induced convergences, could have important repercussions on the distribution of living organisms (e.g. Dandonneau et al., 2003). Finally, the impact of large-scale warming on mesoscale activity needs be evaluated. Attempts at reliable objective classification of these processes will likely require high-resolution regional models forced by realistic atmospheric fields.

Acknowledgements

The authors would like to thank B. Dewitte, G. Eldin, M. Lengaigne, R. Morrow and O. Pizarro, whose expertise has been valuable for the validation of the automated methods. We are also grateful to the two reviewers, K. Takahashi and D. Chelton, for constructive comments. A. Gizolme was supported by the Interdepartmental Thematic Action « Humboldt Current System » from IRD and by the « Peru Chile Climate Change » project funded by the Agence Nationale de la Recherche.

Appendix A. Appendix

As explained in Section 2.2, the winding-angle eddy identification algorithm attempts to locate a vortex by selecting and clustering closed streamlines (Guo, 2004). Let us consider a 2D streamline beginning at a starting point P_1 (Fig. 11) and composed of several segments which the length corresponds to the step size (around 1.35 km in our case). The winding-angle (WA) of the streamline corresponds to the cumulated sum of the angles between all pairs of consecutive segments

$$\mathrm{WA} = \sum_{j=2}^{N-1} \langle P_{j-1}, P_j, P_{j+1} \rangle = \sum_{j=2}^{N-1} \alpha_j,$$

where $\langle P_{j-1}, P_j, P_{j+1} \rangle = \alpha_j$ denotes the signed angle between the segments $[P_{j-1}P_j]$ and $[P_jP_{j+1}]$. Positive values of α correspond to counterclockwise-rotating curves and negative values correspond to clockwise-rotating curves.

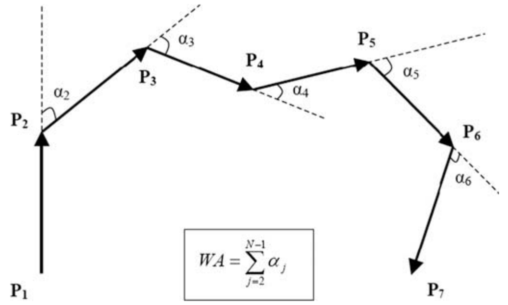

Fig. 11. Winding-angle (WA) schematic representation for a segmented streamline.

In the WA eddy identification method, a streamline is associated with an eddy if its winding-angle is higher than 2π.

References

Bakun, A., 2006. Fronts and eddies as key structures in the habitat of marine fish larvae: opportunity, adaptive response and competitive advantage. Scientia Marina 70 (2), 105–122.

Basdevant, C., Philipovitch, T., 1994. On the validity of the "Weiss criterion" in two-dimensional turbulence. Physica D 113, 17–30.

Bryan, K., 1996. The role of mesoscale eddies in the poleward transport of heat by the oceans: a review. Physica D 98, 249–257.

Buning, P., 1989. Numerical Algorithms in CFD Post-Processing. In: Computer Graphics and Flow Visualization in Computational Fluid Dynamics. Lecture Series 1989–07. Von Karman Institute for Fluid Dynamics, Brussels, Belgium.

Carr, M.-E., Strub, P.T., Thomas, A.C., Blanco, J.L., 2002. Evolution of 1996–1999 La Niña and El Niño conditions off the western coast of South America: a remote sensing perspective. Journal of Geophysical Research – Oceans 107 (12), 3236. doi:10.1029/2001JC001183.

Chaigneau, A., Pizarro, O., 2005a. Surface circulation and fronts of the South Pacific Ocean, east of 120°W. Geophysical Research Letters 32, L08605. doi:10.1029/2004GL022070.

Chaigneau, A., Pizarro, O., 2005b. Mean surface circulation and mesoscale turbulent flow characteristics in the eastern South Pacific from satellite tracked drifters. Journal of Geophysical Research – Oceans 110, C05014. doi:10.1029/2004JC002628.

Chaigneau, A., Pizarro, O., 2005c. Eddy characteristics in the eastern South Pacific. Journal of Geophysical Research – Oceans 110, C06005. doi:10.1029/2004JC002815.

Chavez, F.P., 1995. A comparison of ship and satellite chlorophyll from California and Peru. Journal of Geophysical Research – Oceans 100 (C12), 24855–24862.

Chelton, D.B., Schlax, M.G., 2003. The accuracies of smoothed sea surface height fields constructed from tandem satellite altimeter datasets. Journal of Atmospheric and Oceanic Technology 20, 1276–1302.

Chelton, D.B., de Szoeke, R.A., Schlax, M.G., El Naggar, K., Siwertz, N., 1998. Geographical variability of the first-baroclinic Rossby radius of deformation. Journal of Physical Oceanography 28, 433–460.

Chelton, D.B., Schlax, M.G., Samelson, R.M., de Szoeke, R.A., 2007. Global observations large oceanic eddies. Geophysical Research Letters 34, L15606. doi:10.1029/2007GL030812.

Cushman-Roisin, B., 1994. Introduction to Geophysical Dynamics. Prentice-Hall, Upper Saddle River, NJ. 320 pp.

Dandonneau, Y., Vega, A., Loisel, H., du Penhoat, Y., Menkes, C., 2003. Oceanic Rossby waves acting as a "hay rake" for ecosystem floating by-products. Science 302, 1548–1551.

Ducet, N., Le Traon, P.Y., Reverdin, G., 2000. Global high-resolution mapping of ocean circulation from TOPEX/Poseidon and ERS-1 and -2. Journal of Geophysical Research – Oceans 105, 19477–19498.

ENFEN, 2003. Informe Técnico ENFEN-Enero 2003, Comité Multisectorial para el Estudio Nacional del Fenómeno El Niño <http://www.imarpe.gob.pe>.

Falkowski, P.G., Zieman, D., Kolber, Z., Bienfang, P.K., 1991. Role of eddy pumping in enhancing primary production in the ocean. Nature 352, 55–58.

Fang, F., Morrow, R., 2003. Evolution, movement and decay of warm core Leeuwin Current eddies. Deep-Sea Research II 50, 2245–2261.

Grados, C., 1989. Variabilidad del regimen hidrico del codo Peruano–Chileno. Comisión Permanente del Pacifico Sur, Revista del Pacifico Sur (numero especial), 95–104.

Guo, D., 2004. Automated feature extraction in oceanographic visualization. Master Thesis, Massachusetts Institute of Technology, unpublished.

Hakim, G.J., Canavan, A.K., 2005. Observed cyclone–anticyclone tropopause vortex asymmetries. Journal of Atmospheric Sciences 62, 231–240.

Helly, J.J., Levin, L.A., 2004. Global distribution of naturally occurring marine hypoxia on continental margins. Deep-Sea Research I 51, 1159–1168.

Hormazabal, S., Shaffer, G., Leth, O., 2004. Coastal transition zone off Chile. Journal of Geophysical Research – Oceans (109), C01021. doi:10.1029/2003JC001956.

Hussain, F., Huyakawa, M., 1987. Education of large-scale organized structure in a turbulent plane wake. Journal of Fluid Mechanics 180, 193–204.

IMARPE, 2005. Informe Anual de Metas 2004 de la Unidad de Oceanografía Física. Internal report, unpublished.

Isern-Fontanet, J., García-Ladona, E., Font, J., 2003. Identification of marine eddies from altimetry. Journal of Atmospheric and Oceanic Technology 20, 772–778.

Isern-Fontanet, J.I., Font, J., Garcia-Ladona, E., Emelianov, M., Millot, C., Taupier-Letage, I., 2004. Spatial structure of anticyclonic eddies in the Algerian basin (Mediterranean Sea) analyzed using the Okubo–Weiss parameter. Deep-Sea Research I 51, 3009–3028.

Isern-Fontanet, J.I., García-Ladona, E., Font, J., 2006. Vortices of the Mediterranean Sea: an altimetric perspective. Journal of Physical Oceanography 36, 87–103.

Jayne, S.R., Marotzke, J., 2002. The oceanic eddy heat transport. Journal of Physical Oceanography 32, 3328–3345.

Jeong, J., Hussain, F., 1995. On the identification of a vortex. Journal of Fluid Mechanics 285, 69–94.

Lagerloef, G.S.E., Mitchum, G., Lukas, R., Niiler, P., 1999. Tropical Pacific near-surface currents estimated from altimeter, wind and drifter data. Journal of Geophysical Research – Oceans 104, 23313–23326.

Le Traon, P.Y., Dibarboure, G., 1999. Mesoscale mapping capabilities from multiple altimeter missions. Journal of Atmospheric and Oceanic Technology 16, 1208–1223.

Le Traon, P.-Y., Morrow, R., 2001. Ocean currents and eddies. In: Fu, L.-L., Cazenave, A. (Eds.), Satellite Altimetry and Earth Sciences: A Handbook of Techniques and Applications. Elsevier, New York, p. 57.

Le Traon, P.-Y., Nadal, F., Ducet, N., 1998. An improved mapping method of multi-satellite altimeter data. Journal of Atmospheric and Oceanic Technology 15, 522–534.

Le Traon, P.Y., Dibaboure, G., Ducet, N., 2001. Use of a high-resolution model to analyze the mapping capabilities of multiple-altimeter missions. Journal of Atmospheric and Oceanic Technology 18, 1277–1288.

Leeuw, W.C., Post, F.H., 1995. A Statistical View on Vector Fields. Visualization in scientific Computing. Springer-Verlag.

Logerwell, E.A., Smith, P.E., 2001. Mesoscale eddies and survival of late stage Pacific sardine (*Sardinops sagax*) larvae. Fisheries Oceanography 10 (1), 13–25.

Loubere, P., 2000. Marine control of biological production in the eastern equatorial Pacific. Nature 406, 497–500.

Maharaj, A.M., Cipollini, P., Holbrook, N.J., 2005. Observed variability of the South Pacific westward sea level anomaly signal in the presence of bottom topography. Geophysical Research Letters 32 (4). doi:10.1029/2004GL020966.

McGillicuddy, D.J., Robinson, A.R., Siegel, D.A., Jannasch, H.W., Johnson, R., Dickey, T.D., McNeil, J.D., Michaels, A.F., Knap, A.H., 1998. New evidence for the impact of mesoscale eddies on biogeochemical cycling in the Sargasso Sea. Nature 394, 263–266.

McPhaden, M.J., 2006. ENSO as an integrated concept in Earth science. Science 314, 1740–1745.

Mitchell, T.P., Wallace, J.M., 1992. The annual cycle in equatorial convection and sea-surface temperature. Journal of Climate 5, 1140–1156.

Morrow, R., Donguy, J.-R., Chaigneau, A., Rintoul, S.R., 2004a. Cold-core anomalies at the Subantarctic Front, South of Tasmania. Deep-Sea Research I 51, 1417–1440.

Morrow, R., Birol, F., Griffin, D., Sudre, J., 2004b. Divergent pathways of cyclonic and anti-cyclonic ocean eddies. Geophysical Research Letters 31, L24311. doi:10.1029/2004GL020974.

Nielsen, J.W., Dole, R.M., 1992. A survey of extratropical cyclone characteristics during GALE. Monthly Weather Review 120, 1156–1167.

Okubo, A., 1970. Horizontal dispersion of floatable particles in the vicinity of velocity singularities such as convergences. Deep-Sea Research 17, 445–454.

Pascual, A., Faugère, Y., Larnicol, G., Le Traon, P.Y., 2006. Improved description of the ocean mesoscale variability by combining four satellite altimeters. Geophysical Research Letters 33, L02611. doi:10.1029/2005GL024633.

Penven, P., Echevin, V., Pasapera, J., Colas, F., Tam, J., 2005. Average circulation, seasonal cycle, and mesoscale dynamics of the Peru Current System: a modeling approach. Journal of Geophysical Research – Oceans 110, C10021. doi:10.1029/2005JC002945.

Pizarro, O., Shaffer, G., Dewitte, B., Ramos, M., 2002. Dynamics of seasonal and interannual variability of the Peru–Chile Undercurrent. Geophysical Research Letters 29 (12), 1581. doi:10.1029/2002GL014790.

Qiu, B., Chen, S., 2005. Eddy-induced heat transport in the subtropical North Pacific from Argo, TMI and altimetry measurements. Journal of Physical Oceanography 35, 458–473.

Rio, M.-H., Hernandez, F., 2004. A Mean Dynamic Topography computed over the world ocean fromaltimetry, in-situmeasurements and a geoid model. Journal of Geophysical Research – Oceans 109 (12).

Rio, M.-H., Poulain, P.-M., Pascual, A., Mauri, E., Larnicol, G., Santoleri, R., 2007. A mean dynamic topography of the Mediterranean Sea computed from altimetric data, in-situ measurements and a general circulation model. Journal of Marine Systems 65, 484–508.

Robinson, S.K., 1991. Coherent Motions in the Turbulent Boundary Layer. Annual Review of Fluid Mechanics 23, 601–639.

Roemmich, D., Gilson, J., 2001. Eddy transport of heat and thermocline waters in the North Pacific: a key to interannual/decadal climate variability? Journal of Physical Oceanography 31, 675–687.

Sadarjoen, A., 1999. Extraction and visualization of geometries in fluid flow fields. Ph.D. Thesis, Delft University, Germany, unpublished, 145 pp.

Sadarjoen, A., Post, F.H., 2000. Detection, quantification, and tracking of vortices using streamline geometry. Visualization and Computer Graphics 24, 333–341.

Sadarjoen, A., Post, F. H., Ma, B., Banks, D. C., Pagendarm, H.-G., 1998. Selective visualization of vortices in hydrodynamics flows. In: Proceedings of Visualization'98, Research Triangle Park, NC, pp. 419–422.

Sasai, Y., Ishida, A., Sasaki, H., Kawahara, S., Uehara, H., Yamanaka, Y., 2006. A global eddy-resolving coupled physical-biological model: physical influences on a marine ecosystem in the North Pacific. Simulation 82 (7), 467–474.

Segond, M., 2006. Algorithmes bio-mimétiques pour la reconnaissance de formes et l'apprentissage. Ph.D. thesis, Université de Litoral-côte d'opale, France, 138 pp., unpublished.

Shaffer, G., Pizarro, O., Djurfeldt, L., Salinas, S., Ruttlant, J., 1997. Circulation and low-frequency variability near the Chilean coast: Remotely forced fluctuations during the 1991–1992 El Niño. Journal of Physical Oceanography 27, 217–235.

Siegel, D., McGillicuddy, D., Fields, E., 1999. Mesoscale eddies, satellite altimetry, and new production in the Sargasso Sea. Journal of Geophysical Research – Oceans 104 (C6). doi:10.1029/1999JC900051.

Spear, L.B., Balance, L.T., Ainley, D.G., 2001. Response of seabirds to thermal boundaries in the tropical Pacific: the thermocline versus the Equatorial Front. Marine Ecology Progress Series 219, 275–289.

Stammer, D., 1997. Global characteristics of ocean variability estimated from regional TOPEX/POSEIDON altimeter measurements. Journal of Physical Oceanography 27, 1743–1769.

Stammer, D., 1998. On eddy characteristics, eddy transports, and mean flow properties. Journal of Physical Oceanography 28, 727–739.

Stammer, D., Wunsch, C., 1999. Temporal changes in eddy energy of the oceans. Deep-Sea Research II 46, 77–108.

Stammer, D., Wunsch, C., Ueyoshi, K., 2006. Temporal changes in ocean heat transports. Journal of Physical Oceanography 36, 543–550.

Strub, P.T., Mesias, J.M., Montecino, V., Rutllant, J., Salinas, S., 1998. Coastal ocean circulation off western South America. In: Robinson, A.R., Brink, K.H. (Eds.), The Sea, vol. 11. John Wiley, Hoboken, N. J, pp. 273–313.

Takahashi, K., 2005. The annual cycle of heat content in the Peru-Current region. Journal of Climate 18, 4937–4954.

Thomas, A., 1999. Seasonal distributions of satellite-measured phytoplankton pigment concentration along the Chilean coast. Journal of Geophysical Research – Oceans 104 (C11). doi:10.1029/1999JC900171.

Thomas, A.C., Huang, F., Strub, P.T., James, C., 1994. Comparison of the seasonal and interannual variability of phytoplankton pigment concentrations in the Peru and California Current systems. Journal of Geophysical Research 99 (C4). doi:10.1029/93JC02146.

Vázquez, L., García, W., 2001. Condiciones oceanográficas del mar peruano durante el verano 2000. Informe del Instituto del Mar del Perú 159, 65–72.

Wang, X.L., Swail, V.R., Zwiers, F.W., 2006. Climatology and changes of extratropical cyclone activity: comparison of ERA-40 with NCEP–NCAR reanalysis for 1958–2001. Journal of Climate 19, 3145–3166.

Weiss, J., 1991. The dynamics of enstrophy transfer in two-dimensional hydrodynamics. Physica D 48, 273–294.

Wunsch, C., 1999. Where do ocean eddy heat fluxes matter? Journal of Geophysical Research – Oceans 104, 13235–13249.

Zamudio, L., Leonardi, A.P., Meyers, S.D., O'Bryen, J.J., 2001. ENSO and eddies on the southwest coast of Mexico. Geophysical Research Letters 28, 13–16.

Zhang, X., Walsh, J.E., Zhang, J., Bhatt, U.S., Ikeda, M., 2004. Climatology and interannual variability of Arctic cyclone activity: 1948–2002. Journal of Climate 17, 2300–2317.

Progress in Oceanography 79 (2008) 120–137

Contents lists available at ScienceDirect

Progress in Oceanography

journal homepage: www.elsevier.com/locate/pocean

Vertical structure variability in a seasonal simulation of a medium-resolution regional model of the Eastern South Pacific

Boris Dewitte [a,b,*], Marcel Ramos [c,d], Vincent Echevin [e], Oscar Pizarro [f,g], Yves duPenhoat [a]

[a] LEGOS/IRD/CNES, 14 Av. Edouard Belin, 31400 Toulouse, France
[b] IMARPE, Esquina de Gamarra y General Valle S/N, Chucuito Callao, Peru
[c] Programa de Postgrado en Oceanografía, Departamento de Oceanografía, Universidad de Concepción, Concepción, Chile
[d] Centro de Estudios Avanzados en Zonas Áridas, Facultad de Ciencias del Mar, Universidad Católica del Norte, Chile
[e] LOCEAN/IRD/IPSL, Laboratoire d'Océanographie et de Climatologie: Expérimentation et Approches Numériques, Paris, France
[f] Departamento de Geofísica, Universidad de Concepción, Concepción, Chile
[g] COPAS, Universidad de Concepción, Concepción, Chile

ARTICLE INFO

Article history:
Received 28 February 2007
Received in revised form 2 May 2008
Accepted 14 October 2008
Available online 21 October 2008

Keywords:
Extra-tropical Rossby waves
Critical latitude
Coastal-trapped wave
Peru–Chile Undercurrent

ABSTRACT

A seasonal simulation from a medium-resolution ocean general circulation mode (OGCM) is used to investigate the vertical structure variability of the Southeast Pacific (SEP). The focus is on the extra-tropical Rossby wave (ETRW) variability and associated forcing mechanism. Some aspects of the model mean state are validated from available observations, which justifies a vertical mode decomposition of the model variability. The analysis of the baroclinic mode contributions to sea level indicates that the gravest mode is dominant over most of the domain at all frequencies. Annual variability is on average twice as large as the semi-annual variability which is confined near the coast for all the modes. The first baroclinic mode contribution to the annual cycle exhibits a clear westward propagation north of the critical latitude. The higher-order modes only contribute near the coast where they are associated with vertically propagating energy. The residual variability, which is the energy at all timescales other than annual and semi-annual periods peaks offshore between ~20°S and ~30°S for all baroclinic modes. The third baroclinic mode also exhibits a relative maximum variability off the coast of Peru south of the critical latitude of the annual cycle (~13°S), where the Peru–Chile Undercurrent is the most intense. Sensitivity experiments to the atmospheric and boundary forcing suggest that the residual variability results from the non-linear interaction between annual Rossby waves and the mean flow, while the annual ETRWs in the model result from the summed-contribution from both the local wind stress and remote equatorial forcing. Overall the study extends the classical analysis of sea level variability in the SEP based on linear theory, and suggests that the peculiarities of the baroclinic modes need to be taken into account for interpreting the sea level variability and understanding its connection with the equatorial variability.

1. Introduction

The coastal ocean off Peru and Chile is characterized by permanent upwelling cells in the north due to prevailing trade winds, and by seasonal upwelling in the south. This region also contains the Peru–Chile Current System (PCCS), extending from central Chile (~40°S) to northern Peru (~4°S) (cf. Strub et al., 1998). The PCCS is complex, composed of several surface and subsurface currents, and subject to large seasonal and interannual variabilities. The PCCS has been of interest to the oceanographic and climatic community because climate variability off Peru and Chile is strongly connected to tropical Pacific variability, with the South American coast behaving as an extension of the equatorial wave guide over a wide range of frequencies (Shaffer et al., 1997; Pizarro et al., 2001, 2002; Vega et al., 2003). The PCCS is also intensely productive in terms of fish catch, even when compared to other Eastern Boundary Current (EBC) regions (Strub et al., 1998; Carr, 2002). Thus, the socio-economical impact of climatic events such as ENSO (El Niño Southern Oscillation) has been large over the region. The offshore regional variability (for example as evidenced by the TOPEX/POSEIDON data; Stammer, 1997) also exhibits a strong spatial heterogeneity, reflecting a complex combination of forcing mechanisms of the extra-tropical Rossby waves (ETRW) in a region where mixing processes can significantly impact water mass properties (Yeager and Large, 2004). An important question remains how the extra-tropical Rossby waves 'ventilate' the PCCS.

Altimetric data indicates that ETRWs contribute to sea level variability over a wide range of frequencies (Chelton and Schlax,

---

* Corresponding author. Address: LEGOS/IRD/CNES, 14 Av. Edouard Belin, 31400 Toulouse, France.
E-mail address: bxd@imarpe.gob.pe (B. Dewitte).

0079-6611/$ - see front matter © 2008 Published by Elsevier Ltd.
doi:10.1016/j.pocean.2008.10.014

1996), but also that dispersion from linear theory is likely important (Killworth et al., 1997). As an illustration, Fig. 1 presents the maximum amplitude and phase of the sea level seasonal cycle from altimetric data over 1992–2004. Fig. 1 reveals several interesting features: the phase lines tend to be parallel to the coast north of ~30°S, illustrating the large scale structure and offshore propagation of the signal. The pattern of maximum amplitude for sea level reflects the change in the annual ETRW with latitude with the largest values north of a line from ~30°S at the coast to ~15°S at 90°W, and minimum values south of this line. Further to the south and to the west, the analysis captures prominent mesoscale eddy activity (Chaigneau and Pizarro, 2005). The overall pattern does however not show clear westward propagation suggesting that non-linear processes are at work or that it results from a complex combination of baroclinic modes with different propagation speeds. These observations motivate this study, which attempts to document the ETRW and associated processes at seasonal timescales in the SEP.

ETRW models connected to coastal-trapped wave models have been used to explore sea level and thermocline anomalies near the Chilean coast on a variety of timescales (Vega et al., 2003; Ramos et al., 2006). However, in reduced gravity models of the ocean's response to wind forcing (Qiu et al., 1997), many physical processes are ignored including (1) the coupling of Rossby waves to bottom topography (Killworth and Blundell, 1999), (2) vertical mixing, (3) projection of momentum on the different vertical modes and the coupling among them, and (4) the effects of vertical shear (Killworth et al., 1997; deSzoeke and Chelton, 1999; ColindeVerdiere and Tailleux, 2006) or (5) bottom roughness (Tailleux and McWilliams, 2001). More sophisticated numerical models include these effects but become difficult to interpret.

Here a vertical modal decomposition of a general circulation model is used to explore the seasonal variability in SEP and understand the mechanisms that control the oceanic response to wind and remote forcing. Of particular interest is how the dynamical modes are forced in the model and the connection to equatorial variability via coastal-trapped waves and the radiation of the ETRW north of the critical latitude (Clarke and Shi, 1991). Stated another way, we explore whether the SEP can be considered linear on the different timescales that encompass the seasonal cycle. In addition, the study provides a description of the baroclinic mode variability in the region, as a complement to studies based on linear models (Vega et al., 2003; Ramos et al., 2006). In particular, linear models typically use a single mode with a dissipation term (Rayleigh type) to account for energy lost from the surface to the deep ocean. Such an approach assumes that dissipation occurs through vertical propagation of the Rossby wave (McCreary, 1984; Kessler and McCreary, 1993), a process that, to the author's knowledge has not been investigated for the extra-tropical latitudes in a realistic framework. The modal decomposition used here should provide insights on such process, and extend classical analyses based on the linear theory.

The work is structured as follows. The model, data and method are briefly described in Section 2. In Section 3, mean circulation and the propagating variability are analysed. In Section 4, the vertical mode decomposition is presented and the propagating characteristics of the baroclinic modes are investigated. Section 5 focuses on local and boundary forcing through sensitivity experiments with modified forcing conditions. These experiments permit assessing the degree of 'linearity' of the ESP system as a function of timescale. Section 6 summarizes and discusses relevance of the model findings to our understanding of the ESP dynamics.

2. Model, data and method

2.1. Model

The primitive equation OPA model at 1/3° resolution (fully described by Madec et al., 1998) has been set up for the ESP, in the area between 5°S and 40°S, 92°W and 70°W. This model has 31 z-levels in the vertical with 10 m intervals between 0 and 100 m, and 500 m at 4750 m depth. The model has a rigid lid and the sea surface height is calculated diagnostically. The horizontal diffusion on the tracers and velocity is bilaplacian with a constant coefficient of $1.4 \times 10^{11}\ \mathrm{m}^4/\mathrm{s}$. The model resolution is sufficient to allow some eddies to be resolved explicitly, but the intensity of the resolved mesoscale activity remains low compared to observations.

Open boundary conditions are specified for velocity (barotropic stream function and baroclinic velocities), and for the tracers tem-

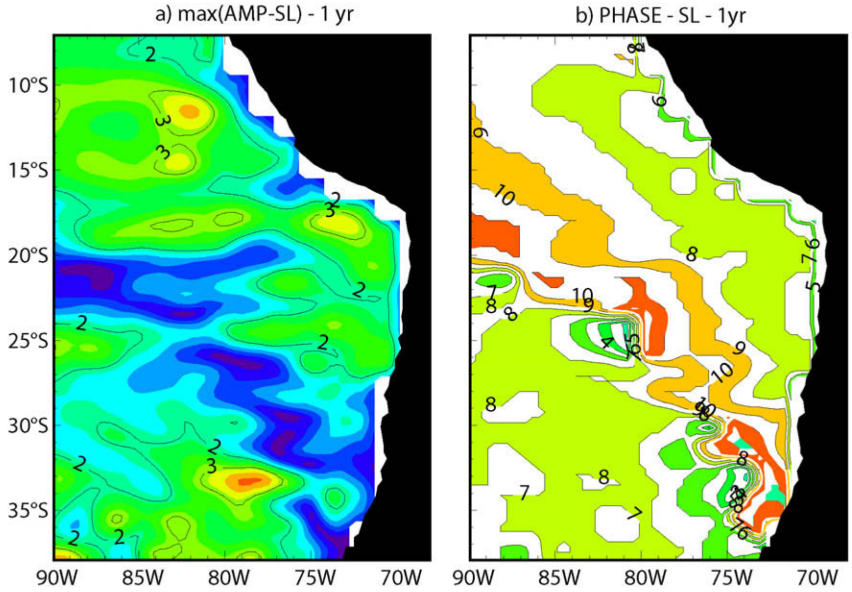

Fig. 1. Maps of the (a) amplitude and (b) phase (annual harmonic) of the seal level as derived from TOPEX/POSEIDON satellite data. Units is cm for the amplitude and calendar month for the phase ('1' corresponds to 'January'). The annual harmonic was smoothed with a three-grid-point-width boxcar average.

perature and salinity for inflow into the model domain. Tracers are advected out of the domain with an upstream advection scheme. A sponge layer is also included to damp propagating waves. The sponge layer is narrow on the north open boundary (1.7°) and wider for the south and west open boundaries (5.3°).

The model is forced at the boundaries with a climatology of the temperature, salinity and velocity fields obtained from an ORCA 2° × 2° global interannual simulation. The global model was forced by ERS winds over 1992–2000 (cf. Lengaigne et al. (2002) for details). The surface forcing of the regional model consists of monthly climatological ERS winds (Bentamy et al., 1996), NCEP heat fluxes (Kalney et al., 1996) and CMAP precipitation fluxes (Xie and Arkin, 1996) over 1992–2000.

Three manipulative experiments used the settings in Table 1, which correspond to different local (heat and momentum fluxes) and open-ocean boundary forcings. The control run simulation, called CR, used a seasonally varying forcing both at the open boundaries (OBs) and at the air–sea interface, whereas the other two simulations explore the impacts of seasonality at the open boundaries (experiment called OBmean) and the momentum fluxes at the air-sea interface (experiment called TXTYmean) by cancelling one or the other. These manipulations OBmean and TXYmean are analysed in Section 5.

Simulations were run for 7 years with climatological forcing. The first 3 years are considered as the spin up period and only the last 4 years are analyzed.

2.2. Data

2.2.1. Gridded satellite winds ERS

Wind products are from CERSAT (http://www.ifremer.fr/cersat) (Bentamy et al., 1996). ERS 1–2 scatterometer measurements have a 50 km spatial resolution and a 500 km-wide swath. These satellites covered the global ocean in 3 days and operated from January 1991 to December 2000. A monthly climatology was computed for 1992–2000 and was used to force the model.

2.2.2. Mixed layer depth (MLD)

Global MLD climatology is from de Boyer Montégut et al. (2004). It was estimated using *in situ* temperature profiles, for which the MLDs are estimated using a difference criterion of 0.2 °C between the surface reference depth (10 m) and the base of the mixed layer. A gridded monthly product is then built on a 2° × 2° spatial grid.

2.2.3. T/P + ERS altimetric data

Sea Level Anomaly (SLA) maps were supplied by AVISO (CLS, Toulouse, France) from 1993 to 2004. The maps result from an optimal interpolation of combined altimetric data from TOPEX/POSEIDON and ERS1/2 missions (Le Traon et al., 1998) on a 1/4° × 1/4° grid every week. The SLAs are built by removing from the measurements the mean sea surface over 7 years (1993–1999). The precision of this product is of about 2–3 cm rms.

2.2.4. Levitus data set

The World Ocean Database 2001 (Conkright et al., 2002) or so-called Levitus data set (Levitus et al., 1998) for temperature was used to derive the mean thermocline depth and to check the model seasonal density structure.

2.2.5. Sea surface temperature (SST)

Two products were used to estimate the mean SST over the model domain: (1) the so-called Reynolds data set (Reynolds and Smith, 1994) on a 1° × 1° resolution grid, with data over 1990–2002; and (2) the 9 km resolution SST from Advanced Very High Resolution Radiometer (AVHRR; Vazquez et al., 1995) from POD-AAC (http://podaac-www.jpl.nasa.gov/products/product102.html) over 1990–2002.

2.3. Method

To understand the dynamic response of the model ocean to variable atmospheric forcing, we used a vertical modal decomposition of ocean density structure. Dynamic vertical modes form a complete orthogonal set that can describe any perturbations of density. We follow Dewitte et al. (1999) who analyzed the interannual variability of equatorial currents and sea level. We have made two simplifying assumptions here. First, we assume that linearization is appropriate. Linearization requires that interface deviations be small relative to mean layer thicknesses, which is probably true on seasonal time scales. Second, we assume that the Wentzel–Kramers–Brillouin (WKB) approximation is appropriate, allowing the analysis to be done independently at each location. This approximation requires that the background state changes over a length scale that is large relative to the wavelength of the perturbations. Although the mean stratification can experience drastic changes over short distances in the region of interest (in particular near the coast where isotherms rise), the method is justified *a posteriori* by the model results, which provide a meaningful dynamical interpretation of the ocean's response to variable atmospheric forcing (see also Thompson et al. (2002) for the North Pacific). The density change length scale off the coast is also much larger than the local Rossby radii (see Fig. 8 of Section 4.1). The WKB approximation in the context of topographic variations is justified by Killworth and Blundell (1999), who argue that while coastal topographic slopes do impact local baroclinic modes and their phase speeds, on a basin-wide average, topographic variations do not influence the overall propagation characteristics of the long-wavelength Rossby waves.

As noted by Wunsch (1997) in his modal decomposition of mooring observations in the World Ocean, modal decomposition has the advantage over, say, Empirical Orthogonal Functions (EOFs) in that it keeps dynamically distinct features separate. EOFs mix the different vertical modes, and only work well when the mode energy levels are very different.

In order to confirm/infirm the propagating nature of the derived baroclinic mode contributions, we used Extended-EOF decomposition (Weare and Nasstrom, 1982). This method often produces pairs of modes with similar spatial structure and explained variance but with a quadrature phase shift. The similar characteristics imply that these paired modes essentially describe the same propagating phenomenon. Modes which are not paired often correspond to non propagating phenomena.

Table 1
Model experiments' description.

Name	Boundary forcing	Wind stress forcing	Heat flux forcing
CR (control run)	Monthly climatology	Monthly varying climatology	Monthly varying climatology
TXYmean	Monthly climatology	Annual mean constant	Monthly varying climatology
OBmean	Mean	Monthly varying climatology	Monthly varying climatology

3. Mean circulation and propagating variability

In this section, we examine the realism of the simulation with regards to the main fields and properties that can influence the wave characteristics. In particular we focus on (1) the mean vertical stratification that determines the vertical mode structure, (2) the characteristics of the Peru–Chile Undercurrent (PCU) that is a major feature of the coastal current circulation in the ESP, and (3) the mixed layer depth that influences how the momentum flux is transmitted to the dynamics and the off-shore and coastal sea level variability.

3.1. Mean state

3.1.1. SST

The mean SST of the CR model is presented in Fig. 2a, where it can be compared to both the Reynolds and AVHRR observations (Fig. 2b and c). The model simulates the main pattern of SST, with a realistic representation of the basin-wide meridional gradients and position of the isotherms. Near the coast, the Peru upwelling (delimited by the 20 °C isotherms) is captured and compares fairly well to the Reynolds estimate. At finer spatial scale, comparison of the two products permits evaluation of the model's ability to simulate the permanent upwelling cells along the Peru–Chile coast. Due to the relatively low resolution of the model (1/3°), the simulated cross-shore SST gradients (not present in the Reynolds SST) are weaker north of ~20°S (Fig. 2a) compared to the observed AVHRR SST (Fig. 2c), which results in substantially cooler SST in the model. On the other hand, off the coasts of central and southern Chile, temperatures are slightly warmer off-shore and cooler on shore, which indicates that the model either overestimates upwelling or that heat fluxes are not realistic or are incorrectly distributed over the mixed layer (too deep at the coast, see Fig. 5). Despites these model flaws, and although the model produces wigglings of the isotherms that are not always present in the high-resolution observations, it provides a generally realistic distribution of SST at

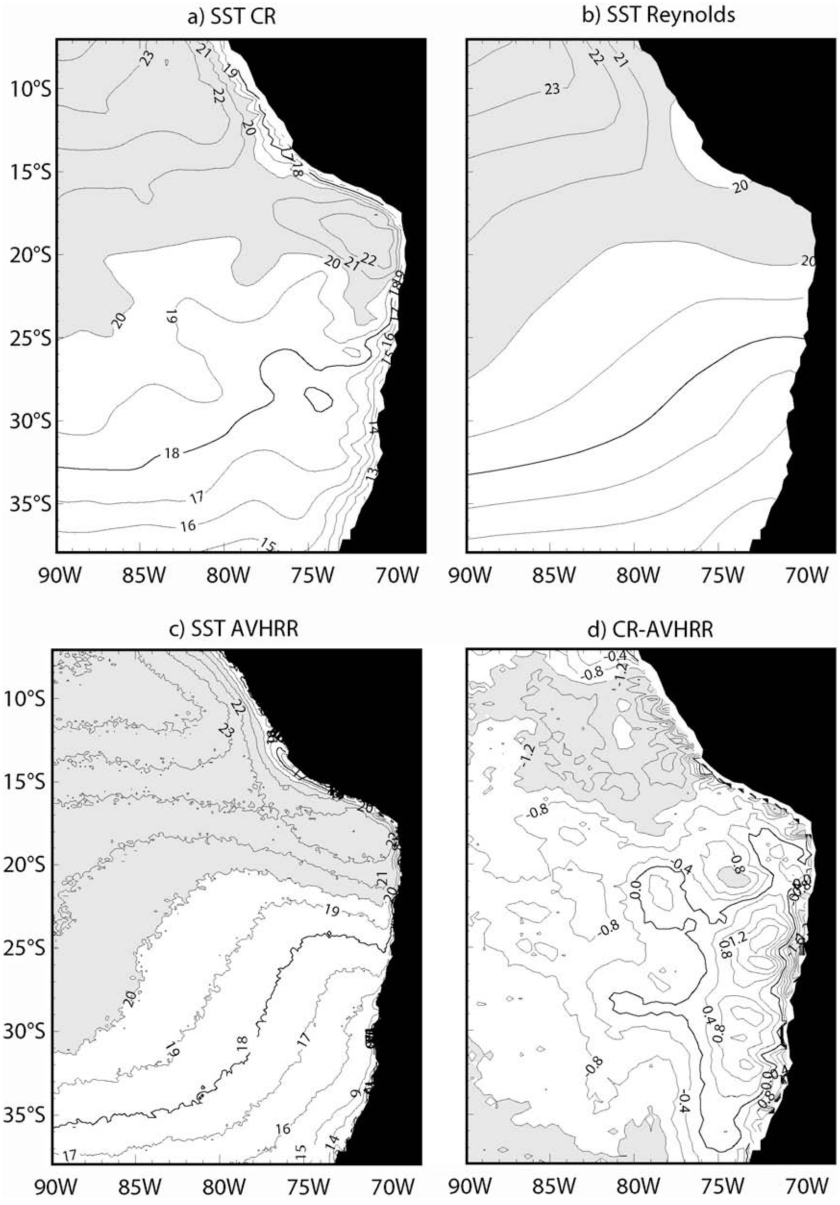

Fig. 2. SST for (a) CR, (b) the Reynolds observations (1° resolution) and (c) the AVHRR observations (9 km resolution). (d) Mean SST difference between CR and AVHRR. Unit is °C. Shading is for temperature above 20 °C and the 18 °C-isotherm is in thick line for (a)–(c). Shading is for temperature anomaly lower than −1.2 °C in (d).

a resolution that cannot be achieved from observations for the subsurface in this region of the world. This also motivates the present study.

3.1.2. Thermocline depth

The thermocline depth in the control run (CR) and in the WOA01 observations was calculated following Pizarro and Montecinos (2004) based on the depth of the maximum temperature gradient (Fig. 3). The comparison is presented in Fig. 3 which highlights the difference in resolution of the two products. The maximum depth is found at 17°S, 89°W in the model, whereas it is at 23°S; 83°W in the observations which may reflect the scarcity of the observed data in this region. Near the coast, the model thermocline does not shoal nearly as much as the observations, which is partly due to the difference in vertical resolution of the two products (higher for the model). Near 500 km offshore the model thermocline tends to be deeper than the observations. However, the mean zonal gradients in thermocline depth, when averaged between 15°S and 35°S, are similar (~0.1 m/km).

3.1.3. Peru–Chile Undercurrent (PCU)

The PCU is a well-defined, poleward, subsurface flow, which extends over the continental shelf and slope off the west coast of South America with a core located between 100 and 300 m depth. The PCU transports warm, salty equatorial subsurface water from the eastern tropical Pacific to at least as far south as 48°S (Silva and Neshyba, 1979). This water mass in turn is the main source for the coastal upwelling off Peru and northern Chile (e.g. Huyer et al., 1987) and is associated with the oxygen minimum (Wyrtki, 1963). A mean poleward flow in the PCU of 5–10 cm s^{-1} has been observed between 5°S and 12°S off Peru (Huyer et al., 1991). At 30°S off Chile, a southward mean flow of about 13 cm s^{-1} (for the period January 1993–February 1999) was observed at 230 m depth, near the PCU core over the upper slope (Pizarro et al., 2002). Like other poleward undercurrents of EBC systems, the PCU may be a return current driven by upwelling-favorable, alongshore winds blowing in the opposite direction (McCreary, 1981). Roden (1962) also showed the relevance of wind-driven Sverdrup dynamics to explain the presence of the rather strong southward transport along the coast of Peru, though he was limited by the poor quality of wind datasets available.

However, seasonal and interannual changes in the PCU off Chile and Peru are not clearly related to these winds (Huyer et al., 1991; Pizarro et al., 2001), and important seasonal variability originates on the equator (Pizarro et al, 2002). It is thus interesting to explore the mean characteristics of the PCU in the model, which will help validate the model and provide insight into PCU dynamics. Fig. 4 displays the mean characteristics (maximum along-shore velocity and depth) of the modelled PCU at 10°S and as a function of latitude. Fig. 4a can be compared to Fig. 11 of Huyer et al. (1991) although the latter is based on data of a peculiar period and corresponds to geostrophic currents only, unlike the climatological model. Despite this limitation, the 1991 figure indicates that the modelled PCU has a realistic pattern at 10°S with a minimum velocity core ~200 km off-shore and a secondary core attached to the continental slope. Its magnitude is weaker than in the observations and decreases southward, while its depth increases southward (Fig. 4b). Considering the relatively low resolution of model with regards to the cross-shore scale of this current (~50 km), the realism of the simulated PCU is encouraging with regards to the connection between equatorial and inner basin variability. In the following, to examine PCU variability, we will consider variability at the core of the mean PCU.

3.1.4. Mixed layer depth

Investigating the mean mixed layer depth in the model may provide insights on the realism of the vertical gradients in the surface layers which impacts the dynamical response of the ocean to momentum and heat flux forcing. Note that the spatial heterogeneity of the model mixed layer will be taken into account to diagnose the theoretical baroclinic mode energy distribution (see Section 4.1). Following de Boyer Montégut et al. (2004), the model mean mixed layer depth was calculated based on the temperature profile with criteria of 0.2 °C (i.e. the depth where temperature equals SST – 0.2 °C). The results are displayed in Fig. 5. The model correctly simulates the offshore deepening of the mixed layer. Further offshore, the model exhibits fine scale structures which may not be resolved by the observations. In particular, near 90°W, 20°S the model simulates a deeper mixed layer than in the observations, whereas near 78°W, 22°S it is shallower.

Summarizing, it appears the model mean state has a reasonably realistic structure that may account for PCU dynamics. It allow further investigation of its variability and associated forcing mecha-

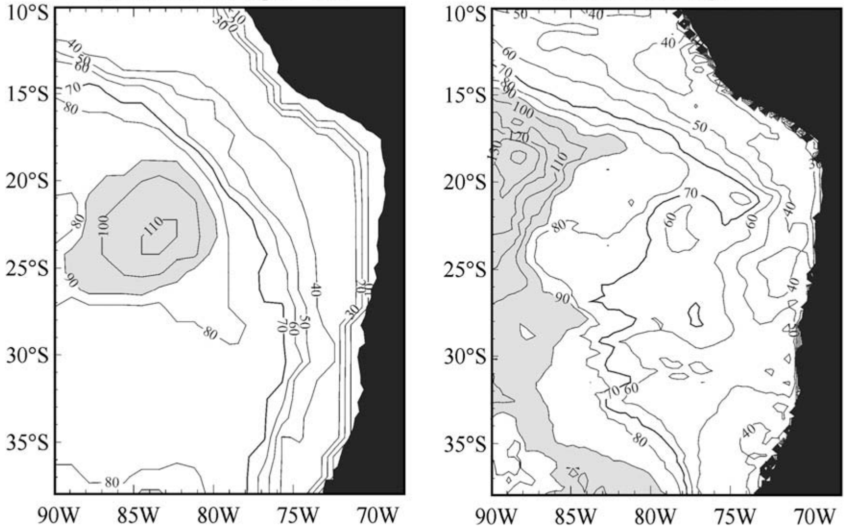

Fig. 3. Mean thermocline depth for (a) Levitus data and (b) CR. Unit is m. Shading is for depth larger than 90 m.

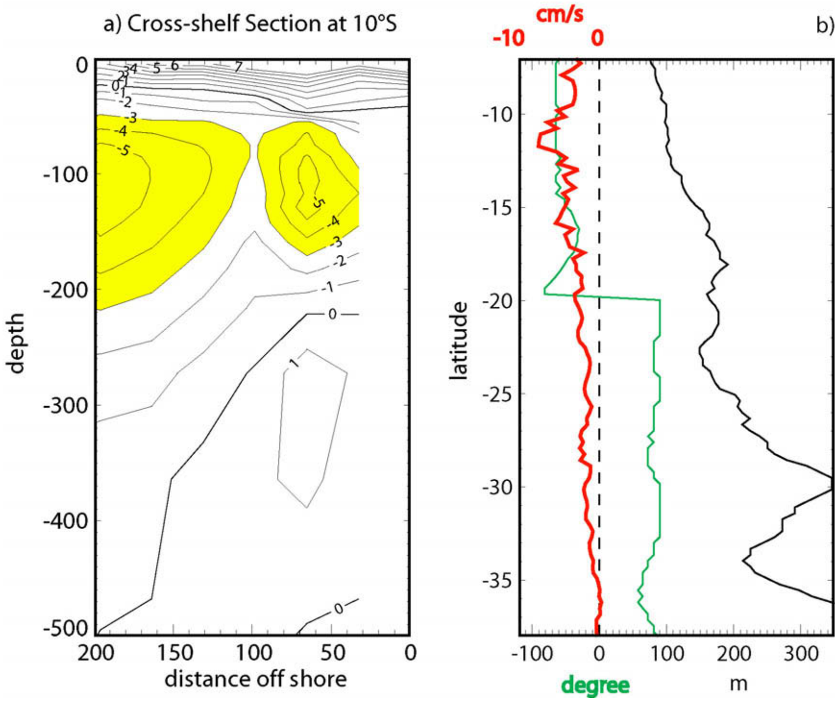

Fig. 4. Mean characteristics of the PCU in CR (negative value for southward current): (a) the cross-shelf section of current at 10°S. This figure can be compared to Fig. 11 of Huyer et al. (1991) who made an estimate of the geostrophic flow from four CTD sections at 10°S [see also Fig. 3 of Strub et al. (1998)]. Yellow shading is for values of current lower than −3 cm s^{-1}. (b) Depth of the core of the PCU (black line) and minimum mean along-shore velocity in the core of the PCU (red line) as a function of latitude (upper scale). The angle of slope of the coastline used to estimate the along-shore velocity is also plotted in green line (lower scale).

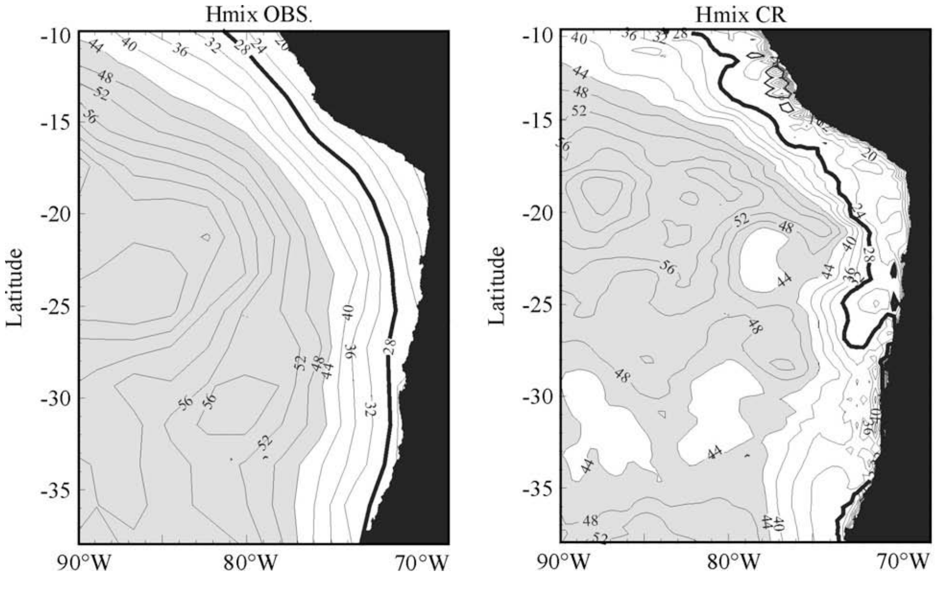

Fig. 5. Mixed layer depth for the observations (left) and the model (right). Unit is *m*. The criteria used is on temperature (*dT* = 0.2 °C). Shading is for depth larger than 44 m.

nisms. In the following, some aspects of the model variability are analysed.

3.2. Variability

3.2.1. Sea level

Fig. 6 displays the results of the EOF analysis of (1) the satellite-derived sea level anomalies and (2) CR. The satellite data were high-pass filtered (cut-off frequency = 1.5-year) in order to dampen interannual variability. Note however that this filtering does not completely remove the low-frequency variability contribution because the satellite seasonal cycle contains a component associated to the rectification of the interannual variability on the mean state and seasonal cycle, which is not the case for CR. This limits the comparison between the simulations and the observations.

The spatial patterns of the dominant EOF are similar for the observations and simulation over a succession of positive and negative anomalies that extend offshore more in the north than in the south. Discrepancies between the observations and the simulation are the largest south of 25°S where the variability associated with

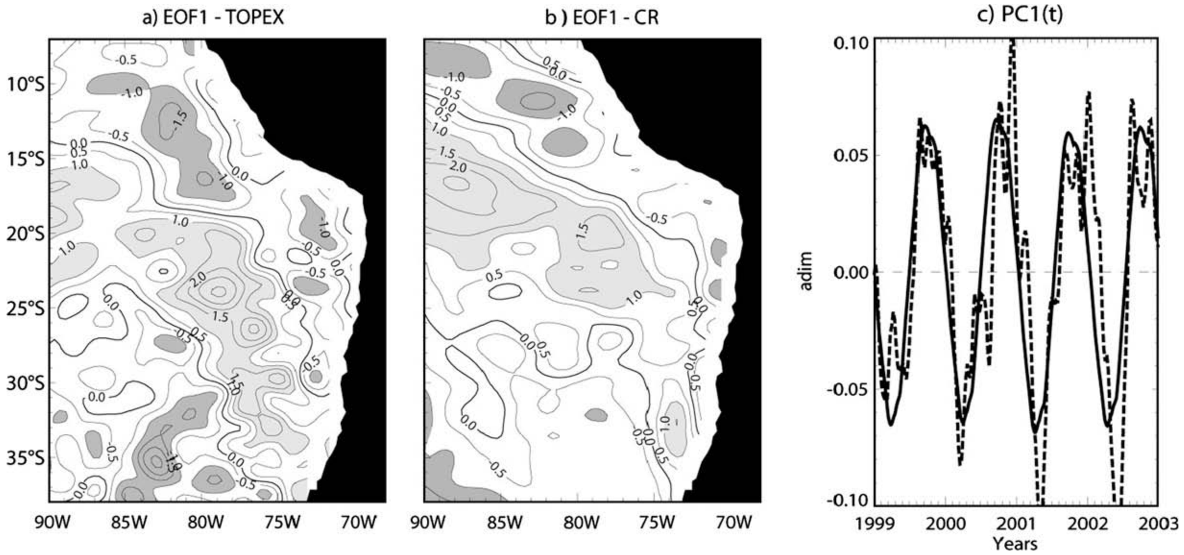

Fig. 6. Maps of the first EOF of sea level for (a) the observations as derived from TOPEX/POSEIDON data and (b) for CR. Units is cm. The associated temporal functions (in non-dimensional units) are shown in the panel (c) in plain line for CR and dashed line for the observations. Darker (lighter) shading is for value lower (larger) than −1 (1) cm. The spatial patterns were smoothed with a seven-grid-point-width boxcar average.

mesoscale eddies is significant in the observations (Chaigneau and Pizarro, 2005). This is partly due to the relatively low resolution of the model which underestimates mesoscale activity by a factor of 3 in terms of eddy kinetic energy as compared to altimetric data (not shown). It may also be related to the fact that monthly mean climatological fields forced the model so that intraseasonal variability in the model is underestimated.

The magnitude of the anomalies is on average slightly higher for the observations than for the simulation. The percentage of explained variance is 20% versus 30% for CR and the altimetric data, respectively. However, because CR uses a repetitive climatological forcing, the EOF analysis is somewhat equivalent to an Extended-EOF (E-EOF) analysis, and, as such, captures the propagating dominant mode of the variability that comes out as a pair of modes. Thus, the pattern of the second dominant mode of the EOF analysis is similar to that of the first, except that the associated temporal functions are shifted by a quarter of a period as in E-EOF analysis (not shown). This implies that the actual percentage of explained variance associated to the seasonal cycle for CR is 30% + 29% = 59%, which is much larger than for the observations. The remaining variance is associated with both the high- and low-frequency variability, which will be discussed in Section 5.

Despite these discrepancies in the spatial pattern, the associated time series of the EOFs are in phase ($c = 0.92$) (Fig. 6c). Other techniques were applied on the sea level time series, which includes E-EOF and Complex-EOF (Horel, 1984), and these lead to comparable results. For instance, the dominant CEOF mode for the model and the observations explained 86% and 53% of the variance, respectively, and exhibit comparable patterns of amplitude and phase (spatial correlation between model and observation reaches 0.50 and 0.45 for the amplitude and phase excluding the region south of a line from (20°S; 90°W) to (38°S; 73°W)).

3.2.2. PCU

As mentioned above, the PCU is a characteristic feature of the SEP. Its existence illustrates the complex vertical structure of the coastal ocean and highlights the peculiar dynamics associated with the connection to equatorial variability through coastal-trapped Kelvin waves. In the following, some aspects of PCU variability are documented through the model, which will later serve as a basis for examination of the connection between the equatorial and the inner basin variability.

The seasonal variability of the PCU has not been well documented due to scarcity of data. Pizarro et al. (2002) however documented PCU variability from a 7-year long current record over the slope and near the core of the PCU at 30°S and showed that this flow is strongly modulated at seasonal and interannual periods by Rossby waves which are in turn forced by equatorial Kelvin waves arriving at the South American coast. Ramos et al. (2006) also noted a connection at semi-annual periods between the coastal and offshore thermocline variability in northern Chile. At these timescales, the PCU, embedded in the coastal ‘wave guide’, exhibits a variability that is documented from the model.

Fig. 7a displays the annual and semi-annual harmonics of the PCU and wind stress along the coast as a function of latitude, with semi-annual harmonics represented over two cycles. It indicates that, whereas the semi-annual cycle of the PCU exhibits a clear southward propagation pattern, the annual cycle exhibits more latitudinal variability, reflecting a more complex forcing mechanism at annual timescale. The amplitudes of the annual and semi-annual cycles are comparable (see plain lines in Fig. 7b) with zones of relative maximum variability for the annual (semi-annual) cycle between 9°S and 13°S (9°S and 11°S) and between 27°S and 37°S (15°S and 19°S). These increases in variability along the coast take place near the critical latitudes of the semi-annual and annual periods for the first and second baroclinic modes as estimated by Clarke and Shi (1991): ~15°S and ~9°S for the semi-annual period and ~37°S and ~23°S for the annual period (see Fig. 7c). Note that the coastline shape and vertical grid configuration of the model (taking into account the changes in the continental shelf width) may explain the deviation from the Clarke and Shi (1991)’s estimate. The latter is based on 300 km segments chosen so that they approximated the deep-sea boundary (source of the topographic data is not mentioned in Clarke and Shi (1991)).

The annual harmonics of the along-shore wind may contribute to the change in propagating characteristics of the PCU variability. As noted in earlier works (Shaffer et al., 1999), the winds off the coast of Peru tend to be phase lagged (lag = ~4–6 months) with the ones of southern Chile with a minimum variability between 17°S and 22°S (Fig. 7b). Moreover, the increase in PUC annual variability south of 25°S seems to be consistent with an increase in

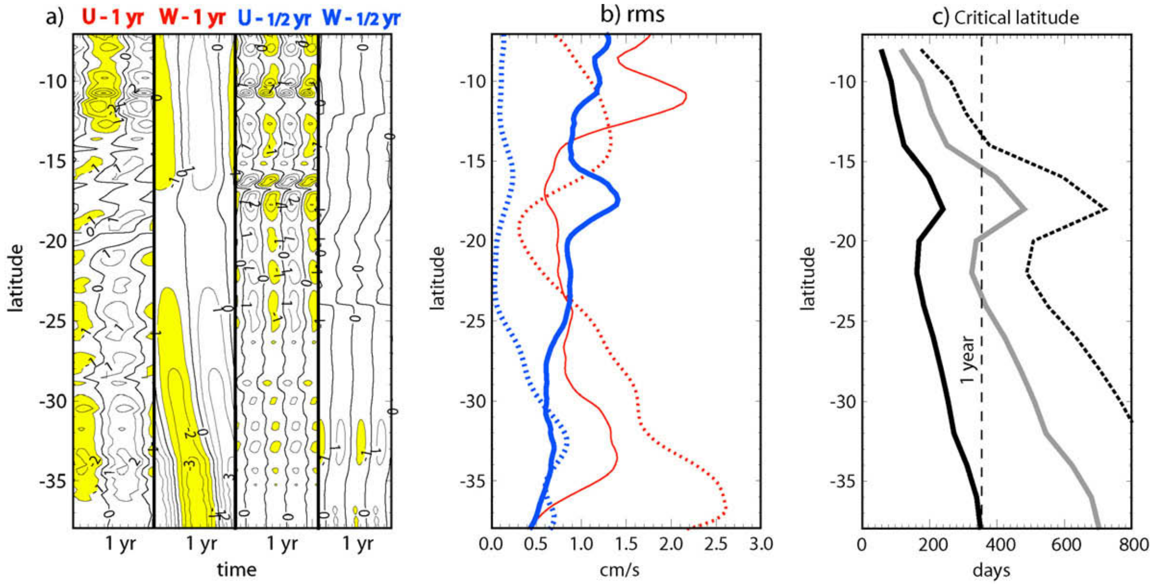

Fig. 7. PUC seasonal cycle: (a) time-latitude sections of the annual and semi-annual components of the PUC and along-shore wind stress. Negative values correspond to southward (northward) current (wind stress). Units are cm s^{-1} for currents and 10^{-2} N m^{-2} for wind stress. Each field are represented over 1-year period. Yellow shading is for values lower than -1. Unit. (b) Variability (RMS) as a function of latitude of the annual (red lines) and semi-annual (blue lines) components of the PUC (plain lines) and wind stress (dotted lines). RMS curves were smoothed with a seven-grid-point-width boxcar average. (c) Critical latitude as a function of the period for the first (black line), second (grey line) and third (dotted line) baroclinic mode as derived from Clarke and Shi (1991).

wind stress, with a lag of several months (Fig. 7a). The semi-annual component of the along-shore wind is much weaker than the annual component, which favours the free poleward propagation of the semi-annual component of the PCU.

With these few aspects of the model variability and mean state in mind, we next investigate the vertical density structure variability and associated dynamical response.

4. Vertical mode decomposition of the model variability

A vertical mode decomposition is sought in order to interpret the dynamical response of the ocean to the heat and momentum forcing and to document the off-shore propagating variability in the model.

4.1. Projection coefficient and forcing

The theoretical projection of the momentum and heat fluxes on a given baroclinic mode can be derived from the vertical mode decomposition of the mean stratification, taking into account both the heterogeneity in mixed layer depth and thermocline depth. For momentum flux, in non-dimensionalized form, the projection coefficient is written as follows, $P_n(x,y) = \frac{\frac{H}{h_{mix}}\int_{-h_{mix}}^{0}\Psi_n(x,y,z)dz}{\int_{-H_{bot}}^{0}\Psi_n^2(x,y,z)dz}$, where H is the mean thermocline depth (cf. Fig. 3b), h_{mix} the mean mixed layer (cf. Fig. 5b), Ψ_n, the vertical mode structures and H_{bot} the depth of the ocean floor. P_n is displayed in Fig. 8 for the first three baroclinic modes. The results indicate that at basin scale, a significant part of the wind stress variability projects on the first and second baroclinic modes. Due to the rising isotherms along the coast, the third baroclinic mode (and high-order modes, not shown here) contributes significantly near the coast especially north of 20°S. However, the pattern of P_n has to be interpreted in the light of the distribution of the local wind stress curl since $P_n \times \vec{\nabla}\Lambda\vec{\tau}$ is the actual forcing term of the linearized momentum equation for each mode. At the annual period, the spatial pattern of the annual harmonic of the wind stress curl forcing (Fig. 8, bottom left panel) reveals that high-order modes are not favoured near the coast between 15°S and 27°S. The region of maximum values for P_2 corresponds also to a region of minimum amplitude of the forcing. On the other hand, the regions of large P_1 are associated with the large amplitude of the annual cycle of the wind forcing, especially in the offshore region.

Note that for heat flux, the projection coefficient has a dependency in $\frac{1}{C_n^3}$ (where c_n is the long wave phase speed for mode n) as compared to P_n (cf. Dewitte (1998)), so that for the high-order vertical modes, heat flux forcing may contribute significantly to the dynamical field variability. However, because of the weak values for phase speed, the dynamical response of the ocean has to remain mostly local and does not radiate from the forcing region.

4.2. Baroclinic mode contribution to sea level

The variability maps for the baroclinic mode contributions to sea level anomalies for the annual and semi-annual cycles and residual are presented in Figs. 9 and 10, which show that the annual cycle projects predominantly on the first baroclinic mode, whereas the semi-annual cycle is less energetic for all the modes in the inner basin. Consistent with critical latitude theory, most of the variability of the annual cycle is confined in the form of coastal-trapped Kelvin waves along the coast south of ~32°S and ~20°S for the first and second baroclinic mode contributions, respectively (see Fig. 7c for an estimation of the critical latitude as a function of baroclinic modes and frequency). The semi-annual cycle has also a maximum in variability offshore, north of ~23°S for the first baroclinic mode, again consistent with the expected theoretical critical latitude. Interestingly, the residual variability projects on all the modes and is as large as the annual variability of the first baroclinic mode. It is by far the largest contribution to the second baroclinic mode. This residual variability extends as far offshore as the annual cycle variability of the first baroclinic mode and exhibits a different spatial pattern for each of the first three modes. In particular, it exhibits a peak in the inner basin at 27°S for the first mode and at 23°S for the second mode, whereas

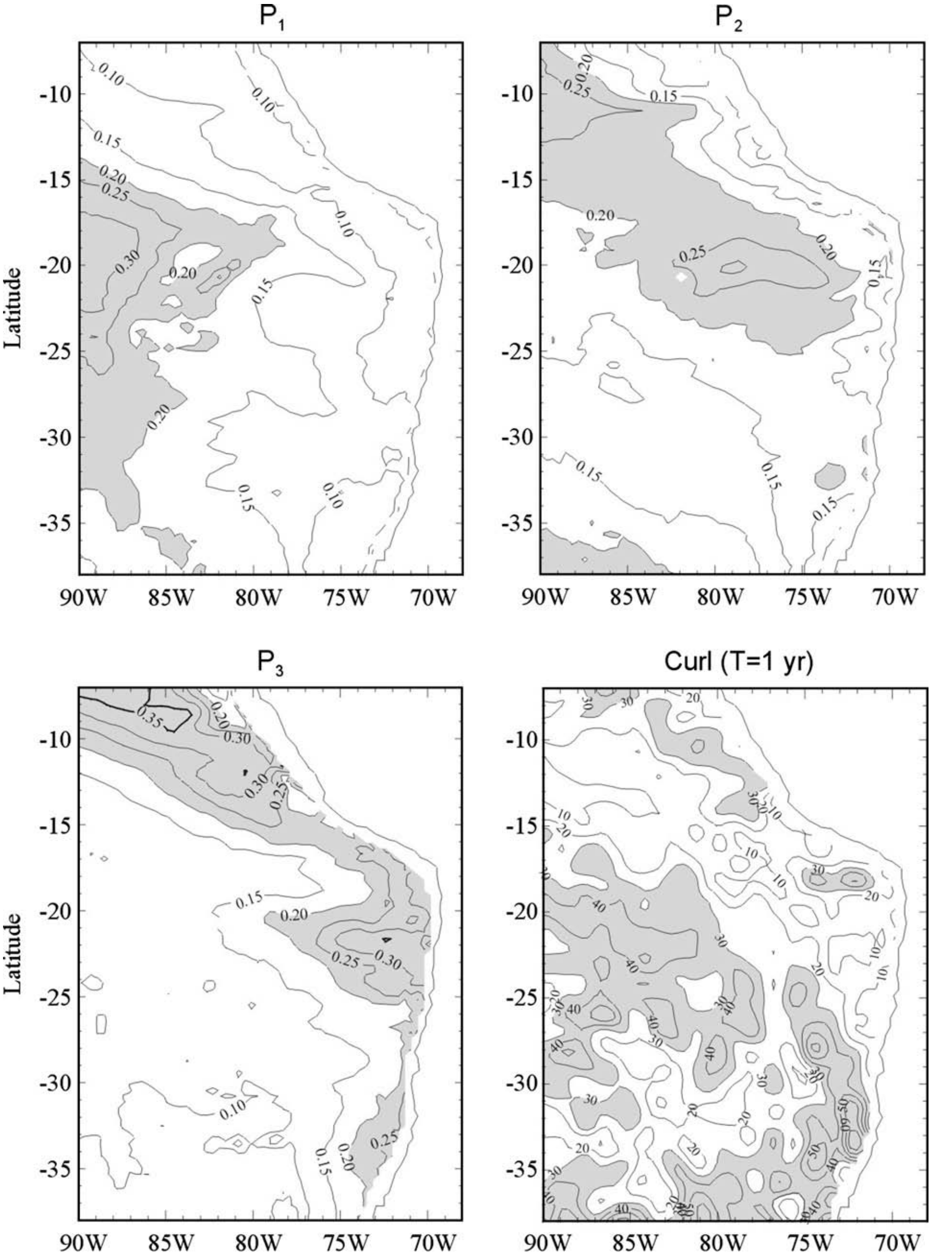

Fig. 8. Non-dimensionalized wind projection coefficient for the first three baroclinic modes and the maximum amplitude of the annual cycle of wind stress curl in 10^{-8} N m^{-3}.

for the third mode, it is the largest near (23°S–80°W) and off the coast of Peru south of ~13°S. Notably, this latter latitude corresponds to the critical latitude of the annual cycle for the third baroclinic mode (cf. Fig 7c), whereas one find the largest amplitude of the PUC along the coast of Southern Peru (Fig. 4b), suggesting wave-mean flow interaction as a source of the residual variability in this region. The summed-contribution of modes 4–18 mostly peaks within ~100 miles of the coast and south of 22°S, which is consistent with theory which predicts energy at these frequencies should remain near the coast as trapped coastal waves. Note the zone of minimum residual variability in a kind of 'shadow zone' off northern Chile for the first and second baroclinic modes and the sharp decrease in variability of the first baroclinic mode south of ~33°S (the critical latitude of the annual cycle of the first baroclinic mode). These complexities reflect the internal variability of the model, which will be further investigated in Section 5.

The first baroclinic mode is dominant over the whole basin for both the annual cycle and the residual variability. The variability of the semi-annual cycle of the first baroclinic mode is about half that of the annual cycle. In the following, we investigate the propagating characteristics of the first baroclinic mode contribution to sea level at the annual period.

4.3. Propagating characteristics

4.3.1. The first baroclinic mode extra-tropical Rossby wave

To investigate the propagating characteristics of the first baroclinic mode contribution to the annual cycle, maximum amplitude and associated phase are estimated at each grid point (Fig. 11a and b). The results indicate clear off-shore propagation of the sea level with the phase lines parallel to each other over most of the basin. Note, however, the spatial heterogeneity of the amplitude of the

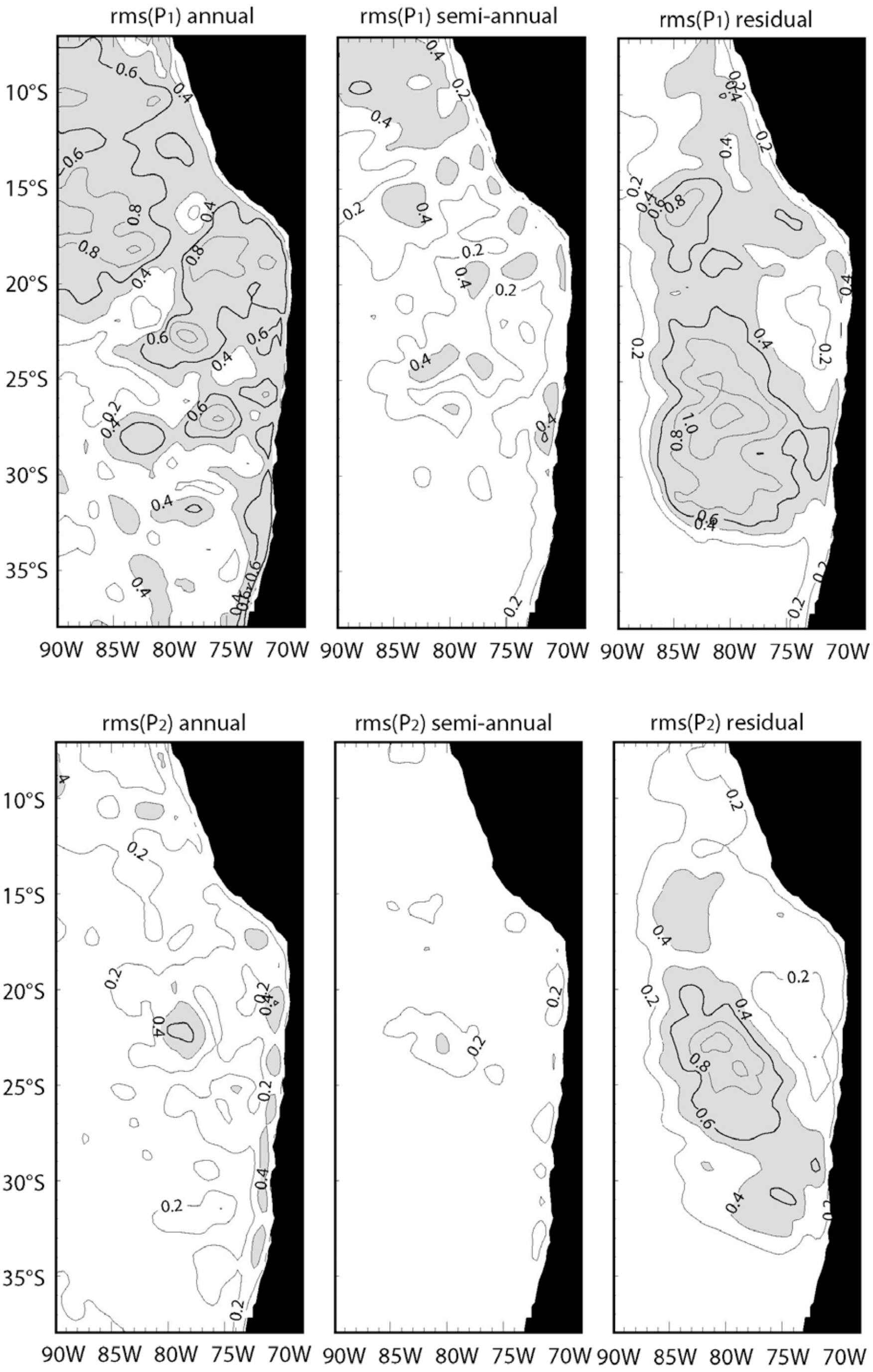

Fig. 9. Baroclinic mode energy distribution: variability (RMS) maps of first (top) and second (bottom) baroclinic contribution to sea level anomaly for the annual and semi-annual frequencies and for the residual. Units are cm. Contour intervals are every 0.2 cm. Shading is for value larger than 0.4 cm. The maps were smoothed with a three-grid-point-width boxcar average.

annual signal which traduces local wind forcing and the likely interaction between modes as suggested by the patterns of wind projection coefficients (Fig. 8). As an indication of the longitudinal extent of the propagation, we computed the distance from the coast reached after 6 months by a theoretical ETRW with phase speed $c(y) = \frac{\beta \cdot c_1^2(y)}{f^2(y)}$ (c_1 is the first baroclinic mode phase speed obtained from the vertical mode decomposition and averaged over a 5° zonal segment starting 1° from the coast). The derived curve mimics the theoretical change of phase speed with latitude (cf. white line in Fig. 11). Interestingly, the curve matches the location of the transition zone between maximum and minimum amplitude of the sea level and the region where phase lines become more erratic (Fig. 11a and b). In order to confirm the propagating nature of the signal, an E-EOF analysis was performed on the recomposed annual harmonic of the first baroclinic mode contribution to sea level. The spatial pattern of the dominant mode (which comes up as a pair) is consistent with off-shore propagation from the coast. A quantitative estimate of the wavelength from Fig. 11c (whether from the phase lines map, taking the distance between phases lines separated by 6 months, or from the E-EOF map, taking the distance of the zero line from the coast) matches the estimate from the dispersion relation of the ERWs ($\omega = -\frac{\beta k c_n^2}{f_0^2}$, see Appendix A), taking

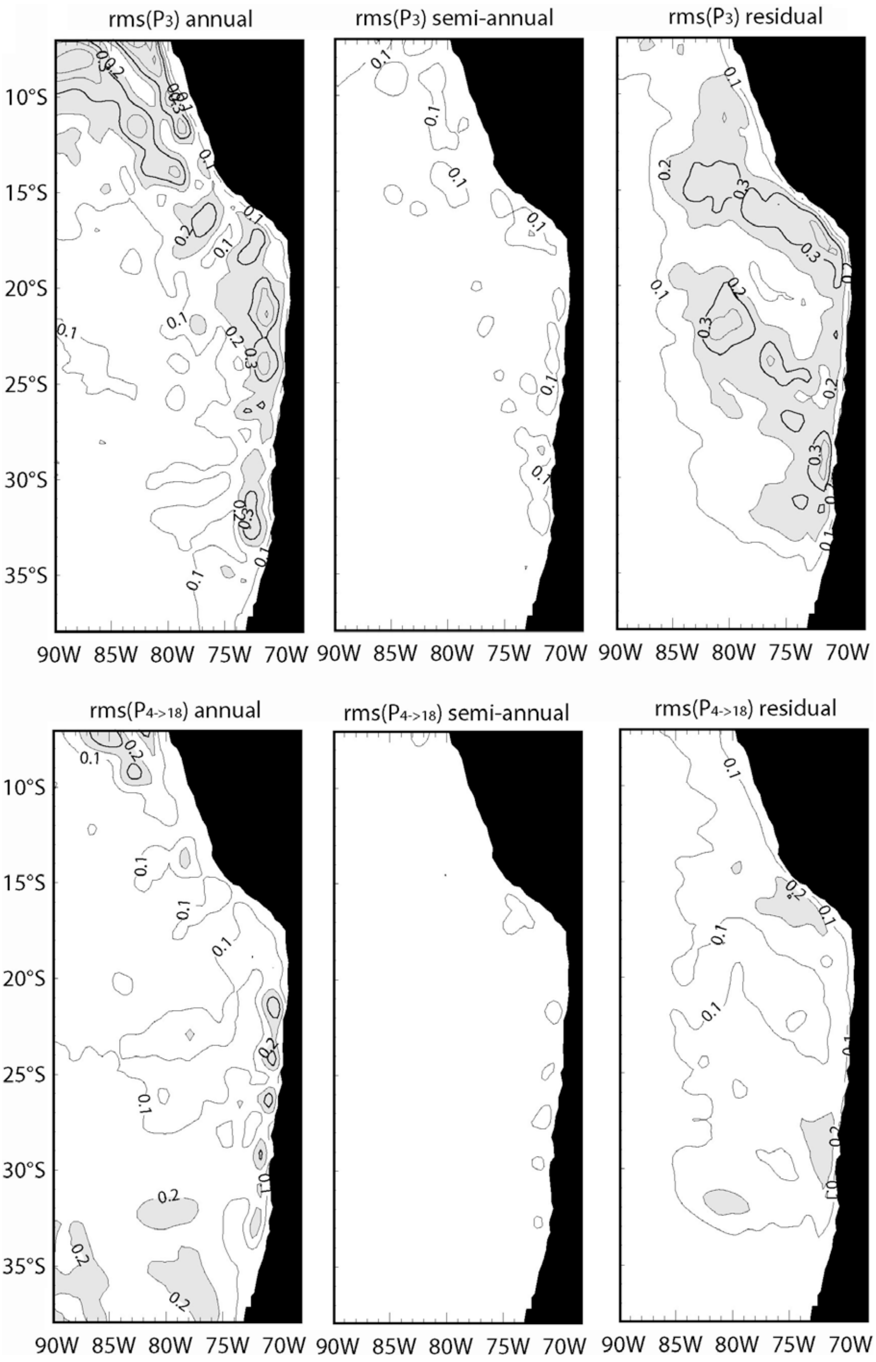

Fig. 10. Same as Fig. 9 but for the third baroclinic modes and the summed-up contributions of modes 4–18. Units are cm. Contour intervals are 0.1 cm. Shading is for value larger than 0.2 cm.

the values for c_1 as derived from the vertical mode decomposition (not shown). These comparisons confirm the off-shore propagation of first baroclinic mode ERW at annual period.

For the second baroclinic mode, off-shore propagation also occurs but is confined near the coast where the amplitude of the annual harmonic is the largest (not shown). For the third baroclinic mode, surface propagation is hardly detectable in the amplitude and phase (not shown) because of the slow phase speed and the coastal restriction of the associated variability.

As a consistency check of the model variability in terms of propagating Rossby wave, we verify in the following that the energy distribution on the baroclinic modes (as described above) is coherent with vertical propagation. Since high-order modes have a strong signature near the coast at the annual period, it is expected that they combine to form 'beams' that transfer energy downwards (McCreary, 1984). Formation of such beams would explain why the first baroclinic mode ETRW dominates the sea level variability in the model.

4.3.2. Vertically propagating energy flux

Following Dewitte and Reverdin (2000), WKB ray path theory is used to interpret wave features identified in the energy flux associated with vertical isotherm displacements. The theoretical background of the WKB ray path theory and the validity of assumptions are extended to extra-tropical latitudes and are presented in Appendix A. Ray paths correspond to the path of the energy flux

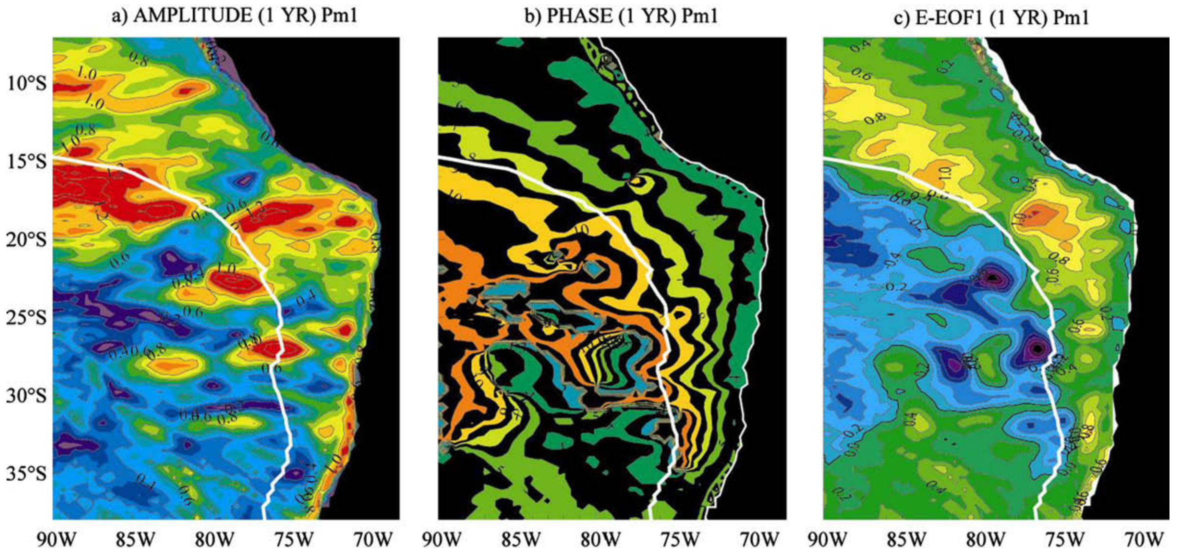

Fig. 11. Maps of the annual harmonic of the first baroclinic mode contributions to sea level anomalies (a) amplitude (in cm) and (b) phase (label '1' corresponds to January). (c) Map of the dominant E-EOF of the recomposed annual harmonic. The thick white line indicates the distance from the coast reached in 6-month by a first baroclinic mode ERW propagating with theoretical phase speed of $c = \frac{\beta \cdot c_1^2}{f^2}$.

$(u \cdot p, v \cdot p, w \cdot p)$ where (u, v, w) is the velocity vector and p is the pressure field (Eliassen and Palm, 1960). Vertical velocity w is estimated as $d\zeta/dt$, where ζ is the vertical displacement of the isotherms $\left(\zeta = \frac{T}{\frac{\partial \bar{T}}{\partial z}}\right)$. The vertical energy flux, $w \cdot p$, should be averaged over long time scales relative to the variability. If there is only one ray path and linear theory applies, the phase of the signal in vertical displacement should be constant along the ray path and the energy flux should be parallel to it. In practice however, the variability is multi-frequency, the signals originating from various areas can interfere, and the simulation is non-linear, so that the ray path concept should only be viewed as a diagnostic tool. The isotherm vertical displacements (ζ) are derived from the simulated temperature field (T) interpolated vertically on a 5 m grid using 1D cubic splines. The vertical convergence of the mean vertical energy flux associated with this field $\left\langle \frac{\partial \zeta'}{\partial t} \cdot p' \right\rangle$ quantifies the anomalous kinetic and potential energy released to the fluid through the (1) dissipation and diffusion terms (not estimated) or (2) advected from surface near the coast (or transferred by non linearities to other frequencies). Brackets denote the time average, and primes denote the annual harmonics of the individual variables.

Fig. 12 displays the annual harmonics for sections at 11°S, 17°S and 27°S. Positive values correspond to downward energy flux and extend westward and downward from the coast in the upper layers. For all sections, maximum amplitude is found near a theoretical WKB trajectory associated to a phase speed between those of the first and second baroclinic modes. The relative maximum for the 11°S section at 2000 m may be due to wave interference within the subthermocline and upward flux originating from the reflection the waves at the ocean bottom. The slope of the energy 'beam' increases with latitude, consistent with theory (cf. Appendix A). The difference between the different sections with respect to the share of energy actually reaching the deep ocean reflects the latitudinal heterogeneity of the high-order mode contribution to variability near the coast (Fig. 10) and the change in critical latitude as a function of mode order.

These results indicate that the weak surface variability of the high-order modes in the offshore region can be explained by the vertical propagation of energy by the ETRW.

5. Role of local wind stress forcing versus boundary forcing

The results presented above may be sensitive to boundary forcing. Of particular interest for the SEP is how local wind contributes to the ETRW variability, as compared to the remote equatorial forcing. Two sensitivity experiments were therefore run with the regional model, with and without seasonal change in boundary and wind forcing. The heat flux was allowed to vary as usual to simplify interpretation. Because heat flux forcing projects preferentially on the higher-order modes, it should not impact results of the manipulations presented here. The configuration of the simulations is summarized in Table 1. The TXYmean stands for the simulation using a mean wind stress forcing, whereas OBmean uses a constant open boundary condition. In order to assure that the baroclinic mode energy distribution in TXYmean and OBmean is not drastically modified by changes in the mean density structure compared to CR, which would limit the comparison between the three simulations, we verified that the mean SST, thermocline depth and mixed layer depth were similar in all the runs. The maps of the difference in mean SST between the simulations and the CR indicates that the changes in boundary forcing configuration impact the mean SST only in the coastal zone and results in SST changes no larger than + or − ~1°C (not shown). The mean thermocline depth of TXYmean and OBmean is also comparable to that in CR in the region of maximum amplitude of the first baroclinic mode (also not shown). The mean structure of the PCU was similar in all the runs (slightly larger amplitude in OBmean).

5.1. Baroclinic mode energy distribution and propagating characteristics

The vertical mode decomposition of the model runs is here described and the baroclinic mode contribution to sea level anomaly is estimated for the annual, semi-annual and residual variability. The results indicate that, as for CR, the variability in TXYmean and OBmean projects preferentially on the annual harmonics of the first mode, with the residual variability of comparable magnitude (or even larger for OBmean) to CR. Also, as for CR, the high-order mode contributions are weaker by an average factor of 2 than that of the first baroclinic mode (not shown).

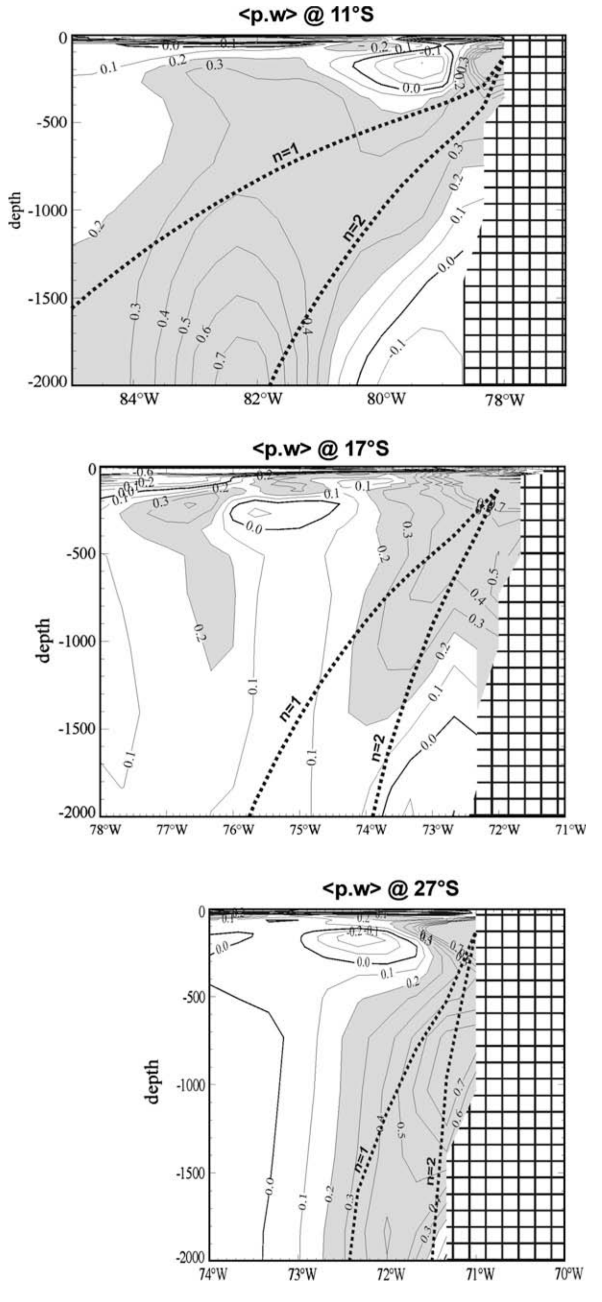

Fig. 12. Sections at 11°S, 17°S and 27°S of the vertical energy flux associated with the annual harmonic. Positive values are for downward flux. The thick dashed lines indicate the theoretical ray paths for phase speed values of the first ($n = 1$) and second ($n = 2$) baroclinic modes, respectively. Unit is 10^{-8} m^2 s^{-2}. Shading is for values larger than 2. Unit is 10^{-9} m^2 s^{-2}.

The propagating characteristic of the gravest baroclinic mode contribution to sea level at the annual period is extracted through E-EOF analysis for TXYmean and OBmean (Fig. 13). For both simulations E-EOF modes emerge as a pair with the associated time series phase-lagged by 3 months (a quarter of a period), indicating that the variability has a propagating nature. Not surprisingly the maximum variability zones of the first baroclinic mode contribution to sea level for the annual cycle are located near the coast for TXYmean (at least north of 20°S), reflecting the connection with equatorial variability. For OBmean, the variability peaks in the inner basin at various locations that are not always associated with the maximum amplitude of the annual harmonics of wind stress curl forcing (Fig. 8, bottom left panel), suggesting that the local wind stress and boundary forcing both contribute to propagation of the ETRW in CR. To illustrate these contributions, the E-EOF maps of TXYmean and OBmean are arbitrarily summed up and presented in Fig. 13c. The resulting pattern strikingly resembles the dominant E-EOF mode of CR (Fig. 11c), which suggests a quasi-linear response by the ocean at annual period. On the other hand, as will be seen in the next section, the similarity of the residual variability in all the runs indicates a non-linear response of the ocean to seasonal forcing.

5.2. Characteristics of the residual variability

The residual variability of the PCU in TYXmean and OBmean is comparable in magnitude and spatial distribution in all the runs (not shown), suggesting that the residual variability mostly results from internal dynamics and only weakly depends on the forcing. More likely, the residual variability depends on the mean alongshore current system.

To further investigate the residual variability, its low- and high-frequency components were 'separated' through filtering (a cut-off period of 1 year is used). E-EOF analysis was then performed on the filtered fields (only the first baroclinic mode contribution to sea level is considered), and the results for the dominant propagating modes plotted in Fig. 14 (only one element of the pair is displayed). For all the simulations, the high-frequency residual variability is maximal near (70°W–27°S). It also exhibits a westward-northward propagating pattern that tends to follow the mean circulation at 100 m, suggesting generation of waves through barotropic and baroclinic instability that extracts energy from the mean flow. The northward propagation may be due to the advection of the waves by the mean flow. Note that the amplitude of the signal in OBmean is more intense than in the other runs, which suggests that the wind stress may damp the instabilities near 25–27°S in CR. Along the coast of Peru, high-frequency variability is also significant for CR and TXYmean but not for OBmean suggesting that this variability mostly originates from equatorial forcing. The dominant periods of the associated time series of the E-EOF mode are ∼140 days for CR and TYmean and ∼250 days for OBmean.

The low-frequency component of the residual exhibits a different spatial pattern, with an 'apparent' propagating feature in the meridional direction. The variability peaks in a region centered around (80°W–30°S) for the all the runs and is larger in OBmean and TXYmean than in CR by a factor of about 2, which suggests that the non-linearities forced by the wind and boundary-forced waves in this region compensate each other and reduce the amount of energy transmitted to the longer time scales.

The characteristics of the residual sea level are suggestive of instability involving interaction between the mean circulation and the ETRWs. Cerovecki and de Szoeke (2006) studied the nature of long baroclinic wave propagation and instability in an idealized unventilated subtropical flow with vertical shear. Interestingly, their solutions from a $2^{1/2}$-layer model, both for the background flow and the perturbations, share many characteristics with the patterns of Fig. 14, which include a well-defined and narrow beam of stable waves emanating from the forcing region and propagation slightly north and westward depending on the background flow cases. These observations again support the interpretation of Fig. 14 as instability process resulting from the interaction between the annual Rossby waves and the mean circulation. Note that the residual variability is enhanced where it overlaps the region of sharp decrease in the first baroclinic mode annual ETRW amplitude, which is again consistent with the above interpretation.

6. Discussion and conclusions

A seasonal simulation from a medium-resolution OGCM is here used to investigate the variability of vertical structure in the SEP. In particular we attempt to determine if surface variability results

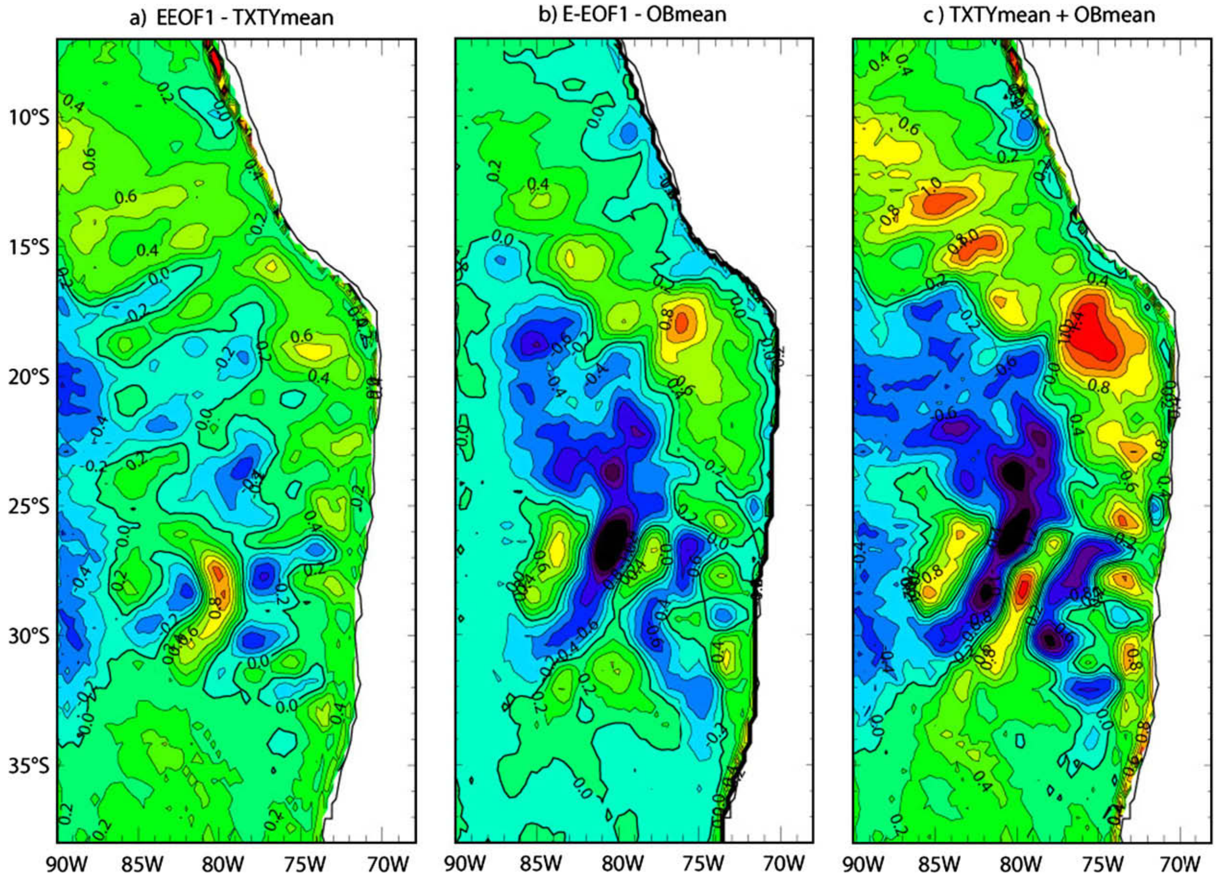

Fig. 13. Maps of the dominant E-EOF of the recomposed annual harmonic of the first baroclinic mode contribution to sea level for (a) TYmean, (b) OBmean, and (c) the sum of (a) and (b). Unit is cm.

from ETRW considering (1) the complex nature of the forcing which is both from equatorial and local origins, and (2) the presence of intraseasonal variability which, to a large extent, accounts for the non-linearity of the system. Although the model does not completely resolve coastal-trapped wave and eddy activity, it simulates much of the observed mean state and variability.

A vertical mode decomposition separated distinct modes of the variability, as evidenced by their different propagating characteristics. The decomposition works efficiently for the low baroclinic modes because the vertical structure is insensitive to the mean flow. The first baroclinic mode is the most energetic for all frequencies. The annual and residual variabilities are the most energetic for each mode (residual is total minus annual and semi-annual harmonics). The semi-annual variability is on average half that of the annual in the inner basin, whereas along the coast within the PCU, the annual and semi-annual are similar in magnitude (Fig. 7). The annual cycle of the first baroclinic mode exhibits clear westward propagation due to ETRWs forced throughout the basin and mostly in the interior. On the other hand, the second and higher-order baroclinic modes are mostly forced near the coast. Interestingly, although we make use of a full physics model, the dynamical adjustment of the ocean at annual frequency is basically linear in the sense that both the local wind stress and the boundary forcings sum to produce the sea level pattern. Another linear process associated with the annual frequency is the vertical propagation of energy that explains the large contribution of the high-order baroclinic modes near the coast, where the modes combine to form 'beams' of energy that propagate downward and westward along ray-paths that are steeper in the south, consistent with theory. Such processes have previously been documented for the equatorial annual Rossby wave (Kessler and McCreary, 1993; Dewitte and Reverdin, 2000), and are generalized here for ETRWs to verify propagation of sea level variability in the model and to interpret characteristics of the coastally trapped high-order baroclinic modes.

The results also reveal the presence of significant 'residual' variability which corresponds mostly to internal dynamics of the model physics (Fig. 14). This residual is largest near the coast and in the transition zone corresponding to the sharp decrease in amplitude and propagation of the ETRW. Interestingly, zonal change of the sea level variability in this transition zone may modulate the meridional circulation through geostrosphical adjustment at a wide range of frequencies since it takes a few months (<~7–8 months) for the first baroclinic annual Rossby wave south of 10°S to cross the basin from the coast up to this zone of minimum amplitude of the annual cycle. The propagating characteristics of the residual variability are consistent with this interpretation, which suggests that the annual ETRW and the mean circulation may interact in this region (ColindeVerdiere and Tailleux, 2006; Cerovecki and de Szoeke, 2006). The possibility of such interaction certainly deserves further investigation from more specific designs of model experiments. Remarkably, results of an idealized exploration of the instability of periodic (including annual) perturbations of oceanic subtropical gyres (Cerovecki and de Szoeke, 2006) are consistent with the more realistic solution of the model.

Results of the medium-resolution model are, however, limited in a number of ways. First, it is not clear to what extent the model can reproduce coastal-trapped waves (and therefore the connection with the equatorial variability), considering that the Rossby

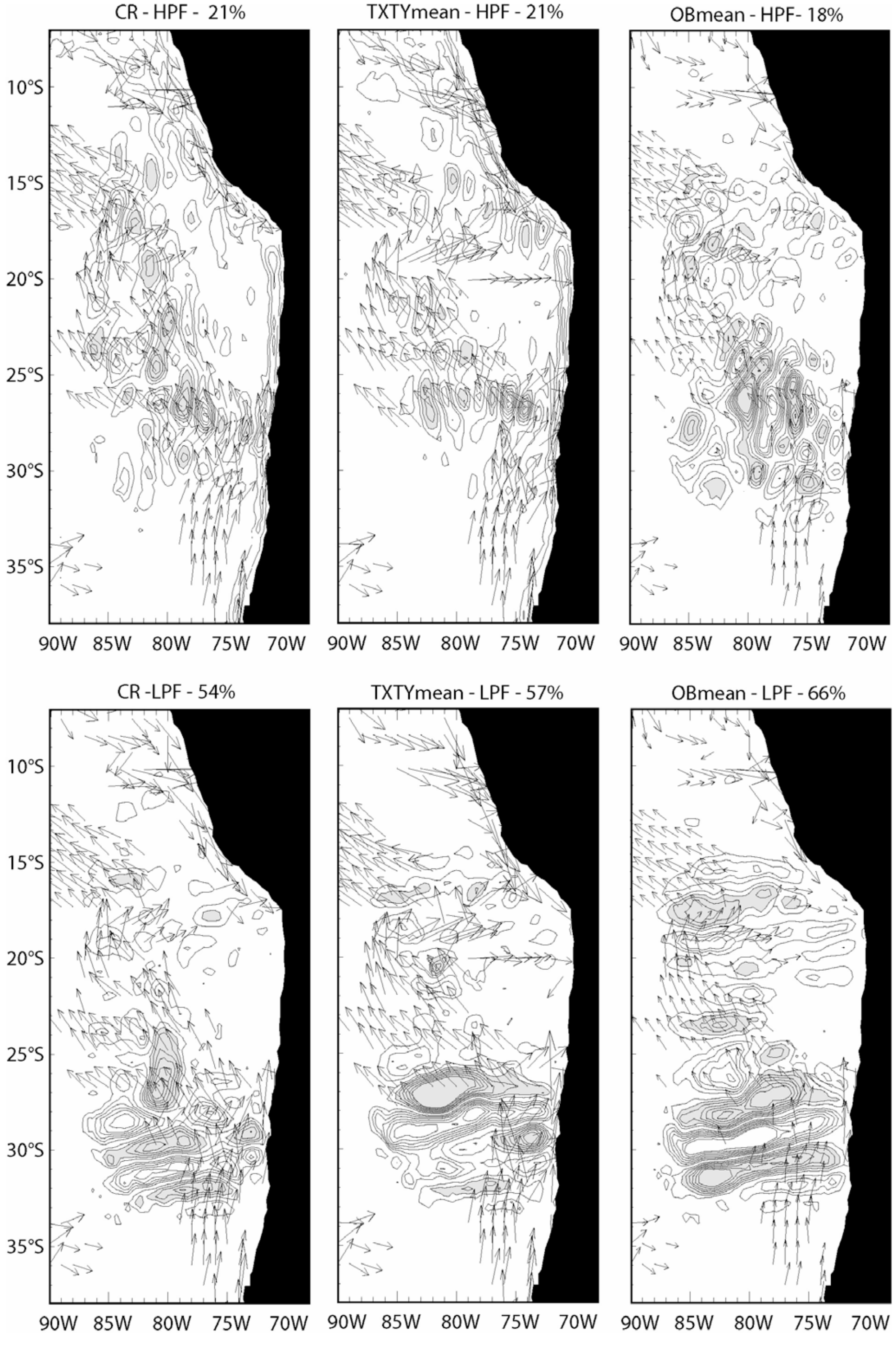

Fig. 14. Dominant E-EOF modes (one element of the pair) of the high-passed (top) and low-passed (bottom) filtered first baroclinic contribution to residual sea level for CR (left panels), TXYmean (middle panels) and OBmean (right panels). Percentage of explained variance (sum of the percentage of variance of the two elements of the pair) is indicated on top of each panel. Unit is cm. Contour interval is every 0.2 cm. Zero contours are not plotted. Shading is for values larger than 0.4 cm. The mean currents (magnitude and direction) at 100 depth are over plotted in each panel. Only the currents which either the zonal or meridional component is larger (lower) than 2 (−2) cm s^{-1} are drawn.

radius of deformation in this region is of the same order as the model resolution (the Rossby radius ranges from 150 to 30 km from ~5°S to ~40°S for the first baroclinic mode – see Chelton et al., 1998). The choice of the medium-resolution was motivated by computational cost considerations. Medium-resolution also permits meaningful interpretation of regional sea level variability. It is worth pointing out that high-resolution models are sensitive to additional parameters such as the spatial resolution of the wind forcing and the characteristics of the open-boundary conditions. For instance, in the regional high-resolution model of Penven et al. (2005), the simulated EKE has a different pattern and amplitude depending on which climatological winds – satellite Quick-

SCAT or Reanalyses product (ERA40) – are used to force the model. Variability scales of wind forcing in this region are therefore important, and the medium-resolution model is less affected by the particular wind stress product used to force the model.

Another important limitation is the seasonal forcing of the model. Considering the non-linearity of the system (as evidenced by the substantial contribution of the 'residual' variability), rectification processes at various timescales are to be expected. For instance, ENSO drastically modifies the regional mean stratification and circulation (Blanco et al., 2002) and consequently may modulate the characteristics of the annual ETRW. Such non-seasonal processes need further investigation. The model results reported here could serve as a background material for the interpretation of simulations including interannual components.

Despite these limitations, our model results show that sea level variability at the annual period consists mostly of a one-baroclinic mode response to wind and equatorial forcing. Takahashi (2005) recently found that the annual cycle of heat content in the Peru region is mainly forced by insolation, and not by the wind stress curl. He notes however that dynamical processes may produce different regional budget characteristics. The apparent conflict between our results and Takahashi's (2005) may suggest regional air–sea coupling on the annual cycle results from compensation among large dynamical signals. For instance, Kessler et al. (1998) found that annual SST in the cold tongue was consistent with solar shortwave forcing alone, but that shortwave forcing is only important because two strong forcings cancel: in their case, cooling via increased upwelling is opposed by warming associated with Tropical Instability Waves. Whether or not the heat flux in our model region is driven by horizontal or vertical advection by the ETRW will need further examination with a medium to high-resolution coupled regional model.

The model's finding of vertically propagating energy on the annual period raises the question whether such propagation might also occur at lower frequencies, including ENSO. If so, energy originating from the equatorial regions may dissipate in the subthermocline at higher latitudes. Long-term medium to high-resolution regional model simulations should provide insight on this issue.

The SEP also contains an oxygen minimum zone (OMZ; Helly and Levin, 2004) which covers a large area off-shore Ecuador, Peru and Chile and is well-marked in the subthermocline. OMZ variability and maintenance processes are poorly understood. In view of our model results, we wonder if the ETRW participates in OMZ formation and maintenance through advection of low oxygen concentration. Interestingly, the bottom of the OMZ at 300 m is located near the zone of intense residual variability in our model (not shown), which also corresponds to the westward limit of the Rossby wave annual variability. More realistic simulation of the ESP using physical–biogeomechical coupled model should help clarify this issue.

Acknowledgements

The preparation and development of this work were made possible thanks to several stays funded by ECOS (grant #C03U05) of Y. duPenhoat, B. Dewitte, O. Pizarro and M. Ramos at PROFC (Laboratorio de Procesos Oceanográficos y Clima) and LEGOS (Laboratoire d'Etude en Géophysique et Océanographie Spatiale). Dr. O. Pizarro was also supported by CNRS (Centre National de la Recherche Scientifique) while visiting LEGOS in 2001 and 2007. O. Pizarro also thanks support from Rings of Science ACT-19 project. M. Ramos was supported by a scholarship from CONICYT (Comisión Nacional de Investigación en Ciencia y Tecnología) and a thesis scholarship (AT-4040200). This study also benefited from support of the ANR (Agence Nationale de la Recherche) within the project PCCC (Peru Chile Climate Change). Computing support for running the OGCM was provided by Institut du Développement et des Ressources en Informatique Scientifique (IDRIS). The two anonymous reviewers are thanked for their constructive comments that helped improve the paper.

Appendix A. Linear formalism for vertically propagating extra-tropical Rossby waves

As shown by Moore and Philander (1977), the linear, inviscid equations for a β-plane ($f = f_0 + \beta y$) can be separated into vertical and horizontal components. The horizontal component yields a dispersion relation for standing wave modes in the meridional and horizontal directions

$$\omega = \frac{-\beta k}{k^2 + l^2 + f_0^2/c_n^2} \tag{A.1}$$

where l and k are the meridional and zonal wavenumbers, respectively, ω the frequency, f_0 the Coriolis parameter at some latitude (y_0) and c_n the separation constant of the vertical structure equation:

$$\frac{d}{dz}\left(\frac{d\Psi_n}{dz}\cdot N^{-2}\right) + \Psi_n c_n^{-2} = F_l \tag{A.2}$$

N is the local Brunt–Vaïsälä (or buoyancy) frequency. F_l is the projection of the forcing onto the latitudinal mode l under consideration. It is usually assumed to be zero below a certain depth close to the surface (Lighthill, 1969). Thus, the vertical structure function Ψ_n is solution of the homogeneous equation with the boundary conditions:

$$\frac{d\Psi_n}{dz} + \frac{N^2}{g}\Psi_n = 0 \quad \text{at } z = 0$$
$$\frac{d\Psi_n}{dz} = 0 \quad \text{at } z = -H \quad (H \text{ is the depth of the ocean bottom})$$

From the vertical equation a local vertical wavenumber can be defined: $m_n(x,z) = \frac{N(x,z)}{c_n(x)}$.

We now consider a motion which is the combination of the solutions of the different vertical modes for a specified l and call m the local vertical wavenumber. It is then interesting to describe the solution as if the vertical scale m^{-1} of the wave was small compared with the scale on which m varies (WKB approximation). (A.1) is then a relation between ω, m and k which can be differentiated to estimate group velocities. In this study, we consider only long zonal wavelengths. In this limit ($k^2 + l^2 \approx 0$), the dispersion relation reduces to:

$$\omega = -\frac{\beta k c_n^2}{f_0^2} \tag{A.3}$$

Given the wave frequency and phase speed, the trajectory that defines wave energy propagation can be obtained by integrating two ordinary differential equation: $\frac{dx}{dt} = C_{ng}^x = \frac{\partial\omega}{\partial k}$ and $\frac{dz}{dt} = C_{ng}^z = \frac{\partial\omega}{\partial m}$. The slope of ray paths in the (x,z) plane becomes:

$$\frac{dz}{dx} = \frac{2k}{m} = \frac{2kc_n}{N} \tag{A.4}$$

Therefore, the wave energy originating at the surface propagates downward towards the west with steeper slope for weaker stratification or lower latitude. Fig. A1 presents the theoretical trajectories for the annual period at various latitudes and for a mean stratification taken from the model (CR). With the definition of the phase propagation in the zonal and vertical directions, and because the dispersion relation is non-dispersive in the long zonal wavelength limit, phase lines are parallel to WKB ray paths. This wave propaga-

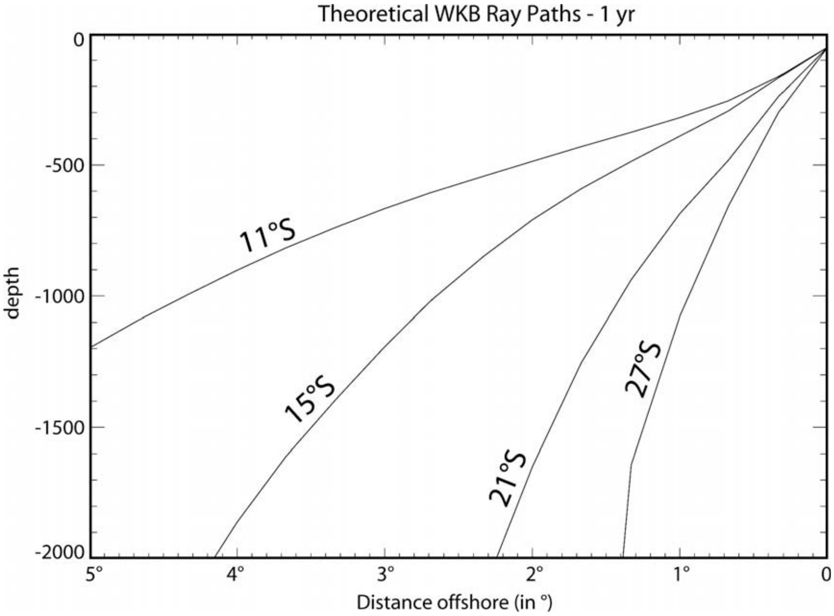

Fig. A1. Theoretical WKB trajectories for the annual period at 11°S, 15°S, 21°S and 27°S. The mean Brunt–vaïsälä frequency of the model and the mean between the first and second baroclinic mode phase speed were used to derive the local slope of the trajectories.

tion provides a mechanism by which low-frequency energy generated by surface wind is transmitted into the deep ocean.

References

Bentamy, A., Quilfen, Y., Gohin, F., Grima, N., Lenaour, M., Servain, J., 1996. Determination and validation of average wind fields from ERS-1 scatterometer measurements. Global Atmos. Ocean Syst. 4, 1–29.

Blanco, J.L., Thomas, A.C., Carr, M.-E., Strub, P.T., 2002. Hydrographic conditions off northern Chile during the 1996–1998 El Niño and La Niña events. J. Geophys. Res. 107 (C3), 89–90. doi:10.1029/2001.JC001002.

Carr, M.-E., 2002. Estimation of potential productivity in eastern boundary currents using remote sensing. Deep Sea Res. Pt. II 49, 59–80.

Cerovecki, I., de Szoeke, R., 2006. Initially forced long planetary waves in the presence of nonzonal mean flow. J. Phys. Oceanogr. 36, 507–525.

Chaigneau, A., Pizarro, O., 2005. Mean surface circulation and mesoscale turbulent flow characteristics in the eastern South Pacific from satellite tracked drifters. J. Geophys. Res. 110 (C5), C05014. doi:10.1029/2004JC002628.

Chelton, D.B., Schlax, M.G., 1996. Global observations of oceanic Rossby waves. Science 272, 234–238.

Chelton, D.B., deSzoeke, R.A., Schlax, M.G., Naggar, K.El., Siwertz, N., 1998. Geographical variability of the first-baroclinic Rossby radius of deformation. J. Phys. Oceanogr. 28, 433–460.

Clarke, A.J., Shi, C., 1991. Critical frequencies at ocean boundaries. J. Geophys. Res. 96, 10731–10738.

ColindeVerdiere, A., Tailleux, R., 2006. The interaction of a baroclinic mean flow with long Rossby waves. J. Phys. Oceanogr. 35, 865–879.

Conkright, M.E., Locarnini, R.A., Garcia, H.E., O'Brien, T.D., Boyer, T.P., Stephens, C., Antonov, J.I., 2002. World Ocean Atlas 2001: Objective Analyses, Data Statistics, and Figures. NOAA, Silver Spring, MD (CD-ROM).

de Boyer Montégut, C., Madec, G., Fischer, A.S., Lazar, A., Iudicone, 2004. Mixed layer depth over the global ocean: an examination of profile data and a profile-based climatology. J. Geophys. Res. 109, C12003. doi:10.1029/2004JC002378.

deSzoeke, R.A., Chelton, D., 1999. The modification of long planetary waves by homogeneous potential vorticity layers. J. Phys. Oceanogr. 29, 500–511.

Dewitte, B., 1998. Rôle de la structure verticale de l'océan sur la variabilité basse fréquence du Pacifique tropical. Ph.D. Thesis, University of Toulouse, 237 pp.

Dewitte, B., Reverdin, G., 2000. Vertically propagating annual and interannual variability in an OGCM simulation of the tropical Pacific in 1985–1994. J. Phys. Oceanogr. 30, 1562–1581.

Dewitte, B., Reverdin, G., Maes, C., 1999. Vertical structure of an OGCM simulation of the equatorial Pacific Ocean in 1985–1994. J. Phys. Oceanogr. 29, 1542–1570.

Eliassen, A., Palm, E., 1960. On the transfer of energy in stationary mountain waves. Geofys. Publ. 22 (3), 1–23.

Helly, J.J., Levin, L.A., 2004. Global distribution of naturally occurring marine hypoxia on continental margins. Deep Sea Res. Pt. I 51, 1159–1168.

Horel, J.D., 1984. Complex principal component analysis: theory and examples. J. Climate Appl. Meteorol. 23, 1660–1673.

Huyer, A., Smith, R.L., Paluszkiewicz, T., 1987. Coastal upwelling off Peru during normal and El Niño times 1981–1984. J. Geophys. Res. 92, 14297–14307.

Huyer, A., Knoll, M., Paluszkiewicz, T., Smith, R.L., 1991. The Peru Undercurrent: a study in variability. Deep Sea Res. 38 (Suppl. 1), 247–279.

Kalney et al., 1996. The NCEP/NCAR 40-year reanalysis project. Bull. Am. Meteorol. Soc. 74, 789–799.

Kessler, W.S., McCreary, J.P., 1993. The annual wind-driven Rossby wave in the subthermocline equatorial Pacific. J. Phys. Oceanogr. 23, 1192–1207.

Kessler, W.S., Rothstein, L.M., Chen, D., 1998. The annual cycle of SST in the eastern tropical Pacific, diagnosed in an ocean GCM. J. Climate 11, 777–799.

Killworth, P.D., Blundell, J.R., 1999. The effect of bottom topography on the speed of long extratropical planetary waves. J. Phys. Oceanogr. 29, 2689–2710.

Killworth, P.D., Chelton, D.B., deSzoeke, R.A., 1997. The speed of observed and theoretical long extra-tropical planetary waves. J. Phys. Oceanogr. 27, 1946–1966.

Le Traon, P.Y., Nadal, F., Ducet, N., 1998. An improved mapping method of multi-satellite altimeter data. J. Atmos. Ocean. Technol. 15, 522–534.

Lengaigne, M., Boulanger, J.-P., Menkes, C., Masson, S., Madec, G., Delecluse, P., 2002. Ocean response to the March 1997 Westerly Wind Event. J. Geophys. Res. 107 (C11). doi:10.1029/2001JC000841.

Levitus, S., Boyer, T.P., Conkright, M.E., O'Brien, T., Antonov, J., Stephens, C., Stathoplos, L., Johnson, D., Gelfeld, R., 1998. World Ocean Database 1998, vol. 1: Introduction. NOAA Atlas NESDIS 18. US Government Printing Office, Washington, DC.

Lighthill, M.J., 1969. Dynamical response of the Indian Ocean to the onset of the southwest monsoon. Philos. Trans. Roy. Soc. London, Ser. A 265, 45–92.

Madec, G., Delecluse, P., Imbard, M., Lévy, C., 1998. OPA 8.1 Ocean General Circulation Model reference manual. Note du Pôle de Modélisation, Institut Pierre-Simon Laplace, No. 11, 99 pp.

McCreary, J.P., 1981. A linear stratified ocean model of the Coastal Undercurrent. Philos. Trans. R. Soc. Lond. 302A, 385–413.

McCreary, J., 1984. Equatorial beams. J. Mar. Res. 42, 395–430.

Moore, D., Philander, S., 1977. Modelling the tropical ocean circulation. Sea 6, 319–361.

Penven, P., Pasapera, J., Tam, J., Echevin, V., 2005. Mean circulation, seasonal cycle and mesoscale dynamics of the Peruvian Upwelling System: a modelling approach. J. Geophys. Res. 110, C10021. doi:10.1029/2005JC002945.

Pizarro, O., Montecinos, A., 2004. Interdecadal variability of the thermocline along the west coast of South America. Geophys. Res. Lett. 31, L20307.

Pizarro, O., Clarke, A.J., Gorder, S.V., 2001. El Niño sea level and currents along the South American coast: comparison of observations with theory. J. Phys. Oceanogr. 31, 1891–1903.

Pizarro, O., Shaffer, G., Dewitte, B., Ramos, M., 2002. Dynamics of seasonal and interannual variability of the Peru–Chile Undercurrent. Geophys. Res. Lett. 29 (12). doi:10.1029/2002GL014790.

Qiu, B., Miao, W., Muller, P., 1997. Propagation and decay of forced and free baroclinic Rossby waves in off-equatorial oceans. J. Phys. Oceanogr. 27, 2405–2417.

Ramos, M., Pizarro, O., Bravo, L., Dewitte, B., 2006. Seasonal variability of the permanent thermocline off northern Chile. Geophys. Res. Lett. 33, L09608. doi:10.1029/2006GL025882.

Reynolds, R.W., Smith, T.M., 1994. Improved global sea surface temperature analyses. J. Climate 7, 929–948.

Roden, G.I., 1962. Oceanographic aspects of the eastern equatorial Pacific. Geophys. Int. 2, 77–92.

Shaffer, G.O., Pizarro, L., Djurfeldt, S., Salinas, Rutlland J., 1997. Circulation and low-frequency variability near the Chilean coast: remotely forced fluctuations during the 1991–1992 El Niño. J. Phys. Oceanogr. 27, 217–235.

Shaffer, G.S., Hormazabal, O., Pizarro, Salinas, S., 1999. Seasonal and interannual variability of currents and temperature off central Chile. J. Geophys. Res. 104 (C12), 29951–29961.

Silva, N., Neshyba, S., 1979. On the southernmost extension of the Perú–Chile Undercurrent. Deep Sea Res. 26, 1387–1393.

Stammer, D., 1997. Global characteristics of ocean variability estimated from regional TOPEX/POSEIDON altimeter measurements. J. Phys. Oceanogr. 27 (8), 1743–1769.

Strub, P.T., Mesias, J.M., Montecino, V., Rutllant, J., Salinas, S., 1998. Coastal ocean circulation off western South America. In: Robinson, A.R., Brink, K.H. (Eds.), The Sea, vol. 11. John Wiley, New York, pp. 273–313.

Tailleux, R., McWilliams, J.C., 2001. The effect of bottom pressure decoupling on the speed of extratropical, baroclinic Rossby waves. J. Phys. Oceanogr. 31, 1461–1476.

Takahashi, K., 2005. The annual cycle of heat content in the Peru Current region. J. Climate 18 (23), 4937–4954.

Thompson, L.K., Kelly, A., Darr, D., Hallberg, R., 2002. Buoyancy and mixed layer effects on the Sea Surface Height Response in an isopycnal model of the North Pacific. J. Phys. Oceanogr. 32, 3657–3670.

Vazquez, J., Tran, A., Sumagaysay, R., Smith, E.A., Hamilton, M., 1995. NOAA/NASA AVHRR oceans pathfinder sea surface temperature data set user's guide version 12. JPL Technical Report, p. 55.

Vega, A., duPenhoat, Y., Dewitte, B., Pizarro, O., 2003. Equatorial forcing of interannual Rossby waves in the South eastern Pacific. Geophys. Res. Lett. 30 (5), 1197–1200.

Weare, B.C., Nasstrom, J.S., 1982. Examples of extended empirical orthogonal function analysis. Mon. Weath. Rev. 110, 481–485.

Wunsch, C., 1997. The vertical partition of oceanic horizontal kinetic energy. J. Phys. Oceanogr. 27, 1770–1794.

Wyrtki, K., 1963. The horizontal and vertical field of motion in the Peru Current. Bull. Scripps Inst. Oceanogr. Univ. Calif. 8 (4), 313–346.

Xie, P., Arkin, P.A., 1996. Analysis of global monthly precipitation using gauge observations, satellite estimates, and numerical model predictions. J. Climate 9, 840–858.

Yeager, S.G., Large, W.G., 2004. Late-winter generation of spiciness on subducted isopycnals. J. Phys. Oceanogr. 34, 1528–1547.

Progress in Oceanography 79 (2008) 138–155

Contents lists available at ScienceDirect

Progress in Oceanography

journal homepage: www.elsevier.com/locate/pocean

1997–1998 El Niño off Peru: A numerical study

F. Colas *, X. Capet, J.C. McWilliams, A. Shchepetkin

Institute of Geophysics and Planetary Physics, University of California, Los Angeles, CA 90095-1567, USA

ARTICLE INFO

Article history:
Accepted 14 October 2008
Available online 21 October 2008

Keywords:
Regional ocean modeling
El Niño phenomena
Eastern-boundary currents
Upwelling
Peru

ABSTRACT

An eddy-resolving numerical simulation for the Peru–Chile system between 1993 and 2000 is analyzed, mainly for the 1997–1998 El Niño. Atmospheric and lateral oceanic forcings are realistic and contain a wide range of scales from days to interannual. The solution is validated against altimetric observations and the few in situ observations available. The simulated 1997–1998 El Niño closely resembles the real 1997–1998 El Niño in its time sequence of events. The two well-marked, sea-level peaks in May–June and November–December 1997 are reproduced with amplitudes close to those observed. Other sub-periods of the El Niño seem to be captured adequately. Simple dynamical analyses are performed to explain the 1997–1998 evolution of the upwelling in the model. The intensity of the upwelling appears to be determined by an interplay between alongshore, poleward advection (related to coastal trapped waves) and wind intensity, but also by the cross-shore geostrophic flow and distribution of the water masses on a scale of 1000 km or more (involving Rossby waves westward propagation and advection from equatorial currents). In particular, the delay of upwelling recovery until fall 1998 (i.e., well after the second El Niño peak) is partly due to the persistent advection of offshore stratified water toward the coast of Peru. Altimetry data suggest that these interpretations of the numerical solution also apply to the real ocean.

1. Introduction

As widely documented in the literature, the El Niño phenomenon has dramatic consequences off the Americas and most particularly in the currents of the Peru–Chile system (PCS) (Strub et al., 1998). Major observational efforts have been deployed to understand the processes at work because of the implications for the ecosystem (Barber and Chavez, 1983), fisheries activity and global climate.

Data obtained for the 1997–1998 El Niño provides a partial picture of the PCS and the changes it went through during this period. It is only partial because in situ observations are condemned to be sparse in time and space and because satellites have a limited view of the subsurface. In this context there is a great need for models to fill the gaps, and many models have, in fact, been developed to understand more fully the PCS functioning. Besides the pioneering work done on the upwelling dynamics in the 1970s and early 1980s, most of the PCS models have focused on the poleward propagation of coastally-trapped waves using linear models. The main reason for this focus is that coastal wave activity alone explains to some degree the intraseasonal variability (Brink, 1982; Ramos et al., 2006), interannual variability (Shaffer et al., 1997; Pizarro et al., 2002), and even lower frequency variability (Clarke and Lebedev, 1999; Pizarro et al., 2001, 2002), at least nearshore. On the other hand, there are indications that the response of the PCS to El Niño conditions simply cannot be fully understood with such coastally-trapped waves models no matter how well they reproduce the sea-level and alongshore-flow fluctuations. In particular, they ignore the Ekman flow modulation that arises from changes in wind patterns during El Niño (Strub et al., 1998). Also onshore flows are known for not being well captured by linear coastally-trapped wave models (Brink, 1982). Observational evidence of the importance of onshore flows is reported by Huyer et al. (1987) for the 1982–1983 El Niño off Peru. More recently, eddy-resolving primitive-equation models have been applied to different sectors of the PCS (Leth and Shaffer, 2001; Leth and Middleton, 2004; Penven et al., 2005). These studies focused on seasonal cycles. The only primitive-equation modeling study we know of that deals with PCS interannual variability is Mesias et al. (2003), but it only incorporates the variability due to the wind. The present work extends that of Penven et al. (2005); it includes the equatorial variability, partly through the boundary conditions and partly explicitly. We use the Regional Oceanic Modeling System (ROMS) to simulate the PCS dynamics over most of the 1990s with realistic atmospheric forcing and boundary conditions provided by a state-of-the-art oceanic general circulation model (OGCM) solution.

Our regional solution is analyzed for its 1997–1998 El Niño period. Special emphasis is put on validation, mainly using sea-level anomalies (SLA) measured from altimeters, and the realism of coastal wave activity in the model is also assessed (Section 3). A qualitative evaluation of the model in terms of subsurface changes undergone by the central Peru upwelling between June 1997 and

---

* Corresponding author.
E-mail address: francois@atmos.ucla.edu (F. Colas).

0079-6611/$ - see front matter © 2008 Elsevier Ltd. All rights reserved.
doi:10.1016/j.pocean.2008.10.015

June 1998 is presented in Section 4. In particular, we define and discuss the succession of stages that characterizes the 1997–1998 El Niño (including the two well-marked sea-level peaks described by Strub and James (2002) using altimetry data): the first peak (P1, May–June 1997); the aftermath of P1 (July–August 1997); the relaxation interval between P1 and P2 (September–October 1997); the second peak (P2, November–December 1998); the aftermath of P2 (January–April 1998); and the recovery from El Niño (May 1998 and afterward). This particular sequencing is devised for our solution analysis, but it approximately coincides with those put forward to describe previous observational analyses (Carr et al., 2002; Blanco et al., 2002). Dynamical analyses show the nature of the complex thermohaline and circulation changes brought about during El Niño. Most importantly we quantify the role played by the alongshore pressure gradient off the Peruvian shelf in counteracting the Ekman transport by driving onshore flow (Section 5). This component of the flow is poorly explained by coastal wave activity alone, and we offer an alternative conceptual model for the thermohaline and circulation evolution over the whole El Niño period (Section 6). In Section 7, a complementary view is given on the effects that geostrophic onshore flow can have on the Peruvian ecosystem. A brief summary is in Section 8.

2. Model set-up

2.1. ROMS hydrodynamic model

The numerical simulations are performed using the Regional Oceanic Modeling System (ROMS; Shchepetkin and McWilliams, 2005). The configuration encompasses a large domain from 15°N to 41°S and from 100°W to the South American coast with open-boundary conditions at its western and southern edges. The open-boundary conditions (Marchesiello et al., 2001) are treated using a combination of an Orlanski scheme for the tracers and baroclinic velocities and a Flather scheme for the barotropic mode. ROMS solves the hydrostatic primitive equations using terrain-following curvilinear vertical coordinates. We use 30 vertical levels stretched toward the surface so that roughly 20 levels cover the first 200 m of the water column over the continental slope at 1500 m depth (vertical stretching parameters are $\theta_s = 6.5$, $\theta_b = 0$, and $T_{\text{cline}} = 10$ m in the notation of Song and Haidvogel (1994)). The bottom topography is interpolated from the Etopo2 database (Smith and Sandwell, 1997) and, to reduce the pressure gradient computation errors, it is smoothed (analogous to Marchesiello et al., 2003) to satisfy the condition $\delta h/h < 0.18$ (Beckman and Haidvogel, 1993). Subgrid-scale vertical mixing is parameterized using the KPP boundary layer formulation (Large et al., 1994).

The configuration is designed taking into consideration several factors. The domain extent allows us to explicitly represent the processes and currents that connect the Peru–Chile system (PCS) with the eastern equatorial Pacific. The premise is that signals of equatorial origin are essential for the functioning of the PCS, in particular coastal waves that can propagate as far south as 35°S along the South American coastal wave guide. The horizontal resolution of $\sim$7.5 km (1/15°) is sufficient to resolve these coastal waves and, more generally, mesoscale processes, given Rossby radii that range from $\sim$200 km in the northern part of the domain down to 25 km in the south (Chelton et al., 1998).

2.2. Model spin-up

The model solution is spun-up for 5 years starting from the Levitus climatology as initial conditions and with climatological atmospheric forcing (ERS for wind stress and COADS for heat and freshwater flux, with a weak restoring toward climatological SST and sea surface salinity; Barnier et al., 1995). Boundary conditions are also climatological from the SODA reanalysis (Carton and Giese, 2008). These forcings are consistent with those used to run the interannual experiment (Section 2.3). The final state of this spin-up is used as the initial condition for the interannual experiment. Little adjustment occurs when restarting with the non-climatological forcing, but we discard the first year (1992) in the analysis. Hereafter, we refer to the interannual solution as RIPC7 (ROMS Interannual Peru–Chile with a 7.5 km horizontal grid resolution).

2.3. Atmospheric forcing

RIPC7 is run from January 1992 to January 2000 using weekly ERS1 and ERS2 scatterometer winds (Bentamy et al., 1996). The 1° resolution ERS wind stress is linearly interpolated onto the model grid. A coastal extrapolation described in Capet et al. (2008) is performed where no data is acquired by the scatterometer, i.e., within 50–100 km from the shore. ERS is chosen because, coastal data gaps aside, it provides well validated accurate wind fields (Quilfen et al., 2000) and was the only scatterometer flying in 1997–1998. The choice of air–sea heat fluxes to force the model is more problematic. Both steep topographies (the Andes are responsible for spurious oscillations in spectral models such as NCEP; Large and Danabasoglu, 2006) and subtle ocean–atmosphere coupling (e.g., the functioning of the extensive stratus cloud deck in the PCS has yet to be fully understood; see VOCALS project http://www.eol.ucar.edu/projects/vocals/) lead to large uncertainties in the heat flux estimates. Forced with NCEP heat fluxes, the model exhibits a climatological 2–3 °C warm bias in SST off southern Peru and northern Chile (not shown). The solution we present is forced with heat fluxes interpolated from the COADS climatology (Da Silva et al., 1994). It yields a much better agreement with SST climatologies. Consequently, the only source of variability (interannual or synoptic) in heat flux forcing comes from the restoring term based on the difference between the model and observed SST (Barnier et al., 1995). For the latter, we rely on the weekly AVHRR-Pathfinder product (http://podaac.jpl.nasa.gov/sst/). The treatment of freshwater is similar but cruder since the observed sea surface salinity used for the restoring is the climatological product from COADS (Da Silva et al., 1994). This means that, for example, the change in rainfall patterns during the El Niño 1997–1998 is not represented.

2.4. Downscaling the Pacific circulation

To study the regional consequences of basin-scale climate changes and the El Niño 1997–1998 event in particular, we do not simulate the whole Pacific but rely on information from an OGCM that is passed on to our regional configuration through the open-boundary conditions. In the solution we present here, the boundary information is extracted offline from a POP-CCSM solution. POP-CCSM is similar to the solution labeled "x1ocn" in Large and Danabasoglu (2006) except that its atmospheric forcing (Large and Yeager, 2004) has interannual variability (and diurnal cycle). Toward the equator POP-CCSM has a horizontal resolution of less than 0.5° in the meridional direction (1° in the zonal direction) to ensure that the system of equatorial currents can be resolved.

A key requirement for this approach is that the open-boundary conditions must input the climate signal to be downscaled. Our boundary conditions are updated every 4 days (the time interval between two POP-CCSM output files) so that equatorial Kelvin waves with frequencies in the intraseasonal band (periods from 50 to 70 days) are transmitted into the regional model. Equatorial wave activity is known to be an essential component of equatorial variability including at the interannual time scale (Kessler and

McPhaden, 1995; Kessler et al., 1995). These equatorial waves trigger coastal waves that propagate poleward along the South American coast (Shaffer et al., 1997). Preliminary simulations with only monthly-varying boundary conditions yielded an overly weak 1997–1998 El Niño, e.g., in SLA (Section 3). Most importantly, POP-CCSM realistically reproduces the evolution of the equatorial thermohaline structure and circulation. Fig. 1 shows a comparison of temperature and zonal velocity between POP-CCSM and the TAO measurements[1] at 110°W, i.e., 10° to the west of our open boundary. Although the POP-CCSM thermocline is too diffuse (a bias commonly seen in OGCMs) the time variability is well captured. The thermocline deepening corresponding to the two 1997–1998 El Niño peaks is approximately the right amplitude and so is the relaxation between them. (Looking closely, notice that the second peak appears to not reach deep enough, and the POP-CCSM evolution seems smoother than of the data; e.g., the sharpness of the two main observed peaks.) The termination phase cannot be assessed at 110°W because the data are missing, but at 95°W good agreement is generally observed, especially during the first half of 1998 (even the weaker third peak in May 1998 – also reported by Carr et al. (2002) – is present in POP-CCSM, albeit weaker than in the data). POP-CCSM shows some skill at reproducing the observed zonal velocities and, in particular, the timing and intensity of the two eastward pulses that correspond to the main El Niño peaks (P2 is centered at greater depths than P1), and it also reproduces the westward currents in winter 1997 and in early 1998. Two notable deficiencies are the weaker-than-observed eastward velocity that prevails through most of 1998 and the systematic westward flow bias near the surface.

3. Sea-level anomaly and coastal wave activity in the Peru–Chile system

3.1. Sea-level evaluation

As a first assessment of RIPC7 realism we compare SLA from our interannual solution to SLA maps derived from satellite altimetric measurements.[2] SLA provides valuable information because of its high spatial and temporal coverage. On the other hand, the SLA has some limitations that need to be kept in mind during this evaluation exercise: most important are the nearshore data gaps and large uncertainty in shallow waters. In addition, the SLA-gridded product we use (DUACS; Ducet et al., 2000) has a nominal resolution of 1/3°. For these reasons caution is required when considering coastal waves whose amplitude is expected to decay exponentially away from the shelf on a scale equal to the first deformation radius.

Fig. 2 shows RIPC7 and DUACS SLAs in a time–latitude diagram, along a line running parallel to the coast 35 km offshore, i.e., far enough at most latitudes to trust the DUACS data. The main characteristics and sequence of events associated with the 1997–1998 El Niño are clearly reproduced in RIPC7 (see also Strub and James, 2002 for a description of the events using altimetry measurements). The simulated July and December peaks have the correct timing and are only slightly weaker (by less than 25%) in amplitude than the observations. Note though that the magnitude of the simulated first peak is closer to the observations and is thus of a strength comparable to the second peak, whereas the first peak is weaker than the second observed one, as also confirmed by tide-gauge measurements (Blanco et al., 2002 and see below). We attribute this model bias to the boundary information at the equator because Fig. 1 suggests that the second peak in POP is weaker than in the observations. The relaxation interval between the two peaks is realistically simulated. More generally, RIPC7 captures the main interannual signals such as the mild El Niño in 1993 and the La Niña conditions that start in mid-1998. For the period 1994–1997, where weak SLAs prevail, the model-data agreement is less clear.

In Fig. 3, we show monthly averaged SLA maps from RIPC7 and DUACS for the months of May and June 1997 (at and shortly after the arrival of the SLA first peak; Fig. 2) and December 1997 (when the SLA second peak has reached its maximum intensity). Notice first the good model-data correspondence in terms of large scale patterns and amplitudes for all three months: the equatorial patch of a large SLA has the correct extension. Toward the south, a positive SLA tends to be increasingly confined nearshore, and this is also nicely captured in RIPC7, especially in May and June. Obviously, the model and data eddy fields are expected to differ since no assimilation constrains their phase correspondence. However, RIPC7 correctly generates a preponderance of anticyclones and some of them (off the main capes and headlands such as Paracas at 14°S) seem to correspond to eddies present in DUACS. One apparent discrepancy is a too strong SLA along central Chile compared to DUACS where the coastal signal is weaker and more broken up; on the other hand, there is no evident amplitude discrepancy in the comparison with coastal tide-gauges in this region (Fig. 4).

DUACS's nearshore SLA needs to be taken cautiously, however, and we perform a complementary evaluation with four tide-gauge records for Paita (5°05′, northern Peru), Callao (12°03′, central Peru), Arica (18°28′, northern Chile), and Caldera (27°04′, central Chile). Daily data were obtained from UHSLC (http://uhslc.soest.hawaii.edu/) and low-passed filtered to be compared with model output, using a Lanczos filter with a 3-day cut-off and 15-day window. Unavoidable sources of model/data discrepancies include the fact that, with ROMS C-grid discretization, sea level at 1/2 grid cell from the coast has to be used as a proxy for coastal sea level; in reality nearshore processes unresolved by our solution might alter the signal somewhat. Despite this caveat, the model-data agreement is good with a rms error (averaged from the four tide-gauges) of 0.05 m over the period 1994–1999 and of 0.03 m if the 1997 El Niño maximum is discarded[3] (Fig. 4). Most importantly the two El Niño peaks have good timing and amplitudes, although the December–January 1997–1998 SLA is underestimated by 20–30% (also noticed in the comparison with DUACS), and some high-frequency peaks are weaker in the model than in the observations. Finally, the signal attenuation going from north to south is also correctly represented in the model with 50% and 40% reductions for the May–June 1997 and December–January 1998 SLA between Paita and Caldera. This statement should be qualified with respect to Fig. 2 that suggests a lack of SLA attenuation in the model around 17°S.

Overall, RIPC7's SLA shows a considerable resemblance to the data, and this gives us some confidence in the realism of the solution because, on scales of the order of the baroclinic Rossby radius, the SLA tends to reflect upper-ocean, depth-integrated thermohaline anomalies (Stammer, 1997). Assessment of the simulated subsurface circulation and thermohaline structure (Section 4.1) tends to reinforce this conclusion.

3.2. Coastal wave activity during El Niño

It is now well established that equatorial variability on a wide range of scales transmits as coastal trapped waves (CTWs) when reaching the eastern end of the Pacific (or other basins). CTWs thus

---

[1] TAO data shown in Fig. 1 were plotted with the TAO Project Office data display interface (http://www.pmel.noaa.gov/tao/realtime.html).

[2] Although there is good agreement; we do not show model-data SST comparisons because satellite SST is partly assimilated in the model through the heat flux restoring term (Section 2.3).

[3] The largest rms error is found at the Arica tide-gauge location with 0.06 m over the period 1994–1999 and 0.05 m if the El Niño maximum is discarded.

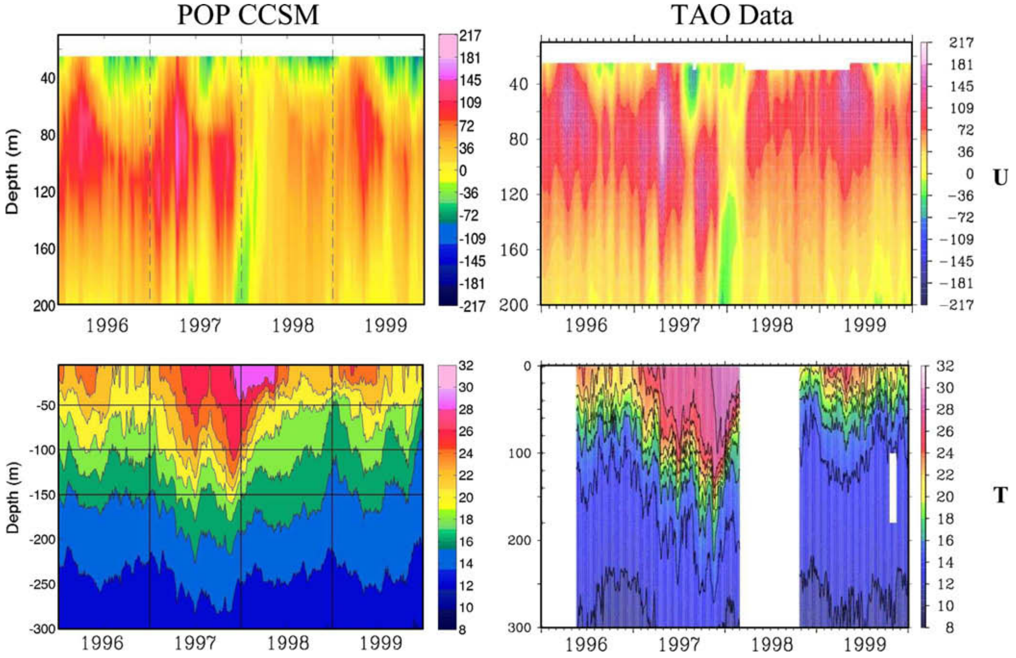

Fig. 1. Zonal velocity U [m s^{-1}] (top) and temperature T [°C] (bottom) time–depth diagram for the POP-CCSM solution (left) and TAO array observations (right) at 110°W at the equator. The white patches indicate missing data, and the model plot for velocity is masked accordingly.

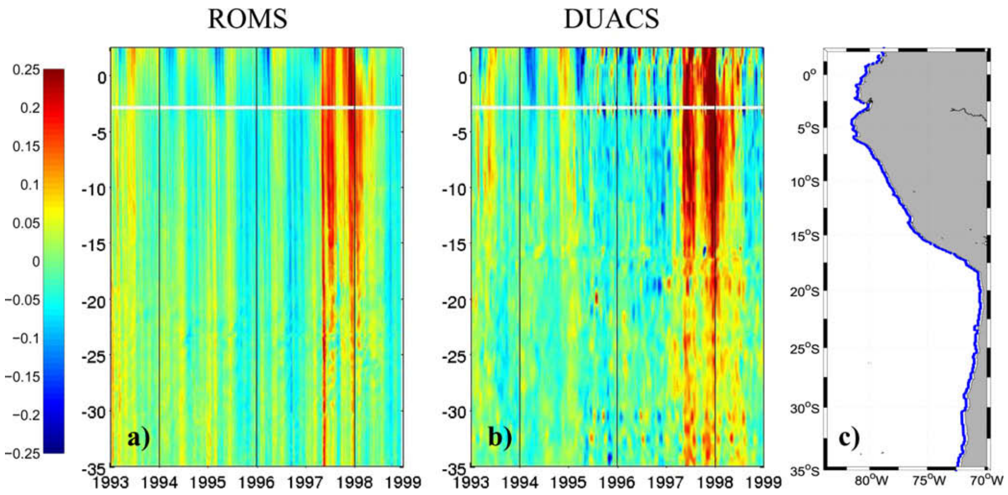

Fig. 2. Time–latitude diagrams of SLA [m] along the west coast of South America from (a) ROMS and (b) DUACS; (c) line where the data are taken, following the coast 35 km offshore.

generated subsequently propagate poleward (Shaffer et al., 1997). Along the west coast of the Americas, the water-mass changes related to El Niño are primarily thought to occur through poleward water-mass advection by the currents accompanying coastal waves (Blanco et al., 2002), especially in the range 50–70 days^{-1}, but also at lower frequencies.

As evident from Fig. 4 the model does not generally follow the tide-gauge signals at high frequency, except in rare instances such as the major SLA pulse in May 1997. On the other hand, the model coastal dynamics is consistent with the description above. Indeed, coastal SLAs spectra have a marked peak at 50–70 days^{-1} that can be traced back into POP but cannot be explained by local wind variability (Fig. 5; on the other hand, the peak at a period of 40 days could be associated with local wind forcing). In addition, subsurface alongshore velocities along the Peruvian Plateau exhibit fluctuations in the same frequency range; they are mainly in geostrophic balance (as expected from idealized Kelvin waves; not shown); and they are strongly correlated with SLA. To get a better sense of the oscillatory behavior associated with different frequency ranges (50–70 days^{-1} and lower frequency corresponding to the two peaks) SLA, alongshore and cross-shore velocities are high-passed or low-passed (resp.). High-pass filtered time-latitude diagrams of SLA and alongshore velocity (Fig. 6) demonstrate poleward propagation for these variables with a phase speed around 3.2 m s^{-1}, i.e., in the upper end of observed CTW phase speed range (Meyers et al., 1998) and roughly consistent with a first-baroclinic Kelvin wave speed. At lower frequency the robustness of spectral estimates is dubious but the low-pass-filtered SLA and alongshore velocity (Fig. 7) reveal again the undulatory nature of El Niño. The propagation speed is about 0.35 m s^{-1} at the 6-month period, not far off the 0.2–0.3 m s^{-1} propagation speed found by Pizarro et al. (2001) for even lower frequency signals.

An outstanding signature of El Niño is thus its underlying CTW activity, both in the high-frequency band 50–70 days^{-1} and at lower frequencies comparable to the two peaks during the event. This wave dynamics is well captured by simple linear models and has

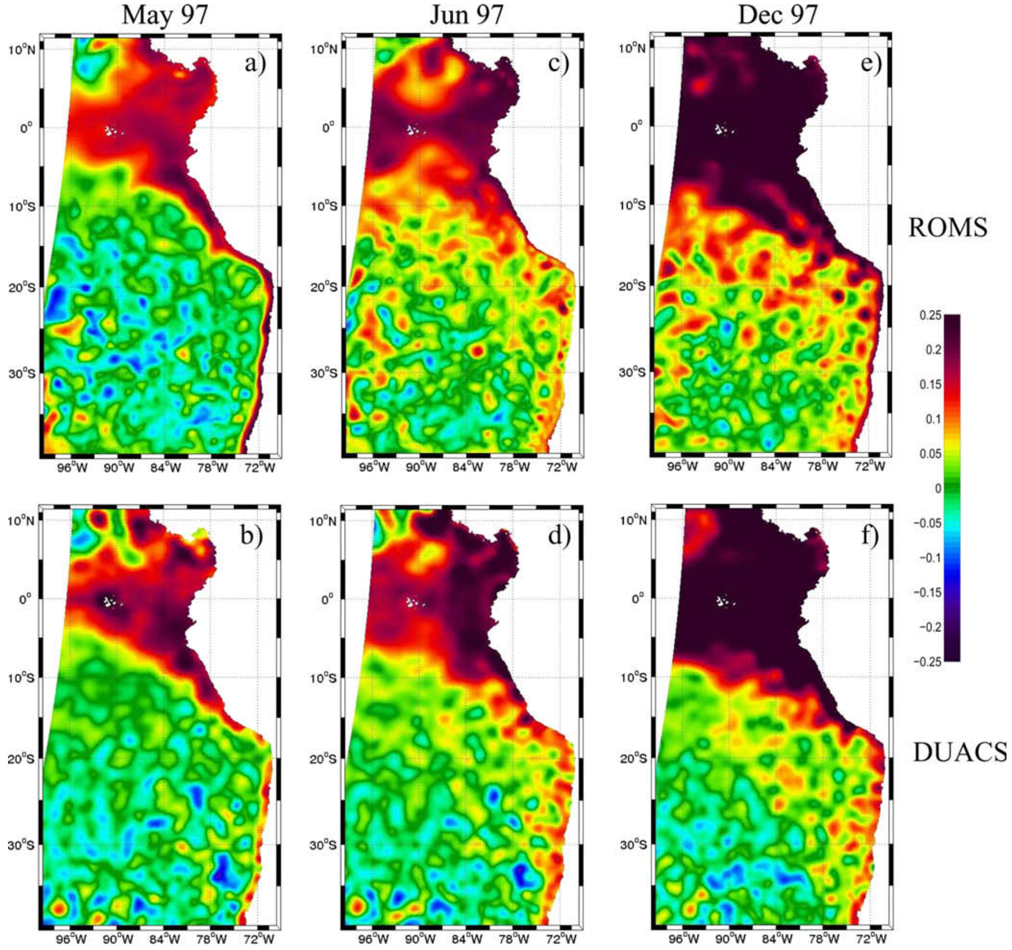

Fig. 3. Monthly mean SLA [m] for the west coast of South America for model (ROMS, top) and observations (DUACS, bottom): (a) ROMS, May 1997; (b) DUACS, May 1997; (c) ROMS, June 1997; (d) DUACS, June 1997; (e) ROMS, December 1997; (f) DUACS, December 1997. Nearly all of the model domain is shown on the maps.

been amply analyzed (Shaffer et al., 1997; Pizarro et al., 2001, 2002). It is also reproduced by RIPC7, but our primitive-equation model allows us to investigate processes going beyond this simple dynamics. On time scales long compared to individual high-frequency pulses (lasting say a few days to a couple of weeks), we expect advection and nonlinear processes to become important. In the remainder of the paper, our focus is to extract such processes from the full signal.

4. El Niño's subsurface signature in Peruvian waters

In this section, we focus on the thermohaline and currents anomalies associated with El Niño in the model. We first describe the persistent changes associated with P2 taken broadly and then examine the modulations on monthly time scales during the whole El Niño period. We focus our attention on central Peru because (1) this region undergoes the largest SLA during El Niño (Fig. 3), and (2) the coastline and the shelf break are nearly straight and run parallel to each other so that physical processes are, to a large degree, invariant alongshore (Penven et al., 2005).

4.1. Second peak

Time-averaged (over the whole second peak from mid-October to mid-February) and alongshore-averaged (from 7°S to 13°S) vertical cross-sections for temperature, Brunt-Väisälä frequency, and alongshore and cross-shore velocities are presented in Fig. 8. The corresponding model climatology between 1993 and 1999 (with 1997 and 1998 excluded) for the same months is also shown and fits the picture of the system for spring–summer (weakening upwelling-favorable winds and increasing atmospheric heat fluxes) as described in Strub et al. (1998) and Huyer et al. (1991) and also simulated by Penven et al. (2005). Upwelling is noticeable during the climatological conditions, with coastal waters around 16 °C and a 100 m upward tilt (from offshore to nearshore) of the corresponding isotherm (Fig. 8b). The water column is weakly stratified but for a thin layer around the boundary layer depth (Fig. 8d). Alongshore velocities (Fig. 8f) reveal a surface-intensified, equatorward coastal current (maximum velocities $\sim$0.20 m s^{-1}) and a Peru–Chile Undercurrent (PCU) underneath. The PCU has its core centered at a depth of 150 m over the slope, with maximum values of 0.10 m s^{-1} (comparable with the observations reported by Brink et al. (1983) and Huyer et al. (1991)), and it extends as far as 150–200 km offshore. Negative cross-shore velocities (Fig. 8h) of $\sim$0.08 m s^{-1} in the first 15–20 m are associated with offshore Ekman transport. Below, a weak onshore return flow at 0.01–0.02 m s^{-1} is present and feeds the coastal divergence.

The picture for the period October 1997–February 1998 differs in many respects. Nearshore surface temperature is 20 °C, i.e., 3 °C warmer than usual; anomalies are even larger offshore (4 °C at 250 km). Maximum subsurface temperature anomalies are still $\sim$2.5 °C at 300 m. Offshore the 60–100 m deepening of the 15 °C isotherm compared to the model climatology is consistent with observed deepenings (Grados, 1998; Sanchez et al., 2000). Except within the first 100 km nearshore, the isotherms below 100 m

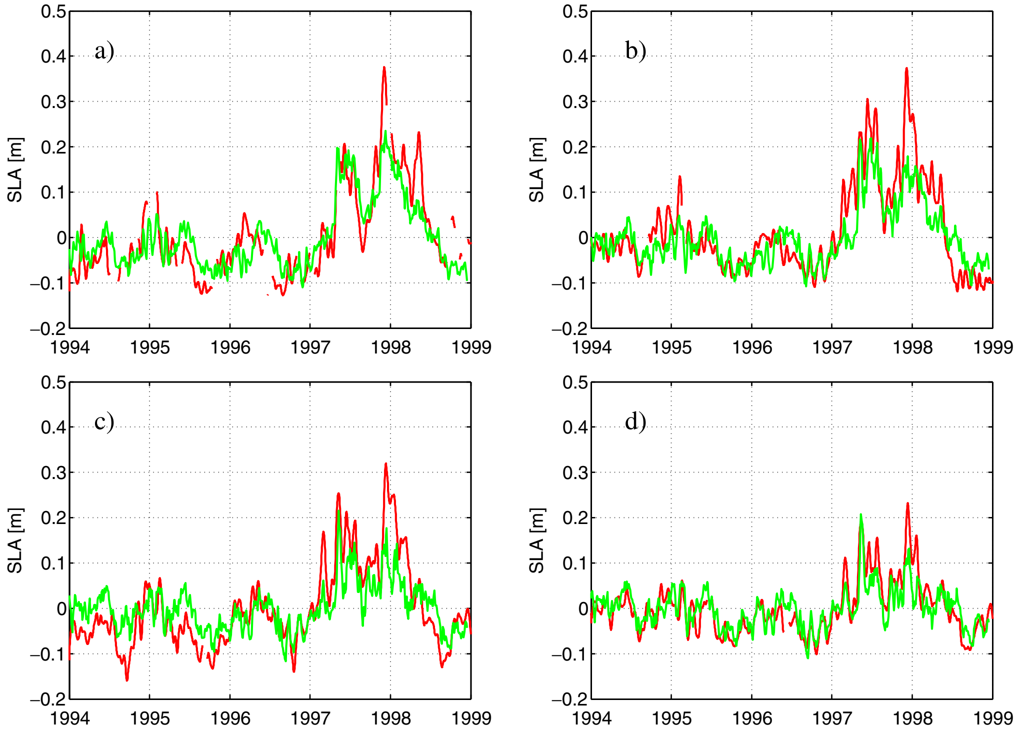

Fig. 4. Tide-gauge (red) and ROMS (green) sea-level time series at four locations along the coast from north to south: (a) Paita (5°05′S), (b) Callao (12°03′S), (c) Arica (18°28′S), (d) Caldera (27°04′S).

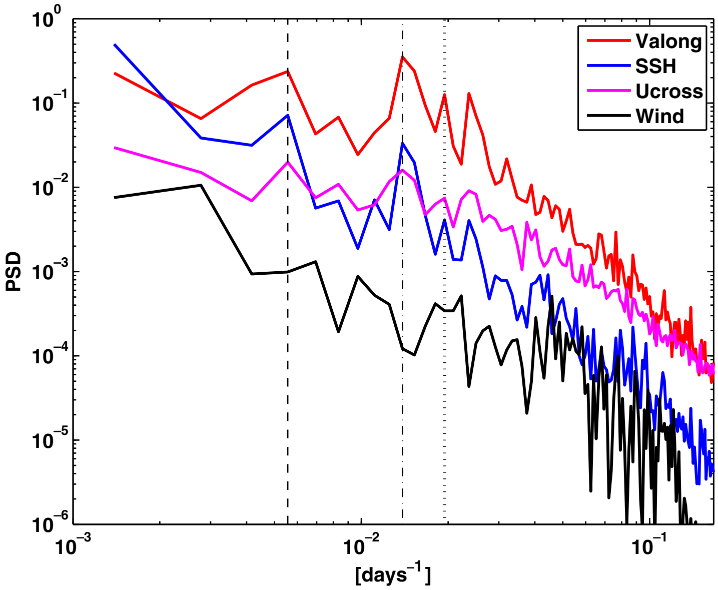

Fig. 5. Power spectra during 1997–1998 of alongshore and cross-shore velocities (150 m depth, 100 km offshore), sea level (at the same grid points) and alongshore wind (50 km offshore). Spectra are computed at every grid points between 7°S and 13°S and then averaged. Vertical lines indicate the frequencies 180 days^{-1} (dashed), 70 days^{-1} (dash-dotted) and 50 days^{-1} (dotted).

bend downward when approaching the coast. Also, the upper 100–150 m of the water column are considerably more stratified (excluding the surface boundary layer, Fig. 8c).

Currents also exhibit major changes (Fig. 8e and g). Velocities in the core of the PCU reach 0.20–0.25 m s^{-1}, in agreement with observations during previous El Niños (Smith, 1983). The poleward flow shows an offshore extension over 250 km. Also notice that the alongshore poleward flow penetrates the nearshore over the shelf, with values of 0.05–0.10 m s^{-1} at a depth around 40–50 m, and that the vertical extent of the equatorward coastal jet is consequently reduced. The lower limit of the PCU remains close to 200 m, i.e., near the zero crossing of the first-baroclinic mode. An equatorward current is underneath the PCU and centered at around 400 m depth, where the velocities are between 0.05 and 0.10 m s^{-1}; it is entirely absent from the model climatology. Although no observations exist to corroborate the existence of such a current off Peru, Kosro (2002) observed a similar equatorward current at depth off northern California during El Niño 1997–1998.

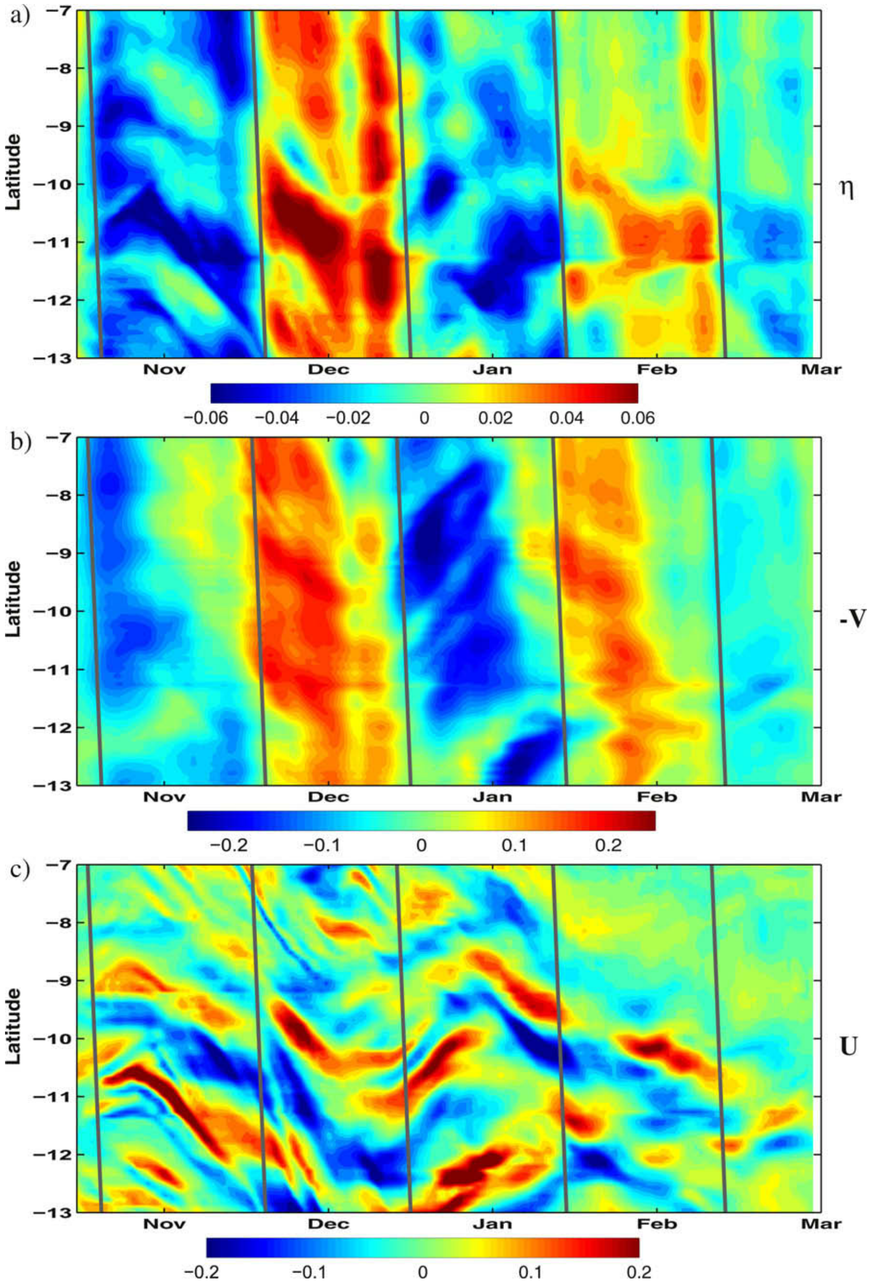

Fig. 6. Time–latitude diagrams from mid-October 1997 to March 1998 of: (a) sea level η [m], (b) negative alongshore velocity $-V$ [m s^{-1}], and (c) cross-shore velocity U [m s^{-1}]. A band-pass filter (with 80 days^{-1} and 12 days^{-1} cut-off frequencies) is applied to reduce the strong signal associated with the ENSO SLA second peak. Model output is saved every 12 h over this period to allow a better estimate of the alongshore propagation speed. Gray lines correspond to $\approx$3.2 m s^{-1}. (Alongshore velocity is averaged between 100 and 200 km offshore and 60 and 180 m depth, as in Fig. 11b.)

4.2. El Niño off Peru on monthly time scales

We now turn to the successive stages that make up the model El Niño event. These bear a close resemblance to the observed sequence, as already suggested by Figs. 2 and 3. This is readily seen in subsurface temperature in Fig. 9. Alongshore averaged temperature sections are shown that are representative of the P1 aftermath period (Fig. 9a); the relaxation interval (Fig. 9b); the P2 period (Fig. 9c); the P2 aftermath period (Fig. 9d); and the El Niño recovery (Fig. 9e). The active P1 period is not shown because it is very much like that of P2. The corresponding figures for the model climatology are shown alongside and provide a sense of the 1997–1998 anomalies.

Right after P1 the offshore temperature has changed and exhibits traits not found in the climatology for the usual conditions for that time of year: an increased stratification with a thicker thermocline and 18 °C water roughly 50 m below its normal depth (i.e., at 120 m depth versus 70 m). These offshore characteristics remain remarkably stable throughout the remainder of 1997 and early part of 1998, with signs of a return to normal only in May–June 1998 (the offshore temperature in Fig. 9e still differs significantly from the climatology Fig. 9j) and with some cooling in the boundary layer (the upper 50 m) in winter 1997 (Fig. 9b). In particular the seasonal cycle, so visible in the climatology, is completely overwhelmed.

As one looks closer to shore and especially over the slope, more variability is observed because the tilt of the thermocline due to

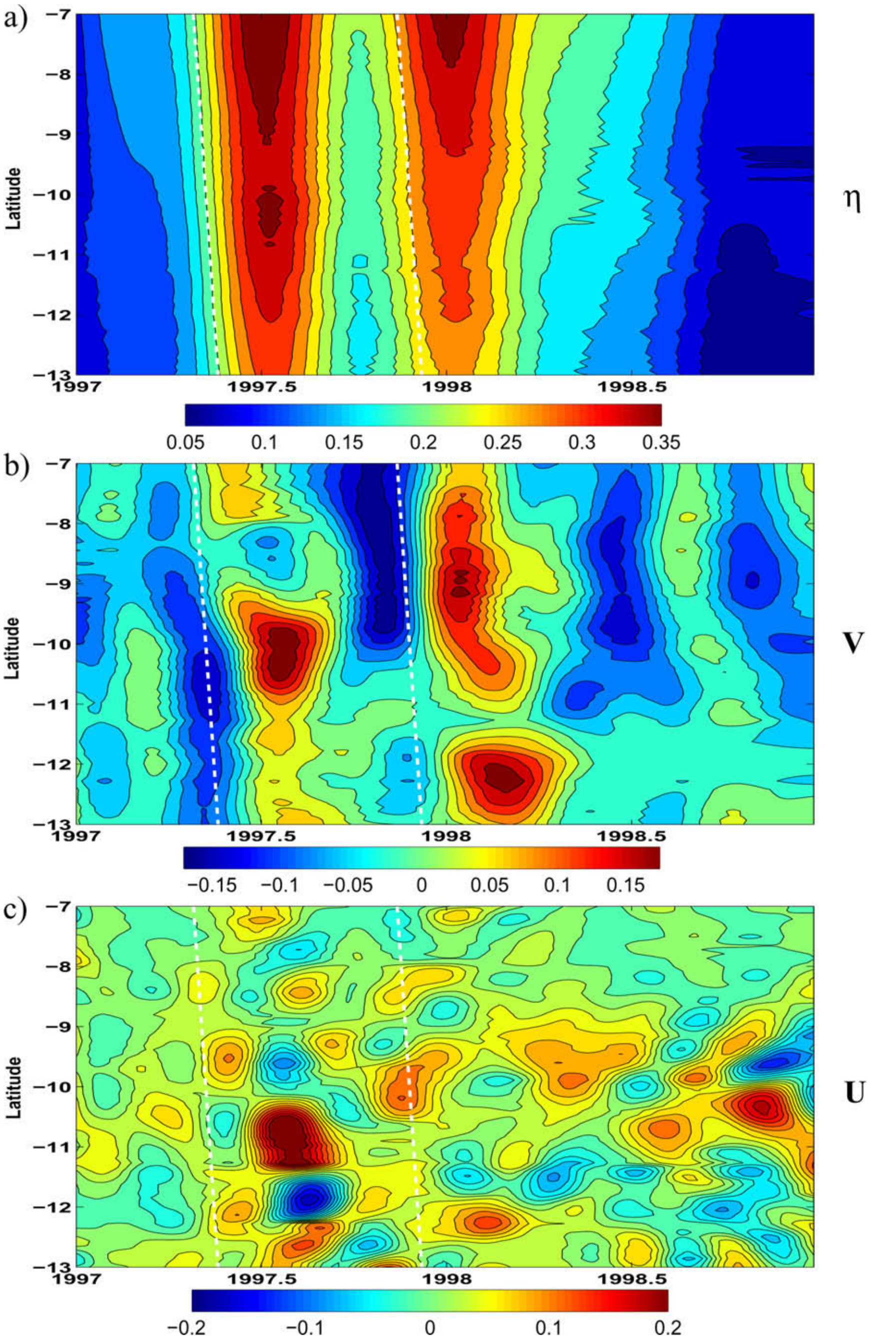

Fig. 7. Time–latitude diagrams for 1997 and 1998 of: (a) sea level [m], (b) alongshore velocity [m s^{-1}], and (c) cross-shore velocity [m s^{-1}]. A low-pass filter (with a 80 $days^{-1}$ cut-off frequency) is applied to reduce the strong signal associated with high-frequency variability (especially in the range 50–70 $days^{-1}$). White lines correspond to ≈0.35 m s^{-1}. (Alongshore velocity is averaged between 100 and 200 km offshore and 60 and 180 m depth, as in Fig. 11b.)

the upwelling activity varies greatly from one phase to another. Yet, these variations do not simply follow those for the mean seasonal climatology. If one compares the upper thermocline tilt within 100 km of the shore between 1997 and 1998 and the climatology, the different months can be classified as follows: from August to December 1997 and from May 1998 on, the tilt is close to normal although the water upwelled at the coast differs significantly. In June 1997 and from February 1998 to April 1998, the thermocline tilt is much less than in climatological conditions (even flat in February and March 1998, Fig. 9d). Sources of upwelled water appear shallower than during climatological situation which may have important biological consequences (on larger scales, Chhak and Di Lorenzo (2007) interpret in these terms the changes undergone by the north Pacific in relation with the PDO oscillation). July 1997 and January 1998 are intermediate by the same measure and tend to have their tilt more confined to the nearshore than the climatology (e.g., compare Fig. 9a and f).

5. Upwelling disruption during El Niño

There are several ways that El Niño can weaken the upwelling.[4] First and perhaps most obviously, the arrival of CTW is associated

---

[4] Note that, in contrast with higher latitudes, the upwelling-favorable wind during El Niño is generally anomalously strong and hence tends to mitigate the weakening effect of the internal oceanic processes.

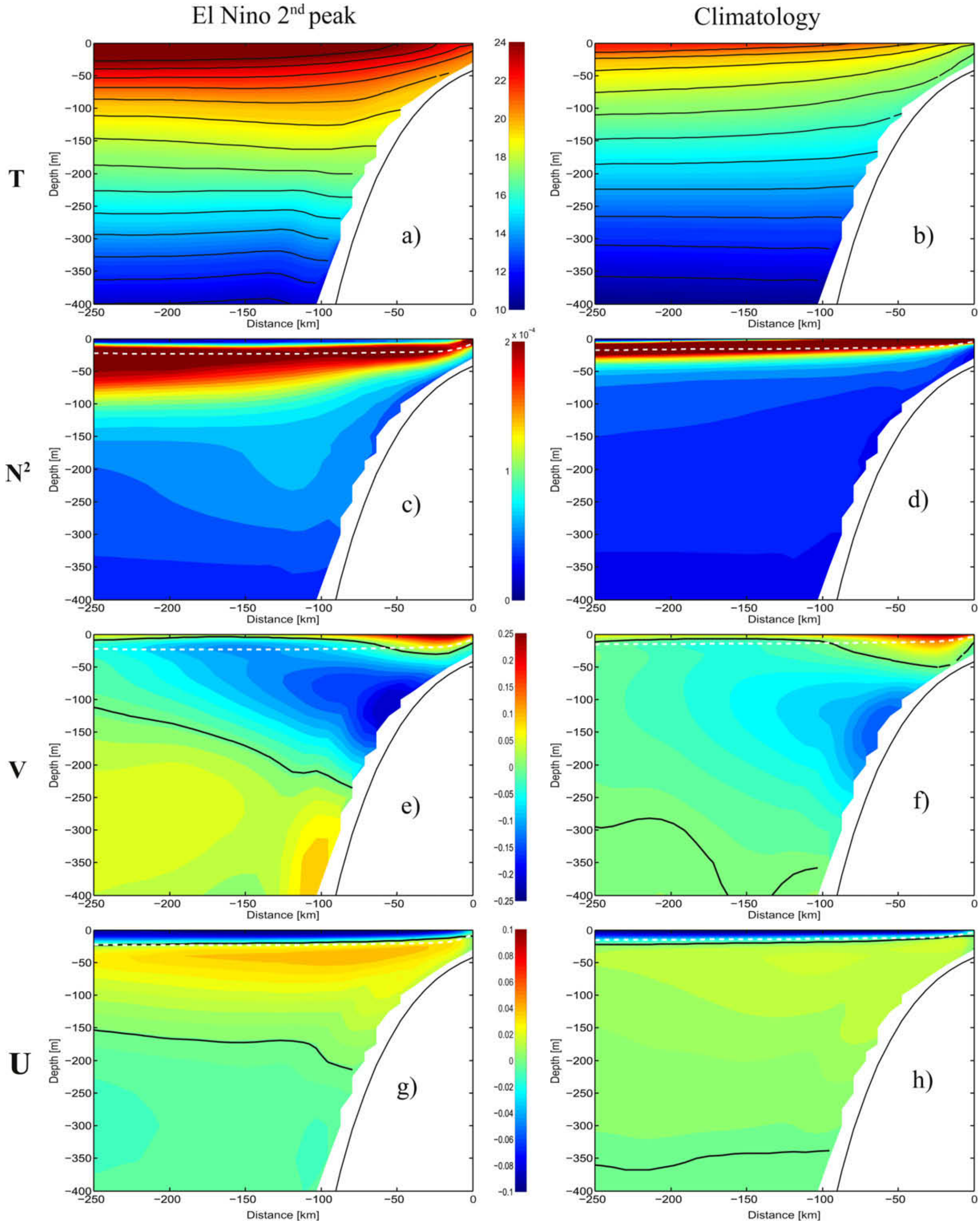

Fig. 8. Vertical sections of (a, b) temperature T [°C], (c, d) Brunt-Väisälä frequency N^2 [s^{-2}], (e, f) alongshore velocity V [$m\ s^{-1}$], and (g, h) cross-shore velocity U [$m\ s^{-1}$] averaged between 7°S and 13°S over the P2 period mid-October 1997 to mid-February 1998 (left column) and in the climatology (right column). Black contours on velocity sections indicate zero velocity. Black contours on temperature sections are every °C. The white dashed line represents the depth of the model mixed layer.

with a depression of the thermocline, i.e., negative vertical velocities that tend to counteract the upwelling driven by Ekman coastal divergence. Second, the anomalously strong PCU and the equatorial water mass it transports tend to increase the upper-ocean stratification. It is highly plausible that, during El Niño, upwelling weakness partly stems from the change in stratification. Although it is difficult to assess the role of this mechanism quantitatively, its relevance is supported by analytical upwelling solutions, e.g., in a 2-layer linear model (Gill, 1982, Section 10.11). Note that this is only for the initial baroclinic response to an upwelling-favorable wind turned on suddenly; nevertheless, the same mechanism is hypothesized to explain the upwelling reduction undergone by the California Current System over the last 50 years (Roemmich and McGowan, 1995; Di Lorenzo et al., 2005; Kim and Miller, 2007). Finally, an equatorward-rising sea level following the coast drives an onshore geostrophic flow that counteracts the Ekman currents, thereby limiting the coastal

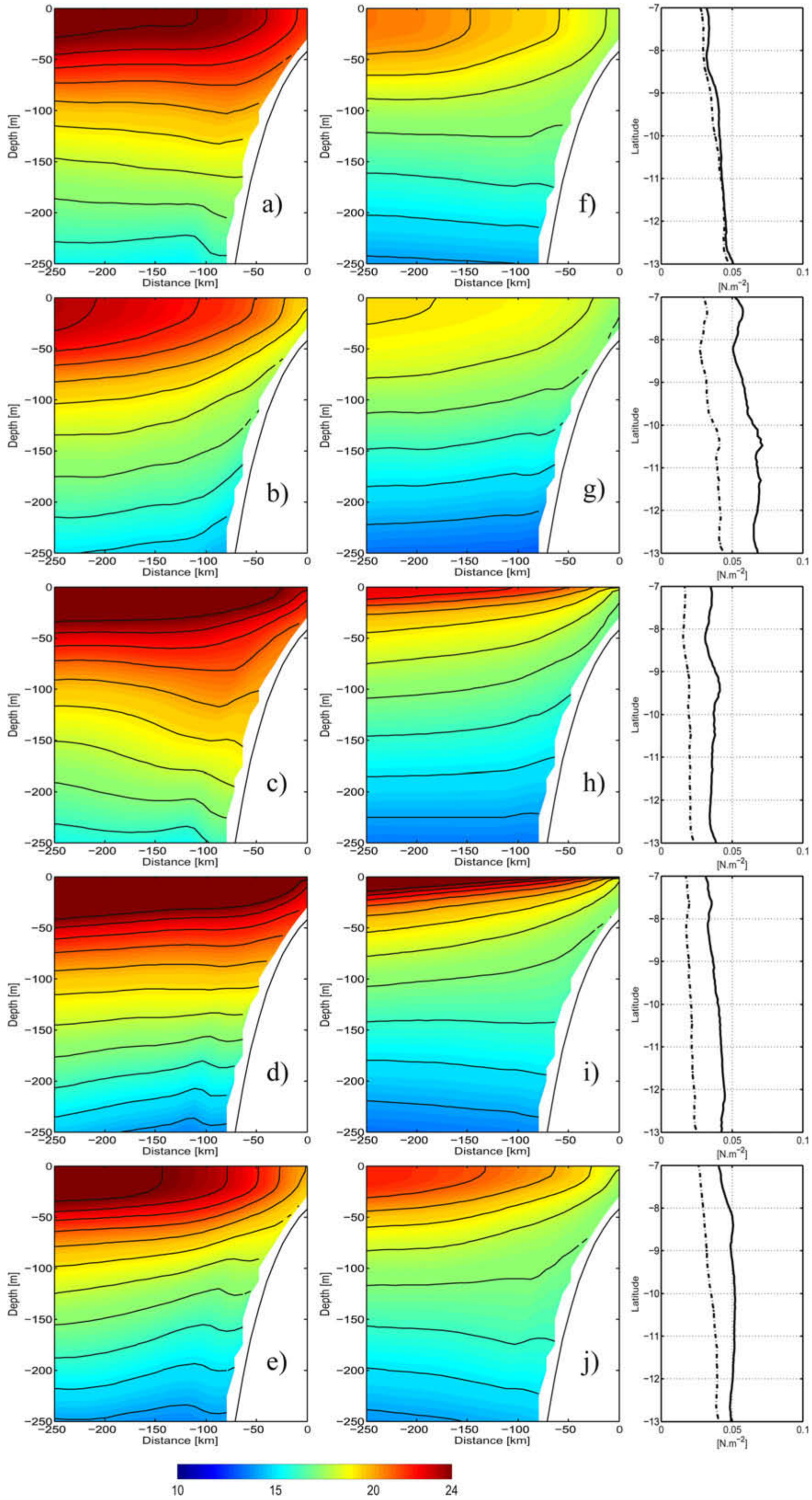

Fig. 9. Vertical sections of temperature [°C] averaged from 7°S to 13°S for different periods of 1997–1998 (left column) as defined in Section 1: (a) P1 aftermath (July 1997); (b) relaxation interval (October 1997); (c) P2 (mid-December 1997 to mid-January 1998) (d) P2 aftermath (March 1998); and (e) recovery from El Niño (June 1998). The model climatology (center column) is shown for the corresponding month: (f) July, (g) October, (h) mid-December to mid-January, (i) March, and (j) June. Alongshore wind stress 30 km offshore between 7°S and 13°S (right column) is shown for the corresponding month in 1997–1998 (black line) and the climatology (dashed line). Positive wind stress is equatorward (i.e., upwelling-favorable). Black contours on temperature sections are every °C.

divergence. In the context of El Niño, this is documented by Huyer et al. (1987) for the Peruvian coast during a few days of 1982–1983. It remains unclear how generic and important this process is.

To some extent the classification done in the previous section between normal and lower than average upwelling conditions off Peru during El Niño can be understood in simple terms involving wind forcing, coastal wave arrivals, and an equatorial water-mass presence off the Peruvian coast. In particular, thermocline tilts comparable to the climatology are seen during periods where the wind intensity is above (sometimes significantly) the maximum climatological values, i.e., 0.06 N m^{-2} reached in July. In the period October 1997–February 1998, the wind anomaly largely compensates for the stratification increase and the CTW induced thermocline deepening until early January 1998. This is also true during late-winter and spring 1997 when winds are strongest and stratification near the surface has been eroded somewhat due to reduced heat fluxes, a combination that results in nearly normal upwelling. Likewise, the recovery starting in May 1998 can be attributed to a conjunction of increasing winds, with values returning to greater than 0.06 N m^{-2}, and some reduction in the stratification. This set of arguments explains at least at a qualitative level the modulations of the Peruvian upwelling intensity on monthly time scales in our solution.

We now turn to the effect of the onshore flow associated with alongshore pressure gradient that can be quantified in a relatively straightforward way using our solution. Fig. 10 shows the Ekman transport estimated from $\tau_y/(\rho f)$ with τy the alongshore wind stress and f the Coriolis frequency. Also shown is the actual transport in the model for similar locations (integrated over the mixed-layer). Important mismatches between the two can be found during P2 and especially P1 (where the El Niño effect combines with a seasonal anomaly) with the offshore transport about half or less of its expected value over periods of several months. Given the resemblance among the time series of equivalent onshore velocity associated with the mismatch (Fig. 10), total onshore velocity at the base of the boundary layer (Fig. 11d), and geostrophic onshore velocity computed from sea level (Fig. 11e), we conclude that the alongshore sea-level gradient plays an important dynamical role during El Niño in our model.

To assess whether this is also true in the real ocean, we computed a cross-shore flow in geostrophic balance using altimeter data. Differences in the treatment of DUACS and ROMS sea levels to deduce velocities are minor. The result is presented in Fig. 11c and closely matches the one for the model for low frequencies (the high-frequency oscillations markedly differ).

Besides strengthening the model credibility it suggests that alongshore sea-level gradient is an important indicator of the health of the Peruvian system. Further thoughts on this are offered in the final section.

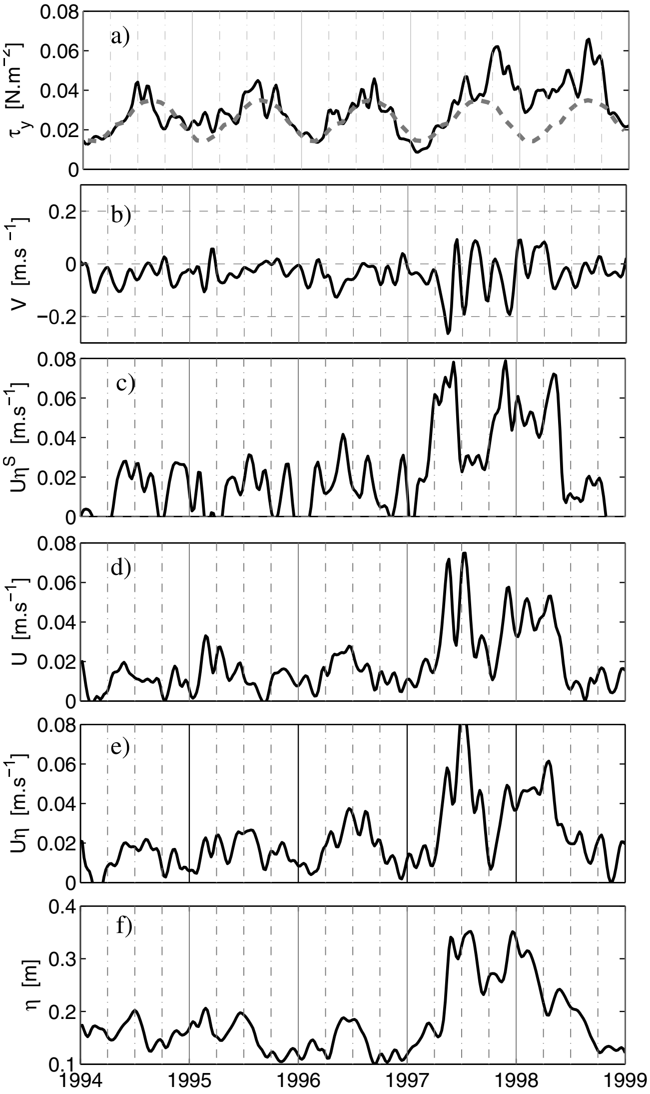

Fig. 11. Time series of (a) alongshore wind stress τ_y, (b) model alongshore velocity V, (c) cross-shore velocity deduced from altimetry data $U\eta S$, (d) model cross-shore velocity U, (e) geostrophic cross-shore velocity deduced from model sea level $U\eta$, and (f) model sea level η. These quantities are for central Peru. (a) is 50 km offshore and averaged between 7°S and 13°S, plotted along with the climatology (dashed gray). (b) is volume-averaged in a tube delimited by the depths 60 m and 180 m, cross-shore distances 100 and 200 km and latitudes 7° and 13°. (c and e) are computed from the alongshore sea-level gradient between 7°S and 13°S at 100 km offshore. (d) is a few meters below the model mixed-layer (i.e., Ekman layer) at 100 km offshore, averaged between 7°S and 1°S. (f) is taken 100 km offshore and between 7°S and 13°S. A low-pass Lanczos temporal filter is applied with a 40 days^{-1} cut-off frequency and a 24-day half-window.

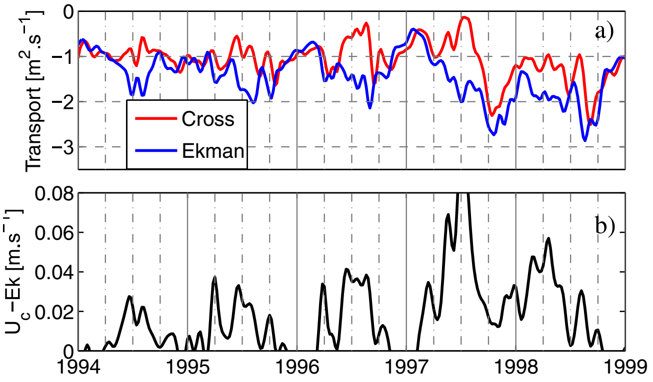

Fig. 10. (a) Ekman transport (blue) estimated from alongshore wind stress and model offshore transport (cross-shore velocity integrated from the surface to the model mixed-layer depth; red). Transports are averaged between 7°S–13°S and 50–150 km offshore. (b) Onshore velocity estimated from the difference between the transports (to be compared with the cross-shore geostrophic velocity in Fig. 11e).

We next inquire into the mechanisms that drive the onshore flow during El Niño. One approach is to connect the cross-shore velocities with the CTWs. Indeed, the power spectrum for the cross-shore velocity (Fig. 5) and even a visual inspection of its time series in Fig. 11d indicate that the cross-shore velocity arises at least in part from the CTW activity. However, the connection to CTWs is not as strong as for alongshore velocities (Figs. 5 and 11b). There is a weaker peak in the cross-shore velocity spectrum for the 50–70 days^{-1} frequency band where CTWs prevail compared to sea level and alongshore velocity. Most convincingly, band-passed, time–latitude diagrams of cross-shore velocity do not exhibit the poleward propagation nearly so clearly as sea level and alongshore velocities do (Figs. 6 and 7). A looser relationship between a CTW and cross-shore velocity is expected on theoretical

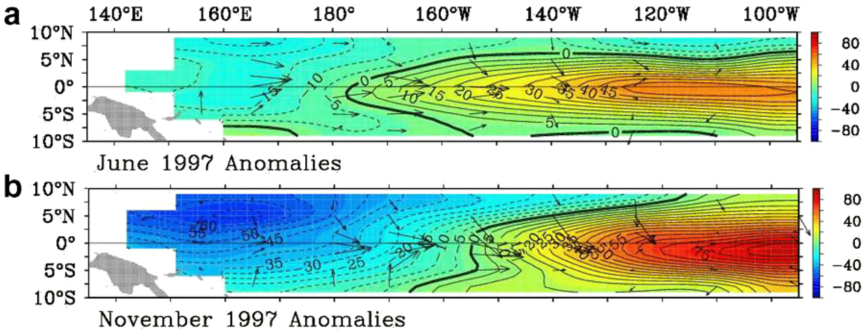

Fig. 12. TAO/TRITON data 20 °C isotherm depth monthly anomaly [m] in: (a) June 97 (top) and (b) November 1997. (From TAO Project Office data display interface; http://www.pmel.noaa.gov/tao/realtime.html.)

grounds; a Kelvin wave in idealized geometry has zero cross-shore velocity, although this result is not expected to hold in the more general case of CTWs along an irregular coast. Further support for this expectation comes from the difficulty that linear wave models have had in capturing observed cross-shore velocities (Brink, 1982, 1991).

6. Delayed El Niño recovery and onshore flow dynamics

In this section we argue that, on a long internal time scale associated with El Niño (~6 months), the anomalous onshore velocity can be understood as a regional downscaling response to the basin-scale circulation and water-mass anomaly, and it has the effect of delaying the recovery to normal conditions throughout the first half of 1998. Its regional manifestation as a warm-water wedge with a northwest/southeast geostrophic frontal-boundary current reaching the Peruvian coast at 14°S is also likely to have upscaling consequences for the whole tropical Pacific, but that demonstration would go beyond our regional modeling study.

It is well known that the eastern equatorial Pacific has an upper-ocean warm anomaly during an El Niño. In the P1 period the warm anomaly is relatively confined in latitude, but in the period approaching the P2 peak the warm anomaly extends well south of the equator throughout the eastern Pacific (Fig. 12). This water-mass anomaly[5] moves into the Peruvian region in late 1997 and early 1998 and remains in place until the next summer, as is evident in a time sequence of horizontal ρ maps within our model domain (Fig. 13). Atypically strong eastward currents south of the equator (Fig. 14) advect anomalously warm water into the region from the central Pacific; they are initially strongest near the equator (around 3°S in July 1997), partly merged with the Equatorial Undercurrent, and later occur as distinct South Equatorial Countercurrents (around 5°S and 10°S in December 1997).

Perhaps the most remarkable aspect of the 1997–1998 El Niño is the slow recovery in the P2 aftermath period in the Peruvian region (Fig. 13). In our simulation the period between mid-January and mid-April 1998 is associated with an almost complete disappearance of cold surface water from coastal upwelling, with isotherm tilts confined to the very nearshore (Fig. 9d). Over this period the anomalous stratification and water-mass characteristics hardly change, despite the facts that the low-frequency SLA is weakening (Fig. 11f) and there is reduced high-frequency CTW activity while the alongshore poleward advection reverses or at least diminishes (Fig. 11b).[6]

Climatologically, the austral summer and early-fall season (coinciding with the P2 after math) is subject to a vigorous upwelling along the South American coast. In 1998 the wind is significantly stronger than its climatology (Figs. 11a and 9), which would tend to increase upwelling. Therefore, some other mechanism(s) must be at work that inhibits upwelling. We find that the onshore velocities associated with the alongshore pressure gradient are in large part responsible for countering the effects of upwelling. This whole period stands out for persistent and sustained geostrophic onshore flow that wipes out about half of the expected Ekman transport. The geostrophic onshore flow has an important side effect that further modifies the Peruvian upwelling. With the spatial distribution of water masses in early 1998, it tends to bring and maintain toward the coast roughly the same equatorial water mass and strongly stratified conditions brought by CTWs at earlier times and accumulated off Peru by early 1998 (e.g., ρ at 50 m depth for January 1998 in Fig. 13d or SLA in Fig. 3). This means that the coastal, upwelled water is itself anomalously warm and light.

We now propose an interpretation for the dynamical mechanisms that control the regional evolution of El Niño during the P2 aftermath, given the occurrence of the basin-scale water-mass and circulation anomalies. It focuses on the interplay between eastern Pacific circulation and Rossby wave generation along the Peruvian coast and subsequent westward propagation.

At and immediately after the time of the P1 arrival (June–July 1997), the extra-equatorial situation is still close to climatological except near the coast where buoyant equatorial water accompanies the poleward-propagating CTWs (Fig. 13a and b). The water mass extends down to the cape south of Paracas at 14°S but does not follow the turn in the coastline (also discussed by Strub and James (2002)). Note that equatorial water hardly reaches beyond this point throughout the El Niño event except for minor intrusions in early 1998. The cape and the portion of coastline south of it are active eddy-generation sites during the whole period with continued poleward advection along the coast and release of coastal water into the interior (cf., Section 7). Near the equator the main pathway for water approaching the coast is in the Equatorial Undercurrent and its southern extension which are significantly

---

[5] The water-mass anomaly cannot be generated as a locally-forced steric response in the model, but must be created by lateral advection into the domain. The air–sea flux specification (Section 2.3) in the offshore anomaly region gives a heating of only 10 s W m^{-2} during the ~2 month anomaly generation phase at the end of 1997, which can account for less than 1 °C increase in the upper-ocean T, whereas the actual increase is more than 3 °C (Fig. 9).

[6] The alongshore advection is measured in the offshore tube defined in Fig. 11b and is intended to capture the first baroclinic mode. The alongshore velocity is poleward but weak in fall 1998. Higher modes may gain importance toward the end of El Niño. We found indeed that the vertical structure of the March–April 1998 alongshore velocities corresponds to a second baroclinic mode. However, changing the averaging method does not change the general conclusion that poleward transport of the equatorial water-mass off the Peruvian Shelf is strongly reduced after December 1998.

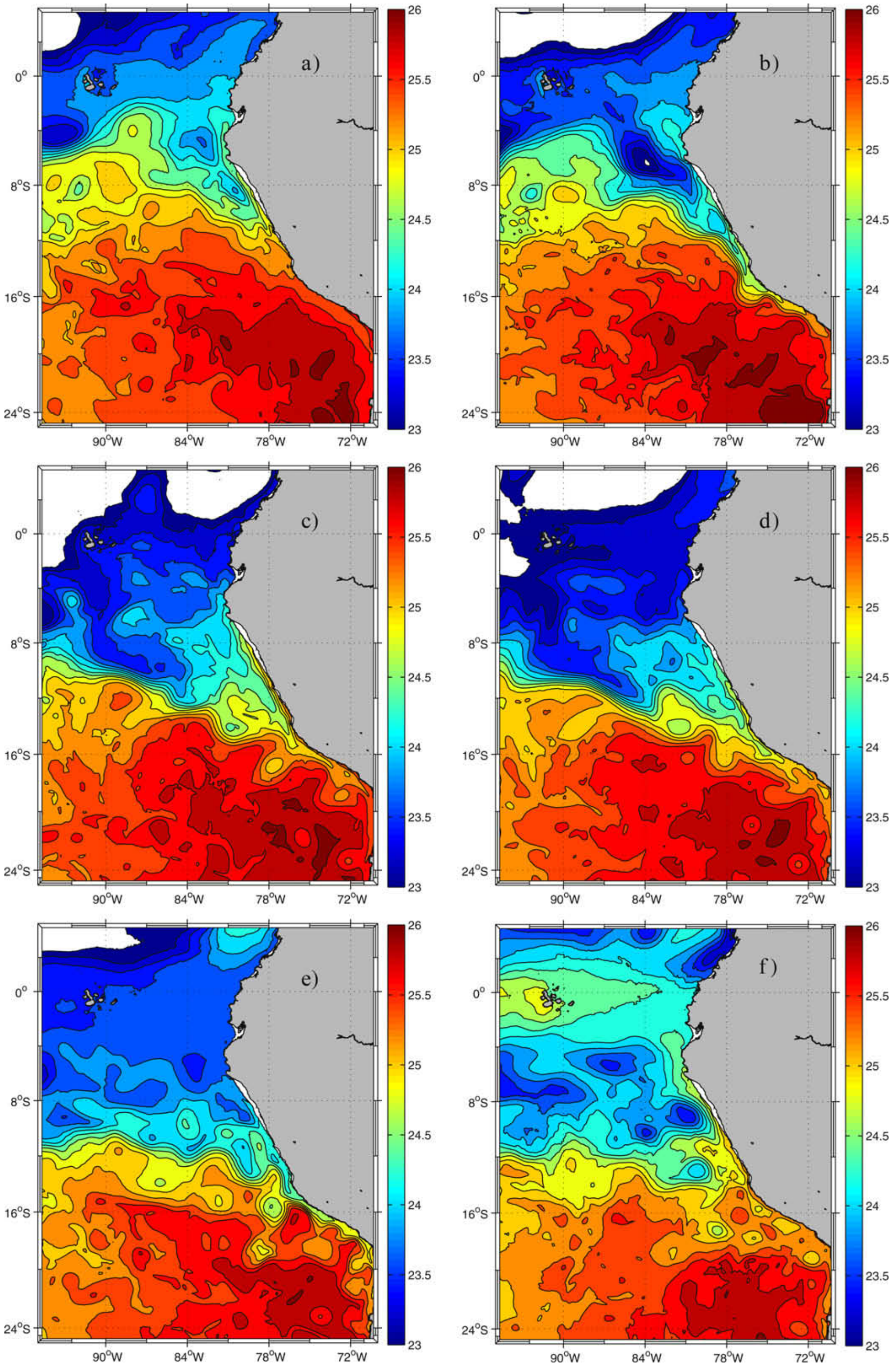

Fig. 13. ρ at 50 m depth off the west coast of South America in: (a) June 1997, (b) July 1997, (c) December 1997, (d) January 1998, (e) March 1998, and (f) June 1998. Color bar indicates $\rho - 1000$ in [kg m^{-3}], each contour is for 0.2 kg m^{-3}.

stronger than their climatological counterparts at 87°W (Fig. 14). The low-frequency poleward pulse P1 of equatorial waters off the coast of Peru triggers a Rossby wave that subsequently propagates offshore (this can be inferred from SLA maps such as in Fig. 3). Off the Peruvian shelf β varies quite rapidly with latitude and so does the phase speed of Rossby waves. The consequence is that the front separating equatorial waters brought by the coastal wave from offshore waters tilts as it progresses offshore. Using time–longitude diagrams (not shown) for subsurface ρ, we estimated the phase speeds at 7°S ($c = 0.25$ m s^{-1}) and 14°S ($c = 0.12$ m s^{-1}). These are in agreement with the observational results of Chelton and Schlax (1996). Progressive clockwise tilting of

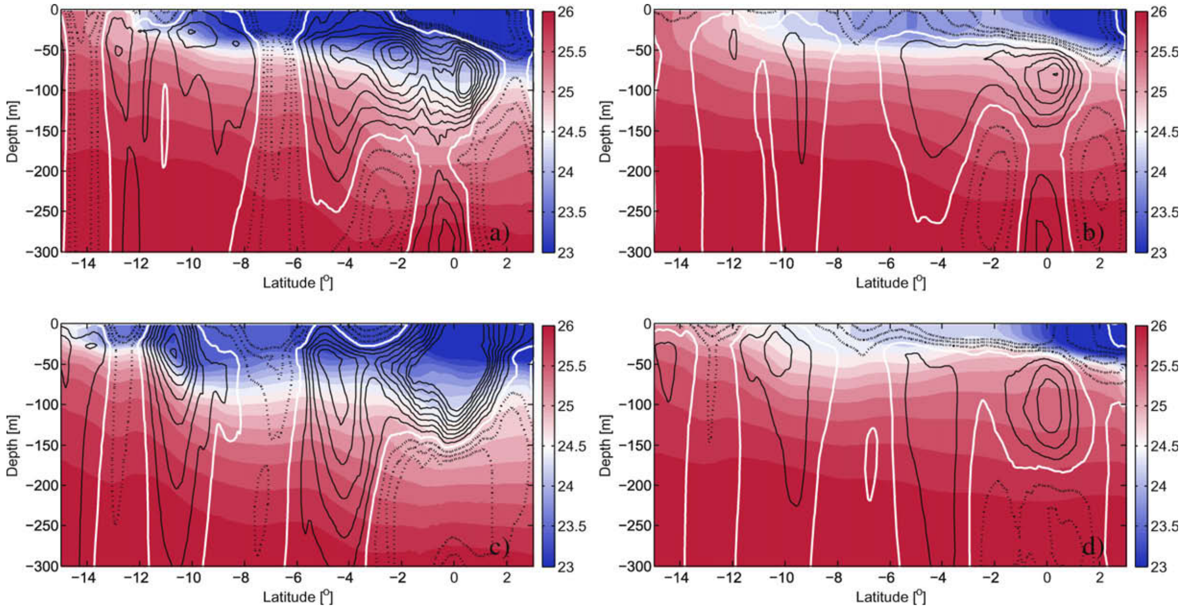

Fig. 14. Vertical sections of model ρ (colored) and zonal velocity (black contours) at 87°W in: (a) July 1997, (b) climatological July, (c) December 1997, and (d) climatological December. Dashed black contours are for negative (westward) zonal velocity. Contours are represented every 0.04 m s^{-1}. White contours stand for zero velocity. Color bar indicates $\rho - 1000$ in [kg m^{-3}].

the pycnocline front and its associated South Equatorial Countercurrent by Rossby waves is in agreement with previous modeling studies by Hulburt et al. (1976) and McCreary et al. (2002), and the scattering of eastern-boundary CTWs waves into westward-propagating Rossby waves is a general process due to β (Milliff and McWilliams, 1994) that is enhanced during the P2 aftermath by the alongshore potential vorticity gradient due to the decreasing thickness of the anomalous water mass along the Peruvian coast.

As the second peak comes in, the front is oriented northwest/southeast, and a wide coastal edge is now filled with equatorial water. This provides a shortcut for this water mass to reach the southern tip of the Peruvian shelf as readily seen in Fig. 15 for the month of December. The plume of buoyant water that follows this pathway is visible on the ρ maps; notice the contours for dark blue colors in Fig. 13c. Zonal eastward currents are anomalously intense at 87°S (Fig. 14), especially the Countercurrent core centered around 10°S. By December 1997 an enormous amount of buoyant equatorial water is sitting in the eastern Pacific (where it will remain until May 1998; McPhaden, 1999) and it keeps flowing toward the Peruvian coast along a now almost zonally oriented front off Central Peru. Nearshore the flow splits into various recirculations and the pressure gradient associated with it tends to spread and weaken when a current encounters a meridional coast (see Weaver and Middleton, 1989; Peliz et al., 2003 for idealized studies of a zonal current encountering a meridional coast).[7]

In fall 1997 this front is the main pathway by which the large scale equatorial climate signal (i.e., at that time the absence of recovery in the eastern Pacific, McPhaden, 1999; Picaut et al., 2002) is being conveyed toward the Peruvian system (Figs. 15c and 14c). This contrasts with earlier times when the basin-scale signals are conveyed primarily through the Equatorial Undercurrent and coastal trapped waves. The southeastern Pacific primarily controls the evolution of the front. In particular, the front is seen to rapidly collapse into a series of recirculations when the basin-scale recovery conditions lead to a shut-down of its upstream source (underway in March 1998; Fig. 15d).

Thus, there are several ways that the regional and coastal dynamics influences the eastern Pacific connection to the equatorial and central Pacific circulations, viz., Rossby wave emission, the existence of preferential sites of eddy generation, and modulated upwelling dynamics. The water-mass front itself may not simply be a passive conduit connecting the offshore equatorial Pacific with the Peru coastal system. Its intrinsic eddy dynamics and its probable enhancement of the coastal wave scattering strongly influence the downscaling of El Niño onto the Peru system. A schematic diagram is presented in Fig. 16 to summarize the scenario outlined in this section.

7. Lagrangian dispersal

A biologically important implication of our analysis is the effect that the geostrophic onshore flow has on enhancing nearshore material retention on the Peruvian shelf during El Niño, and can be hypothesized to aid in the biological recovery (Bertrand et al., 2004). This runs contrary to the increased upwelling-favorable wind, but the persistent geostrophic onshore flow can be dominant, as we have shown for the 1997–1998 El Niño.

To illustrate this retention we perform a Lagrangian diagnostic calculation where floats are released on the Peruvian shelf and tracked during both climatological (1995) and Niño (1997) conditions. More details on the experimental protocol are given in the Appendix. The particle density patterns 30 days after their release on December 1 (Fig. 17) further illustrate several aspects discussed in Section 4.

For 1997 the alongshore extension of the particle distribution reflects the intense poleward currents present during the active P2 phase, whereas in 1995 material is mostly advected equatorward. In the cross-shore direction both years exhibit some particle retention (primarily on the inner part of the shelf) and some offshore loss. The latter is significantly larger in 1995. Also the pathways of offshore loss differ. In 1995 more material is flushed offshore in the upwelling center near Paita (around 6°S) and a central upwelling filament. In 1997 filament-like features drawn by

---

[7] In our case, some details of the recirculation can be related to the El Niño sequence; e.g., notice how the relaxation period is recorded along the front by a large meander (i.e., a Rossby wave) located at 15°S, 82°W in January (Figs. 15c and 13d).

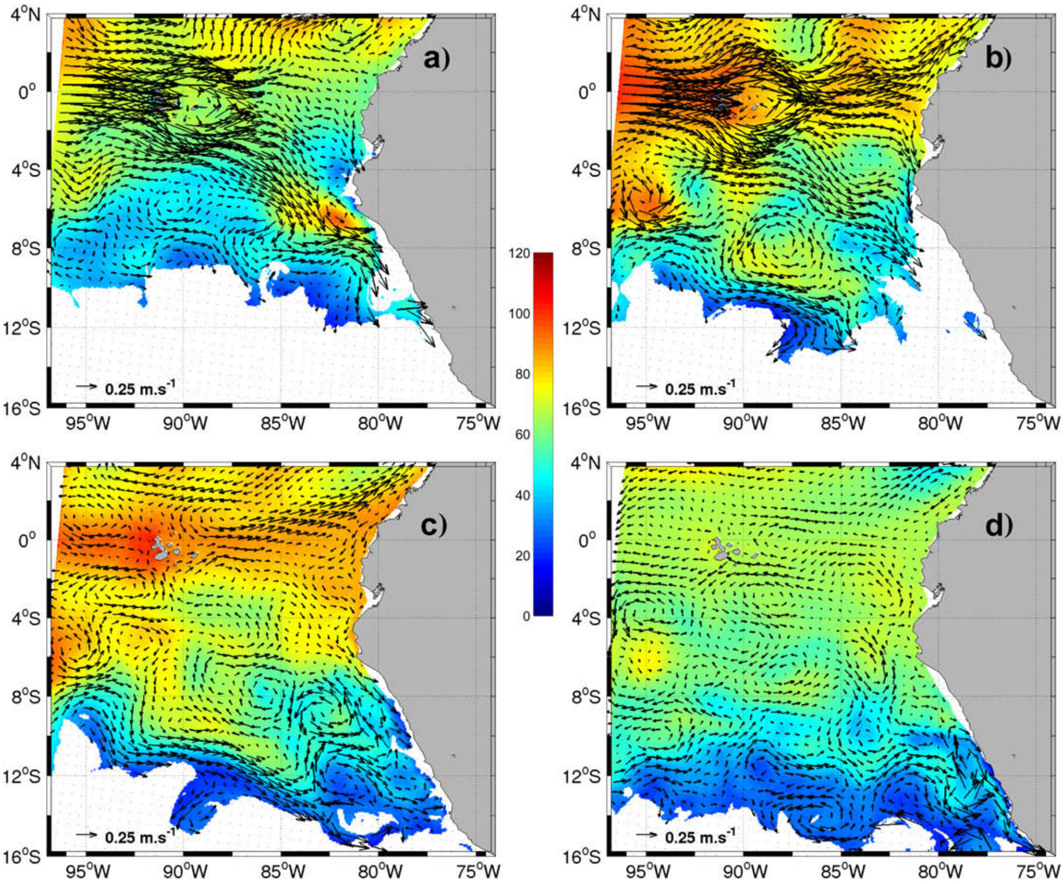

Fig. 15. Velocity on the 1024 kg m^{-3} isopycnal surface for: (a) July 1997, (b) December 1997, (c) January 1998, and (d) March 1998. Color bar indicates the isopycnal depth [m]. Scale for velocity (0.25 m s^{-1}) is indicated in the lower-left corner of each map.

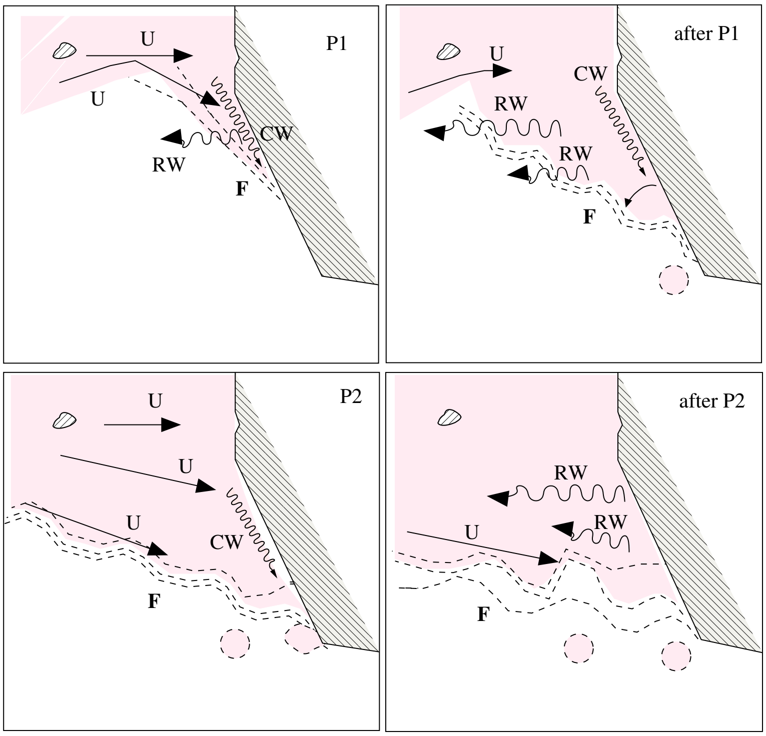

Fig. 16. Sketch of the different phases of 1997–1998 El Niño for the evolution of the anomalous water mass (light red) off Peru. *U* indicates the advection from the west of equatorial origin (straight thick arrows), F the ρ front (dashed lines), RW westward-propagating Rossby waves (long undulating arrows), and CW poleward-propagating coastal waves (short undulating arrows).

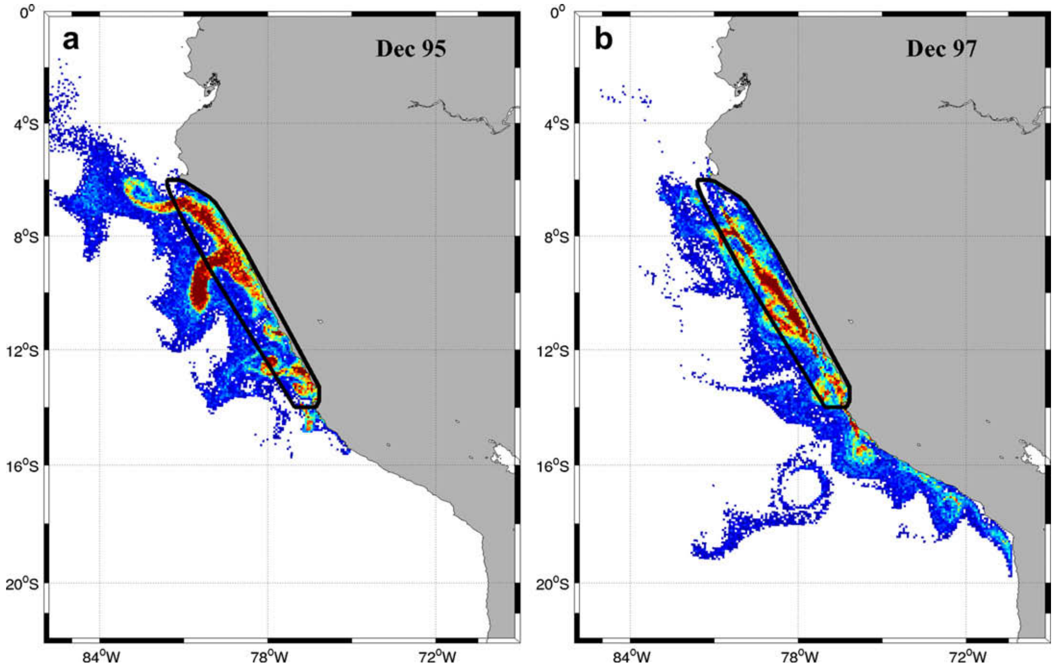

Fig. 17. Particle positions 30 days after release off the west coast of South America in: (a) December 1995 and (b) December 1997. Color indicates particle concentration per model grid cell. Color bars (not shown) are the same for both maps: red is high density, blue is low, and white is none. The black line indicates the area where the 10^5 drifters are initially released.

the particles off the Peruvian shelf are less protuberant. The strongest offshore transport occurs near Paracas (14°S) or farther south, i.e., away from the region directly affected by the geostrophic onshore flow (Sections 5 and 6). The offshore transport involves the generation of eddies that trap particles and carry them as they move offshore.

A more comprehensive study will be required to confirm these results, but it seems that the geostrophic onshore flow can limit the offshore dispersion of material, e.g., organisms. It would be consistent with the alongshore integrated view of a geostrophic onshore flow counteracting the offshore Ekman transport (Section 5). This would mitigate the negative effect exerted by the geostrophic onshore flow on the biology through upwelling reduction.

8. Summary

Our regional numerical simulation for the Peru–Chile system during the most recent strong El Niño event compares favorably with sea level and surface temperature observations. It further provides additional information that help understand the dynamical changes off central Peru during El Niño. The mechanism of Ekman transport reduction by an equatorward, alongshore sea-level gradient, suggested by Huyer et al. (1987) for a short period during El Niño 1983, partly explains the evolution of the upwelling intensity at different stages of El Niño in 1997–1998. In particular, the delayed recovery after the second peak (from mid-January to mid-April 1998) cannot be understood if one considers only the commonly used El Niño indicators based on wind, SLA, or even cross-shore gradient of sea level (i.e., a proxy for poleward geostrophic currents). On the other hand, cross-shore velocity (or, almost equivalently, alongshore sea-level gradient) time series are consistent with the delayed recovery in early fall 1998. Onshore velocities are important because they counteract the upwelling and also because they help maintain anomalously warm water adjacent to the Peruvian shelf. These effects were proposed to explain oceanic conditions off Peru in 1983 (Huyer et al., 1987), and with both model and altimetry data we show that they also apply in 1998. The anomalous alongshore pressure gradient reflects the extensive, persistent water-mass anomaly off Peru in 1998 that is created by eastward advection in the Equatorial Undercurrent and South Equatorial Countercurrent of the basin-scale warm anomaly. The development of this regional anomaly involves Rossby wave emission from coastally-trapped waves. Subsequent Rossby wave offshore propagation keeps the Peruvian system tightly connected to the large scale equatorial circulation even when CTW activity ceases. The connection involves the progressive formation of a northwest/southeast front, separating equatorial waters from eastern subtropical waters, that approaches the Peruvian coast around Paracas. The coastline bend at 14°S is probably critical in controlling the position of the southern extent of the anomalous water mass. The observed SLA also shows the development of a ρ front running between roughly 10°S, 95°W and southern Peru.

Further inquiry is needed to determine how typical the accumulation of an equatorial water mass off central Peru is during the late stages of El Niño events and its controlling processes. Our results imply that an indicator of cross-shore velocity should be added to the other El Niño indicators that are used to estimate the health of the Peruvian system.

Acknowledgments

The AVHRR-Pathfinder SST data were obtained from the Physical Oceanography Distributed Active Archive Center (PO.DAAC) at the NASA Jet Propulsion Laboratory. The altimeter products were produced by Ssalto-Duacs and distributed by Aviso, with support from CNES. Weekly ERS1-2 scatterometers winds were obtained from CERSAT, IFREMER, Plouzané (France). TAO buoys data plots were obtained from the TAO Project Office (http://www.pmel.noaa.gov/tao/realtime.html). E. Curchitser, L. Dobbins, and P. Penven are thanked for providing pre-processing tools, and W. Large is thanked for providing the POP-CCSM solution. Support was provided by the Office of Naval Research in the Grant N0001404-1-0401. Some of the computations were done at the National Center for Supercomputer Applications (NCSA).

Appendix A. Lagrangian experimental protocol

Numerical Lagrangian trajectories are computed using the ROMS-Offline tracking module (Carr et al., 2008). 3D ROMS velocity fields are interpolated in space and time at drifter locations, and trajectories are integrated using a fourth-order accurate time-stepping scheme. The 3D velocity fields are 2-day-averaged model output. This temporal sampling is sufficient to capture the mesoscale activity in the model at this horizontal resolution (7.5 km). Comparison between online (e.g., using velocity fields varying at every model time step) and offline tracking of a set of particles (not shown) shows no significant differences when using 2-day sampling for the model output. In the experiment presented here, we track 100,000 floats released over the Peruvian shelf between the coast and the 200 m isobath and between the surface and the bottom (Lett et al., 2007). Initial positions and the particle density evolution are shown in Fig. 17 for releases in December 1995 and in December 1997. Trajectories are integrated for 60 days, and temperature and salinity are sampled along the trajectories.

References

Barber, R., Chavez, F., 1983. Biological consequences of El Niño. Science 222, 203–210.

Barnier, B., Siefried, L., Marchesiello, P., 1995. Thermal forcing for a global ocean circulation model using a three-year climatology of ECMWF analyses. Journal of Marine Systems 6, 363–380.

Beckman, A., Haidvogel, D., 1993. Numerical simulation of flow around a tall isolated seamount. Journal of Physical Oceanography 23, 1736–1753.

Bentamy, A., Quilfen, Y., Gohin, F., Grima, N., Lenaour, M., Servain, J., 1996. Determination and validation of average wind fields from ERS-1 scatterometer measurements. The Global Atmosphere and Ocean System 4, 1–29.

Bertrand, A., Segura, M., Gutierrez, M., Vasquez, L., 2004. From small-scale habitat loopholes to decadal cycles: a habitat-based hypothesis explaining fluctuation in pelagic fish populations off Peru. Fish and Fisheries 5, 296–316.

Blanco, J., Carr, M., Thomas, A., Strub, P., 2002. Hydrographic conditions off Northern Chile during the 1996–1998 La Niña and El Niño events. Journal of Geophysical Research 107, 3017.

Brink, K., 1982. A comparison of long coastal trapped wave theory with observations off Peru. Journal of Physical Oceanography 12, 897–913.

Brink, K., 1991. Coastal-trapped waves and wind-driven currents over the continental shelf. Annual Review of Fluid Mechanics 23, 389–412.

Brink, K., Halpern, D., Huyer, A., Smith, R., 1983. The physical environment of the Peruvian upwelling system. Progress in Oceanography 12, 285–305.

Capet, X., Colas, F., Kurian, J., McWilliams, J.C., 2008. Response of the North American West Coast to the 1997–1998 El Niño event in ROMS: modulation of mesoscale and submesoscale activity by a basin-scale signal, in preparation.

Carr, M., Strub, P., Thomas, A., Blanco, J., 2002. Evolution of 1996–1999 La Niña and El Niño conditions off the western coast of South America: a remote sensing perspective. Journal of Geophysical Research 107, 3236.

Carr, S., Capet, X., McWilliams, J., Pennington, J.T., Chavez, F.P., 2008. The influence of diel vertical migration on zooplankton transport and recruitment in an upwelling region: Estimates from a coupled behaviorial–physical model. Fisheries Oceanography 17, 1–15.

Carton, J., Giese, B., 2008. A reanalysis of ocean climate using Simple Ocean Data Assimilation (SODA). Monthly Weather Review 136 (8), 2999–3017.

Chelton, D., Schlax, M., 1996. Global observations of oceanic Rossby waves. Science 272, 234–238.

Chelton, D., deSzoeke, R., Schlax, M., El Naggar, K., Siwetrz, N., 1998. Geographical variability of the first-baroclinic Rossby radius of deformation. Journal of Physical Oceanography 28, 433–460.

Chhak, K., Di Lorenzo, E., 2007. Decadal variations in the California Current upwelling cells. Geophysical Research Letters 34, L14604. doi:10.1029/2007GL030203.

Clarke, A., Lebedev, A., 1999. Remotely driven decadal and longer changes in the coastal Pacific waters of the Americas. Journal of Physical Oceanography 29, 828–835.

Da Silva, A., Young, C., Levitus, S., 1994. Atlas of surface marine data 1994. Volume 1: Algorithms and Procedures. NOAA Atlas NESDIS, 6, 74pp.

Di Lorenzo, E., Miller, A., Schneider, N., McWilliams, J., 2005. The warming of the California current: dynamics, thermodynamics and ecosystem implications. Journal of Physical Oceanography 35, 336–362.

Ducet, N., Traon, P.L., Reverdin, G., 2000. Global high-resolution mapping of ocean circulation from TOPEX/Poseidon and ERS-1 and -2. Journal of Geophysical Research 105, 19477–19498.

Gill, A., 1982. Atmosphere-Ocean dynamics. International Geophysics Series, vol. 30. Academic Press.

Grados, C., 1998. Informativo Oceanografico, vol. 8. <http://www.imarpe.gob.pe/oceanin8.html>.

Hulburt, H., Kindle, J., O'Brien, J., 1976. A numerical simulation of the onset of El Niño. Journal of Physical Oceanography 6, 621–631.

Huyer, A., Smith, R., Paluszkiewicz, T., 1987. Coastal upwelling off Peru during normal and El Niño times, 1981–1984. Journal of Geophysical Research 92, 14297–14307.

Huyer, A., Knoll, M., Paluszkiewicz, T., Smith, R., 1991. The Peru Undercurrent: a study in variability. Deep Sea Research 38 (Suppl. 1), 5247–5271.

Kessler, W., McPhaden, M., 1995. Oceanic equatorial waves and the 1991–1993 El Niño. Journal of Climate 8, 1757–1774.

Kessler, W., McPhaden, M., Weickman, K., 1995. Forcing of intraseasonal Kelvin waves in the equatorial Pacific. Journal of Geophysical Research 100, 10613–10631.

Kim, H.-J., Miller, A.J., 2007. Did the thermocline deepen in the southern California Current after the 1976-1977 climate regime shift? Journal of Physical Oceanography 37, 1733–1739.

Kosro, P., 2002. A poleward jet and a equatorward undercurrent observed off Oregon and northern California, during the 1997–1998 El Niño. Progress in Oceanography 54, 343–360.

Large, W., Danabasoglu, G., 2006. Attributions and impacts of upper-ocean biases in CCSM3. Journal of Climate 19, 2325–2346.

Large, W., Yeager, S., 2004. Diurnal to decadal global forcing for ocean and sea-ice models: the data sets and flux climatologies. NCAR Technical Note TN-460+STR, 105pp.

Large, W., McWilliams, J., Doney, S., 1994. Oceanic vertical mixing: a review and a model with a nonlocal boundary layer parameterization. Review of Geophysics 32, 363–403.

Leth, O., Middleton, J., 2004. A mechanism for enhanced upwelling off central Chile: eddy advection. Journal of Geophysical Research C12020. doi:10.1029/2003JC002129.

Leth, O., Shaffer, G., 2001. A numerical study of the seasonal variability in the circulation off central Chile. Journal of Geophysical Research 106 (22), 229.

Lett, C., Penven, P., Ayón, P., Fréon, P., 2007. Enrichment, concentration and retention processes in relation to anchovy (*Engraulis ringens*) eggs and larvae distributions in the Northern Humboldt upwelling ecosystem. Journal of Marine Systems 4, 189–200.

Marchesiello, P., McWilliams, J., Shchepetkin, A., 2001. Open boundary conditions for long-term integration of regional oceanic models. Ocean Modelling 3, 1–20.

Marchesiello, P., McWilliams, J., Shchepetkin, A., 2003. Equilibrium structure and dynamics of the California Current System. Journal of Physical Oceanography 33, 753–783.

McCreary, J., Lu, P., Yu, Z., 2002. Dynamics of the Pacific subsurface countercurrents. Journal of Physical Oceanography 32, 2379–2404.

McPhaden, M., 1999. Genesis and evolution of the 1997–1998 El Niño. Science 283, 950–954.

Mesias, J., Matano, R., Strub, P., 2003. Dynamical analysis of the upwelling circulation off Central Chile. Journal of Geophysical Research 108. doi:10/1029/2001JC001135.

Meyers, S., Melson, A., Mitchum, G., O'Brien, J., 1998. Detection of the fast Kelvin wave teleconnection due to El Niño-southern oscillation. Journal of Geophysical Research 103, 27655–27663.

Milliff, R., McWilliams, J., 1994. The evolution of boundary pressure in ocean basins. Journal of Physical Oceanography 24, 1317–1338.

Peliz, A., Dubert, J., Haidvogel, D., 2003. Subinertial response of a density driven eastern boundary poleward current to wind forcing. Journal of Physical Oceanography 33, 1633–1650.

Penven, P., Echevin, V., Pasapera, J., Colas, F., Tam, J., 2005. Average circulation, seasonal cycle, and mesoscale dynamics of the Peru Current System: a modeling approach. Journal of Geophysical Research 110. doi:10.1029/2005JC002945110.

Picaut, J., Hackert, E., Busalacchi, A., Murtugudde, R., Lagerloef, G., 2002. Mechanisms of the 1997–1998 El Niño–La Niña, as inferred from space-based observations. Journal of Geophysical Research 107, 3037.

Pizarro, O., Clarke, A., VanGorder, S., 2001. El Niño sea level and currents along the South American coast: comparison of observations with theory. Journal of Physical Oceanography 31, 1891–1903.

Pizarro, O., Shaffer, G., Dewitte, B., Ramos, M., 2002. Dynamics of seasonal and interannual variability of the Peru–Chile Undercurrent. Geophysical Research Letters 29, 7–9. doi:10.1029/2002GL014790.

Quilfen, Y., Bentamy, A., Delecluse, P., Katsaros, K., Grima, N., 2000. Prediction of sea level anomalies using ocean circulation model forced by scatterometer wind and validation using TOPEX/Poseidon data. IEEE Transactions on Geosciences and Remote Sensing 38, 1871–1884.

Ramos, M., Pizarro, O., Bravo, L., Dewitte, B., 2006. Seasonal variability of the permanent thermocline off northern Chile. Geophysical Research Letters 33. doi:10.1029/2006GL025882.

Roemmich, D., McGowan, J., 1995. Climatic warming and the decline of zooplankton in the California Current. Science 267, 1324–1326.

Sanchez, G., Calienes, R., Zuta, S., 2000. The 1997–1998 El Niño and its effects on the coastal marine ecosystem off Peru. Calcofi Report 41, 62–86.

Shaffer, G., Pizarro, O., Djurfeldt, L., Salinas, S., Ruttlant, J., 1997. Circulation and low-frequency variability near the Chilean coast: remotely forced fluctuations during the 1991–1992 El Niño. Journal of Physical Oceanography 27, 217–235.

Shchepetkin, A., McWilliams, J., 2005. The regional oceanic modeling system: a split-explicit, free-surface, topography-following-coordinate ocean model. Ocean Modelling 9, 347–404.

Smith, R., 1983. Peru coastal currents during El Niño: 1976 and 1982. Science 221, 1397–1399.

Smith, W.H.F., Sandwell, D., 1997. Global seafloor topography from satellite altimetry and ship depth soundings. Science 277, 1956–1962.

Song, Y., Haidvogel, H., 1994. A semi-implicit ocean circulation model using a generalized topography-following coordinate system. Journal of Computational Physics 115, 228–244.

Stammer, D., 1997. Global characteristics of ocean variability estimated from regional TOPEX/POSEIDON altimeter measurements. Journal of Physical Oceanography 27, 1743–1769.

Strub, P., James, C., 2002. The 1997–1998 oceanic El Niño signal along the southeast and northeast Pacific boundaries – an altimetric view. Progress in Oceanography 54, 439–458.

Strub, P., Mesias, J., Montecino, V., Ruttlant, J., Salinas, S., 1998. The Sea, Coastal Ocean Circulation Off Western South America, vol. 11, John Wiley & Sons, pp. 29–67 (Chapter 10).

Weaver, A., Middleton, J., 1989. On the dynamics of the Leeuwin Current. Journal of Physical Oceanography 19, 626–648.

Progress in Oceanography 79 (2008) 156–166

Contents lists available at ScienceDirect

Progress in Oceanography

journal homepage: www.elsevier.com/locate/pocean

Air–sea carbon dioxide fluxes in the coastal southeastern tropical Pacific

Gernot E. Friederich [a,*], Jesus Ledesma [b], Osvaldo Ulloa [c], Francisco P. Chavez [a]

[a] *Monterey Bay Aquarium Research Institute, 7700 Sandholdt Road, Moss Landing, CA 95039, USA*
[b] *Instituto del Mar del Perú, Esquina Gamarra y Gral. Valle s/n, Apartado 22, Callao, Lima, Peru*
[c] *Universidad de Concepción, Cabina 7 – Barrio Universitario, Casilla 1987, Correo 3, Concepción, Chile*

ARTICLE INFO

Article history:
Available online 21 October 2008

Keywords:
Coastal upwelling
Carbon dioxide
Gas exchange
Seasonality
Eastern South Pacific
Peru
Chile

ABSTRACT

Comprehensive sea surface surveys of the partial pressure of carbon dioxide (pCO_2) have been made in the upwelling system of the coastal (0–200 km from shore) southeastern tropical Pacific since 2004. The shipboard data have been supplemented by mooring and drifter based observations. Air–sea flux estimates were made by combining satellite derived wind fields with the direct sea surface pCO_2 measurements. While there was considerable spatial heterogeneity, there was a significant flux of CO_2 from the ocean to the atmosphere during all survey periods in the region between 4° and 20° south latitude. During periods of strong upwelling the average flux out of the ocean exceeded 10 moles of CO_2 per square meter per year. During periods of weaker upwelling and high productivity the CO_2 evasion rate was near 2.5 $mol/m^2/yr$. The average annual fluxes exceed 5 $mol/m^2/yr$. These findings are in sharp contrast to results obtained in mid-latitude upwelling systems along the west coast of North America where the average air–sea CO_2 flux is low and can often be from the atmosphere into the ocean. In the Peruvian upwelling system there are several likely factors that contribute to sea surface pCO_2 levels that are well above those of the atmosphere in spite of elevated primary productivity: (1) the upwelling source waters contain little pre-formed nitrate and are affected by denitrification, (2) iron limitation of primary production enhanced by offshore upwelling driven by the curl of the wind stress and (3) rapid sea surface warming. The combined carbon, nutrient and oxygen dynamics of this region make it a candidate site for studies of global change.

1. Introduction

The great majority of published sea surface measurements of the partial pressure of carbon dioxide (pCO_2) have come from open ocean waters (Takahashi et al., 2002). As a result there is debate over the role of the coastal ocean as either a source or sink of CO_2 (Cai and Dai, 2004; Thomas et al., 2004; Ver et al., 1999). The coastal ocean has been postulated to be a carbon sink due to high sedimentation rates and carbon export to depth at the shelf edge (Chen, 2004; Walsh, 1991; Wollast, 1998) but a source due to coastal upwelling and runoff of carbon rich waters of terrestrial origin (Chavez et al., 2007; Ver et al., 1999). This situation is changing; for example a compilation of over 2 million measurements from the coasts of North America has recently been synthesized (Chavez et al., 2007). This synthesis suggests that high latitude systems tend to be sinks and low latitude systems tend to be sources of CO_2 to the atmosphere. An analysis of a more limited data set by Borges et al. (2005) and Cai et al. (2006) came to a similar conclusion. These syntheses however only had limited data for low latitude coastal upwelling systems. Here we present the first comprehensive study of air–sea CO_2 flux from a low latitude, tropical eastern boundary coastal upwelling system. The results are in sharp disagreement with the conclusions of Hales et al. (2005) who suggested that eastern boundary coastal upwelling systems in general were strong sinks for atmospheric CO_2.

The equatorial Pacific upwelling system is known to be a strong source of CO_2 to the atmosphere (Chavez et al., 1999; Feely et al., 2002). High local air–sea CO_2 fluxes might also be expected in coastal upwelling regions due to the supply of carbon rich waters from depth combined with rapid surface warming. However, in contrast to the equatorial Pacific, which has low rates of photosynthesis (Chavez et al., 1999), coastal upwelling systems have high rates, which rapidly (days) convert inorganic to organic carbon, and reduces the high air–sea fluxes. Freshly upwelled waters with high pCO_2 and nutrient content can therefore support carbon export to depth and the atmosphere. The resulting spatial and temporal variability has made a comprehensive assessment of the net air–sea exchange of CO_2 difficult in these regions. On a time scale of days to weeks a combination of upwelling, net community production, subduction, wind and surface temperature changes

---

* Corresponding author. Tel.: +1 831 775 1713.
E-mail address: frge@mbari.org (G.E. Friederich).

0079-6611/$ - see front matter © 2008 Elsevier Ltd. All rights reserved.
doi:10.1016/j.pocean.2008.10.001

will determine the direction and magnitude of the air–sea CO_2 flux for a coastal upwelling system.

Observations made in mid-latitude upwelling systems (Borges and Frankignoulle, 2002; Friederich et al., 2002; Hales et al., 2005) indicate that CO_2 sources and sinks may occur in close proximity and biological carbon uptake can frequently produce significant CO_2 under-saturation with respect to the atmosphere. In some upwelling systems such as central California these opposing forces nearly balance each other when appropriate time (one year) and length scales (150 km) are considered. At somewhat higher latitudes such as Oregon (45°N) and Galicia (43°N), the net result appears to be a transfer of CO_2 into the ocean. Observations in the monsoon dominated tropical upwelling system of the northern Arabian Sea indicate a flux of CO_2 from the ocean to the atmosphere with a maximum during the strong upwelling associated with the southwest monsoon (Goyet et al., 1998; Kortzinger et al., 1997). The tropical coastal upwelling system of the Cariaco basin has also reported to be a net source to the atmosphere (Astor et al., 2005).

Observations of sea surface pCO_2 along the Peruvian coast have been too infrequent and spatially isolated to allow a regional estimate of air–sea CO_2 exchange. Measurements of pH in the Peruvian upwelling region near 15°S made by Simpson and Zirino (1980) in May of 1976 indicate that pCO_2 within 40 km of the coast may have had a range between 150 and 950 ppm. In August of 1986 direct measurements of pCO_2 by Copin-Montegut and Raimbault (1994) gave a range of 450–1000 ppm in the same location. During the 1986 expedition measurements extended to about 170 km offshore where pCO_2 was about 500 ppm; considerably above the atmospheric value of 346 ppm (GLOBAL VIEW-CO_2, 2006). Data collected during latitudinal transects in the past decade indicate that high sea surface pCO_2 extends several hundred kilometers offshore (http://www.ldeo.columbia.edu/res/pi/CO2/), thus providing a relatively large area of potential ocean to atmosphere CO_2 transfer. Although the average winds near the Peruvian coast tend to be modest, the wind velocity usually increases away from the coast where it may reach maximum monthly velocities in excess of $10\ \mathrm{m\ s^{-1}}$ during the austral winter. The historical data indicated that the Peruvian upwelling system was probably a source of CO_2 to the atmosphere and in 2004 we began a series of measurements to examine the seasonal and spatial distribution of the air–sea CO_2 exchange between 5° and 15°S along the coast of Peru. These data were gathered during routine fisheries, plankton and hydrographic surveys conducted by the Instituto del Mar del Peru (IMARPE). Additional surveys and mooring deployments extended the coverage to 20°S.

2. Methods

2.1. Shipboard measurements

A continuous stream of seawater was obtained from the ship's seawater system from a depth of about three meters. At the flow rates that were utilized, the time delay between the hull intake and the equilibrator was less than 1 min. A nondispersive infrared gas analyzer (LI-COR model 6262) was utilized to determine the mixing ratio of CO_2 in the atmosphere and in air equilibrated with surface seawater. A commercial CO_2 in dry air standard was calibrated with primary gas standards obtained from the National Oceanic and Atmospheric Administration Climate Monitoring and Diagnostics Laboratory. The result from standard comparisons that were performed with several infrared analyzers over two years indicate that the pCO_2 of the standard that was used in the field was known to at least ±1 ppm. At pCO_2 less than 1000 ppm the average error due to using a single mid-range calibration of the analyzer was estimated to be l ppm or less. Logistics did not allow routine shipboard calibration of the analyzer with compressed gases. In some cases manual calibrations were performed using standards in bags that had been shown to be stable at the 1 ppm level for a month. At other times atmospheric measurements were utilized to validate the sea surface data. Uncontaminated marine air in the sampled area has seasonal variability less than 1 ppm of CO_2 (GLOBAL VIEW-CO_2, 2006) and can be used to check instrument drift. At sea CO_2 free air and atmospheric samples were analyzed every 2 h and we estimate that errors due to blank drift were less than 0.1%. Due to the less than ideal calibration scheme, the measurement uncertainty ranged from 0.5% to 1% depending on cruise and operation conditions. Continuous seawater equilibrated measurements were made every two seconds and averaged at 1 min intervals. Two types of seawater equilibrators were used. Initially a membrane based system (Hales et al., 2004) for seawater equilibration was utilized, however the high phytoplankton densities encountered during bloom conditions necessitated frequent cleaning and caused some data losses. During later cruises a showerhead equilibrator with a total volume of 1 l and a water flow of about 1 l/min was utilized. The gas phase was continuously circulated through the equilibrator and infrared analyzer at a rate of about 250 ml/min. Water vapor, pressure and temperature were measured and appropriate dilution and solubility corrections were applied to estimate in-situ values. The equilibrator temperature was usually measured within ±0.01 C°. Data were adjusted to in-situ values using the temperature offsets observed between the equilibrator and hydrographic station CTD data. The overall system response time to reach 90% of a final equilibrated seawater pCO_2 value was about 1 min. Combining the calibration and measurement uncertainties, the derived sea surface pCO_2 data are probably within ± 1% of the in-situ levels. Values are reported as mixing ratios in dry air at one atmosphere. For part of the analysis the data from each cruise was averaged in 0.25° squares to minimize spatial sampling biases and to allow integration with remotely sensed wind and temperature information.

2.2. Mooring and drifter measurements

In addition to the shipboard measurements, a small mooring was deployed close to the coast near 21°S off northern Chile in July of 2005. CO_2 measurements on the mooring were made using a small low power infrared gas analyzer (Licor 820) following principles similar to those of Friederich et al. (1995). This device measured atmospheric and sea surface pCO_2 every 3 h. Temperature and salinity data was obtained using a Seabird model 47 CT sensor. Data transmission occurred via the Orbcom satellite system and four months of data was collected until the mooring line failed. The same type of system was also deployed as a drifter in October of 2005 off southern Peru at 16.28°S and 75.61°W.

We did not utilize the instantaneous shipboard wind data to estimate air–sea gas exchange since the time scale variability of sea surface pCO_2 distributions is likely to correspond to the upwelling event scale of days to weeks while the local winds can have significant variability on much shorter time scales. Blended interpolated 0.25° satellite wind data was obtained from the NOAA[1] National Climatic Data Center; monthly wind averages were then combined with the shipboard sea surface pCO_2, temperature and salinity data to estimate air–sea carbon exchange. All flux estimates were made using the Wanninkhof (1992) relationship for air–sea gas exchange with long term winds. The flux estimates were made by combining 0.25° spatially averaged shipboard sea surface pCO_2 results with the same resolution satellite wind data. A 30

---

[1] The wind data are acquired from NOAA's National Climatic Data Center, via their website. <http://www.ncdc.noaa.gov/oa/rsad/blendedseawinds.html>.

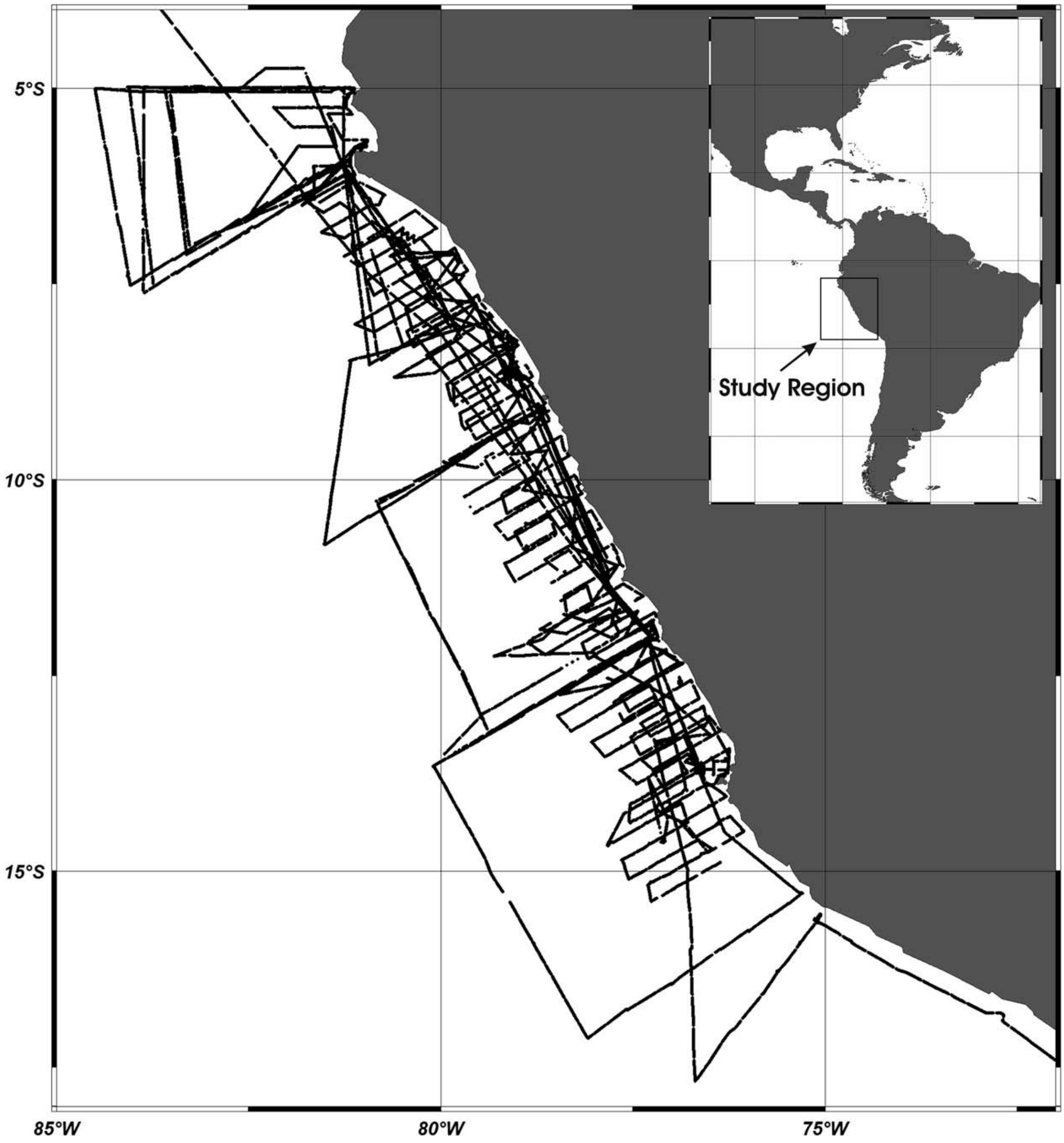

Fig. 1. Study area showing the cruise tracks from eight surveys between August 2004 and October 2006. Data was collected continuously along these tracks and initially averaged in 1 min time bins.

day filter was applied to the wind data and atmospheric pCO_2 was estimated using GLOBAL VIEW-CO_2 (2006). Regional sea surface temperature field was obtained from the NOAA National Climatic Data Center including the anomalies from the long-term mean (Smith and Reynolds, 2005).

3. Results

Between August 2004 and October 2006 sea surface pCO_2 data was collected successfully during 9 cruises off the coast of Peru (Fig. 1). In addition to the shipboard measurements, a coastal mooring in northern Chile recorded pCO_2 for about four months from August to November of 2005. The cruises were not evenly distributed in all seasons; they do however cover much of the Peruvian coast between 15°S and 5°S and in some cases extend out to about 350 km from the coast. While there are numerous interesting small scale features contained in the data, the current analysis is restricted to the general and persistent features of the pCO_2 distribution in the study area.

3.1. Average pCO_2 distribution

The most notable characteristic of this upwelling system is that average sea surface pCO_2 is above atmospheric values at all latitudes between the coastline and the offshore extent of our observations. Only about 5% of the observations contained data that was undersaturated relative to the atmosphere while 74% exceeded atmospheric pCO_2 by more than 100 ppm and 8% had pCO_2 levels more than twice the atmospheric value at the time of the observations (378 ppm). The lowest (~150 ppm) and the

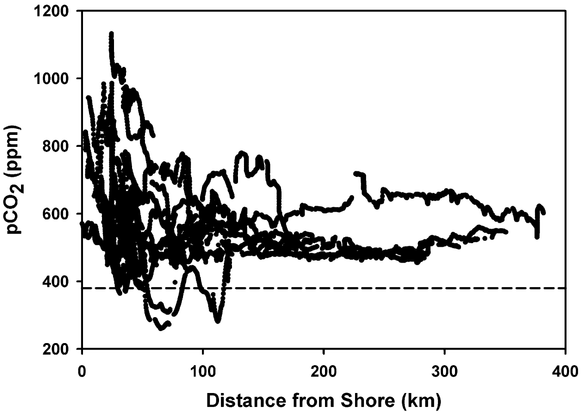

Fig. 2. Sea surface pCO_2 versus distance from shore off central Peru. Most surveys occupied this section which is perpendicular to the coast near 12°S. The dashed line indicates the mean atmospheric pCO_2 of 378 ppm at the time of these cruises.

highest (~1500 ppm) pCO_2 were found over the shelf near the coast. A representative transect of the data collected near 12°S demonstrates the general cross shelf trends (Fig. 2). Sea surface pCO_2 decreases with distance from shore for the first 100 km and then stabilizes but remains well above atmospheric value and does not trend towards equilibrium with the atmosphere over the outer 300 km of this transect (Fig. 2). In the nearshore coastal upwelling zone the highest pCO_2 was associated with local temperature minima. There is a general trend towards higher pCO_2 at low temperatures but this does not constrain the range of values observed at low temperatures. The absolute maxima occurred near 16 °C and the lowest values were observed on the continental shelf near 7°S at a temperature of about 18 °C (Fig. 3).

Latitudinal differences were examined in data collected within 100 km of the coast. While there is a clear decrease in average temperature of about 0.22 °C per degree of latitude towards the south, no significant trend in pCO_2 is evident (Fig. 4). All the very high pCO_2 values south of 15 °C are from a single cruise track.

3.2. Wind patterns

The annual average wind speed derived from 1995 to 2005 monthly climatology is illustrated in Fig. 5. The wind climatology off the Peruvian coast shows a distinct seasonal and spatial pattern. The wind direction is from the southeast or approximately parallel to the coast. There were no wind reversals during our observing period. The mean winds increase with distance from shore and the strongest winds are observed between July and September. This season of strong winds also has an enhanced offshore gradient. There is also a latitudinal gradient; weak winds occur over the shelf between 4°S and 12°S while stronger winds are found to the south. The maximum coastal winds are near 15°S and decrease rapidly south of 16°S. We examined the winds within 150 km of the coast where most of our data was collected and compared them to the climatology (Table 1). During most cruises the monthly mean winds for the coast were near the longer term average for that month. Even though there were north-south trends in the wind anomaly during any given month, these anomalies did not appear to be persistent. One exception was the October 2005 cruises when winds along the entire coast exceeded the climatology by an average of about 0.7 $m\,s^{-1}$.

The 30 day smoothed record of the mean sea surface temperature within 150 km of the coast (Fig. 6) indicates that the period of our observations was slightly colder than the long term average. Although cruise dates were clustered, periods of cold and warm anomalies were sampled. It is not clear at this time whether the low temperatures were the result of enhanced upwelling or if they were related to another large scale process.

The mooring at 21.35°S 70.12°W was deployed on July 26, 2005 and delivered data until November 16, 2005 (Fig. 7). Sea surface pCO_2 for 97% of this deployment was above atmospheric values. The range was from a high 950 ppm during a period of enhanced winds in mid September to a low of 285 ppm in early November when winds had decreased.

4. Discussion

The spatially averaged sea to air fluxes for each cruise make it clear that unlike many other highly productive coastal regions, the Peruvian coastal upwelling system is a source of CO_2 to the atmosphere throughout the year (Table 2). The flux values are high given the modest wind speeds along the Peru coast. There is substantial spatial heterogeneity in the fluxes but the highest values are always found close to the coast. Regions of lowest pCO_2 are also found near the coast, limited evidence suggests that these patches form during relatively stable low wind periods. Fluxes do not decrease as rapidly as pCO_2 as we move offshore due to the increasing average wind. The decrease in pCO_2 as we move offshore is driven primarily by biological uptake, however loss of CO_2 to the atmosphere is a noticeable portion of the carbon transfer out of the upper water column. In the extreme cases the sea to air flux was equivalent to 1 $gm\,C\,m^{-2}\,d^{-1}$. The persistent fluxes out of the ocean, driven by the elevated surface pCO_2, may result from a combination of factors including solar heating, offshore "Ekman pumping", nitrate deficits and iron limitation. Below we will use historical data to examine the possible magnitude of some of these driving forces.

4.1. Influence of heat flux

The greatest net heat flux into the ocean in the tropical Pacific occurs along the Peru coast and in the eastern equatorial Pacific (Weare et al., 1981). The combination of a large positive heat flux with a shallow mixed layer (Lentz, 1992) that is a characteristic of this upwelling region facilitates rapid heating of the surface layer. In the extreme case of a coastal upwelling plume near 15°S the surface heating has been estimated to be 0.8 °C per day (Stevenson et al., 1981). Longer term measurements of heat gain using Lagrangian drifters indicate a more moderate sea surface temperature increase. The results from a drifter released near 16°S in October 2005 (Fig. 8) give an average and nearly linear temperature rise of 0.11 °C per day during the initial 80 days of northwestward drift. During the initial weeks of the deployment this drifter measured sea surface pCO_2 at a depth of less than one meter. This drifter had a more northerly track than the analysis of drifter tracks in this region by Chaigneau and Pizarro (2005), but most drifters have been launched at greater distance from shore. The drifter climatology derived according to the methods of Lumpkin and Garraffo (2005) gives the same initial track as the drifter that we deployed and the tracks of other individual drifters followed similar routes in the NOAA drifter database. The observed temperature rise is a combination of the heat flux, deepening of the mixed layer, horizontal mixing and Ekman pumping. In the absence of biological activity and a constant mixed layer depth of about 10 m, this temperature rise is sufficient to counteract the effect of air–sea exchange on the oceanic pCO_2 when sea surface pCO_2 is below about 460 ppm, given the mean wind speed of about 6.5 $m\,s^{-1}$ along the track of this drifter. This estimate is based on the assumption that there is no change in alkalinity. At greater wind speeds the mixed layer depth would be greater and similar results would be obtained. The actual drifter results shown in Fig. 9 are much more complex since they include the effects of atmospheric

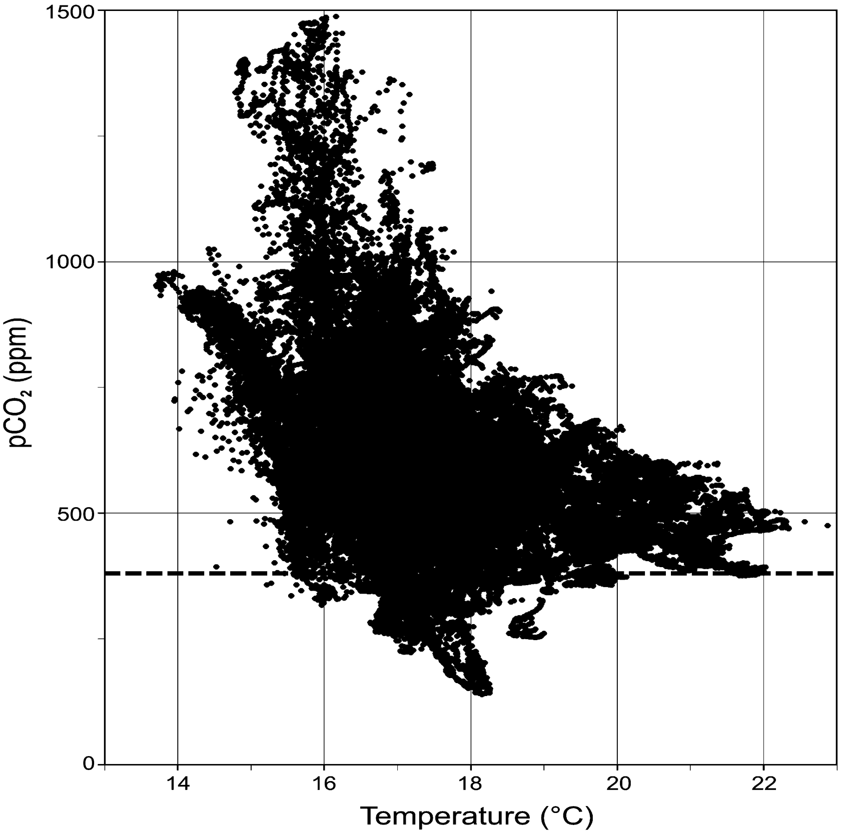

Fig. 3. The pCO_2 versus temperature relationship of all data collected between August 2004 and October 2006. The dashed line indicates the mean atmospheric pCO_2 of 378 ppm at the time of these cruises. There are approximately 125,000 observations and only about 5% of these are undersaturated relative to the overlying atmosphere. About 74% of the values are more than 100 ppm above atmospheric pCO_2.

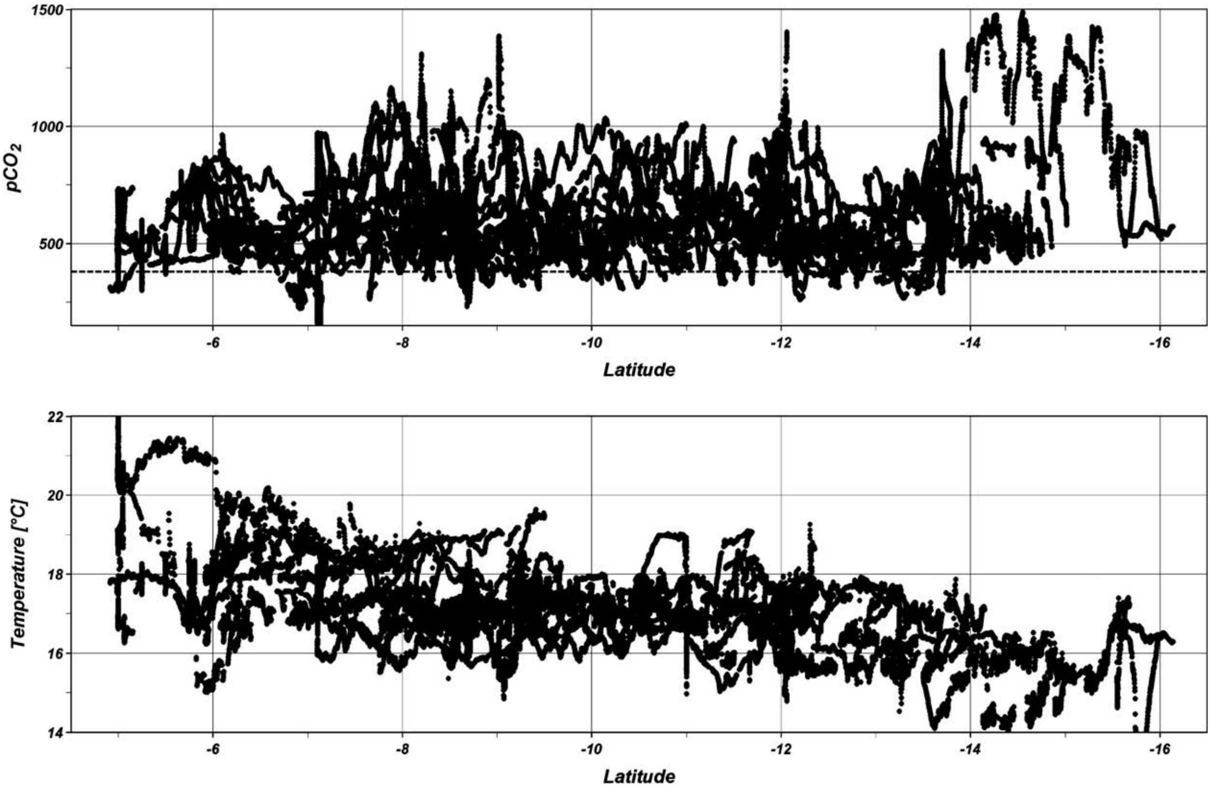

Fig. 4. Latitudinal distribution of temperature and pCO_2 within 100 km of the shore. There is a temperature gradient of about 0.22 °C per degree of latitude but average pCO_2 is similar at all latitudes. The very high values near 15°S are from a single survey.

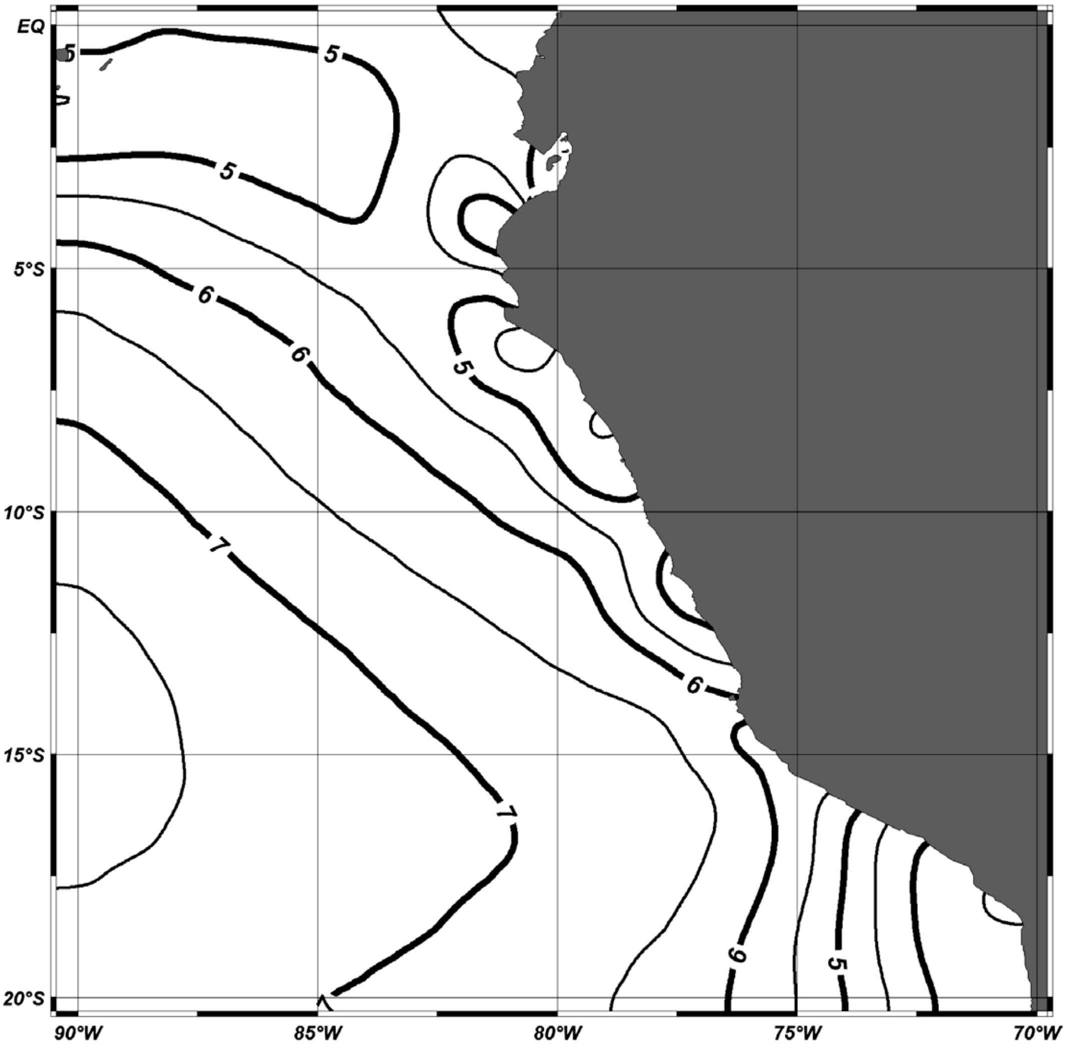

Fig. 5. Annual wind climatology derived from 1995 to 2005 blended satellite derived winds from NOAA's National Climate Data Center. Values are in meters per second.

Table 1
Wind speed and anomalies between 16°S and 5°S from the coast out to 150 km.

Date	Anomalies (m s^{-1})				Wind speed (m s^{-1})		
	Anomaly	Std. dev.	Min	Max	Mean	Min	Max
8/15/2004	0.27	0.39	−1.16	0.88	6.02	5.22	7.46
9/15/2004	−0.22	0.32	−1.4	0.44	5.3	4.46	6.83
11/15/2004	0.16	0.37	−0.95	0.98	5.36	4.19	6.64
2/15/2005	0.27	0.5	−0.98	1.35	4.65	3.14	6.34
10/15/2005	0.69	0.26	−0.18	1.53	6.25	5.02	8.05
4/15/2006	−0.37	0.55	−1.76	1.21	4.9	3.48	7.2
8/15/2006	0.15	0.39	−0.72	1.99	5.9	4.28	8.04
10/15/2006	0.10	0.38	−1.2	1.6	5.64	2.4	9.2

The means and anomalies were calculated from the 0.25° resolution blended satellite derived winds from NOAA's National Climate Data Center. The climatology for estimating the anomalies is based on the years 1995–2005.

exchange, community production, heating and inputs due to mixing or Ekman pumping. During the first nine days of the deployment the estimate of the integrated CO_2 loss from the sea surface was about 0.18 mol m^{-2} (~8 mol m^{-2} y^{-1}) while pCO_2 dropped from about 570 ppm to about 440 ppm. If we again assume a 10 m mixed layer, then the loss to the atmosphere was responsible for about 35% of the CO_2 decrease since the observed change in pCO_2 was approximately equivalent to a total CO_2 decrease of 50 μmol kg^{-1}. During the remainder of the deployment, average pCO_2 increased but the sea to air flux was somewhat diminished due to the lower wind speeds. We can only speculate that the pCO_2 increase during the second half of this deployment was due to offshore mixing and upwelling events combined with the observed warming. Even though pCO_2 climbed during the latter part of this deployment, the sea to air flux decreased due to diminishing winds to a rate of about 4 mol m^{-2} y^{-1}. On an annual basis we can make a rough approximation of the significance of surface heating on the sea to air CO_2 flux in this region. We estimated the change in the inorganic carbon budget of a parcel of upwelled water over time (60 days) due to biological uptake and air–sea exchange over significant range of initial conditions (pCO_2 650–1150) and biological uptake rates. The difference between a constant temperature scenario and a heating rate of 0.1 °C d^{-1} accounted for an annual flux of about 2 mol m^{-2}. This estimate varied by about 10% while the total annual flux in all of scenarios had a range of 2–12 mol m^{-2}.

4.2. Nutrient availability

Coastal upwelling systems that can be sinks for atmospheric CO_2 such as the Oregon coast (Hales et al., 2005), tend to have high levels of preformed nitrate and phosphate. Preformed nutrients are those nutrients present in a water mass during its formation. The assumptions are that oxygen and carbon are near equilibrium with

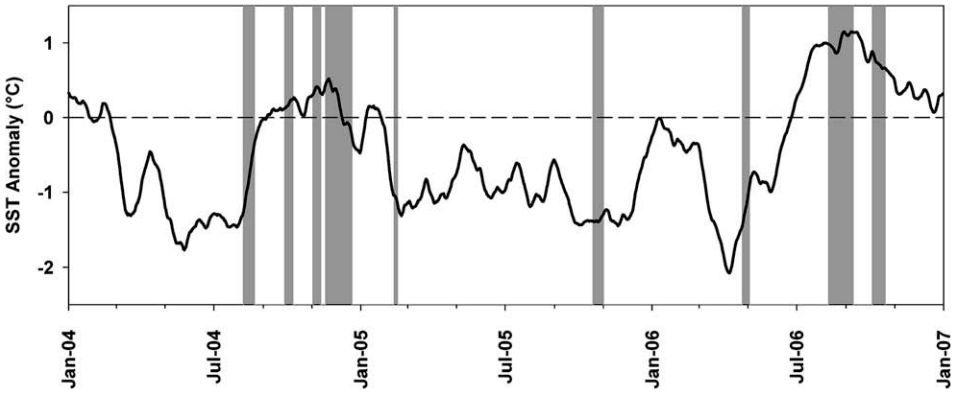

Fig. 6. Sea surface temperature anomaly within 150 km of the coast for the study region. A 30 day smoothing has been applied and the gray shaded bands indicate the times of the ship surveys.

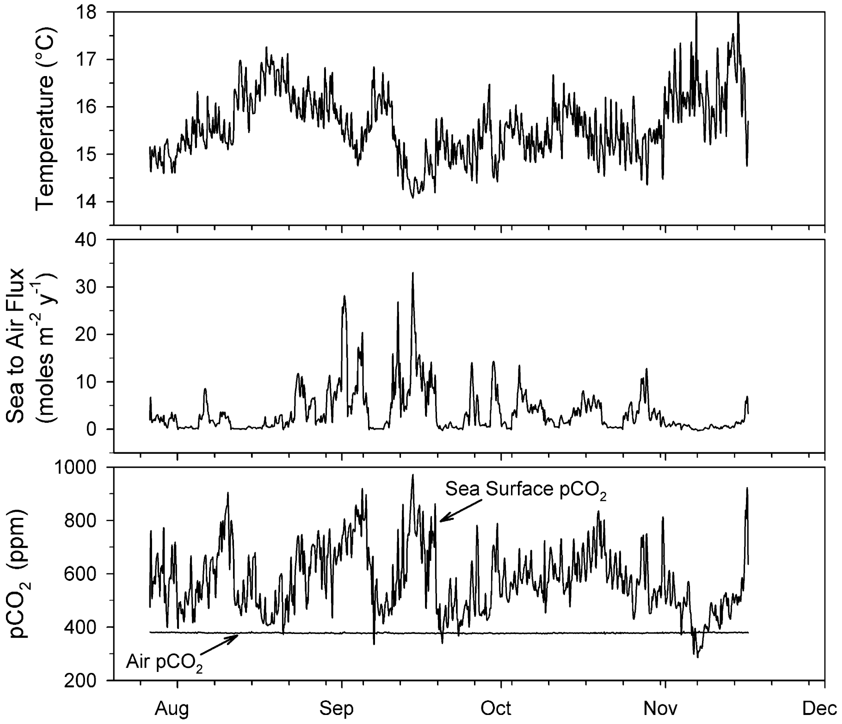

Fig. 7. A mooring deployed close to the coast at 21.35°S on July 26, 2005 produced a record of sea surface and atmospheric pCO_2 every 3 h until November 16, 2005. Temperature and salinity were also measured. The sea to air CO_2 flux was derived by combining the mooring data with daily satellite derived winds.

Table 2
Sea to air CO_2 fluxes (positive indicate degassing from the ocean to the atmosphere) estimates for each of the survey cruises given in units of mol m^{-2} y^{-1}.

Cruise date	Sea to air CO_2 flux (mol m^{-2} y^{-1})			
	Average	Std. dev.	Min	Max
August 2004	6.79	3.28	1.06	18.81
September 2004	4.12	2.62	−0.30	14.78
November 2004	2.10	1.97	−3.14	10.94
December 2004	3.47	2.26	−1.08	14.91
February 2005	2.34	0.83	0.85	4.54
October 2005	6.35	3.84	−0.33	26.82
April 2006	4.26	3.46	−1.87	12.01
August 2006	6.36	4.15	1.61	20.94
October 2006	10.12	9.19	0.03	51.41
Average	5.10	3.51	−0.35	19.46

The data was spatially normalized by first averaging the results in 0.25° squares. The flux calculations used the satellite derived winds and the flux versus wind speed formulation of Wanninkhof (1992).

the atmosphere during water mass formation and that any subsequent respiration has a predictable O_2:C:N ratio (Redfield ratio) (Anderson and Sarmiento, 1994; Li and Peng, 2002; Redfield et al., 1963). Preformed nitrate can be calculated using the simple relationship utilizing the apparent oxygen utilization (AOU) and measured nitrate:

$$\text{preformed} \quad \text{nitrate} = \text{measured} \quad \text{nitrate} - (\text{AOU})(\text{N}/\text{O}_2)$$

where N/O_2 is the Redfield nitrogen to oxygen ratio. When these waters are returned to the surface during upwelling, the consumption of the nutrient released during respiration should return pCO_2 to atmospheric levels and the additional consumption of the preformed nutrients can then produce an additional carbon drawdown. Due to anthropogenic carbon increases in the atmosphere even the consumption of the nutrients released during respiration can produce sea surface pCO_2 slightly below current atmospheric levels. Along the coast of Peru waters with a density of 26.0 σ_t

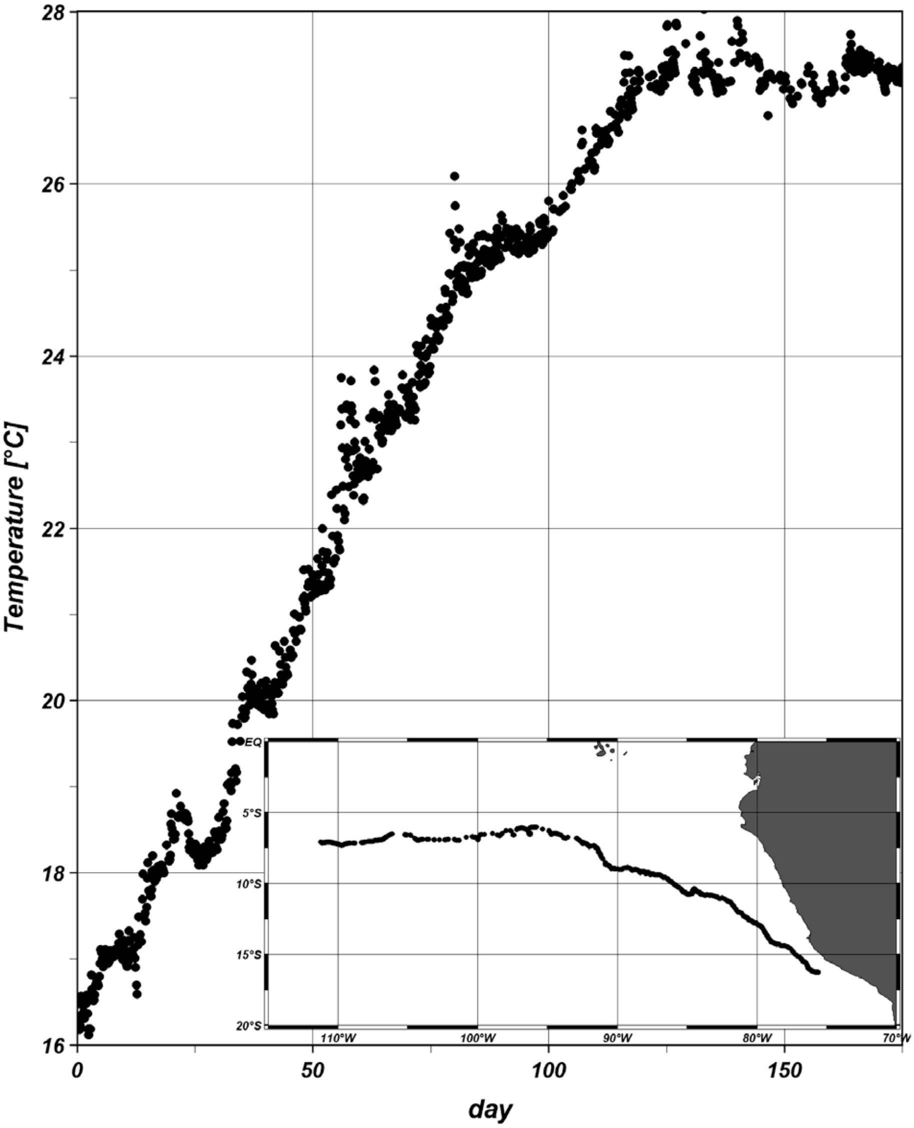

Fig. 8. Sea surface temperature and track of the drifter that was deployed on October 10, 2005 off southern Peru (16.278°S, 75.612°W).

can be considered representative of waters brought to the surface during moderate upwelling (Friederich and Codispoti, 1981; Minas et al., 1986); these waters are advected southward in the coastal undercurrent (Brink et al., 1980) and have a temperature of about 15 °C and a salinity of 35. This water mass was probably formed in the western Pacific (Reid, 1997) where an examination of surface water with these temperature and salinity characteristics indicates that nitrate concentrations during water mass formation was near zero. We have combined all historical hydrographic data available from NODC and estimated preformed nitrate on the 26.0 σ_t surface within 200 km of the coast between 5°S and 16°S. The results indicate an average preformed nitrate value of 0 to $-4\ \mu\text{mol kg}^{-1}$ depending on the chosen Redfield ratio. This calculation indicates that the nutrient levels in the upwelled water in this region are not sufficient to reduce inorganic carbon back to the level that was present when the water mass formed. Since actual preformed nitrate values can not be negative, this is an indication that these source waters have interacted with the underlying denitrification zone (Codispoti et al., 1986; Minas et al., 1986). This estimate of the nitrate deficit based on preformed nitrate is conservative because it is based on oxygen consumption and oxygen is not involved in denitrification. When an estimate of the nitrate deficit based on phosphate (Gruber and Sarmiento, 1997) is made in the upper water column, the average nitrate deficit within 200 km of the coast is closer to $8\ \mu\text{mol kg}^{-1}$; this estimate utilizes a more abundant data set including the results obtained by IMARPE. When water with a preformed nitrate level of zero is upwelled and all nitrate is consumed with a Redfield C:N ratio, the resultant pCO_2 should be close to the atmospheric pCO_2 at the time of water mass formation when adjusted for any heating or cooling. The nitrate deficit in the Peruvian upwelling limits the carbon consumption and a nitrate deficit estimate of $6\ \mu\text{mol kg}^{-1}$ based on the average nitrate deficit calculations using a variety of Redfield ratios results in a pCO_2 that is about 85 ppm above the atmospheric value at the time of water mass formation after all the upwelled nitrate has been consumed. In the eastern tropical North Pacific CFC based age estimates are approximately 20–25 years (Mecking et al., 2004) for the 26.0 σ_t surface. CFC concentrations on this density surface off Peru were similar to those measured in the eastern tropical North Pacific for the same year during the WOCE surveys. In the past twenty years atmospheric pCO_2 has increased by about 35 ppm (GLOBAL VIEW-CO_2, 2006); this has reduced the potential average excess pCO_2 from 85 ppm to 45 ppm. Given the average wind field, the nitrate deficit in

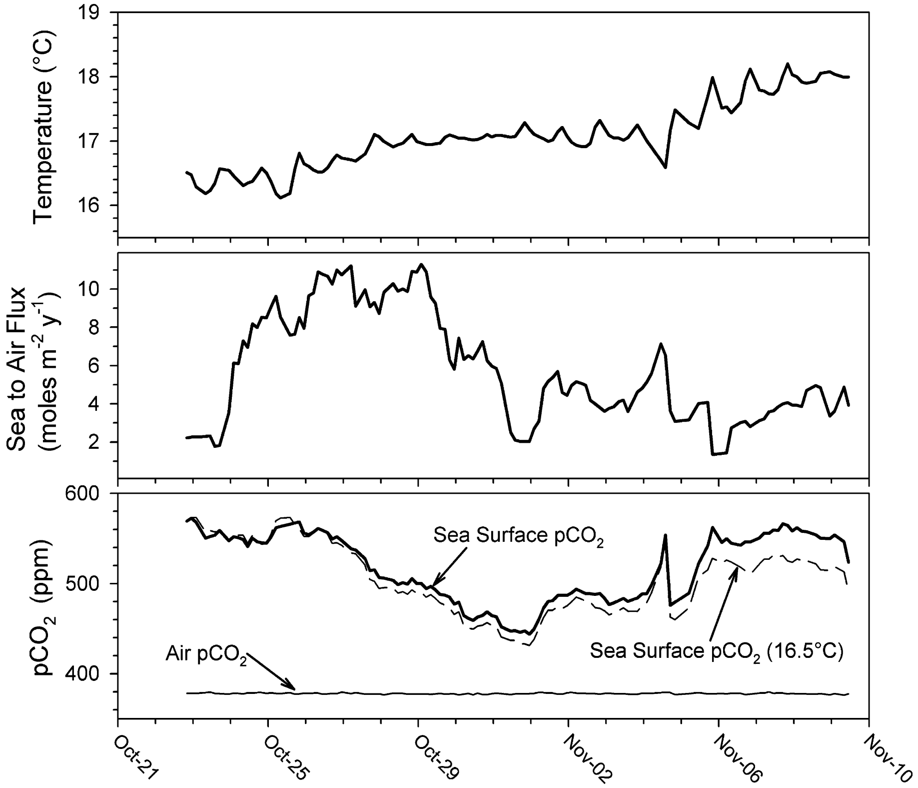

Fig. 9. Temperature, estimated sea to air CO_2 flux and pCO_2 from the initial period of the drifter deployment in October–November 2005. Sea to air CO_2 flux was estimated by combining the satellite derived winds with the drifter pCO_2, temperature and salinity data.

the upwelling waters therefore has the potential of contributing about 1.5 mol m^{-2} to the sea to air CO_2 flux on an annual basis.

4.3. High pCO_2 offshore

The measured levels of pCO_2 in the offshore region were higher than expected and indicate the incomplete utilization of upwelled macro nutrients. It is difficult to estimate and separate the contributions due to iron limitation and Ekman pumping, especially since it is likely that these two factors are coupled. Studies of iron limitation in the Peru upwelling system have noted that the waters over the shelf are replete with available iron, but iron concentrations in offshore waters tend to be low and can lead to the incomplete utilization of macro nutrients (Bruland et al., 2005; Hutchins et al., 2002). The cyclonic curl of the wind stress along the entire Peruvian coast can contribute to oceanic upwelling of iron poor water up to several hundred kilometers from the coast (Bakun and Nielson, 1991). The cyclonic wind stress and curl reaches its maximum during the austral winter when mixed layer depth is also greater and primary productivity is lower. This combination of effects can force the large sea to air fluxes measured in the offshore region.

4.4. Short-term variability

Using the current data set we can not determine the southern boundary of the region where there are persistent high CO_2 fluxes from the ocean to the atmosphere extending a significant distance from the coast. Observations made along the Chilean coast near 30°S and 23°S suggest that high sea surface pCO_2 may be constrained to coastal waters in that region and that biological activity may easily reduce pCO_2 to sub-atmospheric levels (Torres et al., 2003, 1999). A mooring that we deployed from August until November of 2005 near 21°S (Fig. 9) provided a record of continuous high pCO_2 but we do not know the offshore extent of this feature. During the four month deployment the average ΔpCO_2 at the mooring site was close to 200 ppm with a maximum ΔpCO_2 of almost 600 ppm and minimum near −100 ppm. It thus appears as if the crossover from source to sink may occur between 21°S and 27°S. When we combined the mooring data with daily satellite derived winds an average sea to air CO_2 flux of 3.5 mol m^{-2} y^{-1} was estimated using the Wanninkhof (1992) formulation. Some of the periods of high wind coincided with high sea surface pCO_2 resulting in a skewed temporal distribution of the flux. About 50% of the cumulative flux occurred during 16% of the sampling interval and 90% of the total flux can be accounted for by 50% of the days that were sampled. These results indicate that high frequency observations are valuable when we attempt to estimate sea to air CO_2 fluxes in the coastal regime. The major time scales of variability in this record are daily and the wind driven upwelling event scale. Major wind driven upwelling event such as the one in mid September are responsible for much of the total flux but the short-term variability may generate significant modulations. Diurnal heating and primary productivity are the major cause for the high frequency variability in sea surface pCO_2 with an amplitude up to 200 ppm. The average daily heating of the sea surface raised the water temperature by about 0.85 °C and should have raised pCO_2 by an average of about 21 ppm. Rather than rising, pCO_2 usually decreases during the daylight hours when the sea surface temperature is increasing. The average daytime decrease is about 160 ppm and is equivalent to a 50 μmol kg^{-1} decrease of total CO_2 under prevailing conditions. It is likely that the daytime CO_2 decrease is primarily due to phytoplankton carbon uptake at a rate that is greater than the replenishment from upwelling and respiration. A decrease of mixed layer depth due to surface heating may restrict CO_2 flux to the atmosphere to a smaller volume of water and enhance the observed CO_2 decrease, but even in extreme scenarios this effect can only account for a few percent of the daytime decline. This is not surprising since the average sea to air flux of 3.5 mol y^{-1} at this site amounts to about 1 μmol kg^{-1} d^{-1} if distributed over a 10 m mixed layer. During the night the combination of upwelling and respiration tends to restore the high sea surface pCO_2.

5. Conclusions

The Peruvian upwelling system was found to be a source of CO_2 to the atmosphere during all seasons. The spatially normalized annual flux estimate obtained in this study is 5.7 mol m^{-2} y^{-1} from the sea surface to the atmosphere. Table 1 reports the average of the cruises while this value is calculated in a manner analogous to Takahashi et al (2002). When applied to an area of 2000 km of coastline and 400 km from shore this represents a flux of 5.5×10^{13} g or 0.055 Pg C/yr. Feely et al. (2006) estimated a flux of 0.43 Pg C/yr for the period 1998–2004 for a region from 5°N to 10°S and 165°E to 95°W. Extrapolating the coastal values from the coast to 95°W and from the equator to 15°S gives a flux of 0.25 Pg C/yr or over half of the equatorial estimate. This value is certainly too high; when the coastal measurements from this study are combined with the open ocean measurements of Takahashi et al. (2002) a flux of 0.11 Pg C/yr, about 25% of the equatorial flux, is estimated.

The persistent high sea surface pCO_2 observed in this region can be attributed to a combination of the following factors: (1) a nitrate deficit relative to inorganic carbon in the upwelled water; (2) high heat fluxes and rapid warming, and (3) iron limitation of biological uptake of CO_2. The maximum fluxes occurred during the austral winter and spring and the minimum was in summer; this seasonality is driven by a combination of sea surface pCO_2, winds and primary productivity. The higher winds in winter and spring intensify upwelling of CO_2 enriched water and enhance the sea to air transfer. Somewhat paradoxically, primary productivity is lower during the time of maximum upwelling (Pennington et al., 2006). It may be that during the high wind season offshore upwelling, driven by the curl of the wind stress, brings nutrient and CO_2 rich but iron deficient waters to the surface. A similar process was postulated for California by Johnson et al. (1999). The upwelled water may come from greater depths that are lower in oxygen and more deficient in nitrate relative to CO_2 further enhancing degassing. The combination of enhanced upwelling, high winds and iron-limited primary production leads to very high fluxes from the ocean to the atmosphere.

The general trend of low latitude coastal regions as sources of CO_2 to the atmosphere and high latitude regions as sinks is well supported by our observations. Reports from southern South America indicate a change from source to sink that is similar to that found in North America (Torres et al., 2003; Torres et al., 1999). It appears that for South America the crossover from source to sink may occur between 21°S and 27°S. The low latitude coastal upwelling regions in the Cariaco Basin and the Arabian Sea are also reported to be source regions (Astor et al., 2005; Goyet et al., 1998; Kortzinger et al., 1997). Conditions at low latitudes may forecast those that might be found at higher latitudes in the future (due to increased uptake of fossil fuel CO_2).

Acknowledgements

We wish to thank numerous colleagues who assisted in the field efforts as well as the personnel aboard the *R/V Jose Olaya Balandra* and *R/V Knorr*. Dorota Kolber assisted in processing the wind and nutrient data. Financial support for this work was provided by the National Aeronautics and Space Administration under grant NAG5-12392 and by the David and Lucile Packard Foundation.

References

Anderson, L.A., Sarmiento, J.L., 1994. Redfield ratios of remineralization determined by nutrient data analysis. Global Biogeochemical Cycles 8, 65–80.

Astor, Y.M., Scranton, M.I., Muller-Karger, F., Bohrer, R., Garcia, J., 2005. fCO_2 variability at the CARIACO tropical coastal upwelling time series station. Marine Chemistry 97, 245–261.

Bakun, A., Nielson, C.S., 1991. The seasonal cycle of wind-stress curl in subtropical eastern boundary current regions. Journal of Physical Oceanography 21, 1815–1834.

Borges, A.V., Delille, B., Frankignoulle, M., 2005. Budgeting sinks and sources of CO_2 in the coastal ocean: diversity of ecosystems counts. Geophysical Research Letters 32, L14601.

Borges, A.V., Frankignoulle, M., 2002. Aspects of dissolved inorganic carbon dynamics in the upwelling system off the Galician coast. Journal of Marine Systems 32, 181–198.

Brink, K.H., Halpern, D., Smith, R.L., 1980. Circulation in the Peruvian upwelling system near 15°S. Journal of Geophysical Research 85, 4036–4048.

Bruland, K.W., Rue, E.L., Smith, G.J., DiTullio, G.R., 2005. Iron, macronutrients and diatom blooms in the Peru upwelling regime: brown and blue waters of Peru. Marine Chemistry 93, 81–103.

Cai, W.J., 2006. Air–sea exchange of carbon dioxide in ocean margins: a province-based synthesis. Geophysical Research Letters 33, L12603.

Cai, W.J., Dai, M., 2004. Comment on “enhanced open ocean storage of CO_2 from shelf sea pumping”. Science 306, 1477c.

Chaigneau, A., Pizarro, O., 2005. Mean surface circulation and mesoscale turbulent flow characteristics in the eastern South Pacific from satellite tracked drifters. Journal of Geophysical Research 110. doi:10.1029/2004JC002628.

Chavez, F.P., Strutton, P.G., Friederich, G.E., Feely, R.A., Feldman, G.C., Foley, D.G., McPhaden, M.J., 1999. Biological and chemical response of the equatorial pacific ocean to the 1997–98 El Niño. Science 286, 2126–2131.

Chavez, F.P., Takahashi, T., Cai, W.J., Friederich, G., Hales, B., Wanninkhof, R., Feely, R.A. 2007. Coastal Oceans. In: King, A.W., Dilling, L., Zimmerman, G.P., Fairman, D.M., Houghton, R.A., Marland, G., Rose, A.Z., Wilbanks, T.J. (Eds.), The First State of the Carbon Cycle Report (SOCCR): The North American Carbon Budget and Implications for the Global Carbon Cycle. A Report by the US Climate Change Science Program and the Subcommittee on Global Change Research. National Oceanic and Atmospheric Administration, National Climatic Data Center. Asheville, NC, USA, pp. 149–156.

Chen, C.T.A., 2004. Exchanges of carbon in the coastal seas. In: Field, C.B., Raupach, M.R. (Eds.), The Global Carbon Cycle. Island Press, Washington, DC, pp. 341–351.

Codispoti, L.A., Friederich, G.E., Packard, T.T., Glover, H.E., Kelly, P.J., Spinrad, R.W., Barber, R.T., Elkins, J.W., Ward, B.B., Lipschultz, F., Lostaunau, N., 1986. High nitrite levels off northern Peru: a signal of instability in the marine denitrification rate. Science 233, 1200–1202.

Copin-Montegut, C., Raimbault, P., 1994. The Peruvian upwelling near 15°S in August 1986. Results of continuous measurements of physical and chemical properties between 0 and 200 m depth. Deep Sea Research Part I: Oceanographic Research Papers 41, 439–467.

Feely, R.A., Boutin, J., Cosca, C.E., Dandonneau, Y., Etcheto, J., Inoue, H.Y., Ishii, M., Quere, C.L., Mackey, D.J., McPhaden, M., Metzl, N., Poisson, A., Wanninkhof, R., 2002. Seasonal and interannual variability of CO_2 in the equatorial Pacific. Deep Sea Research Part II: Topical Studies in Oceanography 49, 2443–2469.

Feely, R.A., Takahashi, T., Wanninkhof, R., McPhaden, M.J., Cosca, C.E., Sutherland, S.C., Carr, M.-E., 2006. Decadal variability of the air–sea CO_2 fluxes in the equatorial Pacific Ocean. Journal of Geophysical Research 111, C08S90. doi:10.1029/2005JC003129.

Friederich, G.E., Brewer, P.G., Herlien, R., Chavez, F.P., 1995. Measurement of sea surface partial pressure of CO_2 from a moored buoy. Deep Sea Research Part I: Oceanographic Research Papers 42, 1175–1186.

Friederich, G.E., Codispoti, L.A., 1981. The effects of mixing and regeneration on the nutrient content of upwelling waters off Peru. In: Richards, F.A. (Ed.), Coastal Upwelling. American Geophysical Union, Washington, DC, pp. 221–227.

Friederich, G.E., Walz, P.M., Burczynski, M.G., Chavez, F.P., 2002. Inorganic carbon in the central California upwelling system during the 1997–1999 El Nino-La Nina event. Progress In Oceanography 54, 185–203.

GLOBALVIEW-CO_2 2006. Cooperative atmospheric data integration project – carbon dioxide. CD-ROM, NOAA ESRL, Boulder, Colorado.

Goyet, C., Millero, F.J., O’Sullivan, D.W., Eischeid, G., McCue, S.J., Bellerby, R.G.J., 1998. Temporal variations of pCO_2 in surface seawater of the Arabian Sea in 1995. Deep Sea Research Part I: Oceanographic Research Papers 45, 609–623.

Gruber, N., Sarmiento, J.L., 1997. Global patterns of marine nitrogen fixation and denitrification. Global Biogeochemical Cycles 11, 235–266.

Hales, B., Chipman, D.W., Takahashi, T.T., 2004. High-frequency measurement of partial pressure and total concentration of carbon dioxide in seawater using microporous hydrophobic membrane contactors. Limnology and Oceanography: Methods 2, 356–364.

Hales, B., Takahashi, T., Bandstra, L., 2005. Atmospheric CO_2 uptake by a coastal upwelling system. Global Biogeochemical Cycles 19. doi:10.1029/2004GB002295.

Hutchins, D.A., Hare, C.E., Weaver, R.S., Zhang, Y., Firme, G.F., DiTullio, G.R., Alm, M.B., Riseman, S.F., Maucher, J.M., Geesey, M.E., Trick, C.G., Smith, G.J., Rue, E.L., Conn, Bruland, K.W., 1981. Phytoplankton iron limitation in the humboldt current and Peru upwelling. Limnology and Oceanography 47, 997–1011.

Johnson, K.S., Chavez, F.P., Friederich, G.E., 1999. Continental-shelf sediment as a primary source of iron for coastal phytoplankton. Nature 398, 697–700.

Kortzinger, A., Duinker, J.C., Mintrop, L., 1997. Strong CO_2 emissions from the Arabian Sea during south-west monsoon. Geophysical Research Letters 24, 1763–1766.

Lentz, S.J., 1992. The surface boundary layer in coastal upwelling regions. Journal of Physical Oceanography 22, 1517–1539.

Li, Y.H., Peng, T.H., 2002. Latitudinal change of remineralization ratios in the oceans and its implication for nutrient cycles. Global Biogeochemical Cycles 16, 1130.

Lumpkin, R., Garraffo, Z., 2005. Evaluating the decomposition of tropical atlantic drifter observations. Journal of Atmospheric and Oceanic Technology 22, 1403–1415.

Mecking, S., Warner, M.J., Greene, C.E., Hautala, S.L., Sonnerup, R.E., 2004. Influence of mixing on CFC uptake and CFC ages in the North Pacific thermocline. Journal of Geophysical Research 109, C07014.

Minas, H.J., Minas, M., Packard, T.T., 1986. Productivity in upwelling areas deduced from hydrographic and chemical fields. Limnology and Oceanography 31, 1182–1206.

Pennington, J.T., Mahoney, K.L., Kuwahara, V.S., Kolber, D.D., Calienes, R., Chavez, F.P., 2006. Primary production in the eastern tropical Pacific: a review. Progress in Oceanography 69, 285–317.

Redfield, A.C., Ketchum, B.H., Richards, F.A., 1963. The influence of organisms on the composition of seawater. In: Hill, M.N. (Ed.), The Sea: Ideas and Observations on Progress in the Study of the Seas, vol. 2. John Wiley, New York, pp. 26–77.

Reid, J.L., 1997. On the total geostrophic circulation of the Pacific Ocean: flow patterns, tracers, and transports. Progress in Oceanography 39, 263–352.

Simpson, J.J., Zirino, A., 1980. Biological control of pH in the Peruvian upwelling area. Deep Sea Research Part I: Oceanographic Research Papers 27, 733–743.

Smith, T.M., Reynolds, R.W., 2005. A global merged land–air–sea surface temperature reconstruction based on historical observations (1880–1997). Journal of Climate 18, 2021–2036.

Stevenson, M.R., Stuart, D.W., Heburn, G.W., 1981. Short-term variations observed in the circulation, heat content and surface mixed layer of an upwelling plume off Cabo Nazca* Peru. In: Richards, F.A. (Ed.), Coastal Upwelling. American Geophysical Union, Washington, DC, pp. 125–133.

Takahashi, T., Sutherland, S.C., Sweeney, C., Poisson, A., Metzl, N., Tilbrook, B., Bates, N., Wanninkhof, R., Feely, R.A., Sabine, C., Olafsson, J., Nojiri, Y., 2002. Global sea to air CO_2 flux based on climatological surface ocean pCO_2, and seasonal biological and temperature effects. Deep Sea Research Part II: Topical Studies in Oceanography 49, 1601–1622.

Thomas, H., Bozec, Y., Elkalay, K., de Baar, H.J.W., 2004. Enhanced open ocean storage of CO_2 from Shelf Sea pumping. Science 304, 1005–1008.

Torres, R., Turner, D.R., Rutllant, J., Lefèvre, N., 2003. Continued CO_2 outgassing in an upwelling area off northern Chile during the development phase of El Niño 1997–1998 (July 1997). Journal of Geophysical Research, 108.

Torres, R., Turner, D.R., Silva, N., Rutllant, J., 1999. High short-term variability of CO_2 fluxes during an upwelling event off the Chilean coast at 30°S. Deep Sea Research Part I: Oceanographic Research Papers 46, 1161–1179.

Ver, L.M.B., Mackenzie, F.T., Lerman, A., 1999. Carbon cycle in the coastal zone: effects of global perturbations and change in the past three centuries. Chemical Geology 159, 283–304.

Walsh, J.J., 1991. Importance of continental margins in the marine biogeochemical cycling of carbon and nitrogen. Nature 350, 53–55.

Wanninkhof, R., 1992. Relationship between wind speed and gas exchange over the ocean. Journal of Geophysical Research 97, 7373–7382.

Weare, B.C., Strub, P.T., Samuel, M.D., 1981. Annual mean surface heat fluxes in the tropical Pacific Ocean. Journal of Physical Oceanography 11, 705–717.

Wollast, R., 1998. Evaluation and comparison of the global carbon cycle in the coastal zone and in the open ocean. In: Brink, K.H., Robinson, A.R. (Eds.), The Sea, vol. 10. Wiley, New York, pp. 213–252.

Progress in Oceanography 79 (2008) 167–176

Contents lists available at ScienceDirect

Progress in Oceanography

journal homepage: www.elsevier.com/locate/pocean

The seasonal cycle of surface chlorophyll in the Peruvian upwelling system: A modelling study

V. Echevin [a,*], O. Aumont [a,c], J. Ledesma [b], G. Flores [b]

[a] *LOCEAN/IRD/IPSL, Laboratoire d'Océanographie et de Climatologie: Expérimentation et Approches Numériques, IRD/UPMC/IPSL, Paris, France*
[b] *IMARPE, Esquina de Gamarra y General Valle S/N Chucuito Callao, Peru*
[c] *Centre IRD de Bretagne, Plouzané, France*

ARTICLE INFO

Article history:
Accepted 14 October 2008
Available online 21 October 2008

ABSTRACT

The seasonal variability of surface chlorophyll in the northern Humboldt Current System is studied using satellite data, *in situ* observations and model simulations. The data show that surface chlorophyll concentration is highest in austral summer and decreases during austral winter, in phase opposition with coastal upwelling intensity. A regional model coupling ocean dynamics and biogeochemical cycles is used to investigate the processes which control this apparently paradoxical seasonal cycle. Model results suggest that the seasonal variability of the mixed layer depth is the main controlling factor of the seasonality. In winter, the mixed layer deepening reduces the surface chlorophyll accumulation because of a dilution effect and light limitation. In summer, biomass concentrates near the surface in the shallow mixed layer and nitrate limitation occurs, resulting in a biomass decrease in the middle of summer. Intense blooms occur during the spring restratification period, when winter light limitation relaxes, and during the fall destratification period, when the surface layer is supplied with new nutrients. Model sensitivity experiments show that the seasonal variations in insolation and surface temperature have little impact on the surface chlorophyll variability.

1. Introduction

The Peruvian upwelling system (the nearshore 250 km of the Humboldt Current; hereafter PUS) is one of the most intense upwelling systems in the world ocean. Relatively weak, seasonally varying, upwelling-favorable winds drive an offshore Ekman transport and an upward flux of cold, nutrient-rich waters along the coast. The presence of nutrient-rich waters and high insolation at this low latitude generates a year-long but fluctuating phytoplankton bloom which sustains a very rich ecosystem with high stocks of pelagic fish (FAO, 1999). The subsurface waters off Peru have very low oxygen concentrations (Minas et al., 1990), due to low ventilation (Wyrtki, 1962) and to oxygen consumption by the organisms remineralizing the abundant organic matter sinking from the surface (Paulmier et al., 2006). These processes lead to the formation of one of the most intense oxygen minimum zones of the world ocean, whose impact on the surface productivity and on the overlying pelagic ecosystem remains an open question.

The PUS is influenced by the variability of equatorial origin at intraseasonal (Bonhomme et al., 2007) and interannual time scales (Carr et al., 2002). Equatorial variability can propagate along the coast as far south as 40°S (Ulloa et al., 2001) in the form of coastally trapped waves. The upwelling system is also subject to decadal climate variability as shown by the very long time series of ecosystem indices (Chavez et al., 2003). Although the intense nearshore biological activity is related to the wind-driven coastal upwelling, the response of the ecosystem to the wind varies significantly depending on the time scales. Indeed, the seasonal fluctuations of surface productivity, as observed by satellite and *in situ* surface chlorophyll measurements (Chavez et al., 1995, Thomas et al., 2001; Pennington et al., 2006, hereafter PEN06) and of wind intensity, are in opposition. Surface chlorophyll decreases in austral winter, the period during which coastal upwelling and nutrient supply from the subsurface is supposed to be strongest (Calienes et al., 1985). The coupled physical-biogeochemical processes governing this counter-intuitive variability have not been fully investigated, nor their relative impacts quantified. Calienes et al. (1985) suggested that the mixed layer depth increase in winter could reduce surface chlorophyll through light limitation of phytoplankton growth. Guillen and Calienes (1981) also invoke the potential role of low solar insolation in winter. However, other processes may have an impact, such as the seasonal variations of surface macro and micro-nutrient concentrations driven by the upwelling variability, or the surface temperature variations. In the present work, we investigate these processes using ocean color satellite data, *in situ* observations and model simulations. This approach allows evaluation of the relative role of the processes involved. In the following section (Section 2), the data, model and methodology are described. The results are presented in Section 3, and are discussed

---

* Corresponding author.
E-mail address: vincent.echevin@locean-ipsl.upmc.fr (V. Echevin).

0079-6611/$ - see front matter © 2008 Elsevier Ltd. All rights reserved.
doi:10.1016/j.pocean.2008.10.026

in Section 4. Conclusions and perspectives are outlined in Section 5.

2. Materials and methods

Surface chlorophyll concentrations were studied using two different data sets. First, we used *in situ* chlorophyll observations collected by IMARPE (Instituto del Mar del Peru) during 1992–2004 (Fig. 1a). A complete description of the *in situ* data processing and quality control is provided in Appendix A gridded product was constructed as follows: the data for each month of the 1992–2004 period were first binned in a 0.5° × 0.5° grid. Extreme values were filtered out (in log scale) by removing values higher than twice the standard deviation in each spatial bin. The data were then averaged, and transformed into real, i.e. non-log, values, for each month. Data collected during the El Nino years in the 1997–1998 period were included.

Second, we used the SeaWiFS chlorophyll product (version 4 chlorophyll algorithm) for October 1997–December 2004 (Fig. 1b). The data (8-day chlorophyll-*a* composites) were rebinned from the original 0.0879° × 0.0879° grid in a low resolution (0.5° × 0.5°) grid to reduce the noise, the effects of clouds, and the impact of the very high chlorophyll concentrations very close to the shore, which may be unrealistic. The monthly climatology was constructed by removing extreme values (higher than twice the standard deviation in log scale), and averaging log-scale data for each month and for each pixel.

The third data set consists of *in situ* nutrient (nitrate, phosphate, silicate) concentrations collected by IMARPE during 1992–2004. As with the *in situ* chlorophyll data, a gridded product was constructed by binning and averaging the data in a 0.5° × 0.5° grid, after filtering out the extreme values (higher than twice the standard deviation) in each bin. The protocol for processing the nutrient data is also described in the Appendix.

Last, outputs from a numerical model were used to study the different processes governing surface chlorophyll in the upwelling system. To this end, the Regional Ocean Modelling System circulation model (ROMS, Shchepetkin and McWilliams, 2005) and the biogeochemical model (PISCES, Aumont et al., 2003; Aumont and Bopp, 2006) have been coupled:

- The Regional Ocean Modelling System (ROMS) is a free surface, sigma coordinate, primitive equation model. In the present study, the horizontal resolution is 1/6°. ROMS has 30 levels in the vertical, with an increase of resolution near the surface. Because of the use of sigma coordinates, the resolution in the vertical varies depending on the water column depth. The surface layer thickness ranges from a minimum of 10 cm in a 50-m deep nearshore water column, to 6 m in a 4000-m deep water column. Similarly, the bottom layer thickness ranges from 9 m to 900 m. The model configuration used here is very similar to that in Penven et al. (2005), but with a coarser horizontal resolution (1/9° in Penven et al., 2005). For a more complete description of the dynamical model configuration and numerical schemes, the reader is referred to Penven et al. (2005) and to Shchepetkin and McWilliams (2005) respectively.
- PISCES (Pelagic Interaction Scheme for Carbon and Ecosystem Studies) is a biogeochemical model derived from the Hamburg Model of Carbon Cycle, version 5 HAMOCC5 (Aumont et al., 2003). PISCES simulates biological productivity and the biogeochemical cycles of carbon and of the main nutrients (Phosphate, Nitrate, Ammonium, Silicate and Iron). It assumes that phytoplankton growth is directly limited by the external availability in nutrients, and includes two phytoplankton size classes (nanophytoplankton and diatoms), two zooplankton size classes (microzooplankton and mesozooplankton) and two detritus size classes. Diatoms differ from nanophytoplankton by their need for Si, by higher requirements for Fe (Sunda and Huntsman, 1997), and by higher half-saturation constants because of their larger size. PISCES has previously been coupled with the OPA (Madec et al., 1998) ocean general circulation model at coarse spatial resolution (2° and 1/2°) and used in global (Aumont et al., 2003; Aumont and Bopp, 2006) and basin-scale studies (Gorgues et al., 2005).

Here PISCES is coupled to ROMS to address regional and coastal issues. The technical procedure for coupling the ecosystem and dynamical model components follows that of Gruber et al. (2006), who coupled ROMS with a slightly simpler ecological–biogeochemical model than PISCES. Readers are referred to the papers by Aumont et al. (2003) and Aumont and Bopp (2006) for further details on the PISCES model equations.

A climatological simulation has been performed using monthly mean values at the model open boundaries. The dynamical variables (temperature, salinity, velocities) at the boundaries are specified using climatological values of ORCA 0.5° OGCM during 1992–2000. A time series covering the entire 1992–2005 period was not available, but the 1992–2000 series appears sufficiently

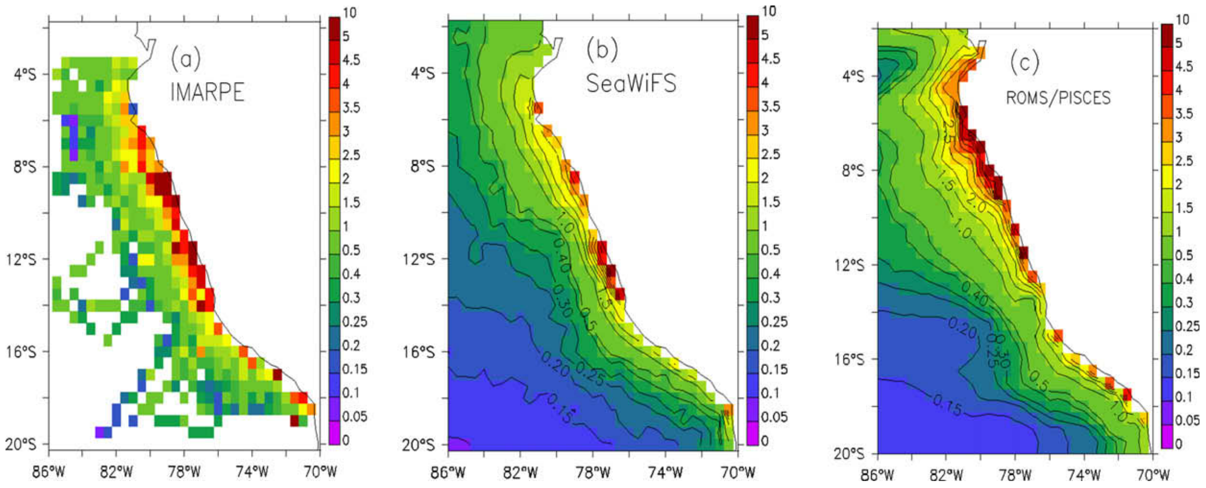

Fig. 1. Average surface chlorophyll (in mgChl/m^3): (a) IMARPE in situ data (1992–2004); (b) SeaWIFs data over the years 1997–2004; (c) ROMS/PISCES model (interpolated onto a 0.5° × 0.5° grid).

long to filter the interannual variability and to represent the large scale dynamical climatological circulation and water mass characteristics. The biogeochemical variables (nutrients and oxygen) are specified using nitrate, phosphate, silicate and oxygen monthly values from the World Ocean Atlas 2001 (Conkright et al., 2002). As boundary estimates of Fe were not available from data climatologies, they were extracted from a climatology of the global, interannual, coupled ORCA-PISCES simulation at 2° resolution, as was performed by Aumont and Bopp (2006).

The surface atmospheric forcing for ROMS consists of a Quikscat wind stress monthly climatology calculated over 1999–2003 as in Penven et al. (2005). This time period was chosen instead of 1992–2000, as the Quikscat product is of better quality than the ERS data because of its higher spatial resolution near the Peruvian coasts (Croquette et al., 2007). Heat fluxes, SST and SSS from the COADS monthly climatology (Da Silva et al., 1994) were also used following Penven et al. (2005). The surface forcing for PISCES includes Fe atmospheric deposition, which was calculated from the model results of Tegen and Fung (1995), assuming constant values for the iron content and the solubility.

ROMS/PISCES was run for a period of eight years, and reached a statistical quasi-equilibrium after a spin-up phase of five years. The final three years of simulation (years 6–8) are used to construct a monthly climatology.

3. Results

3.1. Spatial pattern of surface chlorophyll – in situ, satellite and ROMS/PISCES

The surface chlorophyll maps, averaged over a period of several years, display spatial patterns typical of coastal upwelling (Fig. 1). Chlorophyll concentrations are maximum nearshore (5–10 mgChl/m^3) and decrease gradually offshore, reaching ∼0.5–1.5 mgChl/m^3 at 200–300 km from the coast. The richest nearshore areas are between 6°S and 15°S, with local chlorophyll maxima near 9°S, 12°S and 14°S in the *in situ* map (Fig. 1a), and near 12–14°S in the satellite data (Fig. 1b). Along the coast north of 6°S, surface chlorophyll values are low in both *in situ* and satellite observations, whereas south of 15°S, the satellite chlorophyll is lower than the *in situ* data. The cross-shore gradient of *in situ* chlorophyll seems rather independent of the latitude, whereas chlorophyll-rich waters observed by satellite are closer to the coast.

These time-average values of *in situ* (Fig. 1a) and satellite data (Fig. 1b) are generally consistent with each other, and in agreement with previous studies (Chavez, 1995). The highly productive zone (4–10 mgChl/m^3) is narrower in the satellite data when compared with the *in situ* observations. However, it is well known that the SeaWiFS inverse algorithm used to calculate surface chlorophyll from radiances tends to underestimate the high concentrations in coastal zones (Hooker and McClain, 2000), which may account for part of this bias. Moreover, this nearshore underestimate of chlorophyll by SeaWIFS may be exacerbated by the frequent nearshore cloud coverage, especially in winter, which could prevent the sampling of some of the intense surface blooms.

ROMS/PISCES surface chlorophyll values are shown in Fig. 1c, where the model output has been interpolated onto the same 0.5° by 0.5° horizontal grid as the observations. The modelled chlorophyll concentrations agree reasonably well with the observations in magnitude. Maximum values of ∼5–10 mgChl/m^3 occur within 25–50 km of the coast. Maximum nearshore values are encountered from 5°S to 9°S. The chlorophyll cross-shore gradient is rather similar in the observations and in the model as shown by the cross-shore slope of chlorophyll (Fig. 2) The offshore chlorophyll values are close in the satellite data and *in situ* observations. Modelled large phytoplankton cells (diatoms) are mostly responsible for the biomass increase towards the coast (Fig. 2). This group is known to become dominant in nearshore Peruvian waters (Iriartre and Gonzalez, 2004; DiTullio et al., 2005). Thus the model seems to represent the shift between the nearshore and offshore plankton communities. This contrasts with other modelling studies based on more simple ecosystem models, which are not able to represent this cross-shore transition (Gruber et al., 2006).

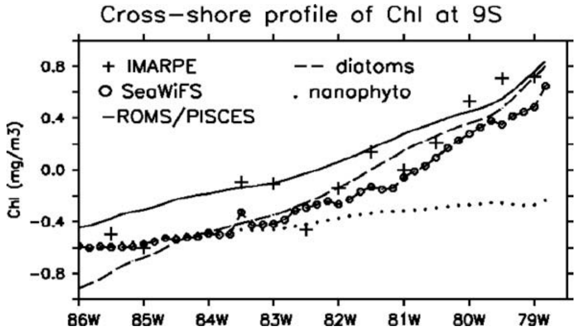

Fig. 2. Cross-shore profile of surface chlorophyll (in mgChl/m^3, in log scale) at 9°S for SeaWiFS (circles) data, IMARPE in situ observations (crosses), and ROMS/PISCES model. The full line corresponds to the model total chlorophyll, the dashed line to the chlorophyll content in diatoms, the dotted line to the chlorophyll content in the nanophytoplankton, respectively.

Some model biases appear in Fig. 1c. North of 6°S, the rather high nearshore chlorophyll (∼3–4 mgChl/m^3) may be caused by excessive coastal upwelling in the model. In contrast, south of 10°S, modelled nearshore chlorophyll is slightly lower than the observations and the productive zone is quite narrow (note the tight isolines near 14°S in Fig. 1c). The nearshore modelled chlorophyll remains rather low as far south as 15°S, despite the strong upwelling center near Paracas (Strub et al., 1998).

3.2. Seasonal variability of surface chlorophyll

3.2.1. Average seasonal cycle

We first study the surface chlorophyll seasonal cycle by averaging all the available data over a coastal box, which roughly defines the boundaries of the PCUbiogeochemical province. In a recent paper, PEN06 defined such a province as a coastal zone of 250 km cross-shore width, ranging from 4°S to 15°S. They computed a seasonal cycle by averaging all the surface chlorophyll *in situ* data available in this box, for each month of the year. The same calculation was repeated with SeaWiFS data during the September 1997–May 2005 period. We proceeded identically by averaging the IMARPE, SeaWiFS and model data over a the same domain. All the *in situ* data collected during 1992–2004 were used in order to compile a sufficient amount of observations. Restricting our data set to the same period studied by PEN06 would have reduced the accuracy of the calculated seasonal cycle (see Table 1).

Results from PEN06 and our study are presented in Fig. 3. The two SeaWiFS time series are very consistent: both display a single chlorophyll maximum in late austral summer and a minimum in austral winter. We verified that the seasonality portrayed in Fig. 3b is not modified when the year 2005 (used in PEN06) is included in our SeaWiFS time series (not shown).

The model seasonal cycle is also consistent. data (Fig. 3b). The modelled chlorophyll is high in austral summer – with a slight decrease in February – and low in austral winter. Note that the model values are significantly higher than the SeaWiFS values, closer to the IMARPE *in situ* data.

Let us now examine the differences in seasonal cycle. The two *in situ* time series display notable differences. The PEN06 *in situ* time series (Fig. 3a) displays two maxima – in early (November) and late austral summer (April), and a minimum in winter

Table 1
Monthly-mean IMARPE *in situ* chlorophyll (in mgChl/m^3) in a 200 km-wide coastal box between 6°S and 15°S during the 1992–2004 period.

	1992	1993	1994	1995	1996	1997	1998	1999	2000	2001	2002	2003	2004
Chjan	2.0(3)	1.7(1)	4.9(1)	1.8(17)	2.9(4)		1.1(1)	1.0(1)	2.4(14)	3.8(1)	1.9(1)	3.4(7)	3.6(12)
Chlfeb	3.1(66)	6.0(47)	2.2(1)	2.3(13)	1.5(7)	2.2(4)	1.1(1)	1.6(20)	2.2(61)	2.5(1)	6.1(4)	6.3(4)	3.8(28)
Chlmar		3.7(20)		3.9(66)	3.4(61)		1.3(3)	1.3(45)	5.4(11)	3.1(42)	4.9(15)		
Chlapr	1.0(2)	3.4(1)	2.1(1)	1.7(3)	7.9(3)	5.0(1)	0.9(13)	2.8(1)	0.66(2)	6.4(3)	3.8(4)	5.8(5)	8.3(4)
Chlmay	1.5(4)	5.6(1)	5.3(1)	1.0(28)	5.4(16)	3.1(1)	0.9(21)	1.4(21)	2.7(18)	4.9(1)	2.1(1)	1.8(15)	2.4(1)
Chljun	1.8(2)	0.5(1)	2.8(1)	0.2(17)	3.6(13)	1.2(11)	1.9(1)	3.5(1)	4.3(3)	7.5(4)	5.0(4)	2.0(6)	2.4(4)
Chljul	1.5(7)	2.6(1)	1.7(1)	0.1(4)	5.9(1)	4.7(14)	1.0(1)	2.4(1)	2.2(1)	0.9(1)	2.4(1)	2.6(4)	1.4(1)
Chlaug	3.1(5)	10.2(1)	2.1(48)	2.3(42)	2.6(44)	1.0(1)	0.9(16)	2.1(1)	3.4(13)	1.4(4)	2.2(77)	2.3(28)	1.6(46)
Chlsep		5.8(1)	3.7(22)	7.8(30)	2.9(49)	1.6(32)	0.8(56)	1.7(21)	3.6(50)	8.6(1)		1.9(23)	3.1(12)
Chloct	7.3(1)	2.3(1)	3.9(4)	1.0(1)	8.3(1)	1.7(16)		1.2(1)	2.9(4)	1.6(3)	1.1(22)	2.3(13)	6.5(11)
Chlnov	1.9(3)		1.3(8)	5.4(32)	1.9(28)		3.2(1)	3.3(25)	5.3(1)	8.7(1)	3.4(3)	2.1(49)	7.0(23)
Chldec		3.5(21)	2.2(16)	6.6(20)	2.8(60)	1.1(1)		4.1(46)	1.1(3)	7.6(4)	3.0(8)	2.8(9)	3.7(47)

The value in brackets indicates the number of 0.5° × 0.5° grid points averaged to compute the monthly mean. When only one grid point is available, the single data point from the Callao (78 °W, 12°S) time series was used.

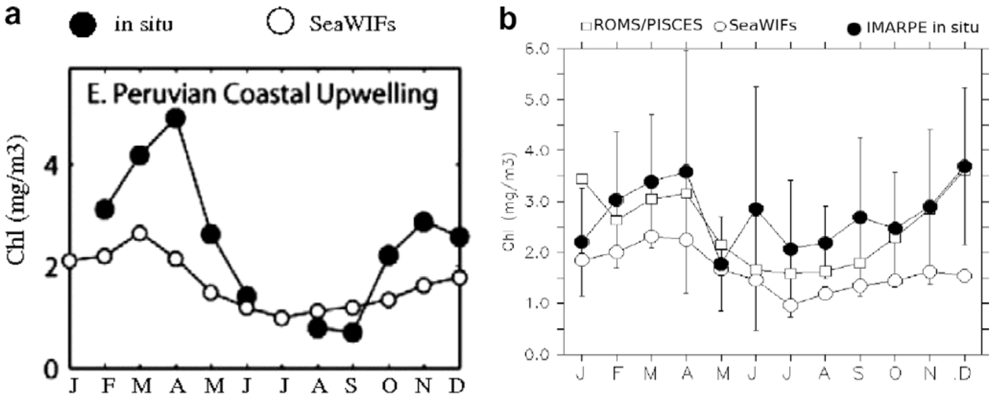

Fig. 3. Seasonal cycle of the surface chlorophyll concentration (in mgChl/m^3) averaged over a coastal box of 250 km zonal width between 4°S and 15°S: (a) in situ (black circles) and SeaWIFs (white circles) data during 1997–2005 (courtesy of Pennington et al., 2006); (b) ROMS/PISCES model (white squares), SeaWIFs (white circles), in situ IMARPE data (black circles), during 1992–2004. Vertical bars correspond to the interannual variability of the in situ data set.

(Fig. 3a). In contrast, the IMARPE time series (Fig. 3b) displays high (but lower than PEN06) values in austral summer, and low values in January, May and in austral winter (July–August). In contrast to PEN06, the IMARPE surface chlorophyll in austral winter remains relatively high (Fig. 3b). These differences during austral winter could be related to differences in data sampling. Indeed, the vertical bars plotted in Fig. 3b indicate the variance of the monthly mean values in the 1992–2004 period, thus the high interannual variability in monthly means. Months with poor sampling (i.e. with less than two observations in the coastal box, see Table 1) were not taken into account in the statistics. Overall, the *in situ* time series are in good agreement with one another, except for the relatively higher values in austral winter in the IMARPE data set.

The model average seasonal cycle is relatively similar to the observed ones. Even though the model values are overestimated in January, the surface phytoplanktonic biomass displays the same seasonal tendency as the observations: chlorophyll is high in austral summer, and reaches a minimum in austral winter as the wind-driven upwelling is supposed to strengthen (Bakun and Nelson, 1991).

3.2.2. Alongshore variations of the seasonal cycle

Alongshore variations of the surface chlorophyll seasonal cycle are portrayed in Fig. 4. The SeaWiFS and model chlorophyll values within a 200 km-wide coastal band were binned for each month and each latitude. The IMARPE data set was not comprehensive enough to study alongshore variations because of low sampling during some months (e.g. April, see Table 1).

Let us first describe the alongshore variability observed by SeaWiFS (Fig. 4a). Several patterns can be emphasized. First, the phase of the seasonal cycle depends little on latitude. From 7°S to 14°S, high values are encountered in late austral spring and early summer (October–November–December). In austral spring (October), chlorophyll is high (greater than 1.5 mgChlm^{-3}) in three narrow latitude bands (6–7°S, 8–9°S and 11–14°S, Fig. 4a), and decreases near 10–11°S. Two isolated points near 10°S and 12°S in August (Fig. 4a) suggest that high chlorophyll values may occur in austral winter as well. However, this signal is not very well sampled because of the higher cloud coverage during this season.

The model alongshore variations of modelled chlorophyll agree relatively well with the satellite data in the north of Peru (Fig. 4b). The modelled values are high during austral spring and summer with a slight decrease in February. Maximum concentrations are reached during late austral spring near 7°S in the model, and during late summer in the observations. The maximum modelled values (~6–7 mgChl/m^3) are higher than the maximum SeaWiFS values (~4 mgChl/m^3). The lowest chlorophyll values are reached during the winter months (July–August–September). Between 10.5°S and 11°S, the model's seasonal variability decreases, consistently with SeaWiFS data. South of 13°S, the model is not realistic, as shown by the low chlorophyll concentration (less than 1.5 mgChl/m^3) all year long.

3.3. Seasonal variability of the chlorophyll content in the euphotic layer

As noted previously, the evolution of surface chlorophyll does not seem to be controlled by lack of nutrients in the surface layer, which increases in austral winter due to the more upwelling-favorable winds during this season (Fig. 5a). The question we now ad-

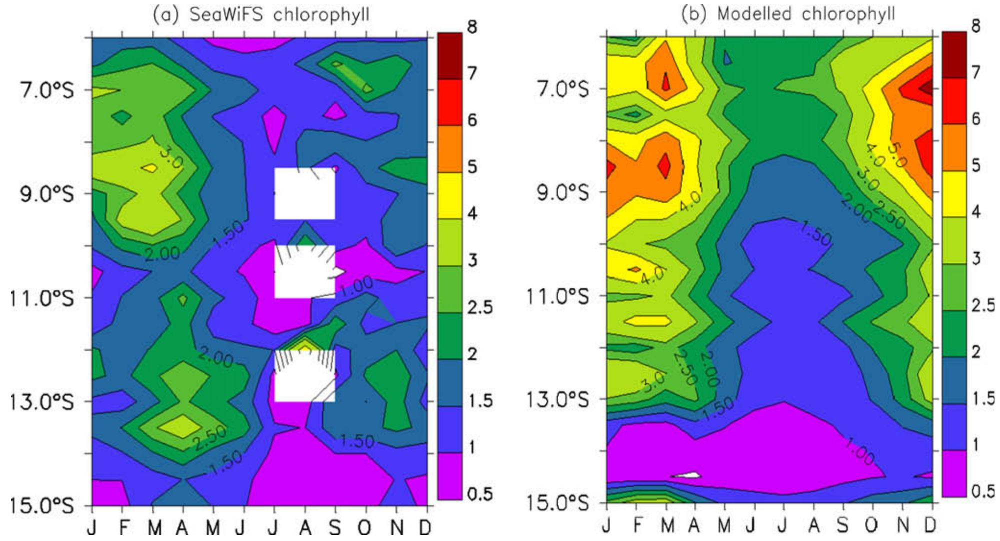

Fig. 4. Latitude-time variations of the surface chlorophyll concentration (in mgChl/m^3) in a 200 km-wide coastal band: (a) SeaWIFs; (b) ROMS/PISCES model. Contour values are identical to the color scales.

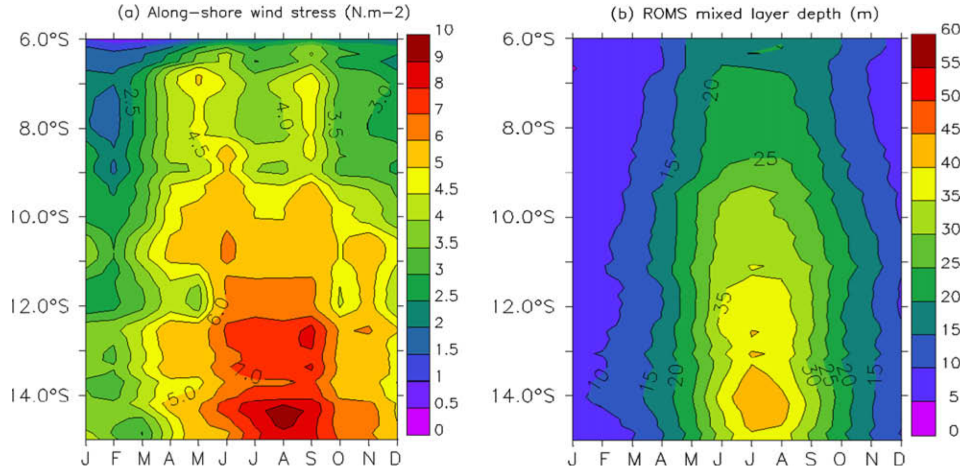

Fig. 5. Time–latitude variations: (a) alongshore wind stress (in N m^{-2}) from a 1999–2003 Quikscat climatology; (b) ROMS/PISCES mixed layer depth (in m). Both variables are averaged in a 200 km-wide coastal band.

dress is the following: what is the impact of vertical mixing due to the winter trade winds increase? Could this process drive a decrease in surface chlorophyll concentrations by distributing phytoplankton over a thicker mixed layer? Fig. 5b displays the evolution in time of the model mixed layer depth (hereafter MLD), defined as the depth where the local Richardson number reaches the critical value of 0.3 (Large et al., 1994). MLD values increase significantly during austral winter and southward, as does alongshore wind(Fig. 5a). The model MLD values are realistic as very similar (not shown) to the climatological values (de Boyer Montegut et al., 2004). To contrast the total chlorophyll content with the surface chlorophyll signal, we averaged chlorophyll vertically over the euphotic layer depth and horizontally in the 200 km coastal band and in the 4–15°S latitude range. The variations are portrayed in Fig. 6a, along with those of surface chlorophyll. The depth-averaged chlorophyll shows a similar variability than the surface chlorophyll, albeit with a lower amplitude. The main difference between the two is that the depth-averaged chlorophyll level in early summer (~2.5 mgChl/m^3 in January–February) is rather close to the winter level (~1.5–2 mgChl/m^3 in July–August–September), whereas the summer surface level (~3.5 mgChl/m^3 in January–February) is roughly equal to twice the winter surface level (~1.5–2 mgChl/m^3 in July–August–September). This difference between the surface values and depth-averaged values illustrates the impact of vertical mixing on the vertical profile of chlorophyll, as suggested by Calienes et al. (1985). Note also that the total phytoplanktonic biomass is not well correlated with the variability of upwelling-favorable winds. Fig. 6a displays two distinct peaks in late austral spring (November–December) and late summer (March), whereas the alongshore wind stress is maximum in April and September (Fig. 5a).

Thus, the paradox of low chlorophyll during strong upwelling can be partly explained by the role of vertical mixing. The surface chlorophyll concentration is higher in early summer partly because of surface stratification permits blooms to accumulate. In winter, the upwelling is stronger than in summer (Fig. 6a) but biomass is distributed vertically over a greater MLD, hence the surface chlorophyll concentration is reduced. MLD variations have thus a major impact on the surface chlorophyll seasonal variability and on the vertical distribution of chlorophyll.

To further investigate the role of vertical mixing, two sensitivity experiments were performed with the model. The first experiment

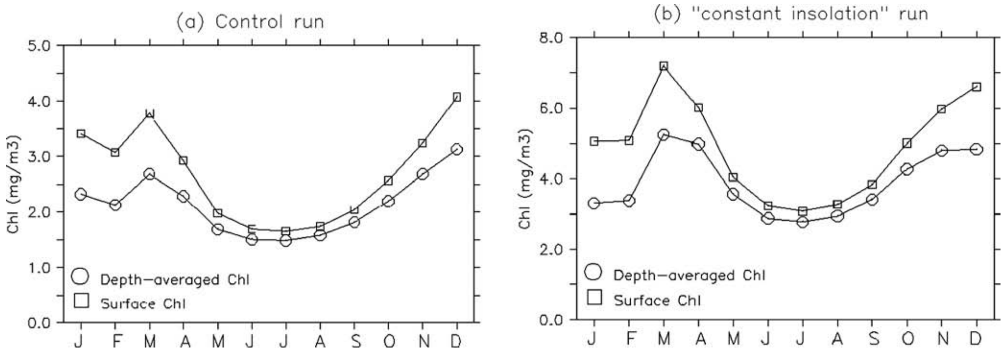

Fig. 6. Time evolution of the ROMS/PISCES surface chlorophyll (squares) and depth-averaged chlorophyll in the euphotic layer (circles) (in mgChl/m^3), horizontally averaged in a 200 km-wide coastal band between 4°S and 15°S: (a) control run; (b) constant insolation run. Note the change of scale between the two figures.

consists in suppressing the seasonality of vertical mixing by imposing a constant MLD and constant vertical mixing coefficients in the biogeochemical part of the model. These model parameters were fixed to annual mean values. In this experiment, the seasonality of the upward nutrient flux is not modified with respect to the control run, and only the mixing coefficients and mixed layer depth used in the biogeochemical tracers equations are kept constant in time. The results of this experiment confirm our hypothesis: with a fixed mixing coefficient and MLD, the seasonality of the surface and depth-averaged chlorophyll is almost totally removed (figure not shown). The signal, averaged over the coastal region defined in Fig. 6, varies between 1.2 and 1.6 mgChl/m^3 throughout the year. This confirms the role of the mixed layer seasonality in driving the seasonality of surface chlorophyll.

Surface temperature may also influence the surface primary productivity through the Q10 effect (Eppley, 1972). Nearshore primary production could reduce in winter because of the surface temperature decrease associated with atmospheric cooling and to the strong wintertime upwelling of cold water. To investigate the impact of this process, we performed an experiment in which the temperature used in the biogeochemical model was kept constant throughout the year, fixed to the annual mean value. As in the previous experiment, the impact of the physics on the ecosystem is unchanged from the control run, except for the temperature effect. The results show a negligible effect (figure not shown). The seasonal variability of surface chlorophyll differs by less than 5% from the control run variability. In conclusion, these two sensitivity experiments show the overwhelming impact of winter vertical mixing on the surface chlorophyll variability at seasonal time scales.

3.4. Nutrient limitation and chlorophyll seasonal variability

Macronutrients such as nitrate, phosphate and silicate were routinely collected during the IMARPE cruises during the 1992–2004 period. The time-latitude evolution of *in situ* and modelled surface nutrients in the 200 km-wide coastal band is shown in Figs. 7 and 8, respectively. Overall, the seasonal cycle of the surface nutrients appears to be in phase by the wind-driven upwelling (Fig. 5a), as high concentrations occur in austral spring and winter. In austral summer, the model macronutrient surface concentrations agree relatively well with the observations, except at latitudes south of 13°S. In winter, the model surface concentrations are higher by a factor of ~2 for nitrate, ~1.5 for silicate and phosphate, than the *in situ* data. This may partly stem from the model biogeochemical tracer initial conditions. PISCES initial and boundary conditions for the macronutrients concentrations were initialized using data from the World Ocean Atlas 2001 (Conkright et al., 2002) data product on a 1° by 1° horizontal grid, which were extrapolated onto the ROMS model 1/6° × 1/6° grid. The model late austral winter (August–September) high nitrate concentrations (~18 μmol/l, Fig. 8a) compare well with WOA data (not shown), but the austral fall and early winter values are much larger than in WOA. A comparison between WOA and IMARPE vertical sections of nitrate shows that the WOA nitrate concentration could be overestimated near the coasts (figure not shown) due to the lack of nearshore profiles in the data base. The high values in the WOA (and hence in the model initial conditions) could be an artefact caused by the extrapolation of offshore high nitrate values towards the coastal margin, where denitrification within the Oxygen Minimum Zone could induce low nitrate concentrations (Wooster et al.,

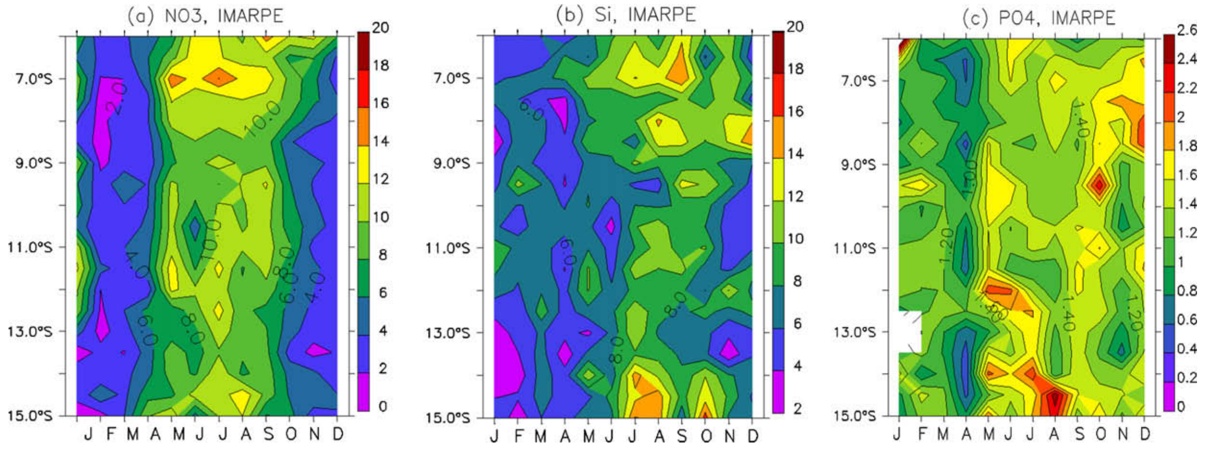

Fig. 7. Time–latitude variations of the surface in situ IMARPE: (a) nitrate; (b) silicate; (c) phosphate surface concentration (in μmol/l) averaged in a 200 km-wide coastal band.

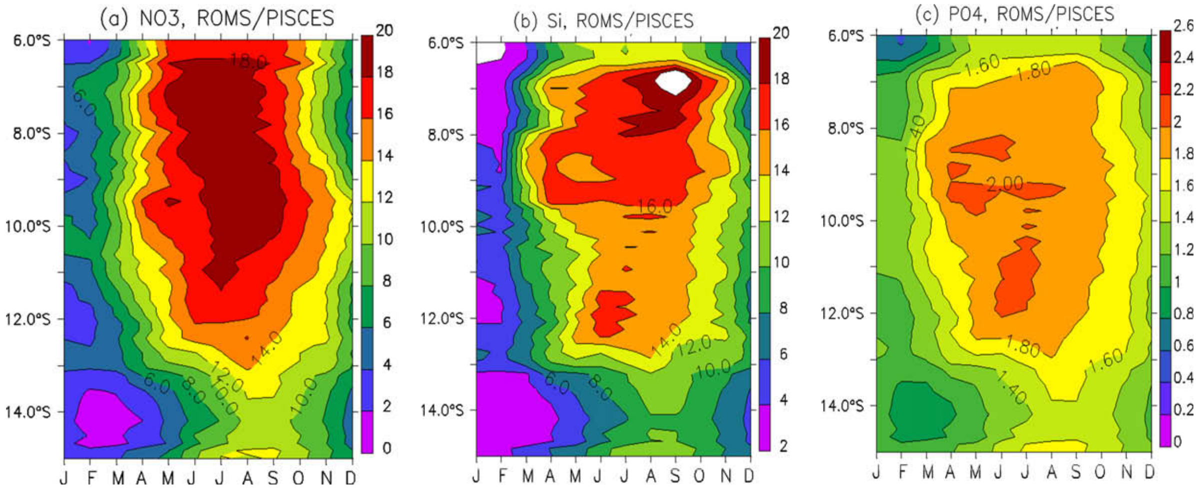

Fig. 8. Same as Fig. 7 for model results.

1965; Ward et al., 1989). On the other hand, the silicate and phosphate concentrations compare well with WOA and IMARPE data (not shown), and the model winter values remain higher than the observations (Figs. 7b–c and 8b–c). This suggests that the austral winter upwelling of nutrients may be too strong in the model, consistent with the higher than observed model surface chlorophyll values (Figs. 3 and 4).

Nutrient and light limitation of the primary production can be quantified by computing explicitly the limitation terms in the primary production model parameterizations. The model primary production is proportional to the product of a light limitation term and a nutrient limitation term. The nutrient limitation term L_{nut} is the minimum of a set of (n) Michaelis–Menten nutrients limitation factors, namely $L_{\mathrm{nut}} = \min_{i=1,\ldots,n}[C_i/(K_i + C_i)]$ where the index (i) denotes a specific nutrient, C_i its concentration and K_i its half-saturation constant. The light limitation term L_{light} is equal to $[1 - \exp(-\alpha\,(\mathrm{Chl/C}) \cdot \mathrm{PAR}/(\mu \mathrm{Lnut})]$ where α is the initial slope of the PI curve, Chl/C the chlorophyll over carbon ratio, PAR the photosynthetically available radiation, μ the growth rate depending on temperature. When enough light is available this term saturates to 1, whereas it remains less than 1 when light limits the growth. We chose to focus on the limitation terms of diatom growth, as they contribute to more than 70% of the total chlorophyll concentration in the region.

The cross-shore vertical structure of the limiting nutrient is portrayed for different time periods in Fig. 9. In the well-lit, shallow mixed layer which establishes during austral summer, diatom growth is limited by nitrate within ~100 km from the coast, and then by silicate further offshore (Fig. 9a–b). Because of the relatively weak upwelling and offshore Ekman transport during summer, phytoplankton growth is constrained by the upward flux of macronutrients such as nitrate and silicate, which are consumed rapidly after they reach the surface. Fe availability limits the growth in a thin subsurface layer located offshore. The nearshore Fe concentration is relatively high since it is supplied by the continental shelf sediments. Due to offshore Ekman transport and shallow mixed layer during summertime, Fe is advected offshore and remains confined near the surface, hence limiting phytoplankton growth below the mixed layer. Note that light limitation occurs at very shallow depths (~2–4 m) nearshore and at greater depths (~10 m) 100 km from the shore (Fig. 9a and 9b) because of the high chlorophyll concentration in the surface layer near the coast.

During austral winter, the limiting factors change drastically (Fig. 9c). Silicate is brought to the surface by the strong coastal upwelling and advected offshore by Ekman currents, thus is no longer limiting offshore as during summertime. At ~100 km from the shore, nutrient limitation shifts to Fe. Note that because of the increased wintertime vertical mixing, Fe is diluted vertically. Its concentration decreases and remains sufficiently high to avoid Fe limitation only within ~100 km from the coast. In the vertical, light availability is the dominant limiting factor over most of the mixed layer.

To further investigate the impact of Fe limitation on phytoplankton growth, it was artificially turned off in the PISCES model in order to evaluate its impact on the ecosystem. This induced a surface chlorophyll increase by ~20–40% north of 9°S during most of the year (Fig. 10). The increase reached ~40–50% in austral spring between 9°S and 11°S. The impact was strongest near 14°S, where the productivity resulted in a two-fold biomass increase, reaching realistic levels of ~1.5–2 mgChl/m^3. However, the late spring–summer model bias was not significantly reduced, suggesting that Fe limitation may not be the only issue near 14°S. In conclusion, this sensitivity experiment confirms that Fe is the main limiting nutrient off the shelf in winter in our model, and that the productivity can be increased when Fe limitation is relaxed. In contrast, nutrient limitation shifts to macronutrients such as nitrate and phosphate during summer. Fe limitation of diatom blooms off the Peruvian shelf has been observed during the late austral winter of 2000 (Hutchins et al., 2002; Bruland et al., 2004; Hare et al., 2005) and these observations support our hypothesis. However, note that the modelled biomass increase due to the relaxation of Fe limitation near 8°S remains moderate (~20–40%, Fig. 10). This suggests that light limitation due to the winter MLD increase or to the lower winter insolation, is the main factor controlling the winter productivity. This will be investigated in more detail in the next section. Moreover, Fe and light conditions are closely related as Fe limitation may be enhanced by the higher Fe requirement of phytoplankton cells when light conditions are less favourable (e.g., Sunda and Huntsman, 1997).

3.5. Light limitation and the seasonal variability of chlorophyll

Insolation displays significant seasonal variations over the Peru area. On average, the COADS climatological nearshore solar flux is maximum in austral summer (between 240 and 280 W/m^2) and minimum in austral winter (between 120 and 160 W/m^2). The amplitude of the insolation cycle is maximum near 15°S (figure not shown). We now investigate the impact of these variations on surface chlorophyll. In a sensitivity experiment, the seasonal variations of insolation were suppressed in the biological model.

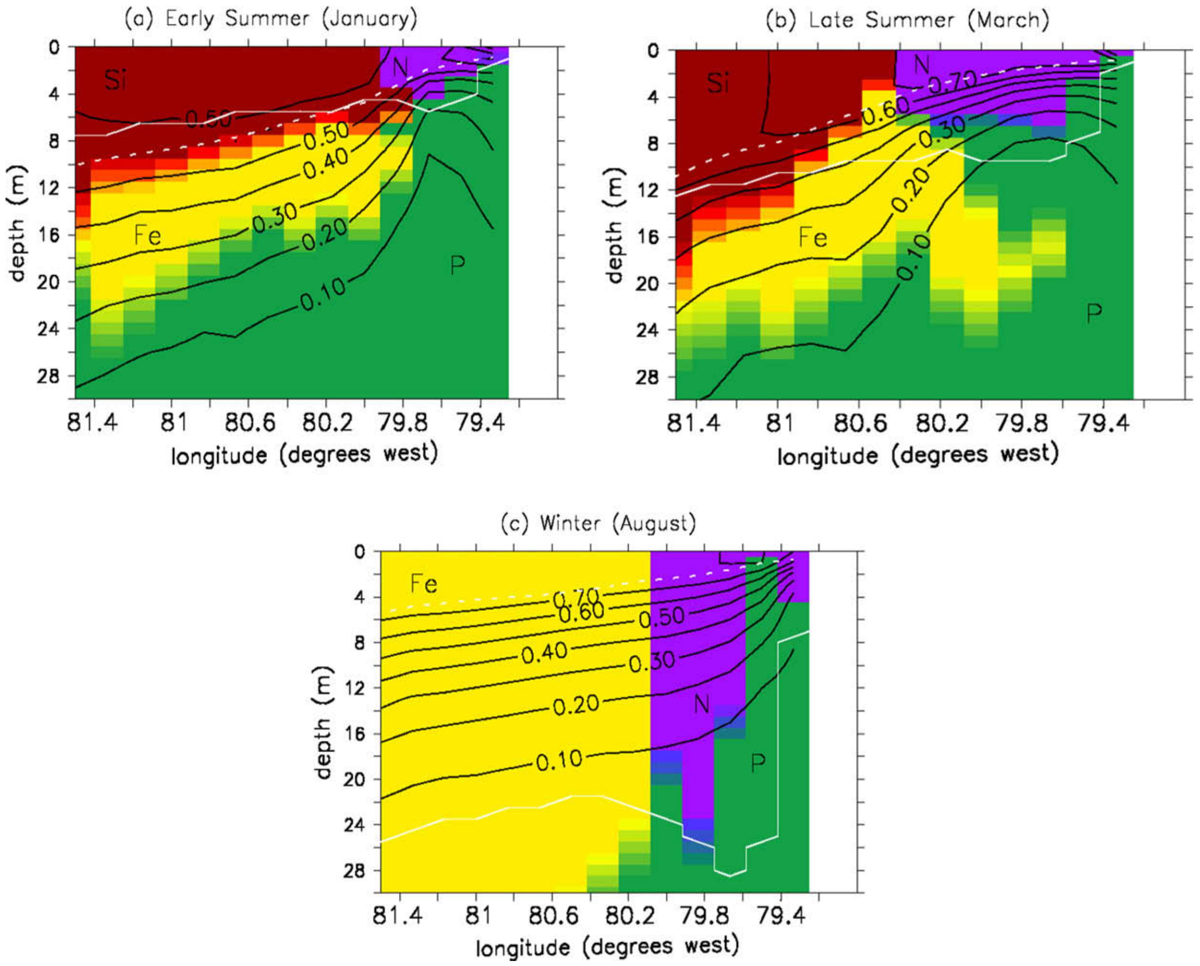

Fig. 9. Diatoms colimitations at 8°S: (a) early summer (January); (b) late summer (March); (c) winter (July). Colors and labels indicate the limiting nutrient (purple: nitrate (N), yellow: iron (Fe), green: phosphate (P), red: silicate (Si)). The dashed white line indicates the depth at which the limitation shifts from nutrients (above the line) to light (below the line). Labeled black contours indicate the value of the light limiting coefficient (L). The full white line indicates the mixed layer depth.

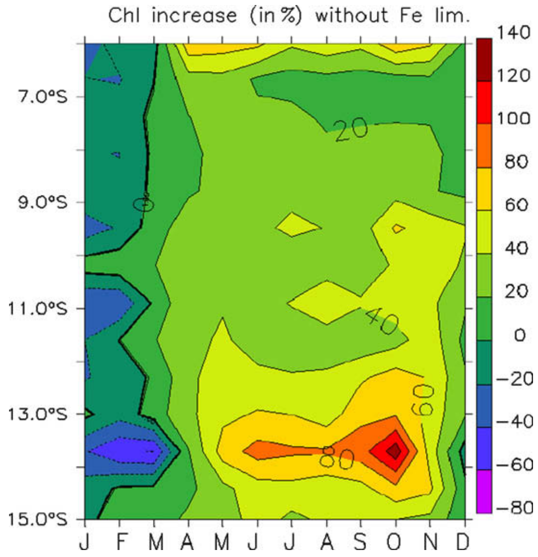

Fig. 10. Time–latitude evolution of the surface chlorophyll increase (in%) when Fe limitation is relaxed in the ROMS/PISCES model.

The heat fluxes (including the heating effect of the short wave solar radiations) vary seasonally in ROMS physical and thermodynamical components, in order to keep the MLD, vertical mixing and thermal stratification unchanged with respect to the control run. In contrast, the solar radiation available for phytoplankton growth is kept constant with time and latitude throughout the simulation. It is fixed to 190 W/m^2, which corresponds to the year-averaged value over a 200-km-wide band of coastal ocean band between 6°S and 15°S.

The average chlorophyll seasonal cycle is represented in Fig. 6b. First, note that the mean level of surface chlorophyll (~4–5 mgCh/m^3) is greater than in the control run (~2.5–3 mgCh/m^3, Fig. 6a). This rather surprising result can be explained by the significant light limitation of winter productivity in the control run. A 25% increase in solar radiation during winter (190 W/m^2 instead of 150 W/m^2) in the "light-pertubed" simulation generates a two-fold increase in depth-averaged biomass during winter (Fig. 6). This accumulated biomass produces a significant pool of ammonium in the subsurface layers (figure not shown), which is consumed during the spring and fall bloom. This effect is substantial as biomass doubles during summer in the "light-perturbed" simulation in spite of a light level lower (by ~30%) than in the control run. The important result of this experiment is that the characteristics of the surface chlorophyll seasonal variations are unchanged (Fig. 6b) with respect to the control run (Fig. 6a). The seasonality remains both in the surface and depth-averaged chlorophyll signals. This indicates that the total phytoplankton biomass varies regardless of the insolation cycle, because of spring restratification and fall destratification induced by vertical mixing, as in open-ocean oligotrophic regions. The effect of vertical mixing can be estimated by comparing the summer and winter depth-averaged biomass in Fig. 6b. They are relatively close (~3.5 and ~2.5 mgCh/m^3, respectively) during the two periods, whereas the surface values differ by ~2–2.5 mgChl/m^3. The sudden rise in depth-averaged biomass of about 1.5 mgChl/m^3 between February and March results from an MLD increase which entrains regenerated nutrients (NH_4) into the shallow, well-lit surface layer, and generates a fall bloom.

To conclude, the model experiments show that the insolation seasonal variations have a weak impact on the seasonal cycle of surface chlorophyll, and that vertical mixing acts in two different ways. Firstly, phytoplankton is distributed over a greater depth in winter than in summer. Hence, the winter surface chlorophyll concentration decrease is caused by a purely physical vertical dilution and by a primary production decrease due to light limitation. Light limitation is mainly caused by the MLD increase, and not by the reduced insolation during winter. The decrease in vertical mixing in late winter-spring induces a restratification phase, during which light limitation is relaxed, allowing phytoplankton to grow until the surface regenerated nutrients are consumed. Secondly, in austral fall, the mixed layer depth increases and entrains new nutrients into the mixed layer, which generates the March bloom.

4. Discussion

Satellite data, *in situ* observations and model results display a surface chlorophyll seasonal variability near the Peruvain coasts which is in phase opposition with the dynamical forcing of the coastal upwelling. The observed variability has been well reproduced with the ROMS/PISCES coupled model, especially off northern Peru (6–10°S). Further south, the simulated amplitude of the seasonal cycle is reduced compared to observations.

Several hypotheses may explain the model's lack of realism south of 10°S. The first one is the morphology of the continental shelf in the model, which could have an impact on the input of Fe from the sediments. A wider continental shelf implies a larger Fe supply from the sediments. As a consequence, the upwelled waters north of 10°S contain more Fe because the shelf is widest there (Bruland et al., 2004). In the ROMS model, bottom topography has been smoothed in order to reduce the slope near the shelf break and verify numerical criteria which limit error on the horizontal pressure gradient (Mellor et al., 1998). Because of this smoothing procedure, the shelf off Peru is narrower in the model than in reality, especially south of 11°S. Since Fe appears to be the limiting nutrient during winter, this model artifact could limit excessively the development of phytoplanktonic biomass south of 10°S.

The absence of intraseasonal variability in the physical forcing of the model (the atmospheric forcing and the model's open boundary conditions (hereafter OBCs)) may also impact chlorophyll variability. Indeed, the OBCs of the model are seasonal and cyclic. In the Equatorial Pacific, the intraseasonal eastward propagating equatorial Kelvin waves, which trigger poleward propagating coastally trapped waves when reaching the American coast, have been filtered from the OBC. These coastal waves may shoal or depress the nutricline along the coast, and generate westward-propagating Rossby waves which advect surface chlorophyll offshore (Bonhomme et al., 2007).

Coastal waves may impact nearshore biological productivity, whereas Rossby waves may extend the biologically productive coastal zone further offshore. To investigate the potential impact of this variability on the seasonal cycle, model experiments should be performed with the full spectrum of variability at the OBCs. Let us now focus on the nutrients issue. On the one hand, the surface and subsurface (not shown) macronutrient (nitrate, silicate and phosphate) concentrations are higher in the model simulation than in the IMARPE *in situ* data (Figs. 7 and 8). On the other hand, the model outputs are consistent with the very high values of NO_3 from the WOA data base, which were used to initialize the model. To explain these differences between the WOA data base and the IMARPE measurements, a dedicated study of the WOA and IMARPE nitrate profiles should be conducted in the future. Furthermore, the physical model may be partly responsible for the nutrient bias. Indeed, the seasonal cycle of the polewards-flowing Peru/Chile Undercurrent, which transports most of the water mass upwelled near the coast, is not well known and may not be very well represented in the model. A vertical section of WOA density in July near 8°S (not shown) shows that the subsurface isopycnals and nitrate isolines tend to deepen toward the coast. This suggests an increase in the PCUC transport which is not reproduced by the model. The question of the impact of the circulation on macronutrient supply remains open and should be addressed in future work.

5. Conclusions

The seasonal variability of the surface chlorophyll concentration in the Peru upwelling system were studied using *in situ* observations, satellite data and results from a three dimensional regional model coupling ocean dynamics (ROMS) and biogeochemical cycles (PISCES). The SeaWiFS satellite data and IMARPE *in situ* observations display a strong seasonality with low values in austral winter and high values in austral spring and summer, in phase opposition to upwelling intensity (Bakun and Nelson, 1991). The modelled surface chlorophyll seasonal cycle is similar in pattern and values are in general between the IMARPE and SeaWIFS data.

The mechanisms controlling the chlorophyll seasonality were investigated using model experiments. The deepening of the mixed layer was shown to be mainly responsible for the decrease of surface chlorophyll in austral winter, confirming previous observational studies (Calienes et al., 1985). The phytoplanktonic biomass increased significantly in austral spring and fall following periods of restratification and destratification, respectively. The PCU system is almost as productive in austral winter as in early summer, and the decrease in surface biomass in winter results from a dilution and light limitation effect, and that the reduced insolation during winter does not affect the amplitude and phase of the surface chlorophyll signal.

Nutrient limitations of phytoplankton growth were studied in the model. Fe appears to be the limiting nutrient off northern Peru during winter in the model, which is consistent with several recent studies based on *in situ* Fe measurements (Hutchins et al., 2002; Bruland et al., 2004). In summer, the upwelling is weaker and the model limitation shifts to macronutrients such as nitrate and silicate. Future studies will investigate the impact of dynamical processes at higher resolution and of an improved atmospheric forcing on the surface productivity, and will address the intraseasonal and interannual variability in the Peru upwelling.

Acknowledgements

Model simulations were performed on NEC-SX5 and NEC-SX8 IDRIS (Institut du Développement et de Ressources en Informatique Scientifique) computers. J. Ledesma was financially supported by the DSF (Département Soutien et Formation) of IRD (Institut de Recherche pour le Développement). The collaborative work between IRD and IMARPE was sponsored by the IRD ATI “Sistema de Humboldt”. We also thank Cyril Lathuilière from LOCEAN for extracting and processing SeaWiFS data.

Appendix A

A.1. IMARPE chlorophyll-***a*** measurements

The chlorophyll measurements are made using the standard fluorometric procedure of Holm-Hansen et al. (1965). Chlorophyll-*a* pigments are retained by micro-filters (Whatman GF/F 0.75 μm). The 100 ml sea water samples are then freezed for further analysis. The pigments are extracted in acetone for periods of 3 h. Chlorophyll is then calculated from results obtained with a Turner Design (AU-10 Model) previously calibrated with commercial Chl-*a* from (Sigma Chemical Co.) This method is adapted for a range of measurements between 0.01 and 200.00 mg/m^3, with a precision of ±0.20 mg/m^3. Quality control consisted in computing a climatology in $0.5^\circ \times 0.5^\circ$ bins, comparing each of the chlorophyll values to the climatology, and filtering the extreme values.

A.2. IMARPE nutrient measurements

The water samples were collected and freezed on board for later measurements. Nutrients were measured following the spectrophotometric method described in Strickland and Parson (1972) using a Perkin–Elmer Lambda 40 double-beam UV/Vis spectrophotometer.

References

Aumont, O., Bopp, L., 2006. Globalizing results from ocean *in situ* iron fertilization studies. Global Biogeochemical Cycles 20 (2). doi:10.1029/2005GB00259.

Aumont, O., Maier-Reimer, E., Blain, S., Monfray, P., 2003. An ecosystem model of the global ocean including Fe, Si, P colimitations. Global Biogeochemical Cycles 17 (2), 1060.

Bakun, A., Nelson, C.S., 1991. The seasonal cycle of wind stress curl in sub-tropical boundary current regions. Journal of Physical Oceanography 21, 1815–1834.

Bonhomme, C., Aumont, O., Echevin, V., 2007. Advective transport caused by intraseasonal Rossby waves: a key player of the high chlorophyll variability off the Peru upwelling region. Journal of Geophysical Research 112, C09018. doi:10.1029/2006JC004022.

Bruland, K.W., Rue, E.L., Smith, G.J., DiTullio, G.R., 2004. Iron, macronutrients and diatom blooms in the Peru Upwelling regime: brown and blue waters of Peru. Marine Chemistry 93, 81–103.

De Boyer Montégut, C., Madec, G., Fisher, A.S., Lazar, A., Iudicone, D., 2004. Mixed layer depth over the global ocean: an examination of profile data and a profile-based climatology. Journal of Geophysical Research 109, C12003. doi:10.1029/2004JC002378.

Calienes, R., Guillen, O., Lostanau, N., 1985. Variabilidad espacio temporal de clorofila, produccion primaria y nutrients frente a la costa peruana. IMARPE bolletin, Callao. 44.

Carr, M.-E., Strub, P.T., Thomas, A.C., Blanco, J.L., 2002. Evolution of 1996–1999 La Nina and El Nino conditions off the western coast of South America: a remote sensing perspective. Journal of Geophysical Research 107 (12), 3236. doi:10.1029/2001JC001183.

Chavez, F.P., 1995. A comparison of ship and satellite chlorophyll from California and Peru. Journal of Geophysical Research 100 (C12), 24855–24862.

Chavez, F.P., Ryan, J., Lluch-Cota, S.E., Niquen, M., 2003. From anchovies to sardines and back: multidecadal change in the Pacific ocean. Nature 299, 217–221.

Conkright, M.E., Locarnini, R.A., Garcia, H. E., O'Brien, T.D., Boyer, T.P., Stephens, C. Antononov, J. (2002). World Ocean Atlas 2001: objectives, analyses, data statistics and figures [CD-ROM], NOAA Atlas NESDIS 42, Silver Spring, Md.

Croquette, M., Eldin, G., Grados, C., Tamayo, M., 2007. On differences in satellite wind products and their effects in estimating coastal upwelling processes in the south-east Pacific. Geophysical Research Letters 34, L11608. doi:10.1029/2006GL027538.

Da Silva, A.M., Young, C.C., Levitus, S., 1994. Atlas of surface marina data 1994, vol. 1, Algorithms and procedures, technical report, Natl. Oceanogr. And Atmos. Admin., Silver Spring, Md.

DiTullio, G., Geesey, M.E., Maucher, J.M., Alm, M.B., Riseman, S.F., Bruland, K.W., 2005. Influence of iron on algal community composition and physiological status in the Peru upwelling system. Limnology Oceanography 50, 1887–1987.

Eppley, R.W., 1972. Temperature and phytoplankton growth in the sea. Fishery Bulletin, 1063–1085.

FAO (Food Administration Organisation), (1999). The state of world fisheries and aquaculture 1998. FAO Documentation Group, Rome, Italy.

Gorgues, T., Menkes, C., Aumont, O., Vialard, J., Dandonneau, Y., Bopp, L., 2005. Biogeochemical impact of tropical instability waves in the Equatorial Pacific. Geophysical Research Letters 32, L24615. doi:10.1029/2005GL024110.

Gruber, N., Frenzel, H., Doney, S.C., Marchesiello, P., McWilliams, J.C., Moisan, J.R., Oram, J.J., Plattner, G.K., Stolzenbach, K.D., 2006. Eddy-resolving simulation of plankton ecosystem dynamics in the California Current System. Deep Sea Research I 53, 1483–1516.

Guillen, O., Calienes, R., 1981. Upwelling off Chimbote. Coastal and Estuarine Science 1, 312–326.

Hare, C.E., DiTullio, G.R., Trick, C.G., Wilhelm, S., Bruland, K.W., Rue, E.L., Hutchins, D.A., 2005. Phytoplankton community structure changes following simulated upwelled iron inputs in the Peru Upwelling region. Aquatic Microbial Ecology 38, 269–282.

Holm-Hansen, O., Lorenzen, C.J., Holmes, R.W., Strickland, J.D.H., 1965. Fluorometric determination of chlorophyll. Journal du Conseil Permanent International pour L'Exploration de la Mer 30 (1), 3–15.

Hooker, S.B., McClain, C.R., 2000. The calibration and validation of SeaWiFS data. Progress in Oceanography 45, 427–465.

Hutchins, D.A., Hare, C.E., Weaver, R.S., Zhang, Y., Firme, G.F., DiTullio, G.R., Alm, M.B., Riseman, S.F., Maucher, J.M., Geesey, M.E., Trick, C.G., Smith, G.J., Rue, E.L., Conn, J., Bruland, K.W., 2002. Phytoplankton iron limitation in the Humboldt Current and Peru Upwelling. Limnology and Oceanography 47, 997–1011.

Iriartre, J.L., Gonzalez, H.E., 2004. Phytoplankton size structure during and after the 1997/1998 El Nino in coastal upwelling area of the northern Humboldt Current System. Marine Ecology Progress Series 269, 83–90.

Large, W.G., McWilliams, J.C., Doney, S.C., 1994. Oceanic vertical mixing: a review and a model with a nonlocal boundary layer parameterization. Review of Geophysics 32, 363–403.

Madec, G., Delecluse, P., Imbard, M., Lévy, C., 1998. OPA 8.1, ocean general circulation model reference manual. *Notes du pôle de Modélisation, 11*, Institut Pierre-Simon Laplace (IPSL).

Mellor, G.L., Oey, L.-Y., Ezer, T., 1998. Sigma coordinate pressure gradient errors and the seamount problem. Journal of Atmospheric and Oceanic Technology 15 (5), 1122–1131.

Minas, H.J., Coste, B., Minas, M., Raimbault, P., 1990. Conditions hydrologiques, chimiques et production primaire dans les upwellings du Pérou et des îles Galapagos, en régime d'hiver austral (campagne Paciprod). Oceanologica Acta (10), 383–391.

Pennington, J.T., Mahoney, K.L., Kuwahara, V.S., Kober, D.D., Calienes, R., Chavez, F.P., 2006. Primary production in the eastern tropical pacific: a review. Progress in Oceanography 69 (2–4), 285–317.

Paulmier, A., Ruiz-Pino, D., Garçon, V., Farias, L., 2006. Maintaining of the Eastern South Pacific Oxygen Minimum Zone (OMZ) off Chile. Geophysical Research Letters 33, L20601. doi:10.1029/2006GL026801.

Penven, P., Echevin, V., Pasapera, J., Colas, F., Tam, J., 2005. Average circulation, seasonal cycle, and mesoscale dynamics of the Peru Current System: a modeling approach. Journal of Geophysical Research 110 (C10), C10021. doi:10.1029/2005JC002945.

Shchepetkin, A.F., McWilliams, J.C., 2005. The regional oceanic modeling system: a split-explicit, free-surface, topography-following-coordinate ocean model. Ocean Modelling (9), 347–404.

Strickland, J., Parson, T., 1972. Practical Handbook of Seawater Analysis. Fisheries Board of Canada Ottawa, Bulletin. 167.

Strub, P.T., Mesías, J.M., Montecino, V., Rutllant, J., 1998. Coastal ocean circulation off western South America. In: Robinson, A.R., Brink, K.H. (Eds.), The Global Coastal Ocean. The Sea, 11, Interscience, New York, pp. 273–313.

Sunda, W.G., Huntsman, S.A., 1997. Interrelated influence of iron, light and cell size on marine phytoplankton growth. Nature 390, 389–392.

Tegen, I., Fung, I., 1995. Contribution to the atmospheric mineral aerosol load from land surface modification. Journal of Geophysical Research 100, 18707–18726.

Thomas, A.C., Carr, M.E., Strub, P.T., 2001. Chlorophyll variability in eastern boundary currents. Geophysical Research Letters 28 (18), 3421–3424.

Ulloa, O., Escribano, R., Hormazabal, S., Quinones, R.A., Gonzalez, R.R., Ramos, M., 2001. Evolution and biological effects of the 1997–1998 El Nino in the upwelling ecosystem off northern Chile. Geophysical Research Letters 28 (8), 1591–1594.

Ward, B.B., Glover, H.E., Lipschultz, F., 1989. Chemoautotrophic activity and nitrification in the oxygen minimum zone off Peru. Deep Sea Research 36, 1031–1051.

Wooster, W.S., Chow, T.J., Barret, I., 1965. Nitrite distribution in the Peru current waters. Journal of Marine Research 23, 210–221.

Wyrtki, K., 1962. The oxygen minima in relation to ocean circulation. Deep Sea Research 9, 11.

Progress in Oceanography 79 (2008) 177–189

Contents lists available at ScienceDirect

Progress in Oceanography

journal homepage: www.elsevier.com/locate/pocean

Oxygenation episodes on the continental shelf of central Peru: Remote forcing and benthic ecosystem response

Dimitri Gutiérrez *, E. Enríquez, S. Purca, L. Quipúzcoa, R. Marquina, G. Flores, M. Graco

Dirección de Investigaciones Oceanográficas, Instituto del Mar del Perú, P.O. Box 22 Callao, Peru

ARTICLE INFO

Article history:
Accepted 14 October 2008
Available online 21 October 2008

Keywords:
Peru margin
Benthic communities
Thioploca
Oxygen minimum zone
ENSO
Remote forcing

ABSTRACT

The interplay between the oxygen minimum zone and remotely-forced oxygenation episodes determines the fate of the benthic subsystem off the Central Peruvian coast. We analyzed a 12 year monthly time-series of oceanographic and benthic parameters at 94 m depth off Callao, Central Peru (12°S), to analyze: (i) near-bottom oxygen level on the continental shelf in relation to dynamic height on the equator (095°W); and (ii) benthic ecosystem responses to oxygen change (macrobiotic infauna, meiofauna, and sulphide-oxidizing bacteria, *Thioploca* spp.). Shelf oxygenation episodes occurred after equatorial dynamic height increases one month before, consistent with the propagation of coastal trapped waves. Several but not all of these episodes occurred during El Niños. The benthic biota responded to oxygenation episodes by undergoing succession through three major ecological states. Under strong oxygen deficiency or anoxia, the sediments were nearly defaunated of macro-invertebrates and *Thioploca* was scarce, such that nematode biomass dominated the macro- and meiobiotas. When frequency of oxygenation events reduced the periods of anoxia, but the prevailing oxygen range was 10–20 μmol L^{-1}, mats of *Thioploca* formed and dominated the biomass. Finally, with frequent and intense (>40 μmol L^{-1}) oxygenation, the sediments were colonized by macrofauna, which then dominated biomass. The *Thioploca* state evolved during the 2002–2003 weak EN, while the macrofauna state was developed during the onset of the strong1997–1998 EN. Repeated episodes of strong oxygen deficiency during the summer of 2004, in parallel with the occurrence of red tides in surface waters, resulted in the collapse of *Thioploca* mats and development of the Nematode state. Ecological interactions may affect persistence or the transition between benthic ecosystem states.

1. Introduction

The upwelling zone off the Central Peruvian coast (8°S–14°S) is characterized by a higher biological production and a thicker and more intense oxygen minimum zone (OMZ) than other latitudinal coastal areas off Peru. In this zone, the main sources of the subsurface dissolved oxygen are the Peru–Chile undercurrent (PUC), which is formed off northern Peru from a southern branch of the Equatorial Undercurrent, and the turbulent diffusion from surface waters; while the main sink is oxygen consumption by the high respiratory demand of the settling and sedimentary organic matter, especially near the coast (Rowe and Howarth, 1985; Codispoti et al., 1989; Fossing, 1990; Strub et al., 1998; Pennington et al., 2006). The combination of these processes causes intense oxygen depletion over the continental shelf (Gutiérrez et al., 2006a). The oxygen regime though is subjected to significant temporal variability, especially by the poleward propagation of coastal trapped waves (CTWs) with periods between 30 and 50 days. These waves have their origin in the Equatorial region and occur more frequently during warm El Niño Southern Oscillation (ENSO) phase periods (Brink, 1982; Strub et al., 1998; Pizarro et al., 2001; Camayo and Campos, 2006). The CTWs can be generated upon Kelvin waves (KW) travelling the equatorial line reach the western coast of South America, but also from the propagation of free Tropical Waves, or even by anomalous activity of the northerly Panama wind jet, crossing the equatorial line (Brink, 1982; Hormazabal, 2001; Camayo and Campos, 2006; Mosquera, 2006). The passage of the CTWs is associated with deepening of the nutricline, oxycline and the OMZ off the Peru–Chile coast (Brink et al., 1981; Morales et al., 1999; Ulloa et al., 2001). The deepened nutricline reduces rates of primary production at the surface and oxygen consumption in subsurface waters. Passage of equatorial waves thus increases oxygen levels on the continental shelves.

Under neutral or cold ENSO phases, oxygen deficiency (<20 μM) occurs over the continental shelf bottoms while surface sediments tend to be anoxic, e.g. with no oxygen and with free hydrogen sulphide (Tyson and Pearson, 1991). Under these conditions benthic macrofauna do not inhabit shelf sediments; such populations only

---

* Corresponding author. Tel./fax: +51 1 6250827.
E-mail addresses: dgutierrez@imarpe.gob.pe (D. Gutiérrez), dim.gutierrez@gmail.com (D. Gutiérrez).

0079-6611/$ - see front matter © 2008 Elsevier Ltd. All rights reserved.
doi:10.1016/j.pocean.2008.10.025

develop if sustained oxygenation occurs, allowing successful recruitment and growth (Tarazona et al., 1988a,b, 2001). Mats of the large sulphide-oxidizing/nitrate-reducing bacteria *Thioploca* spp. develop under some conditions (Tarazona and Arntz, 1986; Zafra et al., 1988; Tarazona, 1990; Gutiérrez et al., 2006a). These bacteria glide up and down in their sheaths, obtaining energy by oxidizing hydrogen sulfide from below the sediment surface with nitrate from the water column. The mats can develop associated to suboxic conditions in the surface sediments and in the overlying water, e.g. very low-oxygen levels but no hydrogen sulphide (Tyson and Pearson, 1991; Bruland, 2006). Thus, oxic conditions or anoxia in the sediment surface are detrimental for *Thioploca* growth (Gallardo, 1977; Jørgensen and Gallardo, 1999; Schulz et al., 1996, 2000). On the other hand, though information on continental shelf meiofauna are scarce, recent work has found dense upper-slope meiofaunal populations within the OMZ off Central Peru, mostly composed of nematodes (Levin et al., 2002; Neira et al., 2001b).

Tarazona et al. (1988a,b, 2001) have described, for coastal embayments of Central Peru, the positive responses of macrofaunal communities to periods of oxygenation associated with El Niño's (EN's). Multi-year observations in the bays of Ancon (11°45′S) and Independencia (14°20′S) indicate that, following oxygenation, a recurrent pattern of colonization by benthic macrofauna occurs – observable as increases in diversity, abundance and biomass – and extending well beyond the termination of the EN (Tarazona et al., 1988a,b, 2001; Arntz et al., 2006). Nevertheless, local processes such as upwelling, phytoplankton blooms followed by sinking, and sediment resuspension due to wave action or erosion may additionally be important in the benthic ecosystem responses to EN or oxygenation episodes (Gutiérrez et al., 2006b). The response of deeper, continental shelf communities to EN off central Peru is less well known (Salzwedel et al., 1988; Arntz et al., 1991; Gutiérrez et al., 2002, 2006a,b). Off Callao (12°S) at 94 m depth, increases of macrofaunal species richness, biomass and bioturbation potential occurred during the 1997–98 EN and lasted a year after EN; near-zero *Thioploca* spp. biomass was recorded during this period (Gutiérrez et al., 2002),

The purpose of the present study is to document the oxygen regime and the benthic ecosystem response on the continental shelf off Central Peru. Since oxygenation events control the benthic ecosystem, we analyze (i) the time variability of the coastal subsurface oxygen content off central Peru in relation to equatorial oceanographic anomalies and (ii) the coupling, sign and duration of biomass and diversity changes of the macrobiota (infauna and *Thioploca* spp., since sizes of colonial trichomes and sheaths correspond to macrobenthos size range) and meiobiota (particularly nematodes) associated with changes in the oxygen regime. We postulate that: (i) Equatorial remote forcing governs the oxygen regime for the benthic ecosystem off Central Peru on monthly to interannual time-scales; and (ii) Frequency and duration of oxygenation episodes trigger succession among major components of the benthic biota (macrofauna, meiofauna and *Thioploca* spp.).

2. Material and methods

We analyzed monthly time-series data from a station 94 m deep, and 10 nautical miles off Callao, central Peru (12°02.8′S, 077°17.1′W; Fig. 1) from October 1992 to December 2005. Temperature, salinity and dissolved oxygen (as determined from the Winkler method; Carrit and Carpenter, 1966) were determined at standard depths. Bottom water dissolved oxygen (BWDO), temperature and density were measured at 90 m water depth. Combined subsampling and titration errors resulted in a precision of ca. ±5 μmol L^{-1}. Therefore an overestimation of dissolved oxygen values was possible, especially at contents $\leqslant$10 μmol L^{-1}, and affected our ability to detect events of anoxia.

Monthly monitoring of benthic parameters did not begin until August 1993. Macrobenthos (>0.5 mm) was sampled using a 0.04 m^2 Van Veen grab in three replicates. Macrofaunal species were identified, counted and weighed, Species richness (S) was calculated and is reported as number of species per 0.04 m^2. Biomass

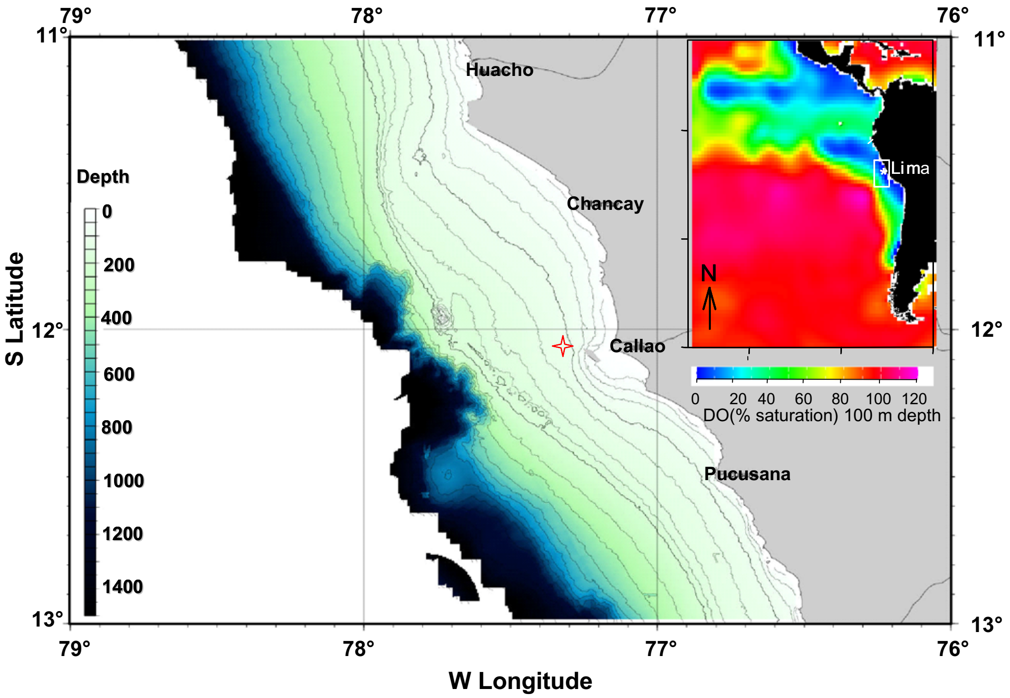

Fig. 1. Map showing the oceanographic station at 94 m depth off Callao (12°02.8′S, 77°17.1′W). The upper right panel shows the percent saturation of dissolved oxygen in the tropical Eastern Pacific Ocean (Source: http://iridl.ldeo.columbia.edu/SOURCES/.NOAA/.NODC/.WOA01/, Levitus 2002).

of *Thioploca* spp. was quantified as wet weight of sheaths containing cell trichomes. Percent of sheaths with trichomes was also determined for each sample. Macrofaunal biomass and abundance, and *Thioploca* spp. biomass is reported as grams per m^2.

Meiofauna was sampled from October 2002 to December 2005, every second month, using a short gravity corer. Three cores were collected by survey and each core was subsampled with a tube of 3.6 cm^{-2} internal diameter, corresponding to a surface area of 10 cm^2; only the top one centimeter was analyzed. Major meiofaunal taxa (excluding foraminifera) were sorted, identified and counted, and the densities were expressed as number of individuals per 10 cm^2 (Neira et al., 2001b). The Simpson dominance index (Simpson, 1949) was calculated on the abundances per major groups.

To further compare biotic components, wet weights of macrofaunal invertebrates were converted to ash-free dry weights (AFDW) using taxon-specific conversions (Brey et al., 1988, and references therein) and then to organic carbon using a factor of 0.518 (Salonen et al., 1976). Biomass of *Thioploca* spp. sheaths + trichomes were converted to carbon by assuming dry weight is 9% of wet weight (Huettel et al., 1996), and carbon is 12.5% of dry weight (Thamdrup and Canfield, 1996). Finally, nematode wet weight was first estimated from biovolume measurements with microscope following Andrassy, 1956), then converted to carbon (12.4%, following Wieser, 1960). Carbon is expressed as g Cm^{-2}.

We used linear interpolation computed from monthly survey profiles to estimate the depth of (1) the 45 $\mu mol\ L^{-1}$ oxygen level, taken as the upper boundary of the oxycline ($\sim$1 $mL\ L^{-1}$), (2) the 22 $\mu mol\ L^{-1}$oxygen level, taken as the upper boundary of the OMZ ($\sim$0.5 $mL\ L^{-1}$), thereafter 'vertical position of the OMZ', and (3) the isopycnals $\sigma_t = 26\ kg\ m^{-3}$ and $\sigma_t = 26.5\ kg\ m^{-3}$. Since these oxygen levels are well above $\leqslant$10 $\mu mol\ L^{-1}$, methodological difficulties associated with low-oxygen estimation using Winkler titration minimally affected oxycline and OMZ depth determination.

The daily, 5-day averaged and monthly time-series of the Equatorial dynamic height at 95°W (TAO project buoy, http://www.pmel.noaa.gov/tao) were employed to track the propagation of sea level anomalies (associated with equatorial Kelvin waves, KW) and their impact on the local water column conditions (as coastal trapped waves). Callao sea surface height was obtained daily from Callao (Dirección de Hidrografía Naval del Perú, DHN). Monthly average wind speed from Callao (Chucuito) was also provided by the DHN. These time-series were filtered with five day averages and interpolated linearly to fill gaps. Anomaly values were computed as standard units, in order to compare variances of the time-series, and also were analyzed with discrete wavelets (Torrence and Compo, 1998) to represent temporal changes in spectra. Pearson cross correlations were calculated to investigate connections between the local and remote time-series with 0, +1 or >1 month lags (Emery and Thomson, 1998).

3. Results

3.1. Oceanographic variability, oxygen and remote forcing

3.1.1. Kelvin waves and the water column

The oceanographic time-series off Callao (sea surface height, temperature, density and oxygen) off Callao record (Fig. 2) the influence of KWs (Table 1), which are more frequent and strong during EN. At least seven episodes during which the Callao thermocline and pycnocline were deepened while sea level in Callao rose can be identified after an increase in the Equatorial dynamic height (arrows over Fig. 2). Five of these episodes occurred during ENs (February–March and June–July 1993; April–May and December 1997; and April 2002). The other two episodes occurred in non-EN years (December 1994 and July 2000). Since 2003, at least two deepening episodes occurred and the relationship with the equatorial dynamic height is clear (Fig. 2). Table 1 links the Callao episodes with equatorial conditions, by comparing the equatorial in situ observations with Kelvin wave signals reported in the bibliography (Cravatte et al., 2003; Kessler and McPhaden, 1995a,b; Kessler and Kleeman, 2000; Dewitte et al., in press).

3.1.2. Oxygen and remote forcing

In comparison with the record of temperature and density, the time-series of dissolved oxygen exhibited more pronounced variations (Fig. 2c). The position of the OMZ oscillated from 10 to more than 90 m depth, and its overall mean depth (±one standard deviation) was 52.3 m (±33.2 m). Seasonal differences in the vertical position of the OMZ are not obvious due to the high interannual variability. All seven pycnocline depressions (above) were also recorded as water column oxygenation episodes, as the OMZ was pushed downwards more than one standard deviation, typically reaching the bottom at the study site. However the oxygen time-series reveal at least four more oxygenation episodes with similar amplitude as the above mentioned events (April 1994, April 1995, December 1995/January 1996 and September 2003). These correspond to moderate increases in dynamic height on the equator and sea surface heights at Callao, with weak changes of the local thermal structure. In addition, several minor oxygenation episodes also occurred, in which the OMZ was depressed to 60–90 m, so that BWDO was 10–20 $\mu mol\ L^{-1}$. These minor oxygenation episodes occurred during the weak 2002–2003 EN. In contrast, from August 1998 to April 2000 (e.g., during the 1998–99 La Niña; LN), there were no oxygenation episodes, nor were there disturbance of Equatorial dynamic height or deepening event within the water column.

3.1.3. Equatorial dynamic height and Callao sea surface height

Cross-correlations yielded significant relationships between the Equatorial dynamic height and the vertical position of the OMZ, and between the Equatorial dynamic height and the 26 $kg\ m^{-3}$ isopycnal depth with a one month lag ($P < 0.05$; Fig. 3a and b). Similar results were obtained with subsurface ($\geqslant$50 m) temperature, density and dissolved oxygen with a one-month lag (Table 2). The wavelet analysis on the difference between the standardized anomalies of the Callao sea surface height and the Equatorial dynamic height revealed two signals, one of them at 30–50 days, in rough agreement with the one-month lag explained above, and the other one at 5–15 days, which was more active during 2002–2003 (Fig. 3c). The linear relationships between Callao oceanographic variables and the Equatorial dynamic height had higher residual variances on subsurface dissolved oxygen (52% and 56% respectively, Table 2) than did density or temperature (28% and 34%, respectively, also Table 2). Similarly, the portion of unexplained variance was higher ($\sim$57%) for the iso-oxygen depths than for the isotherm or isopycnal depths ($\sim$40%). The portion of variance not explained is higher when only the time-series from the 2003–2005 period is analyzed, reaching more than 60% for the subsurface temperature and density, as well as for the isotherm and isopycnal depths, and about 80% for dissolved oxygen and the iso-oxygen depths (data not shown).

3.1.4. Bottom water dissolved oxygen

The missing values of BWDO from some surveys could be extrapolated from its relationship with the OMZ depth, since about 88% of the variance of the BWDO was explained by the OMZ depth via the equation: $BWDO = e^{(0.22 \times Z - OMZ)}$ ($n = 104$). The time-series of BWDO is shown in Fig. 4a. Values above 20 $\mu mol\ L^{-1}$ were characteristic of the mature 1997–98 EN, and also occurred between January and July 1993. Other peaks in BWDO were associated with the oxygenation episodes described above. Values $\leqslant$10 $\mu mol\ L^{-1}$

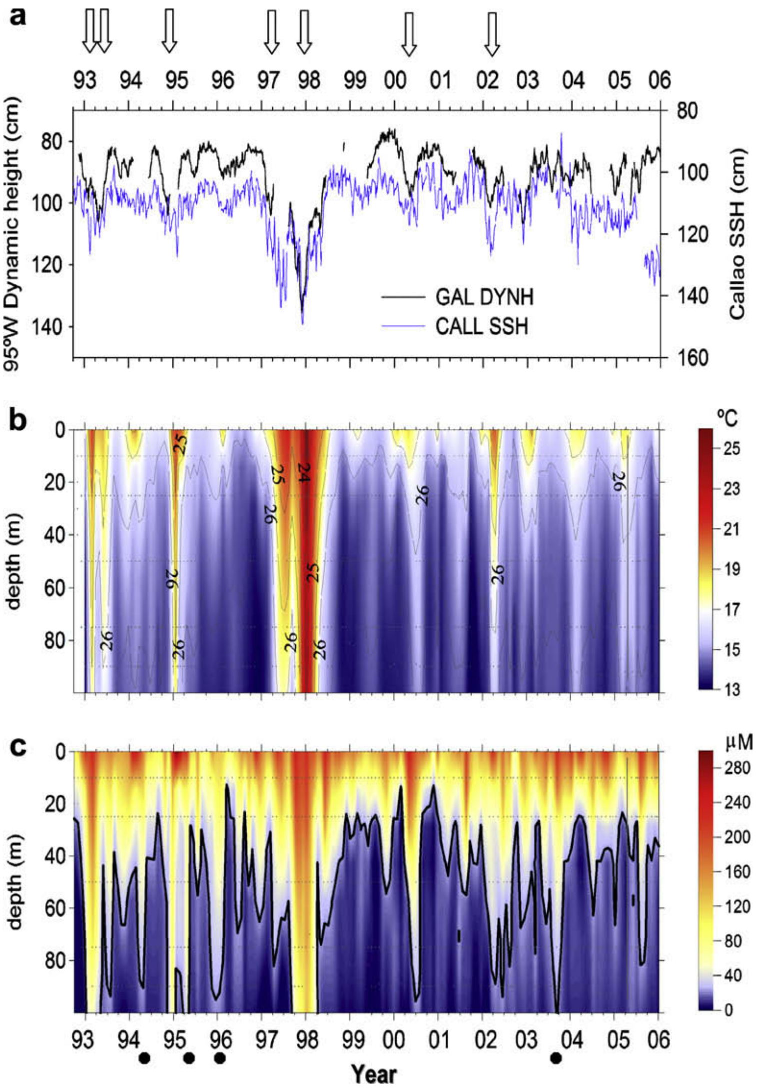

Fig. 2. Time-series of equatorial DH and oceanographic variables off Callao (12°S): (a) 5-day averaged equatorial dynamic height at 95°W (GAL DYNH) (black, scale reversed) and Callao SSH (blue, scale reversed); (b) Temporal variability of temperature (°C, coloured) and density – σ_t (kg m^{-3}; contour lines); (c) Temporal variability of dissolved oxygen (μmol L^{-1}); the thick isoline correspond to the vertical position of the OMZ (oxygen content = 22 μmol L^{-1}). Arrows depict the impact of coastal trapped waves off Callao (see Table 3). Oxygenation episodes uncorrelated with depressions of the thermocline or pycnocline are marked with black circles below the time axis.

dominated during the 1998–1999 LN, and were more frequent than on average during late 1993, in 1996–1997 and since early 2004. Values within the range 10–20 μmol L^{-1} dominated the time-series between 2002 and 2004.

Table 1

Vertical structure and oxygenation episodes off Callao related with increases of dynamic height at 95°W, Equator (Galapagos), from *in situ* data (arrows in Figs. 2 and 4). The first column indicates the date of the episodes. The second column indicates the warm (W) or neutral (N) conditions in the Niño 3 + 4 region in the Equatorial Pacific, according to the Oceanic El Niño Index ONI (NOAA, 2003); the May 97–April 1998 warm episode corresponds to the 1997–98 EN. The third and fourth columns indicate the date of the closest remote forcing wave and its reference, respectively. KW = Equatorial Kelvin wave (Niño 3 + 4 region), CTW = coastal trapped wave; in brackets, significant theoretical wave periods from power spectra.

In situ event	ONI episode	Remote forcing	Reference
February–March 1993	March–July 1993, W	December 1992, KW (60 d) January 1993, CTW (10–50 d)	Kessler and McPhaden, (1995a) and Camayo and Campos (2006)
June–July 1993	March–July 1993, W	December 1992–September 1993, KW (60 d)	Kessler and McPhaden (1995b)
December 1994–February 1995	April 1994–March 1995, W	December 1994, KW (70–120 d)	Cravatte et al. (2003) and Dewitte et al. (in press)
April–May 1997	May 1997–April 1998, W	March 1997, KW(70–120 d) May 1997, CTW (50–180 d)	Cravatte et al. (2003) and Kessler and Kleeman (2000)
December 1997	May 1997–April 1998, W	December 1997, KW (70 d)	Cravatte et al. (2003)
July 2000	July–September 2000, N	May 2000, KW (120 d)	Dewitte et al. (in press)
April 2002	May 2002–March 2003, W	February 2002, KW (120 d)	Dewitte et al. (in press)

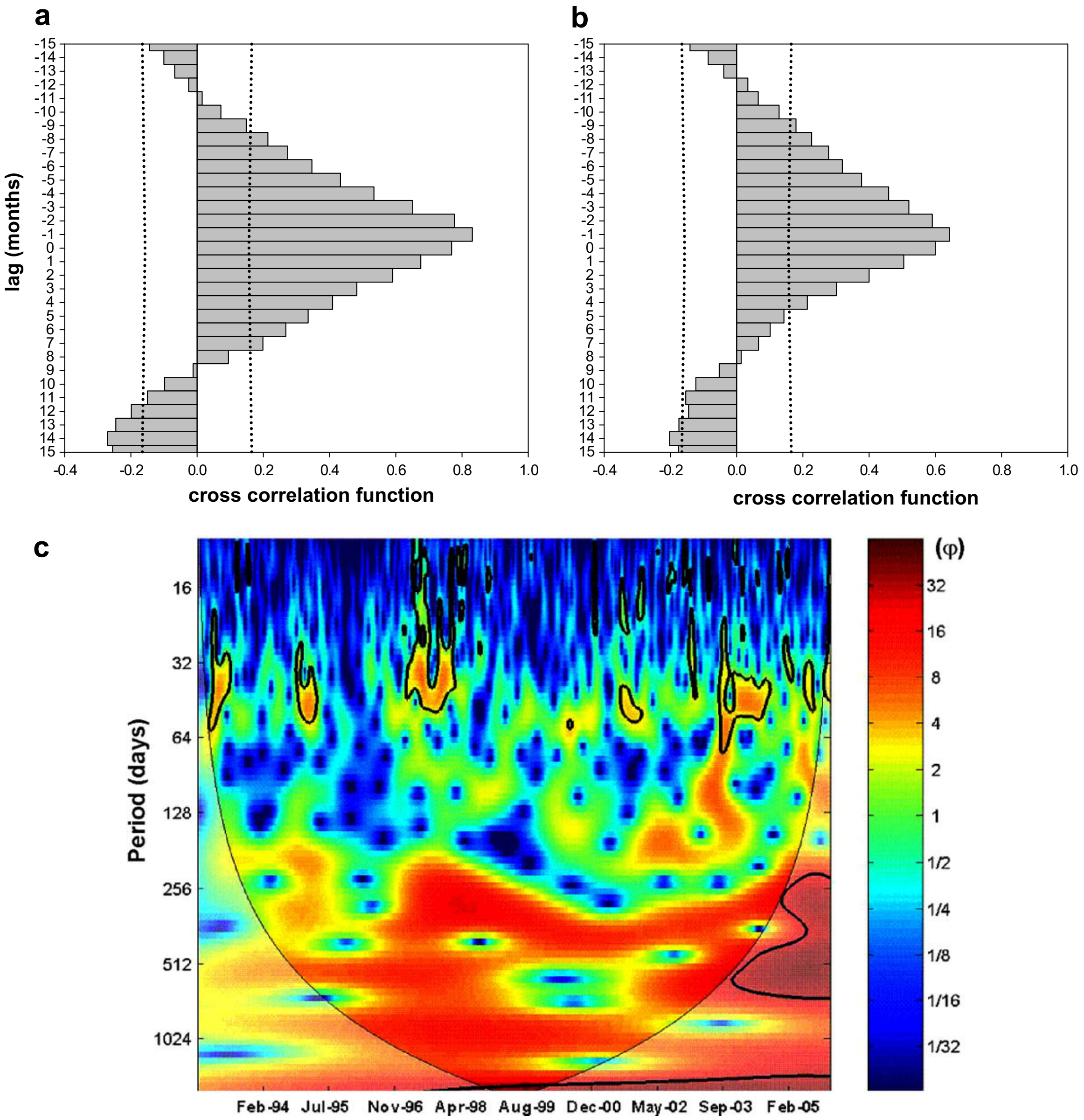

Fig. 3. (a) Cross correlation function between the 95°W equatorial DH and the OMZ depth (22 μmol L^{-1} iso-oxygen) off Callao; (b) Cross correlation function between the the 95°W equatorial DH and the 26 kg m^{-3} isopycnal depth; (c) Wavelet analysis of the difference between the standardized anomalies of the daily Callao SSH and the daily 95°W equatorial DH, showing significant signals at periods of 5–15 days and 30–50 days; the power of spectral density (ϕ) was calculated with Morlet wavelet and is represented in colors, the significant values are enveloped by a black line and the period is represented in days (Torrence and Compo, 1998). Dotted lines in (a) and (b) indicate critical values at significance level $\alpha = 0.05$.

3.2. Benthic ecosystem

Surface sediments at this station are composed of diatomaceous and organic-rich (>4% TOC) mud, with high water content in the top layer (>90%). Over time the sediments release free H_2S or *Thioploca* spp. mats develop on. Water content decreases exponentially below the sediment surface and compact sediments (water content <60%) are present at about 10–15 cm deep.

3.2.1. Macrofauna

Means and standard deviations of species richness (S), total abundance (N) and total biomass (B) were 3 ± 2 spp. per 0.04 m^{-2}, 442 ± 1092 ind. m^{-2} and 4.3 ± 10.3 g m^{-2}, respectively. Fig. 4b shows the temporal variabilities of S and B. Species richness rose from August to October 1993, following the seven-month period of oxygenation. The community was dominated by the amphipod *Ampelisca araucana* and the spionid polychaete *Paraprionospio pinnata*; other species that colonized the bottom were the polychaetes *Nephtys ferruginea* and *Sigambra bassi*, and the bivalve mollusk *Pitar* sp. The switch to strong oxygen deficiency was followed by a rapid decline down to zero values of the community parameters in February 1994. Thereafter S and B oscillated at low levels until the end of 1995, but with transient increases in April 1994 and February 1995, associated with oxygenation events. Near defaunation was observed in late 1996 until February 1997, during strong oxygen deficiency. A rapid and early response of benthic macrofauna to EN-associated oxygenation occurred from April to May 1997, consisting in increases of S, N and B up to 3–10 times their long-term means. This early colonization was dominated by *P. pinnata* and *A. araucana*. From the oxygenated period September 1997 to June 1998, *S. bassi* became dominant, and enteropneusts, nemerteans, several bivalves (e.g., *Pitar* sp.) and small decapods

Table 2
Pearson product-moment correlation coefficients of monthly Equatorial Dynamic Height (1 month lag) at 95°W (DYNH-1), and monthly wind velocity at Callao (CA WINDVEL) with oceanographic parameters during the monthly field surveys off Callao: sea surface height (CASSH), oxygen concentration at 50 m depth (OX50), oxygen concentration at 90 m depth, near the bottom (BWDO), temperature at 50 m depth (TEMP50), temperature near the bottom (TEMP90), sigma-t at 50 m depth (SIGMAT50), sigma-t near the bottom (SIGMAT90), OMZ 22 μmol L^{-1} upper boundary depth (Z-OMZ), 45 μmol L^{-1} iso-oxygen depth (Z-OXYC), 15 °C isotherm depth (Z-15ISOT), 14 °C isotherm depth (Z-14ISOT), 26 kg m^{-3} isopycnal depth (Z-26ISOP), and 26.5 kg m^{-3} isopycnal depth (Z-26.5ISOP). All the coefficients are significant ($p < 0.001$). Number of observations (n) is in brackets.

	DYNH (−1)	CAWINDVEL
CASSH	0.660 ($n = 146$)	0.489 ($n = 112$)
OX50	0.666 ($n = 122$)	0.422 ($n = 87$)
BWDO	0.654 ($n = 102$)	0.384 ($n = 65$)
TEMP50	0.849 (n = 110)	0.460 ($n = 76$)
TEMP90	0.849 ($n = 99$)	0.449 ($n = 65$)
SIGMAT50	−0.811 ($n = 105$)	−0.507 ($n = 7$)
SIGMAT90	−0.806 ($n = 94$)	−0.503 ($n = 60$)
Z-OMZ	0.656 ($n = 119$)	0.418 ($n = 86$)
Z-OXYC	0.643 ($n = 120$)	0.402 ($n = 87$)
Z-15ISOT	0.809 ($n = 109$)	0.448 ($n = 7$)
Z-14ISOT	0.657 ($n = 109$)	0.334 ($n = 76$)
Z-26ISOP	0.789 ($n = 108$)	0.488 ($n = 75$)
Z-26.5ISOP	0.752 ($n = 107$)	0.426 ($n = 74$)

colonized the sediments. S, N and B ranged 4–9 spp. per 0.04 m^{-2}, 336–1348 ind. m^{-2} and 4.2–74.5 g m^{-2}, respectively. Larger organisms, mostly enteropneusts and nemerteans, accounted for the increases in biomass. In spite of the development of strong oxygen deficiency and even anoxia during the 1998–1999 LN, higher-than-mean values of the community parameters persisted for about a year after the onset of the low-oxygen 1998–99 LN conditions. During late1999, community parameters decreased rapidly to near-defaunation from September 2001 to November 2002. Only juvenile specimens of *P. pinnata* or *A. araucana* were found during this period in the sediments. After December 2002, the community parameters have fluctuated from near-zero values to small peaks within the long-term means (e.g., early 2003, early 2004 and late 2005 for biomass).

3.2.2. *Thioploca*

Following Schulz et al. (1996), a ‘mat’ of *Thioploca* is defined as the condition wherein a network of interwoven trichomes and sheaths at sediment:water interface is dense enough to stabilize the sediment. From parallel observations of cores and grab samples, this mat condition occurs when *Thioploca* biomass in grab samples is $\gtrsim 30\,\mathrm{g\,m^{-2}}$. *Thioploca* fluctuated from zero to 131.9 g m^{-2}. The percent of sheaths with trichomes was positively correlated with the wet weight of sheath material ($r = 0.62$, $n = 128$, $p < 0.001$). Zero or nearly zero *Thioploca* biomasses were recorded during 1993. From early 1994 to July 1994, biomass increased slightly as did percent of sheaths with trichromes (Fig. 4c). Over the following year, both biomass and sheaths with trichomes increased but with large fluctuations, and from February 1996 to February 1997, both parameters fell to near-zero. During the 1997–98 EN and the 1998–99 LN, *Thioploca* trichomes almost disappeared, but empty sheaths were found during the EN. *Thioploca* was then absent until September 2000, followed by a gradual increase of biomass occurred from October 2000 to December 2001, when most of the *Thioploca* sheaths contained trichomes. The highest biomasses (>100 g m^{-2}) were found in 2002, and mats with sheaths containing trichomes remained dominant (70–90%) until January 2004. Over the next six months, both parameters decreased with large fluctuations. Since then, from July 2004 to July 2005, reduced levels of both parameters have occurred (30–70% and 0–10.7 g m^{-2}, for percent sheaths with trichomes and biomass, respectively), followed by higher but fluctuating biomass values in the last portion of 2005.

3.2.3. Meiofauna

Because the meiofauna consists mainly of nematodes, Simpson’s dominance index is correlated with nematodes abundance ($r = 0.78$, $n = 20$, $p < 0.001$). From September 2002 until April 2003, low nematode and total meiofaunal abundances occurred (<100 ind. 10 cm^{-2}), and as a consequence of the low nematode numbers, diversity was relatively high (3–7 taxa 10 cm^{-2}; not shown). In addition to nematodes (65–90% of abundance), the meiobiota also consisted of nemerteans, rotifers, ciliates and harpacticoid copepods. Diversity fell suddenly in July 2003, when only nematodes and rotifers were found. From early 2004 to April 2005, nematodes abundance increased to 2052 ± 404 10 cm^{-2}. In parallel the nematode dominance reached 90–100%. Finally, in the second half of 2005, only nematodes were found and those at reduced abundances (5–293 ind. 10 cm^{-2}).

3.3. Correlations with environmental variables and among biological parameters

Among the macrofaunal and meiofaunal community parameters, the macrofaunal biomass and species richness, and the meiofaunal phyletic Simpson Index exhibited significant correlations with the BWDO and the one-month lagged Equatorial dynamic height (Table 3). In contrast, no significant correlation was found between the *Thioploca*’s biomass or percent sheaths with trichomes and these abiotic factors. On the other hand, significant negative correlations were observed between the macrofaunal biomass and species richness with *Thioploca*’s biomass and percent sheaths with trichomes, and between the meiofaunal phyletic Simpson Index and those *Thioploca* parameters. However, meiofaunal and macrofaunal community parameters were not significantly correlated (Table 3).

4. Discussion

4.1. Remote forcing and subsurface dissolved oxygen

The average 50 m depth of the OMZ upper boundary at our Callao station is in agreement with previous estimates for this latitude (Wooster and Gilmartin, 1961; Zuta and Guillén, 1970). However, the temporal variability of OMZ depth is very high, even during non-EN years (Fig. 2). OMZ depth is essentially non-seasonal, as is thermocline depth, SST and other oceanographic parameters off the low-latitude Peruvian coast (Bohle-Carbonell, 1989; Tarazona, 1990). On the other hand, the significant correlation of the OMZ position with the one-month lagged Equatorial dynamic height is almost certainly due to poleward propagation of CTWs from the equator (Brink, 1982; Chavez et al., 1984; Hormazabal et al., 2001). As mentioned above, CTWs can develop from diverse sources, so that a variety of atmospheric/oceanic processes in the Equatorial region can trigger the propagation of the anomalies in the oceanographic conditions along the Peruvian coast.

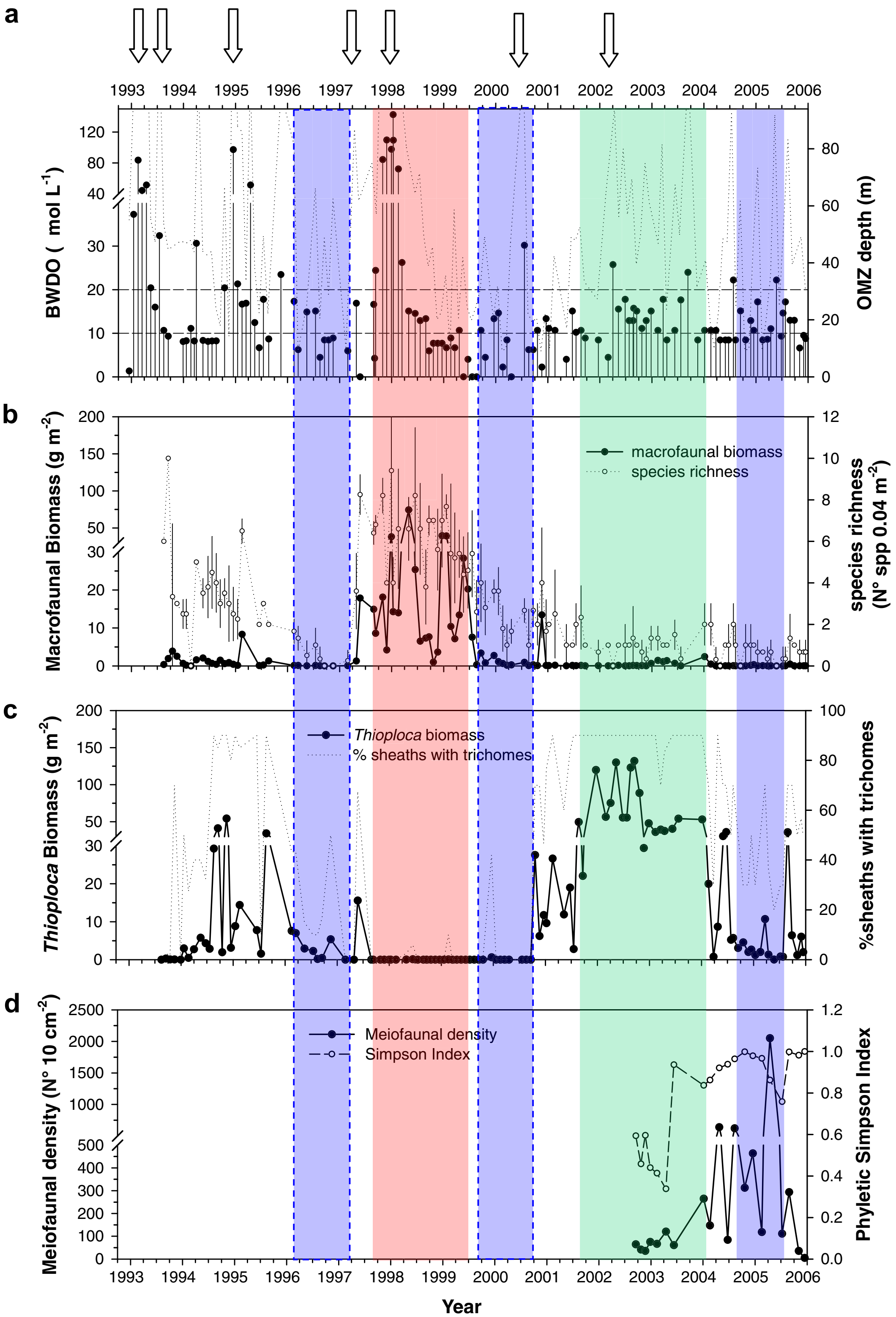

Fig. 4. Time-series of benthic community parameters related to subsurface and bottom dissolved oxygen variability: (a) bottom water dissolved oxygen content (black circles) and Z-OMZ (dotted line); the short – dash lines correspond to the 10 and 20 μmol L^{-1} content levels near the bottom; (b) macrofaunal biomass (black circles) and species richness (mean and ± 1 S.D., open circles); (c) biomass of *Thioploca* spp. (black circles) and percent of *Thioploca* sheath material with trichomes (dotted line); and (d) meiofaunal density and phyletic dominance Simpson Index. Arrows depict the impact of coastal trapped waves off Callao (see Table 3). Shaded red, blue-sky and green boxes envelope the periods of the benthic ecosystem states: macrofauna state, Nematoda state and *Thioploca* state, respectively.

The variance not explained by the relationship between the subsurface dissolved oxygen or the oxycline/OMZ depth with the Equatorial dynamic height is higher than those from the subsurface temperature and density. Some oxygenation episodes were not

Table 3

Pearson product-moment correlation coefficients between abiotic factors BWDO, CA WINDVEL and DYNH(−1) and benthic community parameters, and among benthic community parameters: macrofaunal biomass (MACROF B), macrofaunal density (MACROF N), macrofaunal species richness (MACROF S), meiofaunal density (MEIOF N), meiofaunal phyletic groups richness (MEIOF PHYLS), meiofaunal Simpson Index (SIMPSON INDEX), percent *Thioploca* sheaths with trichomes (% LSHEATHS), *Thioploca* biomass (THIOP B), and Nematoda numerical dominance (NEMAT D). Abiotic factors abbreviations are explained in Table 2. The correlations that are statistically significant at $\alpha = 0.05$ (*), $\alpha = 0.01$ (**) and $\alpha = 0.001$ (***) are indicated.

	MACROF B	MACROF N	MACROF S	MEIOF N	MEIOF PHYLS	SIMPSON INDEX	% LSHEATHS	THIOP B	NEMAT D
CAWINDVEL	0.196 ($n = 77$)	0.190 ($n = 77$)	0.174 ($n = 77$)	–	–	–	−0.098 ($n = 77$)	0.004 ($n = 77$)	
BWDO	0.194* ($n = 110$)	0.032 ($n = 110$)	.240* ($n = 110$)	−.0690 ($n = 20$)	0.205 ($n = 20$)	−0.435 ($p = 0.055$) ($n = 20$)	−0.144 ($n = 110$)	−0.084 ($n = 110$)	−.398 ($n = 20$)
DYNH (−1)	0.292** ($n = 108$)	0.149 ($n = 108$)	0.263** ($n = 108$)	−0.308 ($n = 20$)	0.231 ($n = 20$)	−0.524* ($n = 20$)	−0.072 ($n = 108$)	.0185 ($n = 108$)	−0.363 ($n = 20$)
MACROF B		.234* ($n = 114$)	.6242*** ($n = 114$)	−0.157 ($n = 20$)	0.283 ($n = 20$)	−0.365 ($n = 20$)	−.366*** ($n = 114$)	−.200* ($n = 114$)	−0.199 ($n = 20$)
MACROF N			.417*** ($n = 114$)	−0.034 ($n = 20$)	0.118 ($n = 20$)	0.024 ($n = 20$)	0.051 ($n = 114$)	−0.040 ($n = 114$)	0.014 ($n = 20$)
MACROF S				−0.170 ($n = 20$)	−0.044 ($n = 20$)	−0.030 ($n = 20$)	−.474*** ($n = 114$)	−.311** ($n = 114$)	0.061 ($n = 20$)
MEIOF N					0.288 ($n = 20$)	0.237 ($n = 20$)	−0.341 ($n = 20$)	−0.317 ($n = 20$)	0.203 ($n = 20$)
MEIOF PHYLS						−0.628** ($n = 20$)	0.483* ($n = 20$)	0.262 ($n = 20$)	−0.701*** ($n = 20$)
SIMPSON INDEX							−.556* ($n = 20$)	−0.562** ($n = 20$)	0.776*** ($n = 20$)
% LSHEATHS								.641** ($n = 114$)	−0.476* ($n = 20$)
THIOP B									−.596** ($n = 20$)

accompanied by similar changes of the thermocline and pycnocline, while some periods of strong oxygen deficiency (mostly after 2002) occurred in spite of depressed thermocline and pycnocline. These differences might be explained by the complex and non-linear interactions between coastal upwelling, wind mixing, and red tide formation (Codispoti et al., 1989; Smayda, 2000; Graco et al., 2001). For example, moderate warming of the water column may result in decreased surface primary production followed by lower subsurface oxygen consumption and higher BWDO values.

On the other hand, from 2003 onwards Equatorial dynamic height fluctuations have been weaker and less correlated with the Callao oceanographic parameters, and coherence between the Callao parameters themselves have been non-significant (oxycline, thermocline and pycnocline depths). Since the monthly Callao coastal wind speed exhibits a positive trend since 1992, especially for March–April ($F_{(1,26)} = 12.68$; $p < 0.01$, $R^2 = 0.33$; slope t-test = 3.56; $p < 0.01$), it is likely that coastal upwelling and turbulent mixing have been intensified in late summer and early fall, interfering with any equatorial modulation of oxygen supply. The summer/fall approach of warm, stratified subtropical waters towards the coast (Zuta and Guillén, 1970; Morón, 2006) causes formation of a steep upwelling front during wind events. When winds relax, the front and thermal stratification migrate towards the coast, favoring the development of red tides (Sánchez and Delgado, 1996; Smayda, 2000). In fact, a positive trend in summer/fall SeaWifs chlorophyll-*a* off Callao from 1997 to 2005, and a higher frequency and longer permanency of red tides related with massive algal blooms off the Central Peruvian coast since 2002, have been detected (F. Chávez and S. Sánchez, personal communication). During field surveys we frequently observed red tides during summer and fall in 2004 and 2005. Red tide blooms end in massive phytodetrital sedimentation and decay (Smayda, 2000), which can produce local anoxia on the shelves. Such strong local events decouple the remotely-driven oxygen temperature and density relations in the water column, and likely explain at least some of the variability between the oxycline/OMZ and the thermocline or pycnocline observed since 2002.

4.2. Benthic ecosystem succession and oxygenation

Changes in benthic ecosystems off Peru and Chile have previously been related to ENSO (Arntz et al., 2006; Tarazona et al., 1988a,b, 2001; Gutiérrez et al., 2002, 2006a,b; Sellanes et al., 2007). In the Bay of Ancón, during non-EN years, shallow bottoms (34 m) are dominated by characteristic species that are tolerant to oxygen deficiency, such as the polychaetes *Magelona phyllisae* and *Chaetozone* sp, *Thioploca*, or nematodes. During the EN, short pulses of opportunistic species occur, some developing early (as the polychaete *P. pinnata* and the ophiurid *Ophiactis kroyeri*) and others persisting for at least a year after EN termination (Tarazona et al., 1988a,b, 2001). Off Concepcion (36°S, central Chile), the extreme 1997–1998 EN altered the seasonal regime of oxygen deficiency and carbon flux with a >1 year period of bottom oxygenation and reduced carbon flux. Consequently the macrofaunal assemblage switched from tube-dwelling, interface feeders (*P. pinnata* and *A. araucana*) to burrowing, deposit feeders (the polychaetes *Mediomastus branchiferus* or *Cossura chilensis*; Gutiérrez et al., 2002; Sellanes et al., 2007).

The biomass of the large sulphur-oxidizing bacteria *Thioploca* is strongly reduced during EN. Off Peru, large decreases of biomass have been associated with abundant empty sheaths in the surface sediments (Zafra et al., 1988; Arntz et al., 1991, 2006; Gutiérrez et al., 2002). Off central Chile, Gallardo (1985) found that *Thioploca* mats dominated the macrobenthic biomass in 1975, a non-EN year, but almost disappeared during the 1982–1983 EN. Afterwards in the same location, Schulz et al. (2000) found a reduction in

Table 4
Properties of the oxygen regime and major community descriptors for the different benthic ecosystem states (Macrof = macrofaunal-dominated; Thiop = *Thioploca*-dominated; and Nemat = Nematoda-dominated) in the continental shelf sediments off Callao (see text). For BWDO, it is indicated the frequency distribution (number of cases and percent), according to range in concentrations, for each of the states. For the rest of cases, mean values ± 1 S.D., number of observations (in brackets), and range of values are given. No data = 'n.d.'.

Properties and descriptors	Benthic states		
	Macrof	Thiop	Nemat
Period	August 1997–June 1999	August 2001–January 2004	February 1996–February 1997 August 1999–September 2000 August 2004–July 2005
BWDO ⩽ 10 nmolL^{-1}:n(%)	10(42%)	5(23%)	18(56%)
BWDO 10–20 nmol L^{-1}:n(%)	6(25%)	15(68%)	12(38%)
BWDO > 20 nmol L^{-1}:n(%)	8(33%)	2(9%)	2(6%)
Z-OMZ	71 ± 47 (24)	58 ± 22 (22)	36 ± 27 (32)
	10–159	24–108	9–110
BWDO concentration (nmoL L^{-1})	34 ± 43 (24)	13 ± 5 (22)	10 ± 6 (32)
	0–143	4–26	0–30
Macrofaunal biomass (g m^{-2})	18.9 ± 17.4 (21)	0.4 ± 0.7 (19)	0.4 ± 0.8 (30)
	1.0–74.5	0.0–2.4	0.0–3.4
Macrofaunal biomass (g C m^{-2})	1.148 ± 1.163 (21)	0.029 ± 0.052(19)	0.021 ± 0.038 (30)
	0.069–5.264	0.000–0.197	0.000–0.158
Macrofaunal abundance (N m^{-2})	657 ± 506 (21)	266 ± 746 (19)	124 ± 178 (30)
	160–2300	0–3313	0–833
Macrofaunal species richness (No. spp. 0.04 m^{-2})	6 ± 2(21)	1 ± 1 (19)	1 ± 1 (30)
	4–9	0–2	0–4
Thioploca biomass (g m^{-2})	0.0 ± 0.0 (21)	65.6 ± 35.5 (19)	2.1 ± 2.8 (30)
	0.0–0.1	22.0–131.9	0.0– 10.7
Thioploca biomass (g C m^{-2})	0.000 ± 0.000 (21)	0.738 ± 0.400 (19)	0.023 ± 0.031 (30)
	0.000–0.001	0.248– 1.484	0.000–0.120
Thioploca sheats with trichomes (%)	0.9 ± 2.5 (21)	88.6 ± 4.8 (19)	23.2 ± 22.9 (30)
	0–10	70–90	0–70
Meiofaunal abundance, top 1-cm (N 10 cm^{-2})	n.d.	91 ± 75 (8)	613 ± 732 (6)
		35–265	111–2052
Nematoda biomass, top 1-cm (g C m^{-2})	n.d.	0.016 ± 0.011 (8)	0.152 ± 0.212 (6)
		0.005–0.033	0.005–0.546
Meiofaunal phyletic richness (No. taxa 10 cm^{-2})	n.d.	5 ± 1 (8)	3 ± 2 (6)
		2–7	1–5
Meiofaunal phyletic groups Simpson Index	n.d.	0.58 ± 0.21 (8)	0.92 ± 0.09 (6)
		0.34–0.94	0.76–1.00

Thioploca biomass during the 1997–1998 EN as normally occurs during winter when normally upwelling is less frequent and the OMZ is deeper. For meiofauna, off Central Chile, Sellanes and Neira (2006) have reported an overall increase in abundance during the 1997–1998 EN, though this increase varied along a benthic transect between the Bay of Concepcion and the outer shelf (28–120 m). Harpacticoid copepod abundance increased while nematodes decreased (Neira et al., 2001b; Sellanes and Neira, 2006).

Off Callao the benthic ecosystem was also affected by ENSO-driven oxygen changes. The system varied among three different states, with biomass dominance by: (i) macrofauna; (ii) *Thioploca*; or (iii) Nematoda (Table 4). The total ecosystem biomass differed significantly between these states (Kruskal–Wallis ANOVA and Mann–Whitney tests; see Table 5 and below). The temporal frequency distributions of BWDO also differed (Fig. 5). In the 'macrofauna state', the frequency distribution was bimodal, with the first mode at ⩽10 μmol L^{-1}, and the second mode at >40 μmol L^{-1} (occurring on 42% and 25% of station occupations, respectively). In none of the other states did the >40 μmol L^{-1} class occur. In the '*Thioploca* state', the 10–20 μmol L^{-1} was most common (68%). Finally, in the 'Nematoda state', the ⩽10 μmol L^{-1} occurred during 56% of station occupations. After collapsing the frequency distribution into three classes (⩽10 μmol L^{-1}, 10–20 μmol L^{-1}, and >20 μmol L^{-1}), there was a significant association between ecosystem state and oxygen concentration (chi-square tests, $p < 0.05$).

The macrofauna state evolved after the first coastal trapped wave reached Callao early during the 1997–98 EN, when O_2 values reached 143 μmol L^{-1} near the bottom). Surprisingly, the macrofauna state persisted after EN terminated and into 1999 under the extreme oxygen deficiency or even anoxia that characterized the 1998–2000 LN (Fig. 5). This prolonged survival of macrofauna may be explained by the colonization of bioturbating species

Table 5
Differences between *Thioploca* (Thiop), macrofauna (Macrof) and Nematoda (Nemat) carbon biomasses at each of the benthic ecosystem states, according to the non-parametric Kruskal–Wallis test. Homogenous groups were estimated from the Mann–Whitney U test (underlined). Nematoda biomass data only correspond to the top one centimeter (see text).

State	Kruskal–Wallis ANOVA	p-value	Homogenous groups (oc = 0.05)
Macrof	$H_{(1,42)} = 33.39$	<0.001	Thiop Macrof
Thiop	$H_{(2,46)} = 33.27$	<0.001	Macrof Nemat Thiop
Nemat	$H_{(1,68)} = 6.47$	0.039	Thiop Macrof Nemat

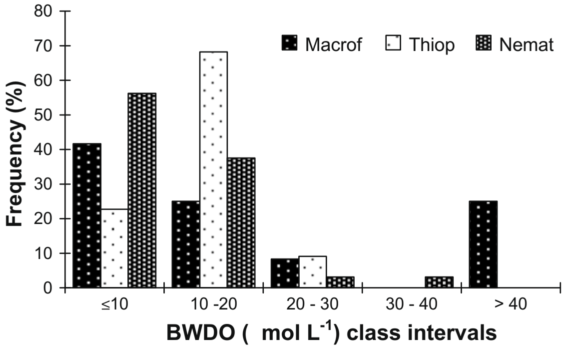

Fig. 5. Frequency distribution (%) of BWDO (μmol L^{-1}) under the macrofauna state (Macrof), *Thioploca*–state (Thiop), and Nematoda state (Nemat).

(mostly enteropneust and nemertean worms) that continued to ventilate surface sediment even with very low-oxygen concentrations in the overlying waters (Gutiérrez et al., 2002). The switch to extreme oxygen deficiency associated to LN also resulted in the depletion of nitrate (that is used for oxidize hydrogen sulphide by *Thioploca*), likely due to enhanced denitrification in the water column (Graco et al., 2006). It was just in late 2000, after a CTW reached Callao depressing moderately the OMZ and increasing subsurface nitrate (Graco et al., 2006), whereby *Thioploca* could colonize the seafloor. Then a *Thioploca* state characterized 2002–2003, during a weak EN. These years were characterized by a moderately deep oxycline and high near-bottom nitrate, but the prevailing oxygen range near the bottom was not enough for macrofaunal colonization (10–20 μmol L^{-1}; Table 4; Fig. 5). By early 2004 under sustained oxygen deficiency (Figs. 2 and 4), the mats were mostly gone, despite a deepening of the thermocline. During this year the macrofauna was also depauperate, while meiofaunal nematodes increased. Our data only assess meiofaunal in the top centimeter of sediment, but other observations indicate that this centimeter contains about 60% of the total meiofauna (<10 cm; E. Enríquez, personal communication). Since nematodes comprise over 90% of the metazoan meiofauna, nematode biomass in the top centimeter represent about 50% of the total meiofaunal biomass. These conditions define the Nematoda state, which was established from 2004 to 2005 (Fig. 4). Similar absence of both macrobenthic animals and *Thioploca* mats occurred during the extreme oxygen-deficient 1999–2000 period (see above). Probably the Nematode state characterized the benthic ecosystem here as well, since Nematoda populations multiply in anoxic settings with high loads of organic matter (Neira et al., 2001a; Levin et al., 2002; Levin, 2003). The Nematoda state may also have developed during 1996–1997, when similar, though less extreme, conditions and reductions of macrobiota were observed (Fig. 4, Table 4).

Other periods exhibited mixed characters. In 2001–2002 and early 2004, the biota was apparently in transition between the *Thioploca* and Nematoda states. Before 1996, macrofauna and *Thioploca* biomasses oscillated, and a general decreasing trend of macrofaunal diversity was observed. Since an extended but moderate EN persisted from 1991 to 1993, it is possible that the variability reflects a late evolution of the macrofauna state associated to the EN (Arntz et al., 2006). Frequent alternation of near-bottom oxygenation and depletion probably precluded development of *Thioploca* mats during these years.

4.3. Response times of the macrobiota

The macrofauna responded to oxygenation episodes with rapid increases in biomass or species richness. Such increases occurred following passage of the mid-1993, early 1995, March 1997 and mid 2000 CTWs. However, the colonizations were short-lived and did not result in a macrofaunal state, as the oxygenated conditions rapidly dissipated, with the exception of the extreme 1997–1998 EN. Direct observation of the macrobiota during these transient oxygenation episodes reveals that most are new juvenile recruits inhabiting the top centimeter of sediments, suggesting that most colonization is via larval settlement rather than immigration of juveniles and adults (Tarazona, 1990).

Thioploca also showed rapid colonization. During the early phase of the *Thioploca* state the population doubling time averaged 34 ± 19 days with a minimum doubling time of 8 days, faster than laboratory growth rates under simulated optimal conditions (26–52 days; Otte et al., 1999) or on Concepcion shelf sediments (22–35 days; Schulz et al., 2000). Given optimal environmental conditions and starting from biomass values $\sim$1 g m^{-2}, it apparently takes <2 months for the establishment of 100 g m^{-2} mats. On average however, mats appear to take about eight months to form. This calculation is in agreement with the nine-month observed duration of the transition to the *Thioploca* state (Fig. 4, Table 4). The pronounced $\sim$monthly fluctuations of *Thioploca* abundance suggest that favorable growth conditions are often not sustained. For instance, the rapid collapse of the mats in early 2004 was associated with the appearance of fluffy, sulphidic layers in the surface sediments. These layers most likely result from massive sedimentation of organic matter, presumably due to senescence and sinking of the red tides mentioned above. Degradation and respiration of this organic matter probably switched redox conditions to anoxic. Experimental and field observations have shown that when the bottom water is oxygen and nitrate-depleted and hydrogen sulphide builds to high concentrations in the sediment-water interface, the *Thioploca* filaments emerge from the sediment and may be entrained in bottom flows, dispersing from their previous habitat (Gallardo, 1985; Huettel et al., 1996).

4.4. A conceptual model of the benthic succession triggered by ENSO-driven oceanographic regimes

Here we frame a conceptual model to explain the variability of the benthic assemblages under contrasting oceanographic regimes, as were recorded in the 1993–2005 period off Callao (Fig. 6). The switch from anoxic (e.g., sulphidic) to suboxic and oxic conditions depends on the frequency and intensity of oxygenation events. The ecological effects of changes in the frequency and in the duration of oxygenation periods are related. For example, it has been described that characteristic infaunal species inhabiting the shelf sediments, such as *P. pinnata*, have respiratory anaerobic pathways (González and Quiñones, 2000) that permit them to survive in the transition between oxygen deficiency and anoxic conditions. *Thioploca* moves up in surface sediments to avoid sulphidic conditions, preferring low-oxygen concentrations in the overlying water (see below; Huettel et al., 1996). In addition, the nitrate storage capacity in its vacuoles should enable *Thioploca* to survive short periods when the bottom waters are anoxic and nitrate-depleted (Huettel et al., 1996). Free sulphide also reduces the ability of benthic animals to survive absence of oxygen (Diaz and Rosenberg, 1995; Gamenick et al., 1996). Therefore, the characteristic shelf macrobiotic species seem to exhibit metabolic and behavioral adaptations to cope with short periods of anoxia and their ability to survive depends on oxygenation episodes. The duration of these episodes is constrained by the characteristic periods of the coastal trapped waves (Table 1) and their frequency is normally increased during the EN phase of ENSO (Strub et al., 1998; Pizarro et al., 2001). During periods of negative Equatorial dynamic height anomalies (e.g., LN conditions),

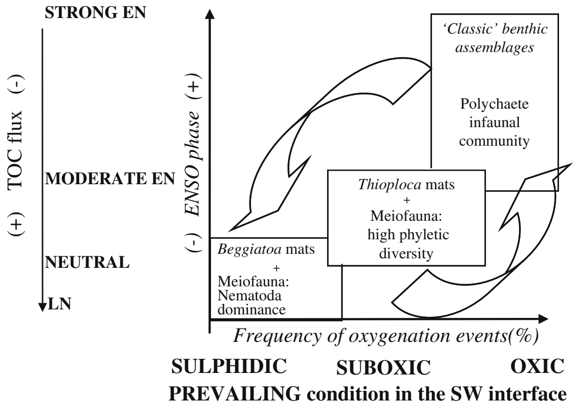

Fig. 6. Conceptual model that explains the succession of shelf benthic communities off Central Peru forced by ENSO and the associated frequency and intensity of oxygenation episodes.

the OMZ shoals and continental shelf oxygen levels are reduced. Carbon fluxes are also likely higher due to a shallower nutricline and enhanced near-surface productivity. Consequently the shelf sediments are loaded with decaying organic matter, become anoxic and become dominated by nematode populations. This Nematoda state is also characteristic of sediments permanently located in the core of the OMZ, where some nematodes contain symbionts which permit sulphide oxidation (Levin, 2003; Neira et al., 2001b).

As long as the benthic environment is subjected to oxygenation events, nitrate is replenished in the bottom water, free sulphide and other reduced compounds are chemically removed and a suboxic layer is established, favoring the colonization by *Thioploca* trichomes, which are easily resuspended and redistributed (Gallardo, 1985). However, the formation of mats will occur only if suboxic conditions persist. A positive feedback may be established when *Thioploca* become abundant enough to significantly reduce sulphide levels by $\gtrsim$ 30%, pushing anoxic conditions deeper into the sediment (Ferdelman et al., 1997; Fossing et al., 1995; Otte et al., 1999).

More frequent as well as more intense oxygenation (>20 μmol L^{-1}) permits development of the macrofaunal state that can reach higher biomasses under oxic conditions, as it occurred during the 1997–1998 EN. The reduction and disappearance of *Thioploca* in oxygenated conditions is consistent with previous reports for the Peru–Chile coast (Zafra et al., 1988; Schulz et al., 2000), but causes are elusive. Though nitrate is the major electron acceptor in *Thioploca* metabolism (Otte et al., 1999), recent experiments have demonstrated that *Thioploca* spp. can also respire aerobically (N.P. Revsbech, personal communication). Others have shown that trichomes retreat into the sediment when oxygen reached 15 μM and nitrate was low (<5 μM), but there was not an avoidance of oxygen under nitrate-rich (>20 μM) conditions (Huettel et al., 1996). Hence, the collapse of *Thioploca* populations seems to be only indirectly controlled by oxygenation. Oxygen can influence nitrate cycling (nitrification or denitrification) and sulphide oxidation. It seems that bottom water was not nitrate-depleted during the oxygenated 1997–1998 EN, varying from 8.8 to 19.8 μM (M. Graco, personal communication). Inspection of the sediments revealed abundant burrows and galleries and no sulphide smell at all, in contrast to conditions in non-EN periods. Possibly a reduction of carbon fluxes during EN and a subsequent decrease of the reactivity of the stored organic matter by aerobic microbial respiration resulted in decreased sulphate reduction rates. In addition, flushing of oxygen into the sediments by benthic fauna could have pushed sulphate reduction deep into the compact sediment layer, hampering *Thioploca* survival. Part of the negative correlation between *Thioploca* and macrofauna biomasses (Table 3) can be interpreted by a differential tolerance to oxygen deficiency. This is supported by the spatial trends of *Thioploca* and macrofauna along the Northern and Central Peruvian shelf, showing that *Thioploca* tends to replace macrofauna at increasing latitude with stronger bottom water oxygen deficiencies (Gutiérrez et al., 2006a).

The negative correlation or the lack of correlation between *Thioploca*, and macrofauna or meiofauna (Table 3) questions the effectiveness of the 'sulphide detoxification' performed by *Thioploca*, particularly for the metazoan communities (Jørgensen and Gallardo, 1999; Neira et al., 2001b; Arntz et al., 2006). The tendency for higher diversity of meiofaunal major taxa to occur under the *Thioploca*-dominated state can also be attributed to similar reduced tolerances to anoxia by *Thioploca* and minor meiofaunal groups, as harpacticoid copepods, rotifers, and others (Neira et al., 2001b; Levin, 2003).

At shallower sites off Callao, absence of macrofauna and *Thioploca* spp., and presence of nematode populations co-occur with sheathless filamentous bacterial mats, probably *Beggiatoa* spp. (D.G. pers. obs.). Sheathless, nitrate-vacuolated, sulphur-oxidizing mats are common in the semi-enclosed and shallow Concepcion Bay (Gallardo, 1979; Schulz et al., 2000; Graco et al., 2001). The sheathless condition may be an adaptation to increase exchange between the bacteria and nitrate-rich and the sulphidic layers (Graco et al., 2001). Under the fluctuating environment off central Peru, this condition is more likely to occur in shallow areas with very high organic load, as coastal embayments, permitting the transient co-existence of sulphide buildup in the sediment surface with oxygenation and nitrate availability in the bottom water. There, the 'Nematoda state' may coexist with mats of sheathless filamentous bacteria.

5. Conclusions

Remote forcing controls the oxygen regime on the continental shelf off Callao at monthly to interannual time-scales, taking into account the characteristic periods associated with the passage of coastal trapped waves. When such forcing is weak (lower frequency and/or energy of coastal trapped waves, e.g. the period 2003–2005), local physical, biological and biogeochemical processes (as those related to the development and fate of red tides) appear to control the level of near-bottom oxygenation.

Both intensity and frequency of oxygenation episodes and anoxia control development of the benthic ecosystems of the Peruvian shelf sediments. Permanent anoxia (e.g., sulphidic) conditions are unfavorable for the macrobiota, including *Thioploca* populations, but nematode populations can attain their highest biomasses under anoxia. Increasing frequency of oxygenation episodes favors the development of *Thioploca* mats as the most characteristic benthic ecosystem 'state'. More intense oxygenation permits recruitment of macrofauna that finally replace the mats as the main component of the macrobiota. Ecological interactions, mediated by the biological activity, as enhanced bioturbation and bio-irrigation, can additionally affect the persistence or transition between these three characteristic ecosystem states.

Acknowledgements

We deeply thank the Instituto del Mar del Perú (IMARPE) for full support of this research. Also we acknowledge the Dirección de Hidrografía y Navegación del Peru (DHN) for kindly providing sea level data and monthly wind records off Callao. We acknowledge Mrs. Víctor Aramayo and José Pasapera who supported analytical and data processing tasks. Dr. Francisco Chávez and Dr. David Foley kindly provided Seawifs chlorophyll-a information from the zone off Callao. The EU-project CENSOR (Climate variability and El Nino Southern Oscillation: Impacts for natural resources and management, contract 511071) financed the post-doc grant of M. Graco. This study was conducted in the frame of the EU-project CENSOR (Climate variability and El Nino Southern Oscillation: Impacts for natural resources and management, contract 511071) and is CENSOR publication 0236.

References

Andrassy, I., 1956. Die rauminhalts- und gewichtsbestimmung der fadenwürmer (Nematoden). Acta Zoologica Academia Scientiarum Hungaricae 2, 1–15.

Arntz, W., Tarazona, J., Gallardo, V.A., Flores, L.A., Salzwedel, H., 1991. Benthos communities in oxygen deficient shelf and upper slope areas of the Peruvian and Chilean Pacific coast and changes caused by El Niño. In: Tyson, R.V., Pearson, T.H. (Eds.), Modern and Ancient Continental Shelf Anoxia, vol. 58. Geological Society Special Publication, London, pp. 131–154.

Arntz, W., Gallardo, V.A., Gutiérrez, D., Isla, E., Levin, L.A., Mendo, J., Neira, C., Rowe, G.T., Tarazona, J., Wolff, M., 2006. El Niño and similar perturbation effects on the benthos of the Humboldt, California, and Benguela Current upwelling ecosystems. Advances in Geosciences 6, 243–265.

Bohle-Carbonell, M., 1989. On the variability of the Peruvian upwelling system. In Pauly, D., Muck, P., Mendo, J., Tsukayama, I. (Eds.). ICLARM Conference Proceedings of The Peruvian Upwelling Ecosystem: 1953–1984, vol. 18, pp. 14–32.

Brey, T., Rumohr, H., Ankar, S., 1988. Energy content of macrobenthic invertebrates: general conversion factors from weight to energy. Journal of Experimental Marine Biology and Ecology 117, 271–278.

Brink, K.H., 1982. A comparison of long coastal trapped wave theory with observations off Peru. Journal of Physical Oceanography 12, 897–913.

Brink, K.H., Jones, B.H., Van Leer, J.C., Mores, D.W., Stuart, C.N.K., Stevenson, M.R., Dugdale, R.C., Herbun, G.W., 1981. Physical and biological structure and variability in an upwelling center off Peru near 15°S during march 1977. In: Richards, F.A. (Ed.), Coastal Upwelling. American Geophysical Union, Washington, DC, pp. 473–495.

Bruland, K., 2006. A review of the chemistries of redox sensitive elements within suboxic zones of oxygen minimum regions. Gayana (Concepc.) 70 (Supplement), 6–13.

Camayo, R., Campos, E.J.D., 2006. Application of wavelet transform in the study of coastal trapped waves off the west coast of South America. Geophysical Research Letters 33, L22601.

Carrit, D., Carpenter, J., 1966. Comparison and evaluation of currently employed modification of the Winkler method for determining dissolved oxygen in sea water. Journal of Marine Research 24, 286–318.

Chavez, F.P., Barber, R.T., Soldi, H., 1984. Propagated temperature changes during onset and recovery of the 1982–83 El Niño. Nature 309, 47–49.

Codispoti, L.A., Barber, R.T., Friederich, G.E., 1989. Do nitrogen transformations in the poleward undercurrent off Peru and Chile have a globally significant influence? In: Neshyba, S.J., Mooers, N.K., Smith, R.L., Barber, R. (Eds.), Poleward Flows Along Eastern Ocean Boundaries. Coastal and Estuarine Studies. Springer-Verlag, pp. 281–310.

Cravatte, S., Picaut, J., Eldin, G., 2003. Second and first baroclinic Kelvin modes in the equatorial Pacific at intraseasonal timescales. Journal of Geophysical Research 108, 3266–3286.

Dewitte, B., Purca, S., Illig S., Reanult, L., Giese, B., in press. Low frequency modulation of intraseasonal equatorial Kelvin wave activity in the Pacific from SODA:1958-2001. Journal of Climate.

Diaz, R.J., Rosenberg, R., 1995. Marine benthic hypoxia: a review of its ecological effects and the behavioral responses of benthic macrofauna. Oceanography and Marine Biology Annual Review 33, 245–303.

Emery, W.J., Thomson, R.E., 1998. Data Analysis Methods in Physical Oceanography. Pergamon, Oxford.

Ferdelman, T.G., Lee, C., Pantoja, S., Harder, J., Bebout, B.B., Fossing, H., 1997. Sulfate reduction and methanogenesis in a Thioploca-dominated sediment off the coast of Chile. Geochimica et Cosmochimica Acta 61, 3065–3079.

Fossing, H., 1990. Sulfate reduction in shelf sediments in the upwelling region off central Peru. Continental Shelf Research 10 (4), 355–367.

Fossing, H., Gallardo, V.A., Jørgensen, B.B., Huettel, M., Nielsen, L.P., Schulz, H., Canfield, D.E., Forster, S., Glud, R.N., Gundersen, J.K., Kuver, J., Ramsing, N.B., Teske, A., Thamdrup, B., Ulloa, O., 1995. Concentration and transport of nitrate by the mat-forming sulphur bacterium *Thioploca*. Nature 374, 713–715.

Gallardo, V.A., 1977. Large benthic microbial communities in sulfide biota under Peru–Chile subsurface countercurrent. Nature 268, 331–332.

Gallardo, V.A., 1979. Peculiaridades bentónicas sublitorales del Pacífico sur oriental. In: Proceedings of the Workshop “Perspectivas en la investigación ecológica marina en Chile (Pacífico sur oriental y Antártica)”. Universidad Austral de Chile, Valdivia, August 23–25, 93 p.

Gallardo, V.A., 1985. Efectos del fenómeno de El Niño sobre el bentos sublitoral frente a Concepción, Chile. In: Arntz, W., Landa, A., Tarazona, J. (Eds.). El Niño y su impacto en la fauna marina, vol. Extraordinario. Boletin Instituto del Mar del Perú, pp. 79–885.

Gamenick, I., Jahn, A., Vopel, K., Giere, O., 1996. Hypoxia and sulphide as structuring factors in a macrozoobenthic community on the Baltic Sea shore: colonization studies and tolerance experiments. Marine Ecology Progress Series 144, 73–85.

González, R.R., Quiñones, R.A., 2000. Pyruvate oxidoreductases involved in glycolytic anaerobic metabolism of polychaetes from the continental shelf off central-south Chile Estuarine. Coastal and Shelf Science 51, 507–519.

Graco, M., Farías, L., Molina, V., Gutiérrez, D., Nielsen, L.P., 2001. Massive developments of microbial mats following phytoplankton blooms in a naturally eutrophic bay: implications for nitrogen cycling. Limnology and Oceanography 46, 821–832.

Graco, M., Flores, G., Ledesma, J., Purca, S., Gutiérrez, D., Girón, M., 2006. Biogeochemical variability in the oxygen minimum zone of the upwelling Humboldt system off central Peru. In: Extended abstracts book, International Conference on the Humboldt Current system, 27 November–2 December, Lima, Peru, IMARPE, IRD and FAO, unpublished.

Gutiérrez, D., Gallardo, V.A., Levin, L., Quipúzcoa, L., Solís, J., 2002. Biomass and bioturbation responses of macrobenthos during El Niño 1997–1998 in continental margin sediments off the southeastern Pacific. In: Salinas, S., Urban, H.J., Arntz, W.E. (Eds.), Impacts of El Niño and Basin-Scale Climate Change on Ecosystems and Living Marine Resources, vol. 30(1). Investigaciones Marinas, Viña del Mar Chile, p. 144.

Gutiérrez, D., Quipúzcoa, L., Enríquez, E., 2006a. Oxygen deficiency and benthic communities in the Peruvian upper continental margin. Gayana (Concepc.) 70 (Supplement), 29–36.

Gutiérrez, D., Aronés, K., Chang, F., Quipúzcoa, L., Villanueva, P., 2006b. Impacto de la variación oceanográfica estacional e inter-anual sobre los ensambles de microfitoplancton, mesozooplancton, ictioplancton y macrozoobentos de dos áreas costeras del norte del Perú entre 1994 y 2002. Boletin Instituto del Mar del Perú. 22 (1–2).

Hormazabal, S., Shaffer, G., Letelier, J., Ulloa, O., 2001. Local and remote forcing of sea surface temperature in the coastal upwelling system off Chile. Journal of Geophysical Research 106, 657–671.

Huettel, M., Forster, S., Klösser, S., Fossing, H., 1996. Vertical migration in sediment-dwelling sulfur bacteria *Thioploca* spp. in overcoming diffusion limitations. Applied and Environmental Microbiology 62, 1863–1872.

Jørgensen, B.B., Gallardo, V.A., 1999. *Thioploca* spp.: filamentous sulfur bacteria with nitrate vacuoles. FEMS Microbiology Ecology 128, 301–313.

Kessler, W.S., McPhaden, M.J., 1995a. Oceanic equatorial waves and the 1991–1993 El Niño. Journal of Climate 8, 1757–1774.

Kessler, W.S., McPhaden, M.J., 1995b. Forcing of intraseasonal Kelvin waves in the equatorial Pacific. Journal of Geophysical Research 100 (10), 613–631.

Kessler, W.S., Kleeman, R., 2000. Rectification of Madden–Julian oscillation into the ENSO cycle. Journal of Climate 13, 3560–3575.

Levin, L.A., Gutiérrez, D., Rathburn, A., Neira, C., Sellanes, J., Muñoz, P., Gallardo, V.A., Salamanca, M., 2002. Benthic processes on the Peru margin: a transect across the oxygen minimum zone during the 1997–98 El Niño. Progress in Oceanography 53, 1–27.

Levin, L.A., 2003. Oxygen minimum zone benthos: adaptation and community response to hypoxia. Oceanography and Marine Biology: An Annual Review 41, 1–45.

Neira, C., Gad, G., Arroyo, N.L., Decraemer, W., 2001a. Glochinema bathyperuviensis sp. n. (Nematoda, Epsilonematidae): a new species from Peruvian bathyal sediments, SE Pacific Ocean. Contributions to Zoology 70, 147–159.

Neira, C., Sellanes, J., Levin, L.A., Arntz, W.E., 2001b. Meiofaunal distributions on the Peru margin: relationship to oxygen and organic matter availability. Deep-Sea Research I 48, 2453–2472.

NOAA, 2003. NOAA gets US consensus for El Niño/La Niña index, definitions. NOAA magazine. september 30. WWW page, <http://www.magazine.noaa.gov/>.

Morales, C.E., Hormazabal, S.E., Blanco, J.L., 1999. Interannual variability in the mesoscale distribution of the depth of the upper boundary of the oxygen minimum layer off northern Chile (18–241S): implications for the pelagic system and biogeochemical cycling. Journal of Marine Research 57, 909–932.

Morón, O., 2006. Monthly sea surface salinity by marsden squares off the Peruvian coast (1960–2004). In: Extended abstracts book, International conference on the Humboldt Current system, 27 November–2 December, Lima, Peru. IMARPE, IRD and FAO, unpublished.

Mosquera, K., 2006. Numerical study of the response of the ocean to a northerly wind-jet in the equatorial eastern Pacific. In: Extended abstracts book, International Conference on the Humboldt Current System, 27 November–2 December, Lima, Peru. IMARPE, IRD and FAO, unpublished.

Otte, S., Kuenen, J.G., Nielsen, L.P., Paerl, H.W., Zopfi, J., Schulz, H.N., Teske, A., Strotmann, B., Gallardo, V.A., Jørgensen, B.B., 1999. Nitrogen, carbon and sulphur metabolism in natural *Thioploca* samples. Applied and Environmental Microbiology 65, 3148–3157.

Pennington, J.T., Mahoney, K.L., Kuwahara, V.S., Kolber, D., Calienes, R., Chavez, F.P., 2006. Primary production in the eastern tropical Pacific: a review. Progress in Oceanography 69, 285–317.

Pizarro, O., Clarke, A.J., Van Gorder, S., 2001. El Niño sea level and current along the South American coast: comparison of observations with theory. Journal of Physical Oceanography 31, 1891–1903.

Rowe, G.T., Howarth, R., 1985. Early diagenesis of organic matter in sediments off the coast of Peru. Deep-Sea Research 32, 43–55.

Salonen, K., Sarlava, J., Hakala, I., Viljanen, M.L., 1976. The relation of energy and organic carbon in aquatic invertebrates. Limnology and Oceanography 21, 724–730.

Salzwedel, H., Flores, L., De Flores, E., Zafra, A., Carbajal, G., 1988. Macrozoobentos del sublitoral peruano, antes, durante y después de El Niño 1982–1983. In: Salzwedel, H., Landa, A. (Eds.), Recursos y dinámica del ecosistema de afloramiento peruano, Vol. Extraordinario. Boletin Instituto del Mar del Perú (pp 77–98).

Sánchez, S., Delgado, E., 1996. Mareas rojas en el área de Callao (12°S), 1980–1995. Informe Progresivo Instituto del Mar del Perú (44), 19–37.

Sellanes, J., Neira, C., 2006. ENSO as a natural experiment to understand environmental control of meiofaunal community structure. Marine Ecology 27, 31–43.

Sellanes, J., Quiroga, E., Neira, C., Gutiérrez, D., 2007. Changes of macrobenthos composition under different ENSO cycle conditions on the continental shelf off central Chile. Continental Shelf Research. doi:10.1016/j/csr.2007.01.001.

Schulz, H., Jørgensen, B.B., Fossing, H., Ramsing, R., 1996. Community structure of filamentous, sheath–building sulfur bacteria, *Thioploca* spp., off the coast of Chile. Applied and Environmental Microbiology 62 (6), 1855–1862.

Schulz, H., Strotmann, B., Gallardo, V.A., Jørgensen, B.B., 2000. Population study of the filamentous sulfur bacteria *Thioploca* spp. off the Bay of Concepción, Chile. Marine Ecology Progress Series 200, 117–126.

Simpson, E.H., 1949. Measurement of diversity. Nature 163, 688.

Smayda, T.J., 2000. Ecological features of harmful algal blooms in coastal upwelling ecosystems. South African Journal of Marine Science 22, 219–253.

Strub, P.T., Mesías, J.M., Montecino, V., Rutllant, J., 1998. Coastal ocean circulation off western South America. In: Robinson, A.R., Brink, K.H. (Eds.), The Global Coastal Ocean: Regional Studies and Syntheses, The Sea, vol. 11. John Wiley & Sons, New York, pp. 237–313.

Tarazona, J., 1990. Disturbance and stress associated to El Niño and their significance for the macrobenthos of shallow areas of the Peruvian upwelling system. Ph.D. Thesis, Bremen Univ., Germany, 181 pp.

Tarazona, J., Arntz, W.E., 1986. Bacterias filamentosas gigantes en fondos someros de la Bahía de Ancón. Revista de Ciencias UNMSM 74, 178–180.

Tarazona, J., Salzwedel, H., Arntz, W.E., 1988a. Oscillations of macrobenthos in shallow waters of the Peruvian central coast induced by El Niño 1982–83. Journal of Marine Research 46, 593–611.

Tarazona, J., Salzwedel, H., Arntz, W.E., 1988b. Positive effects of "El Niño" on macrozoobenthos inhabiting hypoxic areas of the Peruvian upwelling system. Oecologia 76, 184–190.

Tarazona, J., Arntz, W., Valle, S., Peña, T., 2001. Los índices de El Niño y del impacto sobre las comunidades bentónicas. In: Tarazona, J., Arntz, W., Castillo, E. (Eds.), El Niño en América Latina. Impactos biológicos y sociales. Consejo Nacional de Ciencia y Tecnología, Lima , Perú, pp. 113–126.

Thamdrup, B., Canfield, E., 1996. Pathways of carbon oxidation in continental margin sediments off central Chile. Limnology and Oceanography 41 (8), 1629–1650.

Torrence, C., Compo, G.P., 1998. A practical guide to wavelet analysis. Bulletin of the American Meteorological Society 79, 61–78.

Tyson, R.V., Pearson, T.H., 1991. Modern and ancient continental shelf anoxia: an overview. In: Tyson, R.V., Pearson, T.H. (Eds.), Modern and Ancient Continental Shelf Anoxia. Geol. Soc. Spec. Publ. Geological Society of London (Vol. 58, pp. 1–24).

Ulloa, O., Escribano, R., Hormazabal, S., Quiñones, R., Gonzalez, R., Ramos, M., 2001. Evolution and biological effects of the 1997–98 El Niño in the upwelling ecosystem off northern Chile. Geophysical Research Letters 28 (8), 1591–1594.

Wieser, W., 1960. Benthic studies in Buzzards Bay. II. The meiofauna. Limnology and Oceanography 5, 121–137.

Wooster, W., Gilmartin, M., 1961. The Peru–Chile undercurrent. Journal of Marine Research 19, 97–122.

Zafra, A., Salzwedel, H., Flores, L.A., 1988. Distribución y biomasa de bacterias filamentosas (*Thioploca* spp.) en las costas norte del Perú durante 1976–1985. In: Salzweedel, H., Landa, A. (Eds.), Recursos y dinámica del ecosistema de afloramiento peruano, vol. Extraordinario. Boletin Instituto del Mar del Perú, Callao, pp. 99–105.

Zuta, S., Guillén, O., 1970. Oceanografía de las aguas costeras del Perú. Boletin Instituto del Mar del Perú 2, 157–324.

Progress in Oceanography 79 (2008) 190–197

Contents lists available at ScienceDirect

Progress in Oceanography

journal homepage: www.elsevier.com/locate/pocean

Laminated sediments from the central Peruvian continental slope: A 500 year record of upwelling system productivity, terrestrial runoff and redox conditions

A. Sifeddine[a,i,*], D. Gutiérrez[b], L. Ortlieb[a], H. Boucher[a], F. Velazco[b], D. Field[c], G. Vargas[d], M. Boussafir[e], R. Salvatteci[b], V. Ferreira[f], M. García[a], J. Valdés[g], S. Caquineau[a], M. Mandeng Yogo[a], F. Cetin[a], J. Solis[b], P. Soler[h], T. Baumgartner[f]

[a] *IRD, Paleotropique (UR 055), 32 Avenue Henri Varagnat, 93143 Bondy Cedex, France*
[b] *IMARPE, Esquina Gamarra y General Valle s/n, Callao 22000, Peru*
[c] *Monterey Bay Aquarium Research Institute, 7700 Sandholdt Road, Moss Landing, CA 95039, USA*
[d] *Departamento de Geología, Facultad de Ciencias Físicas y Matemáticas, Universidad de Chile, Plaza Ercilla, Santiago, Chile*
[e] *Institut des Sciences de la Terre (ISTO), Université d'Orléans, 45067 Orléans, France*
[f] *CICESE, Km. 107 Carretera Tijuana – Ensenada 22860, Mexico*
[g] *Facultad de Recursos del Mar, Universidad de Antofagasta, Casilla 170, Antofagasta, Chile*
[h] *UMR LOCEAN, 5 Place Jussieu, 75005 Paris, France*
[i] *Departamento de Geoquimica, Universidade Federale Fluminense, RJ-Brasil*

ARTICLE INFO

Article history:
Accepted 14 October 2008
Available online 21 October 2008

Keywords:
Humboldt current system
Laminated sediments
Centennial variability
Recent Holocene
Paleoceanography

ABSTRACT

Sedimentological studies including X-ray digital analyses, mineralogy, inorganic contents, and organic geochemistry on cores of laminated sediments accumulated in the oxygen minimum zone of the central Peruvian margin reveal variable oceanographic and climate conditions during the last 500 yr. Coherent upcore variations in sedimentological and geochemical markers in box cores taken off Pisco (B0405-6) and Callao (B0405-13) indicate that variability in the climate proxies examined has regional significance. Most noteworthy is a large shift in proxies at ~1820 AD, as determined by ^{210}Pb and ^{14}C radiometric dating. This shift is characterized by an increase in total organic carbon (TOC) in parallel with an abrupt increase in the enrichment factor for molybdenum Mo indicating a regional intensification of redox conditions, at least at the sediment water interface. In addition there was lower terrestrial input of quartz, feldspar and clays to the margin. Based on these results, we interpret that during several centuries prior to 1820, which corresponds to the little ice age (LIA), the northern Humboldt current region was less productive and experienced higher terrestrial input related to more humid conditions on the continent. These conditions were probably caused by a southward displacement of the inter-tropical convergence zone and the subtropical high pressure cell during the LIA. Since 1870, increases in TOC and terrigenous mineral fluxes suggest an increase of wind-driven upwelling and higher productivity. These conditions continued to intensify during the late 20th century, as shown by instrumental records of wind forcing.

1. Introduction

The nearshore 200 km of Humboldt current system is strongly influenced by coastal upwelling and is one of the most productive marine ecosystems in the world (Pennington et al., 2006; Zuta and Guillén, 1970). Due to its large latitudinal extension, the upwelling varies in intensity and persistency during the year (Thomas et al., 1994). Off the Peruvian coast, near-continuous upwelling supports high rates of primary production and one of the world's largest fisheries. On the interannual time scale, oceanic circulation and upwelling is modulated by the El Niño-Southern Oscillation (ENSO) cycle, manifested as changes in near surface biological production (Arntz and Fahrbach, 1996) subsurface oxygenation, and terrestrial runoff to the nearshore ocean. Variability on decadal time-scales is observed in instrumental records (Chavez et al., 2003), but understanding the nature of longer-term change is hindered by the absence of long high-resolution records.

Paleoceanographic and paleoclimatic changes can be reconstructed from sedimentological variables, depending on preservation conditions during sedimentation and afterwards. Such variables are used as paleoenvironmental 'proxies', or indicators of past climate and ocean conditions. Preservation of paleoceanographic records is enhanced along portions of the Peruvian margin by occurrence of a strong subsurface oxygen minimum zone (OMZ; Helly and Levin, 2004) which inhibits biological 'reworking' of sediments. This OMZ extends from the southeast to the equatorial Pacific, and its formation and maintenance is supported by basin-

---

[*] Corresponding author.
E-mail address: abdel.sifeddine@ird.fr (A. Sifeddine).

0079-6611/$ - see front matter © 2008 Elsevier Ltd. All rights reserved.
doi:10.1016/j.pocean.2008.10.024

Table 1
Geochemical and mineralogical measurements and their significance in paleoenvironmental reconstructions.

Proxies	Environmental significance
Mineral fraction (quartz, feldspar, clays)	Detrital input
Total organic carbon (TOC)	Productivity
Molybdenum (Mo)	Sediments redox conditions
Oxygen index (OI)	Degradation (aerobic oxidation)

scale circulation processes (Lukas, 1986) and high Humboldt current system (HCS) surface productivity and organic carbon fluxes from the surface into the OMZ, which amplify oxygen consumption in subsurface waters of the Peruvian coastal upwelling (PCU) system.

Paleoceanography of the continental shelves off South America has received little attention and climate over the last 1000 yr remains little studied (see McCaffrey et al., 1990; Rein et al., 2005; Gutiérrez et al., 2006). Changes in temperature, salinity, and paleoproductivity have been examined however at glacial and interglacial time-scales (Suess et al., 1990; Fink et al., 2006; Rein, 2007). Several sedimentary accumulation zones along the central Peruvian continental margin have favorable conditions to preserve past environmental events with high temporal resolution: bottom-water dysoxia, high sedimentation rates, and stable topographical settings (Suess et al., 1990; Reinhardt et al., 2002; Gutiérrez et al., 2006). Gutiérrez et al. (2006) constructed detailed paleoceanographic records of the past several centuries from laminated sediments from the central Peruvian margin. The combination of high productivity and near-anoxic conditions over the Peruvian margin results in the preservation of annual to decade-scale variations in climate and upwelling in organic and inorganic geochemical proxies (Krissek and Scheidegger, 1983; Suess et al., 1990; Böning et al., 2004; McManus et al., 2006).

Here we use mineral content and organic and inorganic markers in sediment cores to examine, at different time-scales, past changes in productivity, sediment redox conditions and terrigenous input (Table 1). We use total organic carbon (TOC) to infer productivity, and an oxygen index (OI) to infer degree of aerobic oxidation of TOC. Redox-sensitive metals (e.g. molybdenum) can be used to indicate redox conditions in the sedimentary environment at the time of deposition. This particular behavior has permitted reconstruction of past bottom-water oxygenation based on molybdenum (Mo) concentration profiles in sediment cores (McManus et al., 2006; Tribovillard et al., 2006, 2008). Finally, the mineralogical composition of sediment cores can provide information on past conditions by recording terrigenous input as related to erosion, aeolian transport, runoff, and deposition onto continental shelf (Vargas et al., 2004; Rein, 2007).

2. Oceanographic setting

Coastal upwelling occurs along the eastern margins of major oceanic basins when predominantly along-shore winds and Coriolis force drive surface waters offshore and these are replaced by deeper, cooler and nutrient-rich waters. The enhanced biological productivity supported by upwelling increases the flux of organic material to the coastal ocean floor. This flux intensifies the OMZ and results a high rate of TOC deposition on the continental shelves, both of which limit organic matter degradation and favor preservation. As a consequence the organic carbon content of sediments beneath upwelling systems may reach 10% (Libes, 1992; Hedges and Keil, 1995), whereas organic carbon in sediments beneath oligotrophic oceans typically varies from 0.2% to 0.4% (Muller and Suess, 1979; Duan, 2000).

Upwelling-favorable along-shore winds are present along the Peruvian coast all year long and maximal between 14°S and 16°S, weakening in the north, near Punta Falsa (6°S; Echevin et al., 2004). Wind strength however varies and 'upwelling events' last from a few days to a week and are stronger and more frequent in winter due to offshore winds associated with a strengthened subtropical high pressure cell. The wind-driven surface circulation consists in a shallow, equatorward, coastal jet (Strub et al., 1998), with maximum intensity in winter, known as the Peruvian coastal current. This current can be identified by the shoaling of isopycnals in the nearshore surface layers. Offshore, the circulation is dominated by poleward flows, identified as the Peru–Chile counter current which advects warm and saline waters from tropical origin (Lukas, 1986). Below the surface coastal current, the subsurface, coastally trapped, Peru–Chile undercurrent advects saline (35.0–35.1 PSU) tropical waters poleward. Its signature is characterized by the deepening of isopycnals towards the coast at 50–200 m depth (Echevin et al., 2004).

Off the central Peruvian coast (9–15°S), the upper margin sediments are organic-rich. Excess ^{210}Pb-derived sedimentation rates vary from 0.04 to 0.15 cm yr^{-1} (Reimers and Suess, 1983; Levin et al., 2003). Based on exploratory surveys and literature, the Callao (~12°S) and Pisco (~14°S) areas were selected as sample sites. Two Soutar-box cores were collected in May 2004 by the R/V Olaya (Instituto del Mar del Peru, IMARPE): The first one from the continental shelf off Callao (B0405-13, 12°00′S, 72°42′S, 184 m water-depth); and the second one from the upper continental slope off Pisco (B0405-06, 14°07′S, 76°30′S, 299 m water-depth; Gutiérrez et al., 2006; Fig. 1).

3. Analytical procedures

Sedimentary structures were documented by X-radiography (SCOPIX, Migeon et al., 1999). Chronological models for the last 130 yr were developed by using the downcore distributions of natural excess ^{210}Pb and ^{230}Th and of the bomb-derived ^{241}Am. The chronology beyond the last 130 yr was inferred from radiocarbon ages, calibrated with local reservoir effects by Gutiérrez et al. (2008).

Mineralogical composition was obtained by X-ray diffraction (XRD) and by Fourier transformed infrared spectrometry (FTIR) respectively. For FTIR analyses, samples were placed in a KBr disc, which ensures that Lambert–Beer's law is valid. A quantitative determination of the mineral content from various blends was performed by making a multi-component analysis of the experimental spectrum using the spectra of each component in the mixture (Bertaux et al., 1998). Mean relative standard deviation was 0.8% for the mineral quantification.

Organic matter characterization and quantification were done using Rock-Eval 6 programmed pyrolysis (Lafargue et al., 1998). Total organic carbon (TOC %) reflects the quantity of organic matter (OM) present in the sediment. Normalized to TOC the hydrogen index is the amount of hydrocarbon (HC) released during pyrolysis (HI, mg HC/g TOC), and the oxygen index similarly gives the oxygen content calculated from the amounts of CO and CO_2 released during pyrolysis (OI, OIRe6, mg O_2/g TOC).

Molybdenum (Mo) and Aluminium (Al) concentrations were analysed by ICP-MS (Ultramass Varian) and ICP-AES, respectively, after hot-plate acid digestion (combination of acids: HF, $HN0_3$, $HClO_4$) which eliminated organic matter and removed silicates (Zwolsman and Van Eck, 1999; Cho et al., 1999). Measurement precision for Al and Mo was determined by comparing duplicate analyses (usually ±0.04% and ±0.03% respectively).

Mo is a trace metal used to asses past redox conditions (Tribovillard et al., 2006, 2008; McManus et al., 2006). As a redox-sensi-

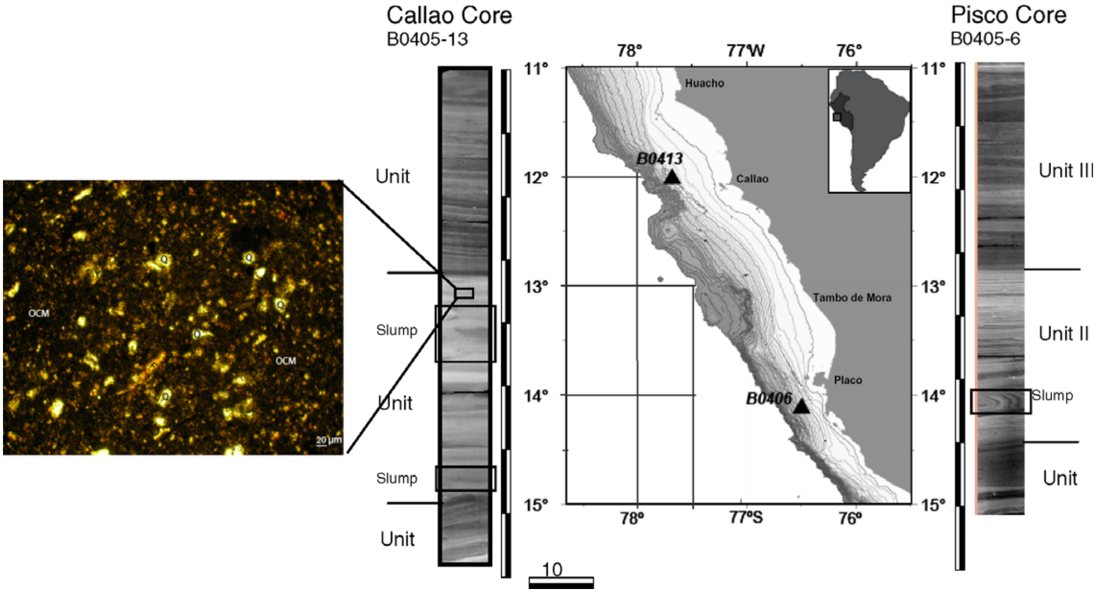

Fig. 1. Location and X-ray images of Pisco core (B0405-06, 14°07.90 S, 76°30.10W, 299 m depth) and Callao Core (B0405-13, 12°00′S, 72°42′S, 184 m depth) off the central-south Peruvian coast. Slumps are considered as instantaneous deposits, and are not considered in chronological development of downcore analyses. Light laminae are "dense", dark laminae are "less dense". The photograph shows the thin section of Callao core observed in polarized light. Q: quartz. F: feldspar, OCM: organic clay matrix.

tive metal, Mo is commonly removed from the ocean and transferred to the sediments via different pathways (McManus et al., 2006; Poulson et al., 2006; Tribovillard et al., 2006, 2008). In oxic sediments, where aerobic respiration decomposes organics, Mo is scavenged from the water column with an association of metal oxides. Under reducing conditions however, where anaerobic processes dominate, Mo is removed from the water column with sulfidized organic material or via sequestration by Fe–S phases. Sediments contain variable amounts of biogenic materials that dilute the trace-elements, most commonly calcium carbonate and opal. Thus, to compare trace-element proportions in samples that contain varying carbonate and opal contents, it is customary to normalize trace-element (here Mo) concentrations to Al content (Tribovillard et al., 2006). Al is a constituent of the aluminosilicate fraction of the sediments and is essentially inert during diagenesis. Moreover, according to Valdés et al. (2005), Al normalization enables regional comparison and the evaluation of terrestrial input of trace metals. The method is also applied to determine Enrichment Factors (EFs) according the equation described by Tribovillard et al. (2006): $EF = (Mo/Al)_{sample}/(Mo/Al)_{average\ shale}$). We used values for average shales from different sources (Turekian and Wedepohl, 1961; McManus et al., 2006). If Mo EF is greater than 1, then Mo is enriched relative to average shales and, if Mo EF is less than 1, it is depleted.

The particulate fluxes for each sediment constituent (TOC, quartz, feldspar and clays) are calculated by multiplying the concentration of each constituent by the overall sediment accumulation rate. In general terms, this relation can be expressed as: sediment flux ($mg\ cm^{-2}\ yr^{-1}$) = element concentration ($mg\ g^{-1}$) × sediment accumulation rate ($g\ cm^{-2}\ yr^{-1}$). The flux estimation for each element has the advantage of providing information on the inputs of the different constituents independently of their relative dilution in the matrix.

Thin sections were constructed from resin-impregnated 10 cm longitudinal segments of the Callao core (B0405-13). Water was replaced by acetone prior to impregnation with resin following Bénard (1996) and Zaragosi et al. (2006). After impregnation with resin, the bonded blocks were cut to approximately 100 µm using a precision saw (ESCIL LT-260) and thereafter hand polished to a thickness of 30 µm using the rotating lapidary unit. Finally, cover slips were fixed on the thin sections using the collage resin mixture. The structure of the laminations was analysed using a polarised light microscope, with a magnification of 20.

In order to estimate the shared variability of the environmental proxies and their relationships with one another, we applied a principal component analysis (PCA).

4. Results

4.1. Lithology and chronology

The observation of the core X-ray images reveals the existence of bands and laminations (<5 mm thickness), formed by the succession of light (dense) and dark (less dense) layers, which appear to have been deposited with negligible bioturbation under nearly anoxic conditions (Fig. 1). Three stratigraphic units are observed in the Pisco Core. The basal unit (unit I) (74–62 cm) is formed by the succession of several primarily banded sediments. The unit II, which starts at 62 cm and extends to 34 cm, presents a slump at the base (55–52 cm). This unit, which is characterized by an overall greater density (lightly colored in the X-radiograph; Fig. 1), contains pairs or 'couplets' of dark and light laminae that range from 2 to 5 mm in thickness. The upper unit (unit III) (34–0 cm), with average lower density (darker in Fig. 1), is marked by a series of thick light and dark band (ca. 1 cm). In the Callao core, the X-ray image also reveals three units that are similar to those of the Pisco core in density and depth. Unit I (84–66 cm) also contains band structures. Unit II (66–34 cm) is denser (lighter color), as in the Pisco core, but is formed by thick bands (~1 cm) rather than fine laminations as observed in the Pisco core and is interrupted by several slumps in the middle part of the unit. Unit III (34–0 cm) is marked by a low density and is formed by the succession of both millimeter-thick laminae and broader bands.

Average sedimentation rates are ~2.2 $mm\ yr^{-1}$ for the Pisco core and ~2.1 $mm\ yr^{-1}$ for the Callao core for the lapse 1870 AD to present. The centuries prior to the late 19th century have average sedimentation rates of 1 and 0.6 $mm\ yr^{-1}$, respectively (Gutiérrez et al., 2008). At these rates the banding patterns in

Fig. 1 do not resolve interannual or even decadal-scale variability (and can be affected by water content and compaction from burial; Gutiérrez et al., 2008). The results are presented as concentrations (%) and fluxes of sediment constituents.

4.2. Mineral fraction

X-ray diffraction (XRD) shows that the terrigenous mineral fraction of both cores is quartz, feldspar, kaolinite, illite and vermiculite. The upcore variations in these fractions are similar in both cores (Fig. 2) and identify three sections which correspond to the units identified through the XRD lithological description of Fig. 1.

Unit I (prior to 1400 AD) is characterized by low quartz, feldspar and clays content (respective mean abundances of 6%, 10% and 10%). Unit II (~1400–1820 AD) begins with an increase of quartz (5–15%), feldspar (10–20%) and clays (10–28%). Concentrations remain relatively stable until the top of the unit. Unit III (1820–2004 AD) starts with a decrease in concentrations of quartz, feldspar and clays that reach minimum values and then increase to the top of this unit reaching values around 10%, 15% and 20%, respectively.

In both cores the variations in upcore fluxes (Fig. 3) are similar to the variations in percent composition (Fig. 2), and again correspond to the three different stratigraphic units. Before 1400 AD fluxes of quartz, feldspar and clays were low around 2, 2 and

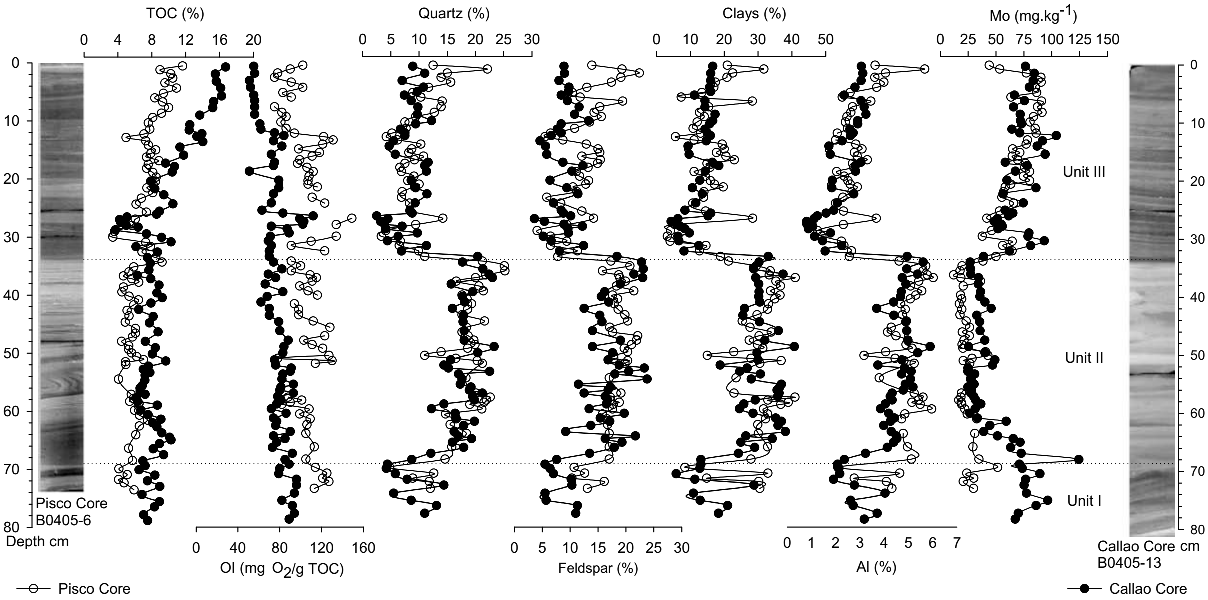

Fig. 2. Upcore variations of TOC content (%), IO (mg O_2/g TOC), mineral (quartz, feldspar) content, clays content, aluminium (%) and molybdenum content of Callao (black dots) and Pisco (open circles).

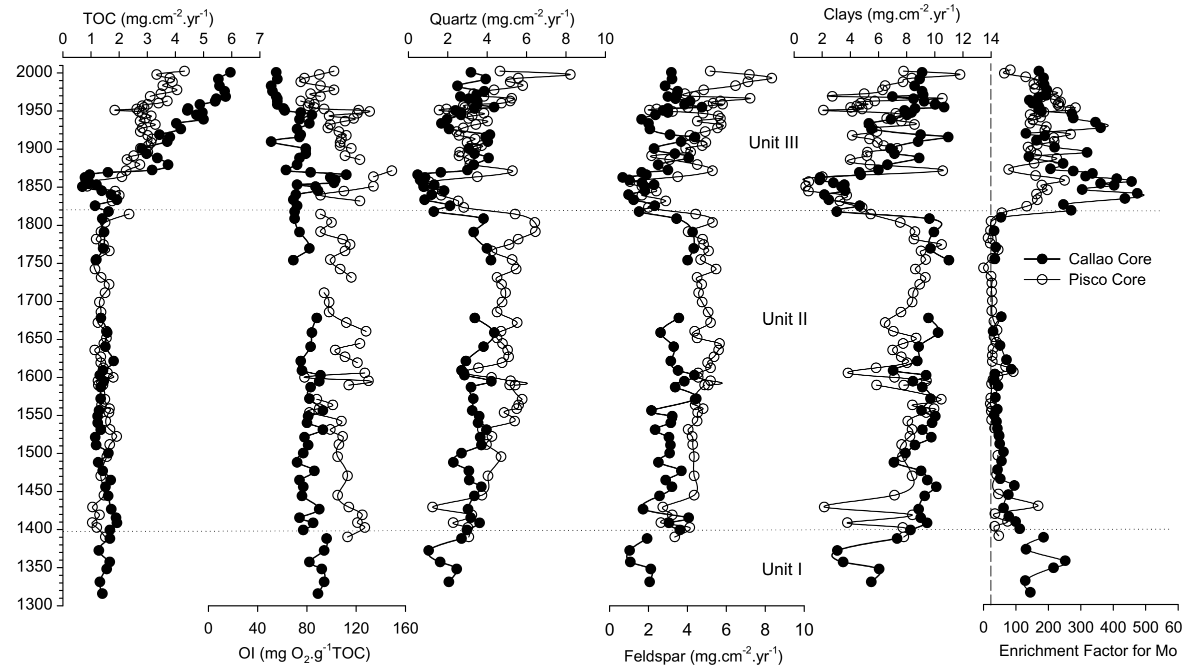

Fig. 3. Upcore variations of TOC fluxes, OI, mineral (quartz, feldspar, clays) fluxes, and EF for Mo of Callao (black dots) and Pisco (open circles).

4 mg cm^{-2} yr^{-1}, respectively. Between 1400 and 1820 AD fluxes of quartz, feldspar and clays were high around 4, 3 and 6 mg cm^{-2} yr^{-1}, respectively. Over 1820–1870, fluxes of quartz (4–0.5 mg cm^{-2} yr^{-1}), feldspar (3–1 mg cm^{-2} yr^{-1}) and clays (6–1 mg cm^{-2} yr^{-1}) decreased abruptly. Finally over 1870–2004 AD, fluxes of quartz, feldspar and clays steadily increased, beginning around 1870 AD and intensifying around 1950 AD with values around 6, 7 and 8 mg cm^{-2} yr^{-1}, respectively, in the superficial sediments.

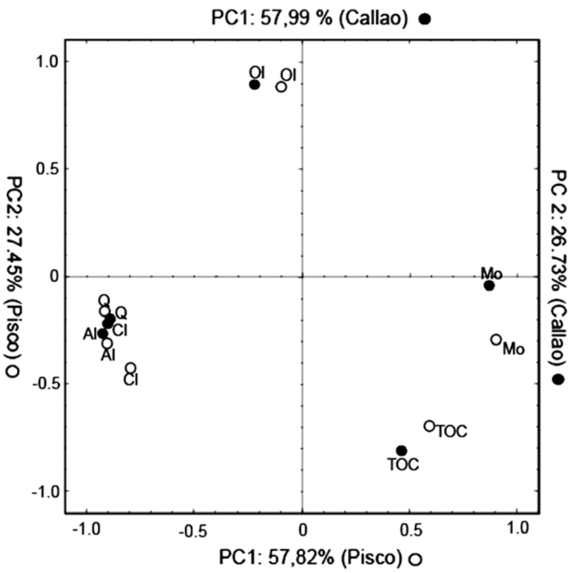

Fig. 4. Projection of the proxy variables on the factor-plane PC1 (quartz, feldspar and clays vs. TOC and Mo) in Callao (black dots) and Pisco (open circles) cores.

4.3. Inorganic fraction

Upcore variations in Al are similar to the variability in clays described above (Fig. 2). Al values are somewhat low (3%) during the first unit and then increase, reaching 5% in unit II. In unit III, Al initially decreases to ~1% around 1870 (1%), and then steadily increases to 6% towards the top of unit III.

Variations in Mo (mg kg^{-1}) are similar to the minerals above only into unit III (Fig. 2). Mo fluctuates around 75 (mg kg^{-1}) before 1400 AD (Unit I) and later decreases and stabilizes around 25 mg kg^{-1} through unit II. In the unit III (1820–2004 AD), Mo increases steadily to 75 mg kg^{-1}.

The Mo enrichment factor in both cores is >1 suggesting a non-terrigenous origin for this metal. The upcore variation in EF for Mo is similar to the variability in mineral fractions only for unit III (Fig. 3). In unit I Mo EF is around 120; and in unit II, it decreases to ~50. Mo EF increases in both cores in unit III, although Callao has a much higher maximum EF than the Pisco core (500 vs. 300). In general, Mo EF values are moderate in the Callao core from 1870 to 2004 AD and in the Pisco core from 1820 to 2004 AD.

4.4. Organic fraction

Upcore variations in TOC correspond to the sedimentological and mineralogical records into Unit III of both cores (Fig. 2). TOCs are near 5% in units I and II of both cores and the OI varies between 120 and 80 for the Pisco and Callao cores, respectively. There is a large increase in TOC within unit III, with higher values in the Callao core (16%) than in the Pisco core (12%). This trend in TOC is accompanied by a progressive decrease in OI towards the core tops, reaching values around 80 in the Pisco core and 70 in the Callao core. TOC fluxes exhibit low values in unit I in both cores (~1.2 mg cm^{-2} yr^{-1}). A transient increase in TOC flux occurs

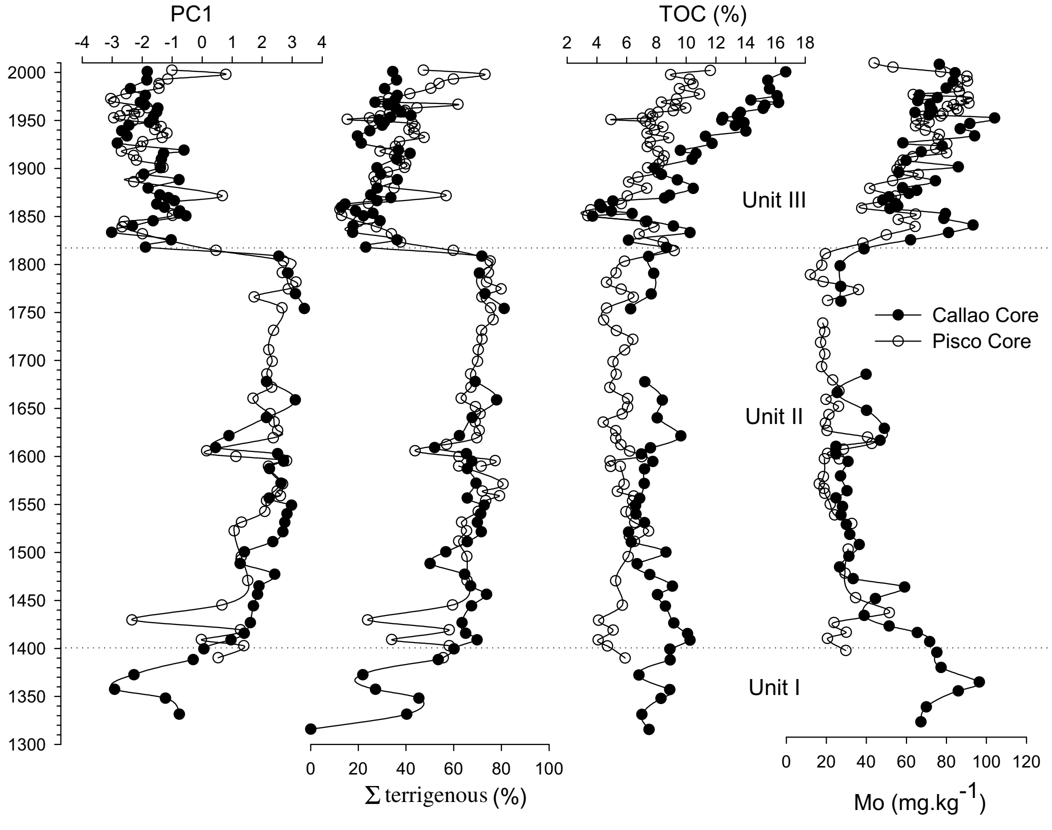

Fig. 5. Upcore variations of PC1, sum of the different terrigenous fractions, TOC and Mo content.

around 1820 AD, associated with decreases in quartz and other minerals fluxes. A positive trend in TOC flux starts at ~1870 AD, reaching ~4 and ~6 mg cm^{-2} yr^{-1}, at Pisco and Callao, respectively, in the 2000s.

4.5. Principal component analysis

A principal component analysis was run on the upcore constituents from each core. Concentrations were used rather than fluxes since uncertainties in chronology can affect estimated flux rates. In particular, if the change in sedimentation rates reported at 1870 is associated with changes in TOC, then the period 1820–1850 AD may have much higher sedimentation rates and consequently, higher fluxes of TOC and other constituents than calculated. At each site, more that 85% of variance is explained by two principal components (Fig. 4). Here, we present only the first component (PC1), which is a negative correlation between the terrigenous fraction (quartz, feldspar, clays and aluminum) and TOC and Molybdenum (Fig. 4).

5. Discussion

The parallel upcore variations of PC1 (Fig. 5) in the Pisco and Callao sites indicate that the environmental proxies exhibit the same pattern in both cores and thus have at least regional significance. The shift at ~1820 AD in both the stratigraphic observations and sedimentological constituents is much stronger than the change at the base of the cores (division between units I and II), which is not apparent in all proxies. A large climatic change apparently occurred at ~1820 AD, which was of greater magnitude than other climate fluctuations throughout the last several centuries. Nevertheless, noteworthy sedimentological fluctuations occur within unit III.

5.1. Little ice age period

High mineral fluxes characterize the 1400–1820 AD period which corresponds to the little ice age (LIA), or rather its South-American counterpart. Examination of thin sections from the Callao core prior to 1820 AD shows that most terrigenous particles (quartz and feldspar; 50–80 μm) present angular to sub-angular aspects, suggesting a fluvial source (Fig. 1) rather than aeolian transport. Similarly, Pisco core particle morphology prior to 1820 suggests river discharge. The similar patterns of flux at both sites are interpreted as resulting from substantial terrestrial input followed by dispersion and transport by the coastal circulation in unit II.

The negative values of PC1 (Fig. 5) during the little ice age (Unit II) reflect both the high mineral content and low Mo content (Fig. 3). Sediments rich in Mo characterize the upper Peruvian margin (<300 m) with high sulphate reduction rates (Böning et al., 2004) under anoxic conditions (see Valdés et al., 2005; McManus et al., 2006; Tribovillard et al., 2006, 2008). Low Mo content during the LIA is probably due to reduced organic loading and suboxic conditions in the surficial sediments.

The LIA period thus appears marked by a low productivity, suboxic sediments and higher terrestrial input of minerals related to rainfall and runoff from the continent. In the Cariaco basin (Venezuela) (Haug et al., 2001; Peterson and Haug, 2006), drier conditions are suggested for the LIA by decreased Ti content in cores linked to decreased detritus from local rivers. Hence, our results are consistent with a global southward migration of the inter-tropical convergence zone (ITCZ), as postulated also by Graham et al. (2007) and Newton et al. (2006).

At seasonal and interannual time-scales, an ITCZ southward shift is associated with the southward projection of surface nutrient poor Equatorial and Tropical water masses. An additional consequence of a southward shift in the ITCZ would be a reduced strength of the subtropical high pressure system that produces upwelling favorable winds. In turn these modifications may cause reductions in coastal upwelling, primary production, and flux of organic material to the continental slope, as observed in the Callao and Pisco cores (Gutiérrez et al., 2008). Note that the variability of efficiency factor (EF) for Mo is inversely related with terrestrial fluxes, suggesting sediment redox conditions changes, which are associated to the organic matter flux changes. This regional response is likely a result of the establishment of new ocean–atmosphere connections that control the position of the ITCZ.

5.2. The modern period

The simultaneous decrease of terrigenous fluxes after 1820 in both cores probably marks a change from rainy to drier conditions. The increase of Mo enrichment factor, in the same period, suggests an enhancement of sediment redox conditions linked to the establishment of a new ocean–atmosphere connection pattern. A transient decrease of TOC flux and an increase of OI are recorded during the lapse 1845–1865 AD. After these two decades, carbon flux exhibits a positive trend while OI decreases, thus suggesting less oxidation of the settling organic matter. This trend coincides with an increase of the dominance of anoxia-tolerant taxa in the benthic foraminiferal assemblage at Pisco, as reported by Morales et al. (2006). Increases in TOC flux are also recorded during the same period in sediments from the continental slope 15°S (McCaffrey et al., 1990) and from Mejillones Bay at 23°S (Valdés et al.,

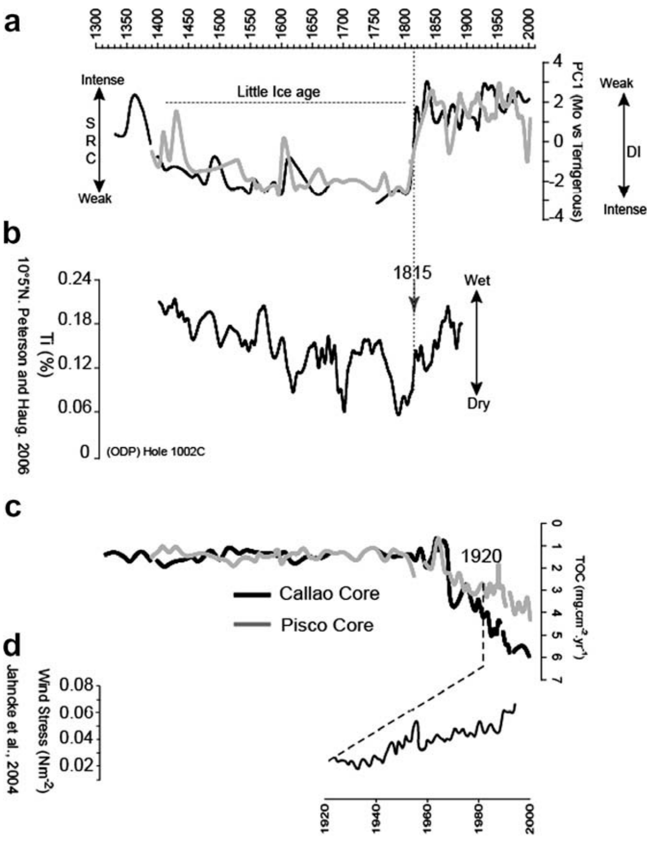

Fig. 6. Comparison between (a) PC1 upcore variation of Callao (black line) and Pisco (grey line), (SRC: sediment redox conditions; DI: detrital input. (b) Ti content of sediments from ODP Hole 1002C (record from Peterson and Haug, 2006), (c) TOC upcore variation of Callao (black line) and Pisco (grey line), (d) instrumental wind stress data from 1925 to 1995 (Jahncke et al., 2004).

2004; Vargas et al., 2004, 2007). These results indicate a regional centennial enhancement of productivity and organic particles export to the sediment. An intensification of this trend is observed since mid-twentieth century, which is likely caused by enhanced upwelling, as recorded instrumentally during the same period (Jahncke et al., 2004; Fig. 6).

6. Conclusion

Laminated sediments from the central Peru continental slope, accumulated under intense upwelling, dysoxia and high sedimentation rates, preserve and record different oceanographic and climatic changes during the last 500 yr. The measurement of different organic, mineral and inorganic variables in cores provides environmental proxies linked to (1) upwelling and productivity, (2) strength of the sediment redox conditions, and (3) terrigenous input to sediments. Changes in the terrigenous input likely correspond to changes in continental rainfall, which affects mineral-laden runoff that is subsequently deposited offshore. A comparison with Cariaco Basin core records of regional precipitation and runoff supports our interpretation that during the little ice age before 1820, the inter-tropical convergence zone (ITCZ) likely occupied a more southerly position and that more humid conditions prevailed in Peru. A more southerly ITCZ would also correspond to a reduced subtropical high pressure system with weaker alongshore winds, and lower primary productivity. Conversely, since the late nineteenth century, increasing TOC fluxes and sediment anoxia are interpreted as caused by the intensification of coastal upwelling, productivity and organic particles delivery to the bottom.

Acknowledgements

This study was supported by the IRD PALEOTROPIQUE research unit (UR 055) and the IMARPE PALEOMAP research program, as well as by the PALEOPECES project (IMARPE-IRD), the IAI small grant project SGP 211-222 (PI: D. Gutiérrez), the Humboldt current system program (ATI-IRD) and finally the PCCC project (French national research agency ANR, P.I. B. Dewitte). We thank the Instituto del Mar del Peru (IMARPE) for full support of this research and acknowledge the crew of the RV José Olaya Balandra and other scientific participants in the box-coring survey.

The authors thank anonymous reviewers and the editors of the special issue for their help in the improvement of the manuscript.

References

Arntz, W., Fahrbach, E., 1996. El Niño: experimento climático de la naturaleza. Causas físicas y efectos biológicos. Fondo de Cultura Económica, México, D.F. 309 p.

Bénard, Y., 1996. Les techniques de fabrication des lames minces de sol. Cahiers Techniques Institut Nationale de Recherche Agronomique 37, 29–42.

Bertaux, J., Frohlich, F., Ildefonse, Ph., 1998. Multicomponent analysis of FTIR spectra: quantification of amorphous silica and crystallized mineral phases in synthetic and natural sediments. Journal of Sedimentary Research 68 (3), 440–447.

Böning, Ph., Brumsack, H.J., Böttcher, M.E., Schnetger, B., Kriete, C., Kallmeyer, J., Borcher, S.L., 2004. Geochemistry of Peruvian near-surface sediments. Geochimica et Cosmochimica Acta 68, 4429–4451.

Chavez, F.P., Ryan, J., Lluch-Cota, S.E., Ñiquen, M.C., 2003. From anchovies to sardines and back-multidecadal change in the Pacific Ocean. Science 299, 217–221.

Cho, Y., Lee, C., Choi, M., 1999. Geochemistry of surface sediments off the southern and western coast of Korea. Marine Geology 159, 111–129.

Duan, Y., 2000. Organic geochemistry of recent marine sediments from the Nansha Sea China. Organic Geochemistry 31, 159–167.

Echevin, V., Puillat, I., Grados, C., Dewitte, B., 2004. Seasonal and mesoscale variability in the Peru upwelling system from in situ data during the years 2000 to 2004. Gayana Concepcion 68, 167–173. ISSN 0717-6538.

Fink, D., Skilbeck, G., Gagan, M., 2006. A 25,000 year inter-annual record of the Peru–Chile current and implications for ENSO variation during deglaciation. In: Nineteenth International Radiocarbon Conference, Oxford April 3–7, 2006, p.174.

Graham, N.E., Hugues, M.K., Ammann, C.M., Cobb, K.M., Hoerling, M.P., Kennett, D.J., Kennett, J.P., Rein, B., Stott, L., Wigand, P.E., Xu, T., 2007. Tropical Pacific – mid-latitude teleconnections in the medieval times. Climatic Change 83, 241–285. doi 10.1007/s10584-007-9239-2.

Gutiérrez, D., Sifeddine, A., Reyss, J.L., Vargas, G., Salvatteci, R., Ferreira, V., Ortlieb, L., Field, D., Baumgartner, T., Boussafir, M., Boucher, H., Valdes, J., Marinovic, L., Soler, P., Tapia, P., 2006. Anoxic sediments off central Peru record interannual to multidecadal changes of climate and upwelling ecosystem during the last two centuries. Advances in Geosciences 6, 119–125.

Gutiérrez, D., Sifeddine, A., Field, D.B., Ortlieb, L., Vargas, G., Chávez, F., Velazco, F., Ferreira, V., Tapia, P., Salvatteci, R., Boucher, H., Morales, M.C., Valdés, J., Reyss, J.L., Campusano, A., Boussafir, M., Mandeng-Yogo, M., García, M., Baumgartner, T., 2008. Rapid reorganization in ocean biogeochemistry off Peru towards the end of the little ice age. Biogeosciences Discuss 5, 3919–3943.

Haug, G.H., Hughen, K.A., Sigman, D.M., Peterson, L.C., Röhl, U., 2001. Southward migration of the intertropical convergence zone through the Holocene. Science 293, 1304–1308.

Hedges, J., Keil, R., 1995. Sedimentary organic matter preservation, an assessment and speculative synthesis. Marine Chemistry 49, 81–115.

Helly, J., Levin, L., 2004. Global distribution of naturally occurring marine hypoxia on continental margins. Deep-Sea Research I 51, 1159–1168.

Jahncke, J., Checkley, D., Hunt, G.L., 2004. Trends in carbon flux to seabirds in the Peruvian upwelling system: effects of wind and fisheries on population regulation. Fisheries Oceanography 13, 208–223.

Krissek, L.A., Scheidegger, K.F., 1983. Environmental controls on sediment texture and composition in low oxygen zones off Peru and Oregon. In: Suess, E., Thiede, J. (Eds.), Coastal Upwelling; Its Sediment Record. Part B: Sedimentary Records of Ancient Coastal Upwelling. Plenum Press, New York, pp. 63–180.

Lafargue, E., Marquis, F., Pillot, D., 1998. Rock-Eval 6 applications in hydrocarbon exploration, production, and soil contamination studies. Revue de l'Institut Français du Pétrole 53 (4), 421–437.

Levin, L.A., Rathburn, A.E.R., Gutiérrez, D., Muñoz, P., Shankle, A., 2003. Bioturbation by symbiont-bearing annelids in near-anoxic sediments: implications for biofacies models and paleo-oxygen assessments. Palaeogeography, Palaeoclimatology, Palaeoecology 199, 120–140.

Libes, S., 1992. An Introduction to Marine Biogeochemistry. John Wiley & Sons, Inc., New York. 289 p.

Lukas, R., 1986. The termination of the equatorial undercurrent in the eastern Pacific. Progress in Oceanography 16, 63–90.

McCaffrey, M.A., Farrington, J.W., Repeta, D.J., 1990. The organic geochemistry of Peru margin surface sediments: I. A comparison of the C3, alkenone and historical El Niño records. Geochimica et Cosmochimica Acta 54, 1671–1682.

McManus, J., Berelson, W.M., Severmann, S., Poulson, R.L., Hammond, D.E., Klinkhammer, G.P., Holm, Ch., 2006. Molybdenum and uranium geochemistry in continental margin sediments: paleoproxy potential. Geochimica et Cosmochimica Acta 70, 4643–4662.

Migeon, S., Weber, O., Faugères, J.-C., Saint-Paul, J., 1999. SCOPIX: a new X-ray imaging system for core analysis. Geo-Marine Letters 18, 225–251.

Morales, M.C., Field, D., Pastor, S.M., Gutiérrez, D., Sifeddine, A., Ortlieb, L., Ferreira, V., Salvatteci, R., Velazco, F., 2006. Variations in foraminifera over the last 460 years from laminated sediments off the coast of Peru. Boletin de la Sociedad Geológica del Perú 101, 5–18.

Muller, P., Suess, E., 1979. Productivity, sedimentation rate, and sedimentary organic matter in the ocean – I. Organic carbon preservation. Deep-Sea Research 26A, 1347–1362.

Newton, A., Thunell, R., Stott, L., 2006. Climate and hydrographic variability in the Indo-Pacific Warm Pool during the last millennium. Geophysical Research Letters 33, L19710. doi:10.1029/2006GL027234.

Pennington, J.T., Mahoney, K.L., Kuwahara, V.S., Kolber, D.D., Calienes, R., Chavez, F.P., 2006. Primary production in the eastern tropical Pacific: a review. Progress in Oceanography 69, 285–317.

Peterson, L.C., Haug, G.H., 2006. Variability in the mean latitude of the Atlantic intertropical convergence zone as recorded by riverine input of sediments to the Cariaco Basin (Venezuela). Palaeogeography, Paeoclimatology, Palaeocology 243, 97–113.

Poulson, R.L., Siebert, Ch., McManus, J., William, M., Berelson, W.M., 2006. Authigenic molybdenum isotope signatures in marine sediments. Geology 34, 617–620.

Reimers, C.E., Suess, E., 1983. Spatial and temporal patterns of organic matter accumulation on the Peru continental margin. In: Thiede, J., Suess, E. (Eds.), Coastal Upwelling: Its Sediment Record. Part B: Sedimentary Records of Ancient Coastal Upwelling. Plenum, New York, pp. 311–346.

Rein, B., 2007. How do the 1982/83 and 1997/98 El Niños rank in a geological record from Peru. Quaternary International 161, 56–66.

Rein, B., Lückge, A., Reinhardt, L., Sirocko, F., Wolf, A., Dullo, W.C., 2005. El Niño variability off Peru during the last 20,000 years. Paleoceanography 20. doi:10.1029/2004PA001099. PA4003.

Reinhardt, L., Kudrass, H.-R., Lückge, A., Wiedicke, M., Wunderlich, J., Wendt, G., 2002. High-resolution sediment echo-sounding off Peru: Late Quaternary depositional sequences and sedimentary structures of a current-dominated shelf. Marine Geophysical Research 23, 335–351.

Strub, P.T., Mesías, J.M., Montecino, V., Rutllant, J., 1998. Coastal ocean circulation off western South America. In: Robinson, A.R., Brink, K.H. (Eds.), The Sea 11, The Global Coastal Ocean. Interscience, New York, pp. 273–313.

Suess, E., Von Huene, R., et al., 1990. Proceedings of the ocean drilling program. Scientific Results 112, 738.

Thomas, A.C., Huang, F., Strub, P.T., James, C., 1994. Comparison of the seasonal and interannual variability of phytoplankton pigment concentrations in the Peru and California Current systems. Journal of Geophysical Research 99, 7355–7370.

Tribovillard, N., Algeo, Th., Lyons, T., Riboulleau, A., 2006. Trace metals as paleoredox and paleoproductivity proxies: an update. Chemical Geology 232, 12–32.

Tribovillard, N., Lyons, T.W., Riboulleau, A., Bout-Roumazeilles, V., 2008. A possible capture of molybdenum during early diagenesis of dysoxic sediments. Bulletin de la Societé Géologique de France 179, 3–12.

Turekian, K., Wedepohl, K., 1961. Distribution of the elements in some major units of the earth's crust. Geological Society of America Bulletin 72, 175–192.

Valdés, J., Sifeddine, A., Lallier-Verges, E., Ortlieb, L., 2004. Petrographic and geochemical study of organic matter in surficial laminated sediments from an upwelling system (Mejillones del Sur Bay, northern Chile). Organic Geochemistry 35, 881–894.

Valdés, J., Vargas, G., Sifeddine, A., Ortlieb, L., Guiñez, M., 2005. Distribution and enrichment evaluation of heavy metals in Mejillones Bay (23 S), Northern Chile: geochemical and statistical approach. Marine Pollution Bulletin 50, 1558–1568.

Vargas, G., Ortlieb, L., Pichon, J.J., Bertaux, J., Pujos, M., 2004. Sedimentary facies and high resolution primary production inferences from laminated diatomaceous sediments off northern Chile (23 S). Marine Geology 211, 79–99.

Vargas, G., Pantoja, S., Rutllant, J.A., Lange, C.B., Ortlieb, L., 2007. Enhancement of coastal upwelling and interdecadal ENSO-like variability in the Peru–Chile current since late 19th century. Geophysical Research Letters 34, L13607. doi:10.1029/2006GL028812.

Zaragosi, S., Bourillet, J.F., Eynaud, F., Toucanne, S., Denhard, B., Van Toer, A., Lanfumey, V., 2006. The impact of the last European deglaciation on the deep-sea turbidite systems of the Celtic-Armorican margin (Bay of Biscay). Geo-Marine Letters 26, 317–329.

Zuta, S., Guillén, O., 1970. Oceanografía de las aguas costeras del Perú, Departamento de Oceanografía. Boletín del Instituto del Mar del Perú 2, 193–196.

Zwolsman, J.J.G., Van Eck, G.T.M., 1999. Geochemistry of major elements and trace metals in suspended matter of the Scheldt estuary, southwest Netherlands. Marine Chemistry 66, 91–111.

Progress in Oceanography 79 (2008) 198–207

Contents lists available at ScienceDirect

Progress in Oceanography

journal homepage: www.elsevier.com/locate/pocean

250 years of sardine and anchovy scale deposition record in Mejillones Bay, northern Chile

Jorge Valdés [a,*], Luc Ortlieb [b], Dimitri Gutierrez [c], Luis Marinovic [d], Gabriel Vargas [e], Abdel Sifeddine [b,f]

[a] *Laboratorio de Sedimentología y Paleoambientes, Instituto de Investigaciones Oceanológicas, Facultad de Recursos del Mar, Universidad de Antofagasta, Casilla 170, Antofagasta, Chile*
[b] *IRD, UR 055, PALEOTROPIQUE, 32 Avenue Henri Varagnat, F-93143 Bondy Cedex, France*
[c] *Instituto del Mar de Perú, IMARPE, P.O. Box, 22, Callao, Peru*
[d] *Departamento de Acuicultura, Facultad de Recursos del Mar, Universidad de Antofagasta, Casilla 170, Antofagasta, Chile*
[e] *Departamento de Geología, Facultad de Ciencias Físicas y Matemáticas, Universidad de Chile, Plaza Ercilla 803, Santiago, Chile*
[f] *Departamento de Geoquimica, Universidade Federale Fluminense, Niteroi, RJ, Brazil*

ARTICLE INFO

Article history:
Accepted 14 October 2008
Available online 21 October 2008

Keywords:
Humboldt ecosystem
Northern Chile
Fish scales record
Sardine
Anchovy

ABSTRACT

Marine oxygen-deficient environments with high sedimentation rates and high primary productivity can provide relevant information regarding variations of ocean–climatic conditions in the past. In the Humboldt current ecosystem, which now hosts huge populations of pelagic fishes (mainly anchovy and sardine), fish scale abundance in the sedimentary record may be useful indicators of environmental change. Here we assess such a proxy record in a 42 cm-long sedimentary core collected from 80 m in Mejillones Bay (23°S, northern Chile). We also analyse fish remains in surface sediment sampled along a bathymetric transect (from 10 to 110 m water depth) in the same bay. In the core-top record, the fluctuations of sardine and anchovy scale deposition rates (SDR) agreed with those of industrial catches for these two species in northern Chile, tending to validate the SDR as a proxy of local fish biomass when bottom anoxic conditions prevail. However, apparent SDR for records prior to 1820 have probably been influenced by dissolution processes linked to the oxygenation of the bottom environment of Mejillones Bay, as suggested by other proxy records. After 1820, the fluctuations in the relative abundance of sardine and anchovy scales point to alternating warm and cold conditions during about 30 years and then a progressively cooler period. Since ca. 1870, marked fluctuations of SDR of both species are observed, probably as a consequence of the onset of a different oceanographic regime characterized by intensified upwelling, stronger subsurface oxygen deficiency, higher primary productivity, and enhanced "ENSO-like" interdecadal variability. While anchovy SDR fluctuated in periods of 25–40 years, only two peak periods of sardine SDR occurred (late 19th century and late 20th century), suggesting that sardine abundance depends on other ocean–climatic factors.

1. Introduction

Pelagic fish catches have exhibited large global fluctuations in the course of the last few decades. These fluctuations have been interpreted variously as depending upon fishing activity or upon natural variations in fish populations as a response to the environmental changes which operate at different time and space scales (Lluch-Belda et al., 1992; Yañez et al., 2001; Chavez et al., 2003; Gutierrez et al., 2007). Historical fluctuations in sardine and anchovy stocks in the Northern Hemisphere, for instance, were principally attributed to climatic changes at a large geographical scale (Lluch-Belda et al., 1989; Baumgartner et al., 1992). A similar situation occurs in the Southern Hemisphere in the Humboldt current ecosystem where the ENSO mode of climatic variability seems to strongly influence the fish stocks (Cañón, 1978, 1985; Cury, 1988; Yañez, 1989; Csirke et al., 1996; Yañez et al., 1998; Schwartzlose et al., 1999; Chavez et al., 2003; Bertrand et al., 2004; Escribano et al., 2004; Ñiquen and Bouchon, 2004).

Past fluctuations of pelagic fish populations and oceanographic conditions can be deduced from analyses of laminated marine sediment sequences when particular physico-chemical conditions are met, particularly in low-oxygen environments (Fitch, 1969; Soutar and Isaacs, 1969; DeVries, 1979; Schwartzlose et al., 1999; O'Connell and Tunnicliffe, 2001). In such environments, which are much less affected by bioturbation and other post-depositional processes, fish remains and particularly their scales are often well-preserved and can provide a record of former fish populations (Gallardo, 1963; Milessi et al., 2005). Relationships between fish remains in sediments and past fluctuations of pelagic populations

---

* Corresponding author. Tel.: +56 55 637401; fax: +56 55 637804.
E-mail address: jvaldes@uantof.cl (J. Valdés).

0079-6611/$ - see front matter © 2008 Elsevier Ltd. All rights reserved.
doi:10.1016/j.pocean.2008.10.002

have mainly been studied in the California Current ecosystem (e.g. Soutar, 1967; Fitch, 1969; Soutar and Isaacs, 1969; Baumgartner et al., 1992; Holmgren-Urba and Baumgartner, 1993; Tunnicliffe et al., 2001; Wright et al., 2005). In the Humboldt current ecosystem of northern Chile and Peru, few studies have examined fish scales as paleoenvironmental and paleoceanographic indicators (DeVries and Pearcy, 1982). Schwartzlose et al. (1999) stressed the need for more detailed studies on fish remains in sediments of the Humboldt current ecosystem to better understand the links between oceanic/climatic phenomena and fish fluctuations.

In northern Chile, a series of previous studies (Ortlieb et al., 2000; Valdés et al., 2000, 2004; Valdés and Ortlieb, 2001; Valdés, 2004; Vargas et al., 2004, 2007) pinpointed the high paleoceanographic potential of sediments accumulated in Mejillones Bay (23°S; Fig. 1). This bay is characterized by a coastal upwelling centered at nearby Punta Angamos, hydrodynamic stability behind a thermal front, high sedimentation rates, and occurrence of the oxygen minimum zone below 40–60 m depth depending on the season (Fig. 1; Zúñiga et al., 1983; Rodríguez et al., 1991; Marín et al., 1993; Valdés et al., 2003). These conditions, which prevail during non-El Niño years, favour the accumulation of abundant biogenic remains and the preservation of primary structure of bottom sediment. In this study we evaluate the quality of the sedimentary record of pelagic fish abundance in Mejillones Bay, with emphasis on the state of preservation of the fish remains, their taxonomic identification, and their potential significance for the reconstruction of former variations of pelagic fish populations.

2. Materials and methods

A 42 cm long sedimentary core (F98-1A) was recovered with a boxcore ("Fuchsia" type) from 80 m of water depth at the center of the Mejillones Bay (Fig. 1). This core was cut transversely every 0.5 cm immediately after sampling, and the samples were disaggregated and sieved through a 250 μm mesh, under a constant flow of water. Fish scales were identified and counted using a microscope. Additionally, superficial modern sediment samples were taken along a bathymetric transect between 14 and 120 m of water depth in the central zone of the bay (Fig. 1) using a small box corer with a 225 cm^2 section. Surface sediment (0.5 cm thick) was taken from each sample and kept at low temperatures during transport and storage.

The identification of the fish scales was restricted to the so-called "typical scales" characteristic of each species; such scales

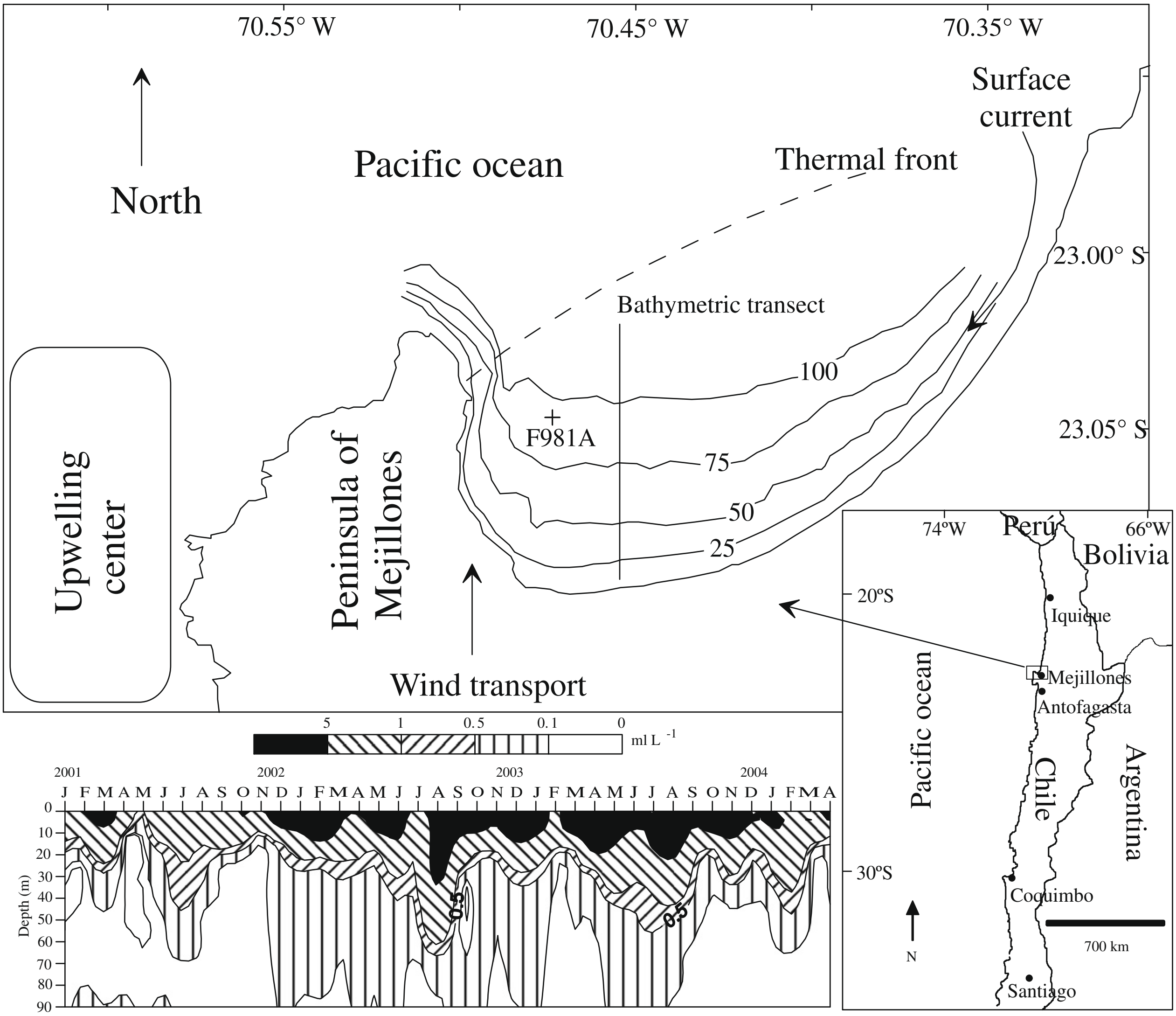

Fig. 1. Schematic geographic and oceanographic setting of the study area, Mejillones Bay, with localization of the sampling zones (bathymetric transects and F98-1A sediment core). Vertical distribution of dissolved oxygen in the water column of Mejillones Bay between 2001 and 2004 (below left) is also shown.

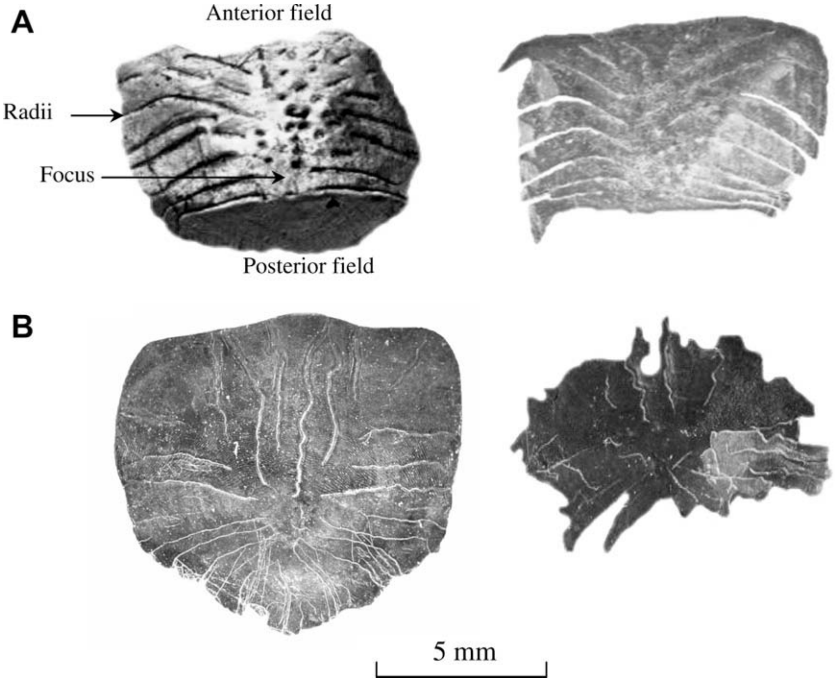

Fig. 2. Sardine (A) and anchovy scales (B). Modern (left) and fossil scales (right) found in the sedimentary core. Principal structures used for the taxonomic identification are indicated (see text).

are those more easily released from the fish body and are found in greater abundance in bottom sediments (Soutar, 1967; Soutar and Isaacs, 1974; DeVries and Pearcy, 1982; Shackleton, 1987; O'Connell and Tunnicliffe, 2001). Typical scales were defined by reference to a preliminary collection of the most important fishes present in the study area, and are characterized by shape, position and shape of scale focus, appearance of the anterior and posterior fields, and radii (Fig. 2).

The most typical scales of both species used in this study present the following characteristics:

- Order: Clupeiformes; Family: Clupeidae; Specie: *Sardinops sagax* (Jenyns, 1842) – sardine.
  Scale type: cycloid (Fig. 2).
  Shape: square, with relatively round edges.
  Focus: diffused aspect, located in the middle part of the scale, close to the posterior field.
  Radii: regular, well-defined and parallel grooves or channels present between the insertion zone and the focal point.
- Order: Clupeiformes; Family: Engraulidae; Specie: *Engraulis ringens* (Jenyns, 1842) – anchovy.
  Scale type: cycloid (Fig. 2).
  Shape: rectangular with oval borders in a shield-like form, and with prominent convex lateral borders around the stuffed area.
  Focus: diffused aspect, located close to the posterior field.
  Radii: longitudinal and external (outer border) position which converge towards the focus, and ornamented with numerous circuli.

The sediment core scales were compared with modern scales from each of the species present in the study area. For the quantification of fish scale abundance in the sediment samples, the following rules were applied: (i) a scale was counted whenever the nucleus and more than one half of the scale were preserved; (ii) counts of 0.5 units were applied for incomplete half-scales which did not show the scale nucleus, provided that no other incomplete scale of the same species was found in the same sample; (iii) the smallest scale fragments were not counted.

The chronological framework of the sediment core was determined through the combination of downcore excess ^{210}Pb activities and ^{14}C ages, as detailed in Vargas (2002) and Vargas et al. (2007). The sedimentation rate was estimated to be 0.131 ± 0.07 cm y^{-1}, which is equivalent to a 2–4 year resolution for 0.5 cm slices obtained from this core. The accumulation of scales down the sediment core is expressed as a scale deposition rate (SDR), according the following formula: $\mathrm{SDR} = (N^{*} T)/A$, in which N represents the number of scales in each sample, T the time interval of such sample, and A is the cross sectional area of the core (cm^2).

3. Results and discussion

3.1. Preservation of fish remains and distribution of sardine and anchovy scales

In this paper we focus on sardine and anchovy scale records because fishery catch and ecological data are available for these two taxa in terms of geographic distribution, importance as fishing resources, and significance for teleconnection studies related to ocean–climatic interactions (Baumgartner et al., 1992; Schwartzlose et al., 1999; Yañez et al., 2001; Chavez et al., 2003;

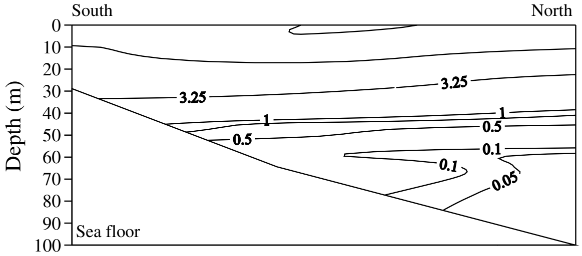

Fig. 3. Dissolved oxygen (in mL L^{-1}) distribution in the water column of Mejillones Bay, in October 2004, along the studied transect (see Fig. 1).

Ñiquen and Bouchon, 2004; Miller et al., 2006). Off northern Chile, anchovy reaches a maximum length of 19 cm, has a short life span (4 years), and is distributed principally within the first 60 nm offshore, and most often the first 25 nm. The sardine is larger (to 40 cm long) and lives longer (25 years), and has a more offshore distribution (0–200 nm) (Gutierrez et al., 2007). Both species commonly live above the thermocline (Yañez et al., 2001). In the study area, the Punta Angamos upwelling center (Fig. 1) adjacent to the bay produces a high biological productivity which favours anchovy and sardine, particularly during their reproductive periods (Barbieri et al., 1995).

The fish remains present in surface sediment and box-core samples correspond to scales, vertebrae, dental pieces, opercula and bones from the scapular zone and otoliths which generally exhibit a low degree of degradation by physical and/or chemical processes. The scales were the most abundant fish debris found in the sediments. Even though they present different degrees of fragmentation, their principal characteristics (shape, anterior and posterior field, head shapes, radii) are well-preserved and allow identification of anchovy, sardine, and mackerel (*Trachurus murphyi*). However, preservation of the fish debris is imperfect and depends on many factors, e.g. their chemical composition and surrounding

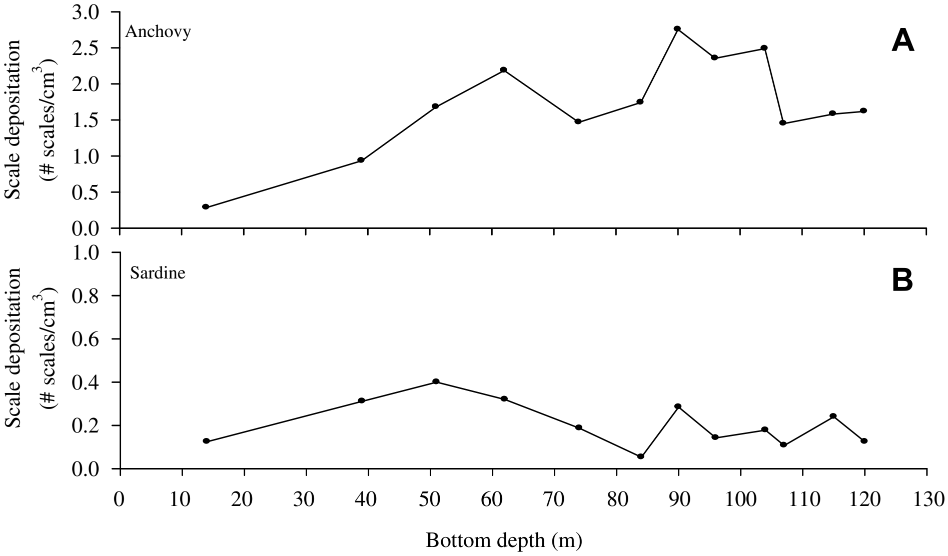

Fig. 4. Sardine and anchovy scale abundances in surface sediments (core top, 0–0.5 cm) along the studied transect (see Fig. 1). Abundance is expressed in number of scales per area of sampling (225 cm^2).

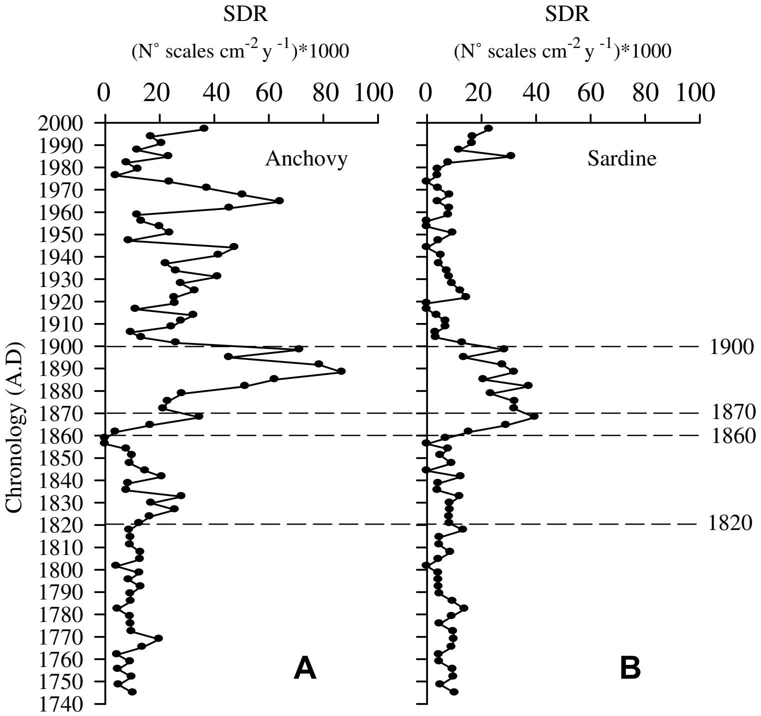

Fig. 5. Anchovy and sardine SDR for the last two decades in Mejillones Bay. The chronology was taken from Vargas et al. (2007). Each point in the curve corresponds to 0.5 cm of sediment (~3 year time range, according to sedimentation rate: see text). SDR is expressed in Number of scales 1000 cm^{-2} y^{-1}. Most important dates cited in the text are highlighted.

sediments, mechanical abrasion, and the rate of bacterial degradation (O'Connell and Tunnicliffe, 2001). Fish bones are compounds of collagen that eventually harden with salts, while the scales are a mixture of microcrystalline apatite within a collagen matrix (Wright et al., 2005) and have greater susceptibility to degradation (Tunnicliffe et al., 2001). Schenau and De Lange (2000) indicate that in aerobic bottom sediments, the acidity generated during organic matter degradation can provoke the dissolution of biogenic apatite, a situation that is strongly reduced in anaerobic environments. The cited authors conclude that the presence of an intense oxygen minimum zone (OMZ) may account for the enhanced preservation of fish debris in sedimentary deposits of the continental margins. Therefore, in Mejillones Bay, the presence of an OMZ diminishes the potential chemical degradation of fish debris. Moreover, the quite limited mechanical abrasion observed in this material coincides with the general lack of benthic organism activity and of bacterial action. The preserved state of fish scales in the sediment of Mejillones Bay is comparable with others sedimentary records of northern Chile (Gallardo, 1963; Milessi et al., 2005); the continental margin of Peru (DeVries, 1979; DeVries and Pearcy, 1982); and the California current ecosystem (Soutar and Isaacs, 1974; Baumgartner et al., 1992; Wright et al., 2005).

To examine the effect of bottom water oxygen concentration on the preservation of fish debris (O'Connell and Tunnicliffe, 2001; Tunnicliffe et al., 2001), we assessed the abundance, composition and preservation state of scales as a function of the oxygenation of the depositional environment within Mejillones Bay. The distribution of dissolved oxygen across a south–north section of the water column in October 2004 is showed in Fig. 3. Based on the oxygenation scale of Bernhard and Sen Gupta (1999) (oxic, >1 mL L^{-1}; disoxic, 0.1–1 mL L^{-1}; microxic, <0.1 mL L^{-1}), most sediments of this bay appear to have been deposited under microxic conditions while, at shallow depth, the environment was more oxygenated.

A total of 2753 scales were counted in the modern core-top sediment samples obtained along the transect (Figs. 1 and 3), with 94% identified as anchovy and sardine. A greater abundance of sardine scales were found between 40 and 60 m, while anchovy scales were most abundant between 50 and 100 m (Fig. 4). One explanation could involve the selective degradation of scales of both species. If this were the case, the anchovy scales would be better preserved under oxygen-deficient conditions (less oxygen, more scales), while the preservation of sardine scales would be less influenced by oxygen (Figs. 3 and 4). Another possibility is that

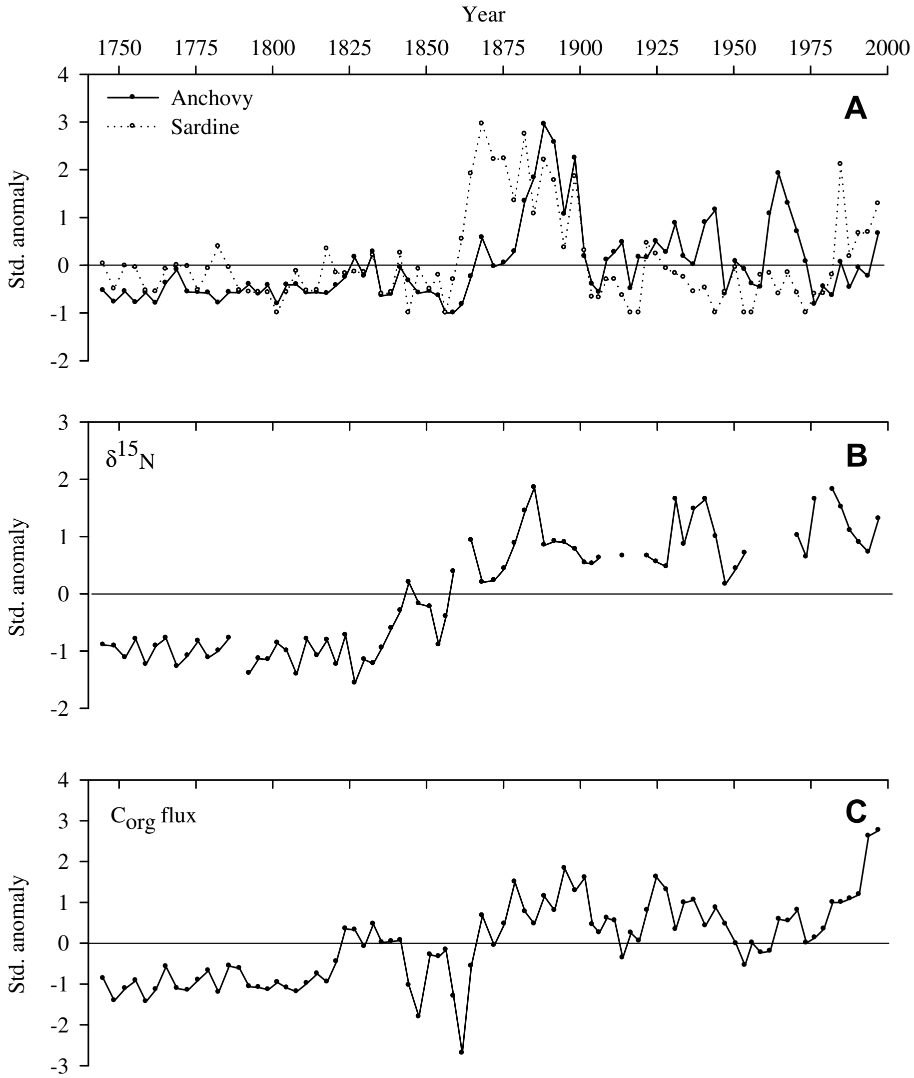

Fig. 6. (A) Standardized SDR anomaly for anchovy and sardine (this work), (B) δ^{15}N and (C) organic carbon flux, in the F98-1A sedimentary record of Mejillones Bay (Vargas et al., 2007). Organic carbon flux is used as an indicator of primary export production and δ^{15}N is used as an indicator of denitrification and oxygen deficiency, according to Vargas et al. (2007).

these patterns of scales distribution result from the circulation of water inside the bay, and from the differences in size and form of the scales of each species, which probably influence their vertical transit through the water column. At present, our interpretation is that the observed distribution of scales of the two species along the bathymetric transect does not reflect the relative abundance of the two fish populations within the embayment, due to the mobility of the populations and the small dimensions of the bay.

In conclusion, this study of the present-day distribution of fish scales suggests that dissolution processes of fish scales are reduced below 50 m water depth and especially at maximal depths (in the center of the bay), characterized by oxygen-deficient conditions. Therefore if it can be assumed that the physical–chemical conditions observed nowadays were similar in a recent past, the downcore records of abundance of fish scales in the center of the bay may reflect fluctuations of fish scale fluxes and related environmental variations.

3.2. Downcore trends of fish scales and preservation issues

The chronology of the core (F98-1A) suggests that the base of the sedimentary sequence has an age of about 250 years, i.e. was deposited around 1740 AD. No indication of interruption of the sedimentation (or of post-depositional erosion) has been observed (more details concerning sedimentological characteristics of this core in Vargas et al. (2007)). The top of the core is assigned the date of extraction, 1998. Assuming a constant sedimentation rate (Vargas, 2002; Vargas et al., 2007), the 0.5 cm slices would yield a succession of time windows of 3 years each.

Sardine and anchovy SDR exhibited low values and variability from 1740 to 1820, when a slight increase in anchovy abundance is observed (Fig. 5). The anchovy SDR exhibited somewhat larger fluctuations from 1820 to 1860, and after 1870, the anchovy SDR increased. The sardine SDR also increased from ca. 1860 AD until 1900 relative to the former period.

Fish debris are susceptible to dissolution in the water column and in the upper part of the sediment column (Schenau and De Lange, 2000). For this reason eventual loss of fish remains due to dissolution is a factor which must be considered in the potential use of scales and bones in sedimentary records. O'Connell and Tunnicliffe, 2001 suggested that scales present in sediments older than 500 years are more susceptible to dissolution, while Wright et al. (2005) indicated that anchovy scales are more heavily mineralized than other species, and thus more resistant to dissolution. On the other hand, it is generally accepted that dissolution processes are much less efficient in depleted oxygen environments (Schenau and De Lange, 2000; O'Connell and Tunnicliffe, 2001; Tunnicliffe et al., 2001; Wright et al., 2005), as observed in the deepest part of Mejillones Bay at present (Fig. 4). However, the profile of δ^{15}N from the same core (Fig. 6) suggests that bottom waters of this bay were more oxygenated prior to 1820. If so, the preservation potential of the fish scale record after deposition may have been reduced, affecting the reliability of the scale deposition rates, as an estimator of true vertical fluxes to the seafloor.

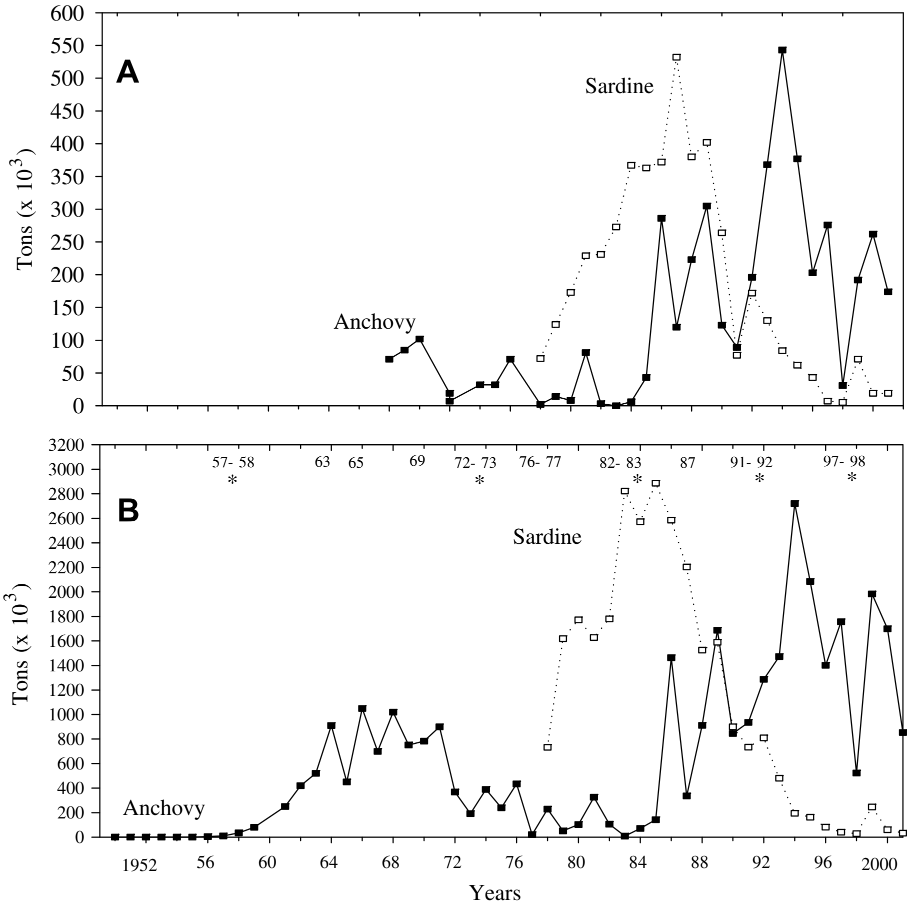

Fig. 7. Anchovy and sardine catch in (A) the Antofagasta region (including Mejillones) and (B) in the whole country, according National Fishing Service, Chile (SERNAPESCA, 1995–2002).

In order to identify changes in SDR which deviate from the mean, we calculated the SDR anomalies (Fig. 6) by subtracting the record mean from each SDR value and normalized the differences by the standard deviation. Fig. 6 also shows the anomalies of organic carbon flux and δ^{15}N, as reported by Vargas et al. (2007) for the same core, which are interpreted to reflect, respectively, fluctuations in biological productivity and intensity of oxygen deficiency in the water column. Negative anomalies, such as those observed between ca. 1744 and ca. 1825 (C_{org}), or ca. 1744 and 1844 (δ^{15}N), are interpreted to indicate lower surface productivity and lower denitrification in the water column (and hence less intense subsurface oxygen deficiency), respectively. Both anchovy and sardine SDR exhibit significant correlations with organic carbon flux and with δ^{15}N (anchovy: $r = 0.551$; $p < 0.01$; and $r = 0.536$; $p < 0.01$, respectively; sardine: $r = 0.350$; $p < 0.01$; $r = 0.340$; $p < 0.01$, respectively). However, when anchovy SDR are compared with both parameters before 1825 and after 1870, which mark two oxygenation regimes, as inferred by δ^{15}N values, no significant correlation was found. Within the transition period (1825–1870), anchovy SDR was significantly correlated with carbon flux ($r = 0.609$; $p < 0.05$) but not with δ^{15}N. For sardine SDR, no correlation was found with δ^{15}N for any period, and only with organic carbon flux after 1870 ($r = 0.395$; $p < 0.01$). All together these comparisons strongly suggest reduced preservation with higher oxygenation in the bay, as in the regime before 1825, but also indicate that within each regime, oxygenation is not a significant factor explaining SDR downcore variability.

3.3. Interdecadal variability of SDR in relation to climate and oceanographic changes

Geochemical, micropaleontological and mineralogical analyses of the core F98-1A (Vargas et al., 2007) suggest a high biological productivity, probably due to an intensification of the upwelling at Punta Angamos (Fig. 1) since 1820. After 1820 the anchovy SDR exhibited larger fluctuations, and after ca. 1870 a general increase is observed. These findings are consistent with the Vargas (2002) study, which depicts two regimes of organic carbon (Fig. 6) and minerals fluxes within the same core, with a transition period between 1820 and 1878. Prior to 1820 a limited biological productivity would have been linked to relatively low-intensity southwest winds, contrasting with an intensification of winds favourable to the upwelling. Time-series of δ^{15}N (Fig. 6), Δ^{14}C, and alkenones-derived sea surface temperature in the same F98-1A core indicate a secular trend in coastal upwelling intensity since AD 1878, characterized by an enhanced influence of the nutrient-rich Equatorial Subsurface Water and a decrease of 2 °C in SST in the zone, as well as enhanced ENSO-like interdecadal variability (Vargas et al., 2007). These oceanographic characteristics correspond to modern upwelling conditions in Mejillones Bay (Strub

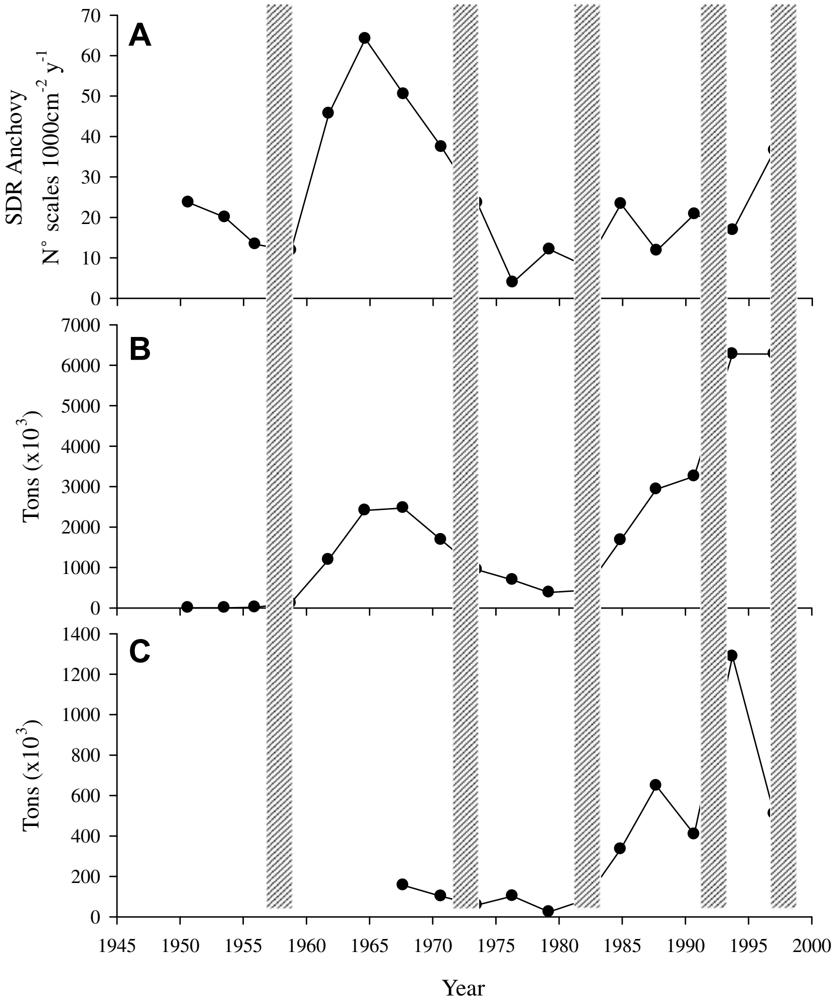

Fig. 8. SDR (A) and catch of anchovy in the Antofagasta Region (B) and in Chile (C), between 1950 and 1998. The dashed bar corresponds to El Niño events.

et al., 1998; Marín et al., 2003). Thus the downcore studies on different proxies point to an interpretation of relatively stable ocean–climate conditions in northern Chile before 1820 unfavourable for anchovy and sardine populations and/or for preservation of fish debris in bottom sediments, either or both resulting in low SDRs, and a higher interdecadal variability overimposed with secular higher productivity since the second half of the 19th century.

Anchovy is generally considered a cool-water fish and sardine a warmer water fish (Chavez et al., 2003; Wright et al., 2005). It is the thermal dependence during the spawning period which may account for these classifications, the anchovy preferring temperatures of 16–18 °C, while sardines prefer temperatures of 19–21 °C (Chong et al., 1991). During strong El Niño events, which are characterized by warming, anchovies tend to disappear while sardine populations increase off Chile and Peru (Zuzunaga, 1985; Csirke et al., 1996; Chavez et al., 2003; Ñiquen and Bouchon, 2004). Bertrand et al. (2004) proposed that climatic variations lead to changes in the range of anchovy and sardine habitat, causing apparent shifts of dominance between anchovy and sardine populations.

The SDR measured in the Mejillones sediment record thus suggests alternating warm and cold periods since 1820 (Figs. 5 and 6). Sardine SDR increased during the second half of the 1800s until ca. 1900, dominating the scale record between ca. 1860 and 1880. Between 1875 and 1905 high values of SDR are recorded for anchovy and sardine and point to a similarity of oceanic regimes with those of 1980s decade (Fig. 7). In both cases, but at slightly different time-scales, high values of sardine SDR preceded peaks of anchovy SDR; for the latter period the SDR pattern followed that of landings (Fig. 7). If this comparison is correct, the lapse comprised between 1860 and 1880 (higher contribution of sardine SDR relative to anchovy SDR) would have been characterized by relatively warm water conditions, and would have been followed by cooler conditions until ca. 1900 as inferred from the replacement of sardine by anchovy. Afterwards an abrupt decline of both species SDR took place in less than a decade.

During the 1900s, the SDR (Figs. 6 and 7) shows variability associated with large-scale changes in the Pacific Ocean. Chavez et al. (2003) proposed an Ecosystem Index for the Southeastern Pacific based on sardine and anchovy landing and seabird abundance for the period 1940–2000. The authors postulated the occurrence of two oceanographic regimes, with a cool phase (“anchovy regime”) from 1950 to 1975, followed by a warm phase (“sardine regime”) from 1975 to the mid-1990s. Our results for the past 50 years agree with this pattern (Fig. 6). During the 1975–1990s period, an increase of sardine SDR (Fig. 5) and a predominance of sardine landings by the Chilean fishery (Fig. 7) between 1982 and 1988, might be interpreted as secondary effects of the 1982–83 El Niño event. The positive anomaly of anchovy SDR observed at the top of the record (1998, Fig. 6) might possibly be related to the shift to an “anchovy regime”, during the 1990s as suggested by Chavez et al. (2003), even though sardines remained abundant.

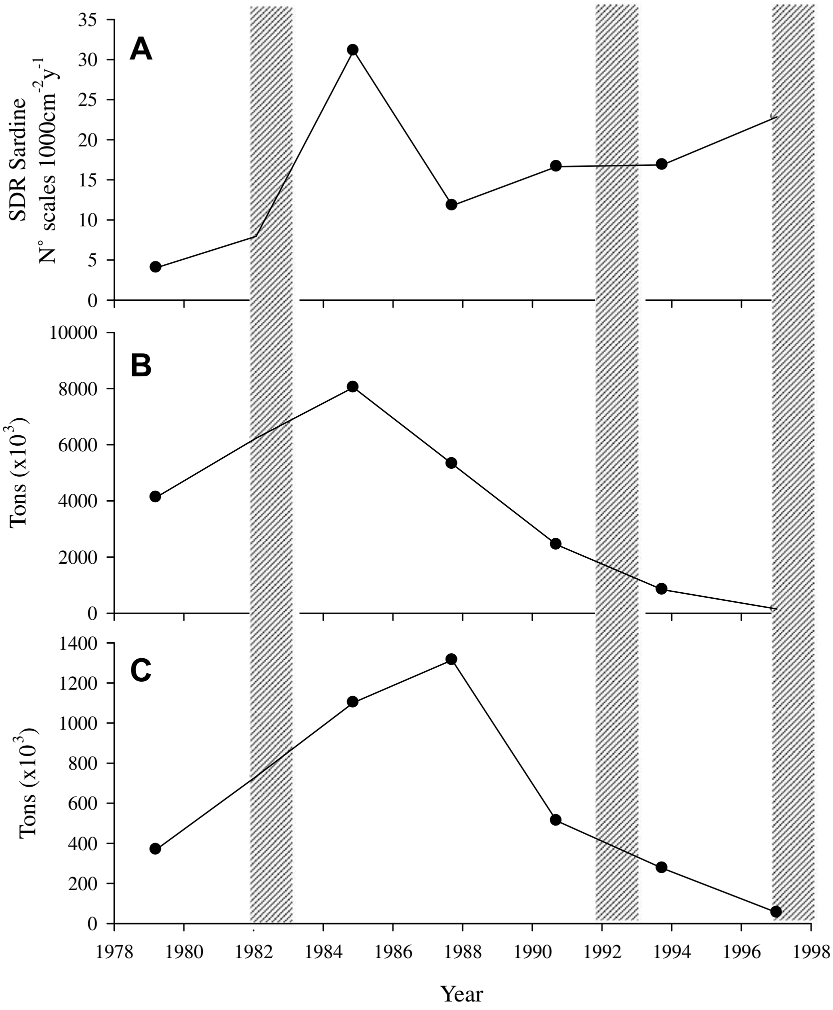

Fig. 9. SDR (A) and catch of sardine in the Antofagasta Region (B) and in Chile (C), between 1978 and 1998. Dashed zone corresponds to El Niño 1982–1983 event.

On the other hand, based on a mineralogical study of the same core, Vargas et al (2007) determined an interdecadal climate variability that roughly follows the Pacific Decadal Oscillation (PDO). The authors deduced that warm interdecadal 'El Niño-like' conditions predominated 1925–1942, and 1976 onward. They propose that during interdecadal warm conditions an increased land–sea thermal contrast along the arid coast of northern Chile and Peru intensifies the equatorward wind stress due to reduced mean low-cloud cover, resulting in enhanced upwelling and primary and export production. According to the thermal preferences of sardine and anchovy, sardine would be better adapted to cope with 'El Niño-like' conditions (Chavez et al., 2003), while anchovies might also benefit from the presence of cold upwelled waters near the coast. Our downcore record shows a positive anomaly of anchovy SDR during the 1925–1942 El Niño-like period, but a positive anomaly of the sardine SDR during the 1976 – El Niño-like period. This apparent contradiction could result from differences between warm periods: the first one less intense than the second one and hence the coastal upwelling response being dominant over the oceanic warming signals.

3.4. SDR and population changes of anchovy and sardine in Northern Chile

The historical data of landing of sardine and anchovy show some correspondence with the respective SDR measured in the sedimentary column (Figs. 8 and 9). This is more evident for anchovy than sardine, probably because there is a longer anchovy landing time series. The strong increase of anchovy SDR in the 1960s coincides with an increase of anchovy catches (Fig. 8). After the fall of anchovy catches between 1975 and 80, the anchovy population recovered as shown by increases both in catches and SDR (Fig. 8). The parallel sequences of both time series are striking even if the magnitude of these fluctuations is different. The sedimentary record indicates that in Mejillones Bay there were more anchovy in the 1960s than in the 1990s, however catches were much greater in the 1990s (Fig. 8) probably due to greater numbers and capacity of fishing ships. The sediment core of this bay can be used to show the higher potential of sedimentary records with respect to landing statistics for an evaluation of pelagic fish populations, even for the last decades.

Anchovy and sardine scales in sediment from the Santa Barbara Basin, California current system, showed changes over the past two millennia (Soutar and Isaacs, 1969; Baumgartner et al., 1992). At time-scales less than 150 years, anchovy SDR appear to fluctuate with periodicities around 60, 70 and 100 years, while sardine SDR fluctuate in periods around 60 and 75 years (Baumgartner et al., 1992). The Mejillones record shows fluctuations in the anchovy SDR of the order of 25–40 years, while the only two observed peaks of sardine SDR were separated about one century one from another, differing to the Santa Barbara Basin records for both species. On the other hand, a positive correlation exists between both species SDR for the whole record ($r = 0.470$, $p < 0.01$), also in the transition period ($r = 0.602$, $p < 0.05$), despite the lag between both, and after 1870 ($r = 0.450$, $p < 0.01$), suggesting that the alternation observed in the late 20th century may not be typical. Baumgartner et al. (1992) noticed that the positive correlation between the California sardine and anchovy SDR is mostly explained by the low-frequency variance (>150 years), and that it vanished at higher frequencies. The sedimentary record of Mejillones Bay, though shorter and limited by preservation issues, suggests different mechanisms governing the population dynamics of the anchovies and sardines off northern Chile than those in California at decadal or longer time-scales, and also different ocean–climatic factors for each species.

Acknowledgements

This study is a contribution of the collaborative PALEOBAME Project between Institut de Recherche pour le Développement and Universidad de Antofagasta, and a product of the JEAI (Jeune Equipe associée à l'IRD) project LASPAL (Laboratorio de Sedimentologia y Paleoambientes) led by the first author (JV). It also benefited from IAI grant No. 03SGP211-222 (Instituto del Mar de Perú, Peru; Universidad de Antofagasta, Chile; Universidad de Chile, Chile; CICESE, México; and the Southwest Fisheries Science Center, USA, PI D. Gutiérrez). The authors thank Vicente Ferreira for his support in improving the analysis of sediment samples, Paola Iratchet and Ismael Kong for their support in the beginning of the studies of sedimentary fish record in Mejillones Bay, and to David Field for his appreciated comments on previous versions of the manuscript. The sedimentary boxcore was obtained through a collaborative action between IRD (programme PVC), Université of Bordeaux (UMR EPOC), Universidad de Antofagasta and Universidad de Chile. Three authors acknowledge the invitation extended by the Organising Committee of the Humboldt Current System Symposium held in Lima in November 2006.

References

Barbieri, M., Bravo, M., Farias, M., Gonzalez, A., Pizarro, O., Yañez, E., 1995. Phenomena associated with the sea surface thermal structure observed through satellite images in the north of Chile. Investigaciones Marinas 23, 99–122.

Baumgartner, T., Soutar, A., Ferreira, V., 1992. Reconstruction of the history of pacific sardine and northern anchovy populations over the past two millennia from sediments of the Santa Barbara Basin, California. California Cooperative Oceanic Fisheries Investigation Reports 33, 24–40.

Bernhard, J., Sen Gupta, B., 1999. Foraminifera of oxygen-depleted environments. In: Sen Gupta, B. (Ed.), Modern Foraminifera. Kluwer Academic Publishers, Cambridge, Great Britain, pp. 201–216.

Bertrand, A., Segura, M., Gutierrez, M., Vasquez, L., 2004. From small-scale habitat loopholes to decadal cycles: a habitat-based hypothesis explaining fluctuation in pelagic fish populations off Peru. Fish and Fisheries 5, 296–316.

Cañón, J., 1978. Distribución de la anchoveta en el norte de Chile en relación a determinadas condiciones oceanográficas. Servicio de Investigación Pesquera, IFOP, Chile, No. 30, p. 65.

Cañón, J., 1985. La variabilidad ambiental en la zona norte de Chile y su influencia en la pesquería pelágica durante El Niño 1982–83. Investigación Pesquera (Chile) 32, 119–128.

Chavez, F., Ryan, J., Lluch-Cota, S., Ñiquen, M., 2003. From Anchovy to Sardine and back: Multidecadal change in the Pacific Ocean. Science 299, 217–221.

Chong, J., Oyarzun, C., Aguilera, E., Arrizaga, A., 1991. Ciclo de maduración y puesta de la sardina española, *Sardinops sagax* (Jenyns, 1842) (Clupeidae), en la zona pesquera de talcahuano, Chile. Scientia Marina 55, 397–404.

Csirke, J., Guevara, R., Cardenas, G., Ñiquen, M., Chipollini, A., 1996. Situation of resources anchovy (*Engraulis ringens*) and sardine (*Sardinops sagax*) at beginning of 1994 and perspective for fishing in Peru, with special reference to northern-center region of Peru. Boletín del Instituto del Mar del Perú 15, 2–23.

Cury, P., 1988. Pressions sélectives et nouveautés évolutives: une hypothèse pour comprendre certains aspects des fluctuations à long terme des poisons pélagiques côtiers. Canadian Journal of Fisheries and Aquatic Sciences 45, 178–191.

DeVries, T., 1979. Nekton remains, diatoms, and Holocene upwelling off Peru. Master Science Thesis, Oregon State University, 85 pp.

DeVries, T., Pearcy, W., 1982. Fish debris in sediments of the upwelling zone off central Peru: a late Quaternary record. Deep-Sea Research 28, 87–109.

Escribano, R., Daneri, G., Farías, L., Gallardo, V., González, H., Gutiérrez, D., Lange, C., Morales, C., Pizarro, O., Ulloa, O., Braun, M., 2004. Biological and chemical consequences of the 1997–1998 El Niño in the Chilean coastal upwelling system: a synthesis. Deep-Sea Research II 51, 2389–2411.

Fitch, J., 1969. Fossil records of certain schooling fishes of the California current system. California Cooperative Oceanic Fisheries Investigation Reports 13, 71–80.

Gallardo, A., 1963. Notas sobre la densidad de la fauna bentonica en el sublitoral del norte de Chile. Gayana (Chile) 10, 1–15.

Gutierrez, M., Swartzman, G., Bertrand, A., Bertrand, S., 2007. Anchovy (*Engraulis ringens*) and sardine (*Sardinops sagax*) spatial dynamics and aggregation patterns in the Humboldt Current ecosystem, Peru, from 1983 to 2003. Fisheries Oceanography 16, 155–168.

Holmgren-Urba, D., Baumgartner, T., 1993. A 250-year history of pelagic fish abundances from the anaerobic sediments of the Central Gulf of California. California Cooperative Oceanic Fisheries Investigations Report 34, 60–68.

Lluch-Belda, D., Crawford, R., Kawasaki, T., Maccall, A., Parrish, R., Schwartzlose, R., Smith, P., 1989. World-wide fluctuations of sardine and anchovy stocks: the regime problem. South African Journal of Marine Science 8, 195–205.

Lluch-Belda, D., Lluc-Cota, D., Hernandez-Vazquez, S., Salinas-Zavala, C., 1992. Sardine population expansion in eastern boundary system of Pacific Ocean as related to sea surface temperature. In: Payne, A., Brink, K., Mann, K., Hilborn, R. (Eds.), Benguela Trophic Functioning. South African Journal of Marine Science 12, 147–155.

Marín, V., Rodríguez, L., Vallejo, L., Fuenteseca, J., Oyarce, E., 1993. Efectos de la surgencia costera sobre la productividad primaria primaveral de la Bahía Mejillones del Sur (Antofagasta, Chile). Revista Chilena de Historia Natural 66, 47–491.

Marín, V., Delgado, L., Escribano, R., 2003. Upwelling shadows at Mejillones Bay (northern Chilean coast): a remote sensing *in situ* analysis. Investigaciones Marinas 31, 47–55.

Milessi, A., Sellanes, J., Gallardo, V., Lange, C., 2005. Osseous skeletal material and fish scales in marine sediments under the oxygen minimum zone off northern and central Chile. Estuarine, Coastal and Shelf Science 64, 185–190.

Miller, D., Moloney, C., van der Lingen, C., Lett, Ch., Mullon, Ch., Field, J., 2006. Modelling the effects of physical–biological interactions and spatial variability in spawning and nursery areas on transport and retention of sardine *Sardinops sagax* eggs and larvae in the southern Benguela ecosystem. Journal of Marine Systems 61, 212–229.

Ñiquen, M., Bouchon, M., 2004. Impact of El Niño events on pelagic fisheries in Peruvian waters. Deep-Sea Research II 51, 563–574.

O'Connell, J., Tunnicliffe, V., 2001. The use of sedimentary fish remains for interpretation of long-term fish population fluctuations. Marine Geology 174, 177–195.

Ortlieb, L., Escribano, R., Follegati, R., Zúñiga, O., Kong, I., Rodríguez, L., Valdés, J., Iratchet, P., Guzmán, N., 2000. Ocean–climatic changes during the last 2000 years in a hypoxic marine environment of Northern Chile (23°S). Revista Chilena de Historia Natural 73, 221–242.

Rodríguez, L., Marin, V., Farias, M., Oyarce, E., 1991. Identification of an upwelling zone by remote sensing and *in situ* measurement. Mejillones del Sur Bay (Antofagasta, Chile). Scientia Marina 55, 467–473.

Schenau, S., De Lange, G., 2000. A novel chemical method to quantify fish debris in marine sediments. Limnology and Oceanography 45, 963–971.

Schwartzlose, R., Alheit, J., Bakun, A., Baumgartner, T., Cloete, R., Crawford, R., Fletcher, W., Green-Ruiz, Y., Hagen, E., Kawasaki, T., Lluch-Belda, D., Lluch-Cota, S., Maccall, A., Matsuura, Y., Nevárez, M., Parrish, R., Roy, C., Serra, R., Shust, K., Ward, M., Zuzunaga, J., 1999. Worldwide large-scale fluctuations of sardine and anchovy populations. South African Journal of Marine Science 21, 289–347.

Shackleton, L., 1987. A comparative study of fossil fish scales from three upwelling regions. South African Journal of Marine Science 5, 79–84.

Soutar, A., 1967. The accumulation of fish debris in certain California coastal sediments. California Cooperative Oceanic Fisheries Investigation Reports 11, 136–139.

Soutar, A., Isaacs, J., 1969. History of fish populations inferred from fish scales in anaerobic sediments off California. California Cooperative Oceanic Fisheries Investigation Reports 13, 63–70.

Soutar, A., Isaacs, J., 1974. Abundance of pelagic fish during the 19th and 20th centuries as recorded in anaerobic sediment off the Californias. Fishery Bulletin 72, 257–273.

Strub, P., Mesias, J., Montecinos, V., Rutlant, J., Salinas, S., 1998. Coastal ocean circulation off western South America. In: Robinson, A., Brink, K. (Eds.), The Sea, vol. 11. John Wiley Sons, New York, pp. 273–313.

Tunnicliffe, V., O'Connell, J., Mcquoid, M., 2001. A Holocene record of marine fish remains from the Northeastern Pacific. Marine Geology 174, 197–210.

Valdés, J., 2004. Evaluación de metales redox-sensitivos como proxies de paleoxigenación en un ambiente marino hipóxico del norte de Chile. Revista Chilena de Historia Natural 77, 121–138.

Valdés, J., Ortlieb, L., 2001. Paleoxigenación subsuperficial de la columna de agua en la bahía Mejillones del Sur (23°S) indicadores geoquímicos en testigos de sedimento marino. Investigaciones Marinas 29, 25–35.

Valdés, J., López, L., Lomónaco, S., Ortlieb, L., 2000. Condiciones paleoambientales de sedimentación y preservación de materia orgánica en bahía Mejillones del Sur (23°S) Chile. Revista Biología Marina y Oceanografía 35, 169–180.

Valdés, J., Ortlieb, L., Sifeddine, A., 2003. Variaciones del sistema de surgencia de Punta Angamos (23°S) y la Zona de Mínimo Oxígeno durante el pasado reciente: Una aproximación desde el registro sedimentario de la Bahía Mejillones del Sur. Revista Chilena de Historia Natural 76, 347–362.

Valdés, J., Sifeddine, A., Lallier-Verges, E., Ortlieb, L., 2004. Petrographic and geochemical study of organic matter in superficial laminated sediments from an upwelling system (Mejillones del Sur Bay, Northern Chile). Organic Geochemistry 35, 881–894.

Vargas, G., 2002. Interactions océan-atmosphère au cours des derniers siècles sur la côte du Désert d' Atacama : analyse multi-proxies des sédiments laminés de la Baie de Mejillones (23° S). Ph.D. Dissertation, Universidad de Bordeaux I, Francia, 270 pp.

Vargas, G., Ortlieb, L., Pichon, J., Bertaux, J., Pujos, M., 2004. Sedimentary facies and high resolution primary production inferences from laminated diatomaceous sediments off northern Chile (23°S). Marine Geology 211, 79–99.

Vargas, G., Pantoja, S., Rutlant, J., Lange, C., Ortlieb, L., 2007. Enhancement of coastal upwelling and interdecadal ENSO-like variability in the Peru–Chile Current since late 19th century. Geophysical Research Letter 34, L13607.

Wright, C., Dallimore, A., Thomson, R., Patterson, R., Ware, D., 2005. Late Holocene paleofish populations in Effingham Inlet British Columbia, Canada. Palaeoceanography Palaeoclimatology Palaeoecology 234, 367–384.

Yañez, E., 1989. Fluctuaciones de los principales recursos pelágicos explotados en la zona norte de Chile y variaciones ambientales asociadas. Comisión Permanente del Pacífico Sur (CPPS), Revista Pacífico Sur (Número Especial), 509–519.

Yañez, E., García, M., Barbieri, M., 1998. Pelagic fish stocks and environmental changes in the south-east Pacific. In: Durand, M., Cury, P., Mendelsohn, R., Roy, C., Bakun, A., Pauly, D. (Eds.), Global Versus Local Changes in Upwelling Systems. ORSTOM Editions, Paris, pp. 275–291.

Yañez, E., Barbieri, M., Silva, C., Nieto, K., Espíndola, F., 2001. Climate variability and pelagic fisheries in northern Chile. Progress in Oceanography 49, 581–596.

Zúñiga, O., Baeza, H., Castro, R., 1983. Análisis de la macrofauna bentónica del sublitoral de la bahía de Mejillones del Sur. Estudios Oceanológicos 3, 41–62.

Zuzunaga, J., 1985. Changes in the equilibrium between the anchoveta and the sardine populations in the upwelling system off Peru. Boletín del Insustituto del Mar del Perú (Extraordinary Volume) El Niño: Its Impacts in The Marine Fauna, 107–117.

Progress in Oceanography 79 (2008) 208–214

Contents lists available at ScienceDirect

Progress in Oceanography

journal homepage: www.elsevier.com/locate/pocean

Zooplankton and forage fish species off Peru: Large-scale bottom-up forcing and local-scale depletion

Patricia Ayón [a], Gordon Swartzman [b,*], Arnaud Bertrand [c,a], Mariano Gutiérrez [a,1], Sophie Bertrand [b,c,a]

[a] *Instituto del Mar del Perú (IMARPE) Gamarra y General Valle s/n Chucuito, Apartado 22, Callao, Lima, Peru*
[b] *University of Washington, School of Aquatic and Fisheries Science, Box 355020, Seattle, WA 98195, USA*
[c] *Institut de recherche pour le développement (IRD), Centre de Recherche Halieutique Méditerranéenne et Tropicale, Avenue Jean Monnet, BP 171, 34203 Sète Cedex, France*

ARTICLE INFO

Article history:
Accepted 14 October 2008
Available online 21 October 2008

ABSTRACT

The Humboldt Current System, like all upwelling systems, has dramatic quantities of plankton-feeding fish, which suggested that their population dynamics may ‘drive’ or ‘control’ ecosystem dynamics. With this in mind we analysed the relationship between forage fish populations and their main prey, zooplankton populations. Our study combined a zooplankton sampling program (1961–2005) with simultaneous acoustic observations on fish from 40 pelagic surveys (1983–2005) conducted by the Peruvian Marine Research Institute (IMARPE) and landing statistics for anchoveta (*Engraulis ringens*) and sardine (*Sardinops sagax*) along the Peruvian coast from 1961 to 2005. The multi-year trend of anchoveta population abundance varied consistently with zooplankton biovolume trend, suggesting bottom-up control on anchovy at the population scale (since oceanographic conditions and phytoplankton production support the changes in zooplankton abundance). For a finer-scale analysis (km) we statistically modelled zooplankton biovolume as a function of geographical (latitude and distance from the 200-m isobath), environmental (sea surface temperature), temporal (year, month and time-of-day) and biological (acoustic anchovy and sardine biomass within 5 km of each zooplankton sample) covariates over all survey using both classification and regression trees (CART) and generalized additive models (GAM). CART showed local anchoveta density to have the strongest effect on zooplankton biovolume, with significantly reduced levels of biovolume for higher neighbourhood anchoveta biomass. Additionally, zooplankton biovolume was higher offshore than on the shelf. GAM results corroborated the CART findings, also showing a clear diel effect on zooplankton biovolume, probably due to diel migration or daytime net avoidance. Apparently, the observed multi-year population scale bottom-up control is not inconsistent with local depletion of zooplankton when anchoveta are locally abundant, since the latter effect was observed over a wide range of overall anchoveta abundance.

1. Introduction

Understanding ecosystem functioning requires identifying the main determinants of species abundance and distribution. Predator–prey relationships are one of these major driving functional processes in marine ecosystem dynamics. The Peruvian coastal upwelling ecosystem is characterized by the presence of two highly abundant, but also highly variable, forage fish species; the Peruvian anchovy or anchoveta (*Engraulis ringens*) and sardine (*Sardinops sagax*). The large fluctuations in abundance of anchoveta and sardine have been the subject of a large number of studies (Csirke et al., 1996; Bakun and Broad, 2003; Chavez et al., 2003; Alheit and Niquen, 2004; Bertrand et al., 2004b; Gutiérrez et al., 2007; Swartzman et al., 2008). These studies show that, at the population and multi-year scale, anchoveta population dynamics appears to depend on the overall productivity of the ecosystem and that they are more abundant when upwelling is enhanced and phytoplankton and zooplankton are abundant. Such bottom-up forcing is a long-term process that can only be observed in smooth trends from long time series (multi-decadal). Indeed the small time scale variability (e.g. seasonal) and the large measurement variance intrinsic to the data that we used (e.g. net plankton sampling, acoustic estimates, landings and associate changes in CPUE) blur these patterns in shorter time series. Such apparent evidence of bottom-up forcing detected at decadal time scales seems confirmed by studies at a centennial scale by Sifeddine et al. (2008) and Valdés et al. (2008) who used laminated sediment cores to show that a large shift in productivity occurred by ~1815. Prior to 1815, during the little ice age, the northern Humboldt Current region was marked by low ecosystem productivity and low anchoveta scale deposition rate. Afterwards, an increase of wind-driven upwelling resulted in higher productivity

---

[*] Corresponding author. Tel.: +1 206 543 5997; fax: +1 206 543 6785.
E-mail address: gordie@apl.washington.edu (G. Swartzman).
[1] Present address: TASA, Av. Néstor Gambeta, Km 14.1, Ventanilla, Callao, Peru.

0079-6611/$ - see front matter © 2008 Elsevier Ltd. All rights reserved.
doi:10.1016/j.pocean.2008.10.023

and increased anchoveta scale deposit. These productive conditions (plankton and fish) intensified during the 20th century. While bottom-up control seems to occur at the population scale, little is known about the potential depletion effect that these vast quantities of pelagic fish may have at a smaller spatiotemporal scale (local scale, 10–100 kms – weeks) on lower trophic levels, particularly on zooplankton, which comprises the bulk of their diet (van der Lingen et al., 2006, in press; Espinoza and Bertrand, 2008). While predator–prey relationships clearly occur at a local scale, an important question is whether fish foraging impacts locally zooplankton biomass and/or if potential local depletion effects are spatially pervasive enough to be detected at the population scale, through, for instance, a top-down control of zooplankton by forage fish as proposed by the wasp-waist hypothesis (Cury et al., 2000, 2003).

To check for bottom-up control on anchoveta we used a long time series available for zooplankton biovolume, i.e. 1961–2005 (extended from Ayón et al., 2004) and commercial pelagic fish landings for the corresponding period. These data allowed us to look at changes in population abundance on large spatial and temporal scales. Concomitantly we examined local-scale questions of distribution and trophic interactions from scientific surveys data over the shorter, but still substantial, time period over which these are available (1983–2005). On this scale we studied the potential depletion effect of pelagic fish on zooplankton. To this end we examined the relative effect on zooplankton biovolume of SST, latitude, bottom depth, diel period, time (year–month) and the abundance of anchoveta and sardine within a neighbourhood of the zooplankton. This small-scale analysis used long term (1983–2005) and fairly high-resolution (1–2 nautical miles) acoustic data from surveys transecting almost the entire Peruvian coastal marine ecosystem, accompanied by an intensive zooplankton sampling program. This time period encompassed large fluctuations in sardine and anchoveta population abundance: the decline of the sardine population and the increase of the anchoveta up to a ‘full anchovy era’ (Gutiérrez et al., 2007) since the end of the 1990s. These data allowed us to look at changes in population abundance at a fine spatial scale over a large spatial region and long time period, permitting examination of local-scale questions of distribution and trophic interactions.

2. Data and methods

2.1. Landing data

Yearly landing data for anchoveta and sardine in Peru between 1961 and 2005 are from the official statistics of the Instituto del Mar del Peru (www.imarpe.gob.pe).

2.2. Acoustic survey data

Acoustic data were collected from 1983 to 2005 by the Instituto del Mar del Perú (IMARPE) on a variety of vessels, most commonly the R/V Humboldt (76 m long), the R/V Olaya (41 m long) and the R/V SNP-1 (36 m long). Surveys consisted of parallel transects averaging 90 nautical miles (167 km) with an inter-transect distance between 14 and 16 nautical miles (26–30 km) depending on the cruise.

The entire observable range of anchoveta distribution was covered (transects shown in Fig. 1 are typical of almost all surveys). Extensive midwater trawl sampling accompanied the acoustic surveys for species identification. The seasonal and temporal distributions of scientific acoustic surveys are: spring (1983, 1996–2005), summer (1990–96, 1999–2005), autumn (1985, 2 surveys in 1998), and winter (1984, 1987–89, 1991, 1998–2003 with 2 winter surveys in 1999, 2000 and 2001). The acoustic surveys deployed Simrad (Kongsberg Simrad AS, Kongsberg, Norway) scientific echosounders EK, EKS, EK400, EY500, EK500 and EK60 (2001–2003 in one vessel). Calibration of the echosounders was done before all surveys. Calibration up until 1992 was done using hydrophones and after 1992 sphere calibration followed a standard procedure (Foote et al., 1987). The acoustic nautical area scattering coefficient (s_A or NASC; see MacLennan et al., 2002 for acoustic definitions), an indicator of fish biomass, was recorded for each geo-referenced elementary sampling distance unit (ESDU) of 1 n. mi. (1994–2003) or 2 n. mi. (1983–1993). Acoustic echo identification was performed using fishing trawl results and echotrace characteristics (see Gutiérrez et al., 2007 for more information on the acoustic protocol). Biomass estimation based on both the trawls and acoustic backscatter for each species was carried out by IMARPE for each survey. Surface temperature and salinity were measured and averaged per ESDU for almost all surveys (exceptions are missing samples in summer of 1990 for both temperature and salinity and additionally summer 1994 and spring 2000 for salinity).

2.3. Zooplankton data

Zooplankton samples were taken with Hensen nets of 0.33 m^2 mouth area with a 300 μm mesh, in vertical hauls between 0 and 50 m. Samples were fixed with 2% formaldehyde buffered with borax. Zooplankton biovolume (mL/sample) was determined at the time of collection using the displacement method (Kramer et al., 1972). Ichthyoplankton and large coelenterates were removed before determining the biovolume. This sampling protocol has been followed consistently for the entire period covered by this study (1961–2005). The hour of sampling was available for most of the data since 1971, for all data since 1983, but for few zooplankton surveys before 1971.

2.4. Zooplankton and forage fish dynamics, population scale

To examine the large-scale relationship between zooplankton biovolume and pelagic fish abundance we used time series on anchoveta and sardine landings and on zooplankton biovolume from 1961 to 2005. Changes in zooplankton biovolume over time were averaged by month (Fig. 2a) and smoothed by fitting a nonparametric spline model to the data in order to reduce the variance and look at rather low frequency patterns (Fig. 2b). Euphausiids, which are an essential part of anchoveta diets (Espinoza and Bertrand, 2008) are not sampled efficiently by Hensen net tows, and this introduced a bias into the data used to estimate fish prey abundance. To reduce this bias we compared the time series using the complete set of zooplankton data with a subset composed of the night-time data (19 h–05 h, local time since 1971). Clearly, euphausiids and other large zooplankton are better sampled at night because of a reduced net avoidance and a shallower distribution (for organisms performing diel migration). The nocturnal data are probably more representative of the anchovy prey community than the entire data set.

2.5. Environmental and fish effects on zooplankton, local scale

To examine the potential effect of anchoveta foraging on zooplankton communities we computed, for each zooplankton net haul, total sardine and anchoveta s_A within 5 km. This threshold was chosen as representative of an ‘accessible’ neighbourhood for fish to zooplankton prey. Because the shape of predator-prey relationships is known to depend on the spatial scale of observation (e.g., Rose and Leggett, 1990; Swartzman et al., 2002; Bertrand et al., 2004a), the analysis was later checked for range of robustness by using neighbourhood ranges between 3 and 30 km. Because results

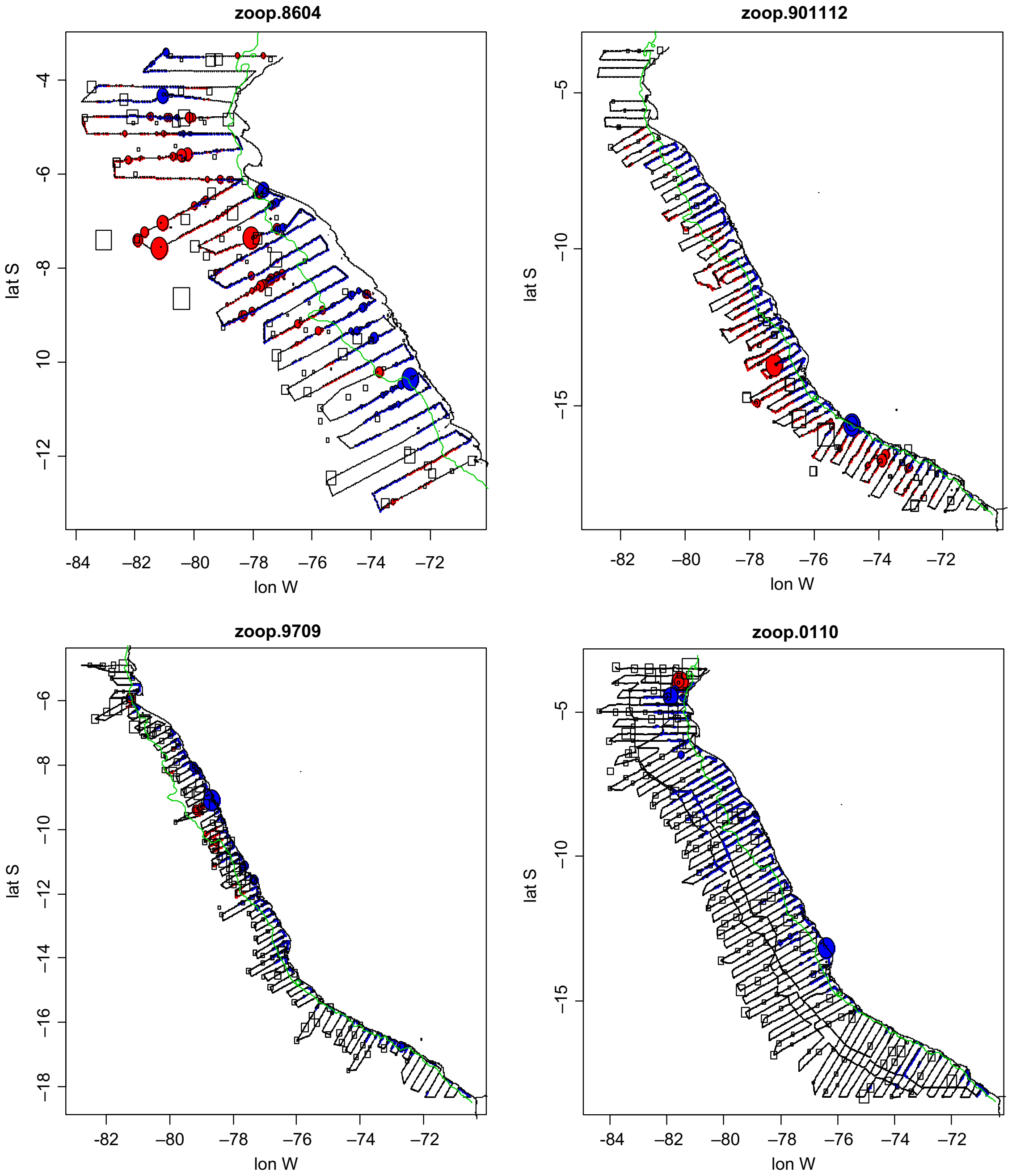

Fig. 1. Graphs of the survey transects along the Peruvian coast in (a) 1986 during a 'warm' period; (b) 1990, later in the 'warm' period; (c) 1997, during the El Nino; and (d) 2001 during a 'cold' period. The sardine and anchovy s_A per ESDU are shown with red and blue filled circles respectively proportional in area to s_A (for that survey). Zooplankton biovolume at zooplankton sampling locations are depicted by squares proportional in area to the biovolume. The 200-m isobath is shown with a green line.

were not significantly different over this range (i.e. they were robust) we only present results for the 5 km neighbourhood.

Since the shelf break location varies markedly along the Peruvian coastline (Fig. 1), we computed the distance in km of each sample location from the 200-m isobath (distance to the closest point at the same latitude). Negative values can be considered to be on-shelf and positive values off-shelf or on the continental slope. Thus, this variable separates the shelf from the abyssal area. Additional covariates associated with each sample location were sea surface temperature (SST), latitude (degrees S), and time of the day, also represented by a categorical day–night variable, and year and month of the sample.

We used classification and regression trees (CART, Brieman et al., 1984) to distinguish the relative importance of environmental and fish (anchoveta and sardine) effects on local zooplankton abundance. We modelled the logarithm of zooplankton biovolume using a regression tree with year, month, latitude, anchoveta and (separately) sardine in the 5 km neighbourhood, distance in km from the 200 m isobath, sea surface temperature (SST) and a day–night categorical covariate. In CART the dependent variable is modelled as a function of covariates. CART divides the data set through a sequence (tree) of binary splits on the values of one of the covariates at a time such that the overall variance in the dependent variable is minimized at each split. The CART tree is usually pruned to fewer nodes for clarity of explanation. For pruning the tree and validating the robustness of the CART results we used the recursive partitioning method (*rpart*; De'ath and Fabricius, 2000). This method divides the data set into a number of sub-

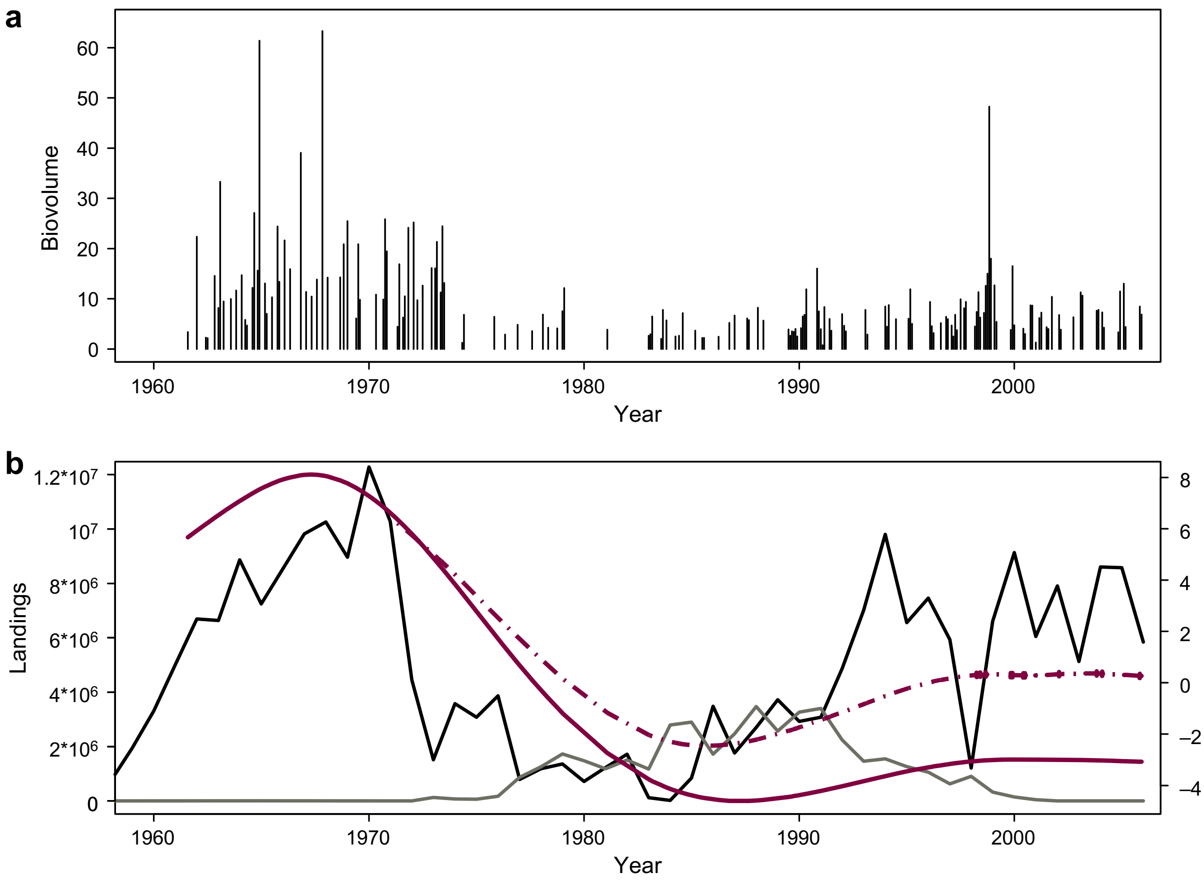

Fig. 2. Time series of (a) zooplankton biovolume (mL/sample) averaged by month; (b) commercial landings for anchovy (black solid line) and sardine (grey solid line), and smoothed trend of biovolume for all zooplankton samples (red continuous line) and night-time samples (red dotted line), the right *y*-axes is relative and corresponds to the spline smoother that was fitted on the data such that a *y*-value of zero is the mean effect of the variable (time) on the response (biovolume). (For interpretation of the references to color in this figure legend, the reader is referred to the web version of this article.)

groups (we used 10 groups following De'ath and Fabricius, 2000) and then repeats the CART analysis sequentially, removing one subgroup each time. This replication gives a measure of robustness in the node splits in CART. Using a graph of the relative performance (i.e., the total model variance plus the number of nodes multiplied by a weighting factor, against the weighting factor) we chose a weighting factor such that the relative performance did not improve markedly with the addition of more nodes. To further examine the overall relationship between mean biovolume and the local covariates used in the CART model we used a Generalized Additive Model (GAM, Hastie and Tibshirani, 1990) regression. We chose the Poisson distribution, which is often used for counts of animals, because the 'link function' for the Poisson distribution requires a logarithmic transformation of the dependent variable, making it similar to the log transformation used in the CART model. The independent variables in the GAM regression were the same as those used for the CART model except instead of day–night we used actual time of day.

3. Results

3.1. Zooplankton and forage fish dynamics, population scale

Time series on pelagic fish landings and zooplankton biovolumes are presented in Fig. 2. Anchoveta and sardine landings according to time (Fig. 2b) have already been presented by several authors (e.g. Chavez et al., 2003; Alheit and Niquen, 2004). Anchovy landings were high during two periods: the 1960s and early 1970s, and the period since the mid-1990s. Sardine captures were highest from the mid 1970s to the mid-1990s. Zooplankton biovolume (Fig. 2a and b) was very high until the early 1970s, then drastically decreased. Biovolume remained low until later in the 1980s and then increased, but without reaching the levels observed during the 1960s. Zooplankton biovolume and anchoveta landings are globally in phase (out of phase with sardine), in particular when considering nocturnal biovolume (Fig. 2b).

3.2. Local effects: CART models

Based on the recursive partitioning method in CART we chose a penalty value cp = 0.0059, which resulted in nine nodes, these being the number of nodes having minimum relative error (total error with a penalty for additional nodes). Neither sardine local abundance (s_A) nor latitude (both included in the CART model) had a major effect on zooplankton biovolume (Table 1), while anchoveta abundance had the strongest effect (i.e. it was the first split in the CART; Table 1). The lowest overall biovolume occurred with high levels of anchoveta ($s_A > 543\ \mathrm{m}^2\ \mathrm{nmi}^{-2}$), particularly on the shelf during winter and summer months. This is an indication of local depletion of zooplankton by anchoveta. Since 1992.5 (mid-1992), the biovolume of zooplankton was lower on the shelf than farther offshore (for anchoveta $s_A < 543\ \mathrm{m}^2\ \mathrm{nmi}^{-2}$). Interestingly, the night-time samples offshore had medium (not low) levels of zooplankton associated with higher levels of anchoveta (Table 1). The low on-shelf zooplankton biovolume associated with high anchoveta abundance may reflect the targeting of zooplankton

Table 1
CART results for logarithm of zooplankton biovolume with year, month, latitude, distance from the 200 m isobath (dist200; in km), sea surface temperature, anchovy and sardine s_A within 5 km of the zooplankton samples, and whether the sample was taken during the daytime or at night. Numbers of observations at each node are in parentheses. Number of splits from the top of the CART tree is shown with bold symbols.

Anchovy s_A(m^2 nmi^{-2})	Year	Dist200	Month	SST	Day–night	Log (vol)
⩾543			spring, autumn			1.38 (364) **2**
“ “		<−26.9 (shelf)	summer, winter			0.04 (307) **3**
“ “		⩾−26.9 (shelf-break, offshore)	“ “		Day	0.53 (269) **4**
“ “		“ “			Night	1.27 (277) **4**
<543	before 1992.5					1.27 (1281) **2**
“ “	since 1992.5	<13.15 (shelf, shelf-break)	June, July, January, March, November	<21.2		0.94 (400) **5**
“ “	“ “	⩾13.15 (offshore)	“ “	“ “		1.51 (542) **5**
“ “	“ “		“ “	⩾21.2		1.85 (649) **4**
“ “	“ “		February, April–May, August–September, December			1.95 (1827) **3**

found near shore by the high abundance anchoveta aggregations. In the off-shelf region the zooplankton abundances near high anchoveta aggregations were greater than on-shelf. There was a notable day–night difference.

3.3. Local effects: GAM models

GAM results (Fig. 3) illustrated the ‘classic’ overall day–night effect as a significant time-of-day change in zooplankton biovolume. The observation in CART of higher biovolume in the spring and autumn near high anchoveta s_A and in selected months under lower anchoveta s_A and different environmental conditions (Table 1) is different than the GAM model which shows a more ‘classic’ winter low, spring and summer high effect on biovolume. These results are not necessary contradictory, since the CART seasonal pattern also depends on local anchoveta abundance, while the GAM pattern does not. The CART observation that off-shelf biovolume was often higher than shelf biovolume was shown in the GAM relationship of the mean biovolume to distance from the 200 m isobath, with peak biovolume occurring at around 150 km offshore of the 200 m isobath, but with not much change between 50 and 200 km offshore of that isobath. The year effect showed an increase in biovolume between the end of the 1980s and 1998, a small dip in 1998–2000 and a further stabilization thereafter. The latitude effect showed a general increase in biovolume north to south. The sea surface temperature effect had two peaks, with a slight dip at about 20 °C. The second peak was significantly higher, which agrees with the CART result, which suggested a temperature effect, with a split around 21° and higher biovolume above this split. Finally, although both neighbourhood (within 5 km) anchoveta and sardine acoustic biomass (s_A) effects on zooplankton biovolume were significant in the GAM, the anchoveta effect was stronger ($p < 10^{-7}$ for anchoveta and $p = 6.0 \times 10^{-4}$ for sardine based on χ^2-values for non-parametric effects). The anchoveta effect sug-

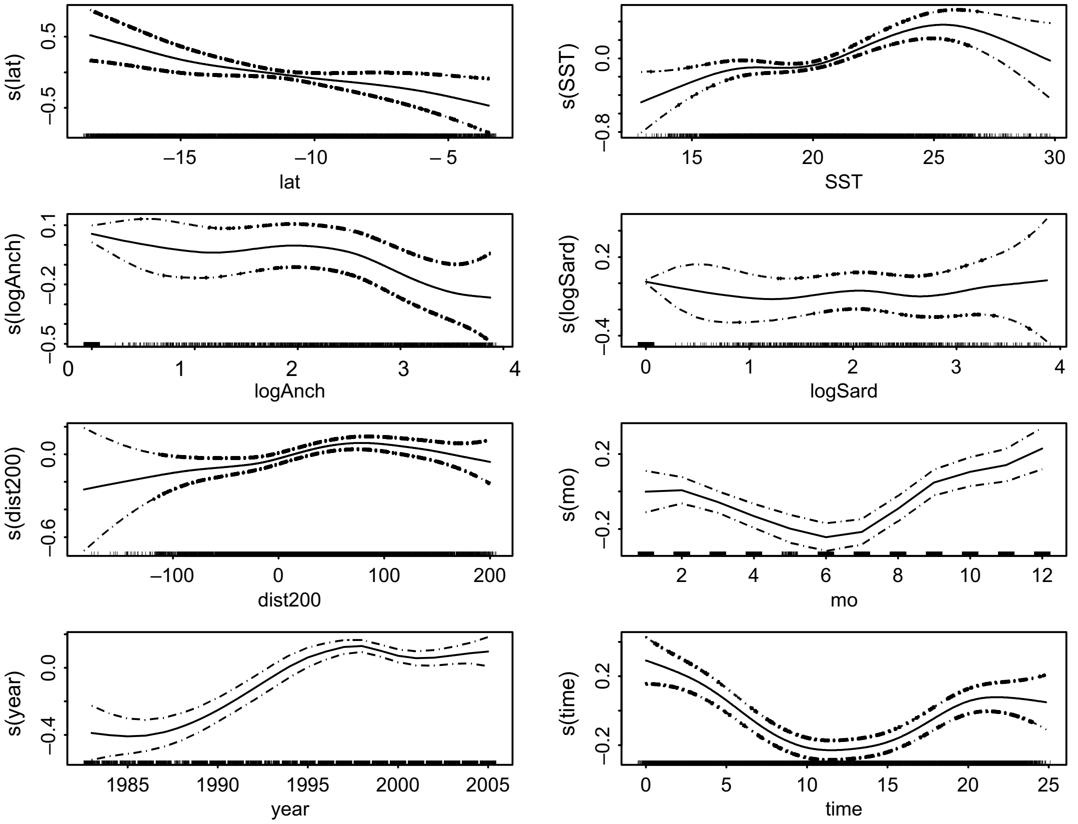

Fig. 3. GAM smooths for the effects on zooplankton biovolume of survey year and month and local variables time of day, sea surface temperature, distance from the 200-m isobath (km), and the logarithm (base 10) acoustic biomass (s_A) of anchovy and sardine within 5 km of the net haul.

gested a decline in local zooplankton biovolume with increasing fish biomass (Fig. 3). The small significance level appears to depend on an extremely large sample size including zooplankton samples for all acoustic surveys (15133 samples).

4. Discussion

4.1. Population abundance: bottom-up control

Our results show that the multi-year trend of both zooplankton biovolume and anchoveta landings are globally in phase (Fig. 2), which provides further evidence for bottom-up control by zooplankton on the anchoveta population, as previously suggested by Alheit and Niquen, 2004. In particular, they indicated that the decrease of the anchoveta population in the early 1970s was caused partially by a decrease of its food source, but they stated that there was no clear indication whether the early phase of the anchoveta recovery during the 1980s was based on an increase of zooplankton. The time series on zooplankton data they relied on was not long enough to show the increasing trend in zooplankton biovolume from the 1980s to nowadays. This was presented by Ayón et al. (2004) and for a somewhat longer time period here (Fig. 2), although absolute values of recent zooplankton biovolume are far below the ones observed during the 1960s. It is difficult to understand these differences (Ayón et al., 2004). Obviously patterns and processes are not simple and ecosystem functioning cannot be reduced to 'simple' trophic controls even if the bottom-up forcing seems dominant. Taylor et al., 2008 also concluded there was bottom-up control for anchoveta using a modelling approach. Others (Alheit and Niquen, 2004; Bertrand et al., 2004b; Swartzman et al., 2008) suggested how water masses, and their intrinsic characteristics in terms of hydrology, and primary and secondary production, drive the abundance and distribution of forage fish species. For instance, the latest anchoveta 'dominance' period we are experiencing since 1992, but particularly since the 1997–1998 El Niño event (Gutiérrez et al., 2007), corresponds to overall colder conditions (Francisco Chavez pers. com.) along the Peruvian coast that led to an extension of cold coastal upwelling waters (Swartzman et al., 2008), high levels of primary production (Francisco Chavez pers. com. and Fig. 5 in Alheit and Niquen, 2004) and high zooplankton abundance (Fig. 2). The typical bottom-up control in the northern HCS does not support the wasp-waist control hypothesis (Cury et al., 2000, 2003), which considers forage fish species to be the driving force in upwelling ecosystems for both higher and lower trophic levels.

4.2. Distribution patterns: local depletion effect

Predation effects of fish on zooplankton are difficult to observe, because predation is a local phenomenon requiring simultaneity in space and time of both predator and prey and the scale of sampling can hardly replicate this simultaneity. On the other hand, the pervasive abundance of anchoveta in some regions may provide an opportunity for observing reduction of zooplankton in regions of high predation. The main uncertainty in such relationships is separating the effect of predation from the effect of production, since some samples may show low abundance due to poor growing conditions rather than higher predation. Our study relies on a large sample which provides an opportunity to find an effect of predation if it exists, and to distinguish it from the noise commonly found in such labile ecosystems due to variability in local conditions, recent history, sampling variability and the mixing of many sizes and species of zooplankton into a single sample number; the biovolume.

Our results strongly suggest local reduction in zooplankton biovolume by anchoveta predation in neighbourhoods where anchoveta abundance is high. This is supported by several pieces of evidence. The CART analysis suggested that when anchoveta abundance within 5 km of the zooplankton samples was high (s_A above 543 $m^2\ nmi^{-2}$) average zooplankton abundance was significantly lower than zooplankton abundance in areas having lower density of anchoveta in the region. The anchoveta effect was the most important effect found by CART, as shown by the highest level split in the data being on anchoveta abundance (Table 1). This suggests that anchoveta abundance has more influence on local zooplankton biovolume than any other covariate, including year, latitude, SST, distance onshore or offshore of the shelf break (200 m isobath), sardine abundance, time of day and month. Furthermore, sensitivity analysis on the distance from samples (currently 5 km) to define the region of influence of anchoveta showed the anchoveta abundance to be the most important factor for distances between 3 km and 30 km suggesting a highly robust effect. These results are also seen in the GAM analysis, which differs from CART in design by considering effects due to smooths of covariates, rather than thresholds and in not explicitly including multivariate interactions. In GAM, zooplankton biovolume decreased with increasing anchoveta abundance over a range of anchoveta s_A from 0 to 4000 $m^2\ nmi^{-2}$ (up to 3.6 in $\log_{10}$ scale), with a stronger effect for high value of s_A ($\log_{10}$ value between 2.5 and 3.0; Fig. 3), close to the threshold observed from the CART analysis ($\log_{10}(543) = 2.73$).

We think the apparent depression of zooplankton near high anchoveta densities is highly unlikely to be due to lower production, since anchoveta is more prevalent in highly productive upwelling and mixed waters than in less productive oceanic or equatorial waters (Alheit and Niquen, 2004; Bertrand et al., 2004b; Gutiérrez et al., 2007; Swartzman et al., 2008). Anchoveta is a plankton predator, depending much more on zooplankton than on phytoplankton. Zooplankton, particularly euphausiids and large copepods, accounts for about 98% of its diet in carbon (Espinoza and Bertrand, 2008). It is therefore not surprising to see a local effect of anchoveta foraging when large fish aggregations are concerned. It is important to note that the results we obtained were limited by the lack of reliability of euphausiid abundance (67.5% of anchoveta diet in carbon) from Hensen net sampling. We probably mainly detected an anchoveta effect on copepods (23.6% of anchoveta diet in carbon), which are better sampled by these nets. Ongoing estimation of euphausiid abundance from historical acoustic data may soon provide better data on euphausiids (Michael Ballón, pers. com.). The depletion effect we observed is only local (i.e. up to 30 km) and does not constitute large-scale or long-term control on plankton population. Finally, sardine, which forages at a lower trophic level than anchoveta (Konchina, 1991; van der Lingen, 2002, 2006, in press), has no evident impact on zooplankton biovolume. The 300 μm mesh net used for plankton sampling allows a rather good representation of the prey community of anchoveta (except for euphausiids) which forage efficiently at sizes higher than 200–250 μm, particularly from 580 μm (van der Lingen et al., 2006) but not for sardine which is able to forage directly on net-phytoplankton (20–200 μm). Studying potential local sardine impact on its prey community would therefore require sampling based on a finer mesh.

Apart from the anchoveta's impact on zooplankton biovolume we observed other covariate effects. We observed a significant and clear diel effect (Table 1, Fig. 3), with higher zooplankton biovolumes during the night. This classic result is likely mainly due to both reduced gear selectivity during the daytime and to diel migration of zooplankton where some zooplankton migrate below the top 50 m of the water column during the daytime. Zooplankton biovolume was higher from the shelf break to 100 km offshore, which corresponds to rather warm temperatures (Table 1; Fig. 3). Such results may be related to the offshore transport of the maturing production, leading that part of the zooplankton community to be distributed away from the coast where the predation is limited as anchoveta has a rather coastal distribution (Bertrand et al., 2004b; Gutiérrez et al., 2007; Swartzman et al., 2008), but also where diel migration can allow zooplankton some daytime protection from anchoveta predation (Bertrand et al., this issue; Escribano et al., in press; Espinoza and Bertrand, 2008). The month effect on zooplankton biovolume was also very clear with higher biovolume in summer than in winter (Fig. 3), which is consistent with enhanced primary production in austral summer (Francisco Chavez, com. pers.).

Other studies illustrated similar direct effects of predation on the distribution and abundance of organisms in the ocean. For instance, Swartzman et al. (2002) and Winter and Swartzman (2006) evidenced an inverse relationship between the local abundance of juvenile pollock (*Theragra chalcogramma*) and zooplankton near the Pribilof Islands, Alaska. Hunt et al., 2002 provided direct evidence of heavy predation of murres (*Uria aalge*) on juvenile pollock upwelled onto a shelf in the Pribilof Canyon, Alaska. Bertrand et al., 2004a found that in the southern part of the HCS, the biomass of the mesopelagic community was lower in areas where high abundance of jack mackerel (*Trachurus murphyi*), their main predator, was observed.

In summary, at the local scale there is clear evidence for a depletion effect on zooplankton biovolume by high neighbourhood densities (spatial range: 3–30 km) of anchoveta. At the population level anchoveta biomass and zooplankton biovolume appeared to co-vary on a multi-year basis. The increase in zooplankton and anchoveta biomass since the 1990s corresponds to a colder period with enhanced primary production in the HCS (Francisco Chavez com. pers.). Thus, although zooplankton likely exerts a bottom-up control on the anchoveta population, when locally abundant anchoveta can induce local depletion (independent of the total anchoveta population level) of zooplankton abundance.

Acknowledgements

The authors gratefully thank the Instituto del Mar del Perú (IMARPE) for having facilitated the use of the data. This work was supported in part by the US National Science Foundation through grant number NSF0075 to two of the investigators (gls and sb). This work is a contribution of the Research Unit 'Upwelling Ecosystems' UR 097 and of the Interdepartmental Thematic Action "Humboldt Current System" from IRD. We also wish to acknowledge and thank the IMARPE staff in the acoustics and zooplankton programs, especially the many zooplankton researchers involved in collecting and analyzing the samples.

References

Alheit, J., Niquen, M., 2004. Regime shifts in the Humboldt Current ecosystem. Progress in Oceanography 60, 201–222.

Ayón, P., Purca, S., Guevara-Carrasco, R., 2004. Zooplankton volumes trends off Peru between 1964 and 2001. ICES Journal of Marine Science 61, 478–484.

Bakun, A., Broad, K., 2003. Environmental 'loopholes' and fish population dynamics: comparative pattern recognition with focus on El Niño effects in the Pacific. Fisheries Oceanography 12, 458–473.

Bertrand, A., Barbieri, M.A., Córdova, J., Hernández, C., Gómez, F., Leiva, F., 2004a. Diel vertical behaviour, predator–prey relationships, and occupation of space by jack mackerel (*Trachurus murphyi*) off Chile. ICES Journal of Marine Science 61, 1105–1112.

Bertrand, A., Segura, M., Gutiérrez, M., Vásquez, L., 2004b. From small-scale habitat loopholes to decadal cycles: a habitat-based hypothesis explaining fluctuation in pelagic fish populations off Peru. Fish and Fisheries 5, 296–316.

Bertrand, A., Gerlotto, F., Bertrand, S., Gutiérrez, M., Alza, L., Chipollini, A., Diaz, E., Espinoza, P., Ledesma, L., Quesquén, R., Peraltilla, S., Chavez, 2008. Schooling behaviour and environmental forcing in relation to anchoveta distribution: an analysis across multiple spatial scales. Progress in Oceanography 79, 264–277.

Brieman, F., Friedman, J.H., Losen, R.A., Stone, C.J., 1984. Classification and Regression Trees. Wadsworth and Brooks/Cole, Monterrey. p. 172.

Chavez, F.P., Ryan, J., Lluch-Cota, S.E., Ñiquen, M., 2003. From anchovies to sardines and back: multidecadal change in the Pacific Ocean. Science 299, 217–221.

Csirke, J., Guevara-Carrasco, R., Cárdenas, G., Ñiquen, M., Chipollini, A., 1996. Situación de los recursos anchoveta (*Engraulis ringens*) y sardina (*Sardinops sagax*) a principios de 1994 y perspectivas para la pesca en el Perú, con particular referencia a las regiones norte y centro de la costa peruana. Boletín del Instituto del Mar del Perú 15, 1–23 (in Spanish, with English abstract).

Cury, P., Bakun, A., Crawford, R.J.M., Jarre, A., Quiñones, R.A., Shannon, L.J., Verheye, H.M., 2000. Small pelagics in upwelling systems: patterns of interaction and structural changes in "wasp-waist" ecosystems. ICES Journal of Marine Science 57, 603–618.

Cury, P., Shannon, L., Shin, Y.-J., 2003. The Functioning of Marine Ecosystems: a Fisheries Perspective In: Sinclair, M., Valdimarsson, G. (Eds.), Responsible Fisheries in the Marine Ecosystem, pp. 103–141.

De'ath, G., Fabricius, K.E., 2000. Classification and regression trees: a powerful yet simple technique for ecological data analysis. Ecology 8, 3178–3192.

Escribano, R, Hidalgo, P., Krautz, C., in press. Zooplankton associated with the oxygen minimum zone system in the northern upwelling region of Chile during March 2000. Deep-Sea Research II.

Espinoza, P., Bertrand, A., 2008. Revisiting Peruvian anchovy (*Engraulis ringens*) trophodynamics provides a new vision of the Humboldt Current system. Progress in Oceanography 79, 215–227.

Foote, K.G., Knudsen, H.P., Vestnes, D.N., MacLennan, D.N., Simmonds, E.J., 1987. Calibration of acoustic instruments for fish density estimation: a practical guide. ICES Cooperative Research Report No. 144, pp. 1–69.

Gutiérrez, M., Swartzman, G., Bertrand, A., Bertrand, S., 2007. Anchovy and sardine spatial dynamics and aggregation patterns in the Humboldt Current ecosystem, Peru, from 1983–2003. Fisheries Oceanography 16, 155–168.

Hastie, T., Tibshirani, R., 1990. Generalized Additive Models. Chapman and Hall, London.

Hunt Jr., G.L., Stabeno, P., Walters, G., Sinclair, E., Brodeur, R.D., Napp, J.M., Bond, N.A., 2002. Climate change and control of the southeastern Bering Sea pelagic ecosystem. Deep Sea Research II 49, 5821–5853.

Konchina, Y.V., 1991. Trophic status of the Peruvian anchovy and sardine. Journal of Ichthyology 31, 59–72.

Kramer, D., Kalin, M., Stevens, E.G., Thrailkill, J.R., Zweifel, J.R., 1972. Collecting and processing data on fish eggs and larvae in the California Current region. NOAA Technical Report NMFS Circ-370, pp. 1–38.

MacLennan, D.N., Fernandes, PG., Dalen, J., 2002. A consistent approach to definitions and symbols in fisheries acoustics. ICES Journal of Marine Science 59, 365–369.

Rose, G.A., Leggett, W.C., 1990. The importance of scale to predator–prey spatial correlation: an example of Atlantic fishes. Ecology 71, 33–43.

Sifeddine, A., Gutiérrez, D., Ortlieb, L., Boucher, H., Velazco, F., Field, D., Vargas, G., Boussafir, M., Salvatteci, R., Ferreira, V., García, M., Valdés, J., Caquineau, S., Mandeng Yogo, M., Cetin, F., Solis, J., Soler, P., Baumgartner, T., 2008. Laminated sediments from the central Peruvian continental slope: a 500 year record of upwelling system productivity, terrestrial runoff and redox conditions. Progress in Oceanography 79, 190–197.

Swartzman, G.L., Napp, J., Brodeur, R., Winter, A., Ciannelli, L., 2002. Spatial patterns of pollock and zooplankton distribution in the Pribilof Islands, Alaska nursery area and their relationship to pollock recruitment. ICES Journal of Marine Science 59, 1167–1186.

Swartzman, G., Bertrand, A., Gutiérrez, M., Bertrand, S., Vasquez, L., 2008. The relationship of anchovy and sardine to water masses in the Peruvian Humboldt Current System from 1983–2005. Progress in Oceanography 79, 228–237.

Taylor, M.H., Tam, J., Blaskovic, V., Espinoza, P., Ballón, M., Wosnitza-Mendo, C., Argüelles, J., Díaz, E., Purca, S., Ochoa, N., Ayón, P., Goya, E., Gutiérrez, D., Quipuzcoa, L., Wolff, M., 2008. Trophic modelling of the Northern Humboldt Current Ecosystem, Part II: Elucidating 2 ecosystem dynamics from 1995–2004 with a focus on the impact of ENSO. Progress in Oceanography 79, 366–378.

Valdés, J., Ortlieb, L., Marinovic, L., Gutiérrez, D., Vargas, D., Sifeddine, A., 2008. 250 years of sardine and anchovy scale deposition record in Mejillones Bay, Northern Chile. Progress in Oceanography 79, 198–207.

Van der Lingen, C.D., 2002. Diet of sardine *Sardinops sagax* in the southern Benguela upwelling ecosystem. South African Journal of Marine Science 24, 301–316.

Van der Lingen, C.D., Hutchings, L., Field, J.G., 2006. Comparative trophodynamics of anchovy *Engraulis encrasicolus* and sardine *Sardinops sagax* in the southern Benguela: are species alternations between small pelagic fish trophodynamically mediated? African Journal of Marine Science 28, 465–477.

Van der Lingen, C.D., Bertrand, A., Bode, A., Brodeur, R., Cubillos, L., Espinoza, P., Friedland, K., Garrido, S., Irigoien, X., Möllman, C., Rodriguez-Sanchez, R., Tanaka, H., Temming, A., in press. Trophic dynamics of small pelagic fish. In: Checkley, D.M.Jr., Roy C., Alheit, J. (Eds.), Climate Change and Small Pelagic Fish (Chapter 8). ISBN:9780521884822.

Winter, A.G., Swartzman, G.L., 2006. Interannual changes in distribution of age-0 walleye Pollock near the Pribilof Islands, Alaska, with reference to the prediction of Pollock year-class strength. ICES Journal of Marine Science 63, 1118–1135.

Progress in Oceanography 79 (2008) 215–227

Contents lists available at ScienceDirect

Progress in Oceanography

journal homepage: www.elsevier.com/locate/pocean

Revisiting Peruvian anchovy (*Engraulis ringens*) trophodynamics provides a new vision of the Humboldt Current system

Pepe Espinoza [a,*], Arnaud Bertrand [a,b]

[a] *Instituto del Mar del Perú, Esquina Gamarra y Gral. Valle s/n, Apartado 22, Callao, Lima, Peru*
[b] *Institut de Recherche pour le Développement (IRD), CRH, Avenue Jean Monnet, BP 171, 34203 Sète Cedex, France*

ARTICLE INFO

Article history:
Accepted 14 October 2008
Available online 21 October 2008

Keywords:
Anchoveta *Engraulis ringens*
Carbon content
Diel feeding behaviour
Trophodynamics
Peru Humboldt Current system
Plankton

ABSTRACT

The Peruvian anchovy or anchoveta (*Engraulis ringens*) forages on plankton and is a main prey for marine mammals, seabirds, fish, and fishers, and is therefore a key element of the food web in the Humboldt Current system (HCS). Here, we present results from the analysis of 21,203 anchoveta stomach contents sampled during 23 acoustic surveys over the period 1996–2003. Prey items were identified to the genus level, and the relative dietary importance of different prey was assessed by determination of their carbon content. Variability in stomach fullness was examined relative to the diel cycle, the distance from the coast, sea surface temperature, and latitude, using generalized additive models (GAMs). Whereas phytoplankton largely dominated anchoveta diets in terms of numerical abundance and comprised >99% of ingested prey items, the carbon content of prey items indicated that zooplankton was by far the most important dietary component, with euphausiids contributing 67.5% of dietary carbon followed by copepods (26.3%). Stomach fullness data showed that anchoveta feed mainly during daytime between 07h00 and 18h00, although night-time feeding also made a substantial contribution to total food consumption. Stomach fullness also varied with latitude, distance from the coast, and temperature, but with substantial variability indicating a high degree of plasticity in anchoveta feeding behaviour. The results suggest an ecological role for anchoveta that challenges current understanding of its position in the foodweb, the functioning of the HCS, and trophic models of the HCS.

1. Introduction

The Peruvian anchovy or anchoveta *Engraulis ringens*, is ecologically and economically the most important pelagic fish species in the Humboldt Current system (HCS). Anchoveta is the major prey of the principal top predators including marine mammals, seabirds, fish and fishers, and more than 250 million tons of anchoveta have been harvested by the purse seine fishery since the 1950s. Anchoveta forage on plankton and is a key element of the marine food web in the HCS and have been the subject of many studies (e.g. the books edited by Pauly and Tsukayama, 1987; Pauly et al., 1989a).

The first trophodynamic studies on anchoveta in Peru concluded that anchoveta subsisted mainly on phytoplankton (Rojas, 1953; Rojas de Mendiola, 1969), and the ability of clupeoids like anchoveta to feed at low trophic levels (directly on primary producers) was suggested as the reason such large populations, biomasses and fisheries could be sustained in upwelling systems (Ryther, 1969). Later studies suggested that in addition to filter-feeding on phytoplankton, anchoveta could also particulate feed on zooplankton (Rojas de Mendiola, 1989; Alamo, 1989), and zooplankton was sometimes considered equally important as phytoplankton in anchoveta diets (Alamo, 1989; Pauly et al., 1989b; Jahncke et al., 2004). With the exception of Konchina (1991), who suggested that anchoveta preferentially consume zooplankton, all other recent work in the HCS has concluded that anchoveta depends mainly on phytoplankton (Alamo et al., 1996a,b, 1997a,b; Alamo and Espinoza, 1998; Espinoza et al., 1998a,b, 1999, 2000). However, these studies were based on counts of anchoveta prey, a method considered to be inadequate for estimating dietary importance (James, 1987; Konchina and Pavlov, 1995). In contrast, methods based on prey weight (e.g. gravimetric) or on nutritional value (e.g. carbon content, caloric or energetic value) may be more ecologically relevant (Hyslop, 1980; Koslow, 1981; James, 1987; Konchina and Pavlov, 1995; van der Lingen et al. 2006, in press). In other upwelling systems, these latter methods indicate that zooplankton, rather than phytoplankton, support clupeoid populations (e.g. Koslow, 1981; James, 1987; James and Chiappa-Carrara, 1990; Chiappa-Carrara and Gallardo-Cabello, 1993; van der Lingen et al., 2006).

Konchina (1991) results highlighting the significance of zooplankton in the diet of anchoveta were based on gravimetric analysis of prey importance, but his study was based on a very small sample size ($n = 65$ fish). Here we revisit Peruvian anchoveta diet

---

[*] Corresponding author. Tel.: +56 1 4202000.
E-mail addresses: pespinoza@imarpe.gob.pe (P. Espinoza), Arnaud.Bertrand@ird.fr (A. Bertrand).

0079-6611/$ - see front matter © 2008 Elsevier Ltd. All rights reserved.
doi:10.1016/j.pocean.2008.10.022

and feeding behaviour in Peru using a database which contains information on the stomach contents of 21,203 anchoveta sampled along the Peruvian coast (1996–2003). In particular we assess the relative importance of different prey types to anchoveta using a method which estimates the carbon content of prey items. We also describe variations in anchoveta stomach fullness in relation to the diel cycle, latitude, distance to the coast, and sea surface temperature, using generalized additive models. Our results confirm Konchina (1991) finding that Peruvian anchoveta subsist primarily on zooplankton, and suggest an ecological role for anchoveta that challenges current understanding of the functioning of the HCS.

2. Materials and methods

2.1. Sampling

Data were collected during 23 IMARPE (Instituto del Mar del Perú) acoustic surveys between 1996 and 2003 with the aim of estimating pelagic fish abundance in the Peruvian EEZ (Table 1). Fish were collected by pelagic trawling conducted throughout the survey area (Fig. 1), and a sub-sample of 10–50 anchoveta was randomly collected from each trawl. At sea, individual anchoveta were measured (total length) to the nearest 0.5 cm and weighed to the nearest 0.1 g, and the cardiac and pyloric sections of their stomachs were extracted fixed in 5% formalin. In the laboratory, stomach contents were extracted and weighed (wet weight, WW) to the nearest 0.01 g for samples collected between 1996 and the summer of 2001, and to the nearest 0.001 g thereafter. Stomach fullness was calculated by dividing individual stomach content weight by fish wet weight and was expressed as a percentage of fish wet weight (Hureau, 1970). The stomach contents of individual fish were then pooled into 2 cm size classes for each sub-sample, and pooled stomach contents were filtered through a 125 μm mesh. The filtered material was diluted to 100 mL using filtered seawater and a 0.1 mL sub-sample was examined under the compound microscope to identify and count phytoplankton prey. The material that remained on the mesh was diluted to 100 mL using filtered seawater and a 10 mL sub-sample was examined using a stereoscopic microscope to identify (to genus) and count zooplankton prey. All prey counts were then standardized to number per 100 mL, except for anchoveta eggs, for which the whole sample was examined.

2.2. Estimation of prey volume, dry weight and carbon content

Different procedures were followed to estimate the carbon content of phytoplankton and zooplankton and hence determine their relative dietary importance. We did not measure the size of any prey items but instead used information from the literature to estimate prey size; the lack of available references on size and volume for planktonic organisms off Peru led us to use a wide range of references published for other ecosystems. Phytoplankton size was converted to phytoplankton cell volume using references describing the organism's geometric shape and providing equations relating shape to volume, with the coefficients for each equation being obtained from the literature or from estimations made by IMARPE (Table 2). To transform volume into carbon content we used equations given in Menden-Deuer and Lessard (2000) and Verity and Langdon (1984) (Table 4). For zooplankton, prosome or total organism length was estimated from the literature or from some direct measurements made by IMARPE on zooplankton from stomach content samples (Table 3). Zooplankton dry weight and carbon content were calculated using equations given by Alexandrov (2001), Deibel (1986), James (1987), van der Lingen (2002), Parsons et al. (1984) and Sameoto (1971) (Table 4). All prey carbon content values were standardized to μg C, and were expressed as a percentage of all fish examined in each cruise.

2.3. Data analysis

For each survey from which anchoveta were collected for trophodynamic analysis we sought potential relationships between stomach fullness and the diel cycle, latitude, distance to the coast, and sea surface temperature. As the relationships are likely to be nonlinear and multivariate, a generalized additive modelling (GAM) approach was used (Hastie and Tibshirani, 1990) using S-Plus software (Insightful Corporation, Seattle, WA, USA). Cubic spline smoothers were used to estimate these nonparametric functions, and separate GAM models were performed for each survey, and also for all the surveys combined.

3. Results

A total of 21,203 anchoveta (*E. ringens*) ranging from 3 to 18 cm total length were analysed (Table 1). In total, 132 prey taxa were

Table 1
Survey code, start and end date, the number of trawls, and the number, length range (in cm) of anchoveta collected for stomach content analysis during this study.

Survey code	Start date	End date	No. of trawls	No. of stomach	Anchoveta length range (Min–Max)
960204	10 February 1996	01 April 1996	49	633	9–19
960809	11 August 1996	27 September 1996	70	1021	5.5–19.5
961112	16 November 1996	19 December 1996	39	639	9.5–19
970204	13 Feb 1997	23 April 1997	45	739	8–19.5
970910	04 September 1997	05 October 1997	51	1259	6.5–19
980305	27 March 1998	01 May 1998	35	687	9.5–18
980809	23 August 1998	17 September 1998	36	624	4–16
981112	30 November 1998	21 December 1998	36	798	4–16.5
990203	14 February 1999	28 March 1999	75	1266	10–17
990809	28 August 1999	17 September 1999	19	336	10–18
991112	12 November 1999	14 December 1999	70	1412	8–18
000102	20 January 2000	26 February 2000	124	2277	6.5–18.5
000607	10 June 2000	06 July 2000	50	928	7.5–18.5
000809	28 August 2000	23 September 2000	38	574	7–18.5
001011	11 October 2000	13 November 2000	45	846	6.5–18
010204	03 March 2001	10 April 2001	78	1630	8.5–18.5
010708	05 July 2001	06 August 2001	83	1596	6.5–19
020203	21 February 2002	18 March 2002	83	1650	7–18
0208	10 August 2002	31 August 2002	30	281	9.5–17
021011	01 October 2002	13 November 2002	36	416	10–17
030203	26 February 2003	31 March 2003	45	524	6.5–17.5
030809	16 August 2003	15 September 2003	26	243	7.5–17.5
031012	24 October 2003	10 December 2003	36	824	4.5–17.5

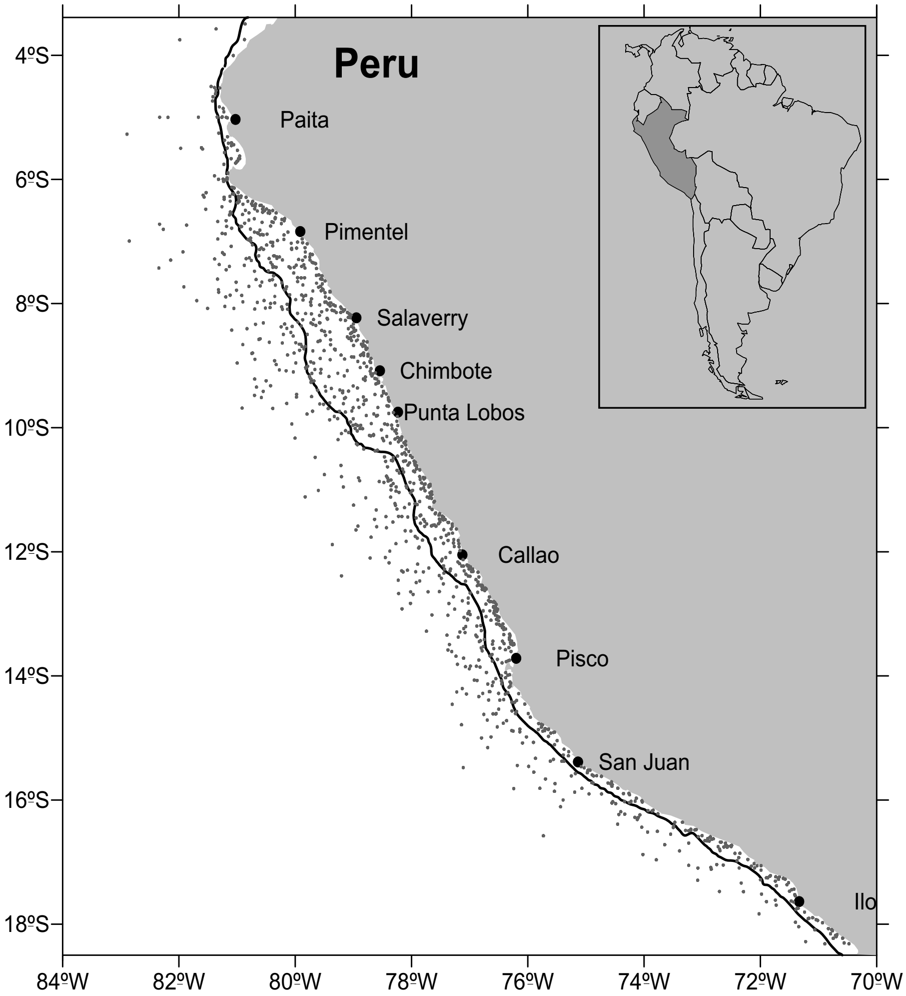

Fig. 1. The locations of trawls (grey dots) from which anchovetas were collected for trophodynamic analysis. The black solid line indicates the 200 m isobaths.

identified: 38 diatoms, 16 dinoflagelates, 2 silicoflagelates, 1 phytoflagelate, 4 microflagellates, 9 tintinnids, 34 copepods, and 28 other items (Tables 2 and 3). Mean stomach fullness was 0.68% of fish WW, and varied between 0.29% WW in February–March 1999 and 1.23% WW in August–September 1998 (Fig. 2).

3.1. Dietary composition

Numerically, phytoplankton dominated anchoveta diet and comprised 99.52% of all ingested prey; copepods represented only 0.07%, euphausiids 0.003%, and other prey items accounted for only 0.40% of the total number of prey (Fig. 2). This view of anchoveta diet changes dramatically when prey carbon content is considered (Fig. 2); zooplankton was by far the most important component and contributed 98.0% of dietary carbon, whilst phytoplankton contributed only 2.0%. Among zooplankters, euphausiids dominated (contributing 67.5% of dietary carbon), followed by copepods (26.3%), and other zooplankton (4.2%). Other groups were much less important in terms of their carbon contribution, including Gastropoda (0.76%), Polychaeta (0.75%), lantern fish (*Vinciguerria lucetia* and myctophids) (0.45%), anchoveta eggs (0.40%), Amphipoda (0.40%), Bivalvia (0.31%), zoea (0.29%), megalopa (0.29%), and the red shrimp *Pleuroncodes monodon* (0.01%), but their presence illustrates the omnivorous feeding behaviour of anchoveta.

The phytoplankton carbon fraction (2%) was dominated by the diatoms *Coscinodiscus* (54.0%), *Thalassiosira* (14.6%), *Ditylum* (8.1%), and by the dinoflagellate *Protoperidinium* (6.7%). The copepod carbon fraction was dominated by the genera *Eucalanus* (69.9%), *Calanus* (12.8%) and *Centropages* (6.6%), whilst *Corycaeus* (1.3%), *Candacia* (1.2%), *Paracalanus* (1.0%) and *Scolecithrix* (1.0%) were of lesser importance.

Our results vary depending on the parameters and relationships used to estimate prey carbon content (Tables 2–4). To test the robustness of our results we re-calculated dietary carbon after increasing twofold the relative volume (and thus carbon content) of phytoplankton items and decreasing the relative size of main zooplankton items by a third. Despite these changes our results were similar to those described above; even in the most ‘extreme’ case where phytoplankton was increased and zooplankton decreased by the maximum amounts the contribution by phytoplankton to anchoveta dietary carbon only reached 6% of the total, which appears to confirm the robustness of our results.

Whereas the relative contribution to anchoveta dietary carbon made by different prey types varied between surveys, no seasonal trend could be identified (Fig. 2). Phytoplankton reached maximum levels (40.7% of total carbon content) in anchoveta diet in August–September 1996, and minimum levels (0.07%) in June–July 2000. The contribution of euphausiids was high (⩾80% of total carbon content) during November–December 1996, February–April and September–October 1997, August–September 1999, January–February and August–September 2000, and July–August 2001,

Table 2

Shape, size and volume of phytoplankton cells recorded from anchoveta stomach contents; cell volume was extracted from the literature (see references) or calculated from published geometric shapes and published or estimated cell sizes.

Genus	Geometric shape	Diameter (μm)	Length (μm)	Height (μm)	m[a] (μm)	Volume formula[b]	Volume values (μm^3)
Diatoms							
Actinoptychus	Cylinder[b]					$(\pi/4) \cdot d^2 \cdot h$	16,828[c]
Amphiprora	Elliptic prism[b]	10	35	10		$(\pi/4) \cdot d \cdot l \cdot h$	2749
Amphora	Cymbelloid[b]					$(1/6) \cdot \pi \cdot (2b)^2 \cdot a \cdot (\beta/360)$[d]	6187[c]
Asterionellopsis	Prism on triangle[b]		30	10[e]	10	$(½) \cdot l \cdot m \cdot h$	1500
Asteromphalus	Cylinder[b]	30		5		$(\pi/4) \cdot d^2 \cdot h$	3534
Bacteriastrum	Cylinder[b]	40		80		$(\pi/4) \cdot d^2 \cdot h$	100,531
Cerataulina	Cylinder[b]					$(\pi/4) \cdot d^2 \cdot h$	30,015[c]
Chaetoceros	Elliptic prism[b]					$(\pi/4) \cdot d \cdot l \cdot h$	3937[c]
Cocconeis	Elliptic prism[b]					$(\pi/4) \cdot d \cdot l \cdot h$	780[c]
Corethron	Cylinder + 2 half spheres[b]	20		100		$\pi \cdot r^2 \cdot l + (4/3) \cdot \pi \cdot r^3$[f]	35,605
Coscinodiscus	Cylinder[b]					$(\pi/4) \cdot d^2 \cdot h$	994,625[c]
Cylindrotheca	Prolate spheroid + 2 cylinders[b]					$(\pi/6) \cdot d^2 \cdot h + 2(\pi/4) \cdot d^2 \cdot h$	158[c]
Detonula	Cylinder[b]	40		40		$(\pi/4) \cdot d^2 \cdot h$	50,265
Ditylum	Prism on triangle[b]					$(1/2) \cdot l \cdot m \cdot h$	60,495[c]
Eucampia	Elliptic prism[b]	24	52	30		$(\pi/4) \cdot d \cdot l \cdot h$	9802
Fragilariopsis	Elliptic prism[b]					$(\pi/4) \cdot d \cdot l \cdot h$	190[c]
Grammatophora	Elliptic prism[b]					$(\pi/4) \cdot d \cdot l \cdot h$	9772[c]
Guinardia	Cylinder[b]					$(\pi/4) \cdot d^2 \cdot h$	144,013[c]
Gyrosigma	Prism on parallelogram[b]					$(1/2) \cdot l \cdot b \cdot h$[g]	63,513[c]
Hemiaulus	Elliptic prism[b]	30	90	10		$(\pi/4) \cdot d \cdot l \cdot h$	21,205.75
Lauderia	Cylinder[b]	50		90		$(\pi/4) \cdot d^2 \cdot h$	176,715
Leptocylindrus	Cylinder[b]					$(\pi/4) \cdot d^2 \cdot h$	1608[c]
Licmophora	Gomphonemoid[b]					[b]	11,870[c]
Lioloma	Box[b]	25	50	25		$l \cdot l' \cdot h$[h]	31,250
Lithodesmium	Prism on triangle[b]		34	20[e]	20	$(1/2) \cdot l \cdot m \cdot h$	6800
Navicula	Elliptic prism[b]					$(\pi/4) \cdot d \cdot l \cdot h$	3013[c]
Odontella	Elliptic prism[b]					$(\pi/4) \cdot d \cdot l \cdot h$	13,081
Planktoniella	Cylinder[b]	80		15		$(\pi/4) \cdot d^2 \cdot h$	75,398
Pleurosigma	Prism on parallelogram[b]					$(1/2) \cdot l \cdot b \cdot h$[g]	36,882
Proboscia	Cylinder[b]					$(\pi/4) \cdot d^2 \cdot h$	13,641
Pseudonitzschia	Prism on parallelogram[b]					$(1/2) \cdot l \cdot b \cdot h$[g]	646
Pseudosolenia	Cylinder[b]	50		300		$(\pi/4) \cdot d^2 \cdot h$	589,049
Rhizosolenia	Cylinder[b]					$(\pi/4) \cdot d^2 \cdot h$	108,532
Skeletonema	Cylinder + 2 half spheres[b]					$(\pi) \cdot r^2 \cdot l + (4/3) \cdot \pi \cdot r^3$[f]	459
Stephanopyxis	Cylinder + 2 half spheres[b]	40		60		$(\pi) \cdot r^2 \cdot l + (4/3) \cdot \pi \cdot r^3$[f]	108,909
Thalassionema	Box[b]					$l \cdot l' \cdot h$[h]	1252
Thalassiosira	Cylinder[b]					$(\pi/4) \cdot d^2 \cdot h$	14,390
Tropidoneis	Prism on triangle[b]		75	18[e]	18	$(1/2) \cdot l \cdot m \cdot h$	12,150
Dinoflagellates							
Ceratium	Ellipsoid + 2 cones + cylinder[b]					$(\pi/6) \cdot a \cdot b \cdot l + 2 \cdot (1/3) \cdot \pi \cdot r^2 \cdot z + (\pi/4) \cdot d^2 \cdot h$[jk]	47,435[i]
Dinophysis	Ellipsoid[b]					$(\pi/6) \cdot a \cdot b \cdot l$[j]	50,000 (assumed)
Diplopelta	Ellipsoid[b]					$(\pi/6) \cdot a \cdot b \cdot l$[j]	50,000 (assumed)
Diplopsalis	Cone + half sphere[b]					$(1/3) \cdot \pi \cdot r^2 \cdot z + (1/2) \cdot (4/3) \cdot \pi \cdot r^3$[fk]	50,000 (assumed)
Dissodium							50,000 (assumed)
Goniodoma	Sphere[b]					$(4/3) \cdot \pi \cdot r^3$[f]	50,000 (assumed)
Gonyaulax	2 cones[b]					$2 \cdot (1/3) \cdot \pi \cdot r^2 \cdot z$[k]	50,000 (assumed)
Gymnodinium	Ellipsoid[b]					$(\pi/6) \cdot a \cdot b \cdot l$[j]	88,099[i]
Oxophysis	2 cones[b]					$2 \cdot (1/3) \cdot \pi \cdot r^2 \cdot z$[j]	50,000 (assumed)
Podolampas	Cone[b]					$(1/3) \cdot \pi \cdot r^2 \cdot z$[k]	50,000 (assumed)
Pronoctiluca	Cone + half sphere[b]					$(1/3) \cdot \pi \cdot r^2 \cdot z + (1/2) \cdot (4/3) \cdot \pi \cdot r^3$[fk]	50,000 (assumed)
Prorocentrum	Ellipsoid[b]					$(\pi/6) \cdot a \cdot b \cdot l$[j]	16,303[i]
Protoperidinium	2 cones[b]					$2 \cdot (1/3) \cdot \pi \cdot r^2 \cdot z$[k]	133,298[i]
Pyrocystis	Ellipsoid[b]					$(\pi/6) \cdot a \cdot b \cdot l$[j]	50,000 (assumed)
Pyrophacus	Ellipsoid[b]					$(\pi/6) \cdot a \cdot b \cdot l$[j]	50,000 (assumed)
Scrippsiella	Ellipsoid[b]					$(\pi/6) \cdot a \cdot b \cdot l$[j]	50,000 (assumed)
Silicoflagellates							
Dictyocha							30,000 (assumed)
Octactis							30,000 (assumed)
Phytoflagellates							
Tetraselmis	Elliptic prism[b]	10	25	5		$(\pi/4) \cdot d \cdot l \cdot h$	1964
Microflagellates							
Olisthodiscus luteus	Prolate spheroid	50	110			$(\pi/6) \cdot d^2 \cdot l$	143,990
Tintinnids							
Amphorellopsis	Cylinder[l]	30		200		$(\pi/4) \cdot d^2 \cdot h$	98,175
Codonella	Cylinder[l]	30		200		$(\pi/4) \cdot d^2 \cdot h$	98,175
Codonellopsis	Cylinder[l]	30		200		$(\pi/4) \cdot d^2 \cdot h$	98,175
Dictyocysta	Cylinder[l]	30		200		$(\pi/4) \cdot d^2 \cdot h$	98,175
Eutintinnus	Cylinder[l]	30		200		$(\pi/4) \cdot d^2 \cdot h$	98,175
Favella	Cylinder[l]	30		200		$(\pi/4) \cdot d^2 \cdot h$	98,175

(*continued on next page*)

Table 2 (*continued*)

Genus	Geometric shape	Diameter (μm)	Length (μm)	Height (μm)	m^a (μm)	Volume formula[b]	Volume values (μm^3)
Helicostomella	Cylinder[l]	30		200		$(\pi/4) \cdot d^2 \cdot h$	98,175
Tintinnopsis	Cylinder[l]	30		200		$(\pi/4) \cdot d^2 \cdot h$	98,175
Xystonella	Cylinder[l]	30		200		$(\pi/4) \cdot d^2 \cdot h$	98,175
Foraminiferida	Ellipsoid[b]		200			$(\pi/6) \cdot a \cdot b \cdot l^j$	523,599
Radiolaria	Ellipsoid[b]		110			$(\pi/6) \cdot a \cdot b \cdot l^j$	88,698
Acanthaires	Prolate spheroid[b]	50	75			$(\pi/6) \cdot d^2 \cdot l^j$	98,175

[a] m: height of even-sided triangle of the transapical section.

[b] Hillebrand et al. (1999).

[c] Snoeijs et al. (2002).

[d] *a*: length; *b*: height.

[e] *h*: base of even-sided triangle of the transapical section.

[f] *r*: radius.

[g] *b*: minor axis; *l*: major axis, similar to length.

[h] *l*′: minor base of rectangle, similar to diameter (*d*).

[i] Menden-Deuer and Lessard (2000).

[j] *a*: main axis; *b*: minor axis of cross section (in Foraminiferida: $a = 100$, $b = 50$; Radiolaria: $a = 55$, $b = 28$).

[k] *z*: height of the cone.

[l] Chiappa-Carrara and Gallardo-Cabello (1993).

and the lowest value (5.8%) was recorded in November–December 1998. The maximum contribution to dietary carbon (86.7%) from copepods occurred during November–December 1998, at the end of the 1997–1998 El Niño event, and the lowest value (2.0%) was observed during November–December 1996.

3.2. Stomach fullness dynamics

GAM computed on the combined data from all surveys (Fig. 3) show that the main ingestion period for anchoveta occurred during daytime, between 07h00 and 18h00, local time, and this general pattern was observed during most of the surveys, although there were several exceptions (Fig. 3). For instance, during four surveys (990809, 000607, 010204, 0208) the feeding period began earlier at about 02h00 and terminated in the early afternoon, whereas during two other surveys (980305, 030809) feeding occurred mainly at night. In some instances (surveys 961112 and 970910) anchoveta showed a longer (>16 h) feeding period with no clear evacuation period.

In addition to showing a diel pattern, stomach fullness also varied with latitude (Fig. 3), with higher values encountered off both Northern (<6 °S) and Southern (>13 °S) Peru although some surveys presented very different patterns. Indeed the global trend does not seem robust and strong variability in the relationship between stomach fullness and latitude occurred during the time series; for example, high stomach fullness values were observed in the central part of Peru in 960204, 960809, 991112 and 000607 (Fig. 3).

Stomach fullness increased with distance from the coast and reached maximal values at distances >120 km (Fig. 3), but again this general trend obscures strong variability between surveys. When anchoveta were distributed close to the coast, high fullness levels could be observed close to shore, in particular during the 1997–1998 El Niño, but this was also seen in 1999, 2000 or 2001.

Anchoveta stomach fullness was related to temperature, with a minimum observed at 22 °C (Fig. 3). However, the range of temperatures varied strongly depending on the timing of a particular survey, suggesting that this general trend is also not robust. In fact, whereas the general trend was observed for 13 surveys it was not observed in six others (960204, 970910, 990809, 020203, 010204, 010708) during which fullness increased with temperature, in two surveys (980305,0208) where dome-shaped relationships between SST and stomach fullness were observed, in two other surveys (960809,030203) where U-shaped patterns between SST and stomach fullness were observed, nor in one survey (980809) where a bimodal pattern was observed.

4. Discussion

4.1. Dietary composition

Our analysis of the stomach content composition of 21,203 anchoveta illustrates its omnivorous foraging character; this species feeds on both phytoplankton and zooplankton and has a large diversity of prey (132 taxa were identified at the genus level). As shown by Konchina (1991), the size range of anchoveta prey varies by several orders of magnitude, from tens of micrometers (microflagellates) to tens of millimetres (fish, e.g. *V. lucetia*).

When considering only prey numbers, anchoveta diet is dominated by phytoplankton which comprise 99.5% of all prey and the zooplankton fraction appears negligible (Fig. 2). However when the carbon content of prey items is considered, zooplankton becomes by far the most important component and contributes 98.0% of dietary carbon, with a strong dominance of euphausiids (67.5%) followed by copepods (26.3%). These results depend on the parameters and relationships used to estimate prey carbon content (Tables 2–4); the analysis seems robust but the exact proportion of specific taxa should be considered with caution.

The phytoplankton carbon fraction was dominated by the large solitary diatoms *Coscinodiscus* and *Ditylum*, and the chain forming *Thalassiosira*. Similar dominance has been reported for anchovy (*E. encrasicolus;* formerly *E. capensis*) in the Benguela Current system, where the most important phytoplanktonic items were the large solitary diatoms *Rhizosolenia*, *Pleurosigma* and *Coscinodiscus* (James, 1987). Previous studies performed off Peru and based on numerical or frequency of occurrence analysis also highlighted the importance of diatoms in anchoveta diet, in particular nine genera of the Coscinodiscineae: *Coscinosdiscus*, *Melosyra*, *Cyclotella*, *Skeletonema*, *Thalassiosira*, *Stephanopyxis*, *Coscinoscira*, *Planktoniella*, and *Asterolampra* (Rojas de Mendiola, 1969, 1971, 1989; Alamo, 1989; Pauly et al., 1989b). Other taxa such as the diatoms *Chaetoceros* and *Asterionellopsis*, and the dinoflagellate *Protoperidinium*, were also considered important to anchoveta diet (Alamo et al., 1996a,b, 1997a,b; Alamo and Espinoza, 1998; Espinoza et al., 1998a,b, 1999, 2000).

Table 3
Type and size of zooplankton recorded from anchoveta stomach contents; length was estimated by IMARPE except where indicated.

Name	Type	Length (mm)
Acartia	Calanoida	0.9375[a]
Aetideus	Calanoida	1.5
Calanus	Calanoida	2[b]
Calocalanus	Calanoida	1[c]
Candacia	Calanoida	1.1666[a]
Centropages	Calanoida	1.5[a]
Clausocalanus	Calanoida	0.65[b]
Clytemnestra	Harpacticoida	0.66[b]
Copilia	Poecilostomatoida	1.75[a]
Corycaeus	Cyclopoida	1[a]
Corycella	Poecilostomatoida	0.65
Euaetideus	Calanoida	0.9[b]
Eucalanus	Calanoida	4
Euchaeta	Calanoida	1.08[b]
Euchirella	Calanoida	2.5[b]
Euterpina	Harpacticoida	0.5[c]
Haloptilus	Calanoida	1.2[a]
Lubbockia	Poecilostomatoida	0.8
Lucicutia	Calanoida	1.03[a]
Macrosetella	Harpacticoida	0.7
Mecynocera	Calanoida	0.899[a]
Microsetella	Harpacticoida	0.7[c]
Nonocalanus	Calanoida	1.5
Oithona	Cyclopoida	0.5[a]
Oncaea	Poecilostomatoida	0.667[a]
Paracalanus	Calanoida	0.8[b]
Phaena	Calanoida	0.8
Pleuromamma	Calanoida	1.2[b]
Pontellina	Calanoida	1.5
Rhincalanus	Calanoida	4
Saphirina	Poecilostomatoida	2.3[b]
Scolecithrix	Calanoida	1.7[b]
Scolecithtricella	Calanoida	1.8[b]
Temora	Calanoida	1.2[b]
Harpacticoida		0.6[c]
Copepoditos		0.5[a]
Restos de copépodos		0.25
Euphausiacea		12[b]
Amphipoda		8[b]
Ostracoda		0.7
Zoea		2
Megalop		3
Cirriped larvae		0.1
Emerita sp. Larvae		5
Decapod undetermined larvae		5
Pagurus sp.		5
Pleuroncodes monodon		7
Decapoda Reptantia n/i		3
Galatheidae		7
Bivalvia		1.25
Gastropoda		1.25
Anchoveta eggs		vol: 0.27 mm^3[d]
Apendicularia		10
Echinoderm larvae		1
Chaetognata		8[b]
Squid remains		10
Polychaeta		10
Anchoa sp. Eggs		vol: 0.27 mm^3
Engraulidae eggs		vol: 0.27 mm^3
Fish eggs		vol: 0.27 mm^3
Fish larvae		15
Fish undetermined		15
Engraulidae		15
Vinciguerria sp.		15
Myctophidae		15

[a] http://earth.leeds.ac.uk/cyclops/data/ncfs-zooplank.xls.
[b] Santander et al. (1981).
[c] Tudela and Palomera (1997).
[d] Llanos-Rivera and Castro (2004).

Zooplankton dietary carbon was dominated by euphausiids and copepods. The most important copepods were *Eucalanus*, *Calanus* and *Centropages*, in partial agreement with Rojas de Mendiola (1971, 1989) and Pauly et al. (1989b) who reported that *Calanus*, *Centropages* and *Corycaeus* were frequently-observed in anchoveta stomach contents. During the 1997–1998 El Niño, various studies confirmed the numerical importance of copepods and euphausiids; whereas amphipods, anchoveta eggs, *Vinciguerria* sp., and Myctophidae were of minor importance (Blaskovic' et al., 1999; Espinoza et al., 1998a,b, 1999, 2000).

In spite of the zooplankton dominance in anchoveta diet described above, the contribution made by different prey items varied strongly during the study period (Fig. 2), illustrating the anchoveta's opportunistic feeding ability. For instance, the phytoplankton fraction was high (up to 40% of carbon content) in 1996, but thereafter was never higher than 5%, irrespective of the overall environmental condition (i.e. El Niño 1997–1998 or La Niña 1999). It is difficult to relate these changes in the proportion of dietary phytoplankton to specific conditions. The proportion of anchoveta dietary carbon derived from copepods increased from November–December 1996 (2.0%) to a maximum in November–December 1998 (86.7%) and February–March 1999 (77.1%), after the 1997–1998 El Niño; the copepod fraction also reached high levels (>40%) in June–July 2000, October–November 2000 and August 2002, making the extraction of any seasonal pattern difficult.

4.2. The anchoveta: a predator

Our results demonstrate that anchoveta is a predator foraging at a higher trophic level than has generally been recognised (e.g. by Pauly et al., 1989b; Rojas de Mendiola, 1989), with its main input of carbon coming from zooplankters such as euphausiids and large copepods. Our results differ from the conventional dogma on clupeoid feeding ecology in the HCS, in which diatoms are considered as the major food source. Such feeding low on the food chain has been invoked to explain how such large anchoveta populations can be supported in this system (Rojas de Mendiola 1971). These conclusions now appear incorrect as they are based on counts of very small (phytoplankton) prey who's caloric (carbon) contribution to anchoveta diet is often trivial (Cushing, 1978; Konchina, 1991). James (1987) demonstrated that assessing fish diet from the number of prey items is unsatisfactory due to the preponderance of minute food items and the great difference on size range between phytoplankton and zooplankton (10^{-3} mm for diatoms to 10 mm for zooplankton), which makes the use of carbon or calorie equivalents for assessing the importance of dietary components essential. The determination of prey carbon content helps in determining the true importance of a food type (James, 1988), and this method has been used to highlight the importance of zooplankton over phytoplankton for *E. mordax* off California (Koslow, 1981; Chiappa-Carrara and Gallardo-Cabello, 1993), *E. encrasicolus* and *Sardinops sagax* in the Benguela Current upwelling system (James, 1987; van der Lingen, 2002; van der Lingen et al., 2006), and *Sardina pilchardus* in the north-eastern Atlantic (Garrido et al., 2008); see van der Lingen et al. (2006, in press), for recent reviews of clupeoid trophic ecology. In the Peruvian case, Konchina (1991) was the only scientist to conclude that anchoveta preferentially consumes zooplankton, and that most anchoveta biomass is supported by copepods and euphausiids. Finally, in Central Chile, using isotope analysis, Hückstädt et al. (2007) estimated the trophic level of anchoveta to 3.63, which confirm the dominance of zooplankton in anchoveta diet.

Anchoveta is therefore a 'predator' who select the largest available prey from the phytoplankton and zooplankton communities (Tables 2, 3 and 5). This is shown for zooplankton with the selection of euphausiids and the large copepods *Eucalanus* and *Calanus*, and for phytoplankton with the selection of the large diatom *Coscinodiscus*. Similar selectivity was observed for other anchovy species (e.g. Koslow, 1981; James, 1987; van der Lingen et al., 2006).

Table 4
Relationships employed to calculate dry weight and carbon content of the different categories of phytoplankton and zooplankton. Carbon contents not in μg were transformed in μg for comparison; PL: prosome length (μm); TL: total length (mm); DW: dry weight (μg); WW: wet weight (μg).

Phytoplankton	Volume (μm^3) to Carbon (pg)	
Diatoms	$C = 0.288\ \mathrm{Vol}^{0.811}$[a]	
Dinoflagellates and other phytop.	$C = 0.760\ \mathrm{Vol}^{0.819}$[a]	
Tintinnids, Foraminifera, Radiolaria	$C = 445.5 + 0.053\ \mathrm{Vol}$[b]	
Zooplankton	Length to dry weight (μg) regression	dry weight (μg) to carbon (μg)
Calanoid copepods	$\mathrm{Ln(DW)} = 2.74\ln(\mathrm{PL}) - 16.41$[c]	$C = 0.424\ \mathrm{DW}$[c]
Cyclopoid copepods	$\mathrm{Ln(DW)} = 1.96\ln(\mathrm{PL}) - 11.64$[c]	$C = 0.424\ \mathrm{DW}$[c]
Harpacticoid copepods	$\mathrm{Ln(DW)} = 1.96\ln(\mathrm{PL}) - 11.64$[c]	$C = 0.424\ \mathrm{DW}$[c]
Poecilostomatoid copepods	$\mathrm{Ln(DW)} = 1.96\ln(\mathrm{PL}) - 11.64$[c]	$C = 0.424\ \mathrm{DW}$[c]
Euphausiacea	$\mathrm{DW} = 0.0012\ \mathrm{TL}^{3.16}$[ci]	$C = 0.424\ \mathrm{DW}$[cj]
Amphipoda, Echinoderm larvae	$\mathrm{DW} = 0.005\ \mathrm{TL}^{2.311}$[di]	$C = 0.370\ \mathrm{DW}$[dj]
Ostracods, zoea, megalops, crustacea larvae, hermit crab and Galatheidae	$\mathrm{DW} = 3.946\ \mathrm{TL}^{2.436}$[c]	$C = 0.424\ \mathrm{DW}$[c]
Bivalvia, Gasteropod	$\mathrm{DW} = 47.386\ \mathrm{TL}^{3.663}$[d]	$C = 0.424\ \mathrm{DW}$[c]
Fish eggs	$\mathrm{DW} = 0.093\ \mathrm{Vol} + 0.0012$[ck]	$C = 0.457\ \mathrm{DW}$[c]
Apendicularia	$\mathrm{DW} = 11.3\mathrm{TL}^{1.77}$[e]	$C = 0.387\ \mathrm{DW}$[e]
Chaetognaths	$\mathrm{DW} = 0.00097\ \mathrm{TL}^{2.2365}$[fi]	$C = 0.290\ \mathrm{DW}$[f]
Fish, squid and fish larvae	$\mathrm{DW} = 0.0001\ \mathrm{TL}^{3.582}$[di]	$C = 0.38\ \mathrm{DW}$[g]
Polychaeta	$\mathrm{WW} = 0.01\ \mathrm{TL}^{2.136}$[h] $\mathrm{DW} = 0.157\ \mathrm{WW}$[hi]	$C = 0.518\ \mathrm{DW}$[h j]

[a] Menden-Deuer and Lessard (2000).
[b] Verity and Langdon (1984).
[c] van der Lingen (2002).
[d] James (1987).
[e] Deibel (1986).
[f] Sameoto (1971).
[g] Parsons et al. (1984).
[h] Alexandrov (2001).
[i] DW in mg.
[j] C in mg.
[k] Volume = 0.27 mm^3, from Llanos-Rivera and Castro (2004) as anchoveta eggs dominated fish egg fraction.

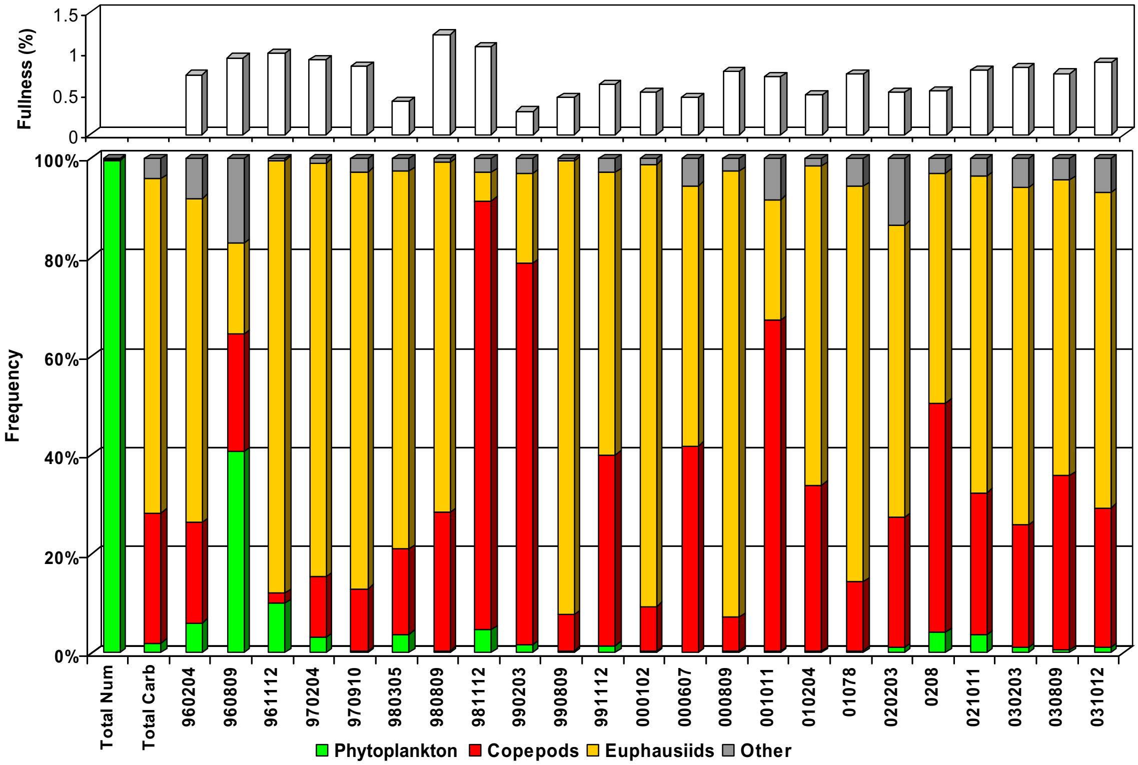

Fig. 2. Percentage contribution of phytoplankton (green), copepods (red), euphausiids (orange) and other zooplankters (grey) by number (total num) and to dietary carbon (total carb) for the total set of 21,203 anchoveta stomach contents. Also shown are the percentage contribution to dietary carbon by prey type for each of the 23 surveys from which anchoveta stomach contents were analyzed; surveys are identified along the *x*-axis, with the first two numbers corresponding to the year, the following two numbers the start month of the survey, and the last two numbers the end month of the survey.

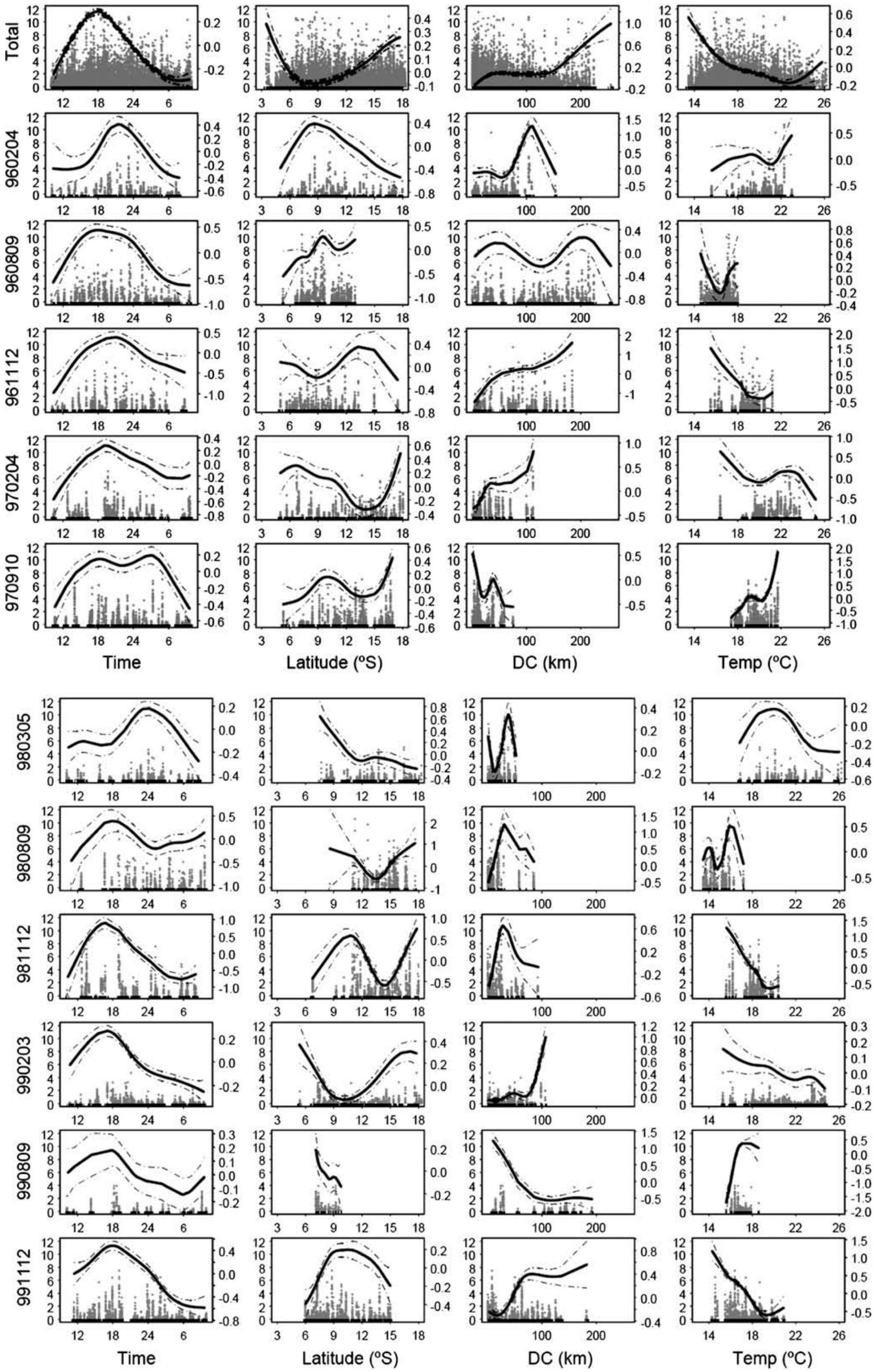

Fig. 3. Scatter plot (grey dots) and cubic spline smoother fits (black solid lines) of GAM models (the black dashed lines show the 95% confidence limits) based on anchoveta stomach fullness according to time of day, latitude, distance from the coast (DC) and sea surface temperature (°C) for the complete set of 21,203 stomach contents (top panel) and for each of the 23 surveys from which stomach contents were analyzed (lower panels); surveys are identified along the *y*-axis, with the first two numbers corresponding to the year, the following two numbers the start month of the survey, and the last two numbers the end month of the survey. The left *y*-axis shows stomach fullness (% WW) and scaling along the right *y*-axes is relative and corresponds to the spline smoother that was fitted on the data such that a *y*-value of zero is the mean effect of the variables on the response.

4.3. Stomach fullness dynamics

As previously observed for *E. encrasicolus* (James, 1987), *E. ringens* displays an extremely high degree of opportunism in fulfilling its dietary requirements and can shift between prey types according to their availability (Table 2). This flexible feeding behaviour was confirmed by the GAM models (Fig. 3) which illustrated the high variability between surveys when relating stomach fullness

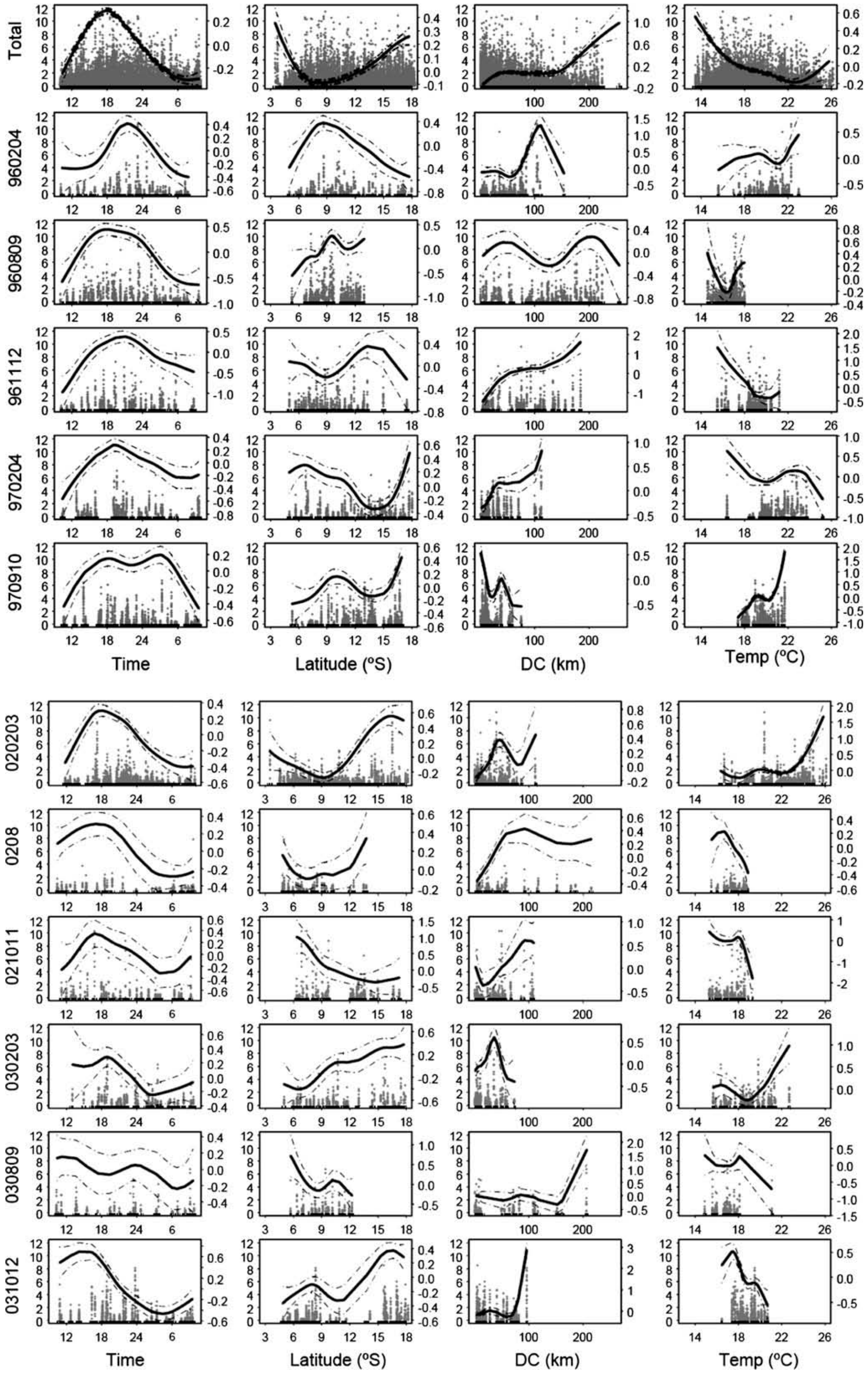

Fig. 3 (*continued*)

to time, latitude, distance to the coast, or SST. In the highly variable HCS anchoveta have had to evolve adaptive strategies in space and time (Bertrand et al., 2004a), including its spawning behaviour (e.g. Buitrón and Perea, 2000), its mode of spatial distribution (e.g. Bertrand et al., 2004b, 2008; Gutiérrez et al., 2007), or its feeding behaviour as illustrated by this study.

Such variability precludes the determination of robust patterns, and indeed results differ strongly between surveys and therefore from one dataset to another. Our study was based on more than 20,000 stomach content samples collected during an 8 year period which is, to our knowledge, the largest database on anchoveta diet, and the results we obtained from all surveys combined (Fig. 3) can

Table 5
Contribution by number and carbon content of anchoveta dietary items (data from all surveys combined).

Dietary items	Total number	Total carbon (μg)
Diatoms		
Actinoptychus	2,249,000	1733
Amphiprora	107,000	19
Amphora	186,000	64
Asterionellopsis	265,043,000	28,742
Asteromphalus	719,000	156
Bacteriastrum	791,000	2597
Cerataulina	26,000	32
Chaetoceros	206,866,000	49,060
Cocconeis	4000	0.26
Corethron	217,000	307
Coscinodiscus	60,994,000	1,284,639
Cylindrotheca	4000	0.07
Detonula	32,551,000	60,910
Ditylum	89,090,000	193,730
Eucampia	16,313,000	8107
Fragilariopsis	1,487,000	30
Grammatophora	3000	1
Guinardia	1,831,000	8045
Gyrosigma	10,822,000	24,481
Hemiaulus	15,000	14
Lauderia	7000	36
Leptocylindrus	2000	0.23
Licmophora	16,000	9
Lioloma	11,757,000	14,963
Lithodesmium	19,686,000	7273
Navicula	5,025,000	959
Odontella	1,513,000	950
Planktoniella	4,557,000	11,847
Pleurosigma	2,266,000	3299
Proboscia	9000	6
Pseudonitzschia	33,495,000	1834
Pseudosolenia	27,000	372
Rhizosolenia	4,494,000	15,699
Skeletonema	972,395,000	40,361
Stephanopyxis	572,000	2004
Thalassionema	39,032,000	3656
Thalassiosira	513,411,000	348,371
Tropidoneis	2000	1
Dinoflagellates		
Ceratium	8,046,000	42,746
Dinophysis	609,000	3399
Diplopelta	17,000	95
Diplopsalis	22,000	123
Dissodium	1,248,000	6966
Goniodoma	1,256,000	7011
Gonyaulax	44,000	246
Gymnodinium	2000	19
Oxophysis	53,000	296
Podolampas	6000	33
Pronoctiluca	1000	6
Prorocentrum	1,340,000	2611
Protoperidinium	11,461,000	160,651
Pyrocystis	704,000	3930
Pyrophacus	16,000	89
Scrippsiella	1,002,000	5593
Silicoflagellates		
Dictyocha	8,469,000	29,262
Octactis	566,000	1956
Phytoflagellates		
Tetraselmis	6000	2
Microflagellates		
Olisthodiscus luteus	1,214,000	9804
Tintinnids		
Amphorellopsis	10,000	79
Codonella	340,000	2699
Codonellopsis	83,000	659
Dictyocysta	337,000	2675
Eutintinnus	216,000	1714
Favella	97,000	770
Helicostomella	3,310,000	26,272
Tintinnopsis	732,000	5810
Xystonella	1,081,000	8580
Foraminiferida	1,040,000	29,323
Radiolaria	1,986,000	10,219
Acanthaires	12,000	68
Zooplankton		
Copepoda		
Acartia	40,020	176,227
Aetideus	16,080	256,667
Calanus	114,300	4,012,932
Calocalanus	2190	11,509
Candacia	47,120	377,775
Centropages	129,440	2,066,103
Clausocalanus	112,340	181,347
Clytemnestra	6810	8543
Copilia	200	1697
Corycaeus	144,420	409,077
Corycella	120	146
Euaetideus	2330	9174
Eucalanus	93,090	21,834,378
Euchaeta	34,450	223,544
Euchirella	280	18,118
Euterpina	19,930	14,510
Haloptilus	10	87
Lubbockia	4910	8981
Lucicutia	18,330	104,803
Macrosetella	10,550	14,853
Mecynocera	3230	12,679
Microsetella	37,960	53,444
Nonocalanus	360	5746
Oithona	126,830	92,338
Oncaea	173,890	222,492
Paracalanus	109,280	311,602
Phaena	8340	23,781
Pleuromamma	400	3464
Pontellina	40	638
Rhincalanus	1070	250,970
Saphirina	570	8261
Scolecithrix	13,390	301,165
Scolecithtricella	740	19,466
Temora	3560	30,832
Harpacticoida	52,970	55,130
Copepoditos	120,290	94,624
Restos de copépodos	285,570	33,625
Euphausiacea	61,319	80,233,346
Amphipoda	2103	475,392
Ostracoda	150	105
Zoea	38,682	350,220
Megalop	14,205	345,328
Cirriped larvae	7170	44
Emerita sp. Larvae	80	6750
Decapod undetermined larvae	1080	91,125
Pagurus sp.	1	84
Pleuroncodes monodon	48	9192
Decapoda Reptantia n/i	3062	74,438
Galatheidae	1	192
Bivalvia	8090	368,083
Gastropoda	19,910	905,876
Anchoveta eggs	39,611	476,270
Apendicularia	180	14,039
Echinoderm larvae	80	0.17
Chaetognata	2830	83,314
Squid remains	5	873
Polychaeta	7992	888,965
Anchoa sp. Eggs	248	2982
Engraulidae eggs	15	180
Fish eggs	1931	23,218
Fish larvae	361	223,898
Fish undetermined	41	25,429
Engraulidae	2	1240
Vinciguerria sp.	809	501,754
Myctophidae	51	31,631

therefore be considered as representative. However, except in the case of their diel feeding behaviour, we think that the mean signal in anchoveta stomach fullness is not a good representation of the biological reality at any one moment. Instead, we consider that the most important point arising from our stomach fullness analysis does not reside in the mean patterns but in the variability from one survey to the other (Fig. 3). This variability is another illustration of anchoveta plasticity.

The general trend of diel temporal variation in stomach fullness was the most consistent, and the main feeding period as determined using GAMs ranged between 07h00 and 18h00 (Fig. 3). This general pattern was observed for most surveys, although night-time feeding behaviour made substantial contributions to total ingestion (moon cycle could play a role). Feeding duration also varied from one survey to another, as also shown by Espinoza and Blaskovic' (2000). The primarily diurnal feeding behaviour we observed differs from results of other studies of anchoveta feeding periodicity based on a large database (5245 individuals) from samples collected over the period 1953–1982 (Pauly et al., 1989b; Jarre et al., 1991), which indicated that most feeding occurred between 11h00 and 24h00. This difference cannot be related to the different methods of analysis used i.e., GAM in this study and Sainsbury's method (Sainsbury, 1986) in previous studies, since applying Sainsbury's method to our data does not change the results.

So why did the main feeding period change? At least two hypotheses can be proposed to explain this difference: a shift in the ecosystem, or a problem of data collection. Anchovies in other upwelling systems are considered as daytime (e.g. northern anchovy *E. mordax*; Baxter, 1967; Loukashkin, 1970; Koslow, 1981) or night-time (e.g. Benguela anchovy *E. encrasicolus*; James 1988) foragers. At first sight the main daytime trend we found appears surprising since zooplankton perform diel migrations and a large fraction of zooplankton is generally distributed within or below the oxycline during the day, out of reach of the anchoveta (e.g. Escribano et al., in press; Bertrand et al., 2008). However our results demonstrate that anchoveta can change their feeding period and forage at night if necessary. The HCS experienced 'cold' and 'warm' years during the period (1996–2003) of our study with a dominance of the upwelling-related cold coastal water along the Peruvian coast, except during the 1997–1998 El Niño (Swartzman et al., 2008). That anchoveta fed mainly during the day suggests that, even with the highly stratified conditions typical of enhanced upwelling periods, there were enough prey available during the day to sustain anchoveta. It seems therefore difficult to ascribe the difference between our results and previous studies to changes in climatic conditions. The period 1953–1982 that was previously studied included a wide range of climatic conditions: 'cold' until the beginning of the 1970s, and 'warm' from then until the mid 1980s. Hence we feel that it is more likely that the differences in anchoveta mean feeding periodicity between our and earlier studies was due to potential problems in the data collection (e.g. data sources varied from scientific cruises to fishing boats) for the 1953–1982 series or by the fact that the mean pattern hides important variability from one period to the other. Indeed a refined analysis of the data set used in previous studies revealed a pattern of several feeding periods per day, including some feeding during late night (Jarre-[Teichmann], 1992).

The plasticity in anchoveta foraging periodicity was even more obvious when considering the distance to the coast, latitude or SST, where mean patterns were not representative of the observations from a single survey. Inside its range of overall viable conditions anchoveta is therefore able to forage efficiently at any time, any place, or any temperature. In other words, inside its cold coastal water-related habitat (see Bertrand et al., 2004a; Gutiérrez et al., 2007; Bertrand et al., 2008; Swartzman et al., 2008), anchoveta were probably distributed where prey were abundant and available, rather independently of other parameters (Bertrand et al., 2008).

4.4. A new vision of HCS functioning

If anchoveta is a predator that uses large zooplankters as the main source of dietary carbon, then our vision of HCS functioning must change. The HCS is by far the most productive eastern boundary current system in the world in terms of fish catches, but these high catches do not appear to be supported by exceptionally rates of primary production far higher than those observed in the other eastern boundary current systems (Carr, 2002; Carr and Kearns, 2003). The high fish production in the HCS could be related to a more efficient use of primary production due to, for example, a short trophic chain, and this assumption has been prevalent in the last few decades since anchoveta was considered to feed directly on primary producers and hence rely on a complete very short and efficient food chain (Ryther, 1969; Walsh, 1981). But if this is not the case, and anchoveta do not, in fact, benefit from a 2-step food chain, then the explanation for the high fish productivity in the HCS must be found elsewhere. Konchina (1991) stated that the ability of anchoveta to utilize food from several trophic levels and to choose energetically advantageous food enables it to achieve enormous biomass in a relatively short time. Yet all trophic models of the HCS developed to date, even recently, still consider that the anchoveta consumes at least as much carbon from phytoplankton as from zooplankton (e.g. Jahncke et al., 2004; Neira et al., 2004). Our results indicate that carbon flows in trophic models of the HCS must be re-evaluated, since the tremendous importance of anchoveta in the coastal pelagic ecosystem means that a major change in its diet should affect all the other components of that system. In particular, the fact that anchoveta forages at a higher trophic level than previously been considered implies that the primary and secondary production of the HCS may be higher than supposed (for primary production see Echevin et al., 2008). No absolute estimation of zooplankton production is available (see Ayón et al., 2004, 2008 for trends in zooplankton biovolume) but we hypothesize that zooplankton production could be higher in the HCS than in other upwelling systems, and this higher secondary production could be related to a more efficient use of primary production by zooplankton and/or a strong connection between the coastal and the offshore pelagic ecosystems. This last argument may particularly apply to the euphausiids, which were the main source of dietary carbon for anchoveta and which inhabit both near- and offshore ecosystems.

The hypothesis of higher zooplankton biomass in the HCS compared to other systems highlights the urgent need for more studies on zooplankton diversity, abundance and dynamics in the HCS, particularly for large zooplankters like euphausiids (Antezana, 2002). Studying these organisms is difficult, however, as they avoid standard samplers such as bongo nets, but new, multi-frequency acoustic measurements permit estimation of the biomass of the main zooplankton groups and facilitate the study of their distribution patterns in 2-D and 3-D (e.g. Lebourges-Dhaussy et al., 2004).

Our results also bring into question current thinking on anchoveta distribution. Because of the westward drift of water masses in the HCS there is usually a spatial separation between areas of peak phytoplankton abundance and areas of peak zooplankton abundance. Hence the relationship between anchoveta distribution and chlorophyll concentration, as observed from satellite, is not necessarily direct, and it is therefore important to take into account the characteristics of the available habitat, including zooplankton abundance, to understand anchoveta distribution patterns and also changes in abundance (cf. the habitat-based hypothesis in Bertrand et al., 2004a). It is not sufficient to use temperature or chlorophyll concentration as indicators of anchoveta distribution, since the plasticity of the genus *Engraulis* in general (Bakun, 1996) and *E. ringens* in particular allows it to feed successfully and distribute across a broad range of environmental variability. The dependence of anchoveta on zooplankton has previously been illustrated by Alheit and Ñiquen (2004) and Ayón et al. (2008), who showed bottom-up control of anchoveta where its abundance in the HCS was linked to overall zooplankton abundance. At a smaller scale, Ayón et al. (2008) also showed that this apparent bottom-up control was accompanied by a local depletion effect, as zooplankton biomass was lower in places were anchoveta was abundant.

4.5. Synthesis: plastic is fantastic!

Our results have demonstrated that the diet of anchoveta in Peru is based primarily on large zooplankters, but also that this species shows tremendous plasticity in its diet and feeding behaviour; anchoveta utilize food from several trophic levels, can choose energetically advantageous food types, and can fit its foraging period and duration to prey. Trophic plasticity is apparently an evolved adaptive strategy; other strategies include the ability to track and concentrate in refuge areas when conditions are adverse (Bertrand et al., 2004a), change its reproductive behaviour (Buitrón and Perea, 2000), and distribute its population over a rather large temperature range (Bertrand et al., 2004a; Gutiérrez et al., 2008). In combination these characteristics may explain the 'anchoveta paradox': how a fish which (i) performs very small migrations and cannot escape adverse conditions, (ii) is mainly distributed in dense surface aggregations and is thus highly accessible to predators (fish, cephalopods, birds, mammals and fishers), and (iii) is very slow in its avoidance reactions to predators (Gerlotto et al., 2006), can achieve such enormous biomass in a relatively short time.

Acknowledgments

The authors gratefully thank the 'laboratorio de ecología trófica' staff from Instituto del Mar del Perú (IMARPE) for having facilitated the use of the data. This work is a contribution of the Research Unit 'Upwelling Ecosystems' UR 097 and of the Interdepartmental Thematic Action "Humboldt Current System" from IRD. We warmly thank Patricia Ayón, François Gerlotto, Mariano Gutiérrez, Astrid Jarre, Salvador Peraltilla, Gordon Swartzman, Jorge Tam and Marc Taylor; particular thanks to Blanca Rojas de Mendiola for her very valuable help when interpreting the results and to Francis Juanes for interesting comments and English edition. Finally we thanks Andrew Bakun and Gary Sharp for their interesting comments and Carl van der Lingen for his continuous and determinant help during all the process of this work.

References

Alamo, A., 1989. Stomach contents of anchoveta (*Engraulis ringens*), 1974–1982. In: Pauly, D., Muck, P., Mendo, J., Tsukayama, I. (Eds.), The Peruvian upwelling ecosystem: dynamics and interactions. ICLARM Conference Proceedings, vol. 18, pp. 105–108.

Alamo, A., Navarro, I., Espinoza, P., Zubiate, P., 1996a. Espectro alimentario y ración de alimentación de *Engraulis ringens* y de *Sardinops sagax* sagax, y mortalidad de huevos de la anchoveta peruana por predación. Informe Instituto del Mar del Perú 119, 34–42 (in Spanish, with abstract in English).

Alamo, A., Navarro, I., Espinoza, P., Zubiate, P., 1996b. Relaciones tróficas, espectro alimentario y ración de alimentación de las principales especies pelágicas en el verano 1996. Informe Instituto del Mar del Perú 122, 36–46 (in Spanish, with abstract in English).

Alamo, A., Espinoza, P., Zubiate, P., Navarro, I., 1997a. Comportamiento alimentario de la anchoveta peruana *Engraulis ringens*, durante el invierno de 1996. Crucero BIC Humboldt 9608-09. Informe Instituto del Mar del Perú 123, 38–46 (in Spanish, with abstract in English).

Alamo, A., Espinoza, P., Zubiate, P., Navarro, I., 1997b. Comportamiento alimentario de los principales recursos pelágicos peruanos en verano y comienzos de otoño 1997. Informe Instituto del Mar del Perú 127, 82–89 (in Spanish, with abstract in English).

Alamo, A., Espinoza, P., 1998. Variaciones alimentarias en *Engraulis ringens* y otros recursos pelágicos durante invierno-primavera de 1997. Informe Instituto del Mar del Perú 130, 45–52 (in Spanish, with abstract in English).

Alexandrov, B.G., 2001. Caloric content of the Black Sea invertebrates: 1 Zooplankton and meiobenthos. In: Ecologiya Morya (Ecology of the Sea), ISSN:1726-6777, pp. 5–10 (in Russian).

Alheit, J., Ñiquen, M., 2004. Regime shifts in the Humboldt Current ecosystem. Progress in Oceanography 60, 201–222.

Antezana, T., 2002. Adaptive behavior of *Euphausia mucronata* in relation to the oxygen minimum layer of the Humboldt Current. In: Färber Lorda, J. (Ed.), Oceanography of the Eastern Pacific. Editorial CICESE, vol. II, pp. 29–40.

Ayón, P., Purca, S., Guevara-Carrasco, R., 2004. Zooplankton volume trends off Peru between 1964 and 2001. ICES Journal of Marine Science 61, 478–484.

Ayón, P., Swartzman, G., Bertrand, A., Gutiérrez, M., Bertrand, S., 2008. Zooplankton and forage fish species off Peru: Large-scale bottom-up forcing and local-scale depletion. Progress in Oceanography 79, 208–214.

Bakun, A., 1996. Patterns in the ocean: ocean process and marine population dynamics. Centro de Investigaciones biológicas del Nordeste. La Paz, Mexico and University of California Sea Grant, San Diego, USA.

Baxter, J.L., 1967. Summary of biological information on the northern anchovy *Engraulis mordax* Girard. California Cooperative Fisheries Investigation Reports 11, pp. 110–116.

Bertrand, A., Segura, M., Gutiérrez, M., Vásquez, L., 2004a. From small-scale habitat loopholes to decadal cycles: a habitat-based hypothesis explaining fluctuation in pelagic fish populations off Peru. Fish and Fisheries 5, 296–316.

Bertrand, S., Díaz, E., Ñiquen, M., 2004b. Interactions between fish and fisher's spatial distribution and behaviour: the anchovy (*Engraulis ringens*) fishery of Peru. ICES Journal of Marine Science 61, 1127–1136.

Bertrand, A., Gerlotto, F., Bertrand, S., Gutiérrez, M., Alza, L., Chipollini, A., Diaz, E., Espinoza, P., Ledesma, L., Quesquén, R., Peraltilla, S., Chavez., 2008. Schooling behaviour and environmental forcing in relation to anchoveta distribution: an analysis across multiple spatial scales. Progress in Oceanography 79, 264–277.

Blaskovic', V., Espinoza, P., Torriani, F., Navarro, I., 1999. Hábitos alimentarios de la anchoveta frente al litoral peruano durante la primavera 1998. Crucero BIC José Olaya Balandra 9811-12. Informe Instituto del Mar del Perú 146, 77–84 (in Spanish, with abstract in English).

Buitrón, B., Perea, A., 2000. Aspectos reproductivos de la anchoveta peruana durante el período 1992–2000. Boletín del Instituto del Mar del Perú 19, 45–54 (in Spanish, with English abstract).

Carr, M.-E., 2002. Estimation of potential productivity in Eastern Boundary Currents using remote sensing. Deep Sea Research II 49, 59–80.

Carr, M.-E., Kearns, E.J., 2003. Production regimes in four Eastern Boundary Current systems. Deep Sea Research II 50, 3199–3221.

Chiappa-Carrara, X., Gallardo-Cabello, M., 1993. Estudio del régimen y hábitos alimentarios de la anchoveta *Engraulis mordax* Girard (Pises: Engraulidae), en Baja California, Mexico. Ciencias Marinas 19, pp. 285–305.

Cushing, D.H., 1978. Upper trophic levels in upwelling areas. In: Boje, R., Tomczak, N. (Eds.), Upwelling Ecosystems. Springer-Verlag, Heidelberg, Berlín, pp. 101–110.

Deibel, D., 1986. Feeding mechanism and house of the appendicularian *Oikopleura vanhoeffeni*. Marine Biology 93, 429–436.

Echevin, V., Aumont, O., Ledesma, J., Flores, G., 2008. The seasonal cycle of surface chlorophyll in the Peru upwelling system: a modelling study. Progress in Oceanography 79, 167–176.

Escribano, R, Hidalgo, P., Krautz, C., in press. Zooplankton associated with the oxygen minimum zone system in the northern upwelling region of Chile during March 2000. Deep Sea Research II.

Espinoza, P., Navarro, I., Torriani, F., 1998a. Variaciones en el espectro alimentario de los principales recursos pelágicos durante otoño 1998. Crucero BIC Humboldt 9803-05 de Tumbes a Tacna. Informe Instituto del Mar del Perú 135, pp. 134–142 (in Spanish, with abstract in English).

Espinoza, P., Blaskovic', V., Navarro, I., 1998b. Comportamiento alimentario de *Engraulis ringens*, a finales del invierno 1998. Crucero de evaluación hidroacústica de recursos pelágicos 9808-09. Informe Instituto del Mar del Perú 141, pp. 67–71 (in Spanish, with abstract in English).

Espinoza, P., Blaskovic', V., Torriani, F., Navarro, I., 1999. Dieta de la anchoveta *Engraulis ringens* según intervalos de talla. Crucero BIC José Olaya Balandra y BIC Humboldt 9906. Informe Instituto del Mar del Perú 149, pp. 41–48 (in Spanish, with abstract in English).

Espinoza, P., Navarro, I., Torriani, F., 2000. Variaciones espaciales en la dieta de la anchoveta a finales de la primavera 1999. Crucero BICs José Olaya Balandra y SNP-2 9911-12. Informe Instituto del Mar del Perú 157, pp. 72–76 (in Spanish, with abstract in English).

Espinoza, P., Blaskovic', V., 2000. Cambios en la dieta de la anchoveta *Engraulis ringens* y su influencia en la dinámica de alimentación. Boletín Instituto del Mar del Perú 19, 21–27 (in Spanish, with abstract in English).

Garrido, S., Ben-Hamadou, R., Oliveira, P.B., Cunha, M.E., Chicharo, M.A., van der Lingen, C.D., 2008. Diet and feeding intensity of sardine *Sardina pilchardus*: correlation with satellite-derived chlorophyll data. Marine Ecology Progress Series 354, 245–256.

Gerlotto, F., Bertrand, S., Bez, N., Gutiérrez, M., 2006. Waves of agitation inside anchovy schools observed with multibeam sonar: a way to transmit information in response to predation. ICES Journal of Marine Science 63, 1405–1417.

Gutiérrez, M., Swartzman, G., Bertrand, A., Bertrand, S., 2007. Anchovy (*Engraulis ringens*) and sardine (*Sardinops sagax*) spatial dynamics and aggregation patterns in the Humboldt Current ecosystem, Peru, from 1983–2003. Fisheries Oceanography 16, 155–168.

Gutiérrez, M., Bertrand, S., Ramirez, A., Morón, O., Bertrand, A., 2008. Ecological niches and areas of overlap of the squat lobster 'munida' (*Pleuroncodes monodon*) and anchoveta (*Engraulis ringens*) off Peru. Progress in Oceanography 79, 256–263.

Hastie, T., Tibshirani, R., 1990. Generalized Additive Models. Chapman and Hall, London.

Hillebrand, H., Dürselen, C.-D., Kirschtel, D., Pollingher, U., Zohary, T., 1999. Biovolume calculations for pelagic and benthic microalgae. Journal of Phycology 35, 403–424.

Hückstädt, L.A., Rojas, C.P., Antezana, T., 2007. Stable isotope analysis reveals pelagic foraging by the Southern sea lion in central Chile. Journal of Experimental Marine Biology and Ecology 347, 123–133.

Hureau, J.-C., 1970. Biologie compare de quelques poissons antarctiques (Nototheniidae). Bulletin de l'Institut Oceanographique Monaco 68, 244.

Hyslop, E.J., 1980. Stomach contents analysis – a review of methods and their application. Journal of Fish Biology 17, 411–429.

Jahncke, J., Checkley, D.M. Jr., Hunt Jr., G.L., 2004. Trends in carbon flux to seabirds in the Peruvian upwelling system: effects of wind and fisheries on population regulation. Fisheries Oceanography 13, 208–223.

James, A.G., 1987. Feeding ecology, diet and field-based studies on feeding selectivity of the Cape anchovy *Engraulis capensis* Gilchrist. In: Payne, A.I.L., Gulland, J.A., Brink K.H. (Eds.), The Benguela and Comparable Ecosystems South African Journal of Marine Science 5, 673–692.

James, A.G., 1988. Are clupeid microphagists herbivorous or omnivorous? A review of the diets of some commercially important clupeids. South African Journal of Marine Science 7, 161–177.

James, A.G., Chiappa-Carrara, X., 1990. A comparison of field based studies on the trophic ecology of *Engraulis capensis* and *E. mordax*. In: Barnes, M., Gibson, R.N. (Eds.), Trophic relationships in the marine environment. Aberdeen University Press. pp. 208–221.

Jarre, A., Muck, P., Pauly, D., 1991. Two approaches for modelling fish stock interactions in the Peruvian upwelling ecosystem. ICES Marine Science Symposia 193, 171–184.

Jarre-[Teichmann], A., 1992. Steady-state modelling of the Peruvian upwelling ecosystem. Doctoral dissertation, University of Bremen, Germany, 153.

Konchina, Y.V., 1991. Trophic status of the Peruvian anchovy and sardine. Journal of Ichthyology 31, 59–72.

Konchina, Y.V., Pavlov, Y.P., 1995. On methods of determining the trophic status of species in ichthyocenes. Journal of Ichthyology 35, 150–166.

Koslow, J.A., 1981. Feeding selectivity of schools of northern anchovy, *Engraulis mordax*, in the southern California. Fishery Bulletin 79, 131–142.

Lebourges-Dhaussy, A., Knutsen, T., Korneliussen, R.J., 2004. Acoustic backscatter from zooplankton and fish explored through an optimised model framework. ICES, CM 2004/R:39.

Llanos-Rivera, A., Castro, L.R., 2004. Latitudinal and seasonal egg-size variation of the anchoveta (*Engraulis ringens*) off the Chilean coast. Fishery Bulletin 102, 207–212.

Loukashkin, A.S., 1970. On the diet and feeding behaviour of the northern anchovy, *Engraulis mordax* (Girard). In: Proceedings of the California Academy of Sciences (Series 4) 37, 419–458.

Menden-Deuer, S., Lessard, E.J., 2000. Carbon to volume relationships for dinoflagellates, diatoms, and other protist plankton. Limnology and Oceanography 45, 569–579.

Neira, S., Arancibia, H., Cubillos, L., 2004. Comparative analysis of trophic structure of commercial fishery species off Central Chile in 1992 and 1998. Ecological Modelling 172, 233–248.

Parsons, T.R., Takahashi, M., Hargraves, B., 1984. Biological Oceanographic Processes. Pergamon, Oxford.

Pauly, D., Tsukayama, I., 1987. The Peruvian anchoveta and its upwelling ecosystem: three decades of change. ICLARM Studies and Reviews, 15.

Pauly, D., Muck, P., Mendo, J., Tsukayama, I., 1989a. The Peruvian upwelling ecosystem: dynamics and interactions. In: ICLARM Conference Proceedings, vol. 18.

Pauly, D., Jarre, A., Luna, S., Sambilay Jr., V., Rojas de Mendiola, B., Alamo, A., 1989b. On the quantity and types of food ingested by Peruvian anchoveta, 1953–1982. In: Pauly, D., Muck, P., Mendo, J., Tsukayama, I. (Eds.), The Peruvian upwelling ecosystem: dynamics and interactions. ICLARM Conference Proceedings, vol. 18, pp. 109–124.

Rojas, B., 1953. Estudios preliminarios del contenido estomacal de las anchovetas. Bol. Cient. Cía. Adm. Guano 1, 33–42.

Rojas de Mendiola, B., 1969. The food of the Peruvian anchovy. Journal du Conseil International pour l'Exploration de la Mer 32, 433–434.

Rojas de Mendiola, B., 1971. Some observations on the feeding of the Peruvian anchoveta *Engraulis ringens* J. in two regions of the Peruvian coast. In: Costlow, J.D. (Ed.), Fertility of the Sea. Gordon and Breach Science Publisher, New York, pp. 17–440.

Rojas de Mendiola, B., 1989. Stomach contents of anchoveta (*Engraulis ringens*), 1953–1974. In: Pauly, D., Muck, P., Mendo, J., Tsukayama, I. (Eds.) The Peruvian upwelling ecosystem: dynamics and interactions. ICLARM Conference Proceedings, vol. 18, pp. 97–104.

Ryther, J.H., 1969. Photosynthesis and fish production in the sea. Science 166, 72–76.

Sainsbury, K.J., 1986. Estimation of food consumption from field observation of fish feeding cycles. Journal of Fish Biology 29, 23–36.

Sameoto, D., 1971. Life history ecological production and empirical mathematical model of the population of *Sagitta elegans* in St. Margaret's Bay Nova Scotia. Journal of Fisheries Research Board of Canada 28, 971–985.

Santander, H., Luyo, G., Carrasco, S., Veliz, M., Sandoval de Castillo, O., 1981. Catalogo de zooplancton en el mar peruano. Boletín Intituto del Mar del Perú 6, 1–75 (in Spanish).

Snoeijs, P., Busse, S., Potapova, M., 2002. The importance of diatom cell size in community analysis. Journal of Phycology 38, 265–272.

Swartzman, G., Bertrand, A., Gutiérrez, M., Bertrand, S., Vasquez, L., 2008. The relationship of anchovy and sardine to water masses in the Peruvian Humboldt Current System from 1983–2005. Progress in Oceanography 79, 228–237.

Tudela, S., Palomera, I., 1997. Trophic ecology of the European anchovy *Engraulis encrasicolus* in the Catalan Sea. Marine Ecology Progress Series 160, 121–134.

van der Lingen, C.D., 2002. Diet of sardine *Sardinops sagax* in the southern Benguela upwelling ecosystem. South African Journal of Marine Science 24, 301–316.

van der Lingen, C.D., Hutchings, L., Field, J.G., 2006. Comparative trophodynamics of anchovy *Engraulis encrasicolus* and sardine *Sardinops sagax* in the southern Benguela: are species alternations between small pelagic fish trophodynamically mediated? African Journal of Marine Science 28, 465–477.

van der Lingen, C.D., Bertrand, A., Bode, A., Brodeur, R., Cubillos, L., Espinoza, P., Friedland, K., Garrido, S., Irigoien, X., Möllman, C., Rodriguez-Sanchez, R., Tanaka, H., Temming, A., in press. Trophic dynamics of small pelagic fish. In: Checkley, D.M., Jr., Roy, C., Alheit, J. (Eds.), Climate Change and Small Pelagic Fish (Chapter 8).

Verity, P.G., Langdon, C., 1984. Relationships between lorica volume, carbon, nitrogen, and ATP content of tintinnids in Narragansett Bay. Journal of Plankton Research 6, 859–868.

Walsh, J.J., 1981. A carbon budget for overfishing off Peru. Nature 290, 300–304.

Progress in Oceanography 79 (2008) 228–237

Contents lists available at ScienceDirect

Progress in Oceanography

journal homepage: www.elsevier.com/locate/pocean

The relationship of anchovy and sardine to water masses in the Peruvian Humboldt Current System from 1983 to 2005

Gordon Swartzman [a,*], Arnaud Bertrand [b,c], Mariano Gutiérrez [c], Sophie Bertrand [a], Luis Vasquez [c]

[a] University of Washington, School of Fisheries, Box 355640, Seattle, WA 98195, USA
[b] IRD, UR097, CRHMT, Avenue Jean Monnet, BP 171, 34203 Sète Cedex, France
[c] Instituto del Mar del Perú (IMARPE), Gamarra y General Valle s/n Chucuito, Callao, Peru

ARTICLE INFO

Article history:
Accepted 14 October 2008
Available online 21 October 2008

Keywords:
Peru-Humboldt Current System
El Niño Southern Oscillation
Pelagic fish spatial distribution
Water masses
Upwelling
Anchoveta
Sardine

ABSTRACT

The Humboldt Current System (HCS) is dominated by two pelagic species; Peruvian anchovy or anchoveta (*Engraulis ringens*) and sardine (*Sardinops sagax*). Using data from 43 acoustic surveys conducted from 1983 through 2005 by the Peruvian Marine Institute (IMARPE), we examined the distribution of these two species relative to water masses. We tested the hypothesis that anchovy was found more frequently in upwelled cold coastal water (CCW) and mixed waters (MCW) than in other water types and that sardine was more associated with more offshore oceanic surface subtropical water (SSW). Surface temperature, salinity, latitude, season and distance to the coast data were used to define water masses. Results using generalized additive models (GAM), modelling sardine and anchovy presence–absence as a function of year, water body, bottom depth and latitude, showed that anchovy were primarily found in CCW and MCS, while sardine were more ubiquitous relative to water masses with some predilection for SSW. These results were supported by various indexes of anchovy and sardine distribution versus water mass as well as temporal and location variables.

1. Introduction

The Humboldt Current System (HCS) off Peru is one of the most productive coastal upwelling systems in the world (Carr, 2002). It supports the world's largest tonnage fishery for Peruvian anchovy or anchoveta (*Engraulis ringens*) (Bouchón et al., 2000) and has in the past also supported a major sardine (*Sardinops sagax*) fishery (Csirke et al., 1996). The HCS experiences year-round upwelling (Thomas et al., 2001). The abundance of anchovy and sardine appears to be linked both to El Niño Southern Oscillation (ENSO) events (frequency of 2–7 years) and to decadal-length regime shifts (Lluch-Belda et al., 1992; McFarlane et al., 2002; Chavez et al., 2003; Alheit and Niquen, 2004). Additionally, the abundance of the anchovy population appears to fluctuate out of phase with sardine in the HCS (Lluch-Belda et al., 1989, 1992; Csirke et al., 1996; Schwartzlose et al., 1999; Bakun and Broad, 2003; Fréon et al., 2003). Chavez et al. (2003) proposed the term 'El Viejo' to define the warm, decadal 'sardine regimes' and 'La Vieja' to define the cold decadal 'anchovy regimes'. However, little is known about the processes underlying the functional response of these species to ENSO events and decadal regime (Bertrand et al., 2004).

It has been hypothesized that cold upwelling water, which supports elevated levels of phytoplankton (Thomas et al., 2001; Chavez et al., 2003), provides overall favourable conditions, in particular for feeding, for anchovy while sardine appears to be favoured in warmer oceanic and frontal waters (Bertrand et al., 2004; Gutiérrez et al., 2007). Sardine is a more efficient filter feeder on phytoplankton and small zooplankton, while anchovy operates more efficiently preying on larger zooplankton (Konchina, 1991; van der Lingen et al., 2006, in press; Espinoza and Bertrand, 2008). Thus, more favourable feeding conditions for sardine may predominate in small and for anchovy in large-zooplankton areas, presumably corresponding to warmer oceanic water and cooler upwelling water, respectively (Mackas et al., 2001; Peterson et al., 2002; Zamon and Welch, 2005). Bertrand et al. (2004) hypothesized that variation in the range of favourable habitat leads to variation in spatial extent of the fish populations. In that sense, dramatic biomasses of anchovy can be concentrated in very small refuge areas when conditions are adverse, as occurred, for instance, during the El Niño event of 1997–1998 (Bertrand et al., 2004). When the range of favourable habitat increases very quickly (at the beginning of La Niña condition for instance) the fish range of distribution can increase drastically even if the population is still not very abundant (Bertrand et al., 2004; Gutiérrez et al., 2007). Gutiérrez et al. (2007) provide evidence that environmentally mediated alterations in habitat range can lead to population changes. In that paper habitat was defined using a very simple proxy, the coast-wide temperature anomaly (Gutiérrez et al., 2007) over a long time period, while the other paper used a more

---

[*] Corresponding author. Tel.: +1 206 543 5997; fax: +1 206 543 6785.
E-mail address: gordie@apl.washington.edu (G. Swartzman).

0079-6611/$ - see front matter © 2008 Elsevier Ltd. All rights reserved.
doi:10.1016/j.pocean.2008.10.021

complex water mass definition but with a short time series (Bertrand et al., 2004).

Here we examine the hypothesized relationships using a complex water mass definition over a long time series. Within this context our objective is to describe the co-variation of water masses and fish spatial distributions and to test hypotheses concerning fish association with water masses. To this end, we used data from 43 acoustic surveys off the Peruvian coast from 1983 to 2005.

2. Data and methods

2.1. Acoustic survey data

Acoustic data were collected from 1983 to 2005 by the Peruvian Marine Institute (IMARPE), most commonly using the R/V Humboldt (76 m long), the R/V Olaya (41 m long) or the R/V SNP-1 (36 m long). At least two acoustic surveys were run in most years. Survey design was composed of parallel transects averaging 90 nautical miles (167 km) long with an inter-transect distance varying between 14 and 16 nautical miles (26–30 km) depending on the cruise.

The surveys intended to cover most of the range of anchovy distribution (transects shown in Fig. 1), which varied from survey to survey. Extensive midwater trawl sampling completed the acoustic surveys for species identification. The seasonal and temporal distributions of scientific acoustic surveys were: spring (1983, 1986, 1989, 1990, 1996–2005), summer (1990–1996, 1999–2005), autumn (1985, 1986, 1997, 2 surveys in 1998), and winter (1984, 1987–1989, 1991, 1998–2005 with 2 winter surveys in 1999, 2000 and 2001). The acoustic surveys deployed Simrad (Kongsberg Simrad AS, Kongsberg, Norway) scientific echosounders EK, EKS, EK400 before 1995, and EY500 and EK500 (the EK60 was also used 2001–2005 in one vessel) thereafter. After 1998 at least two vessels were used for each survey to reduce survey time and the bias from changes in distribution of studied species during the survey. Calibration and intercalibration of the echosounders were undertaken before each survey. Calibration up until 1992 used hydrophones and after 1992 sphere calibration followed a standard procedure (Foote et al., 1987). A bias may exist in acoustic backscatter over the years due to the use of different calibration methods, but more likely due to the use of different acoustic systems. The magnitude of this latter bias is unknown but is assumed to not be a major factor since some calibrations between the systems were made. Acoustic back-scattered energy by surface unit (s_A) was recorded in each geo-referenced elementary sampling distance unit (ESDU) of 2 n.mi. (1983–1993) or 1 n.mi. (1994–2005). Acoustic echo identification was performed using fishing trawl composition and echotrace characteristics. Biomass estimation based on both the trawls and acoustic backscatter for each species was carried out by IMARPE for each survey. There were between 55 and 660 trawls for each survey (average of 190 trawls) .Surface temperature and salinity were measured and interpolated per ESDU for almost all surveys (exceptions are missing samples in summer 1990 for both temperature and salinity and additionally summer 1994 and spring 2000 for salinity), while surface oxygen levels were measured for about half the surveys but were not used because the coverage (number of surveys) was deemed insufficient.

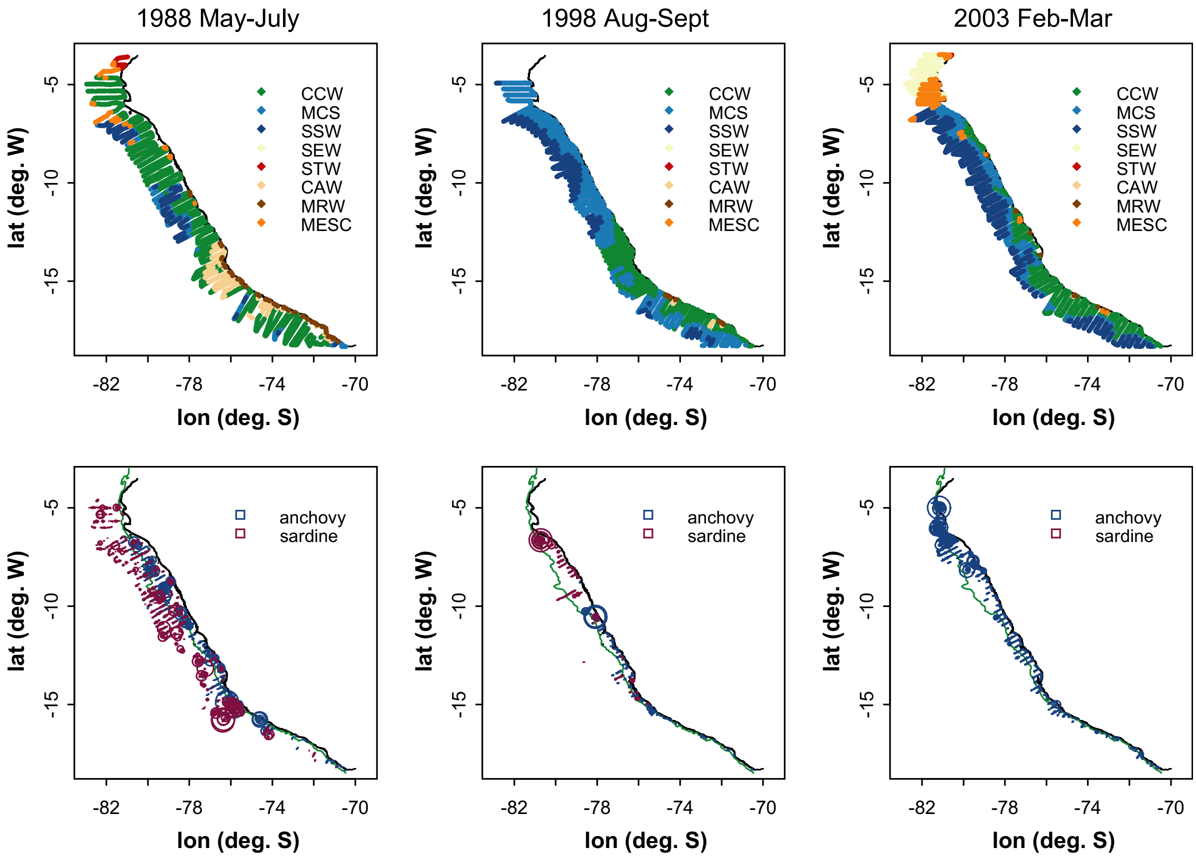

Fig. 1. Plots of the spatial distribution of anchovy (blue circles) and sardine (red circles) abundance (acoustic s_A; lower panels) and of eight water mass categories (upper panels) from acoustic surveys off the coast of Peru in (left to right) 1988, 1998, and 2003. The 200 m isobath is shown on the lower panels.

2.2. Definition of water mass types

Since Peru is a strong upwelling area the water near the coast is generally dominated by upwelled cold coastal water (CCW) which is highly productive. However, over the years the location and extent of this water mass changes considerably and, during periods like El Niño it may completely disappear (Zuta, 1988). The northern region is frequently dominated by warmer water masses coming from the North (Zuta and Guillen, 1970). Offshore, subtropical (oceanic) water, more saline and warmer also mix with the coastal and the equatorial waters (Zuta et al., 1978). Occasionally, Antarctic generated waters reach the Peruvian coast and river water also enters the area. As such, the water masses off Peru are a labile mix of several water types of different temperature and salinity ranges (Urquizo et al., 1987; Strub et al., 1998). We developed in this work an algorithm for defining water masses in one of eight categories based mainly on temperature and salinity ranges but also on season and sometimes latitude ranges as well (Blanco et al., 2001). The algorithm was based on a method discussed in Bertrand et al. (2004) but extended by four additional water mass categories to accommodate the much larger number of survey conditions considered here. To produce an effective categorization, we expect the algorithm to produce contiguous ESDU having the same category (i.e. that the water masses did not appear to be randomly distributed, but represented reasonable sized spatial regions of similar water mass), and unique water mass by ESDU (each ESDU belonged to no more than one water mass type). Also, we intended the categorization to be complete in that very few ESDU would not fit into any category. Because environmental conditions (i.e. temperature and salinity) were highly variable between surveys and due to some missing data, it was not possible to meet these criteria all the time. However, the incidence of uncategorized ESDU was less than 5% of all surveys and, for ESDU without missing temperature or salinity less than 1% was uncategorized. The parameter ranges for defining cold coastal (upwelling) water (CCW), mixed coastal-subtropical (oceanic) water (MCS), surface subtropical water (SSW), surface equatorial water (SEW), surface tropical water (STW), mixed equatorial, subtropical and coastal water (MESC), mixed coastal and river water (MRW) and cold Antarctic water (CAW) are given in Table 1 and were defined according to the literature (Zuta and Guillen, 1970; Morón, 2000). Examples of surveys with water mass distributions compared to sardine and anchovy distributions are given in Fig. 1. Graphs for all surveys are given in Appendix 1 in the web version.

The water masses defined in this paper are dominated by upwelling water (cold coastal water; CCW), this very productive water mass tends to be near the coast and has somewhat lower salinity than the local oceanic or surface subtropical water (SSW) south of 8°S, or lower temperature than the local surface equatorial water (SEW) north of 8°S, which has an intermediate temperature range (Table 1). In the northern region (north of 8°S) very low salinity and warm tropical water is also found (STW), while in the extreme south coast of Peru (south of 13°S and offshore (beyond 5 n.mi from the coast) low temperature and salinity surface Antarctic water (SAW) is found. This is distinguished from low salinity masses of water mixing upwelling water with riverine water (mixed riverine water; MRW) by the latter being closer to the coast (and possibly also farther north to 8°S). Two other masses of water represent mixtures between the primary water types. When spreading CCW mixes with SSW, mixed coastal-subtropical water (MCS) is formed. This water mass is distinguished from SSW by having lower salinities than SSW with potentially higher temperatures or a temperature range similar to CCW, but with higher salinity. North of 8°S CCW can mix both with equatorial

Table 1

Criteria in temperature, salinity, latitude and seasonal ranges used to categorize the eight water mass classes. STW: surface tropical waters; SEW: surface equatorial waters; SSW: surface subtropical waters; CCW: cold coastal water; MESC: mixed equatorial, subtropical and coastal water; MCS: mixed subtropical and coastal water; CAW: coastal Antarctic water; MRW: mixed river and coastal water.

Water mass	Temperature	Salinity	Latitude	Season	Special considerations
CCW	$14 < T < 18$	$34.8 \leqslant S \leqslant 35.0$	S of 8°S[a]	Spring	
	$14 < T < 19$			Summer	
	$14 < T < 18$			Autumn–winter	
	$13.5 < T < 17$			Spring	
	$T \geqslant 18$		N of 8°S	Summer	
	$T \geqslant 19$			Autumn–winter	
	$T \geqslant 18$				
	$T \geqslant 17$				
SSW		$S > 35.1$			
SEW	$20 < T < 26$	$34.0 < S < 34.8$	N of 8°S	Winter–spring	
	$21 < T < 26$			Summer–autumn	
STW	$T > 21$	$S < 34.0$	N of 8°S	Spring	
	$T > 24$			Summer	
	$T > 22$			Autumn–winter	
	$T > 20$				
MCS[b]	$14 < T < 25$	$35.05 \leqslant S < 35.1$		Spring–autumn	
	$13.5 < T < 25$			Winter	
	$14 < T < 18$	$S \geqslant 35.05$		Spring	
	$14 < T < 19$			Summer	
	$14 < T < 18$			Autumn–winter	
	$13.5 < T < 17$				
MESC	$T \geqslant 18$	$34.8 < S < 35.05$	N of 8°S	Spring, autumn	
	$T \geqslant 19$			Summer	
	$T \geqslant 17$			Winter	
	$14 < T \leqslant 18$	$34.0 < S \leqslant 34.8$		Spring, autumn	
	$14 < T \leqslant 19$			Summer	
	$14 < T \leqslant 17$			winter	
MRW	$14 < T < 20$	$S < 34.8$	S of 8°S	Spring–autumn	⩽5 nm of coast
	$13.5 < T < 20$			Winter	
CAW	$13 < T < 18$	$S < 34.8$	S of 13°S		>5 nm of coast

[a] Increase maximum by 1 °C north of 8°S and decrease minimum by 1 °C south of 15°S.

[b] Temperature and salinity ranges are either the top group or second group of the MCS and MESC rows.

SEW and subtropical SSW resulting in a mixed equatorial, subtropical and coastal water (MESC). This water mass has either high temperatures and intermediate salinities or lower temperatures and lower salinities (Table 1). The temperature thresholds defining the ranges of temperature for the different water masses can change between seasons (higher in summer) and the boundary of 8°S between different water masses can shift south (during El Niño) and north (La Niña; Table 1).

2.3. Water mass and fish species centroids and correlation

In order to analyse the effect of water mass dynamic on fish spatial distribution we first examined the distribution of water masses over space and time. We computed the percentage of the survey area in each water mass type in each survey. We divided the coast into 1° latitude bins and computed the dominant water mass in each bin in the 1–10, 10–25 and 25–50 n.mi. distance ranges from the coast. To help the interpretation of water masses time series, we used a temperature anomaly time series from Chicama (8°S), Peru, which is a good surrogate for temperature anomaly (tA) for the entire Peruvian HCS (Gutiérrez et al., 2007). Strong positive anomalies of this index illustrate the El Niño events of 1987, 1992 and 1997–1998 (Fig. 2a; but; the very weak El Niño in 2002 was not detectable in the temperature anomaly data series).

We computed for each survey, fish species and water mass category, the centroid of the distance from the coast and tested for correlation between the fish and water mass centroids. When testing correlation between parameters we took into account autocorrelation (Pyper and Peterman, 1998; *ACF* procedure from S-PLUS) and multiple testing (Bonferroni correction, in Peres-Neto, 1999) potential bias.

To examine a survey-wide measure of the preference of anchovy and sardine for a particular water mass type we computed, for each survey, the ratio of (a) the fraction of the total s_A of anchovy or sardine contained in a particular water mass to (b) the fraction of ESDU of the survey in that water mass. For example, a ratio of 1 represents no preference for that water mass (i.e. the proportion of anchovy in a water mass in the survey is the same as that for the entire survey), while a ratio of 2 represents that the fish abundance is twice as high in this water mass than if the fish had been distributed randomly among the water masses.

2.4. GAM modelling

We modelled the probability of anchovy and sardine presence in an ESDU as a function of latitude, year, bottom depth, and water mass using generalized additive models (GAM; Hastie and Tibshirani, 1990). Since the dependent variable was the probability of fish presence in an ESDU we assumed an underlying binomial distribution. Spline smoothers were used in all cases. Since water mass is a categorical variable ANOVA was used to model it. Thus the full analysis was a mixed model. Additionally, we used the Akaike information criterion to stepwise test whether a variable should be either removed from the GAM or included as a linear factor (rather than a smooth) by examining whether the elimination of a variable or changing from a GAM smooth to a linear factor would reduce the information criterion (or, in case both reduce it, which would most reduce it). This was affected through the S-PLUS function *step.gam*.

3. Results

3.1. Spatio-temporal dynamics of water masses

The percentage of CCW, SSW and MCS water for each survey (Fig. 2b) show that the CCW extent decreased during the El Niño events, while SSW increased and MCS decreased. This pattern was particularly clear during the 1992 and 1997–1998 El Niño (this pattern was not apparent for the 1987 El Niño event probably because there was no survey during the strong positive temperature anomaly part of this event; Fig. 2). The extent of CCW showed a seasonal pattern, more evident since 1998 (as the number of surveys increased from 1 or 2 per year to 2–4 after 1998) with increases during the winter and decreases during summer.

The spatial distribution of water masses north–south but also onshore-offshore (Fig. 3) shows an interesting contrast before and after 1999. During warmer periods (1992–1995 and 1997–1998) SSW dominated the coastal domain (to 25 n.mi.; Fig. 3a

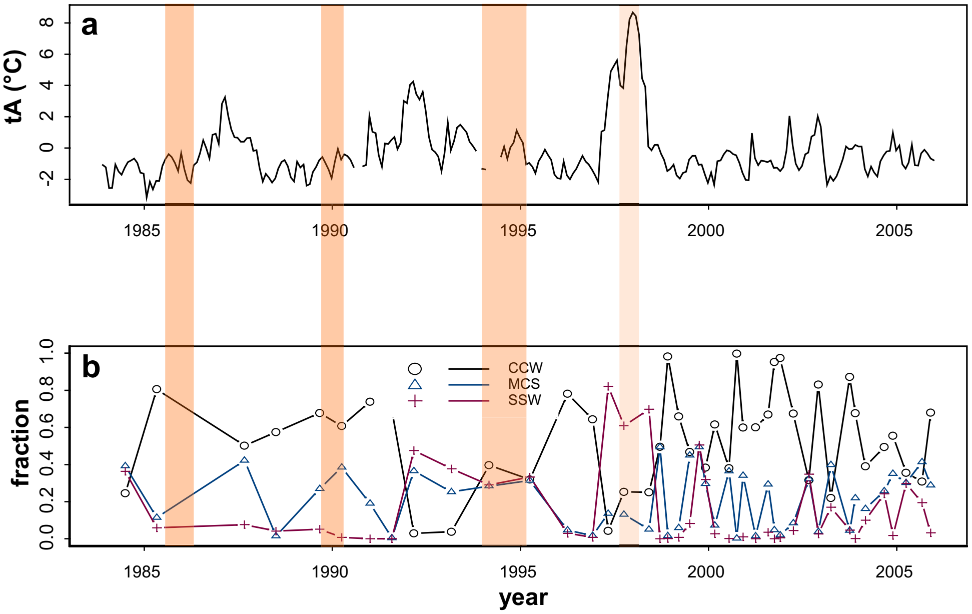

Fig. 2. (a) Temperature anomaly (tA) for surface temperature off the Peruvian coast near Chicama (8°S), Peru (b). Percentage of the survey area covered by CCW, SSW, and MCS from 1983 to 2005. El Niño periods are shown by salmon coloured bands with intensity proportional to opacity.

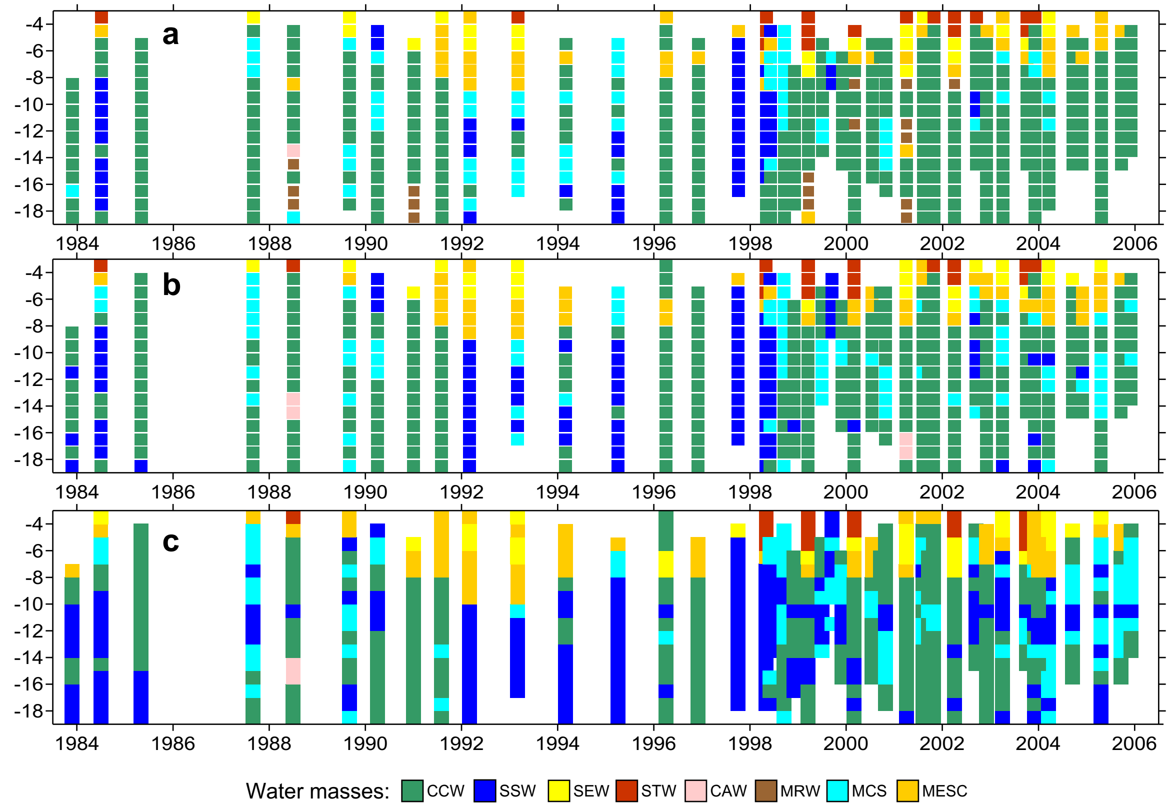

Fig. 3. Dominant water mass by degree of latitude along the Peruvian coast for each survey (a) between 0 and 10 n.mi. from the coast; (b) between 10 and 25 n.mi. from the coast; (c) between 25 and 50 n.mi. from the coast. Year markers refer to January 1. During some years survey results overlap due to intensive temporal coverage.

and b) over a large latitude range, and was even often prevalent close to shore (to 10 n.mi.; Fig. 3a). Since 1999 tropical waters were present in the north in many years. South of 6°S there was dominance by CCW coastward but also offshore to 25 n.mi. and even out to 50 n.mi. for much of the coast. This pattern was also observable for most surveys between 1987 and 1991 (Fig. 3).

3.2. Relating water masses, anchovy and sardine

Anchovy mean distance to the coast (Fig. 4) was significantly correlated with the distance to the coast of the CCW centroid ($r = 0.48$, $p = 0.003$) and the MCS centroid ($r = 0.44$, $p = 0.006$), but not with that of SSW. Sardine mean distance to the coast (Fig. 4) was correlated with the distance to the coast of the SSW centroid ($r = 0.40$, $p = 0.028$) and marginally non-significant with the MCS centroid ($r = 0.38$, $p = 0.058$). This suggests an association of anchovy CCW and MCS water masses and of sardine with SSW. As expected, anchovy was distributed closer to the coast than sardine. The position of the centroid of anchovy distribution was much more variable than that of sardine, which ranged between 40 and 60 km from the coast until the mid 1990s. Thereafter the position of the sardine coast distance centroid distribution showed wider variations. During El Niño periods (except the weak event of 2002), the centroid of anchovy distribution was very close to the coast in 1987, 1992–1993 and 1997–1998 (Fig. 4). The centroid for sardine distribution was also closer to the coast in 1997–1998 but not during the other El Niño periods. As expected, CCW was, on average, closer to the coast during El Niño periods though less so in 1987 (note, however that there was no spring or summer survey in 1987). Similarly, the centroids for SSW and MCS were found closer to the coast during El Niño periods, as they presumably extended their range to include the near coast (Fig. 3). There were no clear patterns in the time series for coast distance of the other water mass categories (not graphed).

The analysis of the preference of anchovy (Fig. 5a) and sardine (Fig. 5b) for a particular water mass according to their availability (based on abundance ratios) shows contrasted results. Results for anchovy are clear with a strong preference for CCW (mean ratio >1.5) all along the time series with a peak during the 1997–98 El Niño. The relationship with MCS (mean ratio ~1) was neutral and negative with SSW (mean ratio <0.5). Results for sardine show three different periods. Until 1991 there was no clear pattern and sardine was distributed in each water mass in proportion to their availability (all mean ratios ~1). From 1992 to the end of 1996, sardine was proportionally more distributed in MCS (mean ratio >1.5) than in other water masses. Since 1997 sardine were usually found preferentially in SSW, although the ratio was quite variable.

3.3. GAM modelling

A GAM model with a binomial link function represented the probability of anchovy presence in any ESDU as a function of latitude, depth, water mass (because water mass is a categorical variable, it is included as an analysis of variance factor in the model) and time of the survey (Fig. 6). The probability of encountering anchovy increased over time, but was relatively constant between the El Niño of 1992 and 1997, followed by further increase after 1998. Relative to latitude, probability of encountering anchovy was highest between 6°S and 14°S and was significantly lower outside this range. There was a decrease in the probability of encounter with increasing water depth (generally fewer anchovy in deeper water). The water mass effect show that anchovy was much more prevalent in CCW (and MRW and CAW), had intermediate encounter probability in mixed waters (MCS and MESC) and was

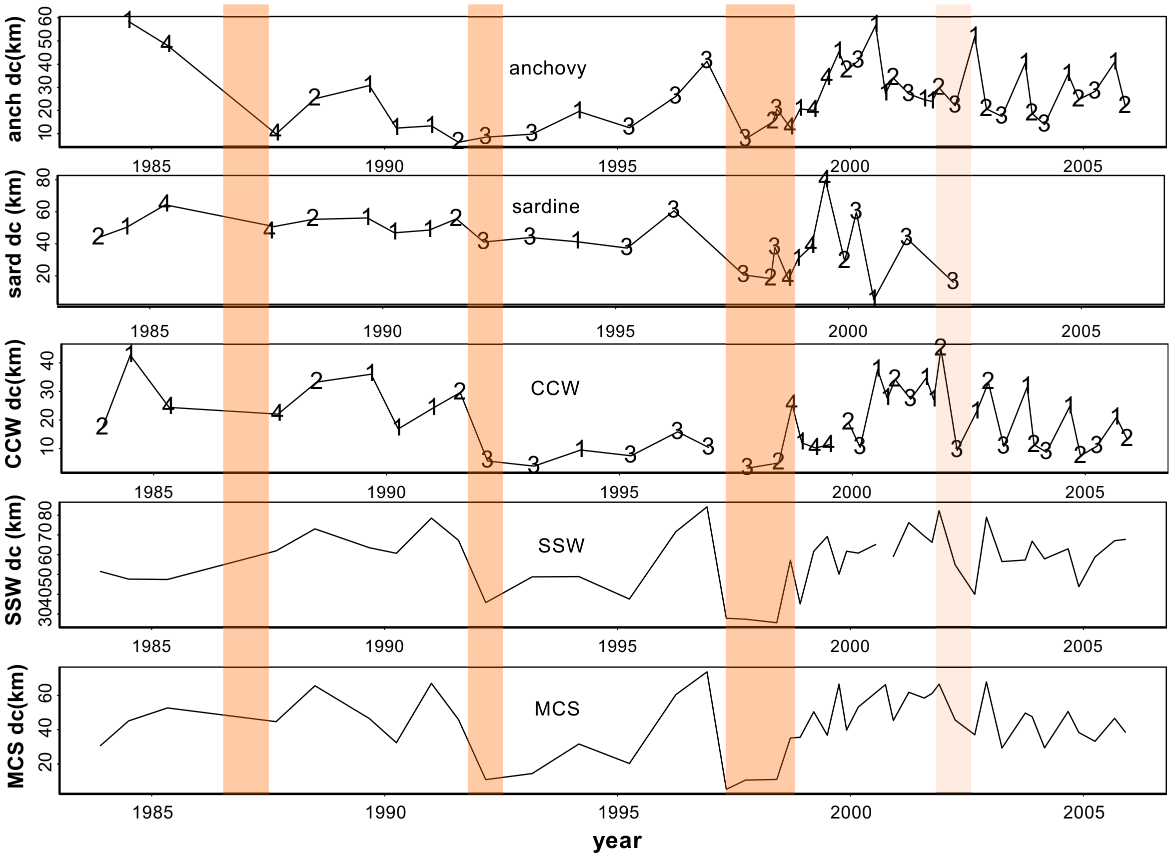

Fig. 4. Distance from the coast (dc; km) of the centroid of distribution of, top to bottom, anchovy s_A, sardine s_A, CCW, SSW and MCS water masses, based on acoustic survey data and concomitant surface temperature and salinity measurements taken from 1983 to 2005 off the coast of Peru. The season is noted by a number 1-4 for winter–spring–summer–autumn. Missing centroids reflect too small a sample size in that category for a survey. El Niño periods are shown by salmon coloured bands with intensity proportional to opacity.

lowest in warmer SSW, SEW and STW. All effects shown were highly significant with *p*-values near 0.

The sardine presence GAM model showed quite different responses to the covariates from those for anchovy (Fig. 7). The temporal effect was markedly different, with constant high probability of sardine ($s_A > 0$) before 1994 and a rapid decline thereafter. Unlike anchovy, sardine probability of encounter was not highest in shallow water, but increased with increasing depth up to 800 m and decreased thereafter. The water mass associations with sardine were weaker than for anchovy. Sardine showed a slight affinity for subtropical and warm waters (SSW, MESC and SEW, but not STW), a slight negative association with colder waters (MRW, CAW and CCW) and intermediate association with MCS and STW (Fig. 7). All GAM main effects were significant with *p-values* close to 0, except depth which had a *p*-value of 0.001. However, most of the water mass differences were not statistically significant (note the overlap in the error bars for the water mass effects). Several of the water mass effects had very wide error bars, reflecting the few data for these water mass types).

4. Discussion

4.1. Water mass dynamics

Inside our "window of observation", the dominant water masses were CCW (highly productive, medium salinity, low temperature), SSW (oligotrophic, high salinity and temperature), and, generally south of 8°S, MCS (mesotrophic, low temperature and high salinity, or medium temperature and medium salinity). An important feature of these water masses is their strong dependence on salinity (Table 1), which makes distinguishing them using satellite products alone problematical. Although the study of the seasonal dynamics of water masses is hampered by unequal seasonal sampling, particularly before 1998 (Figs. 2 and 3), there is a clear increase in the extent of CCW during winter and a reduction in summer. However, the La Niña of 1999–2000 seems to have initiated a period of stronger upwelling all along the coast most of the year (Fig. 3). This change affected the weather of the northern coast, and people complained of "cooler" summers and winters (Mariano Gutierrez, IMARPE, pers. com.). The earlier period, before the El Niño of 1997–1998, was characterised by consistently less cold coastal water and more subtropical water (Figs. 2 and 3). Another notable pattern was the higher percentage of SSW and lower percentages of CCW and MCS during 1992–1995 (note, however, that those surveys were performed in summer, which on average have lower percentages of CCW and MCS waters).

4.2. Anchovy and water masses

The methods we used demonstrated the strong relationship linking anchovy distribution to cold and highly productive water masses in general and CCW in particular. Thus, anchovy distance to the coast was correlated with the distance from the coast of the centroid of CCW and MCS, but not with that of SSW (Fig. 4). Anchovy distance from the coast was consistently lower during 1992–1995, when SSW dominated the Peruvian coast (Figs. 2 and 3); compressing CCW and anchovy distributions closer to the coast (see Gutiérrez et al., 2007 for detailed spatial patterns of anchovy

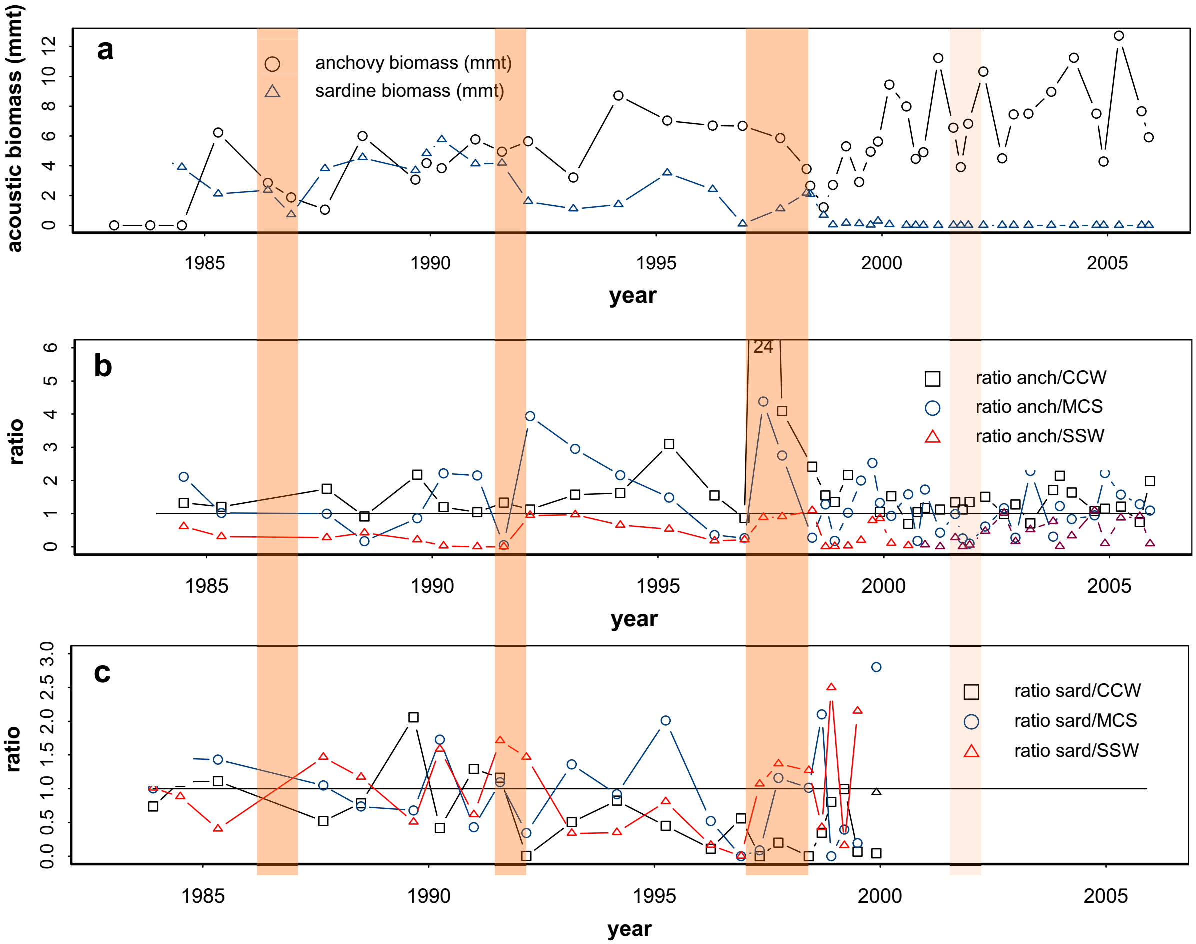

Fig. 5. Acoustic survey estimates for (a) anchovy and sardine biomass. Ratio of the fraction of total s_A of anchovy (b) and sardine (c) in CCW, MCS and SSW respectively to the fraction of total survey ESDU in that water mass. A ratio of 1 (horizontal line shown) represents no preference for that water mass. El Niño periods are shown by salmon coloured bands with intensity proportional to opacity.

and sardine). This pattern was even more marked during the El Niño of 1997–1998. CCW almost disappeared and SSW dominated all along the coast (Fig. 3). Anchovy was then concentrated in few refuge areas (Bertrand et al., 2004) where productive CCW were still present. This affinity of anchovy for colder CCW and MCS is also illustrated by the very high abundance ratios for anchovy in CCW and to a lesser extent in MCS during the 1997–1998 El Niño (Fig. 5a). Anchovy distribution relative to the proportion of water mass available showed a clear and consistent association with CCW, whatever its availability. GAM results (Fig. 6) showed that the probability of anchovy presence in an ESDU was highest in cold and highly productive water masses (CCW, CAW and MRW) and lowest in oceanic and tropical water masses (SSW, SEW, STW). These results are in accordance with previous work (Ñiquen et al., 2000; Bertrand et al., 2004), and, as they are based on longer time series and more exhaustive analysis, they demonstrate with more confidence the affinity of anchovy for CCW. The anchovy range (probability of having anchovy in an ESDU) appears to depend both on water mass type and overall abundance. The relationship of range with abundance can be seen by comparing the year effect for the GAM (Fig. 6) with anchovy acoustic abundance estimates (Fig. 5a; based on the same surveys). The latter show much more variability, though the long-term pattern is similar. As average anchovy abundance increased over time their range also expanded. Because CCW increased particularly in the winter, the range of anchovy, directly associated with CCW, also increased during that season.

4.3. Sardine and water masses

Sardine association with water mass was weaker than anchovy. Sardine distance to the coast was significantly correlated with the distance from the coast of the centroid of SSW but not with that of CCW and MCS (Fig. 4). GAM results (Fig. 7) also illustrate that sardine had a slight (though not statistically significant) preference for SSW compared to CCW. These results seem to support (weakly) a relationship between sardine and SSW (e.g. Castillo et al., 1996; Bertrand et al., 2004). There is no apparent seasonal change in sardine range, possibly due to their lack of or weak association with water masses or possibly due to the insufficiency of seasonal coverage during the period of sardine dominance, Analysis of sardine distribution relative to the proportion of water mass available, suggested three different periods: before 1992; 1992–1997; and after the 1997–1998 El Niño (Fig. 5b). Interestingly, these periods are similar to the ones defined by Gutiérrez et al. (2007) based on fish spatial patterns of distribution (independent of water mass). Before 1992 (a period of mixed sardine and anchovy dominance, Fig. 5a; Gutiérrez et al., 2007), sardine did not have any consistent preference for any of the three dominant water masses (CCS, SSW and MCS) and was distributed between the water masses in proportion to their availability in the study area (i.e. abundance to water mass ratio about 1.0). During this period sardine was mainly distributed between 40 and 60 km from the coast (offshore part of the CCW), centred around the shelf break (GAM results by period not shown) and straddling CCW, SSW and MCS water masses.

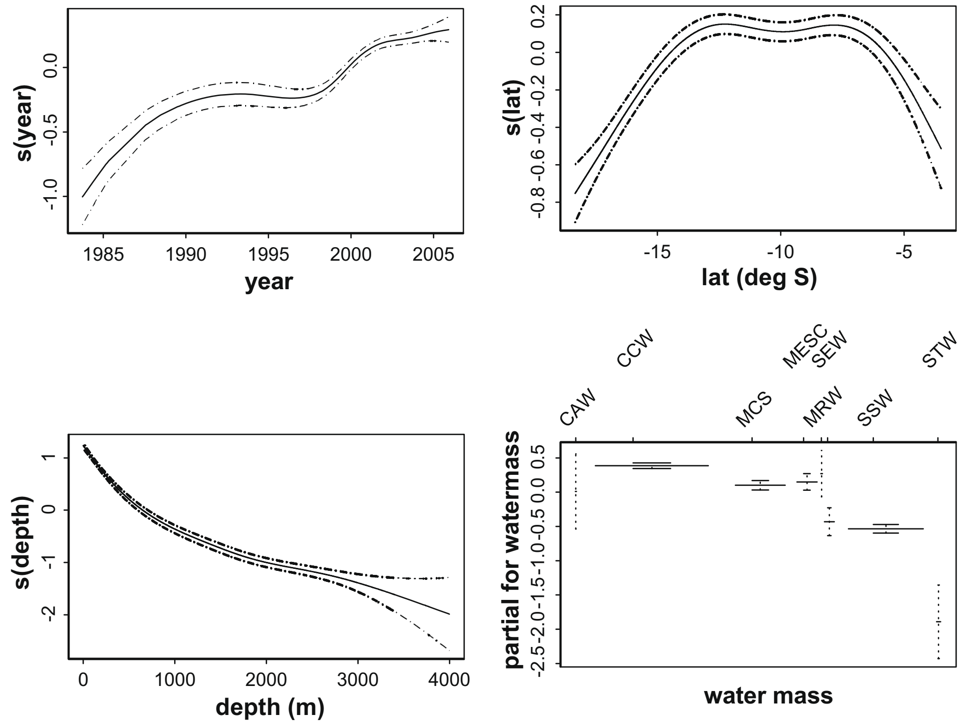

Fig. 6. GAM analysis of anchovy presence probability as a function of water mass, latitude, water column depth and year.

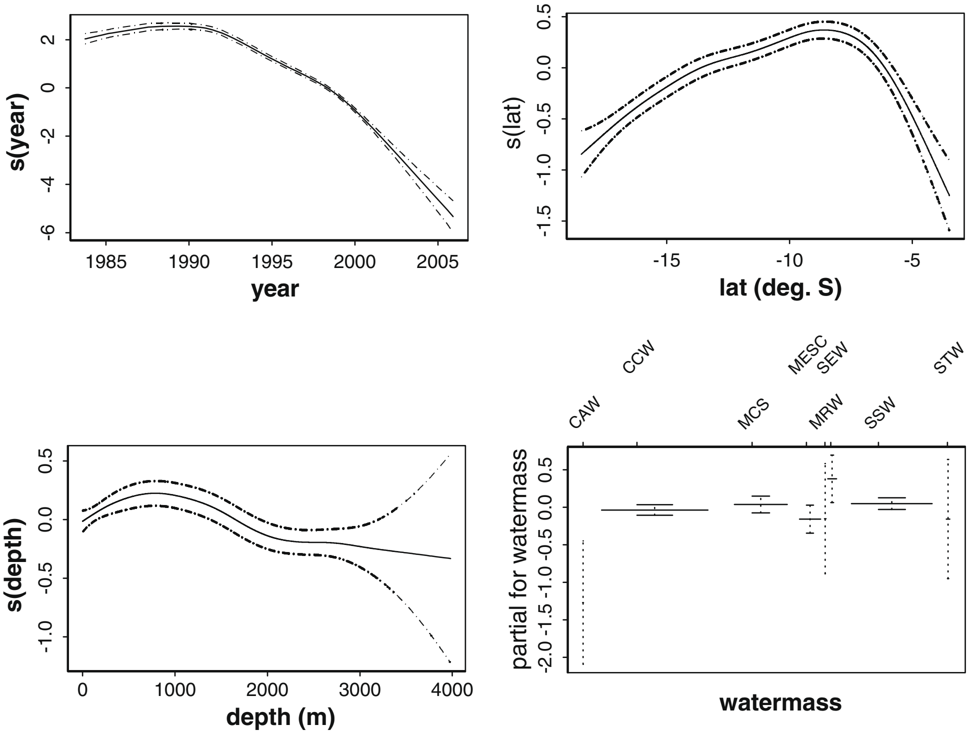

Fig. 7. GAM analysis of sardine presence probability as a function of water mass, latitude, water column depth and year.

The abundant sardine population during this period (Fig. 5a) probably benefited from the enhanced production and retention provided by the shelf break area. From 1992 to 1997 (a period of anchovy dominance; Gutiérrez et al., 2007) the reduced population of sardine (Fig. 5a) was distributed closer to the coast, perhaps associated with the intrusion of SSW toward the coast (Fig. 3) and was found mainly on the shelf (GAM results by period not shown) in the frontal MCS waters between CCW and SSW. Finally, after the 1997–1998 El Niño (period of anchovy dominance; Gutiérrez et al., 2007), sardine was initially distributed preferentially in SSW and then disappeared from the Peruvian coast. We do not know from available evidence whether the absence of sardine after 2000 was due to population depletion or to the migration of sardine out of the survey area. However, the lack of sardine capture by scientific or commercial vessels strongly suggest that sardine population off Peru was depleted (see Bertrand et al. (2004) and Gutiérrez et al. (2007) for more details). A more offshore distribution of sardine-favourable habitat, as found after 1997, should indeed disadvantage sardine since biological enrichment or larval retention and more generally recruitment success would likely be reduced by the offshore Ekman transport of their eggs and larvae which dilute them and diminish their chance of benefiting from aggregations of their most efficiently utilized food sources (see Bakun's triad; Bakun, 1996).

Sardine appears to have a different feeding strategy than anchovy, apparently moving more than anchovy to find large aggregations of small zooplankton and phytoplankton, which they can efficiently filter (van der Lingen et al., 2006). Thus, their presence in a particular water mass may depend more on the availability of small-sized food than on water mass per se, among SSW, MCS and CCW. While CCW is characterised by dominance by large plankton favouring the particulate feeding behaviour of anchovy, and SSW by smaller plankton more appropriate to sardine filter feeding (Mackas et al., 2001; Peterson et al., 2002; van der Lingen et al., 2006), sardine, a more migratory species, may find large aggregations of appropriate sized food in any of the water masses. The fact that sardine is a highly migratory species is supported by the existence of a single sardine species along both East and West Pacific Ocean coasts (Lluch-Belda et al., 1992). It is important to note that, unlike the case with anchovy, our study area may not include the entire range of sardine distribution. It is therefore possible that a proportion of sardine was distributed farther offshore than the survey (i.e. in SSW) and was not considered in our analysis. This problem limits the significance of our results for sardine.

4.4. Synthesis

Peruvian anchovy clearly preferentially inhabits the CCW and other associated cold and productive water masses (CAW and MRW and, to a lesser extent, MCS). Its range of distribution is intimately linked to the area covered by CCW independent of anchovy's abundance as suggested by the habitat-based model proposed by Bertrand et al. (2004). In contrast to previous studies, which suggested anchovy range should be linked primarily to the size of anchovy stock (e.g. Lluch-Belda et al., 1989) it appears that anchovy range of distribution is primarily related to the size of favourable habitat (determined by large scale oceanic forcing, e.g. Kelvin waves, see Bertrand etal. (2008b) and secondarily to the size of the fish stock. These conclusions are supported by our analysis and by examples such as when millions of tons of anchovy were distributed in a very small refuge area during the 1997–1998 El Niño (Bertrand et al., 2004) while a similar anchovy biomass occupied a much larger surface area (>3-fold) in April–May 1986 when CCW was more extensive.

For sardine, even though the results are limited by the fact that we may have only observed a part of the stock (the surveys were designed to focus on the distribution of anchovy, not sardine), the relationship with SSW was weak and varied over time, illustrating a more pervasive distribution.

Sardine and anchovy appear to be ecological neighbours but not ecological analogues (Bertrand et al., 2004; Gutiérrez et al., 2007). Their differences depend not only on differences in their trophic level (e.g. Konchina, 1991; Schwartzlose et al., 1999; van der Lingen et al., 2006), but also on the strength of their association with water mass and their migrating capacities (e.g. Rodríguez-Sánchez et al., 2002). Sardine showed a slight preference for SSW (e.g. Castillo et al., 1996; Bertrand et al., 2004) while anchovy range significantly overlapped with CCW. Both species are able to feed directly on phytoplankton, although sardines are more efficient filter feeders (van der Lingen et al., 2006). Anchovy, which are bite feeders (Konchina, 1991; van der Lingen et al., 2006), are not able to sustain growth on a diet consisting entirely of phytoplankton (Espinoza et al., 2000; van der Lingen et al., 2006) and are mainly zooplanktivorous (98.0% of dietary carbon; Espinoza and Bertrand, 2008). We hypothesize that anchovy associates preferably with CCW because these areas are dominated by the larger zooplankton efficiently ingested by these predominately predators (see Bertrand et al., 2008a for small scale association between anchovy and zooplankton patches); sardine may find better feeding conditions in areas containing abundant aggregations of small filterable zooplankton in their patchy environment, which may predominate in SSW and mixed water masses (e.g. MCS and MESC).

Sardine is a fish that appears well adapted to the Humboldt Current Ecosystem. It has the ability to perform long migrations, to utilize very small particles (van der Lingen, 2002; van der Lingen et al., 2006; Garrido et al., 2007), to feed and spawn in rather low productivity areas (Garrido et al., 2007), to grow to a size less susceptible to predation than anchovy, and to occupy more offshore environments less susceptible to predation on eggs, larvae and early juveniles (Bakun and Broad, 2003). Therefore, it is a challenge to explain why sardine is currently depleted in the HCS? The answer may be in the distribution of sardine habitat in relation to the shelf and the shelf break. When its preferred habitat moves further offshore (i.e. increased upwelling), as happens during cool periods, retention of eggs and larvae of sardine may be reduced, weakening larval feeding success and survival. Also, the depletion of the sardine during high upwelling periods may be due to reduction in its usable habitat through an extremely shallow oxycline associated with an expanded oxygen minimum zone (OMZ), which is known to affect the vertical and horizontal distribution of many marine organisms (Morales et al., 1999). Finally it is important to note that sardine depletion was probably aggravated by overfishing during the 1990s, in particular during El Niño 1997–98 (Csirke et al., 1996; Bertrand et al., 2004).

Acknowledgements

The authors gratefully thank Peruvian Marine Research Institute (IMARPE) for having facilitated the use of the data for this work. This work is a contribution of the Research Unit 'ECO-UP' UR 097 and of the Interdepartmental Thematic Action "Humboldt Current System" from IRD. This work was supported in part by the US National Science Foundation in a grant number NSF0075 to two of the investigators (gls and sb).

Appendix A. Supplementary data

Supplementary data associated with this article can be found, in the online version, at doi:10.1016/j.pocean.2008.10.021.

References

Alheit, J., Niquen, M., 2004. Regime shifts in the Humboldt Current ecosystem. Progress in Oceanography 60, 201–222.

Bakun, A., 1996. Patterns in the ocean: ocean process and marine population dynamics. Centro de Investigaciones biológicas del Nordeste, La Paz, México and University of California Sea Grant, San Diego, USA, 325 p..

Bakun, A., Broad, K., 2003. Environmental 'loopholes' and fish population dynamics: comparative pattern recognition with focus on El Niño effects in the Pacific. Fisheries Oceanography 12, 458–473.

Bertrand, A., Segura, M., Gutiérrez, M., Vásquez, L., 2004. From small-scale habitat loopholes to decadal cycles: a habitat-based hypothesis explaining fluctuation in pelagic fish populations off Peru. Fish and Fisheries 5, 296–316.

Bertrand, A., Gerlotto, F., Bertrand, S., Gutiérrez, M., Alza, L., Chipollini, A., Diaz, E., Espinoza, P., Ledesma, L., Quesquén, R., Peraltilla, S., Chavez, F., 2008a. Aggregation behaviour and environmental forcing as determinisms of fish 3D spatiotemporal distribution across scales: the case for the anchoveta. Progress in Oceanography..

Bertrand, S., Dewitte, B., Pasapera, J., Bertrand, A., 2008b. Spatial re-organisations in the Peru Humboldt Current system under Kelvin waves forcing: contrasting ecological scenarios from physics to fishers. Progress in Oceanography..

Blanco, J.L., Thomas, A., Carr, M.-E., Strub, T., 2001. Seasonal climatology of hydrographic conditions in the upwelling region off northern Chile. Journal of Geophysical Research 106 (C6), 11451–11467.

Bouchón, M., Cahuín, S., Díaz, E., Ñiquen, M., 2000. Captura y esfuerzo pesquero de la pesquería de anchoveta peruana (*Engraulis ringens*). Boletín del Instituto del Mar del Perú 19, 109–115 (in Spanish, with English abstract).

Carr, M.-E., 2002. Estimation of potential productivity in Eastern Boundary Currents using remote sensing. Deep-Sea Research II 49, 59–80.

Castillo, J., Barbieri, M.A., Gonzalez, A., 1996. Relationships between sea surface temperature, salinity, and pelagic fish distribution off northern Chile. ICES Journal of Marine Science 53, 139–146.

Chavez, F.P., Ryan, J., Lluch-Cota, S.E., Niquen, M., 2003. From anchovies to sardines and back: multidecadal change in the Pacific Ocean. Science 299, 217–221.

Csirke, J., Guevara-Carrasco, R., Cárdenas, G., Ñiquen, M., Chipollini, A., 1996. Situación de los recursos anchoveta (*Engraulis ringens*) y sardina (*Sardinops sagax*) a principios de 1994 y perspectivas para la pesca en el Perú, con particular referencia a las regiones norte y centro de la costa peruana. Boletín del Instituto del Mar del Perú 15, 1–23 (in Spanish, with English abstract).

Espinoza, P., Bertrand, A., 2008. Revising anchovy's (*Engraulis ringens*) trophic niche and ecological role reveals its plasticity and lead to a new vision of the Humboldt Current system. Progress in Oceanography..

Espinoza, P., Blascovic, V., Torriani, F., Navarro, I., 2000. Dieta de la anchoveta *Engraulis ringens* según intervalos de talla. Crucero BIC José Olaya Balandra y BIC Humboldt, 9906. Informe del Instituto del Mar del Perú No. 149.

Foote, K.G., Knudsen, H.P., Vestnes, D.N., MacLennan, D.N., Simmonds, E.J., 1987. Calibration of acoustic instruments for fish density estimation: a practical guide. ICES Cooperative Research Report No. 144, pp. 1–69..

Fréon, P., Mullon, C., Voisin, B., 2003. Investigating remote synchronous patterns in fisheries. Fisheries Oceanography 12, 443–457.

Garrido, S., Marçalo, A., Zwolinski, J., van der Lingen, C.D., 2007. Laboratory investigations on the effect of prey size and concentration on the feeding behaviour of *Sardina pilchardus*. Marine Ecology Progress Series 330, 189–199.

Gutiérrez, M., Swartzman, G., Bertrand, A., Bertrand, S., 2007. Anchovy and sardine spatial dynamics and aggregation patterns in the Humboldt Current ecosystem, Peru, from 1983–2003. Fisheries Oceanography 16, 155–168.

Hastie, T., Tibshirani, R., 1990. Generalized Additive Models. Chapman and Hall, London, UK.

Konchina, Y.V., 1991. Trophic status of the Peruvian anchovy and sardine. Journal of Ichthyology 31, 59–72.

Lluch-Belda, D., Crawford, R.J.M., Kawasaki, T., MacCall, A.D., Parrish, R.H., Schwartzlose, R.A., Smith, P.E., 1989. World-wide fluctuations of sardine and anchovy stocks: the regime problem. South African Journal of Marine Science 8, 195–205.

Lluch-Belda, D., Schwartzlose, R.A., Serra, R., Parrish, R., Kawasaki, T., Hedgecock, D., Crawford, R.J.M., 1992. Sardine and anchovy regime fluctuations of abundance in four regions of the world oceans: a workshop report. Fisheries Oceanography 1, 339–347.

Mackas, D.L., Thomson, R.E., Galbraith, M.D., 2001. Changes in the zooplankton community of the British Columbia continental margin, 1985–1999, and their covariation with oceanographic conditions. Canadian Journal of Fisheries and Aquatic Science 58, 685–702.

McFarlane, G.A., Smith, P.E., Baumgartner, T.R., Hunter, J.R., 2002. Climate variability and Pacific sardine population and fisheries. American Fisheries Society Symposium 32, 195–214.

Morales, C.E., Hormazabal, S.E., Blanco, J.L., 1999. Interannual variability in the mesoscale distribution of the depth of the upper boundary of the oxygen minimum layer off northern Chile (18–24°S). Implications for the pelagic system and biogeochemical cycling. Journal of Marine Research 57, 909–932.

Morón, O., 2000. Características del ambiente marino frente a la costa peruana. Boletín del Instituto del Mar del Perú 19, 179–204 (in Spanish, with English abstract).

Ñiquen, M., Bouchón, M., Cahuín, S., Díaz, E., 2000. Pesquería de anchoveta del mar Peruano 1950 – 1999. Boletín del Instituto del Mar del Perú 19, 117–123 (in Spanish, with English abstract).

Peres-Neto, P.R., 1999. How many statistical tests are too many? The problem of conducting multiple ecological inferences revisited. Marine Ecology Progress Series 176, 303–306.

Peterson, W.T., Keister, J.E., Feinberg, L.R., 2002. The effects of the 1997–99 El Niño/La Niña events on hydrography and zooplankton off the central Oregon coast. Progress in Oceanography 54, 381–398.

Pyper, B.J., Peterman, R.M., 1998. Comparison of methods to account for autocorrelation in correlation analyses of fish data. Canadian Journal of Fisheries and Aquatic Sciences 55, 2127–2140.

Rodríguez-Sánchez, R., Lluch-Belda, D., Villalobos, H., Ortega-García, S., 2002. Dynamic geography of small pelagic fish populations in the California Current System on the regime time scale (1931–1997). Canadian Journal of Fisheries and Aquatic Sciences 59, 1980–1988.

Schwartzlose, R.A., Alheit, J., Bakun, A., Baumgartner, T.R., Cloete, R., Crawford, R. J.M., Fletcher, W.J., Green-Ruiz, Y., Hagen, E., Kawasaki, T., Lluch-Belda, D., Lluch-Cota, S.E., MacCall, A.D., Matsuura, Y., et al., 1999. Worldwide large-scale fluctuations of sardine and anchovy populations. South African Journal of Marine Science 21, 289–347.

Strub, T., Mesias, J., Montecino, V., Rutllant, J., Salinas, S., 1998. Coastal ocean circulation off Western South America. In: Robinson, A.R., Brink, K.H. (Eds.), The Sea, vol II. John Wiley, New York, pp. 273–314.

Thomas, A.C., Blanco, J.L., Carr, M.-E., Strub, P.T., Osses, J., 2001. Satellite-measured. Chlorophyll and temperature variability off northern Chile during the 1996–1998 La Nina and El Nino. Journal of Geophysical Research 106 (18), 899–915.

Urquizo, W., Wosnitza-Mendo, C., Valdivia, E., Moreno, C., 1987. Catalogo de datos oceanográficos (T, S y O2) por estaciones del ano en diferentes profundidades frente a la costa peruana. Periodo: 1970–1985. Informe del Instituto del Mar del Perú (in Spanish, with English abstract)..

van der Lingen, C.D., 2002. Diet of sardine *Sardinops sagax* in the southern Benguela upwelling ecosystem. South African Journal of Marine Science 24, 301–316.

van der Lingen, C.D., Hutchings, L., Field, J.G., 2006. Comparative trophodynamics of anchovy *Engraulis encrasicolus* and sardine *Sardinops sagax* in the southern Benguela: are species alternations between small pelagic fish trophodynamically mediated?. African Journal of Marine Science 28, 465–477.

van der Lingen, C.D., Bertrand, A., Bode, A., Brodeur, R., Cubillos, L., Espinoza, P., Friedland, K., Garrido, S., Irigoien, X., Möllman, C., Rodriguez-Sanchez, R., Tanaka, H., Temming, A., in press. Trophic dynamics of small pelagic fish. In: Checkley Jr., D.M., Roy, C., Alheit, J. (Eds.), Climate Change and Small Pelagic Fish..

Zamon, J., Welch, D., 2005. Rapid shift in zooplankton community composition on the Northeast Pacific Shelf during the 1998–1999 El Niño–La Niña event. Canadian Journal of Fisheries and Aquatic Sciences 62, 133–144.

Zuta, S., Guillen, O., 1970. Oceanografía de las Aguas Costeras del Perú. Boletín del Instituto del Mar del Perú 2, 157–324 (in Spanish, with English abstract).

Zuta, S., Rivera, T., Bustamante, A., 1978. Hydrologic aspects of the main upwelling areas off Peru. In: Boje, R., Tomczak, M. (Eds.), Upwelling Ecosystems..

Zuta, S., 1988. Variations of the mass field and currents off the Peru coast. In: IOC. Time Series of Ocean measurements, vol 4. IOC Tech Ser. 33, UNESCO..

Progress in Oceanography 79 (2008) 238–255

Contents lists available at ScienceDirect

Progress in Oceanography

journal homepage: www.elsevier.com/locate/pocean

Zooplankton research off Peru: A review

Patricia Ayón [a,*], Maria I. Criales-Hernandez [a], Ralf Schwamborn [b,c], Hans-Jürgen Hirche [c]

[a] Instituto del Mar del Perú, Apartado 22 Callao, Peru
[b] Department of Zoology, Universidade Federal de Pernambuco, Recife, Brazil
[c] Alfred Wegener Institute for Polar and Marine Research, Bremerhaven, Germany

ARTICLE INFO

Article history:
Accepted 14 October 2008
Available online 21 October 2008

Keywords:
Zooplankton
Review
ENSO
Time series
Humboldt Current
Peru

ABSTRACT

A review of zooplankton studies conducted in Peruvian marine waters is given. After a short history of the development of zooplankton research off Peru, we review zooplankton methodology, taxonomy, biodiversity, spatial distribution, seasonal and interannual variability, trophodynamics, secondary production, and modelling. We review studies on several micro-, meso-, macro-, and meroplankton groups, and give a species list from both published and unpublished reports. Three regional zooplankton groups have been identified: (1) a continental shelf group dominated by *Acartia tonsa* and *Centropages brachiatus*; (2) a continental slope group characterized by siphonophores, bivalves, foraminifera and radiolaria; (3) and a species-rich oceanic group. The highest zooplankton abundances and biomasses were often found between 4–6°S and 14–16°S, where continental shelves are narrow. Species composition changes with distance from the shore. Species composition and biomass also vary strongly on short time scales due to advection, peaks of larval production, trophic interactions, and community succession. The relation of zooplankton to climatic variability (ENSO and multi-decadal) and fish stocks is discussed in the context of ecological regime shifts. An intermediate upwelling hypothesis is proposed, based on the negative effects of low upwelling intensity in summer or extremely strong and enduring winter upwelling on zooplankton abundance off Peru. According to this hypothesis, intermediate upwelling creates an optimal environmental window for zooplankton communities. Finally, we highlight important knowledge gaps that warrant attention in future.

1. Introduction

The coastal upwelling ecosystem off Peru hosts the world's largest single-species fisheries, which is sustained by wind-driven upwelling of nutrient-rich waters to the sunlit surface, where phytoplankton bloom at the base of highly productive pelagic food webs (Bertrand et al., 2005; see also Pennington et al., 2006). Many zooplankton eat phytoplankton, and are in turn preyed upon by fish larvae and many adult planktivorous fish. Conversely, certain zooplankton groups (e.g. medusae) also prey on fish eggs and larvae. Due to their intermediate position in the food web between primary producers and predators, zooplankton serves as a link between bottom-up climate-related control of phytoplankton and fish.

Here we present a short review of zooplankton research off Peru. We focused on meroplankton, macro-, meso-, and microzooplankton, but left the extensive literature on Peruvian ichthyoplankton for a separate review. We build on the short review by Guzmán and Carrasco (1996) of IMARPE ichthyo- and zooplankton studies. Montecino et al. (2006) and Pennington et al. (2006) provided overviews of biological–physical interaction processes off western South America, including several aspects of the Peruvian sector of the Humboldt Current System. More specific reviews of the Peruvian upwelling ecosystem were given by Arntz and Fahrbach (1991), Tarazona and Arntz (2001) and Tarazona et al. (2003), but the main emphasis was on benthic communities and fisheries stocks and zooplankton were mentioned only briefly. An extensive review of zooplankton in the eastern tropical Pacific, however, was recently published by Fernández-Álamo and Färber-Lorda (2006), who focused on large-scale surveys in the eastern tropical Pacific (e.g. EASTROPAC). Our review provides an overview of the work conducted off Peru. In particular, we (1) provide an overview and basis for comparison with other upwelling regions, by (2) summarizing all the literature available, much of which was found in unpublished reports and theses, and (3) identify gaps in our knowledge.

2. History of zooplankton research in Peru

Peruvian marine research was established in 1960 with the Instituto de Investigaciones de los Recursos Marinos (IREMAR) with the financial and technical support of FAO, which in 1964 changed its name to Instituto del Mar de Perú (IMARPE). IMARPE's

---

* Corresponding author. Tel.: +51 14202000x263; fax: +51 14296069.
E-mail address: payon@imarpe.gob.pe (P. Ayón).

0079-6611/$ - see front matter © 2008 Elsevier Ltd. All rights reserved.
doi:10.1016/j.pocean.2008.10.020

initial mission was to compile scientific information about Peru's fish stocks to provide a scientific base for management decisions. With time, events affecting the stocks led to the realization that the scientific base had to be broadened to scale that were previously not regarded as necessary. This lesson was brought home by the catastrophic effects of El Niño's on the anchoveta fishery and Peru's continued dependence on this single-species fishery (Dickie and Valdivia, 1981).

Early zooplankton work concentrated on taxonomy and horizontal distribution (Vásquez, 1967; Alvarado, 1972; Gómez, 1972), especially of euphausiids (Santander, 1967; Santander and Sandoval de Castillo, 1969) and appendicularians (Fenaux, 1968). Additional work followed in the 70s during the International Decade of Ocean Exploration, which coincided with the initial decade of the Law of the Sea. The Law of the Sea emphasized that nations have rights to their coastal resources, including the right of exploration and research (Ancieta, 1981). Interest in the biological production in Peruvian coastal waters was high due to the prosperous anchovy-meal industry.

The international program CUEA (Coastal Upwelling Ecosystem Analysis, 1972–1980) was developed to study the physical, chemical, and biological drivers within upwelling ecosystems. It compared the upwelling systems of Oregon, Baja California, Peru, NW Africa, and Somalia. CUEA was conceived following the "Anton Bruun" Cruise off Peru in 1966 (e.g. Ryther et al., 1966; Ryther, 1967; Barber and Chavez, 1991). Under CUEA, interdisciplinary multiship studies were conducted off Peru during the JOINT-II expedition from March to October 1976 and March to May, 1977. Results were presented in a series of meetings (Barcelona, 1970; Investigaciones Pesqueras 35, 1, 1975; Marseille, 1973; Tethys 6, 1974; Kiel, 1975; Upwelling Ecosystems, 1978) and on the IDOE (International Decade of Ocean Exploration) International Symposium on Coastal Upwelling in Kiel, 1975.

Several cruises of the Institute of Oceanology, Russia, were conducted in 1974 (Vinogradov, 1977) to study the pelagic communities of tropical regions and their zones of intensive upwelling. The majority of the results are published in the journal Oceanology.

In 1975, the Peruvian-German Program PROCOPA (Programa Cooperativo Peruano-Alemán de Investigación Pesquera) was initiated, which lasted until 1985. Its main purpose was to support research in areas that could not be covered sufficiently by Peruvian scientists. Part of the program was the building of RV "Alexander Humboldt", which remains an important vessel in Peruvian fishery research in 1994, Germany funded time series sampling at stations off Paita and San José ("Fixed Coastal Stations Program", Table 2). Sampling at these stations is ongoing.

The bi-country project ICANE (Investigación Cooperativa de la Anchoveta y su Ecosistema) between Peru and Canada began in 1976 during severe changes in the fisheries. The goal was to identify causes of the recent decreases of the anchovy population, with the goal of predicting events in this system on time scales relevant to fishery management (Dickie and Valdivia, 1981). Results were published in Boletín Instituto del Mar del Perú-Callao, Vol. extraordinario (1981). These interdisciplinary programs improved Peruvian field work and data analysis and also established collaborations between Peruvian and foreign scientists.

Table 1
Water masses found in surface waters off Peru.

Water masses	Salinity	Temperature (°C)
Tropical Surface Water (TSW)	<33.8[a]	>25[b]
Equatorial Surface Water (ESW)	33.8–34.8[b]	>20[b]
Subtropical Surface Water (SSW)	35.1–35.7[a]	18–27[b]
Cold Coastal Water (CCW)	34.8–35.1[a]	14–18[c]

[a] Zuta and Guillén (1970).
[b] Gutiérrez et al. (2005).
[c] Morón (2000).

Table 2
Summary of the main types of regular zooplankton surveys off Peru.

Program	Method	Comment
Hensen Net Program	Hensen net (330 μm mesh, 60 cm diameter), towed vertically from 50 m to the surface. Determination of Zooplankton settlement volume → Additional oblique bongo hauls (330 μm mesh, 60 cm diameter) from 200 m to surface	Several times per year since 1964. Hundreds of stations located over the whole marine area off Peru
Fixed Coastal Stations Program	WP2 net (330 μm mesh, 50 cm diameter), horizontal subsurface tows → Since 2004, oblique bongo net samples have been regularly taken at the Fixed Coastal Stations (330 μm mesh, 60 cm diameter for the Callao transect, 330 μm mesh and 22 cm diameter for Paita and San Jose transects) from 200 m to the surface or from the bottom to the surface	Bimonthly since 1994. Stations located on three transects perpendicular to the coast off Paita, San José, and Callao
Intensive Cruises Program (CRIOS)	Experiments for secondary production and grazing, Multinet (330 μm mesh), WP2 net (330 μm mesh) oblique bongo net sampling, laser optical plankton counter	Twice a year since 2005. Stations located on three transects off Callao and inside Bahia de Independencia. Started in the context of the CENSOR project

During the 80s, most of the zooplankton papers published by IMARPE scientists (Table 3) focused on taxonomy (e.g. Santander et al., 1981a,b; Carrasco, 1989), species distributions, water mass indicator species (e.g. Véliz, 1981, 1985; Carrasco de Luyo, 1981; Dextre, 1983; Santander and Carrasco, 1985; Sandoval de Castillo, 1987), effects of El Niño on zooplankton biomass (Santander and Carrasco, 1985), and zooplankton biovolumes (1964–1985; Carrasco and Lozano, 1989). Non-IMARPE researchers published studies (Table 3) on community structure (e.g. Boyd and Smith, 1983; Timonin and Flint, 1986; Vinogradov et al., 1980), diel vertical migration (e.g. Judkins, 1980; Mackas et al., 1981; Smith et al., 1981b) and trophic ecology (e.g. Dagg et al., 1980; Boyd et al., 1980; Herman, 1984).

From the 90s to the present (2007), IMARPE zooplankton scientists have published papers on interaction between zooplankton and the environment (particularly El Niño; Aronés and Ayón, 2002; Castillo et al., 2005), species composition and abundance (Abanto, 2001), diel vertical migration (Escudero, 2003), and zooplankton time series relative to fish stock (Alheit and Niquen, 2004) or hydrographic variability (Gutiérrez et al., 2005; Ayón et al., 2004; Aronés et al., in press; Ayón et al., 2008). This work was supported by the European Community VECEP Program (1993–1999), which supported several fisheries surveys, and World Bank loans to purchase laboratory equipment (1999). In 1998 the research vessel "José Olaya Balandra" was donated by the Japanese government including sampling gear and laboratory equipment. CICESE (Mexico) provided funds from 2004 to 2005 for the analysis of zooplankton time series. In 2005, the multi-country project CENSOR was launched in Peru, funded by the European Union ("Climate variability and El Niño Southern Oscillation: Implications for natural coastal resources and management"; Argentina, Chile, Peru, France, Germany, Spain). CENSOR's zooplankton component focuses on trophodynamic impacts on the time series variability, especially in coastal areas.

Table 3
Overview over selected publications on specific topics related to the zooplankton in marine waters off Peru.

Topics	Main references
Biogeography, distribution, and ecology of specific taxa	Siphonophores (Bigelow, 1911; Véliz, 1985; Sears, 1953)
	Ostracods (Castillo, 2004; Castillo et al., 2005, 2007)
	Copepods (Alvarado, 1972; Gómez, 1972, 1982; Geynrikh, 1973; Santander et al., 1981b; Ayón et al., 1999; Abanto, 2001; Aronés, 2002; Aronés and Ayón, 2002)
	Amphipods (Carrasco de Luyo, 1981; Santander et al., 1981b; Carrasco, 1989; Aronés, 1997)
	Euphausiids (Santander, 1967; Santander and Sandoval de Castillo, 1969; Alvarado, 1972; Antezana, 1978; Santander et al., 1981a,b; Antezana, 2002a)
	Holoplanktonic molluscs (Quesquén and Guzmán, 1999; Quesquén, 2005)
	Chaetognaths (Bieri (1957, 1959); Alvarado, 1972; Santander et al., 1981a,b; Dextre, 1983; Sandoval de Castillo, 1987)
	Appendicularians (Fenaux, 1968)
	Zooplankton guides (Santander, 1981; Santander et al., 1981a,b)
	Horizontal distribution and biogeography (Vásquez, 1967; Beers et al., 1971; Vinogradov, 1977; Guillén, 1978; Santander et al., 1981a,b; Dextre, 1983; Timonin and Flint, 1986; Vasil'ev, 1991; Ayón et al., 1996; Ayón and Girón, 1996; Aronés and Ayón, 2001; Aronés et al., 2001; Quesquén, 2004; Aronés, 2004; Gutiérrez et al., 2005)
Vertical distribution	Judkins (1980), Sameoto (1981), Mackas et al. (1981), Smith et al. (1981a,b), Glebov (1982), Semenova et al. (1982) and Antezana (2002b) (for *Euphausia mucronata*); Escudero (2003) and Criales-Hernández et al. (2008)
Development of plankton communities	Mikheyev (1977a,b), Smith (1978), Vinogradov and Shushkina (1978), Vinogradov et al. (1980) and Boyd and Smith (1983)
Time series	Zooplankton volumes off Peru since 1964 (Carrasco and Lozano, 1989; Ayón et al., 2004)
	Hydrography and mesozooplankton abundance and diversity off Paita 1994–2004 (Aronés et al., in press)
El Niño	Dextre (1983), Santander and Carrasco (1985), Carrasco and Santander (1987), Aronés (1997), Gómez (1997), Ayón et al. (1999), Aronés and Ayón (2002) and Castillo et al. (2005)
Trophic ecology	Grazing and excretion (Cowles, 1978, 1979; Dagg et al., 1980; Boyd et al., 1980; Paffenhöfer, 1982; Arashkevich et al., 1982; Herman, 1984)
	Zooplankton productivity (Shushkina and Kislyakov, 1977)
	Functional characteristics of planktonic communities (Shushkina et al., 1978)
	Microzooplankton production (Sorokin, 1978; Tumantseva and Kopylov, 1985a)

3. Study area – water masses, currents, and upwelling

The distribution of planktonic organisms is dependent on currents and water masses. The waters off Peru are part of the Humboldt Current System (HCS), which dominates most hydrodynamic processes off Chile and Peru (Fig. 1; cite reviews in PIO vol. 69). The Peru Coastal Current (PCC) flows equatorward, while the Peru–Chile Under-Current (PCUC) follows the shelf break towards the pole, and the Peru–Chile Counter-Current (PCCC) flows directly towards the south and veers to the west around 15°S (Penven et al., 2005). The flow of the PCC is strongest in austral winter, when equatorward winds are maximal (Bakun and Nelson, 1991; Echevin et al., 2004a,b; Croquette et al., 2005). It carries colder and saltier upwelled water to the north where they eventually become part of the South Equatorial Current (SEC).

Many oceanographic features vary seasonally and interannually, especially during EN. During "average" years, and especially during La Niña events, the Peruvian shelf is dominated by Cold Coastal Water (CCW, see Table 1), which is strongly influenced by coastal upwelling. Under normal conditions, upwelled waters originate from the PCUC (Echevin et al., 2004a,b). This upwelling of nutrient-rich waters sustains one of the most productive ecosystems of the world, with zooplankton biomasses which are among the highest recorded for large marine ecosystems in lower latitudes (Fernández-Álamo and Färber-Lorda, 2006). Plumes of upwelled water may extend several hundred km offshore at the

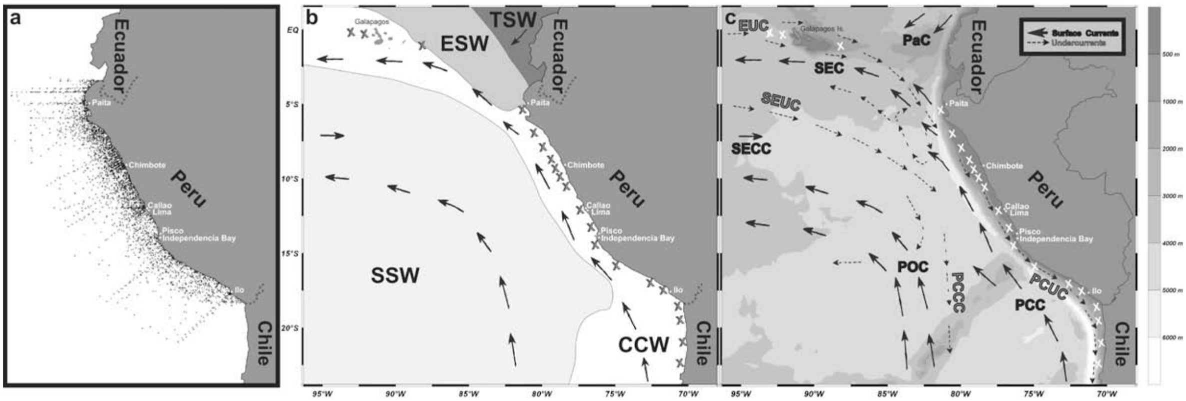

Fig. 1. Study area along the Peruvian coast showing zooplankton sampling stations covered since 1964 (Ayón et al., 2004, modified) (a), schematic distribution of characteristic surface water masses (b), and bathymetry with main currents (c). The approximate locations for main upwelling areas for nutrient-rich waters are indicated ("X"). According to Gunther (1936), Wyrtki (1963, 1967), Zuta and Guillen (1970), Tsuchiya (1981), Huyer et al. (1991), Strub et al. (1998), Schneider et al. (2003), Penven et al. (2005) and Croquette and Eldin (2006), modified. Water masses in b: CCW, Cold Coastal Water and mixed waters under the influence of upwelled cold waters; SSW, Subtropical Surface Water; ESW, Equatorial Surface Water; TSW, Tropical Surface Water. Currents in c: EUC, Equatorial Undercurrent or Cromwell Current; PaC, Panama Current; PCC, Peru Coastal Current, Chile–Peru Current, or Humboldt Current; PCCC, Peru–Chile Counter-Current; PCUC, Peru Coastal Undercurrent, Poleward Undercurrent (PUC), or Gunther Current; POC, Peru Oceanic Current, Oceanic Chile–Peru Current, or Oceanic Humboldt Current.

surface, leading to large-scale offshore blooms, but in general offshore oceanic waters are warmer and contain less nutrients than nearshore upwelled waters. The upwelled and offshore PCC waters interact on several time scales, e.g. the alternation of upwelling and relaxation episodes, seasonal variability upwelling strength, and most drastically by EN. During EN, warm and low-salinity Equatorial Surface Water (ESW) and Tropical Surface Water (TSW) spread southward, and offshore PCC water reaches closer to the coast (Zuta and Guillen, 1970; Fiedler and Talley, 2006). Replacement of nutrient-rich upwelled water by warmer and more oligotrophic offshore water masses leads to drastic changes in pelagic ecosystems.

Sea surface temperatures (SST) increase towards the equator. In northern Peru, equatorward of 14°S, summer SSTs reach 26 °C, while to the south minimum summer SSTs are 17–18 °C (Zuta and Guillen, 1970). In central and sourthern Peru, in winter, SST varies from 13 to 17 °C, and the 19 °C isotherm is found north of 10°S. Stronger than seasonal SST changes, however, ENSO generates a huge interannual variability (Fig. 4). Spatial SST differences are caused by basin scale latitudinal and local (shelf width, water depth) components. The Peruvian shelf is <200 m deep and widest (65 nm) between 7°S and 10°S, and narrowest (3–5 nm) equatorward 7°S and polewardof 15°S (Zuta and Guillen, 1970).

4. Research topics

4.1. Sampling and survey development

IMARPE has always focused on fisheries. Zooplankton samples were a by-product of ichthyoplankton sampling, which was conducted on all surveys, be it pelagic, demersal or hydrographic surveys. Between 1961 and 2006 ~150 surveys were carried out with more than 10,000 samples collected. Surveys covered up to 500 km from the coast between 3°30′S and 18°20′S, although over 95% of the samples were collected within 100 km of the coastline (Fig. 1). Two types of standard surveys for zooplankton sampling have evolved with time (Table 2):

1. In the Hensen Net Program, zooplankton data have been collected since 1964 on Pelagic Fish, Demersal Fish and Oceanographic Surveys, where a Hensen net (330 μm mesh, 60 cm diameter) has been towed vertically from 50 m to the surface. After removal of large coelenterates and ichthyoplankton, the zooplankton settlement volume is measured (Carrasco and Lozano, 1989; Ayón et al., 2004). The stations are located on a predefined meander-shaped cruise track covering the whole coastal area of Peru, although the cruise track was sometimes modified. Zooplankton samples were only taken at stations where echograms indicated fish were present and fish trawling should also be conducted. Since 1996, additional zooplankton sampling has been conducted where distance between trawl positions was >20 nm.
2. In the Fixed Coastal Stations Program, on transects perpendicular to the coast near Paita, San José and Callao horizontal surface tows have been taken since 1994 with a WP2 net (Working Party 2; UNESCO, 1968; 330 μm mesh, 50 cm diameter). Additionally, since 2004, oblique bongo net tows (60 cm diameter, 300 μm mesh size; Table 2) have been included.

During a limited project in 1996/1997, vertically stratified samples with a closing net (200 μm mesh, 85 cm mouth diameter) were taken, usually from 100–50–25–10–0 m on two fixed stations near Callao (12°12.0′S, 077°18.0′W, Escudero, 2003) and Chimbote (09°20.4′S, 79°41.0′W). Since 2000, on Demersal Fish Surveys stratified samples have been taken with a multinet (Hydrobios, 330 μm mesh, 50 × 50 cm mouth size) from 200–150–100–50–10–0 m. More advanced sampling methods have recently been used during the Intensive Cruises Program (CRIOS) that was started under the CENSOR project (Table 2, Section 4).

4.2. Biodiversity

In general, knowledge of the taxonomy of the zooplankton fauna is poor, considering the amount of work invested into sampling (Table 2) and the ecological and economic importance of these ecosystems. Bigelow (1911) and later Sears (1953) worked on siphonophores collected by the US Steamer Albatross in 1904/1905. Santander et al. (1981a,b) catalogued 3 siphonophore, 31 copepod, 35 amphipod, 6 euphausiid, and 6 chaetognath species. Abanto (2001) presented a list of 152 copepod species from 54 genera collected on 15 cruises between 3°30′S and 14°S and 1980–1989. The zooplankton species in Table 4 were identified from the Fixed Coastal Stations Program since 1994, and since 1997 from material sampled in the Hensen Net Program. Previously existing keys have usually been used for identification, which often are based on material from other regions. Organisms have sometimes been mis-identified. For example, during the same expeditions the abundant *Calanus* species were called *Calanus chiliensis* (Sameoto, 1981) and *C. australis* (Santander et al., 1981b). Therefore, a careful taxonomic revision of the fauna of the southeast Pacific is required.

4.3. Spatial patterns

4.3.1. Horizontal distribution and abundance

Santander (1967) provided the first data on major taxa in surface samples from transects perpendicular to the coast between Callao and Chimbote (copepods, euphausiids, appendicularians, siphonophores, and pteropods). In 1987, Carrasco and Santander found that during normal conditions between 6°S and 12°S, copepods were most abundant, followed by siphonophores, chaetognaths, polychaetes, euphausiids, and amphipods. Other studies have found that the main zooplankton groups off Peru were copepods, euphausiids, and chaetognaths (Ayón and Girón, 1996, 1997; Ayón and Aronés, 1997a,b; Ayón et al., 1996; Ayón and Girón, 2004). Off Paita and San José, ca. 98% of the zooplankton were crustaceans, copepods being by far the most abundant group (Gutiérrez et al., 2005).

Santander (1981) studied the zooplankton in an important upwelling area from Pisco to San Juan, in autumm 1976 and 1977. She concluded that food quality and concentration were regulating the zooplankton composition, being low primary production associated to the dominance of euryphagous or carnivorous species, with less herbivourous species. Santander (1981), defined three major zooplankton groups: (1) continental shelf (dominated by *A. tonsa* and *C. brachiatus*); (2) continental slope (siphonophores, bivalves, foraminifera, and radiolaria), (3) oceanic group (*Mecynocera clausi*, *Pleuromamma gracilis*, *Scolecithrix danae*, *Lucicutia flavicornis*, *Euchaeta marina*, *Euchirella bella*, *Oithona plumifera*, *Calocalanus pavo*, *Temora stylifera*, *T. discaudata*, *Nannocalanus minor*, *Eucalanus subtenuis*, *Acrocalanus* sp., *Corycaeus* sp., *Oithona* sp., *Oncaea* sp., *Sapphirina* sp., *Corycella* sp., *Copilia* sp.). Sameoto (1981) confirmed this species composition changes with distance from the shore, but noticed a high variability in species composition and biomass that can occur on daily time.

Planktonic ecosystems of the PCC under the influence of upwelled Cold Coastal Waters (CCW) differ markedly from the subtropical waters to the west by their high concentration of life (fish, birds, mammals, etc.) and by their huge biomass (Ayón et al., 2004). However, a recent analysis of historical data indicates that within the CCW, higher biovolumes are found offshore, prob-

Table 4
List of species identified in Peruvian zooplankton samples (Ayón et al., 2008, status of 2006). References: (1) IMARPE, unpublished; (2) Sears (1953); (3) Véliz (1985); (4) Santander et al. (1981a,b); (5) Quesquén (2005); (6) Castillo (2004); (7) Abanto (2001); (8) Gómez (1982); (9) Carrasco and Santander (1987); (10) Carrasco (1989); (11) Aronés (1997); (12) Santander (1967); (13) Dextre (1983); (14) Sund (1964); (15) Sandoval de Castillo (1987); (16) Fenaux (1968).

Cnidaria
Solmundella bitentaculata 1
Aeginura grimaldii 1
Aequorea coerulescens 1
Aequorea macrodactyla 1
Bougainvillia superciliaris 1
Bouganvillia fulva 1
Heterotiara anonyma 1
Obelia sp. 1
Phialidium uchidai 1
Cladonema sp. 1
Euphysa tentaculata 1
Sarsia eximia 1
Sarsia sp. 1
Cunina octonaria 1
Cunina frugifera 1
Cunina peregrina 1
Cunina globosa 1
Cunina tenella 1
Cunina duplicata 1
Solmissus incisus 1
Cytaeis tetrastyla 1
Geryonia proboscidalis 1
Liriope tetraphylla 1
Halicreas minimum 1
Hydractinia sp. 1
Eucheilota menoni 1
Tiaricodon coerulens 1
Amphinema sp. 1
Leuckartiara octona 1
Leuckartiara zacae 1
Stomotoca pterophylla 1
Stomotoca atra 1
Halitholus intermedia 1
Porpita porpita 1
Vellela velella 1
Pochella polynema 1
Aglaura hemistoma 1
Rhopalonema funerarium 1
Rhopalonema velatum 1
Sminthea eurygaster 1
Amphogona apicata 1
Pantachogon sp. 1
Pegantha laevis 1
Pegantha martagon 1
Pegantha clara 1
Pegantha triloba 1
Solmaris sp. 1
Chromatonema crythrogonon 1
Ectopleura dumortieri 1
Ectopleura sacculifera 1
Atolla wyvillei 1
Nausithoe punctata 1
Nausithoe rubra 1
Pelagia noctiluca 1
Chrysaora plocamia 1
Periphylla periphylla 1
Stomolophus meleagris 1
Phacellophora camtschatic 1
Abyla peruana 2
Ceratocymba leuckarti 1
Abylopsis tetragona 3
Abylopsis eschscholtzi 3
Bassia bassensis 1
Enneagonium hyalinum 1
Nanomia cara 1
Agalma elegans 3
Athoribia rosacea 1
Sulculeolaria biloba 1
Sulculeolaria chuni 1
Sulculeolaria quadrivalvis 1
Sulculeolaria turgida 1
Chelophyes appendiculata 1
Chelophyes contorta 1
Dyphyes bojani 1
Dyphyes dispar 3
Eudoxoides mitra 1
Eudoxoides spiralis 3
Lensia campanella 1
Lensia conoidea 1
Lensia cossack 1
Lensia fowleri 1
Lensia hotspur 1
Muggiaea atlantica 4
Muggiaea kochii 3
Hipopodius hippopus 1
Physophora hydrostatica 1
Rosacea plicata 1
Ctenophora
Bolinopsis infundibulum 1
Velamem sp. 1
Pleurobrachia pileus 1
Hormiphora plumosa 1
Beroe cucumis 1
Annelida
Pelagobia longicirrata 1
Tomopteris sp. 1
Mollusca
Protatanta souloyeti 5
Oxygyrus keraudreni 5
Atlanta turriculata 5
Atlanta helicinoides 1
Atlanta lesueuri 5
Atlanta peroni 5
Atlanta gaudichaudi 5
Atlanta inclinata 5
Carinaria lamarcki 5
Cardiapoda placenta 1
Pterotrachea hippocampus 5
Pterotrachea coronata 5
Firoloida desmaresti 5
Limcina bulimoides 5
Limacina inflata 5
Limacina trochiformis 5
Cavolinia inflexa 5
Cavolinia longirostris 5
Cavolinia uncinata 5
Diacria quadridentata 5
Clio pyramidata 5
Creseis acicula 5
Creseis virgula 5
Hyalocylis striata 5
Cymbulia sibogae 5
Desmopterus papillo 5
Peraclis apacifulva 1
Peraclis reticulata 1
Glaucus sp. 1
Phillirhoe bucephala 1
Cephalopyge trematoides 1
Branchiopoda
Penilia avirostris 1
Pleopis polyphemoides 1
Evadne espinifera 1
Evadne nordmanni 1
Pseudoevadne tergestina 1
Ostracoda
Archiconchoecia striata 6
Halocypris inflata 6
Euconchoecia aculeata 6
Euconchoecia chierchae 1
Conchoecetta giesbrechti 6
Conchoecia aff magna 6
Disconchoecia tamensis 6
Metaconchoecia inflata 6
Metaconchoecia kyrtophora 6
Mataconchoecia teretivalvata 6
Orthoconchoecia agassizi 6
Orthoconchoecia striola 6
Porroecia parthenoda 6
Porroecia porroecia pacifica 6
Porroecia pseudoparthenoda 6
Proceroecia decipiens 6
Copepoda
Acartia danae 7, 8
Acartia erytraea 7
Acartia negligens 7
Acartia lilljeborgii 1
Acartia tonsa 7, 8
Aetideus armatus 7
Aetideus giesbrechti 7
Euaetideus bradyi 7, 8
Euchirella bella 7, 8
Euchirella messinensis 1
Haloptilus acutifrons 7
Haloptilus ornatus 7
Haloptilus oxycephalus 7
Haloptilus sp. 7
Calanus australis 7, 8
Calanus chilensis 8
Calanus darwinii 1
Calanus tenuicornis 7
Canthocalanus pauper 1
Nannocalanus minor 7
Neocalanus robustior 7
Undinula darwinii 7
Undinula sp. 7
Candacia bipinnata 7
Candacia catula 7, 9
Candacia curta 7, 8
Candacia simplex 1
Candacia pachydactyla 7
Paracandacia truncata 7
Centropages brachiatus 7, 8
Centropages elongatus 7
Centropages furcatus 7
Centropages gracilis 7
Clausocalanus arcuicornis 7, 9
Clausocalanus sp. 7
Clausocalanus jobei 1
Clausocalanus furcatus 1
Clytemnestra rostrata 7, 8
Clytemnestra scutellata 7
Corycaeus auronitens 1
Corycaeus dubius 8
Corycaeus catus 7
Corycaeus crassiusculus 7
Corycaeus flaccus 7
Corycaeus furcifer 7
Corycaeus gibulus 10
Corycaeus lautus 1
Corycaeus limbatus 1
Corycaeus longistylis 7
Corycaeus robustus 7
Corycaeus speciosus 7
Corycaeus spp. 7
Farranula gibbula 7
Microsetella gracilis 7
Microsetella rosea 7
Eucalanus inermis 7, 8
Eucalanus elongatus 1
Paraeucalanus attenuatus 7
Rhincalanus cornutus 7
Rhincalanus nasutus 7, 8
Subeucalanus crassus 7
Subeucalanus mucronatus 7
Subeucalanus subcrassus 7
Euchaeta acuta 7, 10
Euchaeta indica 7
Euchaeta longicornis 7
Euchaeta media 1
Euchaeta plana 7
Euchaeta rimana 7
Euchaeta sp. 7
Euterpina acutifrons 10; 7
Heterorhabdus lobatus 1

Table 4 (*continued*)

Heterorhabdus papilliger 7
Lucicutia flavicornis 7, 8
Lucicutia gaussae 7
Mecynocera clausii 7, 8
Pleuromamma borealis 7, 8
Pleuromamma abdominalis 1
Pleuromamma gracilis 8
Pleuromamma piseki 7
Pleuromamma xiphias 7
Oithona sp. 7
Oithona atlantica 1
Otihona fallax 7
Otihona nana 1
Otihona plumifera 7, 8
Otihona setigera 7, 8
Otihona similis 10
Paraoithona parvula 7
Paraoithona sp. 7
Lubbockia squillimana 7
Oncaea conifera 7, 8
Oncaea venusta 7
Pachysoma dentatum 7
Acrocalanus gracilis 7
Acrocalanus monachus 9
Acrocalanus armatus 9
Acrocalanus sp. 7
Calocalanus pavo 7
Calocalanus plumulosus 7
Paracalanus parvus 7, 8
Otihona plumifera 7, 8
Otihona setigera 7, 8
Parvocalanus sp. 7
Phaenna spinifera 7
Calanopia sp. 1
Labidocera acuta 7
Labidocera acutifrons 7
Labidocera sp. 7
Labidocera pavo 1
Pontella sp. 1
Pontellina plumata 7, 8
Pontellopsis armata 7
Pontellopsis perpicans 1
Pontellopsis regalis 1
Pseudodiaptomus sp. 7
Copilia miriabilis 7
Copilia quadrata 1
Sapphirina angusta 1
Sapphirina auronitens 7
Sapphirina darwinii 7
Sapphirina gastrica 7
Sapphirina gemma 7
Sapphirina intestinata 7
Saphirina iris 1
Sapphirina metalina 7
Sapphirina nigromaculata 7
Sapphirina opalina 7
Sapphirina ovatolanceolata 7
Sapphirina spp. 7
Sapphirina stellata 7
Amallothrix sp. 7
Scaphocalanus echinatus 7
Scaphocalanus sp. 7
Scolecithricella abyssalis 7
Scolecithricella aupopecten 7
Scolecithricella bradyi 7, 8
Scolecithricella dentata 7
Scolecithricella minor 7
Scolecithricella spp. 7
Scolecithrix danae 7
Scolecithricella spinipedata 7
Scottocalanus sp. 7
Temeropia mayumbaensis 7
Temora discaudata 7
Temora stylifera 1
Tharybis sp. 7
Amphipoda
Anapronoe sp. 1
Dairella sp. 1
Hyperioides sibaginis 10, 11
Phronimopsis spinifera 10, 11
Hyperia medusarum 10
Hyperietta vosseleri 11
Hyperietta luzoni 11
Hyperietta stephenseni 11
Hyperiodes longipes 11
Hyperoche sp. 1
Lestrigonus bengalensis 11
Lestrigonus macrophthalmus 11
Lestrigonus shoemackeri 11
Lestrigonus schizogeneios 11
Themistella fusca 11
Lanceola sp. 1
Anapronoe sp. 1
Brachyscelus crusculum 10, 11
Lycaea spp. 11
Pseudolycaea sp. 1
Thamneus sp. 1
Tryphana malmi 11
Lycaeopsis themistoides 10, 11
Oxycephalus piscator 10, 11
Oxycephalus armatus 10
Oxycephalus clausi 1
Simorhynchotus antenarius 10
Calamorhynchus sp. 1
Cranocephalus sp. 1
Rhabdosoma armatum 1
Streetsia sp. 1
Turbegella sp. 1
Glossocephalus sp. 1
Leptocotis spinifera 11
Rhabdosoma minor 11
Paraphronima gracilis 11
Thyropus diaphanus 11
Euscelus robustus 11
Schizoscelus ornatus 11
Phronima sedentaria 10
Phronimella elongata 10, 11
Phronima dunbari 11
Phronima colleti 1
Prhronima bowmani 11
Phrosina semilunata 11
Anchylomera sp. 1
Primno macropa 11
Amphithyrus sculpturatus 11
Hemityphis tenuimanus 11
Platyscelus sp. 1
Tetrathyrus forcipatus 11
Parapronoe parva 10
Sympronoe sp. 1
Eupronoe maculata 11
Scina sp. 1
Vibilia armata 11
Vibilia chuni 11
Decapoda
Solenocera sp. 1
Penaeus stylirostris 1
P. vannamei 1
P. californicus 1
P. occidentalis 1
Sergestes sp. 1
Lucifer sp. 1
Callianassa sp. 1
Callichirus sp. 1
Pleuroncodes monodon 1
Pagurus sp. 1
Blefaripoda sp. 1
Lepidopa sp. 1
Emerita analoga 1
Cancer setosus 1
Platyxanthus sp. 1
Libinia sp. 1
Euphausiacea
Euphausia diomedae 1
Euphausia mucronata 12
Euphausia tenera 12
Euphausia eximia 12
Euphausia distinguenda 12
Euphausia lamelligera 12
Euphausia mutica 1
Nyctiphanes simplex 12
Nematoscelis tenella 1
Nematoscelis gracilis 1
Nematoscelis flexipes 1
Stylocheiron affine 1
Stylocheiron carinatum 1
Stylocheiron elongatum 1
Nematobrachium flexipes 1
Mysida
Heteromysis sp. 1
Archaeomysis sp. 1
Mysidopsis 1
Siriella sp. 1
Gybberithrops sp. 1
Metamysidopsis pacifica 1
Chaetognatha
Khronitta pacifica 1
Khronitta subtilis 13
Pterosagitta draco 13
Sagitta bedoti 14
Sagitta decipiens 15
Sagitta enflata 13
Sagitta ferox 14
Sagitta hexaptera 15
Sagitta minima 13
Sagitta maxima 1
Sagitta neglecta 14
Sagitta pacifica 1
Sagitta peruviana 14
Sagitta pulchra 14
Sagitta regularis 13
Thaliacea
Cyclosalpa bakeri 1
Helicosalpa komaii 1
Iasis zonaria 1
Pegea confoederata 1
Ritteriella picteti 1
Salpa fusiformis 1
Thalia democratica 1
Thetys vagina 1
Weelia cylindrica 1
Doliolum gegenbauri 1
Doliolum denticulum 1
Doliolum nationalis 1
Appendicularia
Oikopleura dioica 16
Oikopleira fusiformis 16
Oikopleura albicans 16
Oikopleura cophocerca 16
Oikopleura intermedia 16
Oikopleura longicauda 16
Oikopleura rufescens 16
Stegosoma magnum 16
Cephalochordata
Branchiostoma elongatum 1

ably due to stronger predation nearshore and low biovolumes in freshly upwelled water (Ayón et al., 2008). Also, there is a clear north–south pattern, with high biovolumes mainly between 4°S and 6°S and again poleward of 14°S. These high biovolume areas are characterized by a narrow continental shelf (18–28 km) (Santander, 1981; Carrasco and Lozano, 1989; Ayón et al., 2004). The high biovolumes in the north may be due to the influence of the ESW, which have larger species and higher diversity (Ayón, 1999) than CCW. On the other hand, the number of abundant tropical species greatly decreases toward the coast. In the coastal areas under influence of CCW, large neritic herbivores like *Calanus australis* and *Eucalanus inermis* may grow in mass (Geynrikh, 1973). Off northern and central Peru, euphausiids were less but the remaining mesozooplankton were more abundant (Gunther, 1936).

EN alters mesozooplankton diversity, distribution, and abundance. An increase in diversity is caused by the intrusion of tropical species in the central and southern Peruvian coast (Santander and Carrasco, 1985; Carrasco and Santander, 1987; Carr, 2003). Work off northern Peru during EN shows the intrusion of warm waters with warm water species such as *Centropages furcatus* (Santander et al., 1981b; Aronés et al., 2001). The 1982/1983 EN caused an increase in zooplankton biomass, especially gelatinous species, and diversity (Santander and Carrasco, 1985). In contrast, there was a pronounced decrease in meroplanktonic larvae and ichthyoplankton in the coastal waters during EN.

Specific attention on the regional and seasonal distribution of certain taxonomic groups was drawn by Véliz (1981), who identified ten species of siphonophores between 5°47′ and 9°13′ up to 260 km offshore, and by Castillo (2004) and Castillo et al. (2007) who studied the distribution of 15 ostracod species. During the 1998 EN ostracod species shifted south and their distributions showed positive or negative correlations with salinity and distance to shore.

Some species can be used as water masses indicators (Gómez, 1972; Geynrikh, 1973; Aronés, 2002; Castillo, 2004). Sandoval de Castillo (1987) used chaetognaths as water mass indicators, with *Sagitta bedoti*, *S. neglecta*, *S. peruviana*, and *S. pulchra* associated in ESW, and *S. ferox*, *S. regularis* and *Khronitta pacifica* in SSW. Carrasco and Santander (1987) showed that the copepods *Centropages furcatus*, *Acrocalanus gracilis*, and *A. monachus* were typical in ESW, while CCW species were *Clausocalanus arcuicornis*, *Acartia tonsa*, *Oithona plumifera*, *Paracalanus parvus*, *Centropages brachiatus*, and *Eucalanus inermis*. A recent study conducted off northern Peru (Gutiérrez et al., 2005) recognized several copepod species as indicators of SSW: *Acartia danae*, *Calocalanus pavo*, *Ishnocalanus plumulosus*, *Mecynocera clausii*, and *Oncaea conifera*. Abanto (2001) related the distribution of 152 copepod species to hydrographic data between 3°30′S and 14°S between 1980 and 1989. Examples are presented in Fig. 5. Thus, *Acartia tonsa*, *Calanus australis*, *Clausocalanus* sp., *Paracalanus parvus* are apparently eurythermal and euryhaline and not water mass specific, while *Subeucalanus crassus*, *Sapphirina darwinii*, *Pleuromamma abdominalis* were restricted to SSW, and *C. brachiatus*, *E. inermis*, *Euaetideus bradyi* could be used as indicator species for CCW. During EN, *Centropages furcatus* shifts south and replaced the CCW species *C. brachiatus* and *Eucalanus inermis* (Abanto, 2001). The shift between *C. brachiatus* (non-EN) and *C. furcatus* (EN) was also noticed by Gutiérrez et al. (2005), who related hydrographic parameters to changes in microphytoplankton, mesozooplankton (volume, abundance, and species richness), ichthyoplankton and macrozoobenthos in surface samples collected between 1994 and 2004 on fixed stations off central Peru. They found notable changes in species composition and richness associated with the 1997/1998 EN.

4.3.2. Vertical distribution and migration

The vertical distribution of zooplankton is controlled by their nutritional and physiological requirements; therefore, the structure of the water column with its gradients of temperature and salinity is important. Furthermore, in the Eastern Tropical Pacific, a subsurface OMZ (Pennington et al., 2006) has a profound impact on the distribution of pelagic animals and limits the space available for aerobic life. The upper limit of the OMZ depth is often identified as the depth of the 0.5 ml L^{-1} (Escribano et al., 2000) or 1 ml L^{-1} (Hidalgo et al., 2005; Criales-Hernández et al., 2008) oxygen isopleth. In regions of coastal upwelling, hypoxic water can reach to within a few meters of the surface (Wyrtki, 1966; Judkins, 1980; Escribano et al., 2004). Not many studies have been conducted on the vertical distribution of zooplankton off Peru. Only during international cruises have closing nets, pumps and electronic plankton counters been used (Mackas et al., 1981). Judkins (1980) pumped samples down to 85 m at three stations at the shelf break, over the continental slope, and further offshore. The OMZ appeared to have been the single most important environmental factor structuring and modifying the vertical distribution of zooplankton over the shelf and slope off central Peru. Most mesozooplankton did not occur below the 0.1 ml L^{-1} oxygen isopleth. Onshore shoaling of the OMZ resulted in high near-surface concentrations of mesozooplankton relative to offshore stations. Semenova et al. (1982) described the vertical and horizontal distribution of 37 mesozooplankton species along transects between 7°S and 15°S. Only two species were able to occupy the OMZ: *Eucalanus inermis*, which other studies have shown can with stand 12 h of anoxia (Judkins, 1980; Boyd et al., 1980), and *Euphausia mucronata* (Antezana, 2002a). A thickening of the surface oxygenated layer occurs during EN, and is accompanied by increased vertical migration and habitat expansion for many zooplankton and fish species (Escribano et al., 2004).

Diel vertical migration (DVM) was first demonstrated off Peru by Antezana (1978, 2002a,b). He showed that larvae and juveniles of *Euphausia mucronata* are always in the surface layer, while the adults spend days in the OML and migrate to the surface at night. Smith et al. (1981b) studied the vertical migrations of three copepod families with a 5 m resolution (Oncaeidae, Oithonidae, small Calanoida). The OMZ established a distinct lower boundary. During day-time, all three groups accumulated above the oxycline, while at night, small Calanoida were always higher in the water column than Oncaeidae. These daily excursions seemed sufficient to expose Oncaeidae to onshore/poleward flow by day and offshore/equatorward flow at night. Restriction to the upper 20 m above the OMZ likely influences the onshore–offshore distribution of species (Smith et al., 1981a). Boyd et al. (1980) observed that *Eucalanus inermis*, *Calanus australis*, and *Centropages brachiatus* show different patterns of DVM inshore and offshore, not apparently related to the OMZ. All three species left the upper 5 m during the day inshore, but offshore they remained at the surface both in day and night even though the surface oxygenated layer is thicker offshore. Santander et al. (1981a) found that many mesozooplankton can tolerate oxygen concentrations down to ~0.5 ml L^{-1}, but concentrations <0.2 ml L^{-1} have drastic effects on most taxa. They also found that *Eucalanus inermis*, *Euaetideus bradyi*, *Rhincalanus nasutus*, amphipods, and ostracods occur mainly between 50 and 100 m, where the oxygen content was <0.5 ml L^{-1}. Using a closing net off Callao during three 48 h-periods, Escudero (2003) distinguished four types of migration, with species: (1) spending day at depth and coming to the surface between dusk and midnight; (2) not-migranting; (3) migranting several times each 24 h; and (4) reverse migrating, swimming up in the day and down at night, as in *Lucicutia flavicornis*. Environmental conditions modified the migrations, as O_2 concentrations <0.5 ml L^{-1} were limiting for most taxa.

4.4. Time series: seasonality and interannual variability

Temporal variation of zooplankton abundance can occur as a result of both biological and physical processes. Biological variations occur at a time scale of weeks, associated with the life cycle of zooplankton organisms, and on a diurnal time scale associated with vertical migration. Physical variations can be seasonal and interannual, or also may occur as a result of onshore–offshore and alongshore advection, on a time scale of days. Changes in cross-shelf advection have been observed on a fixed station during 15 days of daily sampling (Smith et al., 1981a). During periods of surface onshore flow, oceanic species were observed, while during offshore flow, coastal species dominated.

Seasonal variability is driven by changes in wind speed and direction, which affect upwelling intensity and coastal circulation. Anchovies and other species release larvae seasonally (Santander and Flores, 1983). Such spawning seasonality suggests that favourable pelagic conditions may also be seasonal. Upwelling off Peru is more intense in winter (Bakun and Nelson, 1991; Echevin et al., 2004a,b; Croquette et al., 2005; Aronés et al., in press). Since primary and secondary production is supported by upwelling nutrient-rich upwelled cold water, maximum phyto- and zooplankton abundances should occur in winter. However, Ayón et al. (2004) found peak zooplankton volumes in spring, especially during the 1960s (Fig. 2). Zooplankton volumes were higher in spring except during the 90s when no seasonal trend was evident. Aronés et al. (in press) analysed the seasonality of zooplankton abundance off Paita (Fig. 2). They generally found highest total abundances in spring and autumn, under moderate upwelling conditions. These observations may suggest that "intermediate-strength upwelling" is favourable for zooplankton, with winter upwelling too strong and summer upwelling too weak. Although coastal upwelling was more intense in winter, zooplankton abundance off Paita was at minimum during winter, and thus displayed a positive correlation with temperature (Aronés et al., in press). Studies off Chile have shown that intermediate monthly wind strengths, with alternating periods of upwelling and relaxation, may best sustain phytoplankton blooms off Chile (Echevin et al., 2004b) and successful recruitment of Peruvian pelagic fish stocks (Walsh et al., 1980; Mendelssohn and Mendo, 1987; Cury and Roy, 1989). Similar concepts have also been called the "optimal environmental window" (Cury and Roy, 1989; Sugimoto and Tadokoro, 1998) or "optimal stability window" (Gargett, 1997). We suggest that the dome-shaped relationship between wind-induced turbulence and zooplankton biomass has an important influence on zooplankton productivity off Peru (Aronés et al., in press), although the dominating mechanisms and processes are not yet clear. Cury and Roy (1989) suggested that strong winds decrease recruitment success by inducing turbulence that hampers the location of zooplankton prey by fish larvae off Peru. This idea is a restatement of "Lasker's hypothesis" (Lasker et al., 1970; Lasker, 1975; Lasker and Smith, 1977) which proposes that strong turbulent mixing (beyond an "optimum") associated with strong wind and coastal upwelling destroys vertical stratification and the prey patchiness required for optimal larval feeding. Under the "optimal window" hypothesis, intermediate upwelling intensity supplies nutrients but below intensity levels where harmful processes become important, such as horizontal advection and the break-up of vertical aggregation layers.

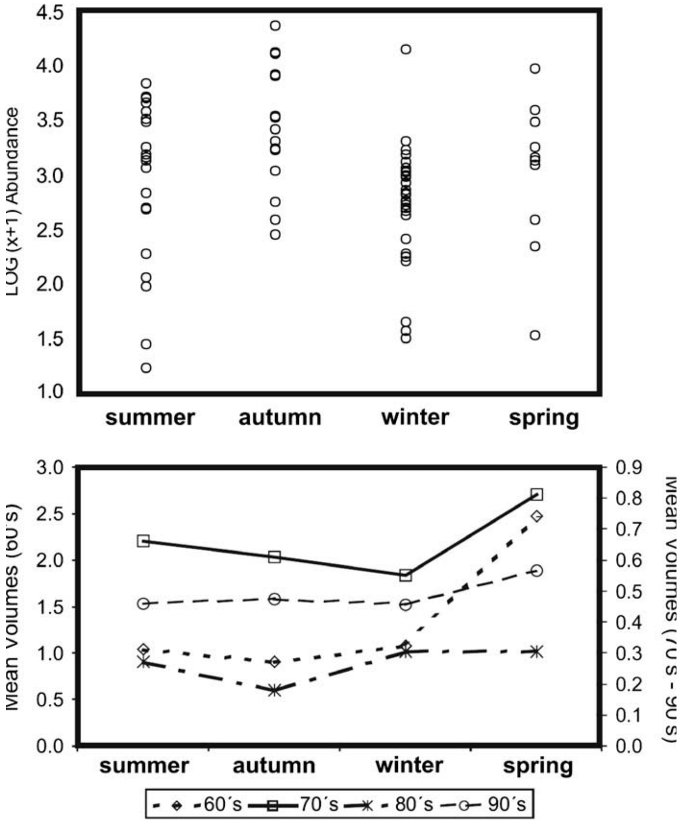

Fig. 2. Seasonality of zooplankton abundance and biovolumes off Peru. Above: seasonal variation of log total zooplankton abundance off Paita, northern Peru, from August 1994 to December 2004 (modified from Aronés et al., in press). Below: mean seasonal zooplankton volumes off Peru for four decades, since 1964. Note that the scale of the ordinate in the 1960s differs from that of the 1970s and 1990s (Ayón et al., 2004).

On the other hand, recent studies suggest that aggregations of zooplankton and fish larvae can be formed by vertical currents (Franks, 1992; Genin et al., 2005). In this case increased vertical turbulence may increase predation intensity by aggregating organisms that are dispersed horizontally, but are able to maintain their depth, such as zooplankton and fish larvae (Hardy, 1936; Franks, 1992; Genin et al., 2005). Increased wind and turbulence could also require increased effort to maintain depth, thus leaving less energy for growth and reproduction (Kloppmann et al., 2002).

The negative effect of strong winter upwelling on zooplankton abundance may also be explained by (1) advective losses, (2) shrinking habitat due to the rise of the oxycline, or (3) match–mismatch during the succession of upwelling → phytoplankton bloom → zooplankton grazing → zooplankton population growth in developing upwelling lenses and filaments. The theoretical implications and possible mechanisms of prey–predator match–mismatch have been reviewed elsewhere (e.g. Durant et al., 2007). Very strong upwelling may also produce adverse physical–chemical conditions in recently upwelled water (steep temperature gradients, low oxygen, high ammonia concentrations, etc.). This "intermediate upwelling" hypothesis may also be relevant to interannual variability. Accordingly, minimum zooplankton abundance from 1970 to 1976 coincided with long periods with strong La Niña (LN) conditions (Fig. 3), when upwelling intensity was maximal.

The large interannual variability in biomass and species composition off Peru was first shown by Santander (1981). Long-term observations are so far only available as zooplankton volumes (1964–2002; Ayón et al., 2004). The relatively large meshed (300 μm) net used to collect these samples does not quantitatively collect smaller zooplankton that likely dominate the nearshore region. Ongoing research is testing capture efficiencies for smaller mesozooplankton (comparing 300 and 200 μm net catches under different conditions), to determine if biases are stable for given taxa. If so, historical zooplankton collections can be reanalyzed. Carrasco and Lozano (1989) presented abundance data from 1964 to 1987 for the northern, central and southern Peruvian coast and recognized a decline. During the 1983 EN copepod abundance between 6°S and 12°S decreased to 1/6 of values for 1977–1981. Nearer the equator (3–6°S), copepod abundance was higher due to advection of larger equatorial species. Ayón et al. (2004) extended this series to 2002 (Fig. 3). The long-term trend of annual mean zooplankton volume, from 1964 to 2001, displayed three different periods: maximum values from 1964 to 1973, a collapse after 1973, low values from 1974 to 1989 (although the recovery seems to start in 1985), and an intermediate level of biovolumes from 1990 to 2002 (Ayón et al., 2004).

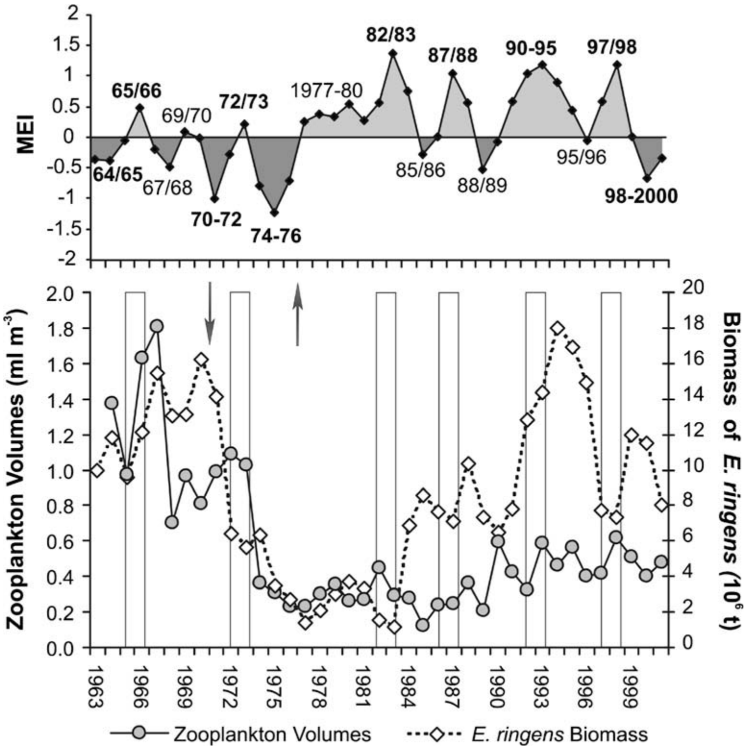

Fig. 3. Mean annual tropical Pacific Multivariate ENSO Index (MEI), zooplankton volumes, and biomass of Peruvian anchoveta (*Engraulis ringens*) from 1963 to 2001. Above: the MEI time series shown is the annual average calculated from the original bimonthly MEI series (Wolter and Timlin, 1998). The variables used to calculate the MEI are: sea-level pressure (P), zonal (U) and meridional (V) components of the surface wind, sea surface temperature (S), surface air temperature (A), and total cloudiness fraction of the sky (C). Original data are 2-degree-cells from the tropical Pacific (30°N–30°S) taken from the COADS data base (http://www.icoads.noaa.gov). El Niño periods are highlighted above; La Niña periods are shown below zero. *Source:* http://www.cdc.noaa.gov. Below: average zooplankton volumes from more than 10,000 samples taken from the Peruvian coast to 300 nautical miles offshore. Values of 1979 and 1988 were interpolated with a 5-year moving average [according to Ayón et al. (2004), modified]. Strong El Niño events are shown as vertical bars. Arrows indicate global sea surface temperature regime shifts in 1970–1971 and 1976–1977 (Yasunaka and Hanawa, 2005).

ENSO and multi-decadal shifts in global sea surface temperature (SST) shifts co-occur (Yasunaka and Hanawa, 2005). Although many other strong ENSO transitions occurred since the early 60s, Yasunaka and Hanawa (2005) detected only two global SST regime shifts in this period, one in 1970–1971 (transition from EN to the strong 1970–1972 LN) and another one in 1976–1977 (transition from the strong 74–76 LN to EN conditions). Coincidently or not, these ENSO-related global SST regime shifts mark the beginning collapse of the anchovy stock in the late 60s to early 70s, and onset of stock recovery in the mid 70s (vertical arrows in Fig. 3). The synchrony of the Peruvian zooplankton and anchovy data with statistically significant global SST regime shifts provide further support for the idea of strong links between regional-scale ecosystem changes and global-scale climatic processes.

Zooplankton volumes and anchovy biomass show a similar pattern (Fig. 3), indicating that multi-decadal oscillations may be affecting both compartments of this ecosystem. There may be valid alternative explanations for the variations in anchovy biomass (e.g. overfishing in the late 60s), but the synchronicity of fisheries and zooplankton data in this and other regions of the Pacific strongly indicate a globally relevant ENSO-like multi-decadal oscillation pattern that is probably triggering these ecological regime shifts. However, there are also three remarkable differences between the time series of anchovy biomass and zooplankton volume: (1) the magnitude of the population collapse in the late 60s and early 70s is similar for both anchovy and zooplankton, but the subsequent recovery was much better for anchovies. Zooplankton never recovered 60s levels; (2) strong EN's do not seem to affect zooplankton communities; there is no clear affect of even the strongest EN events on zooplankton volume; (3) the zooplankton collapse seems to have started 3 or 4 years earlier (in 1968) than for anchovy (in 71 or 72). If real, this association may prove to be a useful early indicator of ecosystem regime shifts. Modelling efforts and time series analyses have shown that mesozooplankton populations respond to subtle climatic signals, and could serve as indicators of climate change (Taylor et al., 2002).

A more recent regime shift in 1999 or 2000 apparently affected pelagic ecosystems in the north-eastern (Greene, 2002; Mackas et al., 2004; Litzow, 2006), north-western (Rebstock and Kang, 2003; Tadokoro et al., 2005), and south-eastern Pacific (Aronés et al., in press). This recent shift, which occurred following the 1997/1998 EN and perhaps during the strong 98/99 LN (Fig. 4), is still under discussion (Bond et al., 2003; Litzow, 2006; Gutiérrez et al., 2007). An analysis of spatial distribution of anchovies and sardines off Peru also showed a dramatic shift after the 1997–1999 ENSO (Gutiérrez et al., 2007). Although sardines were already declining and anchovies had been increasing in biomass before 1999, Gutiérrez et al. (2007) concluded that "since 1999, we have been in a 'full anchovy era' with dramatically low levels of sardine in the HCS". This may be related to an increase in copepod and euphaussiid abundance, which at least off northern Peru, showed an abrupt increase after 1999 (Aronés et al., in press, Fig. 4).

Ayón et al. (2004) and Aronés et al. (in press) demonstrated the importance of long-term zooplankton monitoring in upwelling areas, and confirmed that dramatic changes in pelagic ecosystems occur in the Southeast Pacific. Ayón et al. (2008) used a slightly extended data set (1961–2003) and applied a Generalized Additive Model (GAM) and Classification and Regression Trees (CART) to the zooplankton biovolumes as a function of time of day to examine

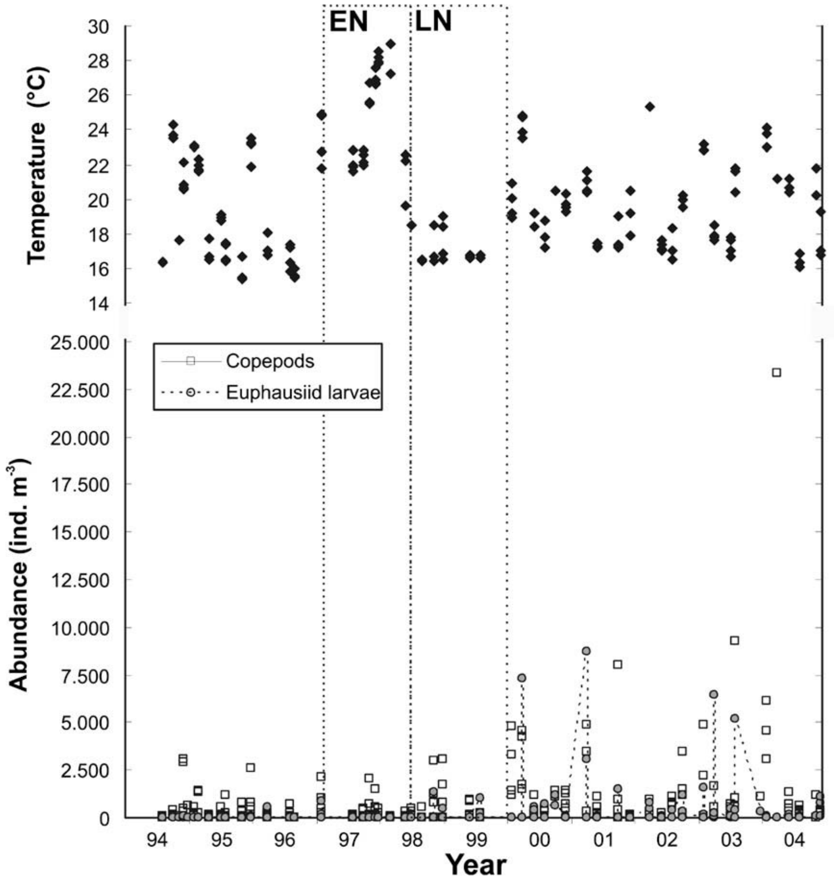

Fig. 4. Temporal variation of surface water temperature and subsurface abundance of copepods and euphausiid larvae off Paita, northern Peru, from August 1994 to December 2004. EN, El Niño 1997/1998; LN, La Niña1998/1999. *Source:* Aronés et al. (in press).

the effect of the diel cycle, other environmental factors, and biological interactions on biovolume. The CART results showed a strong negative impact of anchovy but not sardine biomass on zooplankton. Additionally, zooplankton biovolume was higher offshore than on the shelf and was higher when SST was above 21.2 °C for some years and months. GAM results corroborated the CART.

4.5. Pelagic macrocrustaceans (Euphausiacea and Decapoda)

Two pelagic macrocrustaceans are characteristic of the Peruvian Humboldt Current System (HCS): *Euphausia mucronata* (or 'krill'; Escribano et al., 2000; Antezana, 2006), and the galatheid crab *Pleuroncodes monodon* ('red crab', 'squat lobster', 'langostino colorado', or 'munida'). These species can be very abundant (Antezana, 2002a,b; Bertrand et al., 2005) and thus likely interact with the even larger biomass of *Engraulis ringens* (Peruvian anchovy). Recent data even indicate that krill may be the main food source for adult anchovy (Espinoza and Bertrand, 2008). Many other predators, such as hake, also feed on these pelagic macrocrustaceans (Mejia et al., 1971, 1973, 1980). Although adults, juveniles, post-larvae and larvae of pelagic decapod shrimps are common in plankton catches in tropical and subtropical oceans (Luciferidae, Sergestidae, Penaeidae, and Caridea; Criales and McGowan, 1994; Schwamborn et al., 1999; Schwamborn et al., 2001; Martins et al., 2005; Koettker and Freire, 2006) and occur off Peru (Fernández-Álamo and Färber-Lorda, 2006, Table 4), there is little information on these groups. Hendricks and Estrada-Navarrete (1989) discussed the distribution of pelagic decapod shrimps in the Eastern Pacific, including offshore waters off Peru, but did not give biomass data for these groups off Peru.

Early euphausiid research focused on taxonomy (Santander, 1967; Santander and Sandoval de Castillo, 1969; Ponomareva, 1982). Although sampling with Hensen nets is probably misses adults, euphausiids were nevertheless found to be very abundant, especially at night (e.g. Santander, 1981). Most euphausiids are captured as furcilia and calyptopis larvae (Aronés et al., in press). Antezana (1978, 2002a,b) studied the distribution of *Euphausia mucronata* along the Peruvian and Chilean coasts and the vertical distribution of developmental stages in relation to the oxygen minimum layer (OML). All stages migrated downward during the day, adults migrating deeper than larvae and juveniles. He suggested that these ontogenetic and diel vertical distribution patterns reflect a predator avoidance strategy and may explain the success of this species, which may contribute up to 50% of total zooplankton biomass in the HCS.

The distribution of red crab extends from Chiloe Island (43°S) off Chile to 7°S off Peru (Haig, 1955; Gutiérrez et al., 2008). Red crab individuals are larger in southern end of their range, where they are mostly benthic (Gallardo et al., 1993; Palma, 1994). Off northern Chile and Peru, red crab individuals are smaller and mostly pelagic (Gutiérrez et al., 2008), leading Rivera and Santander (2005) to consider the northern specimens a "dwarf" subspecies (*P. monodon pelagicus*). Most studies on *P. monodon* have been performed off Chile due to its importance for the fisheries in this region (e.g. Haig, 1955; Palma, 1976; Gutiérrez and Zúñiga, 1977; Bustos et al., 1982; Gallardo et al., 1993, 1994; Palma, 1994; Rivera and Santander, 2005). The biology of red crab in Peruvian waters is not well known (Segura and Castillo, 1996; Chimpén, 1999; Franco, 2003), perhaps because red crab have recently increased in biomass (Gutiérrez et al., 2008). *P. monodon* have been occasionally reported as abundant during the last 50 years, mainly off southern Peru. Older reports indicate that *P. monodon* was an important prey item of tunas during the 1930s and

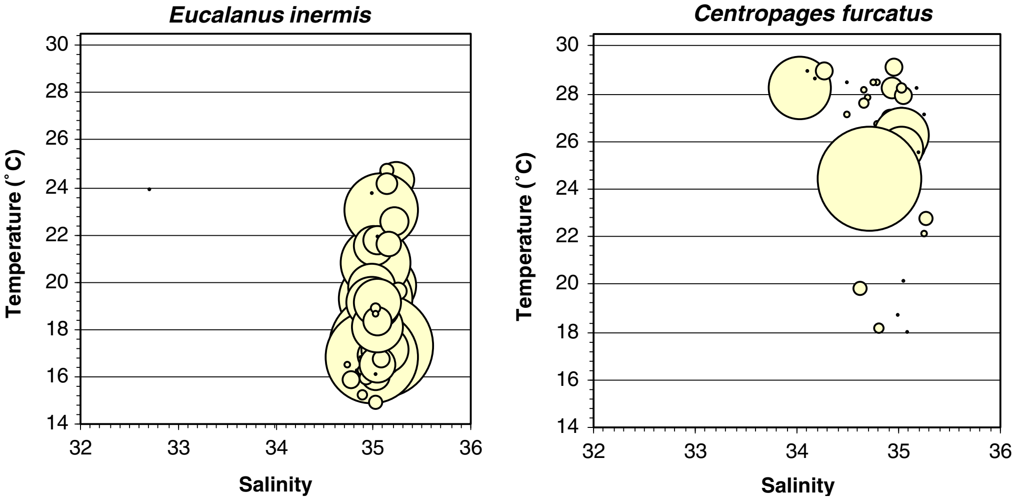

Fig. 5. Temperature–salinity diagrams of waters sampled at surface off Callao and San Jose, Peru, from 1994 to 2004, with superimposed abundances of the copepods *Eucalanus inermis* and *Centropages furcatus*. Samples were taken off Callao, San José from 1994 to 2004 with WP-2 hauls. From Abanto, 2001).

1940s. According to Gutiérrez et al. (2008), *P. monodon* became highly abundant along the Peruvian coast after the 1997–1998 EN. Biomass ranged between 0.6 and 3.4×10^6 t from 1998 to 2005 (acoustic estimates in Gutiérrez et al., 2008) in upwelled nearshore waters where red crab are preyed on by seabirds, mammals, and fish (anchovy preys on red crab zoeae). Gutiérrez et al. (2008) also found that *P. monodon* forage on fish eggs and larvae. Trophic interactions are likely to occur between krill, red crab, and anchoveta.

4.6. Meroplankton

Meroplanktonic larvae of benthic invertebrates (e.g. Decapoda, Cirripedia, Mollusca, Polychaeta) constitute an important fraction of the zooplankton, especially nearshore (Criales-Hernández et al., 2008). Although nearshore food supply may be ample, larvae have to cope with predation, advection, and benthic hypoxia. Important predators are planktivorous fishes and macrocrustaceans, which build up huge biomass in this region. Surface currents in coastal upwelling regions are, on average, directed alongshore or offshore and subsurface waters are anoxic, thus limiting any vertical migration (Shanks and Brink, 2005). Variability in currents exists at various scales, including the upwelling/relaxation cycles, EN and decadal cycles. Shallow-water invertebrates must be able to recruit from larvae retained nearshore or in bays, or, as postulated by Pielou (1975), follow an r-strategy and produce huge numbers of larvae, few few of whom return to shore.

The meroplanktonic larvae of many commercially important benthic organisms remain largely undescribed. The distribution of pelecypod larvae has been described for two cruises in Bahia de Independencia (Mendo et al., 1989; Yamashiro et al., 1990). Increased survival and recruitment of larvae probably explain the dramatic population increases of the scallop *Argopecten purpuratus* that occur during EN. One explanation for "scallop outbursts" is that larval survival increases with temperature (Wolff et al., 2006) and a thicker surface oxic layer, while another idea is that larval predators or competitors disappear from surface waters during EN (e.g. anchovy and crab larvae). Tarazona et al. (1988) studied the bivalve communities of the central Peruvian coast during the 1982–1983 EN. Abundance of bivalve larvae declined during peak EN months in 1983, but recovered immediately afterwards. The meroplankton of Ancón Bay (11°46′S 77°11′W) and Independencia Bay (14°09′S 76°10′W) (Fig. 1) were compared by Tarazona et al. (1989), who found that polychaete larvae dominated Independencia Bay, while bivalve larvae dominated Ancón Bay. Experiments showed that in spite of small tidal amplitude (<1 m), tidal currents dispersed larvae. Scallop larvae may can occur in huge densities nearshore, specifically in Independencia Bay (M. Wolff, personal communication). Yamashiro et al. (1990) evaluated larval stocks in Independencia Bay. The meroplankton was comprised of brachyuran zoeae, brachiopod, gastropod, and polychaete larvae, together with young pteropods and euphausiid larvae. Tidal fluctuations in larval abundance were also observed. Macro-invertebrate settlement in this bay during the 1997–1998 EN has been described by Ramos et al. (1999) by determining recruitment to artificial substrates. *Argopecten purpuratus* only settled during EN, together with warm water turriform gastropods. In contrast, the bivalve *Hiatella solida*, the turbellarian *Notoplana* sp., and the gastropod *Caecum chilense* settled mainly during the preceding cold period. A third group, comprised by the brachiopod *Discinisca lamellosa*, the echinoderm *Ophiactis kroyeri*, and mytilid bivalves, settled only at the very onset of EN (March 1997). This EN-onset settlement peak may be related to unusually strong onshore currents associated with a month-long relaxation of upwelling, or to ecosystem changes. The appearance of unusual tropical species at the end of this EN were also noted (e.g. the bivalve *Pteria sterna* and the gastropod *Epitonium* sp.). Further studies on macro-invertebrate settlement in Peruvian inshore ecosystems have recently been published by Pacheco and Garate (2005).

Larval development has been described for less than 10% of the decapod species that occur off Peru, mostly from other parts of the eastern Pacific (e.g. Costlow and Fagetti, 1967; Quintana, 1983; Dittel and Epifanio, 1984; Quintana and Saelzer, 1986; Báez and Martín, 1992; Báez, 1997; Wehrtmann and Báez, 1997). Although crab larval stages are generally found in zooplankton surveys, there are no species-specific data on decapod larval distributions off Peru. This is one of the focuses in the ongoing CENSOR project.

4.7. Trophodynamics and production of zooplankton

Dugdale and Goering (1970) first studied the trophic role of zooplankton in the Peruvian HCS. Their study of biological production in the Peru Coastal Current during a period of high diatom levels indicated grazing was not the principal source of loss of phytoplankton, with combined anchovy and zooplankton grazing at about 20% of the standing crop. They also suggested that the anchovy were more important grazers than zooplankton. Beers et al. (1971) estimated the consumption by the zooplankton not to exceed 25% of the daily primary production.

During the cruises of the Institute of Oceanology in 1974, attempts were made to describe plankton community dynamics (Vinogradov and Shushkina, 1978; Flint and Timonin, 1985) and to estimate zooplankton production (Shushkina and Kislyakov, 1977). Drits (1985) measured the ingestion rate of *Calanus australis* under natural conditions and studied the content of the gut and faecal pellets. Mikheyev (1977a) described the age structure of dominant copepod species on a transect across the shelf and an upwelling center and compared species number, biomass and species diversity (Mikheyev, 1977b). Flint and Timonin (1985) assessed trophic structure of the crustacean community using mouthpart morphology. In nearshore areas, fine filter-feeders dominated. Over the shelf break area, they found a predominance of coarse filter-feeders and omnivores. Spatial variability in the zooplankton community was explained by the patchy distribution of local upwelling cells, which undergo characteristic changes depending on their age. Secondary production was from experiments following the fate of ^{14}C-labelled phytoplankton and applying a mathematical simulation of a trophic model (Shushkina and Kislyakov, 1977). According to Petipa et al. (1977) excess production on the shelf is utilized in a 200–300 km band of offshore water.

Measurements of grazing and excretion rates of copepods and qualitative descriptions of their prey were conducted during the international projects ICANE and CUEA. According to Cowles (1978, 1979), prey size selection by copepods depended food abundance. Smith et al. (1981a,b) measured ingestion rates of *Acartia tonsa*. Dagg et al. (1980) measured rates of ingestion and excretion of *Calanus chilensis*, *Eucalanus inermis*, and *Centropages brachiatus*, assessing the particle spectrum with a Coulter Counter. As these large species ingested <5% of primary production, the authors suggested that smaller zooplankton must consume most primary production. Boyd et al. (1980) studied prey selectivity by *Eucalanus*, *Calanus*, and *Centropages*. They found that *Calanus* sp. is a non-selective phytophage, while *Centropages* sp. and *Eucalanus* sp. were omnivorous feeders. Furthermore, *Eucalanus* sp. did not feed at the surface at night, but only during the day on OMZ detritus. Nitrogen regeneration during a red tide was measured by Smith (1978), who estimated that mesozooplankton recycled 1–25% of the nitrogen needed to support phytoplankton production. Espinoza and Bertrand (2008) have recently emphasized that in carbon units, anchovies feed primarily on euphausids (66%) and copepods (28%), not diatoms as has traditionally been thought (Pauly et al., 1989).

4.8. Modelling

The first ecological models of the HCS were built by Dugdale and MacIsaac (1971) and Walsh and Dugdale (1971), who simulated nitrate uptake and flow through the Peruvian upwelling system. Energy budgets for the pelagic system were established by Sorokin and Mikheev (1979), using data obtained during the cruises of the Institute of Oceanology in 1974. Walsh (1981) established a carbon budget to understand changes in the carbon flow through the coastal upwelling system after the crash of the anchovy fisheries in the early 70s. Jarre et al. (1991) presented mass balance models (ECOPATH II) for modeling fish stock interactions in the Peruvian upwelling ecosystem, which included also a zooplankton component. Jarre-Teichmann (1998) investigated explored trophic structure with steady-state, mass-balance models (ECOPATH II). The mean transfer efficiency from herbivores to top predators was 4–6%. Comparison of the models for the warm sardine regime versus the cold anchovy regime suggested that anchovy abundance varies with the lower components of the ecosystem (zooplankton and, to some extent, phytoplankton and detritus), while sardine abundance is out of phase. Jarre-Teichmann (1998) concluded that mobility differences between the two species, with sardines relying on their better swimming capability (Bakun and Broad, 2003) to find suitable forage during periods of decreased productivity at lower trophic levels. However, more recent studies emphasize that the major reason for alternation anchovy and sardine abundance is due to is climatic and prey selection mediated (with sardines feeding on phytoplankton and small-sized zooplankton and anchovies on larger copepods and euphausiids), and not related to swimming capability (Bertrand et al., 2004; Gerlotto et al., 2006; van der Lingen et al., 2006; Espinoza and Bertrand, 2008).

Carr (2003) used a numerical model to quantify carbon flow through the upwelling ecosystem from 1996 through 1998 at 9.5° off the coast of Peru. The numerical experiments illustrate ecosystem responses to the evolving conditions associated with EN and LN events.

Ecosystem modelling in the Peruvian upwelling system is only beginning. There is a strong need for theoretical overview, and empirical data is needed as model input. Due to the lack of data, e.g. on the microbial loop, macrocrustaceans and main trophic links, e.g. between anchovies and euphausiids, older models neglect important ecosystem components. Recent trophic models built using the Ecopath with Ecosim (EwE) software focus mainly on commercially important fish and invertebrate stocks. These models do include more recent stomach content data for anchovy (Tam et al., 2006; Taylor et al., 2006; Wolff et al., 2006), yet phytoplankton–zooplankton interactions are not well described and the microbial loop has not yet been integrated. Recent physical–biogeochemical simulations (Echevin et al., 2004b) also do not consider phytoplankton–zooplankton interactions, again showing the need for new data and modelling directed specifically towards the plankton.

5. Knowledge gaps and perspectives

Many topics in zooplankton biology and ecology have been examined off Peru, but a synthetic view of zooplankton dynamics in this part of the HCS and its relation to other components of the system has not yet emerged. There are many important issues still poorly understood, such as the interactions of gelatinous and crustacean plankton, adaptations to life in the OML, microzooplankton dynamics and processes related to the microbial loop. Most urgently, we need concepts, data, and models which may help to link climatic processes to the productivity of the pelagic ecosystem off Peru.

5.1. Taxonomy, life cycles, and cryptic taxa

Taxonomy of zooplankton off Peru is still in its infancy. There is a strong need to combine morphological and genetic studies and compare species with their synonyms in other oceans. Furthermore, little to nothing is known of the ecology of most species. Often, developmental stages of holo- and meroplankton are not described. Basic knowledge of the life cycles is lacking, such as generation times and growth rates, reproductive biology, starvation potential, and life cycle strategies such as dormancy and resting eggs.

Euphausiids may form a large part of the zooplankton biomass. However, due to difficulties in sampling, their biomass may be significantly underestimated. Similarly, gelatinous plankton is often very abundant, but requires dedicated sampling techniques to quantitatively assess its importance. There is little knowledge on bentho-pelagic coupling and the role of meroplankton, especially in the nearshore zone, which is important for artisanal fisheries. This is one of the main focuses of the ongoing CENSOR project.

5.2. Microzooplankton and the microbial loop

The microzooplankton comprises organisms <200 μm (UNESCO, 1968; Smith, 1977; Lenz, 2000), and are typically dominated by protozoa (rotifers, foraminiferans, radiolarians, ciliates, and flagellates) and copepod eggs and nauplii. Protozoan communities are often mixotrophic or of unknown trophic status. They are generally not caught by zooplankton nets, but may be quantified in bacterio- and phytoplankton studies, which may lead to a considerable overlap between bacterio-, phyto-, and zooplankton studies regarding these groups. Microzooplankton can be intense grazers on bacteria and phytoplankton with extremely high production/biomass ratios (Kiørboe, 1997; Agis et al., 2007; McManus et al., 2007), however, little is known about its role off Peru, although it is certainly important, especially during EN, as shown by studies in the adjacent southern HCS (Escribano et al., 2004).

The few studies available are all based on single cruises, usually with few stations. Tumantseva and Kopylov (1985a,b) determined the species composition and biomass of planktonic protozoa and their rates of reproduction and production off Peru. In incubation experiments the average P/B ratio was 1.26 day^{-1}, indicating biomass was more than doubling each day. *Urotricha marina* underwent 8–11 divisions/day. Vinogradov et al. (1980) found similar results and pointed out the importance of microzooplankton production. Heterotrophic microplankton was also studied by Sorokin (1978) and Klekowski et al. (1975), who determined respiration rates of microzooplankton in the equatorial and Peruvian upwelling systems. Sorokin and Kogelschatz (1979) studied the role of heterotrophic microplankton in the flux of organic matter to the benthos near Punta San Juan, Peru. A drogue study showed that the planktonic community in freshly upwelled water was dominated by microheterotrophic bacteria and protozoans, where bacteria ($49\ \text{mg C m}^{-3}$) exceeded by two orders of magnitude the biomass of phytoplankton. Total oxygen used by microheterotrophs exceeded by three-times that produced by primary production, indicating that the heterotrophic respiration was dependent on organic matter pre-existing in the upwelling waters. Tintinnids and their relation to EN were studied by Gómez (1997). The pelagic ecosystem of the equatorial upwelling, including bacteria, several size fractions of phytoplankton, micro- and mesozooplankton, was analyzed by Vinagradov et al. (1977).

Clearly, the studies mentioned above are not nearly sufficient to give even a superficial picture of the processes involving microzooplankton and the microbial loop in the waters off Peru. This shows the urgent need for further studies as to improve our understanding of its highly productive ecosystem.

5.3. Perspectives and suggestions for data acquisition

As it now exists, the Peruvian zooplankton time series is most valuable, and must continue with a consistent methodology and strategy (Table 2). Such time series are essential to study relationships between climate and ecosystems. However, biovolume data alone are often not sufficient to understand regime shifts and their consequences for higher trophic levels. More information is needed on taxonomic composition or at least on size spectra. For estimates of trophic transfer a common unit for biomass (dry mass, carbon content) is essential.

For the short term, the addition of modern optical and acoustical zooplankton sensors to standard large-scale surveys will vastly improve our description of the spatial distribution of zooplankton. The new CRIOS cruises (Table 2) provide a regular monitoring of primary and secondary production and mesozooplankton grazing. These cruises also provide excellent opportunities for process studies (e.g. microbial loop, microzooplankton grazing, the effects of red tides and diatom blooms on zooplankton population dynamics, physical and trophic processes in fronts and upwelling filaments, etc.).

On the long-term, new strategies for data acquisition in real time may yield new perspectives on the dynamics of the Peruvian upwelling ecosystem. To better understand the links between climate and fish, all components of the pelagic system including zooplankton have to be considered, preferably by synchronous interdisciplinary efforts. Still, little is known about many dynamic processes that characterize upwelling systems, such as the evolution of biological communities within upwelled cells. The scale of events controlling the biological–physical interaction is not clear yet. To construct models which effectively encompass the size of the system actually in operation requires at the very least a spectral analysis of the environmental events from the order of days to months, and eventually to years. A powerful device to obtain such information would be an array of autonomous sensors (current meters, ctdo, fluorescence probe, acoustical and optical plankton counters) anchored at appropriate locations along the shelf (Dickie and Valdivia, 1981). Process studies could then be embedded in such a mooring array.

The use of autonomous profiling floats (Roemmich et al., 2004), autonomous underwater vehicles (AUVs, Curtin et al., 1993; Griffiths et al., 2000; Samson et al., 2001; Yu et al., 2002) and enduring autonomous gliders (Sherman et al., 2001; Rudnick et al., 2004) together with satellite imagery may be an additional possibility to generate long-term high-resolution data on important physical, biogeochemical, and biological variables.

5.4. Models

Little attention has been given to the stochastic nature of upwelling systems (Menshutkin et al., 1980), that are influenced by random events that make them shift unpredictably between multiple states (e.g. upwelling and relaxation, red tides versus diatom blooms, etc.). Considering this stochastic nature, early statistical descriptions of meteorological, oceanographic, and fisheries data have concluded that predicting the states of the Peruvian upwelling ecosystem "longer than some months ahead may be beyond reach" (Bohle-Carbonell, 1989). This rather pessimistic view was largely true in the 1970s, considering the unexplained collapse of the anchovy fisheries and ignorance of ENSO and multi-decadal cycles.

Recently, considerable progress has been made in forecasting ENSO (e.g. Penland and Matrosova, 2001; Chen et al., 2004; Cash et al., 2006) and in understanding the intrinsic relationship between ENSO and multi-decadal cycles (Yasunaka and Hanawa, 2005; Ye and Hsieh, 2006). Individual-based Lagrangian models can integrate physical, biogeochemical and biological data (Leising and Franks, 2000; Woods et al., 2005; Croquette and Eldin, 2006). However, only recently this approach has been applied to model zooplankton advection in coastal upwelling regions (Batchelder et al., 2002; Carr et al., 2008). Ecosystem modelling should focus on predicting how future cyclic (e.g. ENSO and multi-decadal variation) and non-cyclic changes (e.g. global warming and ocean acidification) will affect upwelling ecosystems.

Acknowledgements

We would like to thank the Area de Evaluación Producción Secundaria team at IMARPE for their invaluable cooperation in building up the necessary references for this work. Thanks to Mark Taylor, Francisco Chavez, David Mackas, and two anonymous reviewers for improving the original text with important comments and suggestions. This work is a contribution of the Zooplankton Study Group at IMARPE, and was conducted in the frame of the EU-project CENSOR (Climate variability and El Nino Southern Oscillation: impact for natural resources and management, contract 511071). It is CENSOR publication no. 87. This paper forms part of the Ph.D. Thesis of the second author at Bremen University.

References

Abanto, M.R., 2001. Composición, distribución y abundancia de copépodos planctónicos marinos en la costa Norte-Centro (03°30′S–14°00′S) frente al litoral Peruano entre los años 1980 y 1989. Tesis de Licenciatura, Facultad de Ciencias Naturales y Matemáticas, Universidad Nacional Federico Villarreal, Lima (Unpublished).

Agis, M., Granda, A., Dolan, J.R., 2007. A cautionary note: examples of possible microbial community dynamics in dilution grazing experiments. Journal of Experimental Marine Biology and Ecology 341 (2), 176–183.

Alheit, J., Niquen, M., 2004. Regime shifts in the Humboldt Current ecosystem. Progress in Oceanography 60 (2–4), 201–222.

Alvarado, A., 1972. Variación cuantitativa de copépodos, eufáusidos y quetognatos de la zona norte Peruana (07°01′ y 08°56′ Latitud Sur) verano-invierno 1967. Tesis de Biólogo, Universidad Nacional de Trujillo (Unpublished).

Ancieta, F., 1981. The importance of coastal upwelling research for Peru. In: Richards, F.A. (Ed.), Coastal Upwelling Coastal and Estuarine Sciences, vol. 1. American Geophysical Union, Washington, DC, pp. 4–5.

Antezana, T., 1978. Distribution of euphausiids in the Chile-Perú Current with particular reference to the endemic *Euphausia mucronata* and the Oxygen Minimum Layer. Ph.D. Dissertation, San Diego. Scripps Institution of Oceanography, University of California, San Diego, 465 pp.

Antezana, T., 2002a. Adaptative behaviour of *Euphausia mucronata* in relation to the oxygen minimum layer of the Humboldt Current. In: Färber, Jaime (Ed.), Oceanography of the Eastern Pacific II. Centro de Investigación Científica y de Educación Superior de Ensenada CICESE, México, pp. 29–40.

Antezana, T., 2002b. Vertical distribution and diel migration of *Euphausia mucronata* in the oxygen minimum layer of the Humboldt Current. In: Färber, Jaime (Ed.), Oceanography of the Eastern Pacific II. Centro de Investigación Científica y de Educación Superior de Ensenada (CICESE), Mexico, pp. 13–28.

Antezana, T., 2006. *Euphasia mucronata* a keystone and prey of the Humboldt Current. In: Book of Extended Abstracts, International Conference the Humboldt Current System: Climate, Ocean Dynamics, Ecosystem Processes, and Fisheries, Lima, Peru, November 27–December 1, 2006, pp. 51–53 (Unpublished).

Arashkevich, E.G., Flint, M.B., Pelymskij, A.G., 1982. Qualitative characteristics of feeding of abundant zooplankton species in Peruvian coastal waters. Okeanologiya 22 (4), 645–651 (in Russian).

Arntz, W.E., Fahrbach, E., 1991. El Niño Klimaexperiment der Natur: Physikalische Ursachen und biologische Folgen. Birkhäuser Verlag, Basel, Germany. 264pp.

Aronés, K.J., 1997. Distribución horizontal de los amphipoda (crustacea) en el mar Peruano durante el fenómeno "El Niño" verano 1983. Tesis de Licenciatura, Facultad de Ciencias Biológicas, Universidad Ricardo Palma, Lima (Unpublished).

Aronés, K.F., 2002. Estudios comparativos de copépodos costeros frente a Paita y San José. In: Retuerto, F., Talledo, M. (Eds.), XI Reunión Científica Instituto de Investigación de Ciencias Biológicas "Antonio Raimondi" (ICBAR), Lima, p. 74 (Unpublished).

Aronés, K.F., 2004. Zooplancton e ictioplancton del mar Peruano durante el verano 2001. Informe del Instituto del Mar del Perú 32 (1), 47–56.

Aronés, K., Ayón, P., 2001. Variabilidad del zooplancton e ictioplancton frente a Paita entre febrero y diciembre del 2000. In: Retuerto, F., Talledo, M. (Eds.), X Reunión Científica Instituto de Investigación de Ciencias Biológicas "Antonio Raimondi" (ICBAR), Editora EISA SRL, Lima (Unpublished).

Aronés, K., Ayón, P., 2002. Effects of El Niño 1997–1998 on copepods community structure at San Jose Coastal Station (Peru). In: Salinas, S., Urban, H., Arntz, W. (Eds.), Workshop Impacts of El Niño and Basin Scales Climate Changes on Ecosystems and Living Marine Resources: A Comparison between the California and the Humboldt Current Systems. Investigaciones Marinas, Chile, pp. 104–105.

Aronés, K., Girón, M., Ayón, P., 2001. Caracterización del zooplancton en cuatro zonas de la costa Norte-centro del Perú durante el 2000. In: Retuerto, F., Talledo, M. (Eds.), X Reunión Científica Instituto de Investigación de Ciencias Biológicas "Antonio Raimondi" (ICBAR), Lima, p. 60 (Unpublished).

Aronés, K., Ayón, P., Hirche, H.J., Schwamborn, R., in press. Hydrographic structure and zooplankton abundance and diversity off Paita, northern Peru (1994–2004) – ENSO effects, trends and changes. Journal of Marine Science.

Ayón, P., 1999. Volúmenes de zooplancton e ictioplancton frente a la costa peruana en verano e inicios de otoño 1999. Crucero BIC José Olaya Balandra 9902-03, de Tumbes a Tacna. Informe del Instituto del Mar del Perú 147, 59–70.

Ayón, P., Aronés, K., 1997a. Característica generales del zooplancton en la costa norte centro durante el Crucero BIC SNP-1 9607-08. Informe del Instituto del Mar del Perú 124, 51–56.

Ayón, P., Aronés, K., 1997b. Comunidades de zooplancton e ictioplancton frente a la costa norte centro del Perú. Crucero BIC Humboldt 9705-06. Informe del Instituto del Mar del Perú 128, 70–79.

Ayón, P., Aronés, K., Zarate, M., 1999. Variaciones en el comportamiento del copépodo calanoideo *Centropages brachiatus* (Dana, 1849), frente a la costa Peruana durante el evento El Niño 97–98. In: Tresierra, A., Culquichicon, Z. (Eds.), VIII Congreso Latinoamericano Sobre Ciencias del Mar. 1999, Trujillo-Perú, pp. 730–731 (Unpublished).

Ayón, P., Sánchez, S., Girón, M., Villanueva, P., Delgado, E., 1996. Composición y distribución del plancton en el litoral Peruano en el verano de 1996. Crucero de evaluación hidroacustica de recursos pelagicos. BIC SNP-1 9602-04. Informe del Instituto del Mar del Perú 122, 69–78.

Ayón, P., Girón, M., 1996. Características del zooplancton e ictioplancton durante el periodo de verano1995 frente a la costa Peruana crucero de evaluación de recursos pelagicos 9502-04 BIC Snp-1 (13 Febrero–05 Abril 1995). Informe del Instituto del Mar del Perú 116, 73–81.

Ayón, P., Girón, M., 1997. Composición y distribución del zooplancton e ictioplancton frente a la costa peruana durante febrero a abril 1997. Informe del Instituto del Mar del Perú 127, 49–55.

Ayón, P., Girón, M., 2004. El ictioplancton del mar peruano durante la Primavera austral 2001. Informe del Instituto del Mar del Perú 32 (2), 181–187.

Ayón, P., Purca, S., Guevara-Carrasco, R., 2004. Zooplankton volume trends off Peru between 1964 and 2001. ICES Journal of Marine Science 61, 478–484.

Ayón, P., Swartzman, G., Bertrand, A., Gutierrez, M., Bertrand, S., 2008. Zooplankton and forage fish species off Peru: large-scale bottom-up forcing and local-scale depletion. Progress in Oceanography 79, 208–214.

Báez, P., 1997. Clave de larvas de crustáceos decápodos recolectadas frente al norte de Chile durante un fenómeno El Niño. Investigaciones Marinas 25, 167–176.

Báez, P., Martín, J.W., 1992. Decapod Crustacea larvae collected off northern Chile during an El Niño event (February–March, 1983). Contributions in Science, Natural History Museum of Los Angeles County 432, 1–10.

Bakun, A., Broad, K., 2003. Environmental 'loopholes' and fish population dynamics: comparative pattern recognition with focus on El Nino effects in the Pacific. Fisheries Oceanography 12, 458–473.

Bakun, A., Nelson, C.S., 1991. The seasonal cycle of wind stress curl in sub-tropical eastern boundary current regions. Journal of Physical Oceanography 21, 1815–1834.

Barber, R.T., Chavez, F.P., 1991. Regulation of primary productivity rate in the equatorial Pacific Ocean. Limnology and Oceanography 36, 1803–1815.

Batchelder, H.P., Edwards, C.A., Powell, T.M., 2002. Individual-based models of copepod populations in coastal upwelling regions: implications of physiologically and environmentally influenced diel vertical migration on demographic success and nearshore retention. Progress in Oceanography 53, 307–333.

Bertrand, A., Segura, M., Gutiérrez, M., Vásquez, L., 2004. From small-scale habitat loopholes to decadal cycles: a habitat-based hypothesis explaining fluctuation in pelagic fish populations off Peru. Fish and Fisheries 5, 296–316.

Bertrand, A., Segura, M., Gutiérrez, M., Vásquez, L., 2005. From small-scale habitat loopholes to decadal cycles: a habitat-based hypothesis explaining fluctuation in pelagic fish populations off Peru. Fish and Fisheries 5, 296–316.

Beers, J.R., Stevenson, M.R., Eppley, R.W., Brooks, E.R., 1971. Plankton populations and upwelling off the coast of Peru, June 1969. Fishery Bulletin 69, 859–876.

Bieri, R., 1957. The Chaetognath fauna off Peru in 1941. Pacific Science 11, 255–264.

Bieri, R., 1959. The distribution of the planktonic Chaetognatha in the Pacific and their relationship to the water masses. Limnology and Oceanography 4, 1–27.

Bigelow, H.B., 1911. The Siphonophorae Reports on the scientific results of the expedition to the eastern tropical Pacific by the US Fish Commission Steamer Albatross. Memoirs of the Museum of Comparative Zoology at Harvard College 38 (2), 173–401.

Bohle-Carbonell, M., 1989. On the variability of the Peruvian upwelling system. In: Pauly, D., Muck, P., Mendo, J., Tsukayama, I. (Eds.), The Peruvian Upwelling Ecosystem: Dynamic and Interactions, ICLARM, Conference Proceedings, vol. 18, pp. 14–32.

Bond, N.A., Overland, J.E., Spillane, M., Stabeno, P., 2003. Recent shifts in the state of the North Pacific. Geophysical Research Letter Research 30 (23), 2183.

Boyd, C.M., Smith, S.L., Cowles, T.J., 1980. Grazing patterns of copepods in the upwelling system off Peru. Limnology and Oceanography 25, 583–596.

Boyd, C.M., Smith, S.L., 1983. Plankton, upwelling, and coastally trapped waves off Peru. Deep Sea Research Part A 30 (7), 723–742.

Bustos, H., Aracena, O., Mora, S., Palma, W., 1982. Estudio de crecimiento y edad en el recurso langostino colorado (*Pleuroncodes monodon*, H. Milne Edwards, 1837). Instituto de Fomento Pesquero (manuscript), 120p.

Carr, M.E., 2003. Simulation of carbon pathways in the planktonic ecosystem off Peru during the 1997–1998 El Niño and La Niña. Journal of Geophysical Research 108 (10), 1–15.

Carr, S.D., Capet, X.J., McWilliams, J.C., Pennington, T., Chavez, F.P., 2008. The influence of diel vertical migration on zooplankton transport and recruitment in an upwelling region: estimates from a coupled behavioral–physical model. Fisheries Oceanography 17, 1–15.

Carrasco de Luyo, S., 1981. Anfípodos y su relación con mareas rojas. In: Memorias del Seminario Sobre Indicadores Biológicos del Plancton. Instituto del Mar del Peru., Callao-Peru, 8–11 de Septiembre de 1980. UNESCO, pp. 45–53 (Unpublished).

Carrasco, S., 1989. Anfípodos planctónicos del área comprendida ente Paita y norte de Chimbote. Tesis de Licenciatura, Facultad de biología, Universidad Particular Ricardo Palma, Lima (Unpublished).

Carrasco, S., Lozano, O., 1989. Seasonal and long-term variations of zooplankton volumes in the Peruvian sea, 1964–1987. Instituto del Mar del Perú (IMARPE), Deutshe Gesellschafr fur Technische Zusammenarbeit (GTZ) and International Center for Living Aquatic Resources Mangement (ICLARM), Manila, pp. 82–95.

Carrasco, S., Santander, H., 1987. The El Niño event and its influence on the zooplankton off Peru. Journal of Geophysical Research 92 (C13), 14405–14410.

Cash, D.W., Borck, J.C., Patt, A.G., 2006. Countering the loading-dock approach to linking science and decision making – comparative analysis of El Nino/Southern Oscillation (ENSO) forecasting systems. Science Technology and Human Values 31, 465–494.

Castillo, R.F., 2004. Composición especifica, distribución y abundancia de ostracodos epipelagicos en el mar Peruano durante los años 1998 y 2001. Tesis de Licenciatura, Facultad de Ciencias, Departamento de Biología, Universidad Nacional Agraria La Molina, Lima (Unpublished).

Castillo, R.F., Antezana, T., Ayón, P., Mendo, J., 2005. Distribution of ostracods off Peru under the influence of El Niño 1997–1998 First Alexander Von Humboldt. In: International Conference on the El Niño Phenomenon and It's Global Impact, Guayaquil, p. 104 (Unpublished).

Castillo, R., Antezana, T., Ayón, P., 2007. The influence of El Niño 1997–1998 on pelagic ostracods in the Humboldt Current Ecosystem off Peru. Hydrobiologia 585, 29–41.

Chen, D., Cane, M.A., Kaplan, A., Zebiak, S.E., Huang, D.J., 2004. Predictability of El Nino over the past 148 years. Nature 428, 733–736.

Chimpén, C., 1999. Nuevas alternativas tecnológicas para recursos pesqueros no explotados. Revista Focus, Instituto Tecnológico Pesquero del Perú (ITP) Año 2 (1), 36.

Costlow, J., Fagetti, E., 1967. The larval development of the crab, *Cyclograpsus cinereus* Dana, under laboratory conditions. Pacific Science 21 (2), 166–177.

Cowles, T.J., 1978. Copepod feeding in the Peru upwelling system. Ph.D. Thesis, Department of Zoology, Duke University, Durham (Unpublished).

Cowles, T., 1979. The feeding responses of copepods from the Peru upwelling system: food size selection. Journal of Marine Research Research 37, 601–622.

Criales, M.M., McGowan, M.F., 1994. Horizontal and vertical distribution of penaeidean and caridean larvae and micronektonic shrimps in the Florida Keys. Bulletin of Marine Science 54 (3), 843–856.

Criales-Hernández, M.I., Schwamborn, R., Graco, M., Ayón, P., Hirche, H.-J., Wolff, M., 2008. Zooplankon vertical distribution and migration off central Peru in relation to the oxygen minimum layer. Helgoland Marine Research 62 (Suppl. 1), 85–100.

Croquette, M., Eldin, G., Echevin, V., 2005. On the contributions of Ekman transport and pumping to the dynamics of coastal upwelling in the south-east pacific. Gayana 68, 136–140.

Croquette, M., Eldin, G., 2006. A Lagrangian study of the PCUC source waters. In: Book of Extended Abstracts, International Conference The Humboldt Current System: Climate, Ocean Dynamics, Ecosystem Processes, and Fisheries, Lima, Peru, November 27–December 1, 2006, p. 41 (Unpublished).

Curtin, T.B., Bellingham, J.G., Catipovic, J., Webb, D., 1993. Autonomous oceanographic sampling networks. Oceanography 6, 86–94.

Cury, P., Roy, C., 1989. Optimal environmental window and pelagic fish recruitment success in upwelling areas. Canadian Journal of Fisheries and Aquatic Sciences 46 (4), 670–680.

Dagg, M.J., Cowles, T., Whitledge, T., Smith, S., Howe, S., Judkins, D., 1980. Grazing and excretion by zooplankton in the Peru upwelling system during April, 1977. Deep Sea Research 27, 43–59.

Dextre, C., 1983. Distribución horizontal del grupo Chaetognatha y del zooplancton en general en el mar del norte Peruano durante el desarrollo del Fenómeno El Niño en Febrero de 1972. Tesis de Licenciatura, Facultad de Biología, Universidad Nacional Federico Villarreal, Lima (Unpublished).

Dickie, L.M., Valdivia, J.E., 1981. Investigación cooperativa de la Anchoveta y su ecosistema (ICANE) entre Perú y Canadá. Informe sumario. Boletín del Instituto del Mar del Perú Volumen Extraordinario, I–XII.

Dittel, A., Epifanio, C.E., 1984. Growth and development of the portunid crab *Callinectes arcuatus* Ordway: zoeae, megalopae, and juveniles. Journal Crustacean Biology 4, 491–494.

Drits, A.V., 1985. Food ingestion rate of *Calanus australis* as a function of food concentration under natural conditions. Oceanology 25, 116–119.

Dugdale, R.C., Goering, J.J., 1970. Nutrient limitation and the path of nitrogen in Peru Current production. In: Chin, E. (Ed.), A Collection of Manuscripts on the Biological Oceanography of the Southeast Pacific Ocean. U.S. Gov. Print. Off., Washington, DC.

Dugdale, R.C., MacIsaac, J.J., 1971. A computational model for the uptake of nitrate in the Peru upwelling region. Investigation Pesquera 35 (1), 299–308.

Durant, J.M., Hjermann, D.Ø., Ottersen, G., Stenseth, N.C., 2007. Climate and the match or mismatch between predator requirements and resource availability. Climatic Research 33, 271–283.

Echevin, V., Puillat, I., Grados, C., Dewitte, B., 2004a. Seasonal and mesoscale variability in the Peru upwelling system from in situ data during the years 2000–2004. Gayana 68 (Suppl. 2), 167–173.

Echevin, V., Aumont, O., Tam, J., Pasapera, J., 2004b. The seasonal cycle of surface chlorophyll along the Peruvian coast: comparison between SeaWifs satellite observations and dynamical/biogeochemical coupled model simulations. Gayana 68, 325–326.

Escribano, R., Marin, V.H., Irribarren, C., 2000. Distribution of *Euphausia mucronata* at the upwelling area of Peninsula Mejillones, northern Chile: the influence of the oxygen minimum layer. Scientia Marina 64 (1), 69–77.

Escribano, R., Daneri, G., Farías, L., Gallardo, V.A., González, H.E., Gutiérrez, D., Lange, C.B., Morales, C.E., Pizarro, O., Ulloa, O., Braun, M., 2004. Biological and chemical consequences of the 1997–1998 El Nin~o in the Chilean coastal upwelling system: a synthesis. Deep Sea Research II 51, 2389–2411.

Escudero, Y.M., 2003. Migración nictimeral del zooplancton marino en una estación frente al Callao (Perú). Tesis de Licenciatura, Facultad de Ciencias Naturales y Matemática, Universidad Federico Villarreal, Lima (Unpublished).

Espinoza, P., Bertrand, A., 2008. Revising anchovy's (*Engraulis ringens*) trophic niche and ecological role reveals its plasticity provides a new vision of the Humboldt Current system. Progress in Oceanography 79, 215–227.

Fenaux, R., 1968. Algunas apendicularias de la costa Peruana. Boletín Instituto del Mar del Perú 1 (9), 536–552.

Fernández-Álamo, M.A., Färber-Lorda, J., 2006. Zooplankton and the oceanography of the eastern tropical Pacific: a review. Progress in Oceanography 69 (2–4), 318–359.

Fiedler, P.C., Talley, L.D., 2006. Hydrography of the eastern tropical Pacific: a review. Progress in Oceanography 69, 143–180.

Flint, M.V., Timonin, A., 1985. Trophic structure of mesoplankton in the northern part of Peruvian coastal waters. Oceanology 25 (1), 139–145 (in Russian).

Franco, M., 2003. Aspectos biológico-pesqueros del camaroncito rojo *Pleuroncodes monodon* (M. Edwards, 1837) en el litoral Peruano. Tesis de Ingeniero Pesquero, Facultad de Ingeniería Pesquera y de Alimentos, Universidad Nacional del Callao, 225 pp. (Unpublished).

Franks, P.J.S., 1992. Sink or swim, accumulation of biomass at fronts. Marine Ecology Progress Series 82, 1–12.

Gallardo, V., Cañete, I., Enríquez-Brionez, S., Roa, R., Acuña, A., Baltazar, M., 1993. Biología del langostino colorado *Pleuroncodes monodon* H. Milne Edwards, 1837 y especies afines (Crustacea, Decapoda, Anomura, Galatheidae): sinopsis. In: Faranda, F., Parra, O. (Eds.), Elementos Básicos Para la Gestión de Los Recursos Vivos Marinos Costeros de la Región del Biobío. Monografías Científicas, vol. 2. Programa EULA, Universidad de Concepción, pp. 67–113.

Gallardo, V., Cañete, I., Roa, R., Enríquez-Brionez, S., Baltazar, M., 1994. Recruitment of the squat lobster *Pleuroncodes monodon* on the continental shelf off central Chile. Journal of Crustacean Biology 14 (4), 665–669.

Gargett, A., 1997. The optimal stability 'window': a mechanism underlying decadal fluctuations in North Pacific salmon stocks? Fisheries Oceanography 6 (2), 109–117.

Genin, A., Jaffe, J.R., Reef, R., Richter, C., Franks, P.J.S., 2005. Swimming against the flow: a mechanism of zooplankton aggregation. Science 308, 860–862.

Gerlotto, F., Gutierrez, M., Bertrand, S., 2006. The alternation in spatial distribution of sardine and anchovy in the Humboldt Current: effects of climate, behavioral interactions, or data misunderstanding? In: Book of Extended Abstracts, International Conference the Humboldt Current System: Climate, Ocean Dynamics, Ecosystem Processes, and Fisheries, Lima, Peru, November 27–December 1, 2006, pp. 68–69 (Unpublished).

Geynrikh, A.K., 1973. Horizontal distribution of copepods in the Peru Current Region. Oceanology 13, 94–103.

Glebov, B.V., 1982. Diurnal variations in the vertical distribution of zooplankton in Coastal Peru waters. Vestnik Moskovskogo Universiteta, Seriya Biolgiya, Moscow 3, 6–11 (in Russian).

Gómez, O., 1972. Contribución al conocimiento de los copépodos de la costa Peruana. Tesis de Licenciatura, Facultad de Biología, Universidad Nacional Mayor de San Marcos, Lima (Unpublished).

Gómez, O., 1982. Los copépodos planctónicos del Mar Peruano. Boletín de Lima 23, 1–16.

Gómez, I.O., 1997. Los tintinidos (Protozoa: Ciliata) del mar Peruano y sus relaciones con el fenómeno El Niño. Boletín Instituto del Mar del Perú 16 (2), 61–84.

Greene, K., 2002. Ocean sciences meeting: coastal cool-down. Science 295 (5561), 1823.

Griffiths, G., Knap, A., Dickey, T., 2000. Autosub experiment near Bermuda. Sea Technology 41, 35–47.

Guillén, V., 1978. Distribución horizontal de algunos copépodos calonoideos en el area Puerto Pizarro-Callao (03°40′–11°55′LS) en diciembre de 1976. Tesis, Universidad Nacional San Cristóbal de Huamanga, Ayacucho, Peru (Unpublished).

Gunther, E.R., 1936. A report on oceanographical investigations in the Peru Coastal Current. Discovery Reports XIII, 107–276.

Gutiérrez, D., Aronés, K., Chang, F., Quipuzcoa, L., Villanueva, P., 2005. Impacto de la variación oceanográfica estacional e interanual sobre los ensambles de Microfitoplancton, mesozooplancton, ictioplancton y macrozoobentos de dos áreas costeras del norte del Peru entre 1994 y 2002. Boletín Instituto del Mar del Perú 22 (1–2), 1–60.

Gutiérrez, M., Swartman, G., Bertrand, A., Bertrand, S., 2007. Anchovy (*Engraulis ringens*) and sardine (*Sardinops sagax*) spatial dynamics and aggregation patterns in the Humboldt Current ecosystem, Peru, from 1983 to 2003. Fisheries Oceanography 16, 155–168.

Gutiérrez, J., Zúñiga, O., 1977. *Pleuroncodes monodon* H. Milne Edwards, 1837 en la bahía de Mejillones del sur, Chile (Crustacea, Decapoda, Anomura). Revista de Biología Marina, Valparaíso 16 (2), 161–169.

Gutiérrez, M., Bertrand, A., Ramirez, A., Bertrand, S., Gerlotto, F., Moron, O., Peraltilla, S., 2008. Ecological niche, patterns of distribution and overlapping of the squat lobster 'munida' (*Pleuroncodes monodon*) and anchovy (*Engraulis ringens*) off Peru from 1998 to 2006. Progress in Oceanography 79, 256–263.

Guzmán, S., Carrasco, S., 1996. Las investigaciones del ictioplancton y el zooplancton en el IMARPE. Necesidades y perspectivas. Informe Progresivo del Instituto del Mar del Perú, Perú 28, 3–18.

Haig, J., 1955. The crustacean Anomura of Chile. Report of the Lunds University Chile Expedition 1848–1849. Lunds Universitets Arsskrift NF Avd. 2, 51 (12), 1–60.

Hardy, A.C., 1936. Observations on the unequal distribution of oceanic plankton. Discovery Reports 11, 511–538.

Hendricks, M.E., Estrada-Navarrete, F.D., 1989. A checklist of the species of pelagic shrimps (Penoidea and Caridea) from the Eastern Pacific, with notes on their geographic and depth distribution. California Cooperative Oceanic Fisheries Investigation Reports 30, 104–121.

Herman, A.W., 1984. Vertical copepod aggregations and interactions with chlorophyll and production on the Peru Shelf. Continental Shelf Research 3 (2), 131–146.

Hidalgo, P., Escribano, R., Morales, C.E., 2005. Ontogenetic vertical distribution and diel migration of the copepod *Eucalanus inermis* in the oxygen minimum zone off northern Chile (20–21°S). Journal of Plankton Research 27, 519–529.

Huyer, A., Knoll, M., Paluszkiewicz, T., Smith, R.L., 1991. The Peru Undercurrent: a study in variability. Deep Sea Research 38 (Suppl. 1), 247–279.

Jarre-Teichmann, A., 1998. The potential role of mass of balance models for the management of upwelling ecosystems. Ecological Applications 8 (Suppl. 1), s93–s103.

Jarre, A., Muck, P., Pauly, D., 1991. Two approaches for modelling fish stock interactions in the Peruvian upwelling ecosystem. ICES Marine Science Symposium 193, 171–184.

Judkins, D., 1980. Vertical distribution of zooplankton in relation to the oxygen minimum off Peru. Deep Sea Research 27A, 475–487.

Kiørboe, T., 1997. Population regulation and role of mesozooplankton in shaping marine pelagic food webs. Hydrobiologia 363, 13–27.

Klekowski, R.R., Kukina, I.V., Tumantseva, N.I., 1975. Metabolic rate in microzooplankton. Trudy IOAN SSSR, 102 (in Russian).

Koettker, A.G., Freire, A.S., 2006. Spatial and temporal distribution of decapods larvae in the subtropical waters of the Arvoredo archipelago, SC, Brazil. Iheringia: Serie Zoologia 96 (1), 31–39.

Kloppmann, M.H.F., Hillgruber, N., von Westernhagen, H., 2002. Wind-mixing effects on feeding success and condition of blue whiting larvae in the Porcupine Bank area. Marine Ecology Progress Series 235, 263–277.

Lasker, R., 1975. Field criteria for survival of anchovy larvae: the relation between inshore chlorophyll maximum layers and successful first feeding. Fishery Bulletin (United States) 73 (3), 453–462.

Lasker, R., Feder, H.M., Theilacker, G.H., May, R.C., 1970. Feeding, growth and survival of *Engraulis mordax* larvae reared in the laboratory. Marine Biology 5, 345–353.

Lasker, R., Smith, P.E., 1977. Estimation of the effects of environmental variations on the eggs and larvae of the northern anchovy. California Cooperative Oceanic Fishereies Investigation Report 19, 128–137.

Leising, A.W., Franks, P.J.S., 2000. Copepod vertical distribution within a spatially variable food source: a simple foraging-strategy model. Journal of Plankton Research 22, 999–1024.

Litzow, M.A., 2006. Climate regime shifts and community reorganization in the Gulf of Alaska: how do recent shifts compare with 1976/1977. ICES Journal of Marine Science 63, 1386–1396.

Lenz, J., 2000. Introduction. In: Harris, R.P., Wiebe, P.H., Lenz, J., Skjoldal, H.R., Huntley, M. (Eds.), Zooplankton Methodology Manual. Academic Press, UK, pp. 1–32.

Mackas, D.L., Boyd, C.M., Smith, S., Santander, H., 1981. Vertical distributions of plankton in the upper 35 m of the Peruvian upwelling zone – application o a shipboard electronic plankton counting system. Boletín Instituto del Mar del Perú Volumen Extraordinario, 67–71.

Mackas, D.L., Peterson, W.T., Zamon, J.E., 2004. Comparisons of interannual biomass anomalies of zooplankton communities along the continental margins of British Columbia and Oregon. Deep Sea Research Part II 51, 875–896.

Martins, A.S., Haimovici, M., Palacios, R., 2005. Diet and feeding of the cutlass fish *Trichiurus lepturus* in the Subtropical Convergence Ecosystem of southern Brazil. Journal of the Marine Biological Association of the United Kingdom 85 (5), 1223–1229.

McManus, G.B., Costas, B.A., Dam, H.G., Lopes, R.M., Gaeta, S.A., Susini, S.M., Rosetta, C.H., 2007. Microzooplankton grazing of phytoplankton in a tropical upwelling region. Hydrobiologia 575 (1), 69–81.

Mejia, J., Flores, L.A., Segura, G., 1971. Exploración sobre recursos costeros y recursos demersales. Crucero 7104 B/I SNP-1. Serie de Informes Especiales No. IM-88 (Unpublished).

Mejia, J., Flores, L.A., Castillo, J., Hartley, H., 1973. Exploración sobre recursos demersales en el Crucero SNP-1 7205. Un intento de evaluar la cantidad de peces disponibles para la pesca. Serie de Informes Especiales No. IM-149.

Mejia, J., Esquerre, M., Castillo, J., 1980. Situación del recurso merluza y sus características biológicas en la primavera de 1978. Informe del Instituto del Mar del Perú 58, 1–54.

Mendo, J., Yamashiro, C., Rubio, J., Kameya, A., Jurado, E., Maldonado, M., Guzmán, S., 1989. Evaluación de la Población de Concha de Abanico (*Argopecten purpuratus*) en la Bahía Independencia, Pisco, Peru 23 de Setiembre–9 de Octubre de 1987. Informe del Instituto del Mar del Perú 94, 1–65.

Mendelssohn, R., Mendo, J., 1987. Exploratory analysis of Anchoveta recruitment off Peru and related environmental series, pp. 294–306. In: Pauly, D., Tsukayama, I. (Eds.), The Peruvian Anchoveta and its Upwelling Ecosystem: Three Decades of Change. ICLARM Stud. Rev. 15, p. 351.

Menshutkin, V.V., Tseytlin, V.B., Vinogradov, M.Ye., 1980. Stochastic approach to modelling an upwelling ecosystem. Ecosistemy Pelagiali Peruanskogo Rayona (Pelagic Ecosystems of the Peru Area). Nauka Press, Moscow. pp. 257–267.

Mikheyev, V.N., 1977a. Age structure of populations of a zoocoenosis in the Peruvian coastal upwelling. Oceanologia 17, 700–706.

Mikheyev, V.N., 1977b. Structural characteristics of populations of common copepod species in the Peruvian Upwelling Region. Comparison of sampling devices. Oceanology 17 (3), 336–339.

Montecino, V., Strub, T., Chavez, F., Thomas, A., Tarazona, J., Baumgartner, T., 2006. Bio-physical interactions off western South America. In: Robinson, A.R., Brink, K.H. (Eds.), Thesea. Harvard University Press, Cambridge, MA, USA, pp. 329–390.

Morón, O., 2000. Características del ambiente marino frente a la costa peruana. Boletin Instituto del Mar del Peru 19, 179–204.

Pacheco, A., Garate, A., 2005. Bioincrustantes de cultivo de *Argopecten purpuratus* en Bahía Samanco, Perú. Ecologia Aplicada 4 (1–2), 149–152.

Paffenhöfer, G., 1982. Grazing by copepods in the Peru upwelling. Deep Sea Research Part A. 29 (1), 145–146.

Palma, S., 1976. Meroplancton de la región de Valparaíso. Ciencia y Tecnología del Mar 2, 99–116.

Palma, S., 1994. Distribución y abundancia de larvas de langostino colorado *Pleuroncodes monodon* frente a la costa de Concepción, Chile. Investigaciones Marinas, Valparaíso 22, 13–29.

Pauly, D., Jarre, A., Luna, S., 1989. On the quantity and types of food ingested by Peruvian Anchoveta, 1953–1982. In: Pauly, D., Muck, P., Mendo, J., Tsukayama, I. (Eds.), The Peruvian Upwelling Ecosystem: Dynamic and Interactions, ICLARM Conference Proceedings, vol. 18, pp. 109–124.

Penland, C., Matrosova, L., 2001. Expected and actual errors of linear inverse model forecasts. Monthly Weather Review 129, 1740–1745.

Pennington, J.T., Mahoney, K.L., Kuwahara, V.S., Kolber, D.D., Calienes, R., Chavez, F.P., 2006. Primary production in the eastern tropical Pacific: a review. Progress in Oceanography 69, 285–317.

Penven, P., Echevin, V., Pasapera, J., Colas, F., Tam, J., 2005. Average circulation, seasonal cycle, and mesoscale dynamics of the Peru Current System: a modelling approach. Journal of Geophysical Research 110, C10021.

Petipa, T.S., Monakov, A.V., Sorokin, Yu.I., Voloshina, A.V., 1977. Balance of matter and energy in copepods of the tropical upwellings of Pacific Ocean. Polskie Archiwum Hydrobiologii 24, 413–430.

Pielou, E., 1975. Ecological Diversity. John Wiley and Sons. 165pp..

Ponomareva, L.A., 1982. Early stages of larvae Nictyphanes simplex (Euphausiacea) in the Peru Current area. Oceanology XXII, 98–101.

Quesquén, R., 2004. Zooplancton e ictioplancton del mar Peruano durante el invierno 2001. Informe del Instituto del Mar del Perú 32 (1), 81–86.

Quesquén, R., 2005. Moluscos holoplanctonicos heteropoda y pteropoda colectados en noviembre y diciembre de 1996 en el Mar Peruano. Tesis de Licenciatura, Facultad de Ciencias Biológicas, Universidad Ricardo Palma, Lima (Unpublished).

Quesquén, R., Guzmán, S., 1999. Nuevo registro de *Phylliroe bucephala* (Mollusca, Gastropoda: Nudibranchia) para el mar Peruano. In: Tresierra, A., Culquichicon, Z. (Eds.), VIII Congreso Latinoamericano Sobre Ciencias del Mar, Lima, Trujillo, Perú, pp. 374–375 (Unpublished).

Quintana, R., 1983. Larval development of the edible crab, *Cancer edwardsi* Bell, 1835, under laboratory condition (Decapoda, Brachyura). Rep USA Marine Biology Institute Kochi University 5, 1–19.

Quintana, R.Y.H., Saelzer, 1986. The complete larval development of the edible crab, *Cancer setosus* Molina and observations on the prezoeal and first zoeal stages of *C. coronatus* Molina (Decapoda: Brachyura, Cancridae). Journal of the Faculty of Science, Hokkaido University, Series VI, Zoology 24 (4), 267–303.

Ramos, E., Indacochea, A., Tarazona, J., 1999. Impacto de 'El Niño 1997–1998' sobre el asentamiento larval de algunos invertebrados marinos bentónicos de bahía de Independencia, Pisco, Peru. In: Tarazona, J., Castillo, E. (Eds.), El Niño 1997–1998 y su Impacto Sobre los Ecosistemas Marino y Terreste, Revista Peruana de Biología, Volume Extraodinario, pp. 60–68.

Rebstock, G.A., Kang, Y.S., 2003. A comparison of three marine ecosystems surrounding the Korean peninsula: responses to climate change. Progress in Oceanography 59, 357–379.

Rivera, J., Santander, E., 2005. Variabilidad estacional de la distribución y abundancia de larvas de langostino colorado en la zona norte de Chile (Decapoda, Anomura, Galatheidae). Investigaciones Marinas 33 (1), 3–23.

Roemmich, D., Riser, S., Davis, R., Desaubies, Y., 2004. Autonomous profiling floats; workhorse for broad scale ocean observations. Marine Technology Society Journal 38, 31–39.

Rudnick, D.L., Davis, R.E., Eriksen, C.C., Fratantoni, D.M., Perry, M.J., 2004. Underwater gliders for ocean research. Marine Technology Society Journal 38, 73–84.

Ryther, J.H., Hall, J.R., Pease, A.K., Bakun, A., Jones, M.M., 1966. Primary organic production in relation to the chemistry and hydrography of the Western Indian Ocean. Limnology and Oceanography 11 (3), 371–380.

Ryther, J.H., 1967. Occurrence of Red Water off Peru. Nature 214, 1318–1319.

Sameoto, D., 1981. Horizontal and vertical distributions of zooplankton numbers and biomass off the coast of Peru. Boletin Instituto del Mar del Perú Volumen Extraordinario, 164–170.

Samson, S., Hopkins, T., Remsen, A., Langebrake, L., Sutton, T., Patten, J., 2001. A system for high-resolution zooplankton imaging. IEEE Journal of Oceanic Engineering 26, 671–676.

Sandoval de Castillo, O., 1987. Los quetognatos: indicadores zooplanctonicos del fenómeno "El Niño". Boletín de Lima 49, 17–23.

Santander, H., 1967. Los euphausidos en la zona de Callao-Chimbote y la composición general del zooplancton en agosto de 1961. Tesis de Licenciatura, Facultad de Biología, Universidad Nacional Mayor de San Marcos, Lima (Unpublished).

Santander, H., 1981. The zooplankton in an upwelling area off Peru. In: Richards, F.A. (Ed.), Coastal Upwelling Coastal and Estuarine Sciences, vol. 1. American Geophysical Union, Washington, DC, pp. 411–416.

Santander, H., Carrasco, S., 1985. Cambios en el zooplancton durante El Niño 1982–1983 en el área de Chimbote. In: Aguilar, A.E.T. (Ed.), I Congreso Nacional de Biología Pesquera, Trujillo, pp. 201–206.

Santander, H., Flores, R., 1983. Los desoves y distribución larval de cuatro especies pelágicas y sus relaciones con las variaciones del ambiente marino frente al Perú. In: Sharp, G.D., Csirke, J. (Eds.), Proceedings of the Expert Consultation to Examine Changes in Abundance and Species of Neritic Fish Resources, San José, Costa Rica, 18–29 April 1983. FAO Fisheries Report 291 (3), 835–870.

Santander, H., Carrasco, S., Luyo, G., 1981a. El zooplancton del área norte del Perú. Boletin Instituto del Mar del Perú Volumen Extraordinario, 245–253.

Santander, H., Luyo, G., Carrasco, S., Veliz, M., Sandoval, O., 1981b. Catálogo de zooplancton en el mar Peruano, primera parte: Area Pisco-San Juan. Boletin Instituto del Mar del Perú 6, 1–75.

Santander, H., Sandoval de Castillo, O., 1969. La importancia de los Euphausidos y Chaetognatos y resultados de su distribución en base al Crucero de Febrero del 1967. Informe del Instituto del Mar del Perú 49, 1–17.

Schneider, W., Fuenzalida, R., Rodríguez-Rubio, E., Garcés-Vargas, J., Bravo, L., 2003. Characteristics and formation of Eastern South Pacific Intermediate Water. Geophysical Research Letters 30, 1–35.

Schwamborn, R., Ekau, W., Silva, A.P., Silva, T.A., Saint-Paul, U., 1999. The contribution of estuarine decapod larvae to marine zooplankton communities in north-east Brazil. Archive of Fishery and Marine Research 47 (2–3), 167–182.

Schwamborn, R., Neumann-Leitão, S., Silva, T.A., Silva, A.P., Ekau, W., Saint-Paul, U., 2001. Distribution and dispersal of decapod crustacean larvae and other zooplankton in the Itamaracá estuarine system, Brazil. Tropical Oceanography 29 (1), 1–13.

Shanks, A.L., Brink, L., 2005. Upwelling, downwelling, and cross-shelf transport of bivalve larvae: test of a hypothesis. Marine Ecology Progress Series 302, 1–12.

Sears, M., 1953. Notes on the siphonophores. 2. A revision of the Abylinae. Bulletin of the Museum of Comparative Zoology 109 (1), 4–119.

Segura, M., Castillo, R., 1996. Distribución y concentración de la " *Munida*" (*Pleuroncodes monodon*) en el verano 1996. Informe del Instituto del Mar del Perú 122, 79–85.

Semenova, T.N., Timonin, A.G., Flint, M.V., 1982. Horizontal and vertical distribution patterns of mass zooplankton species off Peru. Okeanologiya (Moscow) 22 (2), 297–304 (in Russian).

Sherman, J., Davis, R.E., Owens, W.B., Valdes, J., 2001. The autonomous underwater glider "spray". IEEE Journal of Oceanic Engineering 26, 437–446.

Shushkina, E.A., Kislyakov, Yu.J., 1977. Estimation of the zooplankton production in the equatorial region of the eastern Pacific Ocean and the Peruvian upwelling. Polskie Archiwum Hydrobiologii 24 (Suppl.), 491–502.

Shushkina, E.A., Vinogradov, M.E., Sorokin, Yu.I., Lebedeva, L.P., Mikheyev, V.N., 1978. Functional characteristics of planktonic communities in the Peruvian upwelling region. Oceanology 18, 578–588.

Smith, D.L., 1977. A Guide to Marine Coastal Plankton and Marine Invertebrate Larvae. Kendall Publishing Company, United States. 161pp.

Smith, S.L., 1978. Nutrient regeneration by zooplankton during a red tide off Peru, with notes on biomass and species composition of zooplankton. Marine Biology 49, 125–132.

Smith, S.L., Brink, K.H., Santander, H., Cowles, T.J., Huyer, A., 1981a. The effect of advection on variations in zooplankton at a single location near Cabo Nazca, Perú. In: Richards, F.A. (Ed.), Coastal and Estuarine Sciences, vol. 1, pp. 400–410.

Smith, S.L., Boyd, C.M., Lane, P.V.Z., 1981b. Short term variation in the vertical distribution of copepods off the coast of northern Peru. Boletin Instituto del Mar del Perú Volumen Extraordinario, 112–118.

Sorokin, Y.I., 1978. Description of primary production and of the heterotrophic microplankton in the Peruvian upwelling region. Oceanology 18, 62–71.

Sorokin, Y.I., Kogelschatz, J.E., 1979. Analysis of heterotrophic microplankton in an upwelling area. Hydrobiologia 66, 195–208.

Sorokin, Y.I., Mikheev, V.N., 1979. On characteristics of the Peruvian upwelling ecosystem. Hydrobiologia 62, 165–189.

Strub, P.T., Mesias, J.M., Montecino, V., Rutllant, J., Salinas, S., 1998. Coastal circulation off western South America. In: Robinson, A.R., Brink, K.H. (Eds.), The Sea, vol. 11: The Global Coastal Ocean – Regional Studies and Syntheses, pp. 273–313.

Sugimoto, T., Tadokoro, K., 1998. Interdecadal variations of plankton biomass and physical environment in the North Pacific. Fisheries Oceanography 7, 289–299.

Sund, P., 1964. The Chaetoghnaths of the waters of Peru region. Bulletin Inter-American Tropical Tuna Commission 9, 115–216.

Tadokoro, K., Chiba, S., Ono, T., Midorikawa, T., 2005. Interannual variation in *Neocalanus* biomass in the Oyashio waters of the western North Pacific. Fisheries Oceanography 14 (3), 210–222.

Tam, J., Taylor, M., Baskovic, V., Espinoza, P., Ballon, M., Purca, S., Diaz, S., Gutierrez, D., Quipuzcoa, L., Ayón, P., Sánchez, S., Goya, E., Arguelles, J., Wolff, M., Wosnitza-Mendo, C., 2006. Trophic flows in the Northern Humboldt Current Ecosystem. Part 1: Comparing 1995–1996 and 1997–1998. In: Abstracts of International Conference The Humboldt Current System Climate Ocean Dynamics Ecosystem Processes, and Fisheries, November 27–December 1, 2006 (Unpublished).

Tarazona, J., Paredes, C., Romero, L., Guzmán, S., 1988. La recolonización de las comunidades de Mitílidos en la Costa Central del Perú después de El Niño 1982–1983. In: Salzwedel, H., Landa, A. (Eds.), Recursos y Dinámica del Ecosistema de Afloramiento Peruano. Boletin Instituto del Mar del Perú Volumen Extraordinario, pp. 115–120.

Tarazona, J., Santander, H., Sánchez, S., Carrasco, S., Guzmán, S., 1989. Características del Plancton. In: Tarazona, J., Paredes, C., Romero, L. (Eds.), Mecanismos y Procesos que Controlan la Colonización y Recuperación Post-catastrófica de Recursos Bentónicos de Importancia Económica en dos Áreas de Diferente Productividad del Sistema de Afloramiento Peruano, Informe Final Proyecto AID 936-5542, pp. 69–118 (Unpublished).

Tarazona, J., Arntz, W., 2001. The Peruvian Coastal Upwelling System. In: Seeliger, U., Kjerfve, B. (Eds.), Coastal Marine Ecosystems of Latin America. Ecological Studies, vol. 144. Springer-Verlag, pp. 229–244.

Tarazona, J., Gutiérrez, D., Paredes, C., Indacochea, A., 2003. Overview and challenges of marine biodiversity research in Peru. Gayana 67 (2), 206–231.

Taylor, A.H., Allen, J.I., Clark, P.A., 2002. Extraction of a weak climatic signal by an ecosystem. Nature 416, 629–632.

Taylor, M., Tam, J., Baskovic, V., Espinoza, P., Purca, S., Arguelles, J., Ayón, P., Ballon, M., Díaz, E., Goya, E., Gutierrez, D., Quipuzcoa, L., Sánchez, S., Wolff, M., Wosnitza-Mendo, C., 2006. Trophic flows in the Northern Humboldt Current Ecosystem. Part 2: Elucidating mechanisms of ecosystem change over an ENSO cycle by simulating changes in low trophic level dynamics. In: Abstracts of International Conference The Humboldt Current System Climate Ocean Dynamics Ecosystem Processes, and Fisheries, November 27–December 1, 2006 (Unpublished).

Timonin, A.G., Flint, M.B., 1986. Effect of hydrologic conditions on distribution of zooplankton off the coast of Peru. Oceanology of the Academy of Sciences of the USSR 26 (3), 366–369 (in Russian).

Tsuchiya, M., 1981. The origin of the Pacific equatorial 13 °C water. Journal of Physical Oceanography 11, 794–812.

Tumantseva, N.I., Kopylov, A.I., 1985a. Reproduction and production rates of *Planktic infusoria* in coastal waters of Peru. Oceanology (Academy of Sciences of the USSR) 25 (3), 390–394 (in Russian).

Tumantseva, N.I., Kopylov, A.I., 1985b. Reproductive rate and production of planktonic ciliates in the coastal Peruvian waters. Okeanologiya 25 (3), 503–508.

UNESCO, 1968. UNESCO Report. Monograph on Oceanographic Methodology, vol. 2, pp. 153–159.

van der Lingen, C.D., Hutchings, L., Field, J.G., 2006. Comparative trophodynamics of anchovy *Engraulis encrasicolus* and sardine *Sardinops sagax* in the southern Benguela: are species alternations between small pelagic fish trophodynamically mediated? African Journal of Marine Science 28, 465–477.

Vasil'ev, V.I., 1991. Characteristics of zooplankton in the oceanic zone off Peru. In: Kuz'micheva, V.I. (Ed.), Book Monograph (in Russian).

Vásquez, F., 1967. Ensayo sobre la relación de los factores abióticos con la distribución del zooplancton en la costa sur del Peru. Tesis de Licenciatura, Facultad de Biología, Universidad Nacional de Trujillo (Unpublished).

Véliz, M., 1981. Sifonóforos como posibles indicadores biológicos. In: UNESCO, Memorias del Seminario Sobre Indicadores Biológicos del Plancton. Instituto del Mar del Perú, 8–11 de setiembre de 1980, pp. 104–116.

Véliz, M., 1985. Sifonóforos en el área norte del Peru. In: Aguilar, A.E.T. (Ed.), I Congreso Nacional de Biología Pesquera, Trujillo, pp. 118–121 (Unpublished).

Vinogradov, M.E., 1977. Pelagic ecosystems studies on the upwellings of the eastern Pacific Ocean: cruise 17 of the R/V "Akademik Kurchatov". Polskie Archiwum Hydrobiologii 24 (Suppl.), 7–19.

Vinagradov, M.E., Shushkina, E.A., Kukina, I.N., 1977. Structural and functional analysis of pelagic communities in equatorial upwelling. Polskie Archiwum Hydrobiologia 24, 503–526.

Vinogradov, M.E., Shushkina, E.A., 1978. Some development patterns of plankton communities in the upwelling areas of the Pacific Ocean. Marine Biology 48 (4), 357–366.

Vinogradov, M.E., Shushkina, E.A., Lebedeva, L.P., 1980. Functional characteristics of communities in the northern Peru coastal areas. Peruvian area pelagic ecosystems. Marine Science (in Russian).

Walsh, J., 1981. A carbon budget for overfishing off Peru. Nature 290, 300–304.

Walsh, J.J., Dugdale, R.C., 1971. A simulation model of the nitrogen flow in the Peruvian upwelling system. Investigacion Pesquera 35 (1), 309–330.

Walsh, J.J., Whitledge, T.E., Esaias, W.E., Smith, R.L., Huntsman, S.A., Santander, H., de Mendiola, B.R., 1980. The spawning habitat of the Peruvian anchovy, *Engraulis ringens*. Deep Sea Research 27, 1–27.

Wehrtmann, I.S., Báez, P., 1997. Larvas y estadios tempranos de desarrollo de crustáceos decápodos de Chile: descripciones publicadas. Investigaciones Marinas, Valparaíso 25, 263–276.

Wolff, M., Taylor, M., Mendo, J., 2006. Simulating ecosystem transition from upwelling to El Niño conditions: the case of Independencia Bay, Southern Peru. In: Book of Extended Abstracts, International Conference The Humboldt Current System: Climate, Ocean Dynamics, Ecosystem Processes, and Fisheries, Lima, Peru, November 27–December 1, 2006, pp. 62–63 (Unpublished).

Wyrtki, K., 1963. The horizontal and vertical field of motion in the Peru Current. Bulletin of the Scripps Institution of Oceanography University of California 8 (4), 313–346.

Wyrtki, K., 1966. Oceanography of the eastern equatorial Pacific Ocean. Marine Biology Annual Review 4, 33–68.

Wyrtki, K., 1967. Circulation and water masses in the eastern equatorial Pacific Ocean. International Journal of Oceanology and Limnology 1 (2), 117–147.

Wolter, K., Timlin, M.S., 1998. Measuring the strength of ENSO events: how does 1997/1998 rank? Weather 53, 315–324.

Woods, J., Perilli, A., Barkmann, W., 2005. Stability and predictability of a virtual plankton ecosystem created with an individual-based model. Progress in Oceanography 67, 43–83.

Yamashiro, C., Rubio, J., Jurado, E., Auza, E., Maldonado, M., Ayón, P., Antonietti, E., 1990. Evaluación de la Población de Concha de Abanico en la Bahía Independencia, Pisco, Peru. Informe Instituto del Mar del Peru 98, 1–58.

Yasunaka, S., Hanawa, K., 2005. Regime shift in the global sea-surface temperatures: its relation to El Niño–Southern Oscillation events and dominant variation modes. International Journal of Climatology 25, 913–930.

Ye, Z.Q., Hsieh, W.W., 2006. The influence of climate regime shift on ENSO. Climate Dynamics 26, 823–833.

Yu, X., Dickey, T., Bellingham, J., Manov, D., Streitlien, K., 2002. The application of autonomous underwater vehicles for interdisciplinary measurements in Massachusetts and Cape Cod Bays. Continental Shelf Research 22, 2225–2245.

Zuta, S., Guillén, O., 1970. Oceanografía de las aguas costeras del Perú. Boletín del Instituto del Mar del Perú 5, 157–324.

Progress in Oceanography 79 (2008) 256–263

Contents lists available at ScienceDirect

Progress in Oceanography

journal homepage: www.elsevier.com/locate/pocean

Ecological niches and areas of overlap of the squat lobster ‘munida’ (*Pleuroncodes monodon*) and anchoveta (*Engraulis ringens*) off Peru

Mariano Gutiérrez [a,*], Argiro Ramirez [b], Sophie Bertrand [c,d], Octavio Móron [a], Arnaud Bertrand [a,d,*]

[a] *Instituto del Mar del Perú (IMARPE), Gamarra y General Valle s/n Chucuito, Callao, Peru*
[b] *Instituto Colombiano de Desarrollo Rural – INCODER, Colombia*
[c] *University of Washington, School of Fisheries, Box 355640, Seattle, WA 98195, USA*
[d] *Institut de recherche pour le développement (IRD), CRH, Avenue Jean Monnet, BP 171, 34203 Sète Cedex, France*

ARTICLE INFO

Article history:
Accepted 14 October 2008
Available online 21 October 2008

Keywords:
Munida *Pleuroncodes monodon*
Anchoveta *Engraulis ringens*
Ecological niche
Spatial distribution
Peru Humboldt Current System
Upwelling

ABSTRACT

The world’s largest mono-specific fishery, the Peruvian anchovy or anchoveta (*Engraulis ringens*) fishery, has been the subject of many studies since the 1960s. Details of its relationship with other species have mainly focused on alternations with sardine, *Sardinops sagax*, and little effort has so far been paid to interactions with other species sharing the same ecosystem. This is the case for *Pleuroncodes monodon*, the crustacean squat lobster or ’munida’, which has become highly abundant along the Peruvian coast since the mid-1990s. Munida is now an important prey for seabirds, mammals and coastal predatory fish. Knowledge of patterns of distribution and ecological niche of munida is scarce however off Peru. Here we describe and compare spatial patterns of distribution of anchoveta and munida and their ecological niches based on data from 26 acoustic surveys performed along the Peruvian coast between 1998 and 2006. The results indicate that munida and anchoveta share ecological niches but that munida is restricted to the coldest part of the productive cold coastal waters whereas anchoveta do not present any temperature preference over a large range (14–23 °C). The recent increase in munida abundance off Peru is concomitant with colder conditions; with their onset munida extended its range from central Chile northwards. Off Peru the very shallow oxycline keeps munida from its usual bottom habitat and has forced it to adopt pelagic behaviour.

1. Introduction

The world’s largest mono-specific fishery, the Peruvian anchovy or anchoveta (*Engraulis ringens*) fishery, has been the subject of many ecological studies since the 1960s (e.g., Ryther, 1969; Valdivia, 1978; Csirke, 1980; Walsh, 1981; Pauly and Tsukayama, 1987; Pauly et al., 1989; Alheit and Ñiquen, 2004; Bertrand et al., 2004a, 2005; Gutiérrez et al., 2007; Bertrand et al., 2008a,b; Espinoza and Bertrand, 2008; Swartzman et al., 2008). The strategies of fishers relative to the anchoveta’s spatial distribution have also been documented (Boerema et al., 1965; Bertrand et al., 2004b, 2005, 2007). Studies detailing the relationship of anchoveta to other species focused on its alternation with sardine, *Sardinops sagax*, (e.g., Schwartzlose et al., 1999; Chavez et al., 2003; Massé and Gerlotto, 2003; Alheit and Ñiquen, 2004; Bertrand et al., 2004a; Gutiérrez et al., 2007; Swartzman et al., 2008) with some attention paid to its relationships with plankton (Alheit and Ñiquen, 2004; Ayón et al., 2008; Espinoza and Bertrand, 2008) and birds and mammals (e.g. Jahncke et al., 1997, 1998). Little effort has been yet allocated to study the relationships and interactions of anchoveta with other species. Here we consider the case of the crustacean squat lobster or ’munida’, *Pleuroncodes monodon*, which inhabits the Humboldt Current System (HCS) from Chiloe Island (43°S) in Chile to 7°S off Peru (Haig, 1955). Large numbers of munida have occasionally been reported off southern Peru during the last 70 years. Earliest reports indicate that munida was an important prey item of the diet of apex predators such as tunas during the 1930s and 1940s (Del Solar, 1942 in Schweigger, 1964). Munida has become abundant along the Peruvian coast since the mid-1990s, and particularly after the El Niño in 1997–1998 with acoustic estimates ranging between 0.6 and 3.4 million tons from 1998 to 2005. Even before this surge in abundance Elliott and Paredes (1996) observed munida in stomachs of hake (*Merluccius gayi peruanus*), sharks, mackerel (*Scomber japonicus*), jack mackerel (*Trachurus murphyi*), cachema (*Cynoscion analis*), catfish (*Galeichtys peruvianus*) and anchoveta. Munida also constituted 75% of the diet of sea-lions and was important for sea birds in the zone of the Paracas Peninsula, 14°S (Arias-Schereiber, 1996; Jahncke et al., 1997). Like anchoveta, munida is therefore an

---

[*] Corresponding authors. Present address: TASA, Av. Néstor Gambeta, Km 14.1, Ventanilla, Callao, Peru. Tel.: +51 (1) 4202000.

E-mail addresses: mgutierrez@tasa.com.pe (M. Gutiérrez), Arnaud.Bertrand@ird.fr (A. Bertrand).

0079-6611/$ - see front matter © 2008 Elsevier Ltd. All rights reserved.
doi:10.1016/j.pocean.2008.10.019

important prey for apex predators. Munida is also a predator of plankton (Gallardo et al., 1980; Longhurst et al., 1967). Despite its potential key ecological role as suggested by Schweigger (1964) more than 40 years ago, knowledge of munida's biology and ecology is still poor off Peru. Most references come from Chile where munida has a different behaviour. Indeed, munida's early life stages are pelagic off both Peru and Chile but both juveniles and adults are bentho-demersal off Chile (e.g. Gallardo et al., 1992). Off Peru, the life cycle is all pelagic. *Pleuroncodes planipes*, a closely related squat lobster, is similarly holopelagic in the California Current (Longhurst et al., 1967; Longhurst, 1968; Robinson et al., 2004).

Here we describe and compare spatial patterns of distribution of anchoveta and munida based on 26 acoustic surveys performed along the Peruvian coast between 1998 and 2006. In addition we describe their respective ecological niches with distance to the coast, sea surface temperature, salinity, dissolved oxygen, nutrients and chlorophyll.

2. Material and methods

2.1. Acoustic data

Acoustic data were collected from 26 surveys performed between 1998 and 2006 by the Peruvian Marine Research Institute (IMARPE) on several vessels, most commonly the R/V Olaya (41 m) but also the R/V SNP2 (21 m) and the RV Humboldt (76 m). At least three acoustic surveys were run each year. Survey design was composed of parallel transects averaging 100 nautical miles (182.5 km) long with an inter-transect distance of 14–16 nautical miles (26–30 km). The acoustic elementary sampling distance units (ESDU) were defined as 1 nmi. The entire observable vertical range of anchoveta and munida distributions was covered during most surveys (Fig. 1) even though the surveys performed in winter and spring were often limited to the central and northern part of Peru (5–14°S). Extensive midwater trawling accompanied the acoustic surveys in order to provide biological samples and for species identification. The acoustic surveys used Simrad (Kongsberg Simrad AS, Kongsberg, Norway) scientific echosounders EK500 (RVs Olaya and SNP-2) and EK60 (RV Humboldt) operating at 38 and 120 kHz. The water column was typically insonified till 500 and 150 m at 38 and 120 kHz, respectively. The echosounders were calibrated at least once before each survey with standard procedures (Simmonds and MacLennan, 2005). The acoustic nautical area scattering coefficient (s_A) was recorded for each geo-referenced ESDU. Echo identification was performed by using fishing trawl results and a two-frequencies algorithm on backscattered acoustic volume echograms (S_v) for the surveys performed from 2004 to 2006 using Echoview software (Sonar Data, Tasmania, Australia).

2.2. Environmental data

The measurements of sea surface temperature, salinity and dissolved oxygen (SST, SSS and SSO, respectively) were carried out along the survey transects. Temperature was measured using Furuno MD-500 sensors onboard R/V Olaya and Furuno T-2000 onboard R/V Humboldt. Surface water samples were collected every 2 h for dissolved oxygen (DO) and salinity measurements. Salinity was estimated using a Kahlsico RS 10 sensor until June 1998 then a Portasal 8410A sensor. The concentration of dissolved oxygen was measured using the method of Winkler modified by Carritt and Carpenter (1966). Temperature, salinity and DO data were interpolated by kriging using Surfer software (Golden Software, Colorado, USA). Temperature, salinity and DO values were then averaged for each ESDU. Finally, distance to the coast was determined for each ESDU.

For the survey performed in January–February 2000, data on nitrates, nitrites, silicates and phosphates and chlorophyll were intensively collected. A total of 220 surface water samples obtained from Niskin bottle were frozen onboard and analysed later in laboratory using the method from Strickland and Parsons (1968). Chlorophyll-*a* was fixed in Whatman filters and analysed using the method from Holm-Hansen et al. (1965).

2.3. Spatial analyses

To study the changes in the geographical distributions of munida and anchoveta, for each survey we estimated both the position of the population's centre of gravity (*CG*) and the related inertia. In 2D, the *CG*, which represents the mean location of the population, is a vector with two coordinates. The inertia, whose units are surface units (typically nmi^2), quantifies the spatial dispersion of the population around its *CG*. When sampling is regular, the following equations are used to calculate the centre of gravity (*CG*) and the inertia (*I*):

$$CG = \begin{bmatrix} CG_x = \dfrac{\sum_{i=1}^{n} x_i z_i}{\sum\limits_{i=1}^{n} z_i} \\ \\ CG_y = \dfrac{\sum_{i=1}^{n} y_i z_i}{\sum_{i=1}^{n} z_i} \end{bmatrix} \qquad I = \frac{\sum_{i=1}^{n}\left[(x_i - CG_x)^2 + (y_i - CG_y)^2\right] z_i}{\sum_{i=1}^{n} z_i}$$

with, (x_i, y_i) the location of sample i for $i = 1$ in n with n the total number of samples and z_i the value of the sample at this point. All calculations were performed in orthodromic distances. ESDU from inter-transects were not considered in these calculation.

2.4. Ecological niches

For each of the 131,927 geo-referenced ESDU we examined the following indices for anchoveta and munida: distance to the coast (DC); SST; SSS; SSO; and the acoustic backscattered energy (s_A), an indice of abundance. As the relationships between munida or anchoveta abundance and the environmental parameters were likely to be nonlinear and multivariate, we used a generalized additive model (GAM; Hastie and Tibshirani, 1990) implemented with S-Plus (Insightful Corporation, Seattle, WA, USA). Cubic spline smoothers were used to estimate these nonparametric functions. The response variable, the acoustic energy (s_A) of anchoveta and munida, was log-transformed in order to reduce skewness. Models were obtained for each of the 26 surveys and for the entire data set.

To further characterize the ecological niches of munida and anchoveta we included the nutrients (nitrates, nitrites, silicates and phosphates) and chlorophyll as explanatory variables in the GAM model for the survey performed in January–February 2000.

Finally we constructed a GAM model by relating log transformed s_A of anchoveta and munida to search for relationships between these species at the 1 nmi scale.

3. Results

3.1. Spatiotemporal analyses

Temporal variations of the number of ESDU containing anchoveta, munida and both organisms were similar (Figs. 1 and 2), indicating expansion and contraction of the ranges of these species were also similar. The small difference between the numbers of ESDU with munida alone and with munida and anchoveta illustrates that munida mostly occurs within anchoveta range, as it was particularly clear in spring 1999, summer 2002, winter 2003

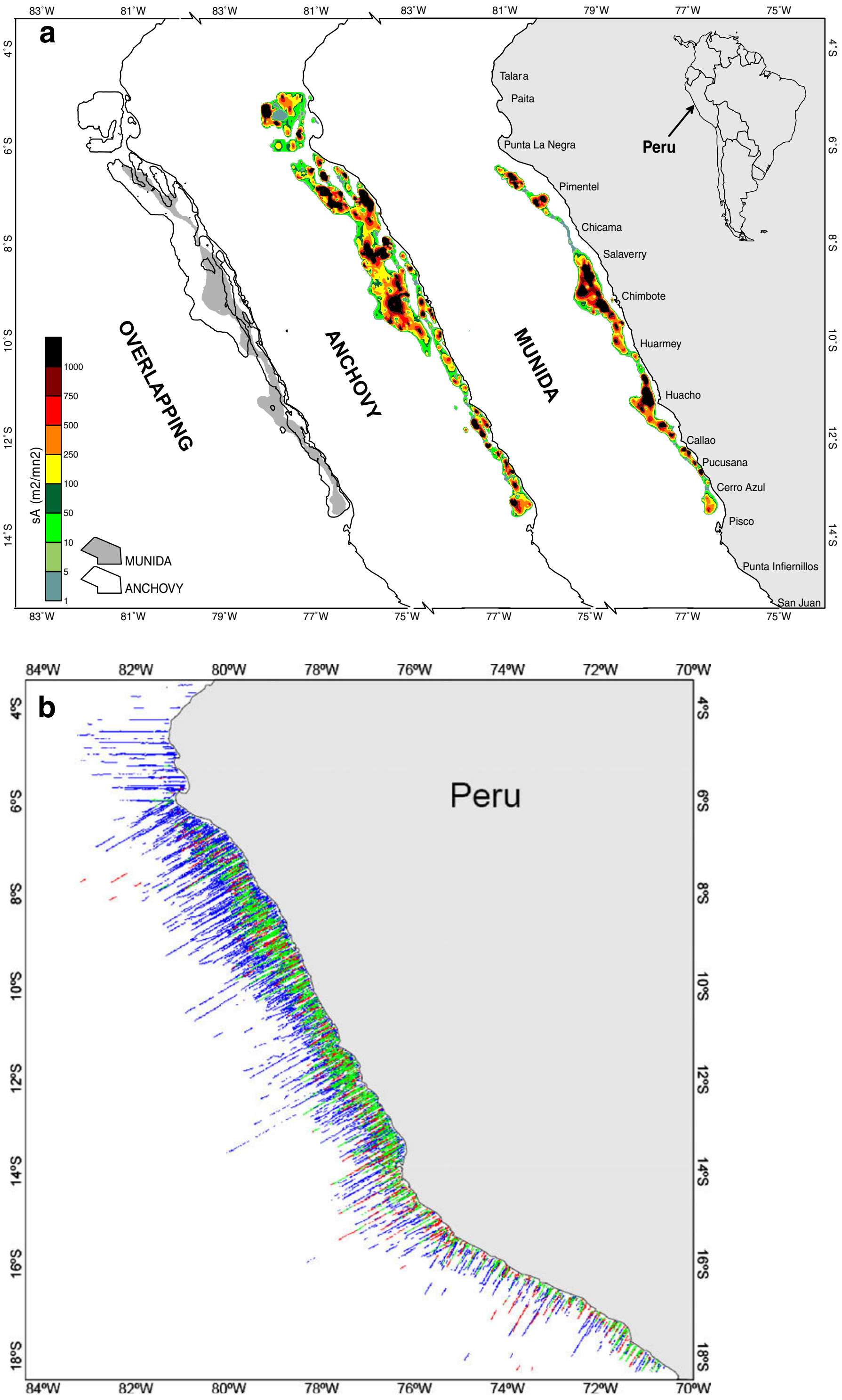

Fig. 1. (a) Study area and example of distribution and relative abundance of munida (*Pleuroncodes monodon*), anchoveta (*Engraulis ringens*) and their horizontal overlapping during Spring 2005 and (b) spatial distribution of all acoustic sampling units (ESDU) from 1998 to 2006 with anchoveta (blue), munida (red) and overlapping of both species (green).

and winter 2006 (Fig. 2). Seasonal patterns however are not clear. Greater area occupancy was observed during summer (February–March) but changes in survey design may have biased the results.

Similar dynamics were observed when considering the population centres of gravity and their inertia (Fig. 3). Changes in centre of gravity and inertia for anchoveta and munida populations were similar. Both species extended their ranges toward the north at the beginning of the time series (Fig. 3a). Then mean latitude was between 8–11°S, and 9–12°S for anchoveta and munida, respectively, with a slightly more southerly distribution in summer compared to winter. This pattern was also observed for longitude (Fig. 3b), due to the orientation of the Peruvian coast, at a given latitude a higher longitude indicates a more offshore distribution. Anchoveta were thus distributed at lower latitudes and further offshore than munida. Variations in inertia were similar for anchoveta and munida (Fig. 3c).

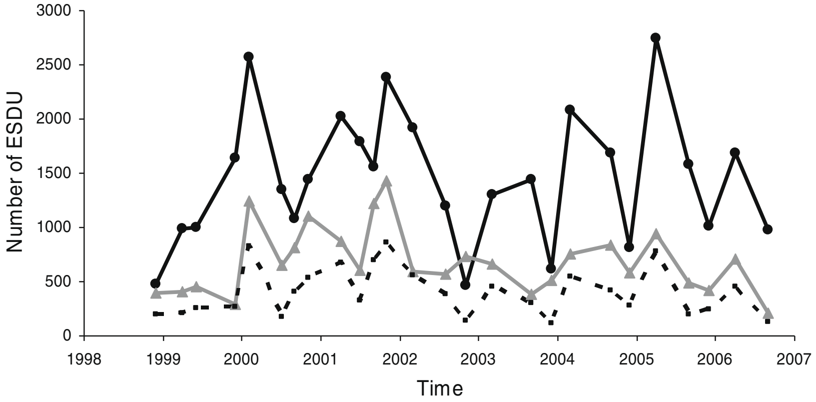

Fig. 2. Time series of the number of acoustic elementary sampling units (ESDU) with presence of anchoveta (black solid line), munida (grey solid line) and both species (black dotted line) during acoustic surveys (1998–2006).

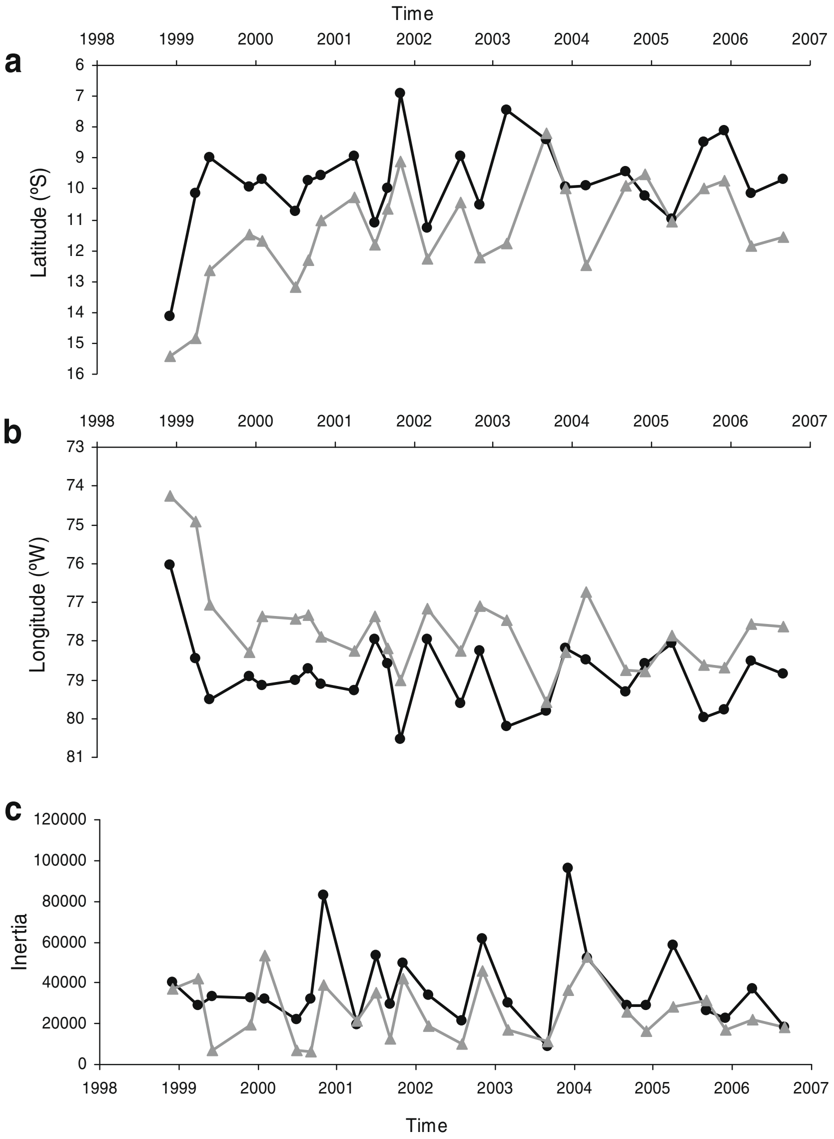

Fig. 3. Time series of the latitudinal (a) and longitudinal (b) location of the centre of gravity and associated inertia of the distribution (c) for anchoveta (black solid line) and munida (grey solid line) during 1998–2006.

3.2. Ecological niches

The abundance relationships between munida and anchoveta at the scale of the ESDU were positive and highly significant ($p < 0.0001$; Fig. 4). Non-linear relationships between munida and anchoveta local abundances and the distance to the coast (DC) and oceanographic parameters (SST, SSS and SSO) for the entire data set are presented Fig. 5. Each plot shows the smoother (spline)

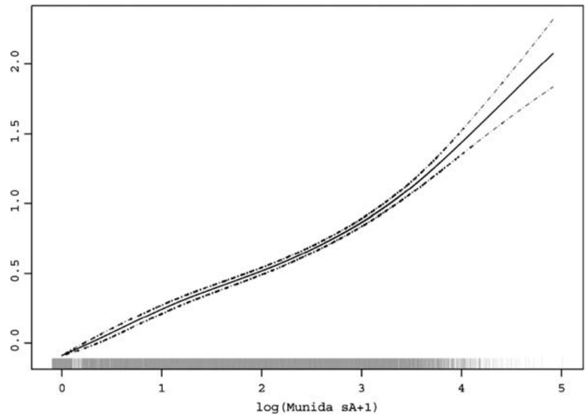

Fig. 4. GAM model based on anchoveta log transformed acoustic abundance (s_A) according to munida log transformed acoustic abundance (s_A). The black dotted lines show the 95% confidence limits of the GAM model. y-Axis is in relative scale, it corresponds to the spline smoother that was fitted on the data, so that a y-value of zero is the mean effect of the variables on the response. Grey tick marks on the x-axis show the location of data points.

that was fitted to the abundance data for munida (left y-axis) and anchoveta (right y-axis). The y-axes are in relative scale, so that a y-value of zero is the mean effect of the explanatory variable on the munida or anchoveta abundance response. Positive and negative y-values indicate positive and negative responses, respectively. The range of the y-axis indicates the relative importance of each predictor. The 95% confidence limits on the estimated relationship are indicated by dotted lines. These lines tend to diverge near the extremes of the range for continuous predictors as a consequence of fewer observations (Agenbag et al., 2003). Tick marks on the x-axis show the location of data points. The main trends of GAM results performed separately for each survey were not significantly different from the models constructed with the entire data set and are not presented.

Results (Fig. 5) illustrate similar patterns in the relations of munida and anchoveta with the distance to the coast (DC), sea surface salinity (SSS) and sea surface oxygen (SSO) but a very different pattern for sea surface temperature. Both species were distributed close to the coast, but munida even closer than anchoveta, in the first 40 km (Figs. 3b and Fig. 5a). Relationships with sea surface oxygen presented a first maximum for low values of dissolved oxygen (<4 mL L^{-1}), a minimum for oxygen concentration between 4 and 6 mL L^{-1} to then increase for high SSO concentrations (Fig. 5b). This bi-modal pattern is an illustration of the non-conservative character of oxygen concentration; oxygen can be either high or low in upwelling areas depending on the relative dominance of photosynthesis and respiration-degradation. Relationships with salinity (Fig. 5c) were very strong and clear for both species with dome-shaped relationships peaking between 34.7 and 35.1 which upwelled cold coastal waters (CCW): 34.80–35.05 (see Morón, 2000; Bertrand et al., 2004a; Swartzman et al., 2008). The curve for munida is contained inside the one for anchoveta illustrating an even more exclusive relationship for munida with the CCW. Finally the relationships with SST (Fig. 5d) showed that anchoveta is broadly distributed over a large range of temperature (14–23 °C) while munida is restricted to colder water (<18 °C).

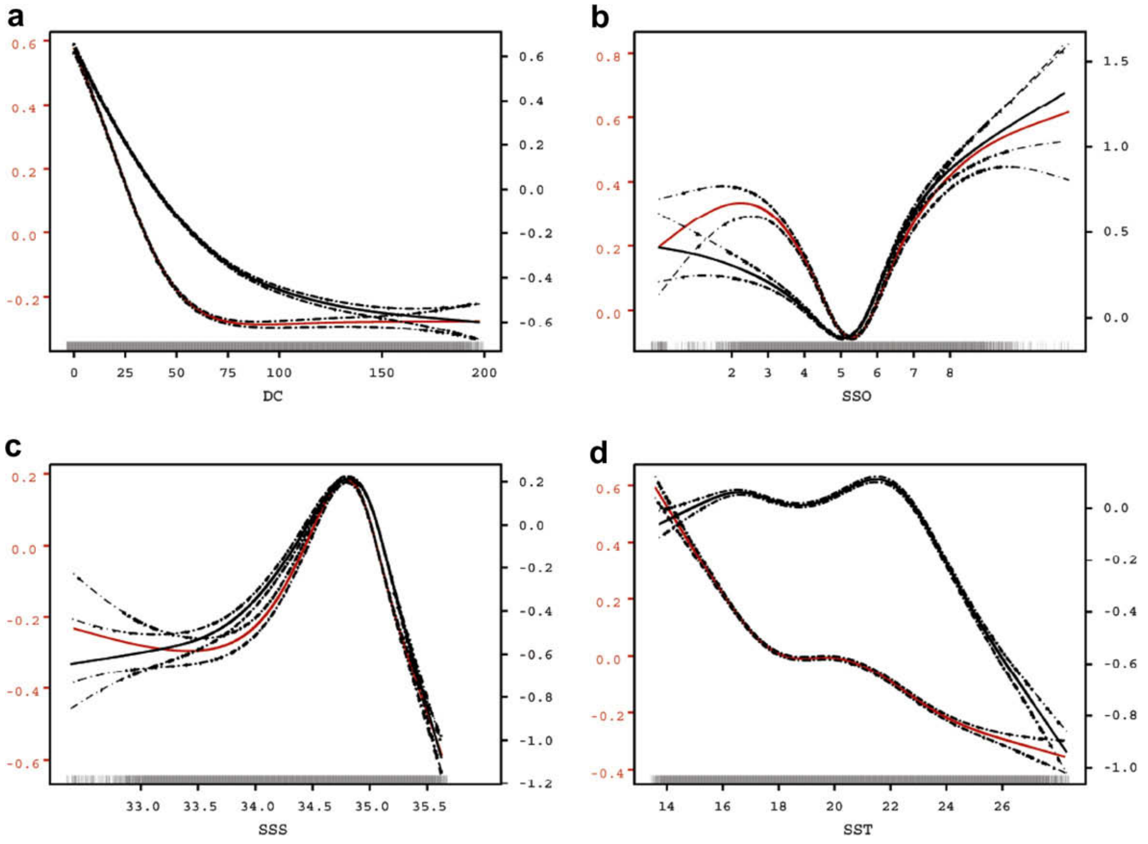

Fig. 5. GAM models based on anchoveta (black lines and right y-axes) and munida (red lines and left y-axes) log transformed acoustic abundance (s_A) according to (a) the distance from the coast (DC), (b) sea surface oxygen (SSO in mL.L^{-1}), (c) sea surface salinity (SSS) and sea surface temperature (SST in °C) for the complete set of 131,927 ESDU. The black dotted lines show the 95% confidence limits of GAM models. y-Axes are in relative scale, they correspond to the spline smoother that was fitted on the data, so that a y-value of zero is the mean effect of the variables on the response. Grey tick marks on the x-axis show the location of data points.

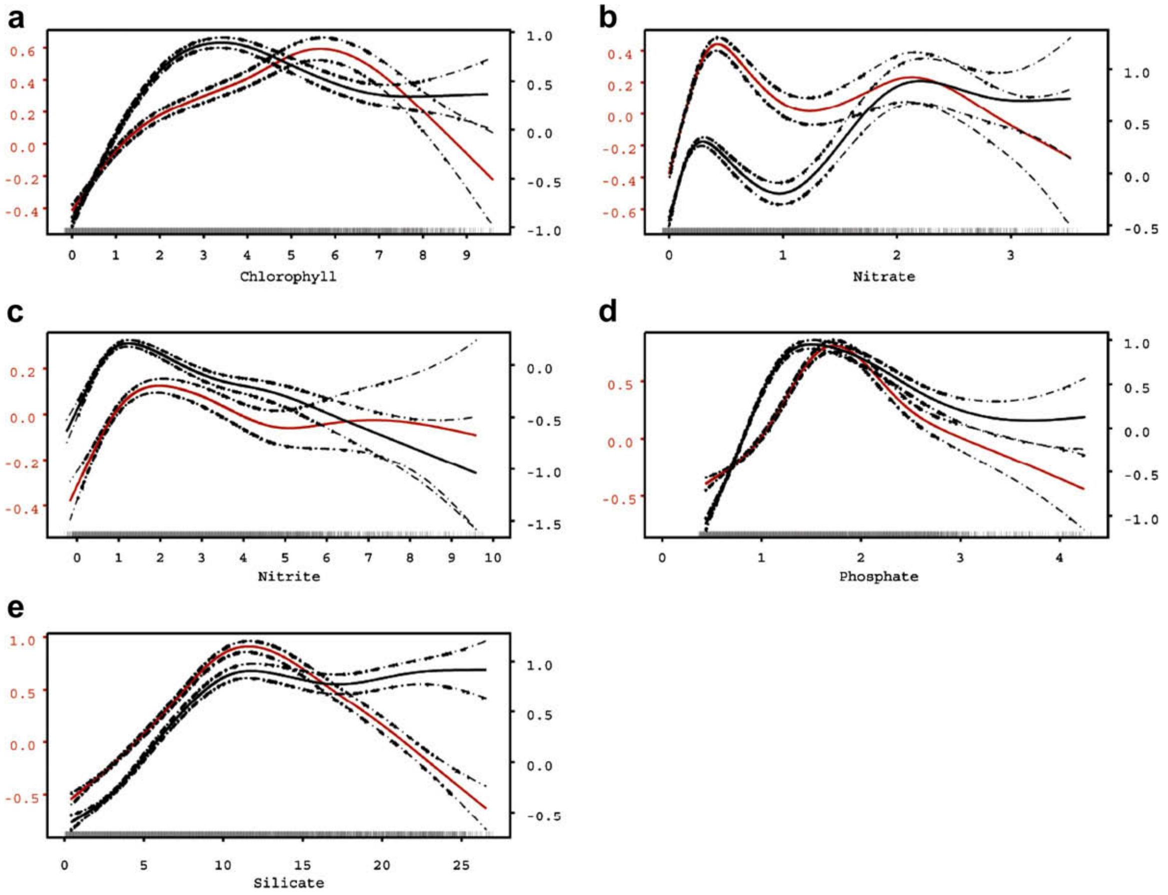

Fig. 6. GAM models based on anchoveta (black lines and right *y*-axes) and munida (red lines and left *y*-axes) log transformed acoustic abundance (s_A) according to (a) chlorophyll (in μg L^{-1}), (b) nitrate (in μg-at L^{-1}), (c) nitrite (in μg-at L^{-1}), (d) phosphate (in μg-at L^{-1}), and (e) silicate (in μg-at L^{-1}) for the survey performed in February–March 2000. The black dotted lines show the 95% confidence limits of GAM models. *y*-Axes are in relative scale, they correspond to the spline smoother that was fitted on the data, so that a *y*-value of zero is the mean effect of the variables on the response. Grey tick marks on the *x*-axis show the location of data points.

Results of GAM models for nutrients and chlorophyll are presented in Fig. 6. Both munida and anchoveta were (i) most abundant in areas with rather low nitrite concentration (0.5–3 μg-at L^{-1}), (ii) bi-modally distributed relative to nitrate concentration (0.2–0.8 and 1.8–2.8 μg-at L^{-1}), and (iii) unimodally distributed relative to phosphate with higher munida and anchoveta biomass for medium phosphate concentration (0.8–2.3 μg-at L^{-1}). The relationship with silicate was dome-shaped for munida (max: 5–20 μg-at L^{-1}) but there was no decline in preference for anchoveta from about 10 μg-at L^{-1}. With chlorophyll, munida was more abundant in areas with higher phytoplankton biomass (4–8 μg L^{-1}) than anchoveta (1–5 μg L^{-1}).

4. Discussion

4.1. Ecological niches

Munida and anchoveta share similar ecological niches and patterns of spatial distribution. Spatial overlapping was strong (Fig. 2). Munida range was smaller but contained within that of anchoveta (Figs. 1 and 2). The centre of gravity of both species shifted toward the north at the beginning of the study period and has remained rather stable since 2000. Relationships with environmental parameters show that both species inhabit cold coastal waters (CCW). Such an association has been described for anchoveta (e.g. Bertrand et al., 2004a; Swartzman et al., 2008) and for pelagic *P. plannipes* in the California Current (Robinson et al., 2004), but not for munida. However, while munida and anchoveta share similar habitats, there are clear differences. Anchoveta do not prefer specific temperatures over a large range (14–23 °C), in accordance with Bertrand et al., 2004a who showed that absolute temperature was not a key parameter determining anchoveta distribution. Munida on the other hand are distributed in the coldest waters available, and in the more coastal part of the anchoveta distribution. Munida therefore mainly occurs in newly upwelled waters. Such waters are highly productive and munida it probably forages on diatoms and zooplankton. Indeed, in the California Current, pelagic *P. planipes* is capable of filter-feeds on diatoms blooms and forage on zooplankton (Longhurst et al., 1967).

The pelagic habitat of munida off Peru differs considerably from its habitat in the central part of Chile where eggs and larvae are pelagic but adults are benthic (Roa et al., 1995, 1997; Bahamonde et al., 1979; Roa and Bahamonde 1993; Roa and Tapia, 1998). Ecological differences are accompanied by biological differences with, for instance, smaller munida in north Chile and Peru than in the central Chile (Guzmán et al., 2002). Another difference relates to the size of the population. Munida is much more abundant off Peru than off Chile. Off Peru biomass estimated acoustically by IMARPE reached several millions of tons over 8 years (maximum: 3.4 millions of tons in winter 2000), compared to the virgin biomass estimated to about 210000 tons off Chile where munida is commonly exploited (Roa et al., 1997). These abundance differences are so large that the presence of a single species vs. two species was debated. Recent genetic analyses confirm that a single species, *Pleuroncodes monodon*, occurs off both Chile and Peru (Pilar Haye and

Elie Poulin, University of Chile, unpublished data). If it is the same species, why are its behaviour and productivity so different? We propose a hypothesis based on dissolved oxygen concentration. Bathymetric distribution of munida ranges between 30 and 400 m off Chile (Haig, 1955; Bustos and Retamal, 1985) but varies according to the latitude. Off northern Chile, adult munida was observed in shallower waters, between 20 and 40 m (Gutiérrez and Zúñiga, 1977), sometimes with a pelagic behaviour (Jorge Castillo, Instituto de Fomento Pesquero, Chile, personal communication). Off Peru, the vertical distribution is restricted to the first 30–40 m and munida is always pelagic. It seems that there is a gradient in the vertical distribution and behaviour of the munida, from bathy-benthonic in central Chile to epi-pelagic in Peru. We propose that this pattern is related to the trend in oxycline depth. Munida is characteristic of areas with moderately low dissolved oxygen concentration (Wolf Arntz, personal communication). Helly and Levin (2004) showed that the depth of the 0.5 mL L^{-1} upper layer diminishes from about 500 m off central Chile (30–40°S), 100 m off northern Chile (20°S) and <100 m off Peru. In Central Chile oxygen concentration is high enough at bottom depth for munida. Further north, the oxygen minimum zone (OMZ) is shallower and the near-absence of oxygen near the bottom prohibits munida's presence. In Peru where the oxycline is very shallow, and the OMZ starts well above the bottom, munida cannot develop any benthonic phase and its life cycle is holopelagic illustrating munida's plasticity (see Espinoza and Bertrand, 2008, for details on anchoveta's plasticity).

4.2. Habitat overlap and interactions

The similarity in their ecological niches and the strong spatial overlap between anchoveta and munida may have potential consequences. On one hand, because both species are prey for apex predators (fish, sea birds and mammals), each species might lessen predation pressure on the other. Conversely, anchoveta and munida forage on plankton and may compete for food. Anchoveta feed primarily on large zooplankton and to a lesser extent on large phytoplankton, particularly diatoms (Espinoza and Bertrand, 2008). The diet of munida has not been studied off Peru. In Chile munida forage on amphipods, zoeas, crustacean eggs, diatoms, foraminifers, bacteria, organic wastes and fish scales (Gallardo et al., 1980). In the California Current, pelagic *P. planipes* feeds on protists, zooplankton (mainly copepods, euphausiids and chaetognaths) and large diatoms; the diatom fraction being higher when diatoms are abundant (Longhurst et al., 1967). It is therefore likely that, off Peru, pelagic munida forage on both phytoplankton and zooplankton and compete for food with anchoveta. In addition competition for food, anchoveta can eat munida eggs, larvae and juveniles, and munida may also forage on anchoveta eggs or larvae. There are therefore potential negative competition and predation between these species. If these interactions occur, they do not seem to have had any strong effect at population scale. Indeed both munida and anchoveta have shown an increase in their population since the beginning-mid 1990s (see Gutiérrez et al., 2007 for anchoveta). This period is characterised by (i) colder conditions related to stronger upwelling (Francisco Chavez, MBARI, personal communication), (ii) dominance of cold coastal waters along the Peruvian coast (Swartzman et al., 2008), (iii) an increase in primary production (Francisco Chavez, MBARI, personal communication) and (iv) an increase in zooplankton production (Ayón et al., 2008). The recent increase in the munida and anchoveta populations associated with cold and productive conditions apparently reflects a bottom-up control (Ayón et al., 2008) and has also been accompanied by a spatial extension of populations to the north.

Any effect of competition for prey could have been dampened by the increased productivity during the last few years. If this productivity declines, competitive interactions between anchoveta and munida may reduce one or both of these populations. Also, their foraging likely impacts other species as well. There is therefore an urgent need for more studies on the huge population of munida off Peru.

4.3. Munida, the species who came in from the cold

In summary, munida and anchoveta share similar ecological niches and overlap spatially but munida is more restricted to the coldest part of the productive cold coastal waters. The recent increase in munida abundance off Peru was concomitant with a change to colder conditions in the HCS (Francisco Chavez, MBARI, personal communication) characterised by rich upwelling waters, the CCW (Swartzman et al., 2008). Munida took advantage of these cold conditions to extend its range north from central Chile to the Peruvian coast (where it probably also occurred in the 1940s; Del Solar, 1942 in Schweigger, 1964). Off Peru the very shallow oxycline keeps munida above its bottom habitat and forced it to become holopelagic off Peru. When the present decadal cold ('La Vieja', see Chavez et al., 2003) conditions end, we may expect that munida population will decrease or even disappear from the Peruvian coast, with its range again contracting southwards into Chilean waters.

Acknowledgements

We wish to sincerely thank to Ing. Georgina Flores from IMARPE for her valuable cooperation in building up the necessary databases for this work. Gordon Swartzman and François Gerlotto are thanked for their comments. Special acknowledgement goes to John Simmonds and Tim Pennington for improving the contents and the English of this work. This work is a contribution of the Study Group 'Cardumen' of IMARPE, the IRD Research Units 'Upwelling Ecosystems' UR 097 and of the Interdepartmental Thematic Action 'Humboldt Current System' from IRD. Many thanks to Larry Hutchings and the anonymous referee for their very valuable comments on the first version of this paper.

References

Agenbag, J.J., Richardson, A.J., Demarcq, H., Fréon, P., Weeks, S., Shillington, F.A., 2003. Estimating environmental preferences of South African pelagic fish species using catch size- and remote sensing data. Progress in Oceanography 59, 275–300.

Alheit, J., Niquen, M., 2004. Regime shifts in the Humboldt Current ecosystem. Progress in Oceanography 60, 201–222.

Arias-Schereiber, M., 1996. Informe sobre el estado de conocimientos y conservación de los mamíferos marinos en el Perú. Informe Provisional del Instituto del Mar del Perú No. 38, 30 pp.

Ayón, P., Swartzman, G., Bertrand, A., Gutierrez, M., Bertrand, S., 2008. Zooplankton and forage fish species off Peru: large-scale bottom-up forcing and local-scale depletion. Progress in Oceanography 79, 208–214.

Bahamonde, R., Henriquez, G., Pavez, P., Ramírez, B., Silva, N., 1979. Evaluación de los recursos de camarón y langostino entre Coquimbo e Isla Mocha. Informe Presentado a la Corporación de Fomento de la producción AP 79-46, 194 pp. (in Spanish).

Bertrand, A., Segura, M., Gutiérrez, M., Vasquez, L., 2004a. From small-scale habitat loopholes to decadal cycles: a habitat-based hypothesis explaining fluctuation in pelagic fish populations off Peru. Fish and Fisheries 5, 296–316.

Bertrand, S., Díaz, E., Ñiquen, M., 2004b. Interactions between fish and fisher's spatial distribution and behaviour: an empirical study of the anchovy (*Engraulis ringens*) fishery of Peru. ICES Journal of Marine Science 61, 1127–1136.

Bertrand, S., Burgos, J., Gerlotto, F., Atiquipa, J., 2005. Lévy trajectories of Peruvian purse-seiners as an indicator of the spatial distribution of anchovy (*Engraulis ringens*). ICES Journal of Marine Science 62, 477–482.

Bertrand, S., Bertrand, A., Guevara-Carrasco, R., Gerlotto, F., 2007. Scale invariant movements of fishermen: the same foraging strategy as natural predators. Ecological Applications 17, 331–337.

Bertrand, A., Gerlotto, F., Bertrand, S., Gutiérrez, M., Alza, L., Chipollini, A., Diaz, E., Espinoza, P., Ledesma, L., Quesquén, R., Peraltilla, S., Chavez, 2008a. Schooling behaviour and environmental forcing in relation to anchoveta distribution: an analysis across multiple spatial scales. Progress in Oceanography 79, 264–277.

Bertrand, S., Dewitte, B., Tam, E., Díaz, E., Bertrand, A., 2008b. Impacts of Kelvin wave forcing in the Peru Humboldt Current system: scenarios of spatial reorganizations from physics to fishers. Progress in Oceanography 79, 278–289.

Boerema, L.K., Saetersdal, G., Tsukayama, I., Valdivia, J. Alegre, B., 1965. Report on the effects of fishing on the Peruvian stock of anchovy. FAO Fisheries Technical Papers 55, 44 pp.

Bustos, H., Retamal, A.M., 1985. Estudio biológico pesquero del langostino colorado *Pleuroncodes monodon* H. Milne Edwards, 1837. Revista Gayana zoología 49, 151–164 (in Spanish, with English abstract).

Carritt, D.E., Carpenter, J.H., 1966. Comparison and evaluation of currently employed modifications of the Winkler method for determining dissolved oxygen in seawater; a NASCD report. Journal of Marine Research 24, 286–318.

Chavez, F.P., Ryan, J., Lluch-Cota, E., Niquen, M., 2003. From anchovies to sardines and back: multidecadal change in the Pacific Ocean. Science 299, 217–221.

Csirke, J., 1980. Recruitment in the Peruvian anchovy and its dependence on the adult population. Rapports et Procès-verbaux des Réunions du Conseil international pour l'Exploration de la Mer 177, 307–313.

Elliott, W., Paredes, F., 1996. Estructura especiológica del subsistema costero, Prospección 9512-9601. Informe del Instituto del Mar del Perú 121, 14–26.

Espinoza, P., Bertrand, A., 2008. Revisiting Peruvian anchovy (*Engraulis ringens*) trophodynamics provides a new vision of the Humboldt Current system. Progress in Oceanography 79, 215–227.

Gallardo, V.A., Bustos, E., Acuña, A., Díaz, L., Erbs, V., Meléndez, R., Oviedo, L., 1980. Relaciones ecológicas de las comunidades bentónicas y bentodemersales de la plataforma continental de Chile central. Informe División de Asistencia Técnica, Dirección de Investigaciones. Universidad de Concepción a Subsecretaria de pesca, 325 p. (in Spanish).

Gallardo, V.A., Henríquez, S., Roa, R., Acuña, A., Cañete, I., Baltazar, M., 1992. Biología del langostino colorado *Pleuroncodes monodon* H Milne Edwards 1837 y especies afines (Crustacea, Decapoda, Anomura, Galatheidae) Sinopsis. In: Faranda, F., Parra, O. (Eds.), Elementos básicos para la gestión de los recursos marinos costeros de la región del Biobio, Serie Monografía Científica, vol. 2. Centro EULA, Chile, pp. 71–113 (in Spanish).

Gutiérrez, M., Swartzman, G., Bertrand, A., Bertrand, S., 2007. Anchovy and sardine spatial dynamics and aggregation patterns in the Humboldt Current ecosystem, Peru, from 1983 to 2003. Fisheries Oceanography 16, 155–168.

Gutiérrez, M.J., Zúñiga, R.O., 1977. *Pleuroncodes monodon* H. Milne Edwards 1837 en la bahía de Mejillones del sur Chile (Crustacea, Decapoda, Anomura). Revista de Biología Marina 16, 161–169.

Guzmán, G., Báez, P., Moreno, R., Rudolph, J.P., 2002. Determinación taxonómica del langostino colorado del norte primera y segunda regiones. Mimeo Universidad Arturo Prat, Iquique, 46 pp. (in Spanish).

Haig J., 1955. The crustacea anomura of Chile. In: Chile Expedition 1948–49, Reports of the Lund University, 68 pp.

Hastie, T., Tibshirani, R., 1990. Generalized Additive Models. Chapman and Hall, London.

Helly, J.J., Levin, L.A., 2004. Global distribution of naturally occurring marine hypoxia on continental margins. Deep Sea Research I 51, 1159–1168.

Holm-Hansen, A., Lorenzen, O., Colmes, R., Strickland, J., 1965. Fluorometric determination of chlorophyll. Journal du Conseil Permanent International pour l'Exploration de la Mer 30, 3–15.

Jahncke, J., Ayala, L., Mendoza, C., 1998. Abundancia relativa y distribución de aves marinas frente a la costa peruana y su relación con la abundancia de anchoveta Crucero BIC Humboldt 9808-09 de Piura a Lima. Informe del Instituto del Mar del Perú No. 141, pp. 85-95 (in Spanish, with English abstract).

Jahncke, J., García-Godos, A., Goya, E., 1997. Dieta del guanay *Leucocarbo boougainvilii* del piquero peruano *Sula variegata* y otras aves de la costa peruana en abril y mayo de 1997. Informe del Instituto del Mar del Perú 126, 75–88 (in Spanish, with English abstract).

Longhurst, A.R., 1968. Distribution of the Larvae of *Pleuroncodes planipes* in the California Current. Limnology and Oceanography 13, 143–155.

Longhurst, A.R., Lorenzen, C.J., Thomas, W.H., 1967. The role of pelagic crabs in the grazing of phytoplankton off Baja California. Ecology 48, 190–200.

Massé, J., Gerlotto, F., 2003. Introducing nature in fisheries research: the use of underwater acoustics for an ecosystem approach of fish population. Aquatic Living Resources 16, 107–112.

Morón, O., 2000. Características del ambiente marino frente a la costa peruana. Boletín del Instituto del Mar del Perú 19, 179–204 (in Spanish, with English abstract).

Pauly, D., Muck, P., Mendo, J., Tsukayama, I., 1989. The Peruvian upwelling ecosystem: dynamics and interactions. In: ICLARM Conference Proceedings, vol. 18, 438 pp.

Pauly, D., Tsukayama, I., 1987. The Peruvian anchoveta and its upwelling ecosystem: three decades of change. ICLARM Studies and Reviews 15. 351 pp..

Roa, R., Bahamonde, R., 1993. Growth and expansion of an exploited population of the squat lobster (*Pleuroncodes monodon*) after 3 years without harvesting. Fisheries Research 18, 305–319.

Roa, R., Tapia, F., Cid, L., Quiñónez, R., Ernst, B., Figueroa, D., Arancibia, H., Galleguillos, R., Retamal, M., 1997. Evaluación directa del stock de langostino colorado en la zona centro sur Informe final proyecto FIP No. 96-23. Universidad de Concepción, Chile. 131 p. (in Spanish).

Roa, R., Gallardo, V.A., Ernst, B., Baltazar, M., Cañete, I., Sandro, E., 1995. Nursery ground, age structure and abundance of juvenile squat lobster *Pleuroncodes monodon* on the continental shelf off central Chile. Marine Ecology Progress Series 116, 47–54.

Roa, R., Tapia, F., 1998. Spatial differences in growth and sexual maturity between branches of a large population of the squat lobster *Pleuroncodes monodon*. Marine Ecology Progress Series 167, 185–196.

Robinson, C.J., Anislado, V., Lopez, A., 2004. The pelagic red crab (*Pleuroncodes planipes*) related to active upwelling sites in the California Current off the west coast of Baja California. Deep Sea Research II 51, 753–766.

Ryther, J.H., 1969. Photosynthesis and fish production in the sea. Science 166, 72–76.

Schwartzlose, R.A., Alheit, J., Bakun, A., Baumgartner, T.R., Cloete, R., Crawford, R.J.M., Fletcher, W.J., Green-Ruiz, Y., Hagen, E., Kawasaki, T., Lluch-Belda, D., Lluch-Cota, S.E., MacCall, A.D., Matsuura, Y., Nevarez-Martinez, M.O., Parrish, R.H., Roy, C., Serra, R., Shust, K.V., Ward, M.N., Zuzunaga, J.Z., 1999. Worldwide large-scale fluctuations of sardine and anchovy populations. South African Journal of Marine Science 21, 289–347.

Schweigger, E., 1964. El litoral peruano, 2da. ed. Editorial de la Universidad Nacional Federico Villarreal. 440 pp. (in Spanish).

Simmonds, J.E., MacLennan, D.N., 2005. Fisheries Acoustics, second ed. Chapman and Hall, London.

Strickland, C.J., Parsons, T., 1968. Manual of the sea water Analysis. Bulletin of the Fisheries Research Board of Canada 125. 310 pp.

Swartzman, G., Bertrand, A., Gutiérrez, M., Bertrand, S., Vasquez, L., 2008. The relationship of anchovy and sardine to water masses in the Peruvian Humboldt Current System from 1983-2005. Progress in Oceanography 79, 228–237.

Valdivia, J.E., 1978. The Anchoveta and El Niño. Rapports et Procès-verbaux des Réunions du Conseil international pour l'Exploration de la Mer 173, 196–202.

Walsh, J.J., 1981. A carbon budget for overfishing off Peru. Nature 290, 300–304.

Progress in Oceanography 79 (2008) 264–277

Contents lists available at ScienceDirect

Progress in Oceanography

journal homepage: www.elsevier.com/locate/pocean

Schooling behaviour and environmental forcing in relation to anchoveta distribution: An analysis across multiple spatial scales

Arnaud Bertrand [a,b,*], François Gerlotto [a,b], Sophie Bertrand [a,b,c], Mariano Gutiérrez [b,1], Luis Alza [b], Andres Chipollini [b], Erich Díaz [b], Pepe Espinoza [b], Jesús Ledesma [b], Roberto Quesquén [b], Salvador Peraltilla [b], Francisco Chavez [d]

[a] IRD, CRH, Avenue Jean Monnet, BP 171, 34203 Sète Cedex, France
[b] Instituto del Mar del Perú, Esquina Gamarra y Gral. Valle s/n, Apartado 22, Callao, Lima, Peru
[c] University of Washington, School of Fisheries, Box 355640, Seattle, WA 98195, USA
[d] Monterey Bay Aquarium Research Institute, 7700 Sandholdt Rd., Moss Landing, CA 95039, USA

ARTICLE INFO

Article history:
Accepted 14 October 2008
Available online 21 October 2008

Keywords:
Fish schooling behaviour
Habitat suitability
Peruvian anchovy *Engraulis ringens*
Spatiotemporal distribution
Predator–prey relationships
Peru Humboldt Current system
Dissolved oxygen and partial pressure of CO_2
Basin model framework

ABSTRACT

The Peruvian anchovy or anchoveta (*Engraulis ringens*) supports the highest worldwide fishery landings and varies in space and time over many scales. Here we present the first comprehensive sub-mesocale study of anchoveta distribution in relation to the environment. During November 2004, we conducted a behavioural ecology survey off central Peru and used a series of observational and sampling tools including SST and CO_2 sensors, Niskin bottles, CTD probes, zooplankton sampling, stomach content analysis, echo-sounder, multibeam sonar, and bird observations. The sub-mesoscale survey areas were chosen from mesoscale acoustic surveys. A routine coast-wide (~2000 km) acoustic survey performed just after the sub-mesoscale surveys, provided information at an even larger population scale. The availability of nearly concurrent sub-mesoscale, mesoscale and coast-wide information on anchoveta distribution allowed for a unique multi-scale synthesis. At the sub-mesoscale (100s m to km) physical processes (internal waves and frontogenesis) concentrated plankton into patches and determined anchoveta spatial distribution. At the mesoscale (10s km) location relative to the zone of active upwelling (and age of the upwelled water) and the depth of the oxycline had strong impacts on the anchoveta. Finally, over 100s km the size of the productive area, as defined by the upwelled cold coastal waters, was the determining factor. We propose a conceptual view of the relative importance of social behaviour and environmental (biotic and abiotic) processes on the spatial distribution of anchoveta. Our ecological space has two *y*-axis; one based on self-organization (social behaviour), and the other based on the environmental processes. At scales from the individual (10s cm), to the nucleus (m), social behaviour (e.g. the need to school) drives spatial organization. At scales larger than the school, environmental forces are the main driver of fish distribution. The conceptual ecosystem models presented in this paper may provide the final links needed to develop accurate forecasts of the spatial distribution of anchoveta over multiple scales.

1. Introduction

Peruvian anchovy or anchoveta (*Engraulis ringens*) is a critical element of the Humboldt Current ecosystem, supporting the largest fishery in the world. Anchoveta is commonly referred to as an *r* species because of its fast growth and time to maturity (~1 year), short life span (~4 years), fast response to environmental variability (Valdivia, 1978; Bertrand et al., 2004a; Gutiérrez et al., 2007), and plasticity in terms of the prey it consumes and foraging behaviour (Espinoza and Bertrand, 2008). Anchoveta is both an important predator of planktonic organisms (Pauly et al., 1989; Espinoza and Bertrand, 2008), a prey for apex predators (Arntz and Fahrbach, 1996; Jancke and Goya, 1998; Arias-Schereiber, 2003) and also shares the productive coastal habitat with the sardine, *Sardinops sagax* and more recently the crustacean squat lobster or 'munida', *Pleuroncodes monodon*, which has been very abundant in the Humboldt Current system (HCS) since the mid 1990s (Gutiérrez et al., 2008).

Anchoveta populations can vary rapidly in both space and time. The variability depends on a number of factors that structure its habitat (e.g. Clark, 1977; Bertrand et al., 2004a, 2008; Swartzman et al., 2008). Gregarious or schooling fish such as the anchoveta are sensitive to processes occurring at spatial scales that impact

---

[*] Corresponding author. Address: IRD, CRH, Avenue Jean Monnet, BP 171, 34203 Sète Cedex, France. Tel.: +33 4 99 57 32 00.
E-mail address: Arnaud.Bertrand@ird.fr (A. Bertrand).
[1] Present address: TASA, Av. Néstor Gambeta, Km 14.1, Ventanilla, Callao, Peru.

0079-6611/$ - see front matter © 2008 Elsevier Ltd. All rights reserved.
doi:10.1016/j.pocean.2008.10.018

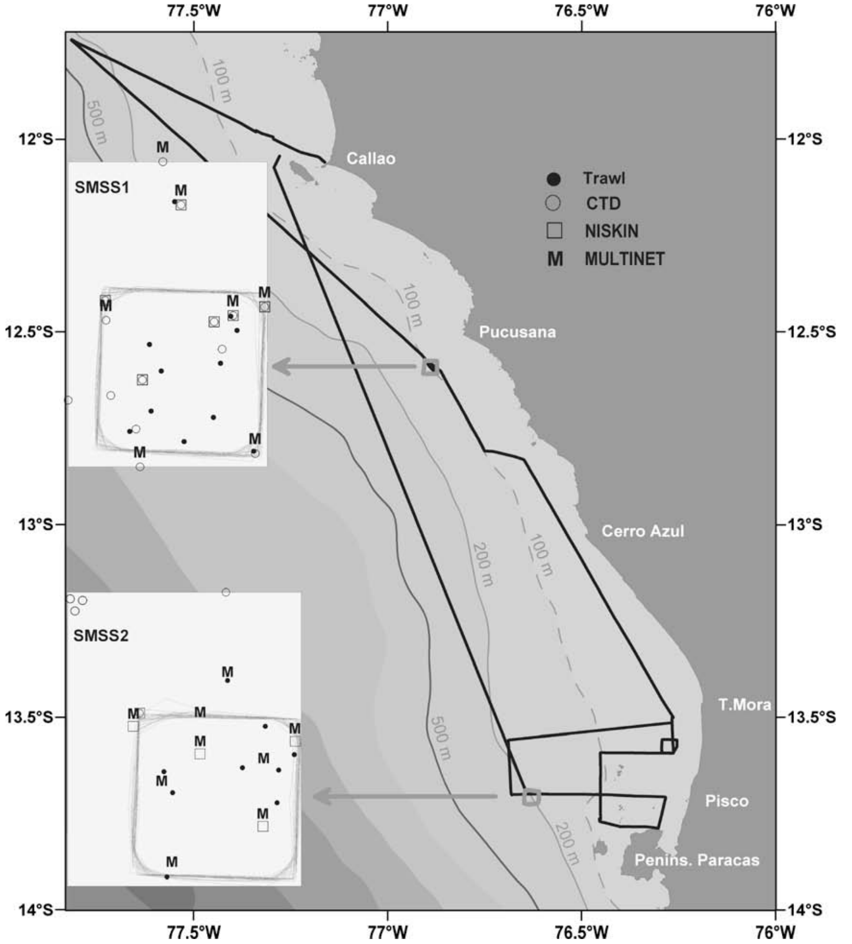

Fig. 1. Survey track (thick line) during the mesoscale ('rake survey') cruise and zooms on the two sub-mesoscale surveys (SMSS1 and SMSS2). Trawl (full circles), CTD (black empty circles), Niskin (black empty squares) and multinet (capital M) positions are also indicated, thin black lines indicates isobaths.

the individual (dm), nuclei (ms), schools (ms to 10s m), clusters of schools (km), clusters of clusters (10s km), and populations (100s km) (Gerlotto and Paramo, 2003; Fréon et al., 2005). For example, Bertrand et al. (2008) described the impact of a coastally trapped Kelvin waves (Clarke, 1983) on the spatial distribution of anchoveta and fishers. The Kelvin waves initiate a bottom-up cascade (Frontier, 1987; Russel et al., 1992) that propagates through the ecosystem from physics to anchoveta and fishers. Physical processes modify the three-dimensional distribution of physical (i.e. temperature), chemical (i.e. oxygen) and biological (i.e. plankton) parameters, the so-called oceanic landscape; then, mobile predators such as anchoveta and fishers respond to these spatial perturbations. At smaller scales, schools are known to self-organize, driven by elementary behavioural rules at the individual level: attraction, repulsion, and cohesion, and produce elaborate collective structures (Soria, 1997; Camazine et al., 2001; Couzin and Krause, 2003). Social rules are critical in school internal structure (Gerlotto and Paramo, 2003; Gerlotto et al., 2004) and can interact with environmental forcing of the oceanic landscape to determine school shape (morphology) so that they are either small dense schools, loose shoals or layers (e.g. Gerlotto et al., 2004; Bertrand et al., 2006). Therefore, school types have been considered good indicators of environmental conditions (Petitgas and Levenez, 1996; Reid, 2000; Petitgas et al, 2003; Bertrand et al., 2006).

While the most notable and dramatic changes in anchoveta are associated with large multi-decadal basin-scale changes in the environment (e.g. Chavez et al., 2003) there are many other scales of variability that are just now emerging. For example a new centennial-scale fluctuation has been elucidated from sediment cores (e.g. Sifeddine et al., 2008; Valdés et al., 2008). Further, upwelling ecosystems are highly heterogeneous with oceanographic and trophic conditions differing strongly on short time and space scales (Lavaniegos et al., 2002; Carr and Kearns, 2003; Bertrand et al., 2004a; Gutiérrez et al., 2007; Chaigneau et al., 2008; Espinoza and Bertrand, 2008; Swartzman et al., 2008). This heterogeneity is the result of mesoscale (10s km) and sub-mesoscale (100s m to km) activity that generates sharp fronts between coastal rich and oceanic poor waters (Chaigneau and Pizarro, 2005a), filaments (Thomas, 1999), eddies (Hormazabal et al., 2004; Chaigneau and Pizarro, 2005b). Internal waves are also emerging as important drivers of the oceanic landscape at these scales (Haury et al., 1978; Pineda, 1999). Studies have already shown that mesoscale activity influences the spatial distribution of fish (e.g. Rogachev et al., 1996; Seki et al., 2002; Fossheim et al., 2005). It is also very likely that sub-mesoscale physics may also influence anchoveta and its interaction with other species (prey, competitors and predators), but there is a paucity of *in situ* observations at this smaller scale.

Here we present the first comprehensive sub-mesocale study of anchoveta distribution in relation to the environment. The environment includes temperature, salinity, dissolved CO_2, dissolved O_2, the vertical and horizontal distribution and abundance of other species (predator, prey and competitors); at the temporal scale we resolve the diel cycle. Sub-mesoscale surveys (SMSSs) (~28 h – 2 nmi) were performed in November 2004 to relate environmental forcing and fish behaviour and distribution in central Peru. SST and

Table 1
Number of samples by sub-mesoscale survey (SMSS) for each parameter.

Parameter	Number of samples	
	SMSS1	SMSS2
Acoustics (anchoveta, munida and zooplankton)	948 ESDUs (0.25 nmi long each)	956 ESDUs (0.25 nmi long each)
Plankton multinet sampling	10 profiles; 436,861 items identified	10 profiles; 154,364 items identified
CTD	14 profiles (2 before and 12 after the acoustic track)	11 profiles (1 before, 10 after the acoustic track)
Sea surface salinity, pCO_2	1568 records (one value each minute except during sensor calibration)	1298 records (one value each minute except during sensor calibration)
Niskin bottles samples	6 profiles (DO, chlorophyll *a*, and phaeopigment)	5 profiles (DO, chlorophyll *a*, and phaeopigment)
Pelagic trawls	11 trawls, 8 with anchovy catch, 1582 anchoveta sampled for biometry and 114 for stomach content analysis	9 trawls, all with anchovy catch, 1525 anchoveta sampled for biometry and 128 for stomach content analysis
Sea bird counting	Along the transects (daylight hours), 9004 seabirds observed over 239 ESDUs	Along the transects (daylight hours), 5878 seabirds observed over 202 ESDUs
Multibeam sonar	6 h of opportunistic recording (when fish was present)	6 h of opportunistic recording (when fish was present)

CO_2 sensors, Niskin bottles, CTD probes, zooplankton sampling, stomach content analysis, echo-sounder, multibeam sonar, bird observations were used to assess interactions between fish behaviour and distribution and the environmental parameters (both oceanographic and biotic). Areas particularly suitable for SMSSs (rake survey were identified from mesoscale acoustic surveys). A routine coast-wide (~2000 km) acoustic survey performed by IMARPE (Instituto del Mar del Perú, www.imarpe.gob.pe) just after the SMSS's, provided information at an even larger population scale.

The availability of nearly concurrent sub-mesoscale, mesoscale and coast-wide information on anchoveta distribution allowed for a unique multi-scale synthesis. A modified basin model framework (BMF) from MacCall (1990), where fish distribute in a theoretical basin (here basin does not refer to ocean basins but to the area over which the fish are distributed) where 'depth' depends on the growth rate per capita in the area, was constructed. MacCall (1990) postulated that fish first colonize favourable areas then move to less favourable areas as they become more abundant (density-dependence). Swartzman et al. (2008) on the other hand showed that anchoveta are restricted to upwelled cold coastal waters (CCW) independent of anchoveta abundance, as suggested by the habitat-based model proposed by Bertrand et al. (2004a). The size of the favoured habitat (CCW) is then an important factor regulating anchoveta populations. Physical (CCW) and chemical (oxygen) parameters define the size of the favoured habitat (quantity) but abundance and distribution of predators and prey determine habitat quality (basin depth). In our 'habitat-based BMF' anchoveta concentration increases in the favoured habitat when quality increases ('deeper basin') rather than expand spatially to less favourable habitats. Basin depth (for the population) increases with habitat quality, determined by multiple biotic and abiotic parameters at our three scales: large/population, meso and sub-meso. We propose conceptual models that explain the spatial distribution of anchoveta at multiple scales as well as the relative influence of social behaviour and the environment.

2. Materials and methods

2.1. Survey design

Two acoustic sub-mesoscale surveys (SMSSs) were carried out on board the IMARPE R/V "Olaya" (41 m long) off the Peruvian coast in November 2004, wherein the ship steamed around two, 2 nautical mile side square boxes (Fig. 1) repeatedly. The average time to run a single square was 1 h at 8 knots. The location of the SMSSs was chosen from anchoveta abundance estimated during a preliminary acoustic rake survey along the coast designed to identify favourable areas (see Fig. 1) at the beginning of the cruise and from the locations of the fishing fleet. The position of the boxes was geographically fixed, i.e. we did not implement a lagrangian tracking system. However, no substantial change in communities was observed during each SMSS and anchovy, the target species was always present. We consider each SMSS as independent.

Acoustic sub-mesoscale survey 1 (SMSS1) was carried out off Pucusana (12°34′S) and consisted of 28 repeated squares (to encompass an entire diel cycle) from November 18th at 04:40 to November 19th at 08:45 (Fig. 1). Acoustic sub-mesoscale survey 2 (SMSS2) was performed 20 nautical miles northwest of Paracas peninsula (13°40′S) and consisted in 28 repeated squares from November 21st at 16:45 to November 22nd at 21:24. After each survey the oceanographic, planktonic and biological features of the area were sampled using CTDs and nets during a 28 h sampling period (Fig. 1). The sampling strategy was designed to capture sub-mesoscale variability over a diel cycle.

2.2. Acoustic observations

Vertical acoustic cross section data were collected in with a 38 and 120 kHz Simrad EK500 split-beam, scientific echo-sounder

Table 2
Mean surface conditions (except for the zooplankton mean density which was integrated over 100 m depth and s_A, which was integrated over 50 m depth) during small-scale surveys 1 and 2.

Parameter	SMSS1	SMSS2
Wind speed ($m\ s^{-1}$)	1.75	3.14
SST (°C)	17.8	16.6
Salinity	35.11	35.06
xCO_2 (ppmv)	359.4	655.3
DO ($mL\ L^{-1}$)	6.6	6.2
Chlo-*a* ($\mu g\ L^{-1}$)	8	21.2
Pheo/Chlo-*a*	0.68	0.32
Main zooplanktonic taxa (% in number)	81.5% of copepods, 10.4% of cladoceras, and 3.7% of ichtyoplankton (clupeids)	76.8% of copepods, 11.7% of ichtyoplankton (clupeids), 4.4% of polychaetes, and 3.6% of cladoceras
Zooplankton mean density (number m^{-3})	121	35.5
Zooplankton s_A ($m^2\ nmi^{-2}$)	22.4	7.2
Munida s_A ($m^2\ nmi^{-2}$)	563.6	0
Anchoveta s_A ($m^2\ nmi^{-2}$)	695.1	407.9
Stomach fullness (%)	0.4	0.27
Number of seabirds species	11	7
Seabirds (number nmi^{-1})	73.3	58.2
% of foraging seabirds	12.5	15.1

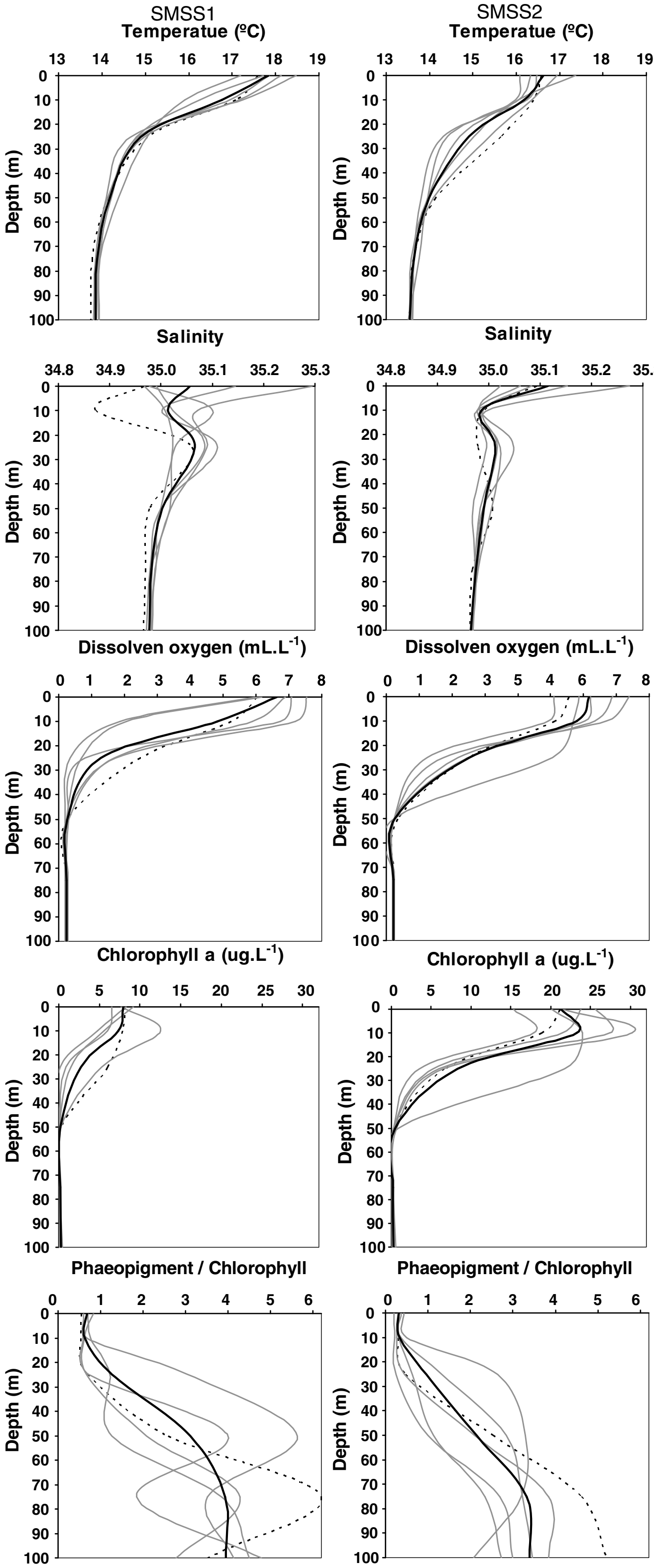

Fig. 2. Vertical profiles from Niskin bottles for temperature, salinity, dissolved oxygen and chlorophyll *a* and the ratio between phaeopigment and chlorophyll *a*. Thick black lines indicate mean profile, dotted black lines indicate the profile performed just before the 28 h acoustic square tracks, grey lines indicate profiles performed after the acoustic tracks.

system (Kongsberg Simrad AS, Kongsberg, Norway), calibrated as in Foote et al. (1987). Data processing was done using Echoview (SonarData Pty. Ltd.) and Movies+ (Weill et al., 1993). Dual frequency analyses were used to discriminate anchoveta, from munida and zooplankton. Species identification was verified with pelagic trawl and plankton net samples. The acoustic nautical area scattering coefficient (s_A or NASC), an indicator of fish biomass, and the acoustic volume backscattering strength (S_v), an indicator of the fish density inside each collective structure (each acoustic echo-trace), were calculated for all echo-traces. Acoustic symbols and units used here follow MacLennan et al. (2002). Acoustic data were recorded by elementary distance sampling unit (ESDU) of 0.25 nmi.

Fish schools were observed in 3D with a scanning multibeam sonar (Reson Seabat 6012). The sonar was mounted on the vessel starboard side, perpendicular to the vessel course, permitting the scanning of a 90° sector from vertical down (below the vessel) to horizontal starboard (parallel to sea surface), with a range of 100 m. Each ping covered this 90° sector, divided into 60 beams of 1.5° (between beams) by 15° (perpendicular) each. The sonar operated at 455 kHz (20 kHz bandwidth) with a ping duration of 0.06 ms. The data was constructed as a 3D image (Gerlotto et al., 1999) with SBI Viewer software (Hamitouche-Djabou et al., 1999).

2.3. Oceanographic data

Sea surface temperature (SST) and the partial pressure of CO_2 were continuously recorded using a resistance temperature detector and a nondispersive infrared gas analyzer (LI-COR model 6262), which determines the partial pressure of CO_2 in the atmosphere and surface seawater (Friederich et al., 2008).

Surface-to-bottom temperature and salinity profiles were obtained with a SEABIRD CTD. Water samples were collected in Niskin bottles at 0, 10, 25, 50, 75, 100, and 150 m and analyzed for dissolved oxygen (DO-modified Winkler method, Carritt and Carpenter, 1966), chlorophyll *a*, and phaeopigment (concentration method of Holm-Hansen et al., 1965).

2.4. Plankton sampling

Zooplankton were collected with a vertically profiling plankton net (multinet) with a 300 μm mesh size in the following depth strata: 0–10 m, 10–25 m, 25–50 m, 50–75 m, and 75–100 m depths. Zooplankton settled volume (mL^3) was determined immediately after collection using the displacement method (Kramer et al., 1972). Samples were fixed in 2% formaldehyde buffered with borax, then examined in laboratory using a stereoscopic microscope to identify and count zooplankton items.

2.5. Fish sampling

Fish were collected by pelagic trawl 'Engel 124/1800' (12 mm codend mesh). For each trawl, a subsample of the catch was collected randomly and anchoveta size was measured to the nearest 0.5 cm. Anchoveta cardiac and fundulus stomachs were extracted onboard and immediately fixed in 5% formalin for later laboratory analysis where stomachs contents were extracted and weighted to the nearest 0.001 g. Stomach fullness index was calculated by dividing fish stomach content weight by body wet weight.

2.6. Seabird counts

Seabird densities were estimated using transects as in Sutherland (1996) during daylight hours (06:00 to 18:00, local time). One trained observer made continuous counts from the ship bridge (10 m above sea level) using binoculars out to 300 m in a 90° arc from the tip of the bow to the starboard. Species identification, counts and behaviour (on water, active feeding, flying, and flight direction) were recorded and the time noted.

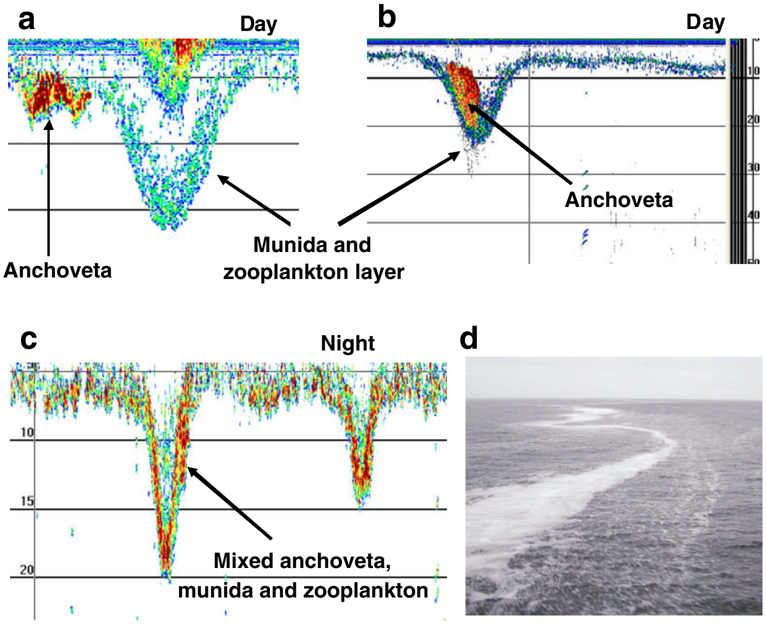

Fig. 3. Vertical features of the water column where internal solitary waves were observed during the day (a, b), the night (c), and surface photograph of a convergence line (d). *Note:* (b) Come from another similar experiment performed in April 2006.

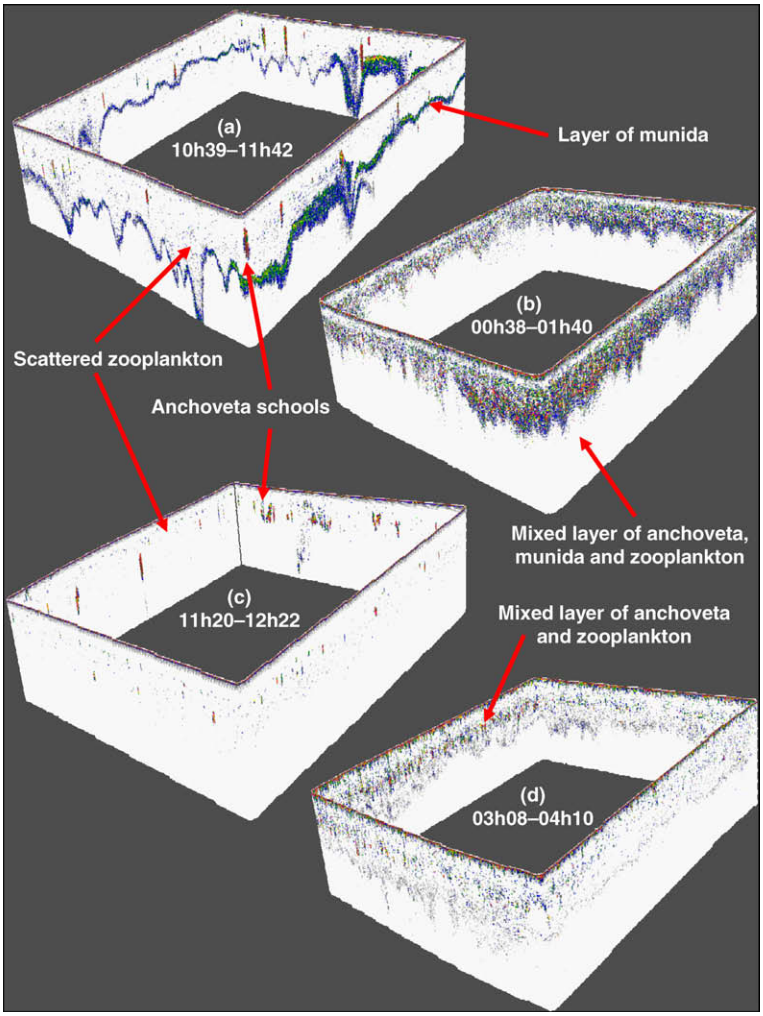

Fig. 4. Examples of acoustic square transects performed during SMSS1 during the day (a), at night (b) and during SMSS2 during the day (c), at night (d). The classical patterns of distribution for anchoveta (*Engraulis ringens*), the squat lobster 'munida' (*Pleuroncodes monodon*) and zooplankton are highlighted.

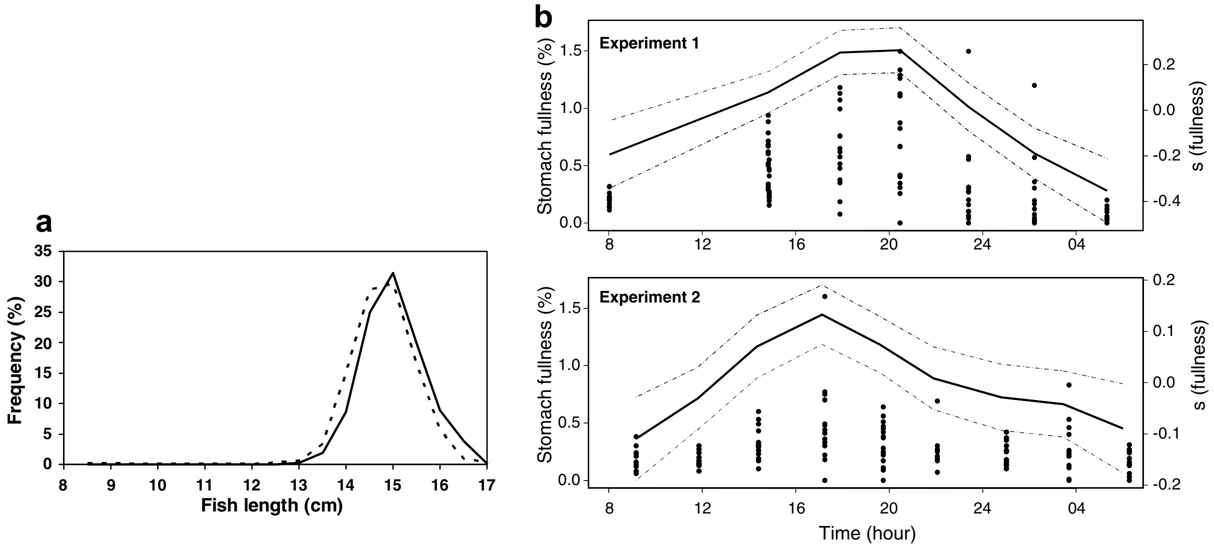

Fig. 5. (a) Fish standard length during SMSS1 (black solid line) and SMSS2 (black dotted line). (b) Scatter plot (black dots) and cubic spline fits (black solid lines) of bivariate GAM models based on anchoveta fullness during SMSS1 and SMSS2 according to the time. The black dotted lines show the 95% confidence limits of GAM models. Left *y*-axis shows the stomach fullness in percentage. The right *y*-axis are in relative scale, they correspond to the cubic spline that was fit to the data, so that a *y*-value of zero is the mean effect of time on the response.

2.7. Data processing

SST, CO_2, the acoustic s_A of zooplankton and to a lesser extent munida and anchoveta abundance showed strong diel variability. This diel pattern was related to diurnal warming of SST that in turn impacts CO_2 solubility and to plankton diurnal vertical migration with a daytime dispersion over a large volume that reduces acoustic detection. We removed the diel pattern using a non-parametric spline model in order to study higher frequency variations.

We used a wavelet approach (Torrence and Compo, 1998) to search for spatiotemporal synchrony between organisms. There are few wavelet applications in marine ecology (Ménard et al., 2007) following the pioneering work by David and Chapron (1990); however this method is appropriate to analyse biological time series, which are often noisy, nonlinear and non-stationary (Cazelles and Stone, 2003); all features that may interfere with correlation or spectral analyses. Wavelet analysis was applied to the acoustic data time series with the diel cycle removed to investigate

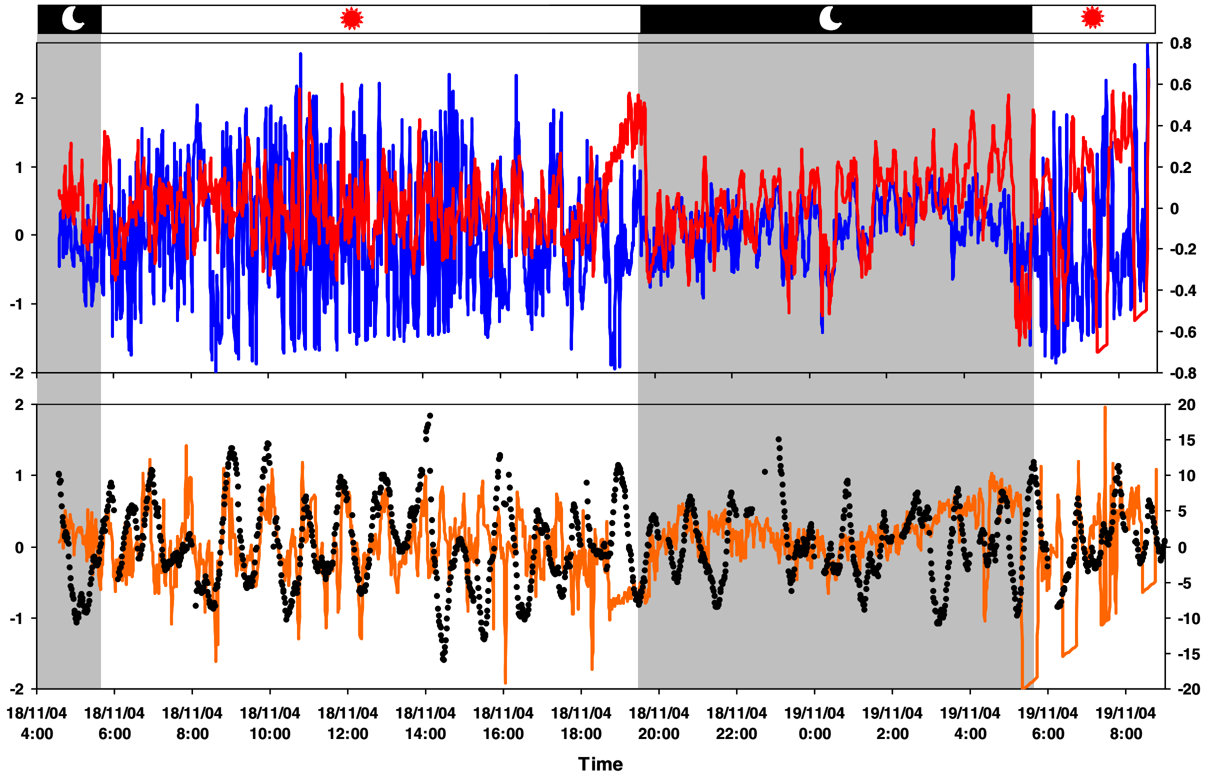

Fig. 6. Time series for anchoveta (blue line), zooplankton (red line), munida (orange line) acoustic abundance and CO_2 (black dots) during SMSS1 where the diel cycle has been removed. Left *y*-axis corresponds to the anchoveta and munida; right *y*-axis corresponds to zooplankton and CO_2.

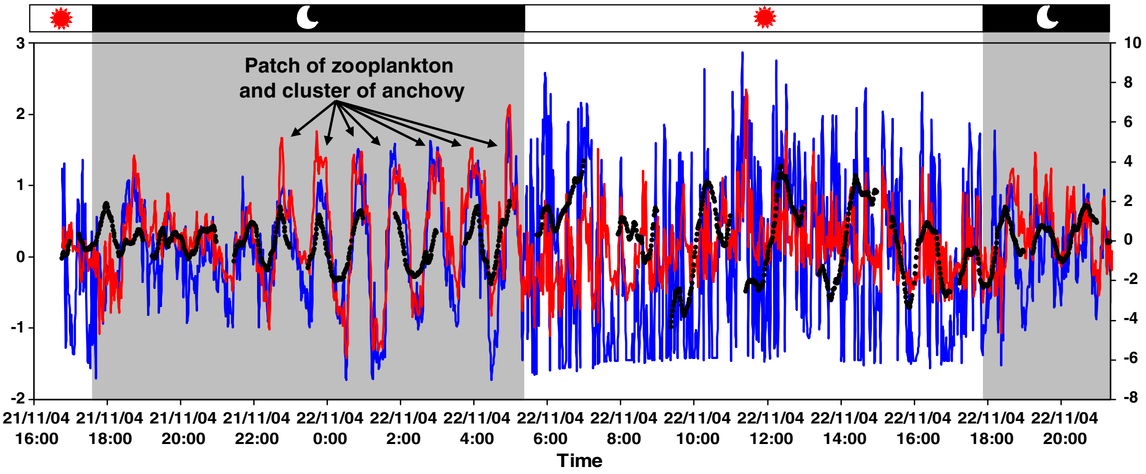

Fig. 7. Time series for anchoveta (blue line), zooplankton (red line) acoustic abundance and CO_2 (black dots) during SMSS2 where the diel cycle has been removed. Left *y*-axis corresponds to anchoveta; right *y*-axis corresponds to zooplankton and CO_2.

other periodic components. Complementary phase analyses characterised spatiotemporal synchrony between signals (Cazelles and Stone, 2003; Ménard et al., 2007). To quantify wavelet statistical significance, we resampled with a Markov bootstrapping (Efron and Tibshirani, 1993) that preserves the short temporal correlations (Cazelles and Stone, 2003). We used the Morlet mother wavelet and original algorithms that were developed in a MATLAB package (version 6.5, The MathWorks Inc.); these incorporate both cross analyses and statistical significance procedures (Cazelles et al., 2007).

Finally, to determine the diel cycle of anchoveta foraging we analysed, for each SMSS, variations in anchoveta stomach fullness over time. As the relationships are likely to be nonlinear, a generalized additive modelling (GAM) approach was used (Hastie and Tibshirani, 1990) using S-Plus (Insightful Corporation, Seattle, WA, USA). Cubic spline smoothers were used to estimate the nonparametric functions.

3. Results

The acoustic track and the positions of pelagic trawls, CTD, multinet, and Niskin sampling stations are indicated in Fig. 1; the total number of samples for each parameter is listed in Table 1.

3.1. Oceanographic conditions

During sub-mesoscale survey 1 (SMSS1), vertical profiles indicated that temperature ranged from about 17.8 °C at 0 m to 14 °C at 100 m. Salinity ranged from 34.9 to 35.3 but mainly between 34.95 and 35.1, values characteristic of upwelled cold coastal waters (Morón, 2000). Dissolved oxygen concentration (DO) ranged between 6 and 7.5 $\mathrm{mL\,L^{-1}}$ at 0 m; the depth of the oxycline (where oxygen changes rapidly from the surface values to close to zero) varied from 15 to 25 m. Chlorophyll concentration was about 8 $\mathrm{\mu g\,L^{-1}}$ at 0 m and very low at 50 m. Finally, the ratio between phaeopigment and chlorophyll was high for surface water (about 0.65), indicating a very active degradation process (Table 2 and Fig. 2). During SMSS1, we crossed convergence lines which were visible as "scum" (accumulations of foam and degraded particulate material) lines (Fig. 3d). These lines, commonly observed off Peru, tend to occur over solitary internal waves (Farmer and Armi, 1999), and during the surveys were associated with two vertical structures observed with the echo-sounder: (i) a deepening of the mixed layer illustrated by the 'v shape' of the munida and plankton layer (Fig. 3a–c), or (ii) in some cases anchoveta were observed inside these structures forming schools during the day (Fig. 3a and b) and layers during the night (Fig. 3c).

During sub-mesoscale survey 2 (SMSS2) temperature ranged from about 16.6 °C at 0 m to 14 °C at 100 m. Salinity ranged from 34.96 to 35.30. Dissolved oxygen concentration decreased from 5–7.5 $\mathrm{mL\,L^{-1}}$ at 0 m to 2 $\mathrm{mL\,L^{-1}}$ at 25–30 m, to 1 $\mathrm{mL\,L^{-1}}$ at 30–45 m and finally to 0.1 $\mathrm{mL\,L^{-1}}$ at 50 m. Chlorophyll concentration was higher (20 $\mathrm{\mu g\,L^{-1}}$) within several meters of the surface and very low at 50 m. Finally, the ratio between phaeopigment and chlorophyll *a* was rather low in the surface waters (about 0.32), indicating very high phytoplankton production and less active degradation processes (Table 2 and Fig. 2).

3.2. Zooplankton, munida, and anchoveta

Fig. 4 shows examples of acoustic square transects performed during SMSSs, illustrating the classic diel patterns of distribution for anchoveta (schools during the day, dispersed at night), munida (layers in the oxycline during the day, dispersed at night) and zooplankton (surface diel vertical migration with nighttime maxima near the surface, and daytime maxima at depth).

The zooplankton community was dominated by copepods; its abundance was three times higher during SMSS1 than SMSS2, regardless to the sampling method, multinet or acoustics (Table 2). The acoustic s_A of zooplankton was lower by day than by night in both areas. This pattern is due to the dispersion of zooplankton over a broader depth range during daily vertical migration (Fig. 4). Dense patches of zooplankton occurred during the first night of SMSS2.

Munida were observed only during SMSS1, scattered close to the surface during night (Fig. 4). During day, munida formed denser layers in the oxycline, and are physically "moved" vertically by the passage of internal waves (Figs. 3 and 4).

During SMSS1 and SMSS2 8 and 9 positive (with anchoveta catch) trawls were performed just after acoustic sampling. Fish size distribution was not significantly different between SMSSs ($\chi^2 = 17.16$, d.f. = 17, $p = 0.44$) and was strongly dominated by one year class of anchovy with a mode of 15 cm (Fig. 5a). Stomach fullness varied according to the time of the day and was significant in both surveys (GAM, $p < 0.0001$). The mean stomach fullness was higher during SMSS1 than SMSS2 (Table 2; *t*-test[1,240] = 3.54, $p = 0.0005$), but in both cases was highest between midday and

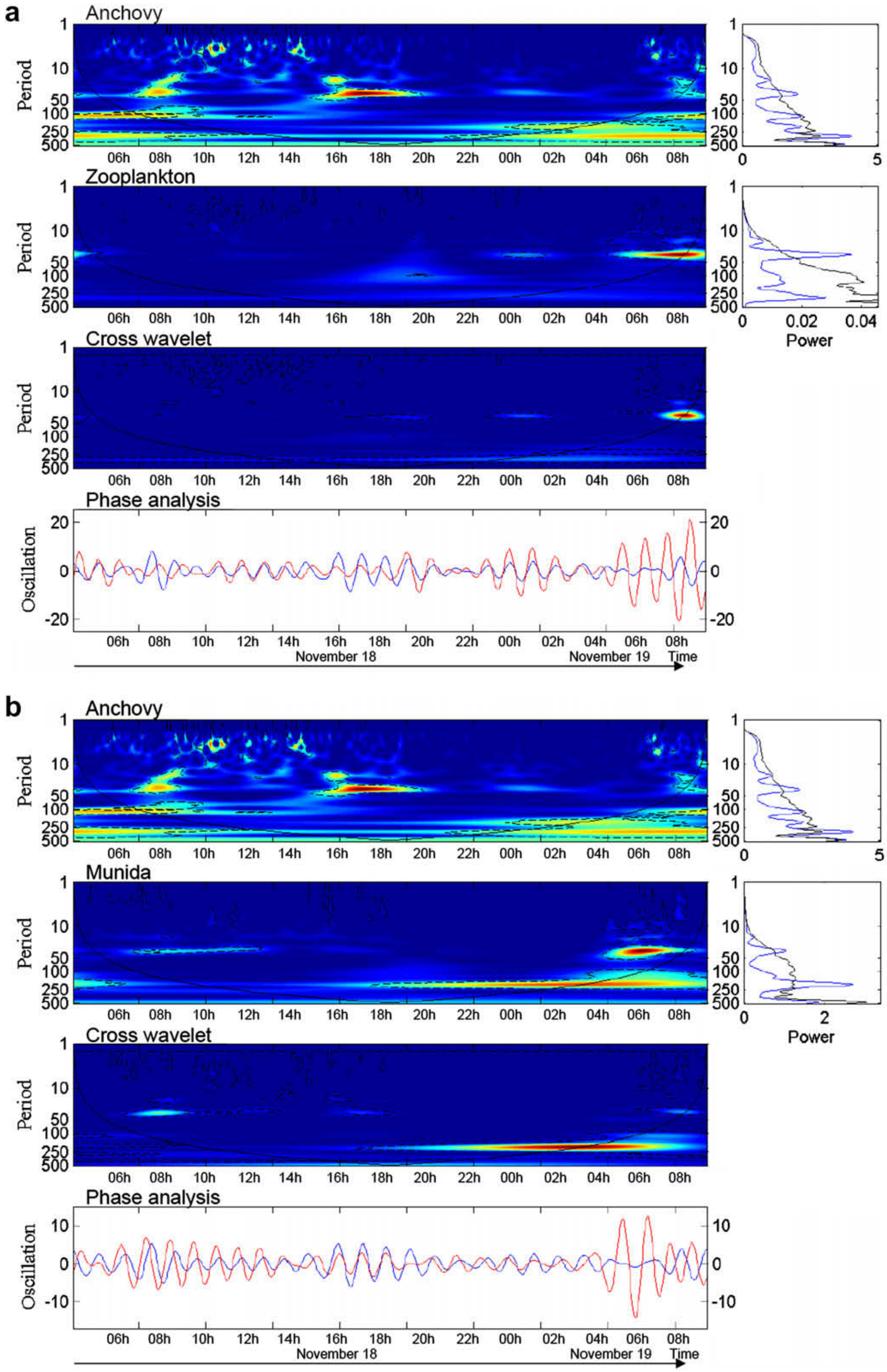

Fig. 8. Wavelet analysis for (a) anchoveta and zooplankton acoustic abundance during SMSS1; (b) anchoveta and munida acoustic abundance during SMSS1; and (c) anchoveta and plankton acoustic abundance during SMSS2. For each case, the upper plots give: on the left the local wavelet power spectrum of anchoveta, zooplankton or munida s_A. The local wavelet power spectrum gives a measure of the variance distribution of the space–time series according to time and for each period; on the right: global wavelet power spectrum of the anchoveta series as a function of period. The cross wavelet plot gives the wavelet cross spectrum between anchoveta and zooplankton or munida series. The wavelet cross spectrum identifies period bands and time intervals within which the two series co-vary. The black solid lines show the cone of influence, i.e. the region where edge effects are present. The black dashed lines show the 5% significance level computed based on 50 bootstrapped series. The lower plot gives the oscillating components computed with the wavelet transform.

18:00–21:00 (Fig. 5b). High stomach fullness was also observed during the night for some (~15%) anchovies. The beginning of the feeding period was not determined for SMSS1, as trawls performed between 08:00 and 14:50 did not catch fish. Anchoveta was always

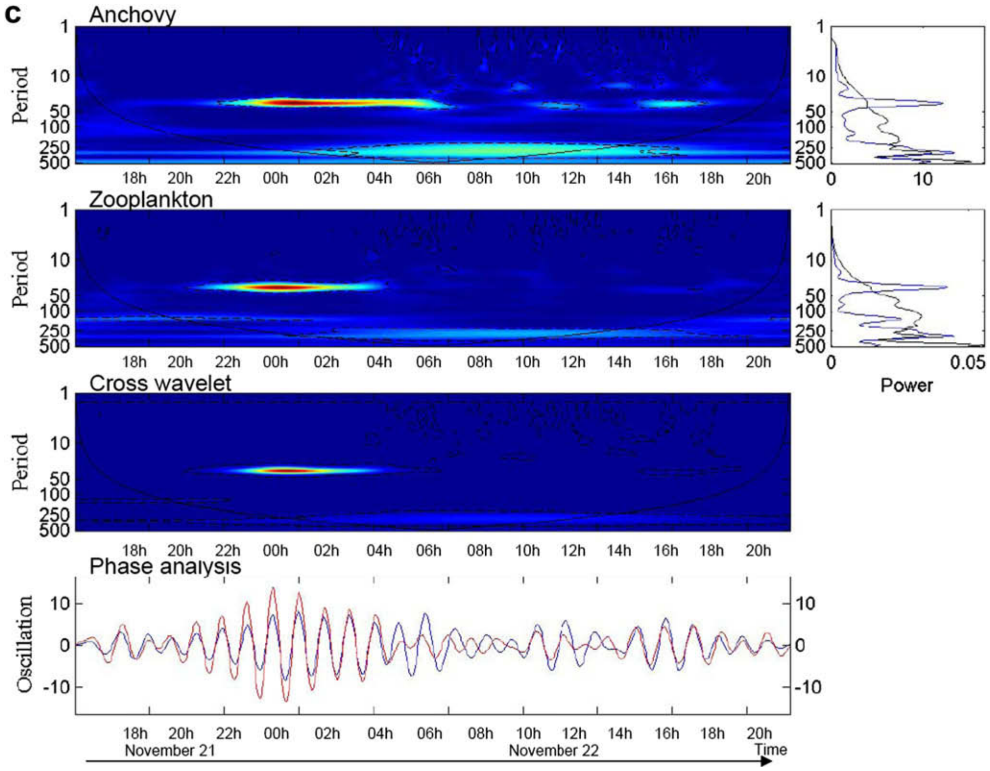

Fig. 8 *(continued)*

above the 2 mL L^{-1} oxygen isoline and the primary diel difference was that they were in schools during the day and scattered at night. The density (S_v) inside anchoveta echo-traces increased from dawn to midday then decreased until dusk and remained stable at a low level during night (ANOVA: $F[3,34467] = 105.5$, $p < 0.00001$ for SMSS1; $F[3,30783] = 390.3$, $p < 0.00001$ for SMSS2). Anchoveta reformed into schools at dawn (Fig. 4).

3.3. Seabirds

Eleven species of seabirds were observed during SMSS1 (mean density: 73.3 individuals/nmi^{-1}). The most abundant were Franklin's gull (*Larus pipixcan*), the Peruvian booby (*Sula variegata*), the Inca tern (*Larosterna inca*), and the Peruvian pelican (*Pelecanus thagus*), listed in decreasing order. Bird abundance was less during SMSS2 with 58.2 individuals/nmi^{-1} with seven species being observed. Listed in decreasing order, the dominant species were the Peruvian booby, the Inca tern, the Guanay cormorant (*Leucocarbo bougainvillii*), and Franklin's gull. The proportion of actively feeding seabirds was 12.5% during SMSS1 and 15.1% during SMSS2. Among these species the Guanay and the Peruvian booby are major predators for anchovy. Others are mainly zooplanktivorous species.

3.4. Space–time series and wavelet analyses

During the SMSSs, SST, and CO_2 presented clear diel variations (not presented) with SST decreasing during the night (magnitude of change: 2.5 °C). CO_2 exhibited the opposite trend, as its solubility increased with decreasing SST. After removing the diel cycle, no relation remained between SST and CO_2. Variation in the SST time series (with the diel cycle removed) could not be related to any other parameter and was eliminated from the analysis. The other space–time series (Figs. 6 and 7) illustrates the varying and dramatically different dynamics between day and night. We observed nocturnal zooplankton patches, in particular during SMSS2, when one patch was sampled repeatedly during 8, 1 h squares during the first night. A cluster of anchoveta and a peak in dissolved CO_2 was always associated with this zooplankton patch (Fig. 7). Such associations were less clear during SMSS1, probably because zooplankton patches were looser or absent in the sampled area. Outside zooplankton patches, anchoveta were also observed but were less abundant and scattered. During the day, both anchoveta schools and zooplankton patches were evenly distributed. Conversely, munida were concentrated in dense layers during daytime, at the depth of the oxycline. Munida local abundance presented a pattern of variation similar to the one of CO_2 (Fig. 6). During night munida was dispersed close to the surface and presented a more homogeneous distribution.

Wavelets, cross wavelets, and phase analyses were applied to reveal possible spatiotemporal synchrony between the organism distributions. Anchoveta and zooplankton acoustic abundances show a clear pattern of synchrony, especially during SMSS2 (Fig. 8a and c). During the afternoon and the night, anchoveta and zooplankton were present in the same 'time–space' period (about 32 ESDU, corresponding to a complete square, i.e. 8 nmi), with the half period indicating the plankton patch size, about 4 nmi. More interestingly, acoustic abundances of these two organisms oscillated perfectly in phase, indicating spatial correlation between anchoveta and zooplankton. At dawn, the spatial periodicity suddenly disappeared, as well as the association between anchoveta and zooplankton (i.e. the zooplankton patch and anchoveta cluster), and irregular small-scale periodicity appeared. Zooplankton and anchoveta stayed out of phase without any clear spatial association until the afternoon, when periodic oscillation and coherent phasing reappeared allowing interactions. During SMSS1 (Fig. 8a), cross wavelet and phase analysis between anchoveta and zooplankton local abundances also showed significant correlation during night (19:00–20:30 and 23:00–02:30), though the signal was weaker than in SMSS2. Note that the phase coherency observed between 10:00 and 14:00 during SMSS1 (Fig. 8a) and between 10:00 and 12:00 during SMSS2 (Fig. 8c) was insignificant, as it did not correspond to any significant cross wavelet (Fig. 8a and c).

Wavelet analyses performed with anchoveta and munida abundance data (Fig. 8b) did not reveal consistent spatial associations between these species. Anchoveta and munida acoustic abundances were in phase only at the end of the day and beginning of the night, i.e. when anchoveta schools were dispersing downwards and munida migrating upwards. Finally, munida and zooplankton distributions were not spatiotemporally associated in wavelet analyses (figure not presented).

3.5. The oceanic landscape

At the anchoveta population scale (100s of km), routine acoustic surveys were conducted in the core of anchoveta distribution by IMARPE just after the SMSSs (November 28–December 21, 2004). Anchoveta were distributed all along the Peruvian coast and the region where SMSSs took place corresponded to a particularly rich area, in an important upwelling cell (www.imarpe.gob.pe).

At a mesoscale (10s of km) the landscape was different between surveys (Table 2) even though both SMSSs' took place in cold coastal waters (see Morón, 2000; Bertrand et al., 2004a; Swartzman et al., 2008). SMSS1 was performed in older upwelled waters characterized by a high proportion of degraded chlorophyll, a very shallow oxycline, and high abundances of zooplankton, munida, anchoveta, and seabirds. The types of seabirds were mostly coastal species (Fraklin's gull and Inca tern) foraging mainly on zooplankton, including munida. SMSS2 was performed in active upwelling waters characterized by lower SST, very high chlorophyll concentration, and medium abundances of zooplankton and anchoveta. Seabirds were less abundant than in SMSS1, but dominated by the Peruvian booby, which forages on anchoveta. During both SMSSs, the main patterns in organisms' distribution over time followed the conventional pelagic diel scheme. Zooplankton performed diel vertical migration and were, during the day, mainly distributed below the oxycline (15–30 m). Munida (Fig. 4) were scattered in the same shallow layer as anchoveta during the night, but migrated deeper than the fish during the day, forming concentrated layers (Fig. 4) at the depth of the oxycline (15–30 m). Anchoveta vertical distribution was restricted to the first 30 m, above the oxycline. Zooplankton apparently finds a daytime refuge from anchoveta within the oxycline.

4. Discussion

4.1. Relative contribution of environment and behaviour in anchoveta schooling dynamics

In both SMSS1 and SMSS2 we observed the classic pattern of fish dispersion at night and aggregation in schools during day (Azzali et al., 1985; Fréon et al., 1996; Fréon and Misund, 1999; Cardinale et al., 2003), with a decrease in school internal density during afternoon and disintegration at dusk. The reduced school internal density during the afternoon appears associated with the beginning of the feeding period (Fig. 5b) as most of zooplankton migrates upwards (30–50 m to 5–20 m) and its availability increases. Indeed, less cohesive fish schools are assumed to be well adapted for feeding on zooplankton as each fish has to catch individual prey (Robinson et al., 1995; Nøttestad et al., 1996; Mackinson et al., 1999). During the night, despite the absence of small-scale (m to 10s of m) fish schools, clear sub-mesoscale (100s of m to km) fish clusters appeared. During the day, fish occurred in dense schools, especially in the morning, but not in larger-scale spatial structures such as clusters (at least on scales observable in our SMSSs). These observations are interpreted below via behavioural constraints and habitat suitability.

During the night, most gregarious pelagic fish do not form dense schools because small-scale collective organisation is generally inhibited by low light intensity [see Fréon and Misund (1999) for a synthesis and Bertrand et al. (2006) for an exception]. At night, environmental features controlled fish distribution. This was particularly clear during the first night of SMSS2, when anchoveta formed a cluster inside a patch of zooplankton (Figs. 7 and 8c). Stomach fullness analyses indicated that the main foraging period was the afternoon and first part of the night (Fig. 5b). Anchoveta were then primarily in the zooplankton patch for foraging, but remained well into the night. Espinoza and Bertrand (2008) showed that even if anchoveta mainly feed during day, they will also feed at other times as long as prey are available. The zooplankton patch probably developed in response to a sub-mesoscale oceanographic feature (e.g. eddy, plume) that we could not identify (see Cotté and Simard, 2005; Croll et al., 2005; Fossheim et al., 2005, for examples of physical forcing on plankton leading to predator concentration or recruitment success). This patch was also characterized by a peak in dissolved CO_2 concentration (Fig. 7) that we relate to respiration by organisms. Indeed, a dense aggregation of organisms has been shown to deplete DO concentration (e.g. McFarland and Moss 1967; Dommasnes et al., 1994); the inverse, increased CO_2 as a result of respiration follows. We think this might be the first observation of this kind.

After dawn, zooplankton migrated down below the oxycline, while anchoveta aggregated in schools. Gerlotto et al. (2006), working with multibeam sonar data obtained after SMSS2 observed that sea birds and sea lions attacked these schools intensively. Indeed sea lions were observed with the multibeam 58% of the time and the attack rate was very high. Schools were in constant reorganization (Gerlotto et al., 2006) and no more spatial structures were evidenced at a scale of 100 s of m to km (Figs. 6 and 7).

4.2. Habitat-based BMF and 3D fish distribution

In an attempt to synthesize the information we adapted the basin model framework (BMF, MacCall, 1990, see also Fréon et al., 2005). As described in Section 1, under our 'habitat-based BMF', the theoretical basin increases in 'depth' with habitat suitability (i.e. not a literal depth but an index of habitat suitability) as determined by physical (e.g. temperature, depth of the oxycline), and biotic (e.g. predation, prey abundance, and spatial distribution) features, independent of density-dependent effects. As the diel cycle is a key factor in anchoveta patterns of aggregation, we constructed a diurnal and a nocturnal representation of the adapted BMF; each BMF being characterized by three different spatial scales: large (100s of km), meso (10s of km) and sub-meso (100s of m to km) (Fig. 9).

The larger basin (100s km) is defined by anchoveta tolerance limits and corresponds to the zone of possible population distribution defined by overall abiotic conditions. The SMSSs took place near the centre of anchoveta species distribution. During the whole cruise survey track (Fig. 1) temperature was not limiting (range of tolerance for anchoveta: ~13–25 °C, Bertrand et al., 2004a; Gutiérrez et al., 2008).

At a mesoscale (10s km), the SMSS1 was performed in aged upwelled waters and SMSS2 in freshly upwelled waters. In both SMSS1 and 2, productivity was high and a shallow oxycline (Fig. 2) limited the depth of anchoveta and prevented diel vertical migration. Zooplankton was abundant (Table 2) and patchily distributed. During the day, part of the zooplankton escaped the anchoveta by migrating into and below the oxycline. The consequence was lower habitat suitability for anchoveta ('shallower' basin, Fig. 9). Predation by seabirds and sea lions also reduced

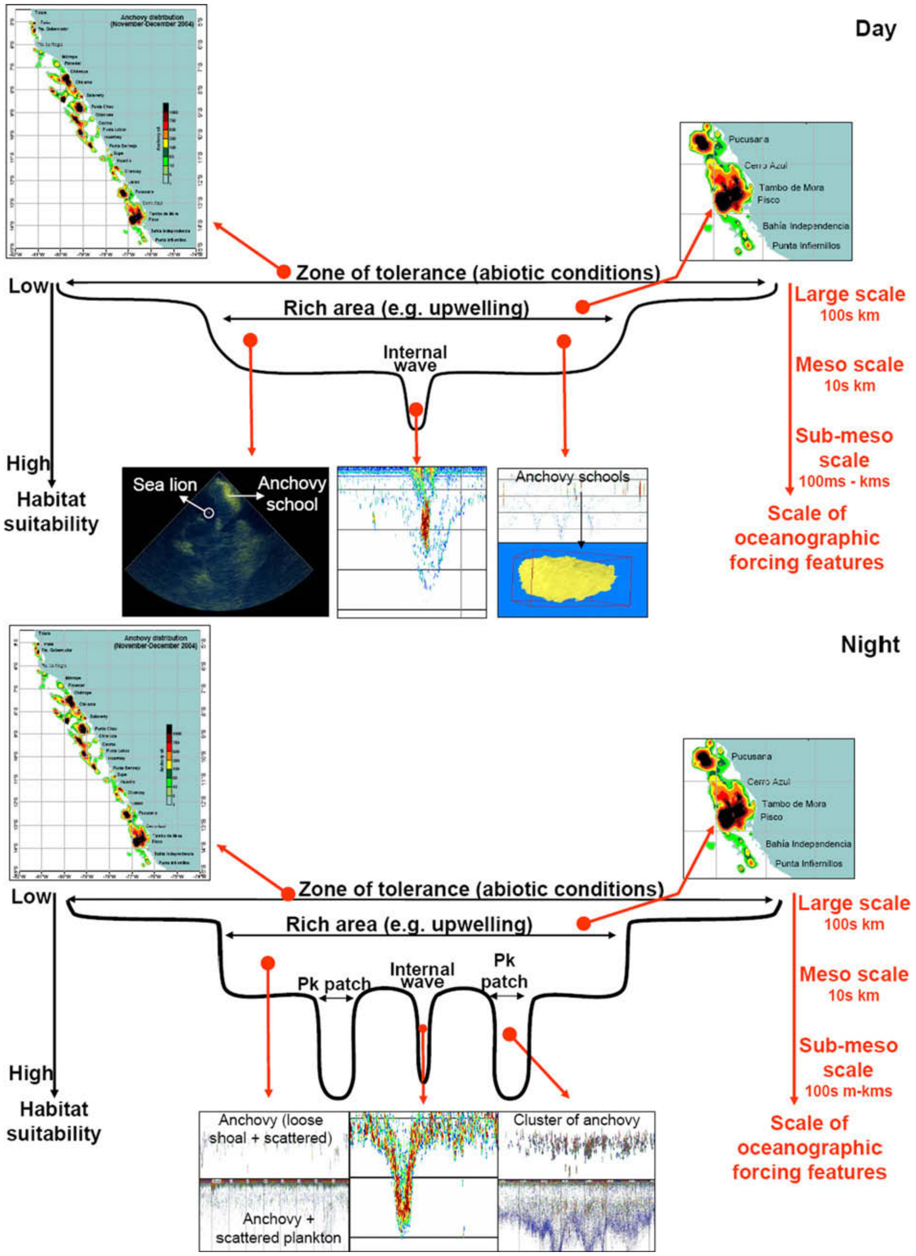

Fig. 9. Synthetic representation of the diel variation of the quality of anchoveta habitat across scales and its consequences on the 3D spatial distribution of anchoveta, adapted from the 'habitat-based basin model framework' of MacCall (1990). The depth of the basin increases with habitat quality in terms of oceanographic (e.g. temperature, depth of the oxycline) and biotic (e.g. predation, prey abundance, and spatial organization) features. The larger basin corresponds to the zone of anchoveta distribution. Inside this general zone, habitat quality increases in areas rich in prey surrounding an upwelling zone for example. Inside the rich areas, sub-mesoscale structures (i.e. internal solitary waves, eddies) can concentrate prey, further increasing habitat quality. During the day (upper figure), the depth of the basin is shallower than during the night since prey are less accessible (some of the plankton have migrated below the oxycline) and predation by visual apex predators (e.g. seabirds) is higher. Anchoveta form schools that are attacked by predators (see Gerlotto et al., 2006). During the night (lower figure) the depth of the basin increases as prey become more available and predation is reduced. Fish are no longer able to construct polarised collective structures (schools) but are concentrated in prey patches or internal waves, when present. Encapsulated figures above the basin figures show anchoveta distribution as evaluated during an acoustic survey performed just after the experiment illustrating the range of distribution of anchoveta off Peru (left) and a zoom in to an upwelling area (right). Encapsulated figures below the basin figures show typical examples of fish collective structure in each case as observed with the multibeam sonar (3D plots and plot showing a sea lion attacking anchoveta schools) or with the echo-sounder.

anchoveta habitat suitability during day. During the day anchoveta was in highly concentrated schools that were irregularly distributed (Figs. 6–8), a response to predators (Gerlotto et al., 2006). During night the vertical upward migration of zooplankton and reduced predation on anchoveta (no seabird attacks) created a 'deeper' (i.e. more suitable) BMF basin (Fig. 9). At night, anchoveta were distributed as loose shoals and scattered fish. It is during the night that the tight coupling between organisms (anchoveta and zooplankton), and their chemical signature (i.e. respiration) develops (Figs. 6 and 7); during the day these relationships dissipate.

At sub-mesoscale (100s m to km) physical processes (internal waves and frontogenesis) concentrated plankton into patches and impacted anchoveta habitat suitability and spatial distribution. Inside the zooplankton patches, conditions were favourable for anchovy so the 'depth' of the BMF basins was high (Fig. 9). During the night, anchoveta cluster size corresponded to zooplankton patch size, suggesting that the size of fish clusters depends on the environment rather than on the total abundance of the fish population. On first order apex predators, fishers included, tend to search for fish clusters, rather than individuals or schools, to forage (Bertrand et al., 2004b; Fréon and Misund, 1999). Surface zooplankton patches were not observed during the day because zooplankton migrated below the oxycline and were less affected by the physical processes. Solitary internal waves (Fig. 3) modified the habitat by deepening the mixed layer and concentrating particulate matter (Haury et al., 1978; Mann and Lazier, 1996; Pineda, 1999; Francks, 2005). Anchoveta habitat suitability was increased by internal waves for at least two reasons. First, solitary internal waves create convergences that concentrate prey above the oxycline, which was particularly important during the day when most zooplankton would otherwise be distributed below the oxycline. Secondly, they increased the available habitat by deepening the oxycline allowing anchoveta to form larger and more elongated (vertically) schools (Fig. 3b).

4.3. Synthesis

We linked levels of fish aggregation (schools, clusters, layers), on a diel basis, to different oceanographic and biological features such as upwelling, zooplankton patches, solitary internal waves, and predators. Based on the observations reported here and published literature we propose a conceptual view of the relative importance of social behaviour and environmental (biotic and abiotic) processes on the spatial distribution of anchoveta. Our ecological space has two *y*-axis; one based on self-organization (social behaviour), and the other based on the environment processes. The importance of the axis to the patterns of fish aggregation depends on spatial scale (Fig. 10). At scales from the individual (10s cm), to the nucleus (m), which are very high density patches inside fish schools that are small enough to allow quasi-instantaneous communication on predator presence, change of direction (Gerlotto and Paramo, 2003), to the school (10s m), social behaviour (e.g. the need to school) drives spatial organization (Fig. 10). At this scale, individual based models, in which individual action is governed by the actions of the individual's immediate neighbours, produce realistic schools (Huth and Wissel, 1994; Couzin and Krause, 2003; Grimm et al., 2005), indicating that inter-individual interactions are crucial. At the school scale or below, social interactions with neighbours (which produce collective structures, e.g. schools, through self organization) are the first priority for an individual. For gregarious fish, the school is "an essential life unit in which fish feed, breed, rest, and flee" (Aoki, 1980).

School size, shape, and location depends (i) on the local habitat characteristics, in particular the presence of prey and their distribution (e.g. Nøttestad et al., 1996; Mackinson et al., 1999; Bertrand et al., 2006), physical forces, like the presence of strong vertical gradients in oxygen (or other "fronts"), or the presence of predators (e.g. Axelsen et al., 2001; Nøttestad et al. 2004; Gerlotto et al., 2006), and (ii) on behaviour related to physiological needs, for instance reproduction in the presence of predators (e.g. Axelsen et al., 2000). At scales larger than the school, environmental forces (from physics to organisms, see Bertrand et al., 2008) are the main driver of fish distribution (Fig. 10). Cluster size depends on submesoscale physical features (e.g. upwelling plumes, eddies) that shape the distribution of zooplankton patches (given that there is motivation for feeding). If the size of the fish cluster depends directly on the physical structures, the number and the internal density of clusters may be more related to intrinsic populational aspects such as total abundance. The size and distribution of larger aggregative units, such as the cluster of clusters, or fish stocks are determined by mesoscale (~100 km) physical features increasing and concentrating productivity such as upwelling cells (high abundance of anchovy in the upwelling cell in our case). Finally, the level of the fish population depends on large scale basin-wide conditions favourable or unfavourable to anchoveta (Chavez et al., 2003) that manifest themselves locally in the physical area occupied by the upwelled cold coastal waters (Swartzman et al., 2008).

Recent advances in space-based real time sensors, high performance computing, robust ecosystem theory, and very high-resolution coupled physical–biological models (e.g. ROMS, Penven et al., 2005) now permit relating the different scales of fish population dynamics over a broad range of scales and make possible operational forecasts of fish availability. Accurate and timely forecasts can provide the information needed to maintain long-term sustainability of fish stocks and protect the ecosystem of which the fish are an integral part, while maximizing social and economic benefits and preventing wasteful overinvestment of economic resources. This new power has been won by hard earned advances in technology and science. Previously, forecasting of how environmental variability and fishing pressure affected fish stocks and their ecosystem was impossible because we lacked efficient, high-resolution ocean observing systems to provide the data for assimilation into operational physical–biological models and final-

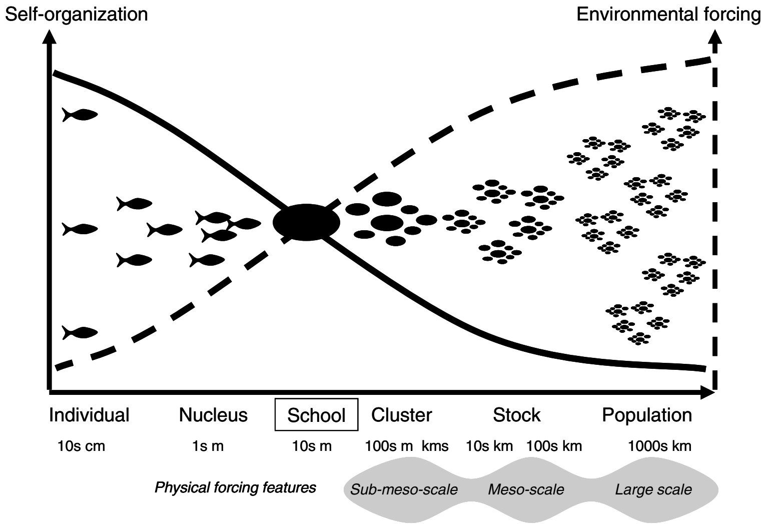

Fig. 10. A conceptual model describing the relative importance of factors regulating aggregation of gregarious fish as a function of scale. There are two *y*-axis one based on self-organization, the other on environmental forcing. The importance of these on fish distribution depends on the spatial scale. At smaller scales, self organization mechanisms are likely to be dominant; at larger-scales adaptation and response to the environment are more important.

ly the ecosystem theory to relate physical forcing all the way from phytoplankton to fish. The conceptual ecosystem models presented in this paper may provide the final links.

Acknowledgments

The authors sincerely thank the Peruvian Marine Research Institute (IMARPE) for the data for this work as well as to Captain Erik Salazar and crew of RV Olaya for their patience and support. We are grateful to Frédéric Ménard for determinant help in wavelet processing. We warmly thank Tim Pennington for very valuable editing work and comments on the manuscript. This work is a contribution of the Research Unit 'Eco Up' UR097, and of the interdepartmental Thematic Action 'Humboldt Current system' from IRD, and of the Study Group 'CARDUMEN' from IMARPE. This work was supported in part by the US National Science Foundation in a grant number NSF0075 to one of the authors (S.B.).

References

Arias-Schereiber, M., 2003. Prey spectrum and feeding behaviour of two sympatric pinnipeds (*Arctocephalus australis* and *Otaria flavescens*) in relation to the 1997–1998 ENSO in southern Peru. M.Sc. Thesis, Faculty for Biology and Chemistry, University of Bremen, Germany.

Arntz, W.E., Fahrbach, E., 1996. El Niño: Experimento Climático de la Naturaleza. Fondo de Cultura Económica, Mexico City (in Spanish).

Aoki, I., 1980. An analysis of the schooling behavior of fish: internal organisation and communication process. Bulletin of the Oceanic Research Institute of the University of Tokyo 12, 1–65.

Axelsen, B.E., Nøttestad, L., Fernö, A., Johannessen, A., Misund, O.A., 2000. 'Await' in the pelagic: dynamic trade-off between reproduction and survival within a herring school splitting vertically during spawning. Marine Ecology Progress Series 205, 259–269.

Axelsen, B.E., Anker-Nilssen, T., Fossum, P., Kvamme, C., Nøttestad, L., 2001. Pretty patterns but a simple strategy: predator–prey interactions between juvenile herring and Atlantic puffins observed with multibeam sonar. Canadian Journal of Zoology 79, 1586–1596.

Azzali, M., Buracchi, G., Conti, S., Gambetti, S., Luna, M., 1985. Relationship between the forms of pelagic fish distribution and nictemeral periods. A tentative model of behaviour. Oebalia 11, 471–488.

Bertrand, A., Barbieri, M.A., Gerlotto, F., Leiva, F., Córdova, J., 2006. Determinism and plasticity of fish schooling behaviour: the example of the South Pacific jack mackerel (*Trachurus murphyi*). Marine Ecology Progress Series 311, 145–156.

Bertrand, A., Segura, M., Gutierrez, M., Vasquez, L., 2004a. From small-scale habitat loopholes to decadal cycles: a habitat-based hypothesis explaining fluctuation in pelagic fish populations off Peru. Fish and Fisheries 5, 296–316.

Bertrand, S., Díaz, E., Ñiquen, M., 2004b. Interactions between fish and fisher's spatial distribution and behaviour: an empirical study of the anchoveta (*Engraulis ringens*) fishery of Peru. ICES Journal of Marine Science 61, 1127–1136.

Bertrand, S., Dewitte, B., Tam, J., Díaz, E., Bertrand A., 2008. Spatial re-organisations in the coastal Humboldt Current system under oceanic climate forcing: portraying contrasted ecological scenarios from physics to fishers. Progress in Oceanography, doi:10.1016/j.pocean.2008.10.017.

Camazine, S., Deneubourg, J.L., Franks, N.R., Sneyd, J., Theraulaz, G., Bonabeau, E., 2001. Self-Organization in Biological Systems. Princeton University Press, Princeton, NJ, USA.

Cardinale, M., Casini, M., Arrhenius, F., Håkansson, N., 2003. Diel spatial distribution and feeding activity of herring (*Clupea harengus*) and sprat (*Sprattus sprattus*) in the Baltic Sea. Aquatic Living Resources 16, 283–292.

Carr, M.-E., Kearns, E.J., 2003. Production regimes in four Eastern Boundary Current systems. Deep Sea Research II 50, 3199–3221.

Carritt, D.E., Carpenter, J.H., 1966. Comparison and evaluation of currently employed modifications of the Winkler method for determining dissolved oxygen in seawater; a NASCD report. Journal of Marine Research 24, 286–318.

Cazelles, B., Chavez, M., Constantin de Magny, G., Géguan, J.-F., Hales, S., 2007. Time-dependent spectral analysis of epidemiological time-series with wavelets. Journal of the Royal Society Interface. doi:10.1098/rsif.2007.0212.

Cazelles, B., Stone, L., 2003. Detection of imperfect population synchrony in an uncertain world. Journal of Animal Ecology 72, 953–968.

Chaigneau, A., Gizolme, A., Grados, C., 2008. Mesoscale eddies off Peru in altimeter records: identification algorithms and eddy spatio-temporal patterns. Progress in Oceanography 79, 106–119.

Chaigneau, A., Pizarro, O., 2005a. Surface circulation and fronts of the South Pacific Ocean, east of 120°W. Geophysical Research Letters 32, L08605. doi:10.1029/2004GL022070.

Chaigneau, A., Pizarro, O., 2005b. Eddy characteristics in the eastern South Pacific. Journal of Geophysical Research: Oceans 110, C06005. doi:10.1029/2004JC002815.

Chavez, F.P., Ryan, J., Lluch-Cota, E., Niquen, M., 2003. From anchovies to sardines and back: multidecadal change in the Pacific Ocean. Science 299, 217–221.

Clark, W.G., 1977. The lessons of the Peruvian anchoveta fishery. California Cooperative Oceanic Fisheries Investigations 19, 57–63.

Clarke, A.J., 1983. The reflection of equatorial waves from oceanic boundaries. Journal of Physical Oceanography 13, 1183–1207.

Cotté, C., Simard, Y., 2005. Formation of dense krill patches under tidal forcing at whale feeding hot spots in the St. Lawrence Estuary. Marine Ecology Progress Series 288, 199–210.

Couzin, I.D., Krause, J., 2003. Self-organization and collective behavior in vertebrates. Advances in the Study of Behavior 32, 1–75.

Croll, D.A., Marinovic, B., Benson, S., Chavez, F.P., Black, N., Ternullo, R., Tershy, B.R., 2005. From wind to whales: trophic links in a coastal upwelling system. Marine Ecology Progress Series 289, 117–130.

David, P.M., Chapron, B., 1990. Underwater acoustic signal analysis with wavelet process. The Journal of the Acoustical Society of America 87, 2118–2121.

Dommasnes, A., Rey, F., Røttingen, I., 1994. Reduced oxygen concentration in herring wintering areas ICES. Journal of Marine Science 51, 63–69.

Efron, B., Tibshirani, R.J., 1993. An Introduction to the Bootstrap. Chapman & Hall, London, UK.

Espinoza, P., Bertrand, A., 2008. Revising Peruvian anchovy (*Engraulis ringens*) trophic niche and ecological role reveals its plasticity and provides a new vision of the Humboldt Current system. Progress in Oceanography 79, 215–227.

Farmer, D., Armi, L., 1999. The generation and trapping of internal solitary waves over topography. Science 283, 188–190.

Foote, K.G., Knudsen, H.P., Vestnes, D.N., MacLennan, D.N., Simmonds, E.J., 1987. Calibration of acoustic instruments for fish density estimation: a practical guide. ICES Cooperative Research Report No. 144.

Fossheim, M., Zhou, M., Tande, K.S., Pedersen, O.-P., Zhu, Y., Edvardsen, A., 2005. Interactions between biological and environmental structures along the coast of northern Norway. Marine Ecology Progress Series 300, 147–158.

Francks, P.J.S., 2005. Plankton patchiness, turbulent transport and spatial spectra. Marine Ecology Progress Series 294, 295–309.

Fréon, P., Cury, P., Shannon, L., Roy, C., 2005. Sustainable exploitation of small pelagic fish stocks challenged by environmental and ecosystem changes: a review. Bulletin of Marine Science 76, 385–462.

Fréon, P., Gerlotto, F., Soria, M., 1996. Diel variability of school structure with special reference to transition periods. ICES Journal of Marine Science 53, 459–464.

Fréon, P., Misund, O.A., 1999. Dynamics of Pelagic Fish Distribution and Behaviour: Effects on Fisheries and Stock Assessment. Blackwell Science, Oxon, UK.

Friederich, G., Ledesma, J., Ulloa, O., Chavez, F., 2008. Air-sea carbon dioxide fluxes in the coastal southeastern tropical Pacific. Progress in Oceanography. doi:10.1016/j.pocean.2008.10.001.

Frontier, S., 1987. Applications of fractal theory to ecology. In: Legendre, P., Legendre, L. (Eds.), Developments in Numerical Ecology. Springer-Verlag, Berlin, pp. 335–378.

Gerlotto, F., Bertrand, S., Bez, N., Gutiérrez, M., 2006. Waves of agitation inside anchovy schools observed with multibeam sonar: a way to transmit information in response to predation. ICES Journal of Marine Science 63, 1405–1417.

Gerlotto, F., Castillo, J., Saavedra, A., Barbieri, M.A., Espejo, M., Cotel, P., 2004. Three-dimensional structure and avoidance behaviour of anchovy and common sardine schools in central southern Chile. ICES Journal of Marine Science 61, 1112–1120.

Gerlotto, F., Paramo, J., 2003. The three-dimensional morphology and internal structure of clupeid schools as observed using vertical scanning multibeam sonar. Aquatic Living Resources 16, 113–122.

Gerlotto, F., Soria, M., Fréon, P., 1999. From two dimensions to three: the use of multibeam sonar for a new approach in fisheries acoustics. Canadian Journal of Fisheries and Aquatic Sciences 56, 6–12.

Grimm, V., Revilla, E., Berger, U., Jeltsch, F., Mooij, W.M., Railsback, S.F., Thulke, H.H., Weiner, J., Wiegand, T., DeAngelis, D.L., 2005. Pattern-oriented modeling of agent-based complex systems: lessons from ecology. Science 310, 987–991.

Gutiérrez, M., Ramirez, A., Bertrand, S., Moron, O., Bertrand, A., 2008. Ecological niches, patterns of distribution and areas of overlap of the squat lobster 'munida' (*Pleuroncodes monodon*) and anchoveta (*Engraulis ringens*) off Peru. Progress in Oceanography 79, 256–263.

Gutiérrez, M., Swartzman, G., Bertrand, A., Bertrand, S., 2007. Anchovy and sardine spatial dynamics and aggregation patterns in the Humboldt Current ecosystem, Peru, from 1983 to 2003. Fisheries Oceanography 16, 155–168.

Hamitouche-Djabou, C., Togni, S., Lecornu, L., Derrode, S., 1999. SBI Viewer: 3D fish schools and sea bottom analysis and visualisation software. User's Guide, AVITIS Contract FAIR CT 96-1717, Development release 3–10 June, 1999 Dpt ITI, ENST-Bretagne, Brest, France.

Hastie, T., Tibshirani, R., 1990. Generalized Additive Models. Chapman & Hall, London, UK.

Haury, L.R., McGowan, J.A., Wiebe, P.H., 1978. Patterns and processes in the time–space scales of plankton distributions. In: Steele, J.H. (Ed.), Spatial Pattern in Plankton Communities. Plenium, New York, USA, pp. 277–327.

Holm-Hansen, A., Lorenzen, O., Colmes, R., Strickland, J., 1965. Fluorometric determination of chlorophyll. Journal du Conseil Permanent International Pour l'Exploration de la Mer 30, 3–15.

Hormazabal, S., Shaffer, G., Leth, O., 2004. Coastal transition zone off Chile. Journal of Geophysical Research: Oceans 109, C01021. doi:10.1029/2003JC001956.

Huth, A., Wissel, C., 1994. The simulation of fish schools in comparison with experimental data. Ecological Modelling 75–76, 135–145.

Jancke, J., Goya, E., 1998. Dietas del guanay y el piquero peruano indicadoras de abundancia y distribución de anchoveta. Boletín del Instituto del Mar del Perú 17, 15–33 (in Spanish, with English abstract).

Kramer, D., Kalin, M.J., Stevens, E.G., Thrailkill, J.R., Zweifel, J.R., 1972. Collecting and processing data on fish eggs and larvae in the California Current region. NOAA Technical Report NMFS Circ-370.

Lavaniegos, B.E., Jiménez-Pérez, L.C., Gaxiola-Castro, G., 2002. Plankton response to El Niño 1997–1998 and La Niña 1999 in the southern region of the California Current. Progress in Oceanography 54, 33–58.

MacCall, A.D., 1990. Dynamic Geography of Marine Fish Populations: Books in Recruitment Fishery Oceanography. University of Washington Press, Washington.

Mackinson, S., Nøttestad, L., Guénette, S., Pitcher, T., Misund, O.A., Ferno, A., 1999. Cross-scale observations on distribution and behavioural dynamics of ocean feeding Norwegian spring-spawning herring (*Clupea harengus* L.). ICES Journal of Marine Science 56, 613–626.

MacLennan, D.N., Fernandes, P.G., Dalen, J., 2002. A consistent approach to definitions and symbols in fisheries acoustics. ICES Journal of Marine Science 59, 365–369.

Mann, K.H., Lazier, J.R.N., 1996. Dynamics of Marine Ecosystems. Blackwell Science, Oxford, UK.

McFarland, W.N., Moss, S.A., 1967. Internal behavior in fish schools. Science 156, 260–262.

Ménard, F., Marsac, F., Bellier, E., Cazelles, B., 2007. Climatic oscillations and tuna catch rates in the Indian Ocean: a wavelet approach to time series analysis. Fisheries Oceanography 16, 95–104.

Morón, O., 2000. Características del ambiente marino frente a la costa peruana. Boletín del Instituto del Mar del Perú 19, 179–204 (in Spanish, with English abstract).

Nøttestad, L., Aksland, M., Beltestad, A., Fernö, A., Johannessen, A., Misund, O.A., 1996. Schooling dynamics of Norwegian spring spawning herring (*Clupea harengus* L.) in a coastal spawning area. Sarsia 80, 277–284.

Nøttestad, L., Fernö, A., Misund, O.A., Vabø, R., 2004. Understanding herring behaviour: linking individual decisions, school patterns, and population distribution. In: Skjoldal, H.R. (Ed.), The Norwegian Sea Ecosystem. Tapir Academic Press, Trondheim, Norway, pp. 227–262.

Pauly, D., Muck, P., Mendo, J., Tsukayama, I., 1989. The Peruvian upwelling ecosystem: dynamics and interactions. In: ICLARM Conference Proceedings, vol. 18.

Penven, P., Echevin, V., Pasapera, J., Colas, F., Tam, J., 2005. Average circulation, seasonal cycle and mesoscale dynamics of the Peru Current System: a modeling approach. Journal of Geophysical Research 110, C10021. doi:10.1029/2005JC002945.

Petitgas, P., Levenez, J.-J., 1996. Spatial organisation of pelagic fish: echogram structure, spatio-temporal condition, and biomass in Senegalese waters. ICES Journal of Marine Science 53, 147–153.

Petitgas, P., Massé, J., Beillois, P., Lebarbier, E., Le Cann, A., 2003. Sampling variance of species identification in fisheries-acoustic surveys based on automated procedures associating acoustic images and trawl hauls. ICES Journal of Marine Research 60, 437–445.

Pineda, J., 1999. Circulation and larval distribution in internal tidal bore warm fronts. Limnology Oceanography 44, 1400–1414.

Reid, D., 2000. Report on echo trace classification. ICES Cooperative Research Report No. 238.

Robinson, C.J., Arenas, F.V., Gomez, G.J., 1995. Diel vertical and offshore–inshore movements of anchovies off the central coast of Baja California. Journal of Fish Biology 47, 877–892.

Rogachev, K.A., Salomatin, A.S., Carmack, E.C., 1996. Concentration of pelagic organisms at mesoscale fronts in the western subarctic Pacific: small fish on long waves. Fisheries Oceanography 5, 153–162.

Russel, R.W., Hunt, G.L., Coyle, K.O., Cooney, R.T., 1992. Foraging in a fractal environment: spatial patterns in a marine predator-prey system. Landscape Ecology 7, 195–209.

Seki, M.P., Polovina, J.J., Kobayashi, D.R., Bidigare, R.R., Mitchum, G.T., 2002. An oceanographic characterization of swordfish (*Xiphias gladius*) longline fishing grounds in the springtime subtropical North Pacific. Fisheries Oceanography 11, 251–266.

Sifeddine, A., Gutierrez, D., Ortlieb, L., Boucher, H., Velazco, F., Field, D., Vargas, G., Boussafir, M., Salvatteci, R., Ferreira, V., García, M., Valdés, J., Caquineau, S., Mandeng Yogo, M., Cetin, F., Solis, J., Soler, P., Baumgartner, T., 2008. Laminated sediments off the Central Peruvian Coast record changes in terrestrial runoff, water mass oxygenation and upwelling productivity over recent centuries. Progress in Oceanography 79, 190–197.

Soria, M., 1997. Le banc de poissons: expression d'une motivation sociale ou comportement collectif d'un groupe auto-organisé? In: Théraulaz, G., Spitz, F. (Eds.), Auto-Organisation et Comportement. Hermes, Paris, pp. 141–156.

Sutherland, W.J., 1996. Ecological Census Techniques: A Handbook. Cambridge University Press, Cambridge.

Swartzman, G., Bertrand, A., Gutiérrez, M., Bertrand, S., Vasquez, L., 2008. The relationship of anchovy and sardine to water masses in the Peruvian Humboldt Current System from 1983 to 2005. Progress in Oceanography 79, 228–237.

Thomas, A., 1999. Seasonal distributions of satellite-measured phytoplankton pigment concentration along the Chilean coast. Journal of Geophysical Research: Oceans 104, C11. doi:10.1029/1999JC900171.

Torrence, C., Compo, G.P., 1998. A practical guide to wavelet analysis. Bulletin of the American Meteorological Society 79, 61–78.

Valdés, J., Ortlieb, L., Marinovic, L., Gutiérrez, D., Vargas, D., Sifeddine, A., 2008. A 250 years sediment record of sardine and anchovy scale deposition in a coastal oxygen deficient environment of the Humboldt ecosystem (Mejillones Bay, 23°S, Northern Chile). Progress in Oceanography 79, 198–207.

Valdivia, J.E., 1978. The Anchoveta and El Niño. Rapports et Procès-verbaux des Réunions du Conseil International Pour l'Exploration de la Mer 173, 196–202.

Weill, A., Scalabrin, C., Diner, N., 1993. MOVIES-B: an acoustic detection description software. Application to shoal species classification. Aquatic Living Resources 6, 255–267.

Progress in Oceanography 79 (2008) 278–289

Contents lists available at ScienceDirect

Progress in Oceanography

journal homepage: www.elsevier.com/locate/pocean

Impacts of Kelvin wave forcing in the Peru Humboldt Current system: Scenarios of spatial reorganizations from physics to fishers

Sophie Bertrand [a,b,c,*], Boris Dewitte [d,c], Jorge Tam [c], Erich Díaz [c], Arnaud Bertrand [b,c]

[a] *University of Washington, School of Fisheries, Box 355640, Seattle, WA 98195, USA*
[b] *IRD, Centre de Recherche Halieutique Méditerranéenne et Tropicale, Avenue Jean Monnet, BP 171, 34203 Sète Cedex, France*
[c] *Instituto del Mar del Perú, CIMOBP, Esquina Gamarra y Gral. Valle s/n, Apartado 22, Callao, Lima, Peru*
[d] *IRD, UMR LEGOS, 14 Av. Edouard Belin, 31401 Toulouse Cedex 4, France*

ARTICLE INFO

Article history:
Accepted 14 October 2008
Available online 21 October 2008

Keywords:
Climate forcing
Ecological scenarios
Fish distribution
Fishers' movements
Kelvin waves
Peru Humboldt Current system

ABSTRACT

Because climate change challenges the sustainability of important fish populations and the fisheries they support, we need to understand how large scale climatic forcing affects the functioning of marine ecosystems. In the Humboldt Current system (HCS), a main driver of climatic variability is coastally-trapped Kelvin waves (KWs), themselves originating as oceanic equatorial KWs. Here we (i) describe the spatial reorganizations of living organisms in the Humboldt coastal system as affected by oceanic KWs forcing, (ii) quantify the strength of the interactions between the physical and biological component dynamics of the system, (iii) formulate hypotheses on the processes which drive the redistributions of the organisms, and (iv) build scenarios of space occupation in the HCS under varying KW forcing. To address these questions we explore, through bivariate lagged correlations and multivariate statistics, the relationships between time series of oceanic KW amplitude (TAO mooring data and model-resolved baroclinic modes) and coastal Peruvian oceanographic data (SST, coastal upwelled waters extent), anchoveta spatial distribution (mean distance to the coast, spatial concentration of the biomass, mean depth of the schools), and fishing fleet statistics (trip duration, searching duration, number of fishing sets and catch per trip, features of the foraging trajectory as observed by satellite vessel monitoring system). Data sets span all or part of January 1983 to September 2006. The results show that the effects of oceanic KW forcing are significant in all the components of the coastal ecosystem, from oceanography to the behaviour of the top predators – fishers. This result provides evidence for a bottom-up transfer of the behaviours and spatial stucturing through the ecosystem. We propose that contrasting scenarios develop during the passage of upwelling versus downwelling KWs. From a predictive point of view, we show that KW amplitudes observed in the mid-Pacific can be used to forecast which system state will dominate the HCS over the next 2–6 months. Such predictions should be integrated in the Peruvian adaptive fishery management.

1. Introduction

Because climate change challenges the sustainability of important fish populations and the fisheries they support, we need to understand how large scale climate/ocean fluctuations affect the functioning of marine ecosystems (Stenseth et al., 2002; Edwards and Richardson, 2004; Worm and Myers, 2004; Burkett et al., 2005; Perry et al., 2005; Lehodey et al., 2006). The Humboldt Current upwelling system (HCS) provides an ideal opportunity to examine the effects of remote climate forcing on a coastal ecosystem as it is influenced by well-described multi-scale climatic forcing (seasonal, inter annual and decadal as well as local, regional and global dynamics, e.g. Chavez et al., 2003). Moreover, owing to the economic importance of the Peruvian anchovy or anchoveta (*Engraulis ringens*) fishery, the world largest monospecific fishery, many components of the ecosystem have been monitored for a relatively long period.

Understanding the response of marine ecosystems to large scale forcing is a difficult task, as climate variability has a stochastic component and biological responses are often non-linear (Hsieh et al., 2005). Such complexity can produce apparently chaotic dynamics at the regional scale, and the responses or evolution of regional systems can appear unpredictable (i.e. deterministic equations cannot describe or predict the succession of states). Still, system states having a high probability of occurrence, or scenarios (Link et al., 2002, use indifferently 'state', 'regime' and 'stanza'), can be statistically characterized (e.g. Knowlton, 2004).

One of the main sources of variability in the Humboldt Current system derives from the passage of coastally-trapped Kelvin waves

---

[*] Corresponding author. Address: IRD, Teruel 357, Miraflores, Casilla 18-1209, Lima 18, Peru. Tel.: +51 1 441 32 23.
E-mail address: Sophie.Bertrand@ird.fr (S. Bertrand).

doi:10.1016/j.pocean.2008.10.017

(KWs), themselves originating in the western and central Pacific as oceanic equatorial KWs (Pizarro et al., 2001). Equatorial KWs are large-amplitude, long-period waves which travel eastwards within the ocean along the equatorial wave guide (Delcroix et al., 2000). They are mostly forced in the central equatorial Pacific by variations in the wind and propagate at 1–3 m s^{-1}. According to the type of wind anomaly (easterlies or westerlies), an equatorial KW can rise (upwell) or deepen (downwell) the thermocline (often 10s of meters) and the sea surface height (centimeters). Because the equatorial thermocline is shallow, especially in the eastern Pacific, non-linear processes affect the speed and the vertical structure of the KW while propagating eastward. These changes in the KW properties can be analytically described by changes in the relative contribution to the overall signal of several linear components, the baroclinic modes (Dewitte et al., 1999). They are obtained by a mathematical decomposition of the KW signal and are the solutions of the linearized dynamical equations of movement on the vertical axis (Cane and Sarachick, 1976). Each of the baroclinic modes has distinct characteristics in terms of propagation, phase speed and meridional scale. As the KW propagate eastward, the relative contribution of each baroclinic mode in the global KW signal changes: KW energy projects more on the first baroclinic mode in the central Pacific, and on the third baroclinic mode close to South America coasts. Because the different baroclinic modes have different speeds and meridional scales (higher-order baroclinic modes propagate slower and are smaller in meridional extent), each may explain better the KW impact on different processes in the coastal ecosystem.

When equatorial KWs reach South America, part of their energy is deflected north and south along the coast where it is trapped by the earth's rotation (Coriolis) force, along the continental shelves or slope (Clarke, 1983, 1992). These coastally-trapped KWs impact the vertical structure of the isotherms along the coast and the location of the upwelling front. They also introduce energy for turbulent flow in the coastal ecosystem and are then likely to impact meso-scale activity and then the spatial structuring of many living communities. Downwelling KWs deepen the thermocline, making coastal upwelling 'inefficient' in terms of nutrient enrichment (brings to surface oceanic warm and low nutrient water; Barber and Chavez, 1983) and is associated with warm conditions (an El Niño-like scenario). Conversely, an upwelling KW raises the thermocline and allows coastal upwelling to bring cold and nutrient-rich water towards the surface. As a consequence, the cold coastal water (CCW) domain expands (a La Niña-like scenario).

The response of populations to climate forcing may be multidimensional: e.g. changes in abundance, in physiology of reproduction, in patterns of migration, in spatial distribution, etc. (e.g. Stenseth et al., 2002; Walther et al., 2002). The response in terms of organism abundance — the most commonly used metric — may be complex and delayed, as abundance is an indirect result of many interacting constraints: e.g. physical conditions, prey availability, reproductive success, competition, and others. Geographic distribution or organism movements are population features that can represent more direct responses to physical forcing (e.g. Perry et al., 2005; Bertrand et al., 2005). Climatic forcing primarily affects the physical habitat and, among other effects, may induce passive (plankton) or active (nekton) spatial redistributions of the living communities (Cotté and Simard, 2005; Croll et al., 2005; Fossheim et al., 2005; Bertrand et al., 2008). Patterns of space occupation, whether for individuals or populations (Margalef, 1979), control ecological interactions such as predation, competition and reproduction which, in turn, feed back to population abundance (e.g. Frontier et al., 2004). Analyzing the spatial redistributions of populations in response to climatic forcing may provide a valuable intermediate step towards understanding changes in population abundance (Keitt et al., 2002).

The purpose of this paper is to define ecological scenarios for the Peruvian coastal ecosystem under varying oceanic equatorial KW forcing. To address these questions, we explore through bivariate lagged correlations and multivariate statistics the relationships between a variety of time series of oceanic KW amplitude (TAO mooring data and model-resolved baroclinic modes) and coastal Peruvian oceanographic data (SST, coastal upwelled waters extent), anchoveta spatial distribution (mean distance to the coast, spatial concentration of the biomass, mean depth of the schools), and fishing fleet statistics (trip duration, searching duration, number of fishing sets and catch per trip, features of the foraging trajectory as observed by satellite vessel monitoring system). Data sets span all or part of January 1983 to September 2006. In particular we (i) describe the spatial reorganizations in the coastal HCS as affected by oceanic KWs forcing, (ii) quantify the strength of the interactions between the dynamics of the physical and biological components of the system, (iii) formulate hypotheses on the processes driving the redistributions of the organisms, and (iv) synthesize the scenarios of space occupation in the HCS under varying KWs forcing.

2. Materials and methods

To quantify oceanic KW forcing, Peruvian coastal oceanography, anchoveta distribution and the foraging behaviour of fishermen, we gathered a large variety of field measurements and model outputs (Table 1). The different data sets were collected over different periods, but always between January 1983 and September 2006 (Table 1, Figs. 1 and 2).

2.1. KW forcing

A proxy for Kelvin wave activity in the equatorial Pacific can be observed through the depth of the 20 °C isotherm (D20) as measured by the TAO/TRITON moorings (Tropical Atmosphere/Ocean, http://www.pmel.noaa.gov/tao/data_deliv/deliv.html). D20 is a robust proxy for KW activity; nevertheless the signal contains also a contribution from reflected Rossby wave (generated by the reflection of part of the KW energy when they hit the South America shore). We analyzed the times series provided by the moorings located at 0°N–95°W and 0°N–155°W. The 95°W mooring was chosen as closest to the coast and the HCS. Data were available from January 1983 to September 2006, with some gaps. The 155°W mooring was chosen as representative of the mid-Pacific, closer to the location of the initiation of the KWs. Data were available from August 1991 to September 2006.

Because the different baroclinic modes of each KW may impact different processes in the coastal ecosystem, it is relevant to analyze their respective contribution to coastal ecosystem variability. Following earlier works (Dewitte et al., 1999, 2003), we consider the first three baroclinic modes (referred hereafter as ak1, ak2 and ak3 for the first three baroclinic modes, respectively); these are the most energetic propagating modes. Their contribution to the total KW amplitude can be resolved from observational data (e.g. wind) input into an ocean model either through direct forcing or through assimilation. For this work we used two model output products.

First, we used output from the simple ocean data assimilation reanalysis of ocean climate variability (SODA, Carton et al., 2000). SODA is an ocean reanalysis product that combines observations (historical archive of hydrographical profiles supplemented by ship intake measurements, moored hydrographical observations, and remotely sensed SST and sea level) with an ocean general circulation model (Geophysical Fluid Dynamics Laboratory MOM2 physics). It creates a grid dataset of ocean features (e.g. temperatures,

Table 1
Acronym, description, data type and time series available for each parameter used in the analysis.

Variable acronym	Description	Data type	Time series available
ak1 SODA 85°W ak2 SODA 85°W ak3 SODA 85°W	First, second and third KW baroclinic mode calculated from SODA at 85°W	Ocean model outputs	January 1983–December 2004
$\sum$ak SODA 85°W	Total KW amplitude from SODA at 85°W (sum of the three first baroclinic modes)		
ak1 SODA 160°W ak2 SODA 160°W ak3 SODA 160°W	First, second and third KW baroclinic mode calculated from SODA at 160°W		
$\sum$ak SODA 160°W	Total KW amplitude from SODA at 160°W (sum of the three first baroclinic modes)		
ak1 LM 80°W ak2 LM 80°W ak3 LM 80°W	First, second and third KW baroclinic mode calculated from linear model at 80°W		January 1983–September 2006
$\sum$ak LM 80°W	Total KW amplitude from linear model at 80°W (sum of the three first baroclinic modes)		
ak1 LM 160°W ak2 LM 160°W ak3 LM 160°W	First, second and third KW baroclinic mode calculated from linear model at 160°W		
$\sum$ak LM 160°W	Total KW amplitude from linear model at 160°W (sum of the three first baroclinic modes)		
D20 95°W	20 °C isotherm depth at 95°W and 155°W	TAO moorings	January 1983–September 2006, with gaps
D20 155°W			August 1991–September 2006
SST	Monthly averaged sea surface temperature off Chicama	IMARPE specific sampling	January 1983–September 2006
DC_{CCW}	Mean distance to the coast of the cold coastal waters centroïd	IMARPE acoustic surveys	October 83–December 2005 Discrete data
MSD	Mean schools depth of anchoveta		
DC_{anch}	Anchoveta mean distance to the coast		
ISO	Percentage of positive (anchoveta $s_A > 0$) elementary sampling distance units		
TD	Monthly averaged travel duration	IMARPE observers at sea aboard fishing vessels	December 1995–September 2006 with gaps (fishery closed)
SD	Monthly averaged searching duration		
NFS	Monthly averaged number of fishing sets		
TC	Monthly averaged trip catch		
μ	Sinuosity and diffusion index from random walk modelling	Model output from satellite fishing vessel monitoring system	November 1999–June 2006, with gaps (fishery closed)

ocean salinities, ocean currents) from which the Kelvin wave contribution to the sea level anomaly for the first three baroclinic modes can be derived (see Dewitte et al., 1999 for more details on the method). To cover 1983–2004, we used two SODA reanalysis experiments which differ by the atmospheric forcing used (see Carton and Giese, 2008): the basic reanalysis, SODA1.4.2, spans the 44 year period from 1958 to 2001; a second reanalysis experiment, SODA1.4.3, spans the period of QuikSCAT scatterometer winds from 2000 to 2004. Carton and Giese (2008) have shown that the agreement between the two products over the 2-year overlapping period (2000–2001) is good. We then built composite time series of monthly mean sea level anomaly originating from the first three baroclinic modes (ak1 SODA, ak2 SODA and ak3 SODA), spanning 1983–2004.

Second, the contribution of these three baroclinic modes was derived from linear model (‘LM’; Dewitte et al., 2002) simulations forced by *in situ* (FSU) and satellite-derived (ERS1 and 2 and QuickSCAT) winds to produce time series spanning January 1983-September 2006 (ak1 LM, ak2 LM and ak3 LM). The LM assumptions are less realistic than SODA (it does not include thermocline dynamics), but this model is much less computationally intensive and allows to generate longer time series of baroclinic modes amplitude from wind product only. As a consequence, LM spans the entire time series from January 1983 to September 2006.

2.2. Coastal oceanography

We used two indicators to describe the physical state of the coastal ocean off Peru. First, the monthly averaged sea surface temperature (SST) off Chicama (collected by IMARPE) presents a long and complete time series and was used as a proxy of the average coastal temperature (Gutiérrez et al., 2007). Second, we estimated offshore extent of the cold coastal waters (CCW) resulting from coastal upwelling. Water masses including CCW were defined with an algorithm using temperature, salinity, season and latitude data collected at regular stations during the scientific surveys performed by IMARPE (see next paragraph and Swartzman et al., 2008 for details). We calculated the mean distance to the coast of the CCW centroid (DCccw) and take this distance to estimate the range of extension or width of the CCW.

2.3. Anchoveta distribution

In Peru, annual acoustic surveys of fish population distribution and abundance have been conducted since 1983 by IMARPE. Surveys occupied on/offshore parallel transects averaging 90 nautical miles (167 km) offshore, with inter-transect distance varying between 14 and 16 nautical miles (26–30 km). Acoustic data were collected by Simrad echosounders (EK, EKS, EK400 before 1995, and EY500, EK500 thereafter, except an EK60 was used 2001–2005 in one vessel). Calibration and intercalibration of the echosounders were undertaken before each survey according to Foote et al. (1987). The acoustic nautical area scattering coefficient (s_A), an index of fish abundance, was recorded in each geo-referenced elementary sampling distance unit (ESDU) of 2 n.mi. (1983–1993) or 1 n.mi. (1994–2006). Anchoveta were identified in the acoustic data with trawl samples. From the acoustic data, we extracted for each survey three metrics of anchoveta distribution:

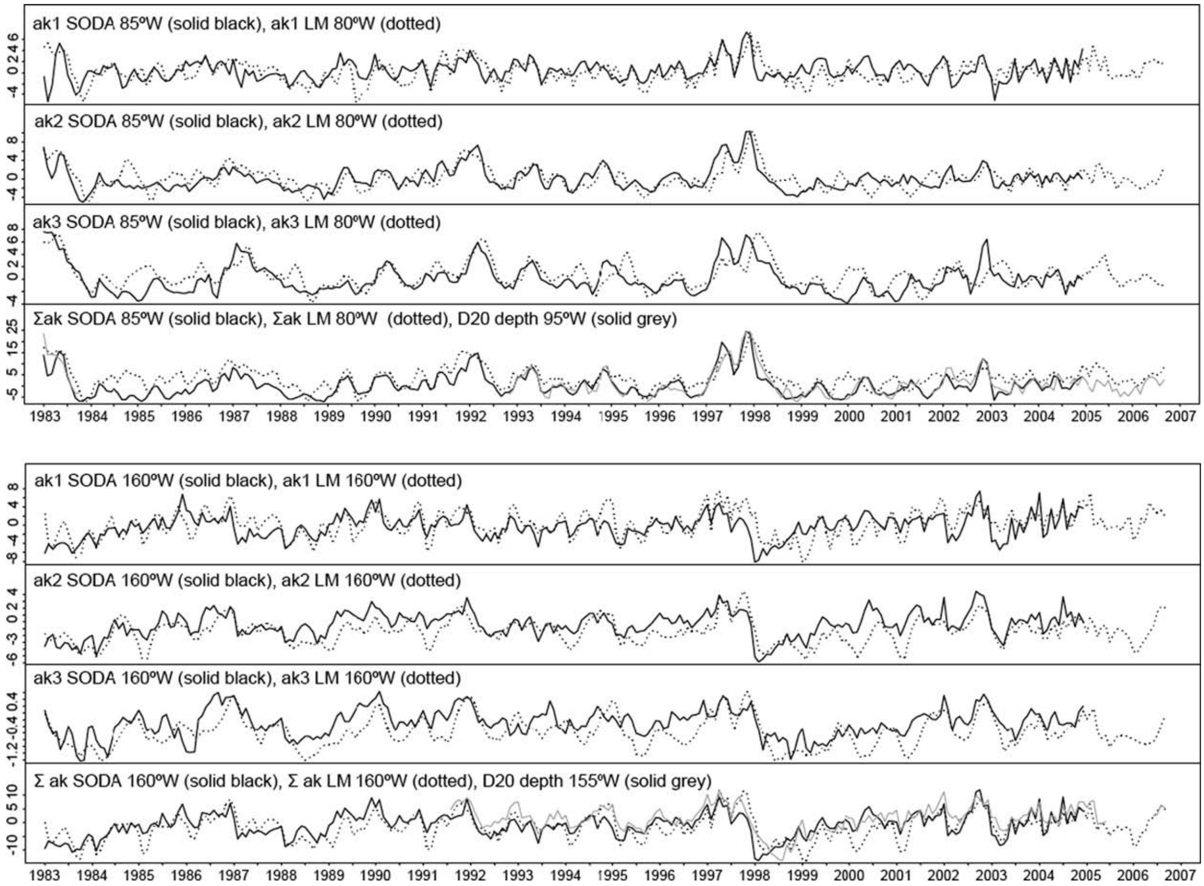

Fig. 1. Time series for the variables describing the Kelvin wave amplitude: first three baroclinic modes (ak1, ak2, ak3) and their sum (∑ak) from SODA and linear model (LM) outputs, and depth of the 20 °C isotherm from TAO moorings (D20).

(i) mean distance to the coast (DCanch; see Swartzman et al., 2008); (ii) an index of spatial occupation (ISO) of fish biomass defined as the percentage of positive (anchoveta $s_A > 0$) ESDU (Bertrand et al., 2004a); and (iii) the mean depth of anchoveta schools (MSD).

2.4. Fishing activity

The description of fishing activity relies on two observation platforms. First we used information collected daily by an onboard IMARPE observers program running since 1996. When the fishery is open, about 25 vessels carry an observer (Bertrand et al., 2004c). Observers record the trip duration (TD), the searching duration (SD), the number of times the net was set (NFS), and the trip catch (TC). These variables, collected for each fishing trip, were averaged by month. Second, we used an index (μ) describing the movements of fishing vessels when foraging for anchoveta (Bertrand et al., 2005, 2007). This index is derived from a Lévy random walk modelling of the fishing trip trajectories as observed by a satellite vessel monitoring system (VMS). This index, whose values range between 1 and 3, describes both the sinuosity and the area explored (diffusion) by a vessel trajectory. When μ is high, the search is close to random, with high sinuosity and low diffusion. In others terms, time allocated to searching and fishing is high and time allocated to steaming is low. When μ is low, the search is close to ballistic or directed, with low sinuosity and high diffusion (Bertrand et al., 2005, 2007). In that case, time allocated to steaming, between fish aggregations, is higher. Data from observers at sea are available from December 1995 to September 2006; data from VMS from November 1999 to September 2006.

2.5. KW impact on coastal ecosystem dynamics: data analysis

We used 18 variables to describe the characteristics of the KWs and their baroclinic modes: (i) the amplitude of baroclinic modes ak1, ak2, ak3, and their sum (∑, showing the global amplitude of the wave and therefore the amplitude of the sea level anomaly) as estimated from SODA at 85°W and 160°W and from LM at 80°W and 160°W, and (ii) D20 at 95°W and 155°W. In addition, 'coastal ecosystem' dynamics were described by 10 variables as defined above: SST, DCccw, MSD, DCanch, ISO, TD, SD, NFS, TC and μ.

2.5.1. Bivariate correlations

The relationships between KW forcing and coastal ecosystem dynamics were explored through two different statistical approaches. First, we used bivariate Pearson correlation tests to quantify the strength of the relationship between each KW baroclinic mode and each coastal ecosystem variable and to identify if these coastal ecosystem variables responded (with delay) to the KW forcing. Each of the coastal ecosystem variables was correlated with 1–4 months lags to SODA at 85°W, LM at 80°W and D20 at 95°W and with 1–6 months lags to SODA and LM at 160°W and D20 at 155°W. Because many variables were only available on a discrete basis (acoustic surveys) and others had a significant number of missing data, no systematic treatment could remove seasonality or autocorrelation. This is not a serious problem for several reasons. First, the raw time series (Figs. 1 and 2) show that, in general, the seasonal cycle is not strong enough to blur lower frequency signals (El Niño 1997–98 event for instance). Second, according to Pyper and Peterman (1998), removing autocorrelation

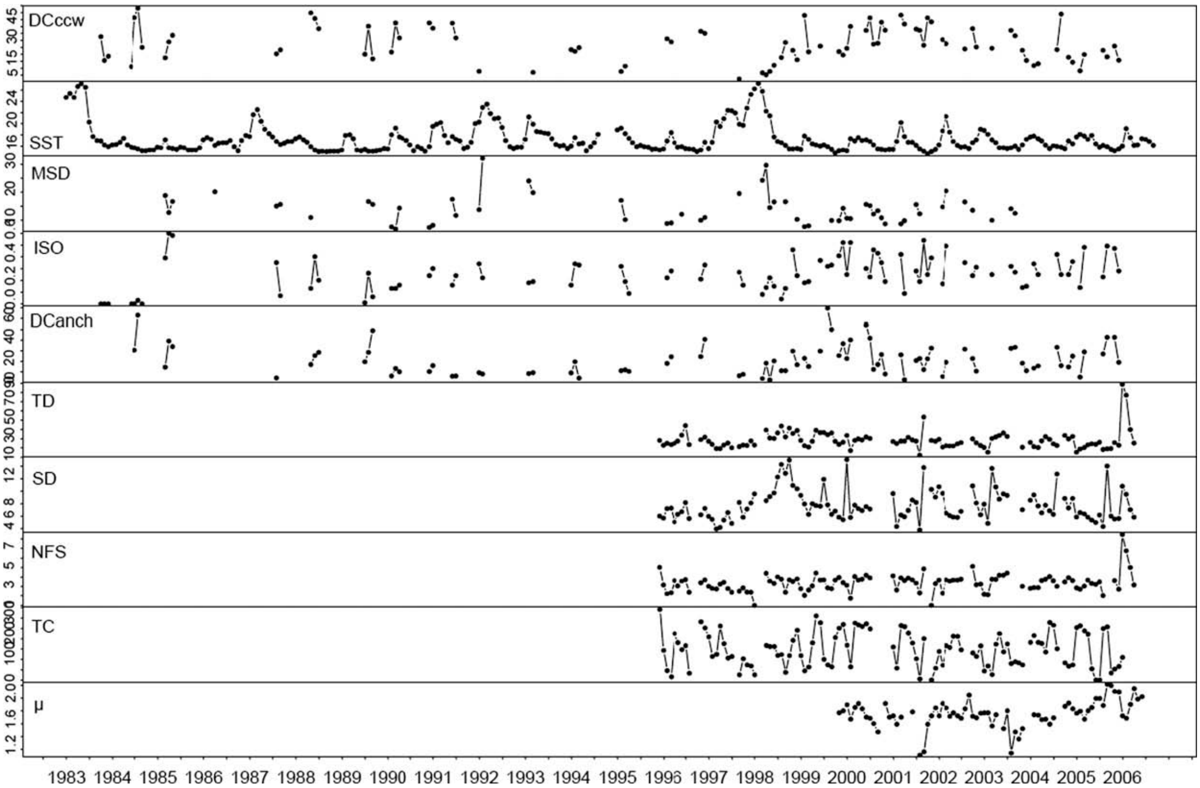

Fig. 2. Time series for the variables describing the Peruvian coastal ecosystem dynamics: mean distance to the coast of the cold coastal waters (DCccw), sea surface temperature off Chicama (SST), mean depth of anchoveta schools (MSD), spatial concentration of anchoveta biomass (ISO), mean distance to the coast of anchoveta (DCanch), mean fishing trip duration (TD), mean searching duration (SD), mean number of fishing sets by trip (NFS), mean catch by trip (TC), and the synthetic index describing fishing trip trajectories (μ).

(for example by ‘prewhitening’, by first differencing) makes implicit assumptions that low-frequency variability is unimportant or may add noise to the time series. The same authors propose an alternative method to account for autocorrelation, which consists of reducing the degrees of freedom with a modified Chelton (1984) method, estimating a lower critical p-value. However, because many of our variables have missing data, we could not estimate the autocorrelation functions required for this method, so we simply considered test results with $p < 0.01$ as significant. As we performed a large number of correlations (1080), we applied the false discovery rate (FDR) multitest correction to avoid inflating Type I error (Benjamini and Hochberg, 1995). For this test, p-values of the n tests are ranked in ascending order. The null hypothesis is rejected for all the tests of rank j inferior to k, k being the rank satisfying:

$$p_k <= k \cdot \alpha \cdot n^{-1} \tag{1}$$

Finally, the overall adequacy of linear modelling (an underlying assumption for a parametric bivariate correlation test) was checked using non-parametric cubic spline smoothers with S-Plus (Insightful Corporation, Seattle, WA, USA).

2.5.2. Multivariate statistical approach

Second, to identify the major scenarios of the coastal ecosystem and to examine its multivariate trajectory in the phase-space of the KW forcing, we completed the investigation through multivariate statistics. We built a principal component analysis (PCA, e.g. Lebart et al., 2000) with the KW forcing variables (ak1, ak2, ak3, SODA 85°W and LM 80°W, D20 at 95°W) as continuous active variables. We projected all the other variables (illustrative) on the factorial space built by the continuous variables to investigate the effect of KW forcing on the coastal ecosystem dynamics. To facilitate the interpretation and to search for non-linear processes, we categorised each illustrative variable in three modalities: low (1), medium (2) and high (3). We finally projected the 285 study months on the factorial space to identify the main scenarios for this ecosystem and to follow the multivariate trajectory of the system through time (Link et al., 2002).

3. Results

Raw time series for the 18 metrics describing the KWs forcing and the 10 metrics describing the coastal ecosystem dynamics are presented in Figs. 1 and 2, respectively. These figures highlight the different time span covered by each of these metrics and clearly show extreme events such as the El Niño of 1997–98.

3.1. Correlations between TAO observations and models outputs

Table 2 synthesises results of correlation tests performed between the data describing the KWs: D20 at 95°W and 155°W, and the corresponding outputs of SODA and LM. SODA output data ($\sum$ak SODA) were globally more correlated to TAO observations (D20; $\rho = 0.90$ and $\rho = 0.80$ for the eastern and western time series, respectively) than LM output ($\sum$ak LM, $\rho = 0.79$ and $\rho = 0.77$ for the eastern and western time series, respectively). This result is consistent with the more realistic assumptions made by SODA on the ocean structure compared with LM (no thermocline dynamics in LM).

Correlation between SODA and LM outputs was approximately the same for the eastern and western time series for ak2 ($\rho = 0.66$ and $\rho = 0.67$, respectively) and ak3 ($\rho = 0.69$ and $\rho = 0.68$, respectively). There was more difference for the first baroclinic mode between the eastern and western time series (ak1;

Table 2
Equatorial KWs forcing, correlations between observations and models outputs: depth of the 20 °C isotherm from TAO moorings (D20), first three baroclinic modes (ak1, ak2, ak3) and their sum ($\sum$) from SODA and the linear model (LM).

Type of test	Variable 1	Variable 2	ρ Pearson	p-Value	df
Correlations between models outputs and observations	$\sum$ak SODA 85°W	D20 depth 95°W	0.90	0	96
	$\sum$ak LM 80°W	D20 depth 95°W	0.79	0	115
	$\sum$ak SODA 160°W	D20 depth 155°W	0.80	0	158
	$\sum$ak LM 160°W	D20 depth 155°W	0.77	0	168
Correlations between SODA outputs and linear model outputs	ak1 SODA 85°W	ak1 LM 80°W	0.48	0	262
	ak2 SODA 85°W	ak2 LM 80°W	0.66	0	262
	ak3 SODA 85°W	ak3 LM 80°W	0.69	0	262
	$\sum$ak SODA 85°W	$\sum$ak LM 80°W	0.76	0	262
	ak1 SODA 160°W	ak1 LM 160°W	0.58	0	262
	ak2 SODA 160°W	ak2 LM 160°W	0.67	0	262
	ak3 SODA 160°W	ak3 LM 160°W	0.68	0	262
	$\sum$ak SODA 160°W	$\sum$ak LM 160°W	0.67	0	262

$\rho = 0.48$ and $\rho = 0.58$ for the eastern and western time series, respectively). The difference between the two models is reduced in the oceanic domain (western time series) where non linear processes are less important. The correlation between SODA and LM was lower for ak1 than for ak2 and ak3. The LM estimate of the first KW baroclinic mode (ak1) also contains over-energetic sub-seasonal variability due to the overestimation of reflection of the Rossby waves at the western boundary (idealized boundaries in LM versus realistic coastline and topography for the SODA model; and simplified formulation for friction in LM).

3.2. Bivariate correlations

Correlations were explored between the 18 metrics describing the KW forcing and the 10 metrics describing the Peruvian coastal ecosystem dynamics, these being lagged either 1–4 or 1–6 months lags for the eastern and western KW forcing, respectively. A total of 414 of 1080 correlations were significant (at $p < 0.01$) after FDR multitest correction. The linear assumption underlying those correlations (see Fig. 3 for examples of bivariate relationships) was acceptable for most of the variables.

Results of significant correlations are synthesised for the eastern KW time series (D20 95°W, SODA 85°W and LM 80°W) in Table 3, and western KW time series (D20 155°W, SODA 160°W and LM 160°W) in Table 4. Only those results corresponding to the baroclinic mode and the time lag maximizing the correlation for each time series are presented. In most cases, significant correlations were also obtained for close lags or modes. Overall trends for each dependent variable are symbolised in the column 3 of Tables 3 and 4.

A downwelling KW near the coast [i.e. a high positive anomaly for the D20 depth at 95°W and high positive anomaly of the sea surface height from SODA (85°W) or LM (80°W)] leads to (Table 3): (i) an increase in SST (max ρ: 1 month lag with D20); (ii) a decrease in the extent of cold coastal waters (DCccw, max ρ: 3 months lag with D20 and $\sum$ak LM); (iii) a deepening of the mean depth of anchoveta schools (MSD, max ρ: 1 month lag with D20); (iv) a reduction in the extent of anchoveta distribution (DCanch, max ρ: no lag with ak3 SODA); (v) an increased spatial concentration of anchoveta biomass (lower ISO, max ρ: 3 months lag with ak3 SODA); (vi) a decrease in the mean fishing trip duration and the time allocated to searching by fishers (TD and SD, max ρ: no lag with ak2 SODA); (vii) a decrease in the mean number of fishing sets per trip (NFS, max ρ: 2 months lag with ak1 SODA); (viii) a decrease in the total catch per trip (TC, max ρ: 3 months lag with ak3 SODA); and (ix) an increase in the sinuosity by fishing trip trajectories (μ, max ρ: 1 month lag with ak2 LM). The strength of these correlations (mean ρ values) generally decreases from the coastal oceanography indices to the fishing activity indices, probably illustrating the increasing complexity or indirect nature relations between the physical forcing and the impacted processes. The trends obtained under an upwelling KW forcing are symmetrically opposite.

A downwelling KW detected far from the coast (155–160°W) leads to similar trends at the coast (85–95°W) but with longer lags (Table 4). The only difference in the overall trends is a decrease in spatial concentration of anchoveta (ISO positive). This result should be considered with caution because only one correlation was significant for ISO. As for the eastern time series, the situation is symmetrically opposite under an upwelling KW forcing.

3.3. Multivariate statistics

The first two factors of the PCA built with ak1, ak2, ak3 from SODA at 85° W and from LM at 80°W and D20 depth from TAO at 95° W represent 63.7% and 12.9% of the total variance, respectively (Fig. 4a). The first factor can be interpreted as a global descriptor of the KW signal and sets the warm events (left panel of the multifactorial plane corresponds to downwelling KWs associated with elevated sea surface and deepened thermocline) against the cold events (right panel of the multifactorial plane corresponds to upwelling KWs associated with reduced sea level and shallowed thermocline). The second factor, which explains much less variance than factor 1, sets mainly the baroclinic modes of higher order (ak3) against the ones of lower order (ak1).

The projections of the modalities of the 10 variables describing the dynamics in the Peruvian coastal ecosystem on this space (Fig. 4b; categorised in three modalities, with time lags maximizing their coordinates on the first factor) shows generally similar patterns to those described by bivariate correlations (Tables 3 and 4), with slightly different lag periods. A warm event, characterized by a downwelling KW (left panel of the multifactorial space) is associated with: (i) an increased SST (modality 3, 1 month lag); (ii) a lower mean distance to the coast of the coastal cold water (CCW; modality 1, 3 months lag); (iii) a increased mean school depth (MSD, modality 3, 3 months lag); (iv) a reduced mean distance to the coast of anchoveta (DCanch, modality 1, no lag); (v) an increased spatial concentration of the fish biomass (ISO, modality 1, 1 month lag); (vi) low fishing trip duration (TD, modalities 1 and 2, no lag); (vii) low searching duration (SD, modalities 1 and 2, 1 month lag); (viii) low number of fishing sets (NFS, modality 1, 1 month lag); (ix) low total catches (TC, modalities 1 and 2, 3 months lag); and (x) fishing trip trajectories characterized by higher sinuosity and lower diffusion (μ, modalities 2 and 3, no month lag). The situation for a cold event, characterized by an upwelling KW forcing, is symmetrically opposite.

The projection of the 285 study months on this multivariate space shows the ecosystem trajectory in the phase-space of the oceanic KW forcing (Fig. 5). A main cloud of points is projected on the central-right part of the first factorial plane and represents the dominant 'cold' ecological scenario where the Peruvian ecosystem has mainly laid for the study period. Apart from this cloud a series of isolated points lie on the left part of the factorial plane. These represent El Niño warm extreme events. When these points are linked through their succession in time (Fig. 5), the trajectories over three El Niño's: 1982–83, 1991–92, 1997–98) are revealed.

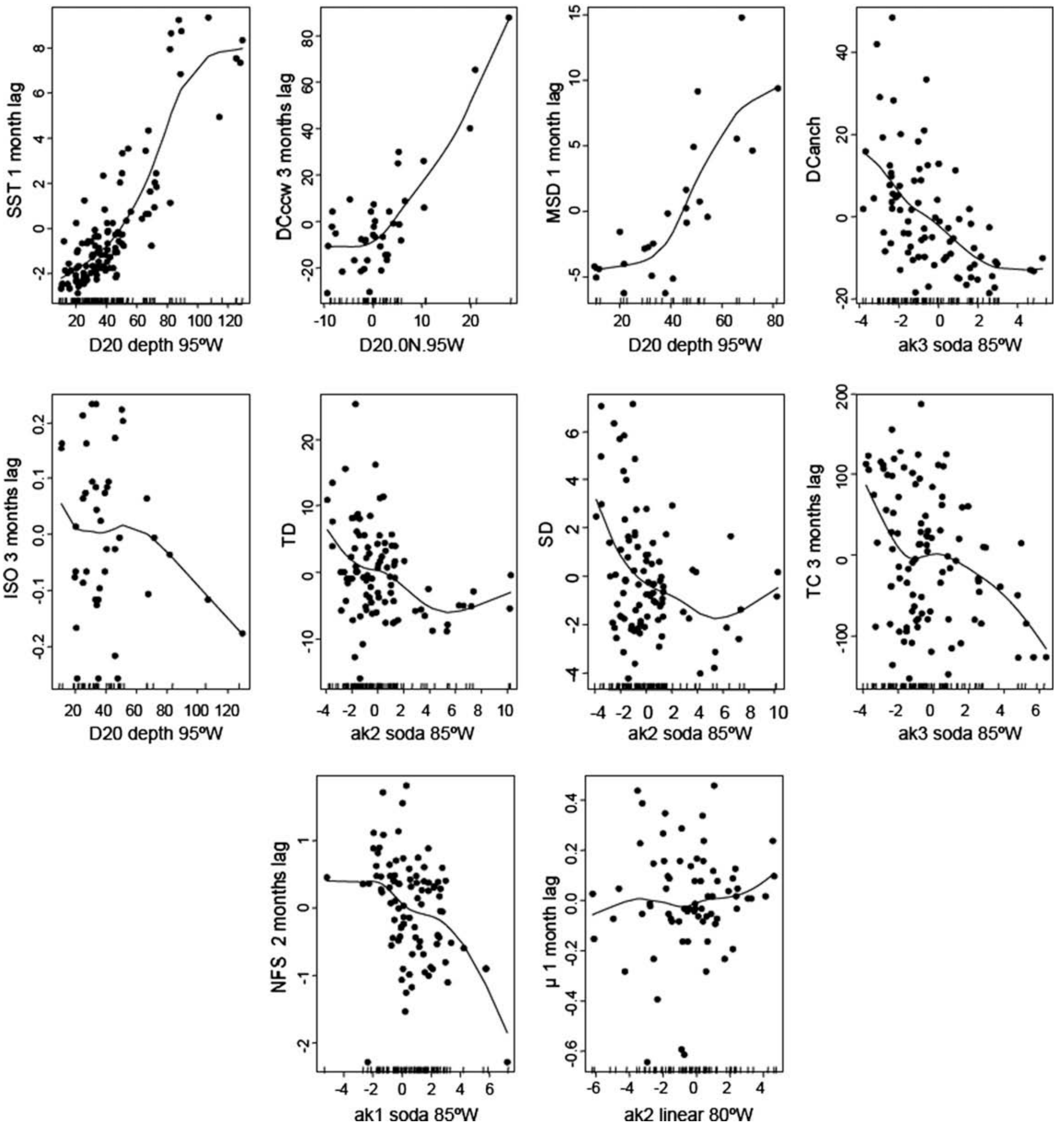

Fig. 3. Examples of non-parametric cubic Spline smoothers applied to the bivariate relationships that maximized the correlation between oceanic KWs signal (D20 at 95°W, SODA 85°W and linear model 80°W) and metrics describing the Peruvian coastal ecosystem dynamics.

Table 3

Synthesis of the bivariate Pearson correlations between the eastern KWs indexes (D20 at 95°W, SODA at 85°W and linear model (LM) at 80°W) and the metrics describing the Peruvian coastal dynamics, each of these being lagged up to 4 months: sea surface temperature off Chicama (SST), mean distance to the coast of the cold coastal waters (DCccw), mean depth of anchoveta schools (MSD), mean distance to the coast of anchoveta (DCanch), index of surface occupation by anchoveta (ISO, lower is ISO, higher is the spatial concentration of anchoveta), mean total duration of the fishing trips (TD), mean time allocated to search for fish (SD), mean number of fishing sets (NFS), mean catch by trip (TC), and an synthetic index of the fishing vessel trajectory (μ). All these results were significant at $p < 0.01$ after multitest correction. Only the statistical results corresponding to the baroclinic mode and the time lag maximizing the correlation for each parameter are presented. In most of cases, close significant results were obtained for a close time lag and/or mode. These overall results are synthesised in the column presenting the general trend of the correlations for each dependent variable.

Impact of oceanic KWs forcing on		General trend	D20 at 95°W			SODA 85°W				LM 80°W			
			ρ	df	Lag	KW baroclinic mode	ρ	df	Lag	KW baroclinic mode	ρ	df	Lag
Peruvian coastal oceanography	SST	↗	0.85	111	1	ak3	0.80	258	0	ak3	0.74	279	0
	DCccw	↘	−0.54	38	3	ak3	−0.51	80	2	$\sum$ak	−0.54	85	3
Anchoveta distribution	MSD	↗	0.80	22	1	ak3	0.53	56	1	$\sum$ak	0.65	56	2
	DCanch	↘	−0.50	37	1	ak3	−0.55	78	0	ak2	−0.46	84	0
	ISO	↘	–	–	–	ak3	−0.32	87	3	–	–	–	–
Fishing fleet behaviour	TD	↘	–	–	–	ak2	−0.34	89	0	–	–	–	–
	SD	↘	–	–	–	ak2	−0.31	89	0	–	–	–	–
	NFS	↘	−0.35	61	3	ak1	−0.40	91	2	ak2	−0.28	103	0
	TC	↘	–	–	–	ak3	−0.35	95	3	ak2	−0.26	105	0
	μ	↗	–	–	–	–	–	–	–	ak3	0.32	69	1

Table 4

Synthesis of the bivariate Pearson correlations between the western KWs indexes (D20 at 155°W, SODA at 160°W and linear model (LM) at 160°W) and the metrics describing the Peruvian coastal dynamics, each of these being lagged up to 4 months: sea surface temperature off Chicama (SST), mean distance to the coast of the cold coastal waters (DCccw), mean depth of anchoveta schools (MSD), mean distance to the coast of anchoveta (DCanch), index of surface occupation by anchoveta (ISO, lower is ISO, higher is the spatial concentration of anchoveta), mean total duration of the fishing trips (TD), mean time allocated to search for fish (SD), mean number of fishing sets (NFS), mean catch by trip (TC), and an synthetic index of the fishing vessel trajectory (μ). All these results were significant at $p < 0.01$ after multitest correction. Only the statistical results corresponding to the baroclinic mode and the time lag (in months) maximising the correlation for each parameter are presented. In most of cases, close significant results were obtained for a close time lag and/or mode. These overall results are synthesised in the column presenting the general trend of the correlations for each dependent variable.

Impact of oceanic KWs forcing on		General trend	D20 at 155°W			SODA 160°W				LM 160°W			
			ρ	df	Lag	Baroclinic KW mode	ρ	df	Lag	Baroclinic KW mode	ρ	df	Lag
Peruvian coastal oceanography	SST	↗	0.46	160	4	ak3	0.39	258	6	ak3	0.62	276	3
	DCccw	↘	–	–	–	–	–	–	–	ak2	−0.42	85	5
Anchoveta distribution	MSD	↗	0.51	38	6	ak3	0.41	56	5	ak3	0.53	56	5
	DCanch	↘	−0.33	63	5	ak3	−0.44	80	5	ak3	−0.45	84	2
	ISO	↗	–	–	–	$\sum$ ak	0.28	86	2	–	–	–	–
Fishing fleet behaviour	TD	↘	−0.57	96	2	$\sum$ak	−0.48	92	3	ak3	−0.33	105	2
	SD	↘	−0.48	96	2	ak1	−0.39	94	5	ak1	−0.26	105	3
	NFS	↘	−0.28	96	2	$\sum$ak	−0.32	92	3	ak2	-0.32	103	3
	TC	↘	–	–	–	–	–	–	–	ak2	−0.34	105	2
	μ	↗	–	–	–	–	–	–	–	ak2	0.35	69	6

The difference in trajectories illustrates the difference in magnitude of the El Niño events (lower for the event of 1991–92).

4. Discussion

Our main objective has been to describe how large scale oceanic forcing via Kelvin waves (KWs) affects the coastal Peruvian ecosystem. How is the global energy of a basin-scale process released when arriving at the coast? It is usually admitted that the arrival of oceanic upwelling or downwelling KWs may have two types of consequences in the coastal domain. First, by changing the thermocline depth, KWs increase or decrease nutrient supply to the surface via upwelling (Barber and Chavez, 1983). If the upwelling pump is less efficient, the consequence is a reduction of the extent of rich and cold coastal surface waters and as a consequence, an apparent intrusion of warm oceanic waters. Additionally, passage of coastally-trapped KWs modifies the cross-shore temperature gradient (upwelling front), may change the stability of the upwelling currents (Morel et al., 2007) and can trigger extra-tropical Rossby waves that radiate offshore. Near the upwelling front, KWs induce meso-scale mixing and diffusion.

This work quantifies the direction and the strength of interaction between oceanic KW forcing and coastal ecosystem dynamics. SODA's underlying assumptions are more realistic than those of LM and in better agreement with TAO observations (D20). However when considering the western oceanic forcing signal, the LM was almost as good as SODA and even better correlated with the coastal parameters (Table 4). The LM time series also identified a correlation between KWs and the spatial behaviour of fishers (μ). This result is probably due to a better coherence between the time series (data allowing μ estimation were only available from 1999). Despite these minor inconsistencies between KWs descriptors, the two statistical approaches — bivariate lagged correlations and multivariate statistics — produced coherent and complementary results.

We could portray contrasting coastal scenarios according to the nature of the oceanic KW forcing (Fig. 6). A downwelling KW, by depressing the thermocline, makes that coastal upwelling brings to surface warmer, low nutrient waters (Barber and Chavez, 1983). Then, the extent of cold and nutrient-rich waters, CCW, is reduced (↘ DCccw), and sea surface temperature increase (↗SST) in the coastal domain. With these changes anchoveta tend to distribute (i) closer to the coast (↘ DCanch), remaining in the CCW (Bertrand et al., 2004b; Swartzman et al., 2008), and (ii) deeper in the water column (↗ MSD) beneath the warm and less productive surface waters (e.g. Arntz and Fahrbach, 1996). Under these conditions anchoveta are concentrated in space (↘ ISO, see Gutiérrez et al., 2007) and the time needed by fishers to find anchoveta aggregations is reduced (↘ SD) and fishing trips are briefer (↘ TD). The number of fishing sets by trip also decreases (↘ NSF) as does the catch per trip (↘ TC). When fish are concentrated in the very coastal fringe the decreased TC seems surprising but may have several explanations: (i) when operating close to the coast, fishers offload more frequently, even when only partly loaded; (ii) anchoveta may be less available to the industrial fleet which, by law, cannot fish nearshore (<5 n.mi.); (iii) anchoveta may move too deep to be available to the purse seine (Bertrand et al., 2004b). Finally, the trajectories followed by the fishing vessels are more sinuous, random-like, and explore smaller areas (↗ μ). This 'Brownian'-like motion occurs because the ships do not need to steam offshore (directed travel) and between clusters when anchoveta are concentrated near the coast in highly contagious aggregations (Clark, 1976; Bertrand et al., 2005). The scenario under the arrival of an upwelling KW is symmetrically opposite to what was described for downwelling KWs (Fig. 5).

Several of these patterns have been described previously (e.g. McPhaden, 1999; Escribano et al., 2004), but the contribution of oceanic KW forcing to the changes in the coastal ecosystem had not been quantified. This work shows that the effect of large scale oceanic KW forcing is detectable and significant in the spatial organization of the ecosystem, including anchoveta and one of their top predators, man. This is an evidence for a bottom-up transfer of the behaviours and spatial structuring (Frontier, 1987; Russel et al., 1992): physics structures the oceanscape and drives the distribution of particles and passive organisms (plankton); then, because living organisms have to meet their prey, they tend to track their distribution (e.g. Frontier et al., 2004) and by the succession of predator–prey relationships, the spatial structuring originally driven by physical forcing tends to be transmitted along the trophic levels of the ecosystem (Fig. 7). Attenuation of the correlations from the oceanographic descriptors (most correlations being in the order of 0.65) to the fishery descriptors (most correlations being in the order of 0.35) reflects the increasing complexity of the factors driving the spatial distributions from physics (water masses redistribution obeying fluid mechanics rules) to living organisms (interplay between physical forcing, biological and ecological constraints).

The multivariate representation of the ecosystem in a factorial plane founded on KW oceanic forcing also showed one state dominated the ecosystem (1983–2006), corresponding basically to an

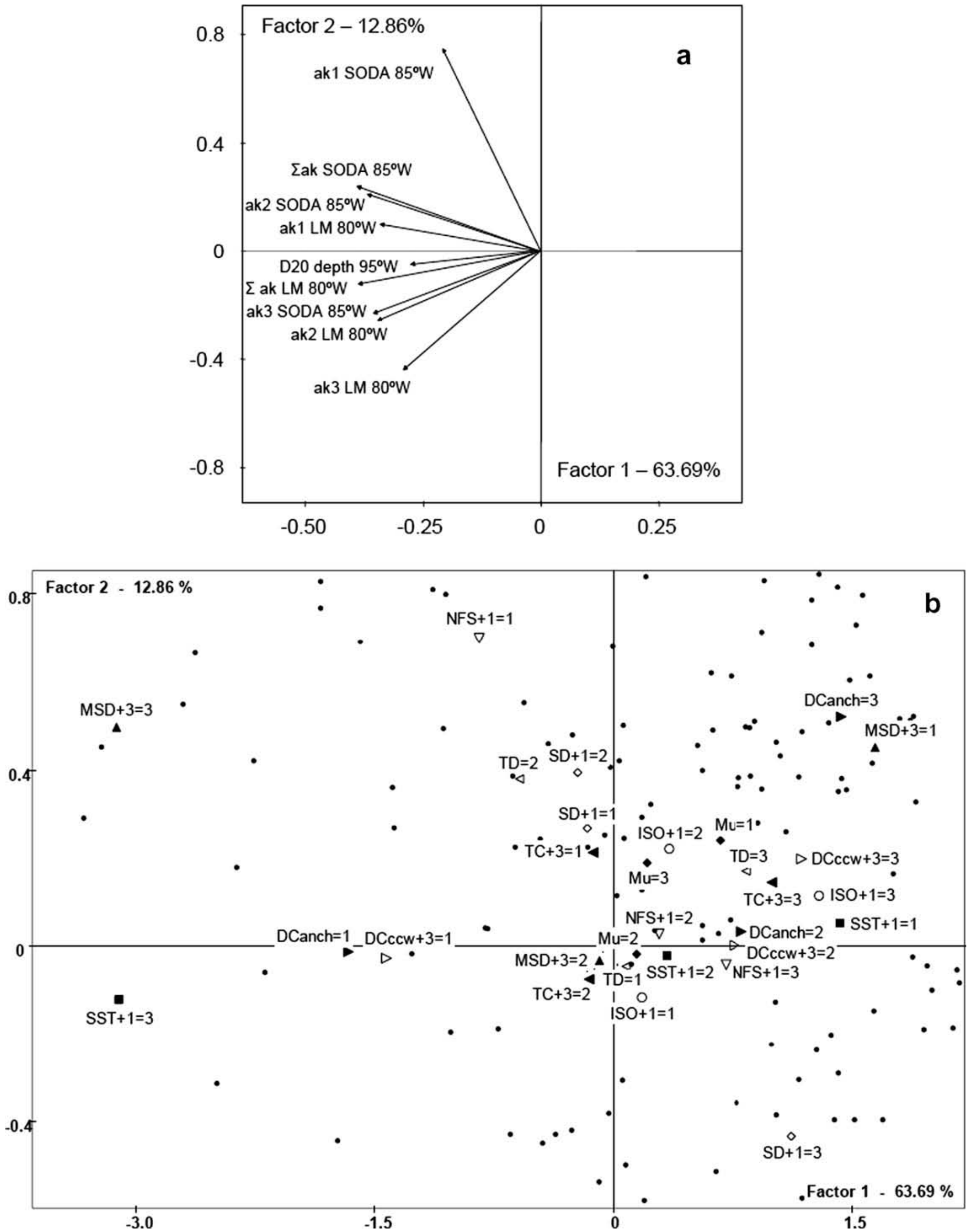

Fig. 4. Results from the PCA analysis: (a) variables describing the large scale oceanic forcing as active variables to build the multifactorial space and (b) the metrics describing the coastal ecosystem dynamics were categorised in three modalities (low = 1, medium = 2 and high = 3) and projected on this factorial plane: sea surface temperature off Chicama (SST), mean distance to the coast of the cold coastal waters (DCccw), mean depth of anchoveta schools (MSD), mean distance to the coast of anchoveta (DCanch), spatial concentration of anchoveta biomass (ISO), fishing trip mean duration (TD), fishing trip mean searching duration (SD), mean number of fishing sets by trip (NFS), mean catch by trip (TC), synthetic index of the vessels trajectories (μ).

average cold or 'upwelling dominant' scenario, with extreme trajectories corresponding to warm but punctual events (El Niño's), generated by downwelling KWs. We hypothesize that one pseudo-stable (cold and productive) state largely dominated our study period because the time series data falls (i) mainly in a cold decadal phase or 'anchovy era'; (ii) the end of a warm regime for the very first years of the time series (Alheit and Ñiquen, 2004; Gutiérrez et al., 2007) and (iii) more generally because whatever is the decadal context (warm or cool), temperature anomalies associated La Niña events (temperature anomaly for Niño 3.4 usually less than 2.5 °C) are on average less than for El Niño events, (temperature anomaly for Niño 3.4 usually less than 4 °C). It would be interesting to extend the multivariate description of the ecosystem to the different Viejo-Vieja decadal periods and anchovy–sardine alternative eras (Chavez et al., 2003). We could then test if during warm decadal periods, upwelling KWs would induce 'cold' events within background warm conditions (see also An, 2004). Additionally, other descriptors could be added in the future to this analysis, such

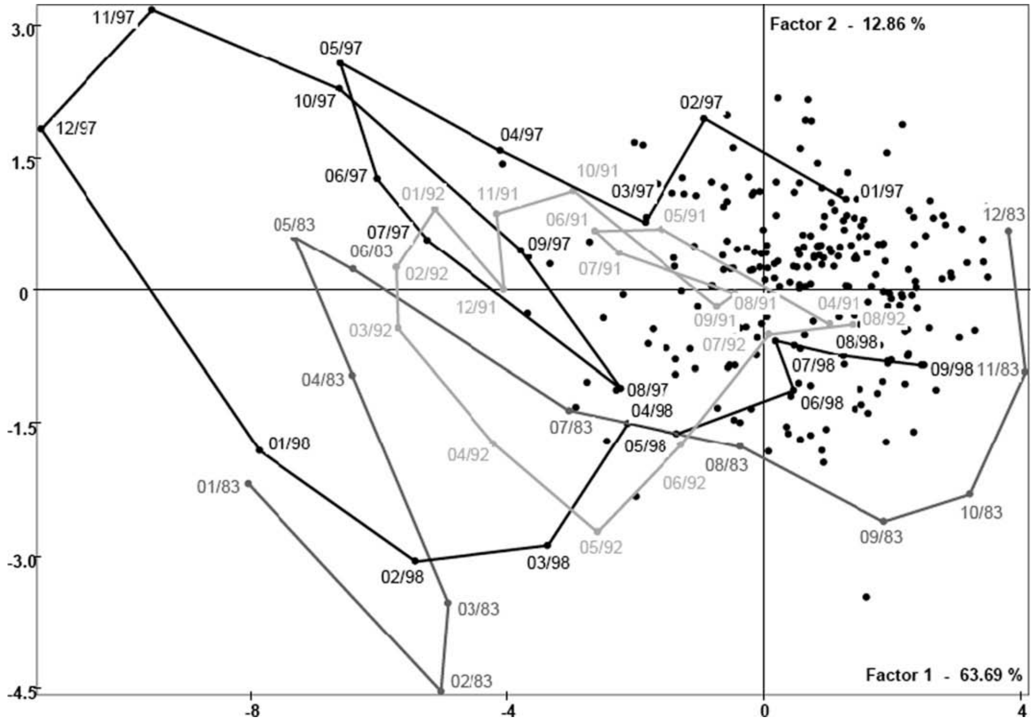

Fig. 5. Projection of the scores for each study month on the first factorial plan. The systemic trajectory for three extreme events in the ecosystem is indicated: El Niño 82–83 (dark grey), El Niño 91–92 (light grey), El Niño 97–98 (black).

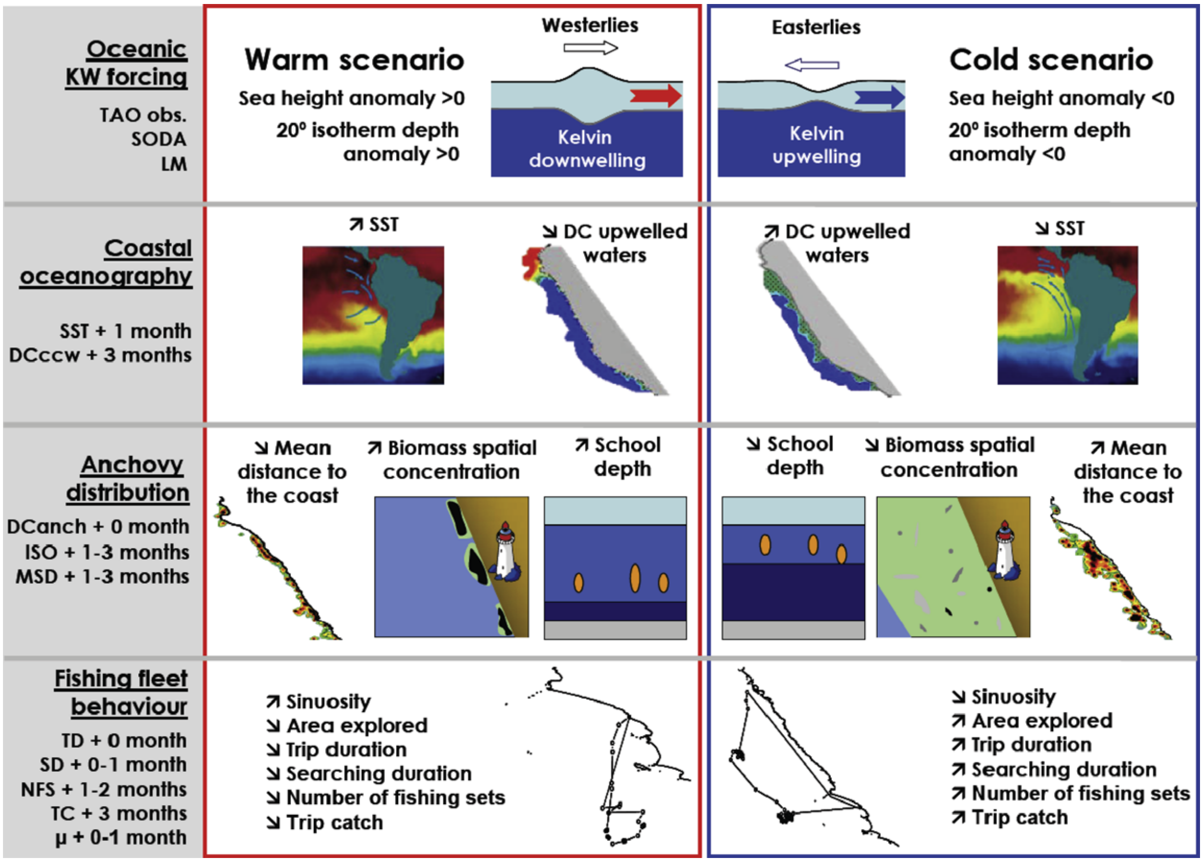

Fig. 6. Synthesis of the warm and cold ecological scenarios driven by oceanic KW forcing observed in the coastal Humboldt Current system. The qualitative response of the metrics describing the coastal ecosystem dynamics are presented for (i) Peruvian coastal oceanography: sea surface temperature (SST), mean distance to the coast of the cold coastal waters (DCccw); (ii) anchoveta distribution: mean distance to the coast (DCanch), index of anchoveta spatial distribution (ISO), mean depth of the schools (MSD); (iii) fishing fleet behaviour: mean travel duration (TD), mean searching duration (SD), mean number of fishing sets (NFS), mean trip catch (TC), synthetic index of fishing trip trajectories (μ).

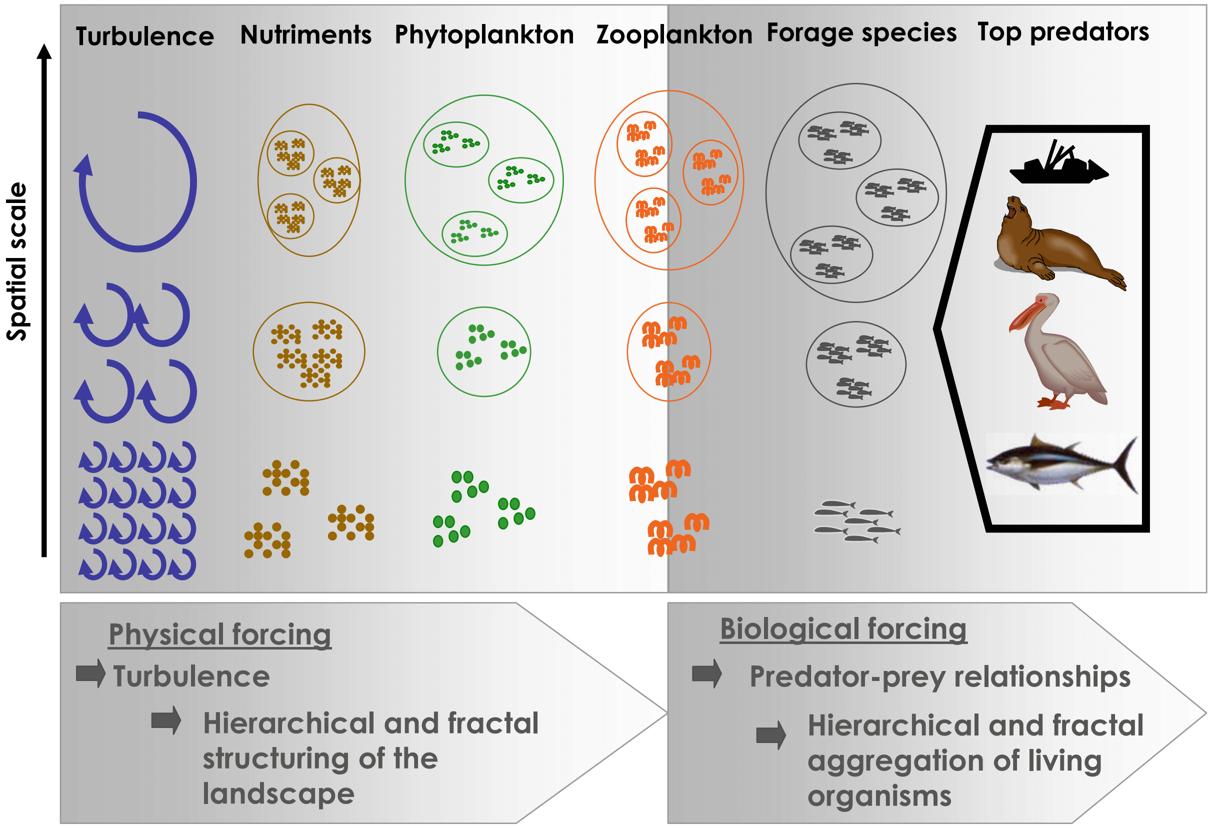

Fig. 7. Schematic representation of the concept of bottom-up transfer of behavious and spatial structuring. The physical forcing structures the pelagic landscape by introducing turbulence in the water mass. The dissipation of this turbulence is fractal by nature and generates a hierarchical structuring of the water mass. The inert particles (nutriments) and part of living organisms (phytoplankton and most of the zooplankton) are passively organized in space by this physical forcing. Then, biological interactions such as predator–prey relationships transmit to a certain extent this spatial structuring along the trophic chain.

as oxycline depth or plankton community or top predator abundances. Using a similar methodology with three decades-long study period, Link et al. (2002) produced a powerful representation of three ecosystem scenarios for the Northeast US continental shelf. As emphasized by Link et al. (2002), if fisheries managers can be more informed of overall ecosystem status they will be empowered to better make operational predictions regarding fluctuations of the resources they are charged with protecting (Pitcher, 2001).

The statistics also showed the existence of a delay between KW signal and coastal ecosystem response. The Eastern Time series that characterized KWs are located on the Equator at 85–90°W. KWs reach and pass along the Peruvian coast from this longitude in less than a week, depending on the relative contribution of the baroclinic modes ($\sim$240 km day^{-1} for the ak1 mode). However, the effects of such KWs remain strong in the Peruvian ecosystem over the next 1–3 months. The existence of these lags may be partly explained by the meso-scale effects of mixing and diffusion mentioned above, or by a 'biological' delay, with the biological system responding over time. However, the details of these lags remain difficult to understand. Lags were not longer for fishing activities than for fish distribution or local physical measures (Fig. 6). For instance, anchoveta reacted (in terms of mean distance to the coast) to a warm event even before that the water masses redistribution was detected (lag 0 for DCanch, 3 months lag for DCccw). If this is not an artifact of the analysis (monthly discretization of the time series, averaging data over the entire Peruvian coast), it may suggest that the KW signal is detected by organisms before the oceanography was substantially impacted or observable (see McFarlane et al., 2000).

Fishery managers need to forecast dynamics of the coastal ecosystem (e.g. Broad et al., 2002). KWs predictably affect coastal processes even when measured 2–6 months in advance in the central Pacific (see western KW time series). The detection of a downwelling KW for instance should be considered as a warning signal of forthcoming adverse conditions for anchoveta (reduced habitat and high vulnerability to the fishing fleet) and fisheries managers should then be prepared to decide temporary management measures reducing fishing pressure (closure or other). This is a piece of answer to Clark who stated as early as 1976 that "to manage the anchoveta stock properly under all the environmental conditions that occur in Peru, particularly during El Niño events, the Peruvian authorities would need to be able to predict environmental changes and their effects on the stock. Variations in upwelling strength along the coast of Peru result from large scale changes across the Pacific Ocean, and may soon be predictable from leading indicators (...)". Not so soon, but thirty years later, we are finally able to propose that KWs amplitude (direct observations and model-resolved baroclinic modes) should be used in the dashboard of the Peruvian fishery adaptive management. Taking into account this large scale oceanic forcing signal should provide a few precious months of anticipation - months indispensable in the decision making process to make anchoveta fishery sustainable.

Acknowledgements

The authors strongly thank the Instituto del Mar del Peru (IMARPE) for having facilitated the use of the data for this work and the SODA team for making available the assimilation products that were used in this study. TAO data Project Office (NOAA/Pacific

Marine Environmental Laboratory 7600 Sand Point Way NE Seattle, WA 98115) is also acknowledged for making available on their website (http://www.pmel.noaa.gov/tao/data_deliv/deliv.html) the D20 depth data. We are also very grateful to Matthieu Lengaigne (IRD – LOCEAN laboratory) for his help in analysing and interpreting these TAO data and for fruitful conversations on this paper. This work is a contribution of the UR 097 'ECO-UP', the UMR 'LEGOS' and the Interdepartmental Thematic Action "Humboldt Current System" from IRD. This work was supported in part by the US National Science Foundation in a grant number NSF0526392 to one of the investigators (Sophie Bertrand).

References

Alheit, J., Ñiquen, M., 2004. Regime shifts in the Humboldt current ecosystem. Progress in Oceanography 60, 201–222.

An, S.I., 2004. Interdecadal changes in the El Niño–La Niña asymmetry. Geophysical Research Letters 31, L23210. doi: 10. 1029/2004GL021699.

Arntz, W.E., Fahrbach, E., 1996. El Niño: experimento climático de la naturaleza. Fondo de Cultura Económica, Mexico City. 312 pp.

Barber, R.T., Chavez, F.P., 1983. Biological consequences of El Niño. Science 222, 1203–1210.

Benjamini, Y., Hochberg, Y., 1995. Controlling the false discovery rate: a practical and powerful approach to multiple testing. Journal of the Royal Statistical Society B 57, 289–300.

Bertrand, A., Barbieri, M.A., Córdova, J., Hernández, C., Gómez, F., Leiva, F., 2004a. Diel vertical behaviour, predator–prey relationships, and occupation of space by jack mackerel (*Trachurus murphyi*) off Chile. ICES Journal of Marine Science 61, 1105–1112.

Bertrand, A., Segura, M., Gutierrez, M., Vasquez, L., 2004b. From small-scale habitat loopholes to decadal cycles: a habitat-based hypothesis explaining fluctuation in pelagic fish populations off Peru. Fish and Fisheries 5, 296–316.

Bertrand, S., Diaz, E., Ñiquen, M., 2004c. Interactions between fish and fisher's spatial distribution and behaviour: an empirical study of the anchovy (*Engraulis ringens*) fishery of Peru. ICES Journal of Marine Science 61, 1127–1136.

Bertrand, S., Burgos, J.M., Gerlotto, F., Atiquipa, J., 2005. Lévy trajectories of Peruvian purse-seiners as an indicator of the spatial distribution of anchovy (*Engraulis ringens*). ICES Journal of Marine Science 62, 477–482.

Bertrand, S., Bertrand, A., Guevara-Carrasco, R., Gerlotto, F., 2007. Scale invariant movements of fishermen: the same foraging strategy as natural predators. Ecological Applications 17, 331–337.

Bertrand, A., Gerlotto, F., Bertrand, S., Gutiérrez, M., Alza, L., Chipollini, A., Diaz, E., Espinoza, P., Ledesma, J., Quesquén, R., Peraltilla, S., Chavez, F., 2008. Aggregation behaviour and environmental forcing as determinisms of fish 3D spatiotemporal distribution across scales: the case for the anchoveta, *Engraulis ringens*. Progress in Oceanography.

Broad, K., Pfaff, S.P., Glantz, M.H., 2002. Effective and equitable dissemination of seasonal to interannual climate forecasts: policy implications from the Peruvian fishery during El Niño 1997–98. Climatic Change 54, 415–438.

Burkett, V.R., Wilcox, D.A., Stottlemyer, R., Barrowa, W., Fagre, D., Baron, J., Price, J., Nielsen, J.L., Allen, C.D., Peterson, D.L., Ruggerone, G., Doyle, T., 2005. Nonlinear dynamics in ecosystem response to climatic change: case studies and policy implications. Ecological complexity 2, 357–394.

Cane, M.A., Sarachick, E.S., 1976. Forced baroclinic ocean motions, I: The linear equatorial unbounded case. Journal of Marine Research 34, 629–665.

Carton, J.A., Chepurin, G., Cao, X., 2000. A simple ocean data assimilation analysis of the global upper ocean 1950–95. Part I: Methodology. Journal of Physical Oceanography 30, 294–309.

Carton, J.A., Giese, B.S., 2008. A reanalysis of ocean climate using Simple Ocean Data Assimilation (SODA). Monthly Weather Review 136 (8), 2999–3017.

Clark, W.G., 1976. The lessons of the Peruvian anchovy fishery. California Cooperative Oceanic Fisheries Investigations Reports XIX, pp. 57–63.

Clarke, A.J., 1983. The reflection of equatorial waves from oceanic boundaries. Journal of Physical Oceanography 13, 1183–1207.

Clarke, A.J., 1992. Low-frequency reflection from a nonmeridional eastern ocean boundary and the use of coastal sea level to monitor eastern Pacific equatorial Kelvin waves. Journal of Physical Oceanography 22, 163–183.

Chavez, F.P., Ryan, J., Lluch-Cota, S.E., Ñiquen, M., 2003. From anchovies to sardines and back: multidecadal change in the Pacific Ocean. Science 299, 217–221.

Chelton, D.B., 1984. Commentary: short-term climatic variability in the Northeast Pacific Ocean. In: Pearcy, W. (Ed.), The Influence of Ocean Conditions on the Production of Salmonids in the North Pacific. Oregon State University Press, Corvallis, Oregon, pp. 87–99.

Cotté, C., Simard, Y., 2005. Formation of dense krill patches under tidal forcing at whale feeding hot spots in the St. Lawrence Estuary. Marine Ecology Progress Series 288, 199–210.

Croll, D.A., Marinovic, B., Benson, S., Chavez, F.P., Black, N., Ternullo, R., Tershy, B.R., 2005. From wind to whales: trophic links in a coastal upwelling system. Marine Ecology Progress Series 289, 117–130.

Delcroix, T., Dewitte, B., duPenhoat, Y., Masia, F., Picaut, J., 2000. Equatorial waves and warm pool displacement during the 1992–1998 El Niño events: observation and modelling. Journal of Geophysical Research 105, 26045–26062.

Dewitte, B., Reverdin, G., Maes, C., 1999. Vertical structure of an OGCM simulation of the equatorial Pacific Ocean in 1985–1994. Journal of Physical Oceanography 29, 1542–1570.

Dewitte, B., Gushchina, D., duPenhoat, Y., Lakeev, S., 2002. On the importance of subsurface variability for ENSO simulation and prediction with intermediate coupled models of the Tropical Pacific: a case study for the 1997–1998 El Niño. Geophysical Research Letters 29 (14). Art. No. 1666.

Dewitte, B., Illig, S., Parent, L., duPenhoat, Y., Gourdeau, L., Verron, J., 2003. Tropical Pacific baroclinic mode contribution and associated long waves for the 1994–1999 period from an assimilation experiment with altimetric data. Journal of Geophysical Research 108 (C4), 3121–3138.

Edwards, M., Richardson, A.J., 2004. Impact of climate change on marine pelagic phenology and trophic mismatch. Nature 430, 881–884.

Escribano, R., Daneria, G., Farías, L., Gallardoa, V.A., González, H.E., Gutiérrez, D., Lange, C.B., Morales, C.E., Pizarro, O., Ulloa, O., Braun, M., 2004. Biological and chemical consequences of the 1997–98 El Niño in the Chilean coastal upwelling system: a synthesis. Deep Sea Research II 51, 2389–2411.

Foote, K.G., Knudsen, H.P., Vestnes, D.N., MacLennan, D.N., Simmonds, E.J., 1987. Calibration of acoustic instruments for fish density estimation: a practical guide. ICES Cooperative Research Report No. 144.

Fossheim, M., Zhou, M., Tande, K.S., Pedersen, O.-P., Zhu, Y., Edvardsen, A., 2005. Interactions between biological and environmental structures along the coast of northern Norway. Marine Ecology Progress Series 300, 147–158.

Frontier, S., Pichod-Viale, D., Leprêtre, A., Davoult, D., Luczak, C., 2004. Ecosystèmes. Dunod, Paris. 550 pp.

Frontier, S., 1987. Applications of fractal theory to ecology. In: Legendre, P., Legendre, L. (Eds.), Developments in Numerical Ecology. Springer-Verlag, Berlin, pp. 335–378.

Gutiérrez, M., Swartzman, G., Bertrand, A., Bertrand, S., 2007. Anchovy and sardine spatial dynamics and aggregation patterns in the Humboldt Current ecosystem, Peru, from 1983–2003. Fisheries Oceanography 16, 155–168.

Hsieh, C.-H., Glaser, S.M., Lucas, A.J., Sugihara, G., 2005. Distinguishing random environmental fluctuations from ecological catastrophes for the North Pacific Ocean. Nature 435, 336–340.

Keitt, T.H., Bjørnstad, O.N., Dixon, P.M., Citron-Pousty, S., 2002. Accounting for spatial pattern when modelling organism–environment interactions. Ecography 25, 155–168.

Knowlton, N., 2004. Multiple "stable" states and the conservation of marine ecosystems. Progress in Oceanography 60, 387–396.

Lebart, L., Morineau, A., Prion, M., 2000. Statistique Exploratoire Multidimensionnelle, third ed. Dunod, Paris. 439 pp.

Lehodey, P., Alheit, J., Barange, M., Baumgartner, T., Beaugrand, G., Drinkwater, K., Fromentin, J.-M., Hare, S.R., Ottersen, G., Perry, R.I., Roy, C., van der Lingen, C.D., Werneri, F., 2006. Climate variability, fish, and fisheries. Journal of Climate 19, 509–530.

Link, J.S., Brodziak, J.K.T., Edwards, S.F., Overholtz, W.J., Mountain, D., Jossi, J.W., Smith, T.D., Fogarty, M.J., 2002. Marine ecosystem assessment in a fisheries management context. Canadian Journal of Fisheries and Aquatic Sciences 59, 1429–1440.

Margalef, R., 1979. The organization of space. Oïkos 33, 152–159.

McFarlane, G.A., King, J.K., Beamish, R.J., 2000. Have there been recent changes in climate? Ask the fish. Progress in Oceanography 47, 147–169.

McPhaden, M., 1999. Genesis and evolution of the 1997–98 El-Niño. Science 283, 950–954.

Morel, G.Y., Darr, D.S., Talendier, C., 2007. Possible sources driving the potential vorticity structure and long-wave instability of coastal upwelling and downwelling currents. Journal of Physical Oceanography 36, 875–896.

Perry, A.L., Low, P.J., Ellis, J.R., Reynolds, J.D., 2005. Climate change and distribution shifts in marine fishes. Science 308, 1912–1915.

Pitcher, T.J., 2001. Fisheries managed to rebuild ecosystems? Reconstructing the past to salvage the future. Ecological Applications 11, 601–617.

Pizarro, O., Clarke, A.J., Van Gorder, S., 2001. El Niño sea level and currents along the South American coast: comparison of observations with theory. Journal of Physical Oceanography 31, 1891–1903.

Pyper, B.J., Peterman, R.M., 1998. Comparison of methods to account for autocorrelation in correlation analysis of fish data. Canadian Journal of Fisheries and Aquatic Sciences 55, 2127–2140.

Russel, R.W., Hunt, G.L., Coyle, O.K., Cooney, R.T., 1992. Foraging in a fractal environment: spatial patterns in a marine predator–prey system. Landscape Ecology 7, 195–209.

Stenseth, N.C., Mysterud, A., Ottersen, G., Hurrell, J.W., Chan, K.-S., Lima, M., 2002. Ecological effects of climate fluctuations. Science 297, 1292–1296.

Swartzman, G., Bertrand, A., Gutiérrez, M., Bertrand, S., Vasquez, L., 2008. The relationship of anchovy and sardine to water masses in the Peruvian Humboldt Current System from 1983–2005. Progress in Oceanography 79, 228–237.

Walther, G.-R., Post, E., Convey, P., Menzel, A., Parmesan, C., Beebee, T.J.C., Fromentin, J.-M., Hoegh-Guldberg, O., Bairlein, F., 2002. Ecological responses to recent climate change. Nature 416, 389–395.

Worm, B., Myers, R.A., 2004. Managing fisheries in a changing climate. Nature 429, 15.

Progress in Oceanography 79 (2008) 290–299

Contents lists available at ScienceDirect

Progress in Oceanography

journal homepage: www.elsevier.com/locate/pocean

The marine ecosystem off Peru: What are the secrets of its fishery productivity and what might its future hold?

Andrew Bakun [a,*], Scarla J. Weeks [b]

[a] *Pew Institute of Ocean Science, Rosenstiel School of Marine and Atmospheric Science, University of Miami, Miami, FL 33149, USA*
[b] *Centre for Marine Studies, University of Queensland, Brisbane, QLD 4072, Australia*

ARTICLE INFO

Article history:
Accepted 14 October 2008
Available online 1 November 2008

Keywords:
Peruvian fisheries
Ecosystem-based management
Climate change
Upwelling
Environmental conditions
El Niño

ABSTRACT

The marine ecosystem located off the coast of central and northern Peru has stood as the "world's champion" producer, by far, of exploitable fish biomass, generally yielding more than 20 times the tonnage of fishery landings produced by other comparable regional large marine ecosystems of the world's oceans that operate under similar dynamic contexts and are characterized by comparable, or even greater, basic primary production. Two potentially contributing aspects are discussed from a framework of interregional comparative pattern recognition: (1) the advantageous low-latitude situation that combines strong upwelling-based nutrient enrichment with low wind-induced turbulence generation and relatively extended mean "residence times" within the favorable upwelling-conditioned near-coastal habitat and (2) the cyclic "re-setting" of the system by ENSO perturbations that may tend to interrupt malignant growth of adverse self-amplifying feedback loops within the nonlinear biological dynamics of the ecosystem.

There is a developing scientific consensus that one of the more probable consequences of impending global climate changes will be a general slowing of the equatorial Pacific Walker Circulation and a consequent weakening of the Pacific trade wind system. Since the upwelling-favorable winds off Peru tend to flow directly into the Pacific southeast trade winds, a question arises as to the likely effect on the upwelling-producing winds that power the productivity of the regional coastal ecosystems of the Peru–Humboldt Current zone. It is argued that the effects will in fact be decoupled to the extent that upwelling-favorable winds will actually tend to increase off Peru. Data demonstrative of this decoupling are presented. A tendency for less intense El Niño episodes in the future is also suggested. These conclusions provide a framework for posing certain imponderables as to the future character of the Peruvian marine ecosystem and of the fisheries it supports.

1. Introduction

Major regional coastal upwelling ecosystems exist in each of the eastern ocean boundary current zones of the Pacific and Atlantic Oceans (Fig. 1). The marine ecosystem off Peru, comprising the northern segment of the Humboldt system, is unequaled in sheer tonnage of fishery landings. In terms of producing fish biomass, it is truly "heavyweight champion of the world".

The rather steady alongshore winds that blow in the equatorward direction along the Peruvian coast drive strong wind-induced coastal upwelling. Just downwind of the upwelling zone, the upwelling-favorable wind flow separates from the coast and turns offshore to feed into the westward trade wind flow that characterizes the near-equatorial band of the Pacific Ocean. As a result, the Peruvian upwelling has been traditionally described as being driven by the trade winds (e.g., Paulik, 1971). The nutrient enrichment and resulting primary productivity associated with this strong upwelling is generally understood to constitute the essential basis for the area's remarkable fishery production.

Growing evidence, modeling findings, and resulting scientific consensus (e.g., Vecchi et al., 2006; Vecchi and Soden, 2007) predict that, as a result of continued buildup of greenhouse gases in the earth's atmosphere, the Pacific trade wind system will tend to decline in intensity. This has led to questions as to whether this implies a simultaneous slowing of the Peruvian upwelling system. Somewhat counter to this idea is a theory (Bakun, 1990), corroboration of which appears to be unfolding as the record of observations continues to lengthen (see Section 5.1), predicting that coastal upwelling should intensify as greenhouse gases increase. These considerations have led to serious questions about the prospects for the Peruvian upwelling ecosystem and its associated fisheries productivity in a future expected to be characterized by (1) greenhouse gas-mediated global climate change and (2) ever

---

* Corresponding author.
E-mail address: abakun@rsmas.miami.edu (A. Bakun).

0079-6611/$ - see front matter © 2008 Elsevier Ltd. All rights reserved.
doi:10.1016/j.pocean.2008.10.027

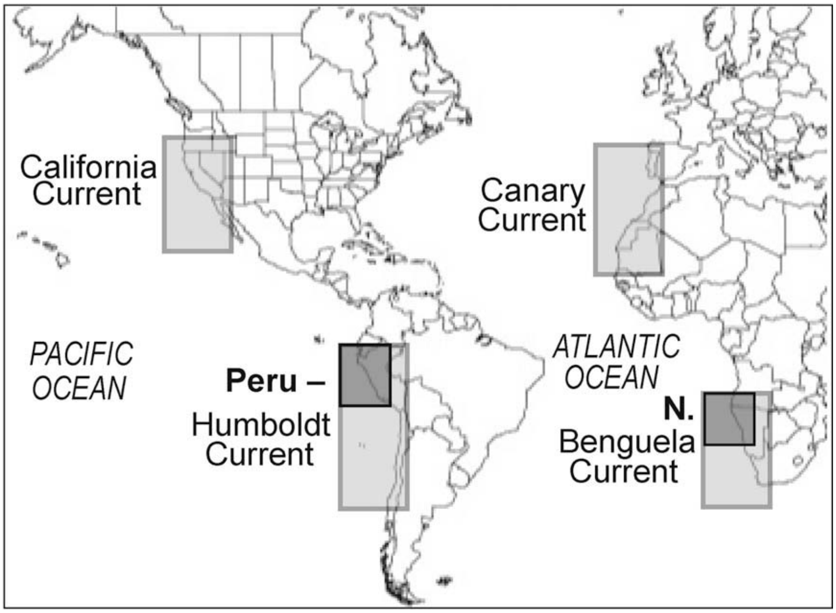

Fig. 1. Locations (shaded rectangles) of major regional eastern ocean upwelling systems; darker-shaded rectangles denote the quasi-separated Peruvian and northern Benguela near-equatorial sub-systems of the respective Humboldt Current and Benguela Current regional upwelling ecosystems.

increasing demand for fisheries products leading to increasing pressures for massive overfishing of a sort that has already adversely impacted other marine ecosystems, notably the northern Benguela upwelling ecosystem which we use in this paper as a logical analog to the Peruvian system (see below).

The great evolutionary biologist, Ernst Mayr, has called the experimental method and the comparative method "the two great methods of science" (Mayr, 1982). The experimental method, where a series of multiple realizations of a process needed to draw scientific inference is assembled from a sequence of controlled experiments, is the one that most people think of first when considering the scientific method. However marine ecosystems, on the scales of large mobile fish populations and the coupled dynamic ocean–atmosphere systems in which they are imbedded, are not amenable to deliberate experimental controls. Fortunately, the comparative method, where the required set of realizations is gathered from naturally occurring spatial or temporal variability, offers an available alternative (Mayr, in fact, credits the power of the comparative method for "nearly all of the revolutionary advances in evolutionary biology", another area where the enormity of scale, notably temporal in that case, tends to preclude application of experimental controls).

In this paper, we apply the comparative method to attempt to identify the specific factors underlying the fishery productivity of the Peru system. We focus particularly on unique characteristics that might potentially explain its unrivaled status as a producer of exploitable fish. Obvious comparative analogs are the other similar eastern ocean boundary upwelling regions (Fig. 1). Of these, the northern Benguela region, being similarly situated as the equatorward sub-region of the other major southern hemisphere regional upwelling system could be considered in many respects to be the most parallel comparative analog to the Peru system. Moreover, having already experienced durable decimation of its fishery productivity, it also might offer an instructive example of what those concerned with the Peru system may wish fervently to avoid.

2. The "world's champion fish-producing ecosystem

The ability of the Peruvian marine ecosystem to produce unparalleled quantities of fish is truly remarkable. For example, in the late 1960s, one single country, Peru, routinely landed more tonnage of one single fish species, the Peruvian anchoveta (*Engraulis ringens*), than the combined total of all the other fished species, both marine and freshwater, landed by all the other countries of North and South America combined. In seeming paradox, the Humboldt system appears to be no more productive in terms of primary productivity than either the Canary or Benguela systems. For example, a recent study by Carr (2001) indicates that it may be only half as productive as the Benguela system. Nevertheless, the Humboldt system routinely has produced more than 20 times as much fish as either of these other two similar systems. Moreover, the Peru system, the smaller near-equatorial sub-segment of the Humboldt Large Marine Ecosystem, often generates the major portion of the entire Humboldt system's fish production.

The northern Benguela system, located off the coasts of the African countries of Namibia and southern Angola, is a logical comparative analog to the Peru system, likewise constituting a more or less connected near-equatorial sub-system of one of the two major southern hemisphere eastern ocean boundary current upwelling regions. It also likewise appears to be the more productive segment of a larger regional LME (the Benguela Current LME) of which it is a component (Carr, 2001). Comparing examples of satellite images of the two regions reveals strong similarities in the pronounced near-coastal ocean surface cooling and high near-coastal phytoplankton production characteristic of intense coastal upwelling zones (Fig. 2). Lüderitz, Namibia, the site of the strongest zone of sustained upwelling in the world, appears as somewhat an analog to Punta San Juan, the location of the strongest upwelling core of the Peru system.

The fact that the Peru system may generate considerably less primary production than the northern Benguela (Carr, 2001), while clearly generating enormously more fish production, demonstrates that higher primary production does not necessarily lead to greater fish production. This conclusion is worth emphasizing. For example, sardines in the eastern Pacific often grow population during El Niño episodes, which are noted for strikingly lowered ocean productivity; using the CalCOFI data set, Agostini et al. (2007) found sardine recruitment to actually be inversely correlated with zooplankton abundance in the larval habitat. This emphasizes the notion that in the ocean, "food heaven" generally coincides with

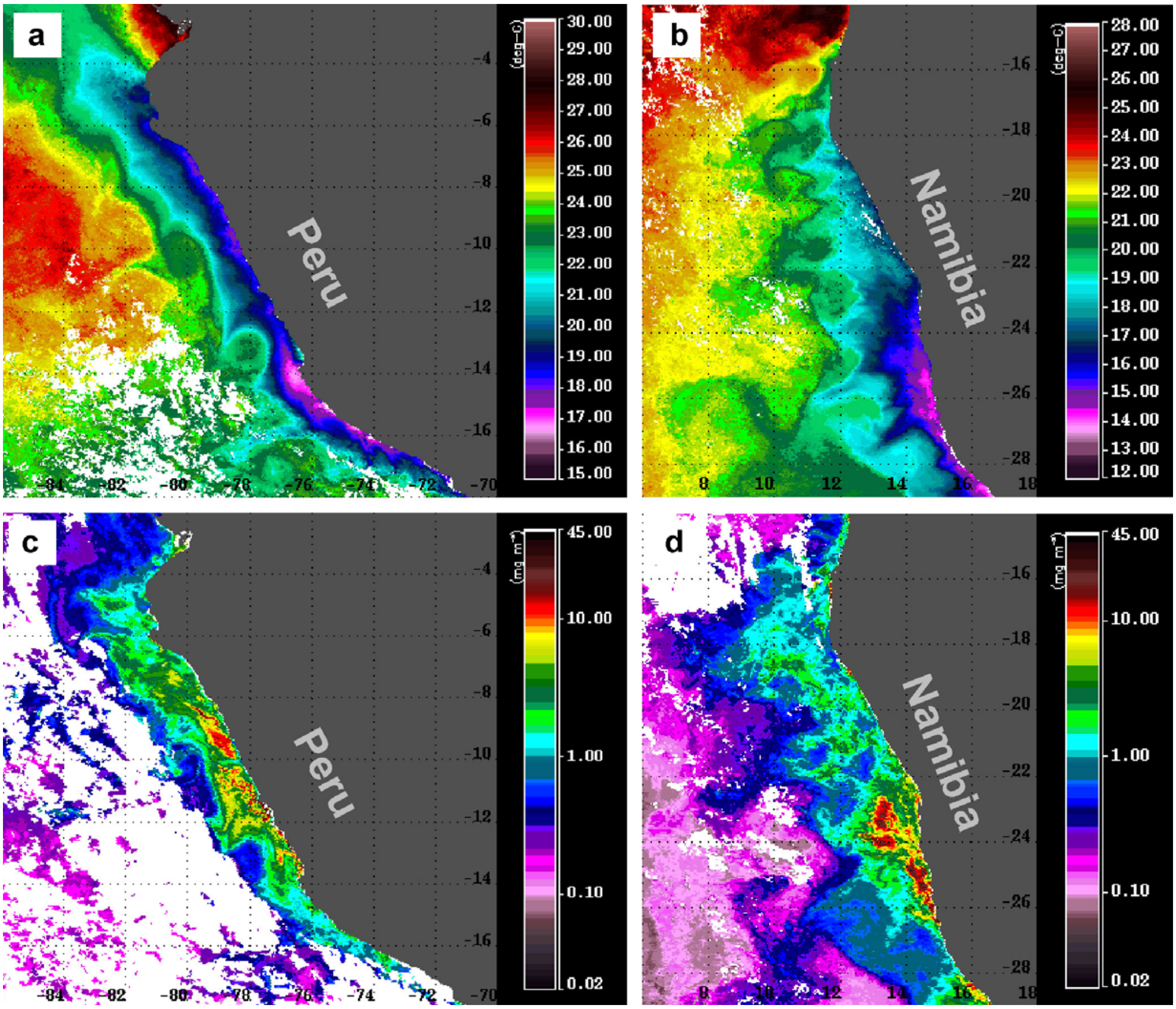

Fig. 2. Satellite imagery examples: (a) SST, Peru system, 7–14 April 2005; (b) SST, N. Benguela system, 7–14 April 2005; (c) Chlorophyll, Peru system, 7–22 April 2005 and (d) Chlorophyll, N. Benguela system, 7–22 April 2005.

"predation hell" (Bakun, 2006). Fish production usually depends more on recruitment success (i.e., successful reproduction) than on food availability (i.e., growth rate). Lowered predation on early life stages appears often to outweigh food availability as a determinant of reproductive success.

Fish production in the Peru system appears normally to be dominated by anchoveta, a particularly efficient species with extremely rapid population responses, even though from time to time (e.g., the late 1970s following the famous initial anchoveta collapse) it has become temporarily dominated by sardines of the genus *Sardinops*. The northern Benguela, on the other hand, appears to have usually been dominated by sardines (*Sardinops*), although following the collapse of the sardine resource in the 1970s, anchovies (*Engraulis capensis*) briefly predominated in fishery landings before likewise collapsing. In the mid-1960, the biomass of Namibian sardines is estimated to have been about 10 million metric tons (Boyer, 1996); annual catches were near 1.5 million MT. Then, in response to intense "pulse" fishing by the Soviet Bloc and other nations, the population collapsed to a much lower level characterized by much reduced productivity, with a biomass of about 1 million MT, and annual catches of 50,000–100,000 MT. More recently, there appears to have been a "regime shift" in which the omnivorous sardines seem to have been largely replaced by zooplanktivores, notably medusae of several species and pelagic gobies (Boyer and Hampton, 2001; Lynam et al., 2006). In remarkable contrast, the Peru system (besides producing 20–100 times as much fish) has managed to repeatedly rebound from multiple declines and from major alternations of dominance between anchovies and sardines.

What could be the secret behind the Peru system's unrivaled capacity to produce fish, and to sustain this production under the continuing pressure of a massive industrial fishery? As has been discussed above, the trophic basis represented by its primary photosynthetic production seems not to be uniquely rich. Evidently, we must thus look beyond such considerations as "bottom-up" trophic flows, ultimate trophic *carrying capacities*, etc., and seek the answer in other characteristics that represent unique aspects that may separate the Peru system from its potential comparative analogs, notably the other similar eastern ocean boundary upwelling regions (Fig. 1).

3. Unique factor #1: Peru is the system nearest to the equator

Of the major regional eastern ocean boundary upwelling regions, the Peru system is the one located at lowest latitudes. This has very important consequences for its physical dynamics. For a given intensity of upwelling-favorable wind, the intensities of wind-driven Ekman transport and resulting upwelling increase rapidly toward lower latitudes, while the input of turbulent mixing energy, which is roughly proportional to the third power (or "cube") of the wind stress (Elsberry and Garwood, 1978), has no dependence on latitude (Fig. 3a). Specifically, a given wind speed will yield about four times as much Ekman transport and associated intensity of upwelling at 9° latitude (the latitude of Chimbote, Peru) as at 39° latitude (the latitude of the center of maximum upwelling on the California coast near Cape Mendocino). To produce a similar rate of upwelling at 39° latitude as at 9° latitude the wind speed would have to double. However, this would entail an eightfold increase in wind-driven turbulent mixing. Thus, the same intensity of wind-driven coastal upwelling would correspond to eight times the rate of turbulence generation in the upwelling center of Northern California (~39° latitude) as in the heart of the anchoveta habitat off Peru (~9° latitude). As a result, the low-latitude location of Peru allows strong continuous enrichment by upwelling with much less disadvantageous turbulence generation than would be a byproduct at higher latitudes (Table 1, column 'c').

Moreover, the offshore extent of a coastal upwelling zone, determined by the baroclinic Rossby radius of deformation (Yoshida, 1967; Mooers and Allen, 1973), likewise increases rapidly toward lower latitudes (Table 1, column 'd'). We can consider this to be a width scale for the favorable near-coastal habitat of organisms adapted to an upwelling zone. An estimate of the average residence time within this favorable habitat of neutrally-bouyant, passively drifting planktonic particles (phytoplankton cells, copepod naplii, fish larvae, etc.) entrained in the Ekman layer, is given by the product of the layer depth and the habitat width scale (Rossby radius: Table 1, column 'd') divided by the Ekman transport (Fig. 3b). If one avoids the issue of potential-latitude dependence of Ekman layer depth (i.e., assumes a constant layer depth in the relative estimation), one sees that the residence time increases dramatically in near-equatorial latitudes (Table 1, column 'e'). But since there would in any case be a tendency for less rapid rotational deflection at lower latitudes, some sort of significance latitude dependence of Ekman layer depth seems intuitively likely. As a very rough gauge of potential latitudinal effects on Ekman layer depth, we can examine the latitude dependence of the theoretical "Ekman depth" (Table 1, column 'f'), the derivation of which presumes a homogenous fluid and depth-independent eddy viscosity (Ekman, 1905), both of which are tenuous assumptions in a real ocean situation. If one accepts this estimate of the layer depth, the increase in residence time at near-equatorial latitudes is even more dramatic (Table 1, column 'g').

Residence times of water parcels and entrained passively drifting particles can be particularly important to the ecosystem dynamics within an upwelling zone. For example, short residence times present great problems to planktonic organisms with complex life cycles, for example making it difficult for copepods, which undergo a fairly lengthy sequence of pre-adult stages prior to becoming reproductively capable, to maintain resident populations in intense upwelling zones; copepod nauplii are important food for fish larvae, which is a probably reason that intense upwelling cores (e.g., Punta San Juan, Lüderitz, Cape Medoncino) are avoided as spawning habitat by mobile fish species. Planktonic herbivores such as copepods are also vital in recycling nutrients in the zone, and in thereby preventing nutrient trapping and sinking of unoxidized organic matter to the sea floor, which may produce hypoxia, etc. Very short residence times tend to shift dominance to the very shortest-lived organisms (e.g., diatoms) that generally represent less nutritious food for other organisms.

The considerations summarized in Table 1 thus appear to present a picture of the Peruvian marine ecosystem as a particularly rich, non-turbulent, "benign" environment, in which relatively weak winds result in large volumes of water being transported offshore and an associated high rate of upwelling which continually enriches a very wide, deep, non-turbulent upper ocean habitat. The associated average offshore transport of larvae and larval food distributed through this thick, slowly moving upper layer would be relatively small, and their loss from a very wide coastal habitat would be minimized. This same ease in maintaining standing stock in the upwelling-enriched environment and lack of exposure to intense turbulent mixing that could exceed *critical depth* (Sverdrup, 1953) would be of similar benefit to primary producers, leading to high concentrations of nutritious food organisms for both larval

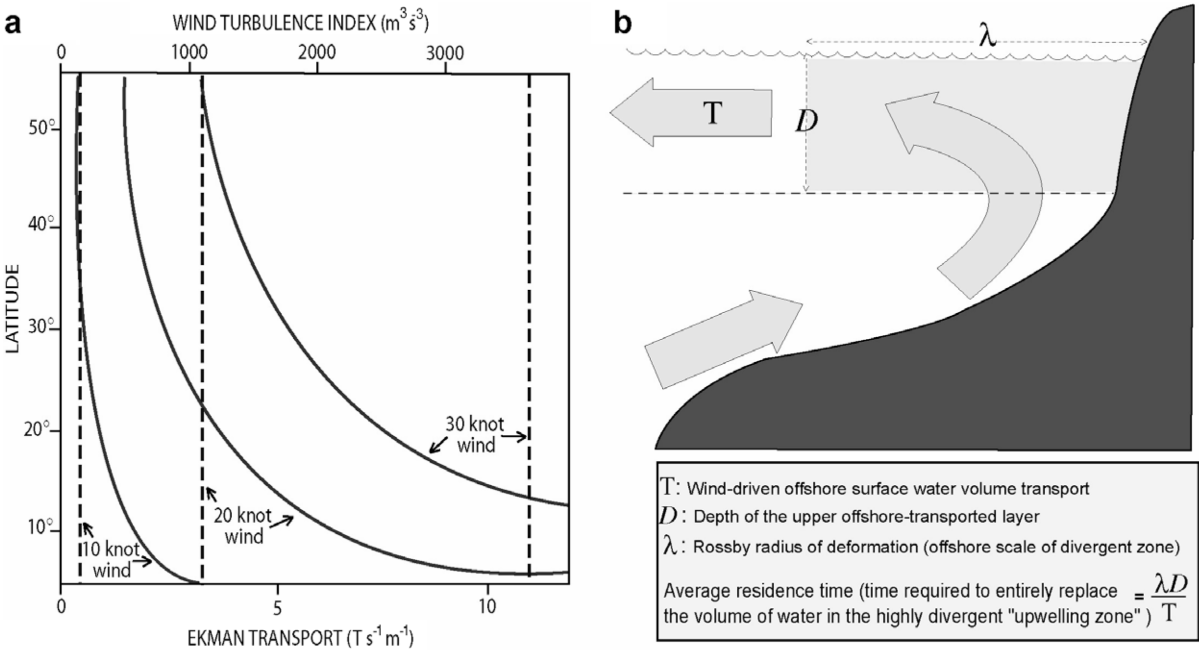

Fig. 3. (a) The "w^3" wind mixing index (3rd power, or "cube", of the wind speed), which is an indicator of wind mixing energy production, versus Ekman transport for several values of wind speed (after Bakun, 1996). (b) Diagram illustrating the computation of the renewal rate of water in the upper layer of the divergent coastal upwelling zone (shaded area).

Table 1
Latitudinal dependencies of various ecologically-significant factors. Selected coastal locations in various eastern ocean boundary upwelling systems are arrayed at the left according to their geographical latitudes.

	a	b	c	d	e	f	g
	Latitude (°)	Wind Speed (m s^{-1})	Mixing index (m^3 s^{-3})	Rossby radius[a] (km)	Residence time[b] (days)	Ekman depth (m)	Residence time[c] (days)
	55	12.3	1842	12.2	1.4	15.6	l.l
	50	11.9	1665	13.1	1.5	16.2	1.2
Vancouver Island ⇒							
Colombia River ⇒							
	45	11.4	1477	14.1	1.6	16.8	1.4
	40	10.9	1280	15.6	1.8	17.7	1.6
Lisbon ⇒							
Talcahoano ⇒							
	35	10.3	1079	17.4	2.0	18.7	1.9
S. California Bight ⇒							
Essaouira (Morocco) ⇒							
	30	9.6	878	20.0	2.3	20.0	2.3
Lüderitz ⇒							
	25	8.8	682	23.7	2.7	21.8	3.0
Walvis Bay ⇒							
	20	7.9	497	29.2	3.4	24.2	4.1
	15	6.9	327	38.6	4.5	27.8	6.2
	10	5.6	180	57.6	6.7	34.0	11.3
Chimbote ⇒							
	5	4.0	64	114.7	13.3	48.0	31.9

[a] Scale width of the coastal habitat.
[b] Time required to traverse a distance of one Rossby radius "habitat width" assuming a latitudinally-constant Ekman layer depth.
[c] Time required to traverse a distance of one Rossby radius assuming a theoretical (homogeneous fluid, constant eddy viscosity) Ekman Mayer depth.

and adult fishes. Nutrient recycling would be efficient and nutrients would thus be effectively retained within the productive upper layers. These considerations, while speculative, provide at least some degree of explanation for the fact that the pelagic fishes of north–central Peru seem to have been able to avoid the apparent reproductive difficulties experienced by fishes attempting to reproduce in other intense upwelling regions and to reach much higher population biomasses than are found in any of the other systems.

Anchovies such as the Peruvian anchoveta possess relative coarse-meshed gillrakers (van der Lingen, 1994). This apparently allows them to deploy a particulary large "filter basket" and thus to efficiently filter quite large water volumes relative to their body size. In addition, other aspects of the anchovy life style enable other efficiencies leading to very rapid population responses (Bakun and Broad, 2003; Bakun, 2006). Moreover, the unique conditions off Peru evidently enable the development of rich concentrations of particularly large multi-celled chains of large diatoms. As a consequence, Peruvian anchoveta may be able to directly filter and consume phytoplankton cells, an ability that in other upwelling systems tends to be possessed only by sardines, while also efficiently consuming the correspondingly large zooplankton either by filtering or particle-feeding (van der Lingen et al., 2006). In contrast, while sardines possess finer filters they incorporate other life-style characteristics that render them less efficient in taking advantage of highly enriched conditions (Bakun and Broad, 2003; Bakun, 2006), even while making them more resilient to, and opportunistic under, less productive, perturbed conditions.

4. Unique factor #2: Being located nearly directly at the terminus of the Pacific equatorial wave guide

However, one still wonders if the favorable aspects that are due primarily to its unique low-latitude position can in themselves be enough to account for the extraordinary fishery productivity of the Peru system. One is led to ponder whether perhaps the other unique aspect of the Peru system, its unique susceptibility to extreme inter-annual ecosystem perturbations associated with El Niño and other ENSO-related episodes could be also an important key to the puzzle (i.e., whether something that at the time is perceived as something extremely bad, might actually in the long run be something extremely good). Being geographically situated very near the eastern terminus of the Pacific equatorial wave guide, the Peru system bears the full immediate brunt of El Niño–Southern Oscillation phenomena, as well as the eventual brunt of every other major perturbation in the enormous Pacific Ocean basin, the remnants of which, through Rossby and Kelvin wave dynamics, must finally arrive to the intersection of the equator with the South American continental coast. These various arriving anomalies are then injected by coastally-trapped wave dynamics directly into the marine ecosystem off Peru, which is thereby subjected to intermittent drastic environmental rearrangements that are more extreme than are known to occur in any other large marine ecosystem on earth.

How could such a situation be viewed as being favorable? Well, for one thing, the extraordinary fishery productivity of the Peru system provides abundant proof that, at the least, it cannot be highly unfavorable. The available explanation would appear to lie in the idea that periodic extreme changes in habitat characteristics may exclude longer-lived, relatively non-productive, suppressive components (predators, competitors, etc.) from the system, as well as interrupt the development of nonlinear "adverse feedback" sequences (Bakun and Weeks, 2006). Such recurrent disruptions could thereby shift the advantage to rapidly-responding populations of small pelagic fishes over more specialized species that in other similar ecosystems may be able to establish and maintain themselves, feeding at a somewhat higher trophic level (i.e., less efficiently with respect to the primary organic production of the ecosystem) than anchovies, while suppressing the growth of lower trophic level populations through their incessant predation. If the impact of El Niño and similar disturbances is such as to expunge such less productive long-lived predatory components from the system, it seems conceivable that much larger biomasses might be attained by a low-trophic-level species having a much shorter life cycle and more rapid population response.

As a counter-example, the California system contains some sixty species of very long-lived predatory rockfish that, as adults, establish themselves in the system, grow very slowly, and remain ever present to immediately predate upon and extinguish incipient outbreaks of more productive, faster growing species (i.e., creating such a deep *predator pit*, according to the terminology of Bakun (1996), that significant population breakouts may be essentially impossible). In terms of tonnage landed, the fishery production of the entire California system is miniscule compared to that of Peru, and even compared to the other major eastern ocean upwelling regions of the world. Moreover, there is an increasingly evident global pattern (Bakun and Weeks, 2006) that suggests that once suppressive effects of predators are sufficiently interrupted so as to permit highly productive small pelagic components of an ecosystem to reach a dominant biomass level, these can then exert *feedback* effects that act to maintain their own dominance and to prevent reestablishment of the formerly dominant predators.

4.1. The Namibian experience

Bakun and Weeks (2006) have recently presented a hypothetical reconstruction of the events that appear to have led to the durable transformation and decimation of the fishery productivity of the northern Benguela marine ecosystem that we have identified in Section 2 as perhaps the most apt comparative analog to the Peru system. To exemplify the sort of negative feedback sequence that has not occurred in the Peru system, we briefly abstract the progression of reconstructed events as follows:

(1) The sardine population off Namibia was subjected to massive overfishing that was imposed in a geographically-biased exploitation pattern (concentrated in the primary reproductive habitat),
(2) fragmenting adapted migrational patterns linking favorable reproductive/nursery and adult feeding,
(3) depriving the population of linked synergistic usage of various favorable segments of the regional ecosystem,
(4) one result being cessation of adult feeding near the intense upwelling core off Lüderitz (Fig. 2b and d).
(5) Without the grazing controls formerly applied by the nektonic omnivorous sardines this allowed phytoplankton to bloom essentially unchecked in the intensely divergent upwelling zone (in which alternative zooplanktonic herbivores tend to be swept out of the system),
(6) causing increased deposition of unoxidized phytoplankton cells on the floor of the continental shelf, and associated increases in hypoxia, toxic gas production, etc.,
(7) as well as massive phytoplankton accumulation in the frontal systems that exist just offshore of the divergent upwelling zone (Fig. 2b and d),
(8) where it was available to nourish growing accumulations of herbivorous zooplankton that are also concentrated in the convergent frontal structures but now freed from the predation pressure formerly applied by the enormous sardine populations that previously concentrated feeding activity in the frontal zones.
(9) this provided a food resource for an explosive outbreak of zooplanktivores (medusae, pelagic gobis, etc.) that are voracious predators not only on larval food-producing zooplankton such as copepods, but also directly on fish eggs and larvae themselves,
(10) that then spread through the entire system, including the favorable reproductive habitats,
(11) durably trapping the northern Benguela system in a transformed, fish-adverse regime, in which fishery productivity has remained drastically depressed to the present day.

4.2. Hypothesis: El Niño — a favorable factor

A marine ecosystem operates as a complex adaptive system (Levin, 1998, 1999; Hsieh et al., 2005). In such systems, nonlinear processes interact in intricate ways to move the systems to configurations that may be much more difficult to reverse than to establish. One can make an analogy to an old Windows computer system that after a period of use begins to bog down and run slower and slower, and essentially cease to operate productively, until one hits the "re-set" button, and re-starts the system from an initial state. According to this hypothetical analogy, El Niño can be considered to represent a figurative "re-set" button for the Peru marine ecosystem of a sort that is not available in the same degree in any of the other similar systems of the world.

Stating the hypothesis more specifically, periodic extreme changes in habitat characteristics may exclude longer-lived, relatively non-productive, suppressive components from the system, as well as interrupt the development of nonlinear "adverse feedback" sequences, continually re-setting the system to initiate a sequence of highly productive transient population responses (note that the following suggested sequence may not be precisely repeatable in all El Niño episodes).

For example, during an El Niño year, sardine may utilize evolved opportunist adaptations to take advantage of the relative distress of other competing or suppressive ecosystem components to find a "loophole" (Bakun and Broad, 2003), particularly in the fields of predation on its early life stages, and produce a major population surge. More tropically-adapted organisms, including shrimp, scallop species, etc., may also arrive under the anomalous warm temperature and poleward flow contexts of an El Niño event.

The year following the El Niño, with many of the normal suppressive organisms having been expunged from the system and the typically rich upwelling-based nutrient supply reestablished, primary production may resume with vigor. Often, rapidly-responding opportunists (scallops, shrimps, etc.), including the temporary tropical immigrant species, may temporarily explode in abundance. Meanwhile, large reproductively-ready anchoveta may be re-arriving from refuges far to the south, and any that may have survived locally (at depth, etc.) will have reemerged into the newly productive upper layer conditions, and local anchovy population re-growth will be re-initiated.

By the second year after the El Niño, the rapidly-responding anchoveta population may already be filtering the water column at such a rate that it may no longer a very viable place for shrimp and scallop larvae, etc. Sardines that may have been hatched in the reproductive surge of the El Niño year will be growing in size and population biomass, even while tending to be outstripped in that respect by the later starting, but exceedingly rapidly-responding, anchoveta. Predatory organisms (seabirds, marine mammals, and predatory fishes) may begin also to respond, but not rapidly enough to appreciably slow the growth of the productive small pelagic fishes. Juvenile jack mackerel, spawned by a resident adult population in the less perturbed wider Pacific, may enter the system in large numbers to share the same role as mobile small pelagic planktivore.

Finally, by the time suppressive ecosystem components are able to build sufficient biomass to begin to pare down this unrestrained production, a new El Niño episode arrives to re-set the system, thereby reinitiating the quasi-repeatable sequence of highly productive transient events.

5. Climate change and upwelling systems

So the Peru system seems to lie within what might be called a "sweet spot" in the spectrum of marine ecosystem configurations.

Moreover, that "sweet spot" appears to be pretty robust, having more than once rebounded from major declines that occurred under exploitation by the largest fishery that has ever existed on earth. But it also appears inevitable that the earth's climate is undergoing accelerating radical changes as a result of unrestrained industrial inputs of greenhouse gases. And climate, as reflected in ENSO variability (Section 4) and latitudinally-regulated balances of enrichment, turbulence, and transport (Section 3), is the inferred basis of the Peru marine ecosystem's "sweet spot". Will the climate changes that appear to be rapidly unfolding be sufficient shift the Peru system out of its current "sweet spot" such that, in the great marine ecosystem "shake-up" that appears to loom just ahead, it may lose its preeminent position and recede back into the mixed crowd of winners and losers?

5.1. Coastal upwelling intensification

One of the reasons that coastal upwelling tends to be a spring-summer phenomenon in the subtropics, and a more year-round phenomena in more near-equatorial regions such as Peru, is that a strong pressure gradient forms between a thermal low-pressure cell that develops over the heated land surface and higher pressure existing over the more slowly warming waters of the ocean. This cross-shore pressure gradient supports an alongshore geostrophic wind that drives an offshore-directed Ekman transport of the ocean surface layer (Fig. 4a). When the surface waters are thereby forced offshore from the solid coastal boundary on spatial scales too large for them to be replaced by waters moving horizontally along the coast, mass balance is maintained by upwelling of subsurface waters.

Eastern sides of oceans are characterized by much drier atmospheres than western sides. Because the most important greenhouse gas in the earth's atmosphere is water vapor, eastern ocean boundary regions tend naturally to experience a much reduced greenhouse effect. Consequently, local nighttime cooling by long wave radiation is rapid and efficient. This tends to relax the thermal low-pressure cells that had built up over the coastal landmass during the day.

As atmospheric greenhouse gas content increases, nighttime radiative cooling will be increasingly suppressed. The average rate of heating over the land will be further enhanced relative to that over the ocean, causing intensification of the low-pressure cells over the coastal interior. This will generate a feedback sequence as the resulting pressure gradient increase is matched by a proportional wind increase, which correspondingly increases the intensity of the upwelling in a nonlinear manner (by a power of 2 or more under these strong wind conditions (Trenberth et al., 1990)) which, in concert with ocean surface cooling produced by the intensified upwelling, further enhances the land-sea temperature contrast, the associated cross-shore pressure gradient, the upwelling-favorable wind, and so on (Fig. 4b). Moreover, an additional potentially contributing set of feedback mechanisms involves greenhouse-associated effects on the vegetal land cover that may regulate the heating of the coastal landmass (Diffenbaugh et al., 2004).

A variety of observational evidence indicates that this projected increase in upwelling intensity is even now unfolding in the major upwelling regions of the world (Bakun, 1990, 1992; Shannon et al., 1992; Schwing and Mendelssohn, 1997; Mendelssohn and Schwing, 2002; Field et al., 2006; Vargas et al., 2006).

5.2. Equatorial relaxation

Countering the prognosis for upwelling intensification is the emerging scientific consensus that a result of impending global climate changes will be a general slowing of the equatorial Pacific Walker circulation (Fig. 5a) and a consequent weakening of the Pacific trade wind system (Vecchi et al., 2006). As stated in Section 1, the major upwelling-favorable wind flow off Peru separates from the South American coast to merge directly into the Pacific southeast trade wind system nearly immediately after exiting the Peruvian upwelling zone. So, is there a paradox? Obviously, for both (1) an increase in upwelling-favorable winds and (2) a decrease in trade winds to occur according to projections, some type of "disjunction" in phases of intensity variation must occur between the two inter-connected systems.

Juxtaposing a low-passed time series of upwelling-favorable winds off Peru (Bakun and Mendelssohn, 1989) published in the 'Peru Upwelling Ecosystem' volumes assembled by Daniel Pauly and his collaborators, with a similar series of the Southern

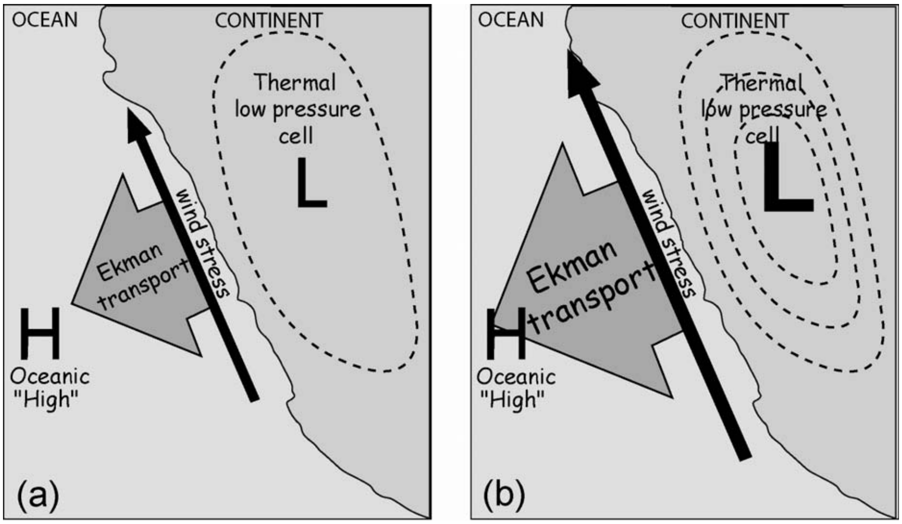

Fig. 4. Diagram of upwelling intensification mechanism: (a) a "thermal" low-pressure cell builds up over the coastal landmass due to heating of the continental surface relative to the more slowly heating ocean, exerting equatorward geostrophic wind stress on the sea surface that, in turn, drives offshore-directed Ekman transport of ocean surface water and corresponding upwelling of deeper waters required to replace the surface waters transported offshore; (b) buildup of greenhouse gases in the atmosphere inhibits nighttime cooling of the heated coastlands, increasing average intensity of the coastal low-pressure cell and associated upwelling-favorable wind, which in terms drives quadratic (or greater) increases in offshore surface transport and resulting upwelling.

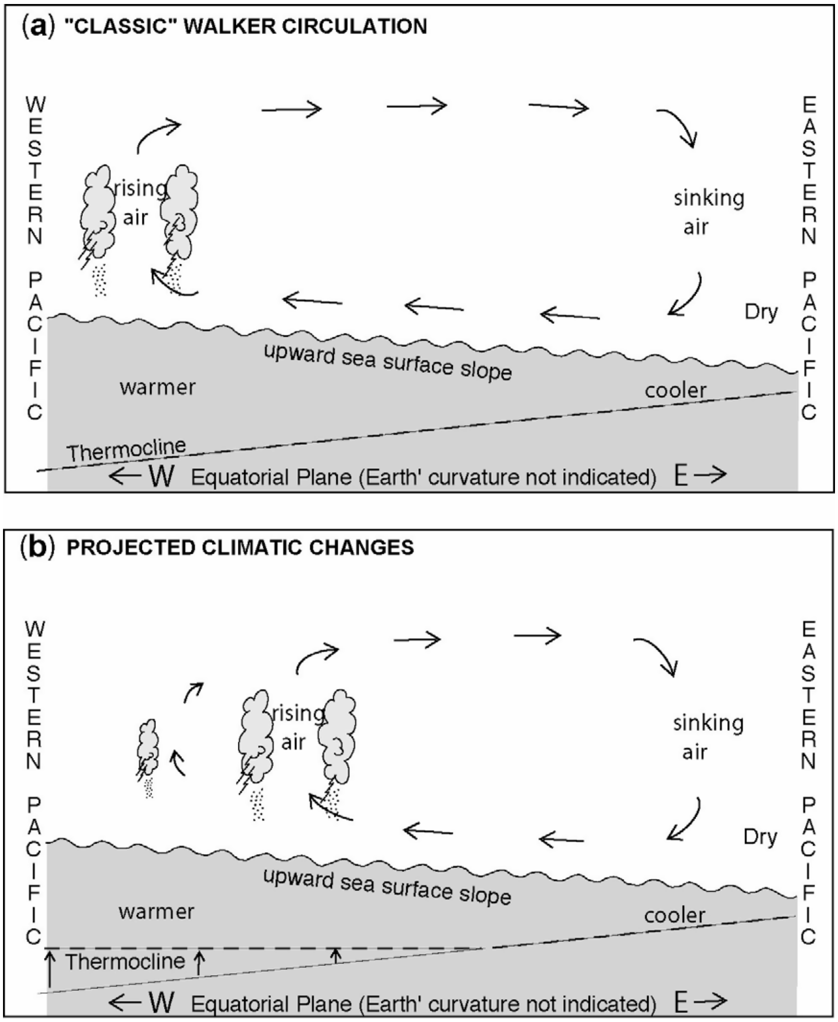

Fig. 5. Diagrams of Pacific Walker circulation: (a) typical La Niña configuration; (b) future climate change tendency predicted by the IPCC model ensemble (Vecchi and Soden, 2007).

Oscillation Index (SOI), which is an index of Pacific trade wind strength (Bjerknes, 1966; Quinn et al., 1978), makes it obvious that such a disjunction does indeed occur (Fig. 6). The strengths of upwelling-favorable winds off Peru and the large scale Pacific trade wind system of the tropical Pacific Ocean are clearly negatively correlated on multi-annual time scales. Moreover, comparison to the sequence of El Niño periods (shaded vertical bars in Fig. 6) makes it also clear that the disjunction occurs on the ENSO time scale. El Niño episodes tend to correspond to reduced strength of the trade winds. This is well known. Less well known is the fact that upwelling-favorable wind off Peru appears to consistently increase, rather than decrease, during virtually all El Niño episodes.

Computed correlations of respective annual- and quarterly-mean series of unfiltered monthly values are not notably high (Fig. 6, right panel) given the obvious synchronies visible in the left panel of Fig. 6, suggesting that the ENSO-scale may be the only scale on which the anti-correlation operates, i.e., suggesting that there may be suppression of the ENSO-related anti-correlation by the more expected opposite positive correlation between the inter-connected wind systems that might be the rule on shorter than ENSO, or longer than ENSO (i.e., the long-term trends visible in Fig. 6) time scales. This idea is supported by the fact that the negative correlations are highest during the austral spring and summer seasons, the seasons when the El Niño mechanisms act with greatest effect.

We propose that this association of increases in locally wind-induced Ekman upwelling off Peru with El Niño constitutes, in itself, a verification of the upwelling intensification hypothesis diagrammed in Fig. 4. Water vapor is the most important of all the greenhouse gases in the earth's atmosphere (Houghton, 2001). The atmosphere of the tropical eastern Pacific boundary zone becomes much more moist during El Niños, implying a much larger combined load of greenhouse gases. Accordingly, this mechanism could reasonably account for the evident increases in upwelling-favorable wind that regularly occur off Peru during El Niño episodes (Fig. 6).

6. Climate change and Peruvian fisheries

So it seems that, beyond the more vague temperature-related prognoses often offered for other types of regional marine ecosystems, there does appear to be some logical and empirical framework on which to base considerations of effects of impending greenhouse-gas-mediated climate change on the Peru marine ecosystem. First, locally wind-induced Ekman upwelling may be expected to increase. Second, the Pacific equatorial system, due to relaxation of the trade wind circulation, may become more chronically "El Niño"-like in its underlying mean background state. If so, the more vigorous local upwelling expected off Peru might have

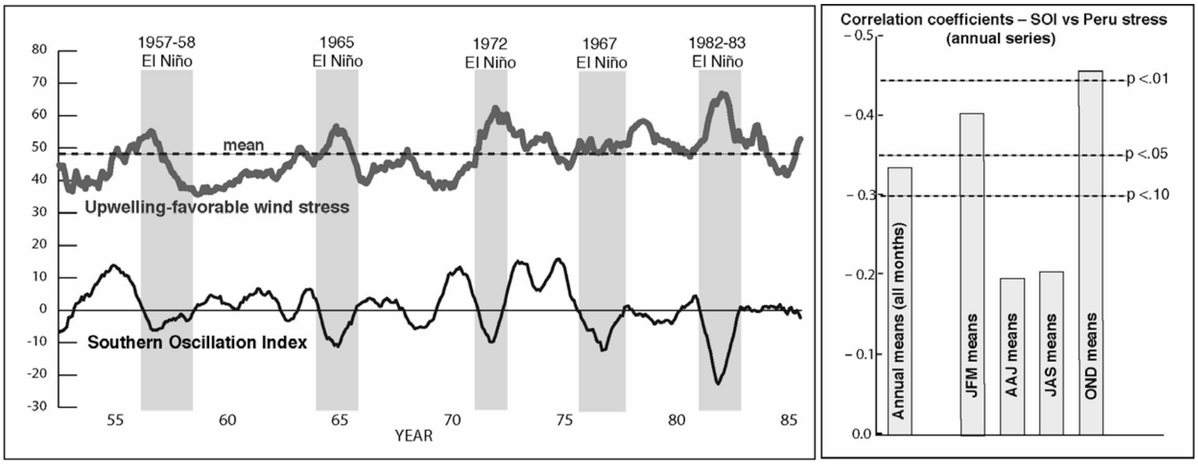

Fig. 6. Left panel: Anti-correlation, on the ENSO time scale, of low-pass-filtered (12-month running means of monthly values) Pacific trade wind strength (Southern Oscillation Index) and intensity of upwelling-favorable wind stress off Peru (as reported by Bakun and Mendelssohn (1989)). Right panel: Correlation coefficients between series of annual and quarterly means of unfiltered monthly values of the two time series. Significance levels (two-tailed tests) are indicated.

less effect due to a deeper thermocline/nutricline structure characteristic of El Niño conditions off Peru.

However, the IPCC model ensemble studies indicate a striking feature in the thermocline response to the weakened trade wind circulation. Rather than simply relaxing the tilt of the trans-Pacific thermocline structure in a linear manner, it appears that the changes will be most intense in the western Pacific, but only rather minor in the eastern Pacific (Vecchi and Soden, 2007). A simplified explanation of this prediction may be posed as follows. The horizontal frictional stress exerted on the ocean surface by the trade winds produces divergence and upwelling in the near vicinity of the equator. But slightly further away from the equator, there is convergence of Ekman transport due to the rapid decline of the coriolis parameter with increasing latitude (Cane and Zebiak, 1985; Philander and Lau, 1988). This produces downwelling to both sides of the near-equatorial zone that, because of the very large baroclinic Rossby radius of deformation (Charney, 1955; Yoshida, 1967; Walin, 1972) at very low latitudes, affects the entire equatorial band, including the near-equatorial zone itself. The projected decrease in trade wind strength would decrease this downwelling tendency produced by the off-equatorial Ekman convergence. Consequently, in terms of “anomaly” (i.e., the future state subtracted from the present state), the expected trade wind relaxation should produce an anomalous upwelling that effects the near-equatorial zone essentially across the entire Pacific, reinforcing the anomalous upward tilt of the near-equatorial thermocline in the western Pacific but tending to counter its anomalous downward tilt in eastern Pacific (Fig. 5b). Accordingly, the effect of the predicted chronic “El Niño”-like state of the tropical Pacific, while leading to a significant shallowing of the thermocline structure in the western equatorial Pacific, may produce only a minimal change in depth of the thermocline structure in the eastern Pacific. Thus effects on the rate of supply nutrients and cooler temperature waters to the local Peruvian upwelling zone may be correspondingly minimal, perhaps even overbalanced by the envisaged increases in locally wind-driven coastal upwelling intensity, such that nutrient inputs and upwelling-induced surface cooling may actually be enhanced.

However, if local coastal upwelling intensifies (Section 5.1) the rates of offshore transport and wind-driven turbulent mixing would increase accordingly. Could that shift Peru’s marine ecosystem out of its current “sweet spot”? Could the currently evident tendency for anchoveta dominance give way to the sardine dominance that seems to characterize the other eastern boundary upwelling systems that are currently subject to relatively stronger winds and more intense turbulence generation? If so, the more wide-ranging sardines would tend to spread the essential fishery productivity of the Peru system beyond the local area, as well as perhaps be less efficient in growing population biomass between ecosystem perturbations.

Moreover, while the potential effect of climate change on the frequency of El Niño episodes remains unclear, the predicted lessened trans-Pacific contrast in depth of the thermocline structure (Fig. 5) suggests that when they do occur they may on average be less intense than currently (i.e., the thermocline-depressing Kelvin waves arriving from the western equatorial Pacific will have lower amplitudes). How would this impact the “re-set button” considerations discussed in Section 4? Could this adversely impact the viability of sardines in the Peru system, which seem to be favored by perturbed conditions (Bakun and Broad, 2003; Agostini et al., 2007). More importantly, could Peru suddenly become subject to growth of debilitating nonlinear feedback instabilities, such as outlined in Section 4.1 as having had devastating effects in the northern Benguela marine ecosystem?

While we are not able with any confidence to answer these last crucial questions, the analysis presented above may offer, at least, a more specific framework for posing them. Moreover, it may suggest the value of widening one’s scope of attention beyond one’s own local system, to a more global view, wherein viewing the future progression of events in the comparative context of a number of regional systems. Each exhibiting varying degrees of similarity and difference, may help to more correctly apprehend and interpret the meaning of the events observed in one’s own “home” marine ecosystem of immediate interest.

Acknowledgment

This paper is a contribution of the PIOS ‘Adverse Eco-Feedbacks’ Project, funded by the Pew Institute for Ocean Science.

References

Agostini, V.N., Bakun, A., Francis, R.C., 2007. Larval stage controls on sardine recruitment variability: the balance between predation and food availability. Marine Ecology Progress Series 345, 237–244.

Bakun, A., 1990. Global climate change and intensification of coastal ocean upwelling. Science 247, 198–201.

Bakun, A., 1992. Global greenhouse effects, multi-decadal wind trends and potential impacts on coastal pelagic fish populations. In: ICES Marine Science Symposia, vol. 195, pp. 316–325.

Bakun, A., 1996. Patterns in the Ocean: Ocean Processes and Marine Population Dynamics. University of California Sea Grant, San Diego, California, USA, in cooperation with Centro de Investigaciones Biológicas de Noroeste, La Paz, Baja California Sur, Mexico, 323pp.

Bakun, A., 2006. Wasp-waist populations and marine ecosystem dynamics: navigating the "predator pit" topographies. Progress in Oceanography 68, 271–288.

Bakun, A., Broad, K., 2003. Environmental loopholes and fish population dynamics: comparative pattern recognition with particular focus on El Niño effects in the Pacific. Fisheries Oceanography 12, 458–473.

Bakun, A., Mendelssohn, R., 1989. Alongshore wind stress 1953–82: correction, reconciliation and update through 1986. In: Pauly, D., Muck, P., Mendo, J., Tsukayama, I. (Eds.), The Peruvian Upwelling Ecosystem: Dynamics and Interactions. International Center for Living Aquatic Resources Management (ICLARM), Manila, Philippines, pp. 77–81.

Bakun, A., Weeks, S.J., 2006. Adverse feedback sequences in exploited marine systems: are deliberate interruptive actions warranted? Fish and Fisheries 7, 316–333.

Bjerknes, J., 1966. A possible response of the atmospheric Hadley circulation to equatorial anomalies of ocean temperature. Tellus 18, 820–829.

Boyer, D., 1996. Stock dynamics and ecology of pilchard in the northern Benguela. In: O'Toole, M.J. (Ed.), The Benguela Current and Comparable Eastern Boundary Upwelling Ecosystems. Deutsche Gesellschaft für Techhnische Zusammenarbeit (GTZ) GmbH, Eschborn, Germany, pp. 79–82.

Boyer, D.C., Hampton, I., 2001. An overview of the living marine resources of Namibia. South African Journal of Marine Science 23, 5–35.

Carr, M.E., 2001. Estimation of potential productivity in eastern boundary currents using remote sensing. Deep-Sea Research 49, 59–80.

Charney, J.G., 1955. The generation of ocean currents by wind. Journal of Marine Research 14, 447–498.

Diffenbaugh, N.S., Snyder, M.A., Sloan, C., 2004. Could CO_2-induced land-cover feedbacks alter near-shore upwelling regimes? Proceedings of the National Academy of Sciences of the United States of America 101, 27–32.

Ekman, V.W., 1905. On the influence of the Earth's rotation on ocean currents. Arkiv för Matematik, astonomi och fysik 2, 1–52.

Elsberry, R.L., Garwood Jr., R.W., 1978. Sea-surface temperature anomaly generation in relation to atmospheric storms. Bulletin of the American Meteorological Society 59, 786–789.

Field, D., Purca, S., Gutierrez, D., Lucas, A. Sifeddine, A., Ortlieb, L., 2006. Is long-term warming off Peru similar to that of the North Pacific. Book of Extended Abstracts, International Conference The Humboldt Current System (HCS195): Climate, Ocean Dynamics, Ecosystem Processes, and Fisheries, Lima, Peru, November 27–December 1, 2006, pp. 26–27.

Houghton, J.T., 2001. IPCC Report. Cambridge University Press, Cambridge, UK.

Hsieh, C., Glaser, S.M., Lucas, A.J., Sugihara, G., 2005. Distinguishing random environmental fluctuations from ecological catastrophes for the North Pacific Ocean. Nature 435, 336–340.

Levin, S.A., 1998. Ecosystems and the biosphere as complex adaptive systems. Ecosystems 1, 431–436.

Levin, S.A., 1999. Fragile Dominion: Complexity and the Commons. Perseus Books, Reading, MA. 250pp.

Lynam, C.P., Gibbons, M.J., Axelsen, B.J., Sparks, C.A.J., Coetzee, J., Heyward, B.J., Bierly, S.S., 2006. Jellyfish overtake fish in a heavily fished ecosystem. Current Biology 16, R492–R493.

Mendelssohn, R., Schwing, F.B., 2002. Common and uncommon trends in SST and wind stress in the California and Peru–Chile current systems. Progress in Oceanography 53, 141–162.

Mayr, E., 1982. The Growth of Biological Thought. Harvard University Press, Cambridge, MA. 974pp.

Mooers, C., Allen, J.S., 1973. Final Report of the Coastal Upwelling Ecosystems Analysis Summer 1973 Theoretical Workshop. School of Oceanography, Oregon State University, Corvallis, OR. 137pp.

Paulik, G.J., 1971. Anchovies, birds, and fisherimen in the Peru Current. In: Murdoch, W.W. (Ed.), Environment: Resources, Pollution and Society. Sinauer Associates, Stanford, CT, pp. 156–185.

Quinn, W.H., Zopf, D.D., Short, K.S., Kuo Yang, T.R.W., 1978. Historical trends and statistics of the Southern Oscillation—El Niño and Indonesian droughts. Fishery Bulletin, US 76, 663–678.

Shannon, V., Crawford, R.J.M., Pollock, D.E., Hutchens, L., Boyd, A.J., Taunton-Clark, J., Badenhorst, A., Melville-Smith, R., Augustin, C.J., Cochrane, K.L., Hampton, I., Nelson, G., Japp, D.W., Tarr, R.J.Q., 1992. The 1980s – a decade of change in the Benguela ecosystem. In: Payne, A.I.L., Brink, K.H., Mann, K.H., Hilborn, R. (Eds.), Benguela Trophic Functioning. South African Journal of Marine Science 12, 271–296.

Schwing, F.B., Mendelssohn, R., 1997. Increased coastal upwelling in the California Current System. Journal of Geophysical Research 102, 3421–3438.

Sverdrup, H.U., 1953. On conditions for vernal blooming of phytoplankton. Journal du Conseil International pour l' Exploration de la Mer 18, 287–295.

Trenberth, K.E., Large, W.G., Olson, J.G., 1990. The mean annual cycle in global ocean wind stress. Journal of Physical Oceanography 20, 1742–1760.

van der Lingen, C.D., 1994. Effect of particle size and concentration on the feeding behavior of adult pilchard, *Sardinops sagax*. Marine Ecology Progress Series 109, 1–13.

van der Lingen, C.D., Hutchings, L., Field, J.G., 2006. Comparative trophodynamics of anchovy *Engraulis encrasicolus* and sardine *Sardinops sagax* in the southern Benguela: are species alternations between small pelagic fish trophodynamically mediated? African Journal of Marine Science 28, 465–477.

Vargas, G., Pantoja, S., Ruttlant, J.A., Lange, C.B., Ortlieb, L., 2006. Enhancement of ENSO-like coastal upwelling variability in the Peru–Chile eastern boundary Current during the 20th century warming. Book of Extended Abstracts, International Conference The Humboldt Current System (HCS115): Climate, Ocean Dynamics, Ecosystem Processes, and Fisheries, Lima, Peru, November 27–December 1, 2006, p. 30.

Vecchi, G.A., Soden, B.J., Wittenberg, A.T., Held, I.M., Leetmaa, A., Harrison, M.J., 2006. Weakening of tropical Pacific atmospheric circulation due to anthropogenic forcing. Nature 441, 73–76.

Vecchi, G.A., Soden, B.J., 2007. Global Warming and the weakening of tropical circulation. Journal of Climate 20, 4316–4340.

Walin, G., 1972. On the hydrographical response to transient meteorological disturbances. Tellus 24, 169–186.

Yoshida, K., 1967. Circulation in the eastern tropical oceans with special reference to upwelling and undercurrents. Japanese Journal of Geophysics 4, 1–75.

Progress in Oceanography 79 (2008) 300–307

Contents lists available at ScienceDirect

Progress in Oceanography

journal homepage: www.elsevier.com/locate/pocean

The impact of overfishing and El Niño on the condition factor and reproductive success of Peruvian hake, *Merluccius gayi peruanus*

Michael Ballón [a,b,*], Claudia Wosnitza-Mendo [a], Renato Guevara-Carrasco [a], Arnaud Bertrand [a,b]

[a] *Instituto del Mar del Perú, Esquina Gamarra y Gral. Valle s/n, Apartado 22, Callao, Lima, Peru*
[b] *IRD, UR097, CRHMT, Avenue Jean Monnet, BP 171, 34203 Sète Cedex, France*

ARTICLE INFO

Article history:
Accepted 14 October 2008
Available online 21 October 2008

Keywords:
Peruvian hake *Merluccius gayi peruanus*
Fish condition factor
Gonad index
Sex ratio
Overfishing
El Niño southern oscillation

ABSTRACT

In this study we examine physiological responses of Peruvian hake (*Merluccius gayi peruanus*) to changes in their population structure and physical environment during the period 1971–2004. In particular, we assess the relative investment of energy in growth and/or reproduction of small (20–35 cm) and large (35–50 cm) hake. We calculated the (i) condition (Fulton's K), (ii) gonad and (iii) gut fullness indices for 42,761 female hakes sampled from commercial landings; these indices indicate fish somatic, reproductive and feeding condition, respectively. Using Generalized Additive Models we then examined potential relationships between these indices and sea surface temperature anomalies and date. Drastic energy exhaustion and a decrease in female hake fecundity were observed during El Niño events. The long-term trend showed a general increase in condition factor and a decrease in gonad index for large hake between 1971 and 2004. Small hake exhibited a different trend with an increase in reproductive activity, which was accompanied by an earlier maturation. We hypothesise that the observed low investment of energy in reproduction by large female hake might be related to the lack of large males, due to a sex-selective fishery and the impact of El Niño. We suggest that fishing diminished hake reproductive capacity, modified the sex ratio in favour of females and increased population vulnerability to environmental stress, in particular to the El Niño. The impact of multidecadal variability and predators like the squid, *Dosidicus gigas*, remain unresolved until longer time series become available.

1. Introduction

Peruvian hake (*Merluccius gayi peruanus*) is the most abundant commercially exploited demersal fish in the northern Humboldt Current System (Peru). Intense fishing pressure was exerted on hake since the early 1970s. Fishing effort increased from an average of 40 active vessels per year before the 1990s to 74 in the early 2000s (Guevara-Carrasco and Lleonart, 2008). It has been hypothesized that fishing caused radical declines in biomass leading to the change of fishery status from fully exploited to overfished and to the closure of the fishery in 2002 (Guevara-Carrasco, 2004). During this period, the population structure changed, exhibiting a drastic reduction in mean hake size (Fig. 1). Large hake (>35 cm) dominated the landings until the late 1980s; after that, smaller hake represented the bulk of the catches. This change was accompanied by an early age of maturation with the percentage of mature hake at the age of 2 years passing from almost zero during the 1980s to more than 60% in the early 2000s (Fig. 1; Wosnitza-Mendo et al., 2004; Guevara-Carrasco and Lleonart, 2008). The fishery was reopened after 18 months in 2004 and total allowable catches and individual non-transferable quotas were implemented to control the exploitation of hake. Although there has been a reduction in fishing effort, hake mean size and abundance remain reduced (Guevara-Carrasco and Lleonart, 2008).

The Peruvian coast is strongly affected by El Niño that alters the physical (e.g. upwelling efficiency, temperature, salinity, oxygen, vertical stratification), and biological (species composition, abundance, distribution and concentration) environment off Peru (Arntz and Fahrbach, 1991; Wolff et al., 2003). El Niño thus affects hake by (i) extending the distribution of hake eggs, larvae (Sandoval de Castillo et al., 1989), juveniles and adults southwards (Samame, 1985), (ii) changing the diet from fish to crustaceans (Sanchez et al., 1985), and (iii) decreasing fishing mortality due to a lower availability (Espino et al., 1985). Many aspects of these changes remain unclear. Indeed, Espino (1990) suggested that El Niño was responsible for the recovery of Peruvian hake population in the 1980s, whereas Wosnitza-Mendo et al. (2004) argued that El Niño was one of the main causes of the decline in hake size during 1991–1992. These opposing views of the possible effects of El Niño on hake (see Espino, 1990; Tam et al., 2006; Wosnitza-Mendo et al., 2004) persist at least partly because of a lack of reliable estimates of natural mortality, making it difficult to separate the effect of the natural environment from that of fishing.

---

[*] Corresponding author. Address: Instituto del Mar del Perú, Esquina Gamarra y Gral. Valle s/n, Apartado 22, Callao, Lima, Peru. Tel.: +56 1 4202000.
E-mail address: michballon@googlemail.com (M. Ballón).

0079-6611/$ - see front matter © 2008 Elsevier Ltd. All rights reserved.
doi:10.1016/j.pocean.2008.10.016

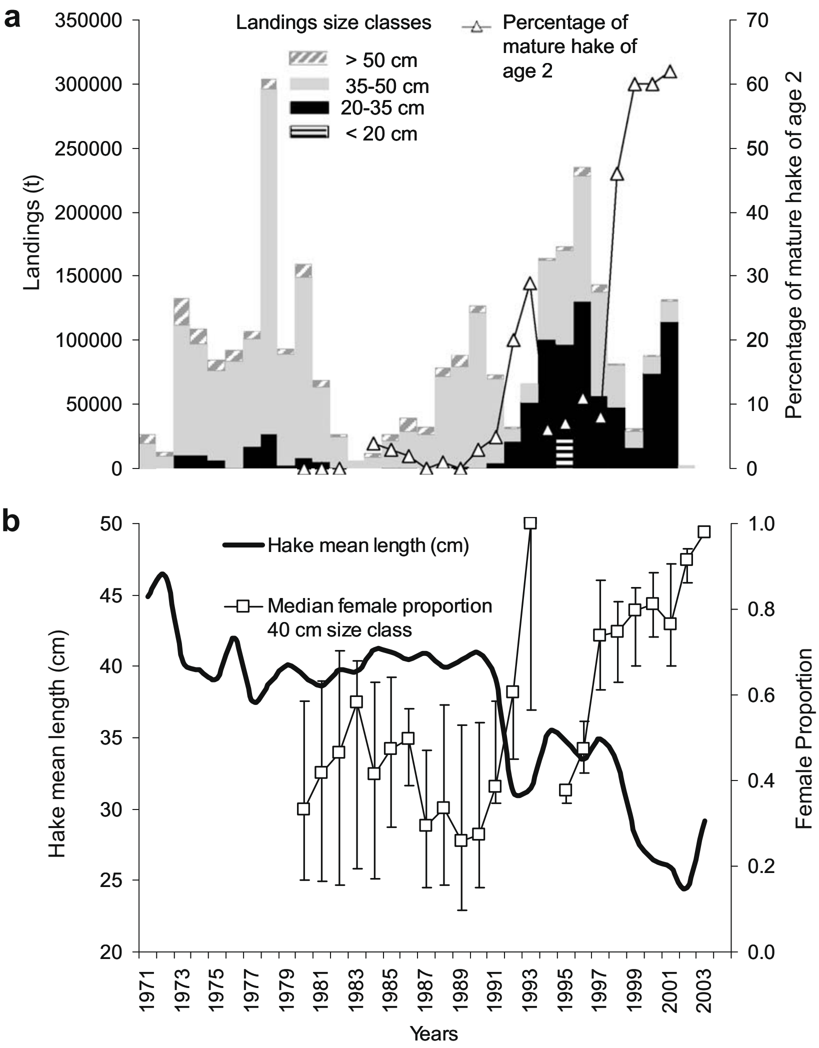

Fig. 1. (a) Annual hake landings by size classes (histograms), and percentage of mature hake of age 2 (solid line with empty triangles; redraw from Wosnitza-Mendo et al. (2004) and Guevara-Carrasco and Lleonart (2008)). (b) Hake mean length in catch over time (smooth black solid line), and median, maximum and minimum hake female proportion in catch for the 37.5–42.5 cm length interval (solid line with empty square).

To determine any overall El Niño effect and to separate it from the long-term effect of fishing we assess the overall condition and reproductive health of hake over time. We assume that El Niño's effect on hake biology can be isolated if an El Niño event provokes a sudden and short term deviation from the long-term trend in hake's condition and reproduction. In this study hake condition and energy investment in reproduction have been assessed using Fulton's condition factor (CF) and gonad index (GI), respectively. Fulton's condition factor indicates the energy budget of the fish (Dutil and Lambert, 1997b), and decreases as a result of starvation (Dutil et al., 2006), investment of energy in reproduction (Lambert and Dutil, 2000), and adverse physical (Takasuka et al., 2005) conditions. The gonad index assesses fish fecundity (Takasuka et al., 2005; Murua et al., 2006). Since fecundity and fish condition are positively correlated (Brooks et al., 1997; Kurita et al., 2003), CF and GI can serve as indices of environmental or feeding conditions (Dutil and Lambert, 1997a). When used in conjunction with fish size data, a compensatory response of small fish to a reduction in overall population size (Trippel, 1995) can be detected.

In this study we calculate the CF, GI and gut Fullness (FI) indices of 42,761 female hake which were sampled between 1971 and 2004, the largest data set ever published on hake. Large and small size classes were assessed to determine if they respond similarly to El Niño and fishing pressure.

We first discuss the effects of El Niño and fishing on CF and GI. Then, long-term trends of fish condition and gonad index are examined with regard to the different responses of large and small hake to a reduction in overall population size and in population size structure, and to the changes in the sex ratio.

2. Materials and methods

Hake mean length in catches and catch size structure by size class (<20 cm; 20–35 cm; 35–50 cm; >50 cm) were determined from sampling performed by IMARPE (Ballón et al., 2007). The female proportion of adult hake in catches between 1980 and 2003 was estimated by the Demersal Fish Department of IMARPE. The median of the female proportion in catches, as well as the minimum and maximum proportions of 37.5–42.5 cm long fish were plotted against time to observe their respective trends (Fig. 1).

The hake biological indices were derived from biological sampling of female hake captured by commercial trawlers off Paita (05° S) from 1971 to 2004. Most of the samplings were performed over the whole year (see electronic supplementary material). Total length, body weight, stomach weight, sex and gonad weight were recorded. Fish smaller than 20 cm and larger than 50 cm were excluded because hake smaller than 20 was almost absent from observations until the mid 1990s and very large hakes were very scarce in samples at the end of the analysed period.

Three indices were calculated for each fish:

1. An indicator of overall health or condition, Fulton's condition factor (CF), with W; the total body weight (in g), and L; the total length (in cm)

   $\mathrm{CF} = W^{*}L^{-3}$

2. An indicator of reproductive health or condition, the gonad index (GI), with Wg; the gonad weight (in g)

   $GI = Wg^{*}W^{-1}$, and

3. An indicator of recent feeding, the fullness index, with Ws; the stomach weight (in g)

   $\mathrm{FI} = Ws^{*}W^{-1}$

In addition to the fish indices, monthly anomalies of sea surface temperature (SSTA) at a coastal station in front of Paita (5° S) were used to assess the physical environment. GI and CF for the entire fish sample and for hake smaller and larger than 35 cm were plotted as monthly averages with their confidence intervals for the period 1971–2004 (Fig. 2). El Niño periods were also indicated in the same graph to visualize the trends of GI and CF during these periods. Regression lines for each series were adjusted to determine the long-term trend of GI and CF.

We sought potential relationships between CF and the other parameters GI, FI, SSTA and date (year–month) using Generalized Additive Modelling (GAM, Hastie and Tibshirani, 1990); a technique that can detect non-linear and multivariate relationships between variables. Cubic spline smoothing was used to estimate the non-parametric function of CF versus the other parameters using S-Plus (Insightful Corporation, Seattle, WA, USA). Since all sets of variables were incomplete before 1980, the GAMs were constructed for 1980–2004. As hake's diet and relative body, gonad and digestive tract weights are known to depend on fish size (Fuentes et al., 1989; Chouinard and Swain, 2002; Lloret et al., 2002), and because large individuals are known to invest more energy in reproduction than small ones (Scott et al., 2006), fish length was not considered in an overall model. Instead a different model was constructed for each 5 cm fish length interval. Results from a first set of GAM analyses performed by 5 cm fish length interval showed that results were similar for fish size ranging from 20 to 35 cm, and from 35 to 50 cm. For this reason, and to avoid repetitive results, we collapsed the six size classes into two larger classes

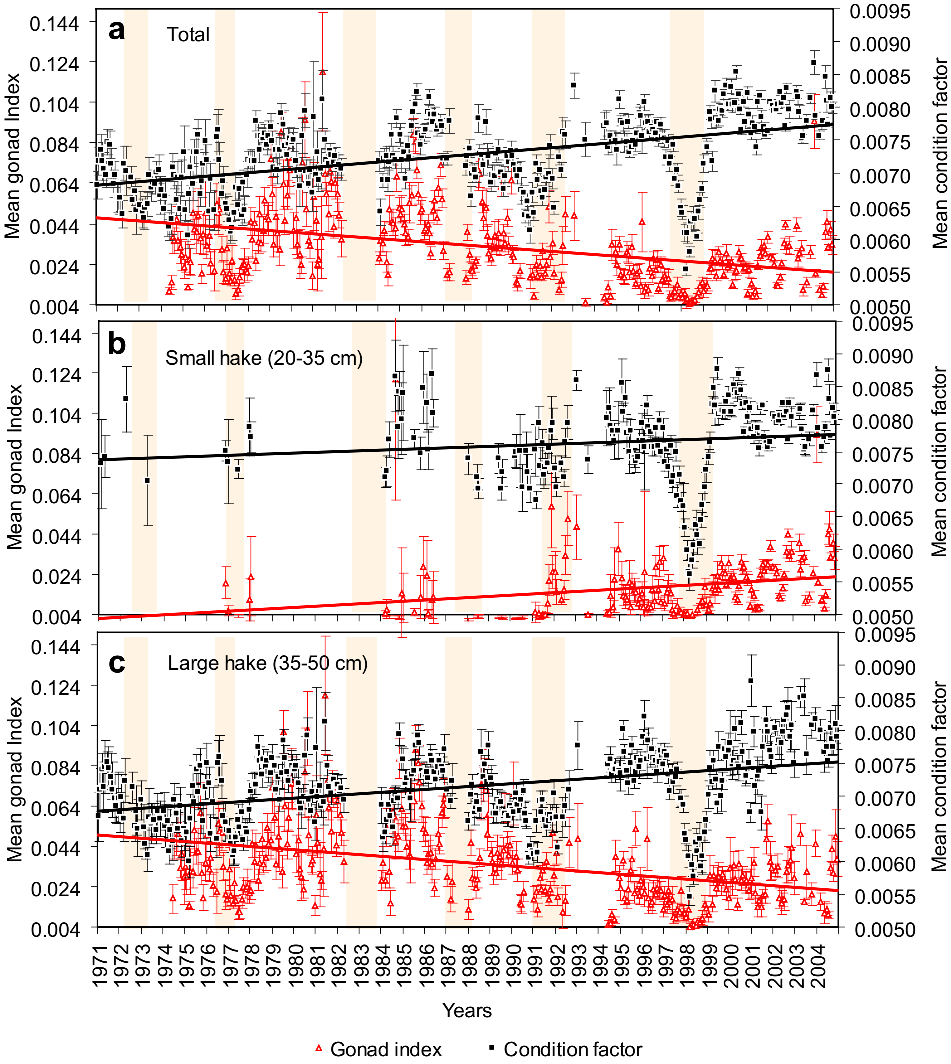

Fig. 2. Monthly mean condition factor (black full squares) ± confidence intervals (black bars), gonad index (red empty triangles) ± confidence intervals (red bars) and lineal trends (black and red solid lines) for (a) all sizes, (b) small (<35 cm) and (c) large (>35 cm) female hake from 1971 to 2004. The overlaid areas in salmon colour correspond to El Niño periods.

(20–35 and 35–50 cm), which encompassed and revealed the main trends.

The GAM described above was repeated using the gonad index (GI) as a dependent variable and CF, FI, SSTA and date as independent variables. Although the relationship between CF and GI was evaluated in the first GAM, it was examined again with GI as the dependent variable, in order to provide the complete matrix of independent variables for each GAM.

3. Results

3.1. Hake size structure and female proportion in catches

Hake size structure in landings showed drastic changes between 1971 and 2003. During this period, hake mean size decreased from over 40 cm to about 25 cm (Fig. 1b). Hake landings were dominated by fish larger than 35 cm during the 1970s–1980s, then by hake smaller than 35 cm. In recent years, hakes larger than 35 cm represented a very small proportion of the catches (Fig. 1a). These changes in size structure coincided with (i) an increase in the female proportion in catches from about 40% at the beginning of 1990 to almost 100% at the beginning of 2000 (Fig. 1b; for more details on changes in sex ratio, see Guevara-Carrasco and Lleonart, 2008), and (ii) an increase in the percentage of mature hake of age 2 from almost zero to about 60% in the early 2000s (Fig. 1a).

3.2. Time series of condition factor versus gonad index

Time series of Fulton's condition factor (CF), gonad index (GI) for all hake showed different trends depending on the time period (Fig. 2a). CF was positively correlated with time ($p < 0.05$) whereas GI was negatively correlated with time ($p < 0.05$). However, it is important to note that the range of hake length has not been constant over time. Samples were dominated by large hakes during the first two decades and by small hakes during the last decades (Fig. 1a), and GI values have been low since the early 1990s. These overall results are similar to those obtained for large hake (35–50 cm) (Fig. 2c). Results for small hake (20–35 cm) are different (Fig. 2b), because both CF and GI increased according to time even if these trends were not statistically significant ($p > 0.05$). Over shorter periods, CF and GI vary in phase, in particular during El Niño events, which had a strong negative effect on both parameters, whatever the size class considered (Fig. 2).

3.3. Generalized additive models

GAM results show that GI, FI, SSTA and time explained 32% and 27% of the deviance of CF for the large and small size classes, respectively. The four tested variables each had significant effects (Table 1). The relationships between CF and the biological indices GI and FI were linear and positive for both size classes (Fig. 3a and b), i.e., large GI and FI values predicted a high CF. The SSTA had negative effects on the CF for both large and small hake (Fig. 3c): positive SSTA, corresponding to El Niño, coincided with reduced CFs for both size classes. To a lesser extent, negative anomalies associated with La Niña might reduce CF. The highest CFs for both size classes occurred with small positive temperature anomalies (~0.3° C). The trend in CF for large hake (Fig. 3d) was similar to that for all hake, with low CF values during the 1980s which increased from the early 1990s. CF for small hake decreased during the 1980s, increased during the 1990s, and then decreased again after 2000 (Fig. 3d).

GAM analysis of gonad index versus CF, FI, SSTA and date explained 28% and 12% of the deviance of the GI for large and small hake, respectively. Significant effects were found for all independent variables (Table 1). Date had a positive effect on GI for small hakes and a negative effect on GI for large hakes. Fish CF had a positive effect on GI whatever the size, while FI negatively affected GI (Fig. 4). As for CF, the lowest GI values for both size classes (Fig. 4c) were related to large positive El Niño-related SSTA. The relation between SSTA and maximum GI varied according to fish size; it was 1° C for large hake and close to 0.3° C for small ones (Fig. 4c). GI variations over time for the two size classes (Fig. 4d) differed. Large hake had a high GI at the beginning of the 1980s which decreased during the mid 1990s and has remained low. Small hake showed a slow increase in GI from the 1980s through 2000; GI then increased more rapidly (Fig. 4d).

Table 1
Statistical characteristics of GAMs based on Fulton's condition factor (CF) and gonad index (GI) for the small (<35 cm) and large hake (>35 cm).

Variable	Source	d.f.	P	Resid. d.f.	Residual deviance	% Explained
Small hake (20–35 cm)						
CF	NULL			21,699	0.0164	
	GI	1	0.00004	21,698	0.0150	8.70
	FI	1	0.00000	21,697	0.0138	6.87
	SSTA	1	0.00000	21,696	0.0130	5.00
	Time	13	0.00000	21,683	0.0120	6.44
	Model			21,683	0.0120	27.01
GI	NULL			21,699	14.2039	
	CF	1	0.00000	21,698	12.9676	8.70
	FI	1	0.00037	21,697	12.9047	0.44
	SSTA	1	0.00000	21,696	12.9012	0.02
	Time	13	0.00000	21,683	12.5235	2.66
	Model			21,683	12.5235	11.83
Large hake (35–50 cm)						
CF	NULL			15,168	0.0118	
	GI	1	0.00000	15,167	0.0110	6.59
	FI	1	0.00000	15,166	0.0100	9.03
	SSTA	1	0.00000	15,165	0.0097	1.85
	Time	13	0.00000	15,152	0.0080	14.56
	Model			15,152	0.0080	32.03
GI	NULL			15,168	16.2778	
	CF	1	0.00000	15,167	15.2059	6.59
	FI	1	0.00000	15,166	14.6550	3.38
	SSTA	1	0.00000	15,165	14.6140	0.25
	Time	13	0.00000	15,152	11.7009	17.90
	Model			15,152	11.7009	28.12

4. Discussion

4.1. Reproduction, starvation and El Niño

Fish in good condition (high CF) had large gonads (high GI), but fish with large gonads had nearly empty stomachs (FI; Figs. 3 and 4). This result suggests that the amount of energy devoted to reproduction depends on overall fish condition, and further suggests that hake with the largest gonads do not feed actively or well. The slope of these relationships was steeper for large hake than small hake, which might be the result of a lower proportion of immature fish in the large size class in comparison to the small size class (Fig. 1a). This indicates that, on average, large hake invests more energy in reproduction and feeds less than small hake, suggesting a higher sensitivity to environmental perturbation (e.g. El Niño) than small hake.

Hake distribution is restricted by the presence of the oxygen minimum zone. During El Niño, the oxygen concentration near the bottom increases, expanding hake's range of distribution and favouring the development of new macrobenthic production (Gutiérrez et al., 2008), in particular the crustaceans that account for a large part of hake diet during El Niño (Tam et al., 2006). Un-

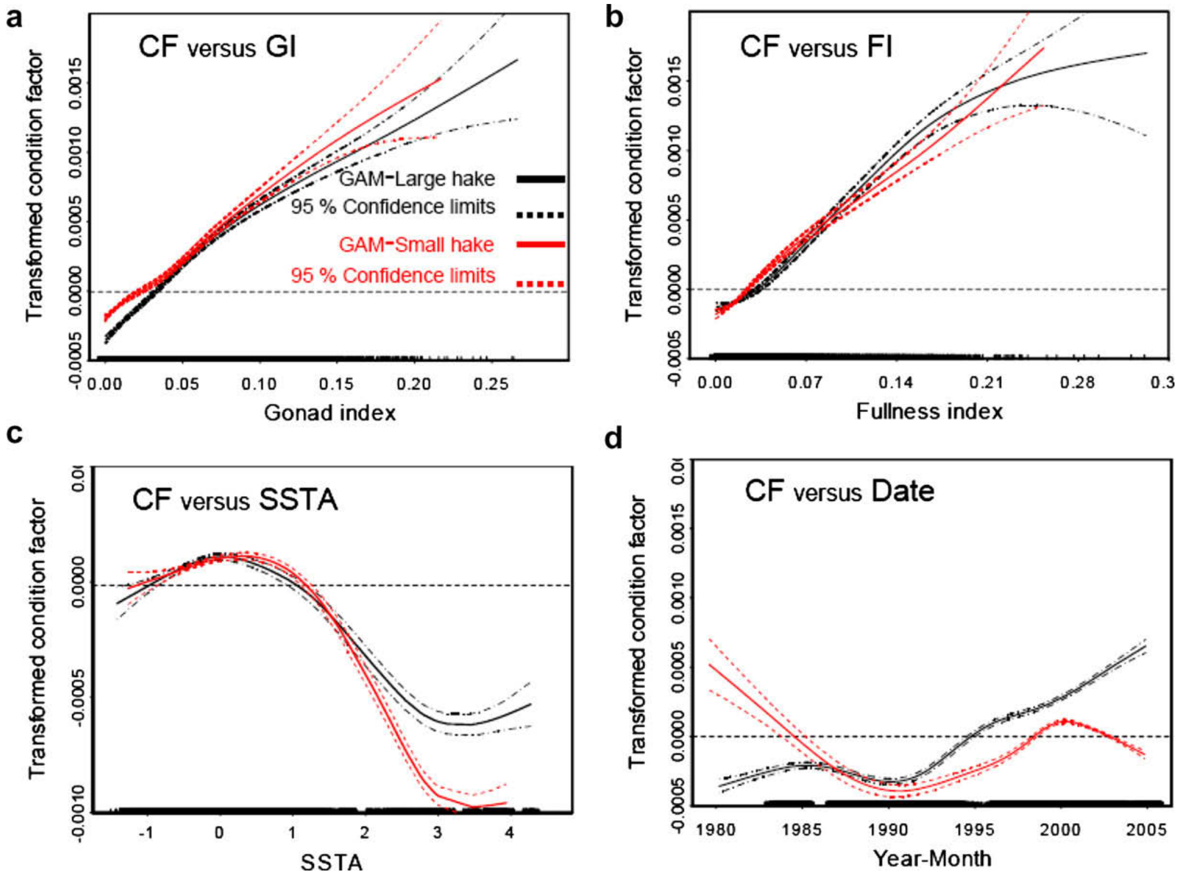

Fig. 3. Cubic spline fits (solid lines) of GAMs based on Fulton's condition factor (CF) according to: Gonad index (a), fullness index (b), sea surface temperature anomaly (c) and date (d) for large (black lines) and small (red lines) hakes. Each panel shows the kind of relationship that exists between the transformed condition factor (*y*-axes) and the *x* variable (*x*-axes). The transformed condition factors are in relative scale and they correspond to the spline smoother that was fitted on the data so that a *y*-value of zero is the mean effect of the *x* variable on the transformed condition factor. Positive and negative *y*-values indicate positive and negative effect respectively on the transformed condition factor. The dotted lines show the 95% confidence limits of GAMs.

der El Niño conditions, apparently favourable, hake condition and reproduction output should improve. However, we observed that El Niño has a strong negative effect on hake biology (depressed CF and GI; Figs. 2–4). The low GI and CF observed during El Niño contradict the idea that these events favour hake (Espino, 1990). Additionally, low hake CFs during El Niño suggest that hake feeding was affected during these events and challenge the idea that hake fully compensates for the lack of small pelagic fish by feeding on alternate prey, for instance by feeding more on crustaceans than fish (Sanchez et al., 1985; Tam et al., 2006). Even if hake adapts foraging during El Niño, the overall effect on CF is negative. Studies on Atlantic cod (*Gadus morhua*) highlighted that extreme environmental conditions, in which food is scarce for a long period, reduce condition factor and reproductive output (Dutil et al., 1999; Dutil and Brander, 2003). A very low condition of adult fish is also associated with a reduction in fecundity (Lambert and Dutil, 2000) and an increase in adult mortality due to reproduction (Dutil and Lambert, 2000). Indeed, reproduction investment could be maintained (even if lower than during favourable periods) at the expense of somatic condition, in which case, the risk of mortality due to exhaustion of energy reserves would increase (Lambert and Dutil, 2000). If hake reproduction took place during or immediately after El Niño, when hake condition and fecundity were minimum and more severe for large hake (Figs. 2–4), mortality and a decrease in recruitment success would likely occur. In any case, El Niño represents a strong environmental stress.

4.2. Overfishing

Overfishing primarily affects large fish (e.g. Pauly et al., 1998) and can aggravate the low abundance periods due to natural variability. If fish concentrate to keep certain density levels in order to form functional spatial aggregation (i.e., for schooling, mating, spawning), a fishery can continue to exploit fish patches even at a low stock level (Rose and Kulka, 1999). Consequently, both mean fish size and distribution area decrease. Indeed, high predation (or fishing) pressure increases the risk of a population collapse (Shoener et al., 2001). This seems to apply to Peruvian hake as intense fishing depleted the population, especially the adult proportion (Fig. 1), and reduced its area of distribution (Guevara-Carrasco and Lleonart, 2008). The probable higher vulnerability of large hake to fishing and to El Niño combined with its depleted population and diminished distribution area could explain the disappearance of adults during and following the El Niños of 1991–1992 and 1997–1998 (Wosnitza-Mendo et al., 2004).

4.3. Long-term changes

The overall trend shows that CF increased and that GI decreased from 1971 to 2005 (Fig. 2a). This trend was observed for large fish but not for small hake (Figs. 2–4). Small hake's reproductive activity increased over time, especially during the last years (Fig. 4), and was accompanied by a decrease in condition factor. A high proportion of immature fish composed the small size class during the

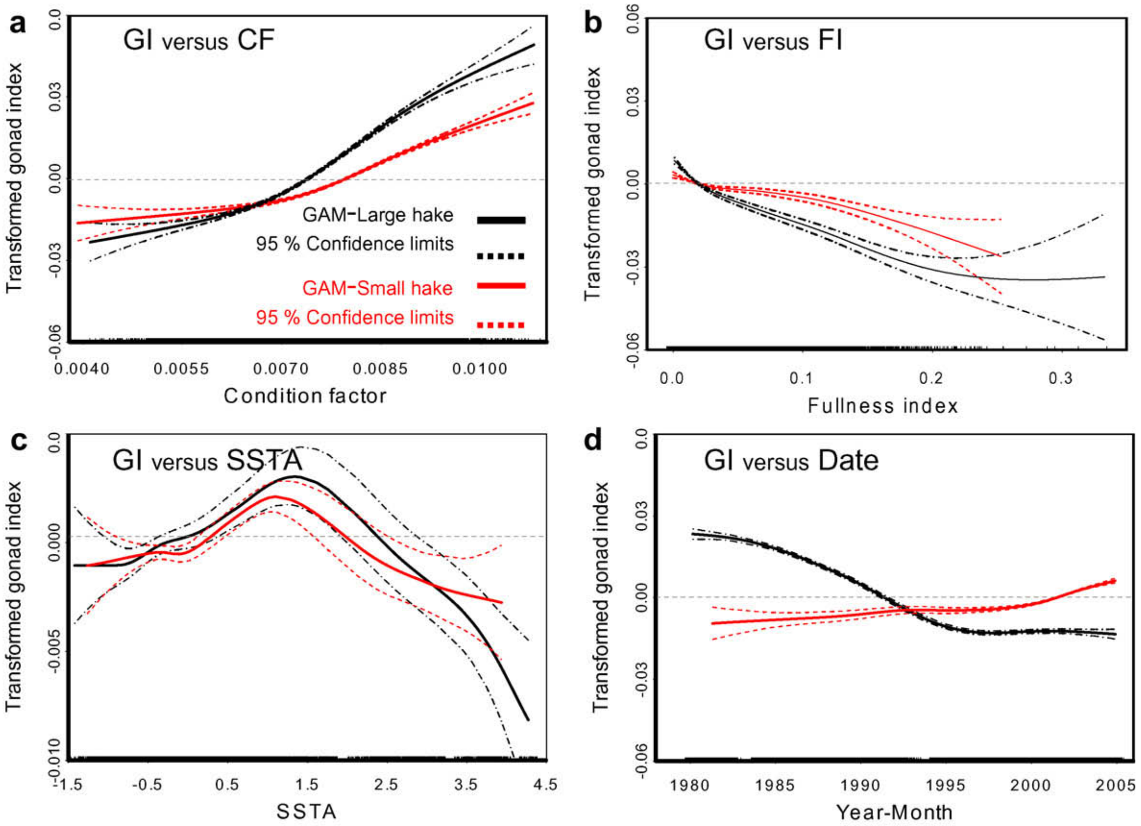

Fig. 4. Cubic spline fits (solid lines) of GAMs based on gonad index (GI) according to: Fulton condition factor (a), fullness index (b), sea surface temperature anomaly (c) and date (d) for large (black lines) and small (red lines) hakes. Each panel shows the kind of relationship that exists between the transformed gonad index (y-axes) and the *x* variable (*x*-axes). The transformed gonad indices are in relative scale and they correspond to the spline smoother that was fitted on the data so that a *y*-value of zero is the mean effect of the *x* variable on the transformed gonad index. Positive and negative *y*-values indicate positive and negative effect respectively on the transformed gonad index. The dotted lines show the 95% confidence limits of GAMs.

early years, and it has substantially reduced in the last years (Fig. 1a; Wosnitza-Mendo et al., 2004; Guevara-Carrasco and Lleonart, 2008). The observed opposite trends of GI and CF suggest that an immature fish reaches a higher CF than a mature fish of similar size. Why did small hake invest relatively more in reproduction than large hake, even with low CFs?

When population biomass is high and close to the carrying capacity, food limitation can lead to a reduction in reproductive output (Hilborn and Walters, 1992). The hake population, however, has been at a low level since the late 1990s (Guevara-Carrasco and Lleonart, 2008) and has exhibited high CFs. Smaller size at maturity (Fig. 1; Wosnitza-Mendo et al., 2004; Guevara-Carrasco and Lleonart, 2008) could compensate for the lack of large adults. Some fish can mature at a smaller size if well-nourished (Trippel, 1995). It is also possible that fishing produces evolutionary pressure for a reduction in size at first maturity (Conover and Munch, 2002; Reznick and Ghalambor, 2005; Swain et al., 2007). These processes may explain the increasing reproductive activity observed in small hake during the last years. They do not, however, explain the still-perplexing low investment in reproduction by those large hakes that have been sampled.

Long term environmental oscillation of the oceanographic condition could have also influenced the CFs and GIs of small and large hake. Warm-to-cool regime shifts have occurred throughout the eastern Pacific during the late 1980s early 1990s and coincide with the changes in the population of several marine organisms (e.g. Chavez et al., 2003; Alheit and Niquen, 2004; Gutiérrez et al., 2007). A change in the trends of CFs and GIs for large and small hake also accured at the beginning of the 1990s (Figs. 3 and 4d), when the last decadal cooling began ('La Vieja' conditions, see Chavez et al., 2003). However, the change in the trends is not 'consistent' (e.g. U-shape for small hake CF, Fig. 3d) indicating that decadal variation is probably not the main effect observed in our data. Furthermore, in this study, neither CF nor GI have been strongly affected by negative SSTA (Figs. 3 and 4c).

Another environmental factor that has not been considered in this study is the expansion of the jumbo squid (*Dosidiscus gigas*), a potential predator for hake, whose biomass increased dramatically during the 1990s off Peru (Taipe et al., 2001). Indeed, off western North America, the expansion of the jumbo squid population coincided with the decline in abundance of the Pacific hake (*Merluccius productus*) (Zeidberg and Robison, 2007), which is the main prey of the jumbo squid over the shelf and slope in this region (Field et al., 2007). However, the evidence for high predation of jumbo squid on the Peruvian hake is inconclusive (Tam et al., 2008). Taylor et al. (2008), in a modelling study, concluded that predation from jumbo squid did not influence the trend in hake abundance. There is a need for further studies to determine if jumbo squid has impacted the Peruvian hake population.

Large fish have higher fecundity (Takasuka et al., 2005; Murua et al., 2006), better egg quality and higher egg viability than small fish (Brooks et al., 1997). For instance, larger Atlantic cod have much higher fecundity and hatching rates than smaller fish (Trippel, 1998). Large individuals contribute disproportionately to the reproductive potential of a stock (i.e. Argentinean hake, *Merluccius hubbsi*; Macchi et al., 2004). Mean length in landings of Peruvian hake decreased from around 40 cm during the 1970s and 1980s to 25 cm in early 2000s (Fig. 1). Thus, the rarity of large female

Peruvian hake and their low GIs since the late 1990s likely indicate diminished reproductive capacity.

4.4. Reproductive failure: a male affair?

Females need males to reproduce, but it has always been assumed that female reproduction does not depend on the number and/or the size of males. Studies on the reproductive behaviour of Atlantic cod (Morgan and Trippel, 1996) and Argentinean hake (Pájaro et al., 2005) have shown that males arrive first, are in higher proportion in the spawning areas and stay longer than females. Females enter the area when ready to spawn and leave it after. This behaviour could make males more vulnerable to fishing. If so, exploitation can alter the sex ratio and potentially reduce the probability that females will encounter mates (Moller and Legendre, 2001).

Trawl data (Paita harbour, 05° S) show that male hake accounted for the majority of the catch early in the fishery. The proportion of females in catch increased from about 40% during the 1980s and early 1990s to 80% in the late 1990s and almost 100% in the early 2000s (Fig. 1; Guevara-Carrasco and Lleonart, 2008). This lack of males could lead to sperm limitation (Rankin and Kokko, 2006). Perhaps more importantly, the shortage of sperm or male pheromone could inhibit females from spawning (Rideout et al., 2005). According to Rowe and Hutchings (2003), individuals unable to gain access to mates might benefit by reallocating energetic resources from reproduction to growth, which might improve reproductive success in subsequent years. We assume that this is the case for large female Peruvian hake, which exhibited high CFs and low GIs when large males were scarce.

We suggest that fishing has diminished hake's reproductive capacity, has modified the sex ratio in favour of females, increased population vulnerability to environmental stress, in particular El Niño, and has lowered population resilience to such an extent that hake population recovery could take longer or even fail altogether if the increase in stock spawning biomass alone (based on a reduction in fishing effort) is to be the main indicator of recovery.

Acknowledgements

The authors gratefully thank the Instituto del Mar del Perú (IMARPE) for having facilitated the use of the data. This work is a contribution of the INCOFISH project (Integrating Multiple Demands on Coastal Zones with Emphasis on Fisheries and Aquatic Ecosystems, of the European Commission, Contract Number 003739) and of the Research Unit 'Upwelling Ecosystems' UR 097 from IRD. We warmly thank Tim Pennington for the English edition and valuable comments on the first version of the MS. We also thank Johanna Holmgren for proofreading many versions of the MS. Finally we thank the anonymous referees for their very helpful comments and suggestions.

References

Arntz, W., Fahrbach, E., 1991. El Niño – Klimaexperiment der Natur: physikalische Ursachen und biologische Folgen. Birkhaeuser, Basel, Boston, Berlin.

Alheit, J., Ñiquen, M., 2004. Regime shifts in the Humboldt Current ecosystem. Progress in Oceanography 60, 201–222.

Ballón, M., Wosnitza-Mendo, C., Guevara-Carrasco, R., Benites, C., 2007. Shifting baseline of demersal species in the humboldt current system. In: Nicholls, J.H., (comp) Incofish Project Database (<http://www.incofish.org>).

Brooks, S., Tyler, C., Sumpter, J., 1997. Egg quality in fish: what makes a good egg? Reviews in Fish Biology and Fisheries 7, 387–416.

Chavez, F.P., Ryan, J., Lluch-Cota, S.E., Ñiquen, M., 2003. From anchovies to sardines and back: multidecadal change in the Pacific Ocean. Science 299, 217–221.

Conover, D., Munch, S.B., 2002. Sustaining fisheries yields over evolutionary time scales. Science 297, 94–96.

Chouinard, G.A., Swain, D.P., 2002. Depth-dependent variation in condition and length-at-age of Atlantic cod (Gadus morhua) in the southern Gulf of St. Lawrence. Canadian Journal of Fisheries and Aquatic Sciences 59, 1451–1459.

Dutil, J.D., Brander, K., 2003. Comparing productivity of North Atlantic cod stocks and limits to growth production. Fisheries Oceanography 12, 502–512.

Dutil, J.D., Castonguay, M., Gilbert, D., Gascon, V., 1999. Growth, condition, and environmental relationships in Atlantic cod (Gadus morhua) in the northern Gulf of St. Lawrence and implications for management strategies in the Northwest Atlantic. Canadian Journal of Fisheries and Aquatic Sciences 56, 1818–1831.

Dutil, J.D., Godbout, G., Blier, P.U., Groman, D., 2006. The effect of energetic condition on growth dynamics and health of Atlantic cod (Gadus morhua). Journal of Applied Ichthyology 22, 138–144.

Dutil, J.D., Lambert, Y., 1997a. Can simple condition indices be used to monitor and quantify seasonal changes in the energy reserves of cod (Gadus morhua)? Canadian Journal of Fisheries and Aquatic Sciences 54, 104–112.

Dutil, J.D., Lambert, Y., 1997b. Condition and energy reserves of Atlantic cod (*Gadus morhua*) during the collapse of the northern Gulf of St. Lawrence stock. Canadian Journal of Fisheries and Aquatic Sciences 54, 2388–2400.

Dutil, J.D., Lambert, Y., 2000. Natural mortality from poor condition in Atlantic cod (*Gadus morhua*). Canadian Journal of Fisheries and Aquatic Sciences 57, 826–836.

Espino, M., 1990. El Niño su impacto sobre los peces demersales del Perú. Boletín Instituto del Mar del Perú 14 (2), 3–10.

Espino, M., Maldonado, M., Benites, C., 1985. Situación de la Población de Merluza (*Merluccius gayi peruanus*) durante El Niño. In: Arntz, W., Landa, A., Tarazona, J. (Eds.), El Niño Su Impacto en la Fauna Marina. Boletín Instituto del Mar del Perú-Callao Volumen Extraordinario, pp. 159–162.

Field, J.C., Baltz, K., Phillips, A.J., Walker, W.A., 2007. Range expansion and trophic interactions of the jumbo squid, Docidicus gigas in the California current. California Cooperative Oceanic Fisheries Investigation Reports 48, 131–146.

Fuentes, F., Antonietti, E., Muck, P., 1989. Alimentación de la merluza (*Merluccius gayi peruanus*) de la zona de Paita. In: Jordán, R., Kelly, R., Mora, O., Vildoso, A., de, Ch., Henriquez, N. (Eds.), Memorias del simposio internacional de los recursos vivos y las pesquerías en el Pacífico Sudeste 9–13 de mayo 1988. Viña del Mar, Chile. CPPS, Revista Pacífico Sur (Número Especial), pp. 276–289.

Guevara-Carrasco, R., 2004. Peruvian hake overfishing: misunderstood lessons. Boletín Instituto del Mar Perú 21, 27–32.

Guevara-Carrasco, R., Lleonart, J., 2008. Dynamics and Fishery of the Peruvian hake: between the nature and the man. Journal of Marine Systems. 71, 249–259.

Gutiérrez, D., Enríquez, E., Purca, S., Quipúzcoa, L., Marquina, R., Flores, G., Graco., M., 2008. Remotely – driven temporal variations of the subsurface dissolved oxygen content and responses of the continental shelf benthic subsystem off Central Peru. Progress in Oceanography 79, 177–189.

Gutiérrez, M., Swartzman, G., Bertrand, A., Bertrand, S., 2007. Anchovy and sardine spatial dynamics and aggregation patterns in the Humboldt Current ecosystem Peru from 1983–2003. Fisheries Oceanography 16, 155–168.

Hastie, T., Tibshirani, R., 1990. Generalized Additive Models. Chapman and Hall, London.

Hilborn, R., Walters, C., 1992. Quantitative Fisheries Stock Assessment: Choice, Dynamics and Uncertainty. Chapman and Hall, New York.

Kurita, Y., Meier, S., Kjesbu, O.S., 2003. Oocyte growth and fecundity regulation by atrsia of Atlantic herring (*Clupea harengus*) in relation to body condition throughout the maturation cycle. Journal of Sea Research 49, 203–219.

Lambert, Y., Dutil, J.-D., 2000. Energetic consequences of reproduction in Atlantic cod (*Gadus morhua*) in relation to spawning level of somatic energy reserves. Canadian Journal of Fisheries and Aquatic Sciences 57, 815–825.

Lloret, J., Gil de Sola, L., Souplet, A., Galzin, R., 2002. Effects of large-scale habitat variability on condition of demersal exploited fish in the north-western Mediterranean. ICES Journal of Marine Science 59, 1215–1227.

Macchi, G.J., Pajaro, M., Ehrlich, M., 2004. Seasonal egg production pattern of the Patagonian stock of Argentine hake (*Merluccius hubbsi*). Fisheries Research 67, 25–38.

Moller, A.P., Legendre, S., 2001. Allee effect, sexual selection and demographic stochasticity. Oikos 92, 27–34.

Morgan, M.J., Trippel, E.A., 1996. Skewed sex ratios in spawning shoals of Atlantic cod (*Gadus morhua*). ICES Journal of Marine Science 53, 820–826.

Murua, H., Lucio, P., Santurtun, M., Motos, L., 2006. Seasonal variation in egg production and batch fecundity of European hake *Merluccius merluccius* (L.) in the Bay of Biscay. Journal of Fish Biology 69, 1304–1316.

Pájaro, M., Macchi, G.J., Martos, P., 2005. Reproductive pattern of the Patagonian stock of Argentine hake (*Merluccius hubbsi*). Fisheries Research 72, 97–108.

Pauly, D., Christensen, V., Dalsgaard, J., Froese, R., Torres Jr., F., 1998. Fishing down the marine food webs. Science 279, 860–863.

Rankin, D.J., Kokko, V., 2006. Do males matter? The role of males in population dynamics. Oikos 116 (2), 335–348.

Reznick, D., Ghalambor, C., 2005. Can commercial fishing cause evolution? Answers from guppies (*Poeclia reticulata*). Canadian Journal of Fisheries and Aquatic Sciences 62, 791–801.

Rideout, R., Rose, G., Burton, M., 2005. Skipped spawning in female iteropaous fishes. Fish and Fisheries 6, 50–72.

Rose, G.A., Kulka, D.W., 1999. Hyperaggregation of fish and fisheries: how catch per unit effort increased as the northern cod (*Gadus morhua*) declined. Canadian Journal of Fisheries and Aquatic Sciences 56, 118–127.

Rowe, S., Hutchings, J.A., 2003. Mating systems and the conservation of commercially exploited marine fish. Trends in Ecology and Evolution 18, 567–572.

Samamé, M., Castillo, J., Mendieta, A., 1985. Situación de las pesquerías Demersales y los Cambios durante El Niño. In: Arntz, W., Landa y, A., Tarazona, J. (Eds.), El Niño su impacato en la fauna marina. Boletín Instituto del Mar del Perú. Extraordinario, pp. 153–158.

Sanchez, G., Alamo, A., Fuentes, F., 1985. Alteraciones de la dieta alimentaria de algunos peces comerciales por efecto del fenómeno El Niño. In: Arntz, W., Landay, A., Tarazona, J. (Eds.), El Niño su impacato en la fauna marina. Boletín Instituto del Mar del Perú. Extraordinario, pp. 135–142.

Sandoval de Castillo, O., Wosnitza-Mendo, C., Muck, P., Carrasco, S. 1989. Abundance of hake larvae and its relationship to hake and anchoveta biomasses off Perú. In: Pauly, D., Muck, P., Mendo, J., Tsukayama, I. (Eds.), The Peruvian Upwelling Ecosystem: Dynamics and Interactions. ICLARM Conference Proceedings 18, pp. 280–296.

Scott, B.E., Marteinsdottir, G., Begg, G., Wright, P., Sigurd Kjesbu, O., 2006. Effects of population size/age structure, condition and temporal dynamics of spawning on reproductive output in Atlantic cod (*Gadus morhua*). Ecological Modelling 191, 383–415.

Shoener, T., Spiller, D., Losos, J., 2001. Predators increase the risk of catastrophic extinction of prey populations. Nature 412, 183–185.

Swain, D., Sinclair, A., Hanson, J., 2007. Evolutionary response to size-selective mortality in an exploited fish population. Proceedings of the Royal Society B 274, 1–8.

Taipe, A., Yamashiro, C., Mariategui, L., Rojas, P., Roque, C., 2001. Distribution and concentration of jumbo flying squid (*Dosidicus gigas*) off the Peruvian coast between 1991 and 1999. Fisheries Research 54, 21–32.

Takasuka, A., Oozeki, Y., Kubota, H., Tsuruta, Y., Funamoto, T., 2005. Temperature impacts on reproductive parameters for Japanese anchovy: comparison between inshore and offshore waters. Fisheries Research 76, 475–482.

Tam, J., Purca, S., Duarte, L.O., Blaskovic, V., Espinoza, P., 2006. Changes in the diet of hake associated with El Niño 1997–1998 in the northern Humboldt Current ecosystem. Advances in Geosciences 6, 63–67.

Tam, J., Taylor, M.H., Blaskovic, V., Espinoza, P., Ballón, R.M., Díaz, E., Wosnitza-Mendo, C., Argüelles, J., Purca, S., Ayón, P., Quipuzcoa, L., Gutiérrez, D., Goya, E., Ochoa, N., Wolff, M., 2008. Trophic modeling of the Northern Humboldt Current Ecosystem, Part I: Comparing trophic linkages under La Niña and El Niño conditions. Progress in Oceanography 79, 352–365.

Taylor, M.H., Tam, J., Blaskovic, V., Espinoza, P., Ballón, R.M., Wosnitza-Mendo, C., Argüelles, J., Díaz, E., Purca, S., Ochoa, N., Ayón, P., Goya, E., Quipuzcoa, L., Gutiérrez, D., Wolff, M., 2008. Trophic flows in the Northern Humboldt Current Ecosystem, Part 2: Elucidating mechanisms of ecosystem change over an ENSO cycle by simulating changes in low trophic level dynamics. Progress in Oceanography 79, 366–378.

Trippel, E.A., 1995. Age at maturity as a stress indicator in fisheries. Bioscience 45, 759–771.

Trippel, E.A., 1998. Egg size and viability and seasonal offspring production of young Atlantic Cod. Transactions of the American Fisheries Society 127, 339–359.

Wolff, M., Wosnitza-Mendo, C., Mendo, J., 2003. The Humboldt Current trends in exploitation protection and research. In: Hempel, G., Sherman, K. (Eds.), Large Marine Ecosystems of the world. Elsevier B.V..

Wosnitza-Mendo, C., Guevara-Carrasco, R., Ballón, M., 2004. Possible causes of the drastic decline in mean length of Peruvian hake in 1992, vol. 21. Boletin Instituto del Mar del Perú. pp. 1–26.

Zeidberg, L.D., Robison, B.H., 2007. Invasive range expansion by the Humboldt squid *Dosidicus gigas* in the eastern North Pacific. Proceedings of the National Academy of Sciences 104, 12948–12950.

Progress in Oceanography 79 (2008) 308–312

Contents lists available at ScienceDirect

Progress in Oceanography

journal homepage: www.elsevier.com/locate/pocean

Size increment of jumbo flying squid *Dosidicus gigas* mature females in Peruvian waters, 1989–2004

Juan Argüelles [a,*], Ricardo Tafur [a], Anatolio Taipe [a], Piero Villegas [a], Friedemann Keyl [b], Noel Dominguez [a], Martín Salazar [a]

[a] *Instituto del Mar del Perú, Callao, Peru*
[b] *Centre for Tropical Marine Ecology, Bremen, Germany*

ARTICLE INFO

Article history:
Accepted 14 October 2008
Available online 21 October 2008

Keywords:
Dosidicus gigas
Length-at-maturity
Population structure
Peru

ABSTRACT

Changes in population structure of the jumbo flying squid *Dosidicus gigas* in Peruvian waters were studied based on size-at-maturity from 1989 to 2004. From 1989 to 1999, mature squid belonging to the medium-sized group prevailed, but from 2001 on, mature squids were larger. This change is not related to the changes in sea surface temperature and we hypothesized that it was caused by the population increase of mesopelagic fishes as prey.

1. Introduction

The jumbo flying squid *Dosidicus gigas* (family Ommastrephidae) is one of the most abundant squids in the eastern Pacific Ocean (Nesis, 1970, 1983; Klett, 1996; Anderson and Rodhouse, 2001; Nigmatullin et al., 2001), and is distributed in the Eastern Pacific from California (USA) to Chile (Nigmatullin et al., 2001). It inhabits a wide range of habitats from epipelagic to mesopelagic (up to 1200 m depth). Like other squid species, *D. gigas* is short-lived with longevity about 1 year (Arkhipkin and Murzov, 1986; Masuda et al., 1998; Argüelles et al., 2001; Markaida et al., 2004) with highly labile populations that exhibit large fluctuations in abundance in response to environmental variability (Waluda et al., 2006). *D. gigas* is an important opportunistic predator in the pelagic ecosystem of the southeastern Pacific Ocean (Nesis, 1970, 1983); myctophid fish compose a large portion of its diet but *D. gigas* also preys on hake, anchovy, mackerel, crustaceans, squid and other organisms (Shchetinnikov, 1986, 1989; Markaida and Sosa-Nishizaki, 2003; Markaida, 2006; Field et al., 2007).

Off Peru, *D. gigas* has been targeted commercially by the artisanal fleet since 1961 (Yamashiro et al., 1998), mainly in the north, and by industrial fleets since 1991 (Taipe et al., 2001). For Chile, landing data of *D. gigas* are available since 1957 (Rocha and Vega, 2003) and there are even older records of stranded individual (Wilhelm, 1954). In Chile *D. gigas* was formerly used as bait in *Genypterus* fisheries due to its very low commercial value. Catches of *D. gigas* were sporadic before 1970, although high abundances have been reported (Schmiede and Acuña, 1992). In the Gulf of California the artisanal fishery targeting *D. gigas* started in 1974 (Ehrhardt et al., 1983), but between 1983 and 1987 the fishery disappeared, perhaps due to the recruitment failure from overfishing or unfavorable environmental conditions following the 1982–1983 El Niño event (Klett, 1996).

The population structure of *D. gigas* is difficult to be assessed due to variability in length-at-maturity. Three sizes of sexually mature squid were defined by Nigmatullin et al. (2001) on the basis of the mantle length (ML) of adult males and females: a small-sized group (13–26 cm and 14–34 cm, respectively), a medium-sized group (24–42 cm and 28–60 cm, respectively) and a large-sized group (>40–50 cm and 55–65 cm to 100–120 cm, respectively). Specimens of the small-sized group are primarily found in the equatorial areas. Individuals of the medium-sized group are found throughout the whole species range (except in the most high-latitudinal parts); while those of the large-sized group occur primarily at the northern and southern peripheries of the range (usually poleward of 10–15° latitude). However, large squids sometimes are found in equatorward-flowing nearshore cold currents, particularly in the coastal branch of Humboldt Current System (Nigmatullin et al., 2001).

In this paper we examine the changes in the size-at-maturity of *D. gigas* adult females off the Peruvian coast during 1989–2004. In particular we test the hypothesis that sea surface temperature controls the size-at-maturity in *D. gigas*.

2. Methods and data

D. gigas biological data (mantle length, sex, maturity) were collected in Peruvian waters (i) during research cruises performed by

---

* Corresponding author.
E-mail address: jarguelles@imarpe.gob.pe (J. Argüelles).

0079-6611/$ - see front matter © 2008 Elsevier Ltd. All rights reserved.
doi:10.1016/j.pocean.2008.10.003

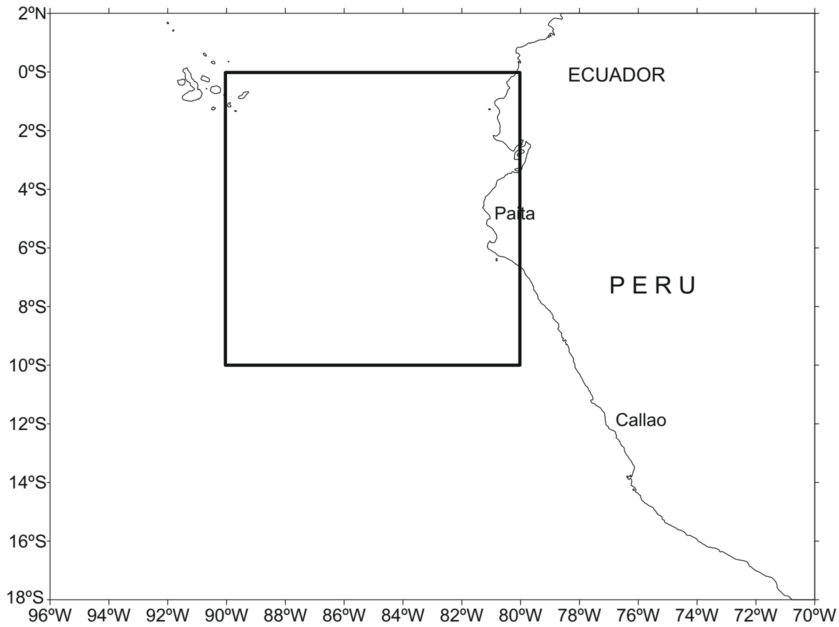

Fig. 1. Areas where sea surface temperature anomalies were obtained: El Niño 1 + 2 area (0°–10°S; 80°–90°W) indicated by square area; and two Peruvian ports: Paita and Callao.

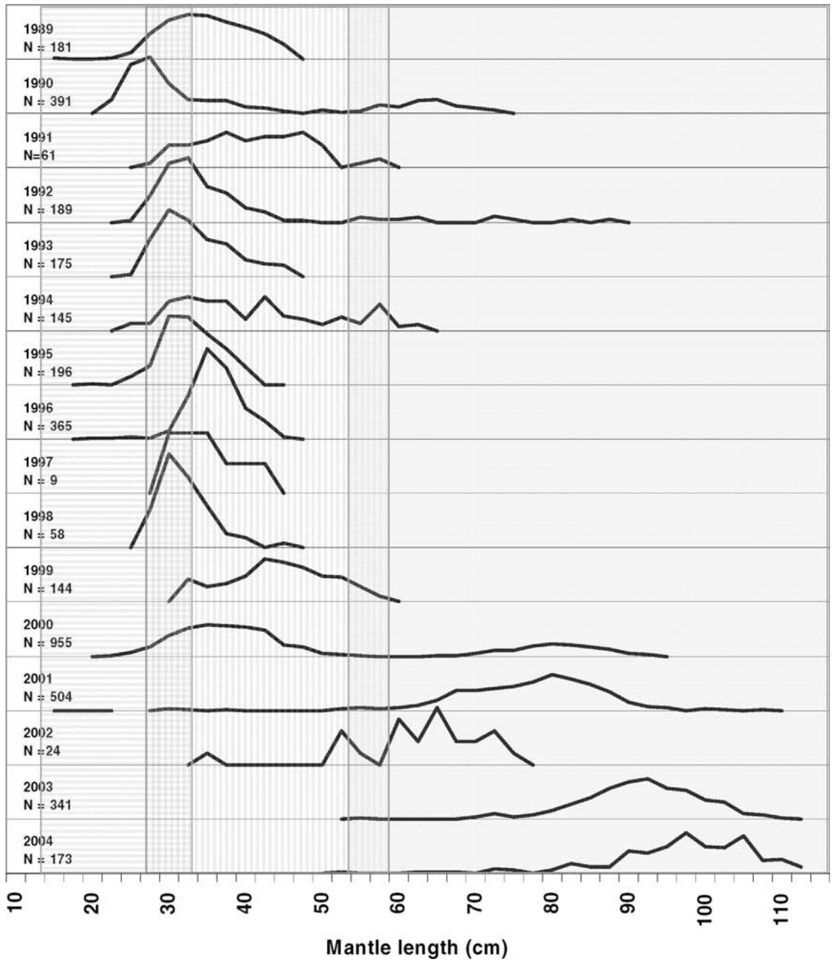

Fig. 2. Annual size structure of mature female of *Dosidicus gigas* in Peruvian waters from 1989 to 2004. Ranges of size-at-maturity according to Nigmatullin et al. (2001) are indicated by different areas, small sized (horizontal lines), medium sized (vertical lines) and large sized (grey).

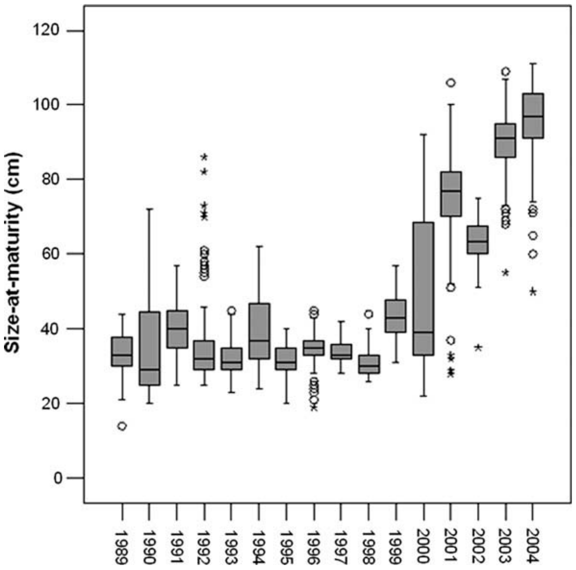

Fig. 3. Annual variation of length-at-maturity (ML) of females in Peruvian waters. Each box shows the median, quartiles, smallest and largest not atypical values. Circles and asterisks indicate extreme and atypical values, respectively.

the Peruvian Institute of the Sea/Instituto del Mar del Perú (IMARPE–http://www.imarpe.gob.pe) and (ii) from the artisanal and industrial fisheries from 1989 to 2004. For the industrial fishery, an observer aboard each vessel collected biological and fishery data. For the artisanal fishery, biological data were obtained from the landings. Mantle length (ML) was measured to the nearest mm. Sexual maturity was assessed with the macroscopic scale proposed by Nesis (1970) and modified by Tafur and Rabí (1997). This scale defines four stages for females: I (immature), II (maturation), III (mature), and IV (spawned). In this paper, mature individuals were those assigned to stages III or IV. The mantle length (ML) of adult females was used to identify the three different length-at-maturity population groups described by Nigmatullin et al. (2001). Length-at-maturity was determined during the main spawning season from October to January (Tafur et al., 2001).

We used monthly sea surface temperature anomalies (SSTA) as a proxy of environmental conditions for the period 1989–2004 in the region El Niño 1 + 2 (0–10° South, 90° west–80° west) and two coastal areas in Peru (Paita: 05°04.9'S–81°06.7'W and Callao: 12°03.3'S–77°08.8'W) (Fig. 1). SSTA for the Niño 1 + 2 were obtained from http://www.cpc.ncep.noaa.gov/data/indices/ssta.indices, while SSTA from Peruvian coastal areas were obtained from IMARPE.

We used classification and regression trees (CART, Brieman et al., 1984) to assess the relative importance of year, month and the different time series of SSTA to length-at-maturity. In CART the dependent variable is modelled as a function of covariates. CART divides the data set through a sequence (tree) of binary splits on the values of one of the covariates at a time such that the overall variance in the dependent variable is minimized at each split. The resulting CART tree is usually simplified ('pruned') for the clarity of explanation.

3. Results

3.1. Female length-at-maturity

During the study period the mantle length (ML) of mature females ranged between 14 and 113 cm (Figs. 2 and 3). According to the length-at-maturity population groups described by Nigmatullin et al. (2001), from 1989 to 1999 a majority of females reached maturity at medium-sizes (28–60 cm). During 2000 medium and large groups of size-at-maturity were observed, but from 2001 on, the large-sized maturing groups were dominating Peruvian waters. Large squid also occurred during 1990 and 1992 but in a lesser frequency. The small-sized maturing group was only abundant in 1990.

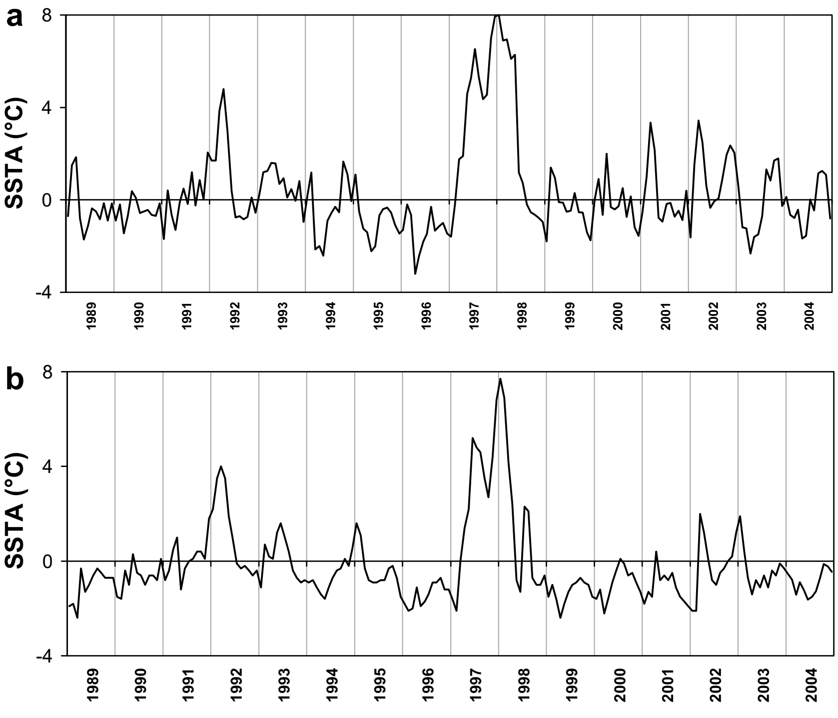

Fig. 4. Monthly time series of SSTA (sea surface temperature anomalies) in two coastal areas in Peru. (a) Paita and (b) Callao, from 1989 to 2004.

3.2. Sea surface temperatures anomalies

The time series of SST anomalies (Fig. 4 shows the time series of SSTA in Paita and Callao) illustrates the strong El Niño of 1997–1998 (Wolter and Timlin, 1998; Morón, 2000), with positive anomalies (>+1 °C) from March 1997 to July 1998 (16 months). Positive SST anomalies also occurred from February to June of 1992, corresponding to moderate El Niño conditions (Morón, 2000). Cool periods were observed, principally during the 1996 La Niña (Morón, 2000), when negative SST anomalies (<−1 °C) occurred from April to December. Negative anomalies were also predominant in Peruvian coastal waters and in the Niño 1 + 2 region after the 1997–1998 El Niño. In the northern coastal waters near Paita, short periods of positive anomalies occurred from 2001 to 2004 (Fig. 4).

3.3. CART analysis

CART results (Fig. 5) indicate that the parameter having by far the strongest effect on the length-at-maturity is year. During 2000 the population transitioned from small to large squid (Figs. 2 and 3). Before January 2001, mature females were medium sized (mean ML 37.4 cm) while after this, the mean mantle length was much larger (mean ML 86.1 cm). In CART the year 1999 and SSTA off Callao had the second most important effects, but these results are much weaker, inconsistent, and not readily interpretable. There was thus no clear link between the length-at-maturity and SSTA.

4. Discussion

The results reported in this paper show a dramatic increase in the length of mature female *D. gigas* in Peruvian waters over the period 1989–2004. From 1989 to 1999 the mean length-at-maturity of females (37.4 cm) fell within the medium-sized group of Nigmatullin et al. (2001). From 2001 on, mean length (85.9 cm) fell within Nigmatullin's et al. (2001) large-sized group. We did not observe the small-sized group reported by Nigmatullin et al. (2001) except in 1990 (Fig. 2). The dominance of the medium-sized group during the 1990s agrees with Nigmatullin et al. (2001) who found this group in the entire distribution area of the jumbo squid except in the most extreme parts of its distribution. We found medium-sized mature squids over a wide range of environmental and temperature conditions, for instance during the El Niño 1992 and 1997–1998 and the La Niña 1996 and 1999 (see Fig. 4 for SSTA). We could not evidence any direct relationships between size-at-maturity and SST, at least at the scale of our study. In the case of the Peruvian waters characterized by their high productivity, in particular in terms of fish (Bakun and Weeks, 2008), other factors such as food availability (Mangold, 1987) could be determined. The increase in length-at-maturity and abundance from 2000 on (Fig. 6) is concomitant with the significant changes for the spatial distribution of anchovy and sardine and the beginning of the 'full anchovy era' in Peruvian waters after 1999 Gutierrez et al. (2007). From 2000 to 2004 the Peruvian upwelling system was characterized by (i) increased areal extent of the upwelled cold coastal waters (Swartzman et al., 2008), (ii) high coastal productivity and recovery of the annual primary production (>0.2 Gt C year^{-1}) after the 1997–98 El Niño (Carr, 2002), (iii) increased in secondary production (Ayón et al., 2008), and (iv) an increased population of one of the most important preys of *D. gigas* (Fig. 6), lanternfish of the genus *Vinciguerria* (Shchetinnikov, 1989; Markaida and Sosa-Nishizaki, 2003). The parallel lanterfish and jumbo squid population trajectories may suggest that an increase in prey availability caused the increase in the length-at-maturity of *D. gigas* off Peru.

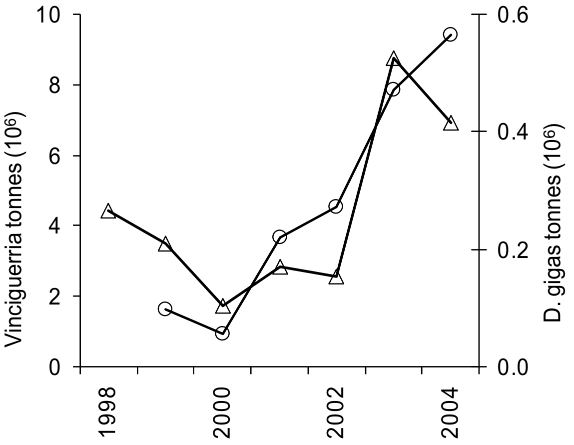

Fig. 6. Annual mean biomass of *D. gigas* and *Vinciguerria lucetia* estimates by acoustic methods during research cruises in Peruvian waters (Imarpe unpublished data). Circle: *Dosidicus gigas*; triangles: *Vinciguerria*.

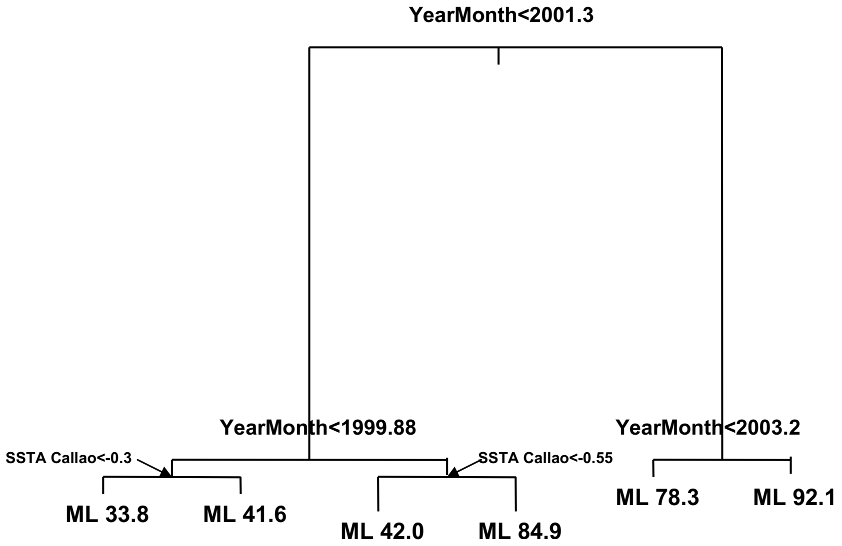

Fig. 5. Result of the classification and regression tree assessing the relative importance of year, month and the different time series of SSTA to length-at-maturity. The tree is split off on the values of one of the covariate at a time such that the overall variance in the dependent variable is minimized at each split.

Fisheries can also affect population size structures, and for jumbo squid a purely industrial fishery slowly changed to a mixed industrial/artisanal fishery from 2000 on (Taipe et al., 2001; IMARPE, unpublished data). But fishing typically produces decrease in size at maturity, in opposition to the abrupt size increase observed in 2000. Additionally, similar large mature groups were also observed off Chile from 2000 on (Zúñiga, 2006), off Mexico from 1995–2004 (excepting 1998–1999; Markaida, 2006; Bazzino et al., 2007), in the northernmost part of the distribution in Oregon in 1997 (Pearcy, 2002), and off the coast of British Columbia in 2004 (Cosgrove and Sendall, http://www.thecephalopodpage.org/Dosidicusgigas.php). In these widely distributed regions the history of the fisheries on *D. gigas* is completely different from that off Peru, suggesting a basin-scale environmental forcing.

Acknowledgements

The authors thank to the anonymous referees whom greatly improved the manuscript through their criticism. A special thank to Dr. Arnaud Bertrand who help us with statistical analysis.

References

Anderson, C.I.H., Rodhouse, P.G., 2001. Life cycles, oceanography and variability: ommastrephid squid in variable oceanographic environments. Fisheries Research 54, 133–143.

Argüelles, J., Rodhouse, P., Villegas, P., Castillo, G., 2001. Age, growth and population structure of the jumbo flying squid *Dosidicus gigas* in Peruvian waters. Fisheries Research 54, 51–61.

Arkhipkin, A., Murzov, S., 1986. Age and growth patterns of *Dosidicus gigas* (Ommastrephidae). In: Ivanov, B. (Ed.), Present State of Fishery for Squids and Prospects of its Development. VNIRO Press, Moscow, pp. 107–123 (in Russian, Spanish Translation).

Ayón, P., Swartzman, G., Bertrand, A., Gutiérrez, M., Bertrand, S., 2008. Zooplankton and forage fish species off Peru: large-scale bottom-up forcing and local-scale depletion. Progress in Oceanography 79, 208–214.

Bakun, A., Weeks, J.S., 2008. The marine ecosystem off Peru: what are the secrets of its fishery productivity and what might its future hold? Progress in Oceanography 79, 290–299.

Bazzino, G., Salinas-Zavala, C., Markaida, U., 2007. Variabilidad en la estructura poblacional del calamar gigante (*Dosidicus gigas*) en Santa Rosalía, región central del Golfo de California. Ciencias Marinas 33, 173–186.

Brieman, F., Friedman, J.H., Losen, R.A., Stone, C.J., 1984. Classification and Regression Trees. Wadsworth and Brooks/Cole, Monterrey. 172 pp.

Carr, M., 2002. Estimation of potential productivity in Eastern Boundary Currents using remote sensing. Deep-Sea Research II 49, 59–80.

Ehrhardt, N.M., Jacquemin, P.S., García, B.F., Gonzáles, D.G., López, B.J.M., Ortiz, C.J., Solís, N.A., 1983. On the fishery and biology of the giant squid *Dosidicus gigas* in the Gulf of California, Mexico. In: Caddy, J.F. (Ed.), Advances in Assessment of World Cephalopod Resources. FAO Fish Technical Paper, vol. 231, pp. 306–340.

Field, J.C., Baltz, K., Phillips, A.J., Walker, W.A., 2007. Range expansion and trophic interactions of the jumbo squid, *Dosidicus gigas,* in the California current. California Cooperative Oceanic Fisheries Investigation Reports 48, 131–146.

Gutierrez, M., Swartzman, G., Bertrand, A., Bertrand, S., 2007. Anchovy (*Engraulis ringens*) and sardine (*Sardinops sagax*) spatial dynamics and aggregation patterns in the Humboldt Current ecosystem, Peru, from 1983–2003. Fisheries Oceanography 16 (2), 155–168.

Klett, A., 1996. Pesquería del calamar gigante Dosidicus gigas. In: Casas-Valdez, M., Ponce-Diaz, G. (Eds.), Estudio del potencial pesquero y acuícola de Baja California Sur, vol, 127–149.

Mangold, K., 1987. Reproduction. In: Boyle, P.R. (Ed.), Cephalopod Life Cycles, Comparative Reviews, vol. 2. Springer, London, pp. 157–200.

Markaida, U., Quiñónez-Velázquez, C., Sosa-Nishizaki, O., 2004. Age, growth and maturation of jumbo squid *Dosidicus gigas* (Cephalopoda: Ommastrephidae) from the Gulf of California, Mexico. Fisheries Research 66, 31–47.

Markaida, U., 2006. Population structure and reproductive biology of jumbo squid *Dosidicus gigas* from the Gulf of California after the 1997–1998 El Niño event. Fisheries Research 79, 28–37.

Markaida, U., Sosa-Nishizaki, O., 2003. Food and feeding habits of jumbo squid *Dosidicus gigas* (Cephalopoda: Ommastrephidae) from the Gulf of California, Mexico. Journal of the Marine Biological Association of the United Kingdom 83, 507–522.

Masuda, S., Yokawa, K., Yatsu, A., Kawahara, S., 1998. Growth and population structure of *Dosidicus gigas* in the Southeastern Pacific. In: Okutani, T. (Ed.), Contributed Papers to International Symposium on Large Pelagic Squid. Japan Marine Fishery Resources Research Center, Tokyo, pp. 107–118.

Morón, O., 2000. Características del ambiente marino frente a la costa Peruana. Boletín Instituto del Mar del Perú 19, 179–204.

Nesis, K.N., 1970. The biology of the giant squid of Perú and Chile, *Dosidicus gigas*. Oceanology 10, 108–118.

Nesis, K.N., 1983. *Dosidicus gigas*. In: Boyle, P.R. (Ed.), Cephalopod Life Cycles, Species Accounts, vol. I. Academic Press, London, pp. 215–231.

Nigmatullin, Ch.M., Nesis, K.N., Arkhipkin, A.I., 2001. A review of the biology of the jumbo squid *Dosidicus gigas* (Cephalopoda: Ommastrephidae). Fisheries Research 54, 9–19.

Pearcy, W.G., 2002. Marine nekton off Oregon and the 1997–1998 El Niño. Progress in Oceanography 54, 399–403.

Rocha, F., Vega, M., 2003. Overview of cephalopod fisheries in Chilean waters. Fisheries Research 60, 151–159.

Schmiede, P., Acuña, A., 1992. Regreso de las jibias (*Dosidicus gigas*) a Coquimbo. Revista Chilena de Historia Natural 65, 389–390.

Shchetinnikov, A.S., 1986. Geographical variability of food spectrum of *Dosidicus gigas* (Ommastrephidae). In: Ivanov, B.G. (Ed.), Resources and Fishery Perspectives of Squid of the World Ocean. VNIRO Press, Moscow, pp. 143–153 (in Russian with English abstract).

Shchetinnikov, A.S., 1989. Food spectrum of *Dosidicus gigas* (Oegopsida) in the ontogenesis. Zoologicheskii Zhurnal 68, 28–39 (in Russian with English abstract).

Swartzman, G., Bertrand, A., Gutiérrez, M., Bertrand, S., Vasquez, L., 2008. The relationship of anchovy and sardine to water masses in the Peruvian Humboldt Current System from 1983–2005. Progress in Oceanography 79, 228–237.

Taipe, A., Yamashiro, C., Mariategui, L., Rojas, P., Roque, C., 2001. Distribution and concentration of jumbo flying squid (*Dosidicus gigas*) off the Peruvian coast between 1991 and 1999. Fisheries Research 54, 21–32.

Tafur, R., Rabí, M., 1997. Reproduction of the jumbo squid *Dosidicus gigas* (Cephalopoda: Ommastrephidae) off Peruvian coast. Scientia Marina 61, 33–37.

Tafur, R., Villegas, P., Rabi, M., Yamashiro, C., 2001. Dynamics of maturation, seasonality of reproduction and spawning grounds of the jumbo squid *Dosidicus gigas* (Cephalopoda: Ommastrephidae) in Peruvian waters. Fisheries Research 54, 33–50.

Waluda, C.M., Yamashiro, C., Rodhouse, P.G., 2006. Influence of the ENSO cycle on the light-fishery for *Dosidicus gigas* in the Peru Current: an analysis of remotely sensed data. Fisheries Research 79, 56–63.

Wilhelm, O., 1954. Algunas observaciones acerca de las mortandades de jibias (*Dosidicus gigas* D'Orbignyi.) en el litoral de Concepción. Revista de Biología Marina 4, 196–201.

Wolter, K., Timlin, M.S., 1998. Measuring the strength of the ENSO events: how does 1997/98 rank? Weather 53, 315–324.

Yamashiro, C., Mariátegui, L., Rubio, J., Argüelles, J., Tafur, R., Taipe, A., Rabí, M., 1998. Jumbo flying squid fishery in Perú. In: Okutani, T. (Ed.), Contributed Papers to International Symposium on Large Pelagic Squid. Japan Marine Fishery Resources Research Center, Tokyo, pp. 119–125.

Zúñiga, M., 2006. Patrón estacional de reclutamiento y abundancia relativa de *Dosidicus gigas* D'O rbigny, 1835 (Cephalopoda: Ommastrephidae) en Chile Centrosur, Tesis para optar el titulo de biólogo marino. Facultad de Ciencias Naturales y Oceanográficas. Universidad de Concepción – Chile, 78 pp.

Progress in Oceanography 79 (2008) 313–325

Contents lists available at ScienceDirect

Progress in Oceanography

journal homepage: www.elsevier.com/locate/pocean

An individual-based model study of anchovy early life history in the northern Humboldt Current system

Timothée Brochier [a],*, Christophe Lett [b], Jorge Tam [c], Pierre Fréon [a], François Colas [c],[1], Patricia Ayón [c]

[a] Institut de Recherche pour le Développement, UR ECO-UP, CRHMT Centre de Recherche Halieutique Méditerranéenne et Tropicale, Avenue Jean Monnet, BP 171 34203 Sète Cedex, France
[b] Institut de Recherche pour le Développement, UR ECO-UP, University of Cape Town, Oceanography Department, Rondebosch 7701, South Africa
[c] Instituto del Mar del Peru (IMARPE), Esquina Gamarra y General Valle S/N Chucuito Callao, Peru

ARTICLE INFO

Article history:
Accepted 14 October 2008
Available online 21 October 2008

Keywords:
Egg buoyancy
DVM
Larval survival
IBM
Engraulis ringens
Hydrodynamic model
Peru
Ichthyoplankton
Biophysical model

ABSTRACT

We used an individual-based model of anchovy (*Engraulis ringens*) early life history coupled with hydrodynamic outputs from the regional oceanic modeling system (ROMS) to investigate the factors driving variability in egg and larval survival rates in the northern Humboldt upwelling region off Peru. Individuals were released within a coastal area and followed for a period of 30 days. Those that were still in the coastal area at that time were considered as retained. We investigated the spatial and temporal variability in the release locations of the individuals retained, and compared these to observed egg concentration patterns reconstructed from a 40-year period of monitoring. A first set of simulations using passive particles to represent anchovy eggs and larvae revealed a large sensitivity of the results to the initial vertical distribution of particles. We then conducted two additional sets of simulations that included the effect of egg buoyancy, larval vertical swimming behavior and lethal temperature. We obtained (1) maximal coastal retention close to the surface in winter and in deeper layers in summer, (2) a large influence of egg buoyancy and of larval vertical behavior on coastal retention in all seasons, (3) a partial match between dates and locations of enhanced retention and observed egg concentration patterns and (4) a low effect of lethal temperature on survival except when associated with high egg density. The model suggests that an optimal temporal spawning pattern for maximizing coastal retention would have two maximums, the most significant in austral winter and the second in summer. This pattern agrees roughly with observed spawning seasonality, but with temporal discrepancy of about two months in the peaks of both series. Spatially, we obtained higher retention from 10 S to 20 S, whereas the observed maximum egg concentration was located between 6°S and 14°S. Among the three sets of simulations, the one taking into account larval vertical swimming behavior lead to the best match with the data.

1. Introduction

Upwelling ecosystems support large populations of small pelagic fish, particularly clupeoids like anchovy and sardine (Fréon et al., 2006). These species are believed to control the trophic dynamics of these systems (Cury et al., 2000) and are often exploited by industrial and artisanal fisheries (Fréon et al., 2005). High levels of recruitment variability make anchovy and sardine stocks particularly difficult to manage (Jacobson et al., 2001). As these fish are short-lived and often heavily exploited the bulk of the biomass comes from one (anchovy) to three (sardine) year-classes. Consequently, fluctuations in recruitment success translate rapidly into fluctuations in population sizes. It is generally accepted that recruitment dependence on the spawning biomass is low, except at very low levels of parental biomass (Fogarty, 1993; Myers, 1998; Myers et al., 1999), and that it depends mainly on survival during the first life stages. Survival is thought to be mainly mediated by environmental conditions rather than by density-dependent processes. Environmental conditions which could influence the survival of the early life stages have been well described (Bakun, 1996; Cury and Roy, 1989; Lasker, 1985). However, forecasting environmentally driven fluctuations in recruitment remains problematic.

The Humboldt Current system is one of the world's major eastern boundary current upwelling systems, and it currently

---

* Corresponding author.
E-mail addresses: timothee.brochier@ifremer.fr (T. Brochier), christophe.lett@ird.fr (C. Lett), jtam@imarpe.gob.pe (J. Tam), Pierre.Freon@ifremer.fr (P. Fréon), francois@atmos.ucla.edu (F. Colas), payon@imarpe.gob.pe (P. Ayón).

[1] Present address: Institute of Geophysics and Planetary Physics (IGPP), University of California Los Angeles, Los Angeles, CA, USA.

0079-6611/$ - see front matter © 2008 Elsevier Ltd. All rights reserved.
doi:10.1016/j.pocean.2008.10.004

sustains a huge stock of anchovy (*Engraulis ringens*), also called anchoveta, that is exploited by thousands of purse-seiners whose annual landing exceeds 5 million tons (Ñiquen and Fréon, 2006). This stock has been monitored since the 1960s by the Peruvian institute IMARPE, providing extensive information on spawning dates and areas despite their large variability (Santander, 1981; Senocak et al., 1989). Anchovy reproduction usually displays two annual peaks, with a major spawning in late winter (August–September) and a secondary spawning in summer (February–March). On average, the winter spawning season is much more intense than the summer one, and the main spawning area is located between 6°S and 14°S. However, inside this large area spawning is both spatially and temporally very irregular. Muck (1989) found a strong negative relationship between the proportion of mature females and temperature but the data were not spatialized. Another study suggested that larvae survived better off the northern coast of Peru during the austral winter season when motile (swimming) algae are available as food (Walsh et al., 1980). Understanding the factors driving anchovy spawning date and location and their impact on eggs and larvae is a key question for local fisheries management.

Realistic numerical hydrodynamic models at a regional scale have recently become available as computational power has rapidly increased over the last decade (Haidvogel and Beckmann, 1998). These models have increasingly been coupled with individual-based models to study the dynamics of early life stages of marine species (Miller, 2007; Werner et al., 2001) and particularly small pelagic fish (Lett et al., in press). Recently, a climatological hydrodynamic simulation of the northern Humboldt upwelling region at a relatively high resolution (1/9°) has been developed and validated (Penven et al., 2005). Lett et al. (2007a) used it to build putative maps of Bakun's triad processes (concentration, retention and enrichment, Bakun, 1996). They showed that the area of largest concentration of anchovy eggs matched the area of optimal simulated enrichment and retention, and that maximum retention rates occurred in summer while enrichment was stronger in winter. Although their results could explain some of the significant anchovy spawning patterns, they could not explain others, like the bimodal seasonal distribution of anchovy egg production usually observed in Peru. In this paper, the same climatological hydrodynamic simulation was used but with a different (and complementary) approach. Instead of mapping separately Bakun's triad elements, we studied the functional impact of anchovy spawning period, vertical egg and larval movements (buoyancy and swimming), and mortality on anchovy retention, following the methodology described by Mullon et al. (2003). We compared the model output with observed data on spawning patterns, following the pattern-oriented modelling (Grimm et al., 2005) approach. Field egg concentration of anchovy eggs as surveyed by IMARPE were used as a proxy for spawning location and period.

It is generally accepted that clupeoids maximize egg and larval retention by spawning in favorable areas (Bakun, 1996), and there is no evidence of the Peruvian anchovy being an exception. Therefore, one of the questions addressed in this paper is whether it is possible, with a simple condition of larval retention in the phytoplankton-rich coastal area, to model features of the observed spawning behavior. In other words, does the Peruvian anchovy spawning maximize the retention condition? We also investigated the impact of egg buoyancy and larval swimming on retention, using different vertical swimming behaviors such as diurnal vertical migration (DVM) and ontogenic migration. Finally, being in an area where the presence of upwelled waters leads to large temperature variations, we also tested different lethal temperatures to analyze how they might interact with other factors to modulate retention.

2. Methods

2.1. The model

The individual-based model (IBM) description below follows the overview-design-details (ODD) protocol for describing individual- and agent-based models (Grimm et al., 2006; Grimm and Railsback, 2005) and consists of six subsections below. The first two subsections provide an overview, the fourth explains general concepts underlying the model design, and the remaining three subsections provide details. The present model is a version of a modeling tool called Ichthyop (Lett et al., 2008) that can be downloaded from http://www.eco-up.ird.fr/projects/ichthyop/.

2.1.1. Purpose

We used a coupled model of transport and survival of anchovy early life stages to assess coastal retention rates depending on spawning tactics, and compared optimized results with the observed reproduction patterns. We also used the model to investigate the relative importance of environmental and behavioral factors on retention.

2.1.2. State variables and scales

The model is composed of virtual individuals and their marine physical environment. Individuals were characterized by the state variables: age (in days), location (in three dimensions, longitude, latitude and depth), life stage (egg or larva) and status (alive or dead). The environment was characterized by three-dimensional fields of state variables: water velocity (in $\mathrm{m\,s^{-1}}$), temperature (in °C) and salinity (PSU).

Environmental conditions were provided by archived simulations of the regional oceanic modeling system (ROMS) (Shchepetkin and McWilliams, 2005) configured for the Peruvian region (Penven et al., 2005). The grid extends from 5°N to 22°S and from 70°W to 92°W with a horizontal resolution of 1/9°. Since ROMS uses terrain-following curvilinear coordinates with 32 layers in this configuration, the vertical resolution ranges from 30 cm to 6.25 m at the surface layer and from 31 cm to 1086 m at the bottom layer. To investigate the seasonal variability of the environment we used a simulation forced with monthly climatological atmospheric fluxes and boundary conditions. Penven et al. (2005) validated the modeled seasonal cycle. Since the mesoscale environment is variable in different simulation years (with the same climatological forcing) due to intrinsic model variability (Batteen, 1997; Marchesiello et al., 2003), a set of three years was chosen randomly among those used by Penven et al. (2005). Water velocity, temperature and salinity fields were averaged and stored every two days. These fields were interpolated in time and space in the IBM to determine values of the environmental state variables at any individual location every two hours. Every simulation lasted for 30 days.

2.1.3. Process overview and scheduling

Virtual eggs were released in the environment following a determined spatial (area, depth and patchiness) and temporal (month, duration and frequency) spawning strategy that constituted the initial conditions (see Sections 2.1.5 and 2.1.6.1). Once released, each egg or larva within each time step was moved, tested for mortality and finally for retention (see Sections 2.1.6.2–2.1.6.4). Depending on the type of simulation, the movement was a passive Lagrangian transport with or without addition of a buoyancy scheme for eggs, or a vertical swimming behavior scheme for larvae.

2.1.4. Design concepts

2.1.4.1. Stochasticity. The release location for each individual was chosen randomly within the specified spawning areas. It aimed at simulating patchy or uniform distributions depending on a patchiness parameter (see Section 2.1.6.1). Instead of testing a repetition effect that largely depended on the initial number of released particles, as did Mullon et al. (2003), the number of individuals chosen was large enough (3000 individuals) to avoid effects due to the random initial location. Therefore only one simulation for each set of parameters was necessary.

2.1.4.2. Observation. A series of simulations were run with different pre-defined sets of parameters. For each simulation the proportion of individuals retained within the coastal area was calculated. We then performed a variance analysis on the proportion of retained individuals. We also investigated the spatial and temporal variability in the release locations of the individuals retained, and compared these to observed egg concentration patterns reconstructed from a 40-year period of monitoring.

2.1.5. Initialization

In each simulation 3000 particles representing virtual eggs were released in the spawning area at the beginning of each month. The spawning area extended from 2°S to 20°S, and from the coast to the 3000 m isobath, which roughly corresponds to the zone of maximum chlorophyll concentrations (Fig. 1). The initial conditions of virtual spawning were defined by year (in the climatological series), month, spawning frequency, area, patchiness and depth (see Section 2.1.6.1). For each simulation, a set of individual characteristics was also chosen: lethal temperature, egg buoyancy and vertical migration behavior (see Sections 2.1.6.2 and 2.1.6.3).

2.1.6. Submodels

2.1.6.1. Spawning strategy. The spawning strategy was defined by the (virtual) spawning area, depth, time, duration, frequency and patchiness. The spawning area was a set of sub-areas covering the coastal zone previously defined (see Section 2.1.5). These sub-areas were defined by three bathymetric intervals (0–100 m, 100–500 m and 500–3000 m) and nine latitudes (every two degrees from 2°S to 20°S). Depth of spawning was defined by an interval (upper and lower depth levels, in m). Spawning time was defined by year and month. Spawning frequency and spawning patchiness were parameters used to set the time and space distribution of the released particles. Spawning frequency was the number of times virtual eggs were released within the spawning period (one month). For this parameter we used values of 1, 3 and 5 to set that all virtual eggs (3000) were released on day 0, 1/3 of them (1000) on days 0, 10 and 20, or 1/5 (600) on days 0, 6, 12, 18 and 24. Spawning patchiness indicated the number of particles released around the same location (±1 m for depth, ±1 1/9° for longitude and latitude). For this parameter we used values of 1, 10 and 100. This last value, for example, indicates that the 3000 particles were released by groups of 100 around any location, i.e., the distribution of particles was patchy, with 30 patches of 100 particles. Locations were randomly chosen within the spawning area.

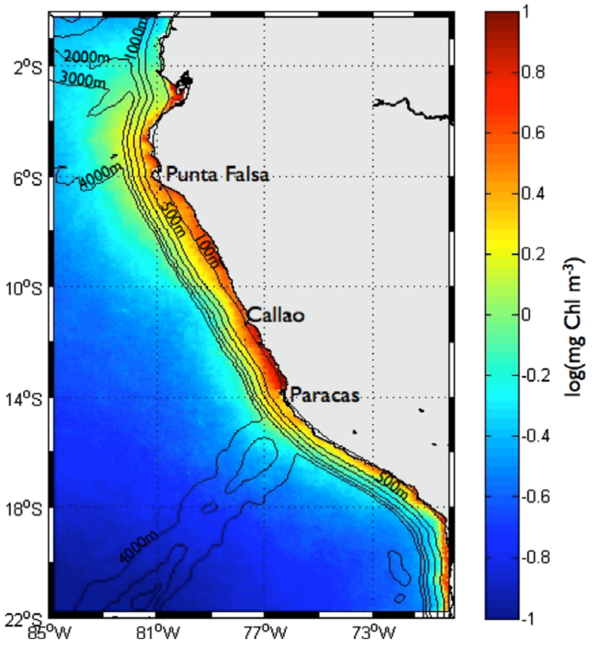

Fig. 1. Superficial chlorophyll *a* concentration annual mean, over the period 1997–2003 (SeaWiFS) superposed with isobaths 100, 500, 1000, 2000, 3000 and 4000 m. The higher chlorophyll *a* concentration is above the continental shelf. Source: ocean Color Web: oceancolor.gsfc.nasa.gov – processing: interanual means – IRD (D. Dagorne).

2.1.6.2. Movement. Depending on the type of simulation, the movement was purely Lagrangian (passive), with buoyancy for eggs or with vertical swimming behavior for larvae (Eq. (1)). Egg buoyancy was calculated as a function of egg density and water density, the latter being calculated as a function of water temperature and salinity (see Parada et al., 2003 for details). The buoyancy scheme was only applied before hatching, i.e., during the first two days after spawning, as suggested by laboratory experiments (Ware et al., 1980). Depending on the type of simulation, the vertical swimming behavior consisted in a diurnal vertical migration (DVM) between two fixed depths (scenario 1) or in maintaining fixed depths at 1, 15 or 30 m (scenario 2, 3 and 4, respectively). The larval vertical swimming scheme was applied 4 days after hatching, i.e., from day 6, roughly corresponding to the time of complete yolk resorption (Ware et al., 1980). In scenario 1 the vertical swimming velocity was an age-dependent function derived from an age-length relationship (Castro and Hernández, 2000) and a length–velocity relationship (Hunter, 1977). The resulting age–velocity relationship was linear for the first month (Eq. (2)). Anchovy larvae swam approximately a distance equal to their size in one second (Hunter, 1977). We considered that this velocity could be applied for vertical migrations

$$\begin{aligned} x(t+\Delta t) &= x(t) + V_u \cdot \Delta t, \\ y(t+\Delta t) &= y(t) + V_v \cdot \Delta t, \\ z(t+\Delta t) &= z(t) + (V_z + V_{buoy}(a) + B \cdot V_{swim}(a)) \cdot \Delta t, \end{aligned} \tag{1}$$

(x,y,z) = individual's position; a = individual's age (days since spawning); t = time, $V_{u,v,z}$ = current velocity along u, v or z axis, $V_{buoy}(a)$ = buoyancy velocity depending on egg and water density, $V_{swim}(a)$ = swimming velocity in cm s^{-1}, B = vertical migration behavior ± 1 depending on depth and time for DVM.

$$\begin{aligned} &\text{for } a \leqslant 6 : V_{swim} = 0, \\ &\text{for } a > 6 : V_{swim} = 0.1 + 0.08 \cdot (a - 6), \end{aligned} \tag{2}$$

a is the time since spawning in days and V_{swim} is the swimming velocity in cm s^{-1}.

2.1.6.3. Mortality. Mortality was temperature-dependent: virtual eggs and larvae died when they were exposed to temperature below a pre-defined threshold value. Although there are few data concerning the lethal temperature for anchovy larvae in Peru, larval survival is known to be strongly dependent on length at hatching, which is usually optimal at intermediate temperature in a given environment (Llanos-Rivera and Castro, 2006; Pauly and Soriano, 1989). Off Peru, the observed temperature range for adults anchovy spawning is 14–21 °C (Jarre et al., 1991), without evidence of temperature selection for spawning (Bertrand et al., 2004). Here we tested the impact of three different arbitrary lethal temperature (12, 14 and 16 °C). These values were selected after preliminary tests in order to obtain contrasted results.

2.1.6.4. Coastal retention. Individuals were considered as retained when they were alive and still in the coastal area after the drift period. We make the generally accepted assumption that the variability of the recruitment is highly correlated to this retention (Bakun, 1996). Based on *in situ* observations (e.g, Ayón, 2004), the coastal area was the same as the spawning area, i.e., the area where high chlorophyll concentrations were observed (Fig. 1). For the drift period we used the ‘‘horizontal-current independent age”, i.e., the age at which larvae can swim fast enough to influence their horizontal motion within the current field. The Peruvian anchovy larval stage duration is about 1.5 months, after which larvae metamorphose into juveniles and recruits (i.e., fish of 37.5–47.5 mm) at 3 months (Palomares et al., 1987). The age-velocity relationship previously described indicated one month-old larvae can swim >2 cm s^{-1}, which might be sufficient to influence motion within currents in the coastal area which typically flow <10 cm s^{-1} (Fig. 10). Therefore we set the drifting time to 30 days after spawning.

Table 1
Parameters tested in each set of simulation.

	Sim I	Sim II	Sim III
Latitude	—2–4 °S, 4–6 °S, 6–8 °S, 8–10 °S, 10–12 °S, 12–14 °S, 14–16 °S, 16–18 °S, 18–20 °S—		
Bathymetry	—0–100 m, 100–500 m, 500–3000 m—		
Month	—Every months—		
Year	3	1	1
Depth of spawning	0–15 m, 15–30 m, 30–45 m	0–50 m	0–50 m
Frequency	1, 3, 5	1	1
Patchiness	1, 10, 100	1	1
Egg density	No	1.023, 1.024, 1.025, 1.026, 1.027	No
Lethal temperature	No	12, 14, 16 °C	No
Vertical swimming behavior	No	No	DVM 0–30 m, Target depth 1 m, 15 m, 30 m

2.2. Simulation experiments, sensitivity analysis and pattern analysis

We performed three sets of simulations (Table 1), which tested the following factors: (1) Considering only Lagrangian drift, the effects of different spawning strategies (location, date, time, depth, etc.) on retention pattern (Simulation I); (2) The effects of varying egg buoyancy (Simulation II) and larval swimming (Simulation III) on retention pattern.

Because our modeling design was similar to that of many experiments, we chose to perform analysis of variance (ANOVA) using retention rates as the dependent variable, the different tested effects (egg density, lethal temperature, spatial and temporal effects) and their first degree interactions as fixed factors. We checked that the error distribution was close to a Gaussian distribution and that the assumption of variance homogeneity was fulfilled. Because the spatio-temporal autocorrelation in the simulated data resulted in an overestimation of the number of degrees of freedom of the ANOVA, and hence of the significance level of the factors, we chose arbitrarily 2% for the explained variance as threshold to discuss the effect of the factors.

Finally, we compared retention spatial and seasonal patterns obtained with the IBM with field observations of anchovy egg concentrations. We derived an egg-distribution climatology with field data from 1961 to 2004. Considering that this observed distribution reflected the average spawning pattern, we compared it with the retention patterns resulting from Simulation III, with a target depth of 15 m, which seems the most realistic in terms of egg and larval depth regulation. If the natural selection has maximized retention within the chlorophyll-rich coastal area for Peruvian anchovy as modeled here, then one would expect observed spawning and retention patterns to be similar in time and space.

3. Results

3.1. Sensitivity analysis

3.1.1. Simulation I

Factors included in the analysis of variance of the simulated retention values were (Table 2): date (year and month) of spawning, area (latitude and bathymetry) and depth of spawning, spawning frequency and patchiness. Spawning depth explained more than 20% of the total variance in the retention values, followed by latitude (7%) and bathymetry (4%). Year, spawning frequency and patchiness explained very little of the variance. On average,

Table 2
ANOVA of IBM’s output for Simulation I show the relative importance of each factor on the variation of the coastal retention rate.

	Df	Sum Sq	Mean Sq	*F* value	% Expl.	Pr(>*F*)
Depth	2	4,074,222	2,037,111	8043.3	22.7	<2.2e−16
Latitude	8	1,290,999	161,375	637.2	7.2	<2.2e−16
Bathymetry	2	694,725	347,362	1371.5	3.9	<2.2e−16
Month	11	250,306	22,755	89.8	1.4	<2.2e−16
Year	2	11,485	5743	22.7	0.1	1.45e−10
Patchiness	2	2490	1245	4.9	0.0	0.0073315
Frequency	2	387	194	0.8	0.0	0.4657411
Depth×latitude	16	385,742	24,109	95.2	2.2	<2.2e−16
Depth×bathymetry	4	71,194	17,798	70.3	0.4	<2.2e−16
Depth×month	22	1,040,158	47,280	186.7	5.8	<2.2e−16
Depth×year	4	5498	1375	5.4	0.0	0.0002299
Latitude×bathymetry	15	1,092,955	72,864	287.7	6.1	<2.2e−16
Latitude×month	88	1,827,175	20,763	82.0	10.2	<2.2e−16
Latitude×year	16	42,677	2667	10.5	0.2	<2.2e−16
Bathymetry×month	22	507,748	23,079	91.1	2.8	<2.2e−16
Bathymetry×year	4	5542	1386	5.5	0.0	0.0002124
Month×year	22	40,613	1846	7.3	0.2	<2.2e−16
Residuals	25,981	6,580,173	253		36.7	
Total		17,924,089			100.0	

retention increased with spawning depth, from ~20% for a spawning at 0–15 m to ~45% at 30–45 m. Retention was higher over the continental shelf (~40% for particles released from the coast to the 100 m isobath) and decreased offshore (~20% for particles released in the area between the 500 m and 3000 m isobaths). Five interactions between factors explained more than 2% of the variability but with high degrees of freedom and therefore relatively low mean square values (Table 2). The most significant was the month×latitude interaction. High (>40%) retention values were found from 8°S to 14°S from June to October. Low (<20%) values were observed all year round from 2°S to 6°S (Fig. 2). The month×depth interaction was observed together with the month×bathymetry interaction (Fig. 3). For the 30–45 m depth level, retention values peaked during late spring (November–January) and were minimal in winter

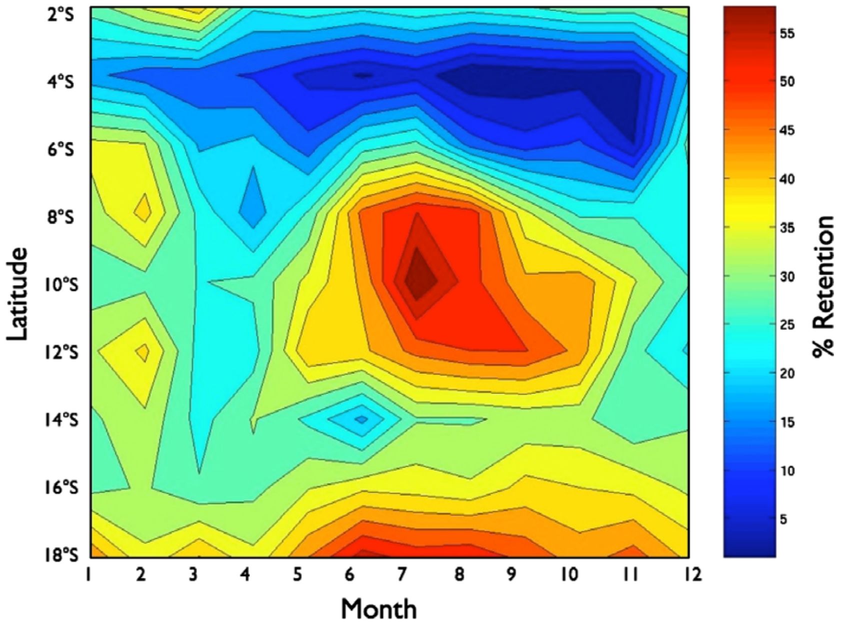

Fig. 2. Hovmuller diagram of the retention rates (Simulation I). The maximum of retention does not occur at the same place in winter and summer.

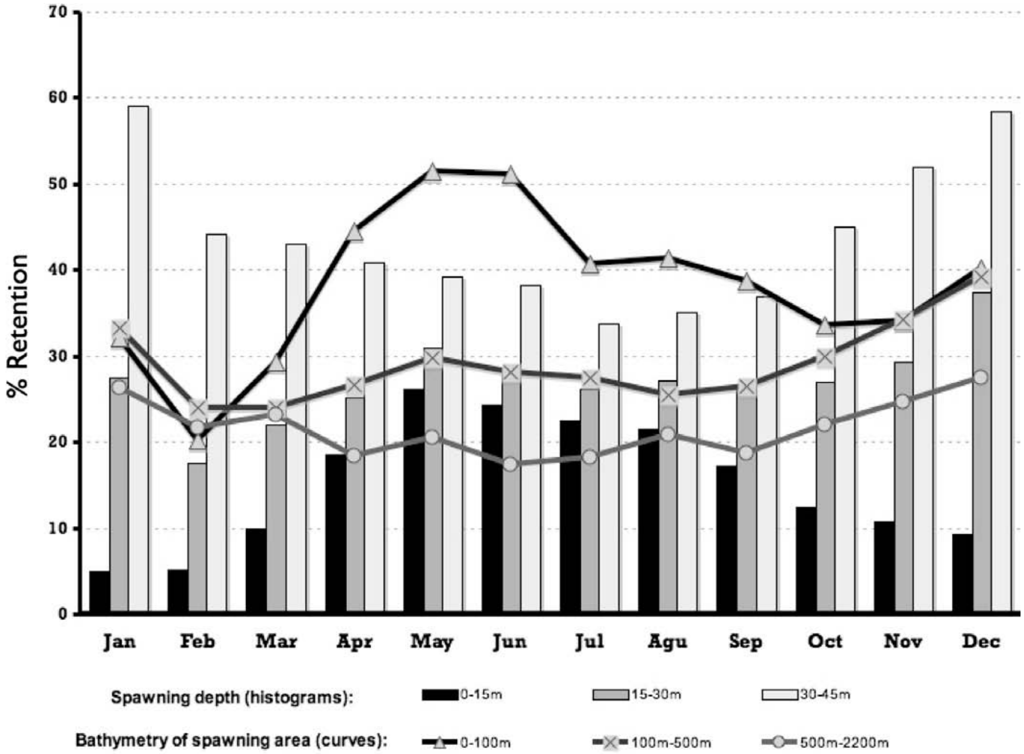

Fig. 3. Monthly retention rates (Simulation I). Histograms: particles released at three different depth ranges (0–15, 15–30 and 30–45 m). Curves**:** particles released at different position above the continental shelf: coast to isobaths 100 m; 100–500 m; 500–3000 m. This figure shows (1) the opposite seasonal pattern of retention for the 0–15 m and the 30–45 m cape, and (2) the higher retention rate in spring and summer over the shallow shelf (0–100 m).

(June–September), while the opposite seasonal pattern was obtained for the 0–15 m level. Maximum values of retention were obtained in fall (May–June) for particles released close to the coast and during late spring (November–January) for particles released further offshore. Because spawning depth was identified as the most sensitive parameter, we conducted two additional sets of simulations which included processes that affected the vertical distribution of eggs and larvae.

3.1.2. Simulation II

We tested the effect of different values of egg buoyancy (egg densities of 1.023, 1.024, 1.025, 1.026 and 1.027 g cm^{-3}) and of lethal temperature (12, 14 and 16 °C) on the simulated retention. We modeled different values only for the single parameters that were found as the most sensitive in the previous simulation, i.e., month, latitude and bathymetry, but held the remaining factors constant (Table 1). The spawning depth was set between 0 and 50 m. ANOVA on the retention values (Table 3) showed that egg buoyancy strongly contributed to the variability in retention values (~30% of the variance) while the lethal temperature contributed only 7.6%. Increased egg density in the range 1.024–1.026 g cm^{-3} strongly increased retention values (Fig. 4). Temperature-dependent mortality was only significant for the highest density class (1.027 g cm^{-3}). A high lethal temperature threshold was detrimental in this case (Fig. 4) suggesting that virtual eggs sank into low temperature waters before hatching. To confirm these hypothesis we analyzed the vertical distribution (averaged over the entire coastal area and over the year) after 2 days of transport for eggs randomly released between 0 and 50 m. For density values of 1.023 and 1.024 g cm^{-3}, eggs concentrated close to the surface. For a density of 1.025 g cm^{-3} they remained mainly between 0 and 50 m, while for larger values, eggs sank rapidly, reaching waters deeper than 150 m for a density of 1.027 g cm^{-3} (not shown). The large mortality observed for an egg density of 1.027 g cm^{-3} was consistent with the annual mean depth of the lethal 16 °C isotherm between 7°S and 13°S from the coast to 500 km offshore, which was about 150 m in the hydrodynamic model (Penven et al., 2005). The density×month interaction (Fig. 5) showed maximum retention in winter (June–August) for densities of 1.023 and 1.024 g cm^{-3}. For larger values there were two maxima, one in winter (June–August) and the other in summer (December–February). The density×bathymetry interaction (Fig. 4) showed that for a egg density of 1.025 g cm^{-3} and higher the largest retention values were obtained for spawning grounds between 100 and 500 m, while for lower values of density retention was maximum for the coastal spawning area. Finally, the density×latitude interaction indicated latitudinal variability of retention values for low density values (1.023 and 1.024 g cm^{-3}). As these densities were the most superficial, this was certainly due to alongshore variations of the upwelling strength.

Table 3
ANOVA of IBM's output for Simulation II show the relative importance of each factor on the variation of the coastal retention rate.

	Df	Sum Sq	Mean Sq	*F* value	% Expl.	Pr(>*F*)
Density	4	1,235,548	308,887	1293.86	29.08	<2.2e−16
Lethal temperature	2	323,280	161,640	677.07	7.61	<2.2e−16
Latitude	8	290,444	36,306	152.08	6.84	<2.2e−16
Month	11	56,661	5151	21.58	1.33	<2.2e−16
Bathymetry	2	51,086	25,543	106.99	1.20	<2.2e−16
Density×lethal temperature	8	369,698	46,212	193.57	8.70	<2.2e−16
Density×latitude	32	323,531	10,110	42.35	7.62	<2.2e−16
Density×month	44	121,762	2767	11.59	2.87	<2.2e−16
Density×bathymetry	8	74,890	9361	39.21	1.76	<2.2e−16
Lethal temperature×latitude	16	26,367	1648	6.90	0.62	6.21e−16
Lethal temperature×month	22	2726	124	0.52	0.06	0.968
Lethal temperature×bathymetry	4	17,465	4366	18.29	0.41	6.51e−15
Latitude×month	88	161,927	1840	7.71	3.81	<2.2e−16
Latitude×bathymetry	15	107,884	7192	30.13	2.54	<2.2e−16
Month×bathymetry	22	36,449	1657	6.94	0.86	<2.2e−16
Residuals	4392	1,048,514	239		24.68	
Total		42,48,232			100.00	

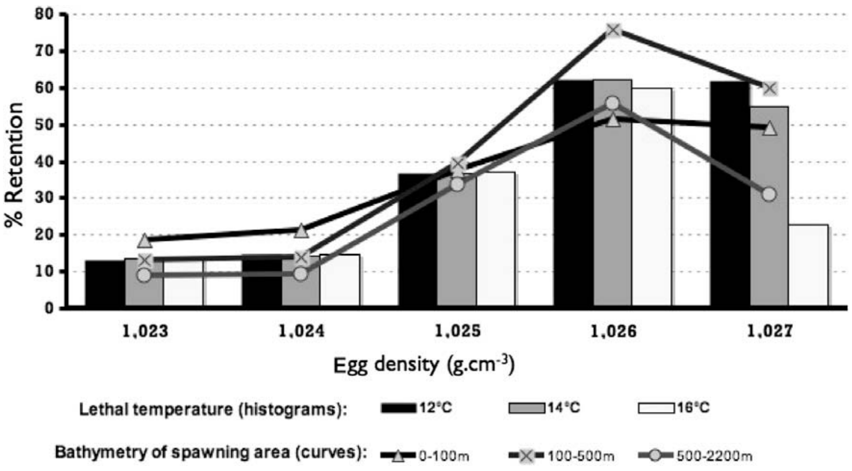

Fig. 4. Retention rates for four different egg buoyancy (Simulation II). Histograms: egg lethal temperatures of 12, 14 and 16 °C; Curves: spawning from coast to isobaths 100 m; 100–500 m; 500–3000 m. Retention increases when buoyancy decreases, but lethal temperature then becomes limitant.

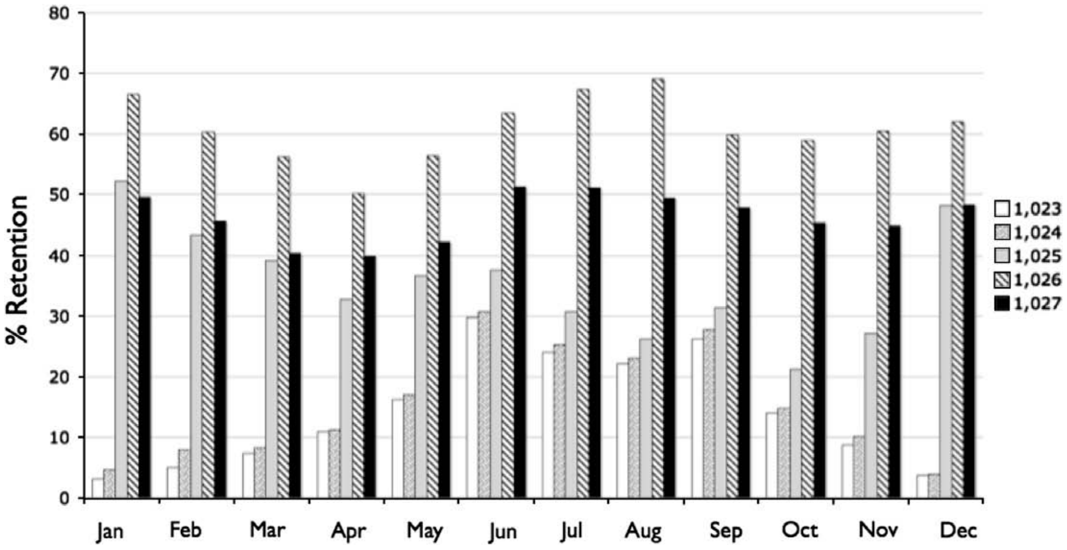

Fig. 5. Monthly retention rate for four egg buoyancy (Simulation II). Heavy eggs (>1.025 g cm^{-3}) retention have two seasonal maxima while light eggs (<1.025 g cm^{-3}) have only one maximum.

3.1.3. Simulation III

Simulated larvae were given depth-regulatory behavior: (1) a diurnal vertical migration (DVM) between 1 and 30 m, or a target depth of (2) 1 m, (3) 15 m, (4) 30 m. In this simulation vertical behavior was the main factor contributing to retention variability (~19%), followed by the latitude (~18%), month (~5%) and bathymetry (~ 4%) factors (Table 4). On average the simulated retention values increased with the target depth from ~30% (at 1 m) to ~55% (at 30 m). The DVM scenario gave an average retention value of ~40%, slightly lower than the scenario using a target depth of 15 m. The vertical behavior×month interaction explained a substantial part of the variance (~8%) but again with a high number of degrees of freedom (33). The retention patterns also changed much with bathymetry. For the coastal area (until 100 m depth) the retention values were maximal during winter for all vertical behavior scenarios. More offshore the scenarios using a target depth of 1 or 30 m showed opposite retention patterns, while the DVM scenario and the 15 m depth one showed two maximums of retention, one during winter and one during summer (Fig. 6).

3.2. Pattern analysis

3.2.1. Seasonal pattern

The two peaks observed in the mean seasonal distribution of collected anchovy eggs could be compared with the two peaks obtained for retention in the simulation using vertical swimming behavior (Simulation III) and a target depth of 15 m with a spawning over the whole area (0–3000 m), or only over the shelf (0–100 m). Although the correlation between maximum observed spawning and enhanced simulated retention was not precise, the main seasonal variation pattern was retrieved (Fig. 7). For spawning over the whole domain, the summer peak was larger than the winter one. By contrast, for spawning over the shelf only, where the majority of the eggs are actually spawned, the winter peak was larger. In both cases a temporal discrepancy of about two months was observed with the field data peaks (for technical reasons the hydrodynamic model started on January 15th so that the temporal shift was actually one month and a half).

3.2.2. Spatial pattern

Field observations indicated that anchovy eggs were found mainly between 6°S and 14°S (Fig. 8). In the areas 6°S–10°S and 14°S–20°S anomalies of egg concentrations and anomalies of retention values were opposite. At 6°S–10°S, the observed egg concentration was significant despite relatively low retention simulated by the model. In contrast, from 14°S to 20°S, field data indicated relatively low egg concentrations despite a high simulated retention (Fig. 8). However, the hydrodynamic model in that region did not reproduce properly the Paracas upwelling cell (Penven et al., 2005), which might lead to an overestimation of retention there.

Table 4
ANOVA of IBM's output for Simulation III show the relative importance of each factor on the variation of the coastal retention rate.

	Df	Sum Sq	Mean Sq	*F* value	% Expl.	Pr(>*F*)
Vertical_behavior	3	73,278	24,426	301.13	19.29	<2.2e−16
Latitude	8	70,184	8773	108.15	18.47	<2.2e−16
Month	11	17,687	1608	19.82	4.66	<2.2e−16
Bathymetry	2	15,911	7956	98.08	4.19	<2.2e−16
Vertical_behavior×latitude	24	4994	208	2.57	1.31	5.53E−05
Vertical_behavior×month	33	31,869	966	11.91	8.39	<2.2e−16
Vertical_behavior×bathymetry	6	1711	285	3.51	0.45	0.0019
Latitude×month	88	53,371	606	7.48	14.05	<2.2e−16
Latitude×bathymetry	15	10,942	729	8.99	2.88	<2.2e−16
Month×bathymetry	22	16,009	728	8.97	4.21	<2.2e−16
Residuals	1035	83,955	81		22.10	
Total		379,911			100.00	

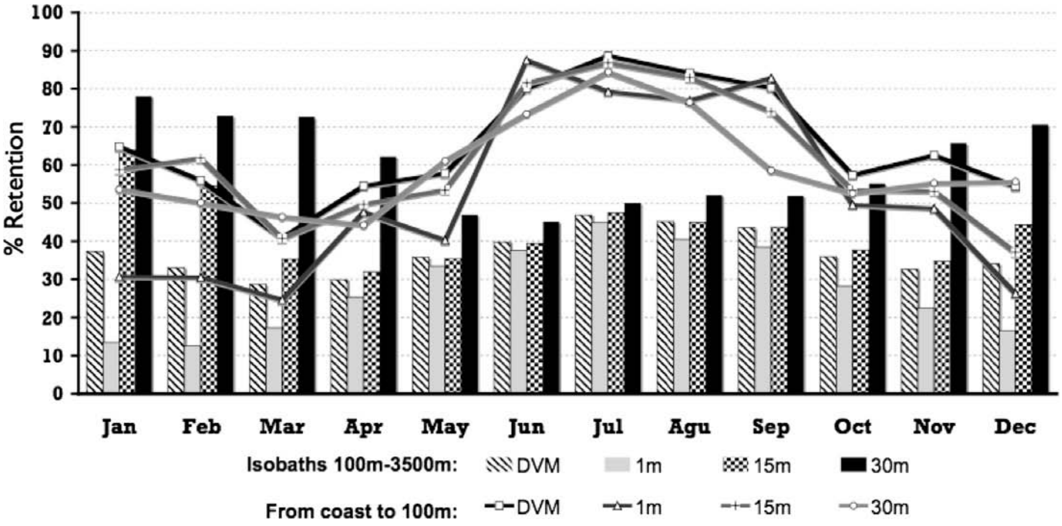

Fig. 6. Monthly retention rate for different scenarios of larval vertical migration (Simulation III). Histograms: eggs released from isobaths 100 m to 3500 m. Curves: eggs released from coast to isobath 100 m. Retention is constant in summer for any vertical swimming behavior while in winter retention is lower for larvae migrating to the near surface and higher for larvae migrating to 30 m depth. For eggs released over the shallow shelf (<100 m), the retention is much stronger in winter.

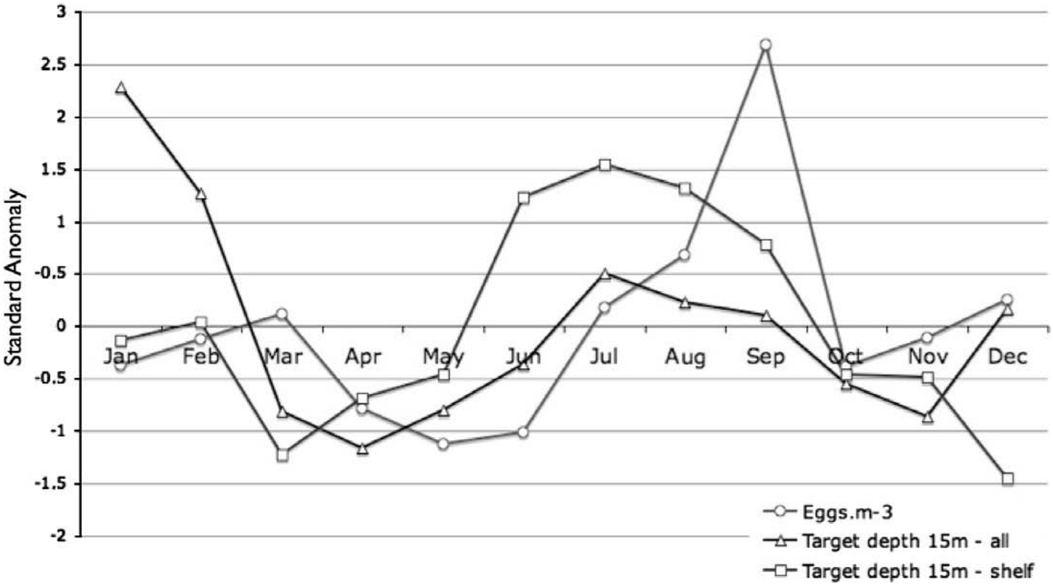

Fig. 7. Standard anomalies of the mean monthly anchovy egg concentrations and the retention for larvae migrating to 15 m depth (Simulation III) released (1) from coast to isobath 3000 m (curve with triangles), (2) from coast to isobath 100 m (curve with squares). The relative importance of the summer and winter peaks of retention depends on whether spawning was sets over the shelf or not.

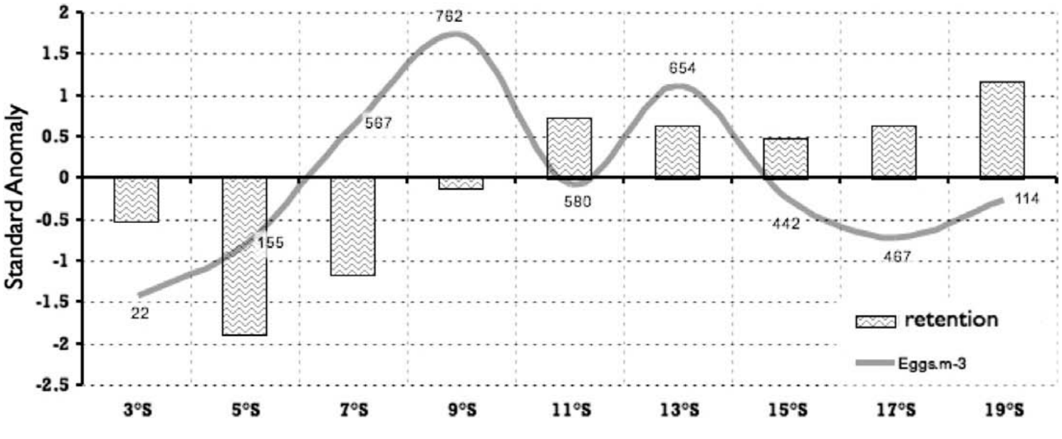

Fig. 8. Spatial comparison between retention (Simulation III) and eggs concentration standardized anomalies. The numbers near the curve indicate the number of data available (square of 1/10° latitude × 1/10° longitude where there is data).

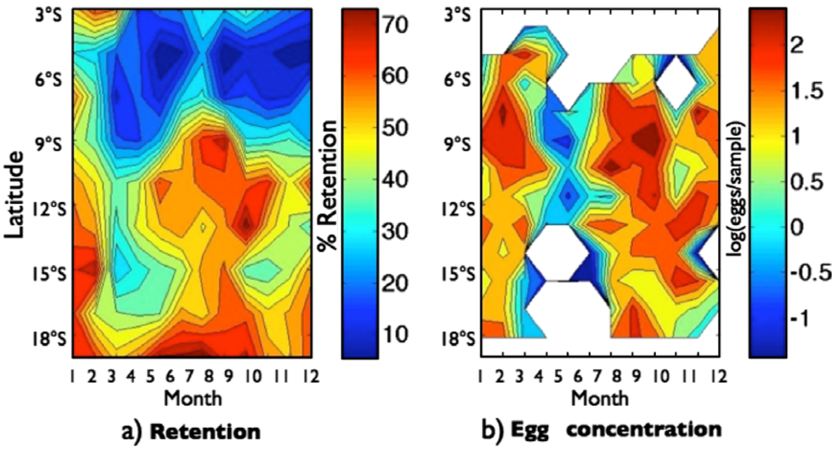

Fig. 9. Spatio-temporal egg concentrations and retention patterns. (a) Hovmuller diagram of retention (Simulation III, target depth 15 m). (b) Hovmuller diagram of anchovy eggs concentration (blank indicates no sufficient data).

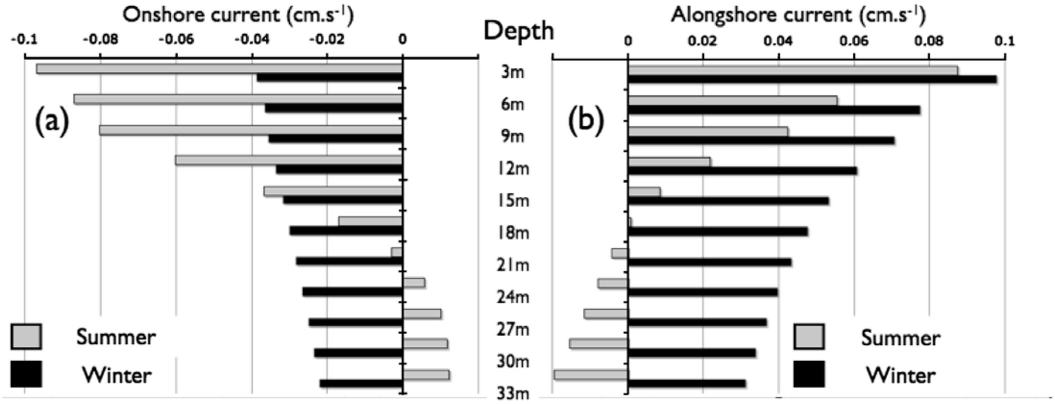

Fig. 10. Average vertical structure (0–30 m) of the flow obtained from the climatological hydrodynamic model simulations (one year) in summer and in winter from 6°S to 14°S over the coastal area (until isobath 2200 m). (a) Onshore current and (b) Alongshore current component. In summer there is a current shear around 20 m that doesn't appear in winter.

3.2.3. Spatio-temporal pattern

We plotted similar Hovmuller representations for both anchovy egg concentrations (field data) and retention values derived from Simulation III with a 15 m depth scenario (Fig. 9). The field data showed a spawning summer peak from 6°S to 10°S, while the model indicated a summer maximum of retention further south at 14°S–16°S. There was a winter spawning peak from 7°S to 12°S and at 18°S, which roughly matched peaks in retention. There was a high simulated retention for eggs released south of 18°S from May to September, but not enough field data allowed to make a comparison, although there was also maximum egg concentrations at 18°S in August. In both egg concentration data and simulated retention values, the summer peak was shorter than the winter peak, and values were low from March to May all along the domain.

4. Discussion

In temperate neritic waters the majority of pelagic fish eggs are spawned at shallow depths (<50 m) and are neutrally or slightly positively buoyant (Sundby, 1991). Our first experiment (Simulation I) consisted in releasing virtual eggs at three depth levels between 0 and 45 m depth all along the Peruvian coast, and considering larvae as retained if they were still in this area after a drifting period of 30 days. Spatially, there were two retention minimums (Fig. 2) corresponding to the abrupt changes in coastal orientation off Punta Falsa (2°S–6°S) and off Paracas (14°S–16°S, Fig. 1). Lett et al. (2007a) used a different criterion for retention, based on the distance traveled by particles from their initial positions, and found maximum retention in summer. Differences in these results are due to currents being more alongshore in winter, which resulted in particles being transported away from their original locations but remaining in the coastal area (Fig. 10b), so that particles were considered as retained by our retention criterion but not by Lett et al.'s (2007a). This was checked by running the simulations described here with both criteria for comparison. Bakun (1987) showed that while the volume of Ekman transport off Peru is much larger in winter, the rate of larval offshore transport is higher in summer. He explained this counter-intuitive result by pointing out that ‘‘drifting organisms which are distributed through the upper mixed layer would experience a faster net offshore drift in the thinner surface mixed layer of austral summer than in the deeper mixed layer of winter, even though the winter transport (by volume) is much larger". Our results agree with this theory, since on average we obtain better retention rates during winter. However, this pattern is sensitive to the spawning depth and location within the upwelling area, and in particular show a summer maximum of retention for particles released between 30 and 45 m (Fig. 3). This maximum occurs because the summer mixed layer is shallower and the offshore Ekman transport layer thinner, with onshore return currents as shallow as 25 m (Fig. 10a).

Spawning frequency and patchiness were not significant factors in the simulations, showing that the non-uniformity in the temporal and spatial distribution of egg release had no effect on retention. Regarding frequency, it might be due to the fact that we used monthly averaged forcing for the hydrodynamic model, which did not allow reproducing significant circulation variability within a month. Regarding patchiness, the null effect could mean that with a patchy spawning, after a short time of drift the eggs were so mixed all along the coast by the mesoscale structures that the final results did not significantly differ from a uniform initial distribution. Clearly these factors would be more important if small-scale biological factors like predation or feeding were included.

Since the currents displayed vertical shears near the surface in the upwelling area (Penven et al., 2005), the vertical distribution of eggs and larvae was a main factor affecting coastal retention. Generally, the factors likely to determine the vertical profile of pelagic fish eggs are spawning depth, buoyancy, vertical mixing, and depth-dependent mortality (Sundby, 1997). Typically, pelagic fish eggs accumulate at the sea surface and decrease in concentration exponentially with depth (Sundby, 1983). In the Bay of Biscay, Coombs et al. (2004) found eggs of both sardine and anchovy predominantly in the upper 20 m of the water column above the pycnocline, increasing in abundance towards the surface. This distribution is expected for buoyant particles under the influence of wind mixing at the surface, by considering the balance of the egg ascent and vertical diffusion (Sundby, 1991), and is consistent with other field reports (Coombs et al., 2003; Dopolo et al., 2005; Olivar et al., 2001). Observations in the northern Humboldt (7°S) for anchovy eggs showed a similar pattern (Ayón, 2004).

In Simulation II we used egg densities ranging from 1.023 to 1.027 g cm^{-3}. For a value of 1.023 g cm^{-3}, buoyancy was positive within the entire spawning area, while for both densities of 1.024 and 1.025 g cm^{-3}, part of the eggs ended up near the surface and another part (spatially segregated) accumulate around 40–50 m, probably near the pycnocline. For 1.026 and 1.027 g cm^{-3}, eggs sank below 50 m. These results suggest that egg densities leading to the typical observed vertical distribution are between 1.024 and 1.025 g cm^{-3}. Measurements of egg densities for *Engraulis ringens* are not available. Measurements for *Engraulis encrasicolus* in the Bay of Biscay gave an egg density around 1.023 g cm^{-3} and a marked increase in density amounting to 1.025 g cm^{-3} in the final quarter of egg development (Coombs et al., 2004). Simulation II also showed that coastal retention increased with egg density. Positive buoyancy of particles led to reduced retention because offshore transport was always faster near the surface. Other simulations (not presented) showed that various spawning depths (0–15, 15–30 or 30–45 m) had no significant effect on retention when the buoyancy scheme was included. We conclude that water density and pycnocline depth are significant parameters for determining egg coastal retention. The incubation time might also be important, since it determines the time during which eggs are exposed to the low retention rates occurring near the surface.

The vertical distribution of larvae is influenced by the same physical factors as for eggs but with the additional variable of swimming. Off Peru anchoveta larvae are typically found deeper than eggs, near the thermocline (Palomera and Sabatés, 1990; Sanchez et al., 1999; Shelton and Hutchings, 1979). Depending on the size of the larvae, they accumulate near the thermocline (Matsuura and Kitahara, 1995), or perform vertical migration between the surface and the thermocline (Shelton and Hutchings, 1979). In the Humboldt upwelling system, oxygen concentrations below 1 ml/l limit the depth of anchovy larvae (Morales et al., 1996) and adults (Mathisen, 1989). As the oxycline is usually found at the base of the thermocline in the central Humboldt (Morales et al., 1999), vertical swimming behavior might be limited by both the thermocline and the oxycline. Preliminary studies of the vertical distributions of anchovy larvae in the northern Humboldt (at 7°S) suggest that they concentrate near the thermocline, between 30 and 50 m depth (Ayón, 2004).

Simulation III investigated the effect of different larval depth-regulatory behaviors: target depths of 1, 15 or 30 m and diurnal vertical migration (DVM) from 1 to 30 m, with age-dependent larval swimming velocities. We found that DVM and a constant depth of 15 m produced similar patterns of retention, typically with retention peaks in winter and summer. Constant 1 and 30 m depth regulation produced opposite seasonal patterns: at 1 m it was maximal while at 30 m it was minimal in winter. This is understandable by looking at the average vertical structures of the flows from the surface to 30 m depth in summer and in winter (Fig. 10). At the surface, during winter, the offshore component of the currents is weaker, leading to a better coastal retention. At 30 m depth currents flow onshore in summer, which also leads to increased retention. The thermocline is shallower during summer and deeper in winter, so that eggs and larvae might be more confined to surface waters during summer. Taking this into account would increase larval retention in winter. Carr et al. (2008) performed DVM modeling experiments in the Californian current system, and showed that the offshore transport experienced by individuals near surface during the night is not compensated by the subsurface onshore flow where individuals migrate during the day time, which is also consistent with Fig. 10.

The sensibility test on lethal temperature showed that temperature is probably not a limiting factor for anchovy early life survival, at least in the climatological case. Of course the actual effect of cold is to slow swimming and growth and indirectly increase mortality rates, but our results show that eggs and larvae usually do not experience temperatures lower than the optimal expected for larval survival. This optimum is given in the literature as being intermediate in the observed temperature range for adults anchovy spawning, which is 14–21 °C in this region (Jarre et al., 1991; Llanos-Rivera and Castro, 2006; Pauly and Soriano, 1989).

Upwelling-favorable wind is generally maximal in winter (Bakun, 1987; Lett et al., 2007a). Chlorophyll displays a first maximum in spring then peaks in summer (Carr and Kearns, 2003; Thomas et al., 2004). Zooplankton concentration peaks in spring (Carrasco and Lozano, 1989). Although anchovy eggs are found all around the year in the northern Humboldt upwelling area, there are usually two peaks of spawning (summer and winter) with winter being much more significant (Fig. 7; Santander, 1981). However, literature (Senocak et al., 1989) and year by year data analysis indicated that the spatio-temporal spawning patterns also showed interannual as well as interdecadal changes, affecting the locations of spawning and the relative intensities of the two spawning peaks. The reason why the major anchovy spawning peak does not coincide with the plankton peak is unclear.

Anchovy eggs are found mostly from the coast to the 100 m isobath, with the greatest abundances from 6°S to 14°S (Ayón et al., 2004), where the continental shelf is wide (Fig. 1). However, our model indicated that coastal retention should be higher from 8°S to 14°S than from 6°S to 8°S, suggesting that eggs spawned south of 8°S may have better chances of survival (Fig. 8). This is consistent with other findings showing that the best conformity between egg abundance and recruitment was between 10°S and 14°S (Einarsson and Rojas de Mendiola, 1966). From 3°S to 6°S little spawning is generally observed. The simulated retention rates were low in this region throughout the year (Fig. 9). This might reflect adaptive behavior to avoid offshore transport of eggs, but also could occur because this area is the limit between warm equatorial waters and cold waters from the coastal upwelling, and is not always suitable anchoveta habitat. In the southern part of the domain, from 14°S to 20°S the model retention rates were good but observed egg concentrations are low. This apparent conflict might be related to the very narrow continental shelf in this region, which could limit the number of spawners in that area or cause the model to overestimate retention.

The existence of two seasons and places of best retention could lead to the existence of multiple anchoveta populations, as suggested by Mathisen (1989). However, the fact that spawning occurs throughout the year lessens the likelihood of functional allopatry and may reflect bet-hedging strategy of the older year-classes, as suggested by McQuinn (1997) in the case of herring. In this case the older anchovy classes, being more fecund, could have a protracted spawning season (wave spawning), as a bet-hedging strategy in a variable environment (Lambert and Ware, 1984; McQuinn, 1997; Muck, 1989). Larval retention rates suggest better larval survival in summer and winter (our results), and generate the corresponding reproduction peaks in the following year with a positive feed-back. The fact that immature fish, spawned six months earlier, dominate the catch in summer while in winter the total biomass is dominated by mature fish (Mathisen, 1989) suggest that winter spawning leads to a more successful recruitment, which is consistent with the maximum modeled retention success for spawning in winter in the 0–100 m area.

Our simulations produced impartial and robustness results. Nevertheless, we have to stress the limitations of the present study. The hydrodynamic model reproduces the mean seasonal circulation and eddy activity, but does not reproduce the strong interannual variability, characteristic of the northern Humboldt in relation with ENSO events (Mackas et al., 2006; Strub et al., 1998). The role of these events on the reproductive success are likely important and will be explored when adequate interannual simulations become available and validated. Moreover, although coastal retention is probably important for larval survival, other important more direct factors like food availability and predation need to be considered. In a first attempt to try to match (1) retention indices derived from a model and (2) IMARPE egg concentration data for anchovy, we adopted the principle of the pattern-oriented modelling approach proposed by Grimm et al. (2005). That approach focused on modeling general pattern rather than on a quantitative estimation of egg-to-anchoveta production. It is difficult to make such quantitative comparisons for many reasons: the modeled and observed quantities compared are not the same, the time series used have different durations, the variability of the datasets are different, etc. However, a qualitative comparison is useful. "Useful patterns need not be striking; qualitative or "weak" patterns can be powerful in combination." (Grimm et al., 2005). Here we used a combination of spatial and seasonal patterns.

A similar modeling methodology has been applied in the Benguela Current system to investigate the dynamics of anchovy (*Engraulis encrasicolus*) and sardine (*Sardinops sagax*) ichthyoplankton. Stenevik et al. (2003) used for sardine in the northern Benguela off Namibia an approach similar to ours. Indeed, because spawning and nursery areas are overlapping in both cases, the main process investigated was retention. In contrast, in the southern Benguela off South Africa, anchovy spawning and nursery areas are about 500 km apart. Therefore, transport between spawning and nursery areas was the process under focus (Huggett et al., 2003). This is less clear for sardine in the southern Benguela, and both transport and retention were considered (Miller et al., 2006). It was shown that egg buoyancy was a determining factor for transport in the southern Benguela (Parada et al., 2003). In the northern Humboldt, we found that this factor was also key for egg retention. In the Benguela, temperature appeared to be an important parameter for ichthyoplankton survival (Lett et al., 2007b; Mullon et al., 2003), but this is not the case in the Canary current system (Brochier et al., 2008), nor in the northern Humboldt as our results suggest. We must however keep in mind that we used climatological hydrodynamic simulations; during a "la niña" episode, the lower sea temperature could limit egg and larval development. Regarding spawning temporal pattern, there is in the southern Benguela one seasonal peak for anchovy and two peaks for sardine (van der Lingen and Huggett, 2003). There are indications that these peaks are related with good transport (Huggett et al., 2003), enrichment and retention (Lett et al., 2006; Miller et al., 2006) conditions in the respective spawning and nursery areas, as we also found for the two spawning peaks of anchovy in the northern Humboldt.

In conclusion, considering only a Lagrangian drift, spawning at different depths (but not frequency, nor patchiness) strongly influenced retention rates (Simulation I); the egg density (Simulation II) and swimming behavior of larvae (Simulation III) also affected the retention rates. In future, we would like to use interannual hydrodynamic simulations to observe ENSO's effects on larval anchoveta early life. This could be done by using a coupled biophysical–biogeochemical model to reproduce the oxygen minimum depth and larval food fields that could enable us to better characterize good recruitment conditions. Finally, it would be interesting to incorporate the effect of small-scale turbulence on larval transport and mortality in the model (Guizien et al., 2006; Lasker et al., 1978; MacKenzie, 2000; Sundby, 1997).

Acknowledgements

The authors are grateful to the technicians and scientists from the IMARPE (Instituto del Mar del Peru) for fruitful discussions, and especially to the whole staff of the CIMOBP (Centro de Investigaciones en Modelado Oceanografico y Biologico Pesquero) for their scientific and technical assistance. We thank Y. Cavallazzi and D.M. Kaplan for editing the text, and D. Dagorne for providing Fig. 1. We are grateful to three anonymous reviewers for their helpful comments, and particularly to the reviewer who also edited the text. This work was supported by EUR-OCEANS, a European Network of Excellence co-funded by the European Commission (6th Framework Programme, Contract No. 511106).

References

Ayón, P., 2004. Informe AEPS Crucero demersales 1994–2004. IMARPE.

Bakun, A., 1987. Monthly variability in the ocean habitat off Peru deduced from maritime observations, 1953–1984. In: Pauly, D., Tsukayama, I. (Eds.), The Peruvian Anchoveta and its Upwelling Ecosystems: Three Decades of Change. ICLARM Studies and Reviews, pp. 46–74.

Bakun, A., 1996. Patterns in the ocean. Ocean processes and marine population dynamics. University of California Sea Grant, California, USA, in cooperation with Centro de Investigaciones Biologicas de Noroeste, La Paz, Baja California Sur, Mexico, 323 pp.

Batteen, M.L., 1997. Wind-forced modeling studies of currents, meanders, and eddies in the California Current System. Journal of Geophysical Research 102, 985–1010.

Bertrand, A., Segura, M., Gutiérrez, M., Vásquez, L., 2004. From small-scale habitat loopholes to decadal cycles: a habitat-based hypothesis explaining fluctuation in pelagic fish populations off Peru. Fish and Fisheries 5 (4), 296–316.

Brochier, T., Ramzi, A., Lett, C., Machu, E., Fréon, P., Hernández-León, S., 2008. Modelling the biophysical dynamics of sardine and anchovy ichthyoplankton in the Canary Upwelling System. Journal of Plankton Research 30, 1133–1146.

Carr, M.E., Kearns, E.J., 2003. Production regimes in four Eastern Boundary Current systems. Deep-Sea Research Part II – Topical Studies in Oceanography 50 (22–26), 3199–3221.

Carr, S.D., Capet, X.J., McWilliams, J.C., Pennnington, J.T., Chavez, F.P., 2008. The influence of diel vertical migration on zooplankton transport and recruitment in an upwelling region: estimates from a coupled behavioral-physical model. Fisheries Oceanography 17 (1), 1–15.

Carrasco, S., Lozano, O., 1989. Seasonal and long-term variations of zooplankton volumes in the Peruvian Sea, 1964–1987. In: Pauly, D., Muck, P., Mendo, J., Tsukayama, I. (Eds.). The peruvian Upwelling Ecosystem: Dynamics and Interactions. Instituto del Mar del Peru (IMARPE), Peru, pp. 82–85.

Castro, L.R., Hernández, E.H., 2000. Early life survival of the anchoveta *Engraulis ringens* off central Chile during the 1995 and 1996 winter spawning seasons. Transactions of the American Fisheries Society 129 (5), 1107–1117.

Coombs, S.H., Boyra, G., Rueda, L.D., Uriarte, A., Santos, M., Conway, D.V.P., Halliday, N.N., 2004. Buoyancy measurements and vertical distribution of eggs of sardine (*Sardina pilchardus*) and anchovy (*Engraulis encrasicolus*). Marine Biology 145 (5), 959–970.

Coombs, S.H., Giovanardi, O., Halliday, N.C., Franceschini, G., Conway, D.V.P., Manzueto, L., Barrett, C.D., McFadzen, I.R.B., 2003. Wind mixing, food availability and mortality of anchovy larvae *Engraulis encrasicolus* in the northern Adriatic Sea. Marine Ecology Progress Series 248, 221–235.

Cury, P., Bakun, A., Crawford, R.J.M., Jarre, A., Quiñones, R.A., Shannon, L.J., Verheye, H.M., 2000. Small pelagics in upwelling systems: patterns of interaction and structural changes in "wasp-waist" ecosystems. Ices Journal of Marine Science 57 (3), 603–618.

Cury, P., Roy, C., 1989. Optimal environmental window and pelagic fish recruitment success in upwelling areas. Canadian Journal of Fisheries and Aquatic Sciences 46, 670–680.

Dopolo, M., Van der Lingen, C., Moloney, C., 2005. Stage-dependent vertical distribution of pelagic fish eggs on the western Agulhas Bank, South Africa. African Journal of Marine Science 27, 249–256.

Einarsson, H., Rojas de Mendiola, B., 1966. An attempt to estimate annual spawning intensity of the anchovy (*Engraulis ringens* jenyns) by means of regional egg and larval survey during 1961–1964. Report volume XI.

Fogarty, M.J., 1993. Recruitment in randomly varying environments. ICES Journal of Marine Science 50, 247–260.

Fréon, P., Alheit, J., Barton, E.D., Kifani, S., Marchesiello, P., 2006. Modelling, forecasting and scenarios in comparable upwelling ecosystems: California, Canary and Humboldt. In: Hempel, G., Moloney, C., Rizzoli, P., Woods, J. (Eds.). The Benguela: Predicting a Large Marine Ecosystem. Elsevier Series, Large Marine Ecosystems.

Fréon, P., Cury, P., Shannon, L., Roy, C., 2005. Sustainable exploitation of small pelagic fish stocks challenged by environmental and ecosystem changes: a review. Bulletin of Marine Science 76 (2), 385–462.

Grimm, V., Berger, U., Bastiansen, F., Eliassen, S., Ginot, V., Giske, J., Goss-Custard, J., Grand, T., Heinz, S.K., Huse, G., Huth, A., Jepsen, J.U., Jørgensen, C., Mooij, W.M., Müller, B., Pe'er, G., Piou, C., Railsback, S.F., Robbins, A.M., Robbins, M.M., Rossmanith, E., Ruger, N., Strand, E., Souissi, S., Stillman, R.A., Vabø, R., Visser, U., DeAngelis, D.L., 2006. A standard protocol for describing individual-based and agent-based models. Ecological Modelling 198, 115–126.

Grimm, V., Railsback, S.F., 2005. Individual-Based Modeling and Ecology. Princeton University Press, Princeton, NJ.

Grimm, V., Revilla, E., Berger, U., Jeltsch, F., Mooij, W.M., Railsback, S.F., Thulke, H.-H., Weiner, J., Wiegand, T., DeAngelis, D.L., 2005. Pattern-oriented modeling of agent-based complex systems: lessons from ecology. Science 310, 987–991.

Guizien, K., Brochier, T., Duchêne, J., Koh, B., Marsaleix, P., 2006. Dispersal of *Owenia fusiformis* larvae by wind-driven currents: turbulence, swimming behaviour and mortality in a three-dimensional stochastic model. Marine Ecology Progress Series 311, 47–66.

Haidvogel, D.B., Beckmann, A., 1998. Numerical modeling of the coastal ocean. In: Brink, K.H., Robinson, A.R. (Eds.). The Sea, vol. 10. Harvard University Press, Cambridge, pp. 457–482.

Huggett, J., Fréon, P., Mullon, C., Penven, P., 2003. Modelling the transport success of anchovy *Engraulis encrasicolus* eggs and larvae in the southern Benguela: the effect of spatio-temporal spawning patterns. Marine Ecology Progress Series 250, 247–262.

Hunter, J.R., 1977. Behavior and survival of northern anchovy *Engraulis Mordax* larvae. California Cooperative Oceanic Fisheries Investigations Reports 19, 138–146.

Jacobson, L.D., De Oliveira, J.A.A., Barange, M., Cisneros-Mata, M.A., Félix-Uraga, R., Hunter, J.R., Kim, J.Y., Matsuura, Y., Ñiquen, M., Porteiro, C., Rothschild, B., Sanchez, R.P., Serra, R., Uriarte, A., Wada, T., 2001. Surplus production, variability, and climate change in the great sardine and anchovy fisheries. Canadian Journal of Fisheries and Aquatic Sciences 58 (9), 1891–1903.

Jarre, A., Muck, P., Pauly, D., 1991. Two approaches for modelling fish stock interactions in the Peruvian upwelling ecosystem. Multispecies Models Relevant to Management of Living Resources, Copenhagen, Denmark, pp. 171–184.

Lambert, T., Ware, D.M., 1984. Reproductive strategies of demersal and pelagic spawning fish. Canadian Journal of Fisheries and Aquatic Sciences 41 (11), 1565–1569.

Lasker, R., 1985. What limits clupeoid production? Canadian Journal of Fisheries and Aquatic Sciences 42 (Suppl. 1), 31–38.

Lasker, R., Parsons, T.R., Jansson, B.O., Longhurst, A.R., Saetersdal, G. (Eds.), 1978. The Relation between Oceanographic Conditions and Larval Anchovy Food in the California Current: Identification of Factors Contributing to Recruitment Failure.

Lett, C., Penven, P., Ayón, P., Fréon, P., 2007a. Enrichment, concentration and retention processes in relation to anchovy (*Engraulis ringens*) eggs and larvae distributions in the northern Humboldt upwelling ecosystem. Journal of Marine Systems 64, 189–200.

Lett, C., Veitch, J., van der Lingen, C.D., Hutchings, L., 2007b. Assessment of an environmental barrier to transport of ichthyoplankton from the southern to the northern Benguela ecosystems. Marine Ecology- Progress Series 347, 247–259.

Lett, C., Rose, K.A., Megrey, B.A., in press. Biophysical models. In: Checkley, D.M., Alheit, J., Oozeki, Y., Roy, C. (Eds.). Climate Change and Small Pelagic Fish, Cambridge University Press (Chapter 6).

Lett, C., Roy, C., Levasseur, A., van der Lingen, C.D., Mullon, C., 2006. Simulation and quantification of enrichment and retention processes in the southern Benguela upwelling ecosystem. Fisheries Oceanography 15, 363–372.

Lett, C., Verley, P., Mullon, C., et al., 2008. A Lagrangian tool for modelling ichthyoplankton dynamics. Environmental Modelling & Software 28, 1210–1214.

Llanos-Rivera, A., Castro, L.R., 2006. Inter-population differences in temperature effects on Engraulis ringensyolk-sac larvae. Marine Ecology Progress Series 312, 245–253.

Mackas, D.L., Strub, P.T., Thomas, A.C., Montecino, V., 2006. Eastern Ocean Boundaries Pan Regional. In: Brink, K.H., Robinson, A.R. (Eds.). The Sea, vol. 14A. Harvard University Press, Cambridge (Chapter 2).

MacKenzie, B.R., 2000. Turbulence, larval fish ecology and fisheries recruitment: a review of field studies. Oceanologica Acta 23 (4), 357–375.

Marchesiello, P., McWilliams, J.C., Shchepetkin, A., 2003. Equilibrium structure and dynamics of the California Current System. Journal of Physical Oceanography 33, 753.

Mathisen, O.A., 1989. Adaptation of the anchoveta (*Engraulis ringens*) to the Peruvian upwelling system. In: Pauly, D., Muck, P., Mendo, J., Tsukayama, I., (Eds.). The Peruvian Upwelling Ecosystem: Dynamics and Interactions. ICLARM Conference Proceedings, pp. 220–234.

Matsuura, Y., Kitahara, E.M., 1995. Horizontal and vertical distribution of anchovy *Engraulis anchoita* eggs and larvae off Cape Santa Marta Grande in southern Brazil. Archive of Fishery and Marine Research 42 (3), 239–250.

McQuinn, I.H., 1997. Metapopulations and the Atlantic herring. Reviews in Fish Biology and Fisheries 7, 297–329.

Miller, D.C.M., Moloney, C.L., van der Lingen, C.D., Lett, C., Mullon, C., Field, J.G., 2006. Modelling the effects of physical–biological interactions and spatial variability in spawning and nursery areas on transport and retention of sardine Sardinops sagax eggs and larvae in the southern Benguela ecosystem. Journal of Marine Systems 61, 212–229.

Miller, T.J., 2007. Contribution of individual-based coupled physical biological models to understanding recruitment in marine fish populations. Marine Ecology Progress Series 347, 127–138.

Morales, C.E., Braun, M., Reyes, H., Blanco, J.L., Davies, A.G., 1996. Anchovy larval distribution in the coastal zone off northern Chile: the effect of low dissolved oxygen concentrations and of a cold-warm sequence (1990–95). Investigaciones Marinas 24, 77–96.

Morales, C.E., Hormazabal, S.E., Luis Blanco, J., 1999. Interannual variability in the mesoscale distribution of the depth of the upper boundary of the oxygen minimum layer off northern Chile (18–24S): implications for the pelagic system and biogeochemical cycling. Journal of Marine Research 57, 909–932.

Muck, P., 1989. Relationships between anchoveta spawning strategies and the spatial variability of sea surface temperature off Peru. In: Workshop on Models for Yield Prediction in the Peruvian Ecosystem, Callao (Peru) 24–28 August 1987, ICLARM Conference Proceedings, pp. 168–173.

Mullon, C., Freon, P., Parada, C., van der lingen, C., Huggett, J., 2003. From particles to individuals: modelling the early stages of anchovy (*Engraulis capensis*/*encrasicolus*) in the southern Benguela. Fisheries Oceanography 12 (4/5), 396–406.

Myers, R.A., 1998. When do environment-recruitment correlations work? Reviews in Fish Biology and Fisheries 8 (3), 285–305.

Myers, R.A., Bowen, K.G., Barrowman, N.J., 1999. Maximum reproductive rate of fish at low population sizes. Canadian Journal of Fisheries and Aquatic Sciences 56, 2404–2419.

Ñiquen, M., Fréon, P., 2006. A new record set by the Peruvian fishery 2.5 million tonnes of anchovy landed in November 2005. GLOBEC International Newsletter, 56–57.

Olivar, M.P., Salat, J., Palomera, I., 2001. Comparative study of spatial distribution patterns of the early stages of anchovy and pilchard in the NW Mediterranean Sea. Marine Ecology Progress Series 217, 111–120.

Palomares, M.L., Muck, P., Mendo, J., Chuman, E., Gomez, O., Pauly, D., 1987. Growth of the Peruvian anchoveta (*Engraulis ringens*), 1953–1982. In: Pauly, D., Tsukayama, I. (Eds.), The Peruvian Anchoveta and its Upwelling Ecosystems: Three Decades of Change. ICLARM Studies and Reviews, Berlin, pp. 117–141.

Palomera, I., Sabatés, A., 1990. Co-occurence of *Engraulis encrasicolus* and *Sardinella aurita* eggs and larvae in the northwestern Mediterranean. Scientia Marina 54 (1), 61–67.

Parada, C., van der Lingen, C.D., Mullon, C., Penven, P., 2003. Modelling the effect of buoyancy on the transport of anchovy (*Engraulis capensis*) eggs from spawning to nursery ground in the southern Benguela: an IBM approach. Fisheries Oceanography 12 (3), 170–184.

Pauly, D., Soriano, M., 1989. Production and mortality of anchoveta (*Engraulis ringens*) eggs off Peru. In: Pauly, D., Muck, P., Mendo, J., Tsukayama, I. (Eds.). The Peruvian Upwelling Ecosystem: Dynamics and Interactions, pp. 155–167.

Penven, P., Echevin, V., Pasapera, J., Colas, F., Tam, J., 2005. Average circulation, seasonal cycle, and mesoscale dynamics of the Peru Current System: a modeling approach. Journal of Geophysical Research 110, C10021.

Sanchez, R.P., Ciechomski, J.D., Lasta, C., Guerrero, R., 1999. A drift study of vertical distribution and mortality of *Engraulis anchoita* eggs and larvae. Revista de Investigacion Desarrollo Pesquero 12, 51–75.

Santander, H., 1981. Distribution patterns and fluctuations in anchovy and sardine spawning. 0378-7699, Callao.

Senocak, T., Schnack, D., Pauly, D., 1989. Mean monthly distribution, abundance and production of anchoveta eggs off Peru (4°S –14°S), 1964–1971 and 1972–1986. In: Pauly, D., Muck, P., Mendo, J., Tsukayama, I. (Eds.). The Peruvian Upwelling Ecosystem: Dynamics and Interactions. ICLARM Conference Proceedings, pp. 143–154.

Shchepetkin, A.F., McWilliams, J.C., 2005. The regional oceanic modeling system (ROMS): a split-explicit, free-surface, topography-following-coordinate oceanic model. Ocean Modelling 9 (4), 347–404.

Shelton, P.A., Hutchings, L., 1979. The Effect of the Environment on Spawning and Recruitment in the Anchovy (Engraulis capensis Gilchrist) ICES Symposium on the Early Life History of Fish. Woods Hole, MA (USA).

Stenevik, E.K., Skogen, M., Sundby, S., Boyer, D., 2003. The effect of vertical and horizontal distribution on retention of sardine (*Sardinops sagax*) larvae in the Northern Benguela – observations and modelling. Fisheries Oceanography 12 (3), 185–200.

Strub, P.T., Mesias, V., Montecino, V., Ruttland, J., Salinas, S., 1998. Coastal ocean circulation off Western South America. The Sea, 11.

Sundby, S., 1983. A one-dimensional model for the vertical distribution of pelagic fish eggs in the mixed layer. Deep-Sea Research 30, 645–661.

Sundby, S., 1991. Factors affecting the vertical distribution of eggs. In: ICES Marine Science Symposia, pp. 33–38.

Sundby, S., 1997. Turbulence and ichthyoplankton: influence on vertical distributions and encounter rates. Scientia Marina 61 (1), 159–176.

Thomas, A.C., Strub, P.T., Carr, M.E., Weatherbee, R., 2004. Comparisons of chlorophyll variability between the four major global eastern boundary currents. International Journal of Remote Sensing 25 (7–8), 1443–1447.

van der Lingen, C.D., Huggett, J.A., 2003. The role of ichthyoplankton surveys in recruitment research and management of South African anchovy and sardine. In: Browman, H.I., Skiftesvik, A.B. (Eds.), The Big Fish Bang. Proceedings of the 26th Annual Larval Fish Conference. Institute of Marine Research, Bergen, Norway, pp. 303–343.

Walsh, J.J., Whitledge, T.E., Esaias, W.E., Smith, R.L., Huntsman, S.A., Santander, H., Rojas de Mendiola, B., 1980. The spawning habitat of the Peruvian anchovy, *Engraulis ringens*. Deep-Sea Research 27A, 1–27.

Ware, D.M., Rojas de Mendiola, B., Newhouse, D.S., 1980. Behaviour of first-feeding Peruvian anchovy larvae, *Engraulis ringens* J. In: Sherman, K., Hempel, G. (Eds.). Symposium on Early Life History of Fish. Conseil International pour l'Exploitation de la Mer, Rapport et procés-verbaux des réunions, pp. 80–87.

Werner, F.E., Quinlan, J.A., Lough, R.G., Lynch, D.R., 2001. Spatially-explicit individual based modeling of marine populations: a review of the advances in the 1990s. Sarsia 86 (6), 411–421.

Progress in Oceanography 79 (2008) 326–335

Contents lists available at ScienceDirect

Progress in Oceanography

journal homepage: www.elsevier.com/locate/pocean

Trophic modelling of the Peruvian upwelling ecosystem: Towards reconciliation of multiple datasets ☆

Sylvie Guénette *, Villy Christensen, Daniel Pauly

Fisheries Centre, University of British Columbia, 2202 Main Mall, Vancouver, BC, Canada V6T 1Z4

ARTICLE INFO

Article history:
Accepted 14 October 2008
Available online 21 October 2008

Keywords:
Clupeoid fisheries
Food webs
Ecosystem modelling
Southern oscillation
Coastal upwelling
Peru

ABSTRACT

In the 1980s, personnel from the Instituto del Mar del Peru collaborated with foreign experts to reconstruct time series of (1) catch and biomass of the Peruvian anchovy *Engraulis ringens* back to 1953, along with parallel time series of (2) abundance of anchovy predators and competitors, and (3) abiotic parameters indicative of the dynamics of the Peruvian upwelling system. This contribution documents an attempt to build an ecosystem model of the Peruvian upwelling ecosystem and recreate the observed biomass trends through the period 1953–1984, using the Ecopath with Ecosim (EwE) software. The time series of biomass, particularly of Peruvian anchovy and its various predators, are not reproduced by the EwE model based solely on the original parameters. Instead, to model the anchovy abundance fluctuations caused by El Niño and other oceanographic events, it is necessary to include mechanisms that were not part of the original description of the ecosystem, which focused on mass-balance. For example, a switch between large and small phytoplankton appears to be required to induce the observed abundance shifts between sardine and anchovy. Similarly, a 'mitigating' relationship must be assumed between bonito (*Sarda chilensis*) and seabirds for the 1965 collapse of seabirds to be reproduced by the model. Mechanisms of this sort, here proposed in a very tentative fashion, will have to be firmly established and quantified before a model can successfully explain both the older data series (1953–1984) as done here, and eventually the new series on the Peruvian upwelling system that became available only recently. With a total of now over 50 years of data, this would represent one of the best documented marine ecosystems in the world, matching its status as one of the most productive.

1. Introduction

In the 1980s, personnel of the Instituto del Mar del Peru (IMARPE) collaborated with foreign experts to construct long (30+ years) monthly time series of catch and biomass of the Peruvian anchovy *Engraulis ringens*, along with time series of abundance of anchovy predators and competitors, and abiotic parameters indicative of the dynamics of the Peruvian upwelling system. These time series, which spanned the years 1953 to the mid-1980s, were documented in two 'data-rich' edited volumes (Pauly, 1993), which presented most of the data upon which the analyses in their chapters were based (see Pauly and Tsukayama, 1987; Pauly et al., 1989). The volume's contributions, while representing the state-of-the-art in fish population dynamics at the time (Cushing, 1988) and leading to a fair description of the Peruvian anchovy population responses to environmental variability, did not allow for any measure of predictability.

Simultaneous efforts at constructing an 'anchovy-centred' model of the Peruvian ecosystem based on coupled differential equations (Jarre et al., 1991; Jarre-Teichmann, 1992) failed. Instead, modelling emphasis shifted to trophic mass-balance (Ecopath) models, for which predecessors existed, notably the model of Walsh (1981). These models could be parameterized for using the data in the above-cited books and other literature (Jarre et al., 1991; Jarre-Teichmann and Pauly, 1993). They provided snapshots of the ecosystem and were useful in that they quantified the food web and documented the main energy pathways leading to anchovy production; but again, they did not allow for predictions.

This contribution has two goals. The first one is to build on previous modelling efforts with the extensive data gathered over 30 years to verify how they could be used directly to reconstruct the observed changes in biomass, and make these results usable by the scientific community. This has now become possible thanks to the Ecopath with Ecosim (EwE) software, which can fit the model to reference time series data (Christensen and Walters, 2005). The second goal is to revisit the original time series (1953–1984)

☆ Based on a keynote address, presented by the last author, at the International Conference on The Humboldt Current System: Climate, Ocean Dynamics, Ecosystem Processes, and Fisheries. Lima, Peru, November 27–December 1, 2006.

* Corresponding author. Tel.: +1 604 822 6348; fax: +1 604 822 8934.
E-mail address: s.guenette@fisheries.ubc.ca (S. Guénette).

0079-6611/$ - see front matter © 2008 Elsevier Ltd. All rights reserved.
doi:10.1016/j.pocean.2008.10.005

in an attempt to provide a different perspective by going back in time and identify critical processes with today's perspective. In doing so, we intend to explore various mechanisms that may be involved and suggest avenues for future research. It is the use of time series to fit a model and the inclusion of mechanisms of interactions that will allow us to move towards evaluating hypotheses about what caused the variations in anchovy biomass. In addition, the use of a long time series provide a better basis to evaluate current events with a larger breadth of experience, going back earlier in time, and thus avoid shifting baselines (Pauly, 1995). We then discuss how to construct a dynamic model potentially capable of making useful predictions for fisheries management.

2. Methods

This model of the Peruvian ecosystem encompasses the coast of Peru between latitudes 4 and 14°S, to 40 nm offshore on average (Jarre et al., 1991) for a total area of 82,000 km^2, and corresponding to the main distribution area of the North-Central stock of Peruvian anchovy. During the period considered here, 1953–1984, anchovy population and catch fluctuated enormously. Major episodes were: (1) onset of the anchovy fisheries in the early 1950s, (2) the increase of anchovy biomass in the late 1950s and 1960s, (3) collapse of the fishery in the early 1970s, and (4) a period of low anchovy catch and biomass. Other species fluctuated similarly, though for several groups (e.g., sea birds and bonito), this was a one-way trip, with high biomasses in the early 1950s coinciding with the onset of the 1973 El Niño, and low biomasses in the 1980s (Muck, 1989b), from which they never recovered.

2.1. The model

Mass-balanced trophic models assign the main species within an ecosystem to functional groups (single species or of a group of ecologically similar species), and account for their (1) biomass (in metric tonnes per square km, $\text{t} \cdot \text{km}^{-2}$) (2) diet (percentage in biomass or volumes), (3) prey consumption per year, per unit of biomass (4) natural and fishing mortality per year, (5) rate accumulation of biomass per year, and (6) net migration. The principle behind this ecosystem modelling approach is that energy is conserved and must be accounted for on a yearly basis (see Walters et al., 1997). Ecosim is a tool for dynamic simulations based on an Ecopath model, whose static representation provides some of the initial-state Ecosim parameters (Walters et al., 1997; Pauly et al., 2000). Ecosim uses a system of differential equations to describe the changes in biomass and flow of biomass within the system over time, by accounting for changes in predation, consumption and fishing rates (Walters et al., 1997; Christensen et al., 2005). Thus, the rate of change of biomass of group i (B_i) is described by

$$\frac{dB_i}{dt} = g_i \sum_j Q_{ji} - \sum_j Q_{ij} + I_i - (m_i + F_i + e_i)B_i \tag{1}$$

where g_i is the net growth efficiency (year^{-1}); Q_{ji} and Q_{ij} are the consumption rate (year^{-1}) of group j by group i and the consumption of group i by group j, respectively (year^{-1}); I_i is the immigration flow in $\text{t} \cdot \text{km}^{-2}$; m_i is non-predation mortality (year^{-1}); F_i is fishing mortality (year^{-1}); and e_i is emigration rate (year^{-1}) (Christensen and Walters, 2004).

Ecopath with Ecosim (EwE) allows the fitting of the model to time series of abundance and catch, and thus allow to evaluate how well the model replicates observed behaviour through time. The time series are used to tune the model. EwE models are generally not 'validated' in the classical sense of using one dataset to tune the model, and using another set of independent data for the validation process. This is not an inherent model problem, but rather a systematic lack of data for most ecosystems. Ecosim is able to incorporate multiple stanzas (ontogenic stages) representing different life history stages of species of special interest (anchovies and sardines in these models). The stanzas of a species are linked and their respective production per unit of biomass (P/B year^{-1}), consumption per unit of biomass (Q/B year^{-1}), and growth calculated from a baseline estimate for a reference group (the adults in our case). Growth for each stanza is calculated from von Bertalanffy growth curves, and a stable survivorship through ages within stanzas is assumed, while natural and fishing mortality is allowed to vary between stanzas (Christensen et al., 2005).

The functional predator–prey relationship is based on the foraging arena theory, which divides the biomass of all prey into vulnerable and invulnerable pools (Walters and Kitchell, 2001). The transfer rate between these two pools (here called 'vulnerability') can range from one to infinity with higher rates implying that the behaviour of both the prey and the predator have less effects on limiting predation rates. A large vulnerability value also means that the predator initial biomass is low compared to its carrying capacity, and that a change in predator biomass will cause a corresponding change in the mortality rate of its prey. The system will thus be more stable when a predator is close to its carrying capacity, and more variable when it is far from it.

Vulnerability values can be specified for each predator–prey pair. Due to uncertainty about how this parameter might change between prey species and to reduce the number of parameters that needs to be estimated, we chose to assume that the vulnerability setting is the same for all species of prey consumed by a given predator. This functional predator–prey response equation predicts changes in diet composition due to changes in relative availability of prey and alternative prey, but it does not allow switching of the diet to new prey that were not consumed initially. Switching between prey items included in the diet can be accommodated.

In addition to the direct trophic relationships mentioned above, it is possible in Ecosim to account for indirect, non-trophic relationships, called 'mediation', that result from a third species modifying the trophic relationship between two other species. The relationships can be negative when increase in biomass of the third species results in a prey becoming less accessible to the predator (i.e., decrease of the vulnerability of the prey to the predator). Conversely, it can be positive, when an increase in the third species abundance increases the vulnerability of the prey to its predator. In the present paper, we explored the hypothesis that bonito feeding activities, which will tend to drive small pelagic fishes to the surface, will tend to make them more vulnerable to seabird predation, similar to the situation described by Au et al. (1999). Other studies have shown that tuna species drive sardines and other schooling fish to surface waters making them available to boobies (Anderson and Ricklefs, 1987).

Environmental influence on the productivity of the ecosystem was also included in the model to improve the fit to time series. The influence of environmental factors is generally included in the model by using a climate index to directly influence the production of primary producers. We assume that the large quantities of nutrients lifted into the euphotic zone by strong upwelling results in the production of larger phytoplankton cells such as diatoms (Iriarte and González, 2004), which in turn favours the production of large zooplankton (calanoids and euphausids) (Alheit and Niquen, 2004). Thus, indices of oceanic changes were included in the model and modified the productivity of diatoms and benthic macrophytes. We added mediation between diatoms and dinoflagellates so that large populations of diatoms would use the nutrients that would otherwise go to small phytoplankton. We used this mediation as a simple proxy for more complex dynamics in which dinoflagellates are favoured over diatoms in less turbulent and warmer temperatures (van der Lingen et al., 2006).

2.2. Data

We structured our model based on the 1950 model presented by Jarre et al. (1991), which was composed of 16 functional groups of organisms including anchovy (*E. ringens*) and sardines (*Sardinops sargax*) and their piscine predators bonito (*Sarda chiliensis*), mackerel (*Scomber japonicus*), horse mackerel (*Trachurus murphyi*), and hake (*Merluccius gayi*), and other consumers, the guano birds, and pinnipeds (Table 1). Guano birds included the cormorant (*Phalacrocorax bougainvillii*), booby (*Sula variegata*), and pelican (*Pelecanus thagus*); the pinnipeds species are the fur seals (*Arctocephalus australis*) and sea lions (*Otaria byronia*). We completed the structure with additional groups: demersal fish (three groups instead of one), other pelagic fish (small and large instead of one group), and invertebrates to include all of the reported catches (Table 1). To this basic structure, we added larval stanzas for sardine and anchovy, and included predation by adult sardine and anchovy on each other's larvae.

Moreover, it soon became obvious that more details in plankton groups needed to be included to account for the respective feeding preferences of sardines and anchovies, as in Jarre-Teichmann (1992). Phytoplankton was divided in two groups, dinoflagellates and diatoms, to account for the fact that sardines are efficient feeders on smaller organisms (which includes cyclopoid copepods) while anchovy prefer calanoids, euphausids and chain-forming diatoms (Jarre-Teichmann, 1992; van der Lingen, 1994). Time series data for zooplankton biomass (Carraso and Lozano, 1989) was assigned to large zooplankton as the sampling has been carried out with a 300 μm plankton net.

Estimates of *P*/*B* and *Q*/*B* were taken from Jarre-Teichmann (1992) for most species. As a starting point, groups not described in her model, (e.g., demersals and 'other pelagic fishes') were attributed estimates based on values generally used for the species in question (Table 1). Diet data were based mainly on Jarre-Teichmann (1992) and completed with information from the literature (Table 2). The fractional diet of anchovy, originally assumed to be composed mainly of diatoms (Jarre-Teichmann, 1992, see her Table 2), was compared with a revised estimate suggested by the reanalysis of Espinoza and Bertrand, 2008, and set at 0.39 diatoms, 0.60 for large zooplankton and 0.01 to other items. This forced a change of the biomass of large zooplankton, which had to be increased to 50 t · km^2 to re-establish mass-balance.

The biomass time series for anchovy (1953–1984), obtained from virtual population analysis, were taken from Pauly et al. (1989). The biomass time series used here for the other species are documented in Muck (1989b). Fishing mortality series were calculated as the ratio catch/biomass. Catches, mainly based on data supplied by Peru to FAO, were obtained from the *Sea Around Us Project* database (Watson et al., 2004, see http://www.seaaroundus.ca), assuming that catches from the study area accounted for 80% of the total catch of Peru as the study area represents about 80% of the total coastline. In absence of biomass data for added demersal and pelagic groups, we derived the biomass estimates from the catch data using a stock reduction analysis (Kimura, 1985). Catches, assumed to be known quantities, are subtracted from the simulated stock size for each time step. This approach is very sensitive to the estimate of initial biomass (or production/biomass ratio – *P*/*B*); if it is too low, there will not be enough production (B^*P/B) estimated over time and this will cause the population to crash. In the fitting, this is seen as an indication that the initial biomass (or *P*/*B*) is too low and should be increased.

The biomass time series of bonito and anchovy were rescaled to avoid values of the ratio catch/biomass higher than 1 year^{-1} in the 1970s. In addition, to balance the model, the 1953 anchovy biomass was increased to 75 t · km^{-2} from an initial value of 68 t · km^{-2} to increase the available production (B^*P/B) to meet the demands and notably those of the predators.

Time series of biomass and catch were used to fit the model for the period 1950–1984. The model was driven with fishing mortality and fitted by varying the vulnerability settings such as to obtain predicted biomass and catch trajectories similar to those observed for the various fish groups, sea birds and pinnipeds. The model was

Table 1
Parameters of the balanced model and vulnerabilities (Vuln.) used as the basic scenario (#1).

	Group name	Trophic level	Biomass (t · km^{-2})	*P*/*B* (year^{-1})	*Q*/*B* (year^{-1})	EE	*P*/*Q*	Vuln.
1	Pinnipeds	**3.39**	0.0044	0.09	28.0	**0.890**	**0.00**	4.82
2	Birds	**3.40**	0.56	0.04	62.0	0.000	**0.00**	2.00
3	Sharks	**3.91**	**0.58**	0.20	**1.0**	0.100	0.20	1.50
4	Rays	**3.77**	**0.42**	0.50	**2.5**	0.050	0.20	3.16
5	Bonito	**3.47**	7.87	0.20	**1.0**	**0.266**	0.20	3.00
6	Mackerel	**3.18**	2.80	0.85	10.0	**0.112**	**0.09**	1.00
7	Horse mackerel	**3.30**	12.68	0.85	10.0	**0.038**	**0.09**	1.00
8	Anchovy larvae	**2.00**	0.23	7.00	102.0	**0.015**	**0.07**	2.00
9	Anchovy	**2.22**	75.00	1.80	15.0	**0.958**	**0.12**	1.00
10	Sardine larvae	**3.00**	0.04	7.00	98.0	**0.390**	**0.07**	1.19
11	Sardine	**2.98**	20.00	1.80	12.0	**0.486**	**0.15**	1.00
12	Pelagic S	**3.08**	**8.36**	1.80	**7.2**	0.900	0.25	1.00
13	Pelagic L	**3.61**	**2.25**	0.10	**0.5**	0.100	0.20	1.78
14	Hake	**3.33**	3.28	0.30	**1.5**	**0.110**	0.20	1.00
15	Demersal L	**3.80**	**0.89**	0.20	**1.0**	0.100	0.20	2.00
16	Demersal M	**3.32**	**3.08**	0.50	**2.5**	0.300	0.20	1.17
17	Demersal S	**3.20**	**5.23**	0.90	**4.5**	0.900	0.20	4.82
18	Cephalopods	**3.38**	**0.69**	2.00	10.0	0.700	**0.20**	1.12
19	Shrimps	**2.79**	**1.99**	2.50	**16.7**	0.900	0.15	1.57
20	Lobster crab	**2.81**	**1.99**	2.00	**13.3**	0.900	0.15	1.01
21	Macrobenthos	**2.41**	**38.29**	3.00	**12.0**	0.500	0.25	1.04
22	Meiobenthos	**2.06**	8.00	9.00	**45.0**	**0.507**	0.20	1.74
23	Lg zoopl	**2.10**	16.00	20.00	**100.0**	**0.824**	0.20	1.08
24	Sm. zoopl	**2.00**	25.00	40.00	**200.0**	**0.633**	0.20	10.00
25	Dinoflagellates	**1.00**	71.00	70.00	–	**0.879**	–	–
26	Diatoms	**1.00**	55.00	70.00	–	**0.797**	–	–
27	Macroalgae	**1.00**	19.72	12.50	–	**0.613**	–	–
28	Detritus	**1.00**	900.00	–	–	**0.147**	–	–

Parameters **in bold** were estimated by Ecopath; the vulnerabilities were estimated in Ecosim.

Table 2

Diet composition used in the balanced model as it was in scenario 1, and the sources of information for each functional group.

	Prey/predator	1	2	3	4	5	6	7	8	9	10	11	12	13	14	15	16	17	18	19	20	21	22	23	24
	Source	1	1	2	2	1	3	3	4	5	4	6	2	2	1	2	2	2	4	4	4	4	1	1	4
1	Pinnipeds	–	–	–	–	–	–	–	–	–	–	–	–	–	–	–	–	–	–	–	–	–	–	–	–
2	Birds	–	–	–	–	–	–	–	–	–	–	–	–	–	–	–	–	–	–	–	–	–	–	–	–
3	Sharks	–	–	–	–	–	–	–	–	–	–	–	–	–	–	–	–	–	–	–	–	–	–	–	–
4	Rays	–	–	0.012	–	–	–	–	–	–	–	–	–	–	–	–	–	–	–	–	–	–	–	–	–
5	Bonito	–	–	0.012	–	–	–	–	–	–	–	–	–	0.020	–	0.002	–	–	–	–	–	–	–	–	–
6	Mackerel	–	–	0.012	–	0.02	–	–	–	–	–	–	–	0.020	0.010	0.003	–	–	–	–	–	–	–	–	–
7	Horse mackerel	–	–	0.005	–	0.02	–	–	–	–	–	–	–	0.040	0.040	0.003	–	–	–	–	–	–	–	–	–
8	Anchovy larvae	–	–	–	–	–	–	–	–	–	–	0.0001	–	–	–	–	–	–	–	–	–	–	–	–	–
9	Anchovy	0.80	0.88	0.033	–	0.70	0.60	0.65	–	–	–	–	–	0.050	0.550	0.161	0.002	–	–	–	–	–	–	–	–
10	Sardine larvae	–	–	–	–	–	–	–	–	0.0001	–	–	–	–	–	–	–	–	–	–	–	–	–	–	–
11	Sardine	0.12	0.05	0.036	–	0.18	0.09	0.10	–	–	–	–	–	0.020	0.050	0.014	0.002	–	0.01	–	–	–	–	–	–
12	Pelagic small	0.02	0.18	0.071	–	0.08	–	–	–	–	–	–	–	0.090	0.010	0.054	0.052	0.02	0.05	–	–	–	–	–	–
13	Pelagic large	–	–	0.012	–	–	–	–	–	–	–	–	–	–	–	0.008	–	–	–	–	–	–	–	–	–
14	Hake	0.01	–	0.012	–	–	–	–	–	–	–	–	–	–	0.020	0.002	–	–	–	–	–	–	–	–	–
15	Demersal large	–	–	0.012	–	–	–	–	–	–	–	–	–	–	–	–	–	–	–	–	–	–	–	–	–
16	Demersal medium	0.02	–	0.036	–	–	–	–	–	–	–	–	–	–	0.002	0.080	–	–	–	–	–	–	–	–	–
17	Demersal small	0.03	0.05	0.102	0.167	–	–	–	–	–	–	–	–	–	0.008	0.139	0.134	0.03	0.05	–	–	–	–	–	–
18	Cephalopods	–	–	0.012	0.056	–	–	–	–	–	–	–	–	0.060	–	0.100	0.007	–	–	–	–	–	–	–	–
19	Shrimps	–	–	0.340	0.222	–	–	–	–	–	–	–	–	0.230	–	0.133	0.100	0.10	0.10	–	–	–	–	–	–
20	Lobster crab	–	–	0.238	0.222	–	–	–	–	–	–	–	–	–	–	0.170	0.046	0.10	0.05	–	–	–	–	–	–
21	Macrobenthos	–	–	0.060	0.333	–	–	–	–	–	–	–	0.200	0.233	0.030	0.103	0.160	0.30	0.34	0.05	0.5	–	–	–	–
22	Meiobenthos	–	–	–	–	–	–	–	–	–	–	–	–	0.233	–	0.042	0.180	0.20	–	0.40	0.1	–	0.01	–	–
23	Large zooplankton	–	–	–	–	–	–	0.14	–	0.192	–	–	0.466	–	0.280	–	0.100	–	–	–	–	–	–	–	–
24	Small zooplankton	–	–	–	–	–	0.25	0.11	–	–	1	0.97	0.285	–	–	0.002	0.120	0.10	0.40	0.30	–	0.35	0.10	0.1	–
25	Dinoflagellates	–	–	–	–	–	–	–	–	–	–	0.02	–	–	–	–	–	–	–	–	–	0.10	0.10	0.2	0.8
26	Diatoms	–	–	–	–	–	0.05	–	1	0.800	–	–	–	–	–	–	0.060	0.05	–	–	–	0.10	–	0.7	0.2
27	Macroalgae	–	–	–	–	–	–	–	–	–	–	–	–	–	–	–	0.023	–	–	–	–	0.25	0.10	–	–
28	Detritus	–	–	–	–	–	–	–	–	0.070	–	0.02	0.050	–	–	0.004	0.055	0.10	–	0.25	0.4	0.25	0.79	–	–
29	Import	–	–	–	–	–	–	–	–	–	–	–	–	–	–	–	–	–	–	–	–	–	–	–	–

1. Jarre-Teichmann (1992); 2. Adapted from Fishbase; 3. Modified from Jarre-Teichmann (1992) to balance the model; 4. Assumed; 5. From Jarre-Teichmann (1992) and Rojas de Mendiola (1989); 6. From Jarre-Teichmann (1992) and Konchina (1992).

first fitted manually to identify where possible solutions were most likely. Formal fitting to the time series was then performed using a non-linear search procedure, allowing vulnerabilities to be modified. We used the knowledge gained in the manual fitting to start the search procedure with different initial parameters to avoid being caught in local optimal solutions. The criterion was a weighted sum of squares of deviations (SS) between the logarithms of observed and predicted biomasses and catches.

3. Results

Given the well known link between El Niño events and anchovy biomass, it was no surprise that fitting the model to time series based on vulnerabilities alone did not lead to good fit to the biomass and catch series of anchovies and sardines (Fig. 1, Basic fit). The only two functional groups that were reasonably well fitted were bonito and pinnipeds. The decrease in bonito seems mainly linked to fishing, although predicted catches were slightly lower than observed. Pinnipeds have been dramatically overexploited since before 1950, their abundance has increased steadily during the study period. All models and fitting strategies suggested that given their initial biomass and production, their abundance had to increase during the study period. The total sum of squares (SS) for this scenario was 206. In the following scenarios, we will monitor the trends in biomass and landings of the species of interest, anchovies, sardines, bonito and seabirds.

Several productivity indicators were successively added in the model, including sea surface temperature, surface NO_3 concentration and flux, upwelling and turbulence (Pauly and Tsukayama, 1987; Pauly et al., 1989) (Table 3), but the index of turbulence off the coast near Trujillo (Mendo et al., 1987) was retained as providing the best fit to the anchovy abundance time series. The turbulence index is calculated as the cube of wind velocity (Mendo et al., 1987). With turbulence index in the model, catches and biomasses of anchovies increased slightly, but they did not reach the peaks observed in the 1960s for anchovies and in the 1980s for sardines (Fig. 1, scenario 1; SS = 188). Note that birds were not influenced directly by the turbulence index.

We tried to recreate the observed decrease in birds using the mediation between bonito and birds which increased the vulnerability of anchovy to guano birds in the presence of bonito (Fig. 2). Considering this mechanism became necessary to model a situation where seabirds were experiencing lower abundance as a consequence of their ‘competitors’, large pelagics, being fished down (see Methods section). Without this mediation effect, the model behaves so that less large pelagics means more small pelagics and hence more food for the seabirds, which then results in higher seabird abundance. In the present model, the mediation caused the bird and bonito biomass’ to decrease in parallel (Fig. 1, scenario 2, SS = 171). Ecosim predicted a decline in guano birds but it did not match observations in steepness and in timing. The reduction of bird predation on anchovy, although small compared to that inflicted by other predators, still allowed anchovy biomass to increase slightly at the end of the study period.

We tried to replicate the observed anchovy and sardine biomass trends by using the mediation and modifying the vulnerabilities. Vulnerabililities are related to the carrying capacity for a given consumer and express the factor by which the predation mortality for a given predator–prey combination can increase if there were many more predators. Low vulnerabilities means that the predator is close to carrying capacity, which results in strong density-dependence for this predator. Vulnerabilities are not completely unknown. For example, we expect a stock that has been fished down to have a high vulnerability, i.e. to be able to increase substantially the predation mortality on its prey. The manipulation of vulnerability values aim at further tuning the model and to make the functional groups respond appropriately. We used the mediation between diatoms and dinoflagellates as a proxy for their presumed competition for nutrients and light. The sigmoid relationship used resulted in less access to nutrients for dinoflagellates when diatom abundance increased, and vice-versa (Fig. 2). By itself, the mediation did not influence the biomass trends for these groups, but this changed when the vulnerabilities were adjusted. First, when the vulnerability for anchovy larvae was decreased from 2 to 1.5 (toward bottom-up control) and the vulnerability for adult anchovy was increased from 1 to 2, an increase in

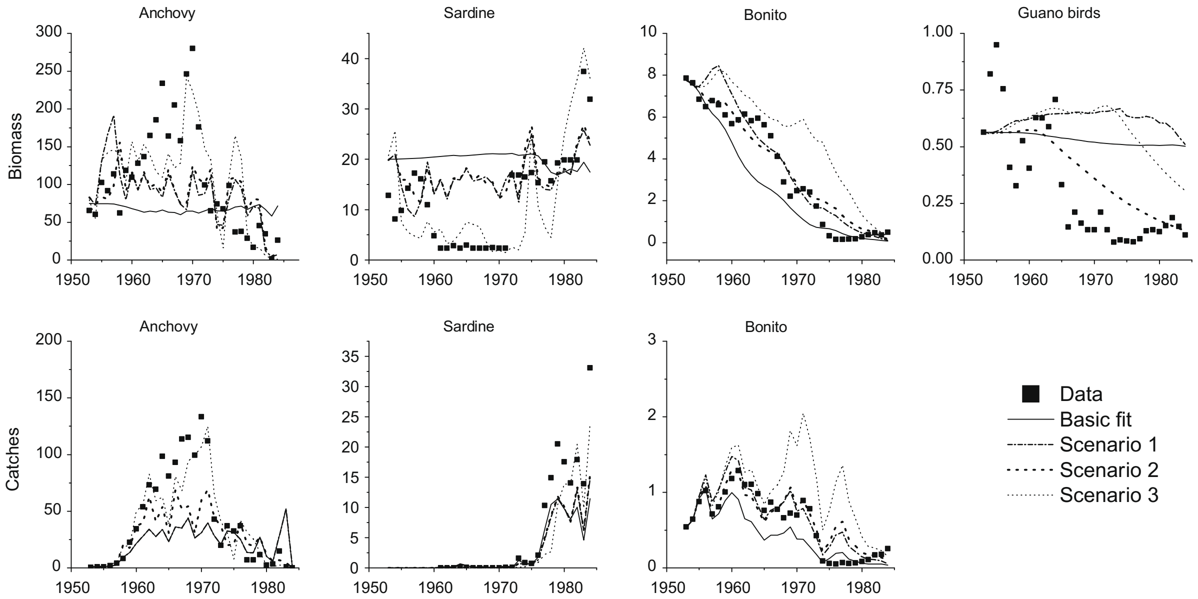

Fig. 1. Comparison of the biomass ($t \cdot km^{-2}$) and catch ($t \cdot km^{-2} \cdot year^{-1}$) time series data (squares) and Ecosim predictions (lines) for four species of the Peruvian upwelling. Thin lines show the result of the basic fit changing vulnerabilities only. Dash-dot lines show the effect of including the turbulence index in the model (scenario 1). Dashed lines show the impact of adding a mediation between bonito and guano birds (scenario 2). Dotted lines show the results of adding a mediation between diatoms and dinoflagellates and modifying some vulnerability values (scenario 3; see text). There were no catches of seabirds included in the model.

Table 3
List and brief description of environmental indices used in the model. The best results were obtained using the turbulence index at Trujillo.

Index name	Unit	Description	Source
Turbulence index at Trujillo	$m^3 \cdot s^{-3}$	Cube of wind velocity	Mendo et al., (1987), Table 4
Alongshore windstress component on the sea surface index	$m^3 \cdot s^{-1} \cdot m^{-1}$ coast	Function of the northward and eastward wind and of the angle of these components from true north	Bakun and Mendelssohn, (1989), Table 1
Upwelling index at Trujillo	$m^3 \cdot s^{-1} \cdot m^{-1}$ coast	Function of Ekman's transport and the difference between the angle of the coast and that of the wind direction	Mendo et al., (1987), Table 1
Upwelling index at Callao	$m^3 \cdot s^{-1} \cdot m^{-1}$ coast	Function of Ekman's transport and the difference between the angle of the coast and that of the wind direction	Mendo et al., (1987), Table 3
Southern Oscillation Index	mbars	Mean pressure difference between Easter Island and Darwin, Australia	Brainard and McLain, (1987), Table 1
Rossby Radius	km	Measure the width of the upwelling zone based on SST and the depth of the 14 °C isotherm	Mendo et al., (1989), Fig. 2
NO_3 concentration in the thermocline	$nM \cdot m^{-3}$	Relies on correlation of the depth of the 14 °C isotherm and nitrates concentration at 60 m depth	Chavez et al., 1989
NO_3 concentration inshore ($\Leftarrow$60 km)	$nM \cdot m^{-3}$	Predicted by using a model that includes a relation between depth and nitrate concentration, wind speed and its effect on the water masses moved, and the size of the Rossby radius	Mendo et al., (1989), Fig. 3
Coastal NO_3 flux per unit area	$mmol \cdot m^{-2} \cdot day^{-1}$	Based on Trujillo upwelling index, using constant upwelling depth model. Closely correlated to the predicted new primary production	Mendo et al., (1989), Fig. 5
Oceanic NO_3 flux per unit area	$mmol \cdot m^{-2} \cdot day^{-1}$	Based on Bakun's upwelling index (Bakun and Mendelssohn, 1989)	Mendo et al., (1989), Fig. 4
Coastal NO_3 flux per unit area	$mmol \cdot m^{-2} \cdot day^{-1}$	Based on Trujillo upwelling index, using variable upwelling depth model	Mendo et al., (1989), Fig. 4

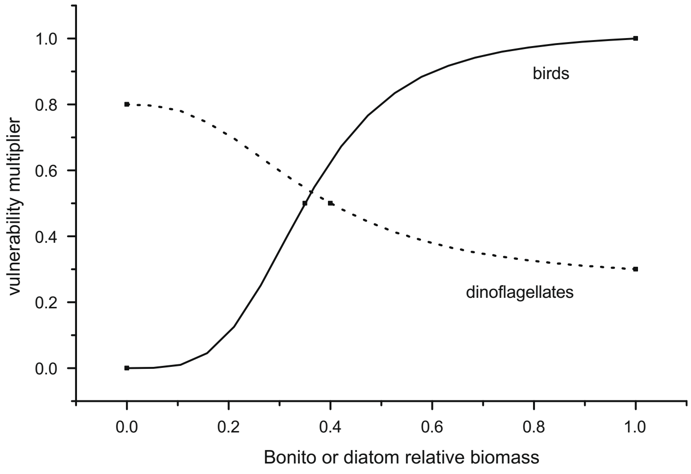

Fig. 2. Shape of the mediation functions used in the model. The solid line shows that, as bonito biomass increases, the vulnerability of prey to birds augments. The dashed line shows that as diatoms' biomass increases, dinoflagellates' access to nutrients decreases.

predicted anchovy biomass and catches occurred, but still not to the levels observed in 1983–1984. Thus, vulnerability was increased to 3 for adult sardine, which resulted in an increase in sardine biomass and a closer fit of predicted and observed anchovy biomass (Fig. 1, scenario 3; SS = 228). The increased sum of squares is due to the decreased fit for birds and bonito biomass.

Anchovies represent 70% of bonito consumption; thus anchovy biomass can be determinant for the trend in bonito biomass. Also, in absence of real time series of sardine and anchovy larvae biomass, the values of vulnerabilities are only dependent on their link with the population dynamics of the adult. Hence, we experimented with several values of vulnerabilities, aiming at obtaining better fits for bonito, sardine and anchovy. We increased the vulnerability of sardine larvae to anchovy (from 2 to 3) and that of anchovy to bonito (from 3 to 4). The resulting trends in biomass and landings came closer to the observed values, with the exception of the bonito which was still overestimated (Fig. 2, scenario 4; SS = 191). Increasing vulnerability of anchovy to bonito again to a value of 10 allowed for a better fit of bonito abundance, but flattened the trend in anchovy biomass (Fig. 3, scenario 5; SS = 171).

Recent results indicate that anchovy feed mainly on large zooplankton rather than diatoms (notably euphausiids, see Espinoza and Bertrand, 2008), and we next attempted to model this. To balance the model with this new diet, the biomass of large zooplankton, and to a lesser extent, diatoms, had to be increased, while the *Q*/*B* for mackerel and horse mackerel were decreased to reduce their intake of zooplankton. It was possible to fit the model to the observed anchovy abundance trends and still obtain the abundance shift from anchovy to sardine starting in the mid-1970s. Under this scenario, however, the anchovy biomass did not reach the levels observed in the late 1960s (Fig. 3, scenario 6; SS = 189).

Of all the scenarios, the best fit was obtained with scenario 4, using a moderate vulnerability of anchovy to bonito, and by increasing the vulnerability of sardine larvae to anchovy. We preferred this solution to that of scenario 5, because it gives more weight to the anchovy time series than to the bonito, which is considered less reliable. The predicted biomass and catch of anchovy and sardine are well predicted by the model (Fig. 4). Predicted catch and biomass of bonito were both overestimated. Observed and predicted biomasses for mackerel and horse mackerel showed little contrast during the study period and although their catches were well predicted by Ecosim, their biomasses were not. The model did not predict the increase in hake biomass that occurred during the 1970s, and thus did not predict the observed peak in

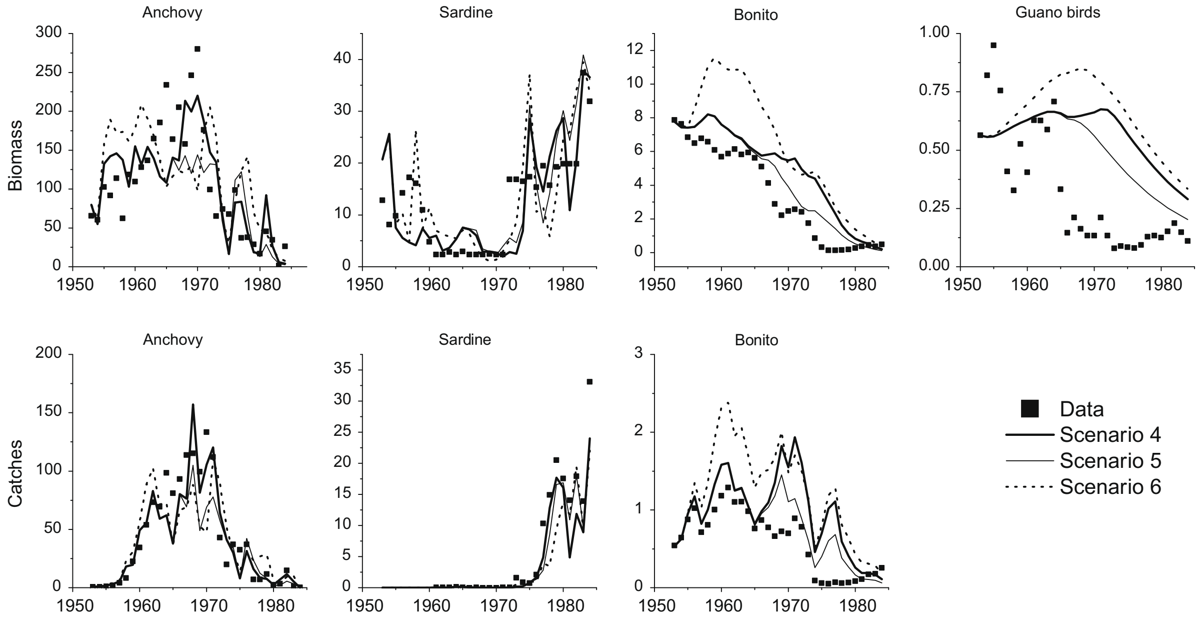

Fig. 3. Comparison of the biomass ($t \cdot km^{-2}$) and catch ($t \cdot km^{-2} \cdot year^{-1}$) time series data (squares) and Ecosim predictions (lines) for four species of the Peruvian upwelling. The thick solid line is the best fit to anchovies and sardines obtained by slightly increasing the vulnerability of anchovy to bonito (scenario 4). The thin line shows the effect of increasing the vulnerability to bonito to a value of 10 (scenario 5). The dotted line shows the effect of assuming that anchovies feeding mainly on large zooplankton (scenario 6). There were no catches of seabirds included in the model.

catches either. Finally, Ecosim did predict the decline in bird populations under this scenario, but starting only in 1972, while the data show a sharp decline between 1964 and 1966 followed by steady low population abundance afterward (Fig. 4).

4. Discussion

The present modelling exercise led to some insights in the Peruvian upwelling ecosystem. The Jarre et al. (1991) model based on 1950s data, constituted the best-snapshot representation of the ecosystem. Nevertheless, the addition of temporal dynamics forced us to reconsider some of the initial parameters of the Jarre et al. (1991) model. For example, the initial biomass of bonito, which appeared acceptable in the Ecopath model, was too low to support the observed catches between 1953 and 1984. In static models, it is impossible to differentiate between a state of large biomass and low production versus a state of low biomass and high production. This can be done by modelling temporal change (now possible with Ecosim), and comparing with observational records (Christensen et al., 2005). As expected, there are still changes that could be made to the Ecopath model to include more recent information of feeding ecology in upwelling ecosystems. For example, the trophic level of anchovy calculated in the model based on a diet mainly composed of diatoms is lower than now believed realistic (van der Lingen et al., 2006; Espinoza and Bertrand, 2008). When a larger proportion of large zooplankton in adult anchovy diet was added (scenario 6), its trophic level increased from 2.22 to 2.67 in Ecopath; a diet completely composed of zooplankton would elevate it further. Diet varies with season, location and prey availability, and sometimes with the analytic technique used. In the model the proportion of prey in the diet of a predator will change through time, depending on changes in prey biomass and the vulnerability of the prey to this predator, and these changes are more important than the initial settings in determining the behaviour of the model (see Guénette et al., 2006 for a detailed discussion on the subject). Obviously, future modelling should add more recent time series (see Taylor et al., 2008 and Tam et al., 2008) and include updated diets, and indeed, doing so should improve the exploration of the system trophodynamics.

The climate index used as a proxy for nutrient concentration and phytoplankton productivity, explained a large fraction of the observed variations in anchovy biomass. This was expected due to the strong relationship between the upwelling strength and productivity (Faure and Cury, 1998; Binet, 1988; Chesney and Alonso-Noval, 1988; Lluch-Belda et al., 1991). It is interesting that a turbulence index yielded the best results, rather than an upwelling index. An increase in either can be expected to increase the production of large phytoplankton and zooplankton, which favours anchovies (van der Lingen et al., 2006). This may be fortuitous, since the relationship between both turbulence and upwelling with the reproductive success of anchovy and sardine are thought to be dome-shaped – ‘optimal windows’ (Cury and Roy, 1989; Roy et al., 1992), not accounted for here. Moreover, reproductive success can be impacted by unfavourable values of one or several of the environmental factors such as turbulence, advection, upwelling intensity, all of which become critical at various times of the year (Guisande et al., 2004). Future versions of the model should include a composite index to more realistically model these oceanographic factors. Alternately, several indices might be applied to different parts of the model. For example, turbulence could modify the level of diatom production, but advection could modify the level of larvae mortality brought by inshore concentration or offshore dispersion.

The assumed negative relationship between diatoms and dinoflagellates helped in fitting the model, but considering this mitigation does not imply that we believe in a direct negative relationship between diatoms and dinoflagellates. Rather, this was a way to introduce a driver for dinoflagellates and favour one phytoplankton type over the other. The addition of a relationship of this type was necessary to model the abundance of sardines, and reflects the idea that sardine and anchovies do not directly compete with each other (Bertrand et al., 2004). Structured this way, the model emphasizes the importance of phytoplankton production and feeding conditions. In addition, instead of including only the relationship between diatoms, large zooplankton and

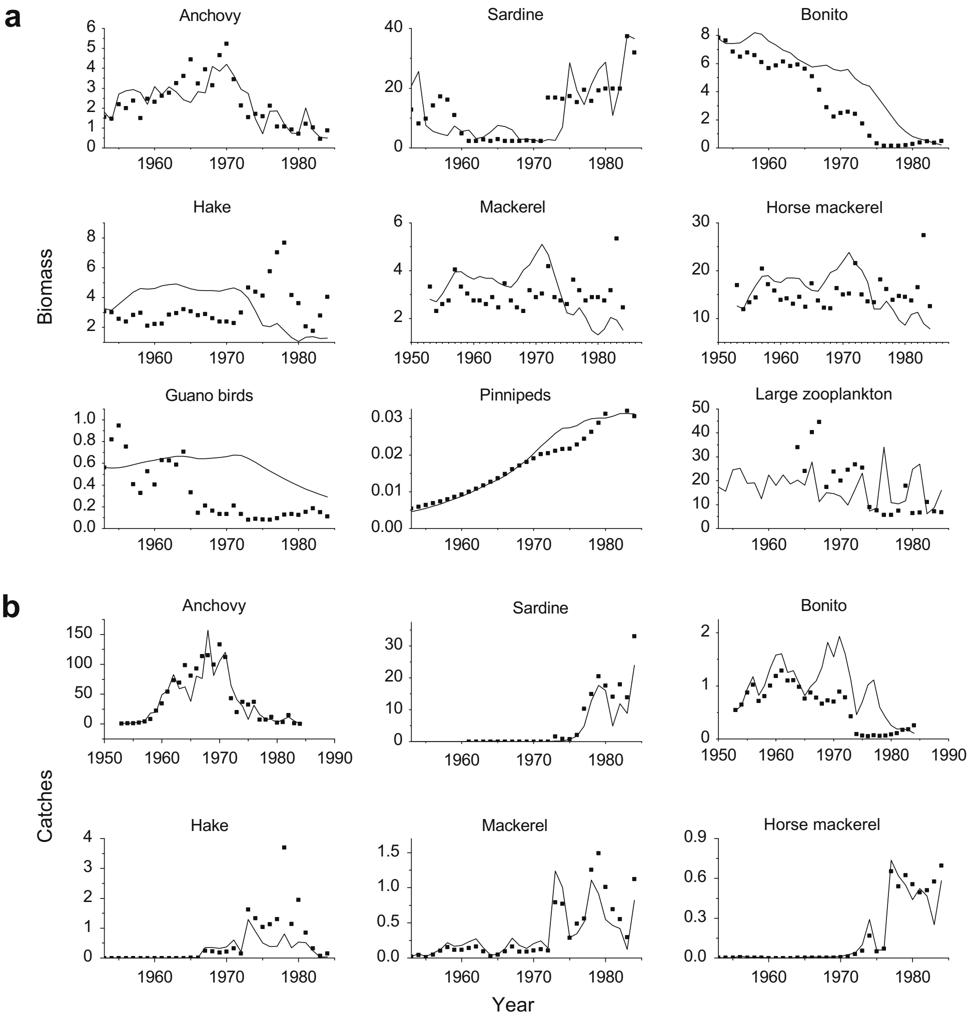

Fig. 4. Comparison of the biomass (t · km^{-2}) and catch (t · km^{-2} · year^{-1}) time series data (squares) and Ecosim predictions (lines), under the best scenario (scenario 4), for all species of the Peruvian upwelling for which we had a time series of biomass.

anchovies, future models should provide mechanisms to link hydrography (calm and warm waters) with nutrients and dinoflagellates, small zooplankton and sardines. This may also involve adding a microbial loop, although such loop is thought to be a minor component of the carbon pathway in upwellings (Moloney et al., 1991).

The division of phytoplankton into two functional groups in the present model is coarse and based, for simplicity's sake, on taxonomic groupings rather than more detailed body size structure (see van der Lingen et al., 2006). Using a model focussed on plankton (and its physiological characteristics) and on carbon and nitrogen flows, Moloney et al. (1991) were able to predict the relative abundance of each size class of phytoplankton in three contrasting systems (oceanic, coastal and upwelling) for 30 days, which emphasizes the importance of size on the rate of nutrients intake and resistance to nitrogen depletion. Such modelling is very useful and described the transfer of energy and nutrients from the upwelling of nutrients to fish (Moloney, 1992) at finer time and space scales. However, the time scale, in such cases, is limited to a few months as opposed to the 30 years considered here.

Part of our model's success is due to the short and direct link between the turbulence index, diatoms, and anchovy on one side, and dinoflagellates, small zooplankton and sardines on the other. However, if anchovy's diet is in fact based more on large zooplankton than diatoms (van der Lingen et al., 2006; Espinoza and Bertrand, 2008), the change in diet can modify the predicted biomass trends. By making such a change in the anchovy diet, scenario 6 was still able to reproduce the main observed trends, but a bit less efficiently. Similarly, the inclusion of a more detailed sized-based zooplankton diet for anchovy and sardine, as suggested in the precedent paragraph (composed of several size-related groups of zooplankton with a small proportion of phytoplankton) (van der Lingen et al., 2006) would likely weaken the link between the turbulence index and fish production unless realistic mechanisms to account for changes in temperature, turbulence and nutrients, and their effects on zooplankton, were added. Ecosim modelling of the Benguela Current, using an anchovy diet based on zooplankton, led to very good results when the vulnerability of zooplankton to anchovy was increased, representing a more top-down dynamics on the plankton (Shannon et al., 2004a). This may be an additional avenue to pursue.

The biomass of horse mackerel and mackerel did not show any major trends. This is mainly because their oceanic distribution only partly overlaps with that of the more coastal anchovy. The distributions of horse mackerel, and mackerel also probably, are related to the amount of prey and dissolved oxygen more than to water temperature (Bertrand et al., 2006), and they are usually found more offshore than anchovies except in El Niño years when they move inshore (Muck and Sanchez, 1987). The model scenarios also did not predict hake biomass correctly, which may be due to its variable latitudinal distribution, and hence variable presence in the model study area. Hake distribution is also strongly influenced by oxygen availability in subsurface waters (Muck, 1989a), a feature not included in this model as implemented.

The positive influence of tuna on bird feeding on anchovy was based on field work (Au et al., 1999), but no quantitative functional relationship has been described. Using what appeared to be a reasonable relationship (Fig. 3), the model predicted a decline in seabirds; this was not nearly as steep as observed, suggesting that our tuna/bird relationship needs improvement or that additional mechanisms explain the decline in seabirds. For example, changes in thermocline and oxycline depth could have the effect driving small pelagics to the surface as well. However, these factors, when included in the model, could help explain the observed decline in seabirds abundance.

Although we focussed on the pelagic community, demersal groups were included in the model in an attempt to suggest a more global view of the ecosystem. Due to the lack of data on these groups, however, they add little value at this point. Demersal groups may eventually be required if the more coastal demersal fisheries are included. The artisanal fisheries operating 'Viking'-type boats are now exploiting both demersal fish and juvenile anchovies (P. Majluf, Universidad Peruana Cayetano Heredia, Lima Peru, personal communication), and as their size and number has increased appreciably since 1998, their impact on the stock may have become strong enough to be included in models otherwise focussing on the pelagic part of the system.

The modelling has also shown the importance of predation of anchovy and sardine on each other's larvae to explain biomass trends. Indeed, the best-fitting model required an increase in vulnerability for the larvae to the adult of the other species, which suggests that the there is little density-dependence at play in the interaction of these species' feeding on the other species' larvae. If one of these species increases, they can eat nearly proportionally more of the other species larvae when vulnerabilities are high. Similarly, empirical work has shown that the contribution of dietary carbon from larvae can be quite important, e.g. carbon from anchovy (*E. encrasicolus*) eggs contributed 15% in the Benguela sardines (Alheit and Niquen, 2004). In the present model, only predation from mackerel and horse mackerel on adult anchovy and sardine has been included, while predation on eggs and larvae (Alheit and Niquen, 2004) has been ignored. Egg cannibalism could also add density-dependent mortality in a future model.

Thus, based on a snapshot of the Peruvian upwelling ecosystem of the early 1950s created in the late 1980s, and time series that spanned during this period, it was possible to recreate the major fluctuations in anchovy and sardine. To do so, however, it was necessary to modify our underlying Ecopath (static) model and, more importantly, it was also necessary to include additional (hypothetical) relationships suggested by empirical studies in other ecosystems. A similar modelling exercise for the Southern Benguela for the period 1997–2002 (Shannon et al., 2004b) was also successful at explaining biomass of trends for sardine and, to a lesser degree anchovy biomasses, using an upwelling index, fishing and changes in vulnerabilities. In this case, environmental variation was the most important factor as well.

Models built with Ecopath with Ecosim are aimed at understanding the dynamics of the upper levels of the food chain, mainly fish, and the impact of fisheries on the ecosystem (Christensen and Walters, 2004; Guénette et al., 2007). Although detailed modelling of the planktonic phase has not been deemed necessary in several models, we have here shown the importance of including processes regulating primary production due to their strong effects on anchovy and sardine populations.

We gave strong emphasis to fitting older time series, although recent, albeit shorter, series are available. All over the world, it is common to see analysis and modelling of relatively short time series which may suffer from the "shifting baseline syndrome" (Pauly, 1995). Here we emphasize long-term time series spanning numerous contrasting events that help identify mechanisms. Recent time series may lack such changes and consequently be too easy to fit a model to. The best situation would be for models to accommodate all the time series available for a given system, i.e., the old, contrast-rich series, and the more precisely estimated new ones. Only when we have models that can accommodate the whole period for which we have data will we be able to use them in a constructive way for fisheries management. To support such work, we have made all data used here, and the books in which they are documented, freely available from the website of the *Sea around Us* Project (http://www.seaaroundus.org).

Acknowledgements

We thank Arnaud Bertrand, I.R.D., for inviting one of us (D.P.) to give the keynote address upon which this contribution is based. V.C. and D.P. acknowledge support through the Sea Around Us Project initiated and funded by the Pew Charitable Trusts. V.C. acknowledges support from the Natural Sciences and Engineering Research Council of Canada Discovery Grants. Finally, we acknowledge the invaluable contribution of the referees who helped strengthen the paper.

References

Alheit, J., Niquen, M., 2004. Regime shifts in the Humboldt Current ecosystem. Progress in Oceanography 60, 201–222.

Anderson, D.J., Ricklefs, R.E., 1987. Radio-tracking masked and blue-footed boobies (*Sula* spp.) in the Galápagos Islands. National Geographic Research 3, 152–163.

Au, D.W., Pitman, R.L., Ballance, L.T., 1999. Yellowfin tuna associations with seabirds and subsurface predators. In: Ecology and Fisheries for Tunas Associated with Floating Objects. Inter-American Tropical Tuna Commission Special Report 11, pp. 327–345.

Bakun, A., Mendelssohn, R., 1989. Alongshore wind stress, 1953–1984: correction, reconciliation and update through 1986. In: Pauly, D., Muck, P., Mendo, J., Tsukayama, I. (Eds.), The Peruvian Upwelling Ecosystem: Dynamics and Interactions. ICLARM Conference Proceedings, vol. 18, pp. 77–81.

Bertrand, A., Segura, M., Gutiérrez, M., Vásquez, L., 2004. From small-scale habitat loopholes to decadal cycles: a habitat-based hypothesis explaining fluctuation in pelagic fish populations off Peru. Fish and Fisheries 5, 296–316.

Bertrand, A., Barbieri, M.A., Gerlotto, F., Leiva, F., Córdova, J., 2006. Determinism and plasticity of fish schooling behaviour as exemplified by the South Pacific jack mackerel *Trachurus murphyi*. Marine Ecology Progress Series 311, 145–156.

Binet, D., 1988. The probable changes in the pattern of sardine and sardinelle distribution along the West African coast, caused by an intensification of the trade winds. Aquatic Living Resources 1, 115–132.

Brainard, R.E., McLain, D.R., 1987. Seasonal and interannual subsurface temperature variability off Peru, 1952 to 1984. In: Pauly D., Tsukayama, I. (Eds.), The Peruvian Anchoveta and its Upwelling Ecosystem: Three Decades of Change. ICLARM Studies and Reviews 15, pp. 14–45.

Carraso, S., Lozano, O., 1989. Seasonal and long-term variations of zooplankton volumes in the Peruvian Sea, 1964–1987. In: Pauly, D., Muck, P., Mendo, J., Tsukayama, I. (Eds.), The Peruvian Upwelling Ecosystem: Dynamics and Interactions. ICLARM Conference Proceedings, vol. 18, pp. 82–88.

Chavez, F.P., Barber, R.T., Sanderson, M.P., 1989. The potential primary production of the Peruvian upwelling ecosystem, 1953–1984. In: Pauly, D., Muck, P., Mendo, J., Tsukayama, I. (Eds.), The Peruvian Upwelling Ecosystem: Dynamics and Interactions. ICLARM Conference Proceedings 18, pp. 50–63.

Chesney, E.J., Alonso-Noval, M., 1988. Coastal upwelling and the early life history of sardines *Sardina pilchardus* along the Galician coast of Spain. In: Blaxter, J.H.S., Gamble, J.C., von Westernhagen, H. (Eds.), ICES Symposium on the Early Life History of Fish 191, pp. 63–69.

Christensen, V., Walters, C.J., 2004. Ecopath with Ecosim: methods, capabilities and limitations. Ecological Modelling 172, 109–139.

Christensen, V., Walters, C.J., 2005. Using Ecosystem Modelling for Fisheries Management: Where are we? ICES CM 2005/M:19.

Christensen, V., Walters, C.J., Pauly, D., 2005. Ecopath with Ecosim: A User's Guide Fisheries Centre, Springer, Berlin, 154p. <http://www.ecopath.org/index.php?name=Publications&sub=ViewPublications&value=ManualsPub>.

Cury, P., Roy, C., 1989. Optimal environmental window and pelagic fish recruitment success in upwelling areas. Canadian Journal of Fisheries and Aquatic Sciences 46, 670–680.

Cushing, D.H., 1988. Review of "The Peruvian Anchoveta and its upwelling ecosystem: three decades of changes". Journal du Conseil International pour l'Exploration de la Mer 44, 297–299.

Espinoza, P., Bertrand, A., 2008. Revisiting Peruvian anchovy (*Engraulis ringens*) trophodynamics provides a new vision of the Humboldt Current system. Progress in Oceanography, doi:10.1016/j.pocean.2008.10.018.

Faure, V., Cury, P., 1998. The climate and eastern ocean systems project (CEOS). In: Durand, M.H., Cury, P., Mendelssohn, R., Bakun, A., Roy, C., Pauly, D. (Eds.), Global Versus Global Change in Upwelling Areas. Séries Colloques et Séminaires. ORSTOM, Paris, pp. 391–407.

Guénette, S., Heymans, S.J.J., Christensen, V., Trites, A.W., 2006. Ecosystem models show combined effects of fishing, predation, competition, and ocean productivity on Steller sea lions (*Eumetopias jubatus*) in Alaska. Canadian Journal of Fisheries and Aquatic Sciences 63, 2495–2517.

Guénette, S., Christensen, V., Hoover, C., Lam, M.E., Preikshot, D., Pauly, D., 2007. A Synthesis of Research Activities at the Fisheries Centre on Ecosystem-based Fisheries Modelling and Assessment with Emphasis on the Northern and Central Coast of BC. Fisheries Centre, UBC, Vancouver, BC, Canada, FCRR 15 (1), 32p.

Guisande, C., Vergara, A.R., Cabanas, J.M., 2004. Climate change and abundance of the Atlantic-Iberian sardine (*Sardina pilchardus*). Fisheries Oceanography 13, 91–101.

Iriarte, J.L., González, H.E., 2004. Phytoplankton size structure during and after the 1997/98 El Niño in a coastal upwelling area of the northern Humboldt Current system. Marine Ecology Progress Series 269, 83–90.

Jarre, A., Muck, P., Pauly, D., 1991. Two approaches for modelling fish stock interactions in the Peruvian upwelling ecosystem. ICES Marine Science Symposia 193, 171–184.

Jarre-Teichmann, A., 1992. Steady-state Modelling of the Peruvian Upwelling Ecosystems. Ph.D. Thesis, University of Bremen, Bremen, 84p. + annexes.

Jarre-Teichmann, A., Pauly, D., 1993. Seasonal changes in the Peruvian upwelling ecosystem. In: Christensen, V., Pauly, D. (Eds.), Trophic Models of Aquatic Ecosystems. ICLARM Conference Proceedings, vol. 26, pp. 307–314.

Kimura, D.K., 1985. Changes to stock reduction analysis indicated by Schnute's general theory. Canadian Journal of Fisheries and Aquatic Sciences 42, 2059–2060.

Konchina, Y.V., 1992. Trophic status of Peruvian pseudoneritic fish in oceanic epipelagic water. Journal of Ichthyology 32, 20–39.

Lluch-Belda, D., Lluch-Cota, D.B., Hernandez-Vazquez, S., Salinas-Zavala, C.A., 1991. Sardine and anchovy spawning as related to temperature and upwelling in the California Current System. Reports of the California Cooperative Oceanic Fisheries Investigations 32, 105–111.

Mendo, J., Pizzarr, L., Castillo, J., 1987. Monthly turbulence and Ekman transport indexes, 1953 to 1985, based on local wind records from Trujillo and Callao, Peru. In: Pauly, D., Tsukayama, I. (Eds.), The Peruvian Anchoveta and its Upwelling Ecosystem: Three Decades of Change. ICLARM Studies and Reviews 15, pp. 75–88.

Mendo, J., Bohle-Carbonell, M., Calienes, R., 1989. Time series of upwelling nitrate and primary production off Peru derived from wind and ancillary data, 1953–1982. In: Pauly, D., Muck, P., Mendo, J., Tsukayama, I. (Eds.), The Peruvian Upwelling Ecosystem: Dynamics and Interactions. ICLARM Conference Proceedings 18, pp. 64–76.

Moloney, C.L., 1992. Simulation studies of trophic flows and nutrient cycles in Benguela upwelling foodwebs. South African Journal of Marine Sciences 12, 457–476.

Moloney, C.L., Field, J.G., Lucas, M.I., 1991. The size-based dynamics of plankton food webs. II. Simulations of three contrasting southern Benguela food webs. Journal of Plankton Research 13, 1092–1339.

Muck, P., 1989a. Anchoveta consumption of Peruvian hake: a distribution and feeding model. In: Pauly, D., Muck, P., Mendo, J., Tsukayama, I. (Eds.), The Peruvian Upwelling Ecosystem: Dynamics and Interactions. ICLARM Conference Proceedings, vol. 18, pp. 306–320.

Muck, P., 1989b. Major trends in the pelagic ecosystem off Peru and their implications for management. In: Pauly, D., Muck, P., Mendo, J., Tsukayama, I. (Eds.), The Peruvian Upwelling Ecosystem: Dynamics and Interactions. ICLARM Conference Proceedings, vol. 18, pp. 386–403.

Muck, P., Sanchez, G., 1987. The importance of mackerel and horse mackerel predation for the Peruvian anchoveta stock (a population and feeding model). In: Pauly, D., Tsukayama, I. (Eds.), The Peruvian Anchoveta and its Upwelling Ecosystem: Three Decades of Change. ICLARM Studies and Reviews 15, pp. 276–293.

Pauly, D., 1993. Data-rich books. BioScience 43, 167–168.

Pauly, D., 1995. Anecdotes and the shifting baseline syndrome of fisheries. Trends in Ecology and Evolution 10, 430.

Pauly, D., Tsukayama, I. (Eds), 1987. The Peruvian Anchoveta and its Upwelling Ecosystem: Three Decades of Change. ICLARM Studies and Reviews, vol. 15.

Pauly, D., Christensen, V., Walters, C., 2000. Ecopath, Ecosim, and Ecospace as tools for evaluating ecosystem impact of fisheries. ICES Journal of Marine Science 57, 697–706.

Pauly, D., Muck, P., Mendo, J., Tsukayama, I. (Eds), 1989. The Peruvian Upwelling Ecosystem: Dynamics and Interactions. ICLARM Conference Proceedings, vol. 18.

Rojas de Mendiola, B., 1989. Stomach contents of anchoveta (*Engraulis ringens*), 1953–1974. In: Pauly, D., Muck, P., Mendo, J., Tsukayama, I. (Eds.), The Peruvian Upwelling Ecosystem: Dynamics and Interactions. ICLARM Conference Proceedings, vol. 18, pp. 97–104.

Roy, C., Cury, P., Kifani, S., 1992. Pelagic fish recruitment success and reproductive strategy in upwelling areas: environmental compromises. South African Journal of Marine Sciences 12, 135–146.

Shannon, L.J., Field, J.G., Moloney, C.L., 2004a. Simulating anchovy-sardine regime shifts in the Southern Benguela ecosystem. Ecological Modelling 172, 269–281.

Shannon, L.J., Christensen, V., Walters, C.J., 2004b. Modelling stock dynamics in the southern Benguela ecosystem for the period 1978–2002. African Journal of Marine Science 26, 179–186.

Tam, J., Taylor, M.H., Blaskovic, V., Espinoza, P., Ballón, R.M., Díaz, E., Wosnitza-Mendo, C., Argüelles, J., Purca, S., Ayón, P., Quipuzcoa, L., Gutiérrez, D., Goya, E., Ochoa, N., Wolff, M., 2008. Trophic flows in the Northern Humboldt Current Ecosystem. Part 1: Comparing 1995–96 and 1997–98. Progress in Oceanography 79, 352–365

Taylor, M.H., Tam, J., Blaskovic, V., Espinoza, P., Ballón, R., Wosnitza-Mendo, C., Argüelles, J., Díaz, E., Purca, S., Ochoa, N., Ayón, A., Goya, E., Quipuzcoa, L., Gutiérrez, D., Wolff, M., 2008. Trophic modeling of the Northern Humboldt Current Ecosystem. Part II: Elucidating ecosystem dynamics from 1995-2004 with a focus on the impact of ENSO. Progress in Oceanography, doi:10.1016/j.pocean.2008.10.008.

van der Lingen, C.D., 1994. Effect of particle size and concentration on the feeding behaviour of adult pilchard *Sardinops sagax*. Marine Ecology Progress Series 109, 1–13.

van der Lingen, C.D., Hutchings, L., Field, J.G., 2006. Comparative trophodynamics of anchovy *Engraulis encrasicolus* and sardine *Sardinops sagax* in the Southern Benguela: are species alternations between small pelagic fish trophodynamically mediated? African Journal of Marine Science 28, 465–477.

Walsh, J., 1981. A carbon budget for overfishing off Peru. Nature 290, 300–302.

Walters, C., Kitchell, J.F., 2001. Cultivation/depensation effects on juvenile survival and recruitment: implications for the theory of fishing. Canadian Journal of Fisheries and Aquatic Sciences 58, 39–50.

Walters, C.J., Christensen, V., Pauly, D., 1997. Structuring dynamic models of exploited ecosystems from trophic mass-balance assessments. Reviews in Fish Biology and Fisheries 7, 139–172.

Watson, R.A., Kitchingman, A., Gelchu, A., Pauly, D., 2004. Mapping global fisheries: sharpening our focus. Fish and Fisheries 5, 168–177.

Progress in Oceanography 79 (2008) 336–351

Contents lists available at ScienceDirect

Progress in Oceanography

journal homepage: www.elsevier.com/locate/pocean

Changes in trophic flow structure of Independence Bay (Peru) over an ENSO cycle

Marc H. Taylor [a,*], Matthias Wolff [a], Jaime Mendo [b], Carmen Yamashiro [c]

[a] Center for Tropical Marine Ecology, Fahrenheitstrasse 6, 28359 Bremen, Germany
[b] Facultad de Pesqueria, Universidad Agraria La Molina, Lima, Peru
[c] Instituto del Mar del Perú, Esq. Gamarra y Gral. Valle s/n, La Punta, Callao, Peru

ARTICLE INFO

Article history:
Accepted 14 October 2008
Available online 21 October 2008

Keywords:
El Nino phenomena
Scallop fisheries
Steady state
Trophic relationships
Humboldt current
Peru
Independence Bay

ABSTRACT

During the strong warm El Niño (EN) that occurred in 1997/98, Independence Bay (14°S, Peru) showed a ca. 10 °C increase in surface temperatures, higher oxygen concentrations, and clearer water due to decreased phytoplankton concentrations. Under these quasi-tropical conditions, many benthic species suffered (e.g. macroalgae, portunid crabs, and polychaetes) while others benefited (e.g. scallop, sea stars, and sea urchins). The most obvious change was the strong recruitment success and subsequent proliferation of the scallop *Argopecten purpuratus*, whose biomass increased fiftyfold. To understand these changes, steady-state models of the bay ecosystem trophic structure were constructed and compared for a normal upwelling year (1996) and during an EN (1998), and longer-term dynamics (1996–2003) were explored based on time series of catch and biomass using Ecopath with Ecosim (EwE) software. Model inputs were based on surveys and landings data collected by the Instituto del Mar del Perú (IMARPE). Results indicate that while ecosystem size (total throughput) is reduced by 18% during EN, mainly as a result of decreased total primary production, benthic biomass remains largely unchanged despite considerable shifts in the dominant benthic taxa (e.g. scallops replace polychaetes as secondary consumers). Under normal upwelling conditions, predation by snails and crabs utilize the production of their prey almost completely, resulting in more efficient energy flow to higher trophic levels than occurs during EN. However during EN, the proliferation of the scallop *A. purpuratus* combined with decreased phytoplankton increased the proportion of directly utilized primary production, while exports and flows to detritus are reduced. The simulations suggest that the main cause for the scallop outburst and for the reduction in crab and macroalgae biomass was a direct temperature effect, whereas other changes are partially explained by trophic interactions. The simulations suggest that bottom-up effects largely control the system.

1. Introduction

The Humboldt Current System (HCS), located in the south east Pacific along the coasts of Chile and Peru, is one of the most productive marine systems in the world. This high productivity is the result of 'coastal upwelling' – a phenomenon driven by southerly trade winds that brings cold, nutrient-rich water from 40 to 80 m up into the euphotic zone where it supports phytoplankton growth (Barber et al., 1985; Arntz et al., 1991; Pennington et al., 2006). As a result, the system supports a large biomass of small planktivorous pelagic fish – comprising the bulk of catches by a large purse seining fleet. An important fishery also exists down to 15–30 m and in the intertidal areas (Arntz and Valdivia, 1985a; Arntz et al., 1988). Despite a relatively low annual harvest (ca. 200,000 t yr^{-1}) compared to the pelagic system, the exploited nearshore species are of high commercial value and the fishery supports thousands of fishers and their families (Wolff et al., 2003).

Under 'normal' upwelling periods, near-seafloor oxygen concentrations <0.5 ml l^{-1} are typical on the continental shelves of Peru (<100 m; Zuta et al., 1983). This is due to the oxygen minimum zone which occurs below the shallow, uplifted Peruvian thermocline (OMZ; 50–600 m) and the sinking of decomposing organic matter from the overlying euphotic zone (Arntz et al., 2006). Bacteria such as the filamentous 'spaghetti' bacteria (genus *Thioplaca*), are commonly found in association with the OMZ (Arntz et al., 1991). At shallower depths, oxygen concentrations increase and are able to support a higher benthic biomass.

These coastal phenomena propagate into Peru's bays, where much artisanal fishing occurs. This is seen in Independence Bay (~14°S) where the deeper regions of the bay (>30 m) are of low biomass while the bay's shallower perimeter is targeted by the artisanal fishery. These shallow areas contain valuable molluscan and crustacean species, but suspension feeding polychaetes dominate biomass (Tarazona et al., 1991).

---

[*] Corresponding author. Tel.: +49 4212380056; fax: +49 4212380030.
E-mail address: marchtaylor@yahoo.com (M.H. Taylor).

0079-6611/$ - see front matter © 2008 Elsevier Ltd. All rights reserved.
doi:10.1016/j.pocean.2008.10.006

The HCS experiences 'natural' climate variations on seasonal, interannual, and decadal time scales, all of which affect the system's productivity and fisheries. Off Peru the strongest interannual perturbation is the warm "El Niño" (EN) phase of the El Niño Southern Oscillation (ENSO). ENs last about 18 months and occur irregularly every 3–5 years. During EN a Kelvin wave travels eastwards on the equator across the Pacific then north and south along the South American coast, where it depresses the normally shallow thermocline and a raises sea level (Pennington et al., 2006). Although Peruvian coastal upwelling continues during EN, water upwells from above the thermocline and is thus nutrient poor (Barber and Chavez, 1983). As a result, the area of 'productive habitat' supported by coastal upwelling is greatly reduced in area (>1.0 mg chl*a* m^{-3}; Nixon and Thomas, 2001), as is overall primary production (Carr, 2002). This reduction in production at the base of the food web negatively impacts many pelagic coastal species (Tam et al., 2008; Taylor et al., 2008).

EN can also produce significant positive faunal changes in benthic habitats, mainly as a result of increased oxygen levels (Arntz et al., 1991). This is especially the case in shallow depths, where faunal density, biomass, species richness, and diversity can all increase during EN (Tarazona et al., 1988). Several species from offshore, equatorial, and subtropical coastal areas also migrate to the Peruvian coast during EN, such as swimming crabs and penaeid shrimps (Arntz et al., 1991). In Independence Bay the resident scallop *Argopecten purpuratus* experiences much higher recruitment and growth during EN. Past El Nino densities have reached up to 8 kg m^{-2} and densities of 129 adult scallops $\cdot$ m^{-2} (Wolff, 1987; Arntz and Tarazona, 1990), which is about 50 times the normal level. Yearly surveys of the macrobenthos of Independence Bay (Fig. 1) conducted by the Instituto del Mar del Perú (IMARPE) have also observed EN biomass decreases in several functional groups (e.g. macroalgae, benthic detritivores, herbivorous gastropods, predatory gastropods, portunid crabs, and polychaetes); while scallops proliferate to nearly replace polychaetes as the main benthic consumer of plankton and detritus (Fig. 2).

During both of the strong ENs of 1982/83 and 1997/98, *A. purpuratus* became the principal target of the diving fishery, which experienced "gold rush" conditions with high catches and enormous revenues (Wolff, 1987, 1988, 1994; Wolff and Mendo, 2000; Mendo and Wolff, 2002). The fishing effort increased mainly due to migration of fishers from other areas. Catches largely reflect actual changes in the scallop population. Other high-price species associated with the scallop habitat are octopus and crab. Crab catches decreased during the 1997/98 EN, but octopus landings increased nearly 5-fold. Pelagic predatory fish migrated towards the coast during EN, such that catch of the line and net fishing fleet increased by about 2.5 times.

While we have a good basic understanding of the main changes to benthic communities associated with EN in Peru, trophic modeling of the effects of EN has not yet been employed. Here we describe and model the Independence Bay ecosystem from an energy flow perspective. First, we compare steady-state trophic models of the system for the upwelling and El Nino conditions, and secondly we explore the drivers of these changes (trophic vs. environmental) using dynamic simulations with performance measured against time series data of changing biomass. In particular, we address the following questions: (i) Are the positive impacts observed in the shallow benthic community during EN (increase in species richness, and diversity) also reflected in the entire ecosystem through indicators of system maturity? (ii) How is the system reorganized during EN? (iii) What insight can be gained into the management of the fishery during EN? (iv) Can changes in biomass and productivities be explained by direct responses to warming, or to trophic interactions? (v) What is the trophic effect of the increased scallop biomass, the reduced primary production (through biomass decrease of phytoplankton as well as macroalgae), and the reduced crab predator biomass on the system?

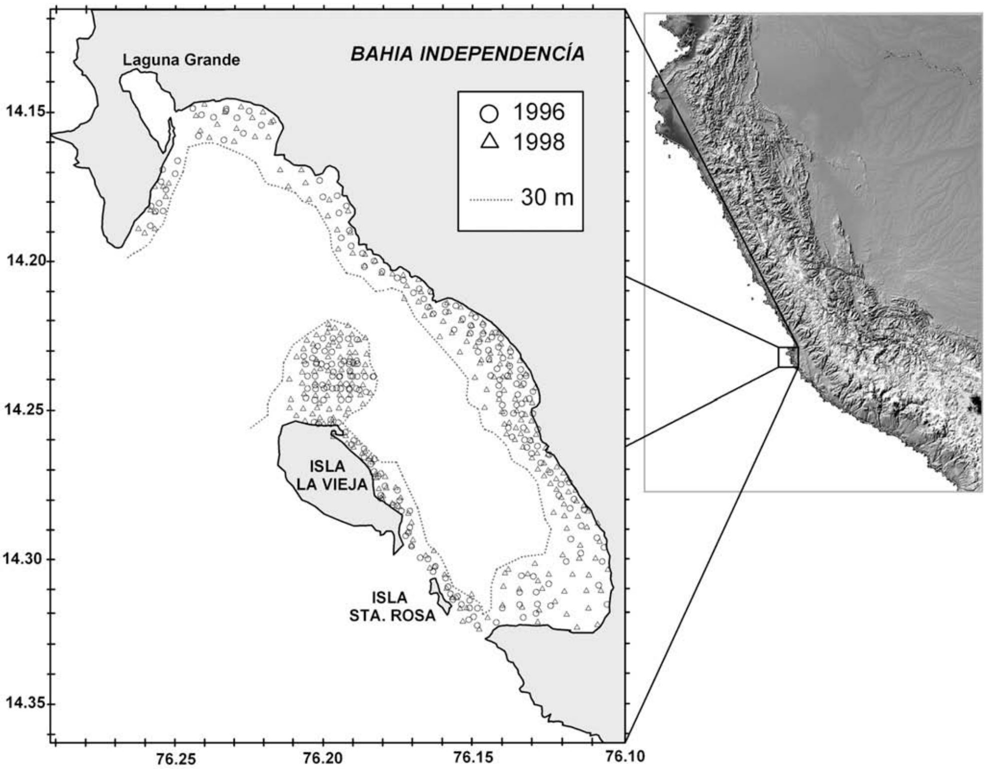

Fig. 1. Map of the Peruvian coast and the study site, Independence Bay. Macrobenthic fauna sampling stations are indicated by circles for 1996 ($n = 223$) and triangles for 1998 ($n = 252$). The 30 m depth isocline is indicated by a dashed line.

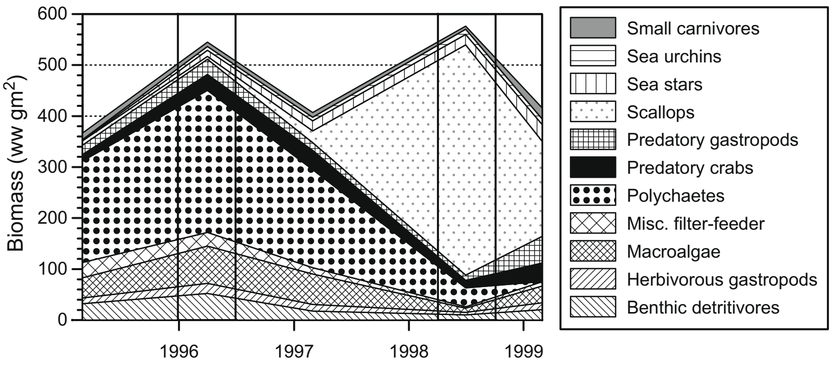

Fig. 2. Biomass changes of benthic macrofauna observed from 1995 to 1999 (IMARPE). Boxes indicate model periods.

2. Materials and methods

2.1. Study area

Independence Bay (14.238°S, 76.194°W) is located approximately 250 km southeast of Lima (Fig. 1). The bay is broadly open to the coastal ocean on either side of 'Isla La Vieja'. Conditions within the bay thus largely reflect the nearshore Peruvian upwelling system, characterized by low surface temperatures (14–18 °C) and high nutrient levels. Bottom (<30 m) oxygen concentrations averaging 3.5 mg L^{-1} during normal upwelling conditions, but in the deeper central part of the bay, low oxygen conditions prevail (<1.0 mg L^{-1}, >30 m) and benthic macrobiota is not abundant and microbial processes dominate. During a strong EN, temperatures increase as much as 10 °C and oxygen conditions are improved at the lower depths. Artisanal fisheries include a diving fishery using hookah and compressor, which operates around the bay's rocky and soft-bottom habitats less than 30 m, and a gillnet and line fishery that targets larger littoral and pelagic fish species.

2.2. Model definition

The two steady-state trophic models of Independence Bay were constructed for the soft-bottom habitats of <30 m depth that fringe the bay, covering about 38% of the total bay area (65.8 km^2 out of a total of 172 km^2; Fig. 1). This area was selected for the following reasons: (i) importance in overall bay macrobiota biomass, (ii) availability of data, and (iii) it encompasses the main activities of the artisanal fishery. Model periods are for 1996, representing a 'normal' upwelling year, and 1998, representing EN (end of the 1997/98 event; Fig. 2). The models were constructed with 20 functional groups including detritus, two primary producers (phytoplankton and macroalgae), zooplankton, six benthic primary consumers (polychaetes, scallops, sea urchins, herbivorous gastropods, benthic detritivores, and miscellaneous filter-feeders), five benthic carnivores (predatory gastropods, small carnivores, predatory crabs, sea stars, and octopus), three fish (littoral fish, small pelagic fish, and pelagic predatory fish), and two top predators (marine mammals and seabirds). These functional groups were designated according to ecological status – organisms within a group are characterized by similar diets, predators, productivities and individual body size (Table 1).

2.3. Basic modeling approach

A mass-balance modeling approach was applied using the software Ecopath with Ecosim 5.0 (EwE) (Christensen and Pauly, 1992; Walters et al., 1997), which quantifies trophic flows among functional groups within an ecosystem and also includes fishery catch. The model also permits the assessment of ecosystem dynamics under different scenarios of use or environmental change (http://www.ecopath.org). Ecopath links the production and consumption of all trophically connected groups within the model ecosystem, as

$$P_i = Y_i + B_i * M2_i + E_i + BA_i + P_i * (1 - EE_i) \tag{1}$$

where P_i is the total production rate of (i), Y_i is the total fishery catch rate of (i), B_i the biomass of the group (wet weight), E_i the net migration rate (emigration–immigration), $M2_i$ is the total predation rate for group (i), BA_i is the biomass accumulation rate for (i). $P_i{}^{*}$ $(1 - EE_i)$ is the 'other mortality' rate ($M0_i$), where EE is the "Ecotrophic efficiency" and is the proportion of the group's production that is consumed by higher trophic levels or is taken by the fishery (for further information, see Christensen et al., 2000). In order to ensure mass balance between the groups, a second master equation is used:

$$\textit{Consumption} = \textit{production} + \textit{respiration} + \textit{unassimilated food}$$

Energy flow in the model requires definition of the diet for all consumers, which determines the fraction of each functional group which will serve as food of the other groups. This diet matrix is further used in the calculation of the trophic level of each group:

$$TL_j = 1 + \sum TL_i * DC_{ij} \tag{2}$$

where DC_{ij} is the fraction of prey (i), in the diet of the predator (j). The trophic level of the predator TL_j is calculated as the mean trophic level of its prey ($\sum TL_i{}^{*} DC_{ij}$) plus 1.0. Primary producers and detritus groups are assigned a trophic level of 1.0.

2.4. Input parameters

Input parameters, detailed below, are derived from a number of sources which are listed in Table 2. Input values for 1996 and 1998 steady-state models can be found in 3.

2.4.1. Biomass

Benthic macrofauna biomass was from IMARPE surveys for the periods 19–29th April, 1996 and 15–24th July, 1998. A total of 223 and 252 1 m^2 quadrants were sampled during the two surveys, respectively. All epifauna and infauna of the upper 5 cm of sediment were collected by hand and placed in mesh bags of 5 mm mesh size. Organisms were later counted and weighed (for further information on sampling, see Samamé et al., 1985; Yamashiro et al., 1990). Groups of small epifauna (herbivorous gastropods, benthic detritivores, scallops, small carnivores) and polychaetes were increased by 25% to correct for undersampling. Miscellaneous filter-feeders (consisting mainly of infaunal bivalves) were increased by 100% to also correct for undersampling—much of this groupṕs biomass is found deeper than 5 cm. These biomass correc-

Table 1
Functional groups and representative species. Species listed are not exhaustive (small benthos groups show the most important species, representing >95% of biomass and/or species averaging >1 g m^2); **, groups/species not found/recorded in captures in 1998; *, groups/species found in 1998 but low in biomass; bold: groups/species not found/recorded in captures in 1996.

Functional group	Species
2. Macroalgae	*Rhodymenia* sp.*, *Macrocystis* sp.*, *Gigartina* sp.*, *Codium* sp.**, *Ulva* sp.*, ***Caulerpa* sp., *Lessonia nigrescens***
4. Polychaetes	*Diopatra* sp., ***Chaetopteridae***
5. Scallops	*Argopecten purpuratus*
6. Sea urchins	*Tetrapigus niger*, *Arbacia spatuligera*, *Arbacia* sp., *Loxechinus albus*, ***Strongylocentrotus*** sp.
7. Herbivorous gastropods	*Crepipatella dilatata*, *Crepipatella* sp., *Tegula euryomphalus*, *Tegula atra*, *Tegula* sp., *Crucibulum* sp., *Aplysia* sp., *Mitrella* sp.
8. Benthic detritivores	*Ophiuroidea**, *Pagurus* sp., *Eurypanopeus sp.**, *Taliepus marginatus* **
9. Misc. filter-feeders	Ascidians, *Aulacomya ater*, *Glycimeris ovata*, *Actinia* sp., *Prothothaca thaca*, *Sponges*, *Semele solida*, *Chama* sp.
10. Predatory gastropods	*Bursa ventricosa*, ***Bursa nana***, *Bursa* sp., *Thais chocolata*, *Thaididae* sp., *Priene rude*, *Cymatium weigmani*, *Cymathidae* sp., *Argobuccinum* sp.**, *Sinum cymba*
11. Small carnivores	*Oliva peruviana*, *Oliva* sp., *Nassarius dentifer*, *Nassarius gayi*, *Nassarius* sp., *Trophon* sp.**, *Crassilabrum crassilabrum*, *Natica* sp.**, *Xantochorus* sp., ***Solenosteria gatesi*, *Solenosteria* sp., *Polinices uber***
12. Predatory crabs	*Cancer setosus*, *Cancer porteri*, *Cancer coronatus***, *Cancer sp.*, *Hepatus chilensis*,, *Platyxanthus cockeri***, ***Callinectes arcuatus***, ***Callinectes sp***.
13. Sea stars	*Luidia bellonae*, *Luidia magallanica*, *Luidia* sp., *Asterina chilensis.***, *Patiria chilensis*, ***Heliaster helianthus***
14. Octopus	*Octopus mimus*
15. Littoral fish	*Isacia conceptionis*, *Seriolella violacea*, *Paralabrax humeralis*, *Cheilodactylus variegatus*, *Labrisomus philippii*, *Hemilutjanus macrophthalmos*, *Acanthistius pictus*, *Paralichthys adspersus*, *Cynoscion analis*, *Sciaena deliciosa*, *Calamus brachysomus*, *Mugiloides chilensis*, *Diplectrum conceptione*, *Chloroscombrus orqueta*, *Sphyraena ensis*, *S. idiastes*, *Myliobatis peruvianus*, *Orthopristis chalceus*, *Mugil cephalus*, ***Diplectrum conceptione***, ***Chloroscombrus orqueta***, ***Sphyraena ensis***, ***Sphyraena idiastes***, ***Myliobatis peruvianus***
16. Small pelagic fish	*Sardinops sagax sagax*, *Ethmidium maculatum*, ***Trachinotus paitensis***
17. Pelagic predatory fish	*Trachurus picturatus murphyi*, *Cilus gilberti*, *Scomber japonicus*, ***Sarda chiliensis chiliensis***, ***Auxis rochei***, ***Scomberomorus sierra***
18. Marine mammals	*Otaria byronia*, *Arctocephalus australis*
19. Seabirds	*Leucocarbo bougainvillii*, *Sula variegata*, *Pelecanus thagus*

tions were based on complementary benthic evaluations conducted by the authors.

Estimates of phytoplankton biomass for the 1996 model were taken from Peruvian coastal averages under ‘typical’ upwelling conditions (settled volume, 3.0 mL m^{-3}) (Rojas de Mendiola et al., 1985) and EN conditions (Delgado and Villanueva, 1998; Villanueva et al., 1998). EN phytoplankton values were increased slightly over coastal averages (+15%) in order to balance the model. Settled volumes were converted to g m^{-2} by assuming 1 mL = 1 g and then multiplying by an average depth for the model area of 15 m by assuming a well-mixed water column.

Information on zooplankton in Independence Bay is of qualitative nature only (Yamashiro et al., 1990); thus zooplankton biomass was left open to be calculated by the steady-state model assuming an Ecotrophic efficiency (*EE*) of 0.95.

Biomass of mobile species such as octopus and fish were estimated from catch data by assuming that the fishery takes 50% of yearly produced biomass. Small pelagic fish are not a principal target of the artisanal fishery and so catch estimates are likely poor indicators of the available biomass. Small pelagic fish biomass was thus left open to be calculated by the steady-state model assuming an *EE* of 0.95 (Table 3).

2.4.2. Catches

Estimates of catch were derived from IMARPE catch statistics for the artisanal fishery from the two main landing sites for Independence Bay – San Andres and Laguna Grande. Unfortunately, landings data do not identify habitat of capture, so that it was necessary to estimate the relative sizes of the bay’s habitats in the model (ca. 10% rocky, 90% soft-bottom) and correct for the fact that most rocky habitat catches are made outside the model area (ca. 10 × greater than within the model). Taking into account the associations of functional groups with particular habitats, their catch statistics were adjusted as follows: scallops and predatory crab catches come *only* from the soft-bottom habitats of the model and thus did not need correction; fish groups, octopus, and miscellaneous filter-feeders, *primarily* found in soft-bottom habitats, were reduced by only 10% to correct catches associated with rocky habitats. Conversely, catches of herbivorous gastropods, predatory gastropods, and sea urchins were mainly associated with broken shell or rocky substrates, and were thus reduced by 80% (Table 3).

2.4.3. Production/biomass (total mortality)

Direct estimates of production to biomass ratios (*P/B*) or Total mortality (*Z*) existed for several benthic invertebrate groups in the model – scallops, predatory crabs, and sea stars. Other groups were estimated using empirical relationships from Brey (2001) taking into account taxonomic group, mean body size, temperature of habitat, feeding modes, and habitat type. In most cases this provided realistic estimates; however, values for polychaetes and misc. filter-feeders were increased to 1.0 based on other estimates from the literature (Table 3).

P/B of phytoplankton was estimated using a modified Eppley curve (Eppley, 1972) as described by Brush et al. (2002):

$$G = G_{\max} * f * LTLIM * NUTLIM \tag{3}$$

where G = realized daily growth rate (d^{-1})(base e), f is the fraction of the day during which there is light, and *LTLIM* and *NUTLIM* are dimensionless ratios from 0 to 1 which describe light and nutrient limitation of growth, respectively (Kremer and Nixon, 1977). $G_{\max}$, as given by Eppley (1972) describes an exponentially-shaped envelope for growth rates of phytoplankton under culture conditions without light or nutrient limitation (as recalculated by Brush et al., 2002):

Table 2
Sources of input data. IE = IMARPE benthic macrofauna evaluation, EM = empirical model (Brey, 2001), EO = Ecopath output, GU = guess estimate, IC = iterative consumption routine (for opportunistic feeding; described herein), IS = IMARPE landings statistics.

Functional group/ parameter	Biomass – B_i (t km^{-2})	Production rate – P_i/B_i (y^{-1})	Consumption rate – Q_i/B_i (y^{-1})	Conversion efficiency – GE_i	Ecotrophic efficiency – EE_i	Catches – Y_i (t km^{-2} y^{-1})	Diet composition – DC
1. Phytoplankton	GU based on Rojas de Mendiola et al. (1985), Delgado and Villanueva (1998)	GU based on modified Eppley curve (Eppley, 1972; Brush et al., 2002)	–	–	EO	–	–
2. Macroalgae	IE	GU based on Macchiavello et al. (1987)	–	–	EO	–	–
3. Zooplankton	EO	GU based on Mendoza (1993), Hutchings et al. (1995)	GU adapted from Polovina and Ow (1985)	EO	GU	–	GU
4. Polychaetes	IE	GU based on Martin and Grémare (1997)	EO	GU	EO	–	GU
5. Scallops	IE	Mendo et al. (1987), Stotz and Gonzalez (1997)	GU based on Wolff (1994)	EO	EO	IS	GU based on Rouillon et al. (2002)
6. Sea urchins	IE	EM	EO	GU	EO	IS	GU
7. Herbivorous gastropods	IE	EM	EO	GU 0.3 based on Mann (1982)	EO	IS	GU
8. Benthic detritivores	IE	EM	EO	GU	EO	–	GU
9. Misc. filter-feeders	IE	GU based on Wolff (1994)	EO	GU	EO	IS	GU
10. Predatory gastropods	IE	EO	GE based on Huebner and Edwards (1981)	GU 0.3 based on Huebner and Edwards (1981)	EO	IS	GU, IC
11. Small carnivores	IE	EM	EO	GU	EO	–	GU partially based on Keen (1972) for gastropod spp., IC
12. Predatory crabs	IE	Wolff and Soto (1992)	Lang (2000), Wolff and Soto (1992)	EO	EO	IS	GU based on Leon and Stotz (2004), IC
13. Sea stars	IE	Ortiz and Wolff (2002)	EO	GU	EO	–	GU, IC
14. Octopus	GU based on catch data	EO	Wolf and Perez (1992), Vega and Mendo (2002)	Wolf and Perez (1992), Vega and Mendo (2002)	EO	IS	GU, IC
15. Littoral fish	GU based on catch data	GU 1.2 based on Wolff (1994)	EO	GU	EO	IS	GU based on FISHBASE (2006)
16. Small pelagic fish	EO	GU	EO	GU 0.1 based on Moloney et al. (2005)	GU	IS	GU based on FISHBASE (2006)
17. Pelagic predatory fish	GU based on catch data	GU 0.85 based on Jarre et al. (1991)	EO	GU 0.1 based on Moloney et al. (2005)	EO	IS	GU based on FISHBASE (2006)
18. Marine mammals	GU	GU based on Jarre et al. (1991)	EO	GU	EO	–	GU
19. Seabirds	GU	GU based on Moloney et al. (2005)	EO	GU based on Moloney et al. (2005)	EO	–	GU
20. Detritus	EO	–	–	–	–	–	–

Table 3

Input-output parameters for steady-state models of Independence Bay in 1996 and 1998 after application of the Ecoranger resampling routine. In bold, Ecopath calculated parameters. B_i = Biomass, P_i/B_i = production rate, Q_i/B_i = consumption rate, EE_i = ecotrophic efficiency, GE_i = gross efficiency or conversion efficiency (P_i/Q_i), F_i = fishing mortality, $M0_i$ = non-predation mortality, $M2_i$ = predation mortality.

Functional group/parameter	Trophic Level		B_i (t km^{-2})		P_i/B_i (y^{-1})		Q_i/B_i (y^{-1})		EE_i		GE_i		Catch (t y^{-1})		F_i		$M0_i$		$M2_i$	
	1996	1998	1996	1998	1996	1998	1996	1998	1996	1998	1996	1998	1996	1998	1996	1998	1996	1998	1996	1998
1. Phytoplankton	**1.00**	**1.00**	51.398	24.816	255.228	366.172	–	–	**0.340**	**0.958**	–	–	0.000	0.000	0.000	0.000	168.495	15.261	86.734	350.911
2. Macroalgae	**1.00**	**1.00**	69.204	8.656	15.840	17.954	–	–	**0.136**	**0.375**	–	–	0.000	0.000	0.000	0.000	13.685	11.217	2.155	6.737
3. Zooplankton	**2.23**	**2.26**	**28.270**	**29.425**	45.827	38.767	175.677	145.755	0.890	0.916	**0.261**	**0.266**	0.000	0.000	0.000	0.000	5.027	3.240	40.800	35.527
4. Polychaetes	**2.06**	**2.06**	324.892	45.927	0.899	1.042	**5.611**	**4.844**	**0.603**	**0.299**	0.160	0.215	0.000	0.000	0.000	0.000	0.357	0.731	0.542	0.311
5. Scallops	**2.00**	**2.00**	7.049	434.504	1.576	2.305	10.037	**14.789**	**0.806**	**0.458**	**0.157**	0.156	2.230	235.421	0.316	0.542	0.306	1.248	0.954	0.515
6. Sea urchins	**2.10**	**2.10**	7.925	11.040	0.551	0.650	**2.589**	**2.891**	**0.949**	**0.563**	0.213	0.225	1.458	0.002	0.184	0.000	0.028	0.284	0.339	0.366
7. Herbivorous gastropods	**2.00**	**2.00**	25.244	5.952	0.925	1.101	**2.778**	**3.793**	**0.788**	**0.943**	0.333	0.290	0.177	0.012	0.007	0.002	0.196	0.063	0.722	1.036
8. Benthic detritivores	**2.00**	**2.00**	70.679	11.314	0.989	1.337	**5.425**	**5.287**	**0.845**	**0.801**	0.182	0.253	0.000	0.146	0.000	0.013	0.153	0.267	0.836	1.057
9. Misc. filter-feeders	**2.24**	**2.22**	82.134	12.111	1.018	0.987	**4.859**	**4.762**	**0.949**	**0.994**	0.210	0.207	1.389	1.935	0.017	0.160	0.052	0.006	0.949	0.821
10. Predatory gastropods	**2.93**	**2.98**	28.104	10.955	**1.653**	**1.407**	4.731	4.549	**0.805**	**0.640**	0.349	0.309	1.326	1.838	0.047	0.168	0.322	0.506	1.284	0.733
11. Small carnivores	**2.96**	**2.99**	9.974	7.595	0.897	0.790	**4.952**	**3.705**	**0.918**	**0.865**	0.181	0.213	0.000	0.000	0.000	0.000	0.073	0.106	0.824	0.684
12. Predatory crabs	**3.35**	**3.09**	27.781	14.870	2.165	2.191	9.889	9.092	**0.930**	**0.191**	**0.219**	**0.241**	3.417	1.673	0.123	0.113	0.151	1.772	1.891	0.306
13. Sea stars	**3.11**	**3.03**	11.567	20.286	0.692	0.734	**3.254**	**3.446**	**0.860**	**0.304**	0.213	0.213	0.000	0.000	0.000	0.000	0.097	0.511	0.595	0.223
14. Octopus	**3.57**	**3.15**	0.315	1.425	4.878	4.809	**11.441**	**12.361**	**0.846**	**0.614**	0.426	0.389	0.749	3.153	2.377	2.212	0.750	1.854	1.750	0.742
15. Littoral fish	**2.86**	**2.99**	1.774	0.353	1.307	1.139	**10.426**	**10.281**	**0.846**	**0.951**	0.125	0.111	0.977	0.206	0.551	0.584	0.201	0.056	0.555	0.500
16. Small pelagic fish	**2.24**	**2.26**	**5.869**	**23.144**	1.939	2.168	**20.868**	**17.957**	0.967	0.867	0.093	0.121	0.298	0.195	0.051	0.008	0.063	0.288	1.825	1.871
17. Pelagic predatory fish	**3.24**	**3.26**	1.360	11.516	0.771	0.845	**7.928**	**7.710**	**0.679**	**0.449**	0.097	0.110	0.584	4.349	0.430	0.378	0.248	0.466	0.093	0.002
18. Marine mammals	**3.45**	**3.39**	0.052	0.010	0.101	0.100	**49.087**	**38.278**	**0.000**	**0.000**	0.002	0.003	0.000	0.000	0.000	0.000	0.101	0.100	0.000	0.000
19. Seabirds	**3.30**	**3.33**	0.056	0.009	0.034	0.036	**62.560**	**52.151**	**0.000**	**0.000**	0.001	0.001	0.000	0.000	0.000	0.000	0.034	0.036	0.000	0.000
20. Detritus	**1.00**	**1.00**	–	–	–	–	–	–	**0.187**	**0.483**	–	–	0.000	0.000	0.000	0.000	0.000	0.000	0.000	0.000

$$G_{\max} = 0.97 * e^{0.0633*T} \tag{4}$$

where T = water temperature. The 'normal' upwelling phytoplankton production 1996 assumed a mean temperature of 16 °C with 50% light (from self-shading) and 0% nutrient limitation factors, while the EN condition of 1998 assumed a mean temperature of 26 °C with 80% light and 50% nutrient limitation factors. Calculated *P*/*B* ratios were high (245 and 365 for 1996 and 1998, respectively) yet the value of total production for the 1996 model in terms of carbon, i.e. ~800 g C m^{-2} yr^{-1}, using a wet weight:C conversion of 14.25:1 from Brown (1991), is conservative with respect to other estimates for the Peruvian coastal system under upwelling conditions, i.e. >1000 and >1500 g C m^{-2} yr^{-1} from Walsh (1981) and Chavez and Barber (1985), respectively. *P*/*B* values for other groups are taken from the literature (Table 2).

2.4.4. Consumption and Conversion efficiency

Direct estimates of consumption rates (*Q*/*B*) were available for a few of the benthic invertebrate groups (octopus, scallops, predatory gastropods, and predatory crabs). For most other groups, ratios of Conversion efficiency (*GE*) or the ratio between Production and Consumption (*P*/*Q*) were applied (Tables 2 and 3).

2.4.5. Diet matrices

Direct diet studies for Independence Bay are limited and thus general knowledge from literature was used in the construction of diet matrices (Table 2). Initial attempts to balance the 1996 model resulted in insufficient production of many smaller epifaunal herbivore and detritivore invertebrate groups (scallops, sea urchins, herbivorous gastropods, benthic detritivores, and misc. filter-feeders) to meet the initial consumption values of the carnivorous benthic invertebrate groups (predatory gastropods, small carnivores, predatory crabs, sea stars, and octopus). As macroinvertebrate groups are described to be rather unselective and opportunistic feeders, limited more by their modes of feeding (Wilson and Parkes, 1998), diet proportions were adjusted to reflect both predatory consumption rates and the available production of prey groups. This was accomplished by iteratively distributing the prey production to the predators in weekly consumption increments, assuming unselectivity. When the production of a single prey group was completely utilized, the following iteration would consider only those prey not fully utilized. Base values of detritus feeding were assumed and the calculated diets resulted in high proportions of polychaetes in their diets – reflecting their high biomass and production in the benthic system in 1996. The 1998 situation was less problematic due to a reduction of carnivorous benthic invertebrate biomass as well as an increase in scallop biomass as prey (see Section 3). Assuming that scallops would be favored prey, their proportion in diet was set high (60–75%) and the remaining diets were calculated as above (Table 4). Diets for fish species were obtained from FishBase (Froese and Pauly, 2006) and were adjusted to the fish groups based on relative species contribution from recorded catches.

2.5. Addressing parameter uncertainty

The balanced steady-state model for 1996 was subjected to the EwE resampling routine *Ecoranger* (Christensen and Walters, 2004) in order to assess the probability distributions of the input parameters. Using a Monte Carlo approach, the routine drew a set of random input variables from normal distributions for each basic parameter, and all resulting combinations that satisfied mass-balanced constraints were recorded. Originally we allowed the routine to use confidence intervals as derived from a pedigree of the data sources, where highest confidence is placed in locally-derived data; however, the initial results often gave parameter values

Table 4
Diet matrices for steady-state trophic models of Independence Bay for 1996 and 1998 after application of the Ecoranger resampling routine (values of 0.000 indicates a proportion of <0.0005).

Prey/predator	Model	3	4	5	6	7	8	9	10	11	12	13	14	15	16	17	18	19
1. Phytoplankton	1996	0.702	0.293	0.787				0.709							0.802			
	1998	0.698	0.301	0.821				0.721							0.795			
2. Macroalgae	1996				0.811	0.783	0.191							0.235				
	1998				0.808	0.801	0.226							0.255				
3. Zooplankton	1996	0.190	0.051					0.195		0.002				0.513	0.198	0.470		
	1998	0.208	0.047					0.175		0.002				0.340	0.205	0.521		
4. Polychaetes	1996				0.090				0.398	0.462	0.292	0.384		0.207				
	1998				0.091				0.052	0.074	0.027	0.039		0.094				
5. Scallops	1996								0.018	0.011	0.011	0.014	0.065					
	1998								0.746	0.613	0.765	0.758	0.743					
6. Sea urchins	1996									0.030		0.032						
	1998									0.059		0.034						
7. Herbivorousgastropods	1996								0.046	0.037	0.032	0.033	0.069					
	1998								0.026	0.031	0.016	0.017	0.033	0.019				
8. Benthic detritivores	1996								0.159	0.149	0.094	0.106	0.194	0.003				
	1998								0.055	0.072	0.028	0.034	0.056	0.015				
9. Misc. filter feeders	1996								0.196	0.164	0.134	0.164	0.220					
	1998								0.049	0.056	0.025	0.029	0.030					
10. Predatory gastropods	1996										0.108	0.145	0.255	0.001				
	1998										0.033	0.037	0.050	0.031				
11. Small carnivores	1996								0.020	0.015	0.015	0.014	0.045	0.000				
	1998								0.021	0.030	0.012	0.016	0.027	0.024				
12. Predatory crabs	1996										0.191			0.001				
	1998										0.033			0.028				
13. Sea stars	1996										0.025			0.000				
	1998										0.031			0.093				
14. Octopods	1996												0.153					
	1998												0.060					
15. Littoral fish	1996													0.001			0.251	0.093
	1998													0.026			0.098	0.100
16. Small pelagic fish	1996													0.001		0.530	0.699	0.907
	1998													0.015		0.479	0.847	0.900
17. Pelagic predatory fish	1996																0.050	
	1998																0.055	
18. Marine mammals	1996																	
	1998																	
19. Seabirds	1996																	
	1998																	
20. Detritus	1996	0.108	0.655	0.213	0.099	0.217	0.809	0.096	0.164	0.129	0.097	0.109		0.038				
	1998	0.094	0.653	0.179	0.101	0.199	0.774	0.104	0.051	0.063	0.032	0.036		0.059				

outside of reasonable biological constraints (e.g. high conversion efficiencies, high cannibalism) and thus we decided to fix all confidence intervals at 20% variation as was similarly done by Arias-González et al. (1997). We allowed resampling until 10,000 runs passed the selection criteria. The 'best' run was then chosen as that with the smallest sum of square residuals between the input parameters and the mean value of all successful runs (for more information, see Christensen et al., 2000).

2.6. Outputs/system statistics

Statistics for comparison of the two system states fall under the categories of community energetics, cycling indices, and system organization. Comparisons of the 'health' and maturity of the two system states drew on statistics from all three areas. Further general descriptive statistics from the calculated outputs of the models included: (i) total throughput (*T*) – measure of the total sum of flows within the system and indicates the 'size' or activity of the system; (ii) contributions to *T* from different types of flows – consumption, export, respiration and flows to detritus; (iii) breakdown of biomass and flows from different components of the system – pelagic vs. benthic biomass and production; and (iv) changes in feeding modes – Herbivory: detritivory ratios.

2.6.1. Community energetics

Several indices of community energetics allowed for the comparison of ecological succession and relative maturity according to Odum (1969) and include: (i) total primary production (*PP*) to total respiration (*R*) ratio (*PP*/*R*); (ii) biomass (*B*) supported by total primary production (*PP*/*B*); (iii) biomass supported by total throughput (*B*/*T*); and iv) energy transfer efficiency (*TE*) between discrete trophic levels.

2.6.2. Cycling indices

The Finn's cycling index (*FCI*) (Finn, 1976) is calculated as *Tc*/*T*, where *Tc* is the amount of system flows that are recycled compared to the total system throughput, *T*. According to Odum (1969) recycling increases in more mature and less stressed systems.

2.6.3. Growth and development indices

Global measurements of system organization are calculated according to a network analysis based on flows among elements in the system as defined by Ulanowicz (1986). Indices include the aforementioned throughput (*T*), along with a measure of ascendancy (*A*), and development capacity (*C*). Ascendancy incorporates both size and organization of flows into a single measure and is calculated as throughput (*T*) multiplied by mutual information (*I*), which concerns the diversity and evenness of flows between compartments (Baird et al., 1998). Development capacity is the theoretical upper limit to ascendancy and thus the dimensionless *A*/*C* ratio allows for a comparable measure of ecosystem development and is predicted to be higher in more mature ecosystems (Ulanowicz, 1986). The difference between development capacity and ascendancy (*C*–*A*) is the system overhead (Φ) and gives a measure of the system's 'strength in reserve' from which it can draw to meet perturbations (Ulanowicz, 1986).

2.6.4. Fishery

Other statistics allow for the assessment of the fishery activity such as its Gross efficiency (catch/net *PP*), mean trophic level of the catch, and primary production needed to sustain the fishery.

2.7. Simulating transition from upwelling to El Niño state

The simulation runs conducted for this study with EwE calculate biomass changes through time by solving the set of differential equations:

$$dB_i/dt = g_i\left[\sum\nolimits_k Q_{ki}(t)\right] - \sum\nolimits_j Q_{ij}(t) - M0_iB_i - \sum F_{if}(t)B_i \tag{5}$$

For species or functional groups $i = 1, \ldots, n$. The first sum represents the food-consumption rate, *Q*, summed over prey types *k* of species *i*, and g_i represents the growth efficiency (proportion of food intake converted into production). The second sum represents the predation loss rates over predators *j* of *i*. $M0_i$ represents the instantaneous natural mortality rate due to factors other than modelled predation. The final sum represents the instantaneous fishing mortality rate, *F*, as a sum of fishing components caused by fishing fleets *f*.

The Q_{ij} are calculated by assuming that the B_i are divided into vulnerable and invulnerable components (Walters et al., 1997), and it is the flux rates v_{ij} and v'_{ij} that move biomass into the vulnerable and invulnerable pools, respectively. This assumption leads to the rate equation:

$$Q_{ij} = \frac{a_{ij}(t)v_{ij}(t)B_iB_j}{v_{ij}(t) + v'_{ij} + a_{ij}(t)B_j} \tag{6}$$

where the v_{ij} and v'_{ij} parameters represent rates of behavioral exchange between vulnerable and invulnerable states and a_{ij} represents rate of effective search by predator *j* for prey type *i*. The exact setting of the v_{ij}, remains uncertain, but the modeling software allows for adjusting the vulnerabilities by a fitting procedure through which the sum of squares between observed and simulated (log) biomasses are minimized (see Walters et al., 1997). In EwE, the vulnerabilities for each predator–prey interaction can be explored by the user and settings will determine if control is top-down (i.e., Lotka-Volterra; >2.0), bottom-up (i.e., donor-driven; <2.0), or intermediate (≈2.0). We applied this fitting routine with our time series, and the computed vulnerabilities were then discussed in the light of possible control mechanisms operating in the ecosystem.

As input for simulations of the ecosystem response to ENSO we used catch per unit of effort (CPUE) time series for the fishery

Table 5
Biomass data for model groups derived from IMARPE benthic surveys in Independence Bay (1996, 1997, 1998, and 1999). Longer time series (1996–2003) were calculated from estimates of catch per unit effort (CPUE). Relative CPUE changes were used to reconstruct the longer time series relative to the 1996 starting values from the steady-state model.

Year/groups	Pp-1	Ma-2	Po-4	Sc-5	Su-6	Hg-7	Bd-8	Mf-9	Pg-10	Sc-11	Pc-12	Ss-13	Oc-14	Lf-15	Ppf-17
1996	51.4	69.2	324.9	7.0	7.9	25.2	70.7	82.1	28.1	10.0	27.8	11.6	0.3	1.8	1.4
1997	28.6	56.6	224.2	28.5	7.4	16.5	24.2	37.7	14.5	10.6	31.4	19.6	0.7	1.5	1.8
1998	28.6	7.6	43.5	564.2	10.9	6.7	13.8	8.2	9.8	6.8	4.5	20.1	0.2	0.2	2.7
1999	51.4	31.1	0.2	233.3	11.7	17.1	27.8	26.7	49.2	25.2	13.9	32.3	0.1	1.7	1.3
2000	51.4			120.6							29.8		0.1	2.4	0.3
2001	51.4			16.1							73.8		0.1	2.4	9.3
2002	51.4			2.7							41.6		0.1	3.5	3.5
2003	51.4			3.7							39.2		0.1	3.8	3.9

resources for the period 1996–2003 (including the EN year 1998) as proxies for stock biomass, together with biomass data obtained from the benthic surveys done by IMARPE for the years 1996, 1997, 1998 and 1999 (Table 5).

To distinguish between trophic and non-trophic effects on functional group biomass changes, we forced biomass changes of several functional groups (drivers) in the model to measure their impact. Drivers included biomass changes in 4 highly-variable functional groups whose abundances are known to be at least partially controlled by non-trophic environmental changes associated with ENSO: phytoplankton (*PP*), macroalgae (*MA*), predatory crabs (*C*) and scallops (*S*). We successively forced the biomass changes of these groups for the simulated time period of 8 years (1996–2003) and recorded the changes in fit as calculated by the sum of squares between the predicted and observed estimates.

An initial exploration of the dynamics using the default predator–prey vulnerability settings for all interactions either decreased the fit of the simulation or made only small improvements. Thus, we decided to first introduce all four drivers in combination and allowed EwE to search for the best predator–prey vulnerability settings. Using these optimized vulnerability settings we again addressed the importance of each driver through single or combined introduction to force the model through time.

3. Results

3.1. General descriptive

Initial parameters of the balanced model can be found on the Pangaea website (Taylor et al., 2007a, b). The Ecoranger resampling routine resulted in balanced models in 0.75% and 2.20% of the runs for the 1996 (normal conditions) and 1998 (EN conditions) models, respectively. The 'best' fitting model parameters are shown in Table 3. Summary statistics are presented in Table 6. The 'size', as measured by the total system throughput (*T*), indicates that the 1996 state was larger than 1998 (34,208 vs. 24,827 t km^{-2} yr^{-1}) mainly as a function of higher primary production. Contributions to *T* from different types of flows indicate that the EN state is characterized by higher absolute and relative flows due to consumption (11,918 t km^{-2} yr^{-1} and 48.0% of *T*) and respiration (7097 t km^{-2} yr^{-1} and 28.6% of *T*) and lower absolute and relative flows into detritus (14.8% of *T*) and as exports (8.6% of *T*). These results indicate better utilization of primary production through increased consumption and decreased losses to detritus as is reflected by the increased *EE* values for phytoplankton and detritus compartments. The overall ratio of herbivory to detritivory feeding decreased slightly during 1998 (6.54 and 5.22 for 1996 and 1998, respectively). Ratios between pelagic and benthic biomass and production were similar for both 1996 and 1998 states with the benthic system dominating in terms of biomass (pelagic/benthic biomass ratios equal 0.13 and 0.14 for 1996 and 1998, respectively) while the pelagic components accounted for most of the production (pelagic/benthic production ratios equal 8.46 and 7.79 for 1996 and 1998, respectively). Besides major changes in primary production between the two periods, which greatly impacted *T*, the overall biomasses of trophic levels II and above are virtually unchanged despite significant changes to several individual functional groups.

3.2. Community energetics

Several statistics on community energetics point to EN conditions as being of a higher 'maturity' than normal conditions. The primary production to total respiration ratio (*PP*/*R*) came closer to the proposed value of 1.0 for mature systems (Odum, 1969) (2.979 in 1996; 1.302 in 1998). Total primary production to biomass (*PP*/*B*) and biomass to total throughput (*B*/*T*) ratios indicated

Table 6
System statistics, cycling indices, and informational indices for the two modeled periods of Independence Bay. Changes in values from the 1996 state to the 1998 state are given as a percent; values in brackets are in percent of total system throughput.

Summary statistics	1996	1998	% Change
Sum of all consumption (t km^{-2} yr^{-1})	8389 (24.5%)	11,919 (48.0%)	42.1
Sum of all exports (t km^{-2} yr^{-1})	9444 (27.6%)	2145 (8.6%)	−77.3
Sum of all respiratory flows (t km^{-2} yr^{-1})	4772 (14.0%)	7097 (28.6%)	48.7
Sum of all flows into detritus (t km^{-2} yr^{-1})	11603 (33.9%)	3666 (14.8%)	−68.4
Total system throughput (t km^{-2} yr^{-1})	34208	24827	−27.4
Sum of all production (t km^{-2} yr^{-1})	16133	11610	−28.0
Calculated total net primary production (t km^{-2} yr^{-1})	14214	9242	−35.0
Net system production (t km^{-2} yr^{-1})	9442	2146	−77.3
Total biomass (excluding detritus) (t km^{-2})	754	674	−10.6
Pelagic/benthic biomass	0.13	0.14	15.6
Pelagic/benthic production	8.46	7.79	−8.0
Connectance index	0.222	0.224	0.9
System omnivory index	0.169	0.122	−27.8
Herbivory/detritivory	6.54	5.22	−20.2
Fishing			
Total catches (t km^{-2} yr^{-1})	12.605	248.930	1874.9
Mean trophic level of the catch	2.73	2.05	−24.9
Gross efficiency (catch/net PP)	0.001	0.027	2936.5
PP required/catch	29.39	9.26	−68.5
PP required/total PP (%)	1.43	17.85	1148.3
Community energetics			
Total primary production/total respiration	2.979	1.302	−56.3
Total primary production/total biomass	18.861	13.715	−27.3
Total biomass/total throughput	0.022	0.027	22.7
Cycling indices			
Finn's cycling index (% of total throughput)	5.11	8.88	73.8
Predatory cycling index (% of throughput w/o detritus)	9.07	5.14	−43.3
System development			
System overhead/capacity (%)	67.0	72.5	−1.2
Ascendancy/capacity (%)	33.0	27.5	−16.7

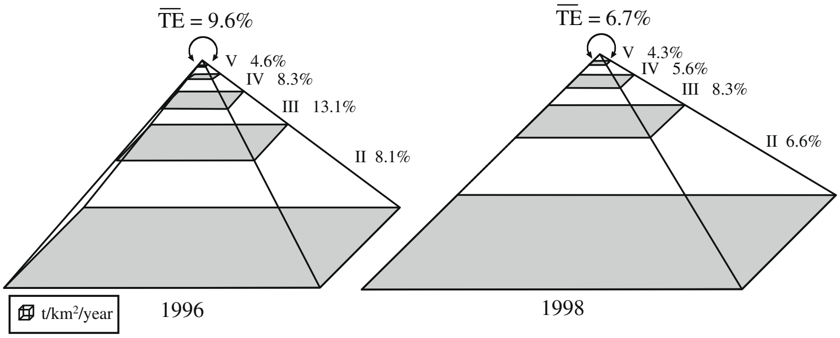

Fig. 3. Modified Lindeman pyramids of flows for steady-state models of Independence Bay. Transfer efficiencies are given for discrete trophic levels. Mean transfer efficiency is the geometric mean of trophic levels II–IV.

that the 1998 state could support a higher relative biomass per unit of primary production and total throughput. On the contrary, mean transfer efficiency (*TE*) was higher for the 1996 state (Fig. 3) due in part to a high utilization of herbivore and detritivore production by predatory invertebrates, as well as higher cannibalism, and can be observed in the high *EE* values for these groups (groups 5–14, Table 3). This 'bottleneck' of flows did not occur in 1998 due both to a decrease in predator biomass and an increase in primary consumer biomass due to the proliferation of scallops. As *TE* can only be calculated for consumer groups, and Ecopath does not quantify solar energy input to producer compartments, mean *TE* reflects the geometric mean of trophic levels II–IV only. Thus, the decrease in *TE* occurred despite an overall improvement in other holistic community energetic indices in 1998; specifically, a higher utilization of primary production and detritus.

3.3. Cycling indices

A higher degree of cycling, as indicated by the Finn's cycling index, was calculated for the EN period (5.11% for 1996; 8.88% for 1998). Again, the higher utilization of primary production and detritus was mainly responsible for this result. Removing this influence is possible with the related Predator cycling index, which showed that the 1996 state had more cycling at the higher trophic levels (9.07% for 1996; 5.14% for 1998).

3.4. Growth and development indices

The ascendancy to development capacity ratio (*A/C*) was slightly higher during normal upwelling conditions in 1996 (33.0% for 1996; 27.5% for 1998) and indicates that this state shows more maturity (i.e. higher total flows and predictability of flows).

3.5. Fishery

The boom of *A. purpuratus* during EN was mostly responsible for the more than 18-fold increase in total catches for the model area, to 248.9 t km^{-2} yr^{-1}. Pelagic predatory fish catches also increased about 7-fold, and as a result the model back-calculated a higher small pelagic fish biomass for 1998. The gross efficiency (catch/net *PP*) of the fishery increased 25-fold and the primary production required per unit of catch decreased, due mainly to the lower trophic level of the scallop (mean *TL* of catch – 2.74 and 2.05 for 1996 and 1998, respectively). The variable nature of the diving effort in response to changing resource abundances also played an important role. As the catch of scallops mainly drove the changes in effort, scallops show fairly similar fishing mortality (*F*) values for the two periods, while other groups that were reduced in biomass during 1998 show higher *F* values (misc. filter-feeders and predatory gastropods) (Table 3). Overall, the expansion of the fishery, combined with the decreased primary productivity, resulted in a value of 18% of total primary production needed to sustain the fishery – an 11-fold increase from 1996.

3.6. Functional group responses to forcing scenarios

The results of the forcing of trophic driver biomasses on the dynamics of remaining functional groups are presented for four scenarios in the following paragraphs.

3.6.1. Scenario 1 (S1): Decrease in primary production during EN (due to lack of nutrient upwelling)

As shown by Fig. 4, a decrease in phytoplankton and macroalgae biomass during EN (1997/98) resulted in decreases in polychaetes, misc. filter-feeders and herbivorous gastropods. A slightly lagged response is also seen in predatory gastropods, which decreased in biomass. While the single addition of the macroalgae driver decreased SS more than did that of the phytoplankton driver (−8.1% for macroalgae; −2.7% for phytoplankton), the average change in combination with other drivers was greater from the phytoplankton driver at −2.8% (Fig. 5).

3.6.2. Scenario 2 (S2): Decrease in predatory crab biomass during EN (due to temperature stress causing mortality and migration to deeper waters)

The application of this driver resulted in a small increase in biomass of the groups sea stars and small carnivores as a result of the reduced crab biomass (Fig. 4). The application of the predatory crab driver resulted in an average change of −4.8% in SS (Fig. 5).

3.6.3. Scenario 3 (S3): Increase in scallop biomass during EN (due to increased recruitment and growth)

Fig. 4 shows the functional group responses to the increased Scallop biomass during the EN warming, which included: (1) abundance increases in predatory gastropods, small carnivores, octopus, sea stars, and (2) abundance decreases in the groups polychaetes, herb. gastropods, benthic detritivores, and misc. filter-feeders. The model also predicts an increase in predatory crab biomass, which is contrary to the observed decrease, supporting the observation that EN warming likely induced a non-trophically mediated mass mortality and emigration of crabs to deeper, cooler waters (Arntz and Fahrbach, 1991). Despite some improvements, the average change from the application of the scallop driver was an increase of 1.8% in SS (Fig. 5), indicating a decrease in fit.

3.6.4. Scenario 4 (S4): Combined forcing of all four drivers (scallops, phytoplankton, macroalgae, and predatory crabs)

The previously mentioned improvements from each driver sum upto explain the dynamics in the majority of groups (Fig. 4). In most cases, the forced dynamics are similar to a dominating individually

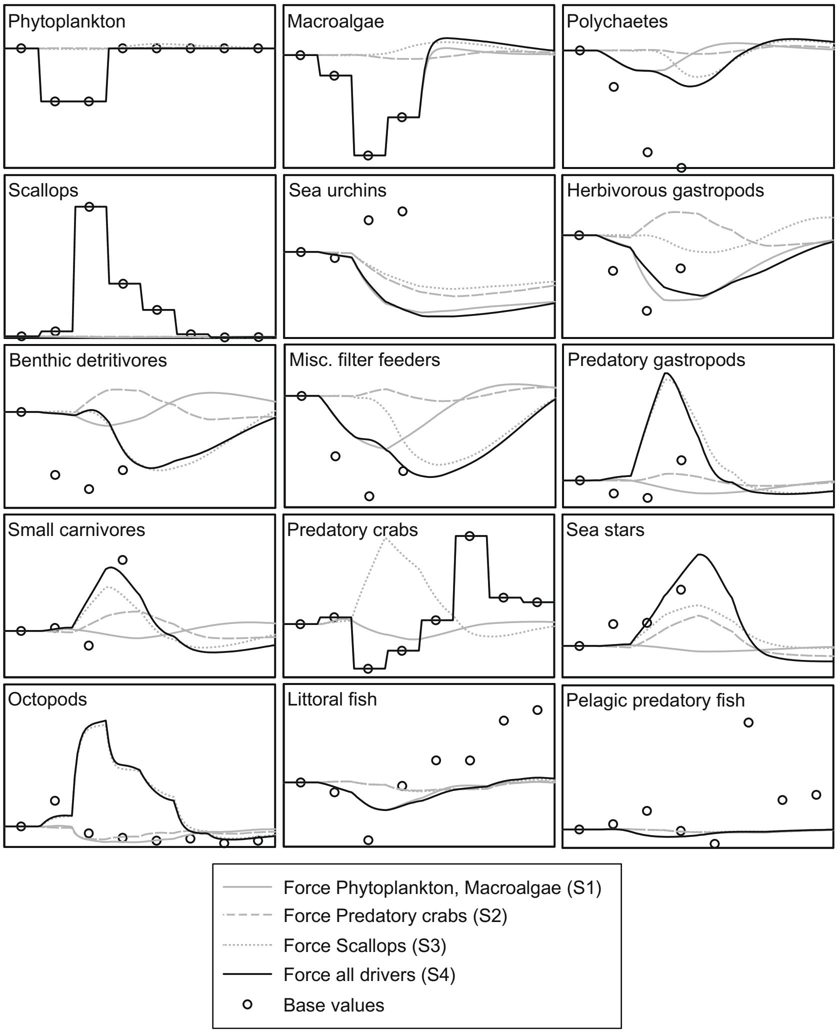

Fig. 4. Simulated versus observed biomass changes. All simulations consider changes in fishing effort (fishing and diving). Simulation trajectories are shown for each of the three scenarios (S1, bottom-up effect of reduced primary production – "Force Phytoplankton, Macroalgae"; S2, top-down effect of reduced benthic predation – "Force predatory crabs"; and S3, effect of scallop proliferation – "Force scallops") plus a combination of all four drivers applied together (S4, "Force all drivers").

forced driver; however, the dynamics of small carnivores and sea stars are improved by the combined application of all four drivers.

3.7. Vulnerability estimates

Table 7 summarizes the vulnerabilities computed for Scenario 4. v-values <1.2 were considered bottom-up control (BU), between 1.2 and 2 (mixed control, MX) and above 2 top-down control (TD).

Accordingly, top-down control is suggested for: (i) predatory gastropods on polychaetes, benthic detritivores and misc. filter-feeders; (ii) predatory crabs on scallops; and (iii) sea stars on predatory gastropods.

Bottom-up control configurations are more dominant and are suggested for: (i) polychaetes to predatory crabs; (ii) scallops to predatory gastropods and octopus; (iii) primary producers and zooplankton prey to fish groups; and (iv) littoral fish and small pelagic fish to marine mammals and seabirds.

4. Discussion

4.1. Summary statistics, flow structure and maturity

The total energy throughput of the Independence Bay ecosystem under normal upwelling conditions (1996 model; T = 34,208 t km^{-2} yr^{-1}) is higher than has been observed for other coastal zones along the Pacific coast, specifically, Gulfo Dulce, Costa Rica (T = 1404) and Tongoy Bay, Chile (T = 20,835 t km^{-2} yr^{-1}) (Wolff, 1994; Wolff et al., 1996), due mainly to its high primary production. When our results are compared to models of specific habitats in Tongoy Bay as constructed by Ortiz and Wolff (2002), the sand-gravel habitat is most similar in terms of total throughput (T = 33,579 t km^{-2} yr^{-1}). This type of substrate is typical of Independence Bay and is associated with strong currents where oxygen concentrations are increased through mixing and circulation and permit higher macrofaunal biomass. Similar values of production, energy flows to detritus, respiration, and exports are also observed between this habitat in Tongoy Bay and the model of Independence Bay under upwelling conditions.

While our estimate of Total throughput is not directly comparable to models that use differing units to describe flows (e.g. dry weight or carbon units), we can compare the proportions of different types of flows. Flow to detritus in Independence Bay during 1996 (33.9%) is similar to that of Tongoy (29%) as well as several US bay systems; e.g. Narragansett Bay (33%), Delaware Bay (30%), and Chesapeake Bay (27%) (Monaco and Ulanowicz, 1997). However, only the models of the South American bays calculated high proportions of exports as well (29–34% vs. 7–10% for US bays). Part of the difference may be attributable to higher exchange rates/low

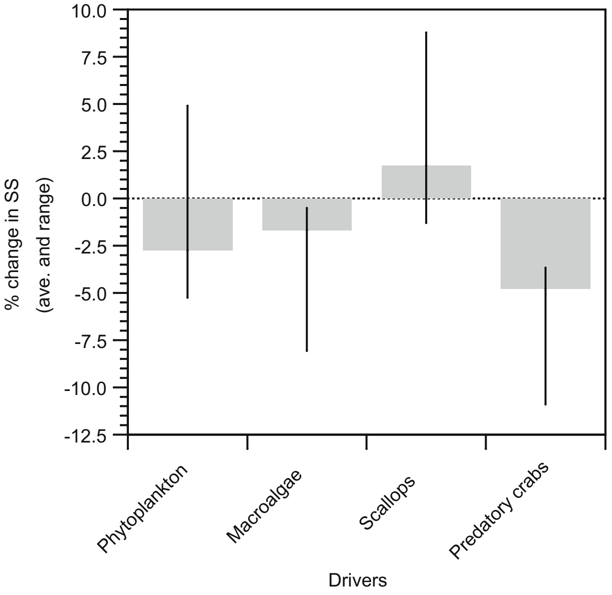

Fig. 5. Percent changes to sum of squares, *SS*, of the 1996–2003 simulation after the forcing of biomass changes of several functional groups 'drivers'. Drivers were applied in all possible sequences and combinations and *SS* was corrected for artificial improvements caused by the fitting of the driver's dynamics. Average change (bar) and range (line) are displayed. Negative values (i.e. decrease in *SS*) indicate an improvement in fit.

residency time of water in relatively open bays like Independence and Tongoy, resulting in more export of production (Rybarczyk et al., 2003); however, the high degree of primary production going unutilized and remaining in the sediments may be more typical of upwelling systems.

The dynamic nature of the artisanal fishery in response to changes in resources helps maintain the ecosystem's efficiency in the face of reduced predation pressure. In response to the scallop boom during EN, fishers migrated to Independence Bay. A main proportion of these migrant fishers were from Sechura Bay in the north of Peru (6 °S), where the largest fishery for scallops is normally found. These fishers were mainly involved in the diving fishery, which increased in effort by 170% in 1998 compared to the previous year. Peak diving effort reached 4932 boat trips per month (October 1998) compared to normal levels of around 750. Fishers also shifted effort to almost exclusively target scallops, yet other soft-bottom species were also taken. Octopus (*Octopus mimus*) is a particularly favored resource due to high price, and also increases in biomass during EN (Arntz et al., 1988). *O. mimus* growth and reproduction have been shown to increase under warmer conditions (Cortez et al., 1999) and embryonic development time is also greatly accelerated under EN-like conditions in the laboratory (Warnke, 1999). The increased catch of octopus is thus likely supported by increased production. Catch of pelagic predatory fish also increased, which may be explained through the overall shrinkage of the upwelling zone during EN and the subsequent intrusion of oceanic waters, which several predatory fish species are associated with (e.g. *Scomber japanicus, Sarda chilensis*, and *Scomberomerus sierra*). This movement may be further related to the pursuit of prey, as anchovy stocks were observed to both concentrate near the coast and then retreat southward to the latitudes near Independence Bay as recorded by acoustic surveys (Ñiquen and Bouchon, 2004).

The expansion of the diving fishery during EN is also observed through much higher indices of gross efficiency (catch/net PP) such that 18% of total primary production required to sustain the fishery. This value is lower than the value (25.1%) calculated by Pauly and Christensen (1995) for upwelling systems, and may reflect low mean trophic level of the fishery (2.05). Nevertheless, for an artisanal fishery, it shows a remarkable efficiency of harvest during EN. On the contrary, the value for normal conditions is extremely low at 1.4%, and illustrates the low level of exploitation of the fishery during normal upwelling periods, likely due to the low abundance of higher priced species like scallops and octopus. As a result, Independence Bay fishers are moving towards a combination of fishing and culture of scallops to maintain income levels between EN "boom times".

Nixon (1982) showed that there is a highly positive correlation between primary production and fishery yield in coastal lagoons, yet Independence Bay catches are highest during the low primary production characteristic of EN. While the fish catches also increased during EN mainly due to immigrations of fish towards the coast, the catch of benthic resources increased the most. Increased oxygen concentration during EN has been suggested as important in the proliferation of benthic species (Arntz and Fahrbach, 1991). Overall consumption of primary production by several primary consumers (i.e. scallops, herbivorous gastropods, and ben-

Table 7
Vulnerabilities calculated by EwE with the application of all four drivers (phytoplankton, macroalgae, scallops, predatory crabs). BU = Bottom-up control (vulnerability ≪ 2.0), TD = top-down control (vulnerability ≫ 2.0), MX = mixed/intermediate control (vulnerability values between 1.2 and 2.0).

	Prey/predator	3	4	5	6	7	8	9	10	11	12	13	14	15	16	17	18	19
1	Phytoplankton	BU	MX	MX				MX							BU			
2	Macroalgae				MX	MX	MX							BU				
3	Zooplankton	TD	MX					MX		MX				BU	BU	BU		
4	Polychaetes				MX				TD	MX	BU	MX		BU				
5	Scallops								BU	MX	TD	MX	BU					
6	Sea urchins									MX		MX						
7	Herbivorous gastropods								MX	MX	MX	MX	MX					
8	Benthic detritivores								TD	MX	MX	MX	BU	MX				
9	Misc. filter-feeders								TD	MX	BU	MX	BU					
10	Predatory gastropods										BU	TD	BU	MX				
11	Small carnivores								MX	MX	MX	MX	MX	MX				
12	Predatory crabs										MX			MX				
13	Sea stars										MX			MX				
14	Octopus												TD					
15	Littoral fish													MX			BU	BU
16	Small pelagic fish													MX		BU	BU	BU
17	Pelagic predatory fish																MX	
18	Marine mammals																	
19	Seabirds																	
20	Detritus	MX	BU	MX	MX	MX	MX	MX	BU	MX	MX	MX		BU				

thic detritivores) increased in order to sustain their increased biomasses – as calculated from *in situ* or empirically-based estimates. As a result, primary production during EN appears to be almost completely consumed in Independence Bay, although several assumptions were made concerning the levels of primary production. However, near-complete use of primary production during EN may be indicated by the clear, tropical-like water and decreases in benthic detrital material observed during EN. Based on the model, recruitment and production increases of scallops account for this result, as scallops consume 58% of phytoplankton production during EN. Wolff et al. (2007) found that the increase in scallops was likely a non-trophic effect resulting from increased larval survival in warmer temperatures. This recruitment success combined with increased oxygen concentrations is likely the main cause of the increase in fisheries yield.

Indicators of system maturity show some contradictions – some suggest normal conditions are more mature and developed while others for the EN state (1998). From a community energetics point of view, the EN state is able to support a similar biomass compared to 1996 despite lower primary production (*PP*/*B* ratio) and total throughput (*B*/*T* ratio), and thus the system's primary production to respiration ratio is closer to the value of 1.0 predicted for mature and efficient systems (Odum, 1969). Similarly, an increased Finn's cycling index is observed during EN due to a better utilization of primary production and detritus by the primary consumers (mainly scallops). These larger energy flows at lower trophic levels offset the negative impacts of EN at the higher trophic levels. During EN the transfer efficiencies (*TE*) of higher trophic levels are decreased and contribute to an overall lower mean *TE*, due to the negative impact of EN on benthic predatory groups (predatory gastropods, small carnivores, and especially predatory crabs). These impacts are also observed through a decreased predatory cycling index and Finn's mean path length during EN, indicating poorer cycling and transfer of energy in the higher trophic levels of the food web.

Relative ascendancy (*A*/*C*) indicates slightly more ecosystem development and maturity during 1996 (33.0% in 1996; 27.5% in EN). Related is the percent overhead (Φ/C), which indicates that the less mature EN state may be better able to withstand perturbation. Baird et al. (1991) found a similar discrepancy when comparing *A*/*C* to *FCI* in several marine ecosystems, where a negative correlation between indices was observed even though both should have increased with system maturity. They suggested that the discrepancy may lie in the fact that stress frequently impacts higher-level species more than lower-level species. As a result, the release of standing biomass of higher trophic levels can be taken up through increased recycling via "short intense loops".

It does appear that the higher trophic levels were more severely impacted by EN in Independence Bay. Furthermore, the most significant short intense loop would be the cycle through detritus, which increases during EN and results in the higher Finn's cycling index (*FCI*). As phytoplankton and macroalgae production were reduced during EN (9247 t m^{-2} y^{-1} during EN; 14,214 t m^{-2} y^{-1} during normal conditions), and consumption of detritus by scallops actually increased, the proportion of recycled detritus is significantly higher in 1998.

This result depends on the decreased primary production during EN. To illustrate, we can increase the primary production in the EN model to the levels of 1996 in order to observe a less-biased comparison (Fig. 6). The EN Finn's cycling index (*FCI*) decreased to a slightly lower value than 1996. However, the relative Ascendancy (*A*/*C*) and Overhead (Φ/C) increase and decrease, respectively, but not to the levels of 1996. Ascendancy is both a function of total throughput (*T*) and system development (i.e. average mutual information, *I*), and while the increase in primary production brings *T* to a similar level as 1996, the EN state still shows lower development, *I*. Under this scenario, EN would appear as of lower maturity despite increased overall community energetics.

Our models do not include information on the microbial loop, which is undoubtedly an important component of ecosystem functioning in Independence Bay. Energy flow through bacteria is likely enhanced during the warm, oxygen-rich conditions of EN. While bacterial functional groups are often removed in other models because their high flows overshadow other groups (Christensen, 1995), they may be of particular importance in our understanding of benthic processes in the Peruvian upwelling system. Thus, future research plans to investigate these important energy pathways for use in future models.

A community analysis for Independence Bay conducted by Wolff and Mendo (2002) indicated that benthic diversity and evenness increased during EN. An initial attempt to model the trophic changes also showed maintenance of flow structure during EN. The authors proposed that this adjustment to abiotic changes might indicate that EN is a condition to which the benthic community has adapted during evolution. This hypothesis is supported by the present study's results, yet may best apply to lower trophic levels that responded quicker to the perturbation. High trophic level benthic predatory groups have been observed to recover quite quickly (e.g. predatory crabs) after EN, but this is likely due to temporary emigrations to deeper waters rather than system adjustment. In this respect we wonder if the post-EN ecosystem, with higher primary production, higher residual scallop biomass, and a return of predatory groups, might not show higher flows or more maturity than the pre-EN state. If so, there may be some long-term

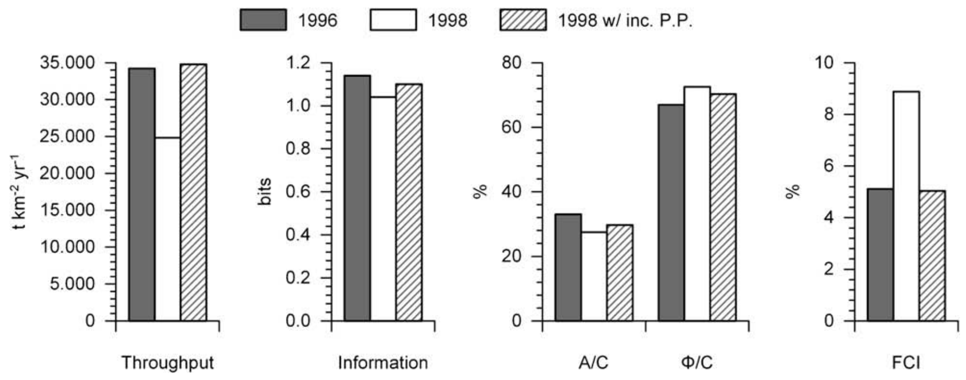

Fig. 6. Simulation of increasing primary production in the 1998 model to normal upwelling levels (1996 model values for macroalgae and phytoplankton) on indices of Ascendancy (*A*/*C*), overhead (Φ/C), mutual information (*I*), and Finn's cycling (*FCI*). Reference values for the 1996 model's indices are given for comparison.

positive impact from EN that may foster the idea that it is an integral part of HCS dynamics (Arntz and Valdivia, 1985b).

4.2. Bottom-up and top-down effects

When the model for normal conditions was forced from below with a reduction in primary producer biomass (phytoplankton and macroalgae to EN levels) the response confirms some of the EN-associated changes observed in functional group biomasses: misc. filter-feeders and herbivorous gastropods strongly decrease, and polychaetes benthic detritivores which also decrease somewhat. Oddly, macroalgae, when used as a single model driver, better explain the observed ecosystem changes (lowering SS) than phytoplankton.

Forcing a reduction in predatory crab biomass (release of top-down control), favors sea stars and small carnivores (competing predators), yet the modeled responses of other groups of the system is insignificant.

Neither EN triggered changes in the bottom-up (phytoplankton and macroalgae), nor the top-down (predatory crabs) forcing improve the fit of scallop dynamics, suggesting that trophic linkages of scallops to their food and predators do not cause proliferation of the scallop stock—an important if negative finding, especially since predatory crabs are well known scallop predators and their biomass reduction during the EN warming has been previously related to the scallop proliferation (Wolff and Alarcon, 1993; Wolff and Mendo, 2000).

While the scallop outburst during EN changed the entire character of the ecosystem, its inclusion as a model driver did not improve the overall fit of the simulation considerably. This may in part be due to lags in the population responses of several functional groups as compared to the reference data; however, the simulation correctly predicts the direction of response for a number of functional groups (positive: predatory gastropods, small carnivores, octopus, sea stars; Negative: polychaetes, herb. gastropods, and misc. filter-feeders), supporting the central role of the scallop in the Independence Bay ecosystem as prey for several consumer groups and as a competitor for other filter-feeders. It is likely that the more immediate decreases in several competing primary consumer groups may be due to the negative effects of competition for space, as the scallop banks became so thick in parts as to obscure the sea floor with several layers of scallops.

The scallop outburst apparently is caused by non-trophic effects (i.e. temperature mediated recruitment). However, once the scallops proliferated, the model suggests great changes to energy flow within the system. During EN scallops proliferated and the biomass of primary producers and predatory crabs decreased, affecting other groups in our simulations (scenario 4) (Fig. 4).

When forcing by the diving and finfish fishery is removed in our simulations, the simulated biomass trajectories of the functional groups were almost identical to those of scenario 4, suggesting that fishing plays a very limited role in the dynamics of the system. This may be explained by the fact that the diving fishery targeted mainly scallops and its increase in catch rate was about proportional to the scallop biomass increase; and the changes in finfish fishing rate were small over the whole period.

4.3. Vulnerabilities

It is important to emphasize that the manipulation of the 'drivers' did not improve the fit of the simulation without first allowing for a fitting of vulnerabilities. This is contrary to the findings of a similar exploration of the larger Peruvian Upwelling system (Taylor et al., 2008) whereby even default vulnerability values reproduced many important dynamics. This may be due to higher data quality in steady-state model (Tam et al., 2008) (as reflected in the Ecopath Pedigree Index, Peru system, 0.638; IB, 0.597; scales between 0 and 1 with highest values for direct measurements of the same system). Furthermore, the less-mobile nature of the benthic organisms in Independence Bay may prevent avoidance of deleterious conditions, thus making the effects of perturbations more pronounced. While the computed vulnerabilities for Independence Bay seem plausible, they should nevertheless be considered with caution since the time series available for the present study was quite short. In future years we will be able to extend the data set over longer periods and may be able to confirm some of the estimated vulnerabilities.

Generally, bottom-up control dominated the fit for the pelagic components such as energetic flow from plankton to small pelagic fish to the higher predators marine mammals and seabirds. Littoral fish also provided an important bottom-up link between benthic production (both macroalgae and invertebrate) to marine mammals. Top-down control was more important in the benthic components of the system. This may be expected given the high Ecological efficiencies calculated for many benthic primary consumers during the normal upwelling year of 1996, due to their high utilization by higher trophic levels. In addition, the fact that only 0.75% of the Ecoranger runs for 1996 resulted in a balanced model (as compared to 2.20% in the 1998 model) illustrates the tightly coupled flows to the benthic predatory groups, which restricted the parameter possibilities for the starting 1996 steady-state model.

A top-down configuration was fit for the predatory crab to scallop interaction. This is possible during normal upwelling periods as the crabs *Cancer setosus* and *Cancer porteri* are the dominant consumers of benthic production; however, the crab decrease during EN is not evidently responsible for the scallop outburst. Furthermore, this vulnerability setting must be taken with caution as the biomass fluctuations of both groups were forced through time and thus the result is likely an artifact. Top-down configurations between predatory snails and several of its prey (polychaetes, benthic detritivores and misc. filter-feeders) help to explain these prey decreases after the EN period. But this result too must be taken with caution as competitive interactions with scallops for space may have also attributed to their declines.

The finding that the abundance of scallop and other Independence Bay filter-feeders exerts bottom-up control on predators' abundance appears plausible and the finding is not new (Wolff and Alarcon, 1993). Despite the negative effects of EN on several higher-level benthic predators, the increased scallop biomass after EN apparently supported the recovery of predatory gastropods, small carnivores, predatory crabs, and sea stars, all of which show higher post-EN biomasses than in 1996. Furthermore, the (possibly normal) bottom-up control of scallops and other filter-feeders by phytoplankton under upwelling conditions may indeed be inverted during EN, when scallops are estimated to have consumed 58% of phytoplankton production alone. A similar role has been identified for the introduced Manila clam *Tapes philippinarum* in the Venice Lagoon system (Pranovi et al., 2003). Furthermore, it was suggested that this strong top-down control of phytoplankton by *T. philippinarum* may be responsible for the system not returning to a phytoplankton-based trophic web (Libralato et al., 2004), although this seems unlikely in Independence Bay given the constant refreshment of productive waters that enter from outside the bay.

4.4. Conclusions

Overall, it appears that the energy flow structure in Independence Bay is more or less maintained during El Niño despite negative impacts at higher benthic trophic levels. In particular, the proliferation of the scallop *A. purpuratus* apparently maintains the energy flow within Independence Bay despite the reduction in primary production. While some alleviation of top-down predation pressure may be felt by benthic primary consumers through the temperature–mediated decreases of crabs, the overall bottom-up affects of reduced primary production (macroalgae and phytoplankton) appears to have reduced the biomass of several functional groups. As seen for many areas along the Peruvian coast, Independence Bay becomes more tropical during EN. Under these conditions the system utilizes most of the (reduced) phytoplankton production so that exports of primary production to detritus are greatly reduced. While the El Niño state appears to show some higher efficiency in overall energetics, the structure and development appears impacted.

The rapid response and adaptation of the artisanal fishery to EN also increases the system's efficiency; however, this increased fishing pressure may have added stress to negatively impacted functional groups through higher fishing mortality. A management plan that allows for the newly recruited *A. purpuratus* population to fully grow and develop may not only reap higher monetary gains as suggested by Wolff and Mendo (2000), but may also enhance post-El Niño system through facilitation of the recovery of benthic predatory groups.

Acknowledgements

The authors are grateful for the support and assistance from the following: Dr. Villy Christensen of the Fisheries Centre, University of British Columbia, for his helpful advice regarding the use of Ecoranger routine within Ecopath with Ecosim; Dr. Tom Brey of the Alfred Wegener Institute for Polar and Marine Research (AWI) for helpful discussions regarding benthic invertebrate energetics and for the use of his somatic production models; Dr. Carl Walters for the use of the Ecosim software. This study was financed and conducted in the frame of the EU-project CENSOR (Climate variability and El Nino Southern Oscillation: Impacts for natural resources and management, Contract 511071) and is CENSOR publication 0050.

References

Arias-González, J.E., Delesalle, B., Salvat, B., Galzin, R., 1997. Trophic functioning of the Tiahura reef sector, Moorea Island, French Polynesia. Coral Reefs 16, 231–246.

Arntz, W., Valdivia, E., 1985a. Incidencia del fenómeno 'El Niño' sobre los mariscos en el litoral peruano. In: Arntz, W., Landa, A., Tarazona, J. (Eds.), 'El Niño' y su impacto en la fauna marina. Instituto del Mar del Perú, Callao, Peru, pp. 91–101.

Arntz, W., Valdivia, E., 1985b. Visión integral del problema 'El Niño': introducción. In: Arntz, W., Landa, A., Tarazona, J. (Eds.), 'El Niño' y su impacto en la fauna marina. Instituto del Mar del Perú, Callao, Peru, pp. 5–10.

Arntz, W., Tarazona, J., 1990. Effects of El Niño on benthos, fish and fisheries off the South American Pacific coast. In: Glynn, P.W. (Ed.), Global ecological consequences of the 1982–83 El Niño-Southern Oscillation. Elsevier Oceanography Series, pp. 323–360.

Arntz, W.E., Fahrbach, E., 1991. El Nino-Klimaexperiment der Natur. Birkhaeuser Verlag, Basel, Switzerland.

Arntz, W.E., Valdivia, E., Zeballos, J., 1988. Impact of El Nino 1982–83 on the commercially exploited invertebrates (mariscos) of the Peruvian shore. Meeresforschung 32, 3–22.

Arntz, W.E., Tarazona, J., Gallardo, V.A., Flores, L.A., Salzwedel, H., 1991. Benthos communities in oxygen deficient shelf and upper slope areas of the Peruvian and Chilean Pacific coast, and changes caused by El Niño. Geological Society 58, 131–154.

Arntz, W.E., Gallardo, V.A., Gutíerrez, D., Isla, E., Levin, L.A., Mendo, J., Neira, C., Rowe, G.T., Tarazona, J., Wolf, M., 2006. El Niño and similar perturbation effects on the benthos of the Humboldt, California, and Benguela Current upwelling ecosystems. Advances in Geosciences 6, 243–265.

Baird, D., McGlade, J.M., Ulanowicz, R.E., 1991. The comparative ecology of six marine ecosystems. Philosophical Transactions: Biological Sciences 333, 15–29.

Baird, D., Luczkovich, J., Christian, R.R., 1998. Assessment of Spatial and Temporal Variability in Ecosystem Attributes of the St Marks National Wildlife Refuge, Apalachee Bay, Florida. Estuarine Coastal and Shelf Science 47, 329–349.

Barber, R.T., Chavez, F.P., 1983. Biological consequences of El Nino. Science 222, 1203–1210.

Barber, R.T., Chavez, F.P., Kogelschatz, J.E., 1985. Biological effects of El Nino. Boletín ERFEN 14, 3–29.

Brey, T., 2001. Population dynamics in benthic invertebrates. Available from: <http://www.awi-bremerhaven.de/Benthic/Ecosystem/FoodWeb/Handbook/main.html>.

Brown, P.C., Painting, S.J., Cochrane, K.L., 1991. Estimates of phytoplankton and bacterial biomass production in the northern and southern Benguela ecosystems. South African Journal of Marine Science 11, 537–564.

Brush, M.J., Brawley, J.W., Nixon, S.W., Kremer, J.N., 2002. Modeling phytoplankton production: Problems with the Eppley curve and an empirical alternative. Marine Ecology Progress Series 238, 31–45.

Carr, M.E., 2002. Estimation of potential productivity in eastern boundary currents using remote sensing. Deep-Sea Research II 49, 59–80.

Chavez, F., Barber, R.T., 1985. La productividad de las aguas frente a la costa del Perú. Boletín ERFEN 15, 9–13.

Christensen, V., 1995. Ecosystem maturity – towards quantification. Ecological Modelling 77, 3–32.

Christensen, V., Pauly, D., 1992. ECOPATH II – a software for balancing steady-state models and calculating network characteristics. Ecological Modelling 61, 169–185.

Christensen, V., Walters, C.J., 2004. Ecopath with Ecosim: methods, capabilities and limitations. Ecological Modelling 172, 109–139.

Christensen, V., Walters, C.J., Pauly, D., 2000. Ecopath with Ecosim Version 4, Help system©.

Cortez, T., Gonzalez, A.F., Guerra, A., 1999. Growth of Octopus mimus (Cephalopoda, Octopodidae) in wild populations. Fisheries Research 42, 31–39.

Delgado, E., Villanueva, P., 1998. Peruvian coastal phytoplankton community during Cruise RV Humboldt 9803–05 from Tumbes to Tacna. Informe. Instituto del Mar del Peru, Callao. pp. 114–120.

Eppley, R.W., 1972. Temperature and phytoplankton growth in the sea. Fish Bulletin 70, 1063–1085.

Finn, J.T., 1976. Measures of ecosystem structure and function derived from analysis of flows. Journal of Theoretical Biology 56, 363–380.

Froese, R., Pauly, D., 2006. FishBase. Available from: <www.fishbase.org>.

Huebner, J.D., Edwards, D.C., 1981. Energy Budget of the Predatory Maine Gastropod *Polinices duplicatus*. Marine Biology 61, 221–226.

Hutchings, L., Verheye, H.M., Mitchell-Innes, B.A., Peterson, W.T., Huggett, J.A., Painting, S.J., 1995. Copepod production in the southern Benguela system. ICES Journal of Marine Science 52, 439–455.

Jarre, A., Muck, P., Pauly, D., 1991. Two approaches for modelling fish stock interactions in the Peruvian upwelling ecosystem. ICES Marine Science Symposia 193, 178–184.

Keen, M.A., 1972. Sea Shells of Tropical West America – Marine Mollusks from Baja California to Peru. Stanford University Press, Stanford, California.

Kremer, J.N., Nixon, S.W., 1977. A Coastal Marine Ecosystem. Simulation and Analysis. Springer-Verlag, New York, USA.

Lang, M., 2000. Populationsstruktur und Konsumverhaltung der decapoden Krebse *Cancer polydon und Cancer porteri* in der Independencia Bucht, Peru. Diplome thesis. Bremen University, Bremen, unpublished.

Leon, R.I., Stotz, W.B., 2004. Diet and prey selection dynamics of Cancer polyodon in three different habitat types in Tongoy Bay, Chile. Journal of the Marine Biological Association of the United Kingdom 84, 751–756.

Libralato, S., Pranovi, F., Raicevich, S., Da Ponte, F., Giovanardi, O., Pastres, R., Torricelli, P., Mainardi, D., 2004. Ecological stages of the Venice Lagoon analysed using landing time series data. Journal of Marine Systems 51, 331–344.

Macchiavello, J., Fonck, E., Edding, M., 1987. Antecedentes y perspectivas del Cultivo de Gracilaria en Coquimbo. In: Arana, P. (Ed.), Manejo y Desarrollo Pesquero. Universidad Catolica de Valparaíso, Valparaiso, Chile, pp. 206–214.

Mann, K.H., 1982. Ecology of Coastal Waters. A Systems Approach. University of California Press, Berkeley, USA.

Martin, D., Grémare, A., 1997. Secondary production of Capitella sp. (Polychaeta: Capitellidae) inhabiting different organically enriched environments. Scientia Marina 61, 99–109.

Mendo, J., Wolff, M., 2002. Pesqueria y manejo de la concha de abanico (*Argopecten purpuratus*) en la Bahia de Independencia. In: Mendo, J., Wolff, M. (Eds.), Bases ecologicas y socioeconomicas para el manejo de los recursos vivos de la Reserva National de Paracas. Universidad Agraria La Molina, Lima, pp. 188–194.

Mendo, J., Valdivieso, V., Yamashiro, C., Jurado, E., Morón, O., Rubio, J., 1987. Evaluación de la población de concha de abanico (*Argopecten purpuratus*) en la Bahía Independencia, Pisco, Peru, 17 de enero – 4 de febrero de 1987 Informe del Instituto del Mar del Perú N°94, Callao, Peru.

Mendoza, J.J., 1993. A preliminary biomass budget for the northeastern Venezuela shelf ecosystem. In: Christensen, V., Pauly, D. (Eds.), Trophic Models of Aquatic Ecosystems, vol. 26. ICLARM Conference Proceedings, pp. 285–297.

Moloney, C.L., Jarre, A., Arancibia, H., Bozec, Y.-M., Neira, S., Jean-Paul Roux, J.-P., Shannon, L.J., 2005. Comparing the Benguela and Humboldt marine upwelling ecosystems with indicators derived from inter-calibrated models. ICES Journal of Marine Science 62, 493–502.

Monaco, M.E., Ulanowicz, R.E., 1997. Comparative ecosystem trophic structure of three US mid-Atlantic estuaries. Marine Ecology Progress Series 161, 239–254.

Ñiquen, M., Bouchon, M., 2004. Impact of El Niño events on pelagic fisheries in Peruvian waters. Deep-Sea Research Part II-Topical Studies in Oceanography 51, 563–574.

Nixon, S.W., 1982. Nutrient dynamics, primary production and fisheries yields of lagoons. Oceanologica Acta Special edition, 357–371.

Nixon, S., Thomas, A., 2001. On the size of the Peru upwelling ecosystem. Deep-Sea Research I 48, 2521–2528.

Odum, E.P., 1969. The strategy of ecosystem development. Science 104, 262–270.

Ortiz, M., Wolff, M., 2002. Spatially explicit trophic modelling of a harvested benthic ecosystem in Tongoy Bay (central northern Chile). Aquatic Conservation: Marine and Freshwater Ecosystems 12, 601–618.

Pauly, D., Christensen, V., 1995. Primary production required to sustain global fisheries. Nature 374, 255–257.

Pennington, J.T., Mahoney, K.L., Kuwahara, V.S., Kolber, D.D., Calienes, R., Chavez, F.P., 2006. Primary production in the eastern tropical Pacific: a review. Progress in Oceanography 69, 285–317.

Polovina, J.J., Ow, M.D., 1985. An approach to estimating an ecosystem box model. Fishery Bulletin 83, 457–460.

Pranovi, F., Libralato, S., Raicevich, S., Granzotto, A., Pastres, R., Giovanardi, O., 2003. Mechanical clam dredging in Venice lagoon: ecosystem effects evaluated with a trophic mass-balance model. Marine Biology 143, 393–403.

Rojas de Mendiola, B., Gómez, O., Ochoa, N., 1985. Efectos del fenómeno El Niño sobre el fitoplancton. In: Arntz, W., Landa, A., Tarazona, J. (Eds.), El Niño: su impacto en la fauna marina. Instituto del Mar del Perú, Callao, Peru.

Rouillon, G., Mendo, J., Ochoa, N., 2002. Fitoplankton en el contenido estomacal de *Argopecten purpuratus* (Mollusca, Bivalvia) suspendida a differentes profundidades en Bahía Independencia. In: Mendo, J., Wolff, M. (Eds.), Memorias I Jornada "Bases Ecológicas y Socioeconómicas para el Manejo de los Recursos Vivos de la Reserva Nacional de Paracas". Universidad Nacional Agraria La Molina, Lima, pp. 60–67.

Rybarczyk, H., Elkaim, B., Ochs, L., Loquet, N., 2003. Analysis of the trophic network of a macrotidal ecosystem: the Bay of Somme (Eastern Channel). Estuarine. Coastal and Shelf Science 58, 405–421.

Samamé, M., Benites, C., Valdivieso, V., Mendez, M., Yamashiro, C., Moron, O., 1985. Evaluacón del recurso concha de abanico (*Argopecten purpuratus*) en la Bahía Independencia, Pisco, en Octubre–Noviembre 1985. Instituto del Mar del Perú.

Stotz, W.B., González, S.A., 1997. Abundance, growth, and production of the sea scallop Argopecten purpuratus (Lamarck 1819): bases for sustainable exploitation of natural scallop beds in north-central Chile. Fisheries Research 32, 173–183.

Tam, J., Taylor, M.H., Blaskovic, V., Espinoza, P., Ballón, R.M., Díaz, E., Wosnitza-Mendo, C., Argüelles, J., Purca, S., Ayón, P., Quipuzcoa, L., Gutiérrez, D., Goya, E., Ochoa, N., Wolff, M., 2008. Trophic flows in the Northern Humboldt Current Ecosystem, Part 1: comparing 1995-96 and 1997–98. Progress in Oceanography 79, 352–365.

Tarazona, J., Salzwedel, H., Arntz, W., 1988. Oscillations of macrobenthos in shallow waters of the Peruvian central coast induced by El Nino 1982–83. Journal of Marine Research 46, 593–611.

Tarazona, J., Canahuire, E., Salzwedel, H., Jeri, T., Arntz, W., Cid, L., 1991. Macrozoobenthos in two shallow areas of the Peruvian Upwelling ecosystem.

Taylor, M.H., Wolff, M., Mendo, J., Yamashiro, C., 2007a. Diet matrix for the steady-state models of Independence Bay for the years 1996 and 1998 before application of the Ecoranger resampling routine. PANGAEA, Available from: <http://www.pangaea.de>.

Taylor, M.H., Wolff, M., Mendo, J., Yamashiro, C., 2007b. Input–output parameters for the steady-state models of Independence Bay for the years 1996 and 1998 before application of the Ecoranger resampling routine. PANGAEA, Available from: <http://www.pangaea.de>.

Taylor, M.H., Tam, J., Blaskovic, V., Espinoza, P., Ballón, R.M., Wosnitza-mendo, C., Argüelles, J., Díaz, E., Purca, S., Ochoa, N., Ayón, P., Goya, E., Quipuzcoa, L., Gutiérrez, D., Wolff, M., 2008. Trophic flows in the Northern Humboldt Current Ecosystem, Part 2: Elucidating mechanisms of ecosystem change over an ENSO cycle by simulating changes in low trophic level dynamics. Progress in Oceanography 79, 366–378.

Ulanowicz, R.E., 1986. Growth and development: ecosystem phenomenology. Springer-Verlag, New York.

Vega, R., Mendo, J., 2002. Consumo de alimento y crecimiento del pulpo *Octopus* spp. alimentado con *Argopecten purpuratus* en la Bahía de Paracas, Pisco. In: Mendo, J., Wolff, M. (Eds.), Memorias I Jornada "Bases Ecológicas y Socioeconómicas para el Manejo de los Recursos Vivos de la Reserva Nacional de Paracas". Universidad Nacional Agraria La Molina, Lima, pp. 212–220.

Villanueva, P., Fernandez, C., Sanchez, S., 1998. Biomasa planctonica como alimento disponible durante el crucero BIC Humboldt y BIC Jose Olaya Balandra 9808–09 de Paita a Los Paltos (Tacna). Informe del Instituto del Mar del Perú 141, 49–54.

Walsh, J.J., 1981. A carbon budget for overfishing off Peru. Nature 290, 300–304.

Walters, C., Christensen, V., Pauly, D., 1997. Structuring dynamic models of exploited ecosystems from trophic mass-balance assessments. Reviews in Fish Biology and Fisheries 7, 139–172.

Warnke, K., 1999. Observations on Embryonic Development of *Octopus mimus* (Mollusca: Cephalopoda) from Northern Chile. The Veliger 42, 211–217.

Wilson, J.G., Parkes, A., 1998. Network analysis of the energy flow through the Dublin ecosystem. Biology and Environment: Proceedings of the Royal Irish Academy 98B, 179–190.

Wolff, M., 1987. Population dynamics of the Peruvian scallop Argopecten purpuratus during the El Nino phenomenon of 1983. Canadian Journal of Fisheries and Aquatic Sciences 44, 1684–1691.

Wolff, M., 1988. Spawning and recruitment in the Peruvian scallop *Argopecten purpuratus*. Marine Ecology Progress Series 42, 213–217.

Wolff, M., 1994. A trophic model for Tongoy Bay – a system exposed to suspended scallop culture (northern Chile). Journal of Experimental Marine Biology and Ecology 182, 149–168.

Wolff, M., Alarcon, E., 1993. Structure of a scallop *Argopecten purpuratus* (Lamarck, 1819)-dominated subtidal macro-invertebrate assemblage in northern Chile. Journal of Shellfish Research 12, 295–304.

Wolff, M., Mendo, J., 2000. Management of the Peruvian bay scallop (*Argopecten purpuratus*) metapopulation with regard to environmental change. Aquatic Conservation: Marine and Freshwater Ecosystems 10, 117–126.

Wolff, M., Mendo, J., 2002. Upwelling is the Disturbance, not El Niño: Insights from Modelling Community Organization and Flow Structure. Investigaciones Marinas 30, 166–167.

Wolff, M., Perez, H., 1992. Population dynamics, food consumption and gross conversion efficiency of *Octopus mimus* Gould, from Antofagasta (northern Chile). ICES Council Meetings Papers. ICES, Copenhagen, Denmark. p. 12.

Wolff, M., Soto, A., 1992. Population dynamics of *Cancer polyodon* in La Herradura Bay, northern Chile. Marine Ecology Progress Series 85, 70–81.

Wolff, M., Hartmann, H.J., Koch, V., 1996. A pilot trophic model for Golfo Dulce, a fjord-like tropical embayment, Costa Rica. Revista de biologia tropical 44, 215–231.

Wolff, M., Wosnitza-Mendo, C., Mendo, J., 2003. The Humboldt current-trends in exploitation, protection and research. In: Hempel, G., Sherman, K. (Eds.), Large Marine Ecosystems of the World. Elsevier, pp. 279–309.

Wolff, M., Taylor, M., Mendo, J., Yamashiro, C., 2007. A catch forecast model for the Peruvian scallop (*Argopecten purpuratus*) based on estimators of spawning stock and settlement rate. Ecological Modelling 209, 333–341. doi:10.1016/j.ecolmodel.2007.07.013.

Yamashiro, C., Rubio, J., Jurado, E., Auza, E., Maldonado, M., Ayon, P., Antonietti, E., 1990. Evaluación de la población de Concha de Abanico (*Argopecten purpuratus*) en la Bahía de Independencia, Pisco, Perú 20 de febrero–04 de marzo de 1988. Informe del Instituto del Mar del Perú N°98, Callao, Peru.

Zuta, S., Tsukayama, I., Villanueva, R., 1983. El ambiente marino y las fluctuaciones de las principales poblaciones pelágicas de la costa peruana. FAO Fisheries Report 291, 179–253.

Progress in Oceanography 79 (2008) 352–365

Contents lists available at ScienceDirect

Progress in Oceanography

journal homepage: www.elsevier.com/locate/pocean

Trophic modeling of the Northern Humboldt Current Ecosystem, Part I: Comparing trophic linkages under La Niña and El Niño conditions

Jorge Tam[a,*], Marc H. Taylor[b], Verónica Blaskovic[a], Pepe Espinoza[a], R. Michael Ballón[c], Erich Díaz[a], Claudia Wosnitza-Mendo[a], Juan Argüelles[a], Sara Purca[a], Patricia Ayón[a], Luis Quipuzcoa[a], Dimitri Gutiérrez[a], Elisa Goya[a], Noemí Ochoa[d], Matthias Wolff[b]

[a] *Instituto del Mar del Perú (IMARPE), Apdo. 22, Callao, Peru*
[b] *Center for Tropical Marine Ecology, Fahrenheitstr. 6, 28359 Bremen, Germany*
[c] *IRD, UR097, CRH, Avenue Jean Monnet, 34203 Sète, France*
[d] *Universidad Nacional Mayor de San Marcos, Apdo. 12, Lima, Peru*

ARTICLE INFO

Article history:
Accepted 14 October 2008
Available online 21 October 2008

Keywords:
Ecotrophic model
Network analysis
El Niño
Peru
Humboldt Current
Trophic energy flow
Upwelling

ABSTRACT

The El Niño of 1997–98 was one of the strongest warming events of the past century; among many other effects, it impacted phytoplankton along the Peruvian coast by changing species composition and reducing biomass. While responses of the main fish resources to this natural perturbation are relatively well known, understanding the ecosystem response as a whole requires an ecotrophic multispecies approach. In this work, we construct trophic models of the Northern Humboldt Current Ecosystem (NHCE) and compare the La Niña (LN) years in 1995–96 with the El Niño (EN) years in 1997–98. The model area extends from 4°S–16°S and to 60 nm from the coast. The model consists of 32 functional groups of organisms and differs from previous trophic models of the Peruvian system through: (i) division of plankton into size classes to account for EN-associated changes and feeding preferences of small pelagic fish, (ii) increased division of demersal groups and separation of life history stages of hake, (iii) inclusion of mesopelagic fish, and (iv) incorporation of the jumbo squid (*Dosidicus gigas*), which became abundant following EN. Results show that EN reduced the size and organization of energy flows of the NHCE, but the overall functioning (proportion of energy flows used for respiration, consumption by predators, detritus and export) of the ecosystem was maintained. The reduction of diatom biomass during EN forced omnivorous planktivorous fish to switch to a more zooplankton-dominated diet, raising their trophic level. Consequently, in the EN model the trophic level increased for several predatory groups (mackerel, other large pelagics, sea birds, pinnipeds) and for fishery catch. A high modeled biomass of macrozooplankton was needed to balance the consumption by planktivores, especially during EN condition when observed diatoms biomass diminished dramatically. Despite overall lower planktivorous fish catches, the higher primary production required-to-catch ratio implied a stronger ecological impact of the fishery and stresses the need for precautionary management of fisheries during and after EN. During EN energetic indicators such as the lower primary production/total biomass ratio suggest a more energetically efficient ecosystem, while reduced network indicators such as the cycling index and relative ascendency indicate of a less organized state of the ecosystem. Compared to previous trophic models of the NHCE we observed: (i) a shrinking of ecosystem size in term of energy flows, (ii) slight changes in overall functioning (proportion of energy flows used for respiration, consumption by predators and detritus), and (iii) the use of alternate pathways leading to a higher ecological impact of the fishery for planktivorous fish.

1. Introduction

The northern part of the Humboldt Current Ecosystem (HCE) off Peru has been modelled with carbon and nitrogen budget models (Dugdale and MacIsaac, 1971; Walsh and Dugdale, 1971; Walsh, 1981), mass balance models (Jarre et al., 1989, 1991; Jarre and Pauly, 1993; Ballón, 2005), a size-based carbon flow model (Carr, 2003) and an empirical carbon flow model (Jahncke et al., 2004). Mass balance models have also been applied in the southern HCE off Chile (Wolff 1994; Ortiz and Wolff, 2002; Arancibia et al., 2003; Neira et al., 2004; Neira and Arancibia, 2004). These models have permitted comparisons between the HCE and other eastern boundary current ecosystems (Jarre, 1998; Jarre and Christensen,

---

* Corresponding author.
E-mail address: jtam@imarpe.gob.pe (J. Tam).

doi:10.1016/j.pocean.2008.10.007

1998; Jarre et al., 1998; Moloney et al., 2005). However, none of these models have focused on the impact of the interannual variability associated with El Niño (EN).

According to Alheit and Niquen (2004), a regime shift occurred in Peruvian waters between 1968 and 1970, wherein waters warmed and zooplankton and anchovy (*Engraulis ringens*) biomass decreased, followed by an increase in sardine (*Sardinops sagax*) stocks. However, another regime shift back to cold conditions occurred during 1984–1986, in this case characterized by an increase of phytoplankton and zooplankton biomasses (see Ayon et al., 2008) associated with excellent recruitment of anchovy but decreases in sardine biomass.

Arntz and Fahrbach (1991) summarized the effects of the 1982–83 EN on the Northern Humbolt Current Ecosystem (NHCE). During EN, in the NHCE near surface temperature increases and the thermocline deepens, causing a collapse of the diatom-based trophic web, with emigration of anchovy and immigration of tropical and oceanic species. Gutierrez (2001) and Bertrand et al. (2004) described the effects of the 1997–98 EN on anchovy distribution and abundance, confirming that anchovy move to deeper waters but finding that the main spatial effect was concentration of stocks very nearshore. These authors attribute an apparent reduction in anchovy biomass to decreased effectiveness of acoustic sampling, unfavorable environmental conditions, increase of natural mortality due to poor feeding conditions, and to a much lesser degree, to mortality due to predation and fishing. Bouchon et al. (2001) analysed the ichthyofauna fluctuations over an El Niño Southern Oscillation (ENSO) cycle and concluded that in cold years the pelagic community is characterized by a high productivity and a low diversity (abundant diatoms and anchovy), but in warm years this pattern is reversed due to the immigration of offshore and tropical species and the reduction of anchovy. While responses of the main fish resources to EN-related perturbations are relatively well known (Aguilar, 1999; Tarazona et al., 2001), understanding the ecosystem response as a whole requires a multispecies ‘ecotrophic’ approach. Given the observed changes in biomass and species composition, it is expected that a strong EN impacts the food web, reducing or redistributing the main energy channel that flows through anchovy under La Niña (LN) conditions.

Previous models of the NHCE (Jarre et al., 1991), which described the flow of energy through the ecosystem during three decades (1953–1959, 1960–1969, 1973–1979), brought great understanding of ecosystem functioning. Now however, biological changes, new data sets, and the advancement of trophodynamic modeling permit construction of more detailed models through the inclusion of additional ‘functional groups’ of organisms (see also Guenette et al., 2008). In this paper we divided the phytoplankton compartment into two groups (diatoms and dino- and silicoflagellates) and zooplankton into three groups (micro-, meso- and macro-zooplankton) to account for the feeding preferences of different small pelagic fish. We incorporated the groups of mesopelagic fish and jumbo squid (*Dosidicus gigas*), which have gained in importance since the last 1997–98 EN. We also increased the detail of demersal groups and separated the hake into three different life history stages. The ecotrophic model framework is a simplified approach where species are aggregated into functional groups. Each group is represented by two linear equations, each of which must balance. One equation ensures balance between groups in the model, the other equation, balances the flows within each group.

The objective of this study is to compare such improved mass balance trophic models for a cold LN conditions (1995–96) versus a warm EN (1997–98) conditions, with the *a priori* hypothesis that the EN perturbation should decrease ecosystem organization. This paper also provides the basis for further explorations of ecosystem dynamics (Taylor et al., this 2008a), wherein non-steady state simulations of ecosystem change during and following the 1997–98 EN are performed and evaluated. In dynamic models, biomass changes are expressed in form of coupled differential equations derived from mass balance models equations.

2. Methods

2.1. Input data

Our models of the Northern Humboldt Current Ecosystem (NHCE) extend from 4°S to 16°S, and 60 nm offshore, covering an area of approximately 165000 km^2 (Fig. 1). In agreement with the ENSO cycle, data from June 1995 to May 1996 and from May 1997 to April 1998 were used as inputs for the cold LN and warm EN mass balance models, respectively, covering a full “biological year” each (*i.e.* starting from about the middle of a calendar year).

The models included 33 functional groups, namely: (1) diatoms, (2) dino- and silicoflagellates, (3) microzooplankton (20–200 μm), (4) mesozooplankton (200–2000 μm), (5) macrozooplankton (2–20 mm), (6) gelatinous zooplankton, (7) macrobenthos, (8) sardine, (9) anchovy, (10) mesopelagics (*Vinciguerria lucetia*, *Lampanyctus* spp., *Leuroglossus* spp.), (11) jumbo squid, (12) other cephalopods (*Loligo gahi*, *Octopus vulgaris*, *Logigunculla* sp.), (13) other small pelagics (e.g. *Anchoa nasus*). (14) horse mackerel (*Trachurus murphyi*), (15) mackerel (*Scomber japonicus*), (16) other large pelagics (e.g. *Sarda chiliensis*, *Coryphaena hippurus*, *Thunnus albacares*), (17) small hake (*Merluccius gayi peruanus*, <29 cm), (18) medium hake (*M. gayi peruanus*, 30–49 cm), (19) large hake (*M. gayi peruanus*, >50 cm), (20) flatfishes (*Paralichthys adspersus*., *Hippoglosina sp.*), (21) small demersals (e.g. *Odonthestes regia*, *Labrisomus philippi*, *Ctenosciaena peruviana*), (22) benthic elasmobranchs, (23) butter fishes (*Trachinotus paitensis*, *Stromateus stellatus*, *Peprilus medius*), (24) congers, (25) medium demersal fishes (e.g. *Paralabrax humeralis*, *Hemanthias peruanus*, *Mugil cephalus*), (26) medium sciaenids, (27) sea robin (*Prionotus stephanophrys)*, (28) catfishes (*Galeichtys*

Fig. 1. Study area covers from 4°S to 16°S, and up to 60 nm (grey shaded area), in the Northern Humboldt Current Ecosystem (dashed line) (modified from Alheit and Ñiquen, 2004).

peruvianus), (29) chondrichthyans, (30) seabirds (*Phalacrocorax bougainvillii*, *Sula variegata*, *Pelecanus thagus*), (31) pinnipeds (*Otaria flavescens*, *Arctocephalus australis*), (32) cetaceans, and (33) detritus.

Models were constructed using the Ecopath software (Ecopath with Ecosim version 5.1; Christensen et al., 2005). Mass balance models are based on two equations for each functional group *i* (Christensen and Pauly, 1992).

The energy balance equation

$$Q_i = P_i + R_i + UF_i \tag{1}$$

where Q_i = prey consumption, P_i = production, R_i = respiration, UF_i = unassimilated food (including excretion and egestion) and, the production components equation

$$P_i = B_i * M0_i + EX_i + B_i * M2_i + BA_i \tag{2}$$

where $M0_i$ = non-predatory mortality (expressed as a function of ecotrophic efficiency, EE_i), $M2_i$ = predatory mortality (expressed as a function of diet composition, *DC*), $\mathrm{EX_i}$ = export (including catch C_i and net migration, NM_i), BA_i = biomass accumulation. EE_i is the proportion of the production that is utilized in the system and is defined as

$$EE_i = (B_i * M2_i + C_i + NM_i + BA_i)/P_i \tag{3}$$

Thus, for each functional group, required input data is: wet weight biomass (*B*, $\mathrm{t\,km^{-2}}$), production/biomass ratio (*P*/*B*, $\mathrm{y^{-1}}$), consumption/biomass ratio (*Q*/*B*, $\mathrm{y^{-1}}$), catch (*C*, $\mathrm{t\,km^{-2}\,y^{-1}}$) and diet composition (*DC*) for each functional group. One unknown parameter (either *B*, *P*/*B*, *Q*/*B* or *EE*) can be estimated when solving the system of linear equations.

Input data for the models were gathered from published and unpublished sources (Table 1). Catch values were obtained from IMARPE (2006) landing statistics and the Sea Around Us (2006) database; some values of production/consumption ratio (*P*/*Q*) and unassimilated food (*UF*) were obtained from Moloney et al. (2005). Sea surface phytoplankton biomass was calculated from relationships of upwelling area vs. chlorophyll *a* (chl. *a*) threshold as calculated by Nixon and Thomas (2001). Conversion factors of carbon/chl. *a* = 40 (Brush et al., 2002) and wet weight/carbon = 14.25 (Brown et al., 1991) were used to estimate wet weights. Proportion of diatoms vs. silico- and dinoflagellates during LN and EN conditions were obtained from a time series (1992–2000) of species cell counts carried out by Universidad Nacional Mayor de San Marcos UNMSM at Ancón Bay, Central Peru (77°11′ W–11°46′ S). Phytoplankton cell counts were converted to biovolumes using the geometric formulas and software of Sun and Liu (2003); cell dimensions were obtained from the literature (*e.g.* Strickland et al., 1969; SERC, 2006; NODC, 2001) or measured under a microscope at the UNMSM. To convert biomass units from $\mathrm{m^3}$ to $\mathrm{m^2}$, a mixed layer depth of 40 m was estimated by averaging vertical profiles of chl. *a* from several latitudes along the Peruvian coast with data from Calienes et al. (1985). Individual zooplankter body masses were estimated from abundance and biomass data (Ayón and Arones, 1997a,b) and zooplankter biovolumes were calculated from individual counts by taxonomic group using length:-weight relationships from Rippe (1996) with body dimensions obtained from Santander et al. (1981) and Wangelin and Wolff (1996). Such biovolume conversions were also needed to convert stomach content data for sardine and anchovy (numbers of phytoplankton cells and zooplankton individuals per stomach by species) into fractions by weight.

In an Ecopath model, the Pedigree Index (*P*) permits assignment of quality or confidence ratings to each parameter. Qualitative pedigree index values were assigned as in Table 2. Based on the individual index values (I_{ij}) an overall Pedigree Index (*P*) is calculated using

$$P = \sum_{i=1}^{n} \frac{I_{ij}}{n} \tag{4}$$

where I_{ij} is the pedigree index value for group *i* and parameter *j* for each of the *n* living groups in the ecosystem. For the models constructed here, *P* was 0.638 (*P* scales between 0 and 1; $t^* = 4.54$, $n = 32$, $p < 0.001$), indicating good model quality with parameters mostly based on local data. For comparison, of 50 Ecopath models reviewed by Morissette (2007), only four models had higher pedigree indices than the present study (upper 7.5%).

Conservative estimates of biomass of some groups were calculated by the software assuming an ecotrophic efficiency of 0.95 (microzooplankton, macrozooplankton, gelatinous zooplankton, small pelagics, small demersals and other cephalopods). Ecotrophic efficiency ($0 < EE < 1$) and gross efficiency ($0 < GE < 0.4$) served as constraints for balancing the models. Gross food conversion efficiency is estimated using

$$GE_i = (P_i/B_i)/(Q_i/B_i) \tag{5}$$

Energy flow balance of models was achieved by tuning the diets of some groups. The dietary composition for functional groups is presented in Table 3. Based on the input data, the Ecopath software calculated ecosystem indicators which describe the state of an ecosystem in terms of energy flows. Behavior of trophic, fishery, energetic and network ecosystem indicators have been related to theories of ecosystem maturity (Odum, 1969) and health (Ulanowicz, 1997) (see Table 4 for a description). The trophic level of a group (*TL*) is calculated as the mean trophic level of its prey plus 1, assuming that primary producers and detritus groups have a trophic level of 1.0. Thus, trophic level is calculated using

$$TL_j = 1 + \sum (TL_i)(DC_{ij}) \tag{6}$$

where DC_{ij} is the fraction of prey *i* in the diet of the predator *j*.

The transfer efficiency (*TE*) of each discrete trophic level is defined as a measure of the fraction of input to each of the aggregated trophic levels that is passed on to the next level, that is, the fraction that is either consumed by predators or harvested

$$TE_n = (Q_{n+1} + EX_n)/Q_n \tag{7}$$

where *n* is the trophic level.

3. Results and discussion

3.1. Biomass and catch changes

Tables 5A and B presents results for LN and EN conditions, respectively. The model synthesizes available data and estimates additional parameters (bold type in Table 5) that define the relationships between the functional groups of organisms in the model. During the LN conditions diatoms, mesozooplankton, anchovy, horse mackerel, mackerel and jumbo squid dominated in biomass in their respective trophic levels. During EN conditions, biomasses of most groups decreased (anchovy, jumbo squid, horse mackerel, hake, demersal fishes, seabirds and pinnipeds), mainly due to a bottom-up control originating from biomass reduction in the lower trophic levels (diatoms, micro- and mesozooplankton). During EN conditions, macrobenthos biomass increased, mainly in the central zone off Peru (10–15°S; Quipuzcoa et al., 2001), probably because bottom oxygen concentrations increased, improving conditions for many organisms. However, biomasses of demersal fish species decreased (e.g. hake, small demersals).

Biomasses of some groups increased during EN (Fig. 2), possibly being favored by low nutrient conditions or higher temperatures (dinoflagellates, macrozooplankton) and/or immigration of some fish (mesopelagics, small pelagics, large pelagics and

Table 1

Input data for the models of the NHCE and their sources. Biomass (*B*), production (*P*), consumption (*Q*) and catch (*C*)

Functional group	*B*		*P*/*B*		*Q*/*B*	*C*		Source
Period	1995–96	1997–98	1995–96	1997–98	1995–98	1995–96	1997–98	
1. Diatoms	53.416	14.761	265	210				*B*, *P*/*B* calculated from Nixon and Thomas (2001) curve, 85% (1995–96) and 46% (1997–98) of diatoms calculated from Ancon, Central Peru (Ochoa, personal communication) and Sanchez (1996) data converted to biovolumes.
2. Silico- and dinoflagellates	9.426	17.328	265	210				*B*, *P*/*B* calculated from Nixon and Thomas (2001) curve, 15% (1995–96) and 86% (1997–98) of silico– and dinoflagellates calculated from data converted to biovolumes from Ancon, Central Peru (Ochoa, personal communication) and Sanchez (1996).
3. Microzooplankton (20–200 um)			256	256				*P*/*B* from Sorokin and Kogelschatz (1979), diet from Shannon et al. (2003).
4. Mesozooplankton (200–2000 um)	31.164	17	40	40				B calculated from IMARPE data (Ayon, personal communication), *P*/*B* from Moloney et al. (2005), diet from Shannon et al. (2003).
5. Macrozooplankton (2–20 mm)					46.55			Q/B from Antezana (2002a), diet from Shannon et al. (2003).
6. Gelatinous zooplankton			0.584	0.584				*P*/*B* from Jarre et al. (1998), diet from Shannon et al. (2003).
7. Macrobenthos	20.729	25.605	1.2	1.2	10			B calculated from IMARPE data (Gutierrez and Quipuzcoa, personal communication), *P*/*B* and *Q*/*B* from Walsh (1981) in Jarre et al. (1989), diet from Shannon and Jarre (1999).
8. Sardine (Sardinops sagax)	7.567	7.909	1.4	1.4		7.97	3.33	B calculated from IMARPE acoustic data (Gutierrez, personal communication), *P*/*B* from Patterson et al. (1992), diet calculated from Alamo et al. (1996a, 1996b), Alamo et al. (1997a, 1997b), Alamo and Espinoza (1998), Blaskovic et al. (1998), Espinoza et al. (1998a, 1998b), Blaskovic et al. (1999).
9. Anchovy (Engraulis ringens)	83.293	33.34	2	2		30.47	14.48	B from IMARPE VPA (Ñiquen, personal communication), *P*/*B* from Csirke et al. (1996), diet calculated from Alamo et al. (1996a, 1996b), Alamo et al. (1997a, 1997b), Alamo and Espinoza (1998), Blaskovic et al. (1998), Espinoza et al. (1998a, 1998b), Blaskovic et al. (1999).
10. Mesopelagics	6.882	22.375	1.4	1.4				B calculated from relationship between *Vinciguerria lucetia* and *Dosidicus gigas* from IMARPE acoustic data 1999–2005 (Gutierrez, personal communication), *P*/*B* calculated from maximum age, diet calculated from IMARPE data (Blaskovic, personal communication)
11. Jumbo squid (*Dosidicus gigas*)	0.524	0.243	8.91	8.91		0.19	0.01	B calculated from relationship between CPUE and B of *Dosidicus gigas* from IMARPE acoustic data 1999–2005 (Gutierrez, personal communication), *P*/*B* from Alegre et al. (2005), diet calculated from IMARPE industrial fleet data (Blaskovic, personal communication), Schetinnikov (1989), Nigmatullin et al. (2001).
12. Other Cephalopods			4.3	4.3		0.05	0.01	*P*/*B* from IMARPE VPA (Arguelles, personal communication), diet from Cardoso et al. (1998) and Villegas (2001).
13. Other small pelagics			1	1		0.69	2.36	*P*/*B* from Shannon et al. (2003) for saury (*Scomberesox saurus*), flying fish (Exocoetidae), pelagic goby (*Sufflogobius bibarbatus*), diet based on Jarre et al. (1989).
14. Horse mackerel (*Trachurus murphyi*)	11.568	3.03	1.2	1.2		1.45	1.94	B from IMARPE acoustic data (Gutierrez, personal communication), *P*/*B* from Moloney (2005), diet calculated from IMARPE data (Blaskovic, personal communication)
15. Mackerel (*Scomber japonicus*)	8.488	6.892	0.85	0.85		0.10	1.34	B from IMARPE acoustic data (Gutierrez, personal communication), *P*/*B* from Jarre et al. (1989), diet calculated from IMARPE data (Blaskovic, personal communication)
16. Other large pelagics	0.589	1.757	0.85	0.4		0.25	0.35	B calculated from catch equal to 50% production, *P*/*B* from Jarre et al. (1989), diet calculated from IMARPE data (Blaskovic, personal communication)

(*continued on next page*)

Table 1 (*continued*)

Functional group	*B*		*P*/*B*		*Q*/*B*	*C*		Source
17. Small hake (Merluccius gayi peruanus, <29 cm)	2.771	1.245	0.928	1.317		0.97	0.56	B from IMARPE VPA (Wosnitza, personal communication), *P*/*B* calculated as average of Z from VPA of the age groups involved (Ballon, personal communication), diet calculated from IMARPE data (Blaskovic, personal communication).
18. Medium hake (M. gayi peruanus, 30–49 cm)	0.414	0.163	1.627	1.946		0.22	0.11	B from IMARPE VPA (Wosnitza, personal communication), *P*/*B* calculated as average of Z from VPA of the age groups involved (Ballon, personal communication), diet calculated from IMARPE data (Blaskovic, personal communication).
19. Large hake (M. gayi peruanus, >50 cm)	0.055	0.028	1.044	1.516		0.02	0.01	B from IMARPE VPA (Wosnitza, personal communication), *P*/*B* calculated as average of Z from VPA of the age groups involved (Ballon, personal communication), diet calculated from IMARPE data (Blaskovic, personal communication)
20. Flatfishes	0.04	0.01	0.304	0.304		0.01	0.00	B from swept area data corrected with hake VPA (Wosnitza, personal communication), *P*/*B* from Neira et al. (2004), diet calculated from IMARPE data (Blaskovic, personal communicaiton)
21. Small demersals			2.3	2.3		0.02	0.02	B from swept area data corrected with hake VPA (Wosnitza, personal communicaiton), *P*/*B* from Wolff et al. (1998), diet calculated from IMARPE data (Blaskovic, personal communication)
22. Benthic elasmobranchs	0.078	0.045	1	1		0.03	0.04	B from swept area data corrected with hake VPA (Wosnitza, personal communication), *P*/*B* based on Shannon et al. (2003), diet calculated from IMARPE data (Blaskovic, personal communication)
23. Butter fishes	0.032	0.006	0.8	0.8				B from swept area data corrected with hake VPA (Wosnitza, personal communication), *P*/*B* from Wolff et al. (1998), diet calculated from IMARPE data (Blaskovic, personal communication)
24. Conger	0.019	0.004	0.75	0.75				B from swept area data corrected with hake VPA (Wosnitza personal communicaiton), *P*/*B* from Wolff et al. (1998), diet calculated from IMARPE data (Blaskovic, personal communication)
25. Medium demersal fish	0.2	0.211	1.32	2.48		0.13	0.14	B from swept area data corrected with hake VPA (Wosnitza, personal communication), *P*/*B* calculated from catch curve for *Paralabrax humeralis* (Ballon, personal communication), diet calculated from IMARPE data (Blaskovic, personal communication)
26. Medium sciaenids	0.369	0.218	0.746	1.085		0.07	0.04	B from swept area data corrected with hake VPA (Wosnitza, personal communication), *P*/*B* calculated from catch curve for Cynoscion analis (Ballon, personal communicaiton), diet calculated from IMARPE data (Blaskovic, personal communication)
27. Sea robin (Prionotus stephanophrys)	0.789	0.319	3.4	3.22				B from swept area data corrected with hake VPA (Wosnitza, personal communication), *P*/*B* calculated from catch curve (Ballon, personal communication), diet calculated from IMARPE data (Blaskovic, personal communication)
28. Catfish	0.577	0.65	0.9	0.9		0.07	0.54	B from swept area data corrected with hake VPA (Wosnitza, personal communication), *P*/*B* from Wolff et al. (1998), diet calculated from IMARPE data (Blaskovic, personal communication)
29. Chondrichthyans	0.027	0.078	0.486	0.486		0.01	0.02	B calculated from catch equal to 50% production, *P*/*B* calculated from Frisk et al. (2001) and Au and Smith (1997), diet calculated from IMARPE data (Blaskovic, personal communicaiton).
30. Seabirds	0.067	0.01	0.04	0.04	60			B from IMARPE abundance data converted to biomass (Goya, personal communicaiton), *P*/*B* and Q/B from Jarre et al. (1989), diet from Guillen (1990).
31. Pinnipeds	0.072	0.053	0.1	0.1	45.9			B from IMARPE abundance data converted to biomass (Goya, personal communicaiton), *P*/*B* from Jarre et al. (1989), Q/B from Muck and Fuentes (1987) in Jarre et al. (1989), diet from Arias (2003).
32. Cetaceans	0.062	0.067	0.1	0.1	20			B calculated from modelled biomass of mysticetes, small and large odontocetes (Kaschner 2004), 1.1 sightings ratio 1997/1995 calculated from Bello et al. (1998). Q/B from Moloney et al. (2005), diet based on Jarre et al. (1998).

Table 2
Pedigree index values qualitatively assigned to model parameters. Biomass (*B*), production (*P*), consumption (*Q*), diet composition (*DC*) and catch (*C*). Lower pedigree index values correspond to guesstimates or other models, while higher pedigree index values correspond to high precision estimates locally based.

Functional group	*B*	*P*/*B*	*Q*/*B*	*DC*	*C*
1. Diatoms	0.7	0.5			
2. Dino- and silicoflagellates	0.7	0.5			
3. Microzooplankton	0	0.6	0.6	0.2	
4. Mesozooplankton	0.7	0.6	0.6	0.2	
5. Macrozooplankton	0.7	0.6	0.6	0.2	
6. Gelatinous zooplankton	0	0.2	0.6	0.2	
7. Macrobenthos	0.7	0.2	0.6	0.2	
8. Sardine	0.4	1	0.6	1	1
9. Anchovy	0.4	1	0.6	1	1
10. Mesopelagics	0.4	0.1	0.6	0.2	
11. Jumbo squid	0.4	1	0.6	0.5	1
12. Other Cephalopods	0.4	0.7	0.6	0	1
13. Other small pelagics	0	0.7	0.6	0	1
14. Horse mackerel	1	0.7	0.6	0.5	1
15. Mackerel	1	0.7	1	0.5	1
16. Other large pelagics	1	0.7	0.6	0.5	1
17. Small hake	1	1	0.6	1	1
18. Medium hake	1	1	0.6	1	1
19. Large hake	1	1	0.6	1	1
20. Flatfishes	0.4	0.8	0.6	0.7	1
21. Small demersals	0.4	0.2	0.6	0	
22. Benthic elasmobranchs	0.4	0.2	0.6	0.7	1
23. Butter fishes	0.4	0.2	0.6	0.7	
24. Conger	0.4	0.6	0.6	0.7	
25. Medium demersal fish	0.4	0.8	0.6	0.7	1
26. Medium sciaenids	0.7	0.8	0.6	0.7	1
27. Sea robin	0.7	0.8	0.6	0.7	
28. Catfish	0.4	0.1	0.6	0.7	1
29. Chondrichthyans	0	0.5	0.6	0.7	1
30. Seabirds	1	1	0.6	1	
31. Pinnipeds	1	1	0.6	1	
32. Cetaceans	0.4	0.6	0.6	0	

chondrichthyans). During the 1997–98 EN, Delgado et al. (2001) found dinoflagellates (*e.g. Ceratium breve, Ceratium praelongum*), and Ayón et al. (1997) found fish larvae (*e.g. Hoplunnis pacifica, Monolene maculipinna*) south of their characteristic ranges, immigrating with the intrusion of warm water masses.

For fish, catch reductions accompanied biomass reductions (Fig. 3), with the exception of sustained high catch changes of mackerel and catfish during EN (whose fishing mortalities were quite low in the cold period). Total catches decreased 41% during EN and the ratio of total catch to biomass decreased 19% (Table 6). A slope < 1.0 in Fig. 3 indicates that biomass changes do not translate immediately or fully into catch changes. Future management measures, should consider that EN-related reduction of catches should be at least proportional to the reduction of biomasses, allowing the exploitation rate (*F*/*Z*) to be maintained. The general biomass and catch reductions during EN can also be appreciated in the pyramids given in Fig. 4.

Separation of phytoplankton into two functional groups (diatoms and silico-dinoflagellates) permits description of alternate pathways and differential responses of consumers. The reduction of diatom biomass during EN forced remaining omnivorous planktivorous fishes (anchovy and other small pelagics) to prey more on zooplankton in the model, (increasing their trophic level). Espinoza and Bertrand (2008) found a higher fraction of zooplankton during EN than in 1996 in anchovy stomachs. Modelled TL of anchovy increased from 2.35 to 3.17 from LN to EN conditions (Table 5). Consequently, the TL of piscivorous groups (large pelagics, seabirds, pinnipeds) also increased. Anchovy biomass reduction left sardine consumption of diatoms and dinoflagellates to increase slightly during EN, possibly in compensation for the increased competition with remaining anchovy for zooplankton, and because sardines are more efficient removers of small particles than anchovy (van der Lingen et al., 2006).

IMARPE zooplankton sampling (300 μm mesh size nets towed from 0 to 50 m depth) captures mainly mesozooplankton, while macrozooplankton, specifically euphausiids, are undersampled due to their deeper distribution. For this reason, biomass of macrozooplankton was estimated within the model, resulting in 21.1 t km^{-2} during 1995–96, and 34.8 t km^{-2} during 1997–98. These high estimates are nevertheless conservative given that they were back-calculated using an ecotrophic efficiency of 0.95. Back calculations must be taken with caution and should ultimately be complemented with dynamic approaches using Ecosim, preferably with long time series of functional groups biomasses, in order to better constrain the estimates (Guenette et al., 2008; Taylor et al., 2008a). Nevertheless, the existence of such a high macrozooplankton biomass is supported by Antezana (2002a) who described *Euphausia mucronata* with SHCE biomass values up to 500 g wet weight per 1000 m^3 within the oxygen minimum layer (Antezana, 2002b). Neira et al. (2004) also estimated high biomasses of euphausiids to meet the consumption requirements of model predators. Their estimates ranged from 73.6 to 106.3 t km^{-2} off central Chile. Moreover, the temporal variation of the diet of anchovy reported by Espinoza and Bertrand (2008) emphasized the importance of zooplankton over phytoplankton. All these evidences point to a high biomass of macrozooplankton in the NHCE as a prey of several species, especially during EN conditions when diatoms biomass diminishes. The apparent paradox of a high macrozooplankton biomass during EN conditions despite low phytoplankton biomass is explained by the lower consumption of diatoms by anchovy, leaving remaining phytoplankton for other species.

3.2. Trophic flows

A comparison of ecosystem indicators of both models (1995–96 and 1997–98) is presented in Table 6. According to Ulanowicz (1997), the 'size' of an ecosystem can be measured by its total activity in terms of energy flows, or by the total system throughput. In addition to the total biomass reduction (−26.7%), total system throughput reduced dramatically (−58.7%), along with a reduction of absolute energy flows for prey consumption, exports, respiration and to detritus. This reduction in the size of the modelled ecosystem in terms of total energy flows during EN is well-reflected in the energy flow pyramids (Fig. 4), where the volume of each compartment representing a trophic level is proportional to the total throughput of that level, and the top angle of the pyramids was made inversely proportional to the geometric mean of the transfer efficiencies between trophic levels.

A large decrease in total primary production during EN (−59.5%) exerted a bottom-up control and decreased ecosystem "size" or total system throughput in the model. During EN the percentage contributions of total system throughput (Table 6) shows slight changes, on one hand an increase in consumption, and on the other hand a reduction in exports and flows into detritus. The relative reduction in exports and flows into detritus apparently reflects an increase in grazing by meso- and macro-zooplankton on phytoplankton in the model. These percentage flow changes were however small, indicating that although EN dramatically alters the system's absolute size, the relative flow of energy between functional groups seems largely unaltered.

While a comparison between ecotrophic models should ideally be based on a common model structure (Moloney et al., 2005), it is noteworthy that the total system throughput (*ca.* 60000 t km^{-2} y^{-1}) in the 1964–71 model before the anchovy collapse (Jarre et al., 1998) is similar to the value (55689 t km^{-2} y^{-1}) obtained here for the LN model. Total system throughput is rather

Table 3
Diet composition of functional groups after the model was balanced, during LN (1995–96) and EN (1997–98). Values represent the fraction of the food intake in wet weight.

Prey/ predator	Years	3	4	5	6	7	8	9	10	11	12	13	14	15	16	17	18	19	20	21	22	23	24	25	26	27	28	29	30	31	32
1. Diatoms	1995–96	0.300	0.850	0.500			0.042	0.692				0.300		0.002						0.600		0.423									
	1997–98	0.200	0.300	0.500			0.123	0.017				0.300								0.600		0.447									
2. Dino- and Silicoflagellates	1995–96	0.100	0.050	0.100			0.003	0.004																							
	1997–98	0.200	0.500	0.400			0.051	0.000																							
3. Microzooplankton	1995–96	0.200	0.100	0.400			0.037	0.000						0.000																	
	1997–98	0.150	0.200	0.100				0.003																							
4. Mesozooplankton	1995–96				0.640		0.704	0.281	0.021	0.075		0.650		0.029						0.400		0.186					0.004				
	1997–98				0.640		0.566	0.603	0.021	0.056		0.650	0.002	0.003						0.400											
5. Macrozooplankton	1995–96				0.120		0.214	0.023	0.979	0.222	0.850		0.560	0.862		0.070	0.003	0.132			0.019	0.028		0.256	0.001	0.975	0.108				0.300
	1997–98				0.120		0.260	0.377	0.979	0.184	0.850		0.469	0.265	0.002	0.201	0.006	0.000			0.061			0.076	0.000	0.611		0.021			0.300
6. Gelatinous zooplankton	1995–96				0.040																				0.004						
	1997–98				0.040																	0.053									
7. Macrobenthos	1995–96					0.070							0.030			0.090	0.001	0.001	0.200		0.565	0.179	0.114	0.383	0.641	0.025	0.572				
	1997–98					0.070							0.020	0.020		0.190	0.069	0.004			0.552	0.500	0.114	0.861	0.473	0.171	0.950	0.083			
8. Sardine	1995–96															0.060					0.031				0.013						
	1997–98													0.017							0.017				0.004				0.447		
9. Anchovy	1995–96									0.043			0.200		0.699	0.358	0.645	0.005	0.500		0.078			0.100	0.184		0.198	0.213	0.877	0.539	0.100
	1997–98									0.040				0.401	0.623	0.069	0.082	0.023	0.455		0.082			0.018	0.190			0.208	0.377	0.377	0.100
10. Mesopelagics	1995–96									0.387				0.005				0.011							0.001					0.004	
	1997–98									0.337				0.001		0.151	0.173	0.002												0.058	
11. Jumbo squid	1995–96									0.120					0.071	0.112					0.022				0.005			0.667			0.200
	1997–98									0.242							0.012	0.111			0.005							0.042			0.200
12. Other Cephalopods	1995–96									0.077			0.120	0.102	0.088	0.070		0.002			0.114		0.037	0.043	0.008			0.009			
	1997–98									0.069						0.035	0.005	0.005			0.015		0.037	0.002	0.031			0.125			
13. Other small pelagics	1995–96									0.044			0.040		0.001	0.005	0.055				0.002			0.001	0.037		0.001		0.036	0.009	
	1997–98									0.040			0.029	0.199	0.210	0.163	0.205	0.020			0.005			0.011	0.051	0.218			0.126	0.008	
14. Horse mackerel	1995–96																				0.001								0.015	0.015	0.200
	1997–98																	0.005			0.005							0.021		0.011	0.200
15. Mackerel	1995–96																														0.200
	1997–98																	0.076													0.200

16. Other large pelagics	1995–96																								0.001					
	1997–98															0.003					0.005				0.002			0.374		
17. Small hake	1995–96									0.032								0.386										0.099		0.013
	1997–98									0.032						0.016	0.147	0.406										0.058		0.050
18. Medium hake	1995–96																				0.049		0.218					0.011		
	1997–98																						0.216					0.004		
19. Large hake	1995–96																											0.001		
	1997–98																											0.001		
20. Flatfishes	1995–96																				0.002		0.009	0.001						
	1997–98																				0.005		0.009							
21. Small demersals	1995–96										0.050		0.040	0.000	0.141	0.165	0.046	0.115			0.099		0.031	0.186	0.031				0.072	0.410
	1997–98										0.050		0.001	0.093	0.165	0.150	0.289	0.069			0.117		0.031	0.030	0.200			0.021	0.050	0.471
22. Benthic elasmobranchs	1995–96																													
	1997–98																													
23. Butter fish	1995–96																								0.001					
	1997–98																				0.003				0.002					
24. Conger	1995–96																	0.030			0.000									
	1997–98																													
25. Medium demersal fish	1995–96																		0.300		0.009		0.324	0.030	0.003					0.006
	1997–98															0.020	0.001	0.014	0.545		0.040		0.326	0.002	0.017			0.021		0.015
26. Medium sciaenids	1995–96																	0.159			0.007				0.050					0.004
	1997–98															0.002	0.011	0.241			0.029				0.030					0.010
27. Sea robin	1995–96															0.070	0.250	0.159					0.233							
	1997–98													0.001				0.024					0.233					0.021		
28. Catfish	1995–96																				0.002						0.114			
	1997–98																				0.014									
29. Chondrichthyans	1995–96																													
	1997–98																													
30. Seabirds	1995–96																													
	1997–98																													
31. Pinnipeds	1995–96																													
	1997–98																													
32. Cetaceans	1995–96																													
	1997–98																													
33. Detritus	1995–96	0.400			0.200	0.800							0.010									0.184	0.034		0.021		0.003			
	1997–98	0.450			0.200	0.800							0.479								0.045		0.034				0.050			
Import	1995–96					0.130					0.100	0.050																		
	1997–98					0.130					0.100	0.050																		

Table 4
Ecosystem indicators and their definitions.

Ecosystem indicator	Definition (Christensen et al. 2005)
Trophic indicators	
Total system throughput	Sum of all flows in a system, represents the size of the system in terms of flows
Total net primary production	Summed production from all primary producers. Primary producers are groups that capture energy through photosynthesis (e.g. phytoplankton and benthic algae)
Mean transfer efficiency	Geometric mean of transfer efficiencies for trophic levels II–IV
Connectance index	Ratio of the number of actual links to the number of possible links. It can be expected to be correlated with maturity
Mixed trophic impact	Combined direct and indirect trophic impacts that an infinitesimal increase of any of the groups is predicted to have on the other groups of the ecosystem
Fishery indicators	
Mean trophic level of the catch	Sum of trophic levels of species in the catch weighted by their contribution to the catch
Gross efficiency of the fishery	The sum of all realized fisheries catches relative to the total net primary production
Primary production required to sustain catches (PPR)	Flows in each path towards the catch of a group are converted to primary production equivalents using the product of catch, production/consumption and the proportion of each group in the path in the diets of the other groups
Energetic indicators	
System primary production/respiration	Ratio between total primary production and total respiration. In mature systems, the ratio should approach 1
System primary production/biomass	Ratio between total primary production and total biomass. In mature systems, the ratio should decline
System biomass/throughput	Ratio between total biomass and total system throughput. In mature systems, the ratio should increase
Network indicators	
Finn's cycling index	Fraction of an ecosystem's throughput that is recycled
Relative ascendency	Ratio between ascendency and developmental capacity, a measure of ecosystem network efficiency (organization)

insensitive to changes in trophic web topology, but is strongly affected by energy flow changes.

Analysis of modeled prey consumption rates of predators (not shown) showed that horse mackerel, mackerel, hake and seabirds, consumed 28% and 46% of anchovy production during LN and EN conditions, respectively. Medium hake mainly preyed upon anchovy, sea robin, small pelagics and small demersals, while jumbo squid preyed upon mesopelagics and macrozooplankton.

Transfer efficiencies during LN conditions were similar as for other upwelling systems with most transfer efficiencies under 10% (Christensen and Pauly, 1995), except for a peak value at trophic level III (17%) due to high utilization of anchovy production (Fig. 5). The slight reductions of transfer efficiencies at high trophic levels during the EN conditions could reflect bottom-up control effects of anchovy over pinnipeds and seabirds. Majluf (1989) mentioned that reductions in the availability of anchoveta cause fur seals have to take a wider range of prey. Tovar et al. (1987) concluded that a lack of food is the ultimate cause for the mass mortalities of seabirds, as for every EN there is a corresponding decline of guano bird numbers. In general, during EN there was an increased utilization of energy at lower levels, while higher trophic levels have similar transfer efficiencies.

Consumption of macrozooplankton increased by 65% during EN conditions, assuming it was the main prey group in both periods for mesopelagic fishes. During EN, several immigrants come from equatorial and oceanic waters, such as chondrichtyans, mesopelagics (lightfish and lanternfish), other small pelagics and other large pelagics, which could impact different trophic levels. Mesopelagic *Vinciguerria* sp. are known to move towards the coast during EN, providing prey for jumbo squid. The increasing trend of jumbo squid, after 1997–98 EN, occurred in parallel to an increase of mesopelagics, thus a possible bottom-up control of mesopelagics over jumbo squid was explored with dynamic simulations (Taylor et al., 2008a).

3.3. Ecosystem indicators

Percentage changes of modelled ecosystem indicators from LN to EN (Table 6) showed that the overall reduction in primary production during EN, produced coherent changes in trophic, fisheries, energetic and network indicators. Fishery indicators showed a reduction in catches, accompanied by lower catch/biomass ratio and pelagic catch/demersal catch ratio, but higher trophic level of the catch and primary production required/catch ratio. In the NHCE, the mean trophic level of the catch increased temporarily (+19%) during EN, mainly due to the increase of anchovy trophic level and a higher proportion of other species in the catch (e.g. mackerel, horse mackerel and other large pelagics). When only demersal fishes are taken into account, trophic level of the catch decreased during EN (from 3.66 to 3.34). However, at a larger spatio-temporal scale, the mean trophic level of the catch showed a decreasing trend from 1980 to 1994 in the South Eastern Pacific (Pauly et al., 1998), suggesting a fishing down the food web process, probably due to the recovery of anchovy, the main target species at low trophic level. Primary production required to sustain the fishery is a function of the trophic level of the species that are caught, as more primary production is required to produce one tonne of a high-level trophic fish, than of a low-level trophic fish.

Thus, despite lower catches during EN (−41%), the increased trophic level of target species resulted in a higher primary production required/catch (+39%), which implies an ecologically costly fishery and stresses the need for precautionary management during and after EN.

Most energetic indicators (net system production, net primary production and primary production/biomass ratio) decreased during EN (Table 4), except the higher system biomass/throughput ratio, apparently indicating a more energetically efficient ecosystem (Odum, 1969) during EN. However, network indicators such as lower Finn's cycling index and relative ascendency indicated a less "organized" ecosystem during EN, which according to Ulanowicz (1986) reflects lower ecosystem growth and development. This result is similar to that of Jarre and Pauly (1993) who estimated a seasonal decrease of cycling in winter and spring, due to lower biomasss and activity of zooplankton and benthos as the principal consumers of detritus. During the LN conditions trophic flows were more articulated, channelling energy flows mainly through anchoveta and showing better adaptation of cold water species to upwelling conditions. Using models before and after the anchovy collapse, Pauly (1987) also mentioned that the Peruvian upwelling ecosystem was better organized before 1972–73 EN than thereaf-

Table 5

Model outputs of the NHCE during (a) LN and (b) EN. Trophic level (*TL*), biomass (*B*), production (*P*), consumption (*Q*), ecotrophic efficiency (*EE*), gross efficiency (*GE*), catch (*C*), fishing mortality (*F*), non-predatory mortality (*M*0) and predatory mortality (*M*2). Parameters in bold were estimated by the model.

(a) LN Functional group/parameter	*TL*	*B* ($t\ km^{-2}$)	*P*/*B* (y^{-1})	*Q*/*B* (y^{-1})	*EE*	*GE*	*C* ($t\ km^{-2}\ y^{-1}$)	*F* (y^{-1})	*M*0 (y^{-1})	*M*2 (y^{-1})
1. Diatoms	1.00	53.416	265.000	–	0.801	–	0.000	0.000	52.690	**212.310**
2. Dino- and silicoflagellates	1.00	9.426	265.000	–	**0.960**	–	0.000	**0.000**	**10.643**	**254.357**
3. Microzooplankton	**2.25**	**20.484**	256.000	**1024.000**	0.950	0.250	0.000	**0.000**	**12.800**	**243.200**
4. Mesozooplankton	**2.13**	31.164	40.000	**125.000**	**0.515**	0.320	0.000	**0.000**	**19.397**	**20.603**
5. Macrozooplankton	**2.50**	**21.096**	**19.085**	46.550	0.950	0.410	0.000	**0.000**	**0.954**	**18.131**
6. Gelatinous zooplankton	**2.98**	**0.017**	0.584	**2.920**	0.950	0.200	0.000	**0.000**	**0.029**	**0.555**
7. Macrobenthos	**2.06**	20.729	1.200	10.000	**0.994**	**0.120**	0.000	**0.000**	**0.007**	**1.193**
8. Sardine	**3.16**	7.567	1.400	**14.000**	**0.853**	0.100	7.969	**1.053**	**0.206**	**0.141**
9. Anchovy	**2.35**	83.293	2.000	**20.000**	**0.469**	0.100	30.474	**0.366**	**1.063**	**0.572**
10. Mesopelagics	**3.49**	6.882	1.400	**14.000**	**0.575**	0.100	0.000	**0.000**	**0.595**	**0.805**
11. Jumbo squid	**4.18**	0.524	8.910	**25.457**	**0.940**	0.350	0.186	**0.354**	**0.534**	**8.021**
12. Other Cephalopods	**3.50**	**6.584**	4.300	**12.286**	0.950	0.350	0.055	**0.008**	**0.215**	**4.077**
13. Other small pelagics	**2.77**	**7.804**	1.000	**10.000**	0.950	0.100	0.688	**0.088**	**0.050**	**0.862**
14. Horse mackerel	**3.57**	11.568	1.200	**12.000**	**0.130**	0.100	1.451	**0.125**	**1.044**	**0.031**
15. Mackerel	**3.59**	8.488	0.850	**8.500**	**0.048**	0.100	0.096	**0.011**	**0.809**	**0.029**
16. Other large pelagics	**3.60**	0.589	0.850	**8.500**	**0.503**	0.100	0.250	**0.425**	**0.422**	**0.003**
17. Small hake	**3.77**	2.771	0.928	**6.187**	**0.623**	0.150	0.975	**0.352**	**0.350**	**0.226**
18. Medium hake	**3.66**	0.414	1.627	**10.847**	**0.394**	0.150	0.218	**0.526**	**0.987**	**0.114**
19. Large hake	**4.32**	0.055	1.044	**6.960**	**0.295**	0.150	0.017	**0.307**	**0.736**	**0.001**
20. Flatfishes	**3.60**	0.040	0.304	**2.027**	**0.821**	0.150	0.006	**0.158**	**0.055**	**0.091**
21. Small demersals	**2.45**	**7.089**	2.300	**15.333**	0.950	0.150	0.019	**0.003**	**0.115**	**2.182**
22. Benthic elasmobranchs	**3.48**	0.078	1.000	**6.667**	**0.401**	0.150	0.031	**0.401**	**0.599**	**0.000**
23. Butter fishes	**2.44**	0.032	0.800	**4.000**	**0.039**	0.200	0.000	**0.000**	**0.768**	**0.032**
24. Conger	**4.21**	0.019	0.750	**5.000**	**0.823**	0.150	0.000	**0.000**	**0.132**	**0.618**
25. Medium demersal fish	**3.38**	0.200	1.320	**8.800**	**0.997**	0.150	0.125	**0.626**	**0.005**	**0.690**
26. Medium sciaenids	**3.24**	0.369	0.746	**4.973**	**0.859**	0.150	0.067	**0.181**	**0.105**	**0.459**
27. Sea robin	**3.49**	0.789	3.400	**17.000**	**0.897**	0.200	0.000	**0.000**	**0.351**	**3.049**
28. Catfish	**3.31**	0.577	0.900	**6.000**	**0.893**	0.150	0.068	**0.118**	**0.096**	**0.686**
29. Chondrichthyans	**4.74**	0.027	0.486	**3.240**	**0.508**	0.150	0.007	**0.247**	**0.239**	**0.000**
30. Seabirds	**3.39**	0.067	0.040	60.000	**0.000**	**0.001**	0.000	**0.000**	**0.040**	**0.000**
31. Pinnipeds	**3.45**	0.072	0.100	45.900	**0.000**	**0.002**	0.000	**0.000**	**0.100**	**0.000**
32. Cetaceans	**4.25**	0.062	0.100	20.000	**0.000**	**0.005**	0.000	**0.000**	**0.100**	**0.000**
33. Detritus	1.00		–	–	**0.814**	–	0.000	**0.000**	**0.000**	**0.000**
(b) EN 1. Diatoms	1.00	14.761	210.000	–	**0.945**	–	0.000	**0.000**	**11.652**	**198.348**
2. Dino- and silicoflagellates	1.00	17.328	210.000	–	**0.841**	–	0.000	**0.000**	**33.286**	**176.714**
3. Microzooplankton	**2.18**	**6.572**	256.000	**1024.000**	0.950	0.250	0.000	**0.000**	**12.800**	**243.200**
4. Mesozooplankton	**2.24**	17.000	40.000	**125.000**	**0.947**	0.320	0.000	**0.000**	**2.104**	**37.896**
5. Macrozooplankton	**2.12**	**34.773**	**19.085**	46.550	0.950	0.410	0.000	**0.000**	**0.954**	**18.131**
6. Gelatinous zooplankton	**3.00**	**0.003**	0.584	**2.920**	0.950	0.200	0.000	**0.000**	**0.029**	**0.555**
7. Macrobenthos	**2.06**	25.605	1.200	10.000	**0.995**	**0.120**	0.000	**0.000**	**0.006**	**1.194**
8. Sardine	**2.99**	8.318	1.400	**14.000**	**0.396**	0.100	3.334	**0.401**	**0.846**	**0.153**
9. Anchovy	**3.17**	33.340	2.000	**20.000**	**0.679**	0.100	14.477	**0.434**	**0.642**	**0.924**
10. Mesopelagics	**3.12**	22.375	1.400	**14.000**	**0.137**	0.100	0.000	**0.000**	**1.208**	**0.192**
11. Jumbo squid	**4.14**	0.243	8.910	**25.457**	**0.853**	0.350	0.014	**0.058**	**1.305**	**7.547**
12. Other Cephalopods	**3.14**	**0.227**	4.300	**12.286**	0.950	0.350	0.012	**0.053**	**0.215**	**4.032**
13. Other small pelagics	**2.85**	**21.419**	1.000	**10.000**	0.950	0.100	2.357	**0.110**	**0.050**	**0.840**
14. Horse mackerel	**2.60**	3.030	1.200	**12.000**	**0.616**	0.100	1.937	**0.639**	**0.461**	**0.100**
15. Mackerel	**3.74**	6.892	0.850	**8.500**	**0.279**	0.100	1.345	**0.195**	**0.613**	**0.042**
16. Other large pelagics	**3.99**	1.757	0.400	**4.000**	**0.687**	0.100	0.351	**0.200**	**0.125**	**0.075**
17. Small hake	**3.59**	1.245	1.317	**8.780**	**0.909**	0.150	0.556	**0.447**	**0.120**	**0.751**
18. Medium hake	**3.89**	0.163	1.946	**12.973**	**0.354**	0.150	0.107	**0.656**	**1.257**	**0.033**
19. Large hake	**4.51**	0.028	1.516	**10.107**	**0.286**	0.150	0.012	**0.429**	**1.082**	**0.005**
20. Flatfishes	**4.14**	0.010	0.304	**2.027**	**0.882**	0.150	0.001	**0.100**	**0.036**	**0.168**
21. Small demersals	**2.49**	**4.897**	2.300	**15.333**	0.950	0.150	0.016	**0.003**	**0.115**	**2.182**
22. Benthic elasmobranchs	**3.33**	0.045	1.000	**6.667**	**0.933**	0.150	0.042	**0.933**	**0.067**	**0.000**
23. Butter fishes	**2.64**	0.006	0.800	**4.000**	**0.845**	0.200	0.000	**0.000**	**0.124**	**0.676**
24. Conger	**4.12**	0.004	0.750	**5.000**	**0.000**	0.150	0.000	**0.000**	**0.750**	**0.000**
25. Medium demersal fish	**3.11**	0.211	2.480	**16.533**	**0.905**	0.150	0.144	**0.682**	**0.236**	**1.561**
26. Medium sciaenids	**3.50**	0.218	1.085	**7.233**	**0.977**	0.150	0.043	**0.197**	**0.024**	**0.863**
27. Sea robin	**3.27**	0.319	3.220	**16.100**	**0.052**	0.200	0.000	**0.000**	**3.054**	**0.166**
28. Catfish	**3.01**	0.650	0.900	**6.000**	**0.937**	0.150	0.544	**0.837**	**0.057**	**0.006**
29. Chondrichthyans	**4.40**	0.078	0.486	**3.240**	**0.501**	0.150	0.019	**0.244**	**0.242**	**0.000**
30. Seabirds	**4.01**	0.010	0.040	60.000	**0.000**	**0.001**	0.000	**0.000**	**0.040**	**0.000**
31. Pinnipeds	**3.86**	0.053	0.100	45.900	**0.000**	**0.002**	0.000	**0.000**	**0.100**	**0.000**
32. Cetaceans	**4.05**	0.067	0.100	20.000	**0.000**	**0.005**	0.000	**0.000**	**0.100**	**0.000**
33. Detritus	1.00	–	–	–	**0.824**	–	0.000	**0.000**	**0.000**	**0.000**

ter. On a smaller spatial scale, Taylor et al. 2008b also found a similar increase in energetic efficiency and decrease in ecosystem organization at Independencia Bay during EN.

In general, biomass and trophodynamic changes indicated that during 1997–98 EN, the ecosystem temporarily moved from its original optimum operating point (Kay, 1991), but returned to it, in

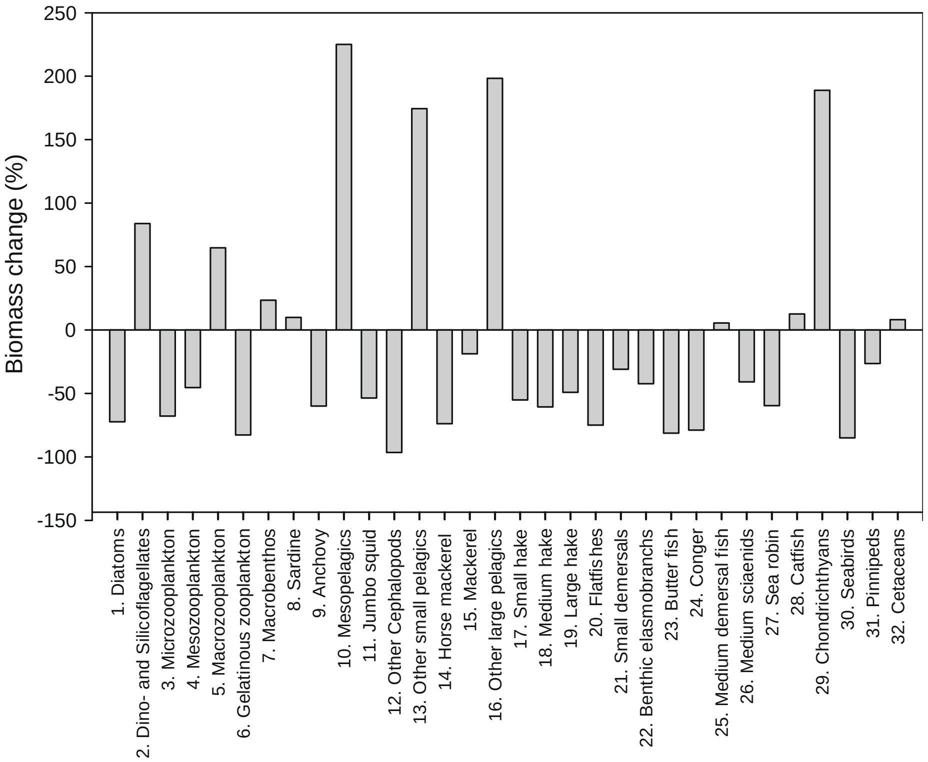

Fig. 2. Percentage biomass changes of functional groups from LN to EN.

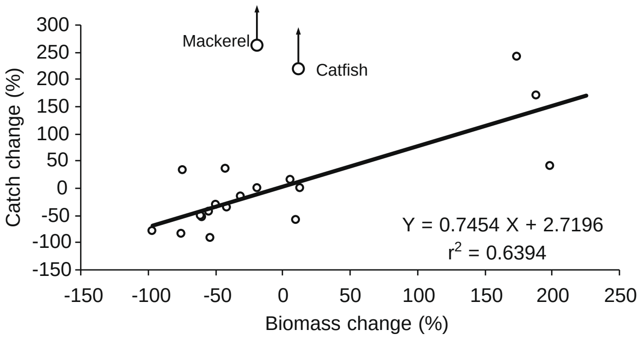

Fig. 3. Relationship between percentage biomass changes and percentage catch changes (excluding mackerel and catfish) from LN to EN.

agreement with the consideration that EN is a typical perturbation to the NHCE.

4. Conclusions

While past ecotrophic modeling efforts in the NHCE dealt with interdecadal changes (Jarre et al., 1991), this study focused on the interannual changes associated with El Niño and the Southern Oscillation (ENSO) cycle. The main finding of previous models was a decrease in relative ascendency from the 1950s to the 1970s, after the decline of the anchoveta, which led to an increase in parallel energy transfer and food web connectance, as energy flows through anchovy were channeled through other species. Our models, with increased details in the planktonic and demersal groups, and incorporation of mesopelagic fishes and jumbo squid, determined three main impacts of EN on the food web: (i) dramatic

Table 6

Comparison of ecosystem indicators from models of the NHCE for both periods, including % change from LN to EN. Values in brackets are in percent of Total system throughput.

Ecosystem indicators	LN	EN	% Change
Trophic indicators			
Total system throughput (t km^{-2} yr^{-1})	55,689	22,986	−58.7
Sum of all consumption (t km^{-2} yr^{-1})	28,478 (51.1%)	12,259 (53.3%)	−57.0
Sum of all exports (t km^{-2} yr^{-1})	2004 (3.6%)	718 (3.1%)	−64.1
Sum of all respiratory flows (t km^{-2} yr^{-1})	14,688 (26.4%)	6065 (26.4%)	−58.7
Sum of all flows into detritus (t km^{-2} yr^{-1})	10,519 (18.9%)	3944 (17.2%)	−62.5
Sum of all production (t km^{-2} yr^{-1})	23,847	9957	−58.2
Total net primary production (t km^{-2} yr^{-1})	16,653	6739	−59.5
Net system production (t km^{-2} yr^{-1})	1965	674	−65.7
Total biomass (excluding detritus) (t km^{-2})	302	222	−26.7
Mean transfer efficiency (II–IV)	10.17	11.72	15.2
Connectance index	0.168	0.174	3.6
System omnivory index	0.203	0.190	−6.4
Fishery indicators			
Total catches (t km^{-2} yr^{-1})	42.70	25.31	−40.7
Mean trophic level of the catch	2.62	3.12	19.1
Gross efficiency (catch/total net primary production)	0.0026	0.0038	46.5
Total catch/total biomass	0.14	0.11	−19.2
Pelagic/demersal catches	26.98	16.28	−39.7
PPR (t km^{-2} yr^{-1})	2420.1	1995.6	−17.5
PPR/total primary produciton (%)	14.5	29.6	103.8
PPR/catch	56.675	78.844	39.1
Energetic indicators			
System primary production/respiration	1.134	1.111	−2.0
System primary production/biomass	55.089	30.403	−44.8
System biomass/throughput	0.005	0.010	100.0
Network indicators			
Finn's cycling index	12.61	7.49	−40.6
Ascendency/development capacity (%)	46.2	40.4	−12.6

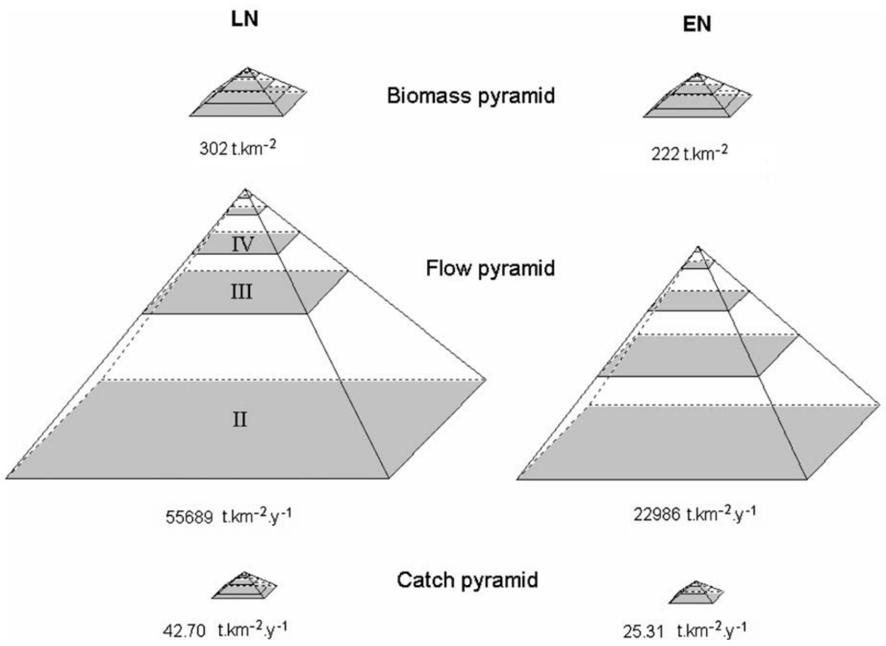

Fig. 4. Biomass (upper), energy flow (middle) and catch (lower) pyramids by discrete trophic levels in LN (left) and EN (right). The size of the pyramids is proportional to the values of biomass, energy flow or catch.

but temporary shrinking of ecosystem size in terms of flows and ecosystem organization, (ii) slight changes in overall functioning (i.e. proportion of energy flows used for respiration, consumption by predators, detritus and export), and (iii) use of alternate pathways through more zooplankton predation on primary producers, leading to a higher impact of the fishery on ecosystem flows. Consequently, trophic level of piscivorous groups also increased. Sardine consumption of diatoms and dinoflagellates increased in order to compensate for the increased competition with anchovy for zooplankton, and because sardines are more efficient removers of small particles than anchovy (van der Lingen et al., 2006). A high biomass of macrozooplankton was needed to balance the con-

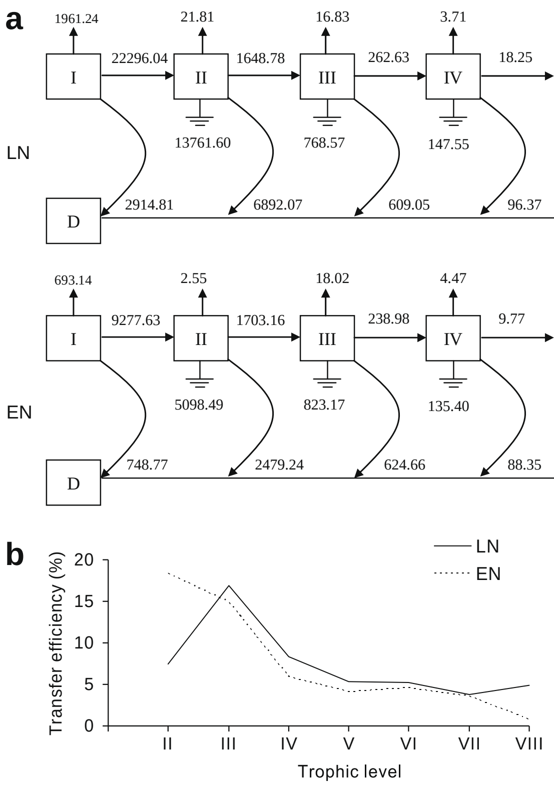

Fig. 5. Comparison of trophic structures in LN and EN: (a) NHCE canonical trophic food chains. Flow networks were aggregated into equivalent trophic chains with distinct trophic levels. Flows are in t.km^{-2}.y^{-1}, straight arrows indicate exports, ground symbols indicate respirational losses, and curved arrows indicate returns to detritus. (b) Transfer efficiencies by discrete trophic levels.

sumption by planktivores, especially during EN conditions when diatoms diminish dramatically. In these conditions, macrozooplankton consumed the remaining phytoplankton left by the reduced anchovy population. EN increased temporarily the trophic level of the catch, and despite lower catches, the higher PPR/catch ratio implied a stronger ecological impact of the fishery, which stresses the need for precautionary management during and after EN. Energetic indicators showed lower system primary production/biomass ratio during EN indicating a more energetically efficient ecosystem, however network indicators showed a lower cycling index, especially at higher trophic levels, and relative ascendency suggesting a less organized ecosystem during EN conditions. These results give support to our general hypothesis that EN is a typical perturbation in the NHCE.

Acknowledgements

We want to thank Renato Guevara, Miguel Ñiquen, Mariano Gutiérrez, Carmen Yamashiro and Sonia Sánchez from IMARPE, for the shared information. We also thank Arnaud Bertrand and Timothée Brochier from the Institute of Research for Development (IRD) for discussions on anchovy ecology, the staff of the Oceanographic and Fishery Biological Modelling Research Center (CIMOBP, IMARPE) and the staff of the CENSOR project for their helpful comments. We also thank Dr. Lynne Shannon, Dr. J. Timothy Pennington and an anonymous referee for their critical suggestions on the manuscript. This study was partly financed and conducted in the frame of the EU-project CENSOR (Climate variability and El Niño Southern Oscillation: Impacts for natural resources and management, contract No. 511071) and is CENSOR publication No. 0085.

References

Aguilar, P. (Ed.), 1999. Fórum El Fenómeno El Niño 1997–98: evolución, pronóstico y mitigación. Informe Final. Publicación Espéciale del Instituto del Mar del Perú, Lima, 150p.

Alamo, A., Navarro, I., Espinoza, P., Zubiate, P., 1996a. Relaciones tróficas, espectro alimentario y ración de alimentación de las principales especies pelágicas en el verano de 1996. Informe del Instituto del Mar del Perú 122, 36–46.

Alamo, A., Navarro, I., Espinoza, P., Zubiate, P., 1996b. Espectro alimentario y ración de alimentación de *Engraulis ringens* y de *Sardinops sagax sagax*, y mortalidad de huevos de la anchoveta peruana por predación. Informe del Instituto del Mar del Perú 119, 34–42.

Alamo, A., Espinoza, P., 1998. Variaciones alimentarias en *Engraulis ringens* y otros recursos pelágicos durante invierno – primavera de 1997. Informe del Instituto del Mar del Perú 130, 45–52.

Alamo, A., Espinoza, P., Zubiate, P., Navarro, I., 1997a. Comportamiento alimentario de la anchoveta peruana, *Engraulis ringens*, durante el invierno de 1996. Crucero BIC Humboldt 9608-09. Informe del Instituto del Mar del Perú 123, 38–96.

Alamo, A., Espinoza, P., Zubiate, P., Navarro, I., 1997b. Comportamiento alimentario de los principales recursos pelágicos peruanos en verano y comienzos de otoño 1997. Informe del Instituto del Mar del Perú 127, 82–89.

Alegre, A., Blaskovic, V., Castillo, C., Espinoza, P., Fernández, F., Flores, R., Peraltilla, S., Tafur, R., Tam, J., Taylor, M., Yamashiro, C., 2005. Comportamiento alimentario del calamar gigante (*Dosidicus gigas*), enfatizando la depredación ejercida sobre la merluza (*Merluccius gayi peruanus*). Informe Interno del Instituto del Mar del Perú, 36p.

Alheit, J., Niquen, M., 2004. Regime shifts in the Humboldt Current Ecosystem. Progress in Oceanography 60, 201–222.

Antezana, T., 2002a. Adaptive behavior of Euphausia mucronata in relation to the oxygen minimum layer of the Humboldt Current. In: Färber Lorda, J. (Ed.), Oceanography of the Eastern Pacific. Editorial CICESE, Mexico, pp. 29–40.

Antezana, T., 2002b. Vertical distribution and diel migration of Euphausia macronata in the oxygen minimum layer of the Humboldt Current. In: Färber Lorda, J. (Ed.), Oceanography of the Eastern Pacific II. Editorial CICESE, Mexico, pp. 13–28.

Arancibia, H., Neira, S., Christensen, V., Olson, R., Arreguín-Sánchez, F., Cubillos, L., Quiñones, R., Gatica, C., Medina, M., 2003. Enfoque metodoldgico para el analisis ecosistemico en la administraction de pesquerias de la zona central de chile. Informe Final Proyecto FIP, 2001-29, 278p.

Arias-Schreiber, M., 2003. Prey spectrum and feeding behaviour of two sympatric pinnipeds (*Arctocephalus australis and Otaria flavencens*) in relation to the 1997-98 ENSO in southern Peru. MSc., University of Bremen, Bremen, Germany.

Arntz, W.E., Fahrbach, E., 1991. El Niño: experimento climático de la naturaleza, causas físicas y efectos biológicos. Fondo de Cultura Económica, Mexico, 309p.

Au, D.W., Smith, S.E., 1997. A demographic method with population density compensation for estimating productivity and yield per recruit of the leopard shark (*Triakis semifasciata*). Canadian Journal of Fisheries and Aquatic Sciences 54, 415–420.

Ayón, P., Arones, K., 1997a. Características generales del zooplancton en la costa norte centro durante el crucero BIC SNP-1 9607-08. Informe del Instituto del Mar del Perú 124, 51–56.

Ayón, P., Arones, K., 1997b. Comunidades de zooplancton e ictioplancton frente a la costa norte-centro del Perú Crucero BIC Humboldt 9705-06. Informe del Instituto del Mar del Perú 128, 70–79.

Ayón, P., Criales-Hernandez, M.I., Schwamborn, R., Hirche., H.-J., 2008. Zooplankton research off Peru: a review. Progress in Oceanography 79, 238–255.

Ballón, M., 2005. Comparative analysis of the community structure and trophic relations of the Peruvian hake *Merluccius gayi peruanus* and its by-catch of the years 1985 and 2001. MSc. Thesis. University of Bremen, 74p.

Bello, R., Arias-Schreiber, M., Sánchez, R., 1998. Distribución y abundancia relativa de cetáceos durante el Crucero BIC Humboldt 9709-10, de Matarani a Paita. Informe del Instituto del Mar del Perú 130, 78–85.

Bertrand, A., Segura, M., Gutiérrez, M., Vásquez, L., 2004. From small-scale habitat loopholes to decadal cycles: a habitat-based hypothesis explaining fluctuation in pelagic fish populations off Peru. Fish and Fisheries 5, 296–316.

Blaskovic, V., Torriani, F., Navarro, I., 1998. Características tróficas de las principales especies pelágicas durante el otoño 1998. Crucero BIC Jose Olaya Balandra 9805-06 de Tacna a Máncora. Informe del Instituto del Mar del Perú 137, 72–79.

Blaskovic, V., Espinoza, P., Torriani, F., Navarro, I., 1999. Hábitos alimentarios de la anchoveta frente al litoral peruano durante la primavera 98. Crucero BIC José Olaya Balandra 9811-12. Informe del Instituto del Mar del Perú 146, 77–86.

Bouchon, M., Cahuin, S., Ñiquen, M., 2001. Fluctuaciones de la ictiofauna pelágica en la región norte-centro del litoral peruano de 1994 a 1998. In: Tarazona, J., Arntz, W., Castillo, E. (Eds.), El Niño en América Latina: impact os biológicos y sociales. Consejo Nacional de Ciencia y Tecnología, Lima, Peru, pp. 73–79.

Brown, P.C., Painting, S.J., Cochrane, K.L., 1991. Estimates of phytoplankton and bacterial biomass production in the northern and southern Benguela ecosystems. South African Journal of Marine Science 11, 537–564.

Brush, M.J., Brawley, J.W., Nixon, S.W., Kremer, J.N., 2002. Modeling phytoplankton production: problems with the Eppley curve and an empirical alternative. Marine Ecology Progress Series 238, 31–45.

Calienes, R., Guillén, O., Lostanau, N., 1985. Variabilidad espacio-temporal de clorofila, producción primaria y nutrientes frente a la costa peruana. Boletín del Instituto del Mar del Perú 10, 1–44.

Cardoso, F., Tarazona, J., Paredes, C., 1998. Biological aspects of the Patagonian squid *Loligo gahi* (Cephalopoda: Loliginidae) in Huarmey, Peru. Revista Peruana de Biología 5, 9–14.

Carr, M.E., 2003. Simulation of carbon pathways in the planktonic ecosystem off Peru during the 1997–1998 El Niño and La Niña. Journal of Geophysical Research 108. 10-1-15.

Christensen, V., Pauly, D., 1992. ECOPATH II a software for balancing steady-state ecosystem models and calculating network characteristics. Ecological Modelling 61, 169–185.

Christensen, V., Pauly, D., 1995. Fish production, catches and the carrying capacity of the world oceans. Naga, The ICLARM Quarterly, 34–40.

Christensen, V., Walters, C., Pauly, D., 2005. Ecopath with Ecosim: a user's guide. Fisheries Centre Research Reports 12, 154.

Csirke, J., Guevara Carrasco, R., Cardenas, G., Niquen, M., Chipollini, A., 1996. Situation of the *Engraulis ringens* and *Sardinops sagax* resources and perspectives to the fishing in the Peruvian waters, north and central regions of the Peru coast. Boletín del Instituto del Mar del Perú 15, 1–23.

Delgado, E., Sánchez, S., Chang, F., Villanueva, P., Fernández, C., 2001. El fitoplancton frente a la costa peruana durante el Niño 1997-98. In: Tarazona, J., Arntz, W., Castillo, E. (Eds.), El Niño América Latina: impactos biológicos y sociales. CONCYTEC, Lima, pp. 29–38.

Dugdale, R.C., MacIsaac, J.J., 1971. A computational model for the uptake of nitrate in the Peru upwelling region. Investigación Pesquera 35, 299–308.

Espinoza, J., Navarro, I., Torriani, F., 1998a. Variaciones en el espacio alimentario de los principales recursos pelágicos durante otoño 1998. Crucero 9803-05 de Tumbes a Tacna. Informe del Instituto del Mar del Perú 135, 134–142.

Espinoza, P., Blaskovic, V., Navarro, I., 1998b. Comportamiento alimentario de Engraulis ringens, a finales del invierno 1998. Crucero de evaluación hidroacústica de recursos pelágicos 9808-09. Informe del Instituto del Mar del Perú 141, 67–71.

Espinoza, P., Bertrand, A., 2008. Revisiting Peruvian anchovy (*Engraulis ringens*) trophodynamics provides a new vision of the Humboldt Current system. Progress in Oceanography 79, 215–227.

Frisk, M.G., Miller, T.J., Dulvy, N.K., 2001. Life histories and vulnerability to exploitation of elasmobranchs: Inferences from elasticity, perturbation and phylogenetic analyses. Elasmobranch fisheries: Managing for sustainable use and biodiversity conservation, Dartmouth, NS (Canada). Northwest Atlantic Fisheries Organization.

Guenette, S., Christensen, V., Pauly, D., 2008. Trophic modelling of the Peruvian upwelling ecosystem: towards reconciliation of múltiple datasets. Progress in Oceanography 79, 352–365.

Guillén, V., 1990. Alimentación del pelícano o alcatraz (*Pelecanus thagus*) en la isla Macabí. Boletín de Lima 67, 85–88.

Gutiérrez, M., 2001. Efectos del evento El Niño 1997–98 sobre la distribución y abundancia de anchoveta (*Engraulis ringens*). In: Tarazona, J., Arntz, W., Castillo,

E. (Eds.), El Niño en América Latina: impact os biológicos y sociales. Consejo Nacional de Ciencia y Tecnología, Lima, pp. 55–72.

IMARPE, 2006. Estadísticas pesqueras. En línea: <http://www.imarpe.gob.pe/imarpe/estadispesquera.php>.

Jahncke, J., Checkley, D.M., Hunt, G.L., 2004. Trends in carbon flux to seabirds in the Peruvian upwelling system: effects of wind and fisheries on population regulation. Fisheries Oceanography 13, 208–223.

Jarre-Teichmann, A., Muck, P., Pauly, D., 1989. Interactions between fish stocks in the Peruvian upwelling ecosystem. ICES 1989 MSM Symposium Paper 27, 24p.

Jarre-Teichmann, A., 1998. The potential role of mass balance models for the management of upwelling ecosystems. Ecological Applications 8, S93–S103.

Jarre, A., Muck, P., Pauly, D., 1991. Two approaches for modelling fish stock interactions in the Peruvian upwelling ecosystem. In: Daanand, N., Sissenwine, M.P. (Eds.), Multispecies Models Relevant to Management of Living Resources. ICES Marine Science Symposium 193, pp. 171–184.

Jarre, A., Pauly, D., 1993. Seasonal changes in the Peruvian upwelling ecosystem. In: Christensen, V., Pauly, D. (Eds.), Trophic Models of Aquatic Ecosystems, ICLARM Conference Proceedings, vol. 26, pp. 307–314.

Jarre-Teichmann, A., Christensen, V., 1998. Comparative modelling of trophic flows in four large upwelling ecosystems: global versus local effects. In: Durand, M.-H., Cury, Ph., Mendelssohn, R., Roy, C., Bakun, A., Pauly, D. (Eds.), Global versus Local Changes in Upwelling Systems. ORSTOM, Paris, pp. 423–443.

Jarre-Teichmann, A., Shannon, L.J., Moloney, C.L., Wickens, P.A., 1998. Comparing trophic flows in the Southern Benguela to those in other upwelling ecosystems. South African Journal of Marine Science 19, 391–414.

Kaschner, K., 2004. Modelling and Mapping Resource Overlap between Marine Mammals and Fisheries on a Global Scale. Ph.D. thesis, The University of British Columbia, Vancouver, BC, Canada.

Kay, J.J., 1991. A non-equilibrium thermodynamic framework for discussing ecosystem integrity. Environmental Management 15, 483–495.

Majluf, P., 1989. Reproductive ecology of South American fur seals in Peru. In: Pauly, D., Muck, P., Mendo, J., Tsukayama, I. (Eds.), The Peruvian Upwelling Ecosystem: Dynamics and Interactions, ICLARM Conference Proceedings, vol. 18, pp. 332–343.

Moloney, C.L., Jarre, A., Arancibia, H., Bozec, Y.-M., Neira, S., Jean-Paul Roux, J.-P., Shannon, L.J., 2005. Comparing the Benguela and Humboldt marine upwelling ecosystems with indicators derived from inter-calibrated models. ICES Journal of Marine Science 62, 493–502.

Morissette, L., 2007. Complexity, cost and quality of ecosystem models and their impact on resilience: a comparative analysis, with emphasis on marine mammals and the Gulf of St. Lawrence. Ph.D. Thesis, University of British Columbia, Canada.

Muck, P., Fuentes, H., 1987. Sea lion and fur seal predation on the Peruvian anchoveta, 1953 to 1982. In: Pauly, D., Tsukayama, I. (Eds.), The Peruvian Anchoveta and its Upwelling Ecosystem: Three Decades of Change, ICLARM Studies and Reviews, vol. 15, pp. 234–247.

Neira, S., Arancibia, H., Cubillos, L., 2004. Comparative analysis of trophic structure of commercial fishery species off Central Chile in 1992 and 1998. Ecological Modelling 172, 233–248.

Neira, S., Arancibia, H., 2004. Trophic interactions and community structure in the Central Chile marine ecosystem (33–39°S). Journal of Experimental Marine Biology and Ecology 312, 349–366.

Nigmatullin, C.M., Nesis, K.N., Arkhipkin, A.I., 2001. A review of the biology of the jumbo squid *Dosidicus gigas* (Cephalopods: Ommastrephidae). Fisheries Research 54, 9–19.

Nixon, S., Thomas, A., 2001. On the size of the Peru upwelling ecosystem. Deep Sea Research I 48, 2521–2528.

NODC (National Oceanographic Data Center), 2001. Taxonomic List of the Arctic Phytoplankton Species. On-line: <http://www.nodc.noaa.gov/OC5/BARPLANK/WWW/HTML/all_list.html>.

Odum, E.P., 1969. The strategy of ecosystem development. Science 164, 262–270.

Ortiz, M., Wolff, M., 2002. Trophic models of four benthic communities in Tongoy bay (Chile): comparative analysis and preliminary assessment of management strategies. Journal of Experimental Marine Biology and Ecology 268, 205–235.

Pauly, D., 1987. Managing the Peruvian upwelling ecosystem: a synthesis. In: Pauly, D., Tsukayama, I. (Eds.), The Peruvian Anchoveta and its Upwelling Ecosystem: Three Decades of Change, ICLARM Studies and Reviews, vol. 15, pp. 325–342.

Pauly, D., Christensen, V., Dalsgaard, J., Froese, R., Torres Jr., F., 1998. Fishing Down Marine Food Webs. Science 279, 860–863.

Patterson, K.R., Zuzunaga, J., Cardenas, G., 1992. Size of the South American sardine (*Sardinops sagax*) population in the northern part of the Peru upwelling ecosystem after collapse of anchoveta (*Engraulis ringens*) stocks. Canadian Journal of Fisheries and Aquatic Sciences 49, 1762–1769.

Quipuzcoa, L., Marquina, R., 2001. La estructura comunitaria del macrozoobentos en la plataforma continental del Peru: un analisis decadal. In: Espino, M., Samame, M., Castillo, R. (Eds.), Forum La merluza peruana (*Merluccius gayi peruanus*) biología y pesquería. Informe del Instituto del Mar Perú, pp. 46–49.

Rippe, L., 1996. Gemeinschaftsanalyse des Küstennahen Mesoplanktons im Flachwassergebiet vor der Kolumbianischen Pazifikküste. Diplom thesis, Bremen University, Bremen, Germany.

Sánchez, S., 1996. La comunidad fitoplanctónica en el área de Tambo de Mora a Paita, agosto-setiembre 1995. Informe del Instituto del Mar del Perú 119, 55–69.

Santander, H., Luyo, G., Carrasco, S., Véliz, M., Castillo, O., 1981. Catálogo de zooplancton en el mar peruano. Boletín del Instituto del Mar del Perú 6, 75.

Schetinnikov, A.S., 1989. Food spectrum of the squid *Dosidicus gigas* (Oegopsida) during ontegenesis. Zoologicheski Zhurnal 68, 28–39.

Sea Around Us, 2006. A global database on marine fisheries and ecosystems. Fisheries Centre, University British Columbia, Vancouver. On-line: <http://www.seaaroundus.org>.

SERC, 2006. Phytoplankton guide to Chesapeake Bay and other regions. On-line: <http://www.serc.si.edu/labs/phytoplankton/guide/index.jsp>.

Shannon, L.J., Jarre, A., 1999. Comparing models of trophic flows in the northern and southern Benguela upwelling systems during the 1980s. In: Ecosystem Approaches for Fisheries Management. University of Alaska Sea Grant, AK-SG-99-01, Fairbanks, pp. 55–68.

Shannon, L.J., Moloney, C.L., Jarre, A., Field, J.G., 2003. Trophic flows in the southern Benguela during the 1980s and 1990s. Journal of Marine Systems 39, 83–116.

Sorokin, Y.I., Kogelschatz, J.E., 1979. Analysis of heterotrophic microplankton in an upwelling area. Hydrobiologia 66, 195–208.

Strickland, J.D., Eppley, R., Mendiola, B., 1969. Poblaciones de fitoplancton, nutrientes y fotosíntesis en aguas costeras peruanas. Boletín del Instituto del Mar del Perú 2, 4–35.

Sun, J., Liu, D., 2003. Geometric models for calculating cell biovolume and surface area for phytoplankton. Journal of Plankton Research 25, 1331–1346.

Tarazona, J., Arntz, W., Castillo, E. (Eds.), 2001. El Niño en América Latina: impactos biológicos y sociales. Consejo Nacional de Ciencia y Tecologia, Lima. 423p.

Taylor, M.H., Tam, J., Blaskovic, V., Espinoza, P., Ballón, R., Wosnitza-Mendo, C., Argüelles, J., Díaz, E., Purca, S., Ochoa, N., Ayón, A., Goya, E., Quipuzcoa, L., Gutiérrez, D., Wolff, M., 2008a. Trophic modeling of the Northern Humboldt Current Ecosystem, Part II: Elucidating ecosystem dynamics from 1995 to 2004 with a focus on the impact of ENSO. Progress in Oceanography 79, 366–378.

Taylor, M., Wolff, M., Mendo, J., Yamashiro, C., 2008b. Comparative analysis of trophic flow structure between normal upwelling and El Niño periods for Bahía Independencia, Peru. Progress in Oceanography.

Tovar, H., Guillen, V., Nakama, M.E., 1987. Monthly population size of three guano bird species off Peru 1953 to 1982. In: Pauly, D., Tsukayama, I. (Eds.), The Peruvian Anchoveta and its Upwelling Ecosystem: Three Decades of Change, ICLARM Studies and Reviews, vol. 15, pp. 208–218.

Ulanowicz, R.E., 1986. Growth and Development: Ecosystems Phenomenology. Springer-Verlag, New York. 203p.

Ulanowicz, R.E., 1997. Ecology, the Ascendent Perspective. Columbia University Press, New York. 201p.

van der Lingen, C.D., Hutchings, L., Field, J.G., 2006. Comparative trophodynamics of anchovy *Engraulis encrasicolus* and sardine *Sardinops sagax* in the southern Benguela: are species alternations between small pelagic fish trophodynamically mediated? African Journal of Marine Science 28, 465–477.

Villegas, P., 2001. Growth, life cycle and fishery biology of *Loligo gahi* (d'Orbigny, 1835) off the Peruvian coast. Fisheries Research 54, 123–131.

Walsh, J.J., Dugdale, R.C., 1971. A simulation model of the nitrogen flow in the Peruvian upwelling system. Investigación Pesquera 35, 309–330.

Walsh, J.J., 1981. A carbon budget for overfishing off Peru. Nature 290, 300–304.

Wangelin, M., Wolff, M., 1996. Comparative biomass of spectra and species composition of the zooplantkton communities in Golfo Dulce and Golfo of Nicoya Pacific coast of Costa Rica. Revista de Biología Tropical 44, 135–156.

Wolff, M., 1994. A trophic model for Tongoy Bay – a system exposed to suspended scallop culture (Northern Chile). Journal of Experimental Marine Biology and Ecology 182, 149–168.

Wolff, M., Koch, V., Bautista Chavarria, J., Vargas, J.A., 1998. A trophic flow model of the Golfo de Nicoya, Costa Rica. Revista de Biología Tropical 46 (Suppl. 6), 63–79.

Progress in Oceanography 79 (2008) 366–378

Contents lists available at ScienceDirect

Progress in Oceanography

journal homepage: www.elsevier.com/locate/pocean

Trophic modeling of the Northern Humboldt Current Ecosystem, Part II: Elucidating ecosystem dynamics from 1995 to 2004 with a focus on the impact of ENSO

Marc H. Taylor[a,*], Jorge Tam[b], Verónica Blaskovic[b], Pepe Espinoza[b], R. Michael Ballón[b,c], Claudia Wosnitza-Mendo[b], Juan Argüelles[b], Erich Díaz[b], Sara Purca[b], Noemi Ochoa[d], Patricia Ayón[b], Elisa Goya[b], Dimitri Gutiérrez[b], Luis Quipuzcoa[b], Matthias Wolff[a]

[a] *Center for Tropical Marine Ecology, Fahrenheitstr. 6, 28359 Bremen, Germany*
[b] *Instituto del Mar del Perú, Esq. Gamarra y Valle s/n, Apartado 22, Callao, Peru*
[c] *IRD, UR097, CRH, Avenue Jean Monnet, 34203 Sete, France*
[d] *Universidad Nacional Mayor de San Marcos, Apartado 12, Lima, Peru*

ARTICLE INFO

Article history:
Accepted 14 October 2008
Available online 21 October 2008

Keywords:
Coastal upwelling
Ecosystem disturbance
El Niño phenomena
Trophic relationships
Trophodynamic model
Peru Humboldt Current

ABSTRACT

The Northern Humboldt Current Ecosystem is one of the most productive in the world in terms of fish production. Its location near to the equator permits strong upwelling under relatively low winds, thus creating optimal conditions for the development of plankton communities. These communities ultimately support abundant populations of grazing fish such as the Peruvian anchoveta, *Engraulis ringens*. The ecosystem is also subject to strong inter-annual environmental variability associated with the El Niño Southern Oscillation (ENSO), which has major effects on nutrient structure, primary production, and higher trophic levels. Here our objective is to model the contributions of several external drivers (i.e. reconstructed phytoplankton changes, fish immigration, and fishing rate) and internal control mechanisms (i.e. predator-prey) to ecosystem dynamics over an ENSO cycle. Steady-state models and time-series data from the Instituto del Mar del Perú (IMARPE) from 1995 to 2004 provide the base data for simulations conducted with the program Ecopath with Ecosim. In simulations all three external drivers contribute to ecosystem dynamics. Changes in phytoplankton quantity and composition (i.e. contribution of diatoms and dino- and silicoflagellates), as affected by upwelling intensity, were important in dynamics of the El Niño of 1997–98 and the subsequent 3 years. The expansion and immigration of mesopelagic fish populations during El Niño was important for dynamics in following years. Fishing rate changes were the most important of the three external drivers tested, helping to explain observed dynamics throughout the modeled period, and particularly during the post-El Niño period. Internal control settings show a mix of predator–prey control settings; however a "wasp-waist" control of the ecosystem by small pelagic fish is not supported.

1. Introduction

Eastern Boundary Current Systems (EBCSs), including the Humboldt, Canary, Benguela, and California Currents, and in particular their nearshore upwelling zones, are among the most productive fishing areas in the world. High primary and secondary productivity support large biomasses of small planktivorous pelagic fish, or "small pelagics", which through predator/prey interactions can influence both higher and lower trophic levels (i.e. "wasp-waist" ecosystem control, Cury et al., 2000).

The Humboldt Current, and specifically, the Peruvian upwelling system, produces more fish landings than the other EBCSs (both total and on a per area basis). However, remote sensing-based estimates of primary production rank the Peruvian upwelling system only third, behind the Benguela and Canary Current systems (Carr, 2002). In a way, this apparent paradox supports early fishery hypotheses that emphasize quantity and quality of upwelling. The Peruvian upwelling system's proximity to the equator and large Rossby radius results in strong and sustained upwelling under relatively mild wind forcing (Cury and Roy, 1989; Bakun, 1996). These conditions create a "particularly rich, non-turbulent, benign environment" by which rich coastal plankton communities develop and persist, in turn supporting abundant populations of small pelagics (Bakun and Weeks, 2008).

Peru's proximity to the equator also means that Kelvin waves traveling eastward along the equator during El Niño (EN) impact Peru almost directly. During EN, the "basin-wide ecosystem" of

---

* Corresponding author. Tel.: +49 4212380056; fax: +49 4212380030.
E-mail address: marchtaylor@yahoo.com (M.H. Taylor).

0079-6611/$ - see front matter © 2008 Elsevier Ltd. All rights reserved.
doi:10.1016/j.pocean.2008.10.008

the Pacific, which normally maintains a slope in sea level, thermal structure, and nutrient structure due to trade winds, is lost or reversed (Chavez et al., 2003; Pennington et al., 2006). While upwelling-favorable wind may continue along the Peruvian coast, water is upwelled from above the now deep thermocline and nutricline. As a result, primary production of the Peruvian upwelling system is reduced, and the "active zone" of high primary production can be 1/10th the size of normal conditions (Nixon and Thomas, 2001).

Under normal conditions diatoms dominate the nearshore phytoplankton community. Diatoms are particularly adapted to upwelling conditions through high doubling rates and their ability to form resting spores, which sink and are subsequently returned to the surface via upwelling (Pitcher et al., 1992). In the Humboldt Current system, EN reduces the upwelling of nutrient-rich water, which results in a reduction of the larger size fraction of the phytoplankton community (e.g. diatoms) (Bidigare and Ondrusek, 1996; Landry et al., 1996; González et al., 1998; Iriarte and González, 2004) and are replaced by subtropical phytoplankton normally found further offshore in nutrient poor waters (Rojas de Mendiola, 1981; Ochoa et al., 1985; Avaria and Muñoz, 1987). These changes in the phytoplankton produce changes throughout the ecosystem, with energy likely passing through different pathways before reaching a particle size suitable for grazing by small pelagics (Sommer et al., 2002; González et al., 2004; Iriarte and González, 2004; Tam et al., 2008).

This straightforward, bottom-up perspective becomes complicated when one considers the effects and interactions of top-down processes such as predation and fishing. Fortunately, trophic modeling of EBCSs has a long history from which to draw upon; including steady-state models of the Peruvian (Walsh, 1981; Baird et al., 1991; Jarre et al., 1991; Jarre-Teichmann, 1992) and other upwelling systems (Shannon et al., 2003; Heymans et al., 2004; Neira and Arancibia, 2004; Neira et al., 2004; Moloney et al., 2005). The development of the program Ecopath with Ecosim (EwE) (Walters et al., 1997) further allows for temporal explorations of dynamics, and has been previously applied to the southern Benguela system (Shannon et al., 2004a,b). A review of these advances (Taylor and Wolff, 2007) has assisted in the construction of new steady-state models for the Peruvian system as presented by Tam et al. (2008), which form the basis for the dynamic simulations presented here.

Our objectives are to elucidate the mechanisms of ecosystem dynamics in the Peruvian upwelling system over an ENSO cycle. We evaluate the importance of three external drivers: (i) changes in phytoplankton biomass and composition, (ii) immigration of mesopelagic fish into the model area, and (iii) changes in fishing rates. We also explore internal predator-prey control settings between functional groups of organisms (e.g. bottom-up, top-down control). We speculate that the degree of upwelling and resulting primary productivity may similarly affect ecosystem dynamics across seasonal, inter-annual (EN), and multi-decadal temporal scales, but use the data-rich period of 1995–2004 as a starting point for model exploration.

2. Methods

Using the temporal dynamic routine of Ecosim within the EwE package (Walters et al., 1997, 2000) we explored the relative importance of external and internal ecosystem drivers in the Northern Humboldt Current Ecosystem from 1995 to 2004. External, non-trophically-mediated drivers considered were changes in phytoplankton biomass, fishing rate (effort and mortality), and oceanic immigrant biomass (mesopelagic fish). Internal, trophically-mediated, factors concerned an exploration of trophic flow controls (e.g. bottom-up, top-down) that govern predator-prey dynamics.

2.1. Description of the model

The steady-state model from Tam et al. (2008) is used here as input describing the initial ecosystem state (1995/96 model), which encompasses a full "biological year" (i.e. starting from about the middle of a calendar year). The spatial domain is from 4°S to 16°S and 60 nm offshore (ca. 111 km; see Fig. 1 in Tam et al., 2008). The models consisted of 33 functional groups including detritus, macrobenthos, 2 phytoplankton groups, 4 zooplankton groups, 8 pelagic fish groups, 2 cephalopod groups, 12 demersal fish groups (including 3 life-history stages for Peruvian hake, *Merluccius gayi peruanus*), seabirds, pinnipeds, and cetaceans. Groups were chosen based on similar trophic connections (both to predator and prey groups), similar production and consumption rates, and importance to fishery resources.

The simulations calculate biomass changes through time by solving the set of differential equations:

$$dB_i/dt = g_i\left[\sum_k Q_{ki}(t)\right] - \sum_j Q_{ij}(t) - MO_iB_i - \sum F_{if}(t)B_i \qquad (1)$$

for functional groups $i = 1,\ldots,n$. The first sum represents the food-consumption rate, Q, summed over prey types k of species i, and g_i represents the growth efficiency (proportion of food intake converted into production). The second sum represents the predation loss rates due to predators j of i. All Q's in these sums are calculated by Eq. (2), below. MO_i represents the instantaneous natural mortal-

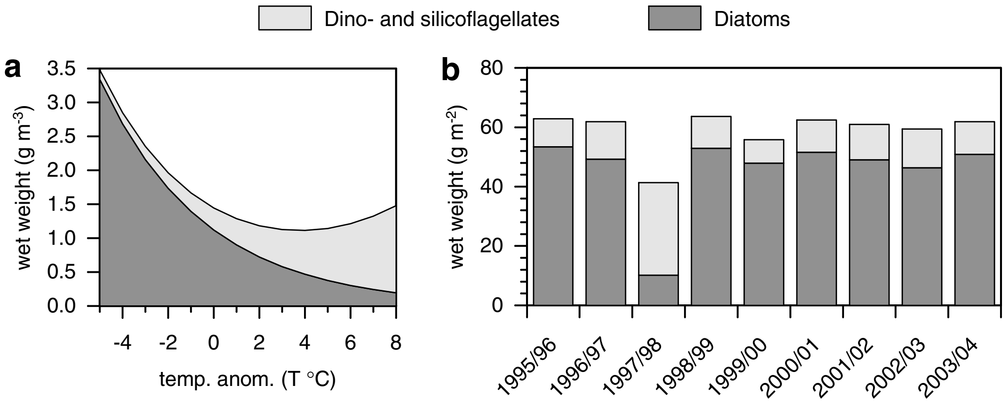

Fig. 1. (a) Relationship between coastal surface phytoplankton biomass (g m^{-3}) as a function of sea surface temperature anomaly (°C) and (b) reconstructed annual phytoplankton biomass values (g m^{-2}) used in the phytoplankton (*PP*) driver.

ity rate due to outside factors other than modeled predation. The final sum represents the instantaneous fishing mortality rate, *F*, as a sum of fishing components caused by fishing fleets *f*.

Consumption rates (Q_{ij}) are calculated by assuming that the biomass of prey *i*, B_i, is divided into vulnerable and safe components, and the flux rates v_{ij} and v'_{ij} move biomass into the vulnerable and safe pools, respectively. This assumption leads to the rate equation:

$$Q_{ij} \frac{a_{ij}(t)v_{ij}(t)B_iB_j}{v_{ij}(t) + v'_{ij} + a_{ij}(t)B_j} \tag{2}$$

where the total consumption rate Q_{ij} varies as a mass action product (avB_iB_j), and is modified downward by a "ratio dependent" effect ($v + v' + aB_j$) representing localized competition among predators. a_{ij} represents the rate of effective search by predator *j* for prey type *i* (for further information, see Walters and Martell, 2004). The vulnerabilities for each predator–prey interaction can be manipulated and settings will determine if control is top-down (i.e. Lotka-Volterra; $v > 2.0$), bottom-up (i.e., donor-driven; $v < 2.0$), or intermediate ($v \approx 2.0$). The EwE software can also fit the vulnerabilities ("fit-to-time-series" routine), where the sum of squares (*SS*) is minimized between observed and predicted log biomasses/catches:

$$SS = \sum[Log(B_{obs}) - Log(B_{pred.})]^2 \tag{3}$$

Simulations measured the importance of three external drivers (see Section 2.2) on dynamics of the Northern Humboldt Current Ecosystem from 1995 to 2004. In addition, we applied the "fit-to-time-series" search routine within EwE to determine a best possible combination of specific predator–prey controls (see Section 2.3). The simulation's performance was measured by *SS* against available time-series data of yearly biomass and catch changes. Time-series data were derived from biomass, catch, fisheries mortality, and fishing effort estimates from IMARPE (Instituto del Mar del Perú) and other sources (Table 1). These data were adapted to the model area and biological year averages.

2.2. External drivers

External drivers were not accounted for within the internal flows of the trophic model. These drivers included: (i) "*PP*", phytoplankton biomass changes due to changes in upwelling and nutrients; (ii) "*F*", fishing rate changes; and (iii) "*I*", Immigrant biomass changes, specifically, the expansion and immigration of mesopelagic fish into the model area. Drivers were introduced successively in all sequences and combinations in order to arrive to an average value of change in *SS* ($n = 15$). External driverś dynamics were defined by available or reconstructed long-term data series as described below.

Phytoplankton, *PP* – Long-term estimates of total phytoplankton biomass are available as total surface chlorophyll *a* (mg m^{-3}) from the SeaWifs satellite. We however needed to divide this total into the small- and large-sized phytoplankton functional groups, and did so by predicting functional group biomass from temperature anomaly, as below. We used a 1992–2000 time-series of coastal phytoplankton sampled by the Universidad Nacional Mayor de San Marcos (Lima, Peru) in Bahía de Ancón (77 39′ W–11 12′ S), Central Peru. The series consisted of cell counts of surface phytoplankton species, which were then converted to biovolume using cell dimensions gathered from literature sources or measured by microscopy. Cell dimensions were applied to geometric-shape assignments as described by Sun and Liu (2003) for the calculation of biovolume. Monthly average biovolume by taxonomic group were plotted against temperature anomalies off Ancón. Biovolume was natural log transformed and yielded the following linear relationships:

$$LN(B) = 17.841 - 0.2184 * T_{anom.} \quad (\text{Diatoms},\ r = -0.20,\ \ p = 0.05) \tag{4}$$

$$LN(B) = 16.603 + 0.1719 * T_{anom.} \quad (\text{Dino- and silicoflagellates},\ r = 0.14,\ \ p = 0.18) \tag{5}$$

where B = biovolume (μm^3 50 ml^{-1}), $T_{anom.}$ = temperature anomaly (°C). Typical of phytoplankton populations, a wide distribution of values was observed; however, diatom biovolume showed a negative trend and dino- and silicoflagellates a positive one, which is consistent with literature concerning the effects of ENSO on phytoplankton communities (Fig. 1a). These relationships were then applied to an index of integrated temperature anomalies for the entire Peruvian coast – the Peruvian Oscillation Index (POI) (Purca, 2005), which allowed for the reconstruction of coastal phytoplankton biovolumes for the years 1995–2003. Despite a non-significant correlation for dino- and silicoflagellates, the temperature-based predictions produce an acceptable range of surface phytoplankton biovolume when compared to the SeaWIFs data. For the simulations we use converted the temperature-based proportions of the two phytoplankton fractions to absolute values with the SeaWifs data for the model domain. Conversion factors used for chlorophyll *a* (Chl *a*) to wet weight were as follows: Chl *a*:Carbon (40:1) (Brush et al., 2002), and Carbon:wet weight (14.25:1) (Brown et al., 1991). Finally, a uniform mixed layer depth of 40 m was assumed to arrive at units of biomass per m^2 as described by Tam et al. (2008) (Fig. 1b).

Fishing rate, *F* – Time-series fishing rate estimates were only available for anchovy, hake and jumbo squid; however, these species represent key fisheries as well as important functional groups in the nearshore pelagic, nearshore demersal, and offshore pelagic ecosystems, respectively. These include fishing mortality rates derived from single species Virtual Population Analyses for anchovy and the three hake functional groups, and changes in fishing effort for jumbo squid (Table 2).

Immigration, I – While biomasses of several oceanic-associated functional groups apparently increased during EN (Tam et al., 2008), long-term data is only available for the mesopelagics functional group – lightfish and lanternfish – as determined by IMARPE acoustic surveys. Distribution of mesopelagics extends far offshore and thus we only considered the portion of the group in the model area. Mesopelagic's biomass increased in the model area following EN, apparently due to immigration; these changes were simulated by forcing mesopelagic biomass as an external driver.

2.3. Internal control

Model settings of prey vulnerability determine whether top-down bottom-up ecosystem dynamics dominate. "Mixed" or intermediate (*MX*; default $v = 2.0$) settings were used for initial explorations of the influence of external drivers. Afterwards, a further fit-to-time-series search routine was run for the 30 most sensitive predator–prey interactions (as determined by a sensitivity routine of the program) to reduce *SS*. The following interactions were also included to assess whether "wasp-waist" ecosystem control occurs around sardine and anchovy: (i) meso- and macrozooplankton as prey of sardine and anchovy; and (ii) all interactions where anchovy and sardine are prey. In total, 49 interactions were included in the search routine.

2.4. Focus on changes in main fishing targets

The dynamics of several main fishing targets and their interactions were also highlighted. Simulated mortality and diet changes for anchovy were examined in detail to help interpret

Table 1
Annual time-series data sets used in the Ecosim simulations.

Functional group	Data set	Comments	Used to force dynamics	Used to measure fit of simulation
1. Diatoms	Biomass (B)	SeaWifs; phytoplankton proportions reconstructed (see Section 2.3)	+	+
2. Dino- and silicoflagellates	Biomass (B)	SeaWifs; phytoplankton proportions reconstructed (see Section 2.3)	+	+
4. Mesozooplankton 200–2000 μm esd.	Biomass (B)	IMARPE survey (Ayón, personal communication) – corrected using seasonal anomalies (1959–2001)		+
7. Macrobenthos	Biomass (B)	IMARPE benthic survey (1995–2003) (Gutierrez and Quipuzcoa, personal communication)		+
8. Sardine – Sardinops sagax	Biomass (B)	IMARPE acoustic survey (1995–1999) (Gutierrez, personal communication)		+
	Catches (C)	Sea Around Us database (2006) (1995–2002)		+
9. Anchovy – *Engraulis ringens*	Biomass (B)	VPA estimates (1995–2003) (Niquen, personal communication)		+
	Fishing mortality (F)	VPA estimates (1995–2003)	+	
	Catches (C)	IMARPE catch statistics (1995–2003)		+
10. Mesopelagics – Lightfish and Lanternfish	Biomass (B)	IMARPE acoustic survey (1999–2003) (Gutierrez, personal communication)	+	+
11. Jumbo squid – Dosidicus gigas	Biomass (B)	IMARPE acoustic survey (1999–2003) (Arguelles, pers. comm.); 1995–1998 reconstructed from CPUE:acoustic ratio from 1999 to 2003		+
	Fishing effort (E)	Korean and Japanese industrial fleet data (1995–2003)	+	
	Catches (C)	Korean and Japanese industrial fleet data (1995–2003)		+
12. Other Cephalopods	Catches (C)	IMARPE catch statistics (1995–1999)		+
13. Other small pelagics – e.g. juvenile demersal fish	Catches (C)	Sea Around Us database (2006) – Engraulidae, Ethmidium maculatum (1995–2002)		+
14. Horse mackerel – Trachurus murphyi	Biomass (B)	IMARPE acoustic survey (1995–2003) (Gutierrez, personal communication)		+
15. Characteristic large pelagic – Scomber japonicus	Biomass (B)	IMARPE acoustic survey (1995–2003) (Gutierrez, personal communication)		+
16. Other large pelagics	Catches (C)	IMARPE catch statistics (1995–1999)		+
17. Small hake – Merluccius gayi peruanus (<29 cm)	Biomass (B)	VPA estimates (1995–2003) (Wosnitza-Mendo, personal communication)		+
	Fishing mortality (F)	VPA estimates (1995–2003)	+	+
	Catches (C)	IMARPE catch statistics (1995–2003)		
18. Med. hake – Merluccius gayi peruanus (30–49 cm)	Biomass (B)	VPA estimates (1995–2003) (Wosnitza-Mendo, personal communication)		+
	Fishing mortality (F)	VPA estimates (1995–2003)	+	
	Catches (C)	IMARPE catch statistics (1995–2003)		+
19. Large hake – Merluccius gayi peruanus (>50 cm)	Biomass (B)	VPA estimates (1995–2003) (Wosnitza-Mendo, personal communication)		+
	Fishing mortality (F)	VPA estimates (1995–2003)	+	
	Catches (C)	IMARPE catch statistics (1995–2003)		+
21. Small demersals	Catches (C)	IMARPE catch statistics (1995–1999)		+
22. Benthic elasmobranchs	Catches (C)	IMARPE catch statistics (1995–1999)		+
25. Medium demersal fish	Catches (C)	IMARPE catch statistics (1995–1999)		+
26. Medium sciaenids	Catches (C)	IMARPE catch statistics (1995–1999)		+
28. Catfish	Catches (C)	IMARPE catch statistics (1995–2002)		+
29. Chondrichthyans	Catches (C)	IMARPE catch statistics (1995–1999)		+
30. Seabirds	Biomass (B)	IMARPE survey (1995–2003) (Goya, personal communication)		+
31. Pinnipeds	Biomass (B)	IMARPE survey (1995–2003) (Goya, personal communication)		+

sources of bottom-up and top-down dynamics. Hake were also of special interest due to the drastic decreases in population size that followed the last strong EN (Guevara-Carrasco, 2004; Ballón et al., 2008). We specifically looked at mortality of the small size class to help interpret possible sources influencing the low recruitment.

3. Results

3.1. External drivers

The driver to phytoplankton biomass and composition improved the overall fit of the simulation, reducing *SS* by 2.7% (Fig. 2b) with greatest improvement during EN and the subsequent 3 year period (Fig. 2a). The driver to immigrant biomass (mesopelagics) reduced *SS* by 9.2% (Fig. 2b) with the greatest improvement in later years when biomasses were highest (Fig. 2a). *SS* for the EN year 1997–98 alone was not improved by the immigrant driver (Fig. 2a). Fishing rate changes proved to be the most important of the three external drivers overall, reducing *SS* by 22.0% (Fig. 2b). Improvements were observed throughout the simulated period except for the final year, and were generally more important during the post-EN years (Fig. 2a).

3.2. Best-fit vulnerabilities

The fit-to-time-series search for vulnerabilities revealed several important predator-prey interactions (Table 2), and further decreased *SS* by 31.2% after the application of the three internal drivers *PP*, *F*, and *I* (total decrease in *SS* of 64.3%). The results did not support a wasp-waist configuration for small pelagics (agrees with Ayón et al., 2008), as bottom-up configurations were estimated for sardines and anchovy on meso- and macrozooplankton; however, a bottom-up configuration was fit for interactions of sardine and anchovy, and their predators. Top-down control of macrozooplankton by mesopelagics and large hake was also suggested. The

Table 2

Predator–prey vulnerabilities searched in the fit-to-time-series routine (in bold); *BU* = bottom-up; *MX* = mixed/intermediate (default setting); *TD* = top-down.

Predator/prey	Diatoms	Silico- and Dinoflagellates	Microzooplankton	Mesozooplankton	Macrozooplankton	Sardine	Anchovy	Mesopelagics	Jumbo squid	Other small pelagics	Small hake	Small demersals	Conger	Med. sciaenids	P. stephanophrys
Mesozooplankton	**1 (BU)**	2 (MX)	2 (MX)												
Macrozooplankton	**1E+10 (TD)**	**1 (BU)**	**1E+10 (TD)**												
Sardine	2 (MX)	2 (MX)	2 (MX)	**1 (BU)**	**1 (BU)**										
Anchovy	**1E+10 (TD)**	2 (MX)	2 (MX)	**1 (BU)**	**1.16 (BU)**										
Mesopelagics				2 (MX)	**1E+10 (TD)**										
Jumbo squid				2 (MX)	2 (MX)		**1 (BU)**	**1 (BU)**	**1E+10 (TD)**	2 (MX)	**1E+10 (TD)**				
Other Cephalopods					**1 (BU)**							2 (MX)			
Horse mackerel					2 (MX)		**1 (BU)**			2 (MX)		2 (MX)			
Mackerel	2 (MX)		2 (MX)	2 (MX)	**1.55 (BU)**			2 (MX)				2 (MX)			
Other large pelagics							**1 (BU)**		2 (MX)	2 (MX)		2 (MX)			
Small hake					2 (MX)	**1 (BU)**	**1 (BU)**		**1 (BU)**	2 (MX)		2 (MX)			**1E+10 (TD)**
Med. Hake					2 (MX)		**1.16 (BU)**			**1E+10 (TD)**		**1E+10 (TD)**			**1.31 (BU)**
Large hake					**1E+10 (TD)**		**1 (BU)**	**1.02 (BU)**			**1E+10 (TD)**	**1.43 (BU)**	**1 (BU)**	**1E+10 (TD)**	**1E+10 (TD)**
Flatfish							**1 (BU)**								
Small demersals	**1E+10 (TD)**			**1E+10 (TD)**											
B. elasmobranchs					2 (MX)	**1 (BU)**	**1 (BU)**		2 (MX)	2 (MX)		2 (MX)	2 (MX)	2 (MX)	
Conger												2 (MX)			**1E+10 (TD)**
Med. demersal fish					2 (MX)		**1 (BU)**			2 (MX)		2 (MX)			
Med. sciaenids					2 (MX)	**1 (BU)**	**1 (BU)**	2 (MX)	2 (MX)	2 (MX)		2 (MX)		2 (MX)	
P. stephanophrys					**1 (BU)**										
Catfish				2 (MX)	2 (MX)		**1 (BU)**			2 (MX)					
Chondrichthyans							**1 (BU)**		2 (MX)		2 (MX)				
Seabirds							**1 (BU)**			2 (MX)		2 (MX)			
Pinnipeds							**1 (BU)**	2 (MX)		2 (MX)	2 (MX)	2 (MX)		2 (MX)	
Cetaceans					2 (MX)		**1 (BU)**		2 (MX)						

control of mesopelagic fish to its main predator, jumbo squid, was 1.0 (bottom-up), helping to explain the increase of squid biomass following the EN of 1997–98. The final time-series trends of the simulation versus the base data is shown in Fig. 3 for biomass and Fig. 4 for catch data.

3.3. Focus on main fishing targets

Anchovy changes during EN were best explained through bottom-up diatom and zooplankton availability, while later changes were more attributable to the fishery. Reduction in diatoms during EN resulted in a higher contribution of zooplankton in the anchovy diet. Dino- and silicoflagellate increases were unimportant as this group contributes only a small proportion to their diet generally (Fig. 5). During EN, modeled predation on anchovy increased – mainly due to horse mackerel – but non-predatory mortality was far stronger (Fig. 6) and seems due to low feeding rates and decreased prey availability. After EN, mortality rates were mainly controlled by fishing.

Decreases in the hake biomasses were well predicted by the simulation for all three size classes (Fig. 3). Mortalities for small juvenile hake indicate that cannibalism did not contribute greatly to the overall mortality even during the pre-crash years of 1995–96 and 1996–97 when adult biomass was higher. Modeled predation of small hake by jumbo squid remains fairly constant despite the squid increases. Squid predation does, however, represent a higher proportion of total hake mortality in the last simulation year following reduction of the hake fishery. Fishing is the most substantial source of mortality for all three hake groups, especially for medium and large hake (Fig. 7).

The immigrant driver simulated the immigration of mesopelagic fish into the model domain. One result is the increase in jumbo squid biomass and a shift in the jumbo squid's diet toward a larger proportion of mesopelagic fish (Fig. 8). Small hake, however, contributed minimally to the squid diet.

4. Discussion

We use the model for the 1995–96 year as a starting point for several reasons: (i) reliable, periodic sampling conducted by IMARPE began in 1995; (ii) 1995–96 was a fairly typical, "normal" upwelling year, several years after the recovery of anchovy; and (iii) 1995–96 preceded the strong EN of 1997–98, offering insight into subsequent dynamics. We asked the question whether this EN event has been a principal perturbation over 1995–2004 and to what degree trophic interactions played a role in the observed ecosystem changes.

4.1. Role of external drivers

Phytoplankton – Given the major decrease in primary production that occurs during EN, it was assumed that the application of this driver would have a major bottom-up impact through the trophic web, and would partially explain the decreased biomass of the coastal ecosystem as a whole. In fact, externally driving phytoplankton downwards did improve the fit of the simulation, especially during EN and the immediately following 3 years. Later years show a reduced importance of the forced phytoplankton changes, likely due to less yearly phytoplankton variability under the more "normal" upwelling conditions (Fig. 1b).

Copepods make up the majority of the mesozooplankton biomass in Peru and are known to be important grazers of the larger microphytoplankton (DeMott, 1989; Sommer et al., 2002, 2005). The model correctly predicts a decrease in mesozooplankton biomass in response to the decreased diatom biomass of 1997–98. Contrary to the sampled changes of mesozooplankton, a rapid recovery is predicted by the model following the resumed higher diatom and total phytoplankton biomass (Fig. 3). Without speculating too much as to the reasons for this discrepancy, we believe that much additional work is required in the modeling of zooplankton. Still, the model predicts at least the correct direction of change for many higher trophic groups, and in some cases predicts change of the correct magnitude as the base data. This is especially true of the trophically-important anchovy dynamics for which data is more widely available.

Of particular importance to small pelagic dynamics are particle size feeding preferences observed for the different species. Sardines possess fine-meshed gillrakers suitable for filtering smaller-sized particles. Anchovy, on the other hand, are more specialized and efficient at feeding on larger-sized particles (James and Findlay, 1989; van der Lingen, 1994; van der Lingen et al., 2006). The result of these adaptations, at least in the Benguelan populations, is that anchovy seem to have higher clearance rates (per weight) than sardine when available particles are larger than about 500–600 μm (van der Lingen, 1994). These feeding differences have been dealt with in other trophic models by defining separate zooplankton compartments by size, and through different vulnerabilities to grazing by small pelagics (Heymans and Baird, 2000; Shannon et al., 2003; Neira and Arancibia, 2004; Shannon et al., 2004a,b). We have further divided phytoplankton into two

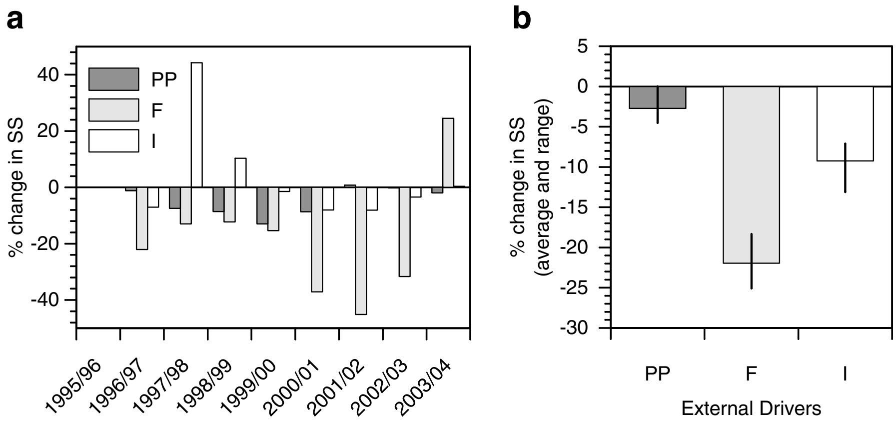

Fig. 2. Percent changes to sum of square differences, *SS*, after the application of different external 'drivers': phytoplankton biomass (*PP*); fishery rates (*F*); and immigrant biomass (*I*). (a) *SS* changes by year after the individual application of each external driver. (b) Average and range of *SS* changes under the application of external drivers in all possible sequences and combinations. All simulations use intermediate, default control settings (i.e. all predator–prey vulnerabilities equal 2.0). Negative values (i.e. decrease in *SS*) indicate an improvement in fit.

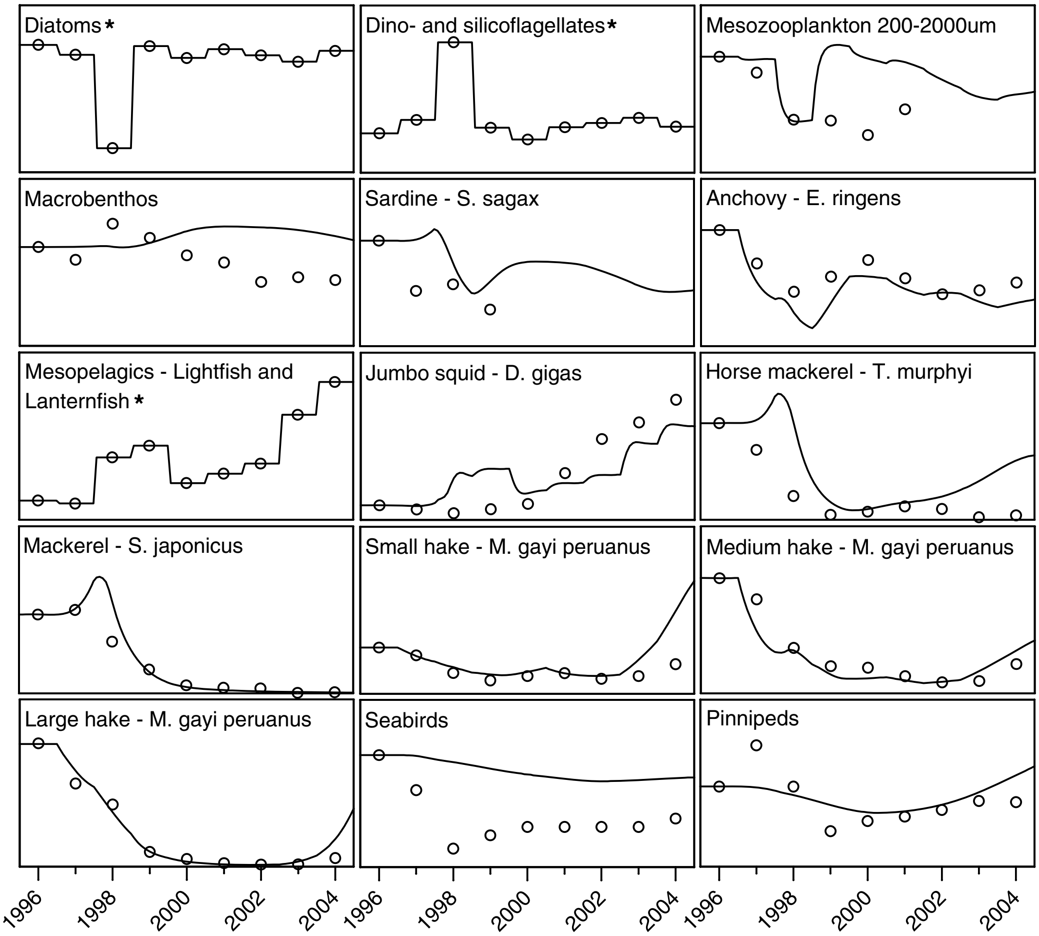

Fig. 3. Time-series trends of biomass changes from the data sets (dots) and Ecosim simulations (lines). Presented is the best-fit simulation (i.e. lowest *SS*), using all drivers (*PP*, *F*, and *I*) followed by a "fit-to-time-series" routine. Yearly data points represent "biological years" (i.e. July-June of following year). Asterisks (∗) indicate artificially-forced functional groups (diatoms, dino - and silicoflagellates, and mesopelagics).

taxonomic groups for a similar reason. According to the biovolume conversions of diet data conducted for our initial steady-state model (Tam et al., 2008) and other authors (Alamo, 1989; Espinoza and Blaskovic, 2000) anchovy feed more on diatoms than flagellates. Although diatoms are more associated with the nearshore cold habitat of the anchovy, they are usually smaller than the cited 500–600 μm optimal particle size; however, it seems likely that aggregates and cell-chains allow anchovies to filter even fairly small diatoms. As a result, anchovy dynamics are well simulated. The initial decrease in anchovy biomass during 1997–98 is mainly reproduced by forcing phytoplankton abundance downwards; specifically, a decrease in diatom biomass and, subsequently, a decrease in the second most important food item, mesozooplankton.

The modeled switch to an anchovy diet dominated by zooplankton was not as complete as was observed from *in situ* samples (Espinoza and Bertrand, 2008; Tam et al., 2008) (Fig. 5), possibly due to: (i) forced biomass decreases of phytoplankton may not have reduced diatoms as dramatically as in reality; (ii) anchovy move closer to the coast and deeper (up to 150 m) during EN (Bertrand et al., 2004), which may be due to non-trophic reasons (e.g. physiological stress associated with the higher surface water temperatures), and possibly prevent feeding upon the remaining diatom biomass; (iii) The modeled starting diet may have been too high (or not) in diatoms, although this cannot explain the lack of change in diet composition as this is calculated mainly from the changes in biomass and vulnerability. Espinoza and Bertrand (2008) have estimated the percent contribution of phytoplankton in carbon units to anchovy diet from stomach contents. Their results indicate that mesozooplankton and macrozooplankton comprise as much as 98% of carbon intake. Although their diet data still needs to be weighted according to the distribution of the anchovy population, it may indicate that our model overestimates the importance of phytoplankton as anchovy prey.

Fishing rates – The application of fishing as an external driver improved the fit of the simulation and helps to explain the long-term dynamics of several main target species. The fishing driver decreased long-term variance by 22%, as compared to a 2–3% decrease in a similar study for the Southern Benguela (Shannon et al., 2004a). This very large difference suggests strong fishery impact on the Peruvian system. In a comparison of trophic models, Moloney et al. (2005) illustrated that the South Benguelan fishery operates on a higher trophic level than in other EBCSs due to the differing diet of small pelagics and composition of the catch; specifically, Benguela small pelagics eat more zooplankton and fishery catches contain more demersal fish. The differences result in a higher mean trophic level of the catch in the Southern Benguela, elevating the statistic of *Flows required per unit of catch* ($[t\ 1°\text{prod}]\ [t\ \text{catch}]^{-1}\ \text{km}^{-2}\ \text{y}^{-1}$) and indicating that the same tonnage catch requires more energetic input from the ecosystem. Despite this cost, the authors determined that the Southern Benguelan fishery required a smaller proportion of total primary production to sustain it when compared to the Peruvian fishery (4% vs. 10%), reflecting the much higher fishing rates in the Peruvian system.

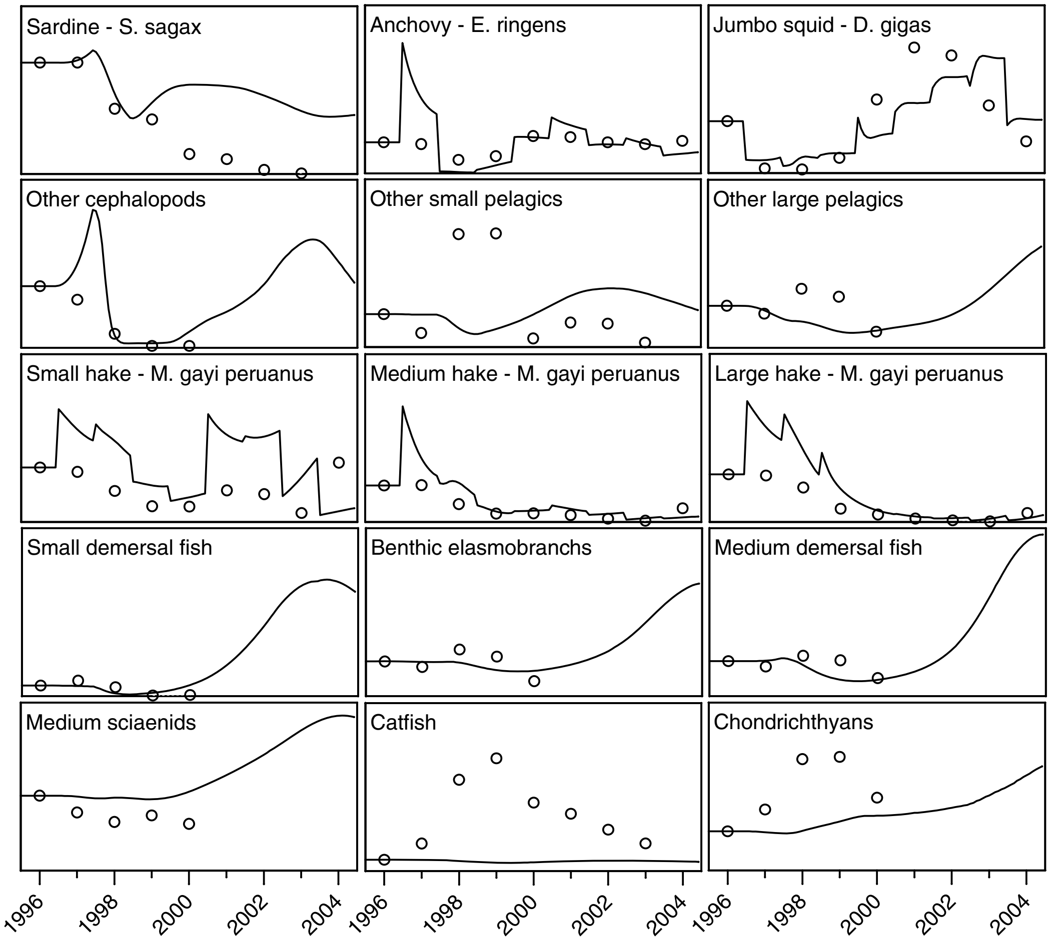

Fig. 4. Time-series trends of fisheries catch changes from the data sets (dots) and Ecosim simulations (lines). Presented is the best-fit simulation (i.e. lowest *SS*), using all drivers (*PP*, *F*, and *I*) followed by a "fit-to-time-series" routine for the 30 most sensitive predator-prey vulnerabilities. Yearly data points represent "biological years" (i.e. July–June of following year).

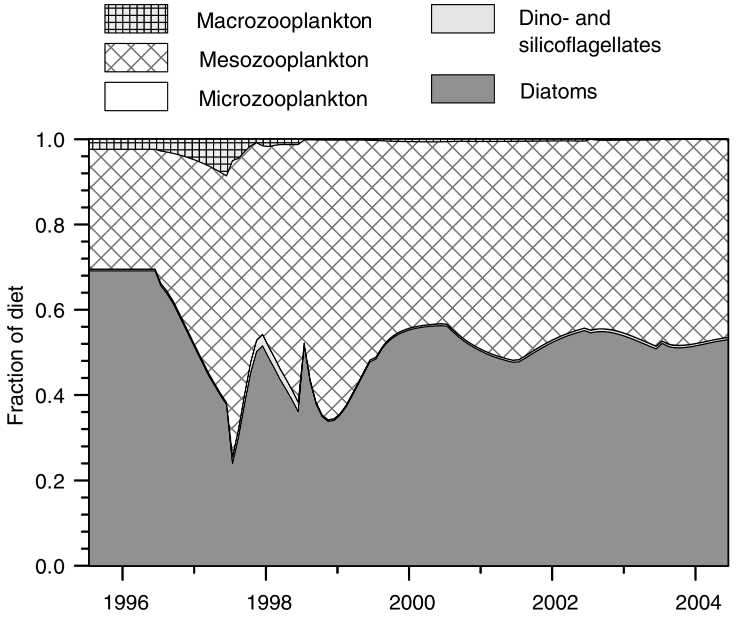

Fig. 5. Contribution of prey items to the diet of anchovy through the Ecosim simulation.

The simulation output calculates mortality rates through time, allowing for the determination of the importance of yearly fishing mortality changes for some key target groups' dynamics as discussed in the following sections. For anchovy, fishing mortality

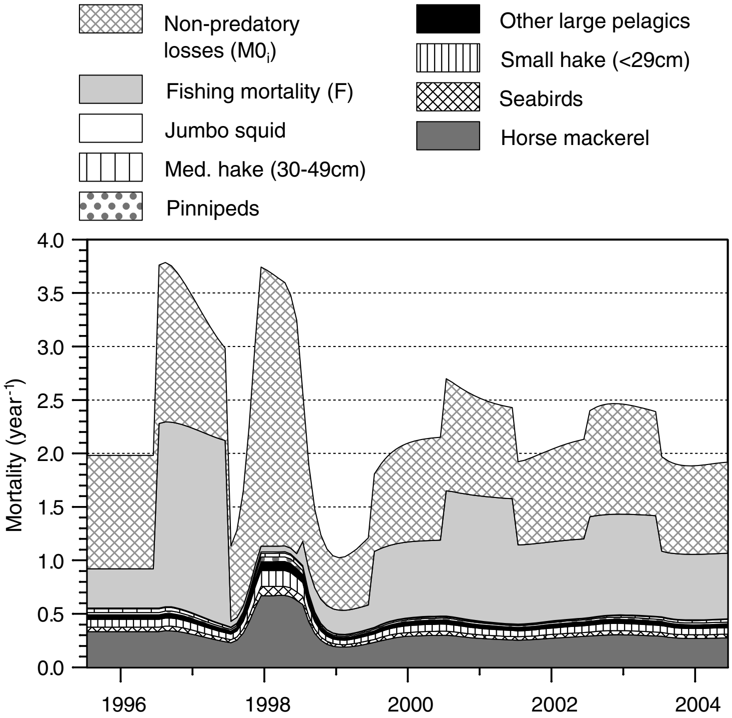

Fig. 6. Sources of mortality of anchovy, *Engraulis ringens*, through the Ecosim simulation. Only the top seven sources of predation mortality are shown (representing >95% of total predation mortality).

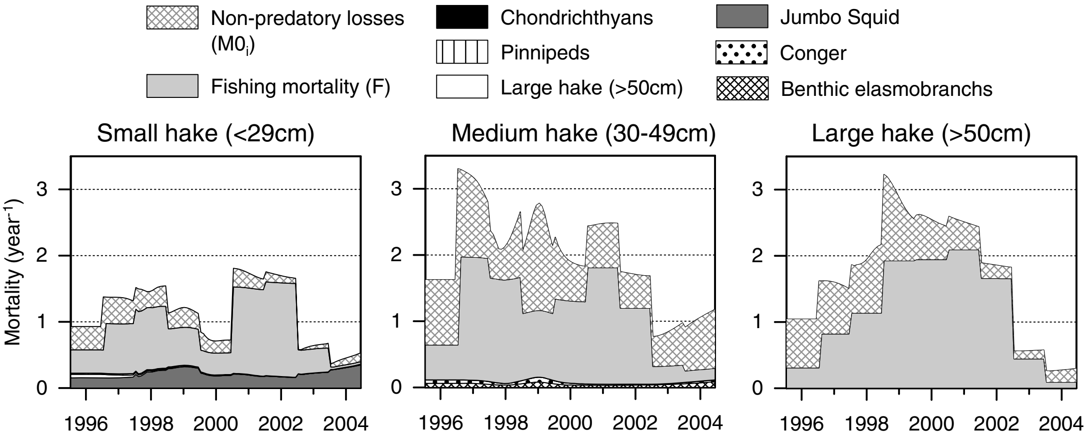

Fig. 7. Sources of mortality for different size classes of hake, *Merluccius gayi peruanus*, through the Ecosim simulation.

(*F*) values are much more variable than mortality from predation (Fig. 7). In 1996–97, before the onset of EN, VPA-derived *F* values more than doubled. This is consistent with past EN events whereby during the first phase of the EN stocks concentrate inshore, increasing their density and catchability (Csirke, 1989), whereas later, during the height of EN and possibly coinciding with the brunt of the arriving Kelvin wave, anchovy stocks are further driven inshore and/or to greater depths (Icochea, 1989; Bertrand et al., 2004). Anchovy had moved closer to the coast and to deeper waters (up to 150 m), which prevented large industrial purse seining (Arntz and Fahrbach, 1991; Bertrand et al., 2004). As the *F* values used are based on a biological year (July–June), the 1996–97 value is influenced by the onset of EN. Positive temperature anomalies for the Peruvian coast were noted as early as March 1997 and more than 2.8 million tonnes were landed during April and May alone. Shortly after these impressive catches, the anchovy fishery was essentially closed until the end of 1998, such that *F* was near zero during EN. Dynamics of the anchovy population in the later years of the simulation show both fishery and predation mortalities elevated as fishing began again and some predators recovered, causing some drop in anchovy biomass over 2000–2003 (Fig. 6).

According to the VPA analysis conducted by IMARPE, hake biomass was very high between 1993 and 96 – levels not seen since the late 1970s – however these levels declined dramatically after the EN of 1997–98 and have remained alarmingly low for the past decade. As a result, the hake fishery closed in September 2002 and now operates at a much smaller scale. Several hypotheses have been offered to explain the crash: (i) low recruitment-success due to cannibalism of juveniles by adult hake (Ballón, 2005), (ii) increased predation pressure on small hake due to the immigration/expansion of jumbo squid, (iii) overfishing (Wosnitza-Mendo et al., 2005), and (iv) demersal community changes affecting the prey of hake (Ballón, 2005). The simulated mortalities for small juvenile hake suggests that cannibalism does not contribute much to

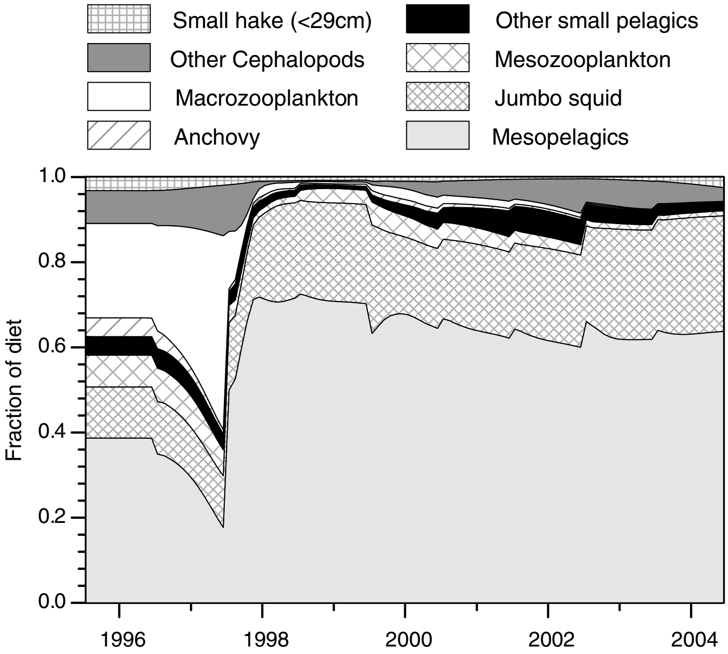

Fig. 8. Contribution of prey items to the diet of jumbo squid, *Dosidicus gigas*, through the Ecosim simulation.

mortality even when adult hake were abundant (1995–97; Fig. 7). Hake fishing mortality, however, increased before EN and remained at high levels for all three hake size groups until the fishery closure in 2002. These increases in *F* over the EN period, in contrast to previous ENs during which *F* generally decreases, were likely due to improved fishing techniques and movement of the trawl fleet southwards in pursuit of hake (Wosnitza-Mendo et al., 2005). The model suggests further mortality occurred due to decreases in prey abundance, especially for medium and large hake. This result is supported by Ballón et al. (2008), who found for 1972–2004 that gonadosomatic and stomach fullness indices decreased with EN-associated positive temperature anomalies, implying food-limited somatic production. The simulation predicts biomass gains for all three hake groups during 2003–04 due to reduced fishing mortality after 2001; however, hake did not recover in reality (Fig. 3). Ballón et al. (2008) offer a non-trophic explanation – reproductive failure. They observed that while large hake (>35 cm) show high condition and stomach fullness indices during the 2000s, gonadosomatic indices have decreased since the mid 1980s. Additionally, sex ratios have shifted toward females (reaching almost 100% for fish larger than 35 cm), leading the authors to hypothesize that long-term fishing pressure from the fishery may have disproportionately depleted males (males comprised 80% of the catches during the 1980s) to the point where females now lack a sufficient number of males to stimulate reproduction. Such a dependence on males to induce spawning is typical in cod-like species (Rowe and Hutchings, 2003). Nevertheless, our simulation supports the results of the VPA: Increases in *F* explain the sharp decline in hake abundance observed from 1997 to 2002. When compared to the baseline natural mortality value ($M = 0.38$) used in the VPA, total mortality values (Z) sum to extremely high levels (above 2.0) for medium and large hake groups, mainly driven by *F*, and illustrate the pressure put on the group during the post-EN period.

Time-series data on fishing rates existed for only three species at the time of this study (anchovy, hake, and jumbo squid). Therefore, simulation results concerning the importance of the fisheries on system dynamics may be somewhat conservative and future simulations may observe an even greater importance by incorporating additional fisheries.

Immigration – The offshore border of the model domain was set at 60 nm (ca. 111 km), which is approximately the mean width of the continental shelf. Previous model domains for the Peruvian upwelling system (Jarre et al., 1991) were narrower due to focus on the nearshore habitat of anchovy. Our wider domain allowed incorporation of the "active zone" or productive upwelling system (Nixon and Thomas, 2001). Our latitudinal range (4–16°S) similarly encompassed the main upwelling region delimited by the equatorial current to the north and a zone of decreased offshore Ekman transport further to the south. This latitudinal extension also corresponds to the main distribution of the northern Humboldt sardine and anchovy stocks (Alheit and Ñiquen, 2004). Despite this care to account for variability of principal functional groups, several less coastal species migrate into the model area, especially during periods of reduced upwelling and subsequent habitat reduction associated with EN. Sardine and mackerels, for example, remain offshore in oceanic water during the strong upwelling of La Niña (Bertrand et al., 2004); and it has been hypothesized that physiological restraints may also limit their distribution (Jarre et al., 1991). These non-trophic effects may help to explain why some more oceanic groups' dynamics are not well predicted by the model, and thus may require additional external forcing in future simulations.

The immigration of mesopelagic fish during EN does not appear to have been a significant factor for the decreased biomass of more coastal species during the EN 1997–98. However, their longer-term growth does appear to impact some more coastal groups in later years of the simulation when their mesopelagic biomass was highest. While the cause of the mesopelagic fish outburst is not known, we speculate that either (i) the euphausiids biomass increased during EN in response to decreased grazing competition with mesozooplankton, and/or (ii) the deepened thermocline during EN may have increased the vulnerability of euphausiids – a principal prey for mesopelagic fish – allowing for an increase in predation by mesopelagic fish. Given euphausiids' strategy of predation avoidance through diel vertical migrations across the Oxygen Minimum Layer (OML, <1.0 ml L^{-1}) (Antezana, 2002), it is possible that a deepening of the upper boundary of the OML may have caused increased vulnerability to predation. In any case, this increase in mesopelagic fish biomass during and after the EN helps to explain the decreases in biomass of both mackerel groups through competition for macrozooplankton, a main prey for all three.

Another link with the mesopelagic fish expansion is the bottom-up response of the key predator, jumbo squid. This has had some benefits in Peru through the sale of fishing permits to foreign offshore Japanese and Korean jigging vessels as well as becoming an important target species for the nearshore artisanal fisheries. Despite this, the fear of negative effects of the jumbo squid outburst on the more valuable hake population has caused alarm. The results of this study indicate that while some competitive effects do occur between jumbo squid and hake, the high fishing rates appear to have more responsibility in the hake's decline. While the direct predation mortality rates on small hake by jumbo squid appear relatively stable in the simulation, is should be noted that it is proportionally larger in the later years possibly due to groups' lower total mortality (Fig. 7).

4.2. Internal control mechanisms

The dramatic improvement in *SS* (31.2%) after the fit-to time-series routine highlights the importance of trophic control to internal dynamics of the ecosystem. Shannon et al. (2004a) also found that fitting of internal dynamics improved the simulation in the Southern Benguela by 40%. Our shorter time-series makes for a less robust analysis; however, we will focus on the most important and interpretable interactions.

One of the more significant results of the vulnerability fitting exploration was that a wasp-waist configuration around small pelagics, typical for other EBCSs, is not supported for the Peruvian system. Cury et al. (2000) found a negative relationship between yearly zooplankton concentrations and small pelagic landings for several upwelling systems (California, Ghana and Ivory Coast, Oyashio (Japan), Black Sea, Southern Benguela) and hypothesized that zooplankton biomass is top-down controlled by pelagic fish. Shannon et al., (2004a), Shannon et al., (2004b) further supported a wasp-waist configuration surrounding small pelagics in the Southern Benguela system. On the other hand, Cury et al. (2000) mentioned that the Peruvian system was one of the few exceptions where zooplankton concentrations and small pelagic landings were positively correlated; specifically, lower zooplankton concentrations (mainly mesozooplankton is sampled) were observed off Peru during the mid 1970s to mid 1980s, coinciding with the period after the anchovy collapse. Zooplankton concentrations have since increased with the recovery of anchovy, but remain lower than the concentrations of the 1960s and early 1970s (Ayón et al., 2004). For the shorter time-series modeled here, we also found a bottom-up relationship between mesozooplankton and the predators – anchovy and sardine (agrees with Ayón et al. 2008).

It has been proposed that Peru's proximity to the equator allows for optimal conditions for upwelling and fish production (Cury and Roy, 1989; Bakun, 1996), by allowing plankton communities to become particularly rich above the stable and relatively shallow thermocline. Furthermore, the shallow oxygen minimum may concentrate plankton above it, thus improving the grazing efficiency of small pelagic fish. We have demonstrated the importance of diatoms in the dynamics the Humboldt Current System, yet to the best of our knowledge a comparison of phytoplankton composition (i.e. based on cell size, taxa, unicellular vs. chain-forming, etc.) between EBCSs is lacking, thus preventing speculation if differences in phytoplankton composition exist. Highly concentrated plankton in Peru would not necessarily explain why zooplankton and small pelagics would both benefit simultaneously during periods of high upwelling. In fact, highly concentrated plankton might make top-down grazing pressure even more pronounced due to more efficient filter-feeding by anchovy. This possibility is supported by Ayón et al. (2008) through evidence of top-down control on smaller scales in Peru, wherein zooplankton biovolume is lower where anchovy and sardine biomass is high (acoustically determined, within a 5 km radius of the zooplankton sample). This finding is contrary to the negative correlation between large-scale trends of zooplankton volumes versus small pelagic fish biomass (Cury et al., 2000); however, Ayón et al. mention the importance of scale in explaining this discrepancy.

Cury et al. (2000) found negative relationships between zooplankton and small pelagics abundances in several upwelling systems (Ghana and Ivory Coast; Southern Benguela; Oyashio, Japan), yet the finding may be in part due to sampling bias, as zooplankton time-series tend to be based on samples restricted to the continental shelf. Where zooplankton over a larger extension from the coast and with evenly spaced sampling stations (California), no significant correlation to small pelagic catches is found. Similarly, zooplankton sampling conducted by IMARPE is fairly uniform and extends to ca. 185 km (100 nm) from the coast. This does not eliminate the possibility of wasp-waist forcing in Peru, but it does imply that it may occur only on smaller scales than our model domain.

Bottom-up configurations were found between sardine and anchovy to all their higher predator groups. In particular, the decreases in anchovy biomass associated with EN contributed to the decreases in several predatory groups, especially horse mackerel and small hake. Over longer time scales (i.e. decadal), both of these fish species show flexibility in their diets, especially during periods of low anchovy biomass (mid 1970s to late 1980s) – horse mackerel shift to zooplankton (Muck, 1989) and hake shift to sardine (Castillo et al., 1989). The shorter simulation period of this study appears to capture the reduction in system size due to the reduced upwelling during EN. As a result, most functional groups of the coastal environment experience reductions in biomass, which may differ from dynamics on decadal time scales such as a regime change. Generally, our results support previous studies presented in Pauly and Tsukayama (1987a), where teleosts, especially horse mackerel, are far more important consumers of anchovy than guano birds and pinnipeds; however acoustic surveys show that teleost spatial overlap with anchovy appears to have decreased significantly since 1997 (A. Bertrand, personal communication).

A more probable bottom-up relationship is that between anchovy and seabirds and pinnipeds, whose distributions strongly overlap with anchovy habitat. Even with a forced bottom-up configuration to anchovy, the model did not reproduce the large decreases in seabirds and pinnipeds that were observed following EN. We believe that a reduction in anchovy vulnerability may explain such a result. Muck and Pauly (1987) first proposed that seabirds are probably more affected by changes in vulnerability resulting from sea surface temperature-mediated distribution changes of anchovy than by changes in anchovy biomass. As mentioned earlier, not only did anchovy retreat to remaining centers of upwelling during EN (Alheit and Ñiquen, 2004), but also moved deeper (up to 150 m) with the thermocline (Bertrand et al., 2004). We believe that this movement made them less vulnerable to these predators. This is well illustrated in a diagram presented by Jarre et al. (1991) whereby changes in the vertical distribution of anchovy affect their vulnerability to predation or capture from seabirds, pinnipeds, and purse seiners. Diving seabirds are specialists on anchovy and have the shallowest effective hunting depth, and so would become the most susceptible to changes in the anchovy's vertical distribution.

Other important internal controls are observed with the more oceanic-associated functional groups. The expansion / immigration of mesopelagic fish into the model area impacted several groups directly, including possible top-down forcing of macrozooplankton and bottom-up forcing to jumbo squid. As mentioned before, this result must be taken with caution given that the diet of mesopelagic fish was not based on *in situ* measurements during the model period; however, the inclusion of several interactions involving macrozooplankton as prey in the vulnerability fitting routine suggests that their dynamics may be of more importance than previously thought. In particular, a top-down configuration between mesopelagics and macrozooplankton helped to explain decreases in macrozooplankton biomass, and subsequent decreases in several competitors for macrozooplankton (other cephalopods, mackerel, horse mackerel). While these groups' are more oceanic, they nevertheless have connections to the coastal zone. Mackerels are known to come closer to the coast both seasonally and during EN in response to decreased upwelling, where they may impact anchovy and other coastal species. Jumbo squid and other cephalopods also occur across the shelf. Cephalopods populations are subject to dramatic fluctuations and their impact on prey populations is equally variable. Their role as predators on fish and crustaceans clearly implicates them as a factor influencing natural mortality and recruitment-success in stocks of commercial exploited species (Rodhouse and Nigmatullin, 1996).

4.3. Conclusions and future prospects

The introduction of external drivers has allowed us to reproduce several key dynamics of the Northern Humboldt Current Ecosystem. Changes in phytoplankton associated with ENSO are important on the short-term while fishing rates and immigration from outside the upwelling region are important dynamics in the long-term. This has helped to elucidate that the dynamics of the Humboldt Current Ecosystem associated with the impact of an El Niño event appear to be relatively restricted to the immediate years following the event, and that once normalization returns, the management of fishing rates will be increasingly important. The separation of principal phytoplankton taxa allows for the simulation of important changes of energy flow in the Northern Humboldt Current Ecosystem over several temporal scales. Additionally, a link between the dynamics of the phytoplankton components and more easily observable environmental parameters, i.e. SST anomalies, takes a first step in the development of predictive models forced in real time.

A larger offshore extension allowed for the incorporation of important interactions between the coastal and more oceanic components of the ecosystem. Nevertheless, artificial forcing of mesopelagic fish was still necessary in reproducing the dynamics of the more oceanic-associated groups. Further investigation into the underlying drivers of the offshore ecosystem may become increasingly important in describing the dynamics of the more economically-important coastal upwelling system.

Internal control settings showed a mix of interactions; however a "wasp-waist" configuration around small pelagic fish is not supported. Specifically, top-down forcing of meso- and macrozooplankton by small pelagic fish is not observed.

Additional non-trophic interactions may also play important roles in dynamics (e.g. changes in vulnerability, recruitment, physiological constraints), and must be considered in future modeling efforts. We have highlighted possibilities of these in cases where the model fails to reproduce the historical trends. This has been an unexpected but extremely positive outcome of the two parts of this work, and has helped to formulate further questions and investigation foci for the future.

Finally, future prospects for trophic modeling include the adaptation of longer reconstructed time-series by Pauly and Tsukayama (1987b), Pauly et al. (1989) and Guenette et al. (this issue) to the model in order to explore dynamics since the development of the industrial fishery around the 1950s. This would create a more robust analysis by which to further tune the internal forcing controls of the model, including the larger-scale dynamics of a regime shift. Ultimately, this will allow for further exploration of fishing scenarios for improved management of the ecosystem.

Acknowledgements

The authors acknowledge assistance from the following people (in alphabetical): Milena Arias-Schreiber, Arnaud Bertrand, David Correa, Michelle Graco, Renato Guevara, Mariano Gutierrez, Kristen Kaschner, Miguel Ñiquen, Ralf Schwamborn, Sonia Sánchez, and Carmen Yamashiro. We also thank Carl Walters for the use of the Ecosim software, and Dr. Lynne Shannon and an anonymous referee for their critical suggestions on the manuscript. This study was financed and conducted in the frame of the EU-project CENSOR (Climate variability and El Niño Southern Oscillation: Impacts for natural resources and management, contract No. 511071) and is CENSOR publication No. 0086.

References

Alamo, A., 1989. Stomach contents of anchoveta (*Engraulis ringens*), 1974–1982. In: Pauly, D., Muck, P., Mendo, J., Tsukayama, I. (Eds.), The Peruvian Upwelling Ecosystem: Dynamics and Interactions, 391. ICLARM, Manila, Philippines, pp. 105–108.

Alheit, J., Ñiquen, M., 2004. Regime shifts in the Humboldt Current ecosystem. Progress in Oceanography 60, 201–222.

Antezana, T., 2002. Adaptive behavior of *Euphausia mucronata* in relation to the oxygen minimum layer of the Humboldt Current. In: Färber Lorda, J. (Ed.), Oceanography of the Eastern Pacific. CICESE, Ensenada, Mexico, pp. 29–40.

Arntz, W.E., Fahrbach, E., 1991. El Nino-Klimaexperiment der Natur. Birkhauser Verlag, Basel, Switzerland.

Avaria, S., Muñoz, P., 1987. Effects of the 1982–1983 El Niño on the marine phytoplankton off northern Chile. Journal of Geophysical Research 92, 14369–14382.

Ayón, P., Purca, S., Guevara-Carrasco, R., 2004. Zooplankton volume trends off Peru between 1964 and 2001. ICES Journal of Marine Science 61, 478–484.

Ayón, P., Swartzman, G., Bertrand, A., Gutierrez, M., Bertrand, S., 2008. Zooplankton and forage fish species off Peru: large-scale bottom-up forcing and local-scale depletion. Progress in Oceanography. 79, 208–214.

Baird, D., McGlade, J.M., Ulanowicz, R.E., 1991. The comparative ecology of six marine ecosystems. Philosophical Transactions: Biological Sciences 333, 15–29.

Bakun, A., 1996. Patterns in the ocean. Ocean processes and marine population dynamics. University of California Sea Grant, California, USA, in cooperation with Centro de Investigaciones Biologicas de Noroeste, La Paz, Baja California Sur, Mexico.

Bakun, A., Weeks, S.J., 2008. The marine ecosystem off Peru: What are the secrets of its fishery productivity and what might its future hold? Progress in Oceanography. 79, 290–299.

Ballón, M., Wosnitza-Mendo, C., Guevara-Carrasco, R., Bertrand, A., 2008. The impact of overfishing and El Niño on the condition factor and reproductive success of Peruvian hake, *Merluccius gayi peruanus*. Progress in Oceanography 79, 300–307.

Ballón, R.M., 2005. Comparative analysis of the community structure and trophic relations of the Peruvian hake *Merluccius gayi peruanus* and its by-catch of the years 1985 and 2001. Masters Thesis, University of Bremen, Bremen, Germany, unpublished.

Bertrand, A., Segura, M., Gutierrez, M., Vasquez, L., 2004. From small-scale habitat loopholes to decadal cycles: a habitat-based hypothesis explaining fluctuation in pelagic fish populations off Peru. Fish and Fisheries 5, 296–316.

Bidigare, R.R., Ondrusek, M.E., 1996. Spatial and temporal variability of phytoplankton pigment distributions in the Central Equatorial Pacific Ocean. Deep-Sea Research II 43, 809–833.

Brown, P.C., Painting, S.J., Cochrane, K.L., 1991. Estimates of phytoplankton and bacterial biomass production in the northern and southern Benguela ecosystems. South African Journal of Marine Science 11, 537–564.

Brush, M.J., Brawley, J.W., Nixon, S.W., Kremer, J.N., 2002. Modeling phytoplankton production: Problems with the Eppley curve and an empirical alternative. Marine Ecology Progress Series 238, 31–45.

Carr, M.E., 2002. Estimation of potential productivity in eastern boundary currents using remote sensing. Deep-Sea Research II 49, 59–80.

Castillo, R., Juárez, L., Higginson, L., 1989. Predación y canibalísmo en la población de la merluza peruana en el área de Paita-Peru. Memorias del Simposio Internacional de los Recursos Vivos y las Pesquerías en el Pacífico Sudeste, Viña del Mar, Chile, Revista Pacífico Sur (Número Especial).

Chavez, F.P., Ryan, J., Lluch-Cota, S.E., Ñiquen, M., 2003. From anchovies to sardines and back: multidecadal change in the Pacific Ocean. Science 299, 217–221.

Csirke, J., 1989. Changes in the catchability coefficient in the Peruvian anchoveta (*Engraulis ringens*) fishery. In: Pauly, D., Muck, P., Mendo, J.,Tsukayama, I. (Eds.), The Peruvian Upwelling Ecosystem: Dynamics and Interactions, vol. 18. ICLARM Conference Proceedings, Manila, Philippines, pp. 207–219.

Cury, P., Roy, C., 1989. Optimal environmental window and pelagic fish recruitment success in upwelling areas. Canadian Journal of Fisheries and Aquatic Sciences 46, 670–680.

Cury, P., Bakun, A., Crawford, R.J., Jarre, A., Quinones, R.A., Shannon, L.J., Verheye, H.M., 2000. Small pelagics in upwelling systems: patterns of interaction and structural changes in "wasp-waist" ecosystems. ICES Journal of Marine Science 57, 603–618.

DeMott, W.R., 1989. Optimal foraging theory as a predictor of chemically mediated food selection by selection by suspension-feeding copepods. Limnology and Oceanography 34, 140–154.

Espinoza, P., Blaskovic, V., 2000. Changes in diet of Peruvian anchoveta *Engraulis ringens* and its influence on feeding dynamics. Boletin del Instituto del Mar del Peru 19, 21–27.

Espinoza, P., Bertrand, A., 2008. Revising Peruvian anchovy (*Engraulis ringens*) trophic niche and ecological role reveals its plasticity and provides a new vision of the Humboldt Current system. Progress in Oceanography. 79, 215–227.

González, H., Daneri, G., Figueroa, D., Iriarte, J., Lefevre, G., Pizarro, G., Nones, R.Q., Sobrazo, M., Troncoso, A., 1998. Producción primaria y su destino en la trama trófica-pelágica y océano profundo e intercambio océano-atmósfera de CO_2 en la zona norte de la Corriente de Humboldt (23 S): Posibles efectos del evento El Niño, 1997– 1998 en Chile. Revista Chilena de Historia Natural 71, 429–458.

González, H.E., Giesecke, R., Vargas, C.A., Pavez, A., Iriarte, J., Santibáñez, P., Castro, L., Escribano, R., Pagès, F., 2004. Carbon cycling through the pelagic foodweb in the northern Humboldt Current off Chile (23° S). ICES Journal of Marine Science 61, 572–584.

Guevara-Carrasco, R., 2004. Peruvian hake overfishing: misunderstood lessons. Boletín del Instituto del Mar del Perú 21, 27–32.

Heymans, J.J., Baird, D., 2000. A carbon flow model and network analysis of the northern Benguela upwelling system, Namibia. Ecological Modelling 126, 9–32.

Heymans, J.J., Shannon, L.J., Jarre, A., 2004. Changes in the northern Benguela ecosystem over three decades: 1970s, 1980s, and 1990s. Ecological Modelling 172, 175–195.

Icochea, L., 1989. Análisis de la pesquería de arrastre pelágica en la costa peruana durante el período 1983–1987 y su relación con los cambios oceanográficos. Flota Pesquera Peruana (FLOPESCA), 51 S.

Iriarte, J.L., González, H.E., 2004. Phytoplankton size structure during and after the 1997/98 El Nino in a coastal upwelling area of the northern Humboldt Current System. Marine Ecology Progress Series 269, 83–90.

James, A.G., Findlay, K.P., 1989. Effect of particle size and concentration on feeding behaviour, selectivity and rates of food ingestion by the Cape Anchovy *Engraulis capensis*. Marine Ecology Progress Series 50, 275–294.

Jarre-Teichmann, A., 1992. Steady-state modelling of the Peruvian upwelling ecosystem. Ph.D. Thesis, University of Bremen, Bremen, Germany, unpublished.

Jarre, A., Muck, P., Pauly, D., 1991. Two approaches for modelling fish stock interactions in the Peruvian upwelling ecosystem. ICES Marine Science Symposia 193, 178–184.

Landry, M.R., Kirshtein, J., Constantinou, J., 1996. Abundances and distributions of picoplankton populations in the Central Equatorial Pacific from 12° N to 12° S, 140° W. Deep-Sea Research II 43, 871–890.

Moloney, C.L., Jarre, A., Arancibia, H., Bozec, Y.-M., Neira, S., Jean-Paul Roux, J.-P., Shannon, L.J., 2005. Comparing the Benguela and Humboldt marine upwelling ecosystems with indicators derived from inter-calibrated models. ICES Journal of Marine Science 62, 493–502.

Muck, P., Pauly, D., 1987. Monthly anchoveta consumption of guano birds, 1953 to 1982. In: Pauly, D., Tsukayama, I. (Eds.), The Peruvian Anchoveta and its Upwelling Ecosystem: Three Decades of Change, vol. 391. ICLARM, Manila, Philippines, pp. 219–233.

Muck, P., 1989. Major trends in the pelagic ecosystem off Peru and their implications for management. In: Pauly, D., Muck, P., Mendo, J., Tsukayama, T. (Eds.), The Peruvian Upwelling Ecosystem: Dynamics and Interactions, vol. 18. ICLARM Conference Proceedings, Manila, Philippines, pp. 386–403.

Neira, S., Arancibia, H., 2004. Trophic interactions and community structure in the upwelling system off Central Chile (33–39° S). Journal of Experimental Marine Biology and Ecology 312, 349–366.

Neira, S., Arancibia, H., Cubillos, L., 2004. Comparative analysis of trophic structure of commercial fishery species off Central Chile in 1992 and 1998. Ecological Modelling 172, 233–248.

Nixon, S., Thomas, A., 2001. On the size of the Peru upwelling ecosystem. Deep-Sea Research I 48, 2521–2528.

Ochoa, N., Rojas de Mendiola, B., Gómez, O., 1985. Identificación del fenómeno El Niño a través de los organismos fitoplanctónicos. Boletin del Instituto del Mar del Perú, Volumen extraordinario. Instituto del Mar del Perú, Callao, Peru. pp. 23–31.

Pauly, D., Tsukayama, I., 1987a. On the implementation of management-oriented fishery research: The case of Peruvian anchoveta. In: Pauly, D., Tsukayama, I. (Eds.), The Peruvian Anchoveta and Its Upweling Ecosystem: Three Decades of Change, vol. 391. ICLARM, Manila, Philippines, pp. 1–13.

Pauly, D., Tsukayama, I., 1987b. The Peruvian anchoveta and its upwelling ecosystem: three decades of change. ICLARM, Manila, Philippines.

Pauly, D., Muck, P., Mendo, J., Tsukayama, I., 1989. The Peruvian upwelling ecosystem: Dynamics and interactions. In: ICLARM Conference Proceedings, Manila, Philippines.

Pennington, J.T., Mahoney, K.L., Kuwahara, V.S., Kolber, D.D., Calienes, R., Chavez, F.P., 2006. Primary production in the eastern tropical Pacific: A review. Progress in Oceanography 69, 285–317.

Pitcher, G.C., Brown, P.C., Mitchell-Innes, B.A. 1992. Spatio-temporal variability of phytoplankton in the southern Benguela Upwelling system. South African Journal of Marine Science/Suid-Afrikaanse Tydskrif vir Seewetenskap.

Purca, S., 2005. Variabilidad temporal de baja frecuencia en el Ecosistema de la Corriente de Humboldt frente a Perú. Ph.D. thesis, Universidad de Concepción, Concepción, Chile, unpublished.

Rodhouse, P.G., Nigmatullin, C.M., 1996. The role of cephalopods in the world's oceans. Role as consumers. Philosophical Transactions: Biological Sciences 351, 1003–1022.

Rojas de Mendiola, S., 1981. Seasonal phytoplankton distribution along the Peruvian coast. In: Richards, F.A. (Ed.), Coastal Upwelling, vol. 20. American Geophysical Union, Washington, DC, pp. 348–356.

Rowe, S., Hutchings, J.A., 2003. Mating systems and the conservation of commercially exploited marine fish. Trends in Ecology and Evolution 18, 567–572.

Sea Around Us, 2006. A global database on marine fisheries and ecosystems. Fisheries Centre, University British Columbia, Vancouver, Available from: <www.seaaroundus.org>.

Shannon, L.J., Moloney, C.L., Jarre, A., Field, J.G., 2003. Trophic flows in the southern Benguela during the 1980s and 1990s. Journal of Marine Systems 39, 83–116.

Shannon, L.J., Christensen, V., Walters, C.J., 2004a. Modelling Stock Dynamics in the Southern Benguela Ecosystem for the Period 1978–2002. African Journal of Marine Science 26, 179–196.

Shannon, L.J., Field, J.G., Moloney, C.L., 2004b. Simulating anchovy-sardine regime shifts in the southern Benguela ecosystem. Ecological Modelling 172, 269–281.

Sommer, U., Stibor, H., Katechakis, A., Sommer, F., Hansen, T., 2002. Pelagic food web configurations at different levels of nutrient richness and their implications for the ratio fish production: primary production. Hydrobiologia 484, 11–20.

Sommer, U., Hansen, T., Blum, O., Holzner, N., Vadstein, O., Stibor, H., 2005. Copepod and microzooplankton grazing in mesocosms fertilised with different Si:N ratios: no overlap between food spectra and Si:N influence on zooplankton trophic level. Oecologia 142, 274–283.

Sun, J., Liu, D., 2003. Geometric models for calculating cell biovolume and surface area for phytoplankton. Journal of Plankton Research 25, 1331–1346.

Tam, J., Taylor, M.H., Blaskovic, V., Espinoza, P., Ballón, R.M., Díaz, E., Wosnitza-Mendo, C., Argüelles, J., Purca, S., Ayón, P., Quipuzcoa, L., Gutiérrez, D., Goya, E., Ochoa, N., Wolff, M., 2008. Trophic flows in the Northern Humboldt Current Ecosystem, Part 1: Comparing 1995–96 and 1997–98. Progress in Oceanography.

Taylor, M.H., Wolff, M., 2007. Trophic modeling of Eastern Boundary Current systems: a review and prospectus for solving the "Peruvian Puzzle". Revista Peruana de Biologia 14, 87–100.

van der Lingen, C.D., 1994. Effect of particle size and concentration on the feeding behaviour of adult pilchard *Sardinops sagax*. Marine Ecology Progress Series 109, 1–13.

van der Lingen, C.D., Hutchings, L., Field, J.G., 2006. Comparative trophodynamics of anchovy *Engraulis encrasicolus* and sardine *Sardinops sagax* in the southern Benguela: are species alternations between small pelagic fish trophodynamically mediated? African Journal of Marine Science 28, 465–477.

Walsh, J.J., 1981. A carbon budget for overfishing off Peru. Nature 290, 300–304.

Walters, C., Christensen, V., Pauly, D., 1997. Structuring dynamic models of exploited ecosystems from trophic mass-balance assessments. Reviews in Fish Biology and Fisheries 7, 139–172.

Walters, C., Pauly, D., Christensen, V., Kitchell, J.F., 2000. Representing density dependent consequences of life history strategies in aquatic ecosystems: EcoSim II. Ecosystems 3, 70–83.

Walters, C.J., Martell, S.J.D., 2004. Fisheries Ecology and Management. Princeton University Press, Princeton, New Jersey.

Wosnitza-Mendo, C., Mendo, J., Guevara-Carrasco, R., 2005. Políticas de gestión para la reducción de la capacidad excesiva de esfuerzo pesquero en Perú: el caso de la pesquería de la merluza. In: Agüero, M. (Ed.) Capacidad de pesca y manejo pesquero en América Latina y el Caribe, vol. 461. FAO Technical Papers, pp. 343–372.

Progress in Oceanography 79 (2008) 379–389

Contents lists available at ScienceDirect

Progress in Oceanography

journal homepage: www.elsevier.com/locate/pocean

Patterns in the spatial distribution of Peruvian anchovy (*Engraulis ringens*) revealed by spatially explicit fishing data

Sophie Bertrand [a,b,c,*], Erich Díaz [b], Matthieu Lengaigne [d]

[a] *University of Washington, School of Aquatic and Fisheries Sciences, Box 355020, Seattle, WA 98195-5020, USA*
[b] *IMARPE, Esquina Gamarra y General Valle S/N, Chuchito, Callao, Lima, Peru*
[c] *Institut de Recherche pour le Developpement (IRD), Centre de Recherche Halieutique Méditerranéenne et Tropicale, Avenue Jean Monnet, BP 171, 34203 Sète Cedex, France*
[d] *IRD, LOCEAN, Tour 45-55, 4ème Etage, 4 Place Jussieu, 75252 Paris Cedex 05, France*

ARTICLE INFO

Article history:
Accepted 14 October 2008
Available online 21 October 2008

Keywords:
Peruvian anchovy
Fish distribution
Vessel monitoring system (VMS)
Neural network
Multilayer perceptron (MLP)
Fishing sets distribution
Clustering index
Purse–seine fleet

ABSTRACT

Peruvian anchovy (*Engraulis ringens*) stock abundance is tightly driven by the high and unpredictable variability of the Humboldt Current Ecosystem. Management of the fishery therefore cannot rely on mid- or long-term management policy alone but needs to be adaptive at relatively short time scales. Regular acoustic surveys are performed on the stock at intervals of 2 to 4 times a year, but there is a need for more time continuous monitoring indicators to ensure that management can respond at suitable time scales. Existing literature suggests that spatially explicit data on the location of fishing activities could be used as a proxy for target stock distribution. Spatially explicit commercial fishing data could therefore guide adaptive management decisions at shorter time scales than is possible through scientific stock surveys. In this study we therefore aim to (1) estimate the position of fishing operations for the entire fleet of Peruvian anchovy purse–seiners using the Peruvian satellite vessel monitoring system (VMS), and (2) quantify the extent to which the distribution of purse–seine sets describes anchovy distribution. To estimate fishing set positions from vessel tracks derived from VMS data we developed a methodology based on artificial neural networks (ANN) trained on a sample of fishing trips with known fishing set positions (exact fishing positions are known for approximately 1.5% of the fleet from an at-sea observer program). The ANN correctly identified 83% of the real fishing sets and largely outperformed comparative linear models. This network is then used to forecast fishing operations for those trips where no observers were onboard. To quantify the extent to which fishing set distribution was correlated to stock distribution we compared three metrics describing features of the distributions (the mean distance to the coast, the total area of distribution, and a clustering index) for concomitant acoustic survey observations and fishing set positions identified from VMS. For two of these metrics (mean distance to the coast and clustering index), fishing and survey data were significantly correlated. We conclude that the location of purse–seine fishing sets yields significant and valuable information on the distribution of the Peruvian anchovy stock and ultimately on its vulnerability to the fishery. For example, a high concentration of sets in the near coastal zone could potentially be used as a warning signal of high levels of stock vulnerability and trigger appropriate management measures aimed at reducing fishing effort.

1. Introduction

The Peruvian pelagic ecosystem is highly dominated by anchovy (*Engraulis ringens*). This species sustains the world's largest single species fishery with 6.5 millions tons landed per year on average over the last decade. Management of the fishery presents a unique challenge as anchovy stock dynamics are tightly driven by the high and unpredictable variability of the Humboldt Current Ecosystem (Alheit and Niquen, 2004). Successful management cannot rely on mid- or long-term policies but needs to be adaptive on weekly or monthly time scales. Decisions on catch and effort limitations within this adaptive management framework need to be based on almost continuous, near real-time estimates of the fish stock condition (available biomass and vulnerability to the fleet), which depend largely on how the fish population is distributed in space (Csirke, 1989; Arreguín-Sánchez, 1996; Harley et al., 2001). Regular scientific acoustic surveys of Peruvian anchovy are performed 2 to 4 times a year by the Instituto del MAR del PEru (IMARPE). To obtain estimates of the condition of the stock at the shorter time steps needed to implement an adaptive management framework, complementary monitoring indicators based on proxies are required.

---

* Corresponding author. Address: IRD, Teruel 357, Miraflores, Casilla 18-1209, Lima 18, Peru. Tel./fax: +51 1 441 32 23.
E-mail address: Sophie.Bertrand@ird.fr (S. Bertrand).

0079-6611/$ - see front matter © 2008 Elsevier Ltd. All rights reserved.
doi:10.1016/j.pocean.2008.10.009

Existing literature suggests that the spatial distribution of fishing operations should reflect to some extent patterns of fish distribution. Fishers constitute, with marine birds and sea lions (Muck and Pauly, 1987; Muck and Fuentes, 1987), the main predators of the Peruvian anchovy population. Although predator–prey spatial relationships may be complex (Fauchald et al., 2000; Davoren et al., 2002), fishers have to search for and find their prey, and their spatial behaviour track the dynamics of prey distribution in a similar way to animal predators (Frontier, 1987; Russel et al., 1992; Bertrand et al., 2005, 2007). Peruvian anchovy are targeted primarily by purse–seiners. Fishing set locations are currently known for a small fraction of the fleet (about 1.5% of the vessels) from an at-sea observer program run by IMARPE. Continuous monitoring of vessel location is obtained via a satellite vessel monitoring system (VMS) called SISESAT (SIstema de SEguimiento SATelital). Implemented in 1999, SISESAT covers the movements of the entire industrial anchovy fishery (approximately 1350 fishing vessels), providing high resolution, real-time, and low cost information on fleet behaviour and spatial dynamics. In this study our aim is to estimate fishing set locations from the one-dimensional geometry of the vessel path provided by the raw VMS data, and to assess the extent to which these estimates are representative of the distribution of anchovy along the Peruvian coast.

A growing number of studies have made use of satellite VMS data to better understand fishery dynamics and behaviour (Bertrand et al., 2005; Bertrand et al., 2007; Deng et al., 2005; Dinmore et al., 2003; Mills et al., 2007; Murawski et al., 2005). In the Peruvian anchovy fishery, purse–seiners fitted with VMS automatically report their position once an hour or less on average. VMS data do not explicitly report whether a vessel is fishing. Each fishing trip lasts from a few hours to 2 days, and one fishing operation (set) lasts on average 2 h. In the course of a fishing trip, between one and five fishing operations may occur on average. Because the time taken for a fishing set is only twice that of the VMS sampling period, identifying fishing set locations from VMS is possible but not trivial. Speed-related criteria have been trialled (speed usually ranges between 0.2 and 1.6 knots, i.e. 0.4–2.9 km h^{-1}, during a fishing set) but tend to over-estimate the number of fishing sets (+182%) due to similarities in vessel speeds when fishing, drifting, and searching.

To improve identification performance, we implement an identification methodology based on artificial neural networks (ANN, Bishop, 1995; Ripley, 1996; Fine, 1999) which have recently become popular tools for non-parametric classification and prediction in many fields of science and engineering. ANNs have proven to be successful at modelling a number of fishery-related variables and to outperform comparable linear models for Pacific herring (*Clupea pallasi*) recruitment (Chen and Ware, 1999), for modelling of virtual fishermen searching behaviour (Dreyfus-León, 1999), and for predicting the relative abundance of bigeye tuna (*Thunus obesus*) from catch and effort data (Maunder and Hinton, 2006) for instance. In this study, we developed an ANN fed with raw VMS data and trained on a sample of fishing trips with known fishing set positions (provided by at-sea observers) to predict a binary response (fishing set/no fishing set). Fishing set positions estimated by the ANN were then compared with acoustic data estimating anchovy biomass to determine the extent to which the spatial distribution of the fleet fishing operations correlates with the patterns displayed by the anchovy stock.

2. Material and methods

2.1. Data

VMS data used to identify fishing set locations were extracted from the SISESAT database, which contains vessel movements for the entire industrial anchovy fleet (about 1350 vessels) since 1999. Each vessel is equipped with an Argos satellite transmitter and global positioning system (GPS) receiver. The transmitter sends a time-referenced position with an accuracy of 100 m on an hourly basis. VMS data extracted from the database covered all of the fishing seasons between 2000 and 2002 (22 months,

Table 1
Summary of the study periods, the corresponding number of fishing sets and elementary sampling distance units (ESDU), and the different indexes computed for describing fish and fishing sets distributions: mean distance to the coast (MDC), total area of the convex polygon enclosing the distribution (TA) and clustering index (Clust).

Month fishing operations	Num fishing sets	MDC (km)	TA (km^2)	Clust.(km^2)	Acoustic survey reference	Date of the survey in the study zone	Number of ESDU		MDC (km)	TA (km^2)	Clust. (km^2)
							s_A > 0	s_A > 500			
March 2000	2376	49.5	39,115	63,323	Sv 2000 01–02	09/02–20/02	1451	765	89.3	73,589	32,985
April 2000	997	61.4	40,332	54,343	–	–	–	–	–	–	–
May 2000	1648	52.4	31,023	55,633	–	–	–	–	–	–	–
June 2000	1592	55.6	53,898	73,026	–	–	–	–	–	–	–
July 2000	2801	80.1	56,713	153,481	Sv 2000 06–07	10/06–22/06	741	131	91.9	82,664	175,378
October 2000	1058	18.9	25,055	279,410	Sv 2000 08–09	30/08–12/09	551	113	23.7	66,022	132,648
November 2000	1902	23.9	39,235	79,306	Sv 2000 10–11	16/10–24/10	646	81	28.7	60,864	113,667
December 2000	1703	79.7	37,190	102,379	–	–	–	–	–	–	–
April 2001	1590	55.4	32,131	61,265	Sv 2001 02–04	09/03–18/03	961	514	60.2	50,317	37,050
June 2001	3455	41.0	45,299	26,836	–	–	–	–	–	–	
July 2001	172	32.8	40,696	77,077	Sv 2001 07–08	11/07–20/07	824	116	70.9	52,899	64,472
October 2001	760	19.1	7 738	64,026	Sv 2001 08–09	30/08–14/09	622	133	18.9	49,442	122,406
November 2001	208	18.0	5 632	191,618	Sv 2001 10–11*	–	–	–	–	–	–
December 2001	129	18.7	10,691	34,618	–	–	–	–	–	–	–
March 2002	1287	31.5	7 851	123,525	–	–	–	–	–	–	–
April 2002	2512	48.2	29,850	39,015	Sv 2002 02–03	01/03–10/03	619	337	40.4	37,105	36,858
May 2002	2880	48.2	33,771	82,736	–	–	–	–	–	–	–
June 2002	1635	77.6	40,487	57,118	–	–	–	–	–	–	–
July 2002	1662	88.4	43,769	170,898	Sv 2002 08	17/08–27/08	679	110	82.8	64,523	135,481
October 2002	407	77.0	28,797	73,383	–	–	–	–	–	–	–
November 2002	3512	58.1	31,439	165,164	Sv 2002 10–11	25/10–09/11	631	99	41.1	53,925	72,227
December 2002	4088	20.5	14,711	155,632	–	–	–	–	–	–	–

* One survey performed during 10-11 2001 was discarded because an important bias between sampling by acoustic and by the fishery was evidenced by IMARPE at this period.

see Table 1 for details) and Peruvian coastal waters from 7°S to 10°S (Fig. 1). SISESAT does not make the distinction between positions at sea or in port. To identify the positions corresponding to fishing trips, and to resample the trajectories into elementary straight moves (Turchin, 1998), we used the set of 3 pre-processing algorithms described in Bertrand et al. (2005, 2007). From the raw positions, we identified 15,975 fishing trips operated by 563 vessels. VMS data held in the database comprises of vessel ID, date, hour, longitude and latitude. From these raw data we derived higher order variables for each elementary straight move: speed (ratio of move length to move duration), speed variation (difference between the speeds of two consecutive moves), and change of direction (absolute angle between the headings of two consecutive moves). Of the raw and derived variables, five were selected as important from the viewpoint of the fishing operation: speed, hour, absolute change of direction, and two calculations of speed variation (current and next position, and current and previous position). All the other available variables that could be deduced from raw latitude–longitude data (distance, heading, etc.) were not included in the set of characterizing variables as they were not found to improve model performance. After pre-processing these variables (standardizing and linearization of the circular variables), they served as inputs to a neural network model.

In order to train the neural network, we needed a reference sample of fishing trips for which we knew where the fishing operations truly occurred. We used information collected by the at-sea observer program run by IMARPE since 1996 and which has sampled an average of 25 vessels almost continuously since that time. The observers collect among other information the exact position of the fishing operations and the corresponding catches. We selected from this data the fishing trips corresponding to the period and area of interest (142 fishing trips, 494 fishing operations). We then extracted the corresponding fishing trips from the VMS database. To build a training dataset, each vessel elementary move generated from the VMS data was assigned the five selected input variables (speed, hour, absolute change of direction, and speed variation $\times$ 2) and a Boolean variable where 1 identified a fishing operation and 0 was assigned to all remaining elementary moves. The remaining VMS elementary moves (the forecast dataset) corresponded to fishing trips where there were no corresponding at-sea observer records.

2.2. Design of the neural network

Neural networks have become a popular tool for classification. The type of neural network used in this study is a multilayer perceptron (MLP), which is probably the most widely used architecture for practical applications. They are supervised networks, so they require a desired output to be trained. They learn how to transform input data into a desired output response, so they are widely used for pattern classification. MLPs have been shown to be able to approximate any continuous function when a sufficient number of hidden nodes are used (Cybenko, 1989; Funahashi, 1989; Hornik et al., 1989). These properties make neural networks good tools for non-parametric classification as they do not assume any parametric form for distinguishing between categories. The MLP used in this study is made up of three neural layers: the input layer, the output layer, and a middle 'hidden' layer. The input layer consisted of the five input neurons, i.e. the speed and hour of the move, the absolute change of heading between the current and the previous move ($|\Delta\theta|$), the speed variation between the current and the previous move (Δv_{-1}) and the speed variation between the current and the next move (Δv_{+1}). The output layer (neuron) consisted of a simple two-class classifier: fishing set or no fishing set.

Fig. 2 displays the topology of a 5-3-1 MLP. In this network typology, the input layer is determined by the input signals. This upper layer sends these signals to neurons in the hidden layer. Each hidden neuron computes the weighted sum of the inputs, i.e. the inner product between its inputs and corresponding weights plus a 'bias' term. This quantity is then transformed using

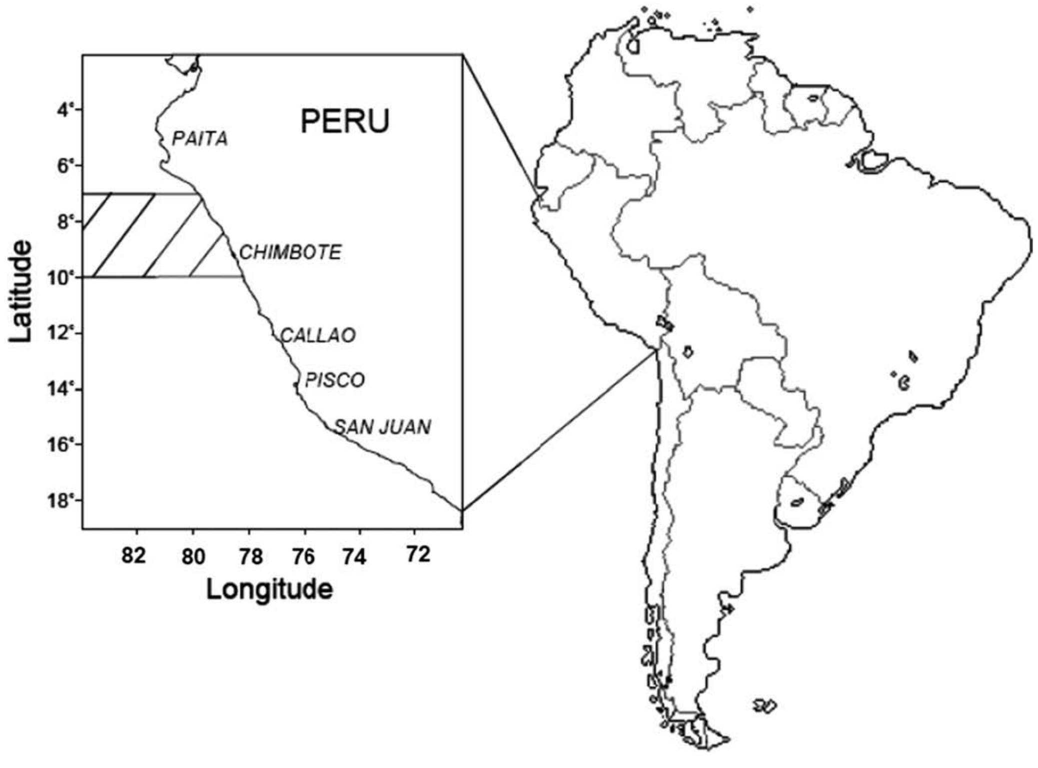

Fig. 1. Map highlighting the region of interest (7°–10° S off Peru).

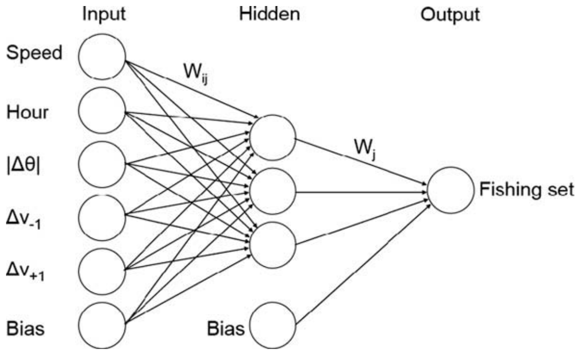

Fig. 2. Topology (5-3-1) of the multilayer perceptron (MLP), a kind of supervised artificial neural network, used to identify fishing sets from VMS data.

an activation function. The output layer processes its signal in the same manner. Therefore, the neural network has multiple inputs (x_i, $i = 1, \ldots, l$) which are non-linearly mapped to m intermediate variables called hidden neurons (h_j, $j = 1, \ldots, m$), and which are then mapped to an output variable y. Mathematically, the relationship linking input to output can be described as follows:

$$h_j = \phi_1\left(\sum_{i=1}^{l} w_{ij}x_i + b_j\right), \quad j = 1, \ \ldots, \ m \tag{1}$$

$$y = \phi_2\left(\sum_{j=1}^{m} \tilde{w}_j h_j + \tilde{b}\right) \tag{2}$$

The characteristics of this empirical model are determined by $m^*(l + 1)$ weight parameters (w_{ij} and w_j) and ($m + 1$) bias parameter (b_j and b). For a two-classes classifier, one output neuron is sufficient. ϕ_1 and ϕ_2 are activation functions for the hidden and output layer. They can be any monotonic smooth function. A multiple linear regression is therefore a special type of neural network with no hidden layer and where ϕ_i are linear functions. By allowing ϕ_i to be monotonic non-linear functions the neural network can model the non-linear relationship that might exist between the input and output signals. In a neural network model, the weights between neurons are the connections between the problem and its solution. The weights and biases contain all the information about the network. Therefore, the objective is to train the network to obtain a combination of weights and biases that minimizes the error between the neural network output signal and the observed output. The most commonly used criterion is to minimize the least mean squares error function (MSE) between the simulated output (y) and the observed output.

To train the network, we used a back-propagation procedure (Reed et al., 1999). This procedure aims at adjusting the weights and biases of the network to minimize the error function. Back-propagation adjusts the weights in the steepest descent direction in which the performance function is decreasing most rapidly. We used the Levenberg–Marquardt algorithm that has the major advantage of speed.

One of the problems that occur during neural network training is called overfitting. The error on the training set is driven to a very small value, but when new data is presented to the network the error is large. The network has memorized the training examples, but not learned to generalize to new situations. We use an efficient technique for improving the generalization performance of the MLP, called early stopping. In this technique the data is divided into three subsets. The first subset is the training set which is used to compute the gradient and update the weights and biases of the network. The second subset, the validation set, is used to stop the training when the error on the validation set begins to rise (i.e. the network begins to over-fit the training data) and the weights and biases at the minimum of the validation error are returned. The test set error is not used during the training, but it is used to compare different models. Another method for improving generalization, called Bayesian regulation (MacKay, 1992) has also been tested but did not give better results than early stopping.

For achieving the balance between data-fitting and model complexity from the proposed performance function, we also aimed to find the best number of hidden nodes. Several statistical criteria were analyzed in order to find the best MLP architecture and generalization performance: (i) mean squared error (MSE), (ii) correlation coefficient (r) and (iii) the correct and incorrect predicted classification rate of fishing operations with respect to the observed fishing operations. The output of the MLP is a real number with range in [0, 1]. We therefore needed to select a threshold on the output to provide the percentage of detections correctly and incorrectly classified. This threshold was chosen so that the total number of identified fishing sets was about the same as the number of observed fishing sets. Its value was set at 0.5.

For each model architecture tested, sensitivity analyses were performed by way of multiple test runs starting from random initial weights to decrease the chance of getting trapped in a local minimum and to find stable results. To compare the results obtained with the MLP, we also used a generalized linear regression model directly adapted using the MLP topology. We used a MLP with one input layer, one output logistic layer and no hidden layer, which is equivalent to a generalized linear regression model with logistic function. The same threshold (0.5) was used to compute the classification.

2.3. Training of the neural network

We trained the MLP described in the previous section with different number of neurons in the hidden layer to find the best architecture to predict fishing operations. The MLP with one hidden layer was tested using hyperbolic tangent sigmoid and logistic sigmoid activation functions for hidden (ϕ_1) and output layers (ϕ_2), respectively. Other activation functions were also used but did not perform as well. The MLP with two hidden layers was also tested but no significant improvement was observed. Training was confined to 2000 iterations, but in most cases there were no significant improvement in the MSE after 300 iterations. The MLP was tested with the number of hidden nodes ranging from 1 to 10, while the training set size was set up randomly as 75% of the sample set. The validation and testing sets each took half of the rest. For reliable results and to better approximate the generalization performance for prediction, each experiment was repeated 50 times with different initial weights, training, validation and testing sets. The reported values were averaged over the 50 independent runs.

2.4. Comparing fish stock and fishing operations distributions

We tested the hypothesis that the distribution of fishing operations was correlated to the distribution of the anchovy stock using two approaches. The first relied on a visual comparison of monthly maps of spatial distribution of fishing sets identified by the neural network with the concomitant spatial distribution of acoustic biomass as observed by 10 IMARPE acoustic surveys (exact dates of these surveys are given in Table 1). The second test was based on a comparison of three spatial indices describing general features of the concomitant distributions of fishing sets and anchovy stock. Acoustic data were collected with a scientific echosounder system (38 and 120 kHz split-beam SIMRAD EK500, Kongsberg SIMRAD AS, Norway), calibrated using standard procedures (Foote et al., 1987). The water column was sampled to depths of 250 and

500 m, for 120 and 38 kHz, respectively. The survey design consisted of parallel transects running from 3.7 km from the coast to approximately 185 km offshore, with inter-transect distances varying between 26 and 30 km. Acoustic backscattered energy by surface unit (s_A) was recorded in each elementary sampling distance unit (ESDU) of 1852 m (1 nautical mile). Species composition was determined from the combination of information from trawling, echo-trace characteristics, and abiotic conditions. Data corresponding to anchovy for the study area were selected, with s_A used as an index of anchovy abundance.

For the comparison of spatial distributions of fishing sets and anchovy abundance (given by non-zero s_A ESDU) we first computed an index of the longitudinal extent covered by each dataset, using mean distance to the coast as a proxy for longitudinal extent. For Peruvian anchovy, longitudinal extent can be used as an indicator of adverse warm conditions (i.e., anchovy highly vulnerable to the fleet) or cold favourable conditions (Mathisen, 1989). A classical illustration for anchovy population relies on the effect of El Niño events on its spatial patterns. Typically, the stock distribution follows the inshore contraction of cold coastal waters (Valdivia 1978; Bertrand et al., 2004), which increases its availability to fishermen, resulting in magnification of catchability when the stock is, at the same time, particularly vulnerable to unfavourable environmental conditions. For fishing sets, the average distance to the coast was estimated with an accuracy of 10 nm (18.5 km) (isoparalitoral areas, IMARPE unpublished data) and then averaged by month. The mean distance to the coast (MDC) for anchovy distribution was estimated as the average distance to the coast of the ESDU associated with anchovy presence. Because fish acoustic data usually include a high proportion of ESDU values with a very low s_A, we weighted the distance estimates by the corresponding ESDU s_A value.

For the second index we estimated the area covered for each distribution (fishing sets and fish abundance). We first determined the minimum convex polygon encompassing all points of the distribution (for an example see Fig. 7), and then estimated the area of these polygons using an algorithm based on a partition of the polygon into a series of elementary triangles.

The third index characterized the patchiness or clustering of the spatial distributions using Ripley's K function (Ripley, 1976). Designed for analysing spatial point processes, the K function is based on the estimation of the average number of events occurring in a disc of radius t

$$\hat{K}(t) = \frac{A}{n^2} \sum_i \sum_{j \neq i} I(d_{ij} \leq t) \tag{3}$$

where $I = 1$ for each point within t distance otherwise $I = 0$, A is an estimate of the area covered by the process, d_{ij} the distance between the ith and the jth point, and n the total number of points of the process. This estimator is biased for large values of t as edge effects may lead to an underestimation of the number of neighbours for the points located at the edges of the process. Several correction factors may be applied (e.g. Dixon, 2002), but one empirical way to limit the impact of these edge effect is to consider only t values smaller than half of the main dimension of the domain. Here we used $t < 18.5$ km as this represented the smallest mean distance to the coast for both anchovy and fishing set distributions. To quantify the degree of clustering of the observed distributions, we calculated the area comprised (the sum of the differences) between the K function estimated from observed data with a random reference K function. The observed distribution of fishing sets is a point process which can be directly compared to a theoretical complete random distribution (homogeneous Poisson process), for which we have

$$K(t) = \pi t^2 \tag{4}$$

For anchovy distribution, we had to adapt this approach in two ways. First, anchovy distribution is essentially a 2D field distribution sampled by a 1D continuous transect. From this data, we defined as a point process the occurrence of ESDU presenting s_A values above 500 m^2 nm^{-2}. This threshold was numerically defined as the median value for the mean non-zero s_A by survey. Empirically, this threshold can be considered to represent fish densities of primary interest to the commercial fleet. Second, because the survey is systematic, the locations where the process may occur are fixed. The random hypothesis as defined here is therefore not a true random spatial process but a random distribution of the selected ESDUs (s_A above 500 m^2 nm^{-2}) among all the existing ESDU locations. For each survey, we generated 100 replicate random distributions of high density ESDUs among transects of the same survey. We defined the clustering index as the area comprised (the sum of the differences) between the experimental K function and the higher K function from the random replicates. Values of K are expressed in nm^2. The clustering index, defined as a difference between two K functions, was therefore also expressed in nm^2.

To explore the potential relationships between fish and fishing sets distributions, we estimated the correlation for these indexes between each survey period and the closest month of fishing activity (see Table 1 for time references). For the tests we calculated Pearson's correlation statistic for normally distributed variables (total area of distribution) and Spearman's non-parametric rank correlation for non-normally distributed variables (mean distance to the coast and the clustering index).

3. Results

3.1. Identification of fishing operations

The performance of a neural network depends on the number of neurons in the hidden layer. Generally speaking, the more neurons there are in the hidden layer, the better the network performs dur-

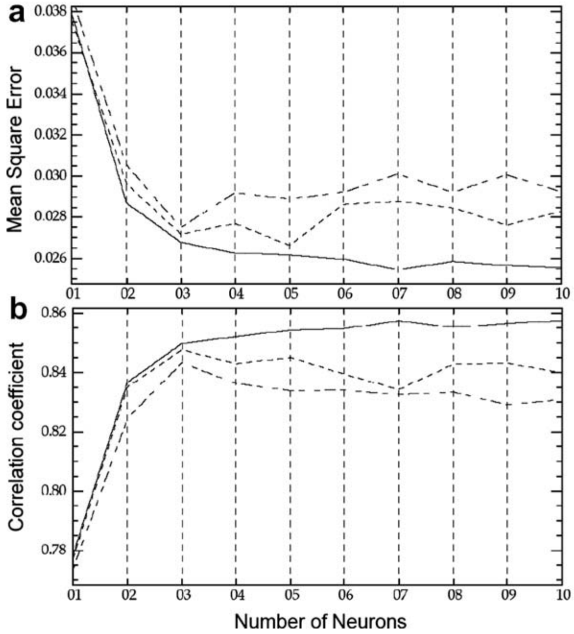

Fig. 3. Performance of the MLP according to the number of neurons in the hidden layer: (a) mean square error (MSE) and (b) correlation coefficient (CC) between observed and predicted fishing sets for the training (solid line), validation (dashed line) and test (dashed-dotted line) dataset. MSE and CC were estimated as an average of 50 independents runs. From this figure, the best MLP used for prediction is chosen to be the one with 3 neurons in the hidden layer.

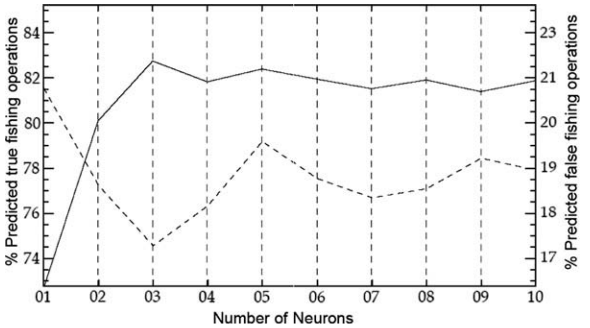

Fig. 4. Correct and incorrect classification rates averaged over 50 independent runs, given different numbers of hidden nodes. The percentage shown represents the number of correctly and incorrectly identified fishing operations divided by the number of real fishing operations. The results were consistent with Fig. 3. MLP with three neurons gave about 83% of correct classification (solid line) and 17% incorrect ones (dashed line) which is a good generalization performance for predicting fishing operations.

ing training. However, the more neurons there are, the higher is the risk of over-fitting, which leads to poorer predictions. This is illustrated by Fig. 3 which gives the average of the MSE (Fig. 3a) and correlation coefficient (Fig. 3b) of 50 runs, given different numbers of hidden neurons for the training, the validation and the test dataset.

While the correlation coefficient monotonically increases with the number of neurons for the training set, it reaches a maximum for both the validation and test set at about three neurons. With more neurons in the hidden layer, this value decreases significantly, indicating that there is over-fitting with more than three neurons. Similar results are obtained with the MSE, with the smallest MSE for the testing set obtained with three neurons. The best MLP network from structural learning is therefore chosen to be three nodes in the hidden layer. Fig. 4 gives the average of the correct and incorrect classification rates of 50 runs, given different numbers of hidden nodes. The results were consistent with Fig. 3. MLP with three neurons gave about 83% of correct classification and 17% incorrect ones which is a good performance for predicting fishing operations. Regardless of the number of neurons considered in the hidden layer, the performance of the MLP exceeded that of the generalized linear regression model (65% correct classification, 16% incorrect classification). Similarly, the speed threshold (Fig. 5) overestimated by 182% the number of observed fishing sets, justifying the use of a more complex tool. The neural network was therefore used to forecast fishing operations for those trips where no observers were onboard. The neural network identified between 129 and 4088 fishing set positions (mean 1744) for the 22 study months and 3 degrees latitude study area (Table 1). Variability in the number of sets per month is largely caused by the imposition of short term access restrictions.

3.2. Spatial distribution of fishing sets and comparison with acoustic biomass

Fig. 6 graphically compares the spatial distribution of fishing sets with concomitant acoustic biomass. In general the patterns are broadly similar. Fishing sets were located near to the shore when high acoustic densities were concentrated along the coast (e.g. October 2000, November 2000 and October 2001), and conversely during times when higher levels of anchovy abundance were recorded offshore (e.g. July 2000). Large clusters of high density fish aggregations are highly coincident with the distribution of fishing sets (e.g. March 2000, April 2001). The degree of spatial coincidence is less apparent as the patch size of fish abundance decreases. At times catches are not seen to occur in areas where anchovy densities appear to be very high (see the small offshore patch of fishing sets in November 2000); conversely some high density but small anchovy patches are not tracked by fishing set distribution (see the offshore anchovy patch in October 2001).

For the distribution of fishing sets, mean distance to the coast varied between 18.5 km (November 2001) and 90.9 km (July 2002). The total area covered by these fishing sets (See Fig. 7a and b for an example of convex polygon used) ranged between

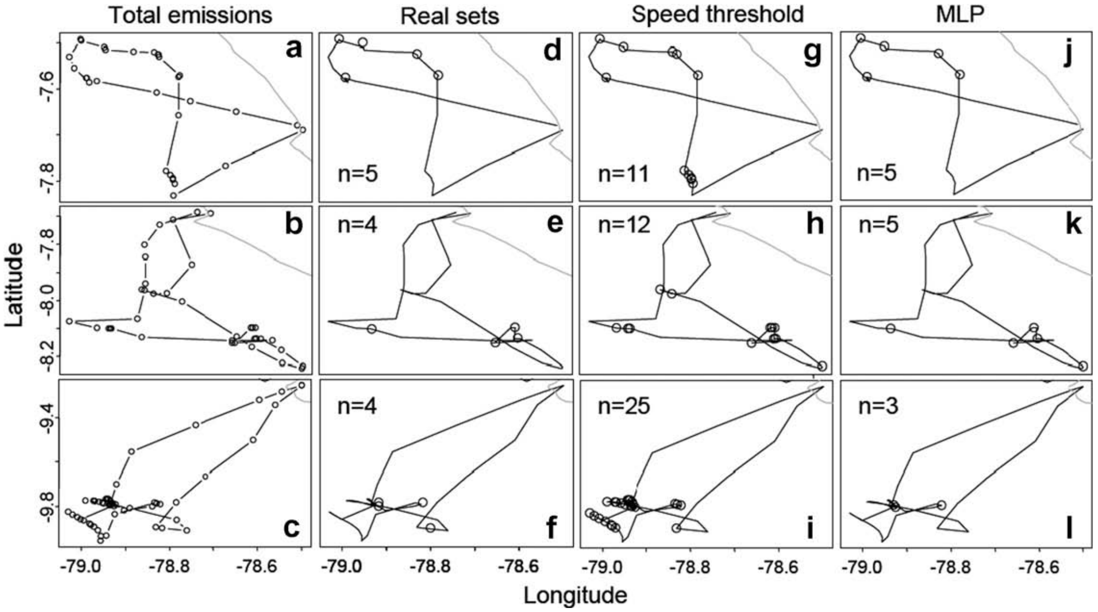

Fig. 5. Tracks of three fishing trips (horizontal succession of pictures) showing the total emissions during the trip (Fig. 5a–c), the number (n) and position of real fishing sets registered by observers on board (Fig. 5d–f), the number (n) and position of the sets estimated only by speed threshold (Fig. 5g–i) and the number (n) and position of the sets estimated by the MLP (Fig. 5j–l). Note that in the first trip the MLP optimized the identification process by successfully finding the real sets, in the second trip the MLP overestimated by one the number of real sets and during the third one the MLP underestimated by one the real sets. Although the last two cases show examples of misclassification, MLP is statistically significantly more powerful than other methods tested for identifying fishing set locations.

5631 km^2 (November 2001) and 56,714 km^2 (July 2000). The clustering index (see Fig. 7c and d for an example of estimated Ripley *K* function) varied between 26,836 km^2 (June 2001) and 279,410 km^2 (October 2000).

There was sufficient data from the acoustic survey to allow a comparison of the indices computed for anchovy distribution for 10 corresponding months (Table 1). The number of ESDU (1.852 km long) with presence of anchovy ($s_A > 0$) varied between 551 and 1451. The corresponding mean distance to the coast varied between 18.9 km (October 2001) and 91.9 km (July 2000). The total area of the polygon enclosing ESDU having anchovy presence varied between 37,105 km^2 (April 2002) and 82,664 km^2 (July 2000). Finally the clustering index was maximum in July 2000 (175,378 km^2) and minimum in April 2002

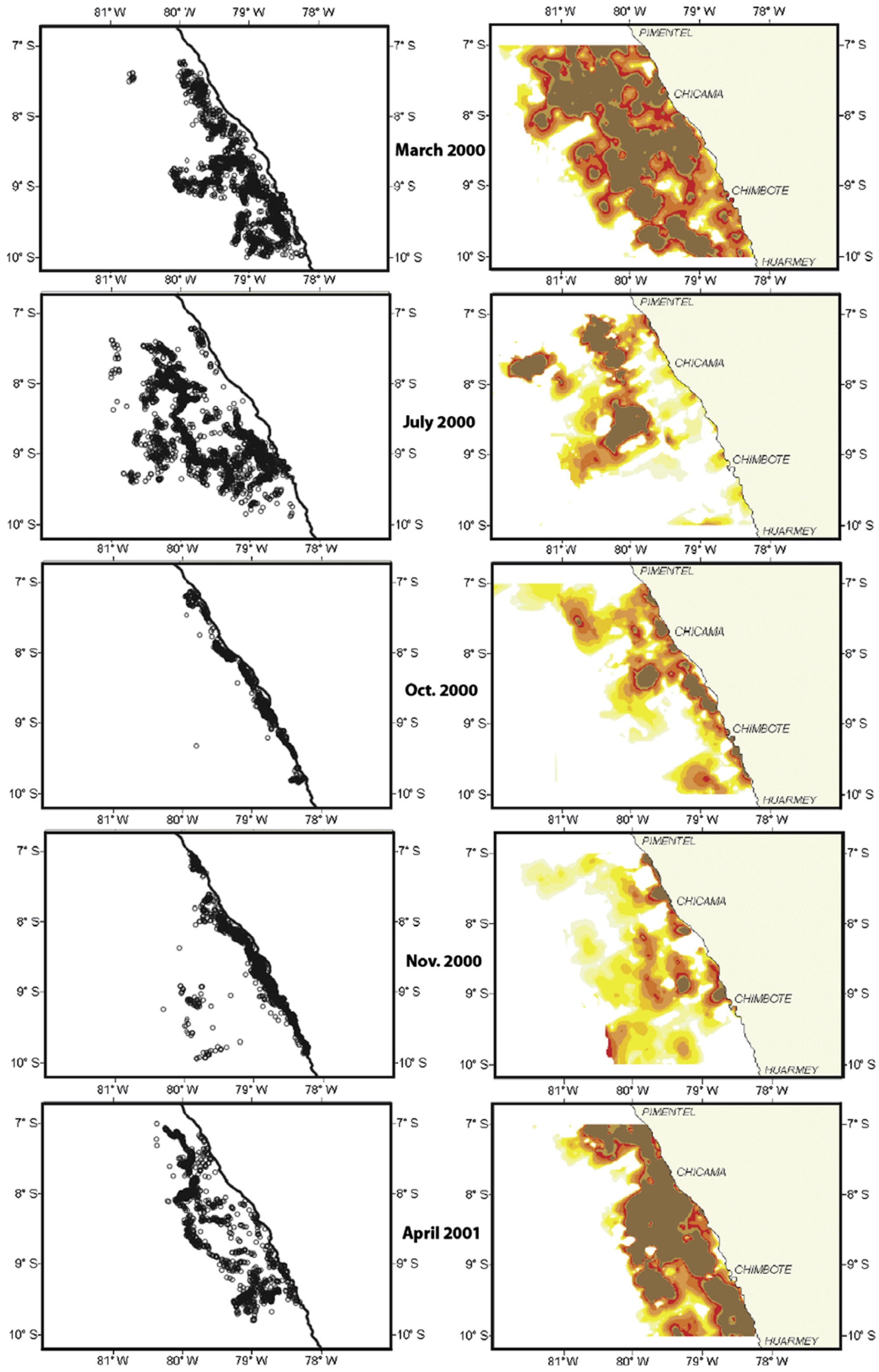

Fig. 6. Monthly maps of spatial distribution of fishing sets identified by the MLP and the corresponding spatial distribution of acoustic biomass as observed by 10 IMARPE scientific survey performed during the periods of interest (exact dates of these surveys are given in Table 1).

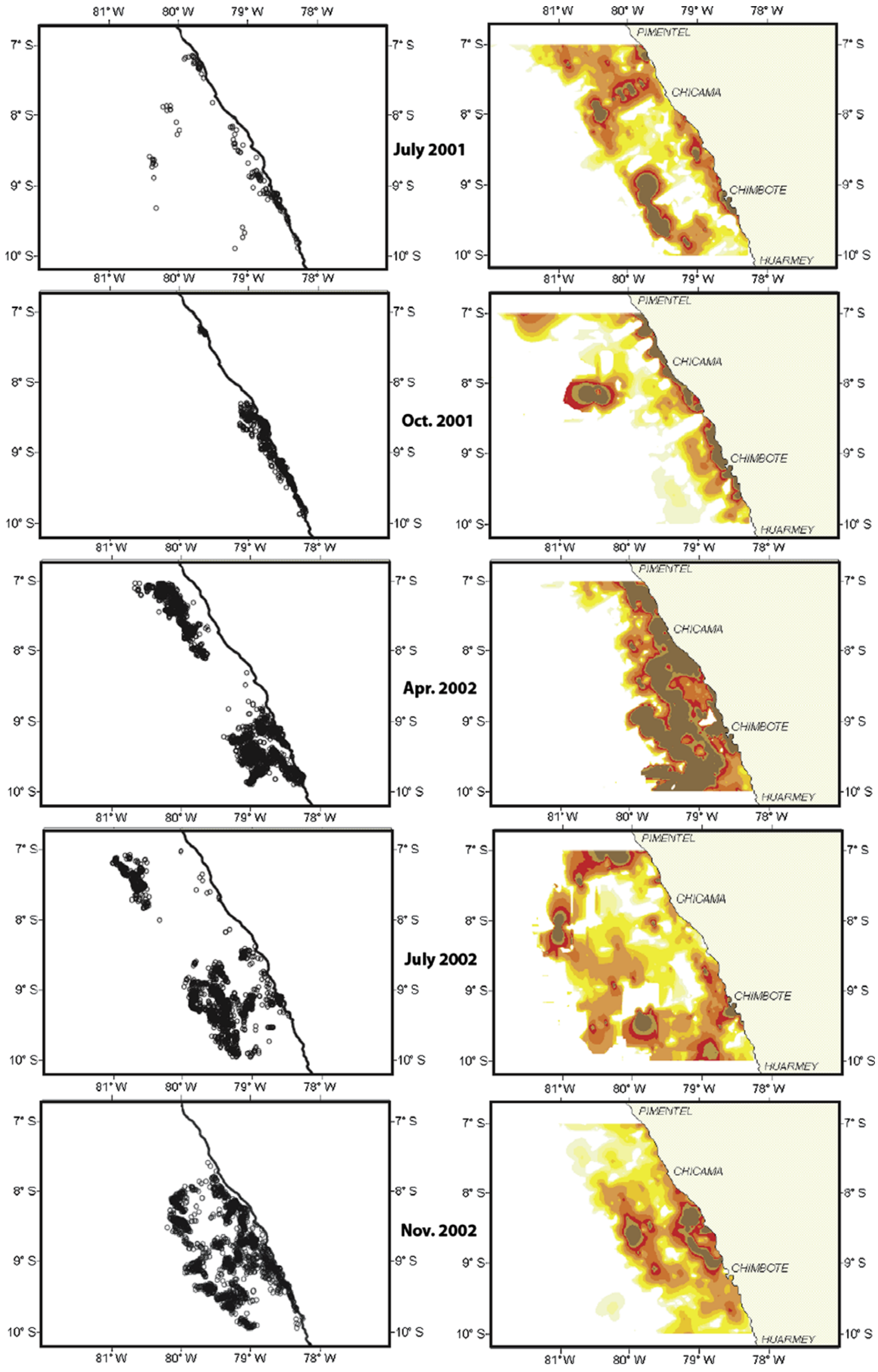

Fig. 6 (*continued*)

($36,858\ km^2$). Correlations between corresponding indices from anchovy and fishing set distributions were significant ($p < 0.05$) for the mean distance to the coast and for the clustering index (Table 2). The correlation between the area of the polygons enclosing fish and fishing set distributions was not found to be significant.

4. Discussion

4.1. On the neural network

In this study we showed the effectiveness of neural networks for identifying the location of fishing operations. The use of a mul-

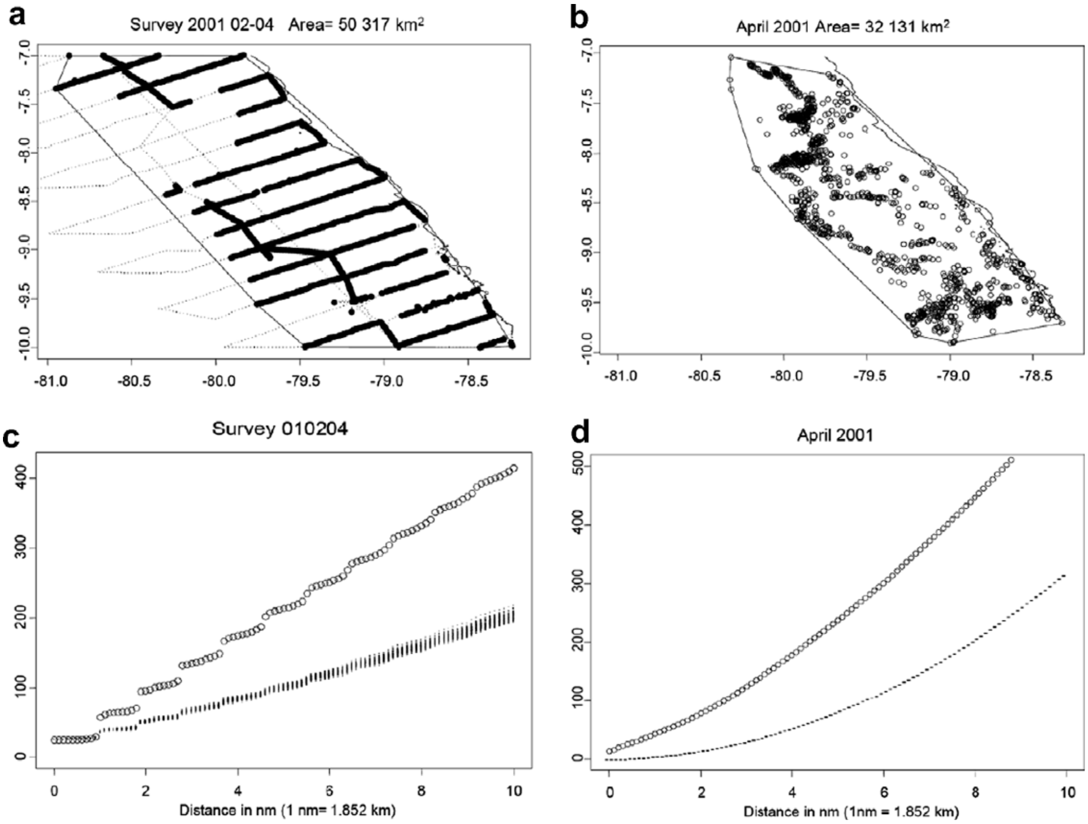

Fig. 7. Example of the minimum convex polygon used to determine the area encompassed by (a) the anchovy distribution and (b) the fishing sets distribution for the month April 2001. Below are represented the corresponding *K* function estimations for fish (c) and for fishing sets (d). In (c), dots represent the empirical *K* function; below are represented the 100 *K* functions corresponding to the 100 replicates of simulated random distributions. In (d), the dotted line represents the empirical *K* function and the dashed line represents the *K* function for a theoretical complete random (Poisson) spatial distribution. The clustering index was estimated as the area comprised between the empirical *K* and the simulated/theoretical random distribution *K*.

Table 2
Correlation results between fishing and fish indicators, n number of individual, ρ Pearson or Spearman correlation coefficient, *p*-value probability of type I error.

Descriptor	*n*	ρ	*p* value
Mean distance to the coast	10	0.78 (Spearman)	0.0200
Total area of distribution	10	0.61 (Pearson)	0.0587
Clustering index	10	0.77 (Spearman)	0.0220

tilayer perceptron allowed us to properly identify 83% of the fishing operations, significantly outperforming linear methods. The ability of neural networks to capture non-linear patterns among a collection of inputs allows them to be robust classifiers for complex systems. The performance values verify that this particular neural network has potential to identify fishing operations. Improvements, however, could still be made. Other types of neural networks, such as Kohonen Maps, as well as different classification techniques, such as support vector machine, could be tested to see whether identification performance can be further improved.

4.2. Fishing activity as an indicator of the fish stock condition

There was generally a high level of visual agreement between the spatial distributions of anchovy and fishing sets. The few discrepancies noted may have several explanations: (1) a slight time lag between acoustic and fishery data (this is the case for October 2001 which was compared to acoustic data collected in September); (2) only few days in a month open to fishing, as in July 2001, where there are too few fishing sets to reliably track anchovy distribution; (3) when anchovy is dramatically abundant, fishers may tend to preferentially exploit the more coastal aggregations (see March 2000 for instance); and (4) the port location may also influence fishing sets distribution, with areas closer to port being preferentially exploited. However, in the Peruvian anchovy fishery, fishing power is so strong (in terms of fleet size: around 1700 vessels for the industrial sector; in terms of number and latitudinal extent of the landing points, spanning all the Peruvian littoral), and anchovy distribution is so narrow in longitude (less than 200 nm), that the effects of these biases are minor and do not affect the overall ability of fishing operations to effectively track the main pattern of anchovy stock distribution.

The distributions of anchovy abundance and fishing sets tend to exhibit a seasonal pattern. Highest values for the mean distance to the coast and the total area of the polygon of presence are found during the austral winter (July). During this time the coastal upwelling is stronger and cold coastal upwelled waters (CCW), the habitat for anchovy, cover a wider extent (Mathisen, 1989; Muck et al., 1989; Bertrand et al., 2004). The reverse situation occurs in austral summer. Despite the clear seasonal patterns in environmental conditions, similar patterns are not apparent for the clustering indexes. Spatial clustering of the anchovy stock is thought to be more dependant on meso-scale physical features, such as eddies (Hyrenbach et al., 2006; Bertrand et al., 2008) which dynamic is influenced by non-periodic oceanic events, such as the arrival of oceanic Kelvin waves in the coastal system (Lengaigne, 2004).

We found significant correlations between fish and fishing set distributions for the mean distance to the coast and for the clustering index. Thus despite the potential biases that may affect the ability of fishing operations to track anchovy distribution (see above), and some spatial discrepancies for small patches of fish abundance, we can assert that the distribution of fishing sets do indeed capture the main features of anchovy stock distribution, such as longitudinal extent and patchiness. Of the three spatial indices, the correlation between the areas covered by anchovy and fishing sets failed to be significant. One explanation could be that surface estimation was more sensitive to the high number of low s_A ESDUs, abundance values that fishers do not consider to be commercially exploitable. It will be interesting in the future to extend the time series to examine in more detail the relationships described by the relatively small sample size available for this study (10 periods could be compared).

Both of the spatial dimensions, longitudinal extent and clustering, are closely related to fish catchability and vulnerability. High clustering and low distance to the coast correspond to situations where fish biomass is concentrated in a small area, and thus make fish aggregations easier to detect, and to catch (e.g. Valdivia, 1978; Csirke, 1989; Fréon and Misund, 1999). In other words, the stock is more vulnerable to the fishing fleet in these situations. Consequently, times when the fleet is found to be highly concentrated in the coastal zone (e. g. October 2001 in Fig. 6), or highly clustered, should be used as a warning signal of anchovy being highly vulnerable to the fishery, and lead to management measures aimed at reducing fishing effort.

4.3. Perspective opened by the use of spatially explicit fishing data

Because fishing activity constitutes, albeit indirectly, the main sampling effort on exploited populations, catch per unit effort (CPUE) has long been and is still widely used as an indicator of stock size by fishery management authorities. The use of CPUE may, however, be questionable with anchovy, because of the strong variability in catchability (e.g. Csirke, 1989). A number of studies have shown that an important part of this variability is explained by the spatial dynamics of fish populations and the fleets that exploit them (e.g. Winters and Wheeler 1985; Csirke, 1989; Crecco and Overholtz 1990; Rose and Leggett, 1991; Hilborn and Walters, 1992; Swain and Sinclair 1994; Petitgas 1998; Gaertner and Dreyfus-Leon 2004). Hilborn and Walters (1992) notes that "spatial mapping of CPUE should be done whenever possible to determine…how the spatial distribution of the stock and effort are changing". Our study has shown that with the advent of VMS technology we are now able to produce routine, near real-time and comprehensive maps (whole fleet) of the distribution of fishing effort. We noted above how information on the location of fishing sets provides useful insights into the condition of the Peruvian anchovy stock and its vulnerability to fishing, and in turn can be used to inform management measures aimed at reducing fishing pressure in an adaptive manner. An important next step will be to combine information on fishing set locations with catch statistics for each trip in order to develop a more complete understanding of the spatial distribution of the catches made by the Peruvian anchovy fishery.

The availability of spatially explicit catch statistics has considerable value in fisheries science, in part to address issues of catchability mentioned above, but also to improve our understanding of fishers' behaviour and to forecast the spatial allocation of effort. These last questions, which constitute an important field of fisheries science, have been addressed mainly through limited observational studies (limited in space, in time and in number of individuals observed) or through numerical models. Allen and McGlade (1986), for instance, were interested in the strategies developed by fishers in searching for fish. They established through a simulation model the existence of two types of fishermen strategies: the stochasts (or risk takers) and the Cartesian (or followers). Millischer and Gascuel (2006) studied, through an individual based model, the impacts of communication and cooperation between vessels during fish searching activities. Spatially explicit catch data will allow a return to the underlying assumptions of this kind of models, to validate or invalidate their general results, and hopefully shed light on the processes contributing to fishers' behaviour. This will be an important step forward as strategies for fishing effort allocation directly impact the effectiveness of fishery management measures. Management measures usually have a spatial component, whether explicit through marine protected areas, marine reserves, or temporary zone closure, or implicit through regional quotas (Babcock et al., 2005). A number of studies have emphasized the importance of testing the effect of different spatially explicit management devices on fisher's behaviour and to forecast their efficiency (e.g. Walters et al., 1999; Sanchirico and Wilen 2001; Smith and Wilen 2003; Hutton et al., 2004; Mahevas and Pelletier, 2004). Spatially explicit fishing data should prove particularly beneficial in this regard by ensuring that the assumptions of the forecasting simulation tools are more realistic and closely adapted to each fishery.

5. Conclusions

This work aimed to assess the extent to which the distribution of fishing operations could track the distribution of the Peruvian anchovy stock, and to assess how fisheries-dependent data could complement acoustic estimates of fish abundance from scientific surveys in an adaptive management process. Fishing set positions were routinely available for only a very small fraction of the fleet (1.5%). We therefore developed an automatic process for the identification of fishing set positions for the entire fishery from vessel trajectories as routinely collected in real-time by VMS. A neural network approach provided the best results, being able to identify 83% of total fishing set locations. Two of the three spatial indices we tested (longitudinal extent and patchiness) found that the distribution of fishing sets and fish abundance were significantly correlated and showed that fishing activity reflects the main features of the spatial dynamics of the stock. These patterns can subsequently be used to inform levels of stock vulnerability. Our results further encourage the use of VMS data as a near real-time monitoring tool for the condition of the Peruvian anchovy stock. The framework is currently being integrated into daily monitoring and management.

Acknowledgments

The authors would like to thank Jaime Atiquipa and Mariano Gutierrez from IMARPE for their valuable aid in providing VMS and acoustic data, respectively, and Arnaud Bertrand from IRD for earliest discussions at the origin of the paper. We are very grateful to Sylvie Thiria, Carlos Mejia and Julie Leloup for fruitful discussions on neural networks. We warmly thank Paul Eastwood for his remarkable editing work and valuable comments on the manuscript. This work is a contribution of the UR 097 'ECO-UP' and the UMR 'LOCEAN' from IRD. This work was supported in part by the US National Science Foundation in Grant No. NSF0526392 to Sophie Bertrand.

References

Allen, P.M., McGlade, J.M., 1986. Dynamics of discovery and exploitation: the case of the Scotian shelf groundfish fisheries. Canadian Journal of Fisheries and Aquatic Sciences 43, 1187–1200.

Alheit, J., Niquen, M., 2004. Regime shifts in the Humboldt Current ecosystem. Progress in Oceanography 60, 201–222.

Arreguín-Sánchez, F., 1996. Catchability: a key parameter for fish stock assessment. Reviews in Fish Biology and Fisheries 6, 221–242.

Babcock, E.A., Pikitch, E.K., McAllister, M.K., Apostolaki, P., Santora, C., 2005. A perspective on the use of spatialized indicators for ecosystem-based fishery management through spatial zoning. ICES Journal of Marine Science 62, 469–476.

Bertrand, A., Segura, M., Gutiérrez, M., Vásquez, L., 2004. From small-scale habitat loopholes to decadal cycles: a habitat-based hypothesis explaining fluctuation in pelagic fish populations off Peru. Fish and Fisheries 5, 296–316.

Bertrand, A., Gerlotto, F., Bertrand, S., Gutiérrez, M., Alza, L., Chipollini, A., Diaz, E., Espinoza, P., Ledesma, J., Quesquén, R., Peraltilla, S., Chavez, F., 2008. Schooling behaviour and environmental forcing in relation to anchoveta distribution: an analysis across multiple spatial scales. Progress in Oceanography 79, 264–277.

Bertrand, S., Burgos, J., Gerlotto, F., Atiquipa, J., 2005. Lévy trajectories of Peruvian purse–seiners as an indicator of the spatial distribution of anchovy (*Engraulis ringens*). ICES Journal of Marine Science 62, 447–482.

Bertrand, S., Bertrand, A., Guevara-Carrasco, R., Gerlotto, F., 2007. Scale invariant movements of fishermen: the same foraging strategy as natural predators. Ecological Applications 17 (2), 331–337.

Bishop, C.M., 1995. Neural Networks for Pattern Recognition. Oxford University Press, Inc., New York, NY. 500p.

Chen, D., Ware, D., 1999. A neural network model for forecasting fish stock recruitment. Canadian Journal of Fisheries and Aquatic Sciences 56, 2385–2396.

Crecco, V., Overholtz, W.J., 1990. Causes of density-dependent catchability for Georges Bank Haddock *Melanogrammus aeglefinus*. Canadian Journal of Fisheries and Aquatic Sciences 47, 385–394.

Csirke, J., 1989. Changes in the catchability coefficient in the Peruvian anchoveta (*Engraulis ringens*) fishery. In: Pauly, D., Muck, P., Mendo, J., Tsukayama, I. (Eds.), The Peruvian Upwelling Ecosystem: Dynamics and Interactions. ICLARM Conference Proceeding, pp. 207–219.

Cybenko, G., 1989. Approximation by superpositions of a sigmoidal function. Mathematics of Control, Signals and Systems 2, 303–314.

Davoren, G.K., Montevecchi, W.A., Anderson, J.T., 2002. Scale-dependent associations of predators and prey: constraints imposed by flightlessness of common murres. Marine Ecology Progress Series 245, 259–272.

Deng, R., Dichmont, C., Milton, D., Haywood, M., Vance, D., Hall, N., Die, D., 2005. Can vessel monitoring system data also be used to study trawling intensity and population depletion? The example of Australia's northern prawn fishery. Canadian Journal of Fisheries and Aquatic Sciences 62, 611–622.

Dinmore, T.A., Duplisea, D.E., Rackham, B.D., Maxwell, D.L., Jennings, S., 2003. Impact of a large-scale area closure on patterns of fishing disturbance and the consequences for benthic communities. ICES Journal of Marine Science 60, 371–380.

Dixon, P.M., 2002. Ripley's K function. In: El-Shaarawi, A.H., Piegorsch, W.W. (Eds.), Encyclopedia of Environmetrics, vol. 3. John Wiley and Sons, Ltd., Chichester, pp. 1796–1803.

Dreyfus-León, M., 1999. Individual-based modeling of fishermen search behaviour with neural networks and reinforcement learning. Ecological Modelling 120, 287–297.

Fauchald, P., Erikstad, K.E., Skarsfjord, H., 2000. Scale-dependent predator–prey interactions: the hierarchical spatial distribution of seabirds and preys. Ecology 81, 773–783.

Fine, T.L., 1999. Feedforward neural network methodology. Springer-Verlag, New York. 356p..

Foote, K.G., Knudsen, H.P., Vestnes, D.N., MacLennan, D.N., Simmonds, E.J., 1987. Calibration of Acoustic Instruments for Fish Density Estimation: A Practical Guide. ICES Cooperative Research Report, No. 144, pp. 1–69.

Fréon, P., Misund, O.A., 1999. Dynamics of Pelagic Fish Distribution and Behaviour: Effects on Fisheries and Stock Assessment. Blackwell Science. 348p.

Frontier, S., 1987. Applications of fractal theory to ecology. In: Legendre, P., Legendre, L. (Eds.), Developments in Numerical Ecology. Springer-Verlag, Berlin, pp. 335–378.

Funahashi, K., 1989. On the approximate realization of continuous mappings by neural networks. Neural Networks 2, 183–192.

Gaertner, D., Dreyfus-Leon, M., 2004. Analysis of non-linear relationships between catch per unit effort and abundance in a tuna purse seine fishery simulated with artificial neural networks. ICES Journal of Marine Science 61, 812–820.

Harley, S.J., Myers, R.A., Dunn, A., 2001. Is catch-per-unit-effort proportional to abundance? Canadian Journal of Fisheries and Aquatic Sciences 58, 1760–1772.

Hilborn, R., Walters, C.J., 1992. Quantitative Fisheries Stock Assessment. Choice Dynamics and Uncertainty. Chapman and Hall, New York, London. 570p..

Hornik, K., Stinchcombe, M., White, H., 1989. Multilayer feedforward networks are universal approximators. Neural Networks 2, 359–366.

Hutton, T., Mardle, S., Pascoe, S., Clark, R.A., 2004. Modelling fishing location choice within mixed fisheries: English North Sea beam trawlers in 2000 and 2001. ICES Journal of Marine Science 61, 1443–1452.

Hyrenbach, K.D., Veit, R.R., Weimerskirch, H., AndHunt Jr., G.L., 2006. Seabird associations with mesoscale eddies: the subtropical Indian Ocean. Marine Ecology Progress Series 324, 271–279.

Lengaigne, M., Boulanger, J.P., Delecluse, P., Menkes, C., Slingo, J., 2004. Westerly wind events and their influence on coupled ocean-atmosphere system: a review. AGU Monograph: Earth Climate: The Ocean-Atmosphere Interaction, pp. 49–71.

MacKay, D.J.C., 1992. Bayesian interpolation. Neural Computation 4 (3), 415–447.

Mahevas, S., Pelletier, D., 2004. ISIS, a generic and spatially explicit simulation tool for evaluating the impact of management measures on fisheries dynamics. Ecological Modelling 171, 65–84.

Mathisen, O.A., 1989. Adaptation of the anchoveta (*Engraulis ringens*) to the Peruvian upwelling system. In: Pauly, D., Muck, P., Mendo, J., Tsukayama, I. (Eds), The Peruvian Upwelling Ecosystem: Dynamics and Interactions. ICLARM Conference Proceeding, pp. 220–234 .

Maunder, M., Hinton, M., 2006. Estimating Relative Abundance from Catch and Effort Data, Using Neural Networks. Inter-American Tropical Tuna Commission, Special Report, 15, 18p.

Millischer, L., Gascuel, D., 2006. Information transfer, behavior of vessels and fishing efficiency: an individual-based simulation approach. Aquatic Living Resources 19, 1–13.

Mills, C.M., Townsend, S.E., Jennings, S., Eastwood, P., Houghton, C.A., 2007. Estimating high resolution trawl fishing effort from satellite-based vessel monitoring system data. ICES Journal of Marine Science 64, 248–255.

Muck, P., Pauly, D., 1987. Monthly anchoveta consumption of guano birds, 1953 to 1982. In: Pauly, D., Tsukayama, I. (Eds.), The Peruvian Anchoveta and its Upwelling Ecosystem: Three Decades of Change. ICLARM Studies and Reviews, vol. 15, pp. 219–233.

Muck, P., Fuentes, H., 1987. Sea lion and fur seal predation on the Peruvian anchoveta, 1953 to 1982. In: Pauly, D., Tsukayama, I. (Eds.), The Peruvian Anchoveta and its Upwelling Ecosystem: Three Decades of Change. ICLARM Studies and Reviews, vol. 15, pp. 234–247.

Muck, P., Zafra de Moreno, A., Aranda, C., 1989. The seasonal dynamics of sea surface temperature and its impact on anchoveta distribution off Peru. In: Pauly, D., Muck, P., Mendo, J., Tsukayama, I. (Eds.), The Peruvian Upwelling Ecosystem: Dynamics and Interactions. ICLARM Conference Proceeding, pp. 33–44.

Murawski, S.A., Wigley, S.E., Fogarty, M.J., Rago, P.J., Mountain, D.G., 2005. Effort distribution and catch patterns adjacent to temperate MPAs. ICES Journal of Marine Science 62, 1150–1167.

Petitgas, P., 1998. Biomass-dependent dynamics of fish spatial distributions characterized by geostatistical aggregation curves. ICES Journal of Marine Science 55, 443–453.

Reed, R.D., Marks II, R.J., 1999. Neural Smithing: Supervised Learning in Feedforward Artificial Neural Networks. The MIT Press, Cambridge, MA. 346p.

Ripley, B.D., 1976. The second-order analysis of stationary point processes. Journal of Applied Probability 13, 255–266.

Ripley, B.D., 1996. Pattern Recognition and Neural Networks. Cambridge University Press. 416p.

Rose, G.A., Leggett, W.C., 1991. Effects of biomass-range interactions on catchability of migratory demersal fish by mobile fisheries: an example of Atlantic cod (*Gadus morhua*). Canadian Journal of Fisheries and Aquatic Sciences 48, 843–848.

Russel, R.W., Hunt, G.L., Coyle, K.O., Cooney, R.T., 1992. Foraging in a fractal environment: spatial patterns in a marine predator–prey system. Landscape Ecology 7, 195–209.

Sanchirico, J.N., Wilen, J.E., 2001. A bioeconomic model of marine reserve creation. Journal of Environmental Economics and Management 42, 257–276.

Smith, M.D., Wilen, J.E., 2003. Economic impacts of marine reserves: the importance of spatial behavior. Journal of Environmental Economics and Management 46, 183–206.

Swain, D.P., Sinclair, A.F., 1994. Fish distribution and catchability: what is the appropriate measure of distribution? Canadian Journal of Fisheries and Aquatic Sciences 51, 1046–1054.

Turchin, P., 1998. Quantitative analysis of movement. Measuring and Modeling Population Redistribution in Animals and Plants. Sinauer Associates, Inc.. 396p..

Valdivia, G.J.E., 1978. The anchoveta and el Niño. Rapports et Procès-verbaux des Réunions du Conseil International pour l'Exploration de la Mer 173, 196–202.

Walters, C., Pauly, D., Christensen, V., 1999. Ecospace: prediction of mesoscale spatial patterns in trophic relationships of exploited ecosystems, with emphasis on the impacts of marine protected areas. Ecosystems 2, 539–554.

Winters, G.H., Wheeler, J.P., 1985. Interactions between stock area, stock abundance and catchability coefficient. Canadian Journal of Fisheries and Aquatic Sciences 42, 989–998.

Progress in Oceanography 79 (2008) 390–400

Contents lists available at ScienceDirect

Progress in Oceanography

journal homepage: www.elsevier.com/locate/pocean

Knowledge-based systems as decision support tools in an ecosystem approach to fisheries: Comparing a fuzzy-logic and a rule-based approach

Astrid Jarre[a,b,*], Barbara Paterson[a], Coleen L. Moloney[a], David C.M. Miller[a,1], John G. Field[a], Anthony M. Starfield[a]

[a] Marine Research (MA-RE) Institute and Zoology Department, University of Cape Town, Private Bag X3, Rondebosch 7701, South Africa
[b] Institute for Aquatic Resources, Denmark's Technical University, North Sea Centre, P.O. Box 101, DK-9850 Hirtshals, Denmark

ARTICLE INFO

Article history:
Accepted 14 October 2008
Available online 21 October 2008

Keywords:
Decision support
Ecosystem approach to fisheries
Pelagic ecosystem
Expert system
Fuzzy logic
Rule-based
Crisp logic
Southern Benguela

ABSTRACT

In an ecosystem approach to fisheries (EAF), management must draw on information of widely different types, and information addressing various scales. Knowledge-based systems assist in the decision-making process by summarising this information in a logical, transparent and reproducible way. Both rule-based Boolean and fuzzy-logic models have been used successfully as knowledge-based decision support tools. This study compares two such systems relevant to fisheries management in an EAF developed for the southern Benguela. The first is a rule-based system for the prediction of anchovy recruitment and the second is a fuzzy-logic tool to monitor implementation of an EAF in the sardine fishery. We construct a fuzzy-logic counterpart to the rule-based model, and a rule-based counterpart to the fuzzy-logic model, compare their results, and include feedback from potential users of these two decision support tools in our evaluation of the two approaches. With respect to the model objectives, no method clearly outperformed the other. The advantages of numerically processing continuous variables, and interpreting the final output, as in fuzzy-logic models, can be weighed up against the advantages of using a few, qualitative, easy-to-understand categories as in rule-based models. The natural language used in rule-based implementations is easily understood by, and communicated among, users of these systems. Users unfamiliar with fuzzy-set theory must "trust" the logic of the model. Graphical visualization of intermediate and end results is an important advantage of any system. Applying the two approaches in parallel improved our understanding of the model as well as of the underlying problems. Even for complex problems, small knowledge-based systems such as the ones explored here are worth developing and using. Their strengths lie in (i) synthesis of the problem in a logical and transparent framework, (ii) helping scientists to deliberate how to apply their science to transdisciplinary issues that are not purely scientific, and (iii) representing vehicles for delivering state-of-the-art science to those who need to use it. Possible applications of this approach for ecosystems of the Humboldt Current are discussed.

1. Introduction

Management of human activities in the ocean is increasingly based on integrated ecosystem considerations, instead of isolated assessments of seemingly disconnected issues such as temperature change, single-species issues in fisheries, and/or pollution. Along with this development, scientific advice in support of ecosystem-based management must encompass a multitude of information sources, evaluate uncertainties and risks, and combine this information into a single, coherent framework in a logically consistent, defendable and transparent way.

The problems of integrating disparate kinds and sources of information are encountered in many arenas. For example, Roetter et al. (2005) describe a system for land use planning in Asia, Paterson et al. (2008) developed a decision support model for wildlife translocations into communal conservancies in Namibia, and Guimarães Pereira et al. (2005) show how an innovative information tool is applied to a groundwater governance issue in France. This last study emphasized the usefulness of knowledge tools for initiating and informing debates, rather than simply for legitimising decisions.

Knowledge-based systems (also termed "expert systems") are a particular class of computer-based decision support systems that can be subdivided into four major components: (i) a structured

---

[*] Corresponding author. Address: Marine Research (MA-RE) Institute and Zoology Department, University of Cape Town, Private Bag X3, Rondebosch 7701, South Africa. Tel.: +27 21 650 5453; fax: +27 21 650 3301.
E-mail address: astrid.jarre@uct.ac.za (A. Jarre).

[1] Present address: Department of Fisheries and Oceans, Northwest Atlantic Fisheries Centre, P.O. Box 5667, St. John's, NL, Canada A1C 5X1.

0079-6611/$ - see front matter © 2008 Elsevier Ltd. All rights reserved.
doi:10.1016/j.pocean.2008.10.010

knowledge base storing the underlying information, (ii) an information system accessing and retrieving the information, (iii) a modelling component predicting the outcome of a problem posed ("inference engine"), and (iv) a framework that facilitates communication between the user, the knowledge base and the inference engine.

Knowledge bases that are formalised within "rule-based models" applying classical, Boolean ("crisp") logic (Starfield and Bleloch, 1983; Noble, 1987; Starfield et al., 1989) are well suited for the integration and interpretation of different knowledge sources. In the context of ecosystems, rule-based models can synthesize different ecosystem indicators so that, as a group, the indicators are interpreted effectively and consistently. For marine ecosystems in particular, Boolean, rule-based models have been constructed to predict recruitment strength of anchovy in the southern Benguela region (e.g., Korrûbel et al., 1998; Miller and Field, 2002).

Decision support tools in general, and knowledge-based systems in particular, have evolved considerably during the past two decades (Belton and Stewart, 2002; Guimarães Pereira et al., 2005). In particular, fuzzy-set theory (Zadeh, 1965; "fuzzy logic") has been promoted to deal with uncertainties in our understanding of aquatic systems (e.g., Mackinson, 2000; Cheung et al., 2005) and in evaluating the performance of a pelagic fishery (Paterson et al., 2007). Fuzzy logic potentially provides an elegant solution in information-rich contexts such as continuously measured variables, in circumventing possible rule proliferation in an attempt to accurately represent the data (e.g., Miller and Saunders, 2002).

In the context of natural resource management in general, and fisheries management in particular, the need for communication of advice among stakeholders is increasingly recognised as an important component of the decision-making process (e.g., FAO, 2003; Degnbol and Jarre, 2004). In preparation of scientific advice for management, and in acknowledging the large uncertainties around seemingly accurate measurements, quantitative information often is categorized into few categories only (e.g., ICES, 2005; Caddy and

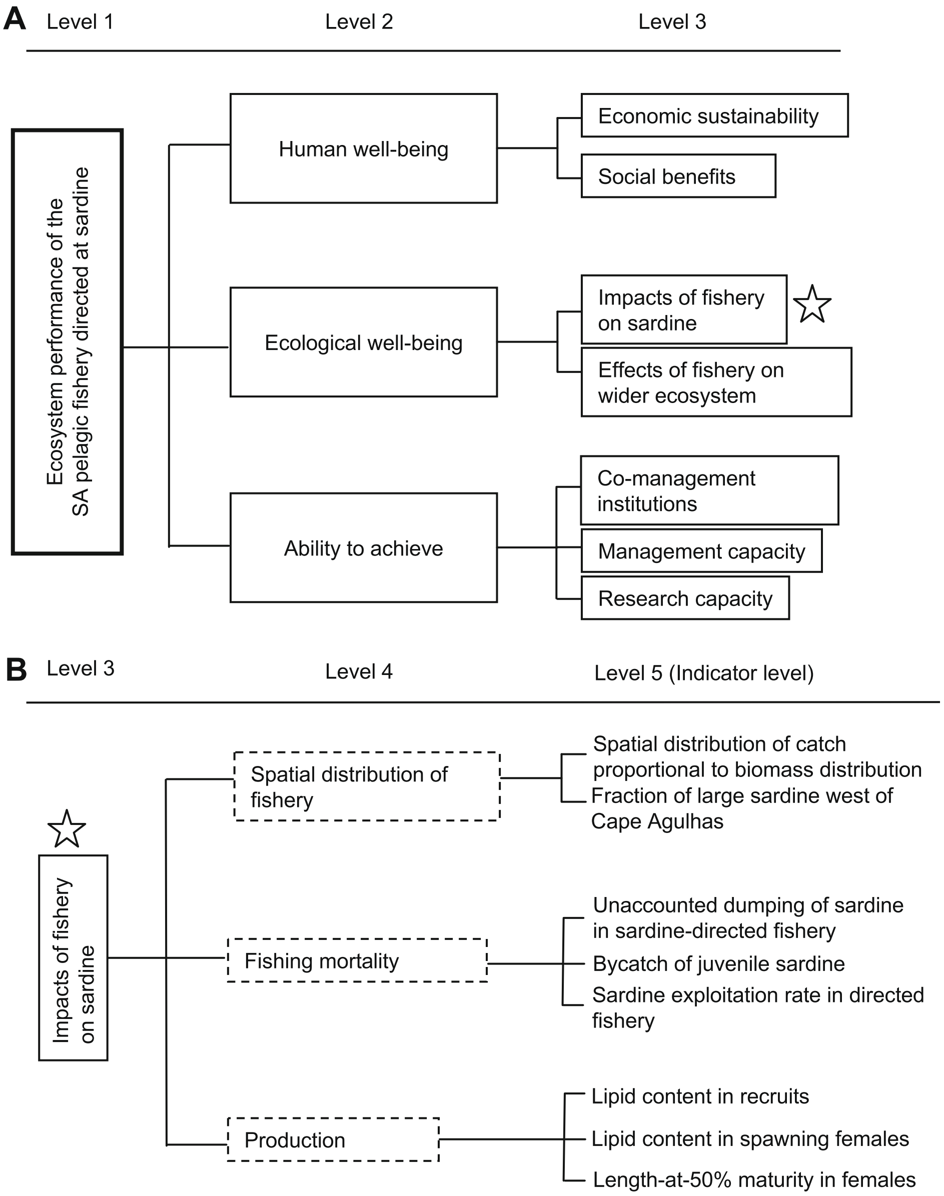

Fig. 1. Objective hierarchy (value tree) for the evaluation of the performance of the South African pelagic fishery directed at sardine in an EAF. (A) High-level objectives. (B) Specific objectives for the direct impacts of the fishery on sardine. Adapted from Paterson et al. (2007).

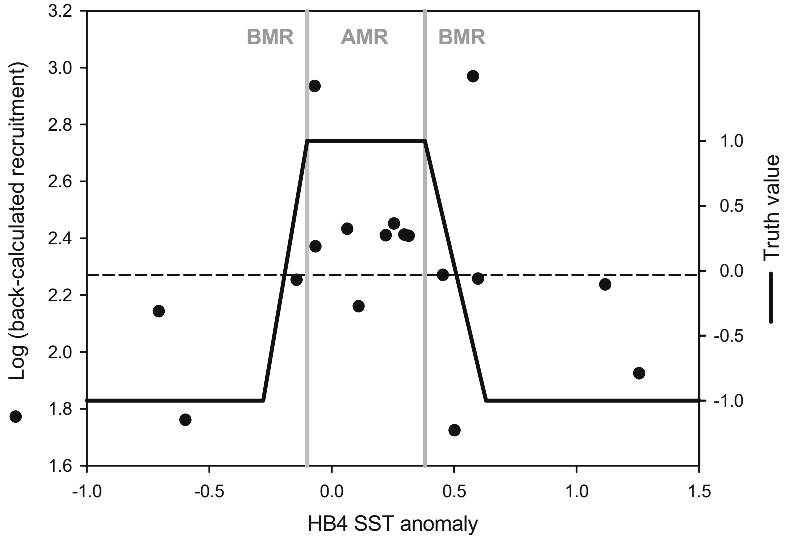

Fig. 2. Transformation of a Boolean classification (Miller and Field, 2002; Sea surface temperature anomaly at Hondeklip Bay, South Africa) into a fuzzy variable as used by NetWeaver. Note that temperature anomalies between −0.1 and 0.38 °C are classified as above-median recruitment (=true), but instead of sharp transitions to "below median recruitment", gradual transitions are modelled using the fuzzy variables.

Table 1
Definition of fuzzy membership functions of the preliminary indicators used to evaluate the impact of the South African pelagic fishery directed at sardine on its target resource (adapted from Paterson et al., 2007).

Indicator	Type	"100% false"	"Undecided"	"100% true"
Spatial distribution fishery: difference between catches relative to biomass at west coast and of total area (%)	Number	20	10	5
Fraction of large sardine west of Cape Agulhas (%)	Number	0	10	20
Sardine exploitation rate (dimensionless)	Number	0.55	0.4	0.2
Bycatch of juvenile sardine (%)	Number	6.1	0.6	0.0
Unaccounted dumping of sardine	Category	0	5	10
Lipid content in recruits (% wet body mass)	Number	2.636	4.140	5.640
Lipid content in spawning females (% wet body mass)	Number	2.384	3.384	4.384
Length at 50% maturity in females (cm)	Number	16.0	17.5	19.0

Agnew, 2004). This raises the question whether the straightforward – and easily communicated – approach of arranging the available information into a small number of categories, and applying classical, Boolean logic in small knowledge-based systems would not be sufficient?

The present study addresses this question by comparing two existing knowledge-based systems relevant to an ecosystem approach to fisheries in the southern Benguela, with potential application to the Humboldt Current system. The aims of the study are to assess whether the two approaches give similar results, and where differences occur, to evaluate the reasons for these. The study also aims to identify advantages and disadvantages of both systems.

2. Material and methods

We constructed a fuzzy counterpart to the Boolean knowledge-based system for anchovy recruitment as developed by Miller and Field (2002), and a Boolean counterpart to the prototype fuzzy knowledge-based system evaluating the performance of the South African pelagic fishery for sardine developed by Paterson et al. (2007). Both Boolean approaches were implemented in WinExp® (Quadling and Quadling, 1995), and both fuzzy-logic approaches were implemented in NetWeaver® (Miller and Saunders, 2002).

The Boolean knowledge-based system developed in Miller and Field (2002) predicts anchovy recruitment based on five variables, with the first variable representing a characteristic of the female spawning population (gonad atresia), and the other four representing the ocean environment as it relates to spawning, transport and recruitment areas for eggs and larvae. A decision is reached predicting recruitment at four levels: above-median recruitment, median recruitment, likely below median recruitment and very likely below median recruitment, and an additional category, "too few data" accounts for serious gaps in the knowledge base in a given year. Boolean thresholds for each of the predictor variables, separating "below" from "above" median recruitment, as well as relative weights of these variables, were derived using classification trees. For each predictor variable, the knowledge-based system requires input of "above", "below" the corresponding threshold, or "not known" for missing data. For inputs indicating "below median recruitment", the model adds the corresponding weights of the predictor variables to arrive at the predicted category. The model is coded using the above five decisions, and with five questions (pertaining to each of the predictor variables) with three possible answers ("below threshold", "above" threshold, or "not known") each. At each step in the interrogation and decision process, the user can retrieve explanatory information on the use of the information, or the reason for the decision reached. A possible "run" is illustrated in Box 1.

Box 1 An illustrative run of a Boolean knowledge-based system on forecasting anchovy recruitment in the southern Benguela, implemented in WinExp (Miller and Field 2002). Text in bold shows user action. See text for details.

Load
This is a deterministic rule-based model created with the intention of predicting years of below median anchovy recruitment (BMR). Rules are based on a decision table created with the use of classification trees for both setting of thresholds and weighting of variables (Miller and Field, 2002).
Five variables have been used in the construction of this rule-based model:
SST AB – the extent of 16–19 °C water (suitable spawning habitat) on the entire Aghulas bank for the period September–October.
CT4 anomaly – the sea surface temperature anomaly off Cape Town for the last four weeks of December.
HB4 anomaly – the sea surface temperature anomaly off Hondeklip Bay for the first four weeks of January.
CAP anomaly – the Cape Agulhas Pressure index anomaly from September to December.
Atresia – the occurrence of alpha oocyte atresia among spawners.
Start
Q1: Does water with a SST of between 16 and 19 °C occupy less than 57% of the Aghulas Bank?
(A1: Yes; A2: No; A3: Unsure/no data available).
A1: Yes
Q2: Is the CT4 SST anomaly for the last four weeks of December low?
(A1: Yes (i.e. less than 0.6 °C); A2: No (i.e. 0.6 °C or more); A3: Unsure/no data available).
Why?
Increased southerly wind frequency (and therefore increased upwelling, decreased CT4 anomaly) is likely to result in many pre-recruits being washed offshore from where they may not be able to return to the productive inshore waters. A positive linear relationship exists between the CT4 anomaly and log-transformed recruitment. A low CT4 anomaly can contribute to below median recruitment.
A2: No (i.e. 0.6 °C or more)
Q3: Is the HB4 SST anomaly for the first four weeks of January extreme?
(A1: Yes (i.e. less than −0.1 or more than 0.38 °C); A2: No (i.e. between −0.1 and 0.38 °C); A3: Unsure/no data available).
Why?
Weak upwelling (high HB4 anomaly) is likely to result in poor feeding conditions on the nursery grounds while too intense upwelling (low HB4 anomaly) could lead to offshore transport and a loss of pre-recruits.
A dome-shaped relationship with an 'optimal environmental window' exists between the HB4 anomaly and log-transformed recruitment. Extreme values of the HB4 anomaly can contribute to below median recruitment.
A2: No (i.e. between −0.1 and 0.38 °C)
Q4: Is the standardised CAP anomaly for September to October low?
(A1: Yes, i.e. less than −0.9 hPa); A2: No (i.e. 0.9 or more HPa); A3: Unsure/no data available).
Why?
The CAP index correlates with the mean daily easterly wind component recorded at Cape Point and is therefore indicative of wind over the Cape Peninsula and marine surroundings. Decreased wind velocity (low CAP index) over the transport area (Cape Point to Cape Columbine) is likely to result in less efficient transport. Low CAP values indicate impeded transport to the nursery grounds, and can contribute to below median recruitment.
A1: Yes (i.e. −0.9 hPa or less)
Q5: Is the incidence of oocyte atresia high?
(A1:Yes (i.e. more than 10%); A2: No (i.e. 10% or less); A3: Unsure/no data available).
Why?
Anchovy showing alpha stage oocyte atresia during the spawning season will only spawn with a 50% likelihood. If a significant proportion of the spawners are affected, reproductive success is likely to be lower due to decreased egg production (or condition). A high frequency of alpha oocyte atresia in anchovy on the spawning grounds is likely to result in reduced spawning success. High atresia can contribute to below median recruitment.
A1: Yes (ie more than 10%)
Decision reached!
The forecast is: BELOW AVERAGE RECRUITMENT – LIKELY.
Why?
You have input that three of the five variables (SST AB, CAP and atresia), between 50% and 67% of the overall weighting, indicate below median recruitment.

The fuzzy knowledge-based system developed by Paterson et al. (2007) evaluates the South African pelagic fishery directed at sardine using the concept of an EAF as laid out in FAO (2003). Overall performance of the fishery is evaluated relative to three overarching objectives, i.e., ecological well-being, socio-economic well-being and institutional feasibility. Each of these objectives is decomposed into a hierarchy of increasingly specific ("operational") objectives which in the end are linked to indicators as illustrated in Fig. 1.

In NetWeaver, indicators can be continuous or categorical variables, and the indicator values are the model inputs. Based on an evaluation of the logical value associated with each input relative to its specific objective, every input is transformed into a real number between −1 (representing the "false" in classical, Boolean logic) and 1 (representing "true" in classical, Boolean logic), where the value of 0 represents "undetermined". The result of the transformation is called a "fuzzy variable", and examples are provided in Figs. 2 and 5. The transformation is defined by assigning input thresholds to these three values. For applications in NetWeaver, a maximum of four thresholds can be used to describe the truth value associated with any input (the "corners" – points of non-differentiability – of the graphs in Figs. 2 and 5), and the transitions between the thresholds are assumed to be linear. For the purpose of this study, we fitted the transformation lines by eye, taking the border between "above" and "below" median recruitment as defined by Miller and Field (2002) as a basis, as depicted in Fig. 2. Ideally, and certainly with a larger database, a robust least-squares method would be employed to define the transformations.

In NetWeaver, the truth values of several inputs ("fuzzy variables") are combined by fuzzy operators called "nodes". Of the several available options, the 'fuzzy AND' and 'UNION' nodes were of interest for our purposes. The fuzzy AND is evaluated as completely false if one or more antecedents are fully false, and completely true if all antecedents are completely true. Intermediate values are obtained according to

$$\mathrm{AND}\{x\} = \mathrm{MIN}\{x\} + (\mathrm{WeightedAve}\{x\} - \mathrm{MIN}\{x\}) * (\mathrm{MIN}\{x\} + 1)/2, \qquad (1)$$

where $\{x\}$ is the set of antecedents of the AND node, MIN is the smallest value in that set, and WeightedAve is the weighted arithmetic mean of that set. It is of particular interest that the last term represents a "penalty" for uncertainty in the knowledge of the feeding information, and (like the Boolean AND) the system will tend towards a conservative evaluation of the truth value of the antecedents. As an example, the combined evaluation of two antecedents, of which one is undetermined and the other one is completely true, returns $\mathrm{AND}\{0,1\} = 0.25$. In contrast, the UNION node performs a weighted average of its antecedents, without inflicting any further penalty, i.e. $\mathrm{UNION}\{0,1\} = 0.5$ if all antecedents are equally weighted. Missing data are transformed into "undetermined", i.e., enter the average with value zero.

All antecedents of the prototype model of Paterson et al. (2007) are connected by AND nodes, following the hierarchy outlined in Fig. 1. For the comparative study, we restricted our scope to the evaluation of the ecological performance of this fishery, and specifically the impacts of the fishery on its target species (Fig. 1B). The specification of the fuzzy variables used for the comparisons is given in Table 1.

After constructing the respective fuzzy and Boolean counterpart models, we demonstrated these models to a small set of potential users for comments on the relative merits of the approaches. This set comprised about 25 persons, all were computer literate and had a higher education. The group comprised modellers and non-modellers.

3. Results

3.1. Anchovy recruitment

As a first step, we implemented a straightforward Boolean translation of the anchovy recruitment model in NetWeaver (Fig. 3). Secondly, we implemented a fuzzy version of this network, by defining the projector ("fuzzy membership") functions for the five predictor variables and combining their weighted values using a UNION node (Fig. 4). We noted that Miller and Field (2002) used weights that were derived from a Boolean classification tree, an approach that does not account for the soft transition from false to true which is the particular feature of fuzzy logic. We therefore had to explore different alternative sets of weights.

For comparison with the Boolean recruitment model, the results were categorized using the following transformation: for each fuzzy truth statement v:

$-1 \leqslant v \leqslant -0.5$ below median recruitment very likely.
$-0.5 < v \leqslant -0.1$ below median recruitment likely.
$-0.1 < v \leqslant 0.33$ median recruitment.
$0.33 < v \leqslant 1$ above-median recruitment.

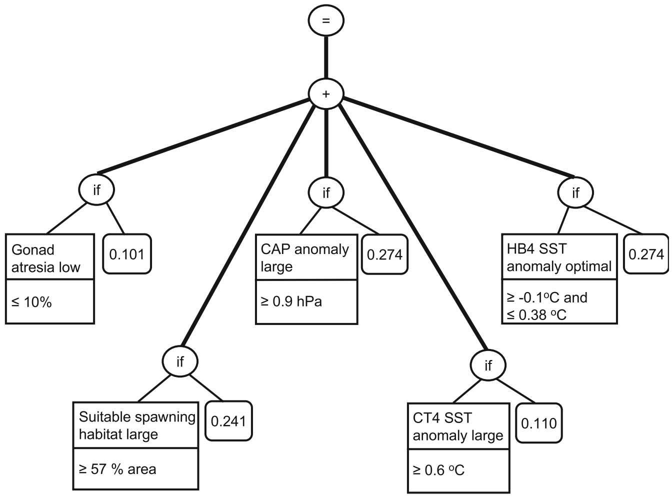

Fig. 3. NetWeaver representation of the Boolean, rule-based model predicting anchovy recruitment in the southern Benguela (1985–2001) developed by Miller and Field (2002). Terms in lower half of boxes represent the condition for which the corresponding statement is true, numbers in rounded boxes give weights in the overall evaluation.

The results of the network runs are summarized in Table 2.

3.2. Ecological performance of the South African pelagic fishery directed at sardine

The (continuous) variables of the fuzzy model were transformed into four categories "critical", "bad", "medium" and "good" using the following thresholds for each fuzzy transformed variable x (Fig. 5):

Critical: $-1 \leqslant f(x) < -0.8$.
Bad: $-0.8 \leqslant f(x) < -0.33$.
Medium: $-0.33 \leqslant f(x) < 0.33$.
Good: $0.33 \leqslant f(x) \leqslant 1$.

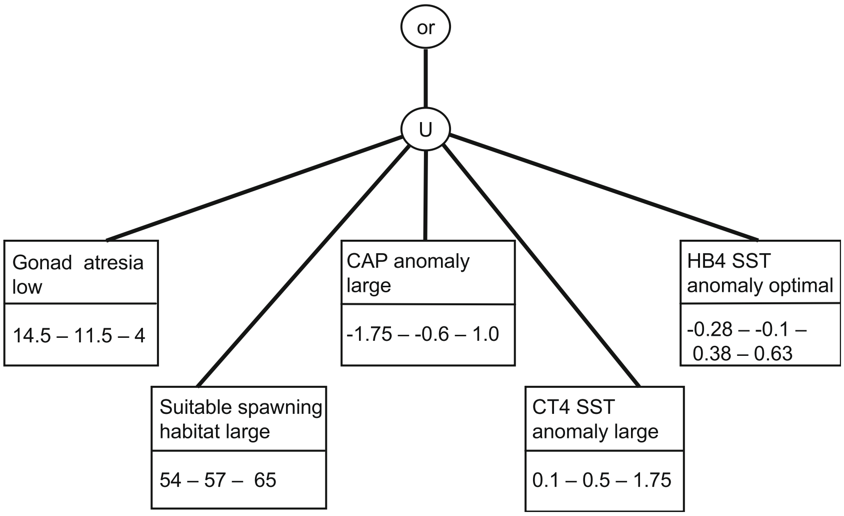

Fig. 4. Definition of the fuzzy Netweaver model predicting anchovy recruitment in the southern Benguela 1985–2001, developed in this study based on Miller and Field (2002). The terms in lower half of the four leftmost boxes represent the condition for which the corresponding statement are completely false – undetermined – completely true. For the rightmost box, the terms represent completely false – completely true – completely true – completely false, see also Fig. 2. "U" represents Netweaver's UNION node, and the "or" is included at the top of the network for reasons of convention.

Table 2
Results of the two knowledge-based systems predicting recruitment of anchovy in the southern Benguela. Recruitment categories from Miller and Field (2002): AM – above median, M – median, BML – below median likely, BMVL – below median very likely. Recruitment estimates are largely based on survey observations, and are calculated back from the time of two dedicated surveys to the beginning of the corresponding fishing season (see Miller and Field, 2002 for details). ✓ denotes agreement between data and our model outputs.

Year	Recruitment categories (=data)	Boolean, rule-based	Fuzzy-logic Weight Set 1[a]	Fuzzy-logic Weight Set 2[b]	Fuzzy-logic Weight Set 3[c]
1985	M	M ✓	M ✓	M ✓	M ✓
1986	AM	M	AM ✓	M	M
1987	AM	AM ✓	AM ✓	AM ✓	AM ✓
1988	AM	AM ✓	AM ✓	AM ✓	AM ✓
1989	BMVL	BMVL ✓	BMVL ✓	BMVL ✓	BMVL ✓
1990	BMVL	BML	BML	BML	BMVL ✓
1991	BMVL	AM	AM	M	M
1992	M	BMVL	M ✓	M ✓	M ✓
1993	BML	BML ✓	BMVL	BML ✓	BML ✓
1994	BMVL	BMVL ✓	BML	BMVL ✓	BMVL ✓
1995	AM	AM ✓	AM ✓	AM ✓	AM ✓
1996	BMVL	BML	M	BML	BML
1997	BML	BMVL	M	M	M
1998	M	AM	AM	M ✓	M ✓
1999	M	AM	AM	AM	AM
2000	AM	AM ✓	AM ✓	AM ✓	M
2001	AM	M	M	M	AM ✓
(M or AM) correct		9 of 10	10 of 10	10 of 10	10 of 10
(BML or BMVL) correct		6 of 7	4 of 7	5 of 7	5 of 7
AM correct		4 of 6	5 of 6	4 of 6	4 of 6
M correct		1 of 4	2 of 4	3 of 4	3 of 4
BML correct		1 of 2	0 of 2	1 of 2	1 of 2
BMVL correct		2 of 5	1 of 5	2 of 5	3 of 5

[a] Weight set 1: Gonad atresia 0.241, Habitat 0.241, CAP Anomaly 0.274, CT4 Anomaly 0.110, HB4 Anomaly 0.274 (Identical to Miller and Field's (2002)).

[b] Weight set 2: Gonad atresia 0.12, Habitat 0.12, CAP Anomaly 0.10, CT4 Anomaly 0.33, HB4 Anomaly 0.33.

[c] Weight set 3: Gonad atresia 0.09, Habitat 0.09, CAP Anomaly 0.07, CT4 Anomaly 0.35, HB4 Anomaly 0.40.

The evaluation was passed through the hierarchy (Fig. 1), applying the precautionary principle "to err on the side of caution in case of uncertainty", where the evaluation rules were derived by evaluating the antecedents following the definition in Table 3. Three sample runs of both models were carried out using realistic input data. The truth values of the inputs after fuzzy transformation are given in Table 4 and the output of the fuzzy and Boolean networks are compared in Table 5. The results show good agreement. The small discrepancy in the overall evaluation of Example 1 is discussed below.

3.3. User feedback

The potential users commented on various aspects of the two approaches related to attainability and flexibility of the software, learning/understanding of the underlying approach, ease of communication of model structure and outputs, and model testing. Their feedback is detailed in Table 6.

Table 3
Evaluation matrix of antecedents in the Boolean version of the knowledge-based system assessing the ecological performance of the South African pelagic fishery directed at sardine.

Antecedent category	Critical	Bad	Medium	Good
Critical	Critical	Critical	Critical	Critical
Bad	Critical	Bad	Bad	Bad
Medium	Critical	Bad	Medium	Medium
Good	Critical	Bad	Medium	Good

Table 4
Truth values after fuzzy transformation (as defined in Table 1) of inputs pertaining to three realistic examples in the evaluation of the ecological performance of the South African pelagic fishery directed at sardine.

Operational objective	Fuzzy transformation output (truth value)		
	Example 1	Example 2	Example 3
Spatial distribution of catch proportional to biomass distribution	1.00	−1.00	−1.00
Large fraction of large sardine west of Cape Agulhas	1.00	−0.17	−0.87
Low sardine exploitation rate	1.00	1.00	−0.99
Low bycatch of juvenile sardine	−0.01	0.95	0.92
No unaccounted dumping of sardine	0.80	0.40	0.00
High lipid content in recruits	0.85	0.69	−0.57
High lipid content in spawning females	−0.07	0.85	0.04
High length at 50% maturity in females	1.00	0.83	−0.37

4. Discussion

4.1. Performance of the fuzzy-logic vs. the Boolean implementation of the knowledge-based systems

Forecasting of "bad" recruitment is important for the management of the anchovy fishery in South Africa, and particular attention must therefore be paid to correct predictions by the knowledge-based system of "bad" recruitment, defined here as likely or very likely below median recruitment. The Boolean implementation of the anchovy recruitment knowledge-based system (Miller and Field, 2002) performed well: on this scale, it misclassified two years out of the 17 years (1991 and 1992, where 1991 was classified too high, and 1992 too low). Here, it is worth remembering that this result exceeds the success rate of 70% postulated by Cochrane and Starfield (1992) for better results in the fishery resulting from improved management. On the finer scale of the four result categories, eight years were classified correctly, four were classified too low (i.e., the knowledge-based system's prediction was lower than the category of the calculated recruitment value) and five were classified too high (i.e., the knowledge-based system's prediction was higher than the category of the calculated recruitment value).

The fuzzy-logic implementation using weight set 3 (Table 2) performed somewhat better: eleven years were classified correctly, two were classified too low and four years were classified too high. On the coarse scale of "ok" vs. "bad" recruitment, both approaches performed the same, i.e., with a success rate of 88%.

With a more detailed focus, the fuzzy models returning the best results placed 66–75% of the weight on processes directly related to the strength of the trade winds as drivers of the upwelling. This stands in contrast to Miller and Field's (2002) result which placed only 38% of the weight on these processes. Consequently, the two approaches suggest different relative importance of the two processes related to anchovy spawning, transport and feeding. This is an interesting outcome, the consequences of which we will explore in a related study. We omit that discussion here, because it falls beyond the objective of the present study which is to compare the relative performance of the models with respect to predicting below median recruitment.

The rule-based knowledge-based system evaluating the ecological effects of the South African pelagic fishery directed on sardine on its target resource performed as well as its fuzzy-logic prototype original. Three points need to be considered in evaluating the result:

1. The weights used can make a difference, as shown by the following example: The fuzzy AND evaluation of {1,0.29,0.24}

Table 5
Comparison of the two knowledge-based systems evaluating the ecological performance of the South African pelagic fishery directed at sardine. ✓ denotes agreement between the two sets of outputs.

Higher-level objective	NetWeaver fuzzy-logic			Boolean, rule-based		
	Example 1	Example 2	Example 3	Example 1	Example 2	Example 3
Appropriate spatial distribution of fishery	1.00	−1.00	−0.831	Good ✓	Critical ✓	Critical ✓
Low sardine mortality due to fishing	0.29	0.67	−0.98	Medium ✓	Good ✓	Critical ✓
High sardine production	0.24	0.77	−0.51	Medium ✓	Good ✓	Bad ✓
Maintain sustainable resource level	0.41	−1.00	−1.00	Medium	Critical ✓	Critical ✓

Table 6
Summary of user feedback on building knowledge-bases using a rule-based (as implemented in WinExp) or fuzzy-logic (as implemented in NetWeaver) approach.

Criterion	Comments, Rule-based / WinExp	Comments, Fuzzy-logic / NetWeaver	Advantage
Cost	WinExp is cheap. Stand-alone versions of knowledge-based systems can be distributed free of charge.	NetWeaver is a commercial software, and is relatively expensive for many stakeholders.	WinExp
Complexity	WinExp is designed for small knowledge-bases.	NetWeaver is a powerful software package that allows the design of complex knowledge-based systems.	NetWeaver
Ease of learning	A small, simple shell like WinExp is learnt very quickly (within a few hours).	NetWeaver has its own "language" which takes a few days to learn. It has a helpful tutorial.	WinExp
Ease of understanding	Rule-based, Boolean reasoning is easily understood by users of the knowledge-based system.	Fuzzy-logic is an intuitively appealing method of taking account of uncertainty in knowledge, e.g., about processes in ecosystems.	Preference-dependent
Ability to communicate among stakeholders	Rule-based reasoning is easily understood and communicated among users of the knowledge-based system. Natural language is used to design and use the system, this makes it easy for users not familiar with quantitative modelling to run the system.	Users unfamiliar with fuzzy-set theory must "trust" the logic of the model.	Rule-based
Visual communication of outputs	WinExp would improve with a graphical interface, e.g. to track partial decisions already reached, and/or to inform the user on progress towards the ultimate decision.	Graphical interface and output are very useful because they summarise a large amount of information in a few images/ diagrammes. [a]	NetWeaver
Flexibility when running the system	The "trail" (log of a particular run) is helpful.	Single inputs can be changed while keeping the others constant, and the sensitivity of the result to that change in that input can be assessed immediately both numerically and visually. Useful for demonstrating the working of the model to stakeholders.	NetWeaver
Ability to add explanations	WinExp strongly encourages (nearly forces) the inclusion of explanations both for questions and decisions. However, the window size would benefit from more flexibility.	Explanations can be entered into NetWeaver knowledge-bases, but the emphasis is on the definition and processing of the truth values, i.e., the numerical information, and their graphical representation. An analyst can omit the explanations from the system, thus detracting from its transparency.	WinExp
Ease of building the knowledge based system	Can be done by an analyst in consultation with stakeholders, Software is sufficiently easy to learn so that stakeholders could use it themselves in a hands-on fashion, e.g. in breakaway sessions.	Typically would be done by analyst in consultation with stakeholders. Stakeholders do not necessarily have to be involved in the technical detail of the software, which include intricacies of fuzzy-set theory and the NetWeaver language.	Preference-dependent
Definition of variables	Categorial inputs do not need to be forced onto a continuous scale, but can be processed with rules straight away.	Converting the inputs (indicators) into fuzzy variables requires careful attention. Numerically literate users probably feel more comfortable than others in this process.	n.a.
Interpretation of model output	Some users expressed their appreciation of having continuous inputs transformed into (few, qualitative, value-interpreted) categories which were easy to understand and work with. Once the rules are agreed upon, the decisions leave little room for additional interpretation (and possible disagreement) with the system output.	Fuzzy network output is a number between -1 and 1, and as such is essentially value-free. Stakeholders can debate (and hopefully agree upon) interpretations of the resulting number.	Preference-dependent
Testing model	Will be guided by an analyst, but can be carried out by users in hands-on fashion.	Will typically be carried out by an analyst.	Preference-dependent

[a] However, the fixed colour-coding can be misleading, e.g., the dark green for truth values of about 0.3 visually indicates a "rather true" outcome, although agreed "true" interpretation may only start for truth values larger than 0.5. Also, the red/green colour scheme is not helpful for colour-blind users. User-defined colour scales on result bars would circumvent both problems, and be a valuable addition to NetWeaver.

(Table 5, Example 1) led to a less conservative result (0.41, category "good") than the rigorous application of the precautionary principle (Table 3) used to the rule-based model ({Good, Medium, Medium} evaluated as "medium". Different sets of weights for the three antecedents of e.g., 0.10/0.75/ 0.15, 0.125/0.625/0.25, 0.15/0.6/0.25, 0.15/0.5/0.35, all would have resulted in the "medium" category under fuzzy evaluation in NetWeaver. These sets of weights are not inconsistent with current fisheries management in general, which (i) tends to place primary emphasis on mortality, (ii) would consider the productivity of the stock next important, and (iii) would consider factors related to the spatial distribution of fishing least important.

2. The choice of weights is tied up with the thresholds or the borderlines between categories or bins. At the lower levels of the network, the choice of weights might well reflect uncertainty around the thresholds for fuzzy membership (Table 1) of a given indicator.

3. If follows that both the weights and the borderlines have to be chosen deliberately to reflect an appropriate level of risk. What represents "good" – A truth value of 0.33? A truth value of 0.50? A truth value of 0.67?

This leads to a number of questions and possibilities. For example; How do we work with managers and stakeholders to

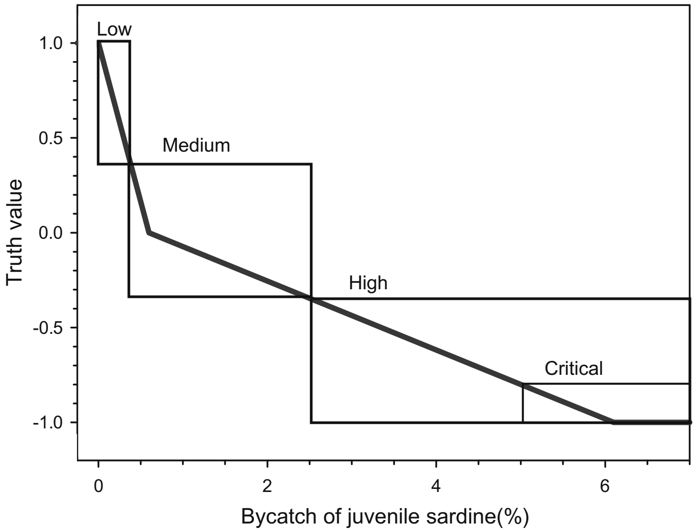

Fig. 5. Illustration of the transformation of a fuzzy variable into categories for the Boolean model. For this example, bycatch of juvenile sardine in the sardine-directed fishery is categorized as "low" (~good) for truth values of 0.33 and higher, corresponding to a bycatch of less than 0.4%, as "medium" for truth values between −0.33 and below +0.33, and as "high" (~bad) for truth values of less than −0.33. The additional category "critical" corresponds to truth values of less than −0.8, i.e. bycatch of juveniles exceeding 5% of the total catch.

determine weights and thresholds that are ecologically sound and reflect their value and risk systems? Would it be useful to offer two alternative sets (more conservative and less conservative)? Would it be useful to model the likely consequences of rigorously applying a knowledge-based system to the South African pelagic fishery, e.g. by building on the approach of Cochrane and Starfield (1992) in an ecosystem context? Does the data base justify sharp borders for Boolean categories? Would it be advantageous to define subsets of rules to improve the decision-making process?

The flexibility of the rule-based approach readily allows the definition of such subsets of rules (e.g., based on additional questions such as "Is the value entered close to the border of the category? How accurate is it? How precise is it?") to circumvent the potential problem of unduly negative evaluation. More generally, Stewart and Joubert (2006) point out that rule-based approaches are more flexible than any other approach in multiple criteria decision analysis. On the other hand they caution that it can take considerable effort to identify a sufficiently rich set of rules to cater for a wide enough range of comparisons of alternatives. Careful applications of other methods, including fuzzy-logic models implemented in NetWeaver, can provide a more elegant model formulation, but the elegance must not come at the expense of extensive sensitivity testing. As far as the two examples presented here are concerned, applying both approaches in parallel has helped us to deepen our understanding of the underlying problem, and to improve our models.

4.2. User feedback and possible stakeholder participation in the decision-making process

As a general observation, modellers and computer scientists tended to respond more positively to the NetWeaver implementation, whereas users who struggle with numerical concepts tended to respond more positively to the natural language implementation in WinExp.

An important difference between the approaches concerns the possibility of stakeholders working with the knowledge tool in a "hands-on" fashion. Stakeholder participation is a paramount component of an ecosystem approach to fisheries management (FAO, 2003; Degnbol and Jarre, 2004). In practical application, a model developer ("analyst" or "knowledge engineer") would be responsible for creating a first prototype system in consultation with stakeholders. The NetWeaver software is expensive and subject to licensing. The WinExp developing software on the other hand is very cheap, and models can be distributed to and used by stakeholders free of charge. The software is simple and easily learnt, making it possible for stakeholders to explore (and probably further refine) the system in a "hands-on" fashion. Because the entire process of designing a knowledge-based system in WinExp uses natural language, rules are straightforward to discuss among users inexperienced in modelling. In this way, all users/stakeholders could participate in the design of the entire knowledge-based system (inputs, rules, and decisions), and contribute actively to sensitivity testing not only of inputs, but also of the functional form and model structure (through the formulation of alternative sets of rules).

The educational aspects of rule-based models have been pointed out by Starfield (1990), and the additional communicative aspect of a model formulated in natural language, and involving good explanations for users, had been expressed earlier (Starfield and Bleloch, 1983; Starfield and Louw, 1986), and confirmed by our test-users. Rule-based models allow interfaces to be designed that could change depending on whether a technical expert or a general user is using the system, e.g. directly through initial questions on the perceived level of expertise, or on the answers given to questions already asked.

The strength of the WinExp software is directly linked to that of *small* knowledge-based systems. In contrast, NetWeaver is a very powerful software package, well suited for complex knowledge-based systems. However, because it is distributed commercially, it has the disadvantage of possibly being beyond the economic reach of some stakeholders. This could restrict its active use by stakeholders in addition to the constraints imposed by having to intellectually master the many possibilities of the software as discussed above.

NetWeaver will best be handled by the model developer ("analyst" or "knowledge engineer"), but the graphic capabilities of the software readily allow demonstration of the consequences of changes to the model in a workshop situation, where the model developer would capture stakeholders suggestions or preferences, implement them in the system, and the discussion would proceed around the system outputs in an interactive way. This implies that testing the sensitivity of the model, other than to initial conditions (as recommended by Platt and Radach (1981), and see Paterson et al. (2007) for an example), would probably be carried out by the analyst in a consultative, but not necessarily participatory, process. This includes testing of sensitivity to (a) parameters (e.g., relative weights of antecedents at each node), (b) functional form (e.g., the steepness of the false–true transitions in defining the fuzzy variables), and (c) model structure (e.g., number of levels in the model hierarchy, and selection of node types).

4.3. Do decisions on complex problems necessitate complex knowledge tools?

It is often stated that ecological systems and human expertise are complex, and the complexity of the real world needs to be reflected in the complexity of the models describing it. If that is true, then designing an integrated and detailed knowledge-based system for the evaluation of the performance of an ecosystem approach to all fisheries in a large and complex marine ecosystem such as the southern Benguela, comprising several different and interacting fisheries, a multitude of stakeholders and large set of different external drivers, would necessitate a large knowledge-based system. A powerful software tool like NetWeaver can be advantageous in this situation, because it allows the development of small and large knowledge-bases alike.

We argue that small knowledge-based systems are worth developing and using. First and foremost, their strength lies in *synthesis* (as opposed to analysis) of complex problems. As models or tools for synthesis, small knowledge-based systems take account of the full complexity of the problem at hand. They force participants in that synthesis (e.g., a decision-making process) to discipline their thoughts on distilling the essence of that complex problem, and to apply Occam's razor. The development of small knowledge-based systems is a process of modelling, of creating a simple model, and is no exception to the general rule that the process of creating the model is as important as the model results (e.g., Belton and Stewart, 2002, Chapter 3.2). Noble (1987) expresses the expectation that knowledge-based systems may contribute to advance ecological theory when the developers are forced to rethink the nature of ecological relationships, thus creating ‘‘deep knowledge”. The rigour of expressing complex problems in an algorithm (however that algorithm may be expressed – numerically, categorically or in natural language) sets straight the thinking of the participants in the modelling process, and thereby improves both process and outcome. The recommendation to keep a model as simple as possible has repeatedly been expressed in both science (e.g., Haidvogel and Bryan, 1992) and at the interface between science and management (e.g., Starfield, 1990, 1997; Degnbol, 2003; Cotter et al., 2004).

Second, as synthesis tools in a management context, small knowledge-based systems can help scientists put their results into a multi-disciplinary perspective, and think through how to apply their science to issues that are not purely scientific. This is particularly relevant in an ecosystem approach to fisheries management, where results of biological oceanography, marine ecology, stock assessment, economics and social sciences need to be considered in a given institutional (political) setting, and under external drivers such as climate change. Jarre et al. (2006: Fig. 11-3) outline how to use a knowledge-based system that indicates the possibility of long-term ecosystem change in a management context.

Third, our experiment of involving users in the evaluation of a prototype system of the sardine fishery has demonstrated the use of small, simple knowledge-based systems as vehicles for delivering state-of-the-art science to those who need to use it. Fuzzy transformation can clearly be advantageous for continuous variables, particularly in situations where the database is sufficiently strong that the shape and slope of the transformation can be defined well. The knowledge underlying even small decision support systems is complex, and requires a rigorous scientific approach to the selection of variables (indicators), and of their categorisation and/or continuous transformation. This underlying science will be documented in the explanations to the questions the user will be asked by the system, whereas stakeholder consensus will be documented in the explanations behind the rules (or nodes, weights) and decisions. Visual aids such as implemented in NetWeaver, can be a great help in this process.

Last but not least, particularly at the interface between science and management, small knowledge-based systems provide a structure for adaptive management (Burgman, 2005, Chapter 12.7; Linkov et al., 2006) and document ‘‘corporate memory”. By facilitating agreement on the components and on the logic of processing the information in a decision-making process, small knowledge-based systems provide a means to think about, communicate, argue about and document, best common practice for all involved (also see Belton and Stewart, 2002, Chapter 1.2). In other words, they provide a methodology for professionals to describe how they make decisions, and hence evaluate and improve how they make decisions. Several methods for structured multiple criteria decision-making exist, and their relative merits have been discussed by Belton and Stewart (2002). For EAF problems in particular, the value of the data base documenting the information, qualitative as well as quantitative, and which forms an intricate part of a knowledge-based system, cannot be overemphasized.

4.4. Possible applications of knowledge-based systems in an ecosystem approach to fisheries management in the ecosystems of the Humboldt Current

This study has introduced two knowledge-based systems implemented for the southern Benguela and compared their results. In a generic fashion, we have highlighted the advantages of continued design and implementation of small knowledge-based systems as tools supporting decision-making on complex problems. Both the Benguela and Humboldt are eastern boundary current systems connected to developing human societies. They show many similarities (e.g., Jarre et al., 1998; Schwartzlose et al., 1999; Moloney et al., 2005), and modelling techniques that are applied successfully in one of them may therefore work in the other.

As an example, our prototype knowledge-based system for evaluating the ecosystem performance of the South African sardine fishery could readily be transferred to the context of pelagic fisheries in the Humboldt Current. However, it is necessary to remember that an important property of multi-criteria decision modelling is the involvement of stakeholders in the process of defining and constructing the model from the very beginning. Therefore, a model constructed in one ecosystem certainly can serve as a platform for discussions in the other, but each knowledge-based system will necessarily be unique. Whereas the high-level objectives may remain very similar, the specific objectives, and particularly the indicators need to be adapted to the specific situation in order to meaningfully represent the knowledge base of the case in focus. Nevertheless, the structures and outputs of different knowledge-based systems built for the same objective can be compared. The comparison will not only enhance our understanding of similarities and differences between ecosystems, it will also contribute to the debate on the necessity for ecosystem-specific sets of objectives and indicators for practical fisheries management, as discussed by Degnbol and Jarre (2004).

A closely related project currently underway aims to design a knowledge-based system for understanding and predicting long-term ecosystem change in the Benguela (Jarre et al., 2006).

Long-term ecosystem change can manifest itself as species dominance alternations, or profound changes in the functioning of marine ecosystems, and also has been documented for the Humboldt Current ecosystems: For the ecosystem off northern-central Peru, long-term ecosystem changes have been observed in the early 1970s and in the mid-1980s (Jarre et al., 1991; Jarre, 1992; Alheit and Ñiquen, 2004). For the ecosystem off central-southern Chile, too, long-term ecosystem change is hypothesized for the mid-1980s Neira (2008). For the southern Benguela, we have characterised the years acting as "turning points" for ecosystem change by using multivariate statistical methodology developed to analyse regime shifts in the North Pacific (Howard, 2007; Howard et al., 2007). In the absence of long time series of primary production for the southern Benguela, we used time series since the 1950s pertaining to zooplankton and two principal species of small pelagic fish (anchovy and sardine) as indicators of ecosystem state, long time series of environmental data (winds, sea surface temperatures) as indicators of environmental pressures, and time series since the 1950s of catches of the principal commercial fish species as indicators of anthropogenic pressures. Building on these results, a first prototype is currently being built. It firstly questions the user with respect to determining the actual "state" of the system, then questions the user with respect to environmental and anthropogenic pressures, and finally arrives at a decision whether these pressures, in the given state, are likely to lead to ecosystem change.

Time series of similar length are available for ecosystems of the Humboldt Current, notably the ecosystem off northern-central Peru, and a similar approach might be followed. In both large eastern boundary current systems, our understanding of the exact mechanisms behind long-term change currently is incomplete (Shannon et al., 2008), and comparative research will likely continue to be fruitful. As illustrated above, knowledge-based systems are able to summarize and indeed integrate various aspects of complex problems, and we expect that they can help us to anticipate ecosystem change, to improve our understanding of the underlying mechanisms, and last but not least contribute to improving the management of human activities in the ocean.

5. Conclusions

- Small knowledge-based systems using fuzzy logic or Boolean logic can readily be translated into one another. The question is not so much on the type of logic used, but on the most appropriate representation of the problem at hand.
- With respect to the model objectives, neither method clearly outperformed the other.
- The advantages of numerically processing continuous variables, and only interpreting the output, such as in the fuzzy-logic NetWeaver implementation, can be weighed up against the advantages of using few, qualitative, easy-to-understand categories such as in the WinExp implementations.
- For purposes of decision model development and academic research into decision support, NetWeaver is powerful software, not the least because of its flexibility (e.g., allowing fuzzy and Boolean logic within the same knowledge-based system) and very attractive user interface.
- Rule-based, Boolean reasoning is easily understood and communicated among users of the knowledge-based system. Users unfamiliar with fuzzy-set theory must "trust" the logic of the model.
- The strengths of Boolean implementations in a small knowledge-based system shell like WinExp lie in communication of the logical reasoning behind a decision process, and in the educational value of a hands-on-approach for stakeholders in that decision-making process.
- Applying the two approaches in parallel improved our understanding of the models as well as of the underlying problems. We advocate using a number of different approaches to tackle a complex problem.
- Even for complex problems, small knowledge-based systems are worth developing and using. Their strengths lie (i) in synthesis of the problem in a logical and transparent framework, (ii) in helping scientists to think through how to apply their science to transdisciplinary issues that are not purely scientific, and (iii) in representing vehicles for delivering state-of-the-art science to those who need to use it.
- We recommend development of similar knowledge-based systems in other large marine ecosystems, including those of the Humboldt Current, for comparison with the Benguela, in order to support the implementation of an ecosystem approach to fisheries management.

Acknowledgements

We would like to thank Marine and Coastal Management, Cape Town, for collecting and providing many of the data that underlie our models. We are particularly grateful to Drs. Lynne Shannon and Carl van der Lingen, as well as Tracey Fairweather and Theressa Akkers of Marine and Coastal Management, Dr. Alison Joubert and Prof. Theodor Stewart of the Department of Statistical Sciences of the University of Cape Town, and the students of the 2006 course in Conservation Biology at the University of Cape Town, for helpful discussions. Dr. Tim D. Smith and two anonymous reviewers provided helpful comments on the manuscript. Partial funding of this work was obtained from the South African Network for Coastal and Oceanic Research, funded by the National Research Foundation and Marine and Coastal Management. AJ gratefully acknowledges support of a mobility grant by the EUR-OCEANS Network of Excellence (CEC FP6 Contract Ref. 511106), as well as support during part of this study by the Institut de recherche pour le développement (IRD, Paris) as a visiting scientist (UR 097 "ECO-UP").

References

Alheit, J., Ñiquen, M., 2004. Regime shifts in the Humboldt Current ecosystem. Progress in Oceanography 60, 201–222.

Belton, V., Stewart, T.J., 2002. Multiple Decision Criteria Analysis: An Integrated Approach. Kluwer Academic Publishers, Dordrecht, The Netherlands.

Burgman, M., 2005. Risks and Decisions for Conservation and Environmental Management. Cambridge University Press, Cambridge, UK.

Caddy, J.F., Agnew, D.J., 2004. An overview of recent global experience with recovery plans for depleted marine resources and suggested guidelines for recovery planning. Reviews in Fish Biology and Fisheries 14, 43–112.

Cheung, W.W.L., Pitcher, T.J., Pauly, D., 2005. A fuzzy-logic expert system to estimate intrinsic extinction vulnerabilities of marine fishes to fishing. Biological Conservation 124, 97–111.

Cochrane, K., Starfield, A.M., 1992. The potential use of predictions of recruitment success in the management of the South African anchovy resource. South African Journal of Marine Science 12, 891–902.

Cotter, A.J.R., Burt, L., Paxton, C.G.M., Fernandez, C., Buckland, S.T., Pan, J.-X., 2004. Are stock assessment methods too complicated? Fish and Fisheries 5, 235–254.

Degnbol, P., 2003. Science and the user perspective: the scale gap and the need for co-management. In: Wilson, D.C., Raakjaer Nielsen, J., Degnbol, P. (Eds.), The Fisheries Co-Management Experience. Accomplishments, Challenges and Prospects. Kluwer Academic Publishers, Dordrecht, The Netherlands, pp. 31–49.

Degnbol, P., Jarre, A., 2004. Indicators in fisheries management: a development perspective. African Journal of Marine Science 26, 303–326.

FAO, 2003. The ecosystem approach to fisheries. FAO Technical Guidelines for Responsible Fisheries. No. 4, Suppl. 2, Food and Agricultural Organisation of the United Nations, Rome, Italy.

Guimarães Pereira, Â., Corral Quitana, S., Funtowicz, S., 2005. GOUVERNe: new trends in decision support for groundwater governance issues. Environmental Modelling and Software 20, 111–118.

Haidvogel, D.B., Bryan, F.O., 1992. Ocean general circulation modeling. In: Trenberth, K.E. (Ed.), Climate System Modelling. Cambridge University Press, Cambridge, UK, pp. 371–412.

Howard, J.A.E., 2007. Application of the sequential *t*-test algorithm for analysing regime shifts to the southern Benguela ecosystem. M.Sc. Thesis, Zoology Department, University of Cape Town, South Africa.

Howard, J.A.E., Jarre, A., Clarke, A., Moloney, C.L., 2007. Application of the sequential *t*-test algorithm for analysing regime shifts to the southern Benguela ecosystem. African Journal of Marine Science 29 (3), 437–451.

ICES, 2005. Report of the ICES Advisory Committee on Fishery Management, Advisory Committee on the Marine Environment and Advisory Committee on Ecosystems, 2005. ICES Advice, vol. 1. International Council for the Exploration of the Sea, Copenhagen, Denmark.

Jarre[-Teichmann], A., 1992. Steady-state modelling of the Peruvian upwelling ecosystem. Ph.D. Thesis, Alfred Wegener Institute for Polar and Marine Research and University of Bremen, Germany.

Jarre, A., Muck, P., Pauly, D., 1991. Two approaches for modelling fish stock interactions in the Peruvian upwelling ecosystem. In: ICES Marine Science Symposia, vol. 193, pp. 171–184.

Jarre, A., Moloney, C.L., Shannon, L.J., Wickens, PA., 1998. Comparing trophic flows in the southern Benguela to those in other upwelling ecosystems. South African Journal of Marine Science 19, 391–414.

Jarre, A., Moloney, C.L., Shannon, L.J., Fréon, P., van der Lingen, C.D., Verheye, H.M., Hutchings, L., Roux, J.-P., Cury, P., 2006. Developing a basis for detecting and predicting long-term ecosystem change. In: Shannon, V., Hempel, G., Malanotte-Rizzoli, P., Moloney, C., Woods, J. (Eds.), Benguela: Predicting a Large Marine Ecosystem, Large Marine Ecosystem Series, vol. 14. Elsevier, Amsterdam, pp. 239–272.

Korrûbel, J.L., Bloomer, S.F., Cochrane, K.L., Hutchings, L., Field, J.G., 1998. Forecasting in South African pelagic fisheries management: the use of expert and decision support systems. South African Journal of Marine Science 19, 415–423.

Linkov, I., Satterstrom, F.K., Kiker, G., Batchelor, C., Bridges, T., Ferguson, E., 2006. From comparative risk assessment to multi-criteria decision analysis and adaptive management: recent developments and applications. Environment International 32, 1072–1093.

Mackinson, S., 2000. An adaptive fuzzy expert system for predicting structure, dynamics and distribution of herring shoals. Ecological Modelling 126, 155–178.

Miller, B.J., Saunders, M.C., 2002. NetWeaver Reference Manual: a compendium aof NetWeaver and NetWeaver related terms, concepts and functions. Penn State University and The Heron Group LLC. Available on <http://www.rules-of-thumb.com> (last accessed December 2006).

Miller, D.C.M., Field, J.G., 2002. Predicting anchovy recruitment in the southern Benguela ecosystem: developing an expert system using classification trees. South African Journal of Science 98, 465–472.

Moloney, C.L., Jarre, A., Arancibia, H., Bozec, Y.-M., Neira, S., Roux, J.-P., Shannon, L.J., 2005. Comparing the Benguela and Humboldt marine ecosystems with indicators derived from inter-calibrated models. ICES Journal of marine Science 62, 493–502.

Neira, S., 2008. Assessing the effects of internal (trophic structure) and external (fishing and environment) forcing factors on fisheries off Central Chile: basis for an Ecosystem Approach to management. PhD thesis, Zoology Department, University of Cape Town, South Africa.

Noble, I.R., 1987. The role of expert systems in vegetation science. Vegetatio 69, 115–121.

Paterson, B., Jarre, A., Moloney, C.L., Fairweather, T., Shannon, L.J., van der Lingen, C.M., Field, J.G., 2007. A fuzzy-logic tool for multicriteria decision-making in the Southern Benguela. Journal of Marine and Freshwater Research 58, 1056–1068.

Paterson, B., Stuart-Hill, G., Underhill, L.G., Dunne, T., Schinzel, B., Brown, C., Beytell, B., Dem, F., Lindeque, P., Tagg, J., Weaver, C., 2008. A fuzzy decision support tool for wildlife translocations into communal conservancies in Namibia. Environmental Modelling and Software 23, 521–534.

Platt, T., Radach, G., 1981. Working with models: sensitivity analysis. In: Platt, T., Mann, K.H., Ulanowicz, R.E. (Eds.), Mathematical Models in Biological Oceanography. United Nations Educational, Scientific and Cultural Organization (UNESCO), Paris, France, pp. 37–46.

Quadling, H., Quadling M., 1995. WinExp–a small expert system for Windows, v. 2.11. Available at: <http://www.howtomodelit.com> (last accessed July 2007).

Roetter, R.P., Hoanh, C.T., Laborte, A.G., Van Keulen, H., Van Ittersum, M.K., Dreiser, C., Van Diepen, C.A., De Ridder, N., Van Laar, H.H., 2005. Integration of systems network (SysNet) tools for regional land use scenario analysis in Asia. Environmental Modelling and Software 20, 291–307.

Schwartzlose, R.A., Alheit, J., Bakun, A., Baumgartner, T.R., Cloete, R., Crawford, R.J.M., Fletcher, W.J., Green-Ruiz, Y., Hagen, E., Kawasaki, T., Lluch-Belda, D., Lluch-Cota, S.E., MacCall, A.D., Matsuura, Y., Nevárez-Martínez, M.O., Parrish, R.H., Roy, C., Serra, R., Shust, K.V., Ward, M.N., Zuzunaga, J.Z., 1999. Wordwide large-scale fluctuations of sardine and anchovy populations. South African Journal of Marine Science 21, 289–347.

Shannon, L.J., Jarre, A., Schwing, F.B., 2008. Regime shifts, ecological aspects. In: Steele, J.H., Thorpe, S., Turekian, K. (Eds.), Encyclopedia of Ocean Sciences 2e. Academic Press, London.

Starfield, A.M., 1990. Rule-based, qualitative modeling. BioScience 40, 601–640.

Starfield, A.M., 1997. A pragmatic approach to modeling for adaptive management. Journal of Wildlife Management 61, 166–174.

Starfield, A.M., Bleloch, A.L., 1983. Expert systems: an approach to problems in ecological management that are difficult to quantify. Journal of Environmental Management 16, 261–268.

Starfield, A.M., Louw, N.J., 1986. Small expert systems: as perceived by a scientist with a computer rather than a computer scientist. South African Journal of Science 82, 552–555.

Starfield, A.M., Farm, B.P., Taylor, R.H., 1989. A rule-based ecological model for the management of an estuarine lake. Ecological Modelling 46, 107–119.

Stewart, T.J., Joubert, A., 2006. Multicriteria support for decision making in the ecosystems approach to fisheries management. Internal Report, Department of Statistical Sciences, University of Cape Town, 27 October 2006, 36 p.

Zadeh, L.A., 1965. Fuzzy sets. Information and Control 8, 338–353.

Progress in Oceanography 79 (2008) 401–412

Contents lists available at ScienceDirect

Progress in Oceanography

journal homepage: www.elsevier.com/locate/pocean

Interdecadal variability of anchoveta abundance and overcapacity of the fishery in Peru

Pierre Fréon [a,*], Marilú Bouchon [b], Christian Mullon [a], Christian García [b], Miguel Ñiquen [b]

[a] *Institut de Recherche pour le Développement (IRD), UR097, CRHMT, BP 171, 34203 Sète, France*
[b] *Instituto del Mar del Peru, (IMARPE), P.O. Box 22, El Callao, Peru*

ARTICLE INFO

Article history:
Accepted 14 October 2008
Available online 21 October 2008

Keywords:
Fishery management
Pelagic fisheries
Fishing effort
Overcapacity
Overexploitation
Temporal variations
Humboldt current
Peru

ABSTRACT

Paleontological and historical stock abundance estimates indicate that pelagic fish populations inhabiting upwelling ecosystems undergo large interdecadal variations in abundance with amplitudes equal to, if not larger than, the interannual variability. The interdecadal variability is characterized by periods of high and low abundance, termed "pseudo-cycles", because of their irregular periodicity. Fisheries targeting small pelagic fish suffer from overall overcapitalization, like many other fisheries, but also from an additional overcapitalization problem: a phase displacement between rapid fish population decreases and a slower disinvestment which follows. This lag produces economic hardship.

Here we document the fish:fishery relationship for the Peruvian anchoveta. Anchoveta pseudo-cycles of 20 to >100 years are observed, with the present stock abundance most likely located near upper part of the cycle. Fleet overcapacity expressed as the proportion of unused present capacity is estimated at 72% and processing overcapacity at 89%. A simple bio-economic model demonstrates the risks associated with the pseudo-periodicity in fish stock abundance in conjunction with fishery investment, open access, and overcapacity: a timing bomb for the fishing sector. The lag between disinvestment and decrease in fish abundance is quantified. A reduction of the fishing and processing capacity and measures to decrease the investment lag are recommended to limit the social, economical and political tensions that will result from the expected decrease in stock abundance. Finally, some management options to reduce these risks are discussed.

1. Introduction

Despite a century of research effort, the major challenge for fishery biologists remains to forecast the abundance of exploited fish stocks. Recently, fisheries have been managed within an ecosystem-based framework (Garcia et al., 2003) but still face the same challenge. Historically, the scientific focus was placed on environmental-forcing or exploitation-forcing (review in Fréon et al., 2005), but until recently, only the interannual scale was taken into account. Historical data on catches and conventional stock abundance estimates show that several fish populations, and especially small pelagic fish inhabiting upwelling ecosystems, undergo large interdecadal variations in abundance with amplitudes equal, if not larger than, the interannual variability (e.g. Bakun, 1996; Spencer and Collie, 1997; Schwartzlose et al., 1999). Paleontological records of scale deposition in anaerobic sediments indicate that this interdecadal variability existed long before fishery exploitation (Baumgartner et al., 1992; Holmgren-Urba and Baumgartener, 1993). The variability alternates between periods of high and low abundance, qualified as "quasiperiodic" (Turchin and Taylor, 1992) or termed "pseudo-cycles" (Fréon et al., 2005) because of their irregularity in periodicity (pseudo-periodic) an shape (often pseudo-sinusoidal or pseudo-U-shaped). Such pseudo-cycles also exist in other environments and systems (Menu et al., 2002). The mean period of the pseudo-cycles in the marine realm varies widely between 10 and 80 years depending on the species and region, but within a system the coefficient of variation of the period is approximately 30% and 50% according to historical and paleontological records, respectively. Because much investment within the fishery industry (and also in small-scale fisheries, see Fréon and Weber, 1983) also occurs on decadal rather than annual or interannual scales, analyses of decade-scale fish:fisheries relations are appropriate.

Fisheries suffer from overcapitalization (Glantz and Tompson, 1981) resulting in the first place from the tragedy of the commons: communal resources suffer from an inexorable process of degradation due to selfishness of "free riders" who use or destroy more than their fair share of common property. In open access fisheries (unlimited number of fishing license), a "race for fishing" is observed where the interest of any individual fisher of fishing company is to invest as much as possible in order to catch the

---

* Corresponding author.
E-mail address: pfreon@ird.fr (P. Fréon).

0079-6611/$ - see front matter © 2008 Published by Elsevier Ltd.
doi:10.1016/j.pocean.2008.10.011

biggest part possible of the annual quota before it is filled. Furthermore two additional factors aggravate fishing overcapacity: the positive feedback between overexploitation and overcapitalization, and misguided subsidies including buy-back programs of old vessels that end up in re-investment of less but much more powerful modern ones (Ludwig et al., 1993; Gréboval, 1999). The fisheries targeting small pelagic fish suffer from an additional overcapitalization problem – the phase displacement between highly variable fish abundance and investment. Investors typically do not anticipate changes in fish abundance, yet there is a long lag between investment and realization of profit (decision-making, factory or boat building delay, accumulation of benefits). Invested capital often peaks and remains committed as stocks enter the declining phase of their interdecadal pseudo-cycle. As stocks decline, the heavy investment has not been recovered and must be reformed, lost, or maintained in hope of a turnaround. Disinvestment in fisheries is slower than investment (Ludwig et al., 1993), which increases losses, i.e. rent dissipation. These powerful economic and political interests that drive fisheries to overcapitalize and overexploit despite scientific evidence that stocks are declining were called the "Ludwig's ratchet" by Hennessey and Healey (2000).

The Peruvian anchoveta fishery is at present the largest single-species fishery in the world, with average landings of *Engraulis ringens* (an anchovy species known as "anchoveta") over 5 million tons annually during the last decade (Ñiquen and Fréon, 2006). The fleet of over 1200 purse-seiners operates from several fishing harbors along the Peruvian coast and performs daily trips of about 20 h. From 1976 to 1999, sardine *Sardinops sagax* was a major secondary target for this fleet with a maximum landing of 3 million tons in 1985. But since then, catches declined, and since 2000, the fleet has been catching around 95% of anchoveta. For this reason the present paper concentrates on anchoveta. More than 99% of the landings of the fleet are processed into fish meal and fish oil, although recently, anchoveta processing for human consumption has started to take place. There was initially a single type of fishing vessel, all with steel hull but of different sizes ranging from 30 to 900 tons of holding capacity (HC), mostly owned by large fishing companies (the 'industrial' fleet). Since 1999 a semi-artisanal fleet of purse-seiners developed using wooden hulls and ranging from 30 to 110 tons HC (denominated the 'artisanal' fleet here, despite the local use of 'industrial wooden fleet'). This fleet is more labor-intensive than the industrial fleet, both for the construction of boat and capture of fish per fisher. Most of the owners have a single boat or share it with co-owners in familial or neighborhood social structures. There are at present about equal numbers of industrial and artisanal boats (~600 in total), but the industrial fleet lands over 85% of the catch.

Despite some official regulation of fishing effort, from a practical point of view the fishery is free access. Anchoveta fishery management is based on seasonal fishing quotas. IMARPE recommendations to the Peruvian Ministry of Fisheries are based on biological years starting on the 1st of October and ending on 30th of the following September. Usually there are two fishing seasons, each with its own quota: a summer season from October to March, and a winter season from April to September. The seasonal quotas are mainly based on acoustic and ichtyoplankton surveys performed at the beginning of every season estimating spawning biomass, recruitment and the age-structure of the stock. Many additional components of the ecosystem are also assessed in an attempt to apply ecosystem-based management: other pelagic species, major predators like birds, sea lions, seals and other fishes. Presently, the immediate goal of management is to maintain spawning biomass above about 5 million tons at the onset of each spawning period (August and February).

In this paper we examine the stock's pseudo-periodicity and relations between Peruvian anchoveta abundance and two main components of the fishery overcapacity: fleet overcapacity and processing overcapacity. We first document the decade-scale variability via literature review and with new data. Then we present a simple bio-economic model demonstrating the risks associated with the pseudo-periodicity of fish stock abundance in conjunction with the open access, the usual patterns of investment, and overcapacity. Finally, management options to reduce these risks are briefly discussed.

2. Material and methods

The study area is the Peruvian continental shelf and margin. It spreads from Tumbes (03°24′S) to (18°21′S), extending offshore up to 90 nautical miles (Fig. 1). Major emphasis is given to the north-central area, from 04°S to 14°S because the bulk of catches comes from the sub-stock located in this area (Pauly and Tsukama, 1987). The catch from the southern area of Peru (from 14°00′S to 18°21′S) are commonly taken to be from a different sub-stock shared by Peru and Chili (Serra, 1983). The issue of stock identity is still debated because individuals from the two sub-stocks sometimes mix (Alheit and Ñiquen, 2004).

Annual time series of catches and effort result from the compilation by IMARPE[1] of daily records of landing by individual purse-seiners, and are associated with sub-sampling of the catch composition as in Bouchon et al. (1997). By combining the information on daily individual landings with the official files on the industrial fleet (characteristics of the vessels), IMARPE produced annual series of holding capacity (HC) and GRT[2]. Because there is a linear relationship between HC and GRT (Tsukayama, 1969), only the first value is used here. The number of fishing days between 1959 and 1996 was obtained by subtracting days of official ("Vedas") and strike closure of the fishery in legal records from 365.

The general definition of overcapacity in fisheries retained here is the "harvesting capacity in excess of the minimum amount required to harvest the desired quantity of fish at the least cost" (OECD, 1996). A conventional expression of excess capacity is the capacity utilisation coefficient (CU) derived from the economy of firms. Applied to fisheries this is

$$\mathrm{CU} = Y/Y' \tag{1}$$

where Y is the fleet harvest desired by the resource managers (e.g. total allowable catch or TAC), and Y' is the potential harvest of the fleet, given the existing stock size. Thus, in a typical situation of overcapacity, $Y' > Y$, hence, we would have $\mathrm{CU} < 1$ (review in Gréboval, 1999). Following Gréboval (1999), we define excess fleet overcapacity as the proportion of the unused present capacity, that is

$$\text{Overcapacity } (\%) = 100 * (1 - \mathrm{CU}) \tag{2}$$

Y and Y' being strictly proportional to fishing effort in case of constant catch per unit of effort, Eqs. (1) and (2) can also apply to effort as in literature examples below. The same equation can apply to processing overcapacity, Y' being here the potential processing capacity.

Stock abundance is estimated by three different methods: the daily egg production method, hydroacoustic surveys, and virtual population analyses (VPA). Only VPA is used here because it covers a longer time period, but acoustic data were used to calibrate VPA estimates. Three VPAs were applied to the north-central stock of anchoveta: one by Pauly and Palomares (1989) for 1953–1985,

---

[1] Instituto del Mar del Perú.

[2] Gross register tonnage, that is the total internal volume of a vessel, with some exemptions for non-productive spaces such as crew quarters.

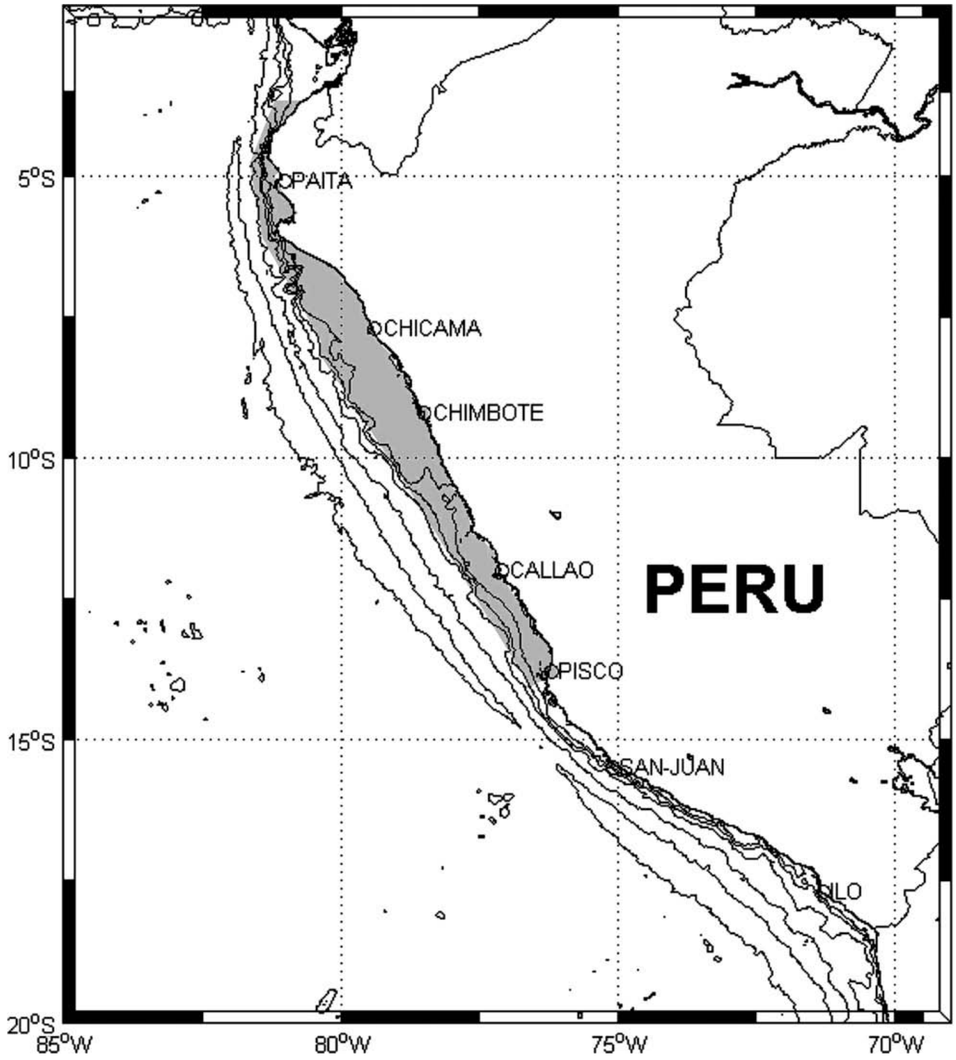

Fig. 1. Studied area. The northern-central stock of anchoveta is mainly located from 4°S to 14°S, within the 200 m isobath (grey area). The Peruvian component of the southern stock (not shown), less abundant and less exploited, is located from 14°S to the southern border around 18°21′S. Source: bathymetry: ETOPO02/coastline: GSHHS/boundary: DCW (produced by Dominique Dagorne, IRD US191).

one by Csirke et al. (1996) for 1960–1994 and one from Ñiquen et al. (2000) for 1961–1999 but updated here up to 2004.

Total fish consumption in Peru from 1999 to 2005 was estimated by multiplying the consumption per capita provided by PRODUCE (2007) by an estimation of the Peruvian population during the same period, assuming that INEI computed its value without using any age threshold. The Peruvian population was estimated by linear interpolation of the INEI census performed in 1993 and 2005.

Five theoretical bio-economic models of increasing complexity are used. All of them are simple implementations of a classical bio-economic model by Smith (Smith, 1968; see also Clark, 2006). In model-I, the carrying capacity of the ecosystem regarding anchoveta (mainly dependent on environmental conditions) is constant and investment and disinvestment patterns symmetrical. In model-II, a time-varying carrying capacity is used to simulate the cyclic character of pelagic stock abundance and investment patterns remain symmetrical. In model-III, the carrying capacity is constant as in model-I, but the investment and disinvestment patterns are dissymmetrical, investment being faster than disinvestment. Model-IV combines the cyclic pattern of abundance in model-II with the asymmetrical investment patterns of model-III (Table 1). Model-V adds total allowable catch (TAC) to model-III.

In models-I and -III, the biological compartment is based on the logistic equation:

$$X'_t = rX_t(1 - X_t/K) - qX_tE_t, \tag{3}$$

where X is the fish stock abundance (and X' its variation), r the natural renewal rate of the population, K the ecosystem carrying capacity, q the coefficient of catchability and E the fishing capacity.

In models-I and -II, we make the assumption that variations of effective fishing capacity (E'_t) are strictly proportional to benefits, such that investment or disinvestment does not lag benefits:

$$E'_t = k(pqX_tE_t - cE_t), \tag{4}$$

where k is the proportion of gains invested or the proportion of losses disinvested, p is a price coefficient and c a cost coefficient. In the second member of Eq. (4), the first part represents sales, proportional to catches (qX_tE_t), whereas the second part represents costs proportional to fishing capacity. One may consider (E'_t) and (X'_t) as annual changes of fishing capacity and fish stock abundance respectively.

In models-II and -IV, a periodic function is associated with the biological compartment:

$$X'_t = rX_t(1 - X_t/K_t) - qX_tE_t, \tag{5}$$

Table 1
Characteristics of the four bio-economic models.

Compartment	Model-I	Model-II	Model-III	Model-IV	Model-V
Biological (variation in K)	Constant (Eq. (3))	Cyclic (Eqs. (5) and (6))	Constant (Eq. (3))	Cyclic (Eqs. (5) and (6))	Constant, then cyclic (Eqs. (5) and (6))
Economical (investment/disinvestment patterns	Symmetrical (Eq. (4))	Symmetrical (Eq. (4))	Asymmetrical (Eq. (7))	Asymmetrical (Eq. (7))	Symmetrical (Eq. (9))
Catch regulation	No	No	No	No	TAC (Eq. (8))

where

$$K_t = K_0(1 + a\mathrm{Sin}(\omega t)) \tag{6}$$

In models-III and -IV, the economic compartment is modified in order to obtain faster investment compared to disinvestment:

$$E'_t = S(pqX_tE_t - cE_t), \tag{7}$$

where S is a function defined such as $S(P) = aP$ for $P < 0$, and $S(P) = bP$ for $P > 0$, with $a < b$, expressing that investment is faster than disinvestment. Indeed we made the strong assumption that capacity is changing proportionate to profits, and being slower to respond where profits are negative. Although we could have used a less drastic asymmetry between investment and disinvestments (S, a nonlinear smooth curve), we have chosen Eq. (7) to keep the model simple, avoid overparameterization, and amplify the differences between dynamics.

In model-V, the catch is regulated by a constant TAC, and the fishing effort is free to increase until the TAC is reached (which does not always occur because of other constraints in the model):

$$X'_t = rX_t(1 - X_t/K_t) - \mathrm{Min}(\mathrm{Tac}, qX_tE_t) \tag{8}$$

and

$$E'_t = k(p\mathrm{Min}(\mathrm{Tac}, qX_tE_t) - cE_t) \tag{9}$$

The bibliographical reviews on pseudo-cycle in abundance and history of the fishery were performed using Internet and direct access to libraries in Peru.

3. Results

Evidence of pseudo-cyclic variation in the Peruvian anchoveta stocks can be found among VPA data (Fig. 2) and paleontological records. VPAs of the north-central Peruvian stock suggest the existence of one full cycle followed by half a cycle since the 1950s. If we consider this series as pseudo-sinusoidal and arbitrarily assume that the starting point of a cycle is its lowest value, then the first cycle was likely to begin around 1948 and to end around 1983. The second cycle follows immediately and continues. The analysis of anoxic sediment cores from the continental shelf off Callao (°00′S, 72°42′S, 184 m depth) and in the upper slope off Pisco (14°07′S, 76°30′S, 299 m) by Gutiérrez et al. (2008) confirm the turning point of the 1980s, but only a local minimum in the early 1940s. Earlier decadal-scale turning points are obvious in the Gutiérrez et al. (2008) data sets of Callo and Pisco that start at the beginning of the 14th Century. The data suggest pseudo-cycles from 20 up to 120 years long, even though the number of turning points could be underestimated due to the low temporal resolution of the data.

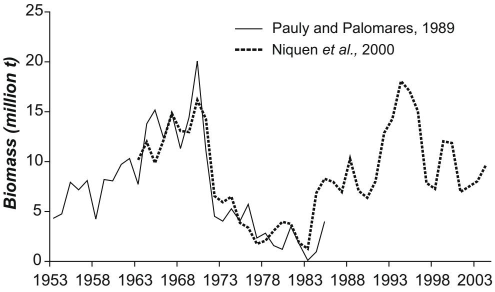

Fig. 2. Anchoveta biomass estimates from two VPA studies. Note the presence of nearly two pseudo-cycles. Sources: Pauly and Palomares (1989) and Ñiquen et al. (2000).

IMARPE (1974) stressed the overcapacity of the pelagic fleet at the beginning of the 1970s, indicating that the fleet could catch a third of the biomass in 1 month (which exceeded by far the turnover rate of the population). Assuming that a commercial fishing vessel can operate 240 days per year, Aguero (1987) estimated that only 364 purse-seiners were necessary to catch the TAC instead of 580 in activity in 1982, resulting in a 37% fishing overcapacity according to Eq. (2). He found a similar value for the processing overcapacity. At that time the total abundance of pelagic stocks was low and the computation was based on sustained catches of 3.5 million tons per year, that is half the production of the 2000–2006 period. More recently, Hatziolos and de Haan (2006) estimated that in 2005 the industrial fleet used only 31% of its fishing capacity and the artisanal fleet 25%, i.e. 69% and 75% of overcapacity respectively; they also estimated the potential catch of the new larger vessels was 95% greater than the old ones (no methodological details provided). A major proof of overcapacity during the following decades appears when comparing trends in fishing capacity and length of fishing seasons between 1987 and 2006. During this period, dominated by anchoveta abundance and landings (Fig. 2), both the number of fishing boats and their mean holding capacity increased dramatically (Fig. 3). As a result, the total fishing capacity of the fleet doubled from about 87,000 to 210,000 tons of holding capacity (Fig. 4). Similarly, the number of processing plants increased from 87 to 140 (Fig. 3a). In the mean time, although the annual quota recommended by IMARPE increased from 1.5 in 1987 to around 6 million tons in 1994, the fishing season decreased from 336 to 49 days because every year the quota was reached earlier due to increased capacity. As a result, the annual number of trips per fishing vessel is now extremely low. Most vessels made less than 50 trips per year in 2006, and a third of the fleet made fewer than 35 trips (Fig. 5). During November 2005, the total catch of anchoveta landings reached a record 2.6 million tons in the north-central area due to increased effort and capacity – there was no evidence of increased anchoveta abundance or availability (Ñiquen and Fréon, 2006). This record demonstrates that the potential catch and processing capacity amount, if the fishery was continually open and fish available, to at least to 31 million tons a year or, more realistically if one take into account the 4 months of fishing closure, 20.8 million tons in 240 days. The processing capacity itself is actually even higher, as total factory capacity is 8 976 ton h^{-1}, which over 240 working days per year amounts to 51.7 million tons processed annually. This processing capacity is about six times more than the average biomass of the stock during the last 5 years.

The recent increase in the number and size of vessels (and to their technical improvements, not discussed here), reflects the

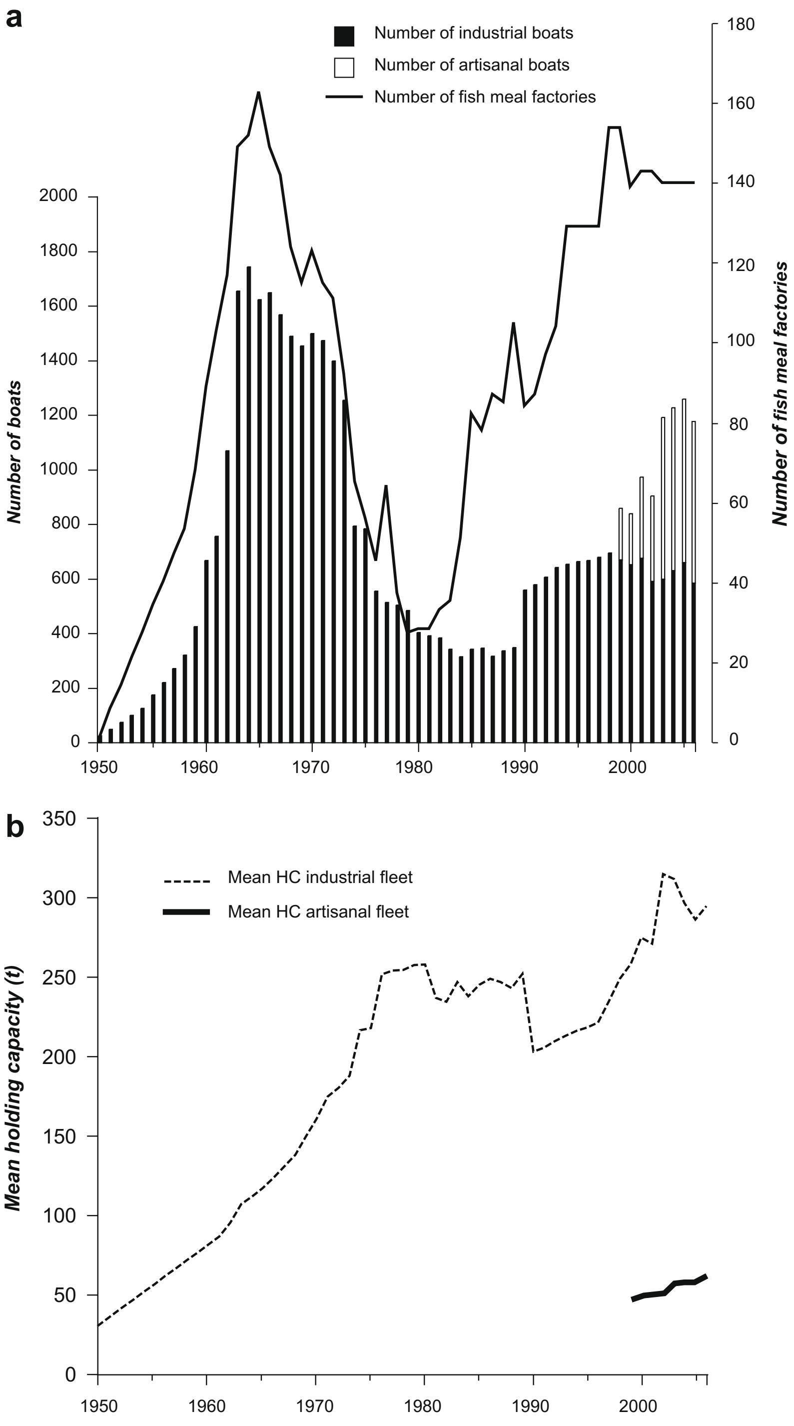

Fig. 3. Dynamics of the Peruvian pelagic industry from 1950 to 2006: (a) number of purse-seiners and number of factories; (b) mean holding capacity (HC) according to type of boat. Note the level off in the number of industrial boats and their mean HC from the mid 70 s. Nonetheless the total fishing power did not decrease due to technological improvements (not shown). Note also the lower mean HC of the artisanal fleet.

response of the fishery to the recovery of the anchoveta stock from 1986 onwards, with rapid and massive investments in more and larger boats (Figs. 3 and 6). In contrast, as shown in Fig. 6, the disinvestment that took place after the collapse of the anchoveta stock in the early 1970s was lagged and less intense than the fish population decrease, and the lag would certainly have been longer without the nationalization of the fishery (into Pesca Perú in 1973; Flores, 1976; Aguilar Ibarra et al., 2000). At that time, part of the fleet was sold to Chile and other countries, and some boats targeted the slow-growing sardine resource, other underexploited species like mackerel and horse mackerel, and the remains of the anchoveta stock. But many boats were idle until the mid 1980s (IMARPE, 1974a,b; Martinez et al., 1990). Pesca Perú was dissolved in 1978 and fishing and processing privatized (Hammergren, 1981). The misbalance between investment and fish abundance increased during the late 1990s and 2000s as stock abundance declined while investment and capacity increased.

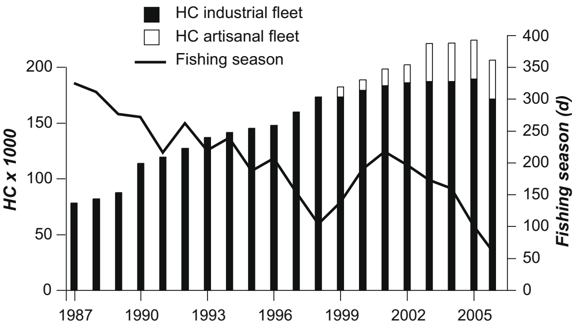

Fig. 4. Dynamics of the Peruvian pelagic fleet compared with the length of the fishing season. Note the opposite trends between the holding capacity (HC) of the fleet and the length of the fishing season.

The bio-economic model shows that, after the realization of a few pseudo-cycles and under stable biological and economical conditions, a stable equilibrium state for all variables develops, which is an attractor of the model dynamics (model-I; Fig. 7). When adding a periodicity to the ecosystem carrying capacity of the previous model (Fig. 8a), the stock, fishing capacity and yield responses are synchronous and stable oscillations (model-II; Fig. 8b–d). When modifying model-I by the incorporation of asymmetry in the investment/disinvestment pattern, the bio-economic system again develops a stable equilibrium on the long term (model-III; Fig. 9). The more dissymmetry in the patterns the larger the oscillations and the longer damping takes. When increasing the investment rate and decreasing the disinvestment rate, the stock average biomass decreases and its standard deviation increases (Table 2). An instable system, with frequent economic losses and collapses, is obtained by combining a periodic variation of ecosystem carrying capacity and an asymmetry in the investment/disinvestment pattern (model-IV; Fig. 10). Finally, adding a constant total allowable catch to model-III results in a relatively stable system where ecosystem carrying capacity is constant (model-V; Fig. 11), but when oscillations of the carrying capacity are added, the system quickly becomes unstable (model-V; Fig. 12). Model-V is extremely sensitive to the amplitude of variations in carrying capacity (not shown).

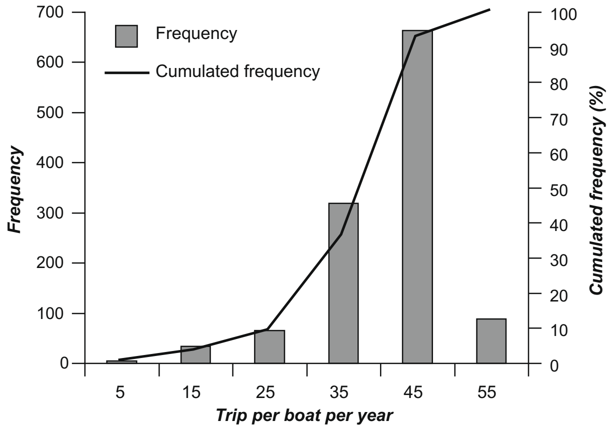

Fig. 5. Frequency distribution histogram of the number of fishing trips per boat in the north-central area in 2006 (the class interval is 10 and the central value of the class is displayed on the x axis). 93% of the vessels made less than 50 trips per year, and 36% made fewer than 35 trips

4. Discussion and conclusion

4.1. Is there a need to decrease fishing and processing capacity?

Paleontological and historical data about conventional stock abundance estimates during the last decades indicate that populations of small pelagic fish inhabiting upwelling ecosystems undergo large interdecadal variations in abundance equal, if not larger, than interannual variations. The anchoveta stock of north-central Peru illustrates such a pseudo-cyclic pattern, which for anchoveta is associated with chronic overcapitalization of its fishery. The situation is aggravated by a phase displacement between fish abundance and investment, characterized by slow disinvestment after declines in fish stocks. It is difficult to predict the length of pseudo-cycles and the cycle-to-cycle variability in stock abundance because (1) few realizations of the pseudo-cycles are available, (2) the process(es) responsible for the pattern of variability are largely unknown, (3) the recent global warming might have an impact on anchoveta.

The reduction in fishing days since 1987 days during a period of relatively stable anchoveta abundance demonstrates the overcapacity of the fishery (Fig. 4). Based on a capture capacity of over 20.8 million ton year^{-1} when average annual quotas was 5.8 million tons since 1987, fleet overcapacity is about 72% according to Eq. (2). Processing overcapacity is even higher ($100 * ((51.7 - 5.8)/51.7) = 89\%$), although only 35% of this capacity can be used to produce first quality fish meal (high protein content) from fresh fish (Hatziolos and de Haan, 2006). The fishery overcapacity problem is not new. Gordon (1954) reported the case of the Pacific halibut fishery and its competitive race for fish: “In 1933 the fishing season was more than 6 month-long. In 1952 it took just 26 days to catch the legal limit in the area from Willapa Harbor to Cape Spence, and 60 days in the Alaska region”. The continuation of this story is provided by Munro (2001). After the 1950s the race for halibut continued until the fishing season decreased to 6 days in 1990, when individual vessel quotas were established. Ten years later the number of active halibut boats had declined by over 50%. As a result, the number of fishing days per annum increased from 6 to 245 (Munro, 2001).

Obviously a fishing fleet must benefit from a certain level of overcapacity to adjust to high abundance periods and/or low availability of the resource. But the present fishing capacity of the Peruvian pelagic fleet is at least three times higher than the average TAC, which does not seem justified. There is now growing evidence that the catchability of pelagic species increases while abundance decreases (review in Fréon et al., 2005), resulting, especially if the quota is not enforced, in a high risk of population collapse. In agreement, Csirke (1989) found a strong negative relationship between the monthly anchoveta biomass estimated by VPA by Pauly et al. (1987) and the coefficient of catchability q resulting from the use of GRT trip^{-1} as a unit of fishing effort.

Since the end of the 1980s, anchoveta off Peru are, despite substantial fishing pressure and interannual variability due to El Niño events, abundant. Decreased abundance must be expected during the next decade(s), and a Peruvian crisis with high social, economical and political tensions will follow. This crisis will occur, even if IMARPE and the Peruvian Ministry of Fishery succeed in preventing a collapse of the resource by unpopular reduced quotas.

This kind of warning and recommendation is not new (review in Glantz and Tompson, 1981). In 1969 a panel of scientific experts recommended decreases to the fleet and processing facilities, 2 years before the stock started to collapse (Bermejo, 2006). At that time the fishing sector was heavily invested and in debt (Bermejo, 2006), illustrating the difficulty of fighting “Ludwig’s ratchet” in an open access fishery (Hennessey and Healey, 2000). Gordon (1954)

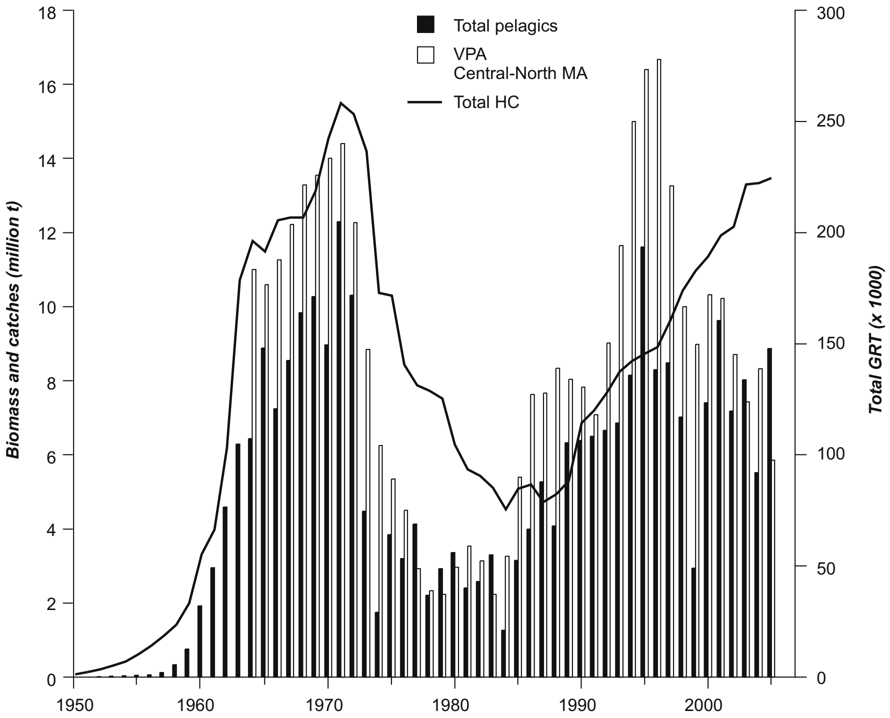

Fig. 6. Comparison of the dynamics of the Peruvian pelagic fleet (expressed in total holding capacity (HC)) with the dynamics of the major exploited resource (3-year moving average of the biomass of the north-central stock of anchoveta estimated by VPA) and the total pelagic catches of the fleet. Note the absence of lag between increasing resource (VPA) and investment (HC) and the positive lag between decreasing resource and disinvestment.

demonstrated that the competition among fishers culminates in the rent dissipation in an open access fishery. The equilibrium condition of uncontrolled exploitation is such that total costs must match total income; hence the net profit is zero, at least in the long run (Scott, 1955, 1993). This was also the base of our bio-economic models. In model-IV we added pseudo-periodicity in the stock abundance and an asymmetrical pattern of investment/disinvestment. It showed that in fisheries, the "conventional capital" *sensu* Munro (i.e. the non-human capital) is essentially "non-malleable" (McKelvey, 1985; Munro, 1999), that is here with some inertia in investment pattern.

4.2. Technical versus economic overcapacity and food security

Even if models-IV and -V demonstrated the risks associated with fishery overcapacity, the usual pattern of investment and pseudo-periodicity in fish stock abundance, they did not treat economic overcapacity – in particular price variability (p is a constant in Eq. (4)). The Peruvian pelagic fishery dominates the global fish meal and oil markets, as Peruvian products constitute ~40% of the world exportations (Tacon, 2003). As a result, price responds to Peruvian rates of production (Aguero, 1987). This production is now limited by fishing quotas and is relatively sta-

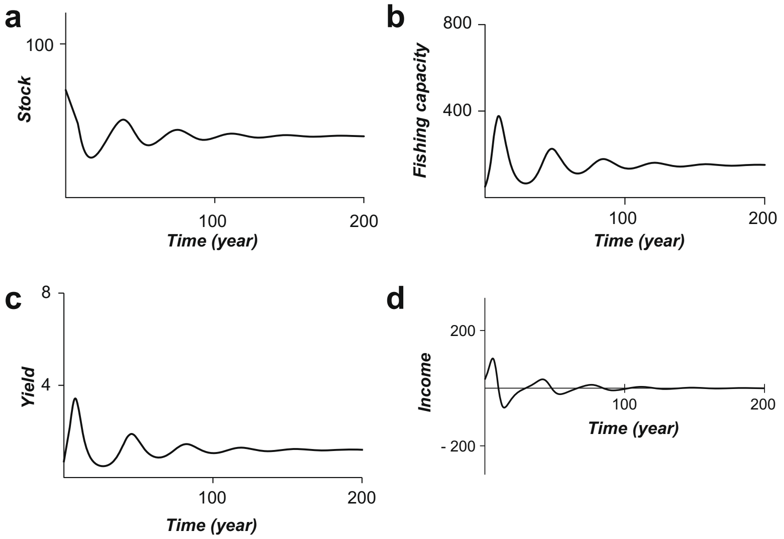

Fig. 7. Theoretical model-I (constant ecosystem carrying capacity; symmetrical investment/disinvestment patterns): (a) time series of stock abundance, (b) fishing capacity, (c) yield and (d) income. Note the long term equilibrium reached after a few oscillations on all time series.

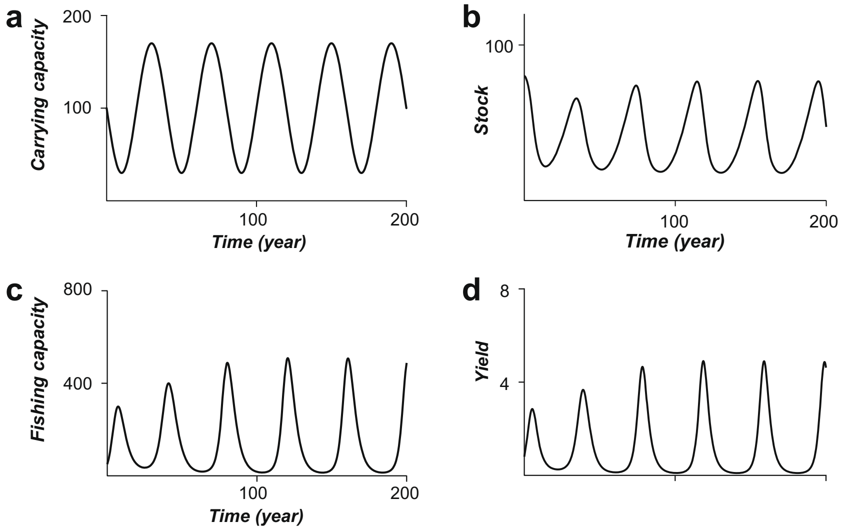

Fig. 8. Theoretical model-II (periodic ecosystem carrying capacity; symmetrical investment/disinvestment patterns): (a) time series of ecosystem carrying capacity, (b) stock abundance, (c) fishing capacity and (d) yield. Note the absence of attenuation of the oscillation generated by the periodic ecosystem carrying capacity.

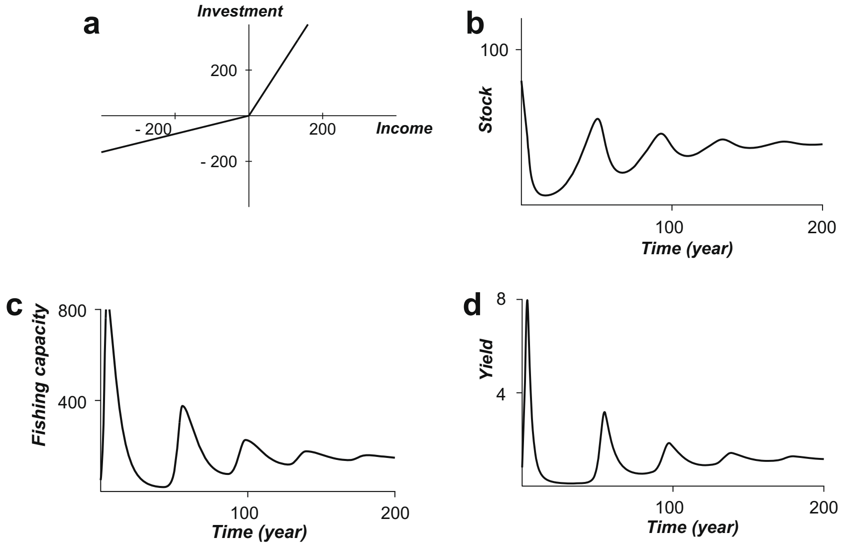

Fig. 9. Theoretical model-III (constant ecosystem carrying capacity; asymmetrical investment/disinvestment patterns): (a) investment/disinvestment behavior according to income, (b) time series of stock abundance, (c) fishing capacity and (d) yield. Note the long term equilibrium reached after a few oscillations on all time series.

Table 2
Simulation of the effect of changing investment and disinvestment rates on the average and standard deviation of the stock biomass.

Investment rate (× 100)	Disinvestment rate (× 100)	Average of the stock biomass	Standard deviation of the stock biomass
20	20	40	7
22	18	40	8
25	16	39	8
28	14	38	8
33	12	37	9
40	10	36	10
50	7	33	12
66	5	28	15
100	3	16	16

ble except during El Niño events. But the demand for both meal and oil has grown during the last 25 years due to the increase of aquaculture, especially for freshwater species in China, and farming of poultry and swine (Tacon, 2003; Asche and Tveterås, 2004). Thus if prices increase, overcapacity might be economically sustainable in Peru providing that fishing quotas are still adequate and enforced to prevent stock collapse. Still, the economic drawbacks of overcapacity in the Peruvian pelagic fishery ought to be better documented, as economic forces can produce a loss of control of the nominal effort or inappropriate

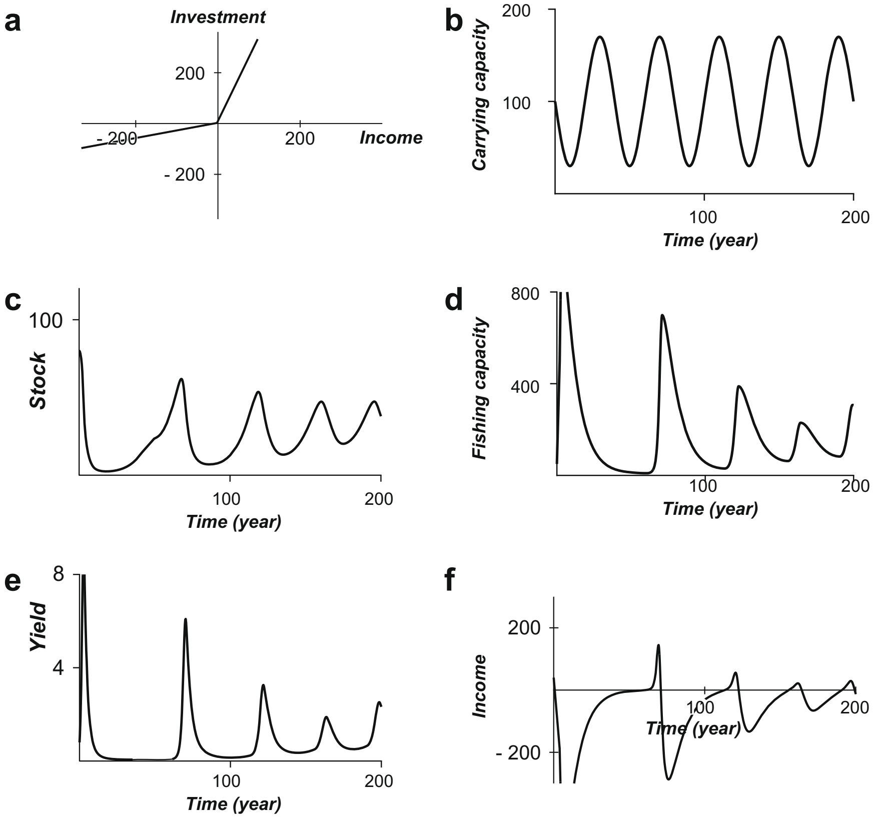

Fig. 10. Theoretical model-IV (periodic ecosystem carrying capacity; asymmetrical investment/disinvestment patterns): (a) investment/disinvestment behavior, (b), time series of ecosystem carrying capacity, (c) stock abundance, (d) fishing capacity, (e) yield and (f) income. Note the instability of the system, with frequent economic losses and collapses.

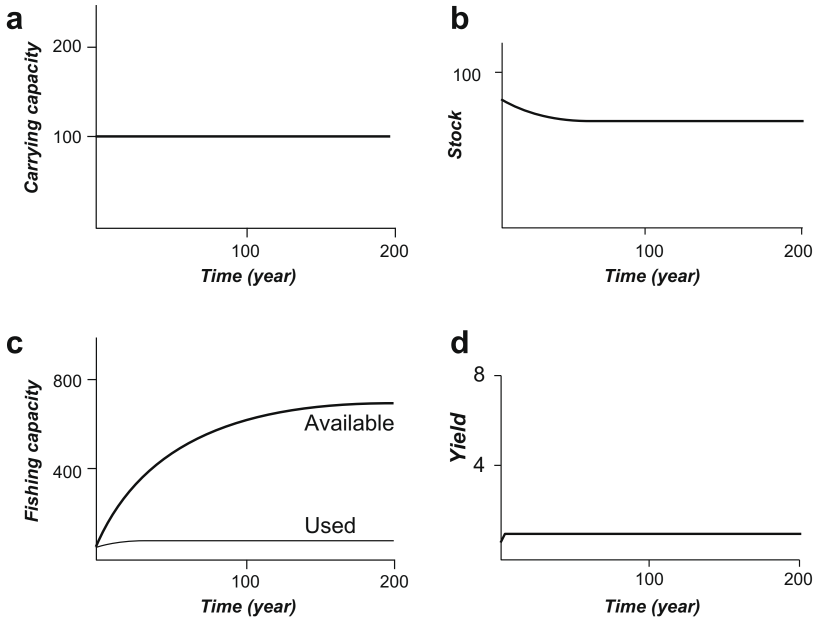

Fig. 11. Theoretical model-V (constant ecosystem carrying capacity; catch controlled by quota): (a) time series of ecosystem carrying capacity, (b) stock abundance, (c) available (bold curve) or used (thin curve) fishing capacity and (e) yield. This is an idealistic situation where, despite a strong overcapacity, the system is stable.

setting of the annual quotas. Sustainable high prices motivate catch under-reporting and poaching, which occur in this fishery as in many others (Castillo and Mendo, 1987; Hatziolos and de Haan, 2006).

Beyond the operational and economic aspects of overcapacity lies the issue of food security, especially in developing countries with high poverty rates such as Peru. Since most Peruvian pelagic catches are processed into fish meal and oil, Peru is a special case.

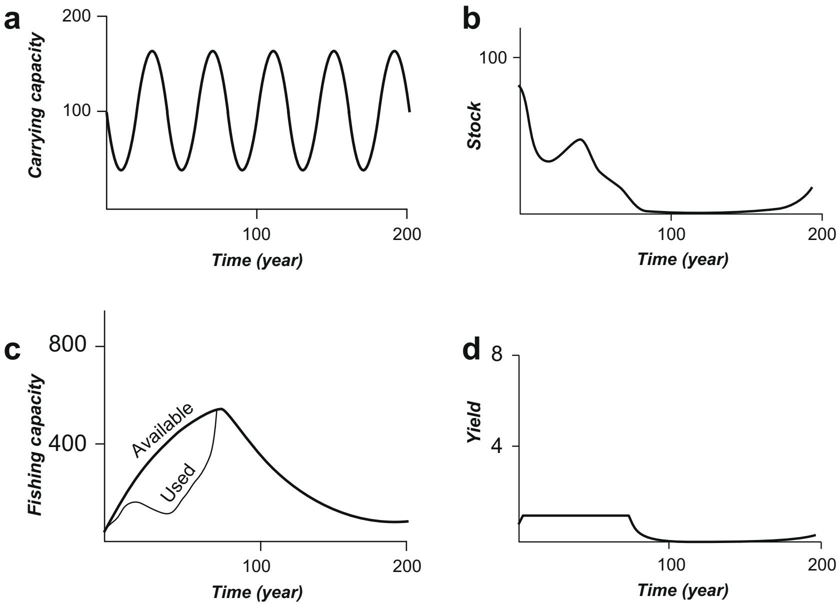

Fig. 12. Theoretical model-V (periodic ecosystem carrying capacity; catch controlled by quota): (a) time series of ecosystem carrying capacity, (b) stock abundance, (c) available (bold curve) or used (thin curve) fishing capacity and (d) yield. The system quickly becomes unstable.

First, within Peru fish meal is largely used to feed poultry and swine which constitute a source of protein. Storz et al. (2005) estimated that Peruvians consume 24 kg of poultry per year. Second, the Peruvian Government has recently encouraged the use of anchoveta products for human consumption, resulting in effective landing of 27,000 ton of fish used for fresh consumption, canning or production of fish pasta in 2005. In both cases the impact of fleet and processing overcapacity on food security is economic. Abundance of pelagic and demersal fish resources off Peru is so high, compared to Peruvian demand, that resource scarcity is not likely to occur within Peru. Only a few percent of the present fishing capacity suffice to secure food: from 1999 to 2005 we estimated that 6% of the total Peruvian production (Table 3), mainly demersal fish, were used for direct human consumption in Peru. But because overcapacity results in higher price of production, it can limit the access of the main source of proteins for the poorest segment of the Peruvian population.

All these negative aspects of fishing overcapacity need be balanced against positive aspects like employment and profits in the fishing sector in the broad sense of the word (construction or importation of fishing gear, boats and plants, etc.). How such positive and negative aspects interact and how profits flow into the overall economy are important economic and political issues that deserve further investigations.

4.3. How to reduce capacity in Peru?

Open access leads to fishery overcapacity and neo-liberalism implemented in Peru from the beginning of the 1990s favored overcapacity (Aguilar Ibarra et al., 2000). Alternative models include (1) establishment of individual quotas (IQ), transferable (ITQ) or not, (2) allocation of specific fishing rights to communities, (3) involving local communities in co-management. These options encourage conservation by fishers (McCay et al., 1998; Clark, 2006). Despite their strong theoretical background, experience to date with these alternative models has been mixed, even to fight the Ludwig's ratchet (review in Hennessey and Healey (2000)). But as pointed out by Troadec and Boncoeur (2003), alternative models to free access are more likely to succeed when national fleets exploit mostly resident stocks. Because the bulk of the resource (north-central anchoveta stock) is mostly a national resource this is presently the case of the Peruvian pelagic fishery.

Important questions remain. Are IQ feasible in Peru, are IQT adapted to a species with a short lifespan such as anchoveta? From an economic point of view, one may suggest that fishery capacity should be strongly reduced. Nonetheless, such a decision must also consider that fishing companies will need to refit older vessels, convert others to alternative users, and hopefully find ways to redeploy personnel. Now that the industrial and artisanal fleets are characterized by a wide range of HC, there are several options regarding the reduction of fishing capacity (Fig. 13). Because the artisanal fleet is more labor-intensive, both at sea and on land, reductions will more strongly affect manpower, whereas reductions to the industrial fleet will decrease invested capital.

All these ecological, economical and management considerations show that if fishery overcapacity must be reduced, solutions are complicated (e.g. effect of continuous technological improvements) and difficult. Nevertheless, a first and urgent measure is to remove the economic incentives that result in ever-increasing investment and fishery overcapacity. Such incentives will surely

Table 3
Estimation of the total annual consumption of fish by the Peruvian population based on the consumption per capita (PRODUCE, 2007) and interpolation of the 1993 and 2005 population census.

Year	1999	2000	2001	2002	2003	2004	2005
Consumption per capita (kg)	18.7	21.3	22.5	19.1	20.7	20.4	19.0
Peruvian population (million)	24.9	25.3	25.7	26.1	26.5	26.8	27.2
Estimated consumption (ton)	466,179	539,124	578,085	498,019	547,638	547,487	517,166

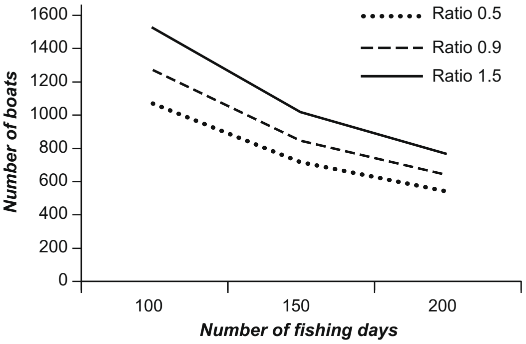

Fig. 13. Simulation of the increase in the number of fishing days and corresponding reduction in the number of boats according to the ratio between the number of artisanal boats and the number of industrial boats (present ratio is 0.9). This simulation is based on year 2005. Note the sensitivity of the total number of boats to the composition of the fleet.

produce economic and political hardship when the Peruvian anchoveta stock, inevitably, begins its next decline.

4.4. How to adjust changes in capacity to abundance fluctuations?

Beyond the need of reducing the overall overcapacity is the need to adjust capacity to the fluctuation of stock abundance. Fréon et al. (2005) proposed a two-level strategy to cope with interannual and interdecadal variations. The first level is the conventional adaptive management approach which incorporates new ecosystem-based thresholds or limit reference points as much as possible. The second level attempts to cope with inter-decadal variations in abundance. Once the turning point in abundance has been documented, uncertainty decreases and management could limit long-term investment in fishing units and related infrastructures and also take into account the entire range of social, economic and political implications. To quantify the associated risks will largely depend on our knowledge of the pseudo-cycle, which remains limited. While better understanding of the interrelated ecological, social, economic, political and governance issues are needed, reduction of the fishing overcapacity is an obvious and immediate need because it represents a timing bomb for the fishing sector.

Acknowledgements

We are grateful to Olivier Thebaud who provided us with references and guidance on the issue of economic overcapacity and to Pierre Lopez who produced the art drawings. This is a contribution to the European network of excellence EUR-OCEANS (EC Contract No. 511106-2) and to the research unit R097 ECO-UP of IRD.

References

Aguero, M., 1987. A bioeconomic model of the Peruvian pelagic fishery. In: Pauly, D., Tsukayama, I. (Eds.), The Peruvian Anchoveta and its Upwelling Ecosystem: Three Decades of Changes ICLARM Studies and Reviews 15, Instituto del Mar del Perú (IMARPE), Callao, Perú; Deutsche Gesellschaft fur Technische Zusammenarbeit (GTZ), Eschborn. Federal Republic of Germany; and International Center for Living Aquatic Resources Management (ICLARM), Manila, Philippines, pp. 307–324.

Aguilar Ibarra, A., Reid, C., Thorpe, A., 2000. Neo-liberalism and its impact on overfishing and overcapitalisation in the marine fisheries of Chile Mexico and Peru. Food Policy 25, 599–622.

Alheit, J., Ñiquen, M., 2004. Regime shifts in the Humboldt Current ecosystem. Progress in Oceanography 60, 201–222.

Asche, F., Tveterås, S., 2004. On the relationship between aquaculture and reduction fisheries. Journal of Agricultural Economics 55 (2), 245–265.

Castillo, S., Mendo, J., 1987. Estimation of unregistered Peruvian anchoveta (*Engraulis ringens*) in official catch statistics, 1951–1982. In: Pauly, D., Tsukayama, I. (Eds.), The Peruvian Anchoveta and its Upwelling Ecosystem: Three Decades of Change . ICLARM Studies and Reviews 15, Instituto del Mar del Perú (IMARPE), Callao, Perú; Deutsche Gesellschaft fur Technische Zusammenarbeit (GTZ), Eschborn. Federal Republic of Germany; and International Center for Living Aquatic Resources Management (ICLARM), Manila, Philippines, pp. 109–116.

Bakun, A., 1996. Patterns in the Ocean: Ocean Processes and Marine Population Dynamics. California Sea Grant College System, Univ. California, La Jolla.

Baumgartner, T.R., Soutar, A., Ferreira-Bartrina, V., 1992. Reconstruction of the history of Pacific sardine and northern anchovy populations over the past two millennia from sediments of the Santa Barbara Basin. California Cooperative Oceanic Fisheries Investigation Reports 33, 24–40.

Bermejo, A., 2006. La década del 70. Pesca Worldwide Circulation Magazine xx, 1–151.

Bouchon, M., Ñiquen, M., Arias Bello, R., 1997. Manual de operaciones del proyecto Bitácoras de Pesca. Informes Progresivos IMARPE 74, 1–44.

Clark, C.W., 2006. The Worldwide Crisis in Fisheries: Economic Models and Human Behaviour. Cambridge University Press, Cambridge, UK.

Csirke, J., 1989. Changes in the catchability coefficient in the Peruvian anchoveta (*Engraulis ringens*) fishery. In: Pauly, D., Tsukayama, I. (Eds.), The Peruvian Anchoveta and its Upwelling Ecosystem: Three Decades of Changes . ICLARM Studies and Reviews 15, Instituto del Mar del Perú (IMARPE), Callao, Perú; Deutsche Gesellschaft fur Technische Zusammenarbeit (GTZ), Eschborn. Federal Republic of Germany; and International Center for Living Aquatic Resources Management (ICLARM), Manila, Philippines, pp. 207–219.

Csirke, J., Guevara, R., Cardenas, G., Ñiquen, M., Chipollini, A., 1996. Situación de los recursos anchoveta (*Engraulis ringens*) y sardina (*Sardinops sagax*) a principios de 1994 y perspectivas para la pesca en el Perú, con especial referencia a la región norte-centro de la costa peruana. Boletín del Instituto del Mar del Perú 15 (1), 1–23.

Flores, M., 1976. El mar peruano como campo de actividad socio-económica. Informe del Instituto del Mar del Perú (unpublished).

Fréon, P., Weber, J., 1983. Djifére au Sénégal: la pêche artisanale en mutation dans un contexte industriel. Revue des Travaux de l'Institut des Pêches maritimes 47 (3–4), 261–304.

Fréon, P., Cury, P., Shannon, L., Roy, C., 2005. Sustainable exploitation of small pelagic fish stocks challenged by environmental and ecosystem changes. Bulletin of Marine Science 76 (2), 385–462.

Garcia, S.M., Zerbi, A., Aliaume, C., Do-Chi, T., Lasserre, G., 2003. The ecosystem approach to fisheries: issues, terminology, principles, institutional foundations, implementation and outlook. FAO Fisheries Technical Paper, vol. 443, 71 pp.

Glantz, M.H., Tompson, J.D. (Eds.), 1981. Resource Management and Environmental Uncertainty; Lessons Form Coastal Upwelling Fisheries. John Wiley and Sons, New York.

Gordon, H.S., 1954. The economic theory of a common property resource: the fishery. The Journal of Political Economy 62, 124–142.

Gréboval, D. (Ed.), 1999. Managing Fishing Capacity: Selected Papers on Underlying Concepts and Issues. FAO Fisheries Technical Paper, vol. 386, 206 pp.

Gutiérrez, D., Sifeddine, A., Field, D.B., Ortlieb, L., Vargas, G., Chávez, F., Velazco, F., Ferreira, V., Tapia, P., Salvatteci, R., Boucher, H., Morales, M.C., Valdés, J., Reyss, J.-L., Campusano, A., Boussafir, M., Mandeng-Yogo, M., García, M., Baumgartner, T., 2008. Rapid reorganization in ocean biogeochemistry off Peru towards the end of the Little Ice Age. Biogeosciences 5, 3919–3943.

Hammergren, L.A., 1981. Peruvian political and administrative response to El Niño. In: Glantz, M.H., Tompson, J.D. (Eds.), Resource Management and Environmental Uncertainty; Lessons form Coastal Upwelling Fisheries. John Wiley and Sons, New York, pp. 317–350 (Chapter 11).

Hatziolos, M., de Haan, C., 2006. Pesca. In: Giugale, M.M., Fretes-Cibils, V., Newman, J.L. (Eds.), Perú: La Oportunidad de un País Diferente: Próspero, Equitativo y Gobernable. World Bank, Washington DC, pp. 427–444.

Hennessey, T., Healey, M., 2000. Ludwig's ratchet and the collapse of New England groundfish stocks. Coastal Management 28, 187–213.

Holmgren-Urba, D., Baumgartener, T.R., 1993. A 250-year history of pelagic fish abundances from the anaerobic sediments of the central Gulf of California. California Cooperative Oceanic Fisheries Investigation Reports 34, 60–68.

IMARPE, 1974a. Informe de la Cuarta cesión del Panel de Expertos de la Evaluación del Stock de Anchoveta Peruana. Boletín del Instituto del Mar del Perú 2 (10), 605–719.

IMARPE, 1974b. Segundo Panel de Expertos: Informe sobre los Efectos Económicos de Diferentes Medidas Regulatorias de la Pesquería de la Anchoveta Peruana. Boletín del Instituto del Mar del Perú 3 (1), 4–40.

Ludwig, D., Hilborn, R., Walters, C., 1993. Uncertainty, resource exploitation, and conservation: lessons from history. Science 260, 17–36.

Martinez, C., Caballero, L., Bohm, G., Gili, R., Bocic, V., Muñoz, H., Barría, P., Serra, R., Hidalgo, H., Saez, P., Ortíz, Y.V., 1990. Diagnóstico de las principales pesquerías nacionales 1990: Estado de situación y perspectivas del recurso. Pesquerías pelágicas Zona Norte (I–IV Región). Corporación de Fomento de la Producción (CORFO) y Instituto de Fomento Pesquero (IFOP), Santiago-Chile, 91 (8), 119 p.

McCay, B.C., Apostle, R., Creed, C., 1998. Individual transferable quotas, comanagement and community. Fisheries 23 (4), 20–23.

McKelvey, R., 1985. Decentralized regulation of a common property renewable resource industry with irreversible investment. Journal of Environmental Economics and Management 12, 287–307.

Menu, S., Gauthier, G., Reed, A., 2002. Changes in survival rates and population dynamics of greater snow geese over a 30-year period: implications for hunting regulations. Journal of Applied Ecology 39, 91–102.

Munro, G.R., 1999. The economics of overcapitalization and fishery resource management: a review. In: Hatcher, A., Robinson, K. (Eds.), Overcapitalization and Subsidies in European Fisheries. Cemare, Portsmouth, pp. 7–23.

Munro, G.R., 2001. The effect of introducing individual harvest quotas upon fleet capacity in the marine fisheries of British Columbia. FAO Fisheries Technical Paper, vol 412, pp. 208–220.

Ñiquen, M., Espino, M., Bouchon, M., 2000. Análisis de la población de anchoveta durante el periodo 1961–1999. Boletín del Instituto del Mar del Perú 19 (1–2), 103–108.

Ñiquen, M., Fréon, P., 2006. A new record set by the Peruvian fishery: 2 5 million tonnes of anchovy landed in November 2005. GLOBEC International Newsletter, 56–57. Oct 2006.

OECD (Organization for Economic Cooperation and Development), 1996. Synthesis Report for the Study on the Economic Aspects of the Management of Marine Living Resources, AGR/FI (96) 12, Paris.

Pauly, D., Palomares, M.L., 1989. New estimates of monthly biomasa, recruitment and related statistics of anchoveta (*Engraulis ringens*), 1953 to 1981. In: Pauly, D., Tsukayama, I. (Eds.), The Peruvian Anchoveta and its Upwelling Ecosystem: Three Decades Of Changes. ICLARM Studies and Reviews 15, Instituto del Mar del Perú (IMARPE), Callao, Perú; Deutsche Gesellschaft fur Technische Zusammenarbeit (GTZ), Eschborn. Federal Republic of Germany; and International Center for Living Aquatic Resources Management (ICLARM), Manila, Philippines, pp. 167–178.

Pauly, D., Palomares, M.L., Gayanilo, F.C., 1987. VPA estimates of the monthly population length composition, recruitment, mortality, bio-mass and related statistics of Peruvian anchoveta 1955–1981. In: Pauly, D., Tsukayama, I. (Eds.), The Peruvian Anchoveta and its Upwelling Ecosystem: Three Decades of Change . ICLARM Studies and Reviews 15, Instituto del Mar del Perú (IMARPE), Callao, Perú; Deutsche Gesellschaft fur Technische Zusammenarbeit (GTZ), Eschborn. Federal Republic of Germany; and International Center for Living Aquatic Resources Management (ICLARM), Manila, Philippines, pp. 142–166.

PRODUCE, 2007. Anuario Estadístico 2006. PRODUCE, Ministerio de la Producción. Oficina General de Tecnología de la Información y Estadística, 220p.

Schwartzlose, R., Alheit, J., Bakun, A., Baumgartner, T., Cloete, R., Crawford, R., Fletcher, W., Green-Ruiz, Y., Hagen, E., Kawasaki, T., Lluch-Belda, D., Lluch-Cota, S., MacCall, A., Matsuura, Y., Nevarez-Martínez, M., Parrish, R., Roy, C., Serra, R., Shust, K., Ward, M., Zuzunaga, J., 1999. Worldwide large-scale fluctuations of sardine and anchovy populations. South African Journal of Marine Science 21, 289–347.

Scott, A., 1955. The fishery: the objectives of sole ownership. Journal of Political Economy 63, 116–124.

Scott, A., 1993. Obstacles to fishery self-government. Marine Resource Economics 8, 187–199.

Serra, R., 1983. Changes in the abundance of pelagic resources along the Chilean coast. FAO Fisheries Report 291, 255–284.

Smith, V.L., 1968. Economics of production from natural resources. American Economic Review 58 (3), 409–431. Part 1.

Spencer, P.D., Collie, J.S., 1997. Patterns of population variability in marine Fish stocks. Fisheries Oceanography 6 (3), 188–204.

Storz, C.D., Taylor, T.G., Fairchild, G.F., 2005. A Primer on Exporting to Peru, EDIS FE521. Department of Food and Resource Economics. University of Florida, Gainesville, FL.

Tacon, A.G.J., 2003. Aquaculture production trends analysis. In: Review of the State of World Aquaculture. FAO Fisheries Circular 886 (2), 5–29. 95 p.

Troadec, J.P., Boncoeur, J., 2003. La régulation de l'accès. In: Laubier, L. (Ed.), Exploitation et Surexploitation des Ressources Marines Vivantes RST, vol. 17. Académie des Sciences. Lavoisier Editions, Paris, pp. 355–394.

Tsukayama, I., 1969. Una nueva medida de la pesca por unidad de esfuerzo en la pesquería de anchoveta. Boletín del Instituto del Mar del Perú 2 (4), 129–156.

Turchin, P., Taylor, A.D., 1992. Complex dynamics in ecological time series. Ecology 73 (1), 289–305.